AD-A065 049 AIR FORCE FLIGHT DYNAMICS LAB WRIGHT-PATTERSON AFB OHIO F/G 1/3
CONFERENCE ON AEROSPACE TRANSPARENT MATERIALS AND ENCLOSURES (1--ETC(U)
DEC 78 R E WITTMAN

UNCLASSIFIED AFFDL-TR-78-168 NL

1 OF 10
ADA
065049



LEVEL II
AD A032 141

AFFDL-TR-78-168

AD A065049

CONFERENCE ON AEROSPACE TRANSPARENT MATERIALS AND ENCLOSURES held 24-28 April 1978, Long Beach, California. (12th) Conference rept.

R. E. WITTMAN
ADVANCED DEVELOPMENT BRANCH
VEHICLE EQUIPMENT DIVISION
Robert E. Wittman

DECEMBER 1978

912 p.

2202, 1926

TECHNICAL REPORT AFFDL-TR-78-168

DDC FILE COPY

Approved for public release; distribution unlimited.

DDC
RECEIVED
FEB 28 1979
D

AIR FORCE FLIGHT DYNAMICS LABORATORY
AIR FORCE WRIGHT AERONAUTICAL LABORATORIES
AIR FORCE SYSTEMS COMMAND
WRIGHT-PATTERSON AIR FORCE BASE, OHIO 45433

012 070
79 02 21 024

NOTICE

When Government drawings, specifications, or other data are used for any purpose other than in connection with a definitely related Government procurement operation, the United States Government thereby incurs no responsibility nor any obligation whatsoever; and the fact that the Government may have formulated, furnished, or in any way supplied the said drawings, specifications, or other data, is not to be regarded by implication or otherwise as in any manner licensing the holder or any other person or corporation, or conveying any rights or permission to manufacture, use, or sell any patented invention that may in any way be related thereto.

This report has been reviewed by the Information Office (IO) and is releasable to the National Technical Information Service (NTIS). At NTIS, it will be available to the general public, including foreign nations.

This technical report has been reviewed and is approved for publication.

ROBERT E. WITTMAN
Project Manager

FOR THE COMMANDER

AMBROSE B. NUTT
Director, Vehicle Equipment Division

Copies of this report should not be returned unless return is required by security considerations, contractual obligations, or notice on a specific document.

AIR FORCE/56780/9 February 1979 — 400

Unclassified

SECURITY CLASSIFICATION OF THIS PAGE (When Data Entered)

REPORT DOCUMENTATION PAGE		READ INSTRUCTIONS BEFORE COMPLETING FORM
1. REPORT NUMBER	2. GOVT ACCESSION NO.	3. RECIPIENT'S CATALOG NUMBER
4. TITLE (and Subtitle) CONFERENCE ON AEROSPACE TRANSPARENT MATERIALS AND ENCLOSURES		5. TYPE OF REPORT & PERIOD COVERED Conference Report - 24-28 April 1978 6. PERFORMING ORG. REPORT NUMBER
7. AUTHOR(s) Compiled by Robert E. Wittman		8. CONTRACT OR GRANT NUMBER(s) F33615-76-C-3076 Task 57
9. PERFORMING ORGANIZATION NAME AND ADDRESS AFFDL/AFML Wright-Patterson Air Force Base, OH 45433		10. PROGRAM ELEMENT, PROJECT, TASK AREA & WORK UNIT NUMBERS Project 2202, Project 1926, and Project 7381
11. CONTROLLING OFFICE NAME AND ADDRESS AFFDL/FEW Wright-Patterson Air Force Base, OH 45433		12. REPORT DATE December 1978 13. NUMBER OF PAGES
14. MONITORING AGENCY NAME & ADDRESS(if different from Controlling Office)		15. SECURITY CLASS. (of this report) Unclassified 15a. DECLASSIFICATION/DOWNGRADING SCHEDULE

16. DISTRIBUTION STATEMENT (of this Report)

Approved for public release; distribution unlimited.

17. DISTRIBUTION STATEMENT (of the abstract entered in Block 20, if different from Report)

18. SUPPLEMENTARY NOTES

19. KEY WORDS (Continue on reverse side if necessary and identify by block number)
Polycarbonate, Interlayers, Aircraft Transparencies, Windshields, Canopies, Acrylic, Bird Impact, Coating, Optical Requirements, Transparent Materials, Environment Resistance

20. ABSTRACT (Continue on reverse side if necessary and identify by block number)
The purpose of this report is to make available the technical papers presented at the Twelfth Conference on 'Aerospace Transparent Materials and Enclosures.' Thirty-eight technical papers are presented in seven sessions that address transparency design and performance, characterization, materials and processes, and bird impact resistance.

The papers contained herein have been reproduced directly from the original manuscripts.

DD FORM 1 JAN 73 1473 EDITION OF 1 NOV 65 IS OBSOLETE

Unclassified

SECURITY CLASSIFICATION OF THIS PAGE (When Data Entered)

79 02 21 024

FOREWORD

This report was prepared by the Improved Windshield Protection Program Office under Project 2202 "Improved Windshield Protection," Project 1926 "Aircraft Windshield Development," and Project 7381 "Materials Application." It was administered under the direction of the Air Force Flight Dynamics Laboratory, Air Force Wright Aeronautical Laboratories, Air Force Systems Command. Mr. R. E. Wittman (AFFDL/FEW) served as Project Manager.

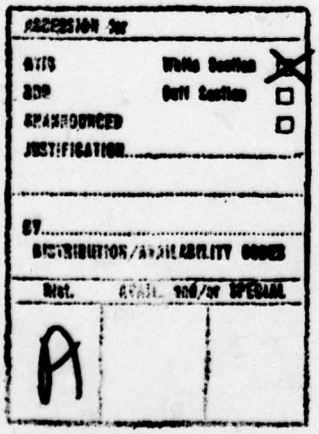
The technical papers contained in this report were presented at the Air Force Materials Laboratory/Air Force Flight Dynamics Laboratory Conference on "Aerospace Transparent Materials and Enclosures," which was held at the Edgewater Hyatt House, Long Beach, California on 24-28 April 1978.

Gratitude and appreciation are expressed to Mr. Samuel A. Marolo, AFML/MXE, and Mr. Joseph Militello and Mrs. Jennie L. Long, University of Dayton, for the excellent job accomplished as Conference Technical Coordinator, Conference Administrator, and Conference Secretary, respectively. Gratitude is also expressed to Colonel G. F. Cudahy, Commander, Air Force Flight Dynamics Laboratory, and Dr. Frank Kelley, Director, Air Force Materials Laboratory for their support of the Conference and their express concern and support of this technical area. Gratitude is expressed also to Dr. Demetrius Zonars, Deputy Director, Air Force Flight Dynamics Laboratory for his introductory remarks at the Conference.

The report was submitted by the author on Contract Number F33615-76-C-3076, Task 57.

Publication of this report does not constitute Air Force approval of the findings or conclusions presented. It is published only for the exchange and stimulation of ideas.

LEVEL II



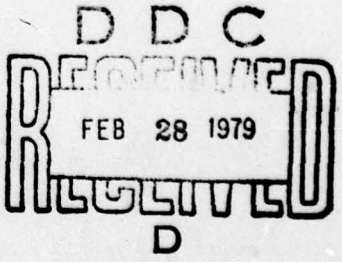


TABLE OF CONTENTS

	PAGE
OPENING REMARKS D. Zonars, Air Force Flight Dynamics Laboratory	1
SESSION I - BIRD IMPACT RESISTANCE	5
A History of Aircraft Transparencies S. R. France and D. Steidl, PPG Industries	7
A Study of Bird Impacts on Monolithic Aircraft Windshields A. J. Bosik, J. B. R. Heath, and R. W. Gould, National Research Council of Canada, National Aeronautical Establishment	11
The Modelling of Bird Impact Loads J. P. Barber and L. I. Boehman, University of Dayton Research Institute, and Capt. J. S. Wilbeck, Air Force Materials Laboratory	63
Biological Control of Birds, An Update 1st Lt. J. S. Kent, Air Force Civil Engineering Center	83
An Analytical Methodology for Defining the Bird Strike Requirements for Aircraft Crew Enclosures J. C. Halpin and J. Griffin, Aeronautical Systems Division	95
Design for Bird Impact: A Structural Systems Problem F. L. Pretzer and R. L. Peterson, Air Force Flight Dynamics Laboratory, and B. S. West, University of Dayton Research Institute	97
SESSION II - ADVANCED TECHNOLOGY DEMONSTRATOR PROGRAM STATUS REVIEW (PART I)	113
Windshield Technology Demonstrator Program - An Overview J. H. Lawrence, Jr., Douglas Aircraft Company, McDonnell Douglas Corporation	115
Environmental Design Criteria for High Performance Aircraft Windshields and Canopies L. P. Koegeboehn, Douglas Aircraft Company, McDonnell Douglas Corporation	141
Evaluation of Windshield Materials Subjected to Simulated Supersonic Flight Environments J. B. Hoffman, Douglas Aircraft Company, McDonnell Douglas Corporation	163

PRECEDING PAGE BLANK-NOT FILMED

TABLE OF CONTENTS (Continued)

PAGE

Aerodynamic Heating and Service Aging Effects on Mechanical Properties of Polycarbonate
M. Coker, Douglas Aircraft Company, McDonnell Douglas Corporation 201

Precipitation Static Electricity and Swept-Stroke Lightning and Their Effects on Windshield Subsystems
R. C. Twomey, Douglas Aircraft Company, McDonnell Douglas Corporation 219

SESSION III - ADVANCED TECHNOLOGY DEMONSTRATOR PROGRAM STATUS REVIEW (PART II) 235

The Development of Statistical Methodologies and a Computer Program for Material Properties
R. H. Magnusson, Douglas Aircraft Company, McDonnell Douglas Corporation 237

Design Mechanical Properties of Processed Polycarbonate and Interlayer Materials for Aircraft Transparencies
F. E. Greene, Douglas Aircraft Company, McDonnell Douglas Corporation 255

Edge Member Testing of Aircraft Transparent Materials
J. B. Hoffman, Douglas Aircraft Company, McDonnell Douglas Corporation 273

High-Speed Bird Impact Testing of Aircraft Transparencies
R. H. Magnusson, Douglas Aircraft Company, McDonnell Douglas Corporation 299

Aircraft Transparent Enclosure Bird Impact Math Model
P. H. Denke and G. R. Eide, Douglas Aircraft Company, McDonnell Douglas Corporation 329

SESSION IV - MATERIALS TESTING AND AIRCREW VISUAL STUDIES 381

Laboratory Screening Tests: A Cost Effective Approach to Aircraft Transparency Design
B. S. West and P. E. Johnson, University of Dayton Research Institute 383

The Fracture Toughness of Polycarbonate: A Preliminary Report
S. A. Sutton, Naval Research Laboratory, Mechanics of Materials Branch 411

TABLE OF CONTENTS (Continued)

PAGE

Abrasion Testing of Transparent Plastics
J. E. Mahaffey, PPG Industries, Incorporated, Aircraft and Specialty Products 433

A Method of Visual Inspection of Aircraft Transparencies
Capt. R. G. Eggleston, Aerospace Medical Research Laboratory 453

F-111 Windscreen Phorias
Lt. Col. B. D. Targove, Aerospace Medical Research Laboratory, Human Engineering Division, and Major W. F. Provines, School of Aerospace Medicine, Physiological Optics 465

The Effects of Windscreen Distortion Upon Pilot Approach and Landing Performance
W. L. Welde, Aerospace Medical Research Laboratory, Visual Display Systems Branch 477

Prediction of Weather-Resistance of Transparent Plastics by Multicondition Accelerated Exposure
J. M. Kolyer, Rockwell International Corporation, Autonetics Strategic Systems Division 491

SESSION V - MATERIALS AND PROCESSES 521

Report on Progress of ASTM F7.08
R. Morrow, Hughes Aircraft Company 523

An Improved Chip Retarder and Seal For Aircraft Windshields
S. H. Herliczek, J. C. Burwell, Sr., and J. G. Marriott, Libbey-Owens-Ford, Automotive Products Development 525

Characterization of Urethane Interlayers
E. M. Brown, Swedlow, Incorporated, Engineering 527

High Temperature Aircraft Glazing
R. Shelton, Swedlow, Incorporated, Engineering 547

Development and Application of Thin High Strength Glass
W. G. Roberts, Triplex Safety Glass Company, Ltd., Aircraft and Special Products Division 579

Superhard Coatings for Army Helicopter Glazings
T. E. Condon, Applied Technology Laboratory, U.S. Army Research and Technology Labs, and R. S. Hassard, Goodyear Aerospace Corporation, Arizona Division 601

TABLE OF CONTENTS (Continued)

	PAGE
Diamond Turning of F-111 Windscreens: Feasibility Study Phase I Major T. T. Saito, Air Force Materials Laboratory, and J. Taboada and Major B. R. Altschuler, USAF School of Aerospace Medicine	637
SESSION VI - DESIGN AND PERFORMANCE - PART I	659
British Airways Experience with Boeing 747 Cockpit and Cabin Windows K. B. Armstrong, British Airways, Structures Group	661
DC-8-60/DC-9. Windshield Attachment J. Christensen, Scandinavian Airlines, Maintenance Engineering	697
Windshield Design for Military Aircraft P. S. Christie, Boeing Aerospace Company, Boeing Military Airplane Development	715
Design, Development and Testing of a Lightweight Bird-Proof Cockpit Enclosure for the F-111 J. B. Olson, Sierracin Corporation, Sylmar Division/ Engineering	739
Glass/Plastic Transparent Armor for Helicopters W. C. McDonald, Goodyear Aerospace Corporation, Arizona Division	765
Design, Development, and Quality Assurance Testing of B-1 Side and Upper Crew Module Windows for Aircraft No. 4 R. E. Shumaker, Goodyear Aerospace Corporation, Arizona Division	787
SESSION VII - DESIGN AND PERFORMANCE - PART II	817
Aircraft Windshield Improvements W. C. Townsley, PPG Industries, Incorporated, Aircraft and Specialty Products	819
The Use of Explosive Cord for 'Through Canopy' Escape Systems G. W. Underwood, British Aerospace Aircraft Group Headquarters (Research)	833
The Windshield Development of a Modern Wide-Body Transport C. R. Mercer, Lockheed-California Company, Engineering	871

TABLE OF CONTENTS (Concluded)

PAGE

Aircraft Transparency Failure and Logistical Cost Analysis
S. Brown, Rockwell International Corporation, Los Angeles Division 905

Aircraft Transparency/Controller System Approach
E. Goller, Sierracin Corporation, Thermal Systems Division 929

OPENING REMARKS

D. Zonars
Air Force Flight Dynamics Laboratory
Wright-Patterson Air Force Base, Ohio

OPENING REMARKS

D. Zonars

Air Force Flight Dynamics Laboratory
Wright-Patterson Air Force Base, Ohio

Good afternoon and welcome to lovely Long Beach! On behalf of the Air Force Systems Command; Colonel Cudahy, Commander of the Air Force Flight Dynamics Laboratory; and Dr. Kelley, Director of the Air Force Materials Laboratory, I extend an official and warm welcome to all of you.

This is the 12th conference sponsored by the Air Force over the past 23 years on the subject of "Transparent Materials and Enclosures," and a registration of over 300 makes it the largest single group to date. I know of two or three people who have been around for just about all of these conferences, and I imagine there are several more in this room today. There are many of you who come from other countries, which speaks well of the reputation of these forums. We appreciate your attendance and look forward to your participation in the technical sessions. Of course, credit must be given to Mr. Wittman, Conference Chairman, Mr. Marolo for Coordination, Mr. Militello for Administration, and McDonnell Douglas for support.

There are several technolgies, each of which are reported through individual technical societies such as the Society of Aerospace and Materials Process Engineers (SAMPE), American Ceramic Society (ACS), American Society for Testing and Materials (ASTM), and so forth, that relate to components of Aerospace Enclosures. However, I believe this is the only conference which totally coordinates these specific technologies and brings them into public view in a "package" forum for the many persons involved in designing, manufacturing, fabricating, and using this knowledge. The consistent high interest in these meetings is proof of this, and I know that the 40 some papers you will hear over the next three days will not disappoint you.

This particular conference affords an added opportunity to the Air Force to include what we refer to as a "Critical Design Review." McDonnell Douglas has been engaged in an Air Force Systems Command (AFSC) sponsored technology program on transparencies for the past two and one-half years. Tomorrow a great portion of the total

PRECEDING PAGE BLANK-NOT FILMED

effort will be summarized and presented. What you will hear certainly will not cover all details of this program, but specific study areas will be reviewed and major technology advances highlighted.

Many years ago an aircraft windshield was simply a piece of plastic or a couple of layers of glass to keep wind and bugs away from the pilot. (Or if he had a leaky engine, it stopped the oil from obscuring his vision thru his goggles.) We have come a long way since then, and today we deal with very sophisticated "systems" that have to provide protection not only from the natural elements, but in the case of the military, hostile environments as well. Truly, transparent steel would be the answer for all of us, however, this technology is not yet in hand. The designing of windshields has become a real challenge, and the fabrication of an end item is turning more from an "art" to a "science." The civilian airline industry has also pushed technology forward because of its continued efforts on longer life and durability of windshields and windows under all conditions. This is not to say the military does not have these same interests because we do, but total flying hours over specific periods of time are much higher for the airlines and the emphasis in the past has been greater from this community.

We are not to the point where a windshield system becomes a "one time" installation on an aircraft and probably will not achieve this capability for a long time. (Never, if some of the fabricators have their way! That's a "joke," son.)

My comments are not meant to have a "deep message," but are just more of an "outsider's observation." In fact, so much of an outsider that retirement this Friday will carry me completely outside. Nevertheless, the Department of Defense will continue to enthusiastically support advances in transparency technology. With that promise, again, welcome to Long Beach, have a very successful symposium, and thank you. Please forgive me for departing, for I must ----

SESSION I

BIRD IMPACT RESISTANCE

Chairman: R. J. Speelman
Air Force Flight Dynamics Laboratory
Wright-Patterson Air Force Base, Ohio

A HISTORY OF AIRCRAFT TRANSPARENCIES

S. R. France and
D. Steidl
PPG Industries
Pittsburgh, Pennsylvania

PRECEDING PAGE BLANK-NOT FILMED

A HISTORY OF AIRCRAFT TRANSPARENCIES

S. R. France and
D. Steidl
PPG Industries

On December 17, 1903, Orville and Wilbur Wright flew their first aeroplane from the wind swept cape at Kitty Hawk, North Carolina. Strapped to the lower wing, in a prone position, Orville's only protection on that first flight was his hat, coat and a pair of automobile goggles. At 60 miles per hour, the wind and engine were deafening. He could feel the lift and see the ground moving down and away beneath the landing skids under his wing.

Today we can watch the ground fall away in total comfort. From 40,000 feet, we can see Kitty Hawk and the Outer Banks reaching north in a thin line toward the Chesapeake Bay. The transparencies that allow us to see out in comfort have changed dramatically in 75 years. The goggles were still essential behind the small windshields of those early open cockpit flights. But, as the aircraft flew higher and faster, we had to enclose ourselves behind a variety of new ideas. From quarter-inch automotive safety glass in flat panels, to today's tempered laminated glass with compound curvatures and critical optical requirements.

Our audio visual presentation on the history of aircraft transparencies is not intended to be an historical document, but rather a fast-paced, entertaining look at the aircraft, its transparencies and the beauty we find looking through them.

PRECEDING PAGE BLANK-NOT FILMED

A STUDY OF BIRD IMPACTS ON MONOLITHIC AIRCRAFT WINDSHIELDS

A. J. Bosik, J. B. R. Heath
and R. W. Gould
National Research Council of Canada
National Aeronautical Establishment
Ottawa, Ontario, Canada

PRECEDING PAGE BLANK-NOT FILMED

A STUDY OF BIRD IMPACTS ON MONOLITHIC AIRCRAFT WINDSHIELDS

A.J. Bosik, J.B.R. Heath and R.W. Gould
Structures and Materials Laboratory
National Aeronautical Establishment
National Research Council of Canada
Ottawa, Ontario, Canada

ABSTRACT

The initial results of an experimental program to generate design information on the bird impact resistance of flat panels of monolithic as-cast acrylic, stretched acrylic and polycarbonate, mounted in a highly rigid frame, were presented at the transparency conference in Atlanta in 1975. In the presentation, data were included for penetration velocity versus panel thickness for one, two and four-pound birds. In addition, a study was made to determine the effects on penetration velocity of varying the panel temperature and impact angle.

The present report contains the results of a continuation of the original program. Studies have been conducted to clarify some of the anomalies existing in the originally presented data. The penetration velocities of polycarbonate panels "clamped" to a highly rigid frame have been determined and empirical equations relating penetration velocity, material thickness and bird weight for the acrylic and polycarbonate panels are given. Studies were also made to determine the effects on penetration velocity of varying the impact position and the cumulative effects of multiple impacts. In addition, studies are being conducted to ascertain correlations between the panel penetration velocities and the material mechanical properties, but only preliminary results are available at present.

PRECEDING PAGE BLANK-NOT FILMED

1.0 Introduction

Along with the continued trend for the design of high performance aircraft, the emphasis on studies of bird resistant aircraft transparencies has generally been directed towards windshields most suitable for aircraft having a high cruise speed. Less prevalent are studies directed at birdproof transparencies for the lower cruise speed type aircraft. As a result, bird impact design data for transparencies of the latter type aircraft are generally lacking, particularly for some of the newer plastic materials such as polycarbonate. There is also some question as to the adequacy of windshields in low cruise speed aircraft not required to be certified in North America to resist bird impact. On this basis, a program was initiated at the Structures and Materials Laboratory of the National Aeronautical Establishment (NAE) to generate bird impact data for windshield materials most applicable to the low speed, unsophisticated and unpressurized aircraft. Although a guideline[1]* in the program was that the aircraft under consideration have a maximum cruise speed of 250 mph, in many instances data have been generated for speeds exceeding the guideline. Because of this and the fact that a number of parameters have been considered, certain parts of the data from the program may also be of interest to investigators of windshields for higher cruise speed aircraft.

Throughout the program, attempts were made to apply standard or widely used procedures for determining the material resistance to bird impact. Specifically, these procedures were applied to bird weights, impact angles, impact positions, material temperatures and use of a highly rigid support structure. Most often in the literature, data has been obtained with the sample panels bolted at the edges although the exact configurations used have not been universal. In the present program, two methods of panel edge attachment were used, loosely defined as "bolted" or "clamped". In the "bolted" case, a panel was restrained primarily by the bearing reactions of the bolts passing through the panel, whereas a "clamped" panel was restrained primarily or totally by the frictional forces on the panel edges. The use of the bolted edges was intended to provide comparative data with the more common practice while clamped edges were used since this method indicated a better utilization of the material. Also, because of the high clamping forces required to retain the panels, the clamped edges are more easily applied to panels impacted at lower speeds than would be the case for higher impact speeds. The plastic materials chosen for the program are commonly used in aircraft transparencies. There appears to be no standard size or shape of panels used in evaluating a material for resistance to bird impact, hence square panels were chosen of a size considered satisfactory.

---

*Superscripts indicate references listed at the end of the paper.

The initial results of the program were presented at the Conference on Aerospace Transparent Materials and Enclosures[2] in 1975. The present paper summarizes the major findings since the aforementioned presentation. A more comprehensive report on the program is being prepared.

2.0 Principal Symbols and Definitions

t - nominal panel thickness (inches)

T - panel temperature (°F)

W - nominal bird weight (lbs) - including bird and packaging

V - velocity (mph)

V_k - velocity (knots)

V_p - penetration velocity (mph) = $\frac{V_a + V_b}{2}$

where V_a = minimum velocity with penetration

V_b = maximum velocity less than V_a without penetration

The error in V_p is expressed $\pm \frac{(V_p - V_b)}{V_p}$

β - impact angle (angle between bird trajectory and plane of panel)

α - sweepback angle (angle between trajectory of bird and normal to panel)

Birds - all birds are real chicken carcasses of one, two or four pound body weight

Edge restraint - refers to type of fastening - "bolted" or "clamped" rather than stiffness of support frame

Penetration - bird impact must result in definite hole or opening in panel.

3.0 Program

The basis of the program was to determine V_p experimentally for flat monolithic panels of as-cast acrylic, stretched acrylic and polycarbonate, mounted in a highly rigid support frame. The parameters, thought to be important in effecting V_p that were investigated, included panel thickness, bird weight, edge restraint, panel temperature, impact angle, impact position and the cumulative effect of multiple impacts. The panel size was nominally two feet by two feet.

In carrying out the program, the first priority was to establish a data base from which the effects of varying the other

parameters could be studied. The data base was established by determining V_p under room temperature conditions for the three materials with the panels mounted at 45° and centrally impacted with one, two and four-pound birds. Panel thicknesses ranging from 0.093 to 0.375 inches were used. The effects on V_p of panel temperature, impact angle, impact position and the cumulative effects of multiple impacts were then investigated for one thickness of each material impacted with only one bird weight.

With the exception of the polycarbonate panels clamped at the edges, the base data and the effects on V_p of varying the panel temperature and impact angle were previously presented[2]. Hence, the emphasis in this paper is to first clarify anomalies existing in the previously presented data, present and compare empirical equations for the base data and present the results of the remainder of the program. In addition, studies are being conducted to ascertain correlations between V_p and the material mechanical properties.

Commercial grades of as-cast acrylic and polycarbonate were procured for the program. The stretched acrylic material was procured to MIL-P-25690A with the optical requirements waived. The manufacturers' quoted mechanical properties as well as the thickness variations encountered during the program are given in Appendix A.

4.0 Test Procedure

The bird impacts were conducted at the NAE/NRC Flight Impact Simulator Facility[3] in which the 10 inch bore compressed air powered gun (Figure 1) was used to propel the birds to the stationary test panels. The facility uses two independently operating optical-electronic timing systems for measuring the projectile velocity just prior to impact. The accuracy of these systems is considered to be within 0.5%.

The birds were real chicken carcasses, previously frozen then thawed to room temperature prior to packaging in polyethylene bags for use. The nominal one, two and four pound chicken carcasses were selected or adjusted so that the respective weights of the packaged projectiles were 1 lb $\pm^{2}_{0}$ oz., 2 lb $\pm^{2}_{0}$ oz. and 4 lb $\pm^{4}_{0}$ oz. The weight adjustments, when necessary, were accomplished by either trimming portions of the extremities of the carcasses or by adding jell (98% water and 2% sodium carboxymethylcellulose by weight) into the packages. The amount of weight adjustment was limited to about 10% of the final projectile weight.

The test panels were obtained from flat sheet stock of the materials. For those panels requiring edge holes, the holes were drilled in a suitable jig for locating the bolt hole positions. No other procedures were used to finish the bolt holes after drilling.

The test panels were attached to a mounting plate which in turn was secured to the structural steel support frame, shown in Figure 2. The various methods used in restraining the panel edges are shown in Figure 3. The method of Figure 3(a) has been termed a "bolted" edge restraint. The remaining methods were termed "clamped" edge restraints. The support frame was first aligned for a centre panel impact and then secured at its base to tie-downs on the floor of the test site. The panel impact position and angle were altered by readjusting the four by four by $\frac{1}{4}$ inch members (supporting the mounting plate) relative to the support frame. Angular alignments were made to within $\frac{1}{2}°$ of the desired values.

An enclosure constructed of styrofoam insulation was erected around a mounted test panel for a low or elevated temperature test. The panel was soaked to the desired temperature by introducing either cooled or heated air into the enclosure with ducts going to each side of the panel. Grid-type copper-constantan thermocouples were used to monitor the panel centre and corner temperatures as well as the temperature of the panel mounting plate during the panel conditioning. A panel was impacted after the centre of the panel reached a temperature of -40 ±5°F for the low temperature tests and +120 ±5°F for the elevated temperature tests. The panels for the low or elevated temperature tests were nominally 1/8 inch thick. Typical panel temperature conditioning durations from room temperature conditions were one hour for cooling and 1/2 hour for heating.

In general three to five impacts were performed to obtain a penetration velocity. Except for the studies pertaining to the determination of the cumulative effects of multiple impacts, it was generally the practice to use a new panel for each impact. A previously impacted panel was used for verification purposes only when there was no visible damage to the panel.

5.0 Discussion of Results

5.1 General

Although the results are given with the nominal material thickness and bird weight, it is recognized that a certain degree of scatter in the results occurred because of their variations from the nominal values. Further scatter in the results, although difficult to quantify, is attributed to the methods of edge restraint. Also it was observed that small changes from the intended impact position produced variations in the results. Finally, some scatter in the results can be attributed to panel-to-panel variations in the material properties. The test data, given in Figures 4 to 19, include all of the impacts performed so as to provide a "band width" of the penetration velocities.

Typical fractured acrylic panels were shown in Reference 2. Typical penetrated polycarbonate panels with the bolted and clamped edge restraints are shown in Figure 20.

5.2 Bird Impacts on Panels Mounted at 45°, Room temperature Conditions, Centre Panel Impacts (Base Data)

5.2.1 Panels "bolted" at edges

The results for the panels tested in the bolted condition are given in Figures 4 to 12. The edge restraint method was that of Figure 3(a) in all cases. The penetration velocities of the panels are approximated by the following empirical equations, which were established by a trial-and-error process of curve fitting;

As-cast acrylic:

$$V_p = \frac{336\ t^{0.52}}{W^{1/3}} \qquad (1)$$

Stretched acrylic:

$$V_p = \frac{369\ t^{0.52}}{W^{1/3}} \qquad (2)$$

Polycarbonate:

$$V_p = \frac{742\ t^{1/3}}{W^{1/3}} \qquad (3)$$

where V_p = penetration velocity (mph)
t = panel thickness (inches)
W = bird weight (lbs)

The results originally presented[2], gave only those data that were necessary to define the penetration velocities. Some of the data contained apparent anomalies. Additional tests were performed to substantiate the data and the present results (Figure 4 to 12) show all of the valid impacts so as to indicate any scatter. In those cases in which anomalies were evident, bird weights, panel thicknesses, static tensile properties of the panel materials and impact positions were checked to ascertain correlations consistent with the discrepancies.

Inconsistencies are particularly evident in the 3/8 inch thick acrylic panel results (Figures 4 and 8) in which the panels were alternately penetrated and non-penetrated with increasing impact velocities. The checks for the acrylic panel tests, indicated no appreciable correlation between the bird weights panel thicknesses or tensile properties (based on tensile strength and elongation) and the discrepancies in the results. Because of the catastrophic manner in which the acrylic panels failed during impact, it could not be determined with any certainty that variations in the impact positions were related to the inconsistencies of the test results.

There was also an apparent anomaly in the original data[2] for the one-pound impacts on 1/4 inch thick polycarbonate panels in that V_p was abnormally high. This anomaly could not be attributed to bird weight, panel thickness or tensile properties. A further examination of the original panels (from which V_p of 569 mph was obtained) showed that the panels had been impacted approximately two inches below the intended impact point (measured in the plane of the panel). The results shown in Figure 10 were with impacts at the approximate centre of the panel and these results indicate a penetration velocity of 466 mph. As a further verification of the above, an additional impact was performed at a point two inches below the centre of the panel at 541 mph and no penetration occurred. Hence, a two inch variation in impact position has a substantial effect on V_p, which led to the anomaly in the previous data.

It is important to note that with the bolted edge restraints, the panel failures initiated at the bolt holes. For that reason, the condition of the bolt holes was important and imperfections could lead to a lower V_p. This would be particularly important for materials which fail in a brittle manner, and is believed to be a factor contributing to the inconsistent results for the acrylic panels. A test in support of this statement is the impact at 177 mph on a 3/8 inch acrylic panel, Figure 4, in which a crack occurred across a corner of the panel with each end of the fracture terminating at a bolt hole. Although no chicken debris penetrated this fracture, the panel was penetrated according to the definition used.

5.2.2 Panels "clamped" at edges

Results for the panels tested in the clamped condition are given in Figures 13 to 19. These results include impacts with one, two and four-pound birds on as-cast and stretched acrylic panels and two-pound bird impacts on polycarbonate panels. The acrylic panels were restrained by the method of Figure 3(b) for all thicknesses. The polycarbonate panels were restrained by the method of Figure 3(c) for 0.093 inch and 0.125 inch thick panels, and by the method of Figure 3(d) for 0.25 inch thick panels.

The penetration velocities are approximated by the following empirical equations:

As-cast acrylic:

$$V_p = \frac{424\ t^{0.52}}{W^{1/3}} \qquad (4)$$

Stretched acrylic:

$$V_p = \frac{587\ t^{0.52}}{W^{1/3}} \qquad (5)$$

Polycarbonate (two-lb bird)

$$V_p = 1374\ t^{2/3} \qquad (6)$$

Of the results previously presented[2], only the data for the two-pound bird impacts on as-cast acrylic panels appeared to contain an anomaly as indicated by a change in curvature of the plotted data. This arose from a misplot of a data point for a 1/4 inch thick panel and the corrected data is shown in Figure 14. The polycarbonate results (Figure 19) were not previously presented.

As compared to the bolted edge results discussed in the previous section, the results of the clamped edge tests are more consistent. This is attributed to the removal of the problem arising from the bolt hole conditions. By clamping the edges, however, a different parameter affecting the V_p is potentially introduced. If insufficient clamping of the edges is achieved, slippage occurs during impact. Depending on the method of edge restraint, the amount of edge slippage can either raise or lower the V_p of a panel. If edge slippage is minimized so as to prevent failure at the bolt holes, V_p is increased. If the clamping force is insufficient, the panel failure occurs at the bolt holes and V_p is decreased. If no bolting through the panel is used, slippage will increase V_p but there is a risk of the panel edge being pulled out of the restraint. In this program, an attempt was made to design the edge restraints to minimize edge slippage and to prevent panel edge failures by machining a radius on the edge of the mounting plate adjacent to the panel. In this manner, the material impact values were obtained with minimal edge effects.

The polycarbonate panels, in particular, required high edge clamping forces to minimize slippage and the required force increased with panel thickness. Nevertheless, panel slippage in varying amounts was still evident for all the materials. The effects of edge clamping are further discussed under Section 5.3.

5.2.3 Comparison of empirical equations with experimental data

A number of empirical equations have appeared in the literature over the years predicting the penetration velocities of transparent materials usually as a function of material thickness, bird weight and impact angle. In general, these equations were based on higher penetration velocity data than was obtained in the present program. In order to ascertain at least an indication of the applicability of these equations to the present data, the equations are compared (for selected conditions) with the data and empirical equations presented in this program. The conditions selected were those found most commonly in the literature: four-pound bird impact, impact angle of 45°, centre panel impact and room temperature conditions.

5.2.3.1 As-cast acrylic

The following empirical equations are used to predict V_p for bird impacts on as-cast acrylic panels:

From a publication[5] prepared at RAE:

$$t = 0.136\ (1-0.348 \cos \alpha)\ \text{antilog}_{10} \frac{V_p \cos \alpha}{202} \qquad (7)$$

Also, Poullain and Clamagirand[6] gave the following equation for a flat panel (converted to English units):

$$t = \left[\frac{(0.447\ V_p)^2 (0.4536\ W)^{2/3} \sin \beta}{18{,}064}\right]^{1/2} \qquad (8)$$

Equations (7) and (8) have been compared with the bolted edge data and equation (1) in Figure 6 and with the clamped edge data and equation (4) in Figure 15. In the relatively small data base of Figures 6 and 15, it is seen that equations (1) and (4) represent the data somewhat more accurately than equation (7) or (8). Equation (8) does however approximate the general slope of the plotted data and is more applicable to the bolted edge condition although it underestimates V_p in both the bolted and clamped edge cases.

5.2.3.2 Stretched acrylic

The following empirical equations are used to predict V_p for stretched acrylic panels:

From Mott[7], based on panels clamped at the edges:

$$V_p = \frac{470\ t^{2/3}}{W^{1/2} \cos \alpha} \qquad (9)$$

From Poullain and Clamagirand[6], as applied to flat panels (converted to English units):

$$t = \left[\frac{(0.447\ V_p)^2 (0.4536\ W)^{2/3} \sin \beta}{20{,}645}\right]^{1/2} \qquad (10)$$

Equations (9) and (10) have been compared with the bolted edge data and equation (2) in Figure 9 and with the clamped edge data and equation (5) in Figure 18.

It is apparent in Figures 9 and 18 that over that relatively small data base, equations (2) and (5) represent the data somewhat better than either equations (9) or (10). Both equations (9) and (10) are somewhat more representative of the bolted edge cases but equation (10) underestimates the V_p of the panels in both the bolted and clamped edge cases.

5.2.3.3 Polycarbonate

Compared to the acrylic materials, relatively little bird impact test data is available in the literature for polycarbonate. A comprehensive study was conducted by Ingelse and Wintermute, a summary of which is given in Reference 8. On the basis of centre panel impacts on 30 inch by 40 inch flat monolithic and laminated panels up to five inches thick, bolted at the edges, and impacted with four-pound birds under room temperature conditions, they obtained the following linear relationship:

$$V_k = 450\ (t_t) + 170 \qquad (11)$$

where V_k = penetration velocity (knots)

t_t = total thickness (inches)

The equation (11) and the experimental data for monolithic panels are compared with the present data and equation (3) in Figure 21.

It is apparent in Figure 21 from both the data presented in Reference 8 and the present data, that a non-linear relationship exists between V_p and t for monolithic panels. For the same panel thicknesses, consistently higher penetration velocities were obtained in Reference 8 than in the present work. The differences in V_p could be attributed to the following:

(i) panel sizes

(ii) panel edge attachment and support structure stiffness

(iii) bird weight tolerance.

Although there are no available data to substantiate an empirical equation which accounts for variation in bird weight for the case of monolithic polycarbonate panels clamped at the edges, on the basis of the two-pound bird impact results (Figure 19), the bolted edge results (Figures 10 to 12), and the assumption that $V_p W^{1/3}$ = constant, it is proposed that for the clamped case in which edge slippage is minimized:

$$V_p = \frac{1731\ t^{2/3}}{W^{1/3}} \qquad (12)$$

5.3 Effects of Impact Position

To determine the effect of impact position on the V_p of the three panel materials, impacts were carried out at the top corner, top edge and bottom edge of the panels. The panels, tested under room temperature conditions, were 1/8 inch thick, mounted at 45° and the bird weight was two pounds. The top corner impacts were carried out with both bolted and clamped edges while only the clamped edge condition was used for the top and bottom edge tests.

The impact positions were as follows (measured in the plane of the panel):

Top corner: five inches from the top and side panel retaining strip inside edge.

Top edge: five inches below the panel top retaining strip inside edge, on the panel centreline.

Bottom edge: five inches above the panel bottom retaining strip inside edge on the panel centreline.

A summary of the results is given in Table 1. In all cases a lower V_p relative to centre panel V_p was obtained. The acrylics exhibited a decrease in V_p ranging from 26% to 46%. The maximum decrease in V_p for polycarbonate was at the upper edge (32%) and the minimum decrease was at the lower edge (7%).

The relative differences between the acrylic and the polycarbonate results are attributed to the differences in deformation which the panels undergo during impact. Compared with the acrylics, polycarbonate panels, particularly when impacted near the bottom edge, undergo large deformations which not only change the panel loading (resulting from the deflected shape) but are also able to absorb more of the impact energy.

The 15% decrease in V_p at the top corner as compared to a 32% decrease in V_p at the top edge in the polycarbonate results could be attributed to the fact that the edge restraint used for the top edge impacts, Figure 3(d), had greater clamping forces than that used for the corner impacts, Figure 3(f). The slippage that could occur because of lower clamping forces might account for the higher V_p of the top corner impact. Preliminary results of the top corner impacts using the highly clamped edge restraint (Figure 3(d)), indicate the V_p for the top corner could be lower.

Edge slippage was found to be an important parameter affecting the results of the stretched acrylic panels impacted at the bottom edge. Initially, the panels were restrained as in the centre panel impacts (Figure 3(b)), and the resulting V_p was 181±8 mph, somewhat higher than the centre panel impact V_p of 165±5 mph. It was observed, however, that edge slippage was occurring. The slippage was observed as a bulge in the panel following a non-penetrating impact. This panel subsequently returned to its normal (flat) shape after the edge clamping was released. With the edges restrained as in Figure 3(e), slippage was minimized and the resulting V_p was 108±3 mph. Hence by reducing the edge slippage, V_p was reduced from 181±8 mph to 108±3 mph, a decrease of 40%.

5.4 Effect of Impact Angle (β) on Clamped Polycarbonate Panels

The effect of impact angle was investigated by centrally impacting 1/8 inch thick panels with two-pound birds for $\beta=25°$

and β=65°. The resulting penetration velocities are compared to those for β=45° in Table 2. It is seen in both cases that V_p decreases when β=25° or 65°. Although the results obtained for β=65° are consistent with the frequently adopted relation that V_p varies inversely as sin β, the opposite is true for the results for β=25°. This phenomenon was also observed by Ingelse and Wintermute[8] for 0.5 inch thick flat polycarbonate panels centrally impacted with four-pound birds in which β=20°. This inconsistency, at the lower impact angles, is attributed at least partly to the severe pocketing which occurs at the rear edge of the panel during impact. Because of the pocketing, loading of the top edge of the panel is highly concentrated and a lower V_p results. The pocketing at the top edge results from the bird sliding to the rear edge because of the low slope of the panel relative to the bird trajectory. The present results and those of Ingelse and Wintermute[8] suggest that V_p is inconsistent at β=20° or 25° only for specific combinations of t and W. The basis for this suggestion is that in Reference 8 with four-pound bird impacts at β=20°, the inconsistencies only occurred for t=0.5 inches. In the present results, the inconsistency occurred for t=0.125 inches at β=25° with two-pound bird impacts.

5.5 Effect of Temperature (T) on Clamped Polycarbonate Panels

The effect of temperature was investigated by impacting panels soaked to -40°F and +120°F with the panels restrained as in Figure 3(d). In each case, the panels were nominally 1/8 inch thick, mounted at 45° and centrally impacted with two-pound birds. The resulting penetration velocities are compared to the room temperature results in Table 3. Additional tests were carried out at room temperature using the same edge restraint as for the low and elevated temperature tests as a verification that no variability was introduced by the edge restraints. The different edge restraints were not found to produce such a variability in that under room temperature conditions, V_p=348±7 mph with the edge restraints as per Figure 3(c) and V_p=340±14 mph with the edge restraints as per Figure 3(d).

After considering the tolerances to which values of V_p were obtained in Table 3, compared with the room temperature results, there appears to be no significant effect on V_p at T=-40°F and only a slight decrease in V_p at T=+120°F.

5.6 Effects of Multiple Impacts

The effects of multiple impacts on V_p for all materials was investigated by repeatedly impacting a panel and comparing these results with the values for V_p derived from tests in which a new panel was used in each impact. In each case, the panels were mounted at 45° and impacts were performed on the centre of the panels under room temperature conditions. Three-eights inch thick panels of as-cast acrylic, stretched acrylic and polycarbonate were impacted with four-pound birds. The acrylic panels

were clamped at the edges (Figure 3(b)) and the polycarbonate panels were restrained by bolting through the edges (Figure 3(a)). In addition, 1/4 inch thick panels of polycarbonate, clamped at the edges (Figure 3(d)), were impacted with two-pound birds.

After each impact, any non-penetrated panel was removed from the mounting plate, visually inspected and any damage recorded. The panel was then remounted.

The penetration velocity of the as-cast acrylic panel, under standard test procedures, was previously found to be 181±7 mph. The results for the multiple impacts on the two as-cast acrylic test panels are given in Table 4.

In the case of the first panel, three impacts were performed at a velocity nominally 30% below V_p, three impacts at nominally 20% below V_p and three impacts at nominally 10% below V_p. Penetration occurred on the ninth impact. In the case of the second panel, two impacts were performed at a velocity nominally 10% below V_p. Penetration resulted from the second impact. Hence, in reviewing the impacts on the two panels, it appears that only those impacts which are at a velocity nominally 10% below the V_p have a damaging effect which leads to a lower V_p for an as-cast acrylic panel.

The results of the multiple impacts on the stretched acrylic panels are given in Table 5. Previously V_p of this panel thickness under standard test procedures, was found to be 209±4 mph. Basically the same procedure was used in the stretched acrylic tests as in the as-cast acrylic panel tests. Impacts were conducted on one panel at velocities nominally 30%, 20% and 10% below V_p and two impacts were performed on a second panel at nominally 10% below V_p. As with the as-cast acrylic panels, it appears that only those impacts at a velocity nominally 10% below V_p had the effect of damaging the panel so as to lower its V_p.

The penetration velocity of a 3/8 inch thick polycarbonate panel bolted at the edges was previously determined to be 344±2 mph. The results of the multiple impacts are given in Table 6. As in the acrylic panel tests, two different panels were impacted; eight impacts on the first and four on the second. In the case of the first panel, three impacts at a velocity nominally 30% below V_p produced no visible damage to the panel. At velocities nominally 20% below V_p, cracks resulted along the upper edge bolt holes after each of the three impacts. At velocities nominally 10% below V_p, the first impact resulted in further cracking around the upper edge holes and the second impact penetrated the panel. In the case of the second panel, four impacts were performed; each at a velocity nominally 10% below V_p. The first impact caused no apparent damage to the panel, the second and third impacts caused cracks to form around the bolt holes at the upper edge and the fourth impact penetrated the panel.

Hence, compared with the acrylic panels, the polycarbonate panels (with bolted edges as per Figure 3(a)), sustained damage at a comparatively lower velocity i.e. 20% below the normal V_p for polycarbonate compared with 10% for the acrylics. In both the acrylic and polycarbonate panels, penetration did not occur until impacts were performed at velocities nominally 10% below V_p. It is well within reason, however, that additional impacts on the polycarbonate panel at velocities nominally 20% below V_p would have resulted in the penetration of the panel, since each impact resulted in additional damage. It is perhaps worthy of mention that at velocities nominally 10% below V_p, more impacts were required to penetrate the polycarbonate panel than the acrylic panels.

The two-pound bird multiple impact results carried out on 1/4 inch thick polycarbonate panels, clamped at the edges, are given in Table 7. The V_p for this panel thickness using standard test procedures was previously determined to be 545 mph. Two panels were impacted. In the case of the first panel, four impacts were performed: the first three at velocities nominally 30% below V_p and the fourth at nominally 20% below V_p. The first three impacts produced progressively greater permanent deformations (in the form of a pocket or bulge) in the panel and the fourth impact resulted in the penetration of the panel. In the case of the second panel, impacted at a velocity nominally 20% below the normal V_p of the panel, the first impact produced a permanent bulge (approximately two and one-half inches deep) in the panel and the second impact penetrated the panel. No further tests were conducted on the polycarbonate panels of this configuration since it is obvious that multiple impacts have a profound effect in lowering V_p. It is equally important to note, however, that it is highly unlikely that in any test procedure, a panel would be retested should it sustain permanent deformation of the type found in these tests.

6.0 Correlation of Material Properties with Penetration Velocity

The objective of this study is to determine the correlation between the material mechanical properties and the bird impact penetration velocities of flat panels.

Although this study is incomplete at present, preliminary indications from bird impact and mechanical property[9] tests of control samples of as-cast, stretched acrylic and polycarbonate materials, confirm that the materials tested in the program exhibited properties which generally agree with those quoted by the manufacturers. Further comments are withheld pending completion of the study.

7.0 Summary and Conclusions

7.1 A substantial data base for bird impacts on flat monolithic panels of as-cast acrylic, stretched acrylic and polycarbonate

materials, ranging in thickness from 0.093 inches to 0.375 inches, and mounted on a highly rigid support frame has been presented. On the bases of the penetration velocities determined from centre panel impacts with one, two and four-pound birds under room temperature conditions and at an impact angle of 45°, the following empirical equations are presented:

(a) For panels bolted at the edges.

- As-cast acrylic

$$V_p = \frac{336\ t^{.52}}{W^{1/3}}$$

- Stretched acrylic

$$V_p = \frac{369\ t^{.52}}{W^{1/3}}$$

- Polycarbonate

$$V_p = \frac{742\ t^{1/3}}{W^{1/3}}$$

(b) For panels clamped at the edges.

- As-cast acrylic

$$V_p = \frac{424\ t^{.52}}{W^{1/3}}$$

- Stretched acrylic

$$V_p = \frac{587\ t^{.52}}{W^{1/3}}$$

- Polycarbonate (2-lb bird impacts)

$$V_p = 1374\ t^{2/3}$$

Although no test data were available to substantiate the effects of bird weight on V_p for clamped polycarbonate panels, it is proposed that for clamped polycarbonate panels

$$V_p = \frac{1731\ t^{2/3}}{W^{1/3}}$$

The data generally confirm the conclusion of a previous investigation[4] that V_p and W are related by

$$V_p W^{1/3} = \text{constant}$$

7.2 Experimental studies were conducted to determine the effects on V_p of varying the impact position, impact angle and panel temperature. The results of these studies for 1/8 inch thick panels and two-pound bird impacts are compared in Figures 22, 23 and 24. For completeness, some of the results previously presented[2] are included in these comparisons. From the comparisons, it is apparent that:

(a) Polycarbonate panels are substantially more resistant to bird impact than the acrylic panels.

(b) Almost without exception, significantly higher resistance to bird impact penetration is obtained with the panels clamped at the edges rather than bolted at the edges.

(c) Of the positions impacted, centre panel impacts are the least severe and panel edge impacts are the most severe.

(d) Compared to V_p for panels at $\beta=45°$, V_p decreased for panels of all the materials at $\beta=65°$ (as would be expected). Although any increase in V_p at $\beta=25°$ for panels of as-cast acrylic and bolted stretched acrylic materials occurred, an unexpected decrease in V_p resulted in the clamped stretched acrylic and the bolted and clamped polycarbonate panels. For polycarbonate panels at $\beta=25°$, this inconsistency appears to be a function of bird weight and panel thickness.

(e) Compared to the room temperature results, the effect on V_p of cooling the panels to -40°F or heating to +120°F differed somewhat with the materials but was not significant for any of the materials.

7.3 Studies were conducted to determine the cumulative effects of multiple impacts. Based on impacts carried out on acrylic panels clamped at the edges, it is concluded that impacts at velocities nominally 90% of the standard V_p have a damaging effect which lowers the V_p of the panel. Impacts at velocities less than 90% of the standard V_p did not appear to affect the resulting V_p for acrylics. Multiple impacts carried out on polycarbonate panels, both bolted and clamped at the edges, showed that damage to the panels occurs at relatively lower impact velocities than for the clamped edge acrylics, resulting in lower penetration velocities. Damage to the bolted polycarbonate panel occurred with impact velocities nominally 80% of V_p, and at 70% of V_p to the clamped polycarbonate panel.

7.4 Although some scatter in the results may be due to tolerances on bird weight and panel thickness as well as other factors, major reasons for the discrepancies are attributed to the edge restraint and small variations in impact position. For panels bolted at the edge with low clamping forces, failures tended to initiate at the bolt holes making the condition of the holes particularly important. Since no special procedures were undertaken to finish or

check the condition of the bolt holes, it is reasonable to assume that imperfections existed which led to some discrepancies. For panels clamped at the edges, the presence of panel edge slippage was found to significantly affect the resulting V_p. Edge slippage could either increase or decrease V_p depending on the specific edge restraint method. Throughout the program panel edge slippage was minimized. There are some indications, however, that the maximum V_p of a panel is obtained when some edge slippage is present. It was found during some impacts on polycarbonate panels that relatively small variations in impact position could significantly affect V_p. Hence, it is important to accurately control the impact position and to verify that the intended position was impacted in order to identify valid and invalid impacts.

7.5 Studies are in progress to ascertain correlations between the penetration velocities of panels and the material mechanical properties. Only preliminary results of this study are available at present.

7.6 A study of the effect on V_p of support structure stiffness would complement the present results.

REFERENCES

1. Report ACASM-TN-1, Associate Committee on Aerospace Structures and Materials, National Research Council of Canada, 1971.

2. Heath, J.B.R. and Bosik, A.J., "Bird Impact Test Program for Windshields of Small, Light Aircraft", Conference on Aerospace Transparent Materials and Enclosures, Technical Report AFML-TR-76-54, pp. 851-885, 1976.

3. Bosik, A.J., Heath, J.B.R. and Gleeson, M.R., "Capabilities of the NAE/NRC Flight Impact Simulator Facility", LTR-ST.701, 8 April, 1974.

4. McNaughtan, I.I., "The Resistance of Transparencies to Bird Impact at High Speeds", Aircraft Engineering, December 1964, pp. 409-413.

5. Staff M.E. Dept., "The Design of Aircraft Transparencies for Resistance Against Impact by Birds and Hailstones", Tech. Note M.E. 106, RAE, Farnborough, April, 1952.

6. Poullain, G. and Clamagirand, M., "Windscreens to Resist Bird Strikes", Proceedings of the Symposium on Optical Transparencies, Royal Aeronautical Society, 9-10 June, 1971.

7. Mott, M.J., "Experimental Investigations into the Bird Resistance of Flat Windscreen Panels with Clamped Edges", Symposium on Optical Transparencies, RAE, 9-10 June, 1971.

8. Ingelse, A.O. and Wintermute, G.E., "Bird Strike Capabilities of Aircraft Transparency Materials", Conference on Aerospace Transparent Materials and Enclosures, Technical Report AFML-TR-76-54, pp. 831-850, 1976.

9. MacKenzie, C., "Mechanical Properties of Polycarbonate Stretched Acrylic and As-Cast Acrylic", Lab. Memo. ST-237, Dec. 1977.

TABLE 1. EFFECT OF IMPACT POSITION

(W=2 lbs, t=1/8", β=45°, T=Room Temp.)

Material	Edge Restraint	V_p(mph)						
		Centre Panel (V_p)	Top Corner (V_{pc})	V_p-V_{pc} %	Top Edge V_{pT}	V_p-V_{pT} %	Bottom Edge V_{pB}	V_p-V_{pB} %
A.C. Acrylic	Bolted[1]	87±3	58±3	33	-		-	
A.C. Acrylic	Clamped[2]	116±3	63±3	46	77±4	34	76±4	35
S. Acrylic	Bolted[1]	99±3	71±3	28	-		-	
S. Acrylic	Clamped[3]	165±5	123±4	26	120±7	27	108±3	35
Polycarbonate	Bolted[1]	265±12	224±11	16	-		-	
Polycarbonate	Clamped[4]	348±7	297±17	15	236±8	32	323±13	7

Notes: (1) As per Figure 3(a).

(2) As per Figure 3(b).

(3) Centre Panel Figure 3(b), Top Corner Figure 3(b), Bottom Edge Figure 3(e), Top Edge Figure 3(b).

(4) Centre Panel Figure 3(c), Top Corner Figure 3(f), Bottom Edge Figure 3(c), Top Edge Figure 3(d).

TABLE 2. EFFECT OF IMPACT ANGLE (β) ON V_p FOR CLAMPED POLYCARBONATE

(W=2 lbs, t=1/8", T=Room Temp.)

V_p (mph)		
β=25°[1]	β=45°[2]	β=65°[2]
316±1	348±7	311±5

Notes: (1) Edge restraint Figure 3(d).
(2) Edge restraint Figure 3(c).

TABLE 3. EFFECT OF TEMPERATURE (T) ON V_p FOR CLAMPED POLYCARBONATE

(W=2 lbs, t=1/8", β=45°)

V_p (mph)			
-40°F	Room Temp.		+120°F
361±11[1]	348±7[2]	340±14[1]	312±7[1]

Notes: (1) Edge restraint Figure 3(d).
(2) Edge restraint Figure 3(c).

TABLE 4. MULTIPLE IMPACTS ON AS-CAST ACRYLIC

(W=4 lbs, t=3/8", β=45°, Clamped Edge Fig. 3(b), Centre Panel Impacts)

Test No.	Panel	Impact Velocity (mph)	Impact Velocity Nominal % Below V_p	Results*
1	A	134	30	NP
2	A	133	30	NP
3	A	131	30	NP
4	A	145	20	NP
5	A	146	20	NP
6	A	148	20	NP
7	A	163	10	NP
8	A	165	10	NP
9	A	167	10	P
10	B	164	10	NP
11	B	164	10	P

*NP - No Penetration; P - Penetration

TABLE 5. MULTIPLE IMPACTS ON STRETCHED ACRYLIC

(W=4 lbs, t=3/8", β=45°, Clamped Edge Fig. 3(b) Centre Panel Impacts)

Test No.	Panel	Impact Velocity (mph)	Impact Velocity Nominal % Below V_p	Results*
1	C	145	30	NP
2	C	149	30	NP
3	C	152	30	NP
4	C	166	20	NP
5	C	163	20	NP
6	C	166	20	NP
7	C	187	10	NP
8	C	185	10	P
9	D	189	10	NP
10	D	188	10	P

*NP - No Penetration; P - Penetration

TABLE 6. MULTIPLE IMPACTS ON POLYCARBONATE
(W=4 lbs, t=3/8", β=45°, Bolted Edges
Fig. 3(a), Centre Panel Impacts)

Test No.	Panel	Impact Velocity (mph)	Impact Velocity Nominal % Below V_p	Results*
1	E	243	30	NP
2	E	245	30	NP
3	E	242	30	NP
4	E	277	20	NP 3 cracked bolt holes
5	E	282	20	NP 4 cracked bolt holes
6	E	278	20	NP 5 cracked bolt holes
7	E	315	10	NP 8 cracked bolt holes
8	E	284	10	P
9	F	325	10	NP
10	F	330	10	NP 2 cracked bolt holes
11	F	321	10	NP 5 cracked bolt holes
12	F	319	10	P

*NP - No Penetration; P - Penetration.

TABLE 7. MULTIPLE IMPACTS ON POLYCARBONATE
(W=2 lbs, t=1/4", β=45°, Clamped Edges
Fig. 3(d), Centre Panel Impacts)

Test No.	Panel	Impact Velocity (mph)	Impact Velocity Nominal % Below V_p	Results*
1	G	409	30	NP 1.4" permanent deformation
2	G	406	30	NP 2.0" permanent deformation
3	G	403	30	NP 3.5" permanent deformation
4	G	429	20	P
5	H	424	20	NP 2.5" permanent deformation
6	H	440	20	P

*NP - No Penetration; P - Penetration

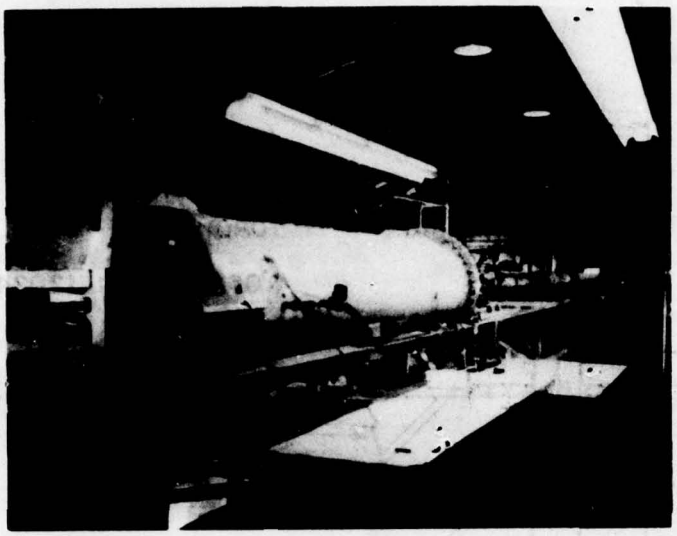


FIG. 1 NRC/NAE FLIGHT IMPACT SIMULATOR



FIG. 2 NRC/NAE TEST PANEL SUPPORT FRAME

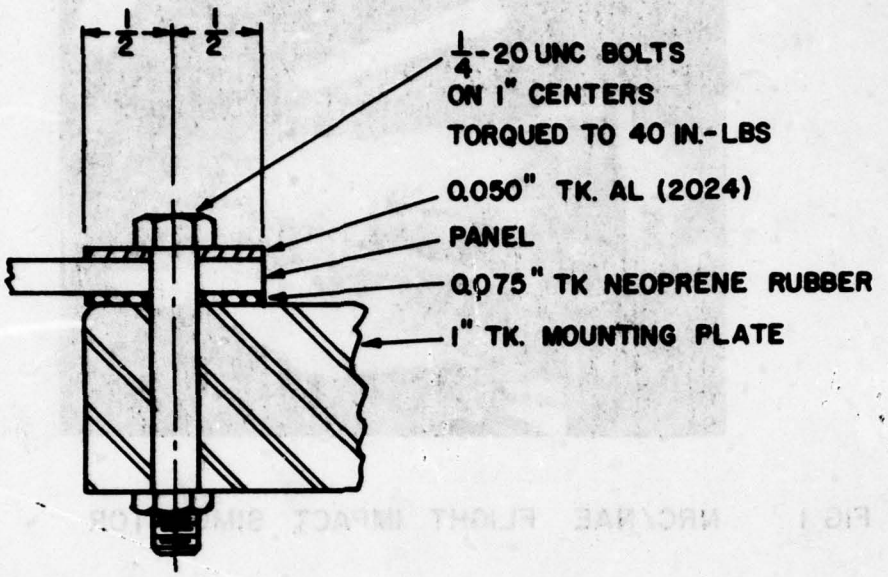


FIG. 3(a)

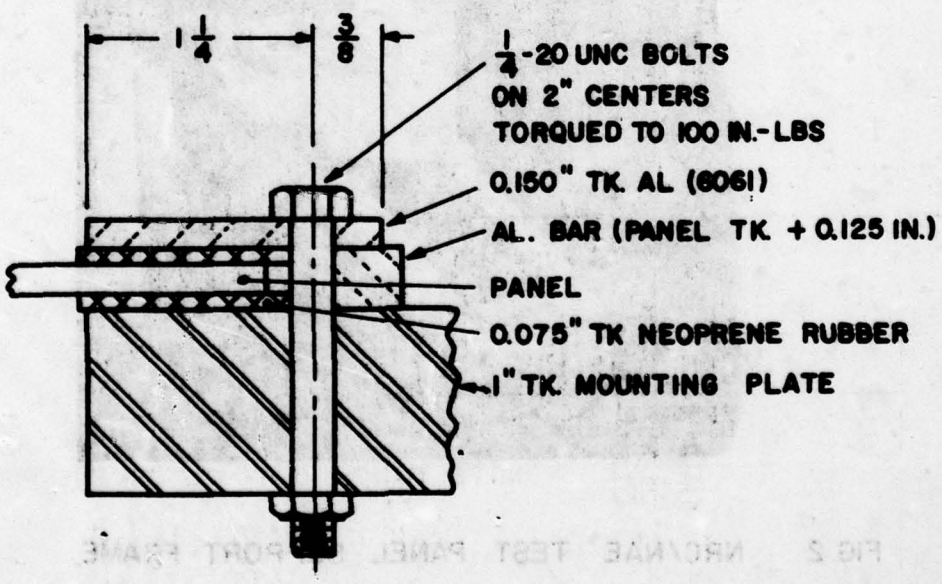


FIG. 3(b)

PANEL EDGE RESTRAINTS

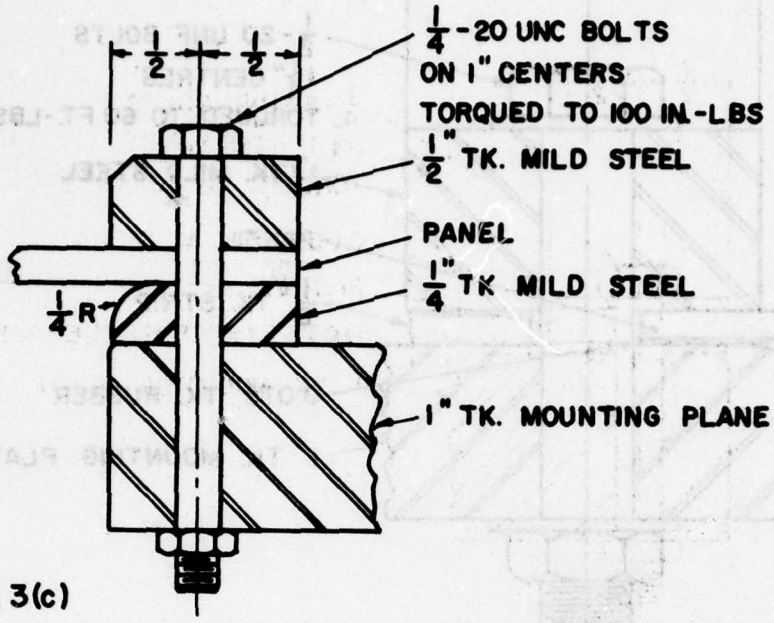
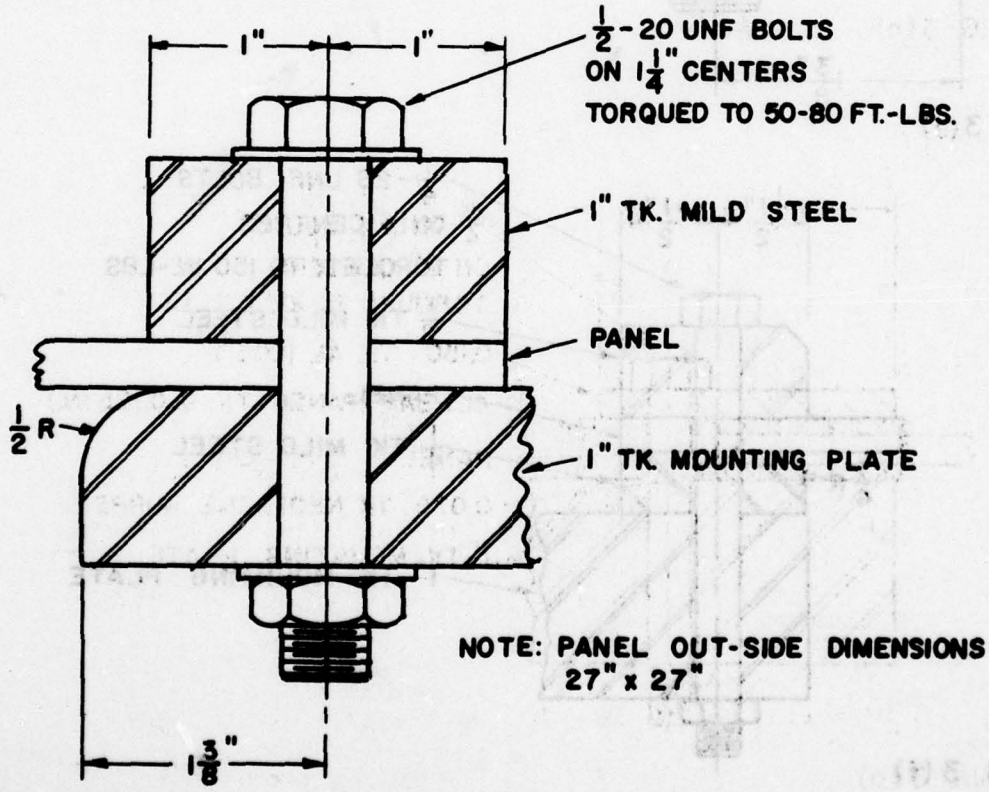


FIG. 3(c)



NOTE: PANEL OUT-SIDE DIMENSIONS
27" x 27"

FIG. 3(d)

PANEL EDGE RESTRAINTS

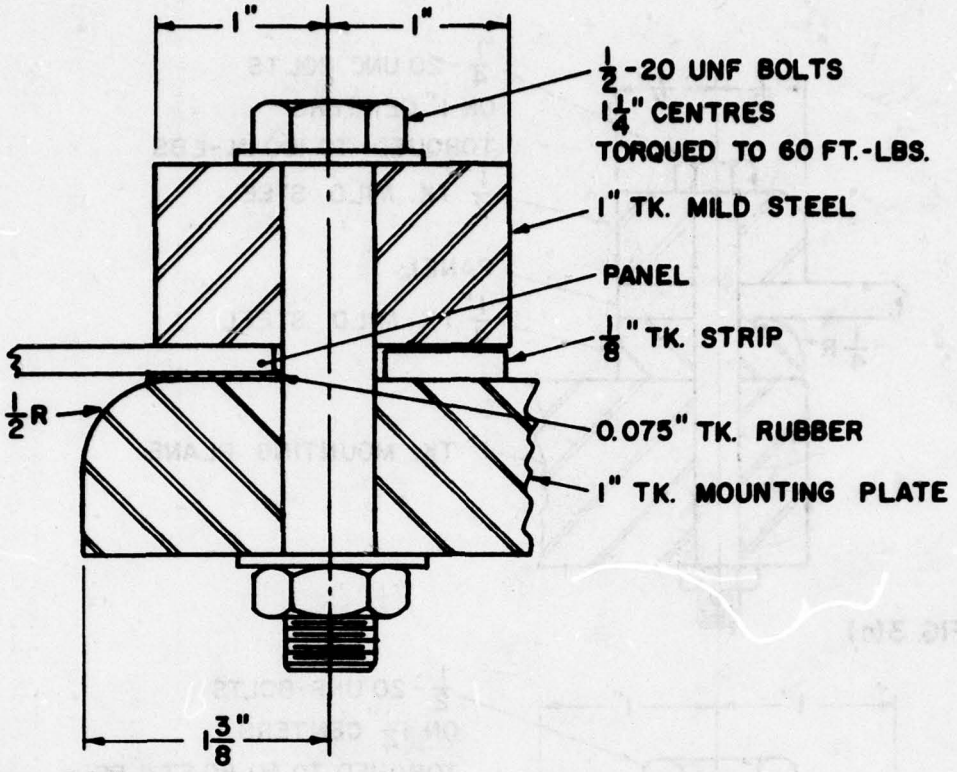


FIG. 3(e)

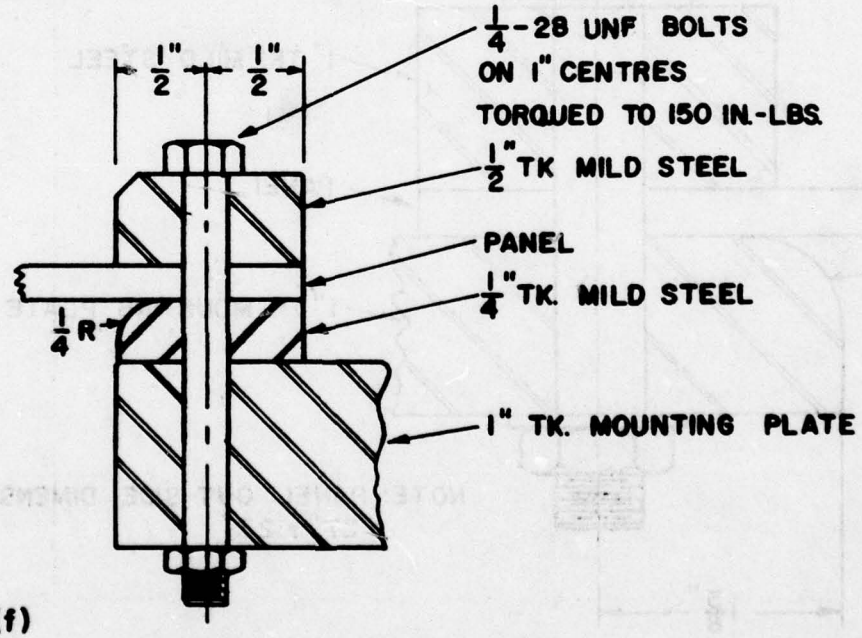


FIG. 3(f)

PANEL EDGE RESTRAINTS

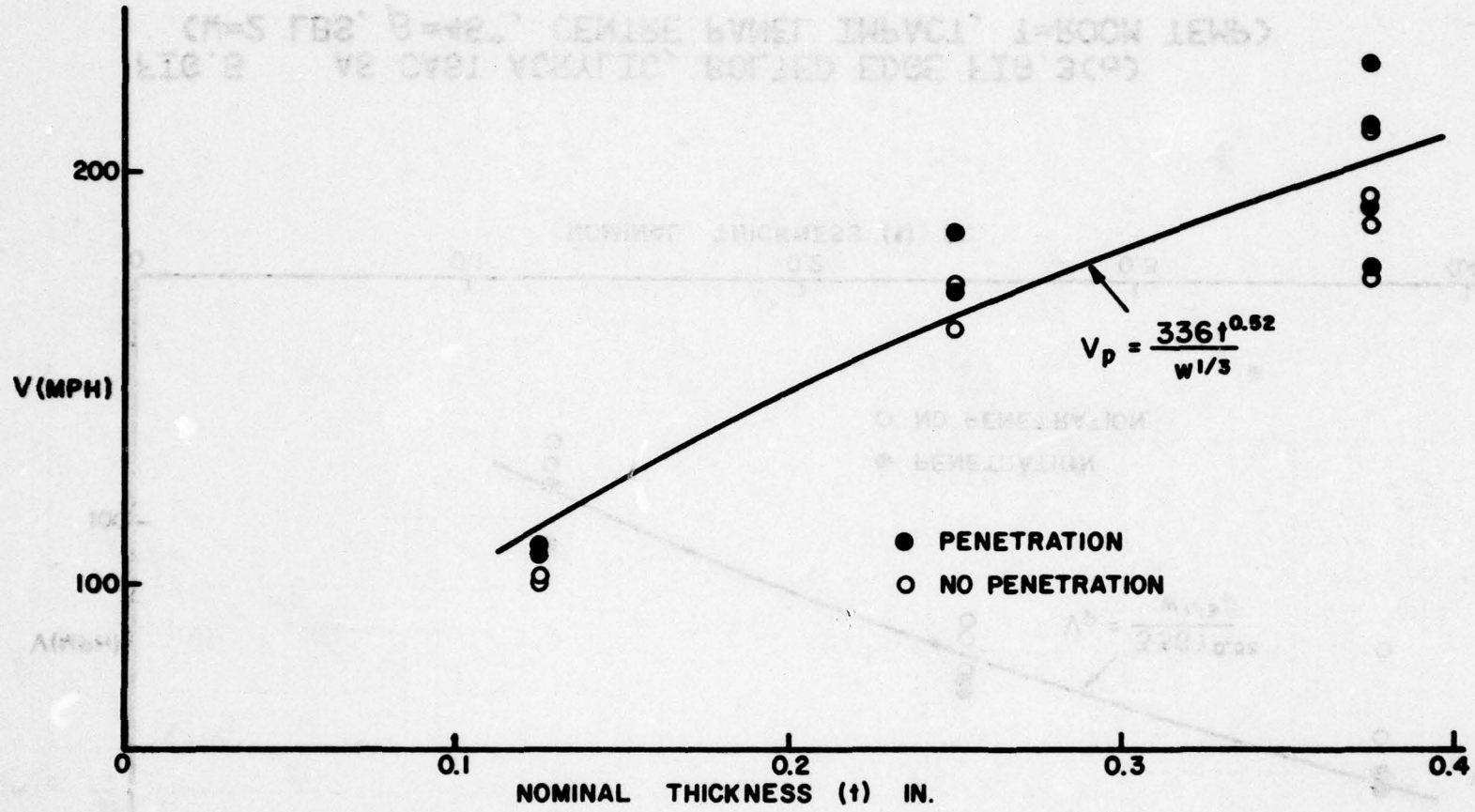


FIG.4 AS CAST ACRYLIC, BOLTED EDGE FIG.3(a)
(W=1 LB, β=45°, CENTRE PANEL IMPACT, T=ROOM TEMP)

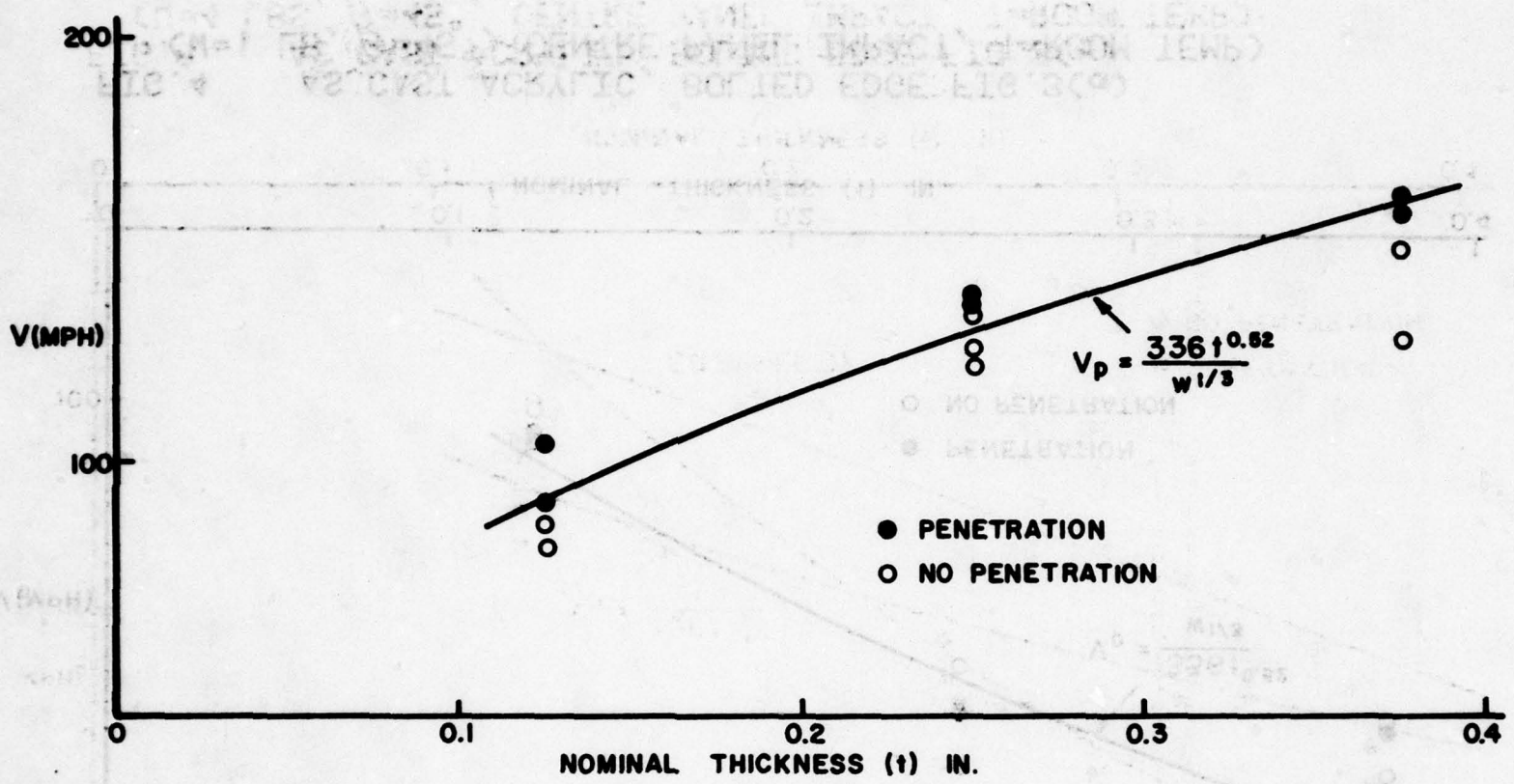


FIG.5 AS CAST ACRYLIC, BOLTED EDGE FIG.3(a)
(W=2 LBS, β=45°, CENTRE PANEL IMPACT, T=ROOM TEMP)

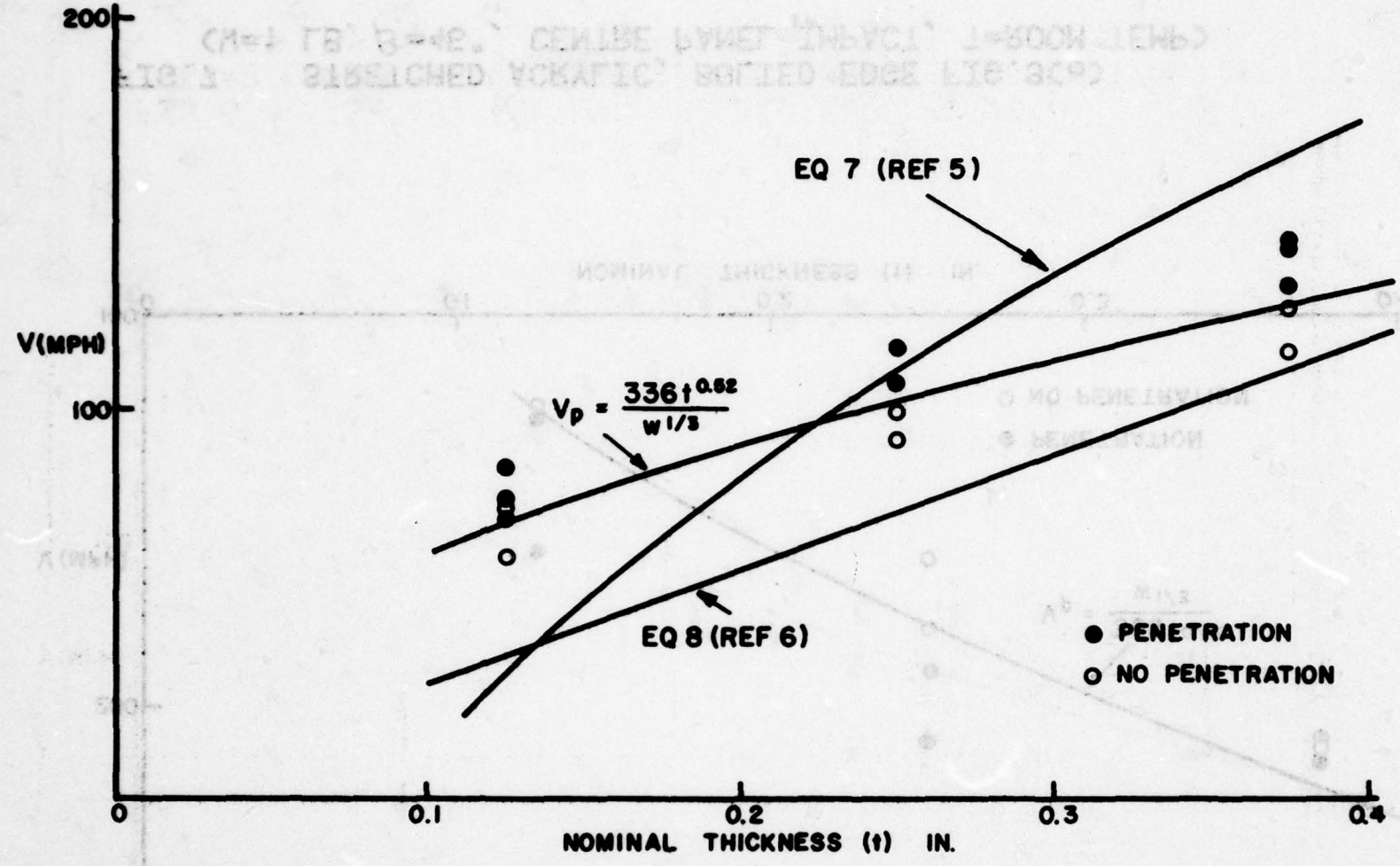


FIG.6 AS CAST ACRYLIC, BOLTED EDGE FIG.3(a)
(W=4 LBS, β=45°, CENTRE PANEL IMPACT, T=ROOM TEMP)

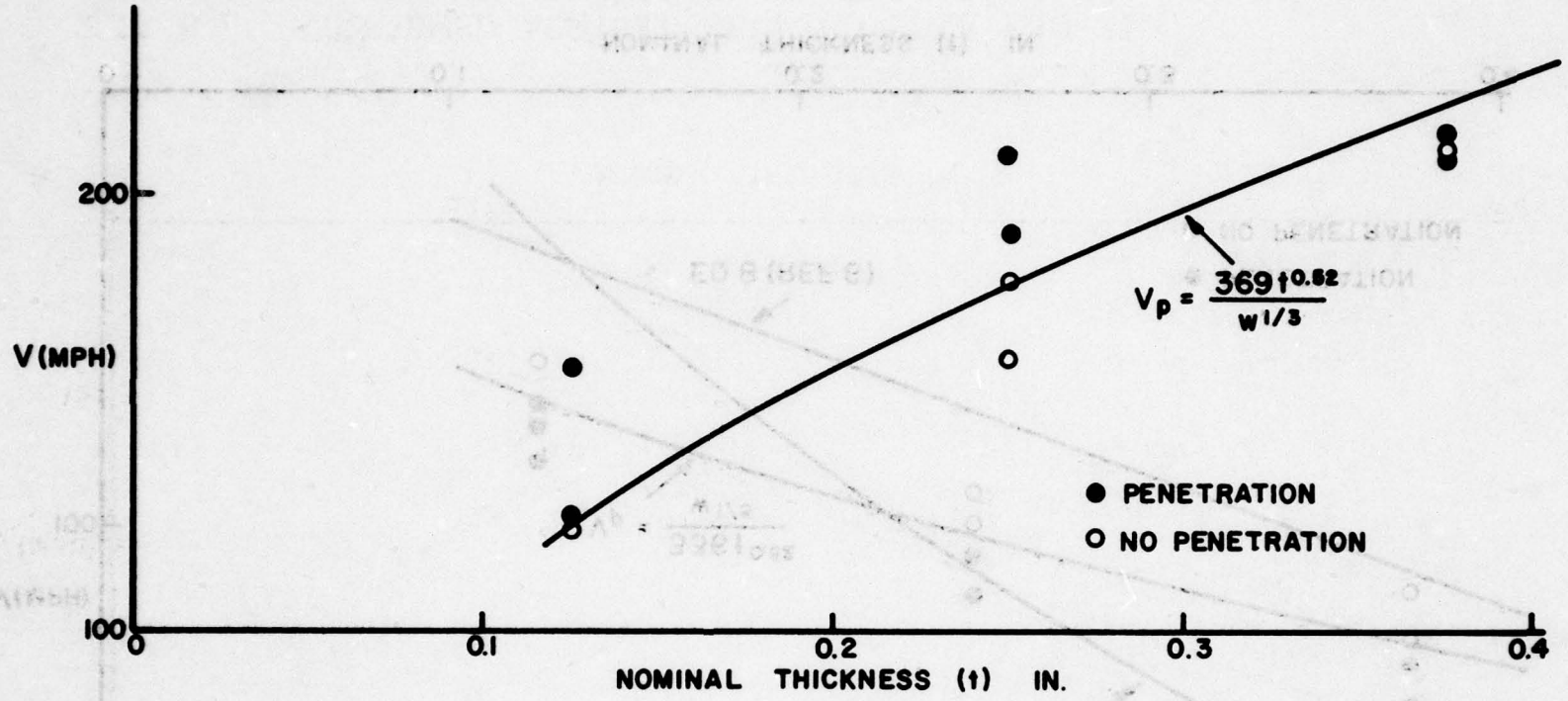


FIG.7 STRETCHED ACRYLIC, BOLTED EDGE FIG.3(a)
(W=1 LB, β=45°, CENTRE PANEL IMPACT, T=ROOM TEMP)

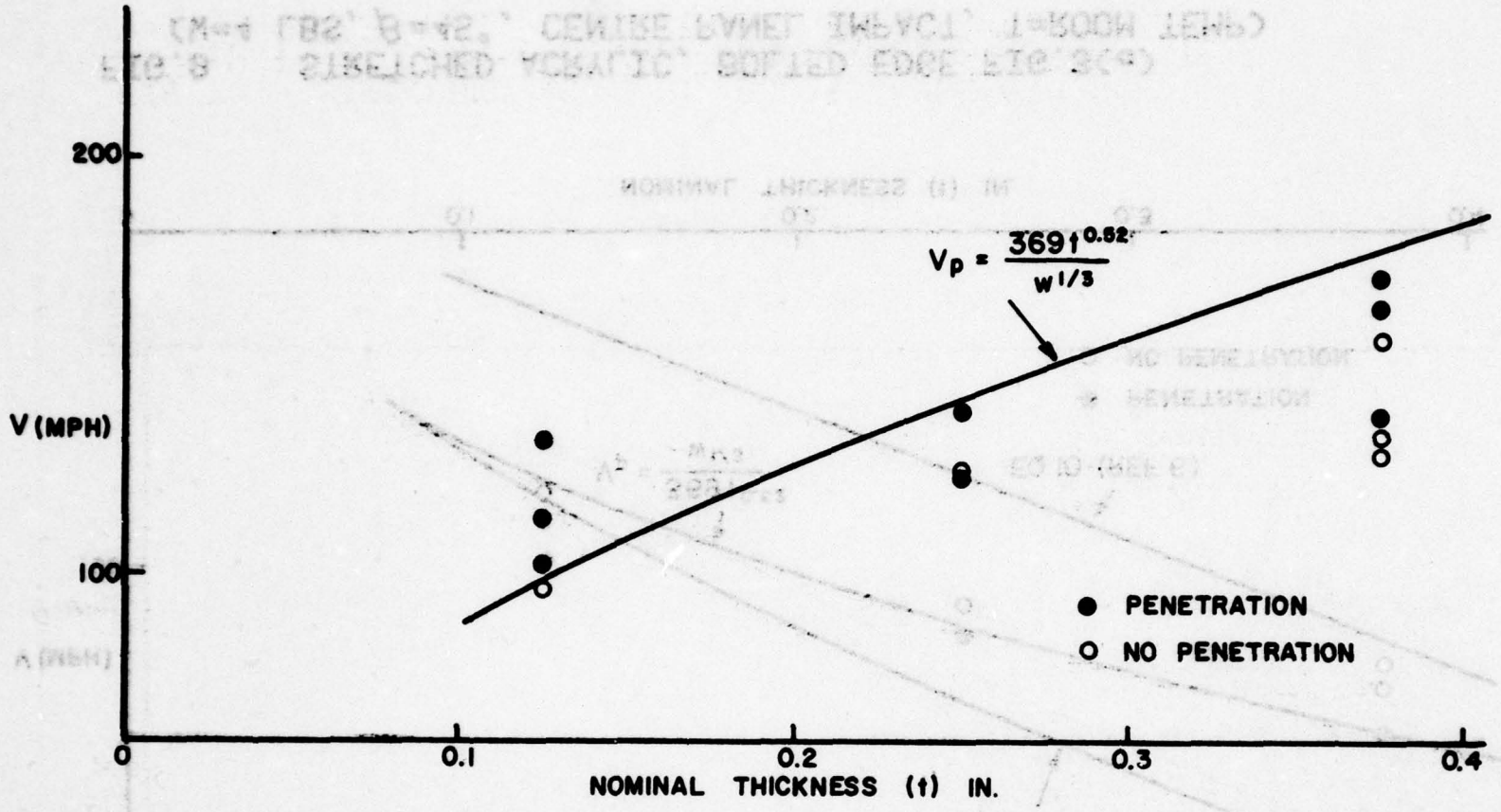


FIG.8 STRETCHED ACRYLIC, BOLTED EDGE FIG.3(a)
(W=2 LBS, β=45°, CENTRE PANEL IMPACT, T=ROOM TEMP)

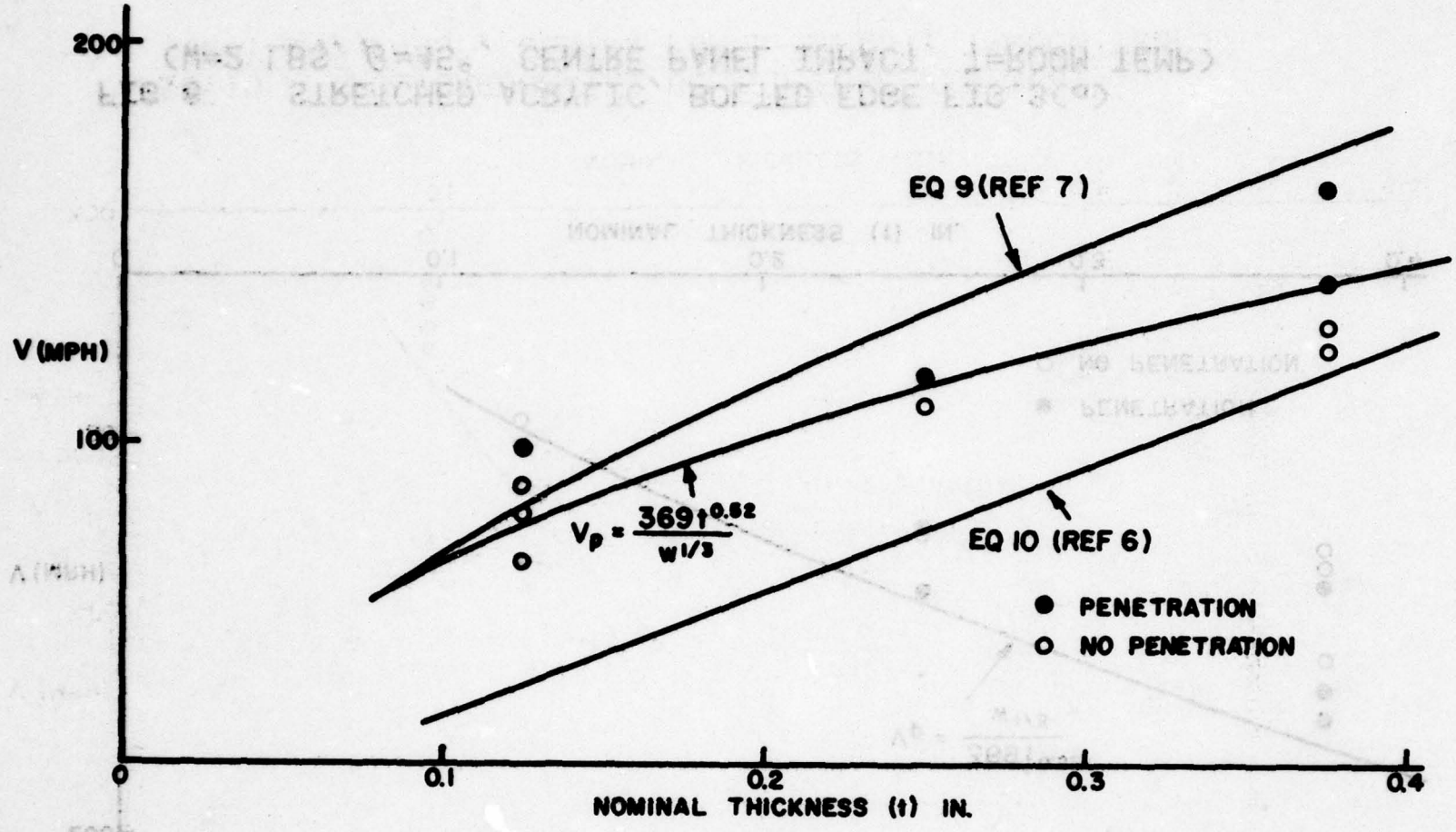


FIG.8 STRETCHED ACRYLIC, BOLTED EDGE FIG.3(a)
(W=4 LBS, β=45°, CENTRE PANEL IMPACT, T=ROOM TEMP)

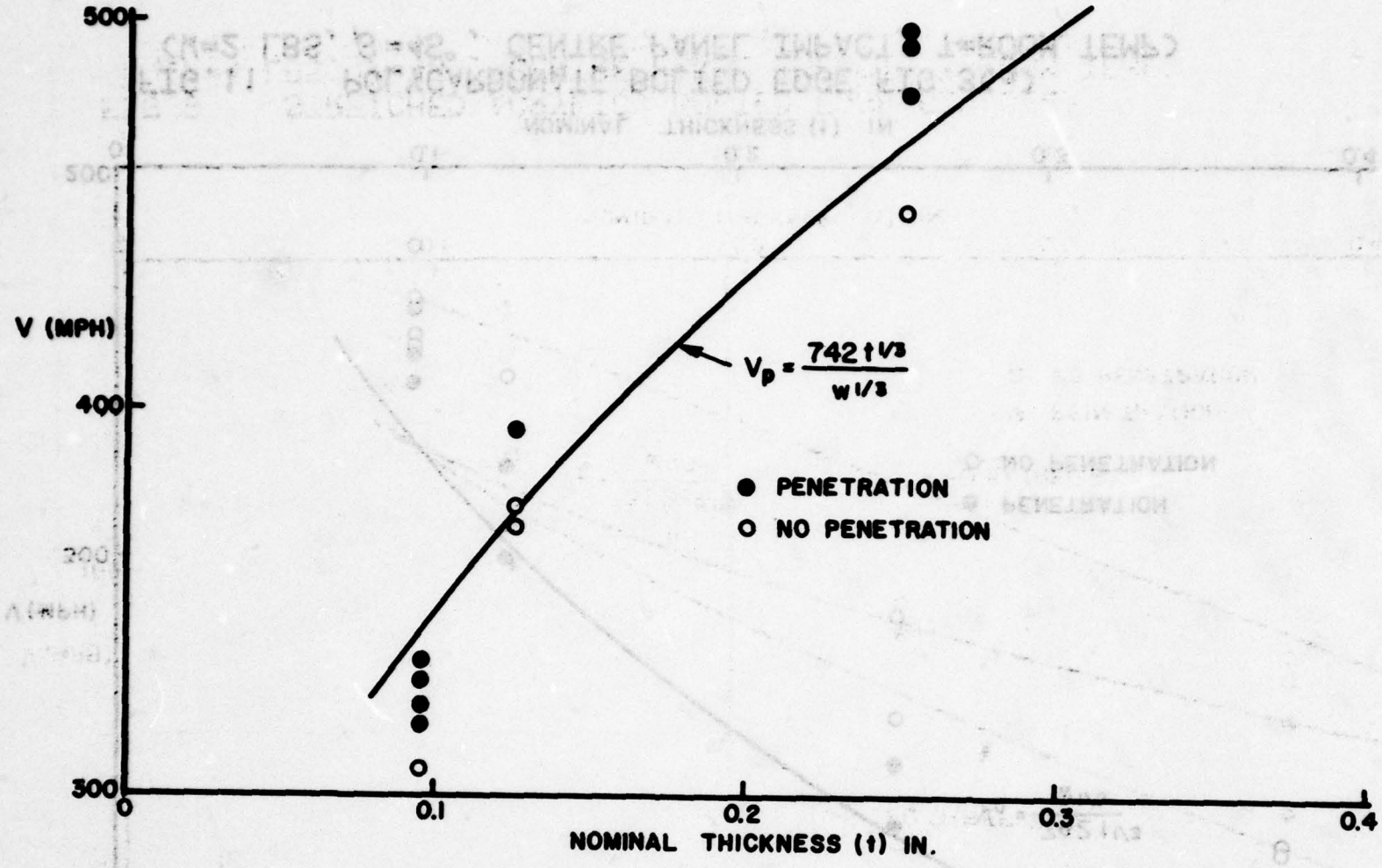


FIG. 10 POLYCARBONATE, BOLTED EDGE FIG. 3(a)
(W=1 LB, β=45°, CENTRE PANEL IMPACT, T=ROOM TEMP)

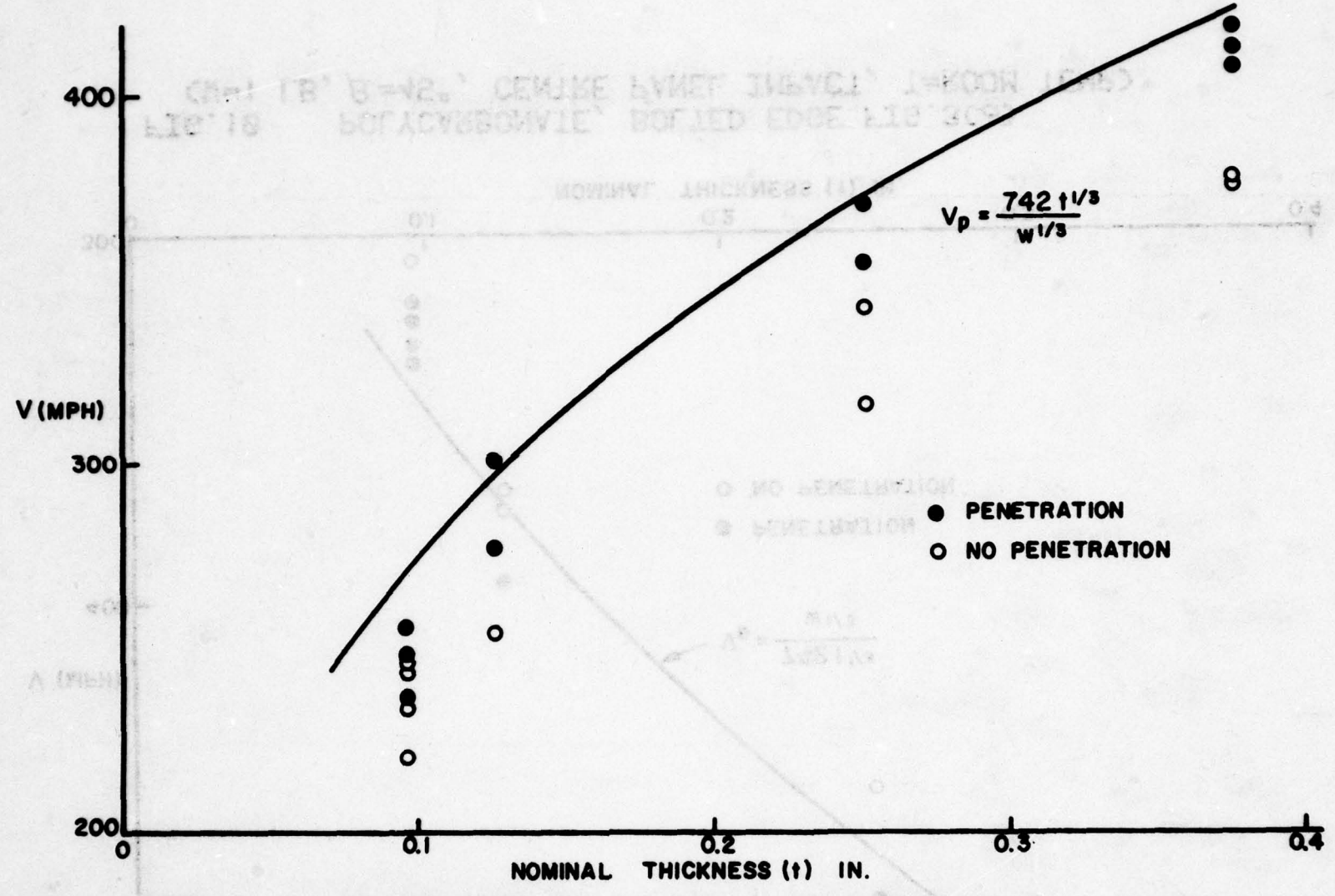


FIG. 11 POLYCARBONATE, BOLTED EDGE FIG. 3(a)
(W=2 LBS, β=45°, CENTRE PANEL IMPACT, T=ROOM TEMP)

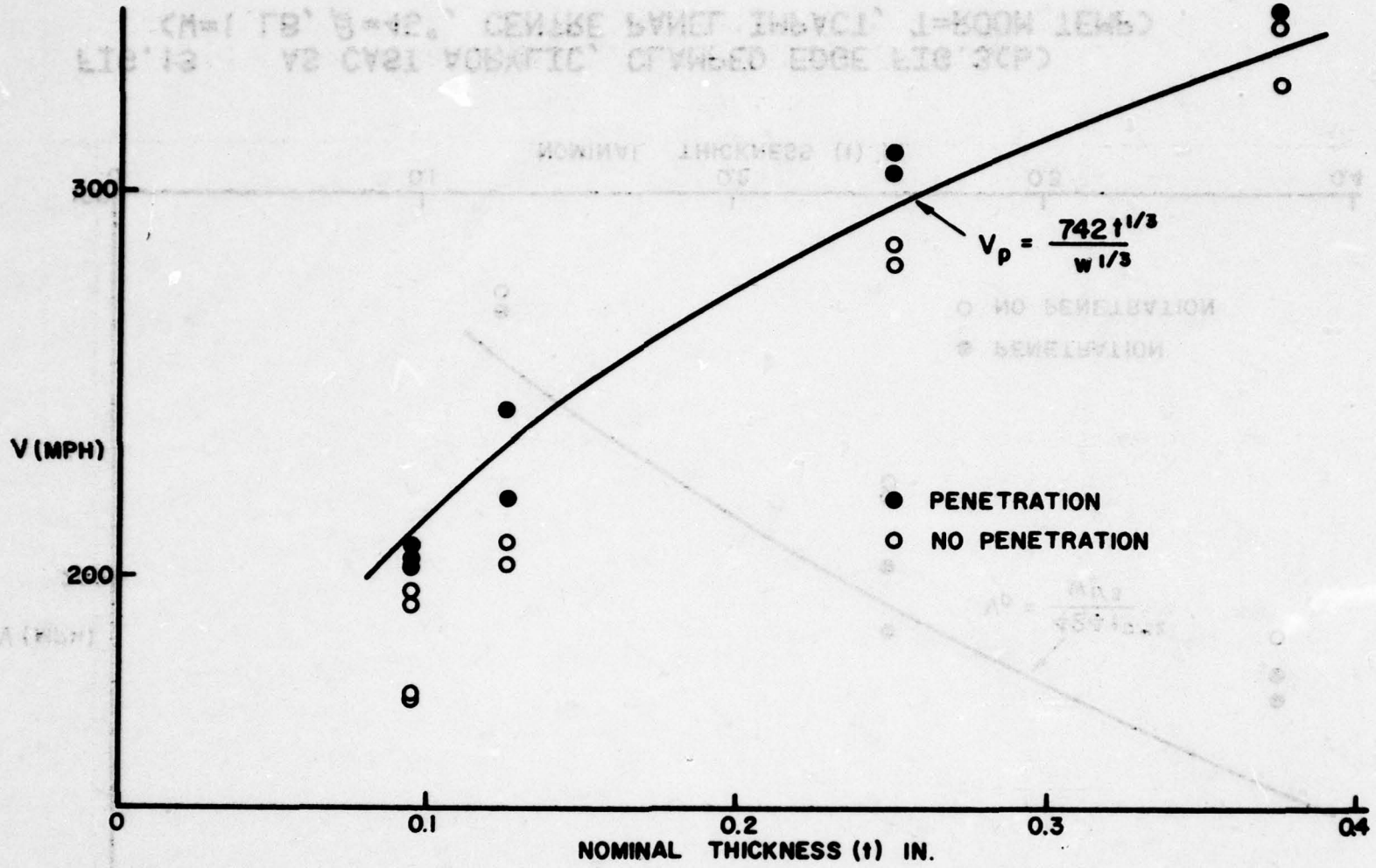


FIG. 12 POLYCARBONATE, BOLTED EDGE FIG, 3(a)
(W=4 LBS, β=45°, CENTRE PANEL IMPACT, T=ROOM TEMP)

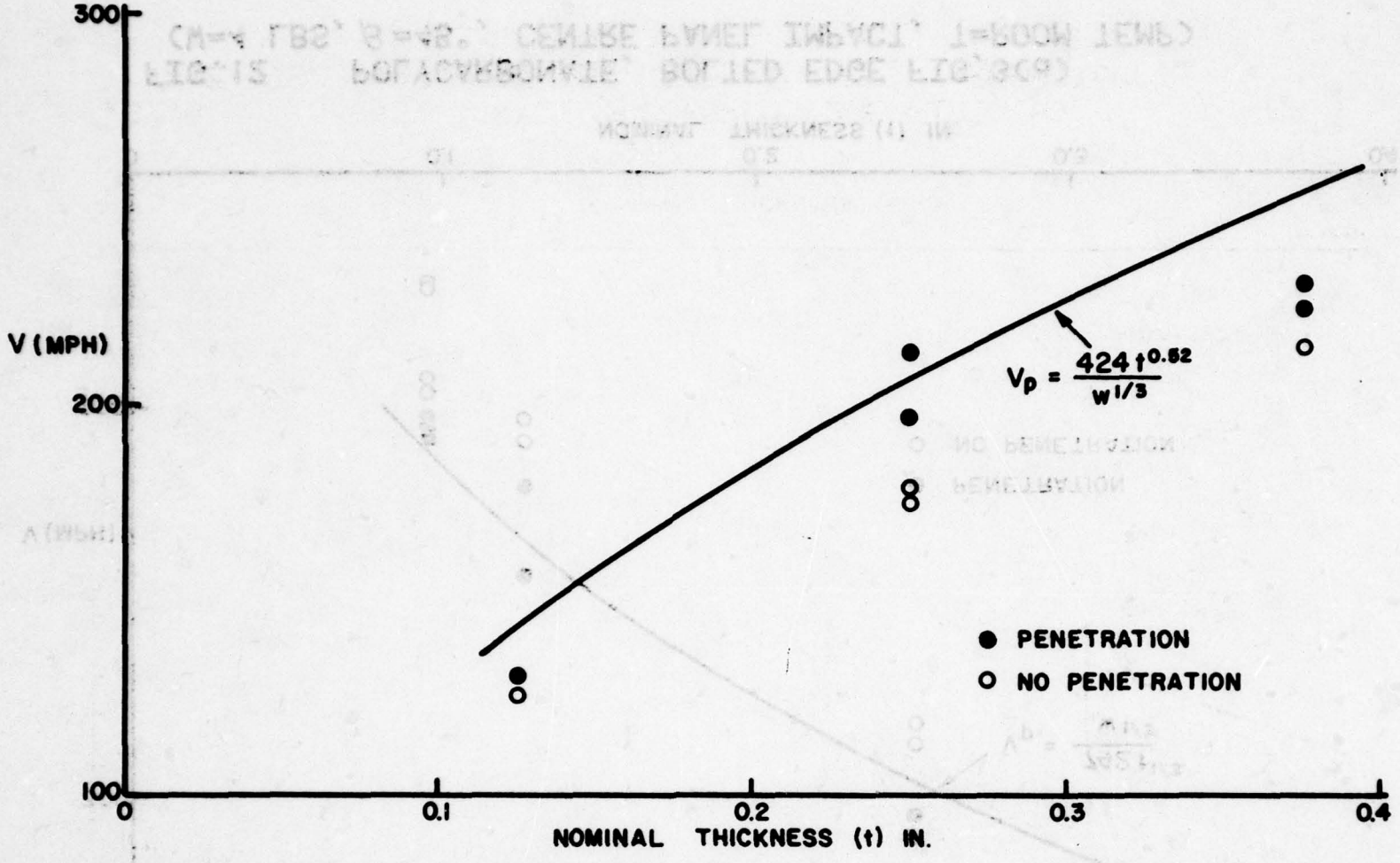


FIG. 13 AS CAST ACRYLIC, CLAMPED EDGE FIG. 3(b)
(W=1 LB, β=45°, CENTRE PANEL IMPACT, T=ROOM TEMP)

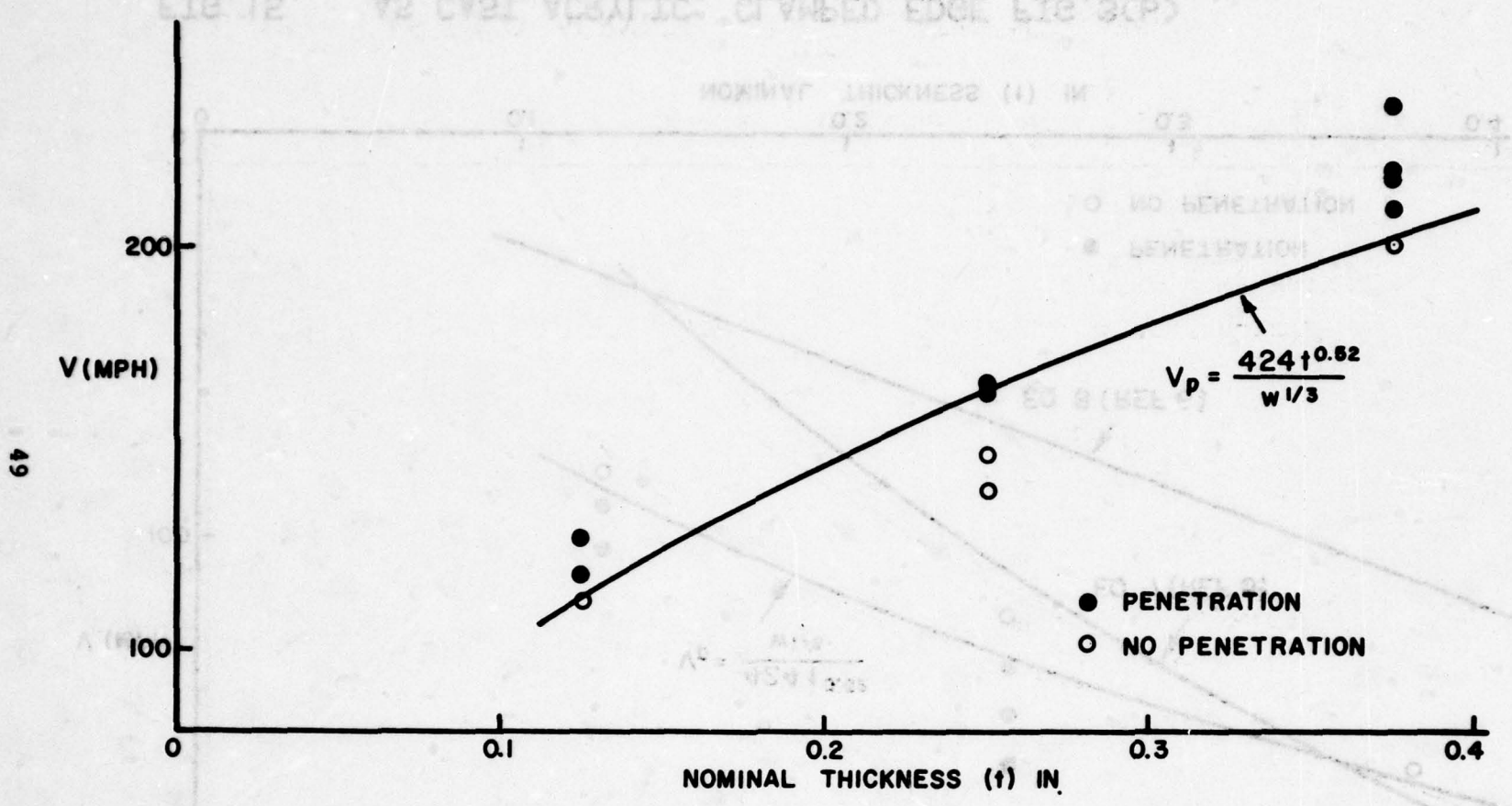


FIG.14 AS CAST ACRYLIC, CLAMPED EDGE FIG.3(b)
(W=2 LBS, β=45°, CENTRE PANEL IMPACT, T=ROOM TEMP)

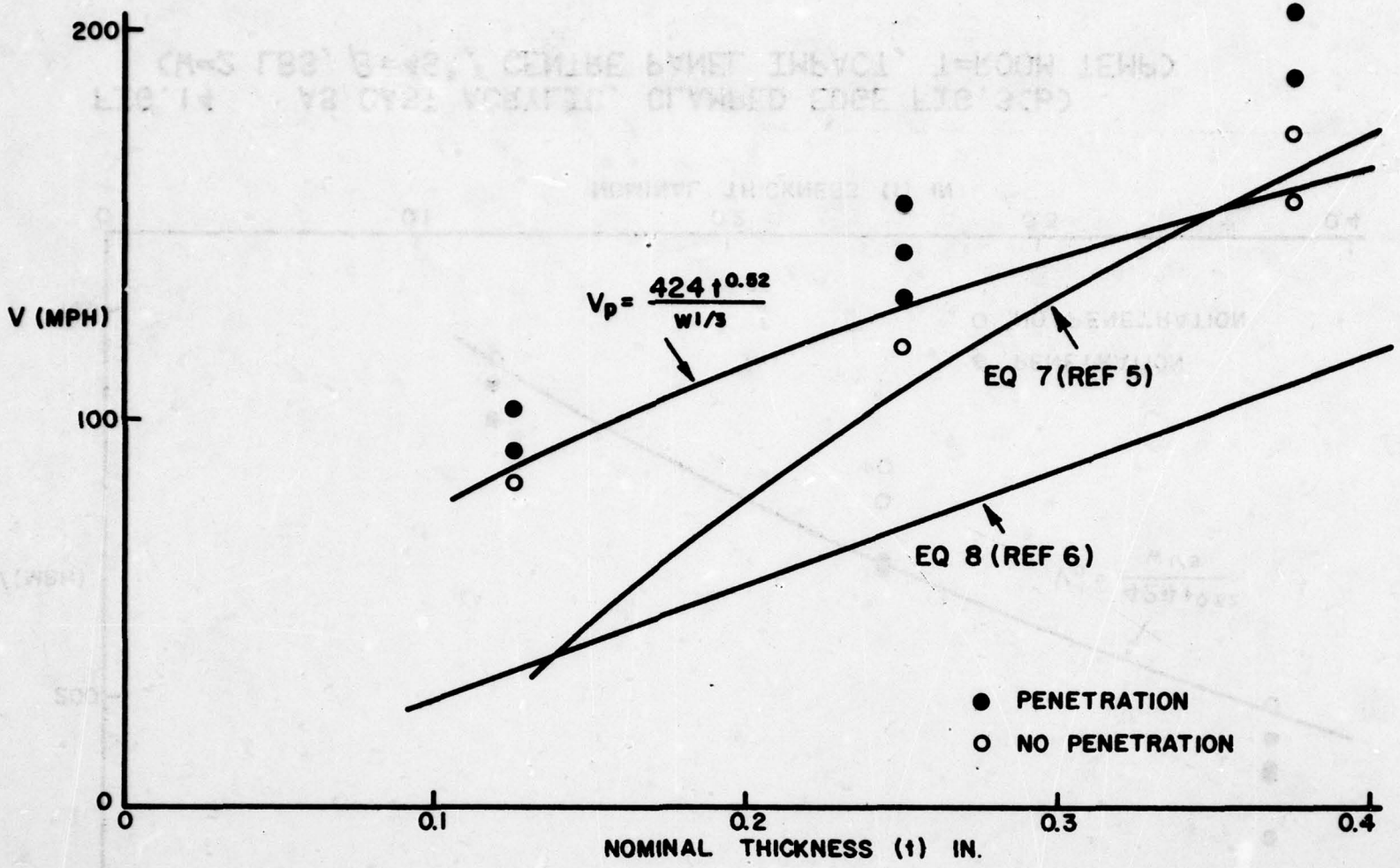


FIG. 15 AS CAST ACRYLIC, CLAMPED EDGE FIG. 3(b)
(W=4 LBS, β=45°, CENTRE PANEL IMPACT, T=ROOM TEMP)

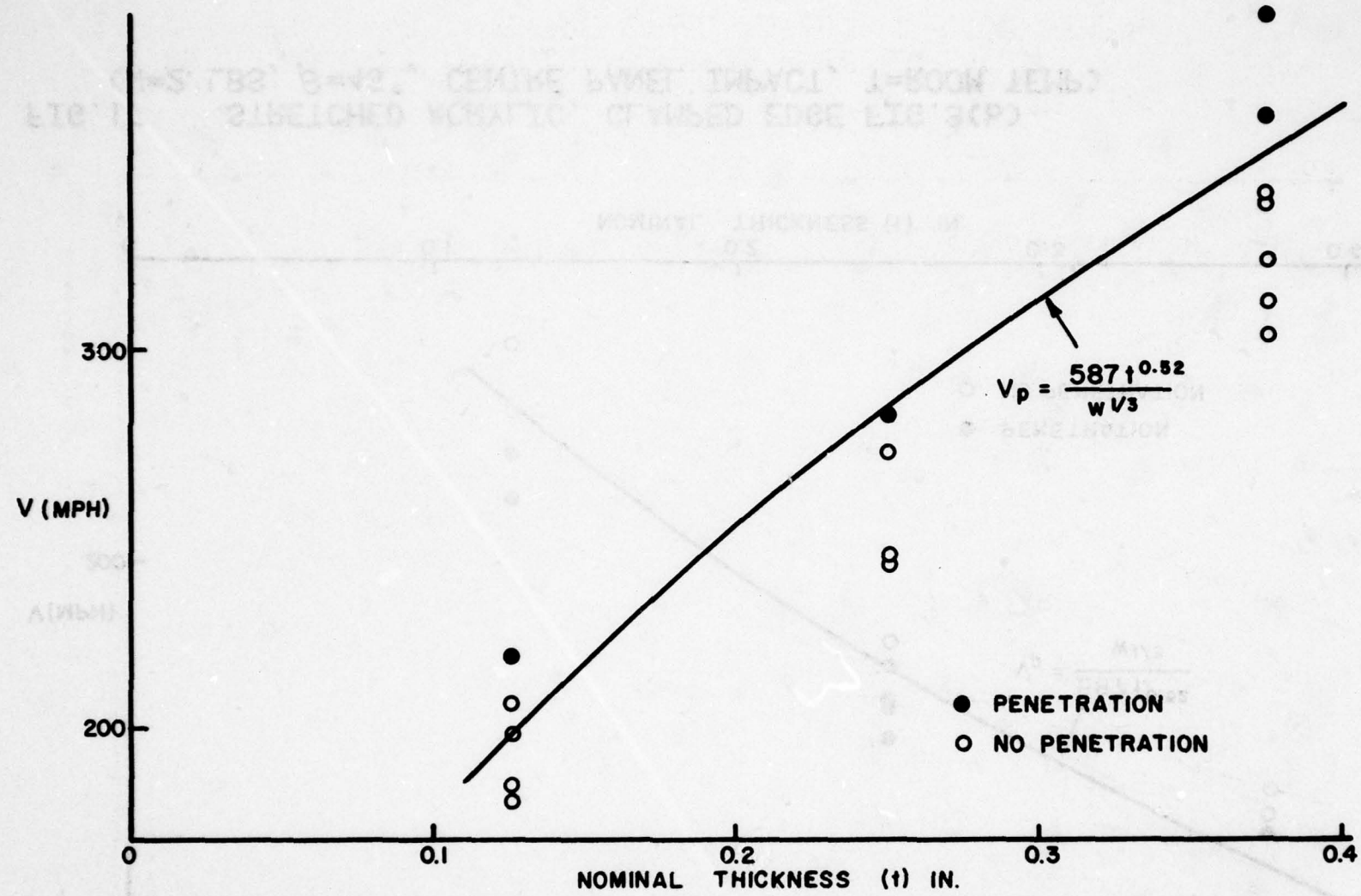


FIG. 16 STRETCHED ACRYLIC, CLAMPED EDGE FIG.3(b)
(W=1 LB, β=45°, CENTRE PANEL IMPACT, T=ROOM TEMP)

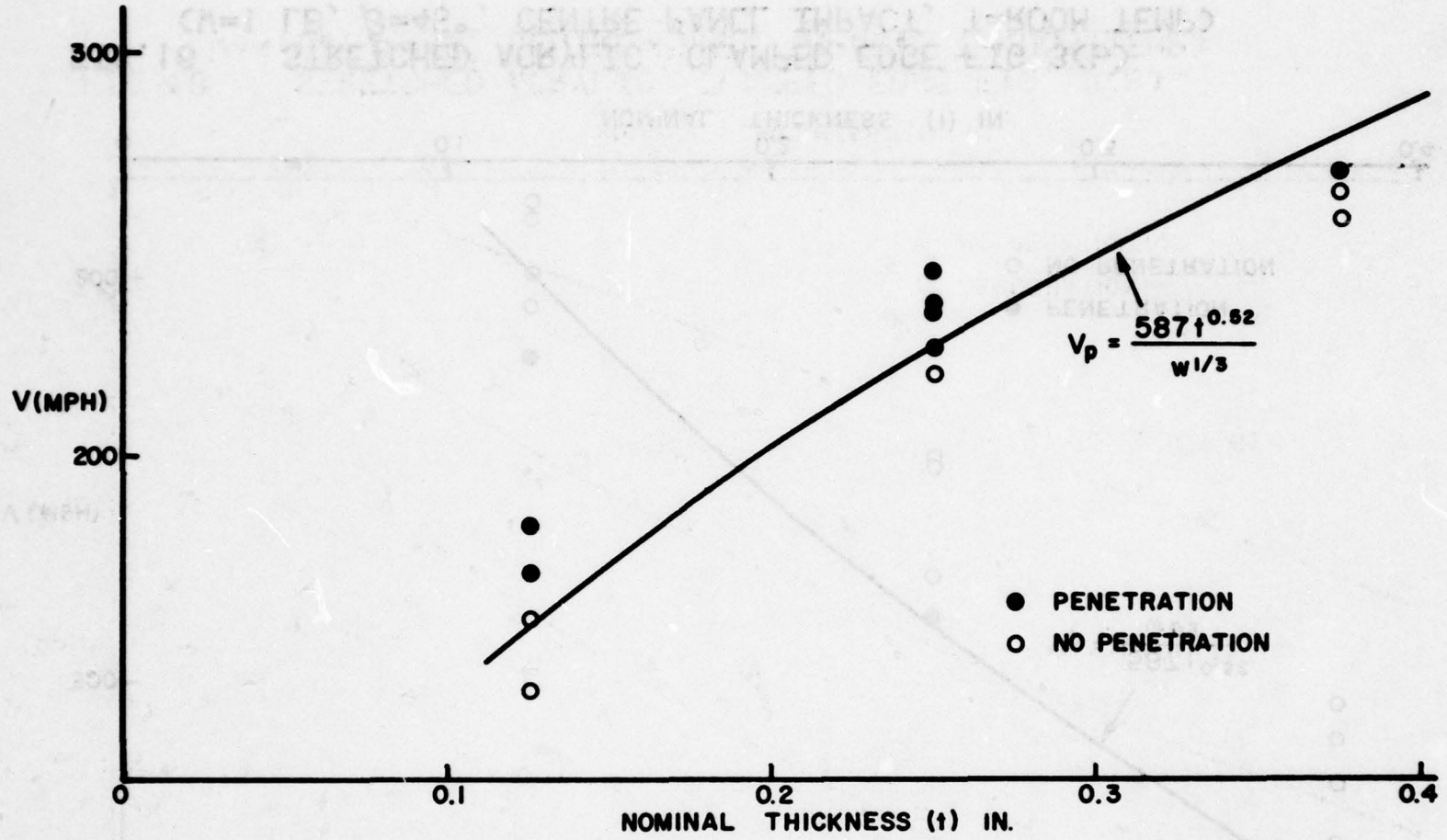


FIG.17 STRETCHED ACRYLIC, CLAMPED EDGE FIG.3(b)
(W=2 LBS, β=45°, CENTRE PANEL IMPACT, T=ROOM TEMP)

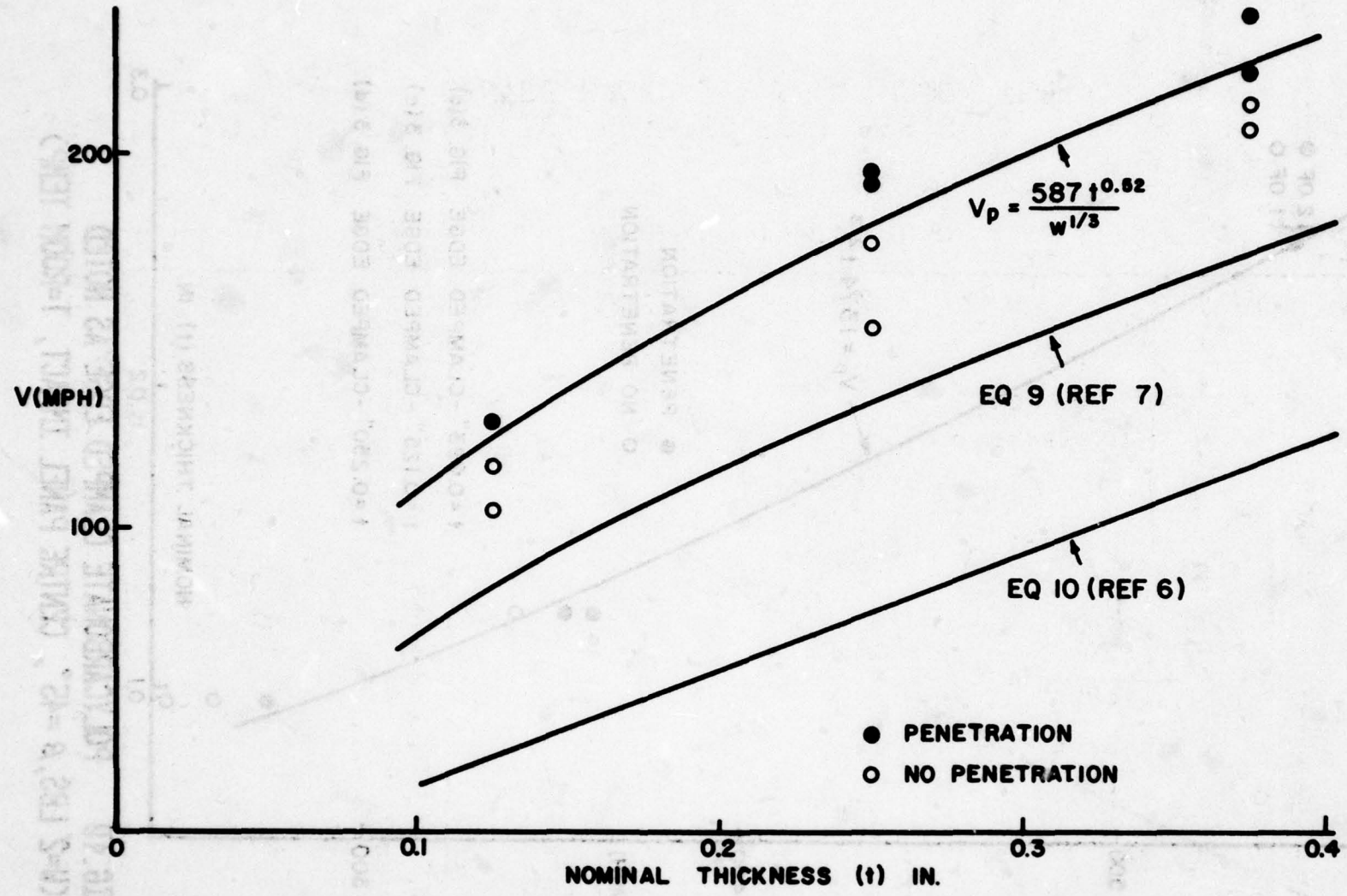


FIG. 18 STRETCHED ACRYLIC, CLAMPED EDGE FIG. 3(b)
(W=4lbs, β=45°, CENTRE PANEL IMPACT, T=ROOM TEMP)

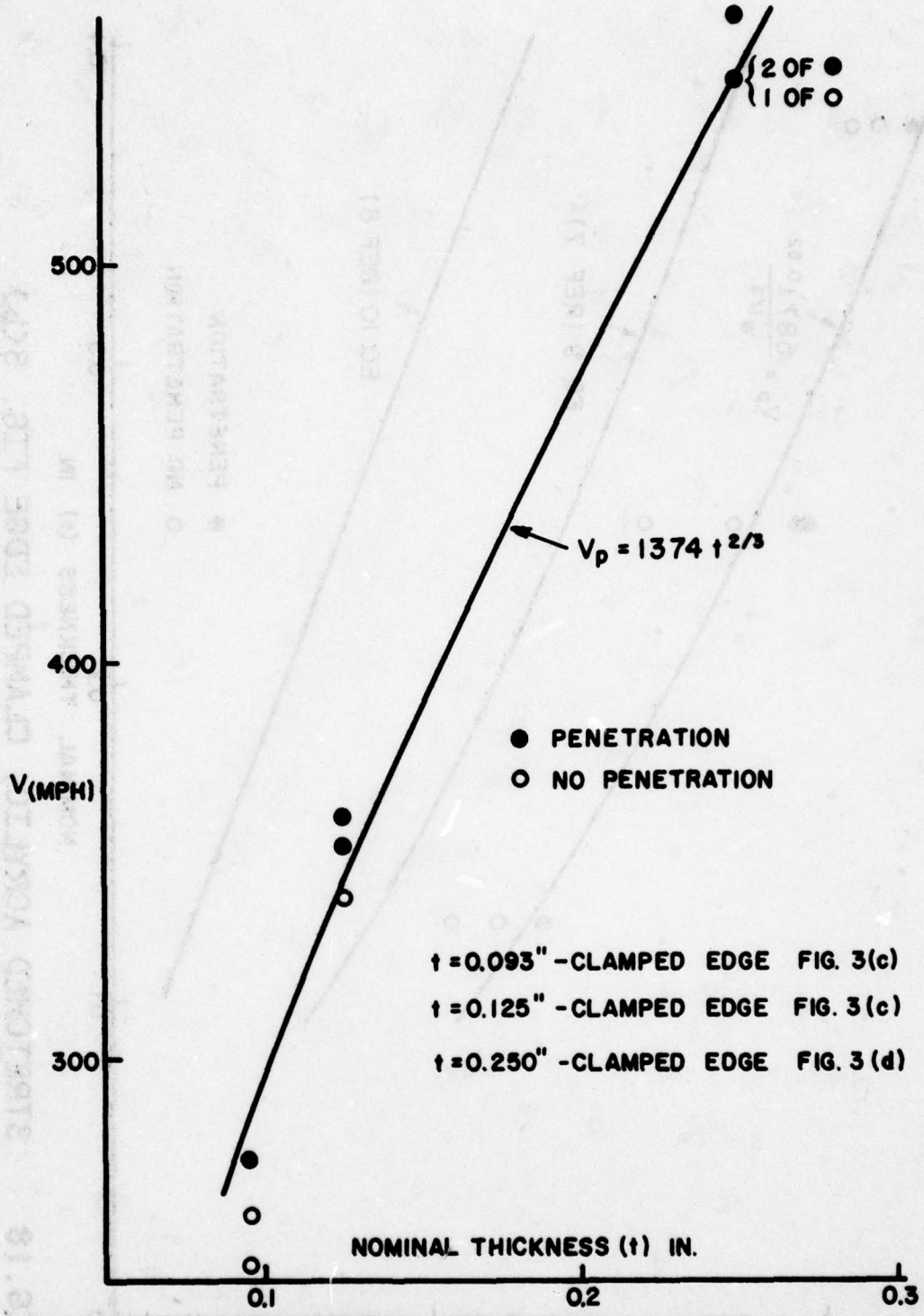
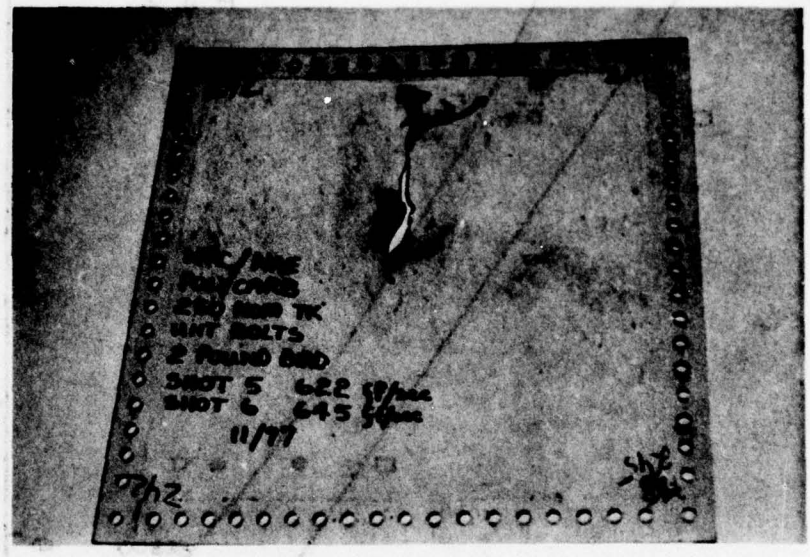


FIG. 19 POLYCARBONATE CLAMPED EDGE AS NOTED
(W=2 LBS, β =45°, CENTRE PANEL IMPACT, T=ROOM TEMP)



(a) BOLTED EDGES



(b) CLAMPED EDGES

FIG.20 TYPICAL POLYCARBONATE PANEL FRACTURES (β=45°, ROOM TEMP)

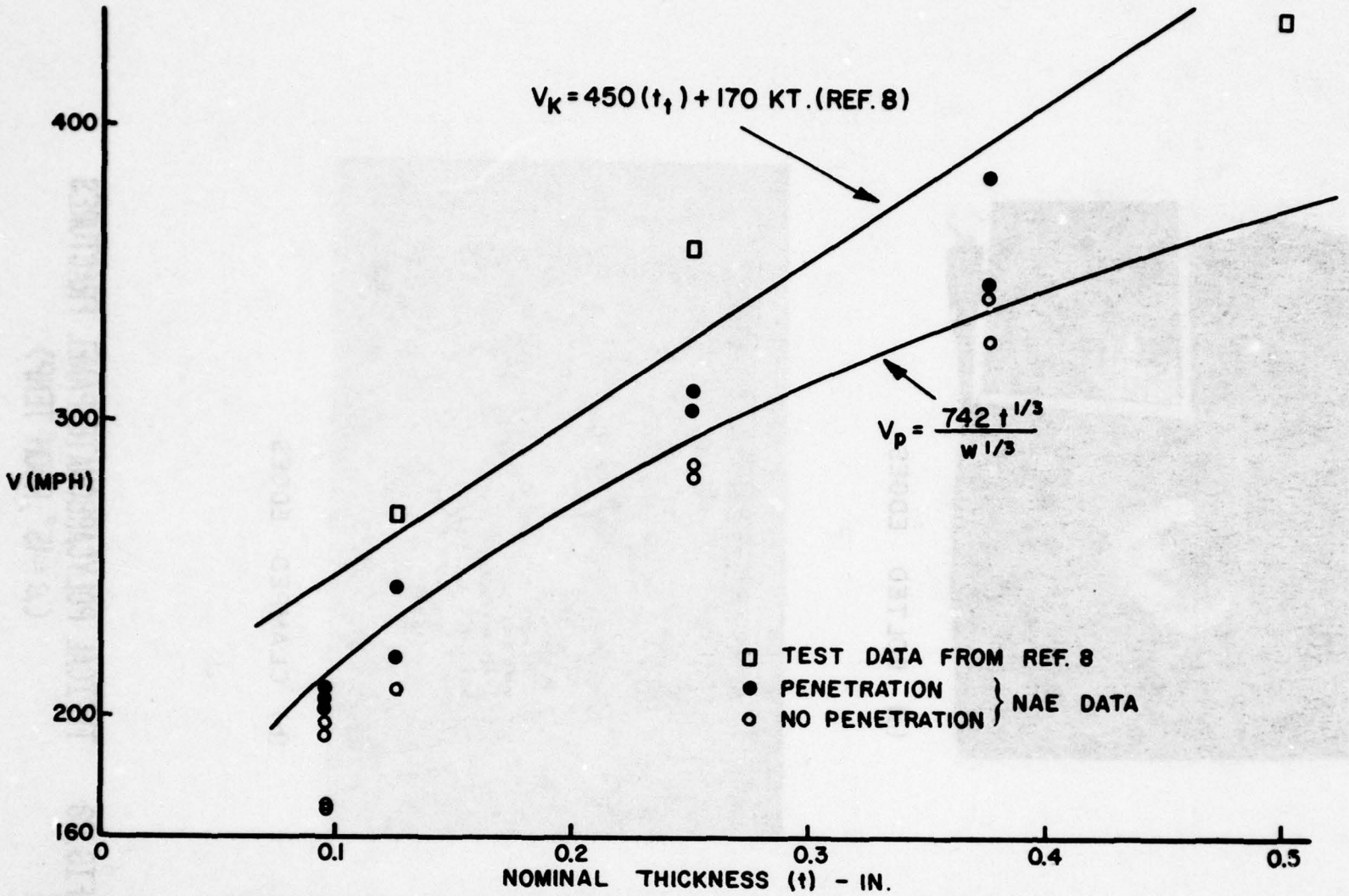


FIG. 21 COMPARISON OF POLYCARBONATE BOLTED EDGE DATA WITH EMPIRICAL EQUATIONS (W=4 LBS, β =45°, CENTRE PANEL IMPACT, T=ROOM TEMP)

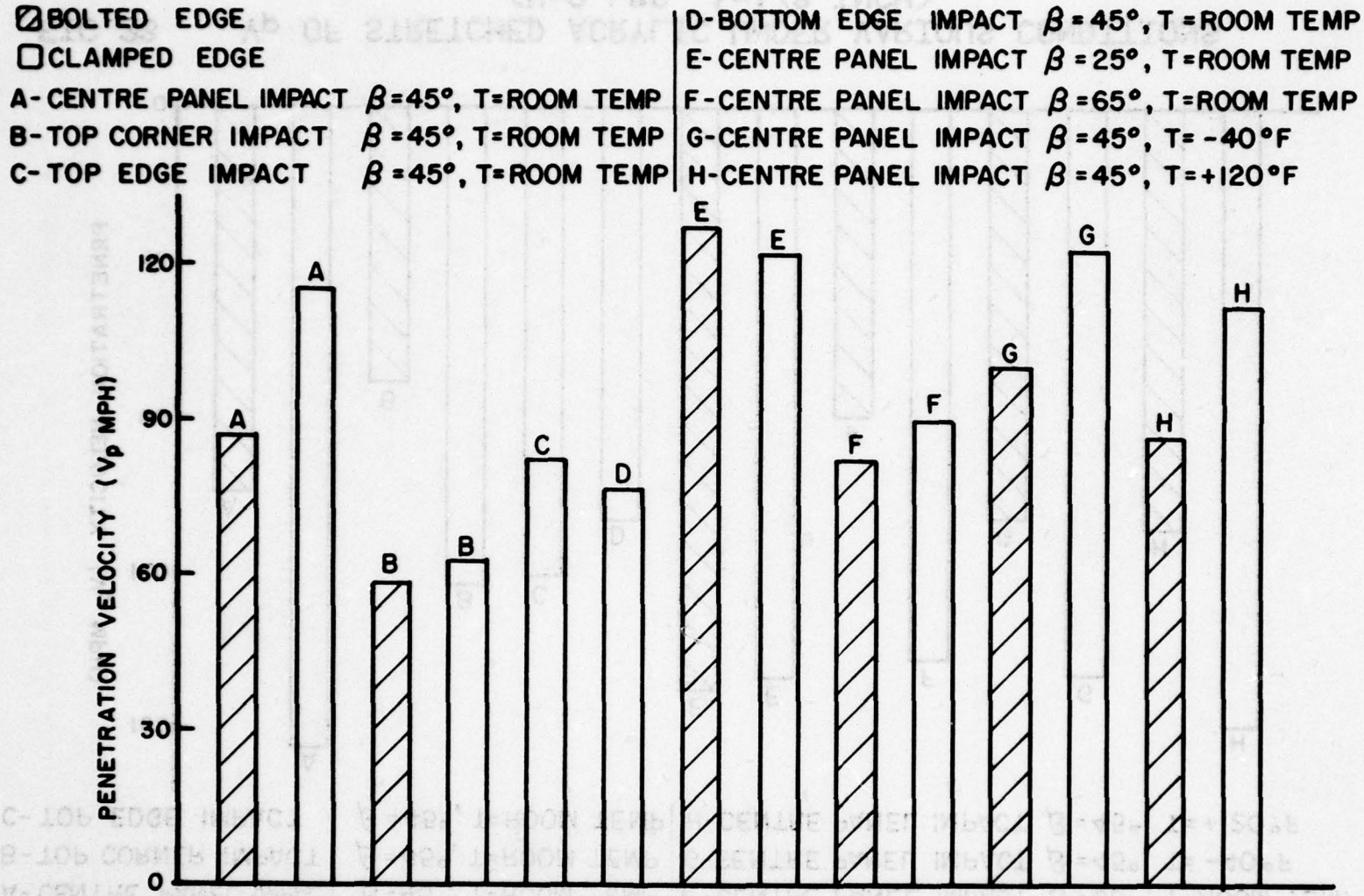


FIG.22 Vp OF AS CAST ACRYLIC UNDER VARIOUS CONDITIONS (W=2 LBS, t=1/8 INCH)

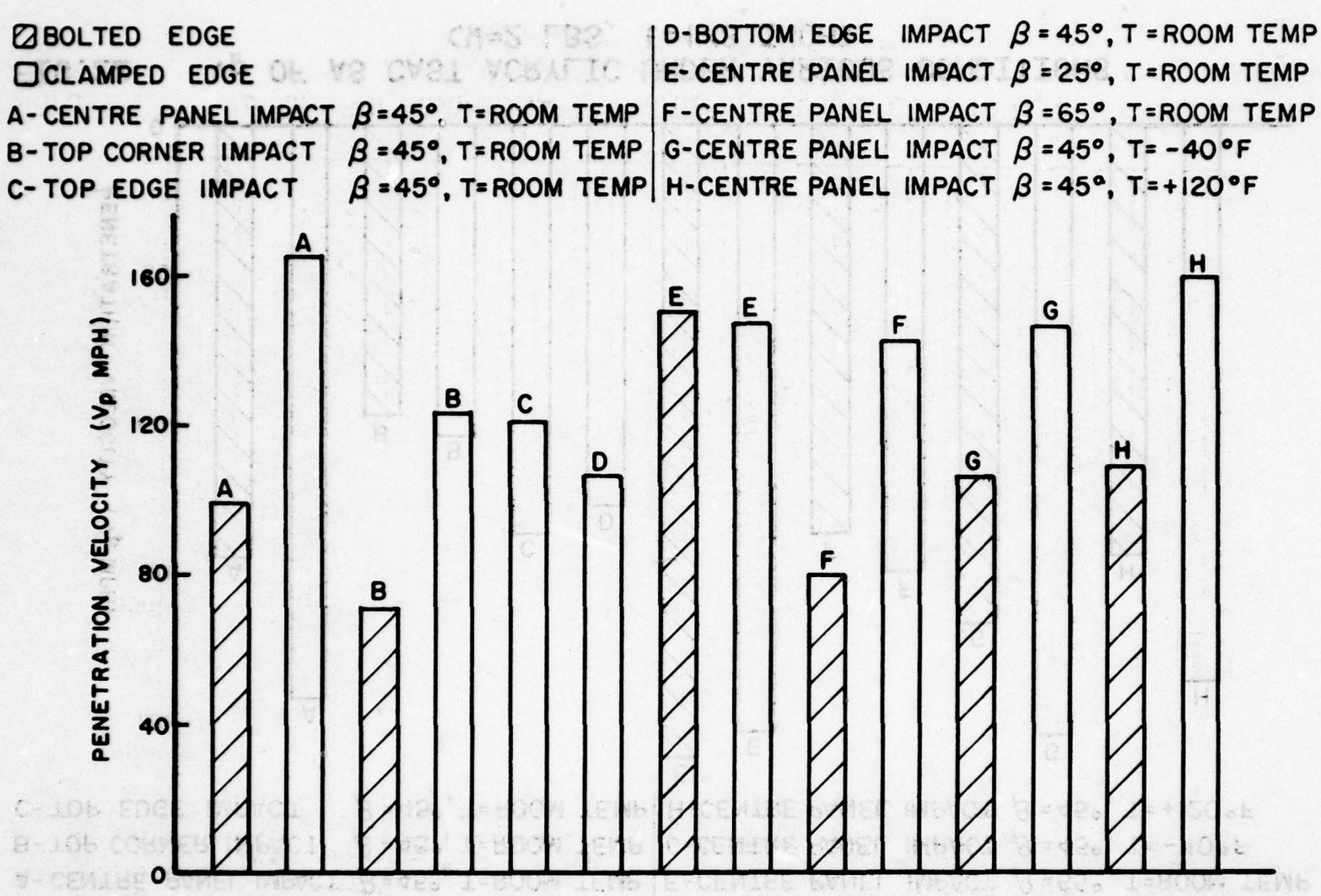


FIG.23 Vp OF STRETCHED ACRYLIC UNDER VARIOUS CONDITIONS (W=2 LBS, t=1/8 INCH)

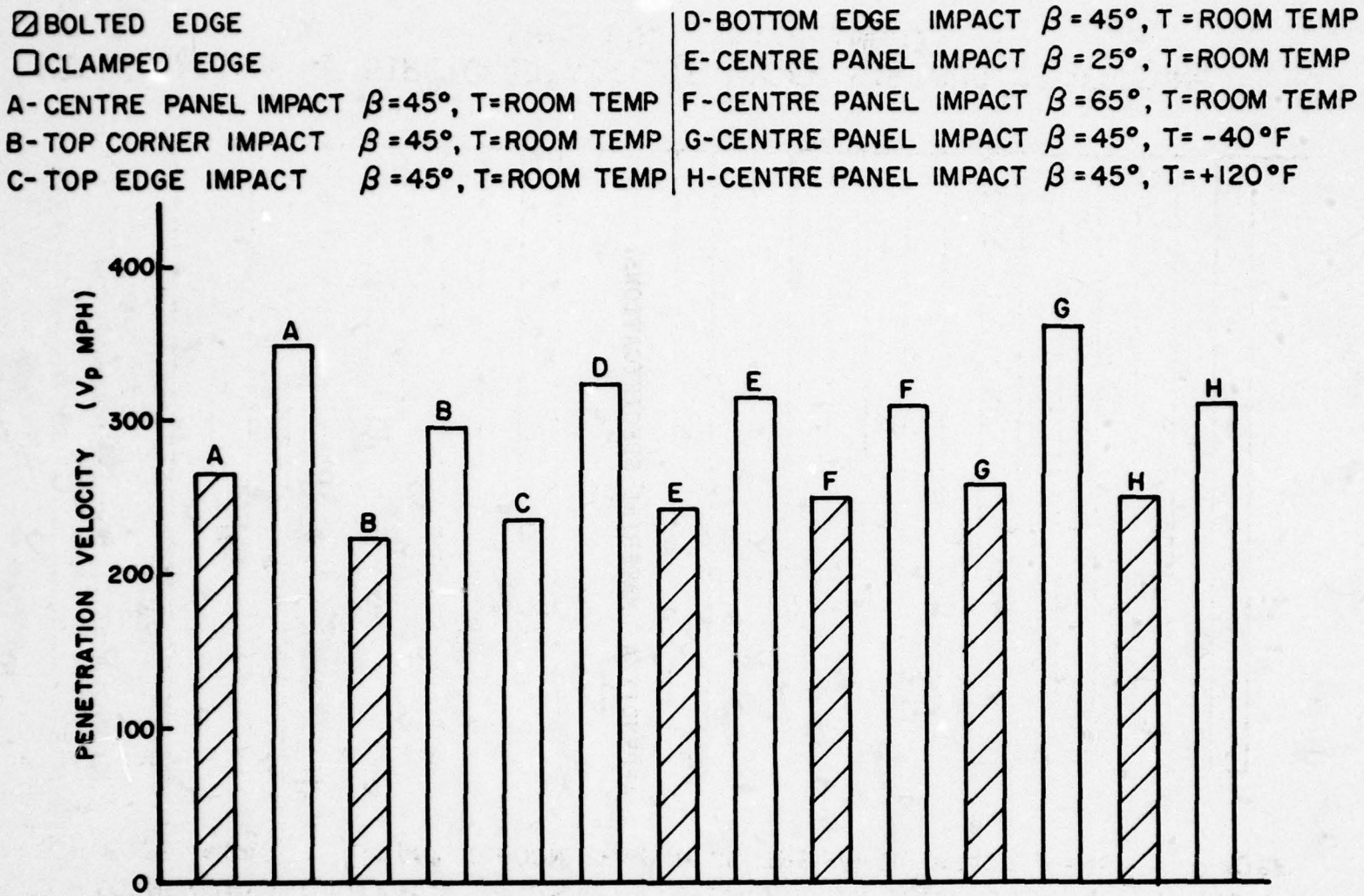
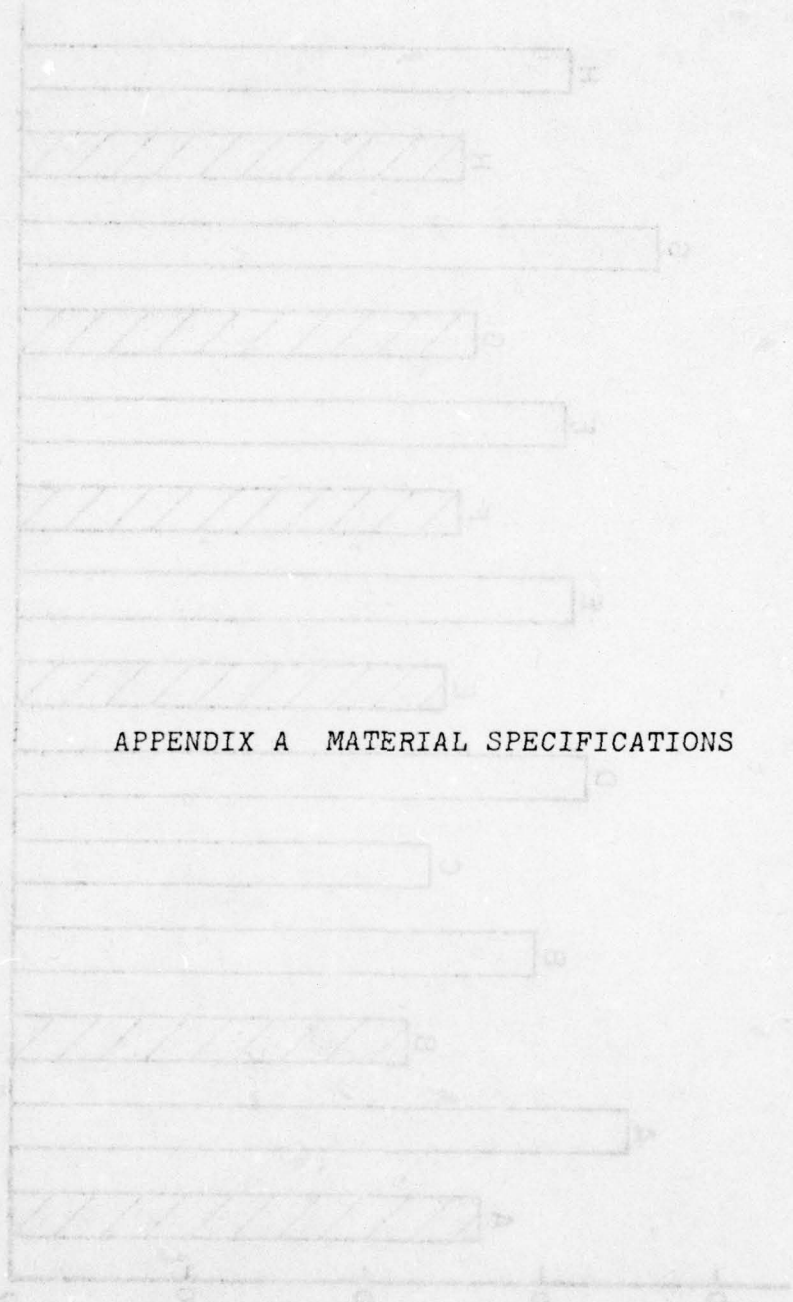


FIG.24 Vp OF POLYCARBONATE UNDER VARIOUS CONDITIONS (W=2 LBS, t=1/8 INCH)



APPENDIX A MATERIAL SPECIFICATIONS

TABLE A-1 MECHANICAL PROPERTIES

Mechanical Properties	ASTM Method	Units	As-Cast Acrylic			Stretched Acrylic	Polycarbonate (Lexan)
			Perspex	Acrylite	Plexiglas		
Tensile Strength	D638	P.S.I.	12,000 Av	10,000 Av	10,500 Max	11,000	9,500 Av
Elongation		%		4.2 Av	4.9 Max		110 Av
Modulus		P.S.I.	475,000 Av	400,000 Av	450,000	450,000	320,000 Av
Flexural Strength	D790	P.S.I.	20,000 Av	16,500 Av	16,000 Max	16,000	13,500 Av
Modulus		P.S.I.	420,000 Av	475,000 Av	450,000		340,000 Av
Compressive Strength	D695	P.S.I.		18,000 Av	18,000 Max	16,000	12,500 Av
Modulus		P.S.I.	440,000 Av	430,000 Av	450,000		345,000 Av
Shear Strength	D732	P.S.I.	11,000 Av	9,000 Av	9,000	11,000	
Impact Strength Izod Milled Notch	D256	Ft. lbs. / in. Notch	0.32 Av	0.4 Av	0.4	0.6	16.0
Rockwell Hardness	R+H P-20		M-90 Av	M-94 Av	M-93	M-97	M-70

TABLE A-2 MATERIAL THICKNESS VARIATIONS ENCOUNTERED

Material	Nominal Thickness (in.)	Thickness Extremes (in.)		Max. Variation in Panel (in.)
		Min.	Max.	
As-Cast Acrylic	0.125	0.087	0.145	0.032
As-Cast Acrylic	0.250	0.229	0.261	0.031
As-Cast Acrylic	0.375	0.347	0.394	0.037
Stretched Acrylic	0.125	0.110	0.148	0.023
Stretched Acrylic	0.250	0.243	0.283	0.023
Stretched Acrylic	0.375	0.351	0.418	0.038
Polycarbonate	0.093	0.089	0.101	0.011
Polycarbonate	0.125	0.118	0.135	0.009
Polycarbonate	0.250	0.242	0.264	0.010
Polycarbonate	0.375	0.367	0.379	0.009

THE MODELLING OF BIRD IMPACT LOADS

J. P. Barber and L. I. Boehman
University of Dayton
Research Institute
Dayton, Ohio

and

Capt. J. S. Wilbeck
Air Force Materials Laboratory
Wright-Patterson Air Force Base, Ohio

THE MODELLING OF BIRD IMPACT LOADS

by

J. P. Barber and L. I. Boehman
University of Dayton

and

Capt. J. S. Wilbeck
Air Force Materials Laboratory

ABSTRACT

The economical design of birdstrike resistant canopies and enclosures for modern, high-performance aircraft requires the use of sophisticated structural analysis techniques. One of the most important aspects of the successful use of these techniques is proper definition of the loads exerted on the structure. This aspect of the analysis is particularly important in dynamic structural response problems such as birdstrike. A three-level approach to the modelling of bird impact loads was selected. The level one model is the simplest and the easiest to implement, but has a limited range of applicability. The level two and three models are increasingly complex and increasingly difficult and costly to implement and operate but extend the range of valid application. Each of the models is described in this paper. Supporting experimental measurements which were used to formulate and validate the models are also presented. The basic principles involved in the proper load model level selection for a given structure are also presented.

PRECEDING PAGE BLANK-NOT FILMED

SECTION I

INTRODUCTION

Birdstrike on aircraft transparencies has proven to be an important consideration in the design of transparent crew enclosures. With the growing deployment of high performance aircraft on low level missions, the severity and importance of the birdstrike problem have grown. The potentially catastrophic effects of birdstrike have resulted in a considerable effort to improve the birdstrike resistance of modern aircraft transparencies. The development of increased birdstrike resistance currently involves an iterative process of building candidate transparencies and testing them. This process usually produces a successful design but is rarely cost effective. The fabrication of candidate transparencies can be very expensive while time and funding limit the testing that can be done. The result is that adequate rather than optimum designs evolve and the design cost is high. Persistent candidate transparency failure escalates the design cost very rapidly.

A more promising approach to the optimum design of birdstrike transparencies involves better analysis and greater understanding of the response of the transparency to bird impact. Recent developemnts in dynamic structural analysis make this approach particularly attractive. These analysis tools are based on finite element structural modelling techniques and are in principle capable of accurately describing the response of transparencies to transient bird loads. Such detailed information on the response of transparencies is of great importance in the design of birdstrike resistant transparencies.

To adequately describe the response of a transparency to bird impact three conditions must be met. First, an accurate mathematical model of the structure must be constructed. This model must be inherently capable of describing the complicated and dynamic characteristics of the transparency and support structure. Secondly, the transparency material must be adequately characterized. In particular, all of the important mechanical properties of the transparency material must be known and suitable mathematical models of that mechanical behavior generated. Finally, an accurate mathematical model of the impact induced loads must be available. The magnitude and the spatial and temporal distribution of the impact loads must all be described adequately to insure that the dynamic response of the transparency will be properly predicted.

Bird impact loading models must have a number of features in order to ensure that the loading will be properly described. Firstly, the model(s) should describe the loading in terms of basic physical processes. This generality is required to ensure applicability of the model(s) over the wide range of structural response modes observed in transparencies. Secondly, the effects of target motion and deformation on the loading should be properly described (i.e., load-target response coupling). Finally, the loading models should be amenable to numerical evaluation to

facilitate operation with the numerical structural analysis tools. This paper describes a series of bird impact loading models which were derived using experimental data and theoretical considerations to meet these requirements.

SECTION II

BACKGROUND

Birds are not simple to model. They are not homogeneous, isotropic, or axi-symmetric. They are not geometrically simple (cylindrical or spherical). The added variable of bird orientation further complicates the modelling problem. To make the problem tractable certain assumptions must be made. From previously reported work, it appears that a bird might be best modelled as a right circular cylinder with a length-to-diameter ratio of two.[1,2,3] Based on a large number of tests, Wilbeck[4] showed that a bird (including flesh and bones) could be adequately simulated by a homogeneous mixture of gelatin with 10 percent porosity. Gelatin was chosen because of its wide historical use as a flesh simulant. Porosity was added to lower the density of the gelatin to that of the birds which were tested. The density of gelatin was taken to be $\rho_f = 1060$ kg/m^3. With the addition of porosity, the porous density, ρ_z, of the gelatin mixture is given by;

$$\rho_z = (1-z)\,\rho_f \tag{1}$$

where z is the porosity. For 10 percent porosity (z = 0.10) the density is $\rho_z = 950$ kg/m^3 (approximately the measured density of chickens used in the impact tests).

Having established a simplified geometric and material model for a bird (right circular cylinder of porous gelatin) the physical phenomena which control the impact process may be identified. Previous work by the authors[1,4] demonstrated that the impact of a bird on a target can be treated as an unsteady fluidynamic process for the impact velocities of interest. They found that the stresses generated during impact greatly exceed the strength of the bird (both flesh and bones) and the bird flows onto the target during the impact. For the impact of a fluid cylinder on a rigid plate, the process may be divided into four phases as illustrated in Figure 1. The first phase is the initial impact in which very high shock pressures are generated in the bird and the target. The release of this shock at the bird free surfaces results in a decaying pressure. The pressure decays until the third phase of the impact is reached. During this phase the bird flows steadily onto the plate. This part of the process may be regarded as jet flow. The final phase of the impact occurs as the trailing end of the bird approaches the plate and the pressures fall to zero.

Figure 2 shows the pressure-time record for the normal impact of a bird on a rigid plate. The transducer was located at the center of the

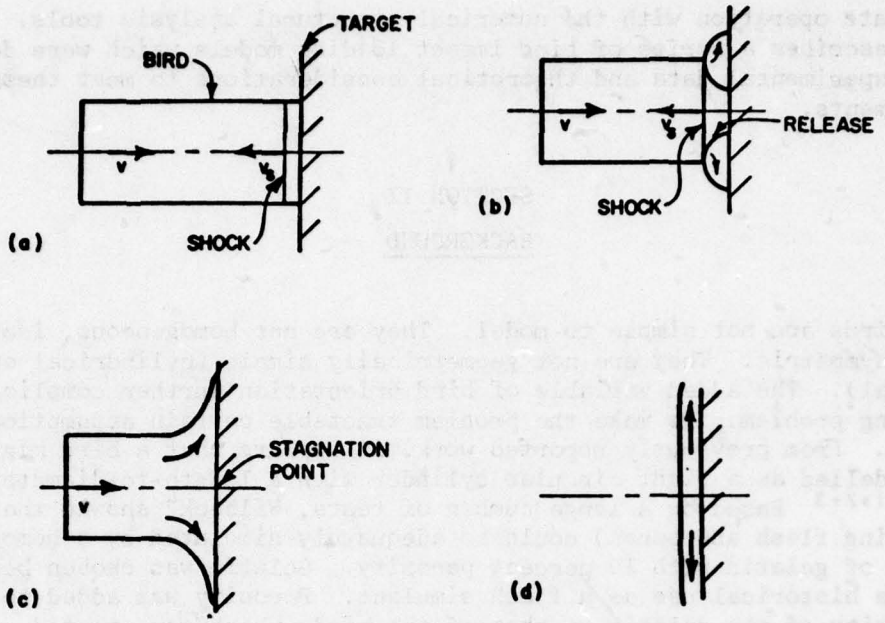


Figure 1. The Phases of a Bird Impact (a) Shock (b) Shock Release (c) Steady Flow (d) Termination

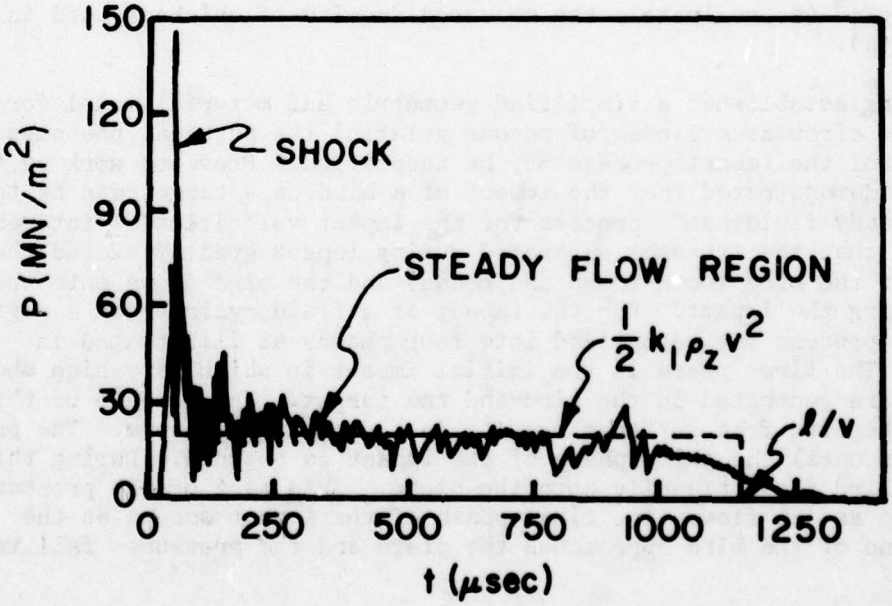


Figure 2. Pressure Time Record for the Normal Impact of a Bird.

impact surface. From this figure it is evident that during the initial shock phase, very high pressures are generated. However, the very short duration of the high pressure results in only a small momentum transfer and this process may have little effect on the overall response of the target. Barber, et al[1], showed that the shock pressures are much lower in oblique impacts. From Figure 2 it is apparent that the dominant phase of bird impact loading appears to be the steady flow phase. By treating the bird as a quasi-steady fluid jet during this phase, Barber, et al[1], calculated the magnitude and distribution of steady flow pressures with remarkable agreement to measurements. The duration was shown to be approximately the time required for the bird to travel its length (i.e., $t_d = \ell/v$).

The pressures generated during bird impact were found by Wilbeck[4] to be sensitive to bird porosity. The shock pressures are the most sensitive and are greatly reduced by even small amounts of porosity. During the steady flow portion of the impact a stagnation point is established in the flow.[1,4] The stagnation pressure is also sensitive to bird porosity. However, for the birds considered in previous studies[1,2,3,4](chickens), which can be modelled with gelatin containing 10 percent porosity, the stagnation pressure can be determined with sufficient accuracy assuming incompressible flow with the porosity removed (i.e., $\rho = \rho_f$). It is concluded that, for chickens at least, porosity must be considered in the determination of the initial shock pressure, but may be ignored in the steady flow regime.

From the large body of previous work[1,2,3,4] it was concluded the birds behave fluidynamically during impacts at the velocities of interest in aircraft design. Bird impacts are dominated by the steady flow phase. For the birds considered (chickens) the porosity of the bird does not appreciably lower the steady flow pressures. These principles were used to formulate a series of bird impact loading models for use with structural analysis tools.

SECTION III
LOAD MODELLING

3.1 Introduction

The loads exerted on a structure during an impact can be characterized in terms of a number of fundamental parameters. The most important of these parameters are the total impulse imparted to the structure, the forces (i.e., the rate of impulse transfer), the pressures (i.e., the spatial distribution of the force) and time variation of forces and pressures (e.g., the duration). The parameters which must be considered in a particular impact are a function of the response regimes of the target. We have identified three response regimes and have developed suitable loading models for each.

The simplest target response regime involves targets which don't respond to the loads during the time of impact. In this case, the target

can be considered to behave as a rigid, immoveable object (from a loading point of view). The most important loading parameter is the impulse transferred to the target. The description of loads for this case is the Level 1 loading model.

If the target translates and rotates during the impact, but doesn't deform locally, the response regime is labelled locally rigid. The process is illustrated in Figure 3. The translation and rotation of the target during impact results in significant changes in the impulse imparted to the target, the duration of the force, the magnitude and direction of the force, and distribution of the pressures exerted on the windshield. The Level 2 loading model was developed to describe the impact loads under these conditions.

If the target not only translates and rotates during impact, but also deforms locally, the response is termed locally deforming. This case is illustrated in Figure 4. The target forms a "pocket" around the bird. This "pocketing" behavior results in greatly increased local loading, local deformation, and momentum transfer to the target. The Level 3 loading model, designed to describe bird impact loading under these conditions, must account for the effects on the impact pressures and pressure distributions of local target shape change and local target motion.

The three levels of loading models are described in more detail in the following paragraphs.

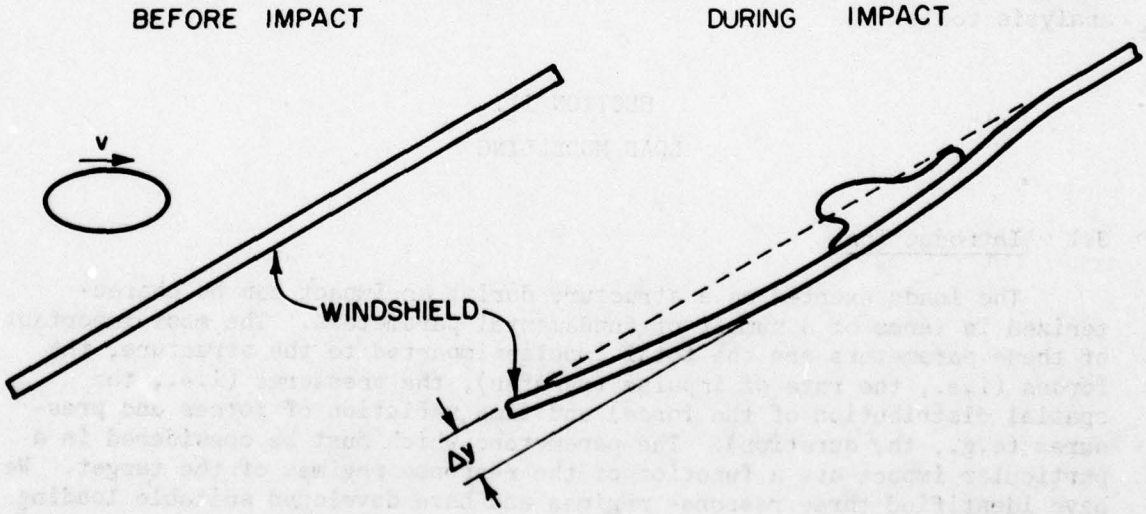


Figure 3. Locally Rigid Windshield Response.

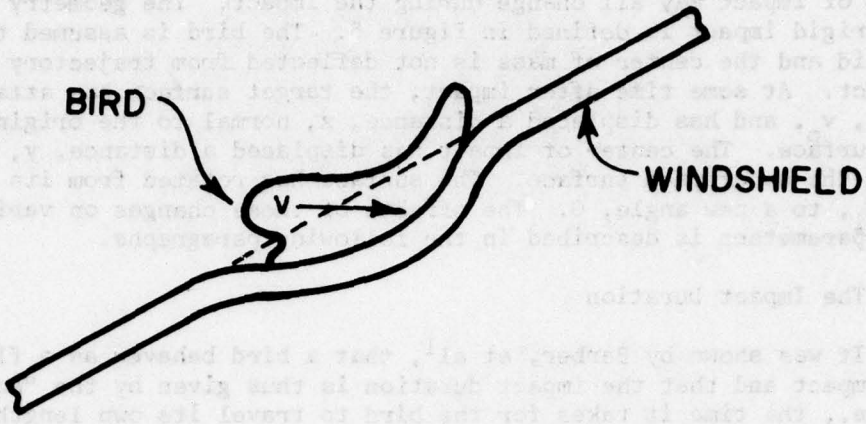


Figure 4. Locally Deforming Windshield Response.

3.2 Level 1 Loading Model

If the target remains locally rigid and doesn't translate or rotate during the impact, then the loads on the target can be adequately characterized in terms of the impulse, I, transferred to the target. For a bird of mass, m, striking a target at velocity, v, with obliquity, θ, the impulse is;

$$I = mv \sin \theta \qquad (2)$$

The impulse may then be simply imparted to the structure at the center of impact in the structural analysis model. This loading model will only be satisfactory for a modal type of structural analyses where the actual duration of the impact is much less than the highest significant modal period excited. (i.e., the impulse approximation must be physically, as well as mathematically, realistic). The more detailed the structural model (higher modes or degrees of freedom) the less applicable this loading model will be. High modes of response must be arbitrarily eliminated in the structural analysis.

Although it has been successfully employed by Tsai, et al[5], this loading model clearly has very limited applicability, and a more accurate description of the time dependent rate of momentum transfer (forces) is required if any significant target motion occurs during impact.

3.3 Level 2 - Loading Model

In a locally rigid impact the impact velocity, impact angle, and location of impact may all change during the impact. The geometry of a locally rigid impact is defined in Figure 5. The bird is assumed to behave as a fluid and the center of mass is not deflected from trajectory during the impact. At some time after impact, the target surface has attained a velocity, v_p, and has displaced a distance, x, normal to the original target surface. The center of impact has displaced a distance, y, in the plane of the undeformed surface. The surface has rotated from its initial angle, θ_i, to a new angle, θ. The effects of these changes on various loading parameters is described in the following paragraphs.

3.3.1 The Impact Duration

It was shown by Barber, et al[1], that a bird behaves as a fluid during impact and that the impact duration is thus given by the "squash-up" time (i.e., the time it takes for the bird to travel its own length). In a locally rigid impact, the length of bird, s, consumed in time, t, is given by the integral equation;

$$s = \int_o^t (v - v_p/\sin\theta)\, dt \qquad (3)$$

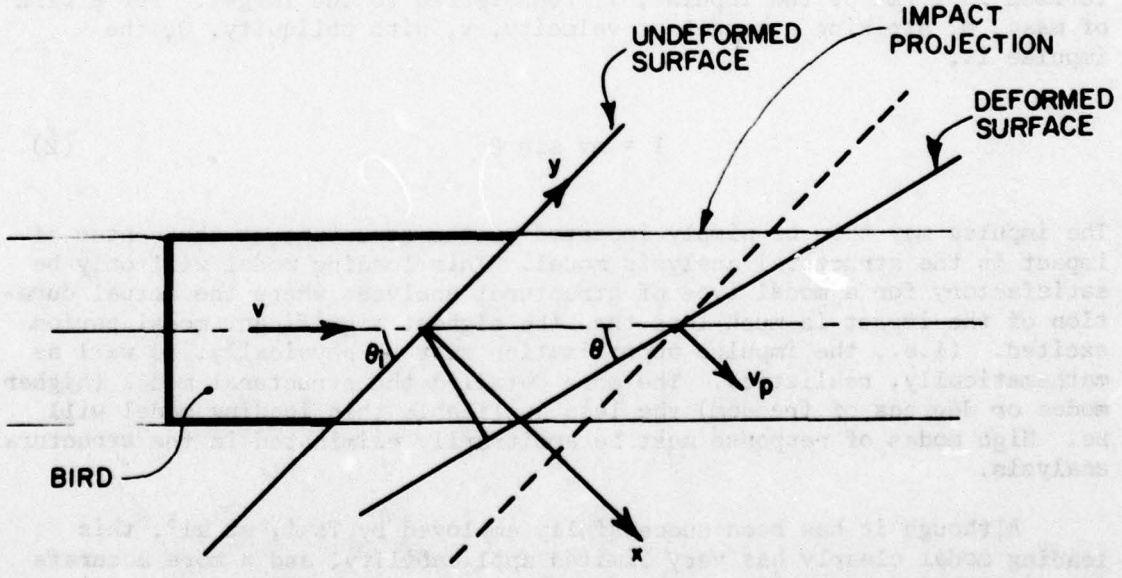


Figure 5. Geometry of a Locally Rigid Impact.

Equation (3) is most easily understood by noting that $v - v_p/\sin\theta$ is simply the relative velocity of the bird with respect to the target along the trajectory. From Equation (3) it is apparent that the "squash-up" time cannot be defined "a priori" in a locally rigid impact. The duration is the time at which the length of bird consumed is equal to the total length of bird available. The progress of a locally rigid impact is not characterized by time but rather the nondimensional length, s/ℓ, which is given by;

$$s/\ell = vt/\ell - \int_o^t (v_p/\ell \sin\theta)\, dt, \qquad (4)$$

where ℓ is the length of the bird. Equation (4) describes the fraction of the bird that has been consumed at time, t, during the impact. When s/ℓ reaches 1.0, the impact is complete and the force drops to zero.

3.3.2 The Impact Force

As pointed out in the background of this paper, the transient shock effects in bird impact are probably not important and the impact may be considered to be a steady flow process. The instantaneous force exerted during the impact may be written as;

$$F = \rho_z A v^2 \sin\theta \qquad (5)$$

where A is the cross-sectional area of the bird at any time during the impact. The non-steady features of the impact, if they are important, can be included empirically. The variation of force with time during the impact on a rigid target may then be regarded as the variation of the cross-sectional area of the bird, A, with time during the impact. The generalized bird impact area-length variation shown in Figure 6 was derived from experimental data obtained by Barber, et al[1]. The average area of the bird, A_{avg}, is simply bird volume divided by bird length. It should be noted that Figure 6 was not intended to imply that the real variation of bird impact area with consumed length was given by this figure, but rather that the loading process could be empirically described in this manner. The non-steady effects of impact, as well as the variations of area, were treated simply as variations of area.

Equation (5) applies to a rigid target and must be modified to properly account for the motion of a locally rigid target. Equation (5) simply equates the force to the momentum flux incident on the target surface. For a locally rigid target surface the momentum flux may be derived by considering Figure 5. The relative velocity of impact normal to the target surface is $\rho_z (v \sin\theta - v_p)^2$. This momentum flux acts over the area of the bird projected on the target surface, or, $A/\sin\theta$. Therefore, the momentum transfer rate, or instantaneous force, exerted on the target is given by;

$$F = \rho_z A(v \sin\theta - v_p)^2/\sin\theta \qquad (6)$$

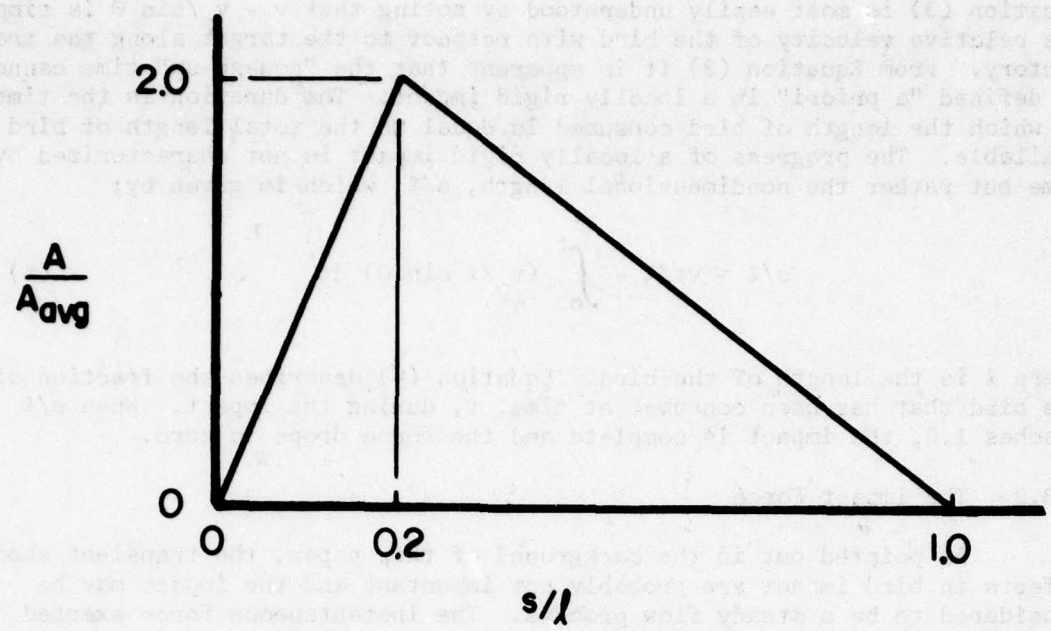


Figure 6. Nondimensional Impact Area Versus Nondimensional Consumed Length.

The area of the bird, A, is considered to be a function of the nondimensional consumed length as shown in Figure 7. During a structural response calculation, the area, A, is evaluated using Figure 6, while v_p and θ are determined from the current calculated position and velocity of the target.

The direction in which the force is applied changes continuously during the impact. However, it is always normal to the target surface and this may be readily determined incrementally during the structural response calculation.

The point of application of the force also changes during the impact and this can be a significant effect. As shown in Figure 5, when the target surface deflects a distance, x, the point of impact translates a distance, y. If the rotation of the target can be neglected then;

$$y = x \cot \theta \qquad (7)$$

If the target also rotates, then the position of impact must be computed by projecting the trajectory onto the surface of the target. In general, the position of impact will be a complicated function of displacement, x, and angle, θ.

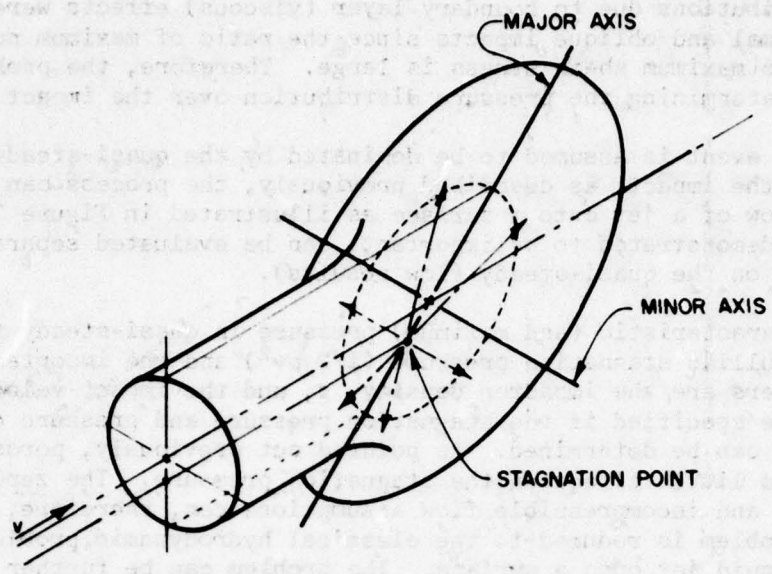


Figure 7. Oblique Impact.

3.3.3 Impact Pressure Distribution

The distribution of pressure in a locally rigid impact has only a minor effect on the response. A point load applied at the center of impact would in principle be adequate. However, many structural analysis techniques require a distributed load in order to obtain reliable solutions. For the Level 2 loading model, the loads may be distributed arbitrarily over the area of the bird projected on the target. For simplicity a uniform distribution of pressure, or some other distribution with a convenient mathematical description, may be used.

If local deformation of the target occurs, this loading model cannot adequately describe the impulse transfer, forces or pressure distribution. As the distribution of local loads (pressures) is arbitrary it should not be expected to accurately predict local deformations, even if they are small. To properly describe the impact loads on a locally deformable target a more sophisticated analysis of loading is required.

3.4 Level 3 Loading Model

If the target deforms locally during the impact, as well as translating and rotating, then a loading model capable of generating the local distribution of loading pressures during the impact is required. As birds behave like a fluid during impact, the distribution of surface pressure during impact is directly related to the fluid nature of the event. To successfully predict the surface stress distributions on deforming surfaces

it is necessary to utilize a fundamental fluidynamic approach. The shear stress distributions due to boundary layer (viscous) effects were ignored for both normal and oblique impacts since the ratio of maximum normal stress (pressure) to maximum shear stress is large. Therefore, the problem was reduced to determining the pressure distribution over the impact area.

If the event is assumed to be dominated by the quasi-steady flow portions of the impact, as described previously, the process can be thought of as the flow of a jet onto a surface as illustrated in Figure 7. (shock effects, if demonstrated to be important, can be evaluated separately and superimposed on the quasi-steady flow results).

The characteristic (and maximum) pressure in quasi-steady fluid flow is the Bernoullian stagnation pressure ($1/2\ \rho v^2$) and the important independent parameters are the impactor density, ρ, and the impact velocity, v. The loads are specified if the stagnation pressure and pressure coefficient distribution can be determined. As pointed out previously, porosity (of chickens) has little effect on the stagnation pressure. The zero porosity density (ρ_f) and incompressible flow assumptions can, therefore, be applied. Thus, the problem is reduced to the classical hydrodynamic problem of the flow of a liquid jet onto a surface. The problem can be further simplified by making the assumption of irrotational flow: an assumption which is supported by the fact that in the impact region fluid inertia forces dominate over viscous forces. With the assumptions of steady, incompressible, irrotational flow, the problem may be treated as a steady, potential flow described by Laplace's equation. A serious complication remains however. The boundary of the jet is a free streamline whose position is not known "a priori". The static pressure is continuous across a free streamline while the velocity normal to this streamline and the stagnation pressure are both discontinuous. Along a free streamline the magnitude of the velocity is constant according to Bernoulli's equation. Thus, even though the governing partial differential equation (Laplace's equation) is linear, the free streamline boundary condition is nonlinear. These conditions can be described, in two-dimensional flows, with complex variable theory and exact analytical solutions for two-dimensional jets impacting on surfaces have been obtained. However, no three-dimensional jet impact flows (such as those of interest here) have been solved analytically. Not even the case of an axi-symmetric (circular) jet impacting normal to a flat plate has been solved, because complex variable theory becomes extremely cumbersome in cylindrical coordinate systems[6]. Approximate analytical solutions are available for predicting the pressure distribution for circular jets impacting normal to flat plates (see Wilbeck[4]). However, not even approximate analytical solutions are available for cylindrical jets impacting flat surfaces obliquely. For this problem, recourse to numerical solutions must be made.

Numerical potential flow solutions for circular jets (jets bounded by free streamlines) are very difficult to obtain because the location of the free streamlines are not, in general, known. For circular jets at normal incidence the position of the free streamlines can be adequately guessed in order to start a solution. For oblique impacts, particularly on curved surfaces, guessing the free streamline position would be a major undertaking in addition to the considerable task of numerically solving

Laplace's equation in three dimensions. Accordingly, an approximate numerical solution which would provide a reasonably accurate description of the pressure distribution (but not necessarily satisfying the free streamline condition) was developed.

Three-dimensional potential flow theory was used to develop a model for predicting the pressure distribution produced by the steady flow of a cylindrical jet impacting on a flat plate. It was assumed that pressure distribution, as calculated for this fluidynamic problem, would provide a reasonable description of the steady flow portion of a bird impact. Incompressible, irrotational flow assumptions were made, but the free streamline boundary condition was not imposed. The method of superposition of solutions was used even though superposition is not strictly valid (although Laplace's equation is linear, the free stream boundary condition is nonlinear). The numerical approach used was based on the method of surface singularities[7].

The approximate numerical solution involved the superposition of two elementary solutions to Laplace's equation. The two solutions used were: (1) the uniform flow of a fluid in an infinite jet of arbitrary but constant cross-sectional area; and (2) the uniform distribution of planar fluid sources over the impact area. The velocity of the fluid within the infinite jet was considered constant, while the fluid outside this region was assumed to be at rest. Surface sources were distributed on the target surface. The strength of the surface sources was selected to provide the correct boundary condition at the target (no flow normal to the target surface). The complete solution to this problem may be found in Reference 1.

The model was exercised and compared with steady flow pressure measurements obtained from the oblique impact of birds. The results are shown in Figure 8 and 9. The nondimensional pressure is the pressure normalized to the stagnation pressure (pressure coefficient), and the nondimensional radius is distance normalized to the bird radius projected onto the surface. The agreement between the measurements and the calculations is remarkably good. The analysis does, however, tend to breakdown in the immediate vicinity of the jet boundary at the target (a sort of "edge effect"). This breakdown occurs because the free streamline boundary condition is not satisfied. This approximate model does, however, predict the pressure distribution quite accurately in the region of maximum pressure, where most of the load (and target deformation) occurs, and does correctly predict the total impulse.

This model can be used for any arbitrarily shaped impact surface. The impact area is divided into small flat elements and a uniform distribution of sources is assumed to cover each element. During the analysis of an impact in which local target deformation takes place, the deformed target shape in the impact zone is calculated at each time interval employed in the dynamic structural analysis. The geometry of the impact zone can then be provided at each time interval to the Level 3 loading model and the pressure distribution appropriate to the target at that time can be determined. As the structural analysis calculation proceeds, the local shape, location and velocity of the impact area is updated and made

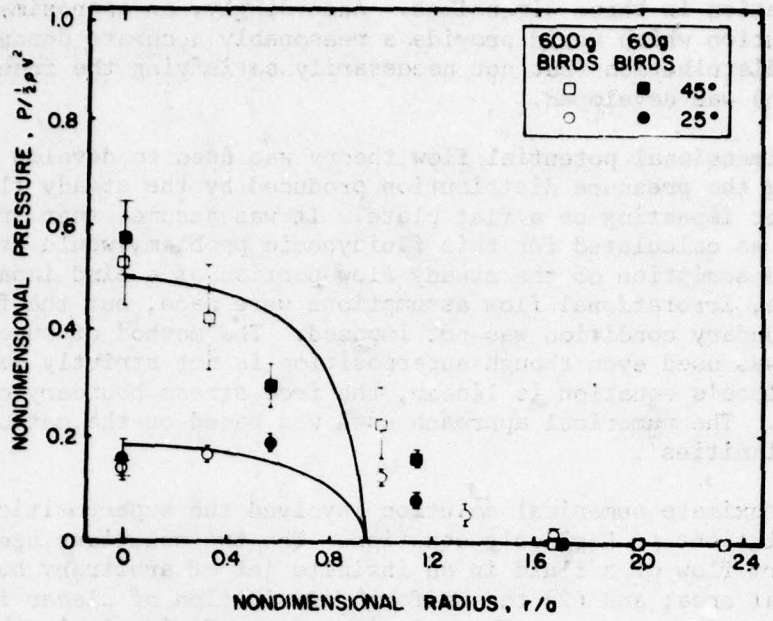


Figure 8. Steady Flow Nondimensional Pressure Distribution Along the Major Axis for Oblique Impact.

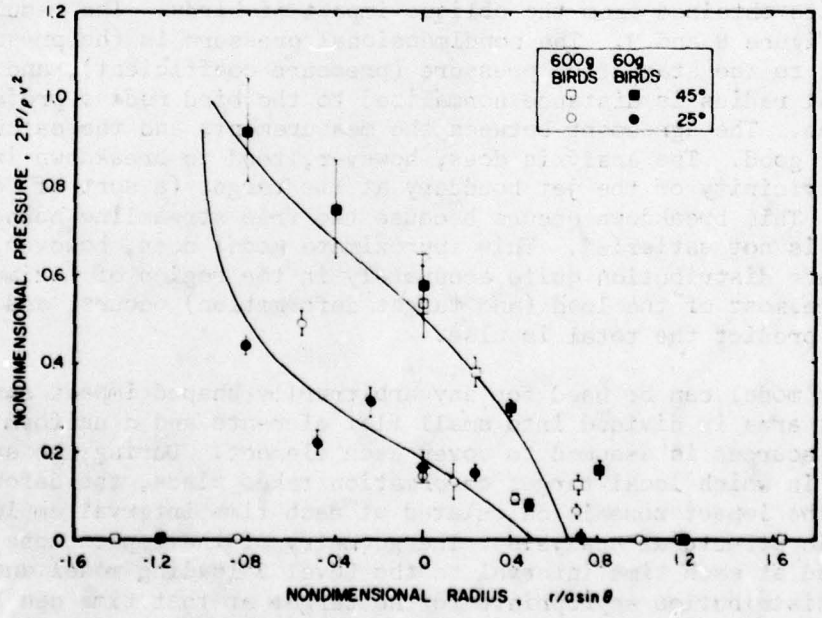


Figure 9. Steady Flow Nondimensional Pressure Distribution Along the Minor Axis for Oblique Impact.

available to the Level 3 loading model. The loading model, in turn, provides updated pressure and pressure distribution information for the structural response computation. The Level 3 loading model is, thus, fully interactive with the structural response calculation. The duration of the impact is computed in the same manner as that described for the Level 2 loading model.

The Level 3 loading model is capable of detailed interaction with the structural response model and is capable of dealing with target translation, rotation and local deformation. The load/response coupling modelled in this formulation should be capable of accurate prediction of both overall target response and local deformation.

The principal limitation of the Level 3 loading model is that it does not include transient effects. The most significant transient effect is the shock process. However, the porosity present in birds appreciably reduces the shock stresses, while the steady flow pressures are not significantly affected. In addition, impact obliquity (transparency impacts are, in general, oblique) also reduces the relative importance of shock stresses. Therefore, it is not obvious that neglect of the shock aspects of bird impact on transparencies is a significant deficiency. Another transient aspect of bird impacts is the variation of bird cross-sectional area at the target surface during impact. This results mainly in a time variation of the impact area. If the flow remains quasi-steady during these variations (i.e., the "velocity" of the variation is low with respect to local sound speed probably a good assumption), then the Level 3 model can be modified to describe these effects. The size and geometry of the "jet" which flows onto the target surface must be updated in time incrementally to describe the variation of impact area with time.

SECTION IV

SUMMARY AND CONCLUSIONS

Birds behave in a fluidynamic manner during impact at the velocities of interest in aircraft design. The transient effects (such as shocks) are relatively unimportant and the bird impact process may be treated as quasi-steady fluid flow. These observations were employed to generate a series of bird impact loading models.

Targets can, in general, respond to bird impact in one of three structural response regimes, rigid, locally rigid, or locally deforming. Loading models with load/response coupling appropriate to each response regime were developed. Each model incorporates the fundamental physics appropriate to the loading and load/response coupling for each response regime. This fundamental approach is necessary to ensure correct description of the loads, especially for the most severe case of load/response coupling, the locally deforming case. For this case an approximate fluidynamic model was developed which can adequately predict pressure distribution for a jet impinging on an arbitrarily shaped surface.

All three models are currently being implemented and rigorously tested. The response to bird impact panels configured like aircraft transparencies will be determined experimentally and compared to predictions made using these loading models.

REFERENCES

[1]Barber, J.P., Wilbeck, J.S., and Taylor, H.R., "Bird Impact Forces and Pressures on Rigid and Compliant Targets," UDRI-TR-77-17, (to be published as AFFDL-TR-77-60.)

[2]Peterson, R.L. and Barber, J.P., "Bird Impact Forces in Aircraft Windshield Design," AFFDL-TR-75-150, March 1976.

[3]Barber, J.P., Taylor, H.R., and Wilbeck, J.S., "Characterization of Bird Impacts on a Rigid Plate: Part I," AFFDL-TR-75-5, January 1975.

[4]Wilbeck J.S., "Impact Behavior of Low Strength Projectiles," PhD Thesis, Texas A&M University, May 1977. (to be published as AFML-TR-77-134.)

[5]Tsai, S.W., Sun, C.T., Hopkins, A.K., Hahn, H.T., and Lee, T.W., "Behavior of Cantilevered Beams Under Impact by a Soft Projectile," AFML-TR-74-94, November 1974.

[6]Milne-Thompson, L.M., Theoretical Hydrodynamics, MacMillan Company, New York, Chapter 11, 1960.

[7]Hess, J.L. and Smith, A.M.O., "Calculation of Potential Flow About Arbitrary Bodies," Progress in Aeronautical Sciences, Vol. 8, Perganon Press, New York, pp 1-138, 1966.

BIOLOGICAL CONTROL OF BIRDS, AN UPDATE

1st Lt. J. S. Kent
Air Force Civil Engineering Center
Tyndall Air Force Base, Florida

PRECEDING PAGE BLANK-NOT FILMED

BIOLOGICAL CONTROL OF BIRDS, AN UPDATE

1st Lt Jim Kent

Environmental Planner Biologist

AFCEC/DEVN Tyndall AFB FL

ABSTRACT

Collisions between aircraft and birds can be lessened, damage reduced, and lives saved, all goals of the USAF Bird/Aircraft Strike Hazard (BASH) Team. Through habitat modification, scaring devices, live trapping, and flight procedure change, we can significantly reduce the probability of bird strikes. Modification of the airdrome environment by removal of roosting, feeding, nesting and loafing areas reduces the attractiveness to birds. Active scaring with pyrotechnics and bird distress calls frightens birds from airfields. Live trapping and relocation of raptors protects these valuable species while maintaining operational safety. Awareness of bird concentrations and locations permits modification of flight procedures to avoid possible strikes. Although complete control is not presently feasible, a knowledge of avian biology and the use of known techniques will reduce safety problems related to bird strikes.

PRECEDING PAGE BLANK-NOT FILMED

BIRD CONTROL ON AIRFIELDS-AN UPDATE

INTRODUCTION

Collisions between aircraft and birds have occurred almost since the beginning of aviation (reference 1). The first fatality from a bird strike dates back to 1912. As aircraft speed and performance have increased, the threat to human life and the amount of damage to planes have also increased. An estimated 1200 bird strikes occur in the United States each year and cost the Air Force over seven million dollars annually (reference 2). The difference between a minor and a severe strike is often the position on the aircraft where the bird strike occurs. The greatest amount of damage from birds usually results from engine ingestion or impacts on the windscreen of the aircraft. Efforts to reduce the hazards of bird strikes have centered in two main areas (1) changes in aircraft design and equipment to avoid collisions, and (2) bird control near airfields.

The Bird Aircraft Strike Hazard (BASH) Team, a division of the Air Force Civil Engineering Center at Tyndall Air Force Base, Florida, is responsible for bird control near airfields. The team advises Air Force Bases on reducing problems associated with birds. Complete bird control is not a realistic goal. Whenever birds and aircraft are in the air the possibility of a bird strike does exist. Recommendations, then, are designed to help reduce the probability of these bird strikes. Control measures provide both short and long term methods of reducing bird hazards. Short-term, immediate response techniques include changing flight operations to avoid high bird concentrations, keeping a watchful eye by airfield personnel for bird activity, and scaring birds from the airfields. Long-term solutions involve habitat management to make airfields less attractive to birds. No single solution appears suitable, but using a combination of methods can significantly reduce bird aircraft strike hazard.

DISCUSSION

OPERATIONAL MODIFICATIONS

Most bird strikes occur at altitudes below 3,000 feet above ground level (AGL). Airdrome environments and low level training routes are subject to the greatest hazard. In most cases, controlling birds in situations away from the airfield is impossible. A knowledge of avian biology can be applied to make operational changes and thus reduce the probability of bird strikes.

Bird activity is greatest during the migration periods each year and during the hours nearest sunrise and sunset each day. The local US Fish and Wildlife Service has current information concerning periods of heaviest migration and areas of high bird densities. This information is valuable to airfield personnel for

designing flight operations. Because a large portion of migration takes place at night, minimumizing night sorties during peak migration reduces the probability of bird strikes. Similarly, because birds are most active during early morning and early evening, a reduction of flights during these portions of the day will help reduce bird strikes.

Airdromes, because of takeoffs, landings, and closed patterns, are the main areas of concern in bird control. Operational changes are sometimes necessary to reduce bird strikes. Takeoffs, because of greater aircraft gross weight and higher power settings needed for climbout, are particularly susceptible to bird strikes. Maximum climbs to 3,000 feet AGL rapidly move aircraft from altitudes where bird strikes are most likely to occur. Landings, though not as critical as takeoffs, still represent significant bird strike problems. As with takeoffs, the more time spent by landing aircraft below 3,000 feet, the higher the risk of a bird strike. In many cases, planes are brought down to glide slope intercept altitudes long before descent for landing. By maintaining aircraft at higher altitudes until descent is necessary for a safe landing, time spent below 3,000 feet is reduced and the hazard lessened. Knowledge of local bird activity is considered for airdrome flight activities. For example, the BASH Team recommended that Dover AFB reduce multiple approaches during periods of high bird activity (reference 3).

In all operational midifications, a good communications system is important to bird strike reduction. Tower personnel need to constantly be aware of bird activity and relay this information to aircrews. If gulls are congregating at the approach end of one runway, aircrews must be alerted so that changes to alternate runways can be considered. If aircrews see birds in the area, tower personnel should be advised so that this information can be passed on to other aircrews. Time is critical in these situations, and communications need to be clear and to the point. The BASH Team often recommends a BIRDWATCH for birds be established similar to a MET watch for weather (reference 4). Bird densities can be relayed to aircrews in increments (ex. BIRDWATCH GREEN, BIRDWATCH YELLOW, or BIRDWATCH RED).

ACTIVE CONTROL

Hazardous birds on airfields must be removed to assure a safe airdrome. For short-term solutions, scaring techniques provide answers for immediate problems. Bird dispersal teams can be equipped and trained to scare birds away from airfields. A uniquely marked/colored vehicle for the team aids in bird dispersal. Birds learn to associate the dispersal team with danger and often leave before scaring activities are necessary (reference 5). Rapid response is the key to bird dispersal team success. If the team cannot respond on short notice (within 5 minutes), team effectiveness is reduced and aircraft are subjected

to either unnecessary and costly delays or increased bird strike potentials. The following equipment has been authorized for active control of airfield bird hazards:

-Binoculars
-Shotgun, single shot
-Pistol, pyrotechnic, M-1
-Simulated airburst, M-74
-Shotgun shells, 12 ga #4 or #6 shot
-Cassette tape player
-Speaker, mobile

Effectively scaring birds requires a combination of techniques to remove birds from the airfield. The M-74 simulated airburst, fired from an M-1 pyrotechnic pistol, sends a projectile about 100 yards before it explodes with a sharp noise (figure 1). Cassette recordings of distress calls made by birds under stress warn birds of danger. These calls are species specific; those emitted by Herring Gulls may not affect Ring-billed Gulls. To use these distress tapes personnel must recognize the various types of birds they wish to disperse. As tapes are played, gulls usually lift off the ground and move closer to investigate the "distressed bird". At this point, a pyrotechnic device (airburst) is fired to hasten dispersal. The bird dispersal team should avoid habituating the birds to scaring techniques. Distress recordings allowed to play too long or airburst fired to often soon teach birds that the danger is not real. To help avoid habituation and reinforce the danger, killing several birds is occasionally necessary.

When scaring techniques are not effective, live trapping and relocation may be used to remove birds from the airfield. Raptors (birds of prey) are often removed in this manner. Agents of the US Fish and Wildlife Service usually have more experience in trapping and relocation than base personnel. They are responsible for protection of raptors (and all protected birds), and their assistance and approval must be sought prior to trapping.

Large concentrations of blackbirds and crows often roost near airfields. Birds entering or leaving the roost area in large flocks create bird strike hazards. Roosts need to be relocated to provide a safe airdrome. When roosts are located on base, personnel use pyrotechnics to scare birds as they attempt to enter the roost. With concentrated efforts over several days, the birds will usually move their roost. It may be necessary to relocate roosts several times until birds pick an area that is not hazardous.



Figure 1. Use of the M-1 pyrotechnic pistol

HABITAT MANAGEMENT

Airfields and their surrounding lands are natural attractants for many birds. Bird reduction on airfields is most effectively accomplished by managing the habitat to make it unattractive for birds. Because long periods are required to realize management effects, initial justification is sometimes difficult. The species of bird causing the bird strike hazard needs to be considered when managing airfield habitat. For example, habitat attractive to gulls and waterfowl (figures 2 and 3) may discourage raptors, or even more specifically, habitat attractive to Red-tailed Hawks may discourage Marsh Hawks.

One of the most frequently used recommendations of the BASH Team deals with grass heights. Short grass and flat surfaces on airfields provide areas for gulls to rest safely with a full field of vision. The short grass also exposes invertebrates which provide a ready food source. Long grass is an effective deterrent for gulls, the group of birds most commonly involved in bird strikes (reference 1). Longer grass heights make invertebrates more difficult for the birds to find and give gulls a poorer field of vision which makes them less likely to rest on the airfield. Optimum grass height is 7-12 inches. This height is tall enough to discourage gulls and yet short enough to keep rodent populations (which attract raptors) down. Grass should be cut short once each year to aid in insect and rodent control, and then grown to the desired height. These longer grass heights not only discourage airfield use by gulls, but also result in better airfield turf and reduced mowing costs.

Sanitary landfills provide excellent food sources for a variety of birds, particularly gulls, blackbirds, Starlings and crows. Landfill locations determine to a large extent the severity of the hazard. If airfields are situated between the landfill and the birds' roosting areas, birds must cross the airfield to feed, thereby creating a hazard. Landfills located close to airfields encourage large bird concentrations in the area. Relocation of sanitary landfills provides the solution for this bird strike hazard. The FAA has recognized this problem, and Order 5200.5 recommends no sanitary landfills within 10,000 feet on an active runway used by jet aircraft. Proper management of landfills will also help reduce the hazard. Completely covering all refuse quickly, and operating the dump as much as possible at night, reduce available food and make the area less attractive to birds. Litter on the airfield itself also attracts birds as they associate garbage with food. Keeping airfields free of litter reduces bird attractants.

Water is another important bird attractant. Eliminating depressions by filling and reseeding reduces standing water on airfields. Wires placed in a zig-zag fashion just above the water line or drainage ditches discourage birds from using these areas (reference 6). Making drainage ditches deep and narrow discourages use

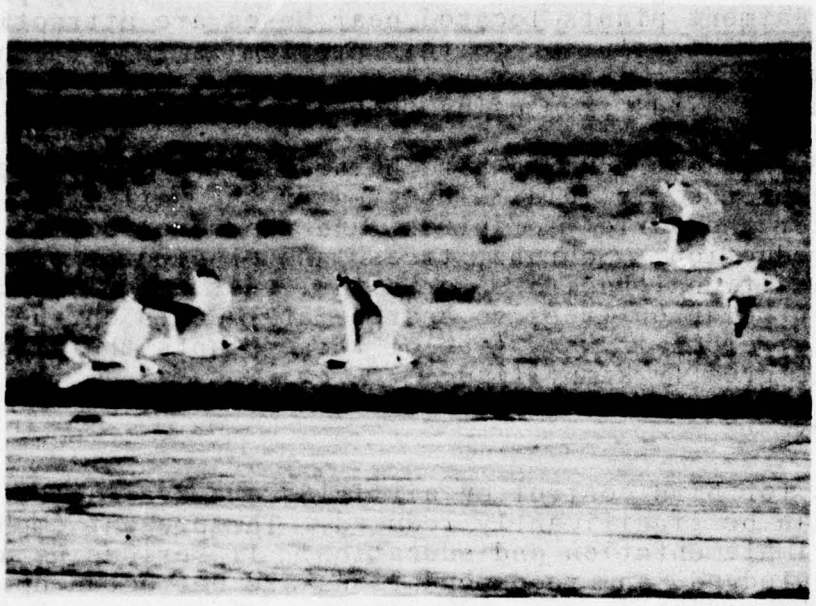


Figure 2. Gulls crossing the airfield at Minot AFB



Figure 3. Ducks loafing on the airfield as a C-5 lands at Dover AFB

by wading birds. Also, removing brush and tall weeds from ditches elinimates nesting habitats for many birds. Holding ponds for sewage treatment plants located near bases are attractive for birds. The best solution to this problem is relocation of sewage ponds. Where this is not feasible, active control is necessary to discourage birds from using these areas.

Another method of reducing bird hazards is to eliminate plant diversity on the airfield. The greater the variety of habitats, the greater the variety of birds, and the more complex the problem of bird reduction. Schrubs, trees, and ornamental plants all provide additional habitats for birds. For example, hawks and owls often perch on trees to search for rodents on the ground. When the airdrome is kept free of these plants the bird reduction problem is greatly simplified.

CONCLUSION

The tools for bird control on airfields are available, and bird strikes can be significantly reduced. The present emphasis involves implementation and education. If serious hazards are not acknowledged, and recommendations are not acted upon, the bird strike reduction program will be ineffective. Programs are underway to make bird control information more available. A handbook describing various bird hazard problems and their solutions is presently being written. Bird hazard risk maps, designed to warn aircrews of areas with high bird densities, are being prepared. Research includes design of gull distress models to scare gulls from airfields, and radar detection and warning of birds. These programs, in addition to BASH surveys of individual bases, help provide a safer flying environment.

REFERENCES

1. Blokpoel, Hans, Bird Hazards to Aircraft, Canadian Wildlife Service, Ottawa, 1975.

2. McCracken, P. R., Bird Strikes and the Air Force, Proceedings of the Seventh Bird Control Seminar, Bowling Green State University, 1976.

3. Clark, Larry T., Lavey, J. M., and Kent, J. S., An Evaluation of the Bird/Aircraft Strike Hazard, Dover Air Force Base, Delaware, unpublished.

4. Harrison, Michael J., and Godsey, E. R., Bird/Aircraft Strike Hazard Survey, Langley Air Force Base, Virginia, Air Force Civil Engineering Center TM-76-4, June 1976.

5. Horsfield, D. J., Owner, Longwings Ltd, London, personal communications.

6. International Civil Aviation Organization, Airport Services Manual, Part 3, Bird Control and Reduction, DOC 9137, AN/898, Part 3, 1975

AN ANALYTICAL METHODOLOGY FOR DEFINING THE BIRD STRIKE REQUIREMENTS FOR AIRCRAFT CREW ENCLOSURES

J. C. Halpin and J. Griffin
Aeronautical Systems Division
Wright-Patterson Air Force Base, Ohio

This paper was not available for printing in this proceedings.

PRECEDING PAGE BLANK-NOT FILMED

DESIGN FOR BIRD IMPACT: A STRUCTURAL SYSTEMS PROBLEM

F. L. Pretzer and R. L. Peterson
Air Force Flight Dynamics Laboratory
Wright-Patterson Air Force Base, Ohio

and

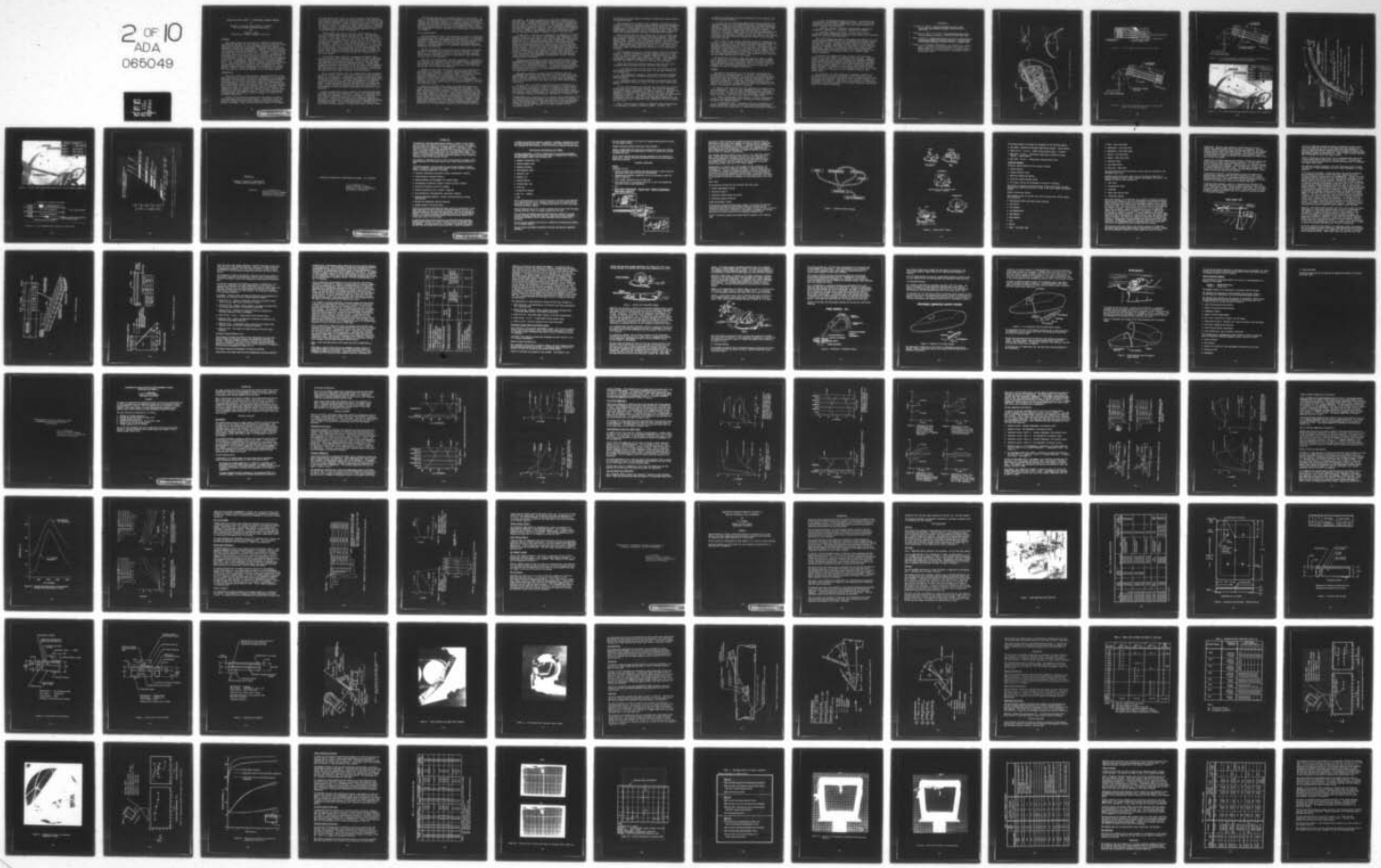
B. S. West
University of Dayton
Research Institute
Dayton, Ohio

PRECEDING PAGE BLANK-NOT FILMED

AD-A065 049 AIR FORCE FLIGHT DYNAMICS LAB WRIGHT-PATTERSON AFB OHIO F/G 1/3
CONFERENCE ON AEROSPACE TRANSPARENT MATERIALS AND ENCLOSURES (1--ETC(U)
DEC 78 R E WITTMAN

UNCLASSIFIED AFFDL-TR-78-168 NL

2 OF 10
ADA
065049



DESIGN FOR BIRD IMPACT: A STRUCTURAL SYSTEMS PROBLEM

by

Forrest L. Pretzer and Richard L. Peterson
Air Force Flight Dynamics Laboratory

and

Blaine S. West
University of Dayton Research Institute

ABSTRACT

This paper points out the need for increased attention by the aircraft designer to the structural design of crew enclosures. Existing low priority for crew enclosure structural design apparently evolved when aerodynamic considerations loomed large relative to structural requirements. However, examples are cited to illustrate that recent emphasis on the design for bird impact resistance has altered this situation. Emphasis is placed on the fact that design for bird impact is a structural systems problem. Development of a bird impact resistant crew enclosure for the F-111 aircraft is used to graphically illustrate the shortcomings of pursuing the design of each component in the system independently (i.e., transparency, support structure, fastener system, etc.). The gains achieved through a systems design approach with no significant change in weight or cost are impressive. The systems design principles suggested are fundamental to aircraft design. However, recent developments are cited which indicate that they are not yet being applied to crew enclosure design.

INTRODUCTION

Since the advent of high altitude, high speed flight it has been necessary to provide aircraft crew members with a protective enclosure. Historically, functional requirements and aerodynamic considerations have been the primary factors influencing crew enclosure design. Good visibility, reliability, maintainability, and a comfortable working environment have received top priority. Structural design loads have generally been the internal pressure-temperature loads for maintaining the working environment, the external aerodynamic pressure and thermal loading, and the loads associated with crew-member ejection. Thus, structural design considerations have generally been relegated to a position of secondary importance.

Studies of the hazards presented by bird impact on transparencies date back to the early 1940's. Since that time, the potential damage resulting from bird/aircraft collisions has greatly increased. This is principally the result of increased

PRECEDING PAGE BLANK-NOT FILMED

aircraft speeds that result in both increased energy densities and impulsive forces during the impact process. The problem has been further aggravated by the introduction of low altitude, high speed mission profiles. These flight profiles place the aircraft in areas of high bird density at speeds approaching or exceeding the speed of sound. Birdstrikes under these conditions increase the probability of serious aircraft damage which may result in an aborted mission or loss of aircraft.

Severe damage and loss of life has, unfortunately, not been an uncommon experience since the 1960's. Two commercial accidents in the early 1960's resulted in the combined loss of 79 lives. Since 1966, the U. S. Air Force has lost more than 10 aircraft worth in excess of $61 million due to bird impacts on transparent enclosures. These include the loss of a T-37B with one fatality, three T-38's with two fatalities, two F-100's with one fatality, and six F-111's with two fatalities. In addition to the $61 million loss in aircraft, and the incalculable loss due to fatalities, an estimated $20 million has been spent in repair costs during the period 1966 through 1972. Further, the role of bird impacts in aircraft losses in Southeast Asia is not fully known.

It has been found, from past incidents and impact tests, that the engines and transparent enclosures are two of the most vulnerable portions of the airplane. The Air Force recognizes the importance of protecting its pilots and at the same time reducing the cost of lost and damaged aircraft. The improved windshield ADPO was established in the Air Force Flight Dynamics Laboratory in 1972. The objective of this office is to promote the development and application of the methodology required for the design of bird impact resistant crew enclosures.

Early studies revealed that the technological base developed during the 1940's, 1950's, and early 1960's for bird resistant design is not adequate. Subsequently, numerous efforts have been undertaken to develop the required technology and to demonstrate it through application. Increased understanding and improved technical tools have emerged, and are emerging in a number of areas. Materials application and manufacturing technology made great strides forward as evidenced by some very significant improvements in the bird impact resistance of operational fleet aircraft.

Other, perhaps more subtle, lessons have resulted from this increased activity and involvement. One is the increased awareness that the response of the crew enclosure to birdstrike is a very complex event which does not lend itself to intuitive solutions. A second is the fact that a piecemeal approach to designing for bird impact resistance does not necessarily produce the desired result. It is this second point, the need for a structural systems approach, to which this paper directs itself.

The systems approach to structural design is not unique. In fact, it is applied routinely to the design of aircraft structure. However, for whatever reasons (i.e., lack of design requirement, consideration of crew enclosure as secondary structure, or lack of emphasis on birdstrike protection), this approach has not been, and is not being applied, to the crew enclosure in many instances. The advantages of such an approach are illustrated in the following example.

F-111 CASE HISTORY

The development of the F-111 birdstrike resistant transparency illustrates the point being made quite dramatically. It has been selected because its developmental history portrays the increased knowledge, understanding, and insight that has been gained. Further, it demonstrates how this learning experience has been applied to the development of a successful structural system for defeating a birdstrike.

Design shortcomings are pointed out for educational purposes and are not intended as criticism of anyone involved. To the contrary, the improvements made in every step of this developmental process represent noteworthy achievements and all those involved are to be commended.

The F-111 is a high speed, low level penetrator. The production aircraft was equipped with glass windshields and canopies in an ejectable crew module as shown in Figure 1. The threshold of failure for this system was a four pound bird at 136 knots and was limited by the glass transparency.

Because of its usage the aircraft proved to be particularly vulnerable to birdstrike. To reduce this vulnerability the Air Force Flight Dynamics Laboratory (AFFDL) initiated a program with PPG Industries, Inc. to develop, test, and evaluate laminated transparency configurations for the F-111[1]. The objective of this effort was to develop F-111 transparencies capable of resisting, without penetration or catastrophic failure, the impact of a four pound bird up to a speed of Mach 1.2 but not less than 500 knots.

Under this program, Bird Impact Resistant Transparencies (BIRT) were developed for the windshield and the canopy. Full scale testing of flight hardware to establish capability of the BIRT transparencies was initiated at Arnold Engineering Development Center (AEDC) in late 1972. These tests indicated that the F-111 BIRT laminated windshield transparencies could withstand center impact of a four pound bird at velocities as high as 780 knots without penetration into the crew module. However, these tests also revealed that bird impact along the aft edge of the windshield resulted in failure of the windshield arch support structure and in catastrophic penetration by the bird into the

crew module. The impact capability of the BIRT windshield and original arch to upper imboard corner impact of a four pound bird was 330 knots. The BIRT cross-section and the edge configuration at this location is shown in Figure 2. The general location of this failure is shown in Figure 3. Thus, laminated transparencies had been developed which exhibited very good potential for defeating a bird. However, the weakest link in the structural system had now become the windshield support flange on the aft arch.

In June 1973, a contract was awarded to the McDonnell Aircraft Company (MCAIR) for the design, development, and fabrication of a structural modification which, with the new BIRT windshield, would improve the F-111 crew module bird impact resistance. The design objective was to provide a structure that could withstand the impact of a four pound bird at a velocity of 793 knots without incurring structural damage that would prevent the aircraft from return to base. Initial full scale bird impact tests conducted on crew modules having a partially reinforced arch* indicated that impact resistance of a four pound bird at 500 knots had been attained. This effort was completed in March 1974 and the use of a full length arch reinforcement for achieving the desired bird impact resistance was recommended by McDonnell Aircraft Company and approved by the AFFDL[2].

Subsequent qualification testing of crew modules having the recommended full length MCAIR arch reinforcement resulted in shear failure of the BIRT windshield when impact occurred in the upper inboard corner (reference Figure 4). A four pound bird produced failure at a velocity of 355 knots. The overall capability of the BIRT transparency and the full length MCAIR arch reinforcement is summarized in Figure 5.

Subsequent analysis of these results indicated that the recommended arch support structure was too stiff relative to the BIRT windshield transparency, and that a more in-depth analytical effort would be required if the desired bird impact resistance were to be achieved within the limits of the F-111 system design constraints.

In April 1975, the AFFDL contracted with the University of Dayton Research Institute to conduct a program to further improve the bird impact resistance of the F-111 windshield system in the arch region. This program[3] involved a review of previous design and testing efforts, development of a design modification supported by structural analysis calculations, fabrication of hardware, and

* These tests were conducted with an interim arch reinforcement configuration which did not extend over the full length of the arch. This reinforcement had the same cross-section as the proposed full length arch reinforcement. However, each part was approximately 13 inches long and was located in the upper inboard corner (reference Figure 4).

verification of bird impact resistance through full-scale testing of flight hardware.

The objective of the effort was to design a structural modification to the F-111 windshield arch support structure (reference Figure 1) to provide impact resistance at any point on the BIRT windshield to a four pound bird at a velocity of 500 knots. More specifically, the objective was to upgrade the impact resistance along the windshield-arch interface as indicated on Figure 5.

Previous test results were studied and it was concluded that the F-111 crew module is a complex structural system. The arch was secondary structure with respect to resisting the original design loads. However, this arch becomes primary structure for resisting the forces resulting from bird impact. The arch, center beam, canopy beam, and transparencies act as a structural unit. Thus, load path analysis for bird impact at a given point on the structure cannot be determined by intuition or by a simplified analysis.

This dictated the use of a finite element structural analysis program. Schedule considerations and program state of the art ruled out the performance of a dynamic response analysis. Thus, it was decided to study the response of the F-111 crew module by performing a parametric study with static loads. This information was then used in the design of the arch reinforcement.

Using the structural analysis data as input the arch reinforcement design was based on the following philosophy.

1. The modification would be such that the strength of the arch support flange would be equivalent to the edge strength of the transparency.

2. The necessary increase in arch support flange stiffness would be provided with a minimum increase in local and overall arch stiffness.

3. The modification would be designed to provide equal bird impact resistance along the length of the arch from center beam to sill.

An arch reinforcement was designed and the design was refined through the aid of full scale testing. The arch reinforcement to optimize system performance is shown in Figure 6. The arch was impacted at three locations along the aft arch and a minimum capability to defeat a four pound bird at 423 knots was established (reference Figure 7). Ultimately, failure occurred in the transparency (at 462 knots) but there was much evidence that the individual structural components were compatible and were responding as a unit.

Thus, a significant increase in capability was achieved with a net decrease in support structure weight. Further, the

windshield transparency edge was identified as the weakest link in the structural design.

In 1976, the Air Force contracted with Sierracin/Sylmar for the development of an alternate design BIRT transparency system (ADBIRT)[4]. Emphasis was placed on improving the edge capability and matching the aft arch reinforcement developed by UDRI. The resulting windshield transparency configuration is shown in Figure 8. Full scale impact tests on this system established the capability to defeat a four pound bird at 491 knots in the aft arch area. Furthermore, analysis of the bird impact film coverage indicated that the structural components formed a near optimum structural system.

The results of the studies described above are summarized in Figure 9. This figure illustrates the tremendous improvement that has been achieved through Air Force efforts to develop a bird resistant crew module for the F-111 aircraft. The capability for defeating a four pound bird, at the most critical impact location, has been increased from an estimated 136 knots to greater than 491 knots. This represents an increase in kinetic energy of the bird of approximately 1000 percent. The capability for resisting two and three pound birds is also shown.

Of particular interest is the fact that all gains in capability above the full length MCAIR reinforcement were achieved with a decrease in total structural weight (reference Figure 9). This demonstrates quite graphically that for complex structural response the indiscriminate addition of material does not necessarily lead to increased capability.

SUMMARY

The design and analysis of crew enclosure structures for birdstrike is a complex problem. In general, the problem will be characterized by geometric and material nonlinearities and by coupling of the bird induced load with the structural response. The failure mode may be fracture, excessive deflection, or ballistic perforation. Large energy transfer occurs during the impact event and the response mode and impact resistance will be greatly influenced by the impact location.

A typical crew enclosure will be comprised of several structural components. Each of these components serves a function in the structural unit and each must be designed with that interaction in mind. A typical listing of structural components and their function in the structural system is shown below.

1. Basic Transparency Cross-Section - resists perforation, fracture, and excess deflection; distributes load to support structure and absorbs energy.

2. Transparency Edge - transfers load from transparency to support structure; can be area of high stress concentrations; design detail very important for maintaining structural integrity.

3. Local Transparency Support Structure - interfaces with transparency and transfers transparency edge loads to airframe structure; stiffness and strength can have great influence in system response and capability.

4. Fastener System - transfers load between interfacing components; essential to structural integrity of system.

5. Airframe Support Structure - may be fixed; can be relatively rigid or somewhat flexible; exact nature will influence design of crew enclosure structure.

The F-111 example was used to illustrate that design for bird impact requires consideration of the response of the crew enclosure structural unit. It was shown that large increases in the strength of a single component, without regard to its effect on the total structure, may result in little or no gain in overall capability. Further, it illustrated that with a structural systems approach, significant gains can be realized using less than ideal structural analysis tools (i.e., static linear elastic analysis).

In reality the response of many aircraft crew enclosure structures to bird impact is transient and nonlinear. Improved tools in the form of bird loading models and nonlinear dynamic finite element digital computer programs are becoming available which will greatly facilitate future design-analysis exercises. These tools, though essential, will never replace the need for sound engineering judgments, particularly with regard to edge design details. Also, it is to be expected that full scale bird impact tests will continue to be an important step in the design cycle.

In conclusion, the most important ingredient required for successful design of crew enclosures is the recognition that the structural analysis practices applied to other primary flight structures are required. Basically, this involves a change in attitudes and priority. With regard to designing for bird impact resistance, the crew enclosure is a primary structural system and should be treated accordingly.

REFERENCES

1. Littell, H. Edward, Improved Windshield and Canopy Protection Development Program, AFFDL-TR-74-75, June 1974.

2. Lewis, A. L. and K. W. Cooke, F-111 Bird-Resistant Windshield Support Structure, AFFDL-TR-74-40, May 1974.

3. West, Blaine S., Design and Testing of F-111 Bird Resistant Windshield/Support Structure, Volume I - Design and Verification Testing, AFFDL-TR-76-101, October 1976.

4. Olson, J. B.,"Design, Development, and Testing of a Lightweight Bird-Proof Cockpit Enclosure for the F-111," paper presented at the Conference on Aerospace Transparent Materials and Enclosures, Long Beach, Calif., 24-28 April 1978.

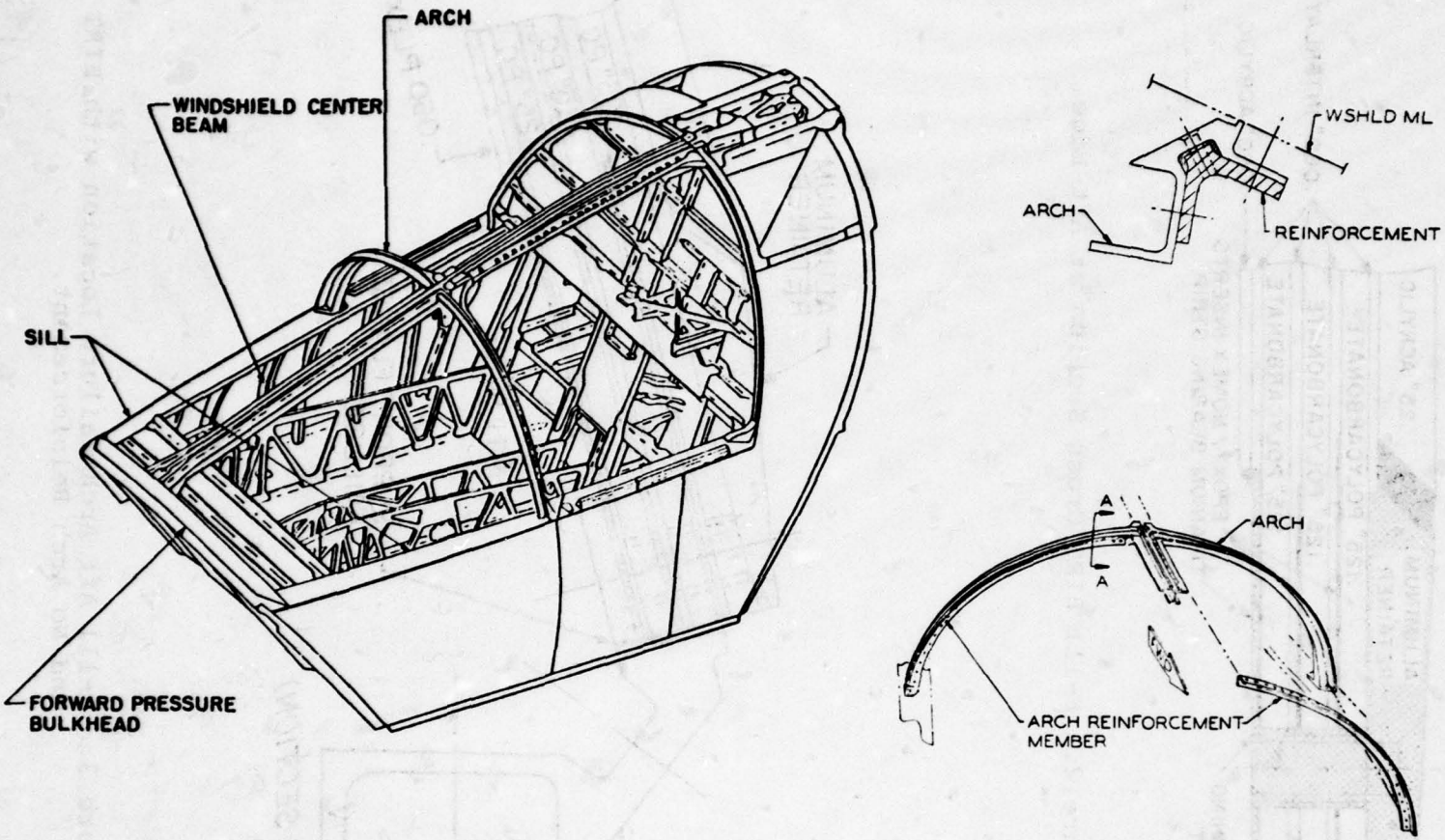


Figure 1. F-111 Crew Module Structure.

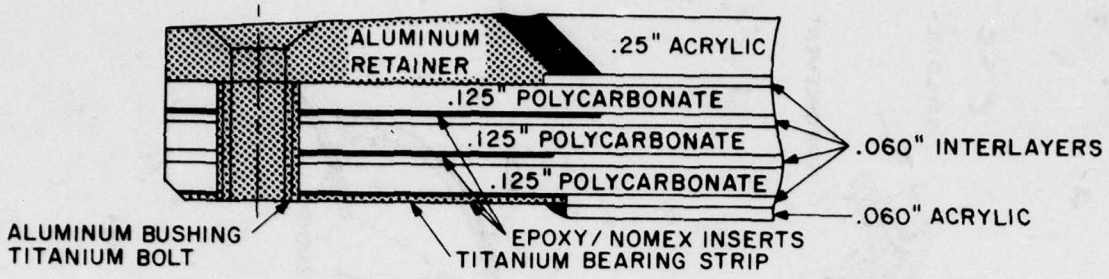


Figure 2. F-111 BIRT Cross Section at Aft Edge.

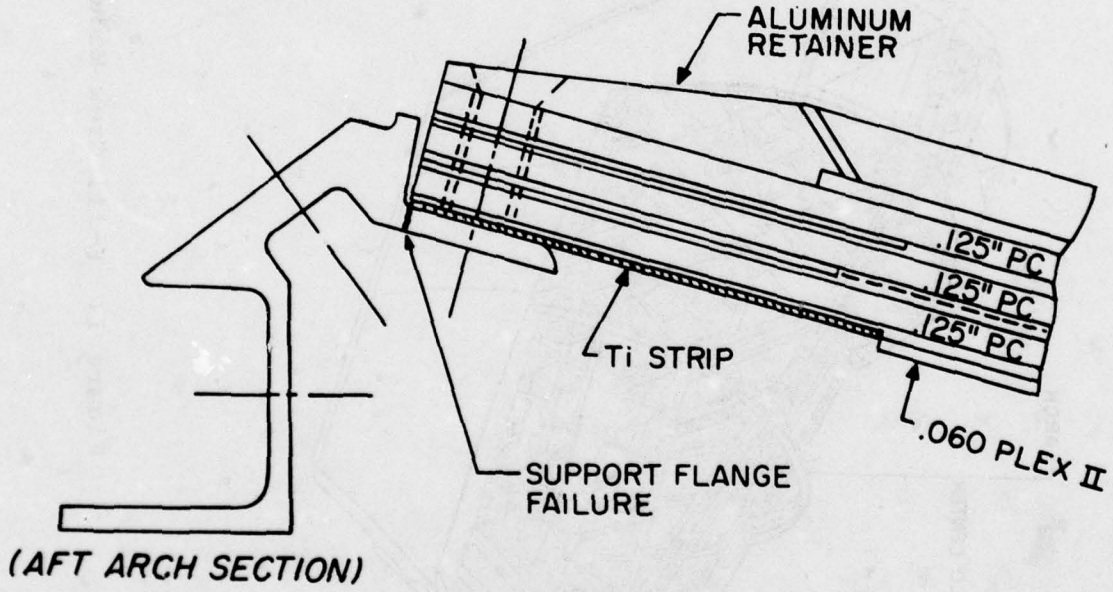


Figure 3. F-111 Aft Arch Failure Location with BIRT and No Arch Reinforcement.

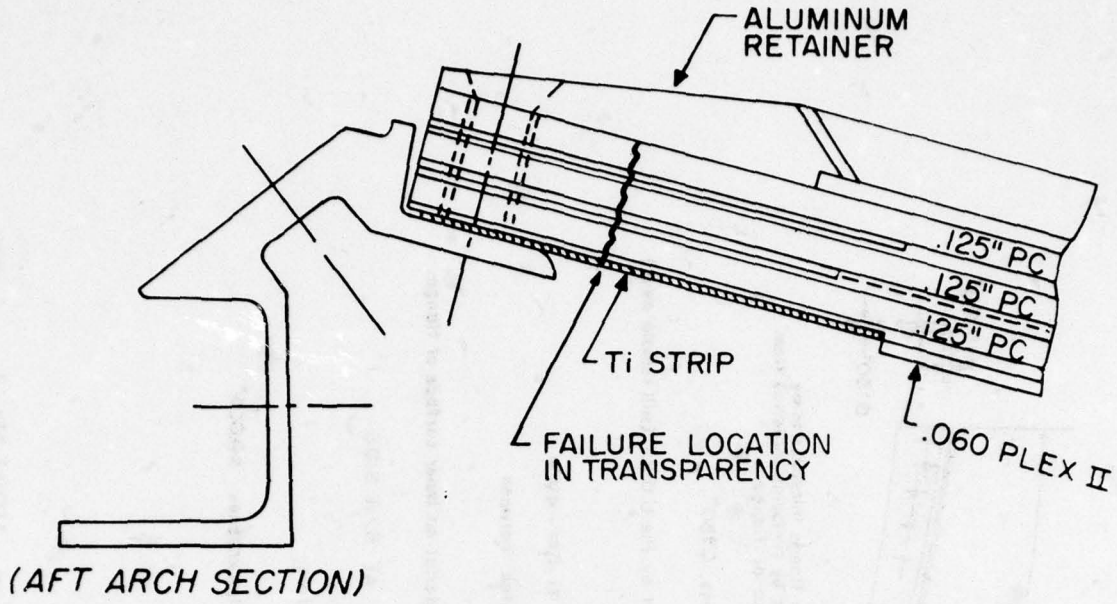


Figure 4. F-111 Transparency Failure Location with BIRT and Full Length MCAIR Arch Reinforcement.

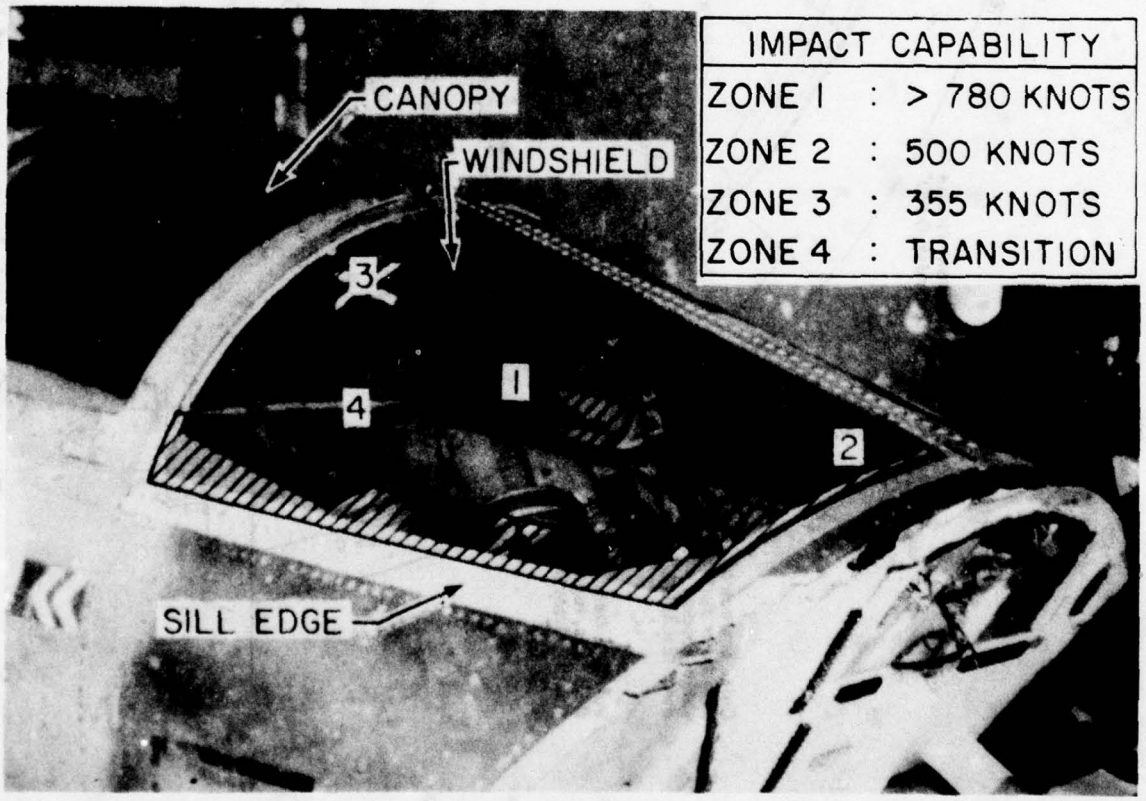


Figure 5. F-111 BIRT Transparency/MCAIR Modified Arch Capability.

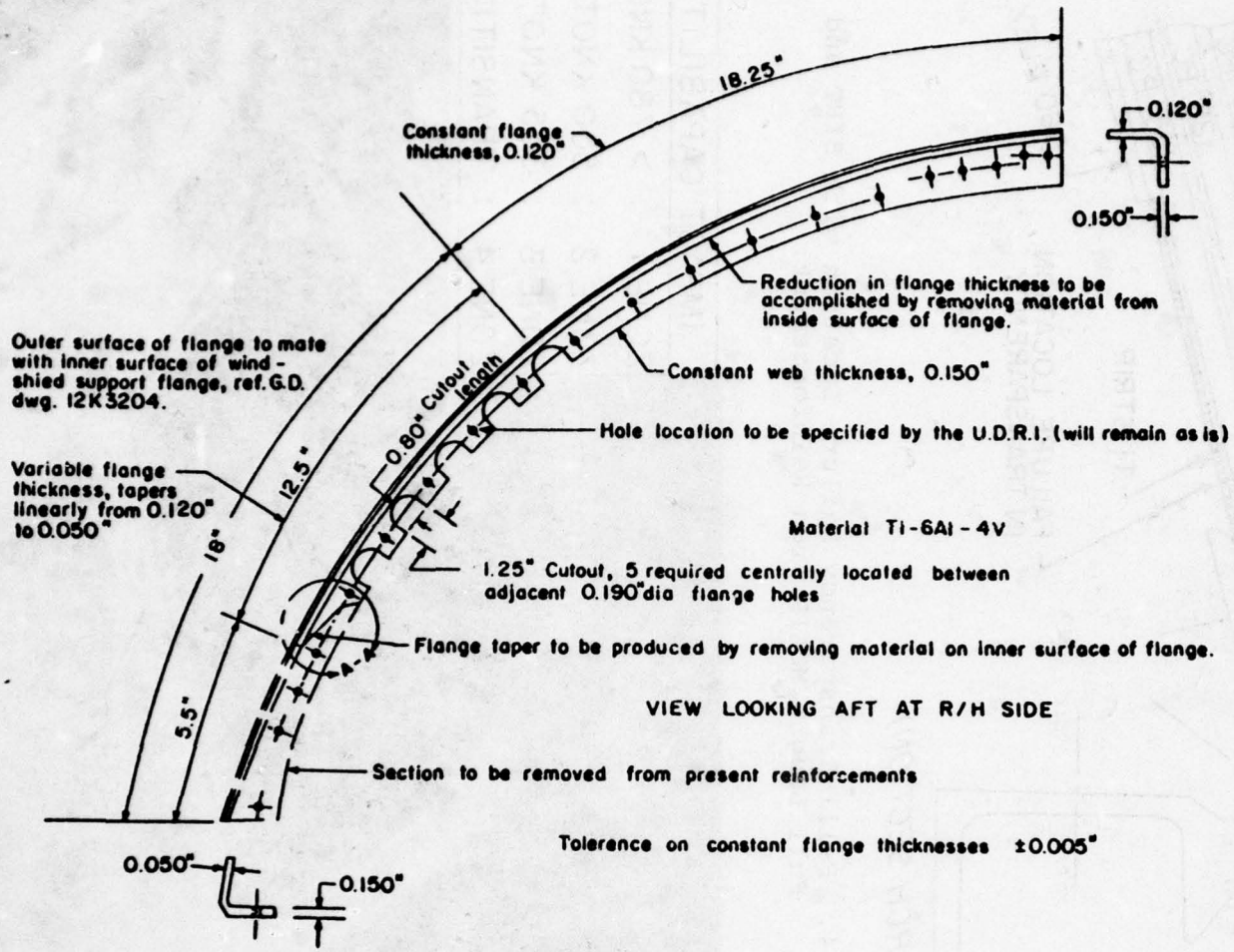


Figure 6. Arch Reinforcement Configuration, UDRI No. 3.

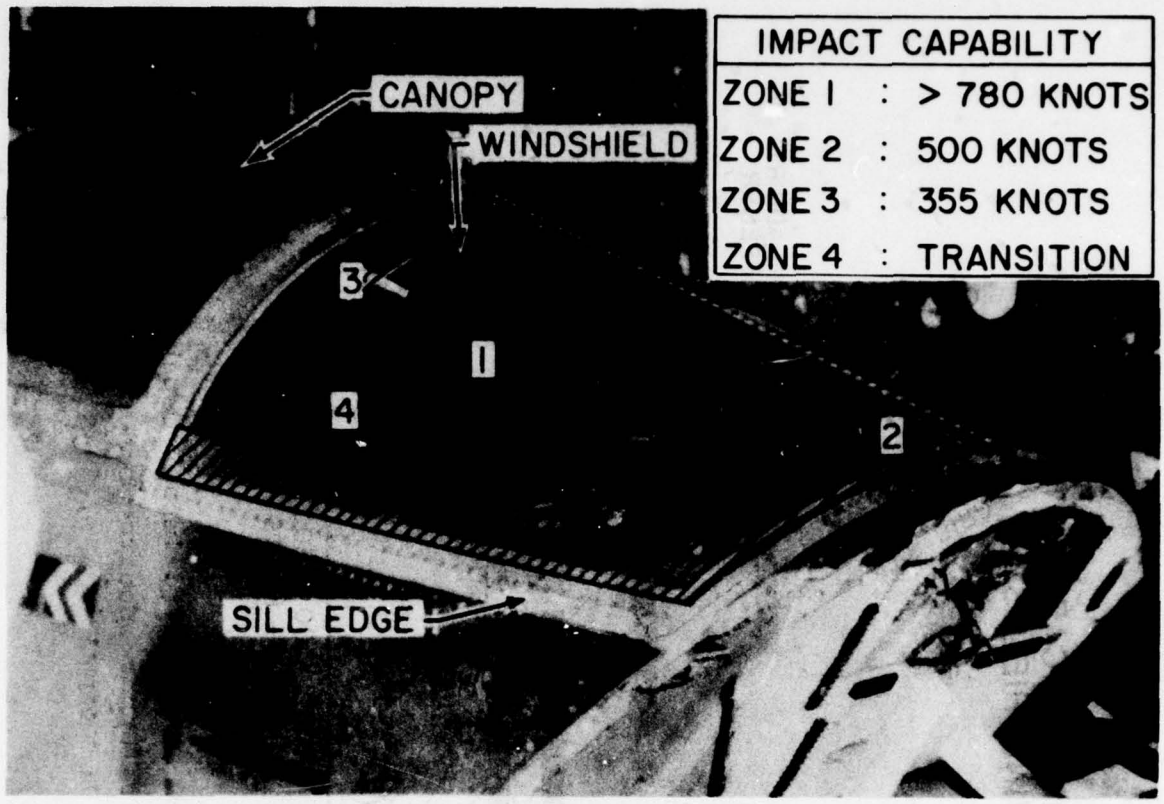


Figure 7. F-111 BIRT Transparency/UDRI Arch Reinforcement Capability.

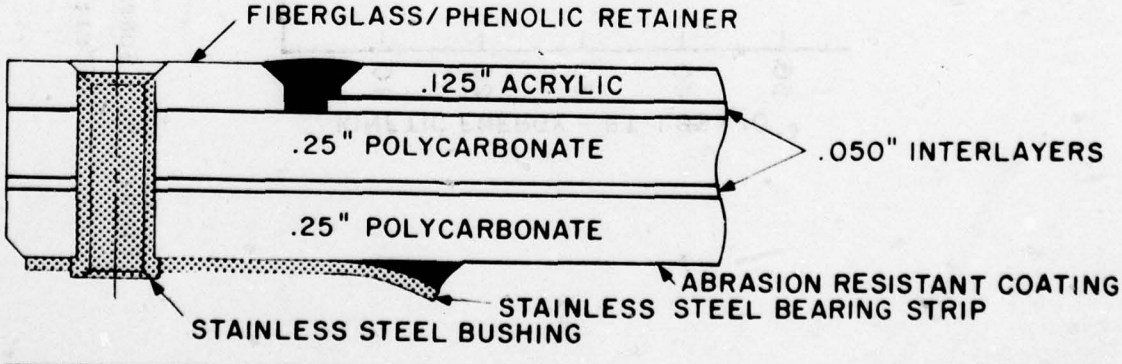


Figure 8. F-111 ADBIRT Cross Section at Aft Arch.

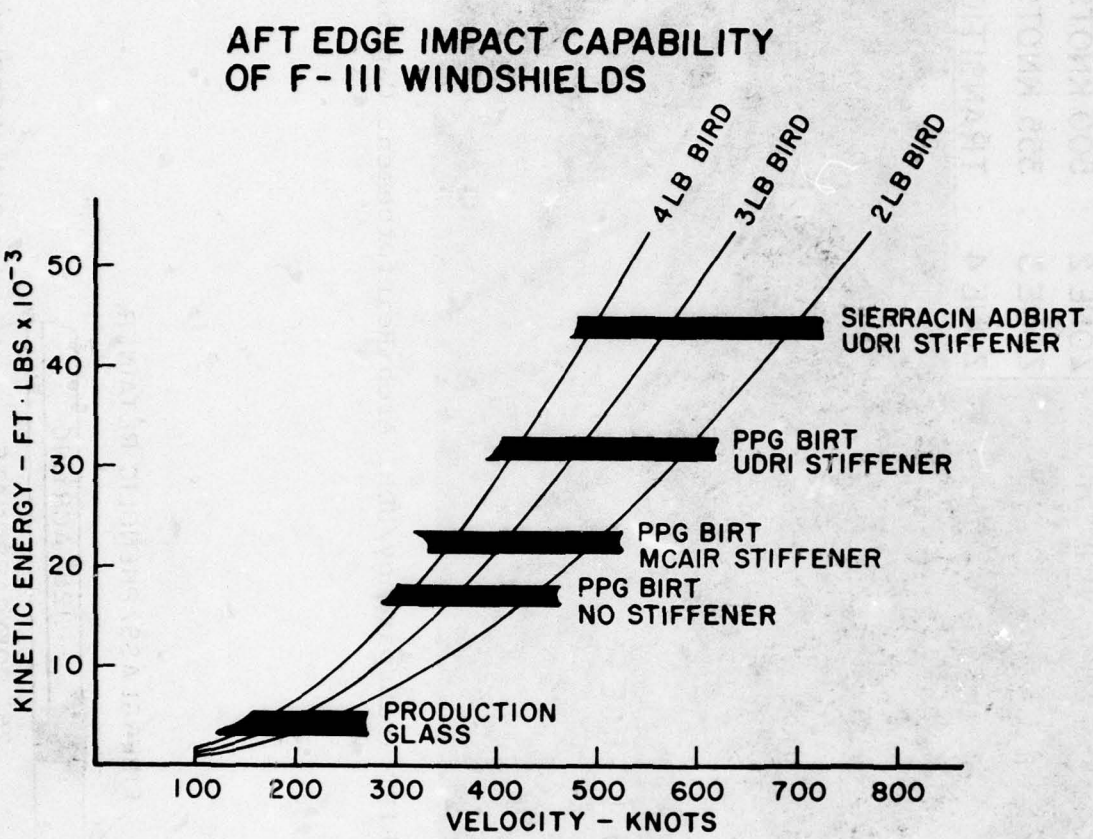


Figure 9. Summary of F-111 Crew Module Bird Impact Capability at Most Critical Impact Point (Upper Inboard Corner).

SESSION II

ADVANCED TECHNOLOGY DEMONSTRATOR PROGRAM STATUS REVIEW (PART I)

Chairman: J. H. Lawrence, Jr.
Douglas Aircraft Company
McDonnell Douglas Corp.
Long Beach, California

WINDSHIELD TECHNOLOGY DEMONSTRATOR PROGRAM - AN OVERVIEW

J. H. Lawrence, Jr.
Douglas Aircraft Company
McDonnell Douglas Corporation
Long Beach, California

PRECEDING PAGE BLANK-NOT FILMED

INTRODUCTION

The Windshield Technology Demonstrator Program is a generic study program directed toward the research and design of transparencies for crew compartment enclosures with emphasis on a systems approach, assessment of materials, laboratory testing of specimens, the development of a bird impact math model, bird impact testing, documentations, and technological applications to two current Air Force aircraft that are in the development stages. In an endeavor to maximize the program goals, the culmination of the efforts will result in the development of a Design Guidelines Handbook in two volumes for subsequent usage by the Aerospace Industry.

This program is sponsored by the Air Force Flight Dynamics Laboratory (FEW), Wright-Patterson Air Force Base, Dayton, Ohio, under contract F33615-75-C-3105.

The Douglas approach to this program has been directed through a project system. Selectively, engineers were chosen from many technical disciplines within the Douglas organization including:

- Structural Engineering (direction, design, documentation, optical)
- Stress Analysis (strength analysis)
- Advanced Methods and Development (bird impact model)
- Environmental Engineering (thermal criteria and heat transfer)
- Electrical Engineering (anti-ice systems)
- Avionics Engineering (RCS, p-static, lightning)
- Test Engineering (instrumentation, tabulation, testing)
- Process Engineering (material, reviews, testing selection, testing applications)
- Reliability Engineering (failure analysis)
- Systems Analysis (life-cycle-cost)

Initially the contract specified that there would be an interim and a final report applicable to each of the two Air Force development aircraft and a three-part report for the Bird Impact Math Model. But, as the program progressed, in an effort to inform the Aerospace Industry of new developments, a total of 24 reports (three-part reports counted as three reports) on a timely basis have or will be issued.

To provide the Douglas Program Director and AFFDL/FEW Project Engineers maximum program visibility, a Master Planning and Control Document (MPCD) was prepared. The major portions of the program were divided into tasks and each task was divided into various work units. Noted in the MPCD is

PRECEDING PAGE BLANK-NOT FILMED

a schedule and budget for manpower, materials, specimens, subcontractor costs, and miscellaneous expenditures. Subsequently, the Program Director and Project Engineer had the latitude to alter the efforts to maximize program goals.

PARTICIPATING SUBCONTRACTORS AND VENDORS

To meet program goals, a series of subcontracts and purchasing agreements were made between Douglas and the participants or between the Air Force and the participants noted in the following list:

- Rockwell International (RI)
- General Dynamics (GD)
- Goodyear Aerospace
- PPG Industries (PPG)
- Sierracin, Inc.
- Swedlow, Inc.
- Texstar Plastics
- Triplex Glass, Ltd.
- Terra Tek
- University of Dayton
- ARO, Inc. - Swedrup
- AEDC

The RI subcontract was an all inclusive contract with Douglas that committed RI to supply microfilm of all drawings relative to the B-1 windshields and supporting structure reports to perform coordination functions, and supply loft data and master plasters.

The GD subcontract was an all inclusive contract with the Air Force to supply drawings relative to the F-16 canopy, reports and loft data.

PPG, Sierracin and Swedlow supplied proprietary data relevant to various studies, performed coordination functions, supplied laboratory specimens, wind tunnel specimens, and bird impact specimens under purchase parts agreements.

The Air Force/RI supplied full-sized B-1 windshields manufactured by Swedlow for bird impact testing.

Texstar Plastics performed coordination functions and supplied laboratory specimens.

The Air Force/GD supplied full-sized F-16 canopies manufactured by Texstar for bird impact testing.

Goodyear Aerospace supplied wind tunnel test specimens.

Douglas subcontracted with Terra Tek to perform high strain rate testing, including preparation and documentation of tensile, compression and shear specimens test data.

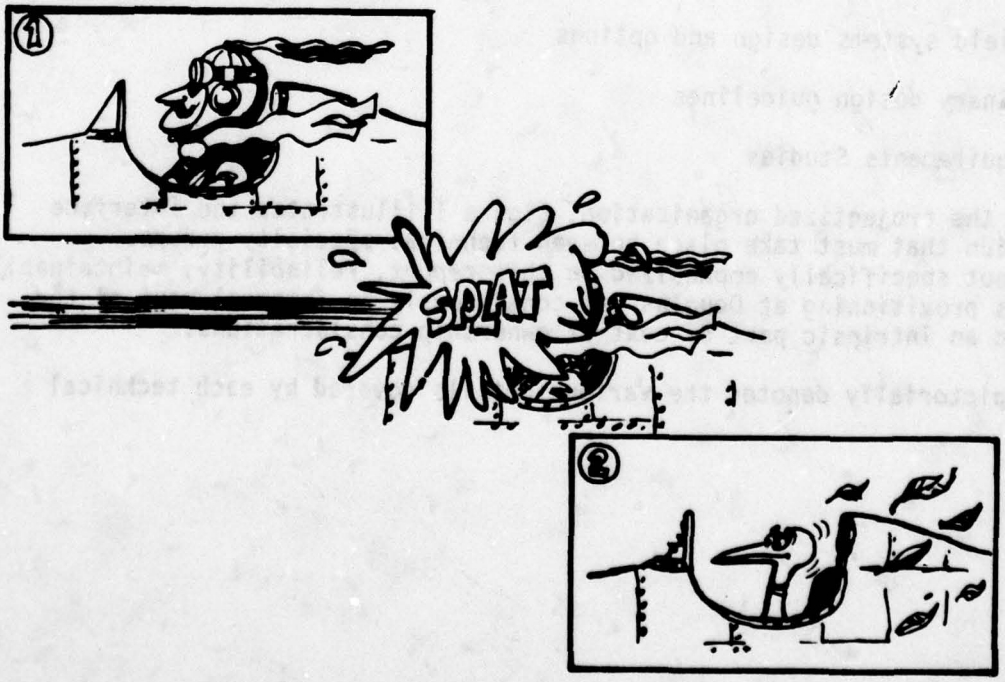
The Air Force supplied data that had been generated by the University of Dayton (UD). UD also performed coordination functions and participated in technical discussions.

TECHNICAL DISCUSSIONS

General

Statements of Fact:

- Cockpit enclosures and canopies have been designed by state-of-the-art approaches rather than by scientific methodologies
- Transparencies materials properties are not as accurate as those for metallic materials
- Total systems approaches have not been used
- Best combinations of transparency materials to meet high temperature conditions have not been determined
- And . . .
- **MILITARY AIRCRAFT "HAVE NOT" BEEN DESIGNED FOR BIRD IMPACT**



Historically, NACA and NASA have expended billions of dollars since 1911 developing aircraft structural concepts, and metallic materials properties that are well documented on MIL HANDBOOK 5. Supplementing MIL HANDBOOK 5 are many excellent textbooks on strength of materials, engineering mechanics, metallurgy and corrosion protection. Currently, vast expenditures are being underwritten for the development of composite materials by NASA and the Air Force for structural applications.

Yet, the most important portion of an aircraft is the flight crew compartment. Within the flight crew work area, not only is it important for efficient arrangement of instruments and ease of systems operations, but the transparency areas must have integral systems that resist all major environmental factors, yet the designs must be lightweight and provide maximum unrestricted visibility in all flight regimes.

Comparatively, in industry very little budget has been expended on the development of materials, materials allowables, or design concepts for transparencies. It must be pointed out, however, that once transparencies are in-service, frequently it becomes necessary to improve the designs for reliability, anti-icing, defogging, and bird impact. Since these improvements are then directed toward a specific aircraft transparency, very little of the analysis and testing is documented for subsequent usage by the industry.

Major Tasks

The program was divided into the following four major tasks:

- Systems requirements studies
- Structural analysis
- Windshield systems design and options
- Preliminary design guidelines

System Requirements Studies

Utilizing the projectized organization, Figure 1 illustrates the interface coordination that must take place between technical specialty groups. Although not specifically emphasized in this report, reliability, maintainability and spares provisioning at Douglas are continuously an integral part of the design and an intrinsic part of cost of ownership considerations.

Figure 2 pictorially denotes the various details covered by each technical area.

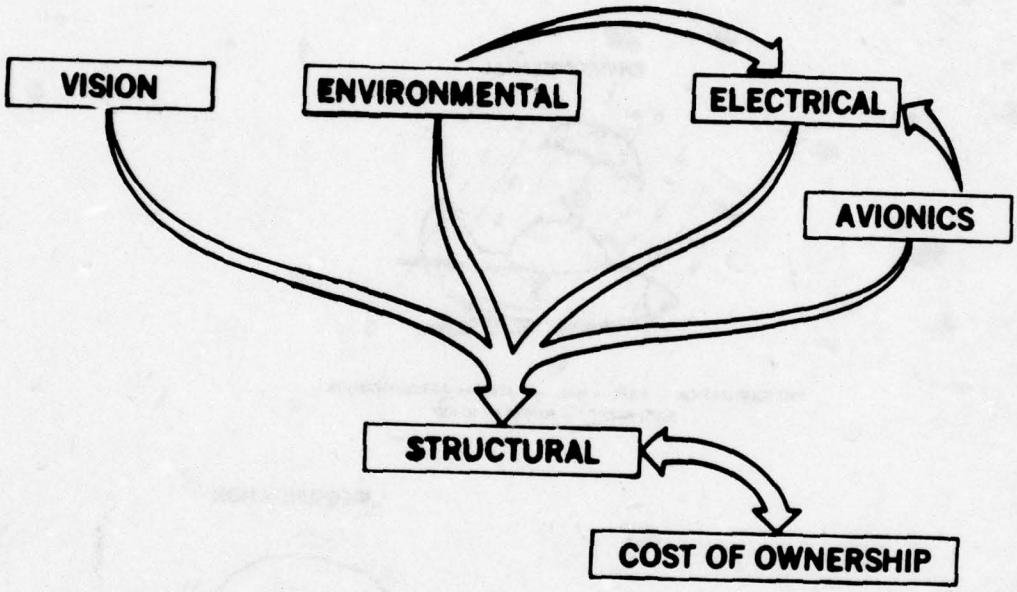


Figure 1. Systems Interface Diagram.

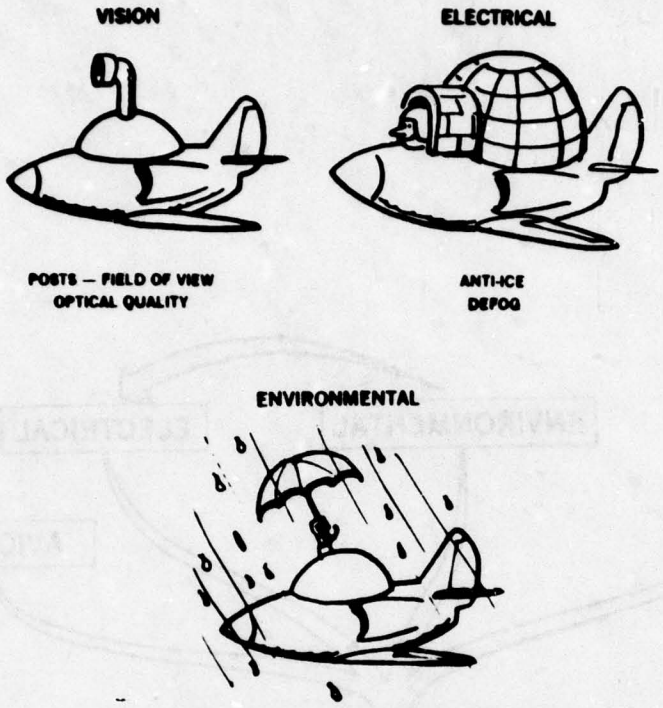


Figure 2. Systems Detail Design.

The various studies for Systems are documented in the following reports:

- MDC J6949: Windshield Technology Demonstrator Program - Interim Report
- AFFDL-TR-77-1: W.T.D.P. - Detail Design Options Study - 3 Volumes
- MDC J7175: W.T.D.P. - Preliminary Investigative Studies of Canopy Designs - Interim Report
- MDC J7176: W.T.D.P. - Canopy Detail Design Options Study

Structural Analysis

Structural design studies for this program included:

- Thermal Analysis
- Internal/External Loads
- Materials Studies and Testing
- Structural Support Optimum Sizing
- Bird Impact Testing and Development of Analytical Techniques

The effects of thermal and internal/external loads on the design of transparencies must interface with and be a part of the total Systems Requirements Studies.

Material Studies and Testing

The following series of specimen tests were conducted under various laboratory conditions:

- Precipitation Static and Swept Stroke Lightning
- Wind Tunnel
- Salt Abrader
- Instrumented Beam
- Beam Damping
- Beam Bending
- Izod
- Optical
- Shear - Low Strain Rate

- Shear - High Strain Rate
- Compression - Low Strain Rate
- Compression - High Strain Rate
- Tension - Low Strain Rate
- Tension - High Strain Rate
- Interlayer Shear
- True Stress/Strain
- Cycle Load - Edge Joint

The justification for performing these various tests are contained in the paragraphs that follow.

Coatings intrinsically play a major role in the choice of materials in design selection to fulfill vastly different requirements for service. The purposes for some of these coatings are:

1. Anti-icing
2. Precipitation Static
3. Lightning
4. Radar Cross Section (RCS)
5. Protective Coatings

Anti-icing coatings, to be effective, must conduct an electrical current to provide the heat needed to keep ice from forming on the windshield surface. These coatings are proprietary to the transparency vendors, such as stannic oxide by PPG Industries, Corning Glass and Libbey-Owens-Ford; gold coatings by Sierracin Corp., and Liberty Mirror; and indium oxides by PPG Industries and Triplex of England. Each coating must be rated at 4-1/2 watts per square inch minimum to prevent ice from forming and must be applied to a surface that is internal to the windshield; consequently, a 200 to 400 volt electrical system is required. To further complicate the design, most windshields must be designed with irregular shapes; thus, the entire surface cannot be coated. This results in trade-offs to position the coatings and bus bars to provide the pilot with maximum visibility during maximum icing conditions. Consequently, elaborate electrical windshield anti-ice systems controllers and transformers must be integrated into a total system that also has to be compatible with the aircraft electrical system.

Precipitation static that forms on the exterior surfaces of windshields and swept-stroke lightning pose problems to windshields in-service. Depending on the selection of materials, either effect can result in failed

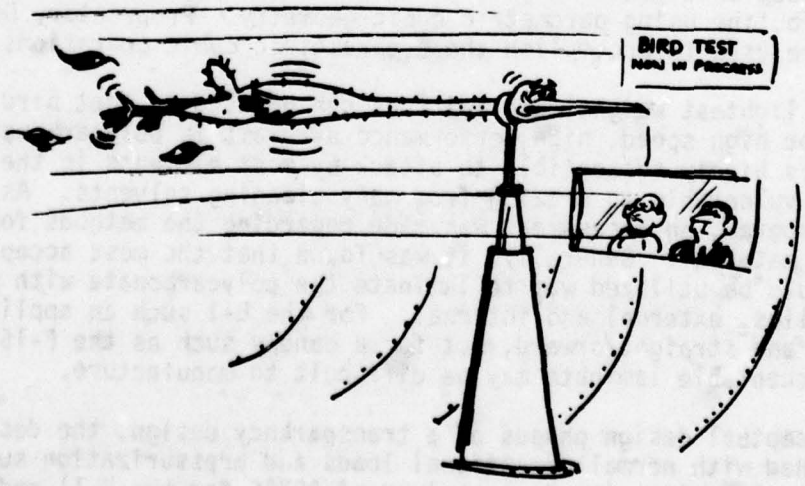
windshields. Some thin glass selected is justification for putting a stannic oxide coating on the exterior surface of a windshield. For this program a series of monolithic coated and non-coated materials were selected and precipitation static tests were conducted. The design and integration of coated exterior surfaces for precipitation static conditions must include grounding the coating to structure and the prevention of current flows into the anti-ice systems.

Another series of coated specimens were designed, purchased and tested under precipitation and swept stroke lightning conditions. For this effort a series of coatings were designed to represent anti-ice or defogging coatings that are embedded within laminates. These specimens had continuous coatings or coatings separated by deletion lines. The parts were purchased from Sierracin and were tested under conditions of precipitation static, thermal effects and simulated swept stroke lightning.

Transparencies installed in high-performance aircraft are subjected to extreme thermal conditions that can cause the materials to fail, create temporary optical distortion or permanently damage the optical quality of the windshield/canopy. The forces of the high speed aerodynamics can cause erosion of the transparency surface and can destroy edge seals.

To evaluate these problems a series of 18 representative windshield and canopy specimens were ordered from four vendors and tested at Mach 1.6 and 2.2 in a wind tunnel at AEDC. Douglas witnessed these tests, collected data, analyzed the data, and documented the results. From the 18 parts, six were selected to perform salt abrader tests in an attempt to simulate the effect of ice crystal impingement.

WIND TUNNEL TEST



A series of beams were designed and tested to determine the damping ratios for various materials for use in a bird impact math model analysis, and a series of laminated beams were designed with strain gages laminated in each beam and tested under static, dynamic and impact conditions to develop strain measurements through the laminated plies. Figure 3 shows a typical laminated beam instrumented for static and impact testing.

Figure 4 illustrates the test results for an instrumented beam relative to a finite element model analysis and a typical analysis. The strain gage installation techniques developed for the beam tests were used for subsequent bird impact tests at AEDC.

The edges were purposely designed so that the installation could be varied from two rows of tight attachments, one row of loose attachments, or simply supported.

At the onset of the program, a survey was made of the various transparency and raw materials suppliers to obtain their data regarding materials, materials allowables, testing data, and recommendations. The most revealing information that was ascertained was that the materials properties of transparency materials was not very accurate. Comparatively, MIL-HDBK-5 for metallic materials has evolved since 1911 with billions of dollars expended in research to develop the guaranteed values noted, while only a few million dollars had been expended developing MIL-HDBK-17, Part II, used by transparency designers. These allowables noted in MIL-HDBK-17 were average values obtained from only a few tests and the data had not been treated statistically to establish acceptable values for designers. It was decided for this program that the specimens selected would be made and tested in sufficient numbers so that they could be statistically analyzed similar to MIL-HDBK-5, Chapter 9. Utilizing this approach, test data collected could be digitized to develop true stress-strain curves through use of a Tektronix 4014-1CRT terminal with a Tektronix 4953 tablet attachment. The software involved in the Douglas digitizing program utilized Fortran IV and Tektronix Plot 10 routine. The Douglas digitizing program connects the digitized points by a curve fitting routine using parametric cubic geometry. Proprietary Douglas subroutines were used to accomplish these parametric cubic operations.

Generally, the lightest weight material that can be used to meet bird impact requirements for high speed, high performance aircraft is polycarbonate. This material is highly susceptible to attack by most elements in the atmosphere and vulnerable to crazing from many cleaning solvents. As a part of this program, an assessment was made regarding the methods for protecting the material. Generally, it was found that the most acceptable method that could be utilized was to laminate the polycarbonate with protective face plies, external and internal. For the B-1 such an application is fairly easy and straightforward, but for a canopy such as the F-16 canopy an optically acceptable laminate may be difficult to manufacture.

During the conceptual design phases of a transparency design, the designer must be concerned with normal operational loads and pressurization subjected to varying thermal regimes (up to a maximum of 307°F for the B-1) and bird impact loading conditions. Under normal loads, the materials would react

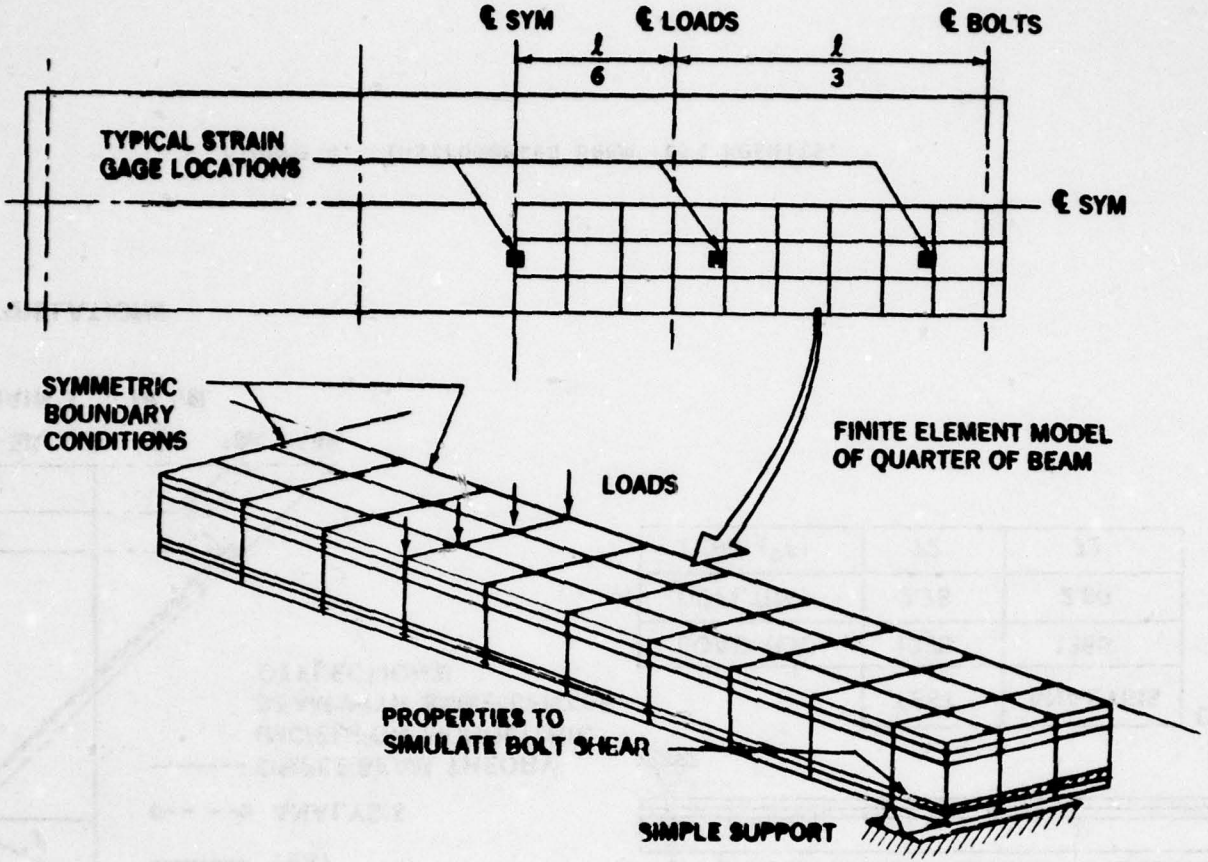
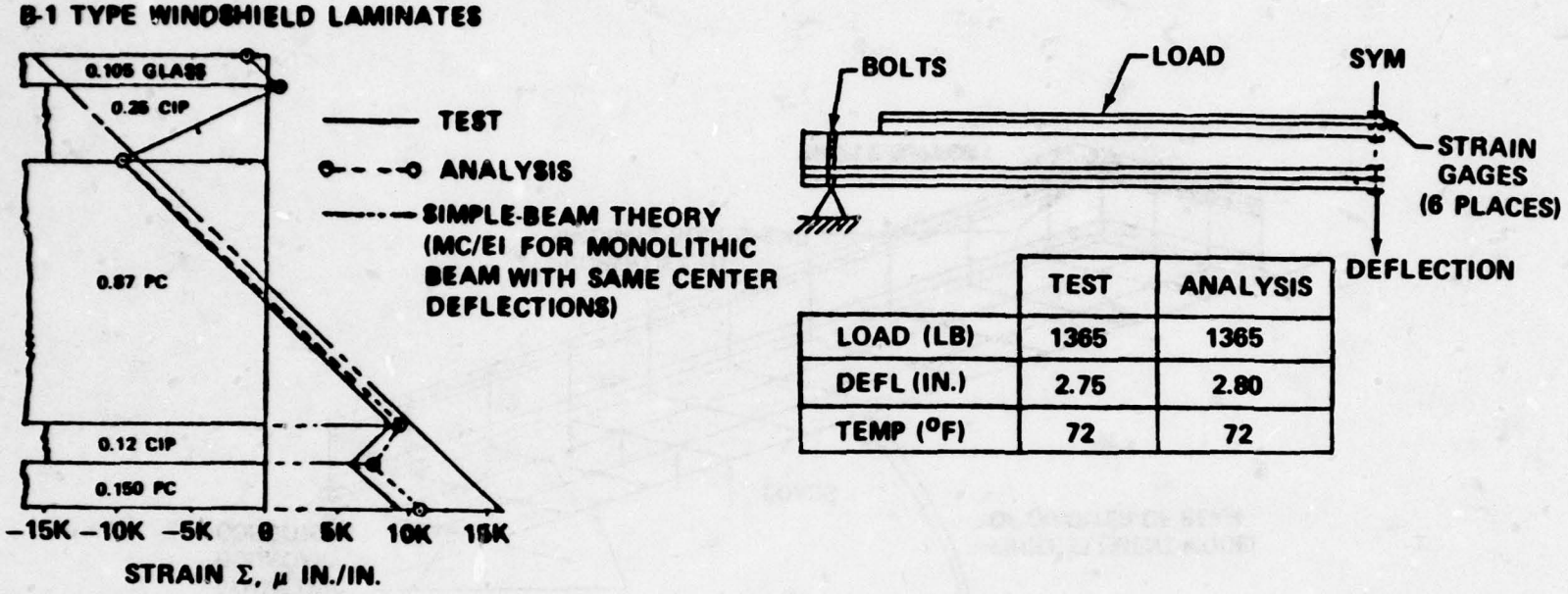


Figure 3. Instrumented Beam.



	TEST	ANALYSIS
LOAD (LB)	1365	1365
DEFL (IN.)	2.75	2.80
TEMP (°F)	72	72

Figure 4. Instrumented Beam Test Results.

under low strain rate loading conditions, and under bird impact would react under high strain rate loading conditions. Both would be greatly affected by temperature conditions. As a part of this program, a series of tests were defined to develop materials properties that could be used by the designer.

In an endeavor to identify the specific items that could have an effect on the material properties of polycarbonate, various types of specimens were obtained from several vendors that represented various phases of manufacturing.

A series of 18 specimens were designed and tested to represent four life cycles under temperatures and loads representative of F-16 conditions. Specimens were cut from F-16 canopies that would represent Texstar monolithic specimens, laminated specimens were obtained from Sierracin and Swedlow with silicone interlayers, and from Sierracin, utilizing their proprietary S-130 interlayer materials.

In summary, a series of tests have been conducted, and the documentation of these tests are contained in the following technical reports:

- AFFDL-TR-76-75: Effects of Laboratory Simulated Precipitation Static Electricity and Swept Stroke Lightning on Aircraft
- AFFDL-TR-76-156: Damping, Static, Dynamic, and Impact Characteristics of Laminated Beams Typical of Windshield Construction
- AFFDL-TR-77-92: Evaluation of Windshield Materials Subjected to Simulated Supersonic Flight Environments
- AFFDL-TR-TBD: W.T.D.P. - Canopy Detail Design Options Study
- AFFDL-TR-77-96: Testing for Mechanical Properties of Monolithic and Laminated Polycarbonate Materials
- AFFDL-TR-77-141: Precipitation Static Electricity and Swept-Stroke Lightning Effects on Aircraft Transparency Coatings
- AFFDL-TR-77-98: High Speed Bird Impact Testing of Aircraft Transparencies

Structural Support Optimum Sizing

The University of Dayton and AFFDL/FEW have demonstrated that the interactions between the structural supports and transparency stiffness is critical. They have extensively studied, developed and tested concepts for the F-111 aircraft. As a part of this program, Douglas studied and tested the stiffness relationships for 36- x 36-inch and the B-1 windshield and the study was documented in AFFDL-TR-77-1.

Bird Impact Testing and Development of Analytical Technique

Historically, bird impact tests had been accomplished to provide pass/fail

conditions for a transparency design, measuring only bird impacted specimens at room temperatures. To be meaningful, studies were conducted and extensive coordination with the AEDC was accomplished that ensured development of installations of thermocouples and strain gages on transparencies and support structure to measure and record testing temperatures and strains. Concurrently, AEDC developed a method, utilizing movie coverage to measure deflections of the transparency at bird impact and the techniques developed were utilized for bird testing the B-1 enclosure, the 36- x 36-inch curved specimens and the F-16 canopies.

The B-1 windshields were determined to be a very high cost item from the standpoint of installation. Because of common windshield retainers between two or more windshields, each edge of the windshield had to be installed with two rows of attachments, and there was great difficulty aligning the attachment holes between the windshield and structure, due to tight fitting holes. To alleviate some of the problems and reduce installation costs, Douglas modified the design and developed modifications of the edge designs to utilize only one row of attachments installed in loose holes with wet sealant applied. A series of six bird impact shots were made to validate the theories developed. Shots were made with four- and six-pound birds at 562 knots, and it was shown that the theories were valid.

In an attempt to optimize windshields, structural support and edge designs, a series of five specimens were designed, utilizing materials proprietary to three transparency vendors, for bird impact testing. A total of ten specimens were ordered that were 36- x 36-inches and curved to a constant 60-inch radius. Two structural fixtures were designed and built to support these specimens for bird tests. The structural arrangement was purposely sized with varying degrees of stiffness and variable corner configurations. Twenty bird impact tests were conducted at AEDC. To maximize the data obtained during the testing, the three vendors laminated various strain gages and thermocouples within each specimen and additional external instrumentation was accomplished by both Douglas and AEDC. The bird impact tests were conducted at extreme hot or cold temperatures that a B-1 aircraft would encounter in service at velocities up to 562 knots.

Prior to completion of these bird tests, the computer resizing effort had progressed to the extent that it was determined that the structural stiffness could be further reduced. Subsequently, for the last shots, the structure was reworked at AEDC to accomplish this effort. Although time consuming, with the extensive amount of instrumentation of these specimens, accurate steady-state temperatures that represented aircraft flight conditions were achievable at AEDC. AEDC was able to document strain readings, steady-state temperatures through the specimens, bird weights, bird velocities, provide movie coverage, and deflections measured from the movies.

Table 1 lists the three series of bird tests and results accomplished at AEDC.

Often times, several million dollars are expended to design aircraft to withstand the impact of four-pound birds at the operational speeds and temperature regimes of the aircraft. These costs are accrued as a result of design and bird testing and more frequently than not, redesigned and

TABLE 1. RESULTS OF BIRD TESTS CONDUCTED AT AEDC

	B-1	36 x 36 IN.	F-16A
NUMBER OF SPECIMENS TESTED	2	9	9
NUMBER OF BIRD SHOTS o AT AMBIENT TEMPERATURE o AT COLD TEMPERATURES o AT HOT TEMPERATURES	6 6 – –	20 8 6 6	30 22 4 4
NUMBER SHOTS/BIRD WEIGHT	5/4 LB 1/6 LB	20/4 LB	28/4 LB 2/2 LB
NUMBER SHOTS/BIRD VELOCITY	6/565 KNOTS	1/218 KNOTS 1/306 KNOTS 3/430-505 KNOTS 15/565 KNOTS	10/123-160 KNOTS 12/161-200 KNOTS 4/201-250 KNOTS 4/350 KNOTS
NUMBER CONFIGURATIONS TESTED	5	11	4
INSTRUMENTATION o NO. OF STRAIN GAGES o NO. OF THERMOCOUPLES o NO. OF HIGH-SPEED CAMERAS	 30 4 3	 38 17 3	 72 12 6

retested to satisfy the bird impact requirements. As a major portion of this program, an effort was undertaken to develop a computerized math model that could be used as a tool by designers to design for bird impact conditions. Since this was an initial effort, a lot of trial and error went into the development. Variously, 36- x 36-inch flat specimens, 36- x 36-inch curved specimens, B-1 air vehicle number 4, and 8 x 36-inch beams were modeled. The finite element modeling effort was accomplished on a Computer Aided Design Drafting (CADD) system so that the computer, after modeling, would print out full-sized drawings. Initially, the math model was developed utilizing McDonnell Douglas Automation System Computers, but was changed to utilize the Air Force Computers at Wright-Patterson AFB, Dayton. To develop initial concepts for the program, the 8 x 36-inch beams were utilized and compared to the test results which are documented in AFFDL-TR-76-156. Since it was determined early that a math model computer program would be extensive to develop and time consuming to apply during initial design phases, a scaled down computer program was developed that would aid the designer in making several estimates of various designs with minimum time expended for an initial approach. This program and theory was developed and is shown in AFFDL-TR-76-114. The concepts developed for the design of the B-1 windshield are noted in AFFDL-TR-77-1.

The documentation of these analytical studies and tests are contained in:

- AFFDL-TR-76-114: The Determination of Deflection and Stress Distribution for a Laminated Beam
- AFFDL-TR-76-156: Damping, Static, Dynamic and Impact Characteristics of Laminated Beams Typical of Windshield Construction
- AFFDL-TR-77-98: High Speed Impact Testing of Aircraft Transparencies
- AFFDL-TR-TBD: W.T.D.P. - Canopy Detail Design Options Study
- AFFDL-TR-77-99: Aircraft Windshield Bird Impact Math Model

Windshield Systems Design and Options Studies

Upon completion of the systems requirements studies, the structural analysis studies, the various materials tests, and the bird impact tests, utilizing the knowledge gained, assessments were made of the B-1 windshields and the F-16 canopies.

A minimum of two alternate designs were developed for each aircraft to fulfill contract requirements.

General Systems Considerations

Many approaches can be taken to develop a design, but once alternate designs are available and choices can be made, it frequently becomes difficult to establish criteria for selecting the one most optimum design.

Figure 5 illustrates the optimum for two extremes. One extreme is the

aircraft and the other extreme represents the ultimate for pilot vision. Neither approach is achievable which causes many compromises to be made.

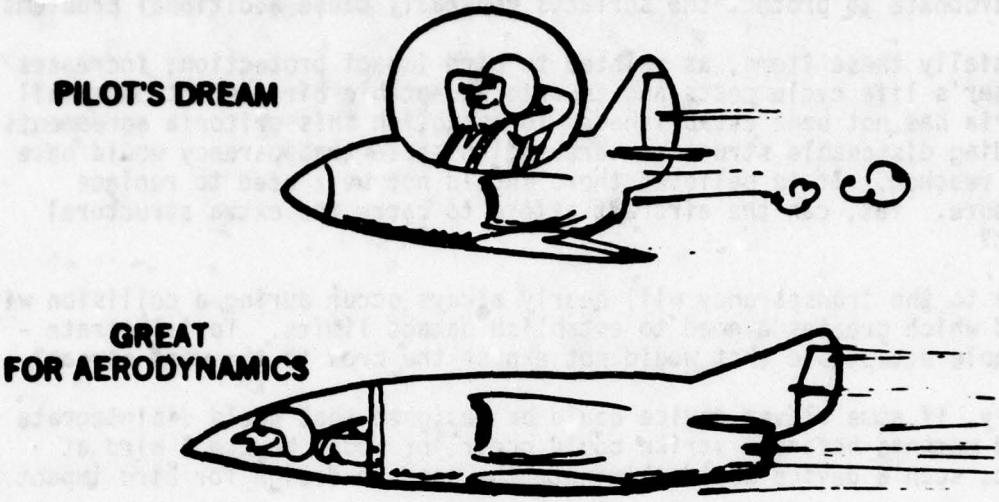


Figure 5. Optimum Crew Compartment Shapes

Generally, the aircraft is shaped by an engineering advanced design section where styling and aerodynamics, generally, are the predominate requirements even though visibility clearances may be provided in accordance with MIL-STD-850. Frequently, the limitations for transparency requirements, such as angle of incidence, distortion, light reflection, light transmission, and haze, are not considered. Yet, if shaping only considered the requirements for the transparency, then drag and noise problems could be created. Further, the stability of the aircraft might be in jeopardy, the drag might cause excessive fuel consumption that could result in the aircraft not completing its intended missions, or fuel consumption might be too costly.

It is believed then that the transparency design at inception should be the best compromise obtainable between the two sets of requirements, otherwise, the optical quality of the windshields could be marginal like the B-1 and F-111 aircraft.

It is possible, however, that the future dictates for high performance aircraft may be such that we can no longer rely on transparencies because of the aerodynamic requirements and may be forced to develop electro-optical systems as replacements.

The high costs associated with loss of lives and military aircraft as the results of mid-air collisions with birds has been justification for the Air Force in the 1970's to make transparencies bird impact resistant. Bird resistant transparencies introduce many new problems that must be compromised. Generally, the transparency has to be thicker; thus, causing a weight increase in addition to creative optical problems. Many times the supporting structure must have additional strength that causes added

weight. The lightest weight transparency material that will withstand bird impact is polycarbonate that is subject to attack by the elements in the atmosphere unless adequately protected. Yet, most coatings applied to polycarbonate to protect the surfaces generally cause additional problems.

Potentially these items, as related to bird impact protection, increases the user's life cycle costs and to date acceptable bird impact pass/fail criteria has not been established. To establish this criteria agreements regarding disposable structure versus disposable transparency would have to be reached. It is believed there should not be a need to replace structure. Yet, can the aircraft afford to carry the extra structural weight?

Damage to the transparency will nearly always occur during a collision with a bird which creates a need to establish damage limits. To illustrate - is a hole acceptable that would not expose the crew to the wind stream?

Ideally, if some clever device could be designed that would disintegrate a bird moments before a strike could occur, or would bounce a bird at impact, such a device would eliminate the need to design for bird impact.



IMPACT

While the preceding paragraphs briefly related some compromising problems associated with the design of a crew compartment transparency, to specify all the compromises required to meet all systems requirements would generate a voluminous listing.

B-1 Alternate Designs

An assessment was made of the B-1 windshield because of the high life cycle costs associated with the production parts, including manufacturing and installation costs.

The existing design had a 7/8 inch thick polycarbonate ply as the main load carrying member of the laminate. Since polycarbonate is not manufactured in the 7/8 inch thickness, two or more sheets of polycarbonate must be fusion bonded together to obtain this thickness.

Test results indicated that the fusion bonded materials may delaminate during thermal and pressurization cycling. Subsequently, multi-layers of thin polycarbonate were considered as an alternate to the heavier ply. Since the program goals were to develop two alternate designs, glass laminates were also designed and tested.

The B-1 windshields as originally designed were determined to be a very high cost item from the standpoint of installation. Because of common windshield retainers between two or more windshields, each edge of the windshield had to be installed with two rows of attachments, and there was great difficulty aligning the attachment holes between the windshield and structure due to tight fitting holes. To alleviate some of the problems and reduce installation costs, Douglas modified the design and developed modifications to utilize only one row of attachments installed in loose holes with wet sealant. Bird shots were made with four- and 6-pound birds at 562 knots.

Figure 6 illustrates the multilayered laminate and the one bolt installation technique.

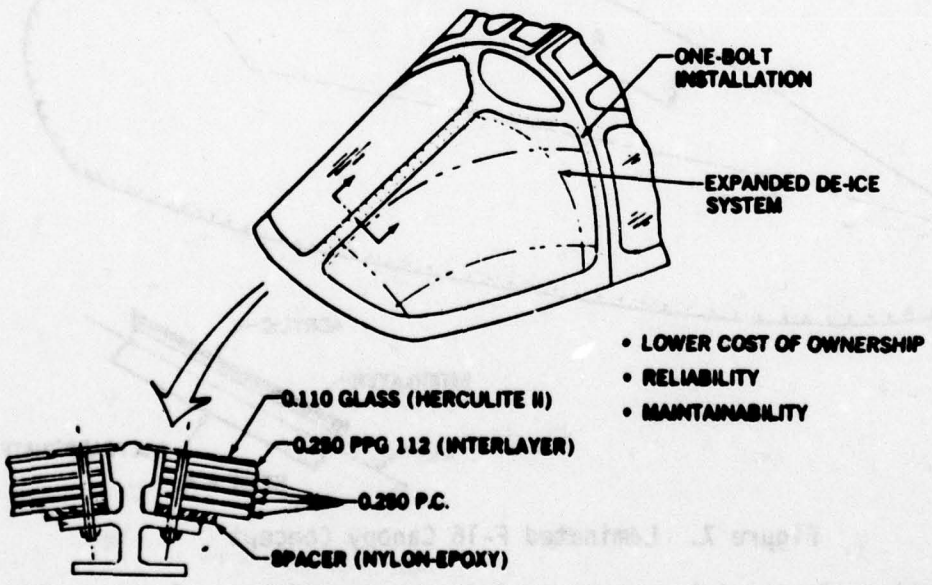


Figure 6. Alternate B-1 Windshield Design

The results of the various studies for this effort are contained in the three volume technical report AFFDL-TR-77-1 that has been released to industry.

The bird impact testing and analysis accomplished by Douglas at AEDC for the B-1 and a series of 36 x 36 inch specimens are contained in AFFDL-TR-77-98.

F-16 Alternate Designs

As a contract requirement an assessment was made of the F-16 canopy. The basic F-16 design is a coated monolithic polycarbonate canopy that was capable of withstanding bird impacts to 350 knots, but it is believed that the coatings on the polycarbonate would have a very short service life.

The direction for this task was to design an alternate canopy capable of withstanding 350 knots and to recommend canopy designs capable of withstanding bird impacts to 565 knots. From the lessons learned during the previous efforts a laminated configuration was deemed preferable and is illustrated in Figure 7.

PROPOSED LAMINATED CANOPY DESIGN

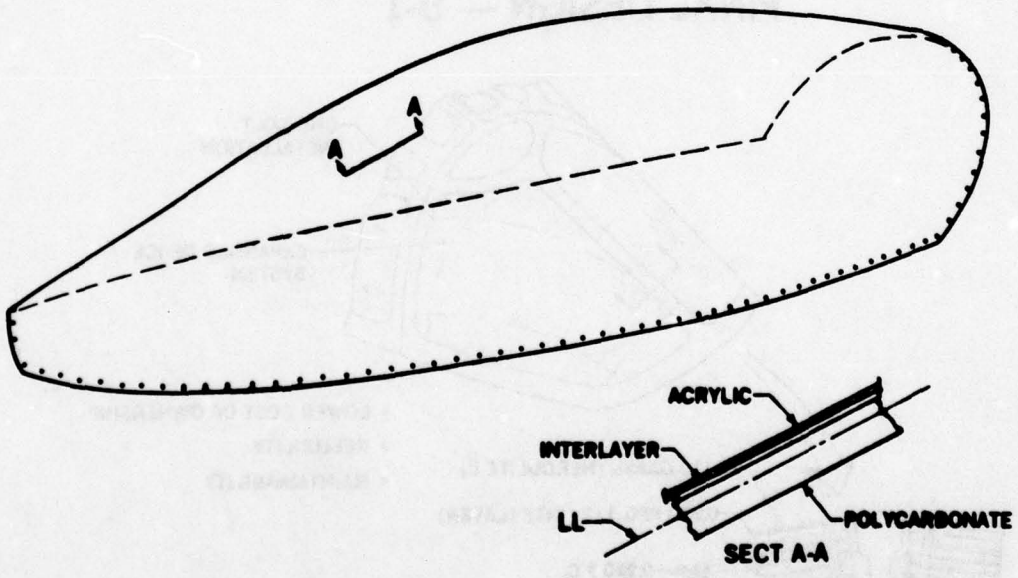


Figure 7. Laminated F-16 Canopy Concept

The combination of materials can be varied to accommodate various speed regimes, thermal restrictions, and can be altered to provide maximum use of available raw materials.

Currently, the acrylic material is manufactured only in 0.125 inch thickness; large enough to make an F-16 canopy. Tradeoff analysis has shown that it would be more desirable for the thickness to be either 0.10 inch thick or less. The main load carrying member minimum thickness at this time is considered to be 0.68 inch and the interlayer to compensate for the expansion/contraction rates of the varying materials was selected as 0.80 inch thick cast-in-place silicone.

In order to limit the weight increase for a laminated canopy a bow frame could be installed as shown in Figure 8. The polycarbonate in the forward canopy could then be increased for higher aircraft speeds without increasing the total canopy weight excessively.

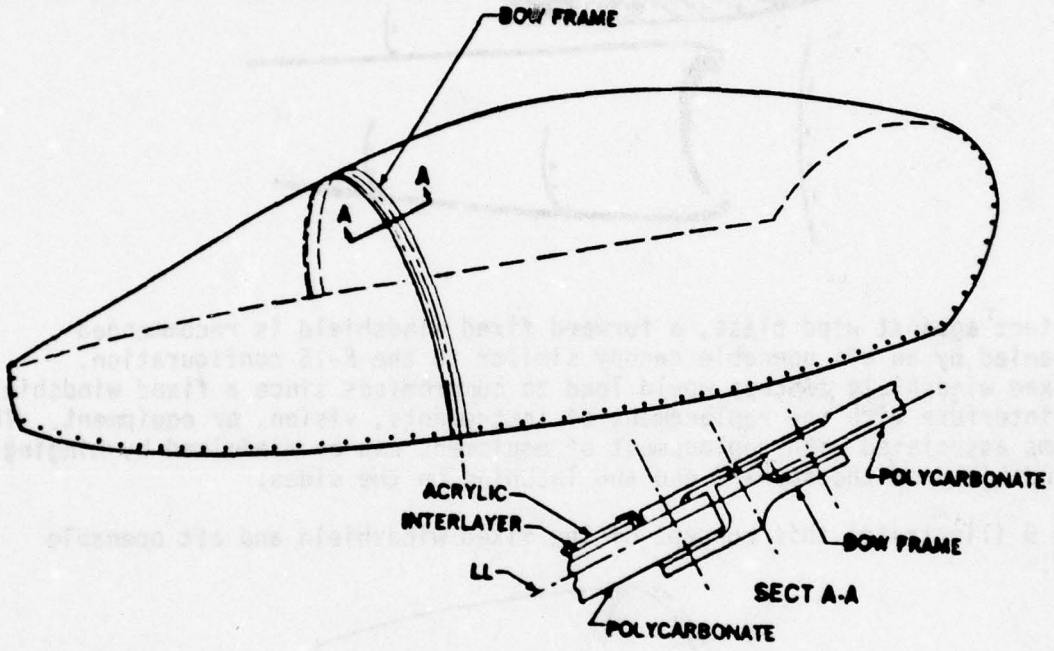
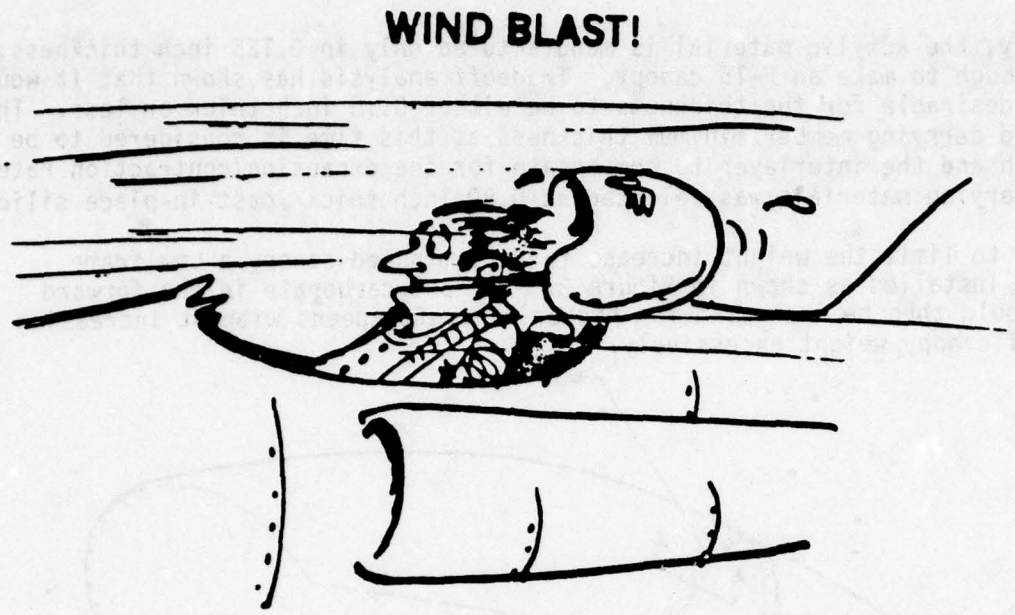


Figure 8. F-16 Canopy/Bow Frame Alternate Design Concept

The compromises that must be considered include the use of coated monolithic polycarbonate on the aft canopy, the pilot's visibility may be obstructed as a result of the bow frame.

Through the years many military aircraft have lost hatches and canopies in flight. The crews, however, were protected because each aircraft had forward fixed windshields. Afforded that protection from windblast, the crew could get the aircraft back to homebase.

In the event an F-16 canopy were lost, the wind blast would be prohibitive and catastrophic.



To protect against wind blast, a forward fixed windshield is recommended accompanied by an aft openable canopy similar to the F-15 configuration. The fixed windshield concept would lead to compromises since a fixed windshield would interfere with the replacement of instruments, vision, or equipment. The problems associated with replacement of equipment can be minimized by hinging the windshield on the forward end and latching on the sides.

Figure 9 illustrates this concept of the fixed windshield and aft openable canopy.

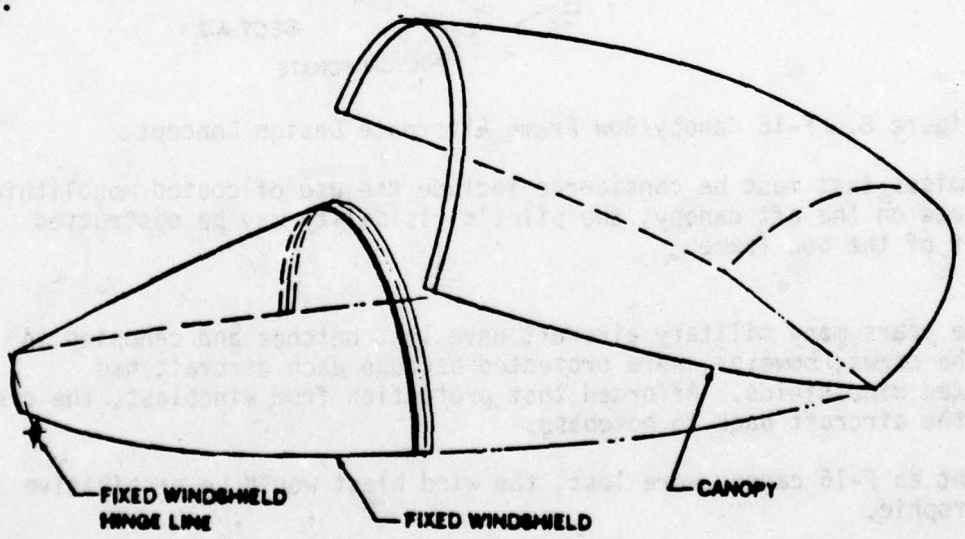


Figure 9. Fixed Windshield and Aft Openable Canopy Concept

The studies and testing conducted for determination of the alternate F-16 canopy designs are contained in technical report AFFDL-TR-(TBD) (MDC J7176) that will be released by the Air Force to industry.

Design Guidelines Handbook

The culmination of the program effort is to result in the development of a handbook in two volumes:

Volume I - Design Methodology
Volume II - Design Data

The handbook format will be developed in accordance with MIL-STD-490.

The handbook will eventually be used throughout the aerospace industry for the design and fabrication of aircraft windshield/canopy systems.

The handbook shall address the full spectrum of transparency systems design and test methodology for optimum performance while minimizng total cost of ownership and to include, but not be limited to:

- Space Allocations/Aircraft Shaping
- Material Characteristics/Performance
- Edgemember Concepts
- Support Structure Requirements
- Hail, Bird, Projectiles, Shrapnel, and FOD Impacts
- Precipitation Static, Lightning, EMP, Laser and Nuclear Flash Resistance
- Anti-icing, Defogging and Demisting
- Visibility and Optical Requirements
- Light Transmission, Haze, Deviation, Distortion

This handbook may be supplemented by other technical reports as necessary such as a separately reported edgemember analysis that will include:

- Scaling concepts
- Bolt spacing
- Sizing as a function of load requirements and materials to be used
- Pressure sealing
- Attachments

- Torque techniques

A technical report may also be required to document the results of additional wind tunnel tests.

ENVIRONMENTAL DESIGN CRITERIA FOR HIGH PERFORMANCE AIRCRAFT WINDSHIELDS AND CANOPIES

L. P. Koegeboehn
Douglas Aircraft Company
McDonnell Douglas Corporation
Long Beach, California

ENVIRONMENTAL DESIGN CRITERIA FOR HIGH PERFORMANCE AIRCRAFT WINDSHIELDS AND CANOPIES

L. P. Koegeboehn
Douglas Aircraft Company
Long Beach, California

ABSTRACT

The design of windshields and canopies and their reliability and maintainability is highly dependent upon the temperature regime that is experienced by these glazing materials in service. This is especially true of supersonic aircraft. Therefore, the thermal analysis is being considered more and more as the industry seeks a more reliable and lower maintenance windshield system.

The areas that must be addressed are as follows:

1. Maximum and minimum temperature
2. Maximum and minimum birdstrike temperature
3. Extreme thermal transients
4. Temperature differentials at the attachment areas
5. Design of anti-ice and defog systems
6. Thermal expansion and its effects

The use of this information and its incorporation into design and testing, results in a better windshield and/or canopy design with longer life and therefore lower overall cost.

PRECEDING PAGE BLANK-NOT FILMED

INTRODUCTION

This paper presents the results of the analytical effort to define the environmental design criteria for high performance aircraft windshields, namely the B-1 and F-16. This work was accomplished in support of the Windshield Technology Demonstrator Program sponsored by the Air Force.

Most of the analyses was thermal in nature. Also included were other environmental effects which included design for hail resistance and rain removal. Most of the thermal analyses were either in support of stress analysis or for establishing test conditions. These analyses include definitions of the temperature distributions for the many expected operating conditions, consideration of transient temperatures, temperature ranges when bird strikes might be expected, thermal aging of the windshield materials, windshield edge temperatures at attachment areas, thermal expansion, thermal factors related to anti-icing and defogging system performance, and the effects of thermal nuclear and solar heating.

TECHNICAL DISCUSSION

Requirements

The windshield must survive all normal thermal conditions to which the aircraft is exposed and it must suffer no degrading effects as a consequence. This includes both the cold atmospheres on the ground and those at high-altitude low-speed cruise. It must also withstand the hot atmosphere conditions during high-speed low-altitude terrain following, the conditions encountered during supersonic dash operations, plus the solar heating which is most significant on the ground. Another requirement is that the inboard surface of the transparency does not exceed 160°F during flight. This requirement is given in MIL-E-38453A.

The windshield defogging system must maintain the windshield surface fog free during operation in the atmosphere defined in MIL-T-5842. If the aircraft is to be designed to operate during icing conditions, as is the case for the B-1, the anti-icing system must meet the requirements specified in MIL-T 5842 and MIL-E-38453A. The rain removal system must also meet the requirements of MIL-E-38453A. If the aircraft is designed for a certain nuclear hardness, the windshield must also be designed to withstand the thermal effects of the blast. The requirements for hail impact were adopted from MIL-STD-210B considering the 1 percent risk factor.

Aircraft Characteristics

To determine if a windshield meets the above stated design requirements, several operational characteristics of the aircraft must be known:

The maximum and minimum temperatures as a function of altitude to which the aircraft is to be exposed, must be defined. To compute minimum windshield temperatures, the maximum subsonic steady stead aircraft velocity is needed as a function of altitude during exposure to the minimum air temperatures.

To compute maximum windshield temperatures, the maximum aircraft velocities are needed as a function of time and altitude during exposure to

the maximum temperatures.

Due to the low thermal conductivity in combination with the high thermal mass of aircraft windshields, high thermal stresses are set up by the large temperature differentials within the canopy. It is important, therefore, to know the transient states of the aircraft, such as descent, climb and acceleration and deceleration rates.

Other factors which affect the transient state of the windshield are anti-ice and defog system performance and effect of a thermal nuclear blast. Therefore the heatup rates of the anti-ice and defog systems must be known and also the magnitude of nuclear blast, if any, that the aircraft is to be designed to withstand.

ANALYSES PERFORMED

Prior to selecting a production design, many windshield configurations must be considered. During this effort, thermal analyses of approximately 20 separate B-1 windshield configurations for the B-1 were made. For the F-16, approximately five configurations were analyzed. The resultant thermal analysis often dictated a change in the windshield configuration, due to the requirements mentioned.

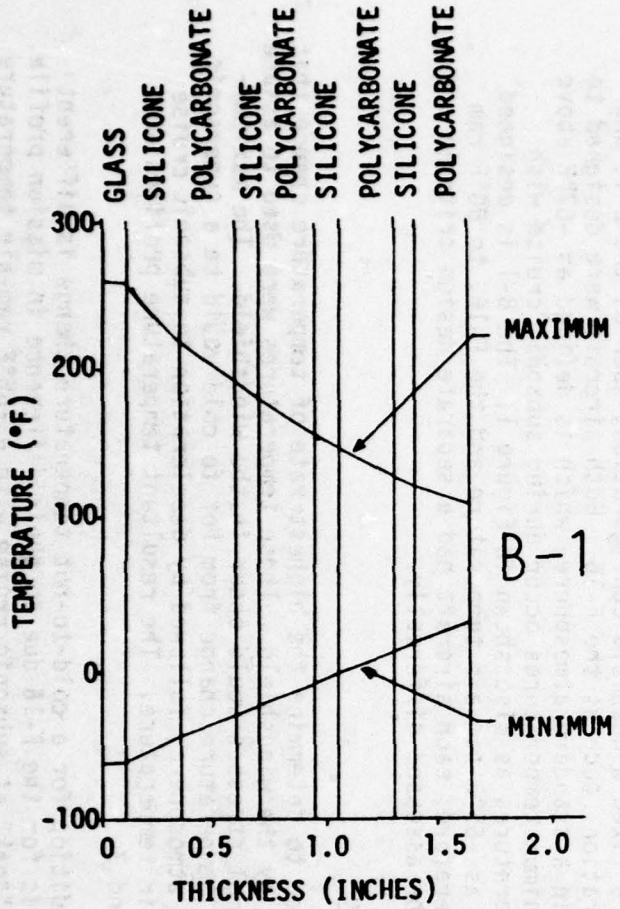
Temperature Distribution

Studies were conducted to determine the temperature distributions within the candidate windshields during maximum and minimum steady state temperature conditions. These temperatures were used to determine what materials would be compatible with a particular installation. The maximum windshield temperatures occur subsequent to a supersonic cruise as shown in Figure 1. Figure 1 shows the temperatures for a fixed windshield configuration, such as the B-1, and for a canopy configuration, such as the F-16. Both aircraft were designed to cruise at max speed in a standard atmosphere, which is defined as -67°F above 36,000 feet. The minimum temperatures occur during subsonic cruise with minimum ram-air temperatures as also shown in Figure 1. The B-1 is designed for operation as low as -65°F ram air temperature and the F-16, to 80°F ram air temperature. Therefore, each aircraft had a separate design criteria and therefore needed to be assessed differently.

Transient Temperature

Studies were conducted to determine the highest rate of temperature change that would be experienced by the windshield. These temperatures were used to assure that no harmful thermal stresses would occur in the windshield. The maximum-rate condition for a temperature change from hot to cold would be a supersonic cruise in a standard atmosphere, followed by deceleration to subsonic cruise at the minimum ram-air temperature. The resultant temperature profiles are shown in Figures 2 and 3.

The maximum-rate condition for a cold-to-hot temperature change is different for the B-1 than it is for the F-16 due to their difference in mission profile. For the B-1 it is a "soak" at subsonic cruise with a -65°F ram-air temperature and anti-ice OFF, followed by an emergency descent to high-speed low-altitude



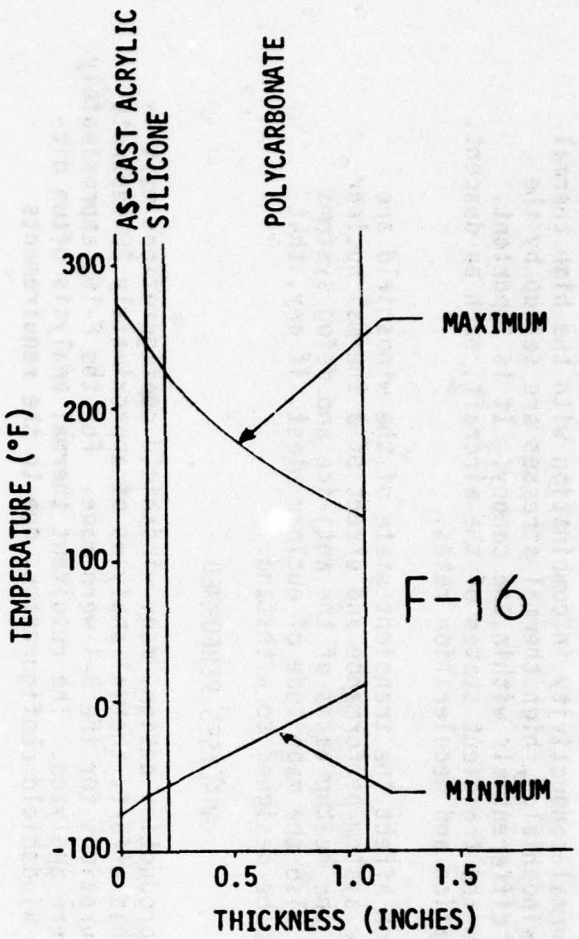


Figure 1. Maximum and Minimum Windshield/Canopy Temperatures

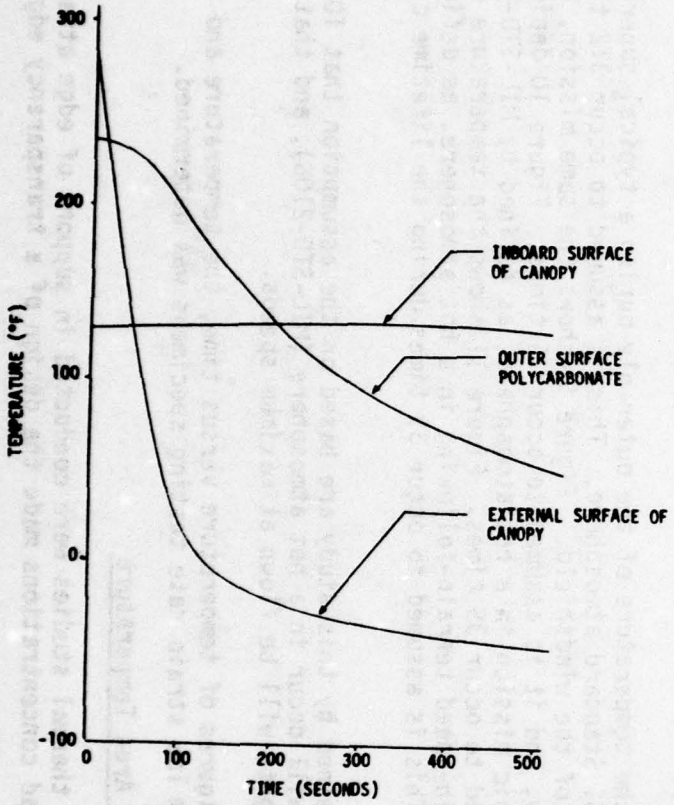


Figure 2. Canopy Temperature Profile During Deceleration from Supersonic Speed to Subsonic Speed.

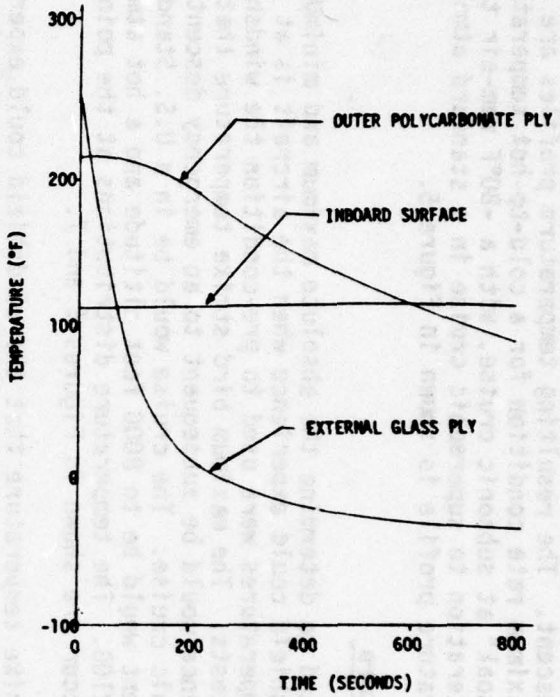


Figure 3. Temperature Profile for Four-Ply Polycarbonate Windshield with CIP Silicone Interlayer During Emergency Descent from Supersonic Cruise to Subsonic Cruise.

terrain following. The windshield anti-ice system would be selected ON at the initiation of the descent. The resulting temperature profiles are shown in Figure 4. The maximum rate condition for a cold-to-hot temperature change for the F-16 is a "soak" at subsonic cruise, with a -80°F ram-air temperature followed by an acceleration to supersonic cruise in a standard atmosphere. The resulting temperature profile is shown in Figure 5.

Bird Strike Temperature

Studies were conducted to determine the absolute maximum and minimum temperatures that the windshield could experience when the aircraft is at 8000 feet or below. These temperatures were used to pre-condition the windshield prior to the bird-impact tests. The maximum bird strike temperature that the windshield could experience would be subsequent to an emergency descent to 8000 feet from a supersonic cruise. The cruise would be in a U.S. Standard atmosphere, and the descent would be to 8000 feet altitude and a hot atmosphere, as defined by MIL-STD-210B. The temperature distributions at the point were the bird strike might occur are shown in Figures 6 and 7.

The minimum bird strike temperature that the windshield could experience would be subsequent to an emergency descent to 8000 feet from a subsonic cruise in a cold atmosphere. The temperature distribution at the point where the bird strike might occur are also shown in Figures 6 and 7.

Time/Temperature Study For Thermal Aging

In support of the low-strain-rate testing of polycarbonates, a thermal study was made on the B-1 type four-ply polycarbonate windshield with a CIP silicone interlayer. For these tests, it was necessary to determine the amount of time that the outer polycarbonate ply would exceed 80°C during the projected life of the windshield.

Figure 8 shows the temperature of the outer ply during a typical supersonic mission in a U.S. Standard atmosphere. This is assumed to occur 312 times during the life of the windshield. Figure 9 shows the same mission, but at maximum velocity, and it is assumed to occur 35 times. Figure 10 depicts a typical supersonic mission in a hot atmosphere, as defined by MIL-STD-210B, and it is assumed to occur 39 times. Figure 11 shows the temperature due to low-altitude high-speed terrain-following in a hot atmosphere, as defined by MIL-STD-210B. This is assumed to occur 39 times during the lifetime of the windshield.

The times determined by this study are based on the assumption that 10 percent of the flights will occur in a hot atmosphere (MIL-STD-210B), and that 10 percent of the flights will be flown at maximum speeds.

From the four figures of temperature versus time, the temperature and time exposure for the low strain rate testing specimens was determined.

Edge Attachment Area Temperature

Edge attachment thermal studies were conducted in support of edge attachment tests. High load concentrations made the design of a transparency edge attach-

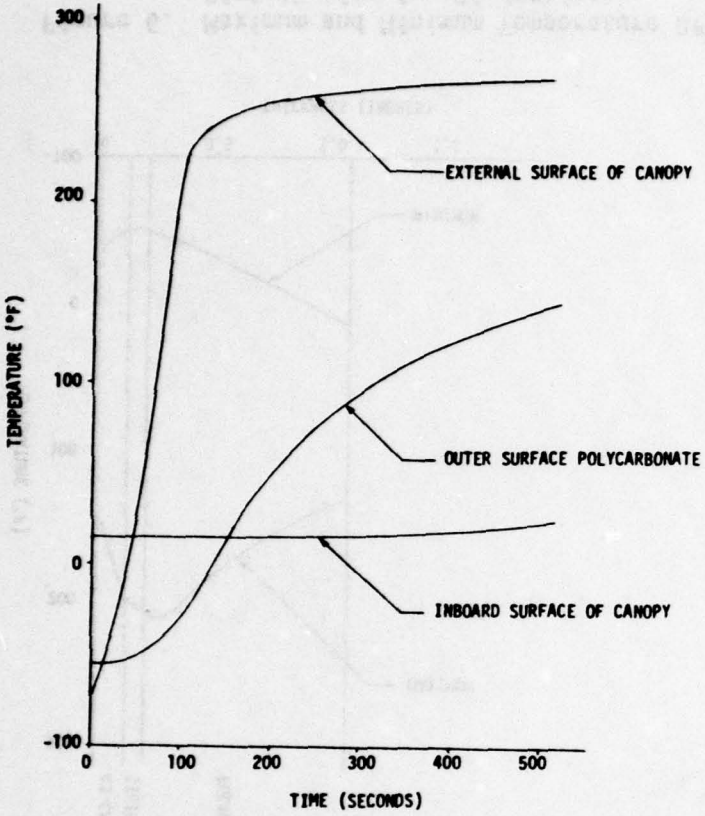


Figure 4. Canopy Temperature Profile During Acceleration from Subsonic to Supersonic Speed.

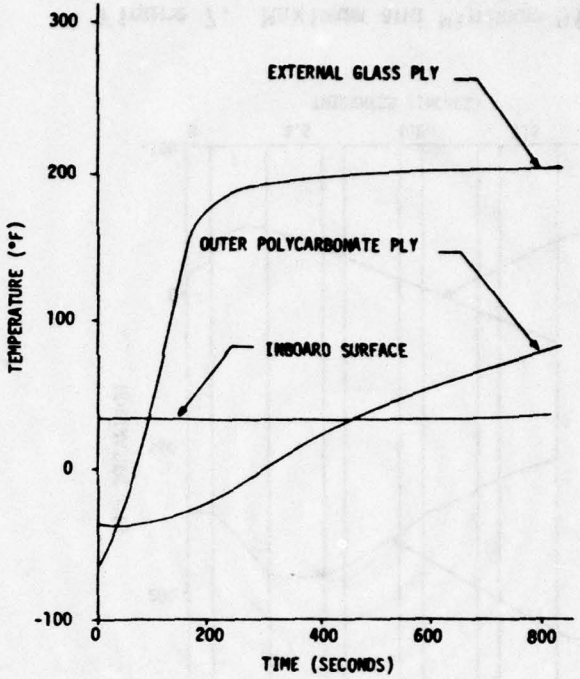


Figure 5. Temperature Profile for Four-Ply Polycarbonate Windshield with CIP Silicone Interlayer During Emergency Descent from Subsonic Cruise to Low Altitude Terrain Following.

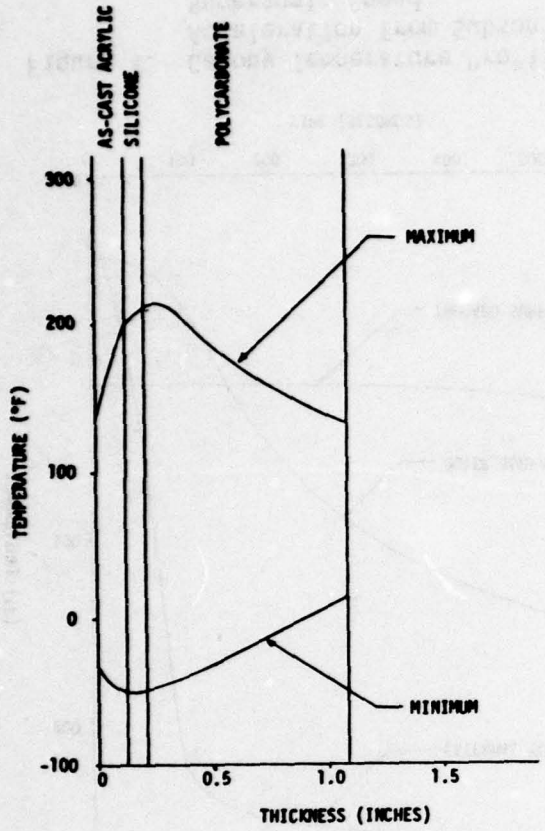


Figure 6. Maximum and Minimum Temperature Distribution Distribution for Birdstrike.

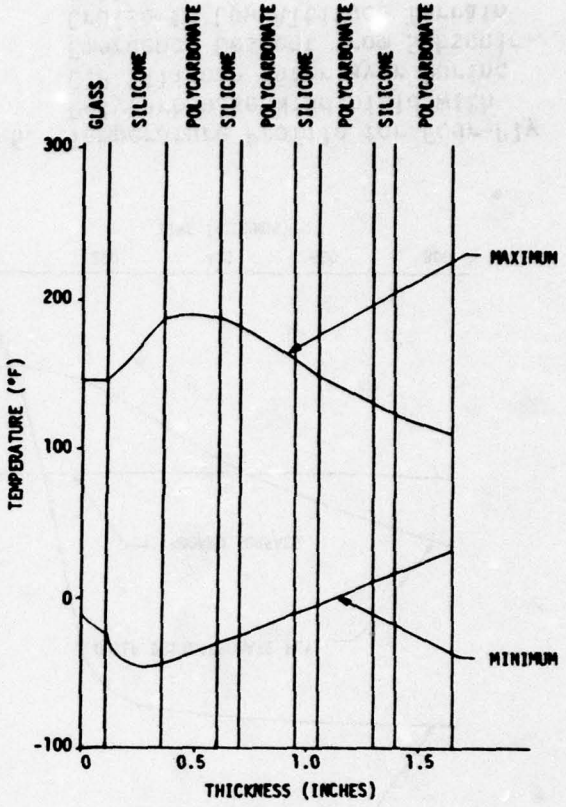


Figure 7. Maximum and Minimum Birdstrike Temperature For Four-Ply Polycarbonate Windshield with CIP Silicone Interlayer.

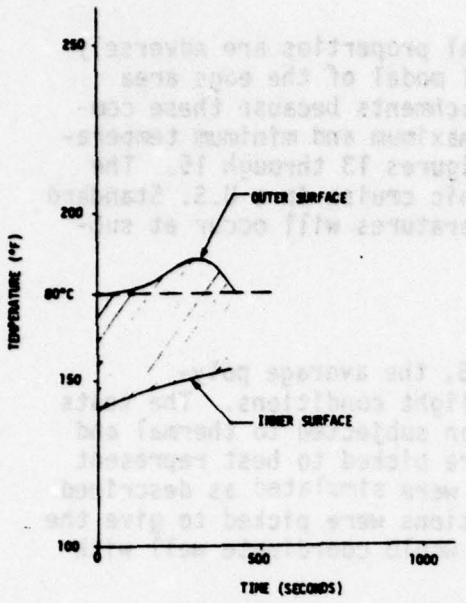


Figure 8. Temperature of Outer Polycarbonate Ply of Four-Ply Windshield During Typical Supersonic Cruise in a Standard Atmosphere.

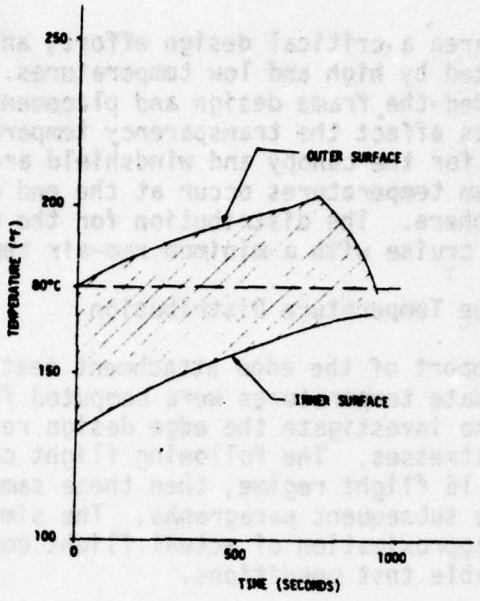


Figure 9. Temperature of Outer Polycarbonate Ply of Four-Ply Windshield During High Speed Supersonic Cruise in a Standard Atmosphere.

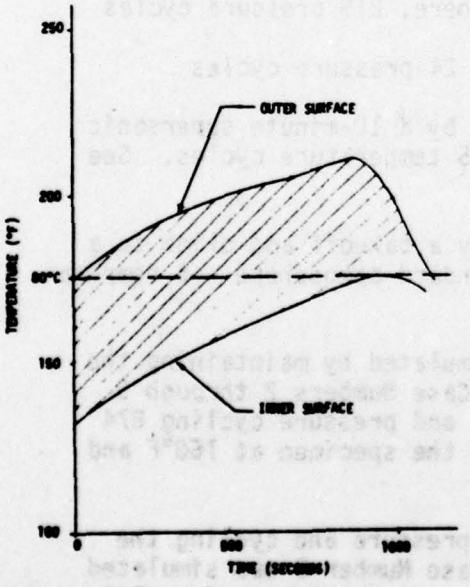


Figure 10. Temperature of Outer Polycarbonate Ply of Four-Ply Windshield During Typical Supersonic Cruise in a Hot Atmosphere.

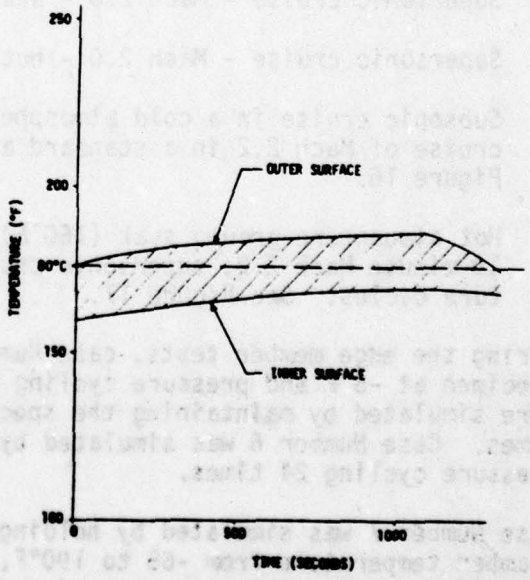


Figure 11. Temperature of Outer Polycarbonate Ply of Four-Ply Windshield During High Speed Low Altitude, Terrain Following in a Hot Atmosphere.

ment area a critical design effort, and the material properties are adversely affected by high and low temperatures. The thermal model of the edge area included the frame design and placement of the attachments because these components affect the transparency temperature. The maximum and minimum temperatures for the canopy and windshield are shown in Figures 13 through 15. The maximum temperatures occur at the end of a supersonic cruise in a U.S. Standard atmosphere. The distribution for the minimum temperatures will occur at subsonic cruise with a minimum ram-air temperature.

Average Temperature Distribution

In support of the edge attachment test for the F-16, the average polycarbonate temperatures were computed for several flight conditions. The tests were to investigate the edge design reliability when subjected to thermal and load stresses. The following flight conditions were picked to best represent the F-16 flight regime, then these same conditions were simulated as described in the subsequent paragraphs. The simulated conditions were picked to give the best approximation of actual flight conditions and would coordinate well with available test conditions.

1. Subsonic cruise - standard atmosphere, 916 pressure cycles

2. Subsonic cruise - hot atmosphere, 102 pressure cycles

3. Supersonic cruise - Mach 1.6 - standard atmosphere, 498 pressure cycles

4. Supersonic cruise - Mach 1.6 - hot atmosphere, 55 pressure cycles

5. Supersonic cruise - Mach 2.0 - standard atmosphere, 219 pressure cycles

6. Supersonic cruise - Mach 2.0 - hot atmosphere, 24 pressure cycles

7. Subsonic cruise in a cold atmosphere, followed by a 10-minute supersonic cruise of Mach 2.2 in a standard atmosphere - 5 temperature cycles. See Figure 16.

8. Hot atmosphere ground soak (160°F), followed by a takeoff and climb to a 10-minute Mach 2.2, supersonic cruise in a standard atmosphere - 5 temperature cycles. See Figure 17.

During the edge member tests, case Number 1 was simulated by maintaining the specimen at -5°F and pressure cycling 916 times. Case Numbers 2 through 5 were simulated by maintaining the specimen at 75°F and pressure cycling 874 times. Case Number 6 was simulated by maintaining the specimen at 160°F and pressure cycling 24 times.

Case Number 7 was simulated by holding a constant pressure and cycling the chamber temperature from -65 to 190°F, 5 times. Case Number 8 was simulated by holding a constant pressure and cycling the chamber temperature from 160 to 245°F, 5 times.

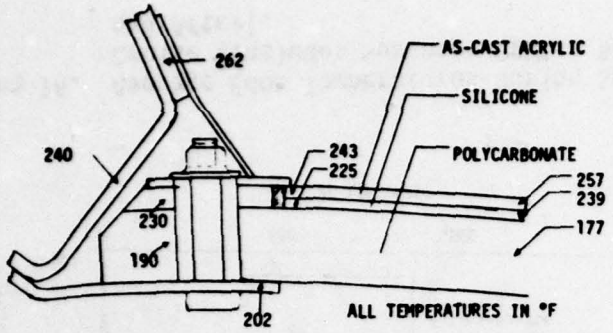


Figure 12. Maximum Temperatures at Canopy Edge.

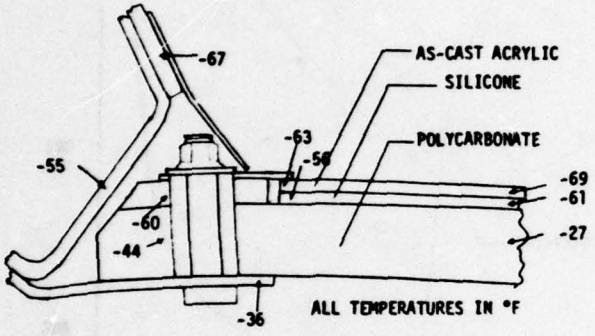


Figure 13. Minimum Temperatures at Canopy Edge

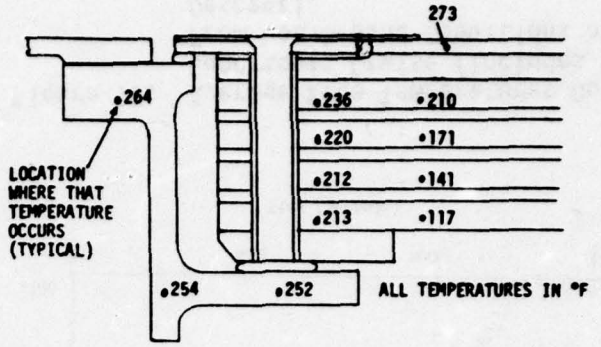


Figure 14. Maximum Temperatures at Edge of Four-Ply Polycarbonate Windshield.

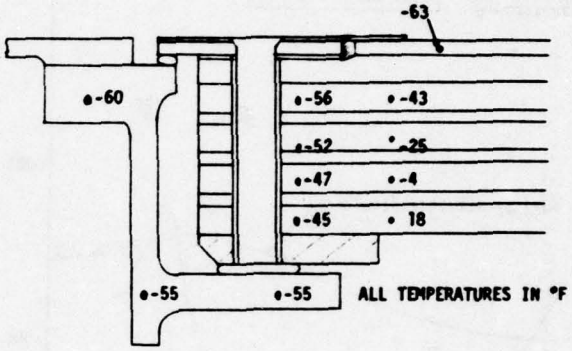


Figure 15. Minimum Temperatures at Edge of Four-Ply Polycarbonate Windshield.

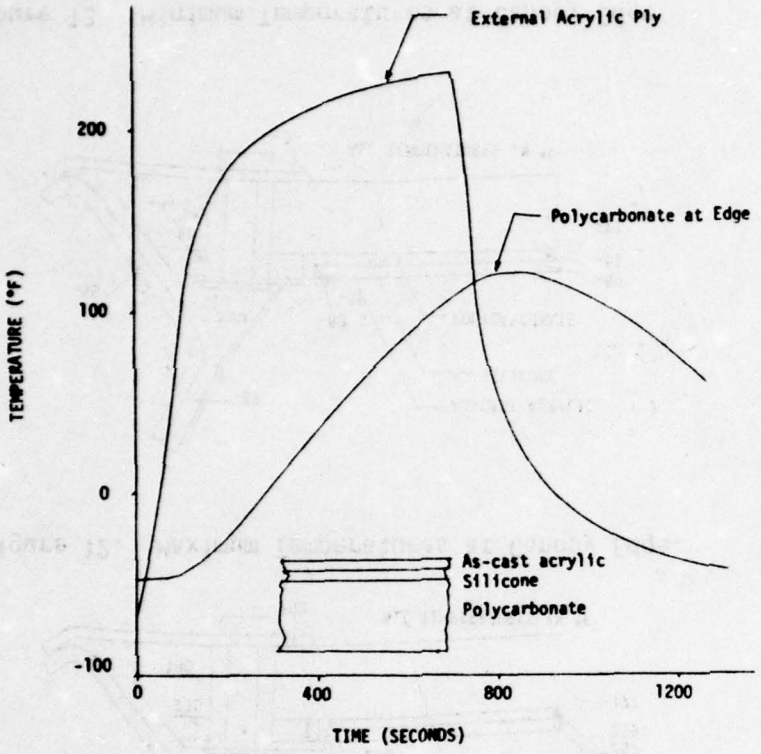


Figure 16. Average Edge Temperatures During Supersonic Cruise (Includes Subsonic Cruise Before and After).

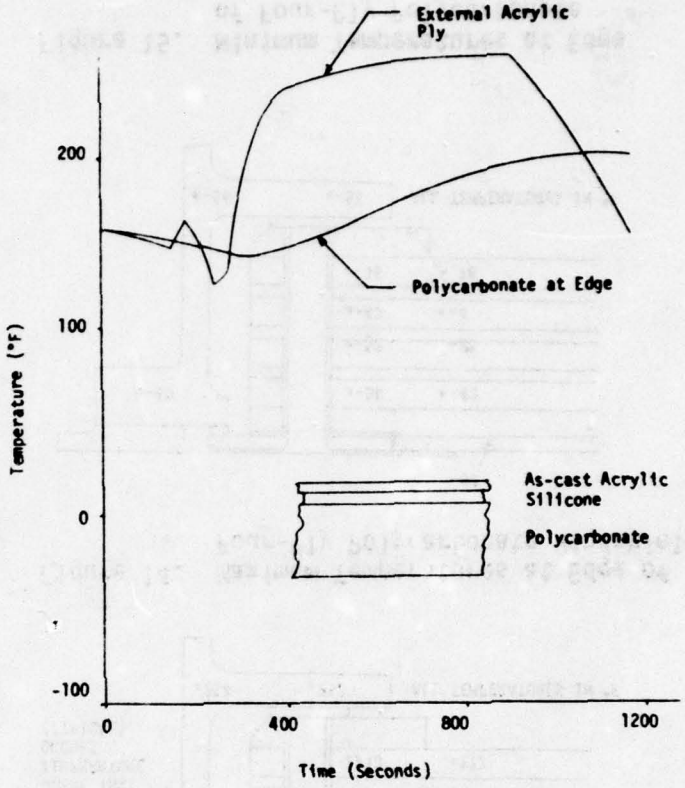


Figure 17. Average Edge Temperatures During Supersonic Cruise (Includes Climb From Hot Ground Conditions and Descent).

Study of Average Temperature Distributions

Also, in support of an edge-attachment test for the B-1, the average maximum temperature and the average minimum temperature of the polycarbonate plies in the windshield were required. The average maximum temperature of the windshield at the edge was assumed as that temperature which occurs during a typical supersonic mission in a U.S. Standard atmosphere. The same condition was analyzed for operation in a hot atmosphere, as defined by MIL-STD-210B; this was assumed to occur 10 percent of the flights. The curves shown in Figure 18 are the profiles of the mathematical average temperatures of the four polycarbonate plies in the U.S. Standard atmosphere and the hot atmosphere during the supersonic portion of a typical mission. The maximum temperature differential among the four plies is 55°F.

The average minimum temperature was assumed to occur during subsonic cruise in a U.S. Standard atmosphere with the anti-ice system selected ON. The arithmetic average temperature of the four polycarbonate plies at the edge was calculated to be -15°F. The maximum temperature differential across the four plies is 5°F.

Study of Maximum Temperature Differentials

Another study for the B-1 was made in support of the edge attachment tests to determine the maximum temperature differentials that could occur in the vicinity of the attachments during heat-up and cool-down conditions. The heat-up condition which would cause the highest temperature differentials would be a climb from subsonic cruise with a -65°F ram-air temperature and the anti-ice system OFF, to a high-speed supersonic cruise in a U.S. Standard atmosphere. The resultant temperatures are shown in Figure 19. Figure 20 shows the maximum temperature differentials for a high-speed descent from a high-speed supersonic cruise to a subsonic cruise with a -65°F ram-air temperature and the anti-ice system ON.

Study of Electrical Edge Heating

A further B-1 study conducted, involving the windshield edge attachment area, was an analysis to determine how the interlayer next to the external glass ply might be electrically heated to help alleviate the possibility of cold-chipping the glass outerply. One method considered to heat the edge is shown in Figure 21. The power applied is 30 watts per linear inch of windshield edge. This value was chosen because it is approximately as high a value as is available. The numbers shown in parentheses are the temperatures without heat, and the numbers shown outside the parentheses are the temperatures with heat applied. The operating condition assumed is a subsonic cruise with a -65°F ram-air temperature and with the anti-ice system ON.

It is apparent that the heat must be applied directly to the edge of the external glass ply to affect the temperature of the interlayer in that area. This objective is not a simple task to accomplish. Heating of this type has been attempted in the past by using wires imbedded in the interlayer. These have broken during operation of the aircraft. A design of this type would require further investigation and possible heating system development in order to solve this heating and failure problem. Douglas has decided not to

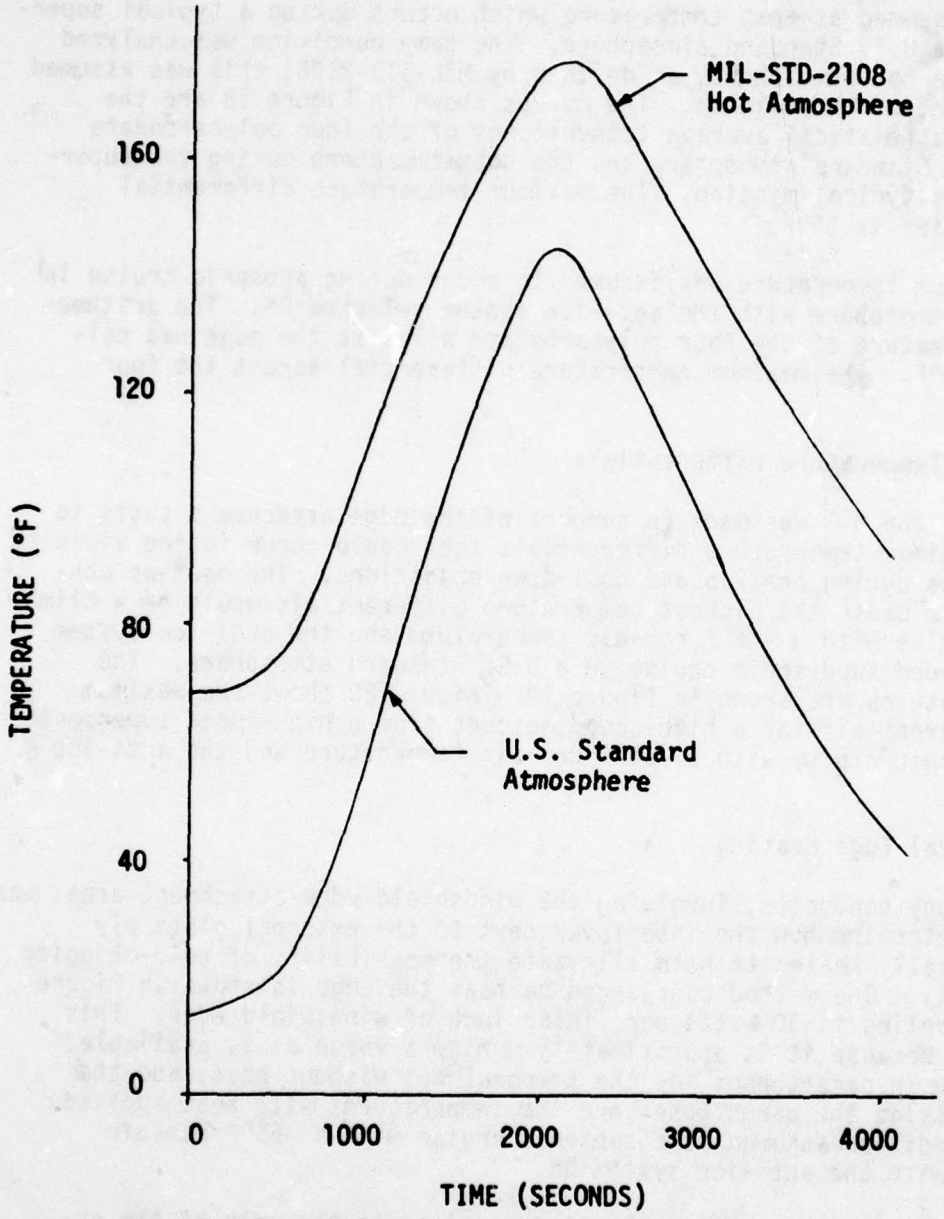


Figure 18 - Average Edge Temperature of Polycarbonate Windshield During Supersonic Flight

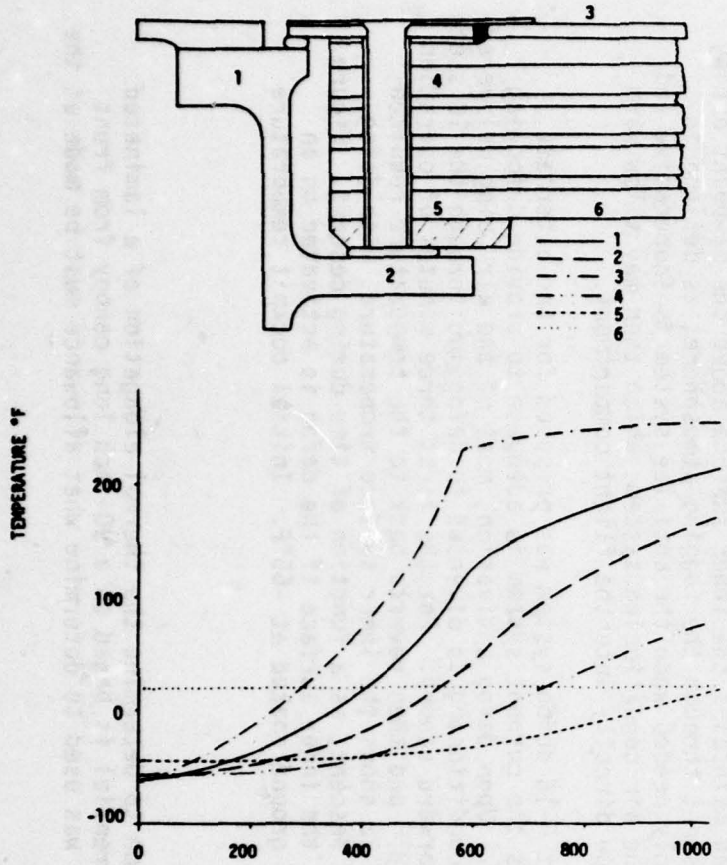


Figure 19. Temperature Differentials at Edge of Polycarbonate Windshield During Climb to Supersonic Cruise.

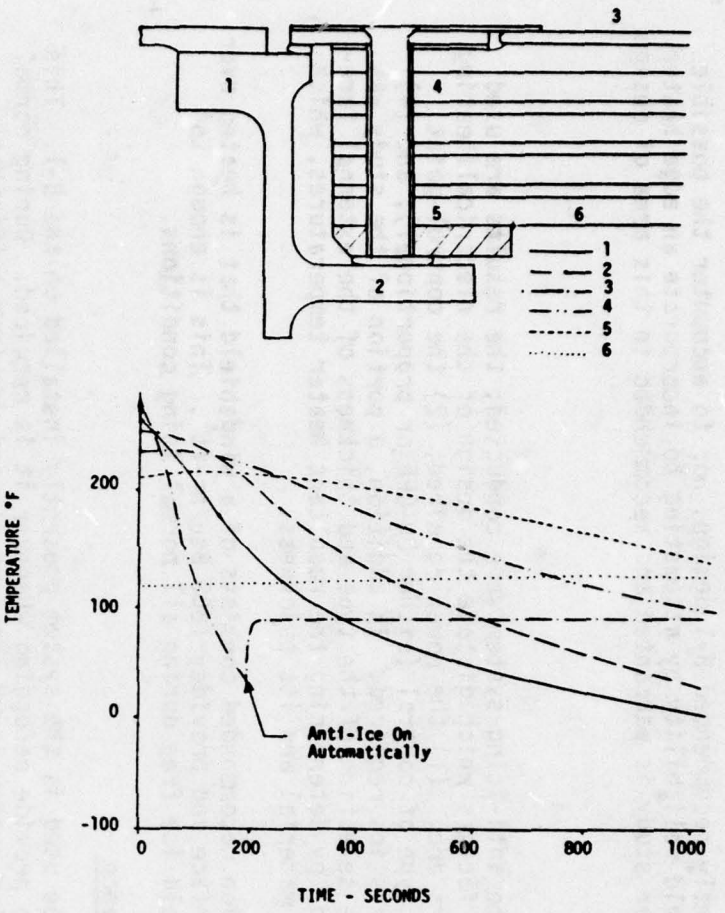


Figure 20. Temperature Differentials at Edge of Polycarbonate Windshield During Descent from Supersonic Cruise.

complicate the presently recommended B-1 design, nor to encounter the possible reduction in windshield reliability by attempting to incorporate an edge heater at this time. Further study is warranted and recommended in this area of design technology.

Anti-Icing System

Thermal studies of the anti-icing system were conducted; the results are used to determine several factors which dictate the design of the electrical heating system. These factors are: (1) the power required; (2) the control-point temperature; (3) the type of control (either ON-OFF or proportional); and (4) the warm-up characteristics required. In addition, a portion of the study was used to assist in the selection of the type and thickness of the external face-ply of the windshield; by determining the resultant heater temperatures, which are functions of the material and its thickness.

The final configuration recommended consists of a windshield that is heated over 90 percent of the surface and provides 1600 Btu/hr-ft^2. This is enough to maintain the windshield ice free during all normal icing conditions.

Defog System Performance

The defog system to be used is the system presently installed on the B-1. This system is adequate to provide defogging whenever it is required. During normal operation, the anti-ice system is ON continuously and provides sufficiently high inner surface temperatures to maintain the surface fog free. The defog system provides 10.6 lb/min. to 213°F air through 22 holes, each 3/16 inch in diameter, at the forward edge of the windshield. After energizing, this air clears the windshield and maintains the inner surface above the dewpoint during the remainder of the descent through the fogging atmosphere, as defined in MIL-T-5842A. This is only needed when the anti-ice system is inoperative and there is a failure of the air conditioning system, which then may allow warm humid outside air to flow directly into the flight compartment.

No change to the current F-16 defog system was proposed for the alternate canopy system design, as the current system is adequate to provide defogging whenever it is required. Upon defog activation, most of the air being delivered to the cockpit for air conditioning is diverted to defogging through the 10 slots on either side of the forward canopy. For the first three minutes of operation the air is heated to 158°F and then reverts back to the temperature required by the cockpit. Figure 22 shows the inner surface temperature, with defog activated at the top of descent, as a function of time during descent. Figure 23 shows the heat up of the inner surface if the defog is activated on an aircraft which has been ground soaked at -65°F. Initial cockpit temperature is assumed at -20°F.

Thermal Expansion

An investigation was made to determine the thermal elongation of a laminated F-16 canopy. The differential is based on a 90-inch long canopy from front to back. This analysis was used to determine what allowance must be made at the

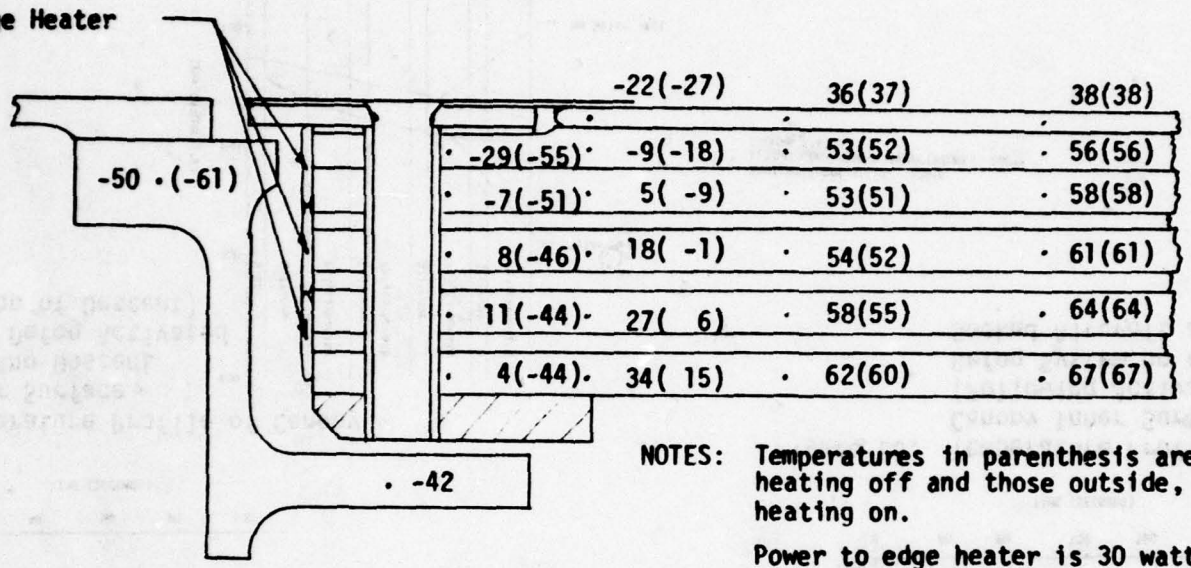


Figure 21 - Temperature at Edge of Polycarbonate Windshield with and without Edge Heating

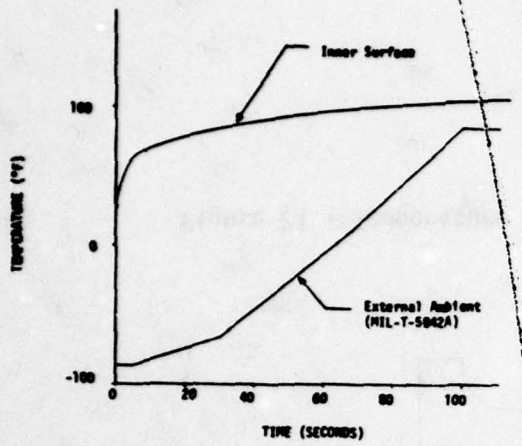


Figure 22. Temperature Profile of Canopy Inner Surface (During Descent With Defog Activated at Top of Descent).

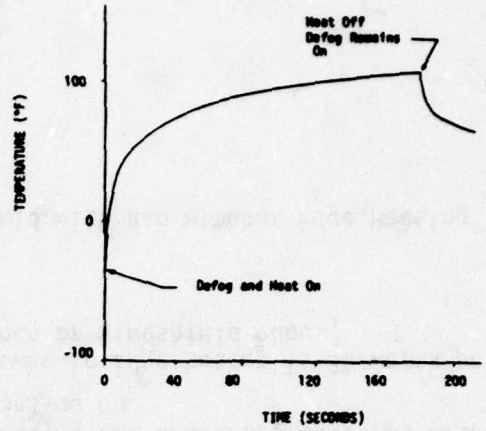
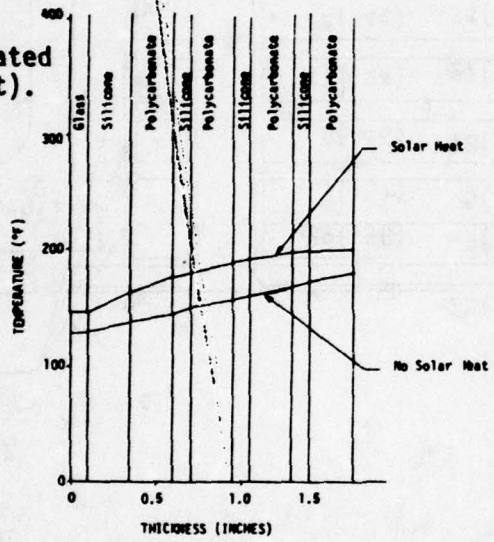


Figure 23. Temperature Profile of Canopy Inner Surface (Following Activation of the Defog System on a Cold Soaked Aircraft at -65°F).



AMBIENT TEMPERATURE: 120°F
FLIGHT COMPARTMENT TEMPERATURE: 200°F
GROUND STATIC

Figure 24. Temperature Distribution for Four-Ply Polycarbonate Windshield with and without Solar Heat.

canopy edge for thermal growth of the outer acrylic ply. Due to the F-16 maximum and minimum temperatures, the allowance at the edge was determined to be 0.33 inch. The minimum thickness of the interlayer was also determined by increasing the thickness so that the interlayer shear strain was not exceeded due to thermal expansion.

Thermal Nuclear Effects

The windshield, when exposed to the heating of a blast, as defined in B-1 Specification L190C2015A, is not adversely affected. This is based on the assumption that 50 percent of the incident thermal energy is absorbed equally among the various plies of the windshield. The windshield temperatures will increase less than 50°F for a windshield initially at 130°F.

Solar Heating Effects

Figure 24 shows the temperature distribution through a four-ply poly-carbonate windshield with CIP silicone interlayers. The two curves show the temperatures both with and without solar heat on a 120°F day with a 200°F flight compartment temperature. It also assumes that 30 percent of the solar energy is absorbed equally through out the windshield. The solar energy incident is assumed to be 360 BTU/hr-ft .

Rain Removal Systems

The B-1 rain removal system is a jet-blast in conjunction with an inflight applied rain repellant system. This is the original design by Rockwell. This system meets the requirements of MIL-E-38453A. Other methods of rain removal were not compatible with the B-1.

The rain removal system for the F-16 consists of ground applied rain repellant. This was selected because windshield wipers and jet blast in conjunction with rain repellant was not compatible with an acrylic or polycarbonate face sheet. The canopy is also easily accessible on the ground.

Hail Protection

Experience has shown that there is very little hail damage with 0.188 inch soda lime glass face sheets. In the event of failure there is still sufficient visibility to complete the mission. This is not true for thinner glass sheets, especially 0.050 chemically strengthened glass. Triplex Glass Company studies have shown that the 0.119 inch chemically tempered glass is equivalent to the 0.188 inch soda lime glass. This information was used in selecting the face sheet for the B-1 windshield. The as-cast acrylic and stretched acrylic face plies are more ductile and thus more hail resistant and therefore thinner face plies are acceptable.

EVALUATION OF WINDSHIELD MATERIALS SUBJECTED TO SIMULATED SUPERSONIC FLIGHT ENVIRONMENTS

J. B. Hoffman
Douglas Aircraft Company
McDonnell Douglas Corporation
Long Beach, California

PRECEDING PAGE BLANK-NOT FILMED

EVALUATION OF WINDSHIELD MATERIALS SUBJECTED TO SIMULATED SUPERSONIC FLIGHT ENVIRONMENTS

by

J. B. HOFFMAN

Douglas Aircraft Company
Long Beach, California

ABSTRACT

The performance of various transparent materials for potential use in the design of aircraft windshields was determined by subjecting test specimens to supersonic Mach number conditions in a wind tunnel.

Flight conditions corresponding to Mach numbers 1.6, 2.0 and 2.2 were simulated.

The test procedure and test results for this program are reported fully in AFFDL-TR-77-92, Reference 1.

PRECEDING PAGE BLANK-NOT FILMED

INTRODUCTION

Relatively short exposure to rain and ice crystal abrasion precipitated erosion of the exterior surface coating used to protect the polycarbonate canopy on the YF-16 prototype aircraft. Similar experience on the F-111F and F-15 canopies substantiated the necessity of further development to provide improvements in protecting polycarbonate from the environment.

The configuration selected to provide optimum erosion resistance and high optical quality for current Air Force inventory aircraft and for application to future aircraft windshield designs was a three-ply laminated transparency which consisted of an acrylic outer ply and a polycarbonate structural ply separated by a soft interlayer.

This report describes a wind tunnel test initiated to obtain comparative performance, reliability and capability information for the laminated design as well as for currently used stretched acrylics and exterior protective coatings on polycarbonate. The program was expanded to test edge member concepts for glass face ply designs and precipitation-static coatings on glass in order to determine the effect of the high speed environment on the edge materials and to investigate degradation of the P-static coating.

A realistic flight environment based on current Air Force supersonic aircraft operating conditions at Mach 1.6, 2.0 and 2.2 was used to calculate the wind tunnel test environment. The 7.4 x 11.4 inch flat test specimens were supported in the wind tunnel by an enclosure designed to permit simulation of realistic cockpit temperatures and pressures. A camera was mounted in the tunnel wall to view the specimens through the normal aircrew viewing angle to monitor the windshield optical distortion that would be observed during flight.

The goals of this test program were to determine face-ply material reliability for selected materials; to ascertain what effect the aircraft operational environment would have on the optics of the transparent materials; to evaluate the performance of two specific edge designs and the use of a precipitation static coating on glass when subjected to a high speed environment. These goals were to be achieved by simulating the operational environment of current Air Force supersonic aircraft in inventory.

The goals of this program were accomplished in a modified tunnel test environment when it became necessary to revise the test conditions to be compatible with the tunnel capability.

An appraisal was made of the materials at the revised conditions and an evaluation of in-tunnel optical distortion and permanent optical distortion was performed. Pre-test and post-test light transmission and haze data were compared. A limited assessment was achieved for the edge designs. The precipitation static glass face ply coating was not evaluated.

This test series was completed in three days in the Hypersonic Wind Tunnel (B) at the Von Karman Gas Dynamics Facility (VKF) located at the Arnold Engineering Development Center (AEDC), Tennessee.

Reference 2 was the final report prepared by the ARO, Inc., for this program.

A previous experimental investigation, Reference 3, provided a valuable source of information for this program.

TEST DESCRIPTION

Facility

These tests were conducted in the Hypersonic Wind Tunnel (B) of the Von Karman Gas Dynamics Facility (VKF). Tunnel B, Figure 1, is a continuous, closed-circuit, variable density wind tunnel with an axisymmetric contoured nozzle and a 50-inch diameter test section. The tunnel can be operated at a nominal Mach number of 6 and 8 at stagnation pressures from 20 PSIA to 300 PSIA and 50 PSIA to 900 PSIA, respectively, and stagnation temperatures up to 890°F. The model can be injected into the tunnel for a test run and then retracted for model cooling or model changes without interrupting the tunnel flow. A complete description of the tunnel may be found in Reference 4.

Specimens

Table 1 identifies the 22 potential test specimens. All but four were tested.

The test specimens were flat, rectangular in shape, and approximately 1 x 7.4 x 11.4 inches in size, as shown in Figure 2. The specimens were instrumented with high temperature thermocouples. Half of the exterior surface of selected specimens were coated with a rain repellant. Measurements were made to determine the light transmission and haze for each configuration prior to testing. Typical specimens are described in detail in Figure 3 through 6.

Hardware

The test hardware consisted of a cabin simulator, a wedge and an instrumented panel. The test setup is shown in Figure 7.

The purpose of the cabin simulator, Figure 8, was to provide both support for the test specimens and a simulated cabin environment on the back side of the test specimens. A specimen was installed in the simulator by laying the specimen in the top of the box and installing a cover with six bolts. Regulated air at ambient temperature was supplied to the simulator at a constant flow rate and was discharged to the tunnel free stream through vents located on the bottom of the simulator. A silicone rubber seal between the specimen and the support frame prevented air leakage and provided room for thermal expansion. A quartz port in the rear of the simulator, Figure 9, made it possible to photograph through the specimen during the test.

The cabin simulator was attached to a wedge which served as the flow generator and which was used to reduce the wind tunnel free-stream Mach number from 6 to a number consistent with the aircraft windshield environment. The wedge was mounted to the sting. The slope of the front surface of the wedge was varied to meet the Mach number requirements by manipulating the sting.

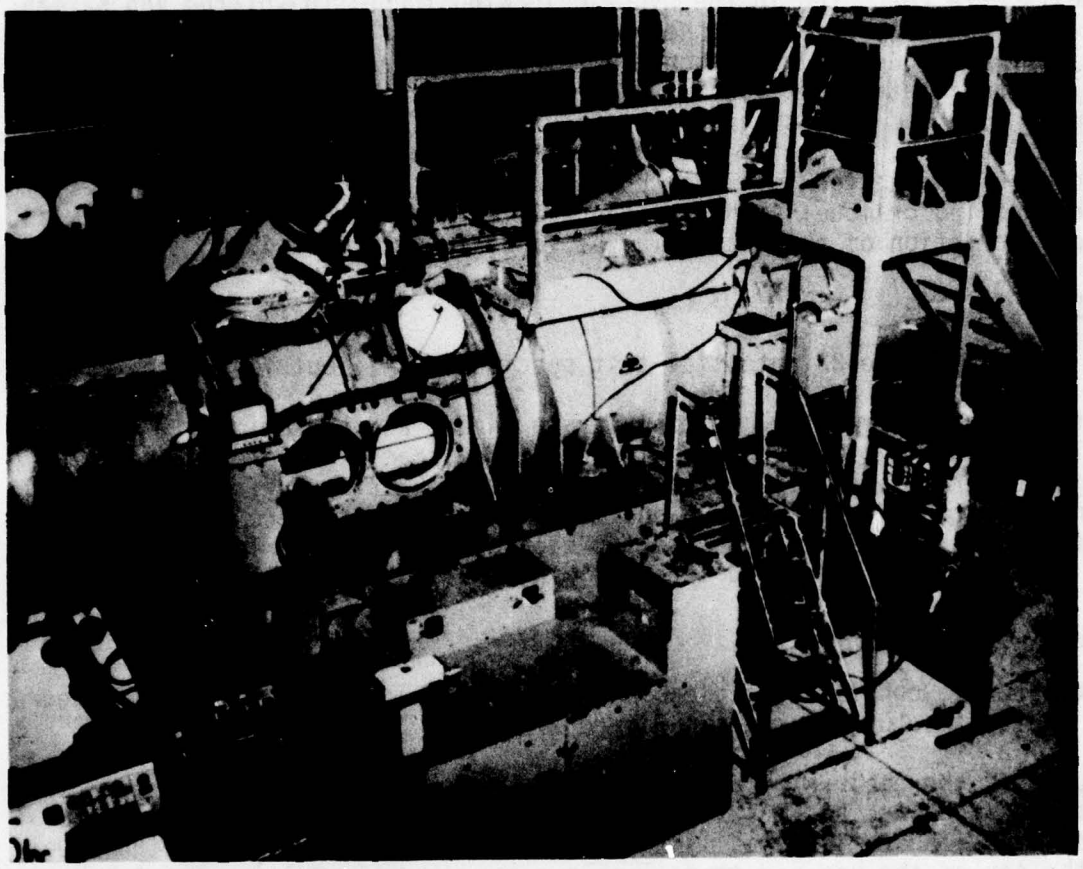


Figure 1. AEDC Hypersonic Wind Tunnel (B)

TABLE 1. TEST SPECIMEN IDENTIFICATION

DAC PART NUMBER	DAC SERIAL NUMBER	VENDOR SERIAL NUMBER	MANUFACTURER	TYPE	THICKNESS OF STRUCTURAL PLY	TOTAL LAMINATE THICKNESS
Z5943260-1	SK01	001	Sierracin	Laminated As-Cast	.50	.68
Z5943260-1	SK02	002	Sierracin	Acrylic/Interlayer	.50	.68
Z5943260-1	SK03	003	Sierracin	Polycarbonate	.50	.68
Z5943260-501	SK04	001	Sierracin		.62	.80
Z5943260-501	*SK05	002	Sierracin		.62	.80
Z5943260-501	*SK06	003	Sierracin		.62	.80
Z5943260-505	SK10	001	Sierracin	Coated Monolithic	.50	
Z5943260-505	*SK11	002	Sierracin	Polycarbonate	.50	
Z5943260-505	*SK12	003	Sierracin		.50	
Z5943260-507	SK13	001	Sierracin		.62	
Z5943260-507	SK14	002	Sierracin		.62	
Z5943260-507	SK15	003	Sierracin		.62	
Z5943260-517	SK16		Sierracin	Stretched Acrylic	.90	
Z5943260-517	SK17		Sierracin		.90	
Z5943260-517	SK18		Sierracin		.90	
Z5943260-513	PPG01		PPG	Glass/Interlayer	.50	.860
Z5943260-515	SWU01		Swedlow	Polycarbonate	.50	.868
Z5943260-519	GY01		Goodyear	Laminated	.25 (Two Ply)	.698
Z5943260-521	GY02		Goodyear	Polycarbonate	.25 (Two Ply)	.692
Z5943260-523	GY03		Goodyear		.25 (Two Ply)	.785
Z5943260-525	GY04		Goodyear		.25 (Two Ply)	.813
Z5943260-527	GY05		Goodyear		.25 (Two Ply)	.777

*Were not tested.

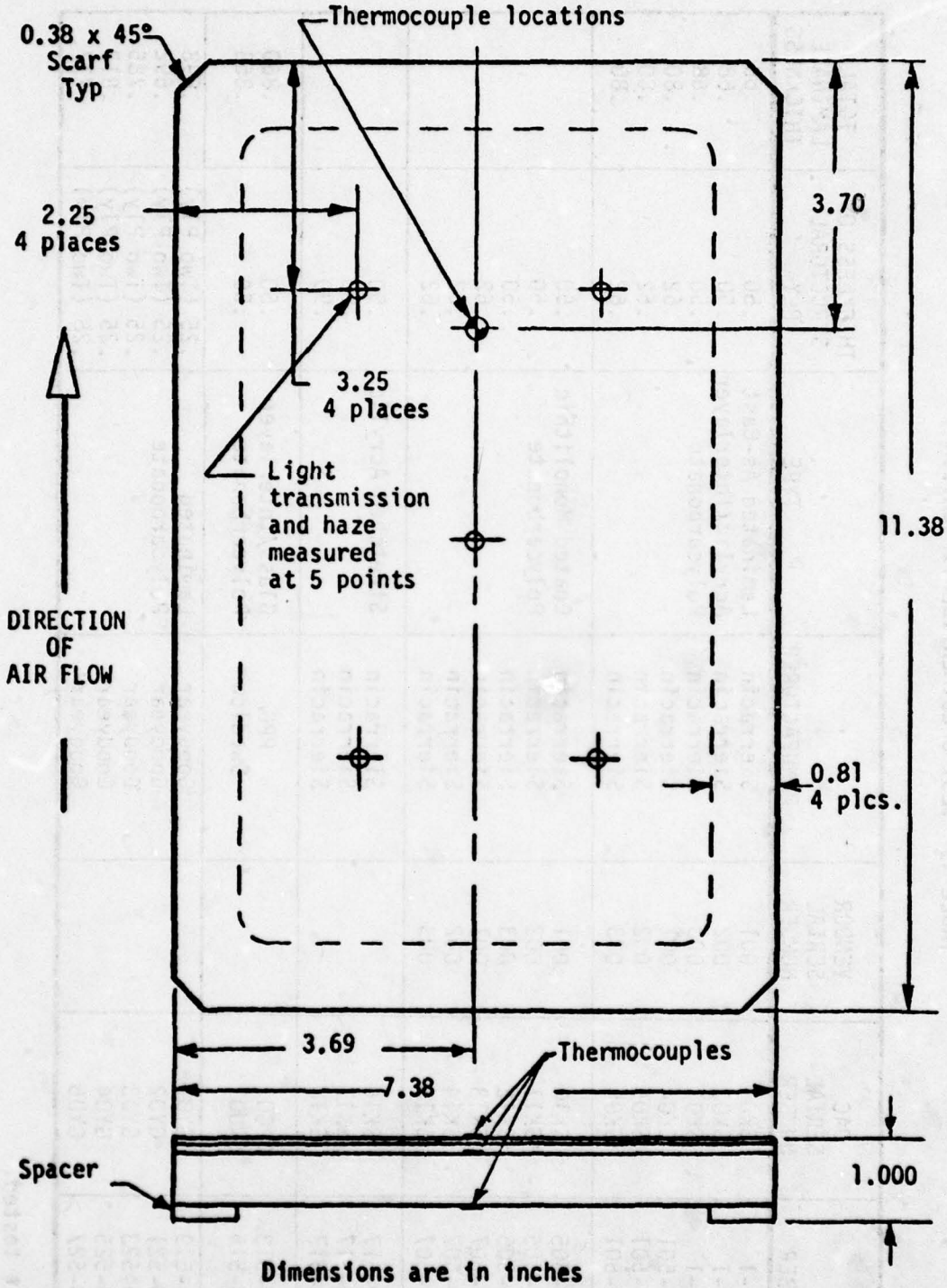
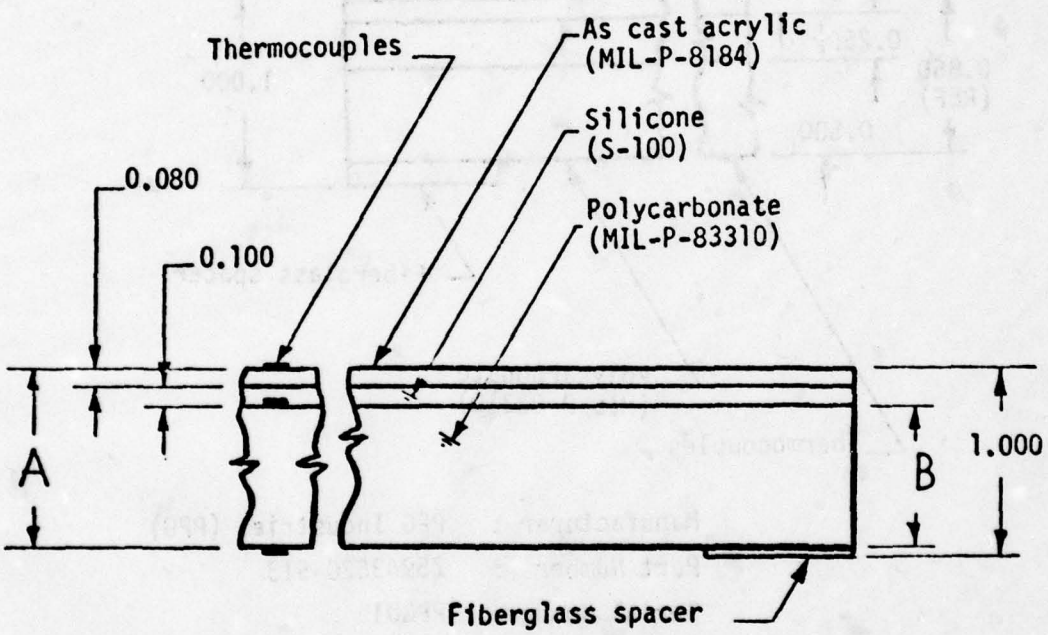


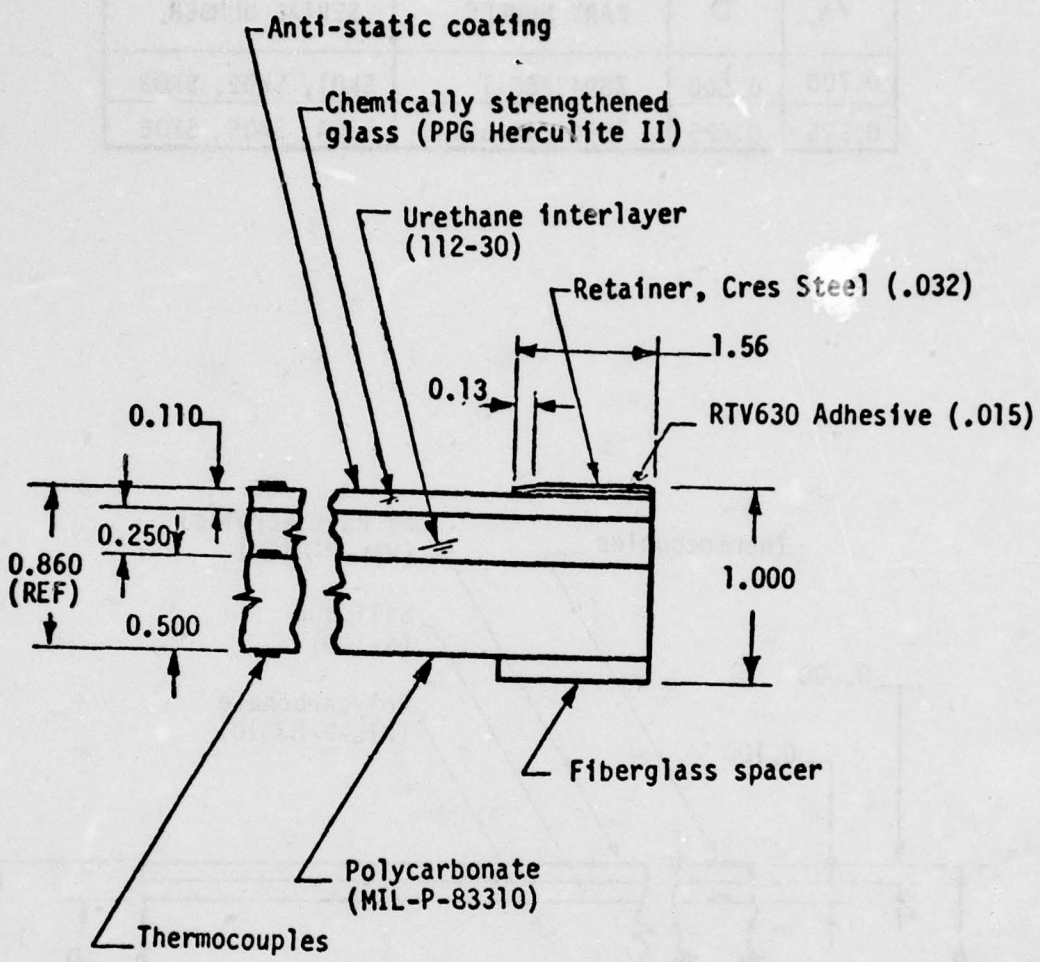
Figure 2. Windshield Test Specimen - General Outline.

A	B	PART NUMBER	SERIAL NUMBER
0.700	0.500	Z5943260-1	SK01, SK02, SK03
0.825	0.625	Z5943260-501	SJ04, SK05, SK06



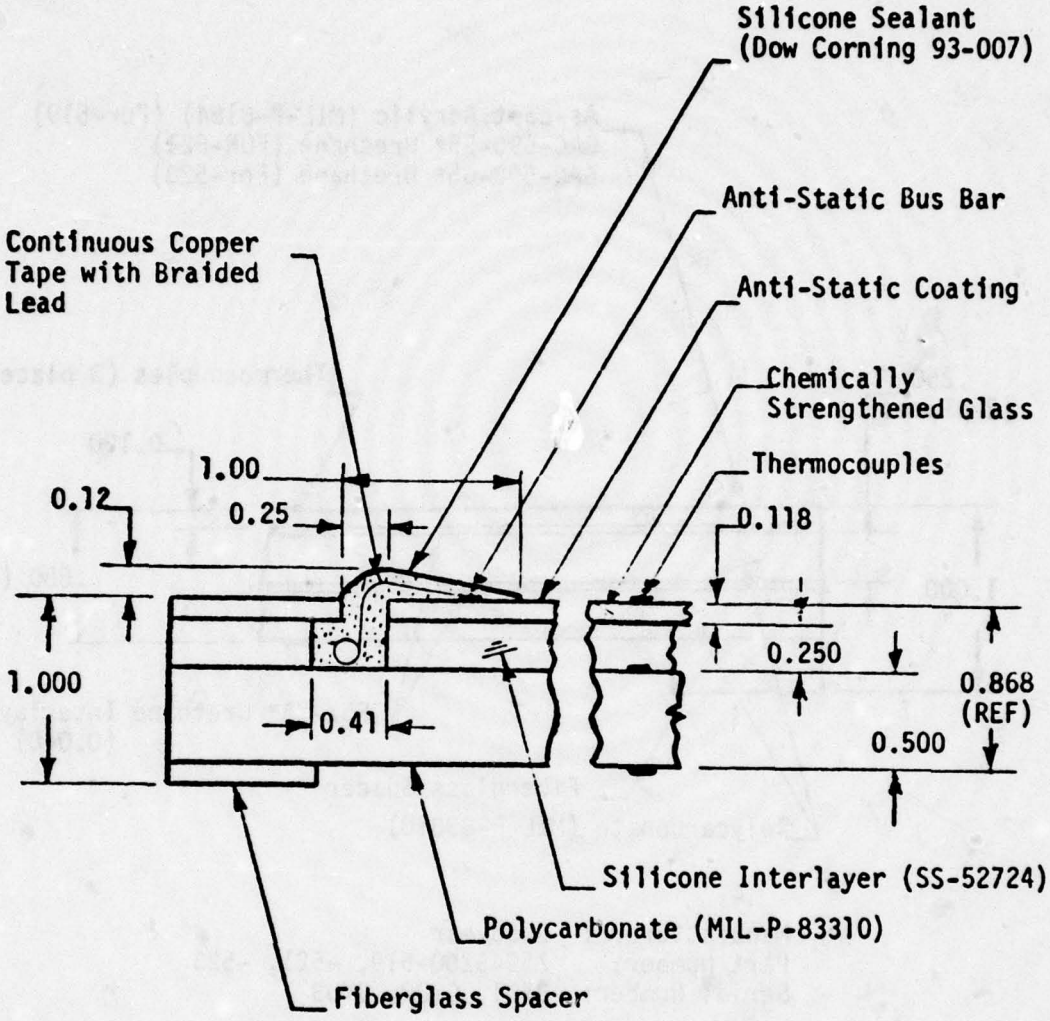
Manufacturer: Sierracin Corporation (SK)
Dimensions are nominal and in inches

Figure 3. Laminated Test Specimen.



Manufacturer : PPG Industries (PPG)
Part Number : Z5943620-513
Serial Number: PPG01
Dimensions are nominal and in inches.

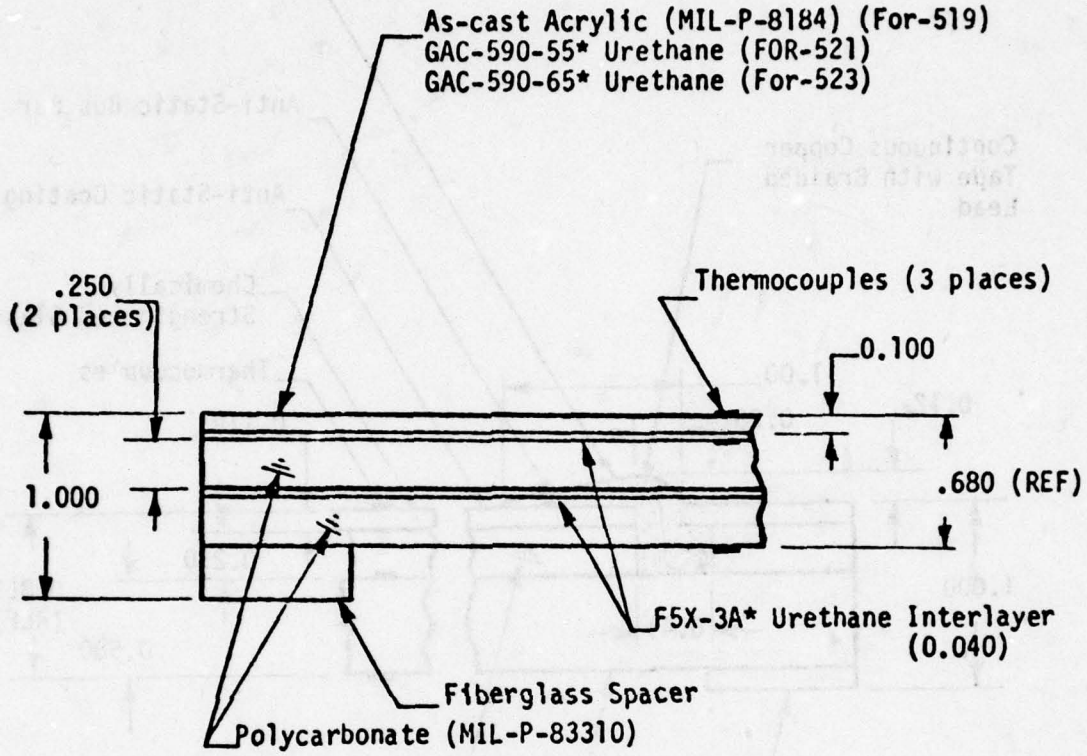
Figure 4. Glass Face Ply Test Specimen.



Manufacturer : Swedlow (SWU)
Part Number : Z5943260-515
Serial Number: SWU01

Dimensions are nominal and in inches

Figure 5. Glass Face Ply Test Specimen.



Manufacturer : Goodyear
Part Number: Z5943260-519, -521, -523
Serial Number: GY01, GY02, GY03

Dimensions are nominal and in inches

GAC-590-65 Urethane is more castable than GAC-590-55 Urethane

*Goodyear Aerospace

Figure 6. Laminated Test Specimen.

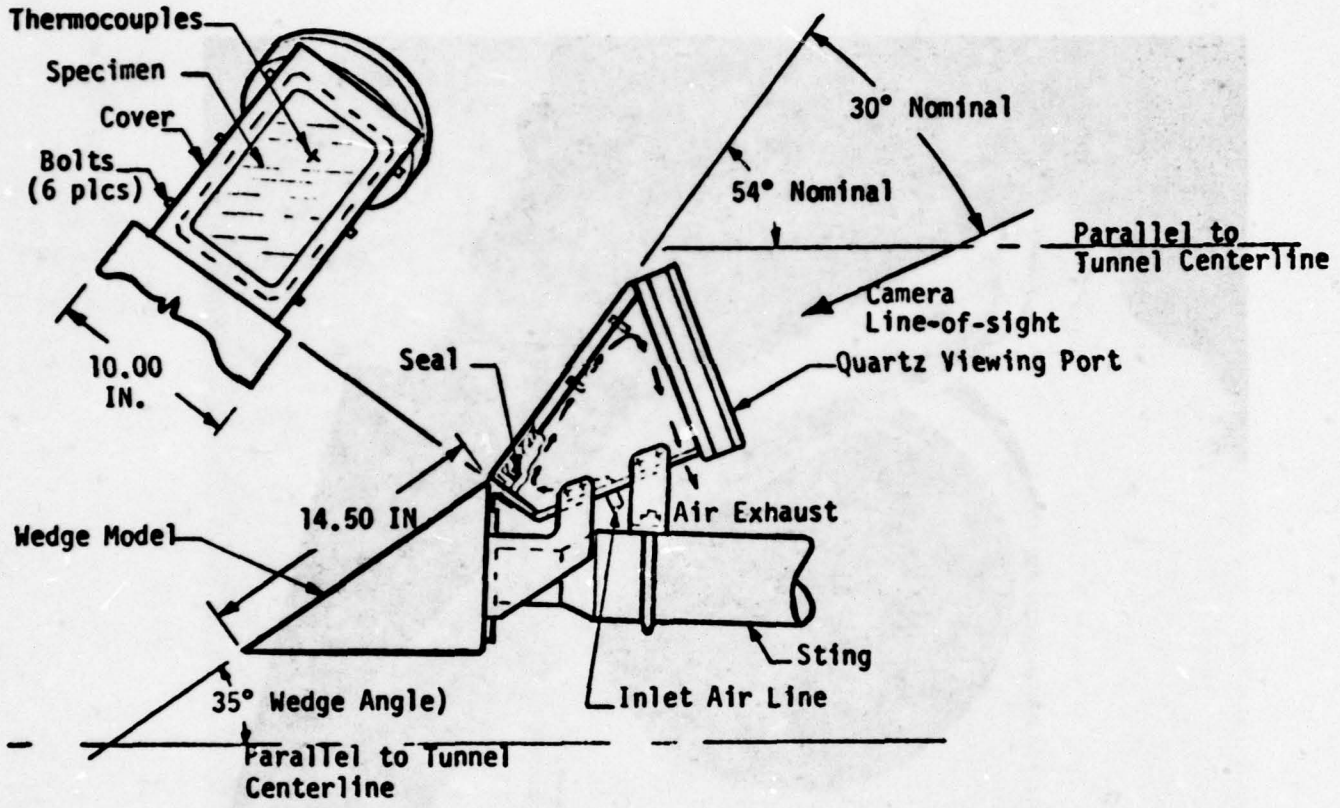


Figure 7. Cabin Simulator and Wedge Model Attached to Sting.
(Angles are for Mach 2.2 Simulation)

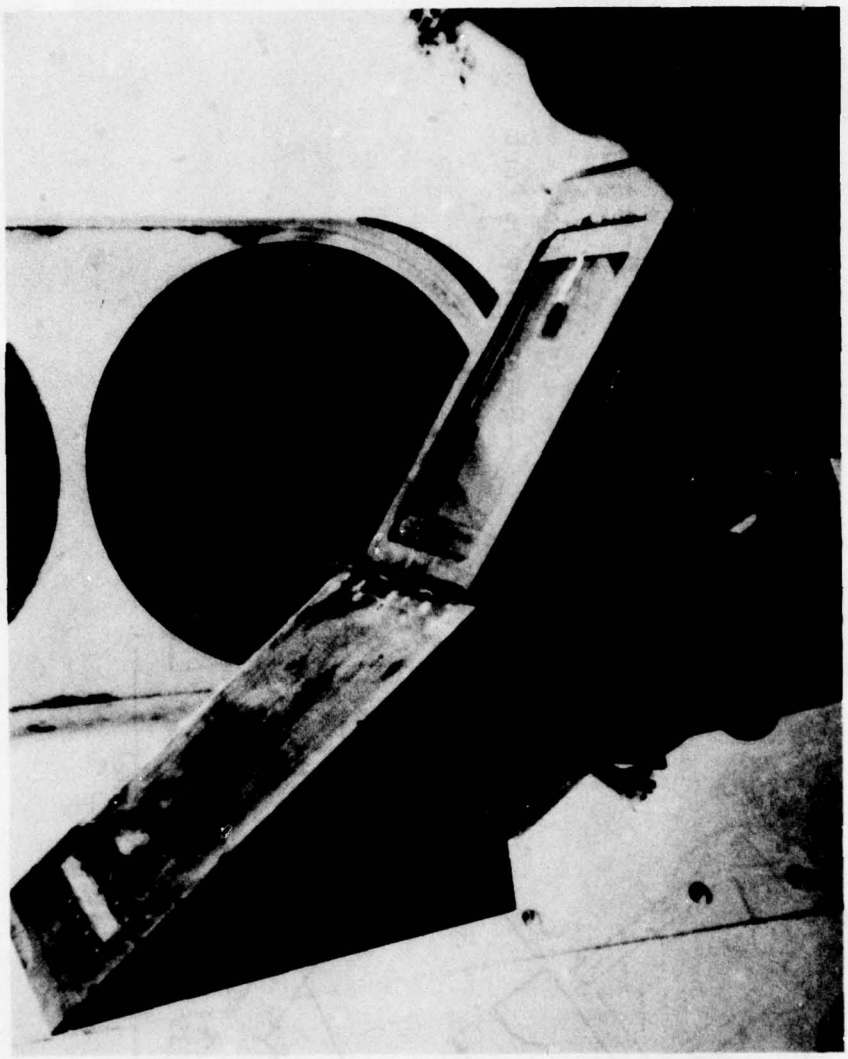


Figure 8. Cabin Simulator and Wedge Model Assembly.

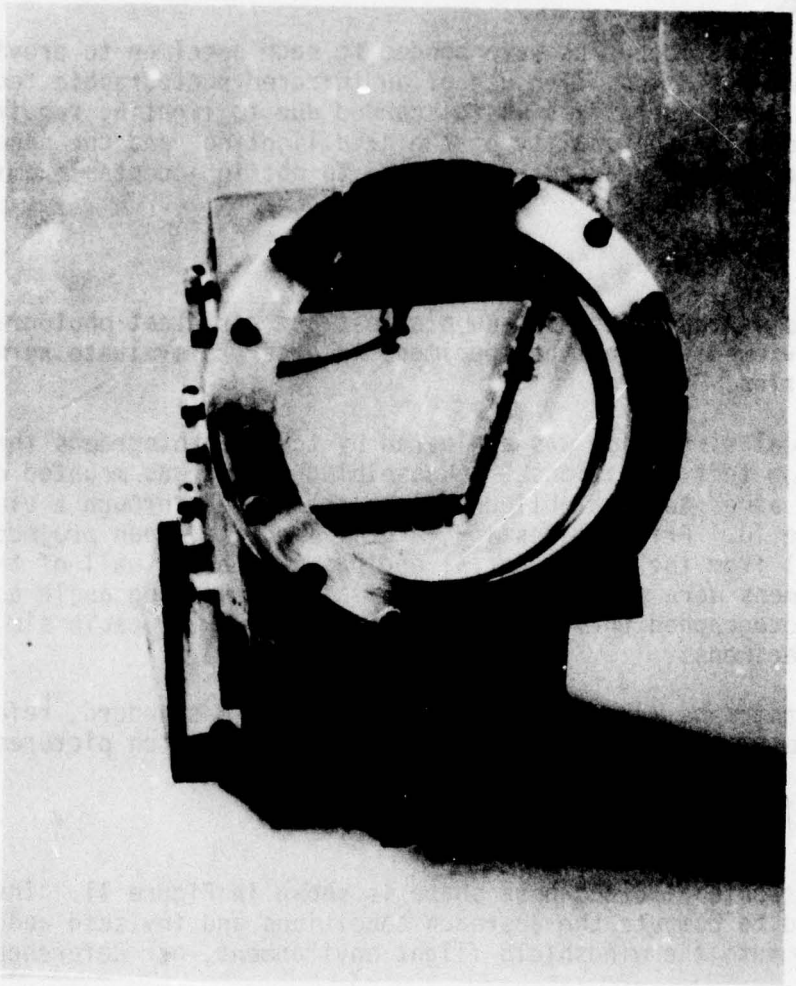


Figure 9. View Through Cabin Simulator Quartz Window.

An instrumented panel was used to determine the heat transfer rate and pressure distribution on the outboard surface of the test specimens. This steel panel had the same planform dimensions as the test specimens. There were 15 pressure orifices and 11 heat-transfer-rate Gardon gages located on the panel surface.

Instrumentation

High temperature thermocouples were bonded to each specimen to provide temperature-time histories. The use of an infrared photographic technique to monitor surface temperatures was discarded due to lighting requirements which interfered with the quality of the grid lighting, and the necessity of coating the specimen with an opaque coating to obtain acceptable emissivity characteristics.

Photography

A Hasselblad camera was used to take pre-test and post-test photographs of a grid board as viewed through the specimens in order to evaluate permanent optical distortion.

In-tunnel optical distortion was evaluated by taking photographs through the specimens during test operations. A Hasselblad camera was mounted outside the tunnel and aimed to look obliquely into the tunnel through a viewing port, shown in Figure 10. Prior to testing, a grid image had been projected onto the tunnel wall from the camera portal and painted on the wall of the tunnel. The test specimens were viewed at a nominal aircrew viewing angle and the grid pattern was photographed through the quartz window in the cabin simulator and through the specimens.

Flow-field photographs were taken periodically with a standard, refocused shadowgraph system, and general coverage 16-mm color motion pictures were also obtained.

Conditions

A typical supersonic aircraft nose shape is shown in Figure 11. Inviscid cone theory was used to compute the approach conditions and inviscid wedge theory was used to compute the windshield flight environment, per Reference 5.

The test environment is shown in Figure 12 for the Mach 2.2 simulation. A two-dimensioned inviscid, oblique-shock solution was assumed to determine the appropriate Mach numbers and pressures to simulate the flight environments. Because of size limitations, a representative approach length of an aircraft nose could not be simulated which resulted in a complex flow field that forced approximations in the test conditions.

The selected flight environment and test environment were calculated for the three conditions. Initially the desired altitudes were 15,000, 25,000 and 36,000 feet, but tunnel capability dictated simulated altitudes of 34,600, 39,200 and 42,200 feet for Mach 1.6, 2.0 and 2.2. During the test the altitude for Mach 1.6 condition was raised to 42,400 feet in order to limit the stagnation temperature to 243°F.

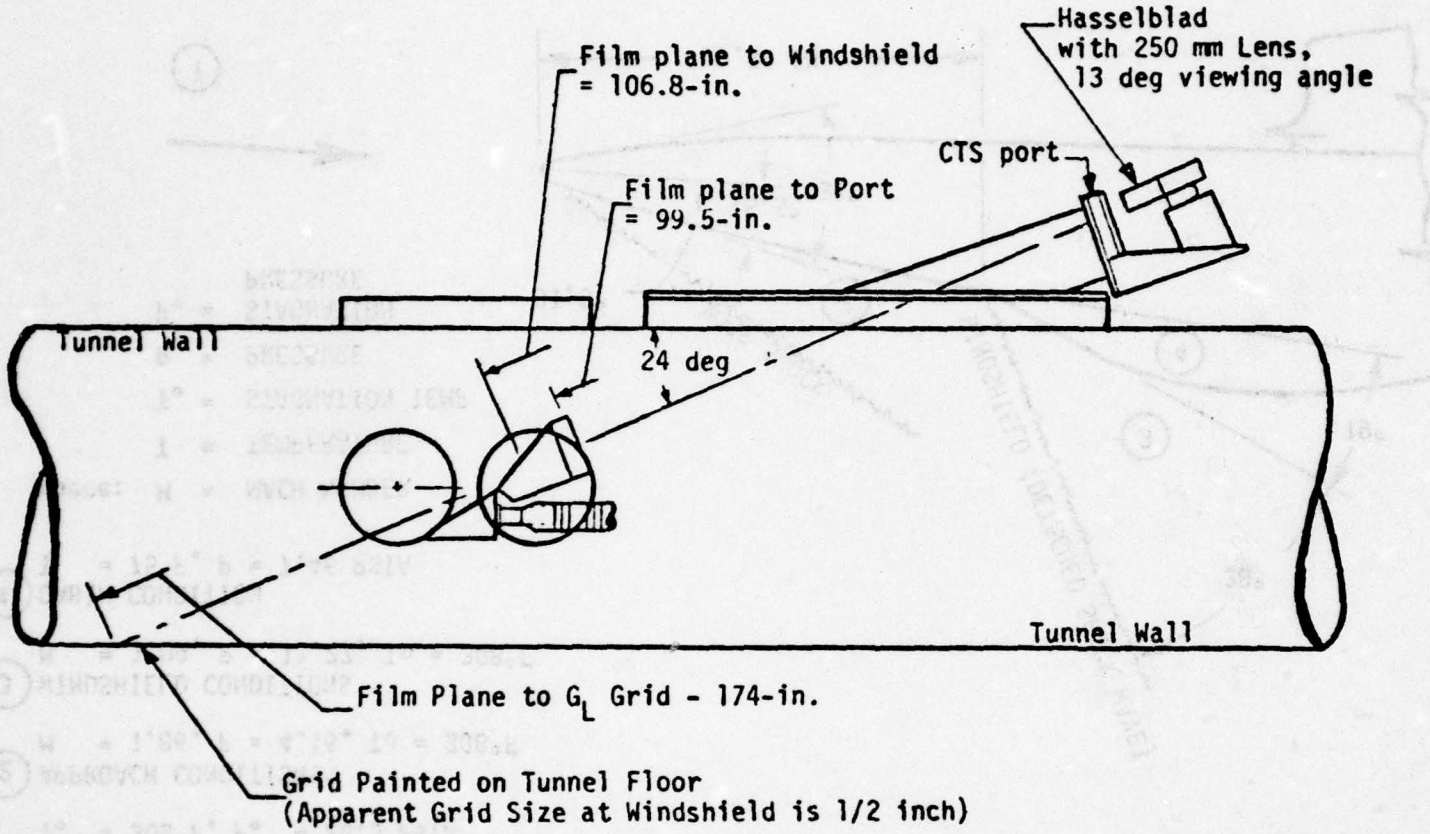


Figure 10. Camera Arrangement for Tunnel Grid Viewing.

FREE-STREAM CONDITIONS

(1) M = 2.2 AT 42,200 FT
T = -70°F, P = 2.46 PSIA
T_o = 308°F, P_o = 26.3 PSIA

(2) APPROACH CONDITIONS
M = 1.86, P = 4.16, To = 308°F

(3) WINDSHIELD CONDITIONS
M = 1.09, P = 11.27, To = 308°F

(4) CABIN CONDITION
T = 75°F, P = 7.46 PSIA

where: M = MACH NUMBER
T = TEMPERATURE
T_o = STAGNATION TEMP
P = PRESSURE
P_o = STAGNATION PRESSURE

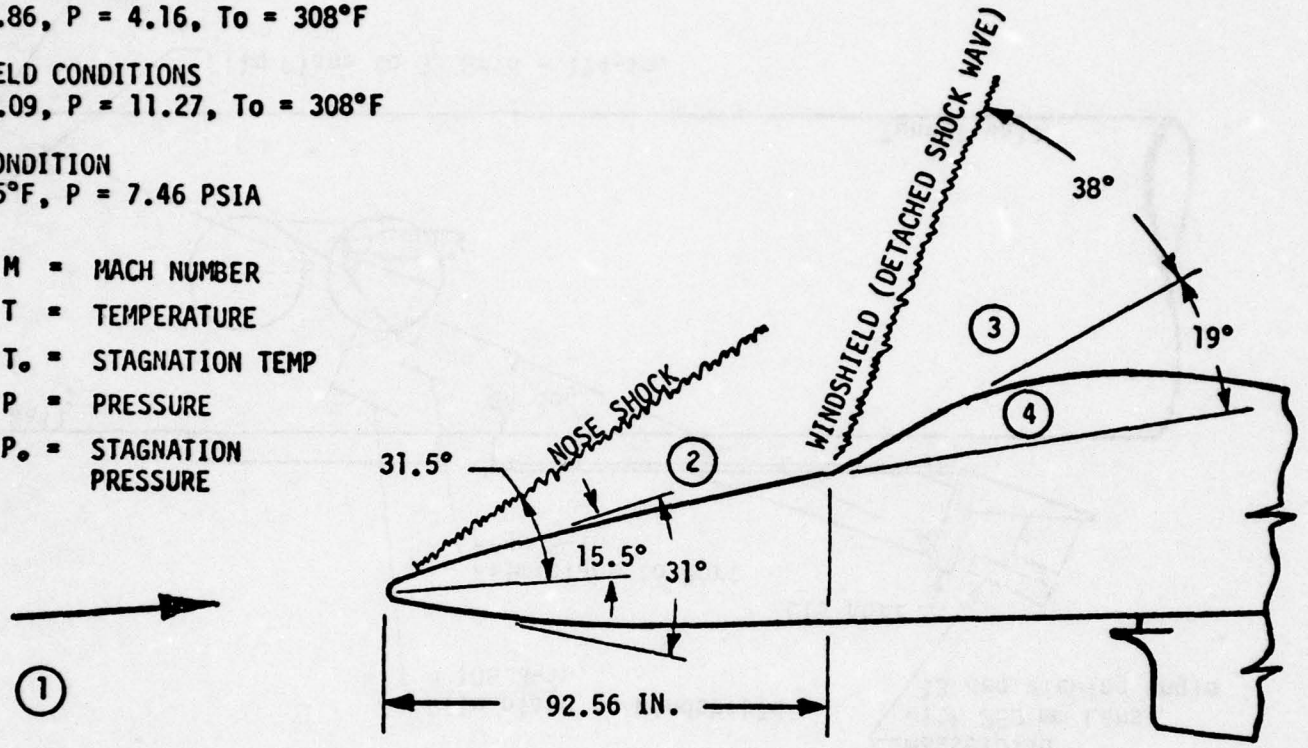


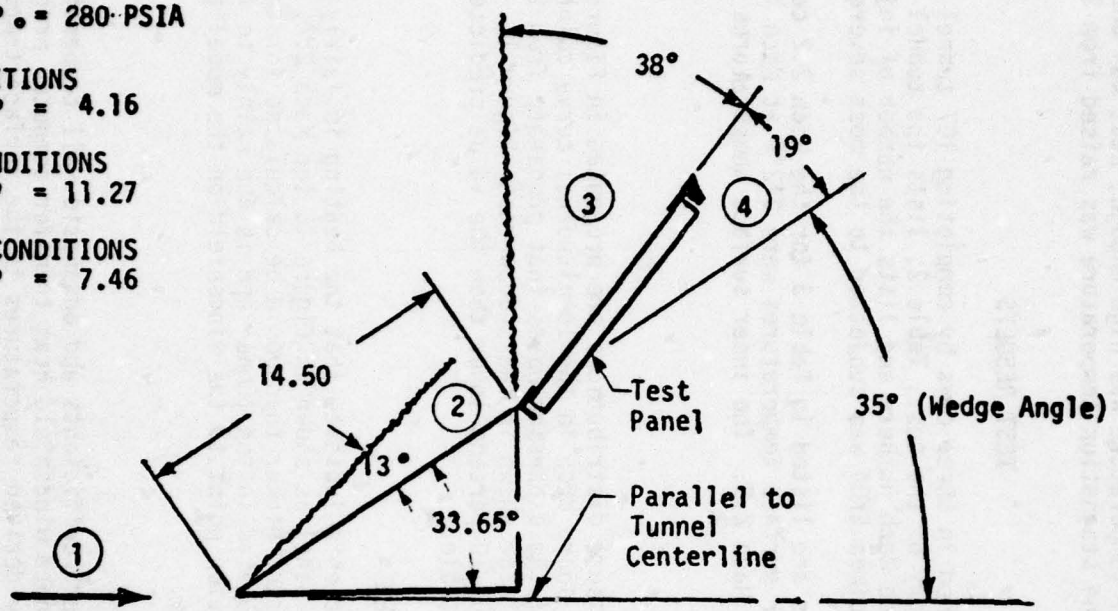
Figure 11. Windshield Flight Environment at Mach 2.2.

① FREE-STREAM CONDITIONS
M = 6
T_o = 308°F, P_o = 280 PSIA

② APPROACH CONDITIONS
M = 1.86, P = 4.16

③ WINDSHIELD CONDITIONS
M = 1.09, P = 11.27

④ INBOARD FACE CONDITIONS
T = 75°F, P = 7.46



where: M = MACH NUMBER
T = TEMPERATURE
T_o = STAGNATION TEMPERATURE
P = PRESSURE
P_o = STAGNATION PRESSURE

Figure 12. Specimen Test Environment at Mach 2.2.

The existence of a detached shock wave precluded the computation of the windshield Mach numbers and ambient pressures for the Mach 1.6 and 2.0 simulations.

The recovery factor that was to be simulated was 95 percent. To assure that the actual adiabatic wall temperature was high enough, heat was added to the Mach 2.2 condition and the stagnation temperature was raised from 308°F to 328°F.

TEST RESULTS

The tests were accomplished in three days by completing 107 tunnel injections on 18 specimens. A summary of the test, Table 2, lists the tunnel time for each specimen at the three Mach numbers and lists the number of injections for each condition. Specimen SK04 was subjected to the most severe environment.

The specimen temperatures are listed in Table 3 for the Mach 2.2 condition. The average maximum outer surface temperatures were 212°F at Mach 1.6, 255°F at Mach 2.0 and 272°F at Mach 2.2. The inner surface temperatures varied from 77°F to 134°F.

Pressure Distribution

The measured surface pressure distributions are presented in Figure 13 for the Mach 2.2 condition. The sharp drop in the longitudinal curve coincides with the intersection point of the expansion waves that propagate from the front corner of the cabin simulator shown in the shadowgraph, Figure 14. The maximum measured pressure is about 10 percent lower than the value predicted by inviscid flow theory and is acceptable.

Heat Transfer Distribution

The heat transfer coefficients indicate that the heating is fairly unfirom over the outer surface of the panel as shown in Figure 15 for Mach 2.2. The values are approximately 65 percent higher than would be calculated for the flight conditions that were simulated in the tunnel and is due mainly to the shorter distance from the stagnation point to the windshield on the model than on the aircraft.

Temperature Correlation

The measured heat transfer coefficients and adiabatic wall temperatures were fed thru a Douglas developed windshield heat transfer computer program to correlate the emperically derived temperatures to the surface temperatures that were measured. The correlation was acceptable at Mach 1.6 (<2% difference), but at Mach 2.2, Figure 16, the difference increased to 9% for the surface ply.

Radiation accounted for approximately 4°F. The remaining discrepancy could be the result of inaccurate physical property data or errors in testing.

SPECIMEN EVALUATION

A test specimen evaluation was made by comparing the change in light transmission and haze, appraising in-tunnel optical distortion and permanent distortion, and documenting physical changes to the specimens.

TABLE 2. TUNNEL TIME IN MINUTES AND NUMBER OF INJECTIONS

SPECIMEN	MACH 1.6 (Min. - Inj.)	MACH 2.0 (Min. - Inj.)	MACH 2.2 (Min. - Inj.)	TOTAL TIME (MINUTES)
SK01	30 - 3			30
SK04	20 - 2	40 - 7	40 - 7	100 (Max)
SK13	30 - 3			30
SK16	30 - 3			30
GY02	30 - 3			30
PPG01	30 - 3	8 (2) - 2		38
SWU01	10 (1) - 1			10 (Min)
GY03	10 - 1	40 - 7	10 - 1	60
SK02		41 - 8		41
SK14		40 - 7		40
SK17		37 (3) - 7		37
GY05		40 - 7		40
GY01		20 - 3	10 - 1	30
SK03			40 - 7	40
SK15			37 - 7	37
SK18			30 - 6	30
GY04			40 - 7	40
SK10			25 - 4	25
TOTAL TUNNEL TIME (4)	3.2 hrs.	4.4 hrs.	3.9 hrs.	11.5 hrs.

NOTES: (1) Face ply cracked after retraction.
(2) Face ply cracked in tunnel.
(3) Lost cabin pressure on second injection.
(4) Instrumented panel injection consumed 4 hours.
The average time between injections was 7 minutes.
The average time to change a specimen was 15 minutes.

TABLE 3. MAXIMUM SPECIMEN TEMPERATURES (MACH 2.2)

SPECIMEN NUMBER	THERMOCOUPLE LOCATION	TEMPERATURE (DEGREES FAHRENHEIT)						
		1	2	3	4	5	6	7
SK04	Outside	(1)						
	Interlayer	204	218	220	223	222	220	233
	Inside	83	92	94	93	96	94	102
GY03	Outside	273						
	Interlayer	217						
	Inside	102						
GY01	Outside	274						
	Interlayer	224						
	Inside	106						
SK03	Outside	266	268	270	271	271	272	
	Interlayer	195	202	204	202	205	217	
	Inside	91	93	100	99	101	109	
SK15	Outside	269	270	235	270	271	273	275
	Inside	95	106	100	99	116	112	134
SK18	Outside	270	272	272	(2)			
	Inside	88	104	110	81	90	95	
GY04	Outside	270	272	272	272	272	272	274
	Interlayer	166	188	194	195	195	195	205
	Inside	86	97	100	102	102	102	104
SK10	Outside	267	269	269	271			
	Inside	97	105	107	115			

NOTES:

(1) Thermocouple Missing
(2) Thermocouple peeled off

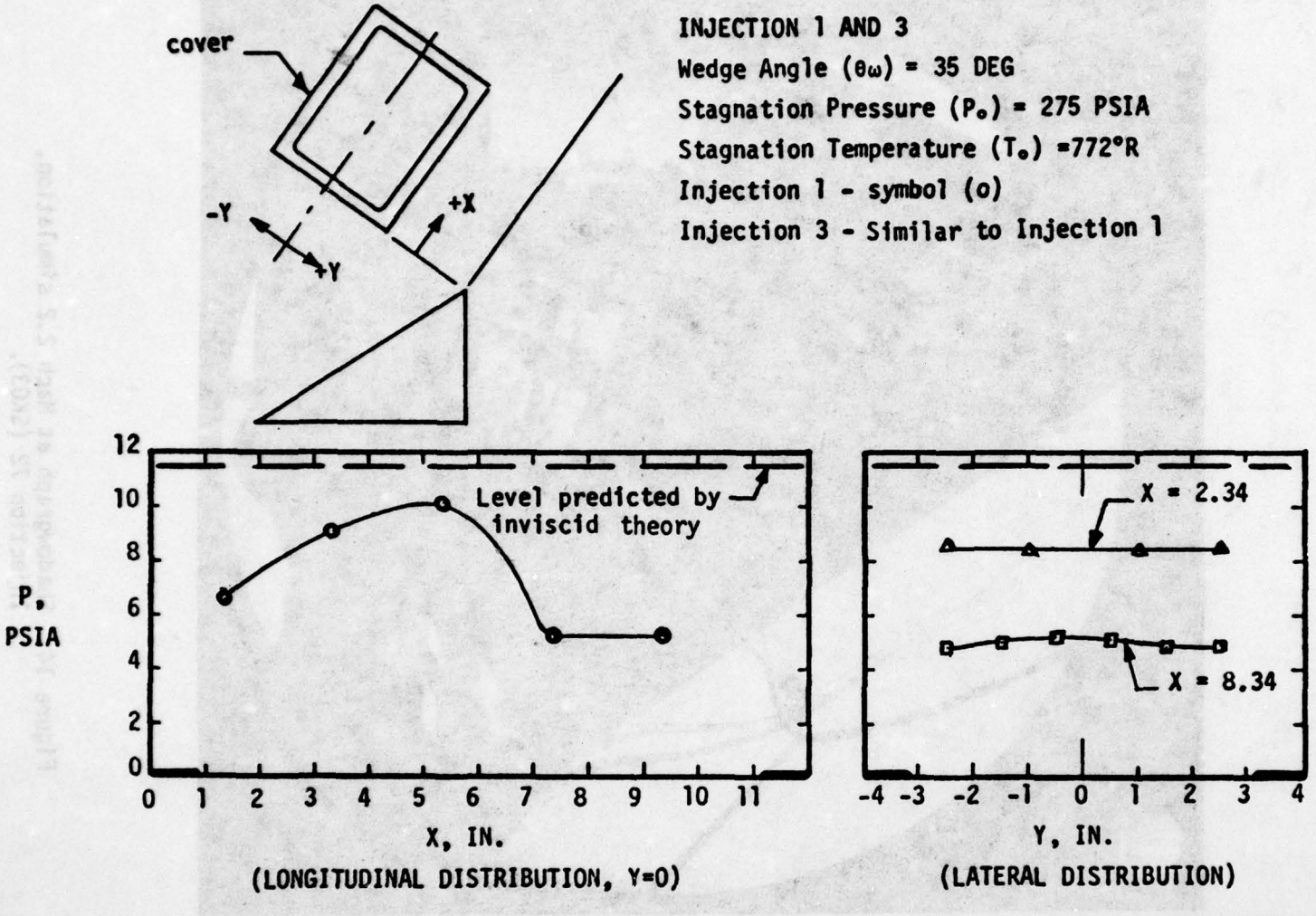


Figure 13. Specimen Pressure Distribution, Mach 2.2 Simulation.

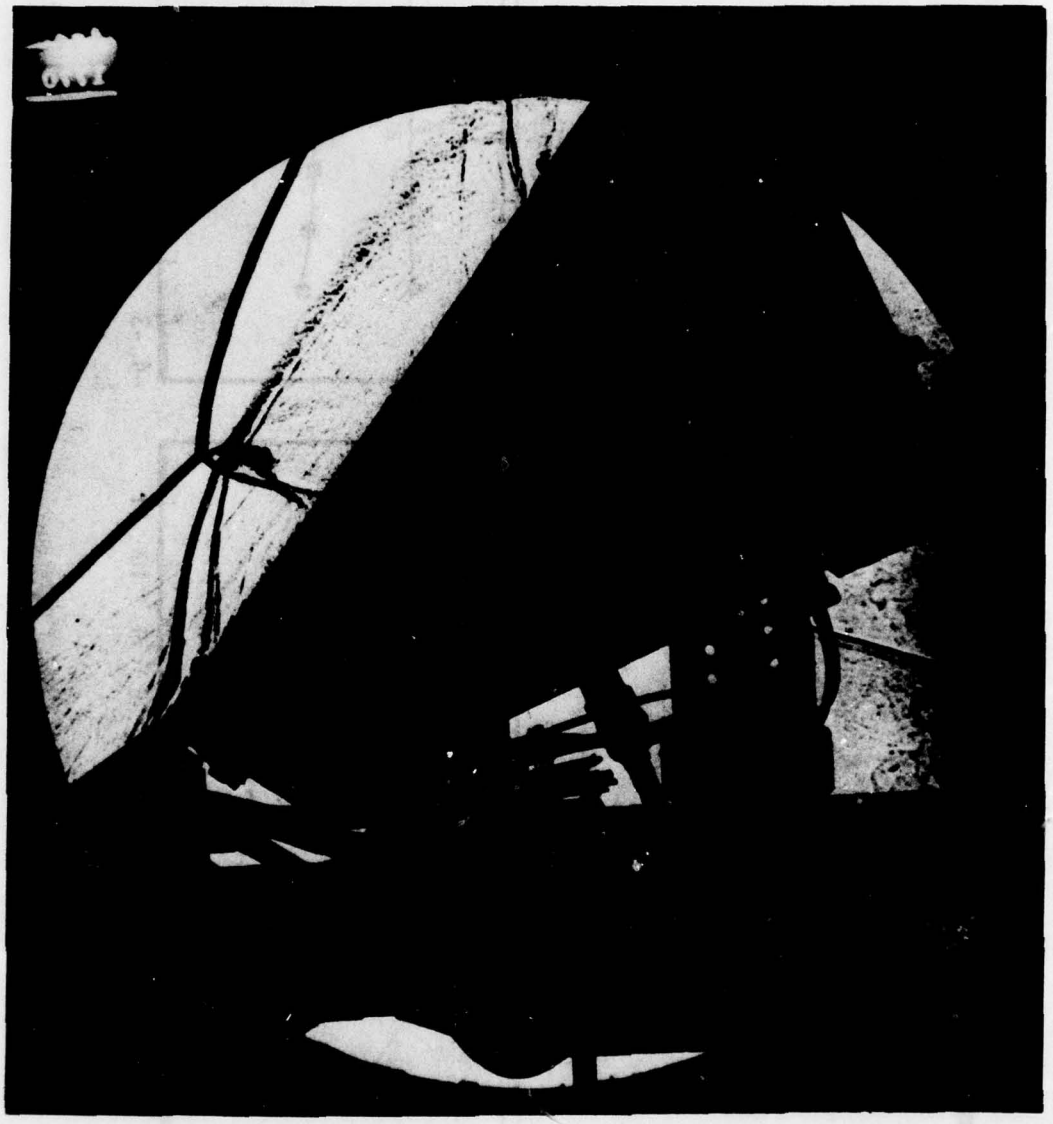
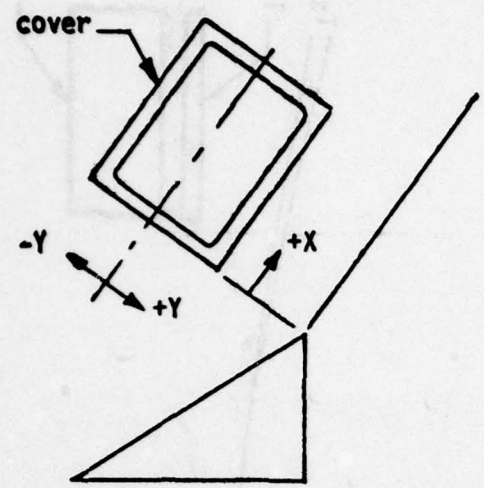


Figure 14. Shadowgraph at Mach 2.2 simulation, Injection 72 (SK03).



INJECTION 1 AND 3
Wedge Angle ($\theta\omega$) = 35 Deg.
Stagnation Pressure (P_o) = 275 PSIA
Stagnation Temperature (T_o) = 772°R
Injection 1 - Symbol (o)
Injection 3 - Symbol (●)

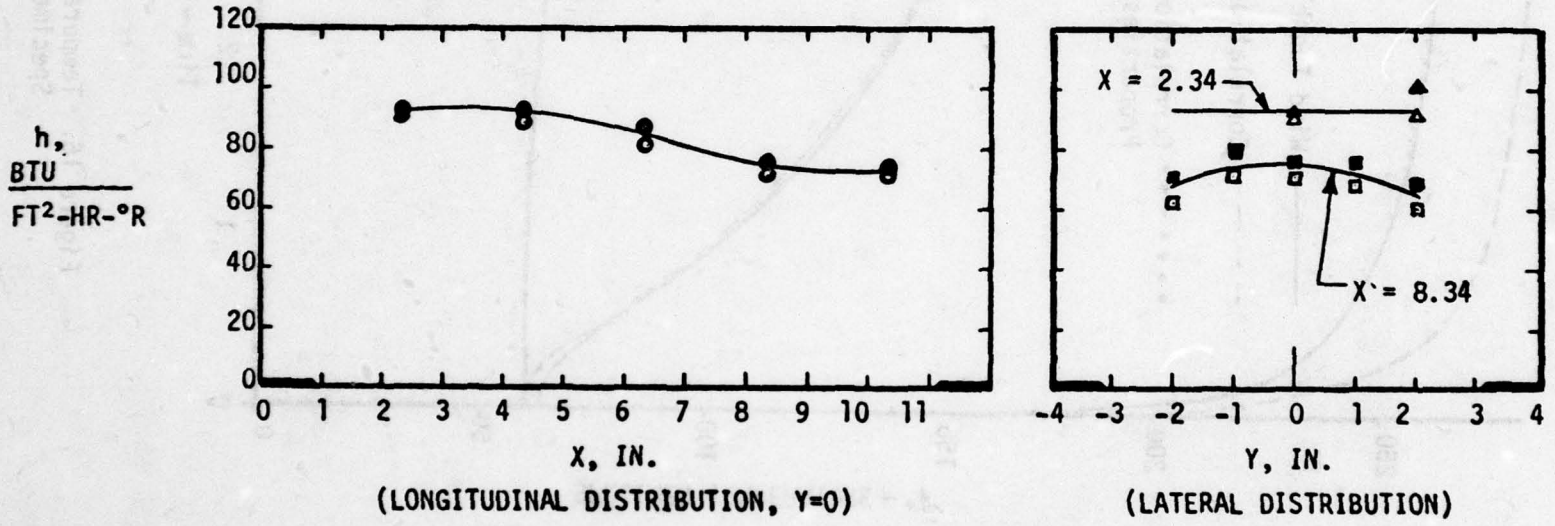


Figure 15. Specimen Heat Transfer Distribution, Mach 2.2 Simulation.

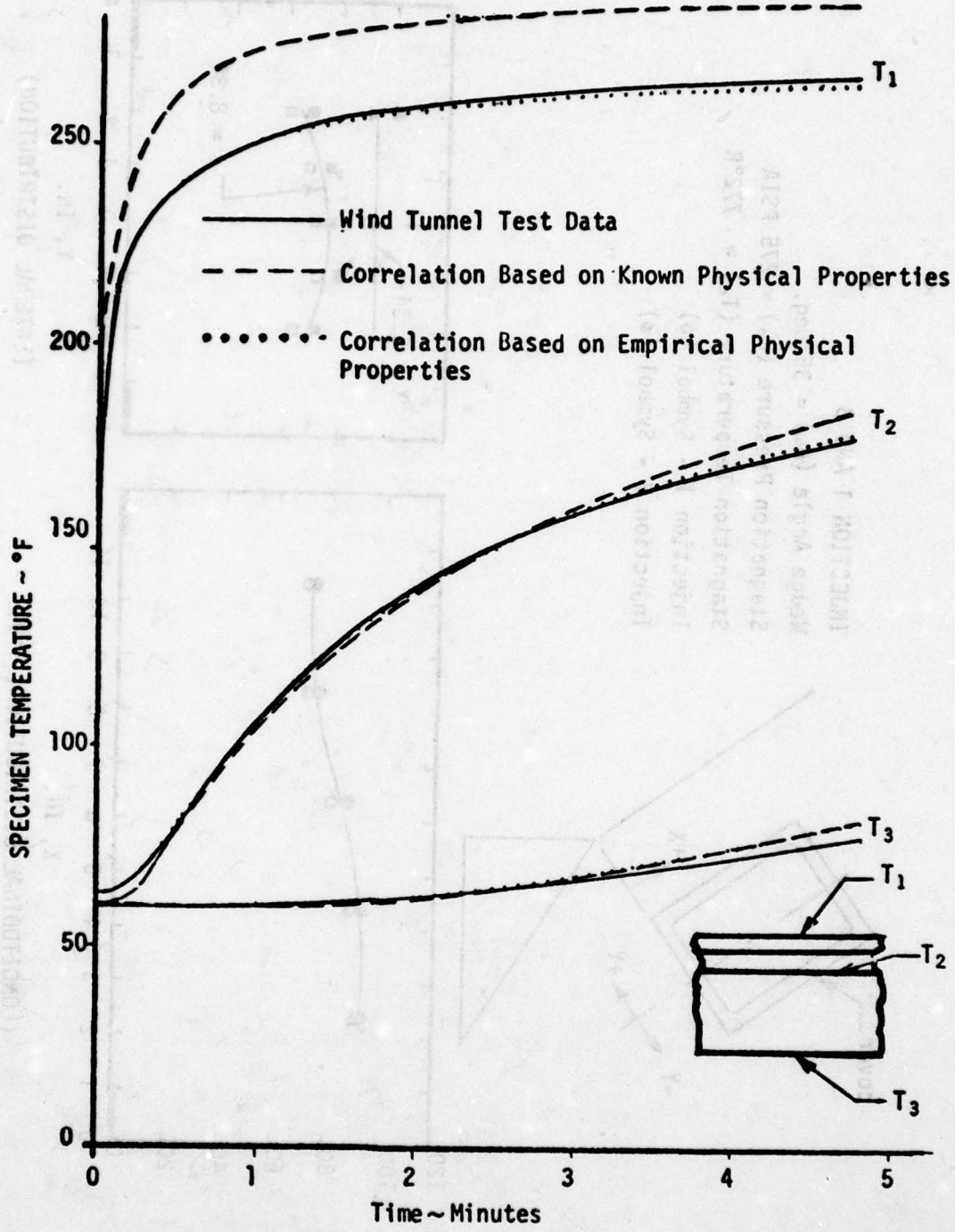


Figure 16. Temperature Correlation, Injection 72, Specimen SK03 (Mach 2.2).

Light Transmission and Haze

A record of the pre-test and post-test measurements for light transmission and haze are shown in Table 4. These values were measured at a zero angle of incidence by the vendors using a Gardner unit. The maximum reduction in light transmission was slightly over one percent. Unexpectedly, half of the specimens show an increase in light transmission after testing.

The maximum increase in haze was 9.62 percent for specimen SK01, an acrylic/silicone/polycarbonate configuration. The monolithic stretched acrylic specimens (SK16, SK17 and SK18) registered an increase of up to 6.7 percent in haze. The coated polycarbonate specimens (SK10 through SK15) increased up to 4.0 percent in haze. Specimens GY01 through GY05 (acrylic and urethane face plies) showed the smallest increase in haze, less than three percent. The variations did not increase as the Mach number was increased.

An increase in light transmission after testing is not considered realistic and these results indicate a tolerance in the methods used to measure light transmission and haze. It is recommended that: future specimens be handled more carefully to avoid dirt and scratches; tight specification requirements be imposed on the method of locating the spots where the measures are to be made; variations in the operator techniques and calibration be eliminated or controlled.

The AEDC/ARO measured light transmission by using a densitometer to read film density from a series of grid photographs taken at a 60-degree angle of incidence. The results of the densitometer method showed a variation in the amount of light transmission from plus 4.2 percent to minus 5.8 percent and more light transmission through some specimens at a 60-degree angle of incidence than was recorded at a zero angle by the Gardner Unit, contrary to what should be expected.

In-Tunnel Optical Distortion

A qualitative optical evaluation of in-tunnel specimen distortion, caused by heat and pressure, was made by comparing a final in-tunnel specimen photograph with one taken seconds after the specimen was installed in the tunnel, as shown in Figure 17. Line distortion was measured and plotted on a grid by overlaying the final in-tunnel photograph with a transparent positive of the first photo. The results are shown in Figure 18 for specimen SK04. Similar comparisons were made for every specimen and the results are documented in Table 5.

Permanent Optical Distortion

An evaluation of perment optical distortion was made by comparing pre-test and post-test grid photographs taken through each specimen at an angle of incidence of 60 degrees. The percent distortion was calculated by measuring the distance between the grid board lines and dividing this measurement by the true line distance. Typical grid photographs are shown in Figures 19 and 20. Table 6 is a summary of permanent distortion.

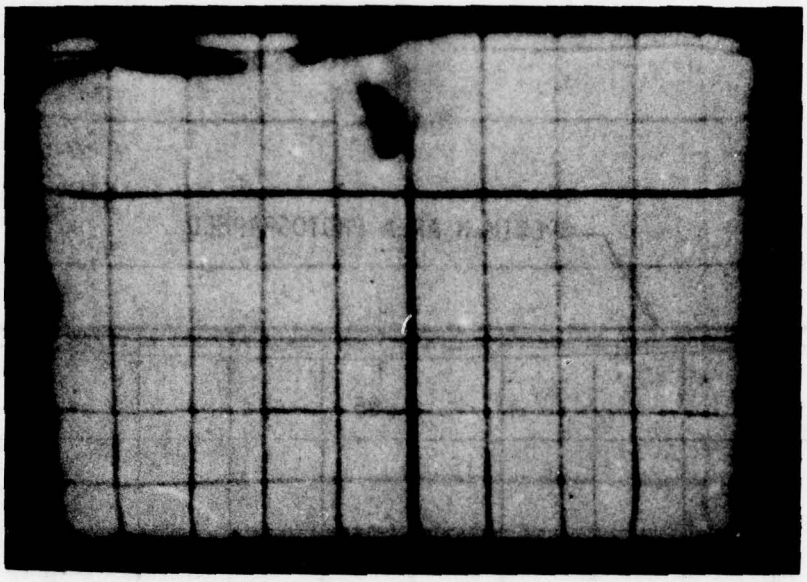
The amount of permanent optical distortion observed in the tested specimens was most significant in the stretched acrylic specimens (SK17 and SK18).

TABLE 4. LIGHT TRANSMISSION AND HAZE DATA.

SPECIMEN NUMBER	TRANSMISSION IN PERCENT			HAZE IN PERCENT			REFERENCE	DATA
	PRETEST (5)	POST-TEST (5)	CHANGE	PRETEST (5)	POST-TEST (5)	CHANGE	TEST MACH NO.	SPECIMEN THICKNESS
SK01	87.50	88.10	+0.60	4.24	13.86	+9.62	1.6	.700
SK02	86.44	88.22	+1.78	2.12	7.84	+5.72	2.0	.700
SK03	87.32	87.34	+0.02	6.48	6.26	-0.22	2.2	.700
SK04	87.60	86.50	-1.10	4.38	7.98	+3.60	1.6/2/2.2	.825
SK05	87.60	(3)		3.40	(3)			.825
SK06	87.90	(3)		5.72	(3)			.825
SK10	87.55	87.16	-0.39	3.28	7.24	+3.96	2.2	.500
SK11	87.78	(3)		2.88	(3)			.500
SK12	87.34	(3)		2.88	(3)			.500
SK13	80.98	81.08	+0.10	1.26	4.76	+3.50	1.6	.625
SK14	82.24	82.10	-0.14	2.84	3.22	+0.38	2.0	.625
SK15	81.52	82.20	+0.68	1.50	2.80	+1.30	2.2	.625
SK16	91.72	91.98	+0.26	2.84	9.54	+6.70	1.6	.900
SK17	92.40	92.38	-0.02	2.08	5.62	+3.54	2.0	.900
SK18	91.50	92.32	+0.82	2.40	8.84	+6.44	2.2	.900
PPG01	75.50	(4)		(4)	(4)			.860
SWU01	72.0	(4)		4.12	(4)			.868
GY01	82.4	82.2	-0.2	3.6	6.2	+2.6	2.0/2.2	.680
GY02	81.0	80.9	-0.1	4.6	6.3	+1.7	1.6	.680
GY03	81.2	80.9	-0.3	3.7	6.4	+2.7	1.6/2/2.2	.680
GY04	80.4	80.6	+0.2	4.9	5.9	+1.0	2.2	.740
GY05	81.1	80.9	-0.2	3.1	4.0	+0.9	2.0	.740

NOTES: (1) Measurements were made by the vendors per ASTM D1003 or FSTM406.
(2) Angle of incidence = 0 degrees.
(3) Specimens were not tested.
(4) No post-test measurements were made.
(5) These values are the average of values measured at five points.

FIRST



LAST

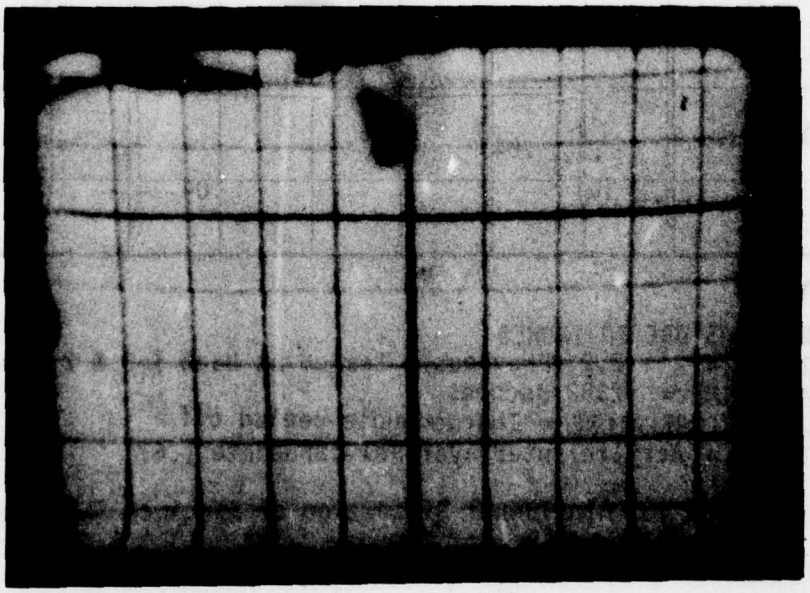
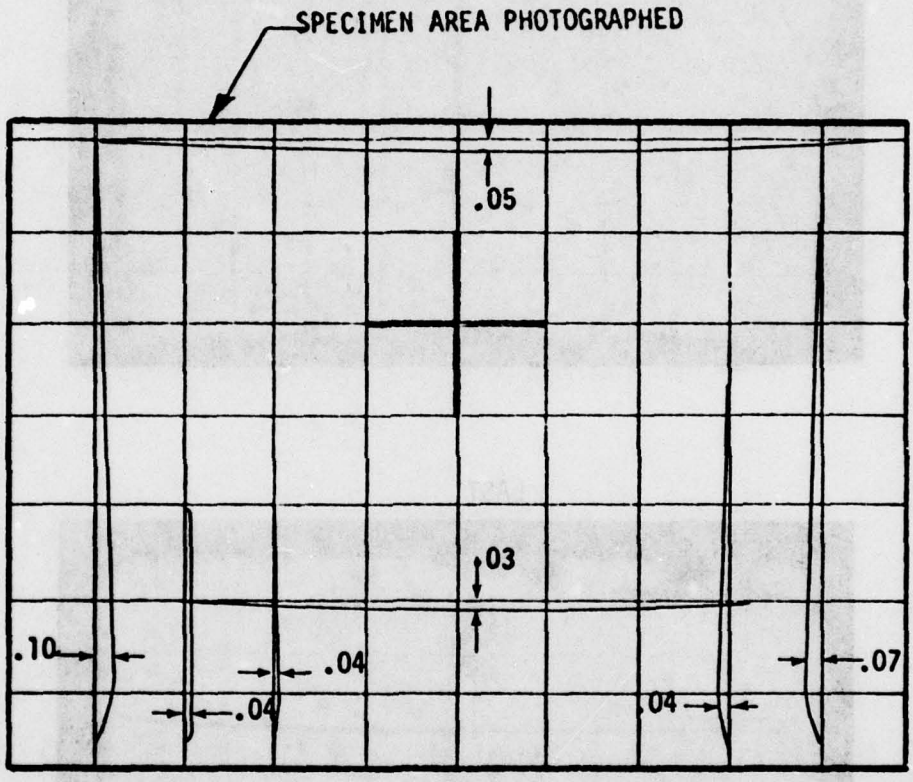


Figure 17. First and Last In-Tunnel Grid Photo for Specimen SK04 at Mach 2.2.



NOTES:

DIMENSIONS ARE IN INCHES
MACH NO. = 2.2 (Previously tested at Mach 1.6 & 2.0)
TUNNEL TIME = 2382 seconds
SURFACE TEMPERATURE = Thermocouple peeled off
MATERIAL - Acrylic/Interlayer/Polycarbonate (.62)

Figure 18. In-Tunnel Distortion of Specimen SK04.

TABLE 5. SPECIMENS RATED BY IN-TUNNEL DISTORTION

(Least distortion is listed first.)

Mach 1.6 SK01 and SK04 (acrylic/interlayer/polycarbonate) GY02 and GY03 (urethane/two polycarbonate plies) and SK13 (coated polycarbonate). SK16 (stretched acrylic)
Mach 2.0 GY01 (acrylic/two polycarbonate plies) SK02 and SK04 (acrylic/interlayer/polycarbonate) GY03 and GY05 (urethane/two polycarbonate plies) and SK14 (coated polycarbonate) SK17 (stretched acrylic)
Mach 2.2 GY01 (acrylic/two polycarbonate plies) and GY04 (urethane/two polycarbonate plies) SK03 and SK04 (acrylic/interlayer/polycarbonate) GY03 (urethane/two polycarbonate plies) SK10 and SK15 (coated polycarbonate) and SK18 (stretched acrylic)

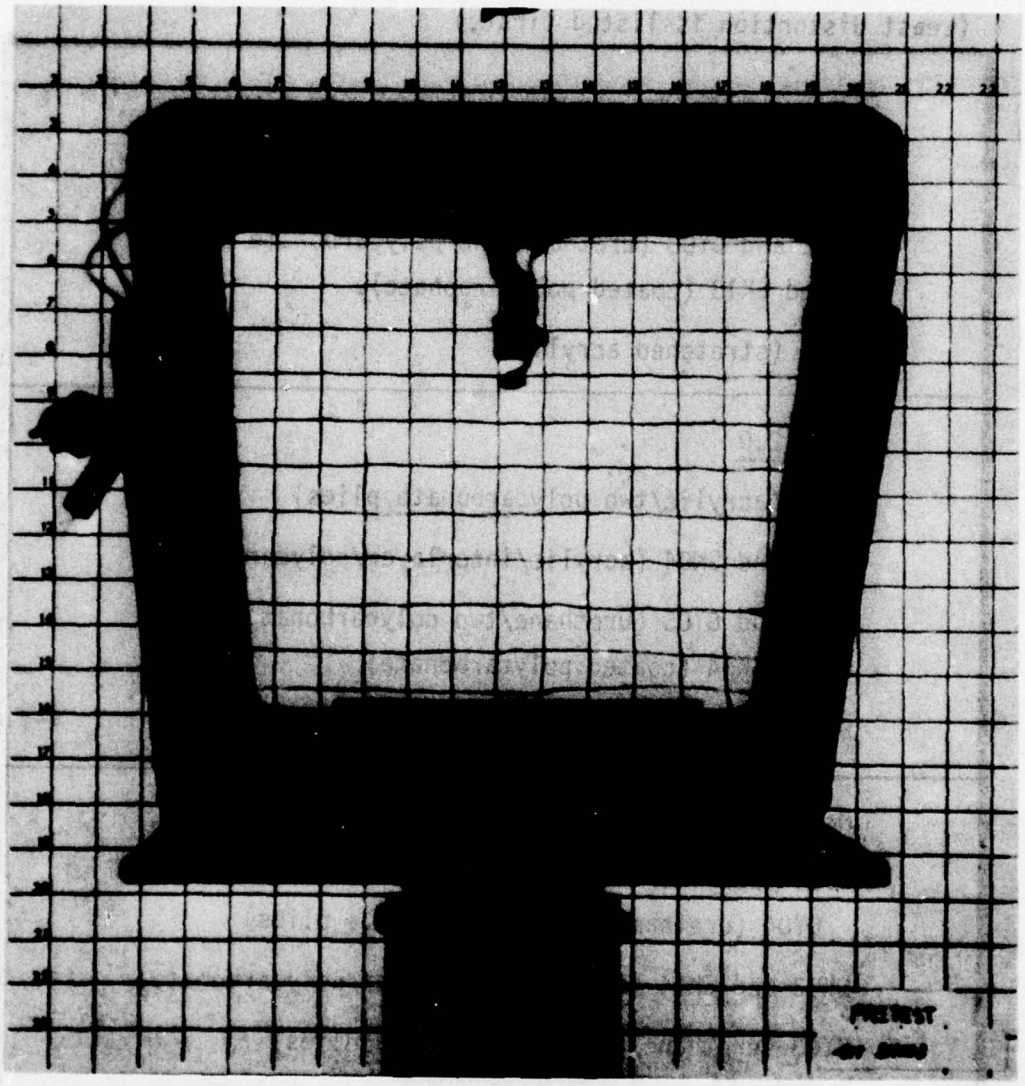


Figure 19. Pre-Test Grid Photograph of Specimen SK18 (Stretched Acrylic).

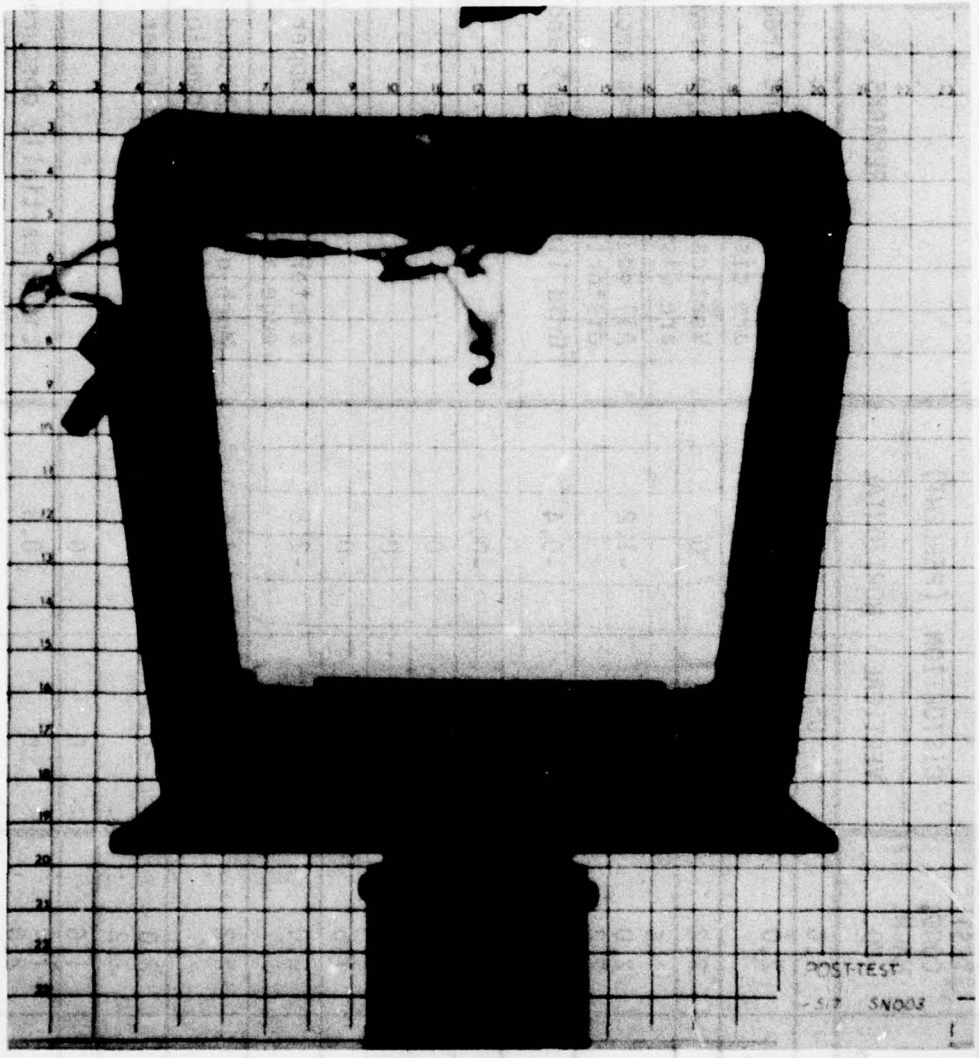


Figure 20. Post-Test Grid Photo of Specimen SK18.

TABLE 6. SUMMARY OF PERMANENT DISTORTION

SPECIMEN NUMBER	TEST COND. MACH. NO.	DISTORTION (PERCENT)		REMARKS
		VERTICAL	HORIZONTAL	
SK01	1.6	0	0	
SK02	2.0	0	0	Vertical edges and area around TC are distorted.
SK03	2.2	0	0	Vertical edges and area around TC are distorted
SK04	1.6 2.0 2.2	0	-1.2	All edges and area around TC are distorted.
SK10	2.2	1.0	-0.4	Grid lines are wavy and dull
SK13	1.6	0.6	-0.7	
SK14	2.0	-0.4	0	
SK15	2.2	0	0	
SK16	1.6	0	0	
SK17	2.0	-6.8	-2.8	Distortion along upper and lower edge and at TC.
SK18	2.2	-1.0	4.6	Much distortion around entire perimeter and thermocouple.
GY01	2.0 2.2	-0.5	-0.8	Distortion along lower edge and at TC.
GY02	1.6	0	0	
GY03	1.6 2.0 2.2	0	0.8	Lines partially obscured along lower edge
GY04	2.2	0.7	0.5	Slight cloudiness near lower edge.
GY05	2.0	-0.5	-0.4	

Moderate optical distortion was sustained by two of the coated specimens (SK10 and SK13) and three of the laminated specimens (GY01, GY04 and GY05). The remaining specimens exhibited very little optical distortion.

Physical Changes

A materials evaluation was made by observing and comparing physical changes to the specimens. The results are shown in Table 7 for selected specimens.

Table 7 delineates thickness change, face ply pitting, thermocouple peel-off, and notes adhesive residue. The maximum change in thickness was less than four percent and affected the laminated specimen, SK02, an acrylic/interlayer/polycarbonate configuration. Pitting was caused by tunnel debris and was most visible in the stretched acrylic materials. Thermocouple peel-off was peculiar to the as-cast and stretched acrylic materials and was attributed to high temperature exfoliation of the adhesive bond. The adhesive residue came from silicone tape on the cover that held the specimens in the cabin simulator.

Examination revealed edge deformation for the acrylic face ply materials caused by compression of the cabin simulator cover. Neither the urethane face ply material nor the polycarbonate material showed any visible effect of the clamping force.

Thermal relaxation of the stretched acrylic materials resulted from the high temperatures. The thermal differential produced sufficient stress in Specimen SK18 to fail the material in shear along one edge and resulted in delamination.

The glass face ply of Specimen SWU01 cracked upon retraction from the tunnel at the termination of its first injection. It is theorized that the failure was precipitated by strain induced at cool down. The silicone sealant edge material was slightly discolored and less pliable but no erosion was visible at the completion of this brief test.

The glass face ply of Specimen PPG01 cracked during its fifth tunnel injection. The circular failure pattern and distortion visible in the pre-test photograph indicates a failure due to pre-test strain coupled with the strain induced by the temperature and pressure environment. Erosion of the sealant under the aft retainer did occur at the center of the specimen.

Performance data for the precipitation static coating was not obtained.

Rain Repellant

The use of rain repellant did not show evidence of a difference in water repelling qualities for the coated and uncoated area; nor was there a difference in surface deterioration.

CONCLUSIONS

The purpose of this test program was to subject candidate windshield materials to a simulated supersonic environment compatible with the performance range of current Air Force inventory supersonic aircraft and to evaluate the ensuing effect of this environment on candidate windshield materials.

TABLE 7. SUMMARY OF PHYSICAL CHANGES

SERIAL NUMBER	MACH NO.	MATERIAL	AVERAGE THICKNESS (INCHES)			POST-TEST THICKNESS (INCHES)		FACE PLY PITTING	TC PEELED OFF	RESIDUE FROM COVER
			PRETEST	POST TEST	CHANGE	MAX	MIN			
SK04	1.6 2.0 2.2	AC/IN/PC	,800	.806	+.006	.811	.801	FINE	YES	
SK03	2.2	AC/IN/PC	.660	.666	+.006	.673	.661	FINE		
GY04	2.2	URETHANE FACE PLY	.813	.815	+.002	.820	.808	FINE		
SK15	2.2	POLYCARBONATE	.630	.632	+.002	.640	.624	FINE		HEAVY
SK18	2.2	ACRYLIC	.905	.905	0	.909	.901	HEAVY	YES	
SK10	2.2	POLYCARBONATE	.570	.576	+.006	.584	.569	MEDIUM		MEDIUM
GY03	1.6 2.0 2.2	URETHANE FACE PLY	.785	.782	-.003	.786	.777	FINE		HEAVY
GY01	2.0 2.2	ACRYLIC FACE PLY	.698	.698	0	.700	.697	FINE		HEAVY
SK02	2.0	AC/IN/PC	.655	.680	+.015	.685	.674	FINE	YES	
SK14	2.0	POLYCARBONATE	.635	.636	+.001	.643	.626	FINE		
GY05	2.0	URETHANE FACE PLY	.777	.779	+.002	.785	.770	FINE		
SK17	2.0	ACRYLIC	.895	.893	-.002	.893	.892	HEAVY	YES	
PPG01	1.6 2.0	GLASS FACE PLY	.861	.863	+.002	.875	.861	FINE. GLASS CRACKED		

The windshield materials were subjected to an acceptable modified test environment of Mach 1.6 at 42,400 feet, Mach 2.0 at 39,200 feet, and Mach 2.2 at 42,200 feet. An evaluation was achieved by appraising the face ply materials, by evaluating the optical distortion of the candidate windshields, both temporary distortion and permanent distortion, and by measuring the change in light transmission and haze in the transparent materials after being subjected to the modified simulated flight environment. The assessment of the edge designs for the glass face ply was incomplete due to early termination of the tests. It was not possible to evaluate the coating on the cracked glass plies.

The light transmission measurements made by the vendors did not exhibit a significant loss of transmission for any of the tested specimens. The maximum loss was slightly over one percent. The largest increase in haze was recorded for the stretched acrylic material; the laminated specimens with the urethane face ply demonstrated the least increase in haze.

Analysis of the in-tunnel optical distortion indicated that the laminated specimens with the acrylic face ply distorted slightly less than those with the urethane face ply, and generally, the laminated specimens displayed less distortion than the monolithic specimens, both polycarbonate and acrylic. The stretched acrylic specimens displayed the most severe distortion which was greatest at the Mach 1.6 condition.

The amount of permanent optical distortion observed in the tested specimens was most significant in the stretched acrylic material. Moderate optical distortion was sustained by two of the coated specimens and three of the laminated specimens. The remaining specimens varied from moderate to no measurable change.

The most conspicuous physical changes occurred to the stretched acrylic material and the glass face ply specimens. Thermal relaxation of the stretched acrylic specimens was obvious.

The two specimens with glass face plies cracked. It is theorized that temperature induced strain precipitated these failures. Erosion of the sealant occurred under the steel edge retainer.

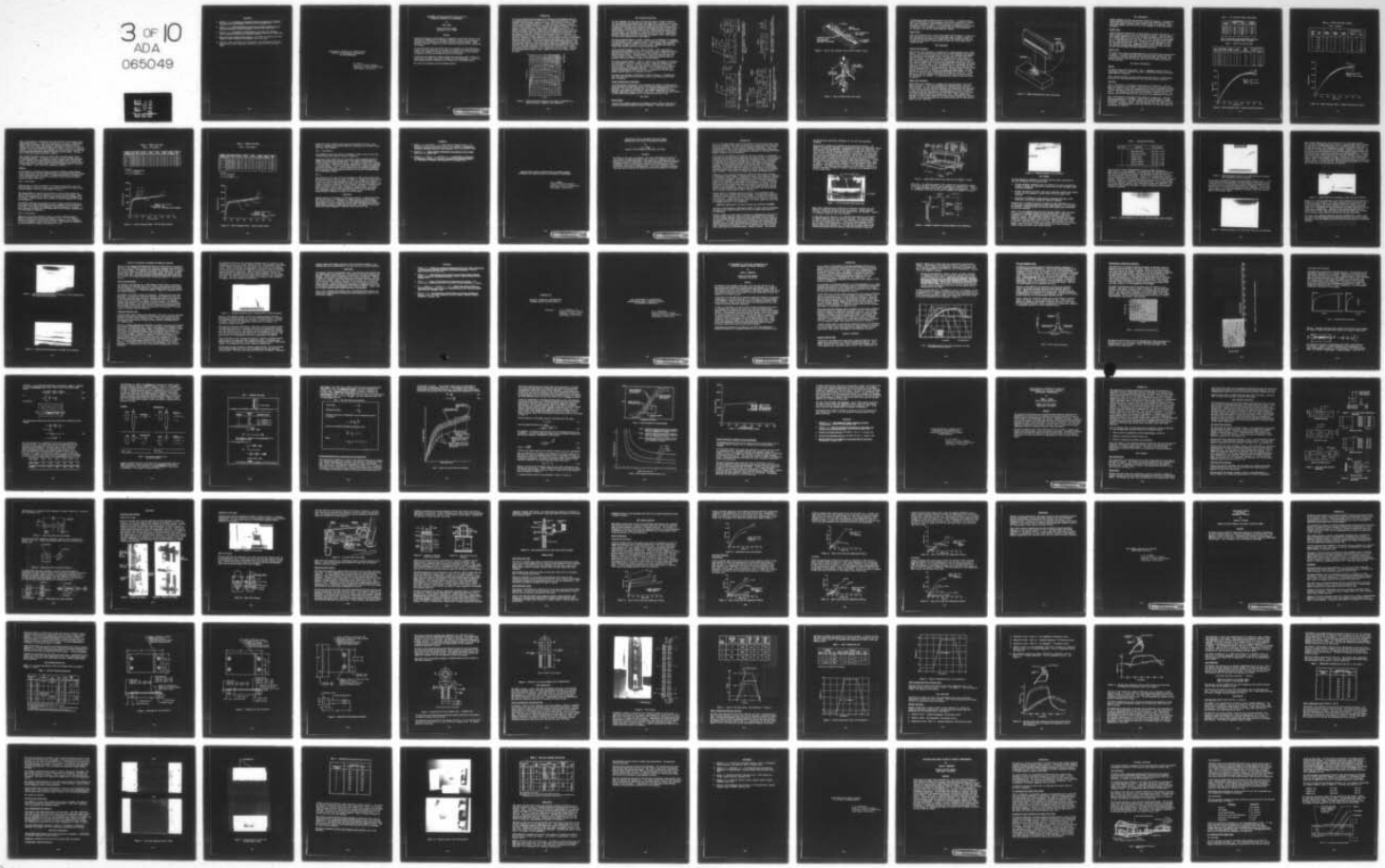
Pitting was most evident in the stretched acrylic material and least visible in the urethane material.

The laminated cast acrylic face ply specimens were deformed at the edges due to the clamping force of the cabin simulator lid and the high temperatures.

AD-A065 049 AIR FORCE FLIGHT DYNAMICS LAB WRIGHT-PATTERSON AFB OHIO F/G 1/3
CONFERENCE ON AEROSPACE TRANSPARENT MATERIALS AND ENCLOSURES (1--ETC(U)
DEC 78 R E WITTMAN

UNCLASSIFIED AFFDL-TR-78-168 NL

3 OF 10
ADA
065049



REFERENCES

1. Hoffman, J. B., Evaluation of Windshield Materials Subjected to Simulated Supersonic Flight Environments, AFFDL-TR-77-92, September 1977

2. Carver, D. B., Aerothermodynamic Evaluation of Windshield Materials in a Simulated Supersonic Flight Environment, AEDC-TR-77-68, June 1977.

3. Carver, D. B., Experimental Aerothermodynamic Evaluation of Laminated Plastic Windshield Materials at Supersonic Speeds, AEDC-TR-74-11, July 1974.

4. Test Facilities Handbook (Tenth Edition), Von Karman Gas Dynamics Facility, Volume 3, Arnold Engineering Development Center, May 1974.

5. Equations, Tables and Charts for Compressible Flow, NACA Report 1135, Ames Research Staff, Ames Aeronautical Laboratory, Moffett Field, California, 1953.

AERODYNAMIC HEATING AND SERVICE AGING EFFECTS ON MECHANICAL PROPERTIES OF POLYCARBONATE

M. Coker
Douglas Aircraft Company
McDonnell Douglas Corporation
Long Beach, California

AERODYNAMIC HEATING AND SERVICE AGING EFFECTS ON MECHANICAL PROPERTIES OF POLYCARBONATE

by

MURL COKER

Douglas Aircraft Company
Long Beach, Calif. 90846

ABSTRACT

Exposure of bisphenol A polycarbonate to temperatures above 80°C results in the accumulative deterioration in the impact strength. There is also a decrease in the extension to break and an increase in the tensile yield strength. Other evidences indicated a degrading of these mechanical properties due to weathering and storage.

A series of tensile and izod impact tests were conducted, at room temperature, on monolithic polycarbonate test specimens to determine the mechanical property changes after exposure to thermal conditioning representative of the exposure a supersonic aircraft would encounter during its life span.

To determine the mechanical property changes due to service aging, a series of tensile and izod impact tests were conducted, at room temperature, on monolithic polycarbonate specimens removed from a four-year-old service-aged canopy.

The tests were conducted per ASTM standard methods.

PRECEDING PAGE BLANK-NOT FILMED

INTRODUCTION

It has been demonstrated that exposure of bisphenol A polycarbonate materials to temperatures above 80°C (176°F) results in accumulative decreases in impact strength, fracture energy, extension to break, and increases in tensile and flexural yield strength (Reference 1). Other evidences indicate a change in these mechanical properties due to weathering and storage (References 2 and 3). Figure 1, from Reference 3, depicts changes that occurred in storage. To determine mechanical property changes due to aerodynamic heating, a series of tensile and impact tests were conducted at room temperature on monolithic polycarbonate specimens after exposure to thermal conditioning representative of the exposure a supersonic aircraft would encounter during its life span. To determine mechanical property changes due to service aging, a series of tensile tests were conducted at room temperature on fusion bonded monolithic polycarbonate specimens removed from a four-year-old service-aged canopy, and from a stretch formed bird test canopy. Tests were conducted per ASTM standard methods. The test specimens used in this test series were fabricated in accordance with ASTM standards from 0.250-inch thick polycarbonate sheet, representative of the core plies in a laminated windshield, and from 0.50 and 0.87 thick fusion bonded polycarbonate sheet representative of a monolithic aircraft canopy. Two types of polycarbonate were tested, "Lexan" (General Electric) and "Tuffak" (Rohm and Haas).

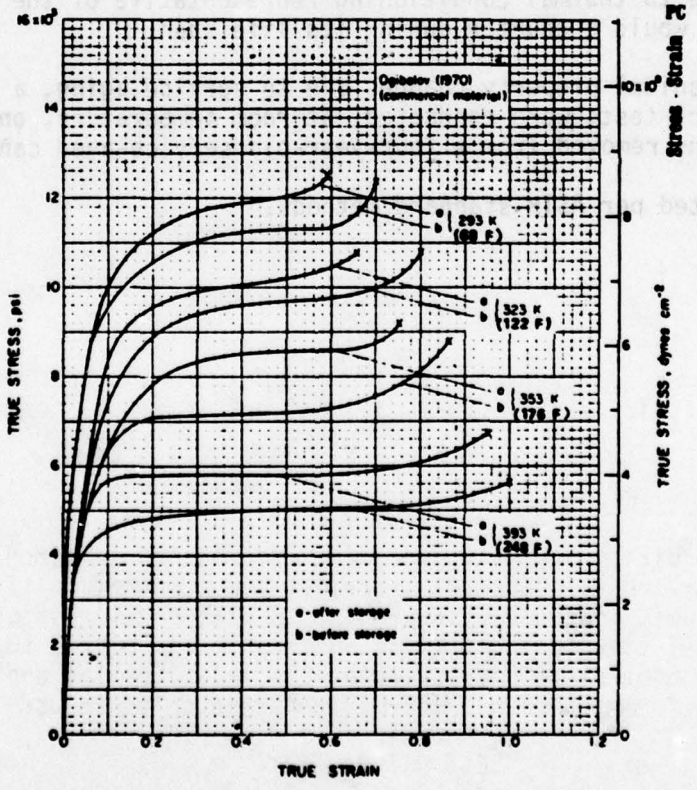


Figure 1. Before and After Storage for Four Years at 293-393K in a Dark Dry Location. (Adapted from Reference 3)

TEST SPECIMEN DESCRIPTION

The test specimens for this series of tests are shown in Figures 2 through 5. All test specimens were examined under polarized light to expose stress risers from machining operations which could have affected the test results. Specimens displaying stress risers were refinished (sanded and polished) to remove such discrepancies. Machine cutting speed and feed rates were controlled to prevent heating parts above 150°F during machining to eliminate adverse thermal conditioning effects. The specimens of a particular test series were orientated in the same length-width relation with respect to the basic stock. Polycarbonate materials tested were required to meet the requirements of MIL-P-83310 except for optical and strength testing requirements.

The tensile specimen Number 1, shown in Figure 2, was constructed in accordance with ASTM D638-72, Type 1, except the overall length was extended to accommodate the Douglas indexing and alignment fixture. Sixty specimens were thermally conditioned, as shown in Table 1 prior to testing. Specimens were made from "Lexan" and "Tuffak" monolithic polycarbonate materials.

Tensile specimens Numbers 2 and 3, shown in Figure 3, were constructed in accordance with ASTM D638-72, Type III, except the overall length was extended, and holes were provided in each end of the test specimen to provide for the Douglas holding fixture. Specimen Number 2 (0.87 inch thick) was made from a service-aged F-15 canopy of "Lexan" fusion bonded polycarbonate material. Specimen 3 (0.50 inch thick) was made by various vendors.

The tensile specimen Number 4, shown in Figure 4, was constructed in accordance with ASTM D638-72, Type III, except the overall length was extended and holes were provided in each end of the test specimen to provide for the Douglas holding fixture. Specimens were made from an F-16 transparency of stretched, fusion bonded Lexan polycarbonate material. Five of these specimens were thermally conditioned at 185°F for 36 hours to simulate the life span aerodynamic heating effects of a supersonic aircraft.

The impact test specimen configuration is shown in Figure 5. Specimens were made from Lexan monolithic polycarbonate material and thermally conditioned prior to testing.

Thermal Conditioning of Specimens

To provide thermal conditioning, test specimens were heated in circulating air ovens equipped with temperature control overrides and temperature/time recording apparatus. Each oven was equipped with iron constantan thermocouples for monitoring the internal circulating air and specimen temperatures to provide automatic temperature control of ovens within +5°F. Calibration and certification of these ovens was performed within a six-month period prior to use.

TEST SETUP

Tensile Tests

A tensile test specimen indexing and alignment fixture, Figure 6, was used to provide for positive clamping and proper alignment. Tests were conducted on

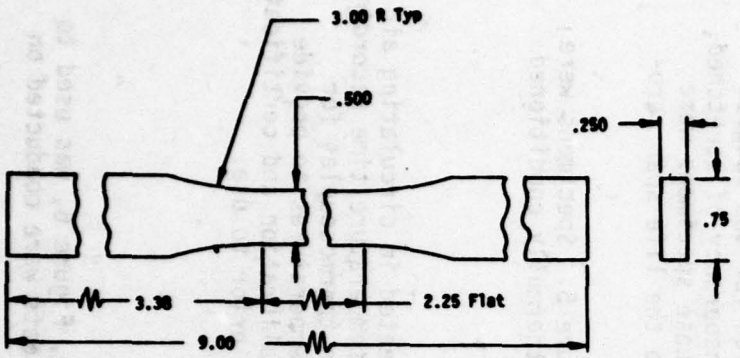


Figure 2. Tensile Specimen Configuration Number 1 (Lexan and Tuffak) (Dimensions are in inches).

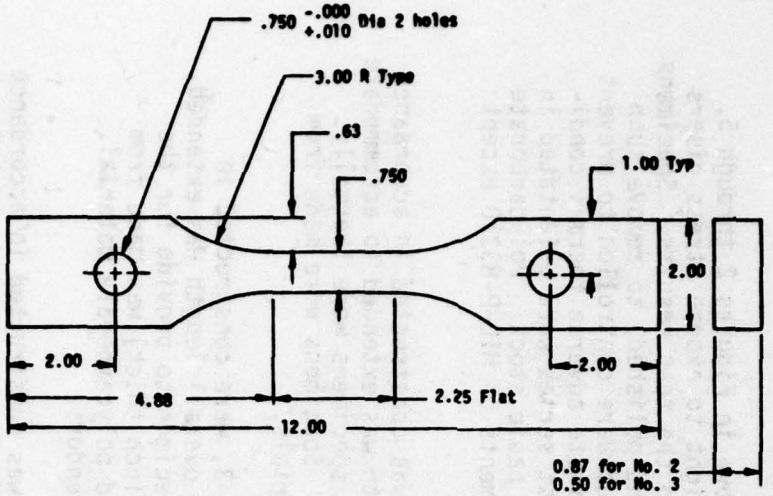
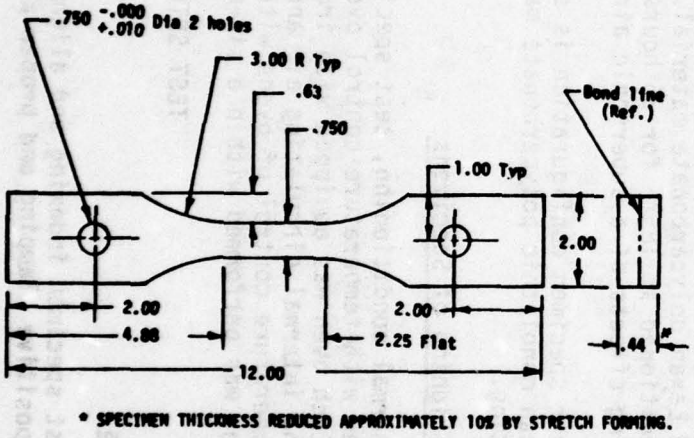


Figure 3. Tensile Specimen Configuration Numbers 2 and 3 (Lexan) -571. (Dimensions are in inches)



* SPECIMEN THICKNESS REDUCED APPROXIMATELY 10% BY STRETCH FORMING.

Figure 4. Tensile Test Specimen Configuration Number 4 (Dimensions are in inches).

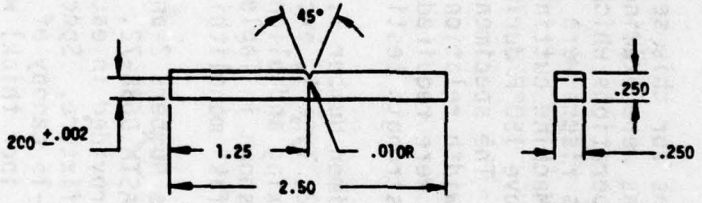


Figure 5. Impact Test Specimen Configuration Number 5 (Lexan and Tuffak). (Dimensions are in inches)

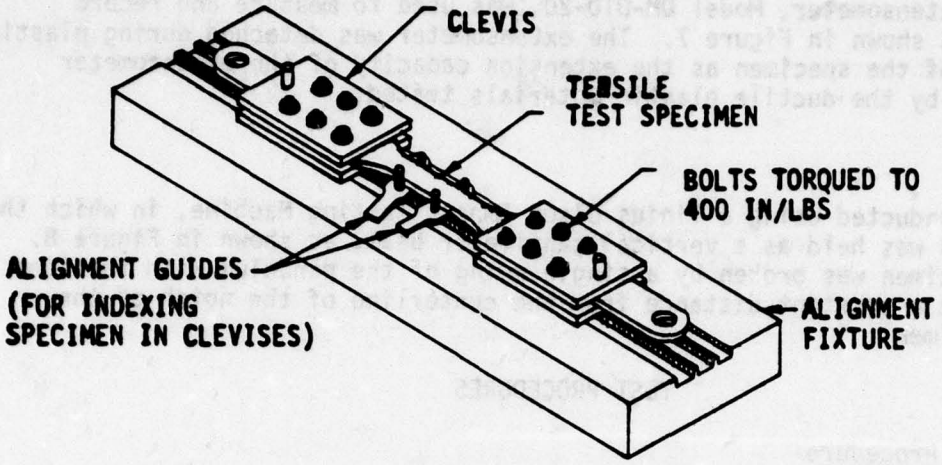


Figure 6. Tensile Test Specimen Indexing and Alignment Fixture.

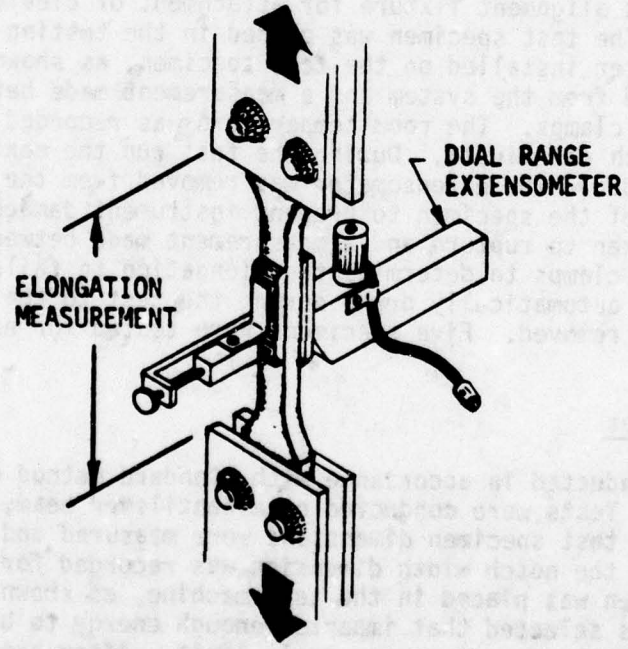


Figure 7. Tensile Stress-Strain Test Setup.

a 30,000-pound capacity Riehle universal test machine. To provide accurate means of determining strain measurements during elastic deformation, a Riehle dual range extensometer, Model DM-D10-20, was used to measure and record elongation as shown in Figure 7. The extensometer was detached during plastic deformation of the specimen as the extension capacity of the extensometer was exceeded by the ductile plastic materials tested.

Impact Tests

Tests were conducted using a Tinius Olsen Impact Testing Machine, in which the test specimen was held as a vertical cantilever beam, as shown in Figure 8. The test specimen was broken by a single swing of the pendulum with the line of contact at a constant distance from the centerline of the notch of the clamped specimen.

TEST PROCEDURES

Tensile Test Procedure

Tensile tests were conducted in accordance with standard method of test, ASTM D638-72. The test specimen gage length cross section dimensions were measured and recorded for each specimen prior to testing. The specimens were mounted into the indexing and alignment fixture for attachment of clevis ends, as shown in Figure 6. The test specimen was placed in the testing machine and a dual range extensometer installed on the test specimen, as shown in Figure 7. The slack was removed from the system and a measurement made between the clevis ends of the specimen clamps. The room temperature was recorded and the machine speed set at 0.05-inch per minute. During the test run the maximum load was determined and recorded. The extensometer was removed from the specimen during plastic deformation of the specimen to prevent instrument damage. The test specimen was then taken to rupture and a measurement made between the clevis ends of the specimen clamps to determine the elongation to failure. A load deflection curve was automatically drawn during the test to the point where the extensometer was removed. Five specimens were tested for each test batch of material.

Impact Test Procedures

Impact tests were conducted in accordance with standard method of test ASTM D256-72a, Method C. Tests were conducted on a cantilever beam, izod type impact machine. The test specimen dimensions were measured and verified to be within tolerance and the notch width dimension was recorded for each specimen. A sample test specimen was placed in the test machine, as shown in Figure 8. A pendulum weight was selected that imparted enough energy to break the specimen without exceeding the excess energy scale limit. After breaking each specimen, the total impact energy and the excess energy readings were recorded. Specimens in the same test batch were run consecutively with the same pendulum weight and test conditions.

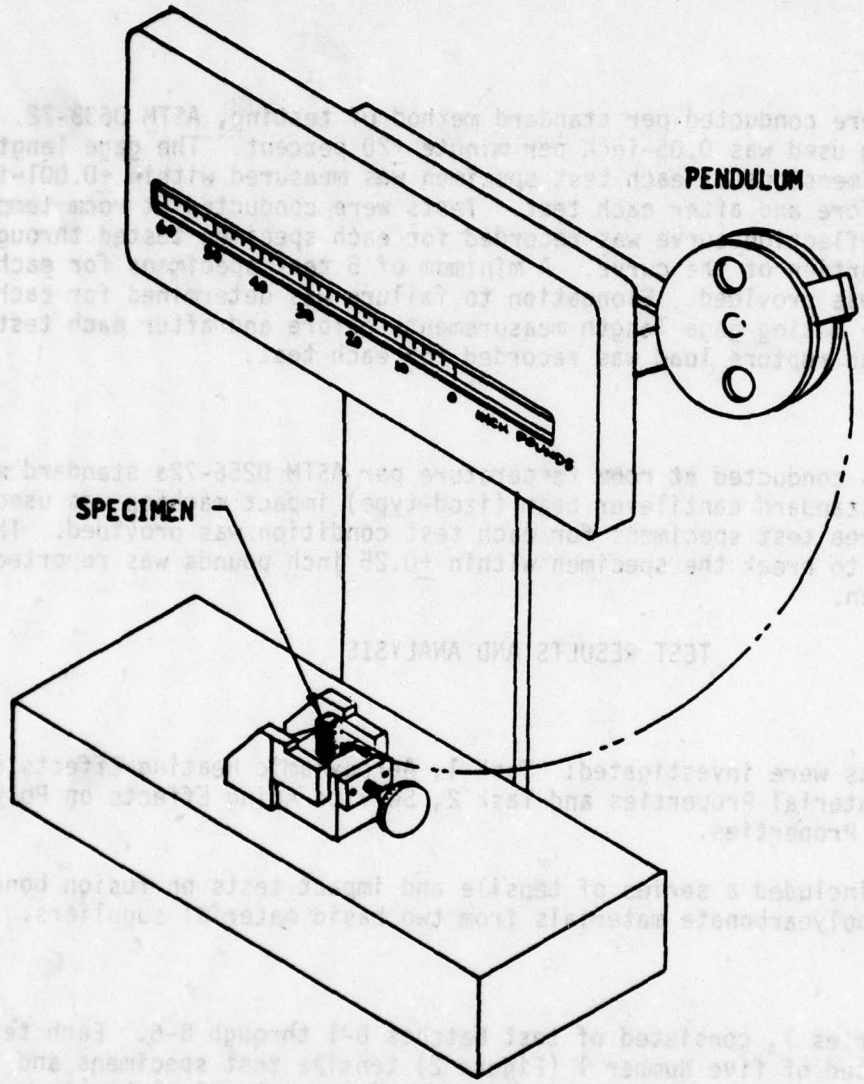


Figure 8. Impact Resistance Test Setup (Izod Type).

TEST REQUIREMENTS

Douglas provided facilities and services required for testing. The mechanical testing machines used were verified for accuracy per ASTM E4-72 procedures within ±0.5 percent traceable to NBS (National Bureau of Standards). Instrumentation equipment was verified for a class accuracy of B1 per ASTM E83-67 procedures.

Tensile Tests

Tensile tests were conducted per standard method of testing, ASTM D638-72. The speed of testing used was 0.05-inch per minute ±20 percent. The gage length cross section dimensions of each test specimen was measured within ±0.001-inch and recorded before and after each test. Tests were conducted at room temperature. A load-deflection curve was recorded for each specimen tested through the peak load portion of the curve. A minimum of 5 test specimens for each test condition was provided. Elongation to failure was determined for each test specimen by making gage length measurements before and after each test. The peak load and rupture load was recorded for each test.

Impact Tests

The impact tests conducted at room temperature per ASTM D256-72a standard method of testing. A standard cantilever beam (izod-type) impact machine was used. A minimum of three test specimens for each test condition was provided. The energy required to break the specimen within ±0.25 inch pounds was reported for each specimen.

TEST RESULTS AND ANALYSIS

General

Two general tasks were investigated: Task 1, Aerodynamic Heating Effects on Polycarbonate Material Properties and Task 2, Service Aging Effects on Polycarbonate Material Properties.

Task 1 testing included a series of tensile and impact tests on fusion bonded and monolithic polycarbonate materials from two basic material suppliers.

Test Data

Task 1, Test Series 1, consisted of test batches B-1 through B-6. Each test batch was composed of five Number 1 (Figure 2) tensile test specimens and three Number 5 (Figure 5) impact test specimens made of "Lexan" polycarbonate material. The test specimens for each test batch were thermally conditioned as shown in Table 1. The average test data for this test series is given in Table 2. The average stress-strain curves for this test series are superimposed in Figure 9.

Task 1, Test Series 2, consisted of test batches T-1 through T-6. Each test batch was comprised of five Number 1 tensile test specimens made of "Tuffak" polycarbonate material. The test specimens for each test batch were thermally conditioned, as shown in Table 1. The test data for this test series are given in Table 3. The average stress-strain curve histories for this test series are superimposed in Figure 10.

TABLE 1. TEST SPECIMEN THERMAL CONDITIONING

TEST BATCH* NUMBER		THERMAL CONDITIONING TEMPERATURE (°F)	THERMAL CONDITIONING TIME (HR:MIN)	APPROXIMATE NUMBER OF FLIGHT EXPOSURES
B-1	T-1	0	0	0
B-2	T-2	180	2:00	35
B-3	T-3	180	12:00	312
B-4	T-4	180	30:00	350
B-5	T-5	185	16:30	75
B-6	T-6	180 185	30:00 16:30	425

*Each "B" test batch consists of five configuration Number 1 (Lexan) test specimens and three configuration Number 5 impact test specimens. Each "T" test batch consists of five configuration Number 1 test specimens.

TABLE 2. TENSILE TEST DATA (LEXAN)

TEST BATCH NUMBER	YIELD STRESS (PSI)	PERCENT ELONGATION TO YIELD	PERCENT ELONGATION TO BREAK	ELASTIC MODULUS ($PSI \times 10^{-5}$)	IMPACT ENERGY TO BREAK (FT-LB/IN. OF NOTCH)	THERMAL CONDITIONING TEMPERATURE (°F)	THERMAL CONDITIONING TIME (HR: MIN)
B-1	9287	2.53	124	3.21	9.77	---	---
B-2	9355	2.59	136	3.12	3.86	180	2:00
B-3	9511	2.55	82	3.28	4.60	180	12:00
B-4	9508	2.53	104	3.19	2.56	180	30:00
B-5	9446	2.45	48	3.22	2.75	185	16:30
B-6	9561	2.43	89	3.36	2.71	180 185	30:00 16:30

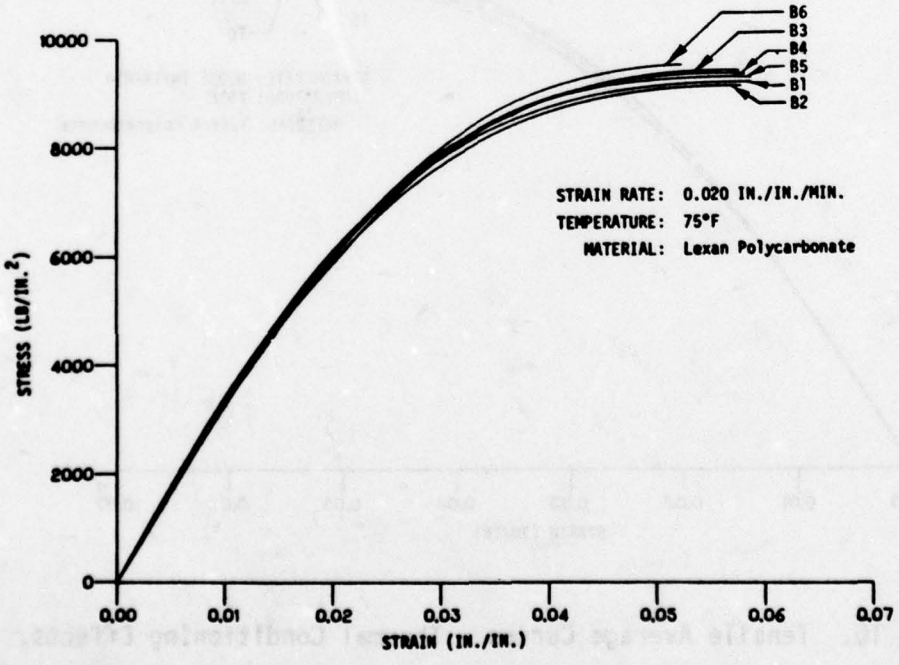


Figure 9. Tensile Average Curves - Thermal Conditioning Effects.

TABLE 3. TENSILE TEST DATA (TUFFAK)

TASK 1, SERIES 2

SPECIMEN TEST BATCH NUMBER	YIELD STRESS (PSI)	PERCENT ELONGATION TO YIELD	PERCENT ELONGATION TO BREAK	ELASTIC MODULUS (PSIx10-5)	THERMAL CONDITIONING	
					TEMPERATURE (°F)	TIME (HR: MIN)
T-1	8858	2.79	140	3.08	---	---
T-2	8926	2.75	137	3.16	180	2:00
T-3	9037	2.73	124	3.12	180	12:00
T-4	8918	2.71	125	3.06	180	30:00
T-5	8819	2.47	113	3.08	185	16:30
T-6	8950	2.48	118	3.13	180 185	30:00 16:30

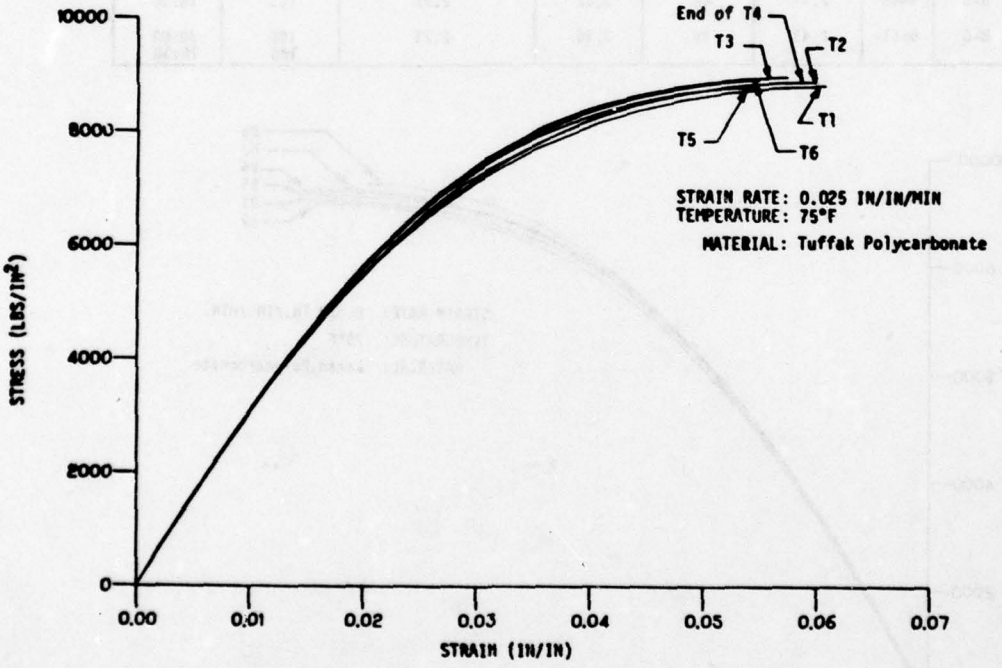


Figure 10. Tensile Average Curves - Thermal Conditioning Effects.

Task 1, Test Series 3, consisted of five test batches of fusion bonded "Lexan" polycarbonate material. A test batch consisted of five each of configuration Number 4 tensile specimens made from fusion bonded polycarbonate material removed from a test canopy, and thermally conditioned at 185°F for 36 hours to simulate the life span aerodynamic heating of a canopy installed on a supersonic aircraft. These test results were compared with the test results obtained from fusion bonded polycarbonate specimens processed by other vendors. The test data for this test series are given in Table 4.

Task 2 testing included a series of tensile tests on fusion bonded "Lexan" polycarbonate material. Five Number 2 (Figure 2) tensile specimens were made of fusion bonded "Lexan" polycarbonate material removed from a service-aged canopy. The results of these tests were compared with the test results on tensile specimens made of fusion bonded "Lexan" polycarbonate material processed by other vendors. Tests results are presented in Table 5.

Analysis

In this analysis, all data are based on averages; therefore, spread between stress-strain curves and other comparable data are considered within the average limits presented for each test batch. Although some data may be superfluous, it was considered better to collect and record all data that was available, should any unusual trend occur.

Task 1, Test Series 1

Referring back to Table 2 and Figure 9, the average stress-strain curve for each test batch, a definite change in some material properties is seen to have occurred between B-1 and B-2, and between B-2 and B-3.

The change between B-1 and B-2 can be noted by a drop in impact energy and tensile modulus while tensile elongation to failure shows an increase. These results are incompatible, as a drop in impact energy should be accompanied by an increase in tensile modulus and a decrease in tensile elongation for a more brittle material.

The material properties data between B-3 and B-6 remain constant except for a small decrease in impact energy and the erratic movement of tensile elongation to failure. These results are compatible (ignoring elongation to failure) which indicates a plateau has been reached where further thermal treatment does not effect material properties.

Task 1, Test Series 2

Comparison of the data presented in Table 3, reveals a gradual change in material properties that has occurred between T-1 and T-6. This change is noted by an increase in tensile yield, and tensile modulus, with a decrease in tensile elongation to both yield and failure. These results are compatible and are indicative of a more brittle material at T-6.

TABLE 4. TENSILE TEST DATA
TASK 1, TEST SERIES 3

SPECIMEN PROCESSOR AND NUMBER*	YIELD STRESS (PSI)	ULTIMATE STRESS (PSI)	ULTIMATE TRUE STRAIN (IN./IN.)	ELASTIC MODULUS (PSI x 10^5)	SECANT MODULUS (PSI x 10^5)	PERCENT ELONGATION TO YIELD	PERCENT ELONGATION TO FAILURE	FRACTURE ENERGY (PSI)
A4 TC	10,293	11,556	0.423	3.30	1.74	2.79	53	4403
A4	9,981	12,411	0.561	3.17	1.50	2.84	75	6020
D3	9,780	11,950	0.474	3.64	1.60	2.54	61	4910
B4	9,509	12,497	0.568	3.21	1.50	2.72	76	5986
C2	9,729	12,525	0.530	3.29	1.61	2.53	70	5635

* A 4 TC
- TC — Thermal Conditioned
- 4 — Part Number
- A — Processor: A, B, C, D

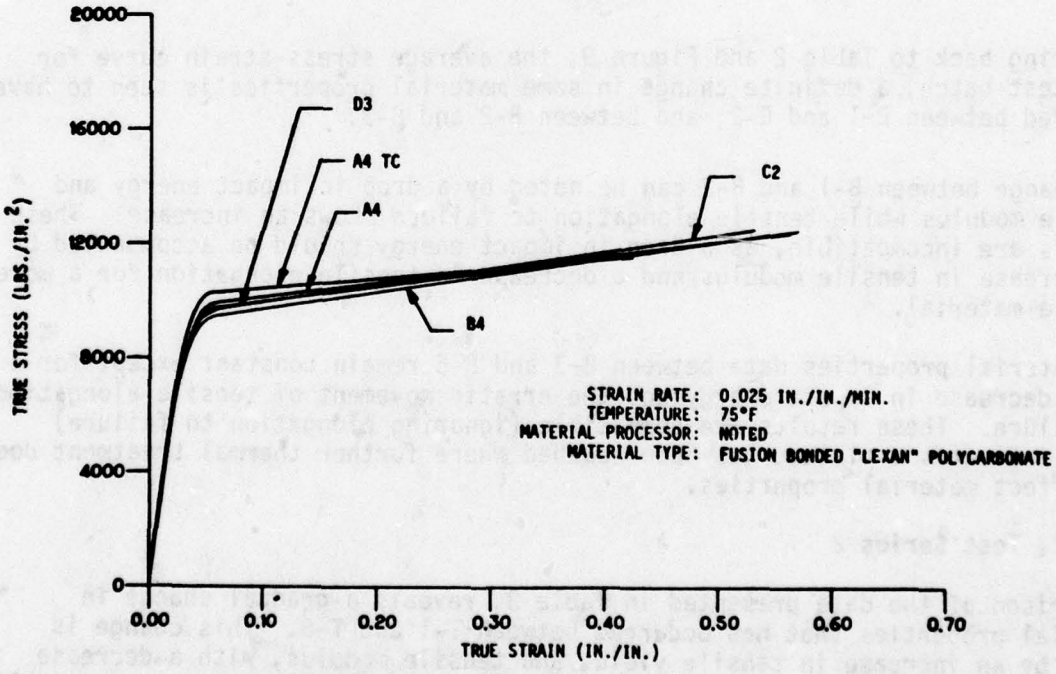


Figure 13. Tensile Average Curves - Service Aging Effects.

TABLE 5. TENSILE TEST DATA

TASK 1, TEST SERIES 3

SPECIMEN PROCESSOR AND NUMBER*	YIELD STRESS (PSI)	ULTIMATE STRESS (PSI)	ULTIMATE TRUE STRAIN (IN./IN.)	ELASTIC MODULUS (PSI x 10^{-5})	SECANT MODULUS (PSI x 10^{-5})	PERCENT ELONGATION TO YIELD	PERCENT ELONGATION TO FAILURE	FRACTURE ENERGY (PSI)
B2 SA	10,092	12,268	0.432	3.42	1.66	2.51	54	4579
B2	10,105	13,283	0.596	3.65	1.77	2.54	81	6707
A3	9,362	12,360	0.539	3.09	1.53	2.68	71	5590
C2	9,729	12,525	0.530	3.29	1.61	2.53	70	5635
D3	9,780	11,950	0.474	3.64	1.60	2.54	61	4910

* A 4 SA
- SA — Service Aged
- 4 — Part Number
- A — Processor: A, B, C, D

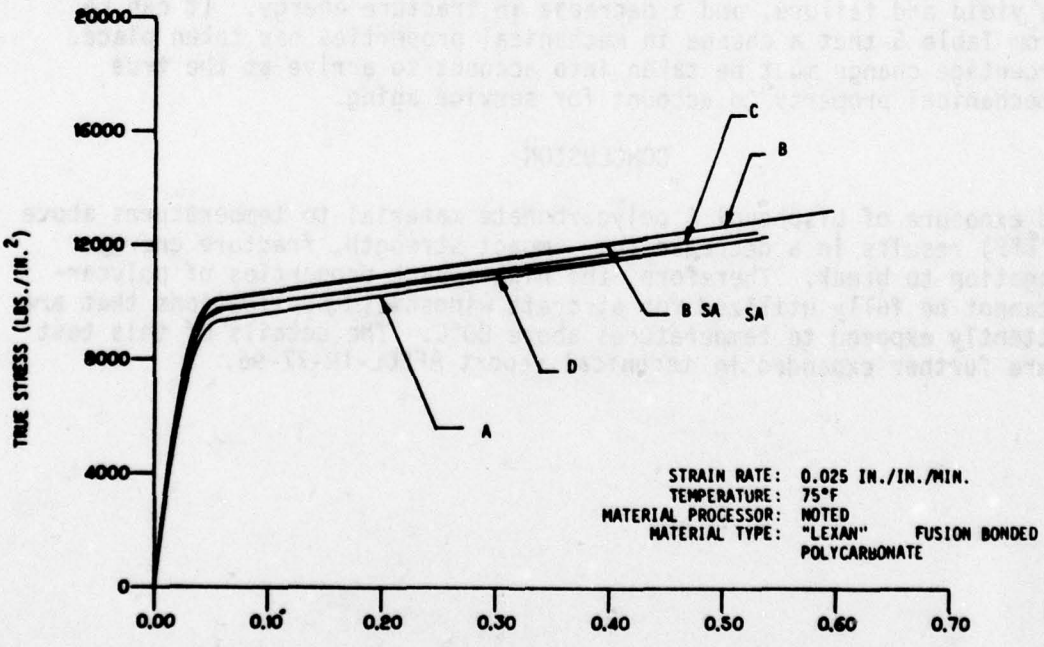


Figure 14. Tensile Average Curves - Service Aging Effects.

Comparison of test results in this test series with that of Task 1, Test Series 1, indicates that "Tuffak" material is affected less by thermal treatment than "Lexan" material.

Task 1, Test Series 3

Test results for this test series is presented in Table 4 and a plot of the average stress-strain curves is given in Figure 13.

Comparison of test results for A4, D3, B4 and C2 test specimens with A4 TC thermal conditioned test specimen reveals that material embrittlement has taken place due to thermal conditioning. This change is noted by an increase in yield strength, a decrease in percent elongation to failure, and a decrease in fracture energy. It can be noted from Table 4 that a change in mechanical properties has taken place. This percentage change in mechanical properties must be applied to design mechanical properties to account for embrittlement due to aerodynamic heating.

Task 2

Test results for this test series are presented in Table 5 and a plot of the average stress-strain curves is given in Figure 14. Comparison of test results for A3, B2, C2 and D3 test specimens with B2 SA service-aged test specimen, reveals that material embrittlement has taken place due to service aging. This change is noted by an increase in yield strength, a decrease in percent elongation to yield and failure, and a decrease in fracture energy. It can be noted from Table 5 that a change in mechanical properties has taken place. This percentage change must be taken into account to arrive at the true design mechanical property to account for service aging.

CONCLUSION

Repeated exposure of bisphenol A polycarbonate material to temperatures above 80°C (176°F) results in a decrease in: impact strength, fracture energy, and elongation to break. Therefore, the high-impact properties of polycarbonate cannot be fully utilized for aircraft windshield applications that are intermittently exposed to temperatures above 80°C. The details of this test effort are further expanded in technical report AFFDL-TR-77-96.

REFERENCES

1. Morgan, R. J. and O'Neal, J. E., "The Effect of Thermal History on the Mechanical Properties and Crystallinity of Polycarbonate", Conference on Aerospace Transparent Materials and Enclosures, AFML-TR-76-54, April 1976.

2. Hassard, R. S., Design Criteria Transparent Polycarbonate Plastic Sheet, ASML-TR-72-117, August 1972.

3. Schram, R. E. Clark, A. F., and Reed, R. P., A Compilation of Evaluation of Mechanical, Thermal, and Electrical Properties of Selected Polymers, U.S. Department of Commerce, NBS Monograph 132, September 1973.

PRECIPITATION STATIC ELECTRICITY AND SWEPT-STROKE LIGHTNING AND THEIR EFFECTS ON WINDSHIELD SUBSYSTEMS

R. C. Twomey
Douglas Aircraft Company
McDonnell Douglas Corporation
Long Beach, California

PRECEDING PAGE BLANK-NOT FILMED

PRECIPITATION STATIC ELECTRICITY AND SWEPT-STROKE LIGHTNING AND THEIR EFFECTS ON WINDSHIELD SUBSYSTEMS

by

R. C. TWOMEY
Douglas Aircraft Company, Long Beach, California

ABSTRACT

Two phases of this work are reported. The first investigated the effects of static electric charging and swept-stroke lightning on candidate outer ply materials for aircraft windshields. The second phase investigated the potential detrimental effects of these natural electrical environments on the optically transparent, electrically conductive coatings which are frequently used to provide anti-icing heat for transparencies. The special laboratory techniques which were used to simulate the separate electrical environments are covered.

PRECEDING PAGE BLANK-NOT FILMED

INTRODUCTION

This is an abridged summary report of the effects of precipitation static electricity and lightning on aircraft windshields and canopies and their supporting electrical subsystems. The full work is reported in References 1 and 2, and was performed as a part of the Windshield Technology Demonstrator Program conducted for the U.S. Air Force Flight Dynamics Laboratory by the Douglas Aircraft Company, McDonnell Douglas Corporation.

Static electric (triboelectric) charging of the outer surface of a windshield or canopy can take place during flight when ice crystals, dust, or other particles impact with the electrically non-conductive windshield surface. This charging can continue until a very high voltage level is achieved. If the windshield or canopy has an electrically conductive anti-icing coating under the outer face ply, the static charge can stress the face ply until it is physically punctured. An alternate possibility, which can also occur on a transparency that does not use buried conductive coatings, is that the air on the charged windshield surface will ionize and conduct the electric charge to the aircraft metal structure. Either type of discharge can produce detrimental effects.

Lightning is also a possible problem and contains far more energy than does a triboelectric static charge. Lightning may attach to the canopy or windshield of an aircraft and puncture the transparency or flash across the outer surface to the aircraft structure. A more probable but still infrequent occurrence, especially on transport or large bomber configurations, is that lightning may attach to the metal nose section ahead of the windshield or canopy. The forward motion of the aircraft then blows the ionized arc channel back over the surface of the transparency. This is called swept stroke lightning, and may include a restrike during the passage or the arc channel over the windshield. (Most lightning flashes contain several restrikes.)

The end results of lightning activity are similar to but potentially more violent than those of static electric discharges. In either event, punctured windshields can be dangerous, and surface flashes can temporarily distract or blind the pilot. Either activity can induce destructive electrical transients into electrical equipment that connects to or is closely coupled to anti-icing or defogging coatings in the transparency.

LABORATORY SIMULATION OF THE STATIC ELECTRIC AND LIGHTNING ENVIRONMENT

Solutions to the potentially detrimental effects of static electric discharges and swept stroke lightning require the ability to produce these effects in the laboratory.

Previous attempts at static electric charging of transparencies have met with limited success, especially where large area transparencies were involved. One early attempt employed a specially cooled wind tunnel in which shaved ice was injected into the wind stream to later impinge on a small glass specimen (Reference 3). This experiment produced true triboelectric charging but the approach presents serious limitations when planned for full size windshields. Other innovative work (References 4 and 5) has employed blown dust or flour which, upon impact with the transparency, produces a charge. This approach

has had practical application (Reference 5), but still has some major drawbacks.

Static electric charge can be applied by non-triboelectric methods. One approach is especially adaptable to transparencies which use a conductive coating within a multi-ply configuration, representative of anti-iced windshields. In this approach a pointed electrode connected to a multikilovolt direct current source is held near the transparency surface to be charged. The return electrical circuit is connected to the conductive coating within the transparency. The single electrode charging technique works, but it has the disadvantage that the charge is applied locally and may overstress some areas of the transparency close to the pointed electrode and under-charge remote areas. To overcome these deficiencies Douglas developed a multi-electrode technique, shown in Figure 1. This uncomplicated, inexpensive approach employs a large number of ordinary lead pencils as the electrodes. It is described in detail in Reference 1. This method has been successfully used to deposit electrostatic charge on specimens as large as 4 feet by 6 feet and can be expanded for use on even larger areas.

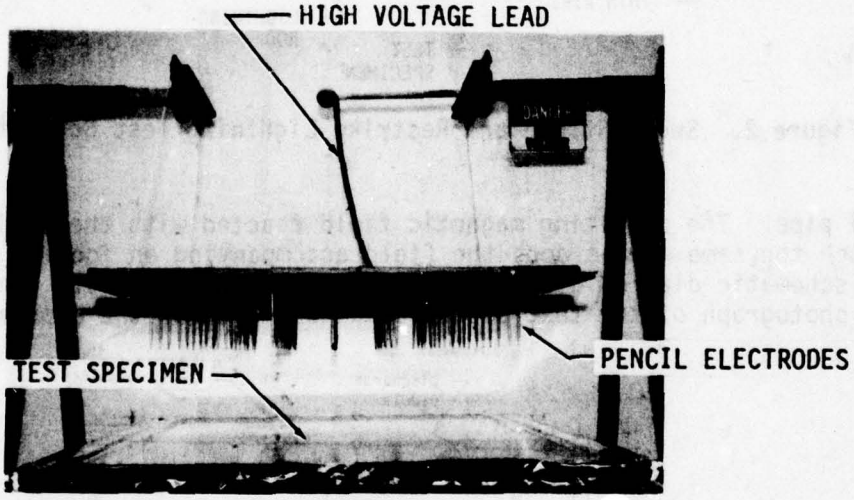


Figure 1. Multi-Electrode Charge Spray Head.

Swept stroke lightning can be simulated by initiating a discharge and then physically passing the specimen through the discharge. Another approach initiates a discharge and then blows the discharge over the specimen. Figure 2 is a schematic drawing of the latter approach.

A later phase of this work required a detailed investigation of the effects of lightning magnetic fields on conductive coatings. The technique shown in Figure 2 could have been used for this evaluation, but a more convenient and less costly approach was used. A metal pipe located adjacent to the outer surface of the windshield outer ply specimen was substituted for the ionized (conducting) discharge arc. The high rate-of-change, high current discharge was passed from the lightning simulation generator through the

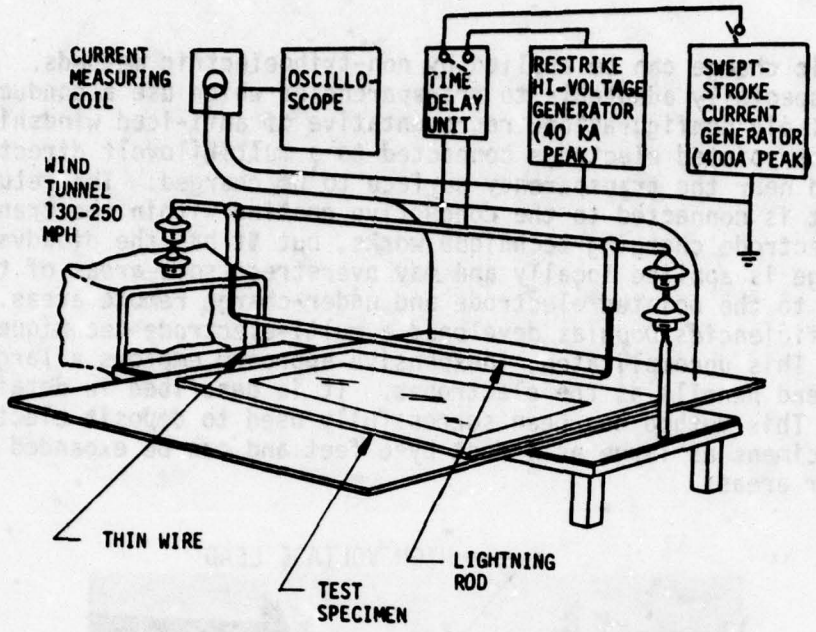


Figure 2. Swept-Stroke and Restrike Lightning Test Schematic Diagram.

metal pipe. The resulting magnetic field reacted with the conductive coating in much the same way as does the field accompanying an ionized flash. Figure 3 is a schematic diagram of this swept stroke lightning field generator. Figure 4 is a photograph of the test set up used to implement the approach of Figure 3.

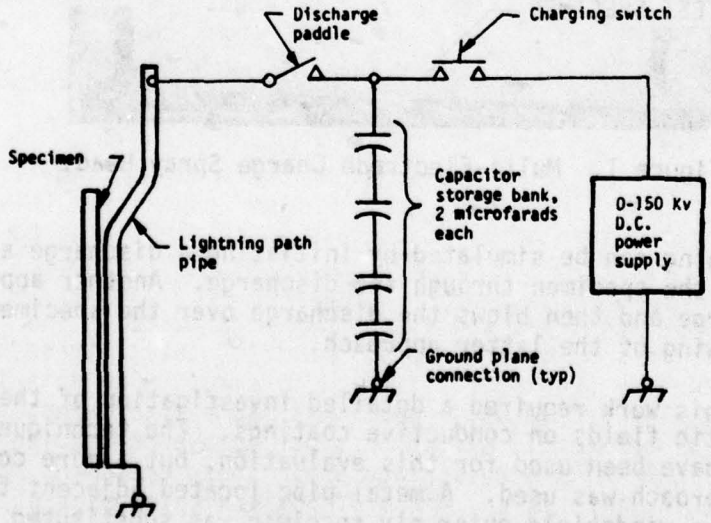


Figure 3. Schematic Diagram of Lightning Magnetic Field Simulator.

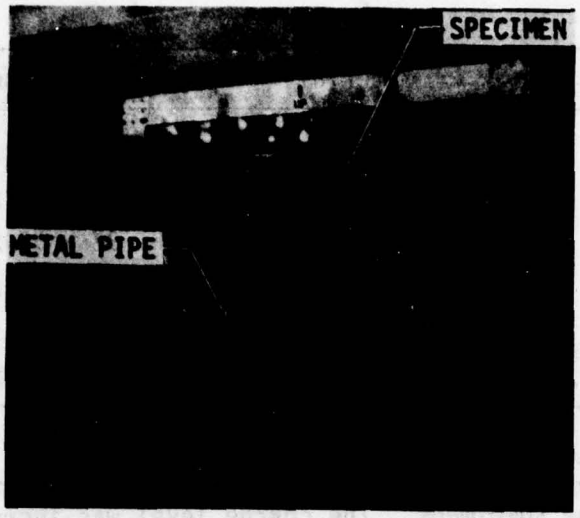


Figure 4. Lightning Magnetic Field Simulator.

TEST PROGRAM

The test program was conducted in two phases and had several objectives of which the following will be discussed here:

- Evaluate candidate windshield outer ply materials for their susceptibility to physical damage when subjected to precipitation static and swept stroke lightning environments.

- Evaluate the effect of external anti-static conductive coatings with respect to their possible tendancy to create attach points for swept stroke lightning.

- Investigate the effects of static electric discharges and swept stroke lightning on sub-surface transparent conductive coatings.

Candidate face ply materials were pre-screened for their suitability for use on high speed, large area windshields or high speed canopies. This mechanical pre-screening eliminated thinner ply materials which might also be more prone to electrical puncture.

Table 1 lists the specimen types and sizes that were tested. The first phase of testing used specimens of outer face ply material only. These had an aluminum foil on the back (unexposed) surface to simulate an anti-icing electrical coating. The second phase specimens had a transparent gold based conductive coating of between 15 and 20 ohms per square on the inner surface of the outer 0.085 inch thick acrylic face ply. These specimens had a cast in place 0.1 inch thick interlayer, and a 0.250 inch thick back ply of polycarbonate. Some of the glass, first-phase specimens had a high resistance stannous oxide anti-static outer surface coating.

TABLE 1. SPECIMEN DESCRIPTIONS

Test Phase	Material	Size (Inches)
I	Soda Lime Glass	48 x 62 x 0.187
I	Herculite II Glass	48 x 62 x 0.110
I	Chemcor Glass	37 x 53 x 0.105
I	Chemcor Glass	37 x 53 x 0.085
I	Acrylic Plastic	48 x 62 x 0.125
II	Acrylic Plastic	34 x 46 x 0.085

Static electric charge, representative of severe inflight charging was deposited on all of the specimens. The charge level was increased to the point where surface discharges took place on the specimens that did not have the anti-static exterior surface coating. The anti-static coating was fully effective in preventing surface flashover. Figure 5 is a representative surface flashover photograph of the first phase testing on a 37 x 53 x 0.085 inch Chemcor specimen. Figure 6 is a photograph of surface flashover on a 34 x 46 x 0.085 inch acrylic specimen as used in the second phase tests. The transparent anti-icing type conductive coating used on the phase two specimens permitted a see-through test setup wherein the camera is viewing through the specimen toward the pencil electrodes.



Figure 5. Surface Flashover on 37 x 53 x 0.085 Inch Chemcor Glass Specimen.

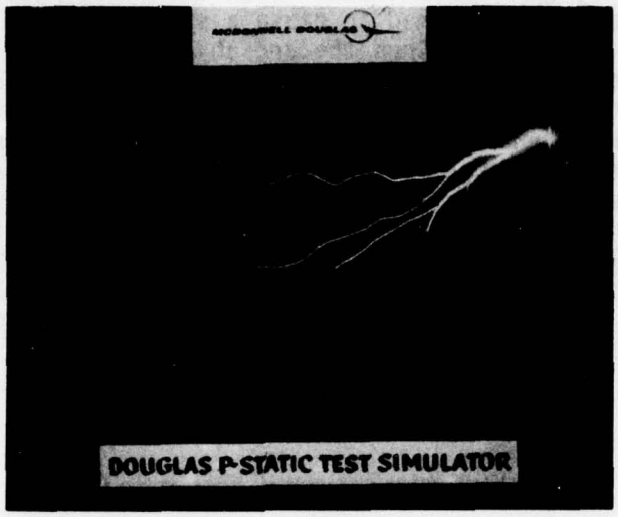


Figure 6. Surface Flashover on 34 x 46 x 0.085 Inch Acrylic Specimen With Transparent Conductive Coating.

No specimens were punctured during the electrostatic charging tests. A high charge condition always resulted in surface flashover of the type pictured in Figures 5 and 6. Faint etching or surface tracking was detected on the exposed surface of the soda lime and Herculite II specimens. One etch pattern, Figure 7, on a soda lime specimen was highly indicative of a pin-hole surface puncture, but detailed inspection using both visual and electrical means did not reveal a hole.

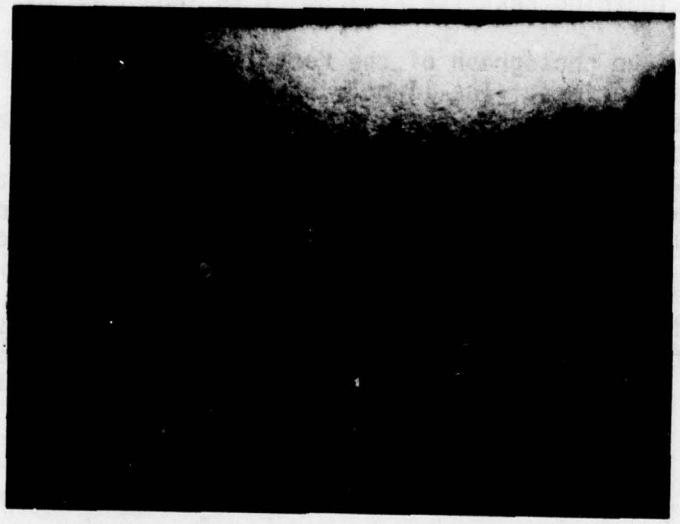


Figure 7. Surface Tracking on 0.187 Inch Thick Soda Lime Glass Specimen.

Swept stroke lightning tests were conducted on the first phase specimens. The lightning discharges were timed to cause a simulated high current restrike to occur during the time period when the arc channel was being blown across the specimen surface. This represented a severe, but possible condition. At no time did the lightning puncture the specimens. However, on occasions, the high current restrike caused the arc to hug the exposed specimen surface prior to being conducted to the metal periphery of the specimen mounting. This hugging action caused surface etching of all the glass specimens, but no etching could be detected on the acrylic specimen. Figure 8 is a time exposure photograph of swept stroke lightning on a soda lime specimen with an anti-static surface coating. The brilliant hook-shaped trace on the downstream (left) edge occurred during the restrike period. The hook pattern was etched into the surface of the glass, but the glass did not fracture.

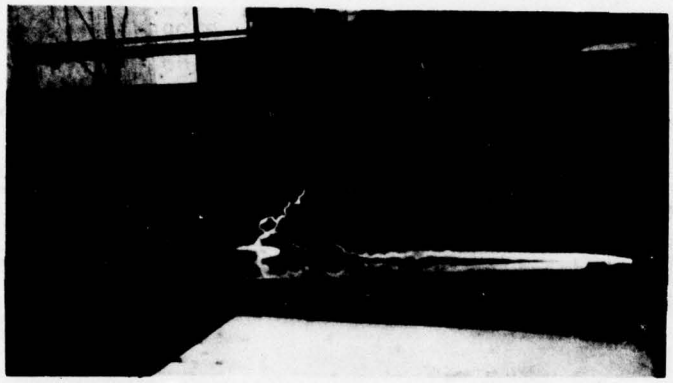


Figure 8. Lightning Restrike Attachment to Soda Lime Glass Specimen.

Figure 9 is a close-up photograph of the restrike markings on the surface of a Herculite II glass specimen. The lightly shaded portion in the central area is the etched glass. The darker shading bordering the lighter area is the burned and discolored anti-static coatings, which was no longer conductive. Figure 10 is a photograph of restrike markings on a Chemcor specimen resulting from several repeated tests. Some multi-trace markings occurred during a single restrike flash. Note that some of the restrike traces took a shorter path to ground at right angles to the 220-mile per hour wind stream.

The swept stroke lightning specimens which were treated with a stannus oxide anti-static resistive coating on the exposed surface did not show any greater tendency to cause the lightning flash to hug the surface than did the untreated specimens.

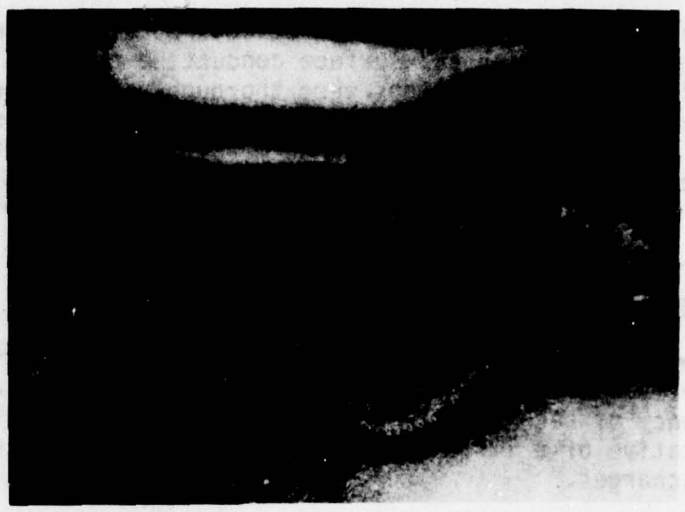


Figure 9. Lightning Restrike Markings on Herculite II Glass Specimen With Anti-Static Resistive Coating.

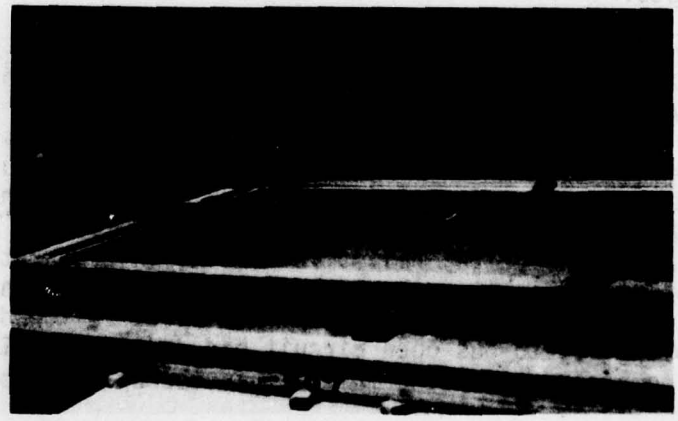


Figure 10. Lightning Restrike Markings on Chemcor Glass Specimen.

EFFECTS OF ELECTRICAL DISCHARGES ON CONDUCTIVE COATINGS

Phase II of the program investigated the effects of static electric discharges and swept stroke lightning on sub-surface conductive coatings representative of anti-icing coatings. Test specimens were thoroughly inspected prior to exposure to the static electric or lightning environment. Visual inspections in normal and polarized light, electrical resistance measurements, and thermal gradient patterns were made. The latter employed the AGA Thermovision 680 System which is, in effect, an infrared closed circuit television system with a multi-color display.

Static Discharge Tests

Two specimens were subjected to a large number of static electric discharges; one specimen to 192 and the other to 163. While no data are available on the inflight frequency of such occurrences, these exposure quantities were thought to be representative of a lifetime of exposure. Figure 6 is representative of the surface discharges.

The exposures were made in groups of discharges. Inspections were made after each group. The electrical transients induced in the conductive film by the individual discharges were measured by instrumenting external wires connected to the conductive film buses. Typical transients for this size specimen reached a peak amplitude of 100 Amperes in one microsecond. The inspection revealed some changes in the resistance uniformity of the conductive coatings, but no changes caused by the static electric discharges were considered significant enough to adversely affect the usefulness of the material if it were a part of an actual aircraft windshield.

Lightning Discharge Tests

Simulated swept stroke lightning electromagnetic field tests using the technique previously discussed were conducted on two specimens which duplicated those used for the static electric discharge tests. Duplicate specimens were used to exclude any possibility of having the static electric discharges affect the lightning tests.

The first lightning specimen was subjected to a number of low current discharges during early instrumentation runs. Visual, resistance, and Thermograph inspections did not show any significant changes in the specimen as a result of these preliminary, low current discharges. Next, the specimen was subjected to a high current (48 kiloampere) discharge, which produced no visual indications of sparking or damage. Therefore, a second high current discharge was run, after which detailed inspection was conducted. When electric power was applied between the buses of the resistive coating in preparation for the Thermovision inspection, a hot spot developed in the coating near an edge bus bar. The acrylic sheet began to bubble in this spot, followed by a rapid cooling. A complete bus-to-bus open circuit had developed. This would be equivalent to a complete anti-icing failure had the specimen been an actual windshield.

The electrical failure in the bus-coating interface area was visible on close examination, but was still rather difficult to see. This specimen, which failed in the lightning environment, was then placed in the P-static test simulator. Figure 11 shows a single oak tree discharge in the central area, and numerous low intensity sparks tracing the length of the electrical failure in the right hand bus-conductive coating area. After the static electric exposure, the coating failure line appeared to have been visually enhanced. It had a pink halo around the conductive coating fracture line which made visual observation very easy. The static electric discharges did not appear to have increased the damage, they only enhanced the visibility.

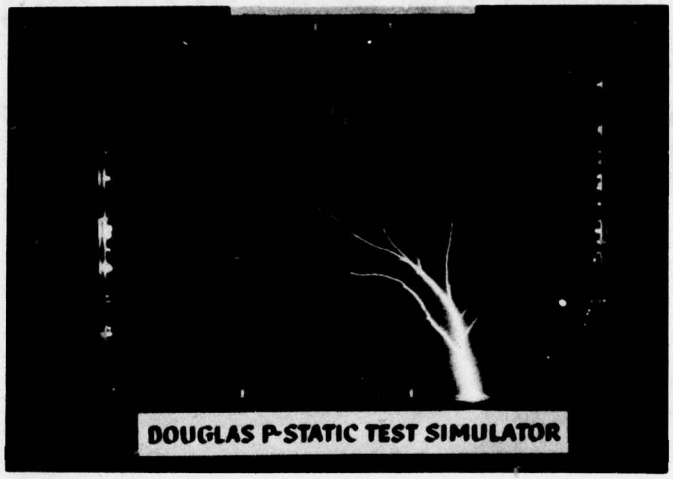


Figure 11. Specimen Undergoing Static Discharge After Lightning Exposure.

Because of the complete failure of the first lightning exposure specimen, a more cautious exposure schedule was used with the second specimen. Low level instrumentation discharges were run, as before. But this time a full series of visual, resistance, and Thermograph inspections were conducted. No significant changes were noted.

Following the preliminary discharges a single high current discharge was made. The conductive coating on this specimen was made in two symmetrical sections with four electrical buses. The buses for one section were directly grounded, while the two buses for the other section were interconnected with a wire and the pulse current induced by the lightning in this section was measured. The peak current in the instrumented section was approximately 130 amperes.

Visual inspection of this specimen following the lightning discharge revealed some burning of the buses and nearby conductive coating. No sparking was observed during the discharge. The Thermovision inspection showed a significant change in the temperature distribution around the damaged area.

The specimen was then subjected to another lightning pulse, with the simulated flash directed symmetrically over the instrumented half of the conductive coating section. The peak pulse current was now about 150 amperes. Inspection

revealed significant damage along most of the bus-coating interface. The specimen would not be satisfactory if it were a part of an actual windshield.

CONCLUSIONS

The external electrical environments such as precipitation static electricity and lightning must be accounted for in the design of aircraft windshields and canopies. Static electric discharges on outer face ply material of adequate thickness and dielectric strength should not puncture the material. The discharges will, however, induce large electrical transients into connected anti-icing circuitry when conductive coatings for this purpose are a part of the face ply design. These induced transients should not damage the electrical coating when the coating-bus design and manufacture are adequate and the size of the charged surface is approximately 3 by 4 feet or smaller. Larger sizes and different material would require additional investigation.

Swept stroke lightning that flashes across a transparency which employs subsurface anti-icing electrical coatings can induce destructive current in the coating-bus assembly.

REFERENCES

1. Twomey, R. C., Effects of Laboratory Simulated Precipitation Static Electricity and Swept-Stroke Lightning on Aircraft Windshield Subsystems, Technical Report AFFDL-TR-76-75, May 1976.

2. Twomey, R. C., Precipitation Static Electricity and Swept-Stroke Lightning Effects on Aircraft Transparency Coatings, Technical Report AFFDL-TR-77-141, December 1977.

3. Sharp, P. J., Static Electrification of Windscreens and Canopies, 1975 Conference on Lightning and Static Electricity, Culham Laboratories, England.

4. Oh, L., Huang, G. C., Goldman, R., et al., Natural and Induced Effects on Integrated Antennas and Circuits at Frequencies to 10 G Hz, Technical Report AFAL-TR-69-210, September 1969.

5. Munsell, M. B., TPS Electrostatic Charge Effects on Avionics Systems and Antennas, Report MDC A3673, McDonnell Aircraft Company, McDonnell Douglas Corporation, November 1975.

SESSION III

ADVANCED TECHNOLOGY DEMONSTRATOR PROGRAM STATUS REVIEW (PART II)

Chairman: J. H. Lawrence, Jr.
Douglas Aircraft Company
McDonnell Douglas Corp.
Long Beach, California

PRECEDING PAGE BLANK-NOT FILMED

THE DEVELOPMENT OF STATISTICAL METHODOLOGIES AND A COMPUTER PROGRAM FOR MATERIAL PROPERTIES

R. H. Magnusson
Douglas Aircraft Company
McDonnell Douglas Corporation
Long Beach, California

PRECEDING PAGE BLANK-NOT FILMED

THE DEVELOPMENT OF STATISTICAL METHODOLOGIES AND A COMPUTER PROGRAM FOR MATERIAL PROPERTIES

by

RALPH H. MAGNUSSON

Douglas Aircraft Company
Long Beach, California

ABSTRACT

MIL-HDBK-5B is the standard source book in the aircraft industry for the design mechanical properties of various metals and elements. As a means of maintaining uniformity in the presentation of mechanical-property values in that document and a high level of assurance in the values reported, statistical techniques are employed and requirements have been established to ensure the adequacy of the supporting data.

A basic effort of the WTDP was to establish mechanical properties of pertinent transparency and interlayer materials on a similar basis to the requirements of MIL-HDBK-5B. Because of the high levels of elongation achieved in these plastic materials, true stress-strain curves were developed from test, thus allowing an accurate behavior description.

To meet the requirements for statistically minimum guaranteed design curves, the developed true stress-strain curves for a series of repeated tests were statistically analyzed for normal (Gaussian) distribution using standard methods. Since budgetary constrains were ever-present, a much smaller sample was utilized rather than the many observations required for the usual normality checks and general design values. The smaller sample was adequately tested for normal distribution using the Kolmogorov-Smirnov test. These procedures allow the development of specific design stress-strain curves taking into account the sample size, and desired confidence level. These curves were developed utilizing a Douglas proprietary computer program to process stress-strain data from the tested specimens.

These methods have proved to be effective in allowing the generation of mechanical properties of transparency materials on a solid statistical basis.

PRECEDING PAGE BLANK-NOT FILMED

INTRODUCTION

A basic effort of the Windshield Technology Development Program was to establish usable mechanical properties of certain pertinent transparency materials on a statistical basis suitable for use in transparency design of high-performance aircraft. The necessity of such property-determination for stringent design requirements is indicated in Reference 1. This paper briefly presents the background of methods involved in the proper determination of transparency material properties such that advantage may be taken of the materials' full capabilities. The testing and methodologies employed by the Douglas Aircraft Company is fully covered in Reference 2.

Past standards of transparent materials are listed (References 3, 4). These handbooks were prepared by the National Bureau of Standards and the Goodyear Aerospace Corporation to provide information for the selection of transparent glazing materials and the factors to be considered in their installation and use in military and commercial aircraft.

In the recent past, aircraft glazing configurations have become increasingly complex, to the extent of not only performing as structural members, but also as protective coverings in a wide variety of situations. Structural loading in the flight profiles of high-performance aircraft involves not only differentials between cockpit pressurization and outer ram air loading, but also transient thermal conditions that tax the lower extremities of material strength spectrums. In addition to these loads are the stringent requirement of withstanding the impact of birds.

Adding the protective features usually increases the transparency thickness and weight beyond that required for structural integrity. If a special coating is required, an additional transparent coating or sheet is often necessary to protect the active coating from damage. In situations where differences of thermal expansion coefficients are critical between two rigid materials, a separating elastic interlayer is added as a further complexity. With one exception, any of the additional protective features will act negatively toward light transmission and optical integrity.

A design engineer needs to have material properties he can, with confidence, utilize in achieving an aircraft transparency design adequate to withstand the critical loads. Also, the design must be compatible with the basic mission and flight optical requirements of the particular aircraft.

TECHNICAL DISCUSSION

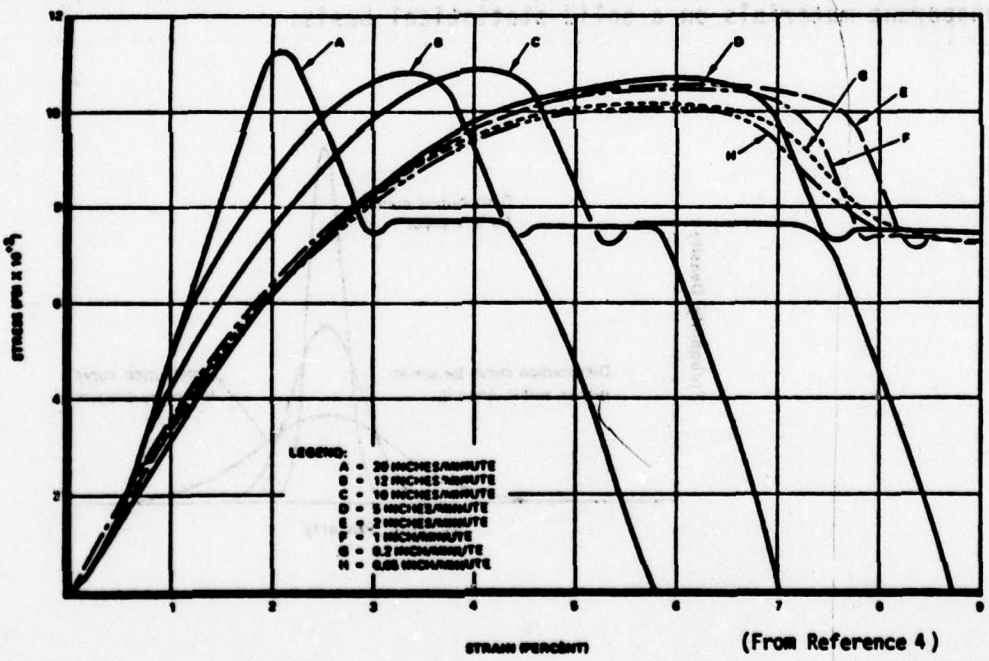
Material Property Data

Historically, the oldest way of describing a material property is by one number which characterizes the "average" property quantiatively. This number indicates the "ball park" value of the material property, but has little meaning from a statistical point of view. Such a description of a

material property tells nothing about the variability of the particular property. Unfortunately, many transparent material properties are listed in this fashion in vendor's and processor's literature, in textbooks and even in the lastest edition of MIL-HDBK-17A, Part II (Reference 4). On page 1-2 of this handbook is stated:

> "The data on the mechanical, thermal, optical, and other properties of transparent plastics and glass have been selected from a number of specifications and reports. Sufficient test data were not available on all materials for establishing design allowables. Therefore, some material property data are only representative values and should be considered as such. Because most configurations are complex, the designer should prepare test specimens of the final design configuration and conduct confirmation tests of all critical design factors." (Underlining by the author.)

It should be mentioned that in MIL-HDBK-17A, Part II, no indication is given for any material as to whether "sufficient test data" was available for it, or whether or not its "material property data are only representative values." As any transparency designer is aware, many times these "ball park" values are the only information easily available. (Figure 1.)



(From Reference 4)

Figure 1. Stress Versus Strain for 1/4-Inch Thick Polycarbonate, MIL-P-83310 Room Temperature (Thermal Condition)

Military-Handbook-5 Data

An example of an excellent source for metallic material properties is Military-Handbook-5B (Reference 5). This military design handbook is the standard source book in the aircraft industry for the design strength properties of various metals and elements. Much of the strength information is based on statistical data and is listed for certain materials of various forms (sheets, bars, castings, etc.) and of various treatments. In most cases, a design allowable value for the material strength properties are given such a certain high percentage of all like material is expected to exceed these values. The statistical techniques employed are a means of maintaining a high level of assurance in the reported values. They also insure the adequacy of the supporting test data.

Section 9 of MIL-HDBK-5B fully describes the statistical techniques required to present acceptable design-allowable material property values. Again, only by proper utilization of such techniques, can the design-allowables of these materials be generated. Douglas followed the recommendations of MIL-HDBK-5B in the preparation of statistically-accurate design-allowables for the polycarbonate specimens tested.

Figure 2 shows the distributive effects when various numbers of material samples are tested. It may be appreciated that when a large number of samples are considered, the material properties can cover a large range. The techniques of MIL-HDBK-5 permit the generation of mechanical properties of transparent materials on a solid statistical basis.

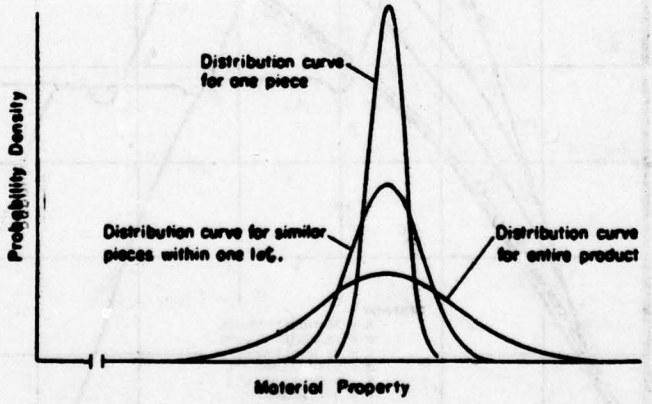


Figure 2. Material Property Distributions.

Determination of Material Properties

The variability of transparent material allowables at different levels of temperature and strain-rate is well known. Hence, to arrive at realistic material properties for design testing must reflect the applicable temperature and/or strain-rate regimes. However, in the case of polymers in general, and polycarbonate specifically, other factors must be considered such as the embrittling effect of thermal conditioning and prior work history. "Thermal conditioning" is a term applied to the net effect of all processes which subject polycarbonate to temperatures between 80°C (176°F) and the glass transition temperature for a certain amount of time. These temperature-time effects are cumulative whether due to optical processing, press-polishing, forming, or a high-temperature flight regime.

The shape of stress-strain curves for metals are quite familiar to any designer. Some typical curves are shown in Figure 3. The top curves show that metals can endure a maximum strain in the neighborhood of 15% before failure. The lower curves are details in the elastic region of the same metals. Most designers are comfortable with the way curves, such as these, were generated. The fact that these stress-strain curves are, in reality, load-deflection curves doesn't seem important.

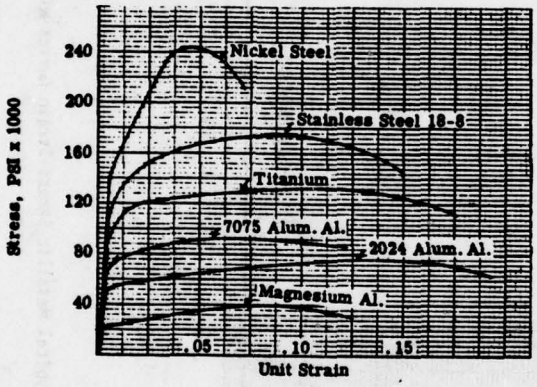


Figure 3. Typical Metallic Stress-Strain Curves.

Now when the "stress-strain" curve of polycarbonate is shown superimposed on the metals curves, as in Figure 4, the designer should appreciate that, perhaps, there's a new "ball-game" in town. This new "ball-game" is the concept of true stress-strain.

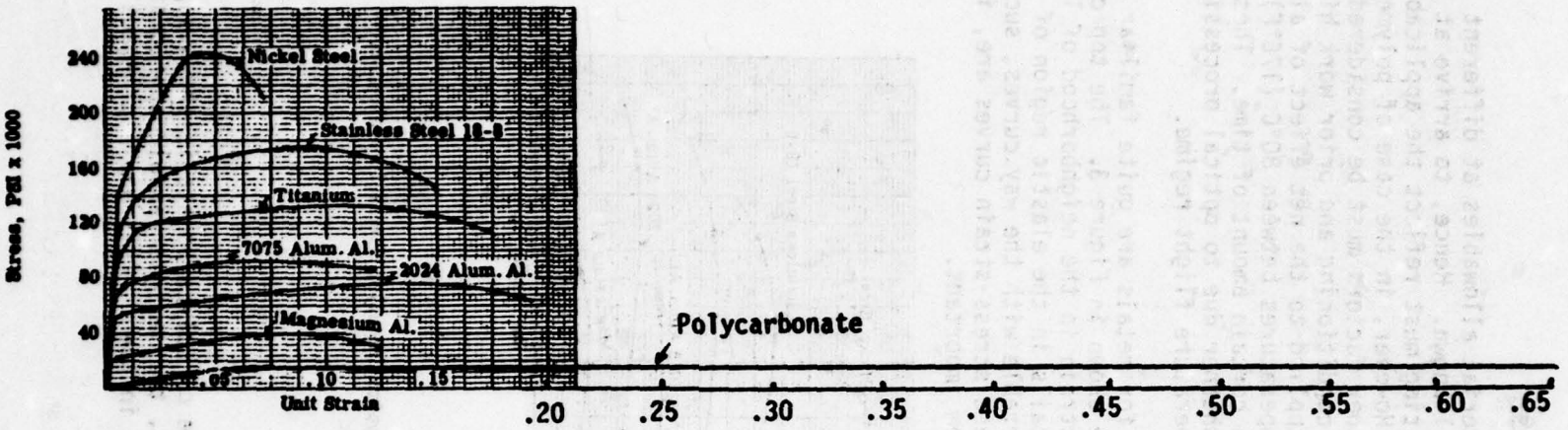


Figure 4. Typical Metallic Stress-Strain Curves with Polycarbonate Comparison.

True Stress and True Strain

The engineering stress-strain curve does not give a true indication of the deformation characteristics of a material because it is based entirely on the original dimensions of the specimen. These dimensions change continuously during the test (Figure 5). This dimensional change is quite noticeable when the specimen undergoes appreciable change in cross-sectional area. This commonly occurs in the highly elongated regions of ductile metals, as in wire drawing or deep-formed parts. Thus, measures of stress and strain which are based on the instantaneous dimensions are needed. Since dimensional changes are small in elastic deformation, it is not necessary to make this distinction in this region.

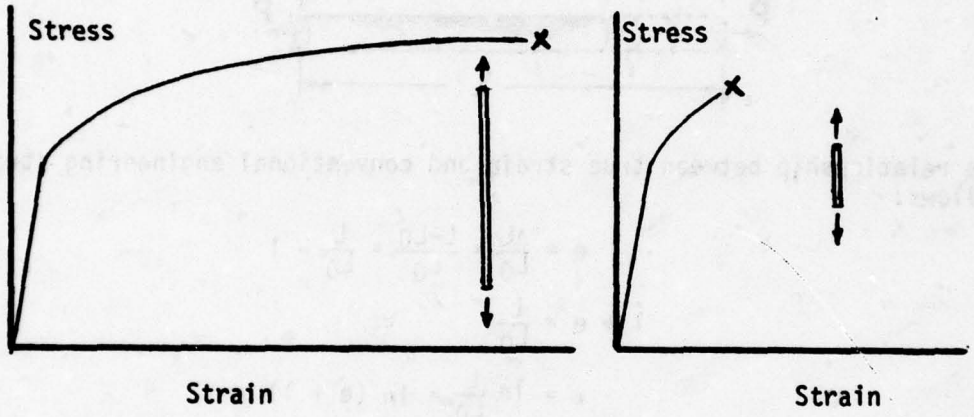
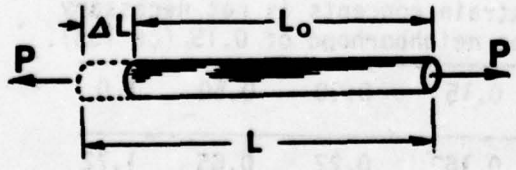


Figure 5. Representative Material Behavior.

Equation 1 describes the conventional concept of unit linear strain, namely, the change in length referred to the original unit length as shown below.



$$e = \frac{L-L_o}{L_o} = \frac{\Delta L}{L_o} = \frac{1}{L_o}\int_{L_o}^{L} dL$$

This definition of strain is satisfactory for elastic strains where ΔL is very small. However, in plastic deformation of polycarbonates and other glassy polymers, as well as in ductile metals, the strain are quite large. The concept of <u>true strain</u>, or <u>natural strain</u>, ϵ, elminates this

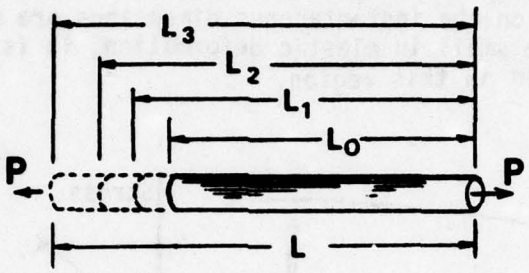
difficulty. In the following definition, the change in length is referred to as the instantaneous gage length, rather than to the original gage length:

$$\varepsilon = \sum \frac{L_1 - L_0}{L_0} + \frac{L_2 - L_1}{L_1} + \frac{L_3 - L_2}{L_2} + \ldots . \qquad (2)$$

or

$$\varepsilon = \int_{L_0}^{L} \frac{dL}{L} = \ln \frac{L}{L_0} \qquad (3)$$

Pictorially:



The relationship between true strain and conventional engineering strain follows:

$$e = \frac{\Delta L}{L_0} = \frac{L - L_0}{L_0} = \frac{L}{L_0} - 1$$

$$1 + e = \frac{L}{L_0}$$

$$\varepsilon = \ln \frac{L}{L_0} = \ln (e + 1) \qquad (4)$$

$$e = (2.71828)^{\varepsilon} - 1$$

Utilizing Equation (4), a comparison of true strain and engineering strain may be made. The table below shows such a comparison and also indicates the percentage error which will be incurred utilizing the engineering-strain approach. This table shows a very sizable error (30%) in engineering strain at an achievable true strain of 0.50, while both measures of strain give nearly identical results up to a strain of 0.10. Again, by referring to Figure 4, it may be seen that for metals, in general, the use of true strain concepts is not necessary as fracture occurs at strain levels in the neighborhood of 0.15 (or 15%).

TRUE STRAIN	0.01	0.10	0.15	0.20	0.50	1.0
ENGRG STRAIN	0.01	0.105	0.162	0.22	0.65	1.72
% ERROR	0	5%	8%	10%	30%	72%

The advantage, or, rather, the necessity of using the true strain concept should be apparent from the example as shown in Figure 6. This example considers a uniform cylinder which is extended to twice its original length. The tensile engineering strain is then $e = (2L_0 - L_0)/L_0 = 1.0$, or a strain of 100%. To achieve the same amount of compressive engineering strain, the cylinder would have to be squeezed to zero thickness. Intuitively, however, one senses that the strain produced in compressing a cylinder to half its original length should have the same absolute value as the strain produced by extending the cylinder to twice its length. Figure 6 shows this. If the true strain concept is used, equivalence is obtained for the two cases as shown.

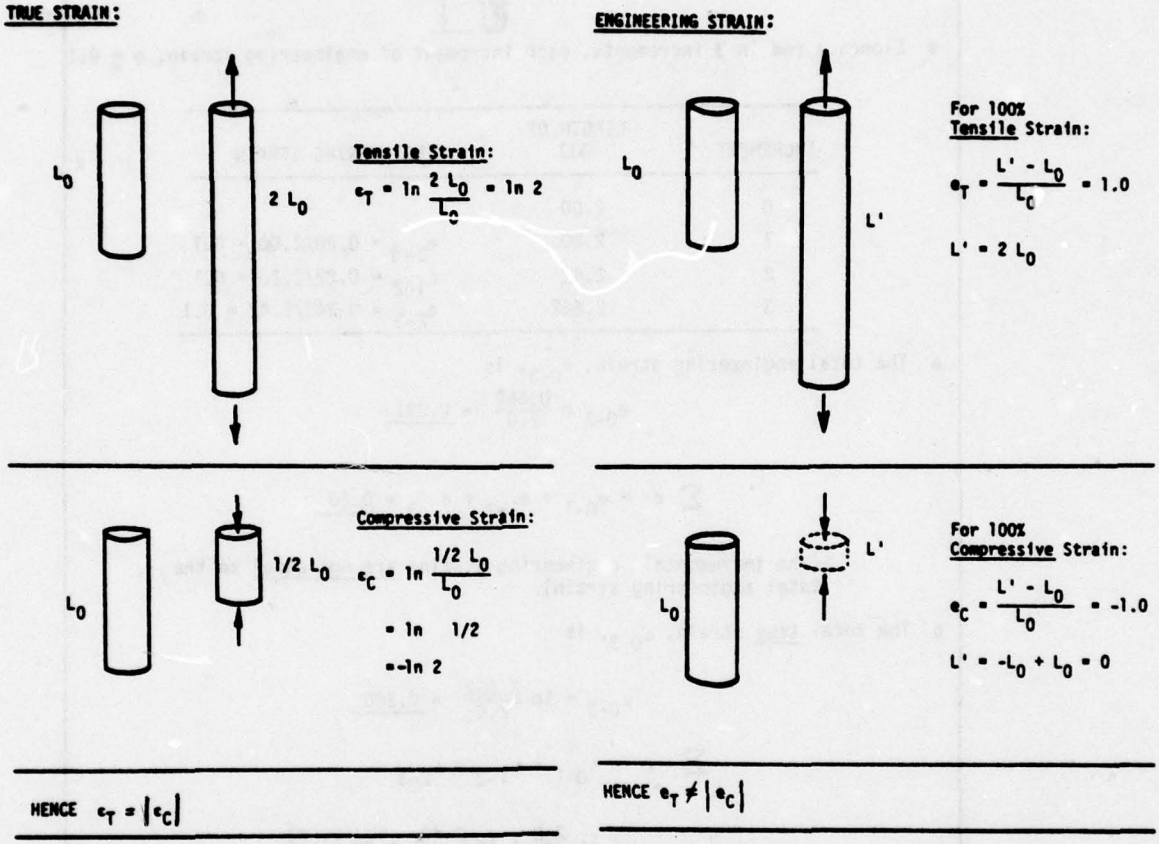


Figure 6. True Strain vs. Engineering Strain for Large Displacements.

Another important reason for using true strain is the advantage that the TOTAL true strain is equal to the sum of the INCREMENTAL true strains. This consideration is all important in computer coding of stress-strain relationships. This concept is covered in Table 1.

TABLE 1. INCREMENTAL TRUE STRAINS



- Elongate rod in 3 increments, each increment of engineering strain, e = 0.1

INCREMENT	LENGTH OF ROD	ENGINEERING STRAIN
0	2.00	
1	2.20	$e_{0-1} = 0.20/2.00 = 0.1$
2	2.42	$e_{1-2} = 0.22/2.20 = 0.1$
3	2.662	$e_{2-3} = 0.242/2.42 = 0.1$

- The total engineering strain, e_{0-3}, is

$$e_{0-3} = \frac{0.662}{2.0} = \underline{0.331}$$

$$\Sigma e = e_{0-1} + e_{1-2} + e_{2-3} = \underline{0.30}$$

(The incremental engineering strains <u>are not equal</u> to the total engineering strain)

- The total <u>true</u> strain, ϵ_{0-3}, is

$$\epsilon_{0-3} = \ln \frac{2.662}{2.0} = \underline{0.286}$$

$$\Sigma \epsilon = \epsilon_{0-1} + \epsilon_{1-2} + \epsilon_{2-3}$$

$$= \ln \frac{2.2}{2.0} + \ln \frac{2.42}{2.2} + \ln \frac{2.662}{2.42}$$

$$= 0.095 + 0.095 + 0.095$$

$$= \underline{0.286}$$

(The incremental true strains <u>are equal</u> to the total true strains)

True stress is the load at any instant divided by the cross-sectional area over which it acts. The engineering stress is the load divided by the original area. These relations are covered in Table 2. Generally, as has been stated, engineering stress-strain curves may be visualized as load-deflection curves. This is the reason for the "drop" in the engineering-stress value at yield; that is, the LOAD in the tested specimen drops, but the TRUE STRESS does not.

TABLE 2. TRUE STRESS DEFINITION AND EQUIVALENCY

True Stress $\sigma = \frac{P}{A}$

Engineering Stress $s = \frac{P}{A_0}$

The true stress may be determined from the engineering stress as follows:

$$\sigma = \frac{P}{A} = \frac{P}{A_0} \frac{A_0}{A}$$

Since the constancy-of-volume relationship holds

$$\frac{A_0}{A} = \frac{L}{L_0} = e + 1$$

hence,

$$\sigma = \frac{P}{A_0} (e + 1) = s (e + 1)$$

Minimum Guaranteed Design Stress-Strain Curve Development

Test curve data is received as a plot of load (pounds) versus strain (inches). Test specimen measurement data furnished with each curve includes gage length (ℓ_g), initial cross-sectional area (A_0), cross-sectional area measured after rupture (A_p), and elongation of specimen to rupture (ℓ_r). The tensile load-strain curve is converted to a tensile stress-strain curve by establishing stress (σ) and strain (ε) scales, plotting the rupture point, and drawing a line tangent to the elastic portion of the curve to the rupture point as

illustrated in Figure 7. The vertical stress scale is established by dividing the load increment (ΔP) by A_o. The horizontal strain scale is established by dividing strain ($\Delta \ell$) by ℓ_g. The tensile curve rupture point true stress (σ_r) and true strain (ε_r) coordinates were determined as follows:

$$\bar{\sigma}_r = \frac{P}{A_p} \tag{5}$$

$$\bar{\varepsilon}_r = \ln \frac{\ell_r}{\ell_g} \tag{6}$$

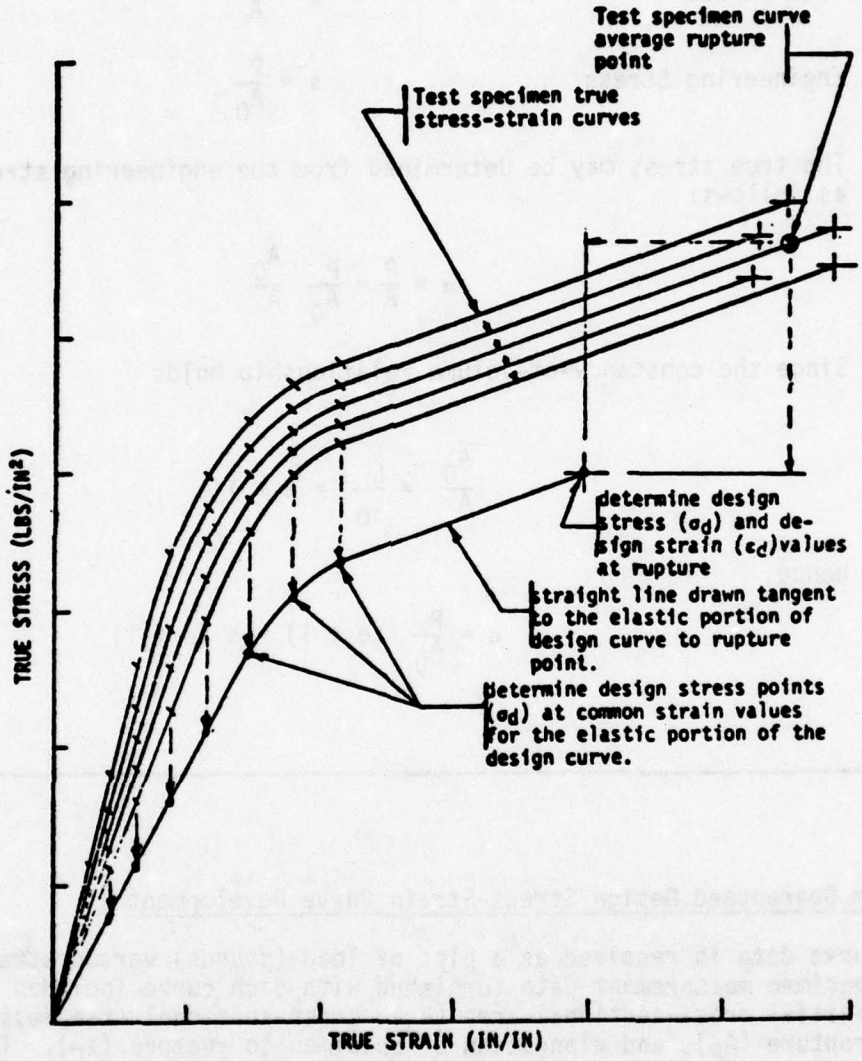


Figure 7. Design Tensile Stress-Strain Curve Development

The plastic range of the true stress-strain curve was drawn as a straight line as this was determined to reflect the test specimen cross-sectional area reduction versus load during plastic elongation. The straight line assumption for the plastic portion of the curve is considered conservative as the final area, A_p, was calculated after the observed elastic snap-back. An approximation of the cross-sectional area reduction based on the observed gap after snap-back gives a ten per cent higher value for <u>stress</u> at rupture.

To meet the requirement for minimum guarantee design curves, the developed true stress-strain curves for a series of repeated tests were statistically analyzed using methods outlined in MIL-HDBK-5B for normal (or Gaussian) distribution. The statistical methods used in MIL-HDBK-5B are normally used in determining specific design strength values such as tensile ultimate strength, tensile yield strengths, compressive yield strength, etc. In a similar manner these methods were adapted to determine specific stress or strain values on the minimum guarantee design curve for a number (n) of stress or strain values (X_i) on the tensile stress-strain curve as illustrated in Figure 11.

From the analysis of the sample size (N), the mean stress ($\bar{X}$), where,

$$\bar{X} = \Sigma X_i / N \quad , \tag{7}$$

and the standard deviation (s), where,

$$s = \sqrt{\Sigma (X_i - \bar{X})^2 / N - 1}, \tag{8}$$

are computed. A normality check was made using the Kolomgorov-Smirnov test as follows: a plot of the cumulative normal curve distribution function was determined by numerical integration of the function

$$\frac{1}{(2\pi)^{1/2}} e^{-\frac{T^2}{2}} \tag{9}$$

where, $T = \frac{(X-\bar{X})}{S}$ (10)

a plot of the sample cumulative distribution function $S_n(X)$ was superimposed upon the normal curve distribution and compared with critical values of D in the table of values for Kolmogorov-Smirnov test as illustrated in Figure 8. Sample stress values that are within the critical values of D are considered as normally distributed. The normally distributed stress points are then analyzed to determine the minimum guarantee design stress point

$$(\sigma_d) = \bar{X} - ks, \tag{11}$$

where k is the one-sided tolerance factor for the normal distribution from MIL-HDBK-5B, Table 9.6.4.1. These k values take into account both the sample size and desired confidence level for A basis, B basis, or C basis curves as shown and defined in Figure 9.

A completed design curve for polycarbonate is shown in Figure 10.

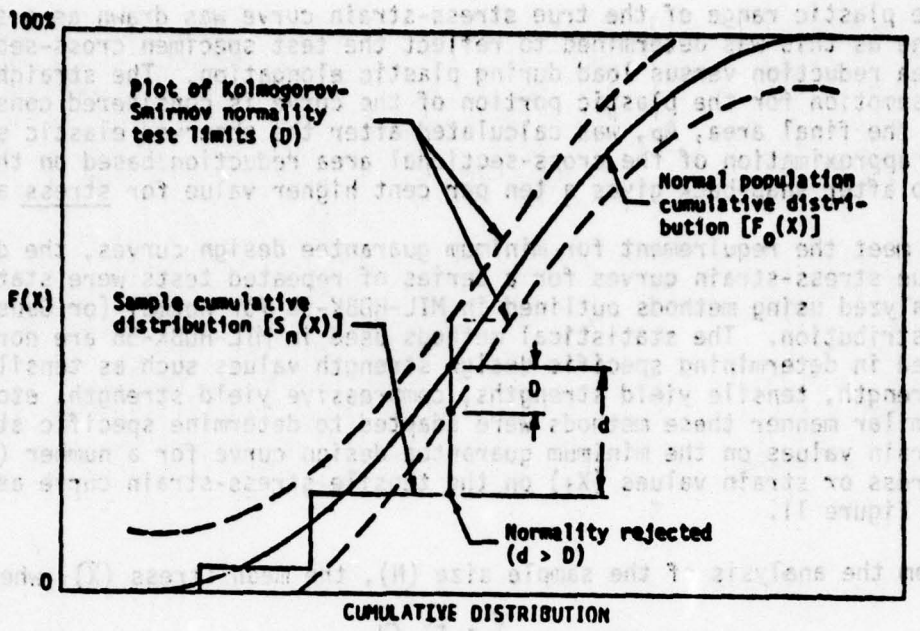


Figure 8. Graphical presentation of normality check.

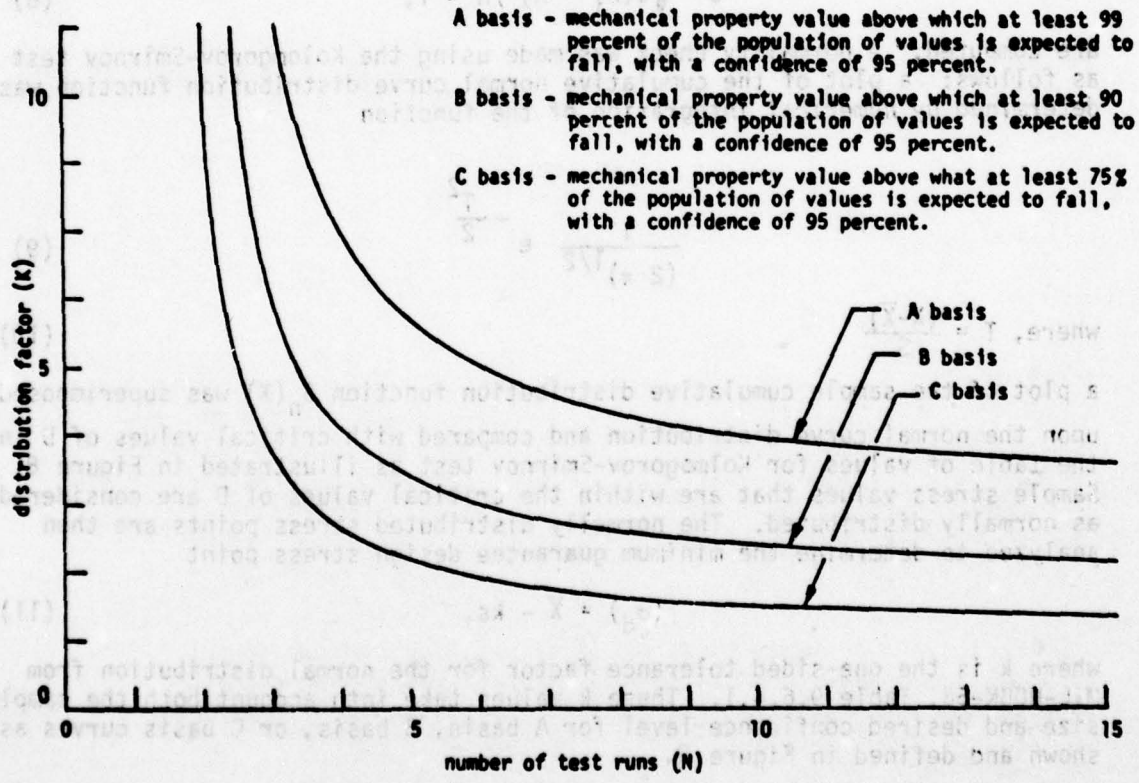


Figure 9. Normal population distribution factor K vs N.

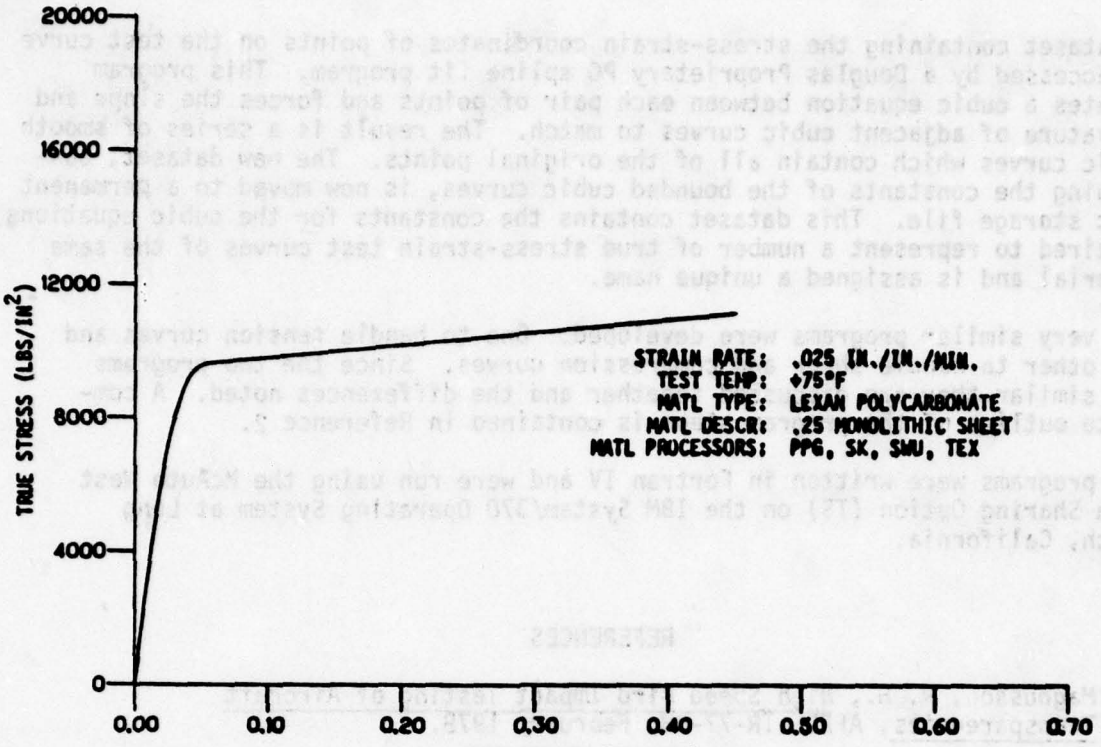


Figure 10. Tensile design (C) curve - General

Material Properties Computer Program Development

The minimum guaranteed stress-strain design curves are constructed by use of developed computer programs used in conjunction with existing Douglas programs.

The true stress-strain test curves were converted to a format that was usable in a computer program. The method selected uses parametric cubic (PC) geometry, which is a mathematical technique for describing bounded 3-dimensional curves and surfaces in a form that satisfies the need for speed, accuracy and manipulative flexibility. This particular case was limited to 2-dimensional curves. Proprietary Douglas subroutines were used to accomplish these parametric cubic operations.

The true stress-strain test curves must first be "digitized", that is, a sufficient number of points to ensure accuracy must be selected on each curve and the stress-strain coordinates determined. A Gerber Flat Bed Plotter with an optical line follower was used to do this. A T.V. camera transmits a picture of the curve with a cross-hair superimposed to a remote screen. Because PC curves were used, relatively few points were required and the operator moves the cross-hair manually to each point to be digitized. The datasets generated are then moved to a file for later use.

A dataset containing the stress-strain coordinates of points on the test curve is accessed by a Douglas Proprietary PC spline fit program. This program creates a cubic equation between each pair of points and forces the slope and curvature of adjacent cubic curves to match. The result is a series of smooth cubic curves which contain all of the original points. The new dataset, containing the constants of the bounded cubic curves, is now moved to a permanent disc storage file. This dataset contains the constants for the cubic equations required to represent a number of true stress-strain test curves of the same material and is assigned a unique name.

Two very similar programs were developed. One to handle tension curves and the other to handle shear and compression curves. Since the two programs are similar they are discussed together and the differences noted. A complete outline of the program steps is contained in Reference 2.

The programs were written in Fortran IV and were run using the McAuto West Time Sharing Option (TS) on the IBM System/370 Operating System at Long Beach, California.

REFERENCES

1. Magnusson, R. H., High Speed Bird Impact Testing of Aircraft Transparencies, AFFDL-TR-77-98, February 1978.

2. Greene, F. E., Testing for Mechanical Properties of Monolithic and Laminated Polycarbonate Materials, AFFDL-TR-77-96, March 1978.

3. Plastics for Flight Vehicles, MIL-HDBK-17, Part II, 14 August 1961.

4. Plastics for Aerospace Vehicles, MIL-HDBK-17A,Part II, January 1973.

5. Metallic Materials and Elements for Aerospace Vehicle Structures, MIL-HDBK-5B, 15 August 1974.

DESIGN MECHANICAL PROPERTIES OF PROCESSED POLYCARBONATE AND INTERLAYER MATERIALS FOR AIRCRAFT TRANSPARENCIES

F. E. Greene
Douglas Aircraft Company
McDonnell Douglas Corporation
Long Beach, California

DESIGN MECHANICAL PROPERTIES OF PROCESSED POLYCARBONATE AND INTERLAYER MATERIALS FOR AIRCRAFT TRANSPARENCIES

by

FRANK E. GREENE
Senior Engineer/Scientist

Douglas Aircraft Company
Long Beach, California

ABSTRACT

The purpose of this program was to develop design mechanical properties of processed polycarbonate and high temperature interlayer materials for use in design analysis of transparencies for low level supersonic aircraft. To provide for both static and dynamic load analysis, complete stress-strain histories of processed materials were developed from tensile, compression and shear tests conducted at strain rates from 0.025 to 12,000 in./in./minute. Tests were conducted at temperature ranges between -30°F and 190°F to simulate the extreme temperature range of the design aircraft flight environment.

The paper presented gives a brief description of test criteria, testing techniques, and test specimens used to accomplish these tasks. A review of problems involved in accomplishing these tasks are discussed along with highlights of tests results to show the effects of temperature and strain rates on materials tested.

PRECEDING PAGE BLANK-NOT FILMED

INTRODUCTION

The determination of design mechanical properties for the structure of a supersonic aircraft transparency involves a knowledge of the load-carrying ability of the transparency materials under low strain-rate and high strain-rate loading conditions at wide temperature extremes. The low strain-rate (0.025 in./in./min. to 20 in./in./min.) mechanical properties of aircraft transparency materials are required to design for cabin pressure, thermodynamic loads, aerodynamic loads, and structural carry-through loading. The high strain-rate (10 in./in./sec to 200 in./in./sec) mechanical properties of the aircraft transparency materials are required to design for bird strike impact loading. In the case of low strain-rate loading, the inherent load-carrying ability of a transparency must be such that the limit load can be sustained without excessive deformation or permanent set, requiring a knowledge of the elastic properties of the materials. The load-carrying ability of a transparency under high strain-rate conditions requires a knowledge of the material in the plastic range, where excessive deformation is a design asset due to energy absorption of the bird impact shock load. To provide these design mechanical properties the complete stress-strain histories of candidate materials are required. The critical design mechanical property requirements for a laminated transparency were determined to be predominately tensile and compressive in the main load carrying plies, and shear in the inner-layer materials.

To be of maximum usage, the required material properties should be generated in a test program that considers effects on the material due to:

1. Rate of strain at appropriate testing temperatures, as well as
2. Effects of processing thermal history and
3. Effects of manufacturing methods and procedures.

Also, the number of tests conducted should be sufficient such that the material properties, allowables, and/or stress-strain curves thus generated may be presented on a minimum guarantee basis. The tests as herein outlined appropriately considered these items in the generation of design mechanical properties.

TEST CRITERIA

Test Temperatures

Test temperatures were determined from aircraft flight profiles in the area of possible bird strike. The minimum and maximum temperatures were determined to be -30°F and 190°F average at the outer structural core ply and adjacent interlayer ply. Based on these criteria, test temperatures used were -30 $\pm$ 5°F, 75 $\pm$ 5°F, and 190 $\pm$ 5°F.

Strain Rates

Minimum low strain rates were determined by the best load-rate to obtain an accurate reading from the dual range extensometer for the 50 to 1 magnification factor. The maximum low strain rate was determined by the maximum chart speed

and load rate that would give an acceptable load-deflection chart for digitizing. High strain rate ranges were determined from strain gage readings of full size transparencies during bird tests to be from 10 in./in./sec. to 200 in./in./sec.

Based on these criteria, strain rates used were 0.025 in./in./min., 5 in./in./min., 10 in./in./sec. and 200 in./in./sec. ±25 percent.

TEST SPECIMEN CONSTRUCTION

All polycarbonate test specimens were examined under polarized light to expose stress risers from machining operations which could affect test results. Specimens displaying stress were refinished (sanded and polished) to remove such discrepancies. Machine cutting speed and feed rates were controlled to prevent heating parts above 150°F during machining to eliminate adverse thermal conditioning effects. Specimens of a particular test series were orientated in the same length-width relation with respect to the basic stock. Polycarbonate materials tested were required to meet the requirements of MIL-P-83310 except for optical and izod testing. Sheet material used for test specimens was pressed or ground polished and subject to thermal temperatures and frequencies required in the normal forming and fabrication processes of a laminated and/or stretch formed transparency.

Low Strain Rate Specimens

The low strain rate tensile specimens, Figure 1, were constructed in accordance with ASTM D638-72, except the overall lengths were extended to accommodate the MDC holding fixtures. Specimens were made from General Electric Co., SL3000, or from Rohm and Haas Co., "Tuffak" monolithic polycarbonate sheet materials. The processed materials tested were from PPG Industries, Texstar Plastics, Sierracin Inc., and Swedlow, Inc.

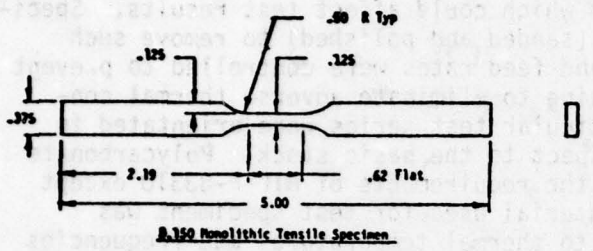
The low strain rate compression specimens, Figure 2, were constructed of General Electric Co., SL3000 monolithic polycarbonate sheet material. The processed materials tested were from PPG Industries, Sierracin, Inc., and Swedlow, Inc.

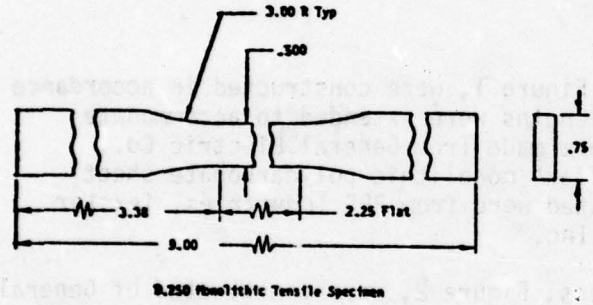
The low strain rate shear specimens, Figure 3, were constructed of a proprietary interlayer material which was laminated between two plies of SL3000 polycarbonate material. Two basic types of shear specimens were tested, a five ply compressive shear test specimen and a torsional shear test specimen. The 2.00 x 2.00 compressive shear test specimen was cut from laminated beams and test transparencies. The interlayer materials tested included polyurethane types from PPG Industries (PPG-112), and Sierracin, Inc. (S-120), silicone types from Swedlow, Inc. (SS 5272Y(HT)), and Sierracin, Inc. (S-100), and a copolymer type (S-130) from Sierracin, Inc.

High Strain Rate Specimens

High strain rate test specimens were constructed in accordance with design criteria specified by Terra Tek, Salt Lake City, Utah, under contract to Douglas for high strain rate testing.

The high strain rate tensile specimens, Figure 4, were constructed of General Electric Co.'s SL3000 and Rohm and Haas Co.'s "Tuffak" polycarbonate





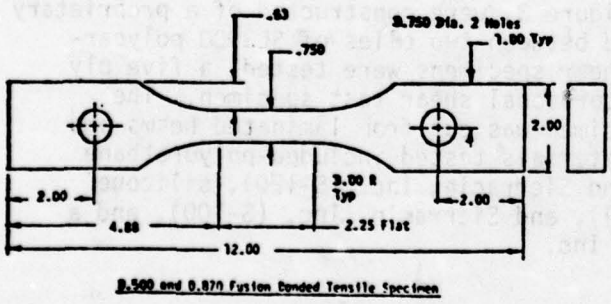


Figure 1. Low Strain Rate Tensile Specimens.

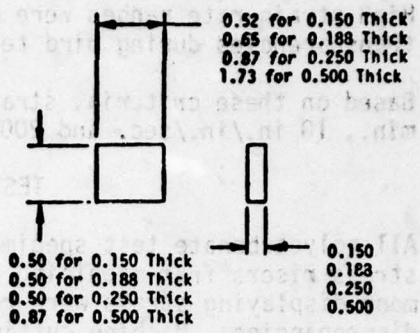
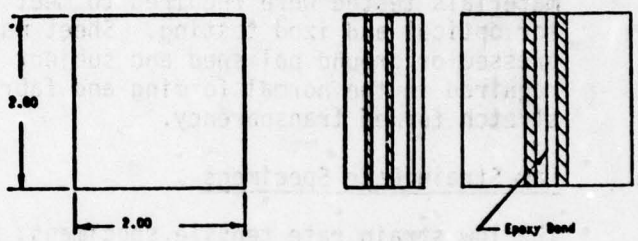
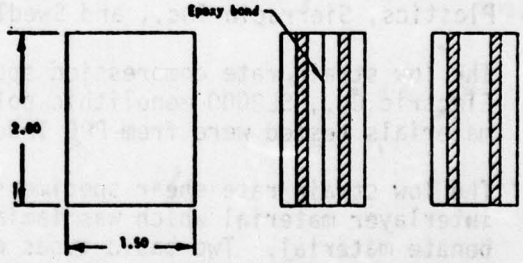


Figure 2. Low Strain Rate Compression Specimens.





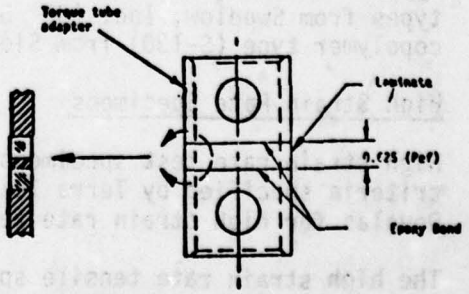


Figure 3. Low Strain Rate Shear Specimens.

sheet material, as processed by PPG Industries, Texstar Plastics Co., Sierracin, Inc., and Swedlow, Inc.

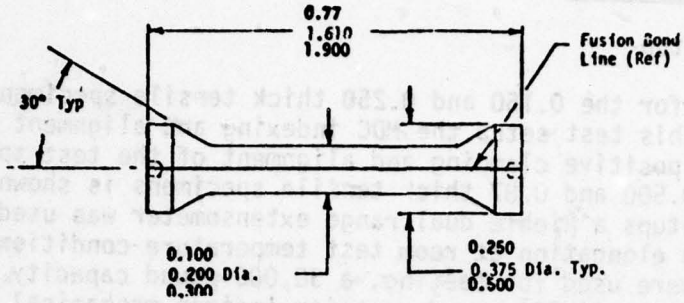


Figure 4. High Strain Rate Tensile Specimen.

The high strain rate compression specimens, Figure 5, were constructed of General Electric Co., SL3000 polycarbonate sheet material as processed by Swedlow, Inc.

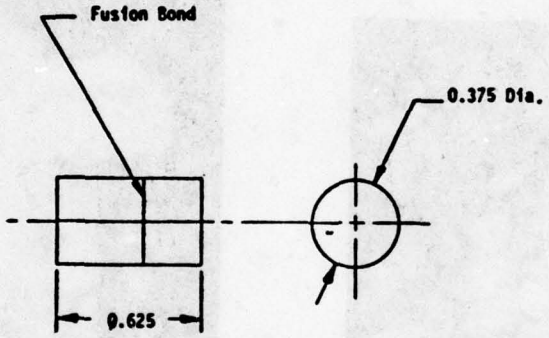


Figure 5. High Strain Rate Compression Specimen.

The high strain rate shear specimens, Figure 6, were constructed of a proprietary interlayer material laminated to two plies of SL3000 polycarbonate materials or to shear adapter fittings. The interlayer materials tested included polyurethane types from PPG Industries (PPG112), and Sierracin, Inc. (S-120); silicone types from Swedlow, Inc: (SS 5272Y (HT)), and Sierracin, Inc. (S-100) and a copolymer type (S-130) from Sierracin, Inc.

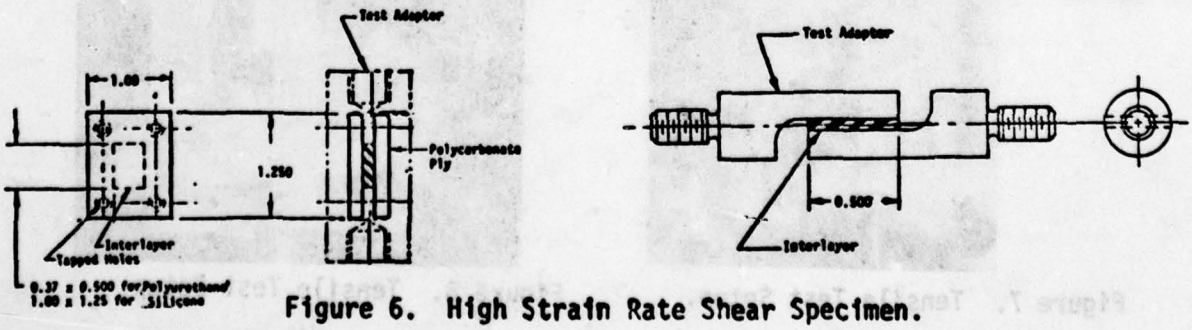


Figure 6. High Strain Rate Shear Specimen.

TEST SETUP

Low Strain Rate Testing

Tensile Test Setup

The test setup for the 0.150 and 0.250 thick tensile specimens is shown in Figure 7. In this test setup the MDC indexing and alignment fixture is used to provide for positive clamping and alignment of the test specimen. The test setup for the 0.500 and 0.87 thick tensile specimens is shown in Figure 8. In both test setups a Riehle dual range extensometer was used to measure and record specimen elongation at room test temperature conditions. Two types of test machines were used for testing, a 30,000-pound capacity Riehle mechanical test machine, and a 10,000-pound capacity Instron mechanical test machine. Test temperatures of -30°F and 190°F were achieved in a Missimers test chamber. The lower temperature was accomplished by injecting a spray of liquid nitrogen. The high temperature was achieved by a electric heating element in the test chamber. Temperatures were maintained within the test chamber by a thermo-couple power controller

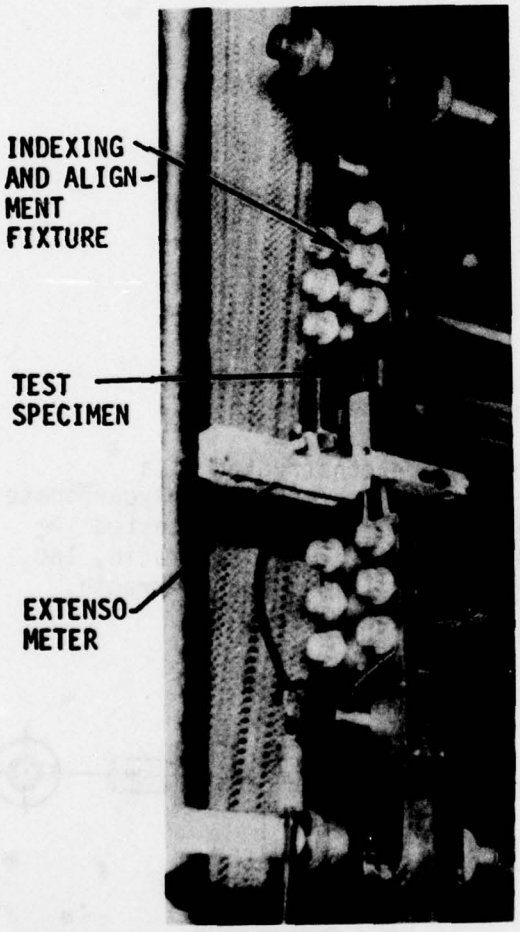


Figure 7. Tensile Test Setup.

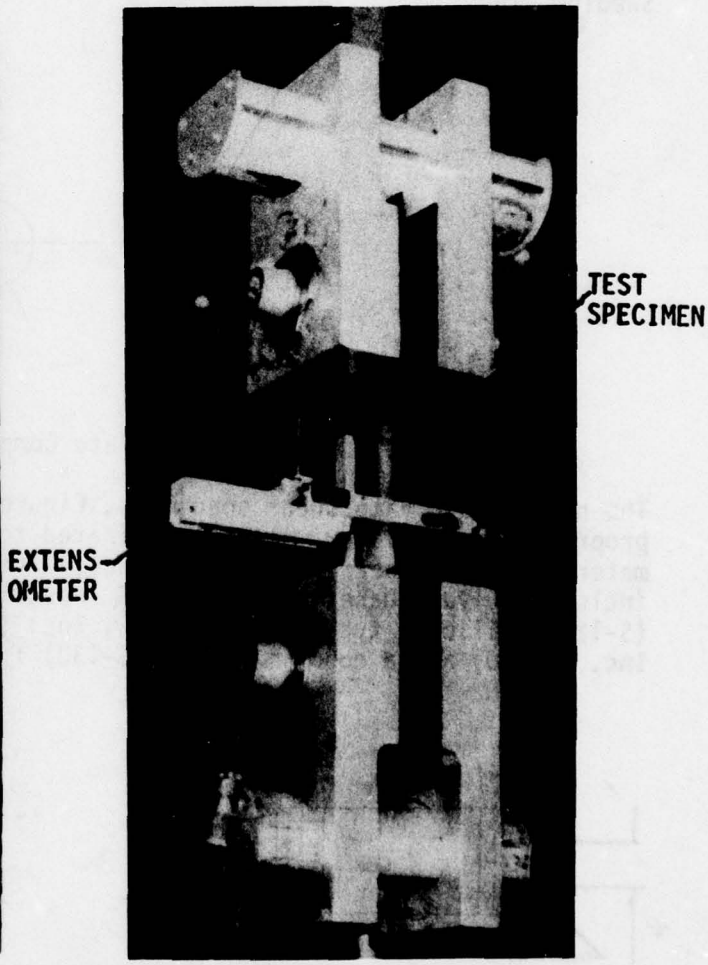


Figure 8. Tensile Test Setup.

Compression Test Setup

The test setup used for compression testing is shown in Figure 9. A Baldwin deflectometer was used to measure and record crosshead movement during specimen compression. The test machine used was a 60,000-pound capacity Baldwin mechanical test machine.

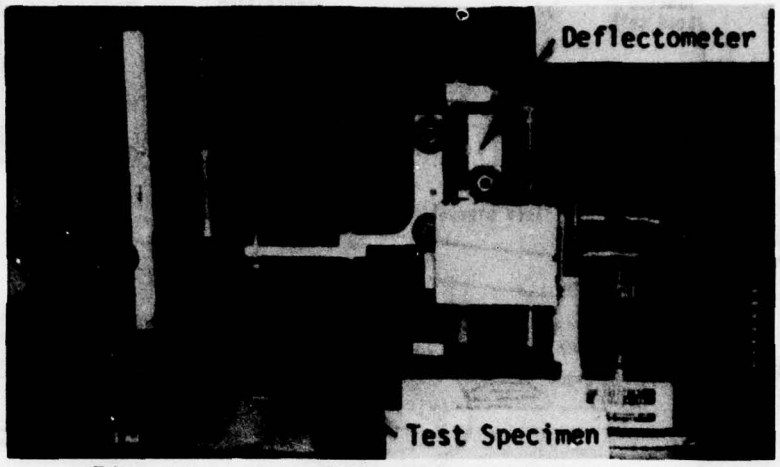


Figure 9. Compression Test Setup.

Shear Test Setup

The test setup for the compressive shear test used the same loading scheme as in the compression test. In this test setup an Instron test machine was used for testing and an Instron deflectometer was used to measure specimen elongation. A shear text fixture, Figure 10, was used to hold the test specimen during test to provide support and proper alignment.

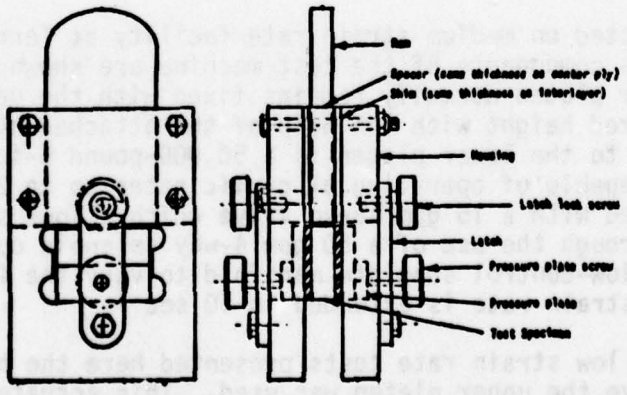


Figure 10. Shear Test Fixture.

The test setup for the torsional shear test is shown in Figure 11. In this test setup the test specimen was attached to the test machine carriage drive gear. Load measurements were made through balanced compression and tensile load cells adapted to the test machine.

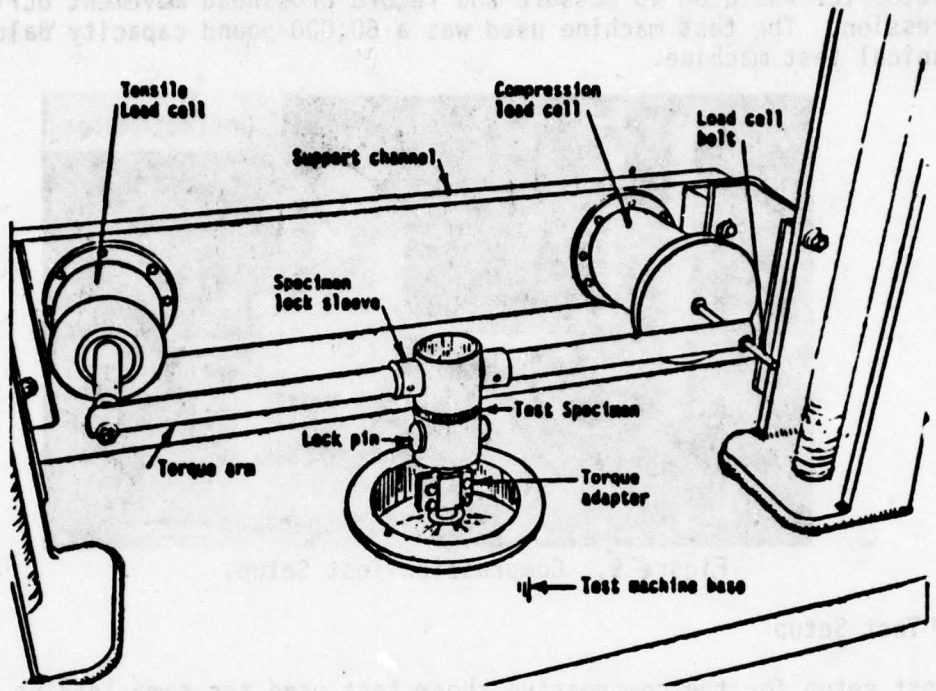


Figure 11. Torsional Shear Test Setup.

Shear tests were conducted on a 10,000-pound capacity Instron mechanical test machine. Load deflection graphs were provided for each test by using the Instron continuous recorder.

High Strain Rate Testing

All tests were conducted on medium strain rate facility at TerraTek, Salt Lake City, Utah. The main components of the test machine are shown schematically in Figure 12. The lower platen normally remains fixed with the upper platen adjusted to the desired height with the help of the attached hydraulic lift cylinders. Attached to the lower platen is a 50,000-pound 6-inch stroke linear hydraulic actuator capable of operating at cyclic rates up to 20 Hz. This actuator is controlled with a 15 gpm servo valve which allows strain rates of 10^{-6} to 1 sec^{-1}. Through the use of a 50 gpm 4-way solenoid operated valve, in conjunction with a flow-control subplate manifold to vary the flow during open-loop operation, the strain rate is extended to 10 sec^{-1}.

For all but the very low strain rate tests presented here the high pressure gas actuator mounted above the upper platen was used. This actuator, Figure 13, is operated by charging a reservoir on either side of the piston to equal pressure. The piston is accelerated when the gas is released from one reservoir, with the direction toward the one that is exhausted. The orifice size can be adjusted to control the exhaust rate. Motion is initiated through a fast acting solenoid valve mounted downstream from the orifice. Piston velocity, and hence rate of

loading, is controlled by the gas charging pressure, the orifice size, and to some extent, the specimen. Piston velocities up to 500 in./sec. can be achieved. Actuators are supplied by a 100 h.p. 50 gpm hydraulic power supply. Accumulators are provided to supply the peak flow rates.

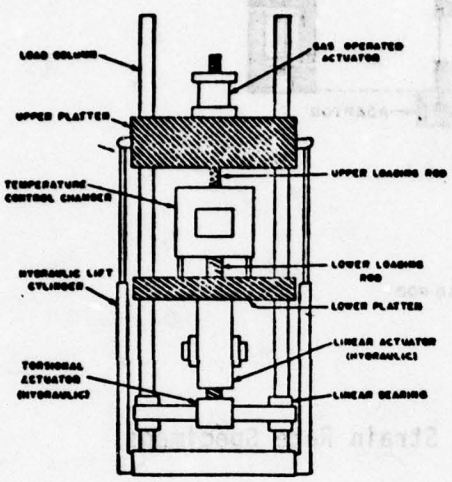


Figure 12. Schematic of Medium Strain Rate Machine.

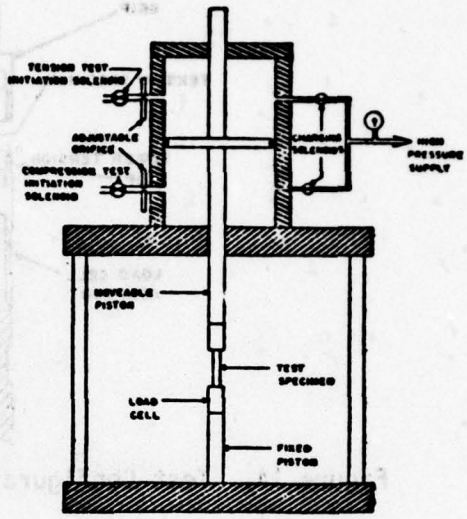


Figure 13. High Strain Rate Gas Actuator.

Controls for the medium strain rate machine are located in adjacent cabinets. These cabinets house servo controllers for the hydraulic actuators, each capable of three feedback modes of operation (displacement, strain, load), thus allowing independent selection of the feedback control. Digital ramp generators and a function generator are also available for test control. The pneumatic controls for the fast acting gas actuator system are also housed in the cabinets.

Specimen temperatures can be maintained in the range of -100°F to 300°F with the use of the temperature chamber shown in Figure 12. The system operates in a closed loop mode with a thermocouple, attached to the sample, providing a feedback signal to a Research Incorporated series 6000 Termac combined temperature-power controller which in turn controls a solenoid for the lower temperature configuration. The solenoid controls the spray of a liquid nitrogen supply. High temperatures are maintained in a similar fashion except that a nicrome wire heater encased in Iconel sheath is substituted for the solenoid valve. In this case, the error signal controls the amount of power supplied to the heaters by the power controller.

The test configuration for tension, compression, and shear tests is illustrated in Figure 14. Sample load was measured with a Sundstrand Data Control, Inc., Quartz Load Cell, Model 923F2, interfaced to a charge amplifier. Strains were measured during the tension and compression tests by strain gages bonded directly to the test specimen. Strains were obtained on shear tests by the use of a linear displacement potentiometer. Both the load and strain were recorder as a function of time on a Nicolet Model 1090AR Digital Equipment Corporation Multiuser

timesharer computer (PDP 11/34). The strain data was plotted as a function of stress on a cathode-ray tube terminal (Tektronix 3030) and copied on a hard copy unit (Tektronix 4610).

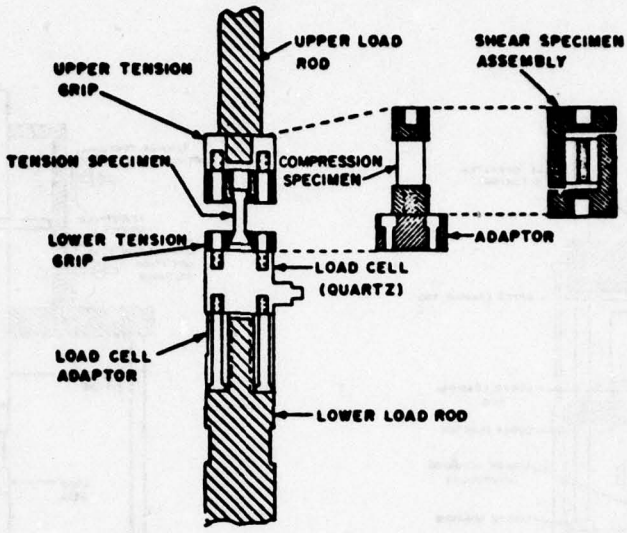


Figure 14. Test Configuration for High Strain Rate Specimens.

PROBLEM AREAS

Low Strain Rate Tests

The use of a specimen gage length in determining strain measurements was found to be in error when compared to tests using an extensionmeter of known extension gage length. A correction factor was determined for each test setup by comparing strain values of identical tensile tests with and without the extensionmeter.

The torsional shear testing was found to give poor results due to a displacement of the specimen during test.

Shear test specimens for polyurethane type materials were found to show evidence of bearing failure of the outer face plies due to loading that exceeded the bearing strength of polycarbonate materials at low test temperatures. The interlayer was undercut to reduce the load to rupture.

High Strain Rate Tests

The load cell calibration was found to be in error due to the test setup attachment method. The load cell was recalibrated in the new configuration, and all previous test curves were corrected for this error.

Strain rates obtained during tests depend on actuator charge pressure, yoke adjustments, and accurately machined test specimens without material flaws. A combination of these items resulted in a larger scatter in strain rates than anticipated.

Premature failure in test specimens were found to be caused by machining flaws or material defects.

TEST RESULTS ANALYSIS

The average stress-strain curves in the following brief analysis was generated from test data contained in technical Report AFFDL-TR-77-96 for the establishment of design mechanical properties of selected materials. This analysis is presented to illustrate strain rate and temperature effects on selected materials to demonstrate the change in mechanical properties due to the design aircraft flight environment and loading conditions.

Core Ply Materials

Processed Polycarbonate

A plot of average tensile true stress-strain curves is presented in Figure 15 comparing processed "Lexan" SL3000 polycarbonate at three test temperatures, -30°F, 75°F and 190°F for low and high strain rates. The true stress-strain curves plotted are a test average of the processed polycarbonate materials from Sierracin Inc., (SK), Swedlow, Inc., (SWU), and Texstar Plastics, Inc., (TEX) aircraft transparency fabricators. It can be seen that temperature effects plastic properties of the processed polycarbonate to a large extent when compared to results at room temperatures at low and high strain rates. The plot reveals a larger gain in yield and rupture strength at -30°F at high strain rates than for low strain rates. A loss in strain to rupture is evident for 190°F at high strain rates that is not evident at low strain rates. Comparison of average curves at low and high strain rates for the three temperature conditions indicate that a change in elastic and plastic properties has taken place. A larger change in properties due to strain rate effects is noted at -30°F than at room temperature and 190°F test conditions.

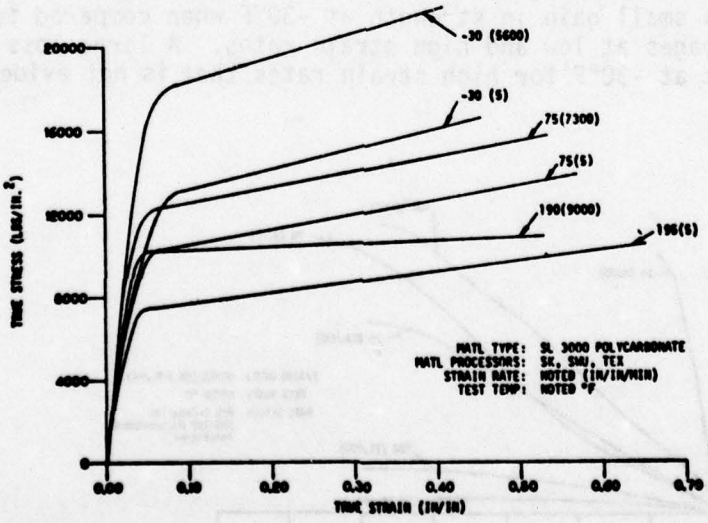


Figure 15. Tensile Strain Rate and Temperature Effects.

A plot of average compression curves comparing processed monolithic SL3000 polycarbonate at room temperatures for low and high strain rates is presented in Figure 16. Separation of curves for low and high strain rates is indicative of strain rate effects on elastic and plastic properties of polycarbonate. These effects are in agreement with effects for tensile tests shown in Figure 15.

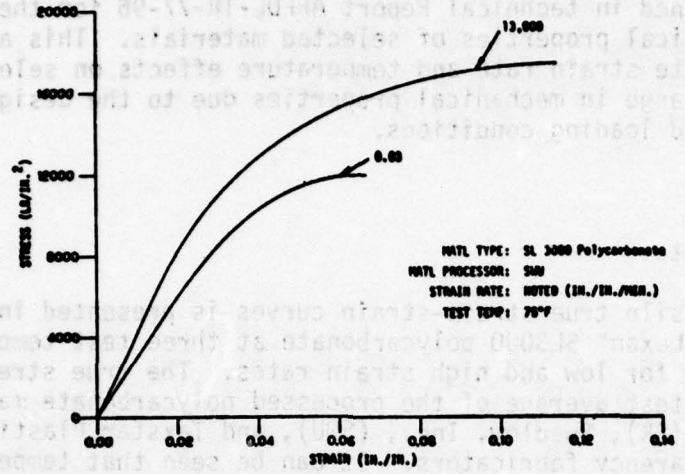


Figure 16. Compression Strain Rate Effects.

Interlayer Materials

Polyurethanes

A plot of average shear stress-strain curves for PPG Industries "PPG112" interlayer material at three test temperatures for low and high strain rates is shown in Figure 17. Test results indicate a large loss in strength at 190°F when compared to room temperature test results at low and high strain rates. Test results reveal a small gain in strength at -30°F when compared to room temperature test averages at low and high strain rates. A large loss in strain to rupture is evident at -30°F for high strain rates that is not evident at low strain rates.

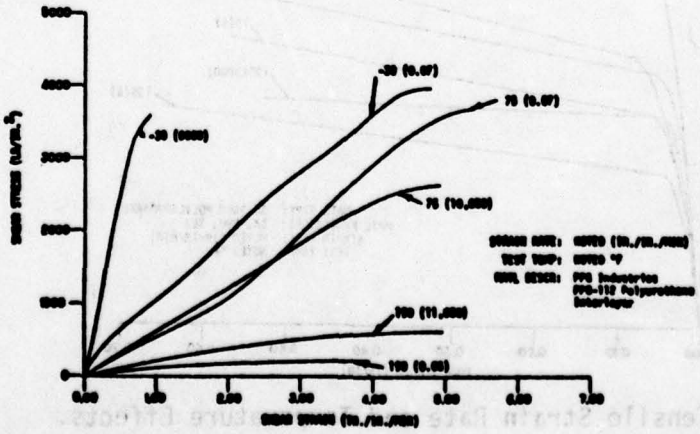


Figure 17. Shear Strain Rate and Temperature Effects.

A plot of average shear stress-strain curves for Sierracin, Inc., "S-120" interlayer material at three test temperatures for high strain rate and one temperature at low strain rate is shown in Figure 18. Test results indicate a large strength loss at -30°F and 190°F when compared to room temperature tests at high strain rates, a large gain in strength and rupture strain is noted for high strain rate when compared to low strain rate tests at room temperatures.

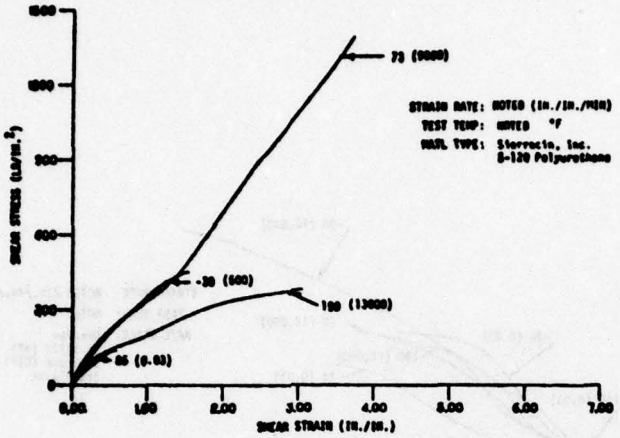


Figure 18. Shear Strain Rate and Temperature Effects.

Silicones

A plot of average shear stress-strain curves for Sierracin "S-100" cast-in-place silicone interlayer material at three test temperatures for low and high strain rates are shown in Figure 19. Test results indicate a loss in strength at 190°F and a gain in strength at -30°F when compared to room temperature tests at low and high strain rates. A gain in elongation to failure at -30°F for low strain rates is not evidenced at high strain rates. The loss in strain to rupture at 190°F for high strain rates is not evident at low strain rates.

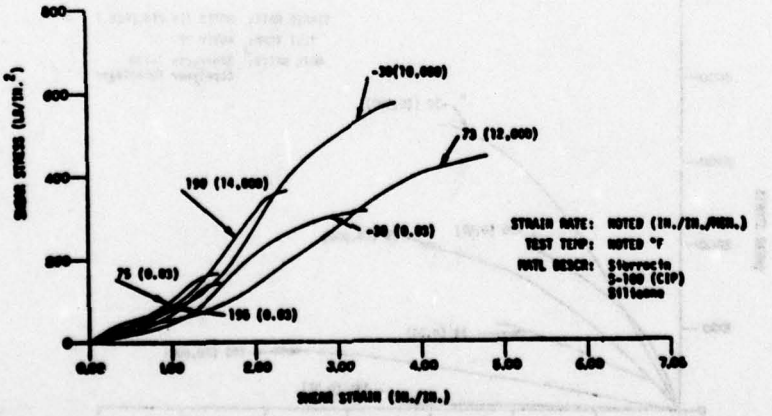


Figure 19. Shear Strain Rate and Temperature Effects.

A plot of average shear stress-strain curves for Swedlow SS5262(HT) cast-in-place silicone interlayer material at three test temperatures for low and high strain rates is presented in Figure 20. Test results indicate a loss in strength at 190°F and a gain in strength at -30°F when compared to room temperature test averages at low and high strain rates. A gain in elongation to failure at -30°F is indicated for high strain rates which is not evidenced at low strain rates. The loss in strain to rupture at 190°F for low strain rates is not evident at high strain rates.

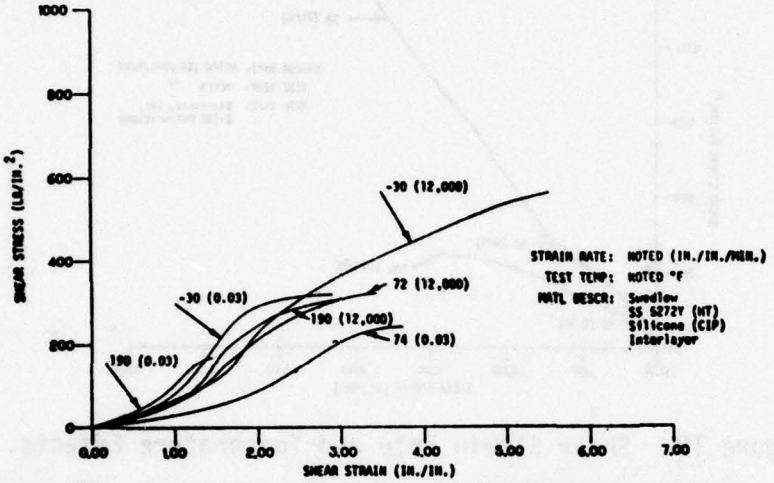


Figure 20. Shear Strain Rate and Temperature Effects.

Co-Polymer

A plot of average shear stress-strain curves for Sierracin S-130 co-polymer interlayer material at three temperatures for low and high strain rates is shown in Figure 21. Test results indicate a loss in strength properties at -30°F when compared to room temperature tests at low and high strain rates. A gain in strain to rupture is evident at 190°F when compared to room temperature tests at both low and high strain rates.

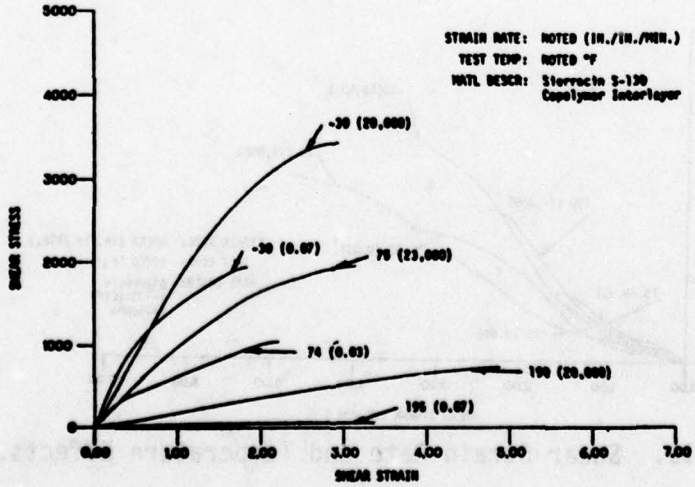


Figure 21. Shear Strain Rate and Temperature Effects.

CONCLUSIONS

Methods of testing described in this report proved to give satisfactory results for the establishment of design mechanical properties for the transparency materials tested with the exception of the torsional shear tests. It is recommended that a minimum of ten tests be conducted for each material and test condition at high strain rates to establish design mechanical properties due to the large scatter in test results and test failures.

Test results analysis demonstrates the need to establish design mechanical properties of transparency materials at all flight environment and loading conditions of the design aircraft. It can be seen that large errors in design analysis of a transparency can result where material properties determined at moderate temperatures and incorrect strain rates are used for design allowables.

EDGE MEMBER TESTING OF AIRCRAFT TRANSPARENT MATERIALS

J. B. Hoffman
Douglas Aircraft Company
McDonnell Douglas Corporation
Long Beach, California

PRECEDING PAGE BLANK-NOT FILMED

EDGE MEMBER TESTING OF AIRCRAFT TRANSPARENT MATERIALS

by

Joseph B. Hoffman

Douglas Aircraft Company, Long Beach, California 90846

ABSTRACT

A series of cyclic durability tests were performed on specimens representing the edge attachment area of a laminated transparency for potential use in the design of aircraft windshields. Simulated flight conditions were based on a 2000-hour design life at typical high performance aircraft operating temperatures and pressures. Four lifetimes of cyclic testing were performed.

PRECEDING PAGE BLANK-NOT FILMED

INTRODUCTION

Relatively short exposure to rain and ice crystal abrasion precipitated erosion of the exterior surface coating used to protect the polycarbonate canopy on the YF-16 prototype aircraft. Similar experience on the F-111F and F-15 canopies substantiated the necessity of further development to provide improvements in protecting polycarbonate from the environment.

The configuration selected to provide optimum erosion resistance and high optical quality for current Air Force inventory aircraft and for application to future aircraft windshield designs was a three-ply laminated transparency which consisted of an acrylic outer ply and a polycarbonate structural ply separated by a soft interlayer.

This report describes a series of edge member durability tests initiated to obtain performance reliability and capability information for a variety of three-ply laminated designs. A realistic flight environment based on current Air Force supersonic aircraft operating conditions was used to calculate the test environment and transparency design life.

The test specimens were assembled in two parallel chains, enclosed in an environmental chamber to permit application of high and low temperatures, and loaded simultaneously by a hydraulic jack.

The goals of this test were to evaluate the edge attachment area of laminated transparency designs for materials obtained from several sources and to verify that the materials and the edge attachment area of a laminated transparency design would sustain without structural failure or delamination the equivalent of four lifetimes of internal pressure cycling at aircraft operating temperatures based on a 2000 hour transparency design life. These goals were achieved.

Background

The prime purpose of an edge attachment is to join an aircraft transparent enclosure to the primary structure. The edge attachment serves to transmit the loads developed in the transparent material to the airframe.

The edge attachment area of a transparent enclosure is exposed to a harsh environment, and must be capable of withstanding extreme temperature gradients, cyclic loads, and stress concentration. An inadequate edge attachment design will result in a reduced service life and high life cycle costs.

Two prime causes of windshield/canopy failures are delamination of the interlayer for a laminated design, and ruptured attachment holes in polycarbonate material generated by crazing and/or excessive bearing load.

A method of minimizing delamination is to use a retainer at the edge of the laminated transparency. Tests were made to compare edges with steel retainers versus edges without retainers.

Improper drilling of attachment holes will produce stress crazing in polycarbonate material at low tensile stress levels under exposure to many common solvents, fluids and environments. Crazing has been defined in Reference 1 as fine cracks

which may extend in a network over or under the surface or through a plastic. Crazing of polycarbonate can significantly lower the impact strength of the material. Bolt hole drilling methods and hole finish must be controlled. Reference 2 notes the following requirements for proper hole drilling. The first requirement is to keep the part cool by using slow to medium cutting speeds and feed rates, and the use of a coolant. The second requirement is to maintain a sharp cutting edge at all times.

Prime consideration must be given to the spacing between bolt holes as noted in Reference 3. A minimum number of bolts is desirable to enhance maintainability. However, bearing stress is inversely proportional to the number of bolts and the bearing stress must not exceed the critical stress level for polycarbonate.

Windshield interchangeability influences life cycle cost. Consideration must be given to bolt hole size (loose versus tight holes), hole sealing (wet or dry), and the type of bushing used to distribute the load. Adequate edge distance must be provided.

TEST SPECIMEN DESCRIPTION

Table 1 is a pre-test description of the test specimens which are shown in Figures 1, 2 and 3.

TABLE 1. PRE-TEST SPECIMEN DESCRIPTION

CONFIGURATION OF Z5943266	MFG.	TYPE OF CONSTRUCTION	TYPE OF INTERLAYER	HOLE SIZE (IN.)	THICKNESS OF POLYCARBONATE	TAPE UNDER BOLTS (4)	REMARKS
-521	SK	Laminated	Silicone	1/4	0.62		(6)
-523	SK		(0.100 In.)	1/4	0.72		(5) (6)
-523	SWU			1/4	0.70	Yes	(6)
-525	SK			1/4	0.94	Yes	(6)
-525	SWU			1/4	0.87		(6)
-527	SK			3/16	0.62		
-529	SK			3/16	0.75		
-529	SWU			3/16	0.70	Yes	
-531	SK			3/16	0.94		(5)
-531	SWU			3/16	0.87	Yes	
-533	TEX	Monolithic (2)	-	1/4	0.50		
-535	TEX	Monolithic (2)	-	3/16	0.50		
-537	SK	Laminated	S-130 (3)	1/4	0.62		(6)
-539	SK		(0.030 In.)	1/4	0.75		(6)
-541	SK			1/4	0.87		(6)
-543	SK			3/16	0.62		
-545	SK			3/16	0.75		
-547	SK			3/16	0.87		

(1) SK = Sierracin, SWU = Swedlow, TEX = Texstar
(2) Specimens taken from canopy impacted as part of bird test program
(3) S-130 - Sierracin Copolymer
(4) 3M Polyurethane tape used to reduce crazing (Ref. 3). Installed between polycarbonate and aluminum plates
(5) Cracks in acrylic ply emanating from holes drilled in end without retainer.
(6) Washers were installed under head of bolts (acrylic side) to eliminate bushing pull out.

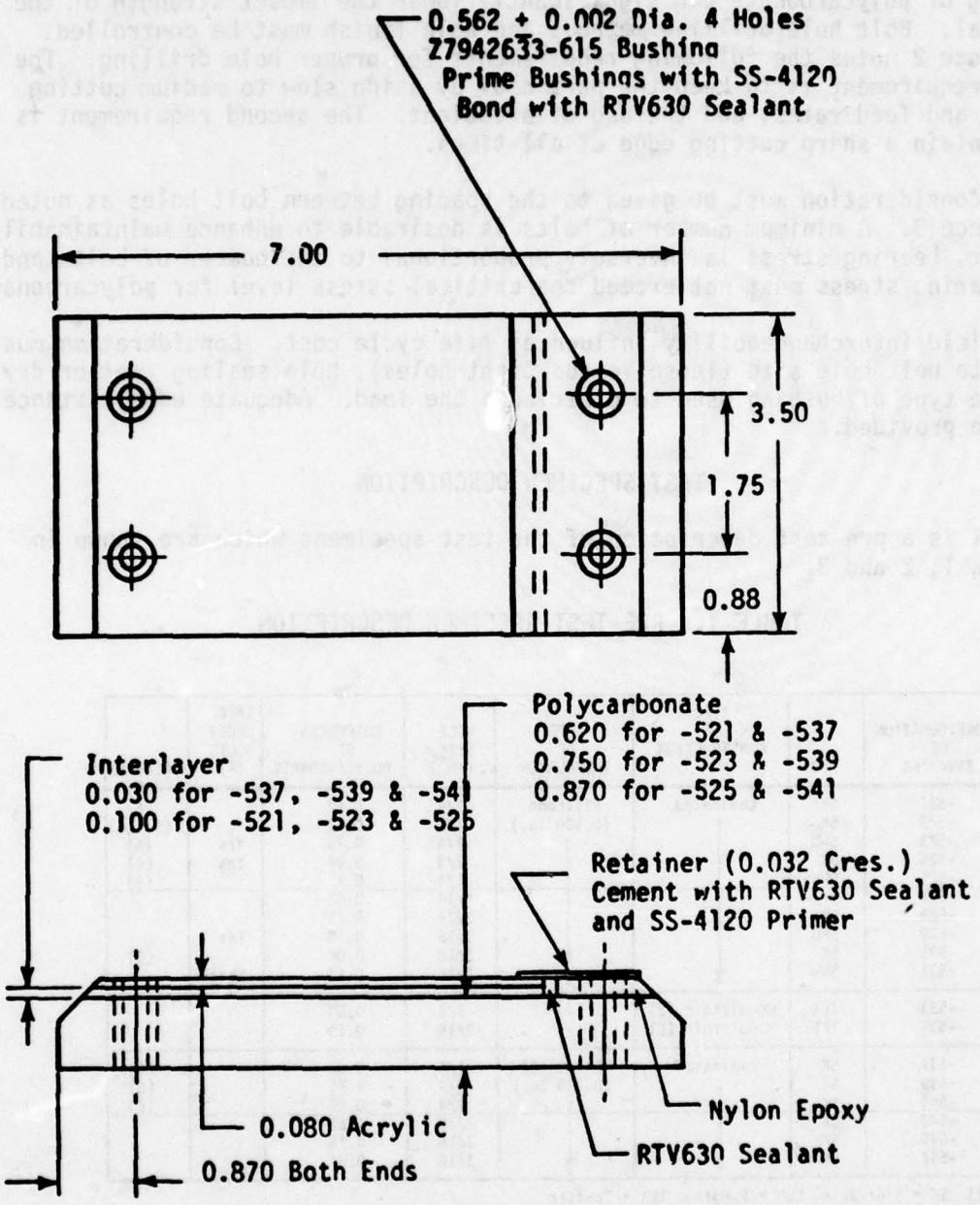


Figure 1. Specimens for 1/4 Inch Bolts

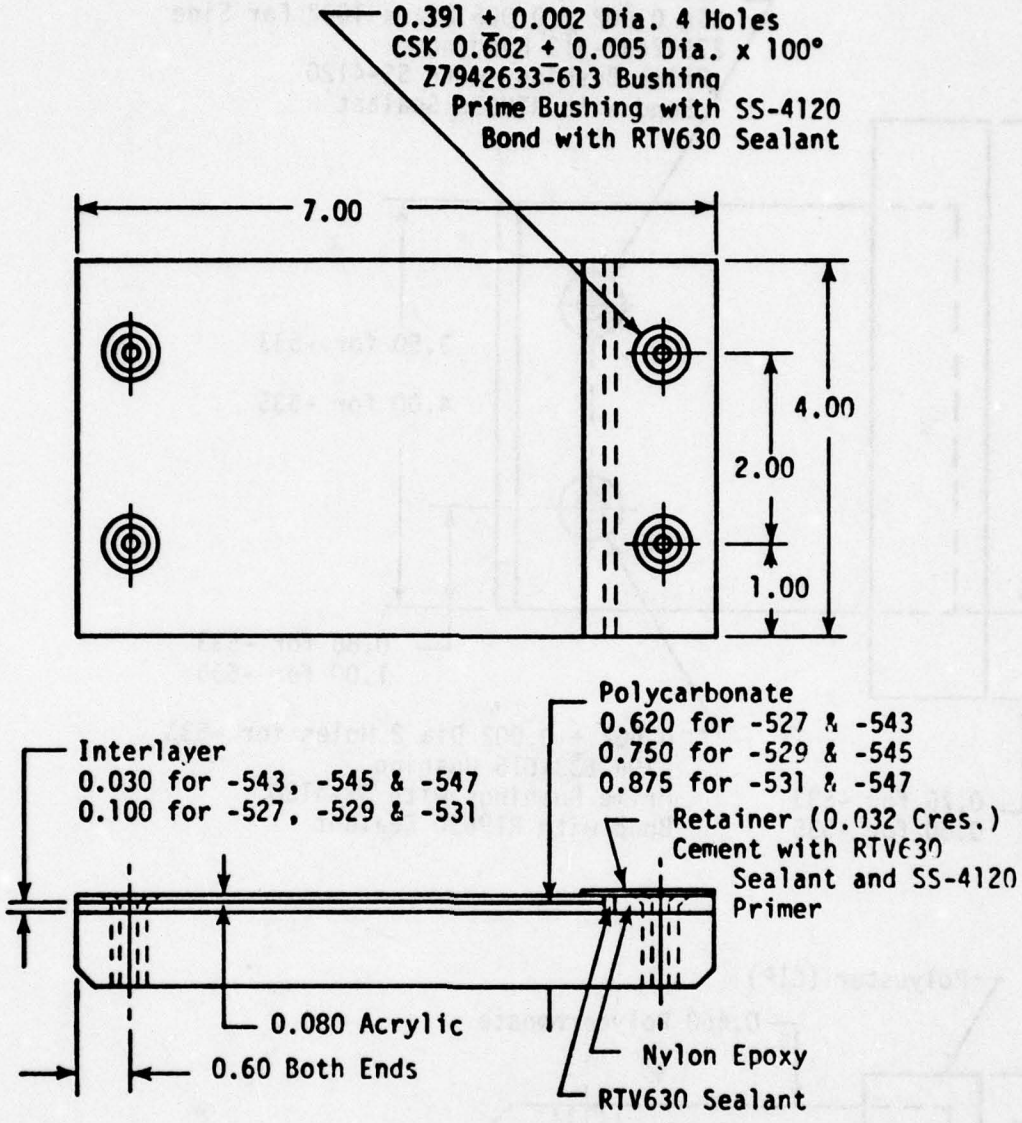
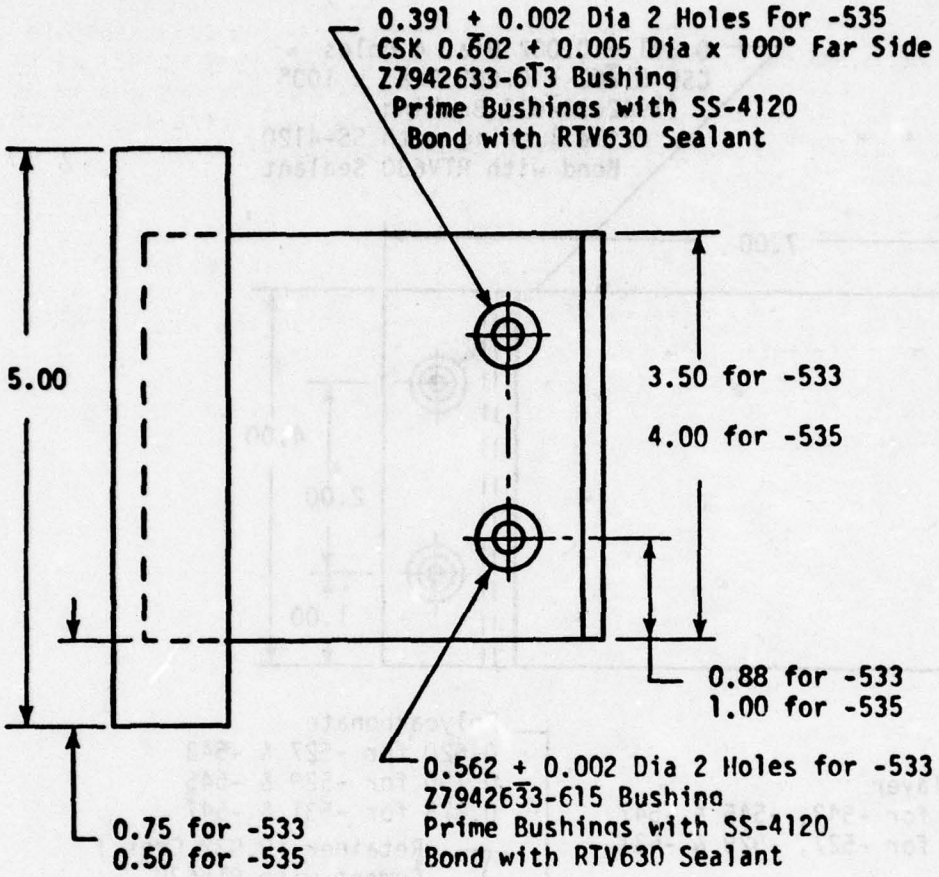


Figure 2. Specimens for 3/16 Inch Bolts



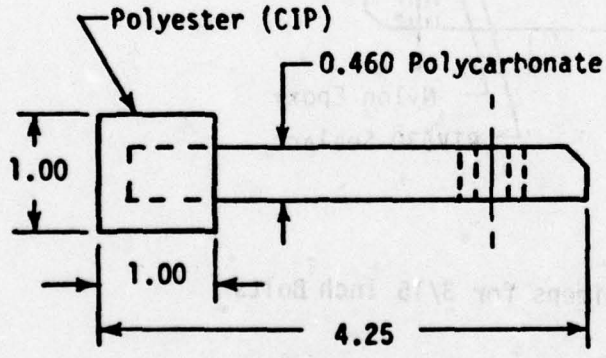


Figure 3. Monolithic Polycarbonate Specimens

The uncoated laminated specimens were comprised of an 0.080-inch as-cast acrylic outer ply and a polycarbonate structural inner ply. The polycarbonate was 0.62, 0.75 and 0.87 inch thick. Two types of interlayers were used: cast-in-place silicone, 0.10 inch thick, and 0.03 inch thick copolymer designated as S-130 by Sierracin. Two monolithic coated specimens, Figure 3, were taken from a canopy that had previously been bird impact tested for the Windshield Technology Demonstrator Program.

The glass filled polycarbonate bushings defined in Figures 4 and 5 were based on the bushings defined in Reference 3. These bushings were installed in oversize holes (0.014 inch maximum to 0.005 inch minimum) and bonded in place with RTV630 after being primed with SS-4120. The oversize hole in the bushing provided bolt clearance of 0.025 inch minimum to 0.030 inch maximum.

Each end of the test specimen presented a different method of load transfer to the bolted connection.

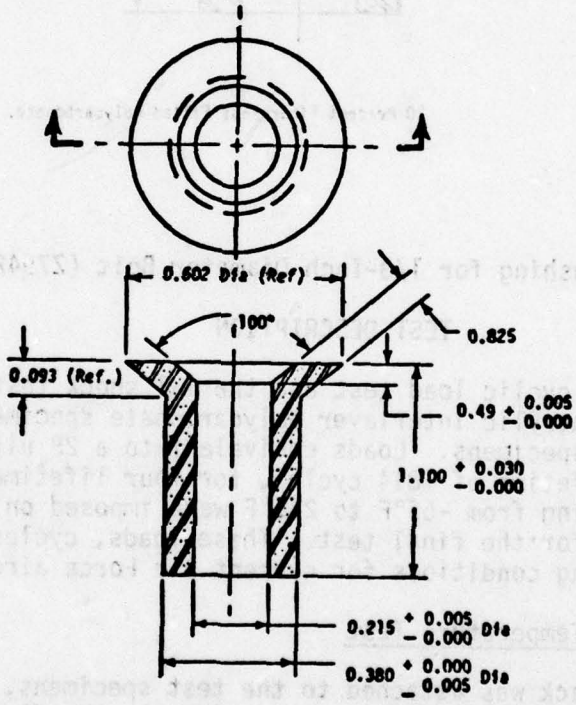
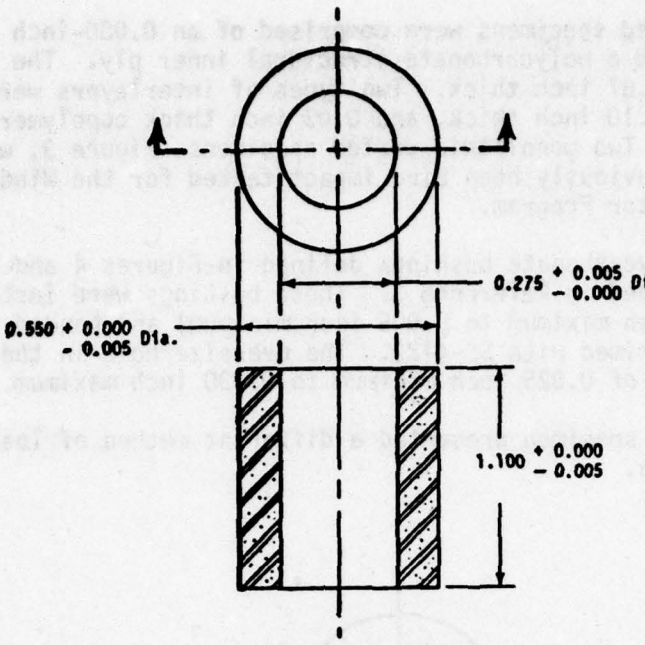


Figure 4. Bushing for 3/16-Inch Diameter Bolt. (Z7942633-613).

The bolt holes were drilled using proprietary methods developed by the vendors to prevent crazing in the bolt holes.

The fasteners were installed dry and torqued to 25-35 in.-lb. for the 3/16 inch diameter bolts and 69-80 in.-lb. for the 1/4 inch diameter bolts. No sealant was used in the holes.



20 Percent Fiberglass Filled Polycarbonate.

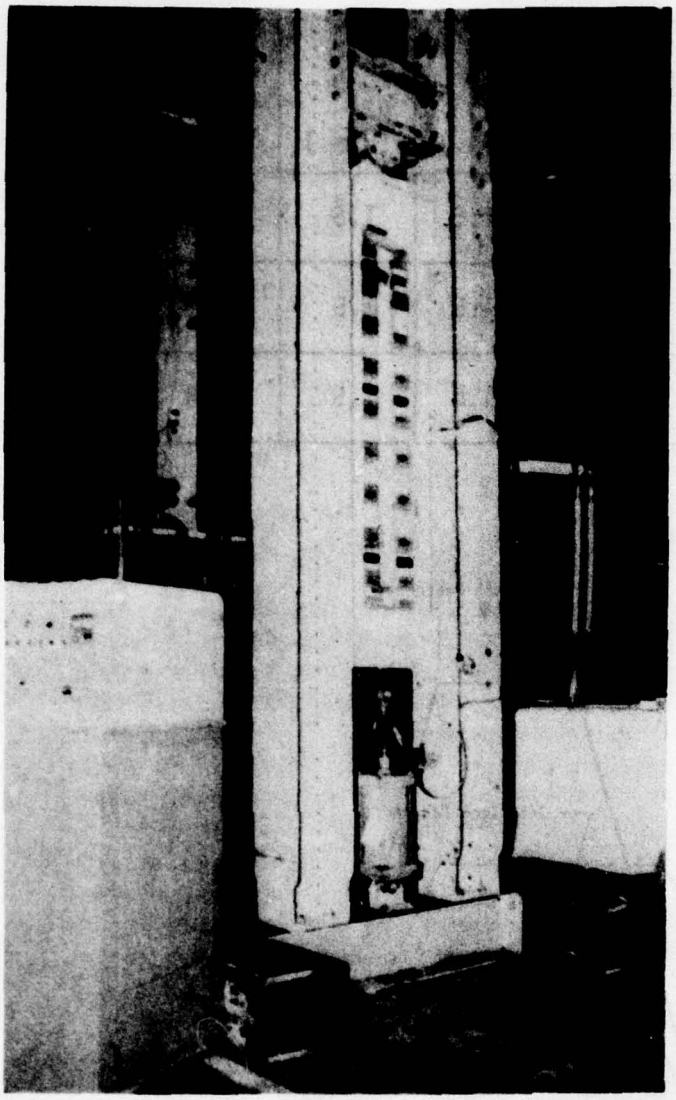
Figure 5. Bushing for 1/3-Inch Diameter Bolt (Z7942633-615).

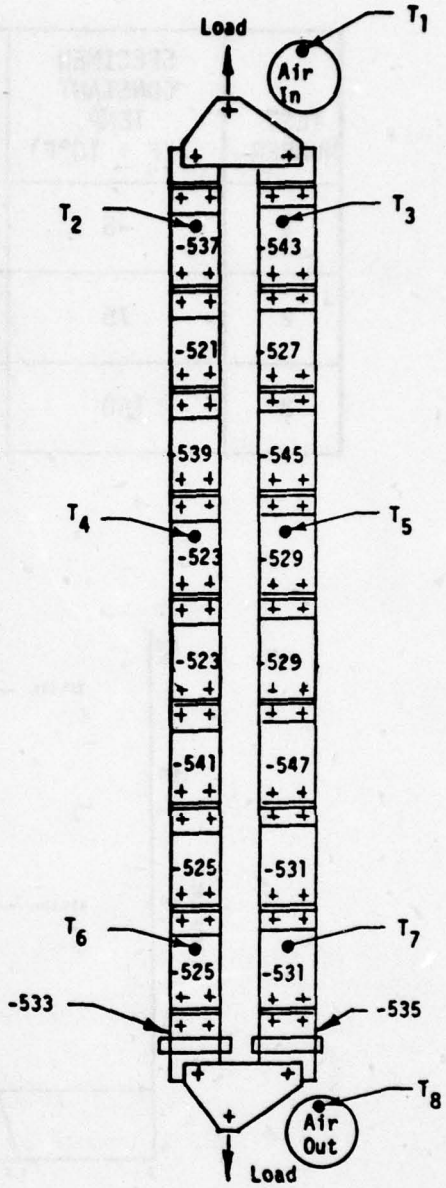
TEST DESCRIPTION

Two types of tests, a cyclic load test and thermal shock test, were conducted on sixteen laminated acrylic interlayer polycarbonate specimens, and two monolithic polycarbonate specimens. Loads equivalent to a 2P ultimate condition were applied for a lifetime of 1814 cycles, for four lifetimes (7256 cycles), and temperatures ranging from -65°F to 245°F were imposed on the specimens. The load was doubled for the final test. These loads, cycles and temperatures were based on operating conditions for current Air Force aircraft.

Cyclic Load/Constant Temperature Test

A pneumatic loading jack was attached to the test specimens, Figure 6, supported in an erector set type test frame made from 12 inch wide-flange beams. A clock timer triggered a solenoid valve in a pneumatic loading system which introduced pressurized air to the loading jack for a given time period. The load level was established by a pressure reducing valve in the air input line to the loading jack. The time rate of loading and unloading was established by a needle valve throttle adjustment of a special solenoid valve in each in/out air line. An electronic load cell installed in the load link with a strip-chart recorder read-out provided the load versus time trace of the cyclic load test.





T = Thermocouple

Figure 6. Test Fixture.

A mechanical counter in each test link records the number of load cycles. A polystyrene environmental test chamber, approximately 12 inches wide, 14 inches deep, and 7 feet high, was installed on the test machine to provide ducting for hot or cold air around the test specimens. Temperatures were monitored through thermocouples attached to the test specimens, and located in the test chamber. Three cyclic load tests were conducted at constant temperatures typical of flight conditions as shown in Figure 7. Typical load cycles are shown for all loading conditions except Test Number 6.

TEST NUMBER	SPECIMEN CONSTANT TEMP (°F ± 10°F)	NUMBER LOAD CYCLES	TIME LOAD ON (Min.)	TIME LOAD OFF (Min.)	TOTAL TEST TIME (Hours)
1	-5	916	4.5	1.5	91.6
2	75	874	4.5	1.5	87.4
3	160	24	4.5	1.5	2.4

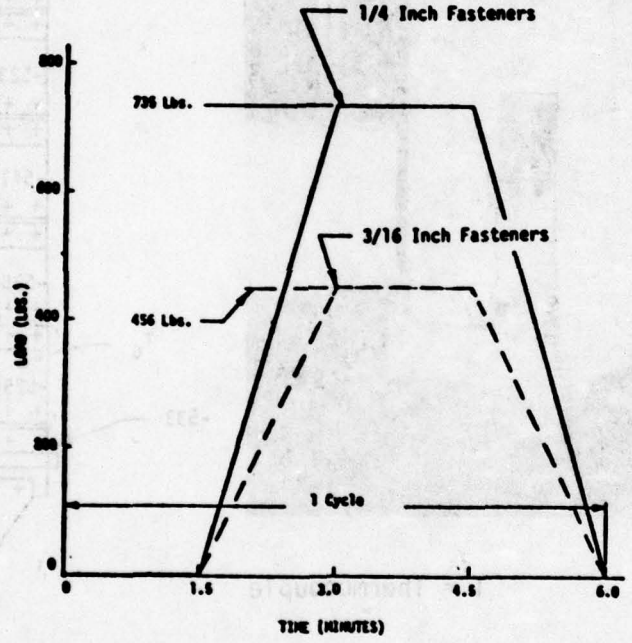


Figure 7. Typical Time Load Cycles, Test Conditions 1 Through 3.

Cyclic Temperature/Constant Load Test

The test setup described for the cyclic load test was used. A constant pneumatic load was imparted to the two links of test specimens through the loading jack. A Wilson environmental testing machine was used to deliver a cold air and hot air supply to the environmental chamber to provide the required specimen temperature conditions noted in Table 2. Temperatures for two sets (Test Numbers 4 and 5) were monitored through thermocouples attached to the test

specimens and chamber and recorded on a slow rate recorder. A typical cold-hot air cycle showing the temperature versus time cycles for conditions 4 and 5 are shown in Figures 8 and 9. The specimens were subjected to a total of ten temperature cycles.

TABLE 2. CYCLIC TEMPERATURE TEST

TEST NUMBER	AIR CYCLIC TEMPERATURE (°F ± 10°F) MIN	MAX	LOAD (LB)	TIME AT LOW TEMP (MINUTES)	TIME AT HIGH TEMP (MINUTES)	TRANSITION TIME LOW TO HIGH TEMP (MINUTES)	NUMBER OF TEMP CYCLES	TOTAL TEST TIME (HOURS)
4	-65	190	$\frac{735}{456}$	20*	20	12 or Less	5	4.33
5	160	245	$\frac{735}{456}$	20*	20	12 or Less	5	4.33
6	AMBIENT	245	$\frac{1470}{912}$	5	20	12 or Less	10	-

*First cycle at low temperature to be 60 minutes.

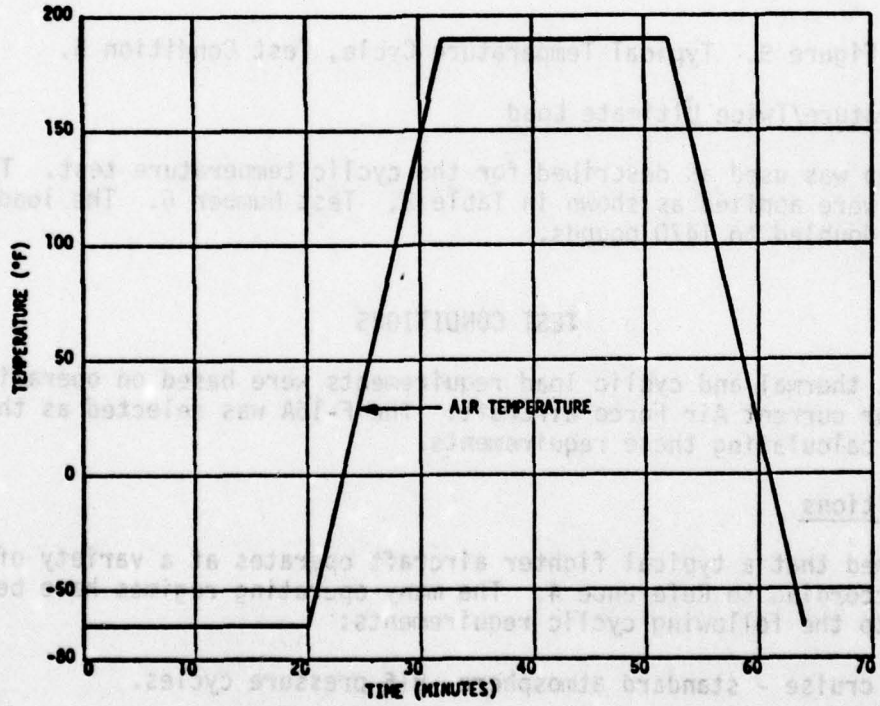


Figure 8. Typical Temperature Cycle, Test Condition 4.

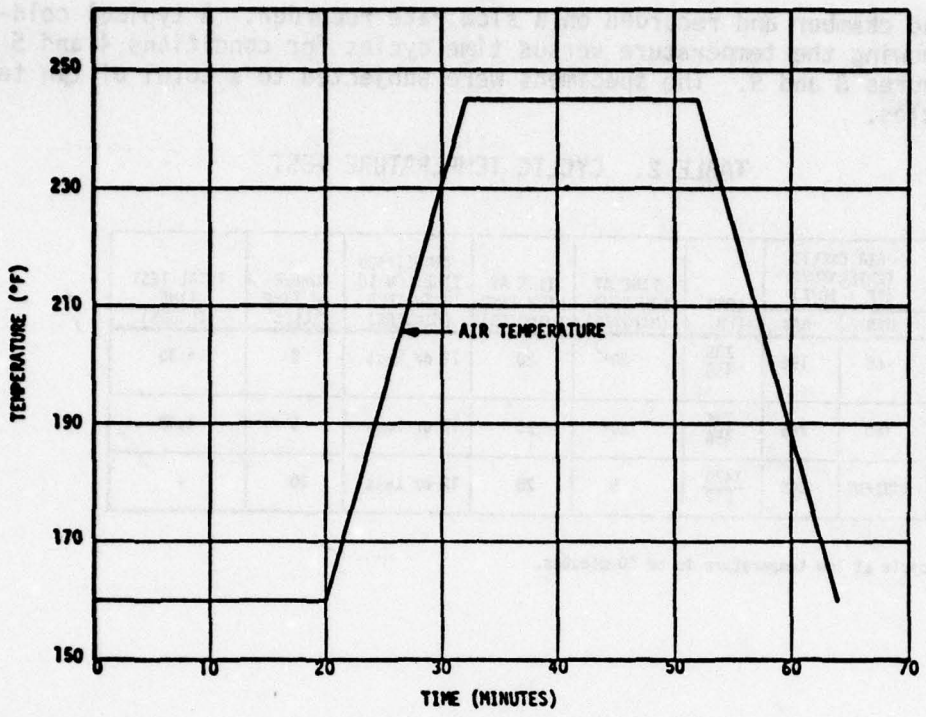


Figure 9. Typical Temperature Cycle, Test Condition 5.

Cyclic Temperature/Twice Ultimate Load

The test setup was used as described for the cyclic temperature test. The temperatures were applied as shown in Table 2, Test Number 6. The load noted in Figure 7 was doubled to 1470 pounds.

TEST CONDITIONS

The pressure, thermal and cyclic load requirements were based on operating conditions for current Air Force aircraft. The F-16A was selected as the typical aircraft for calculating these requirements.

Thermal Conditions

Douglas assumed that a typical fighter aircraft operates at a variety of conditions according to Reference 4. The many operating regimes have been condensed into the following cyclic requirements:

1. Subsonic cruise - standard atmosphere, 916 pressure cycles.

2. Subsonic cruise - hot atmosphere, 102 pressure cycles.

3. Supersonic cruise - Mach 1.6 - standard atmosphere, 498 pressure cycles.

4. Supersonic cruise - Mach 1.6 - hot atmosphere, 55 pressure cycles.

5. Supersonic cruise - Mach 2.0 - standard atmosphere - 219 pressure cycles.

6. Supersonic cruise - Mach 2.0 - hot atmosphere - 24 pressure cycles.

7. Subsonic cruise in a cold atmosphere (-65°F soak) followed by a supersonic cruise of Mach 2.2 in a standard atmosphere - five (5) temperature cycles. See Figure 10.

8. Hot atmosphere ground soak (160°F) followed by a supersonic cruise of Mach 2.2 in a standard atmosphere - five (5) temperature cycles. See Figure 11.

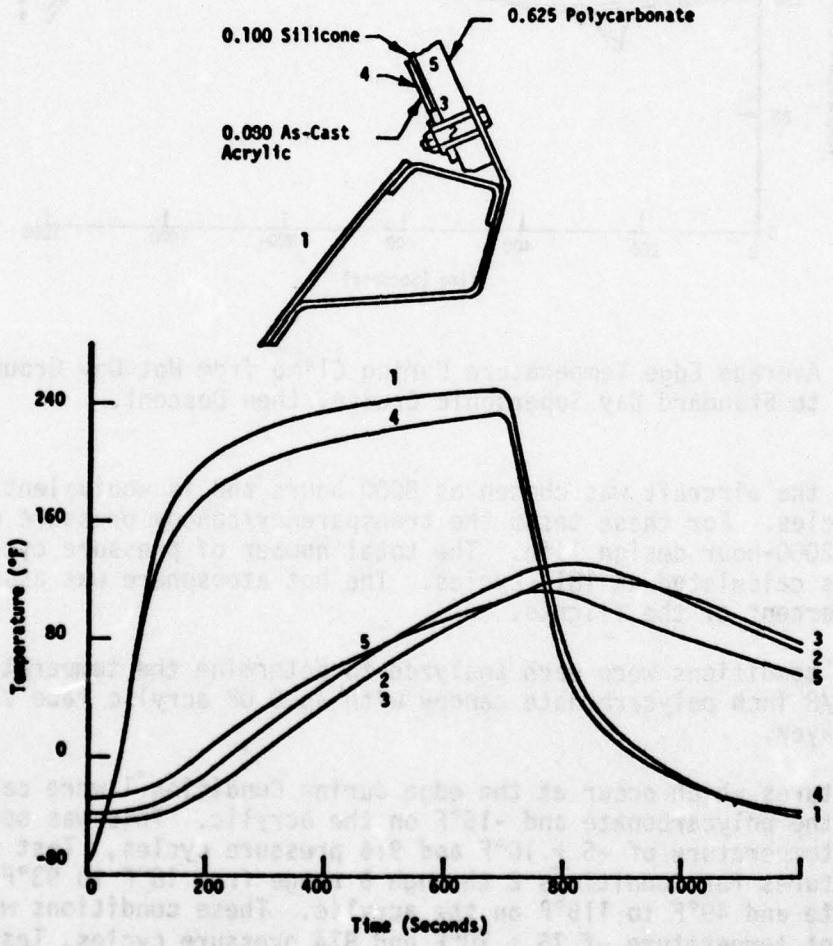


Figure 10. Average Canopy Edge Temperature During Acceleration From Cold Subsonic Cruise to Standard Day Supersonic Cruise, then Decelerate.

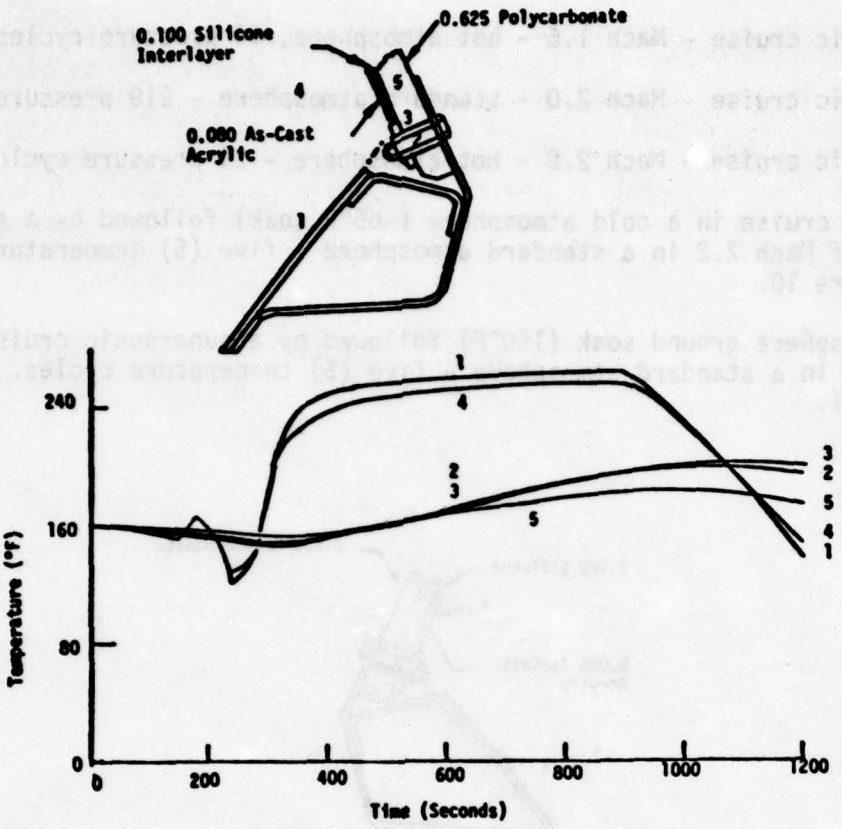


Figure 11. Average Edge Temperature During Climb from Hot Day Ground Soak to Standard Day Supersonic Cruise, then Descent.

The life of the aircraft was chosen as 8000 hours and is equivalent to 7256 pressure cycles. For these tests the transparency/canopy pressure cycles were based on a 2000-hour design life. The total number of pressure cycles for one lifetime was calculated as 1814 cycles. The hot atmosphere was assumed to occur during 10 percent of the flights.

The thermal conditions were each analyzed to determine the temperature at the edge of a 5/8 inch polycarbonate canopy with an 0.08 acrylic face sheet and 0.10 interlayer.

The temperatures which occur at the edge during Condition 1 were calculated to be -5°F on the polycarbonate and -15°F on the acrylic. This was specified as a constant temperature of -5 ± 10°F and 916 pressure cycles, Test number 1. The temperatures for Conditions 2 through 5 range from 18°F to 93°F on the polycarbonate and 49°F to 115°F on the acrylic. These conditions were defined as a constant temperature of 75 ± 10°F and 874 pressure cycles, Test Number 2. The temperatures for Condition 6 are 110°F on the polycarbonate and 160°F on the acrylic. This condition was defined as 24 pressure cycles at a constant temperature of 160 ± 10°F.

Two conditions, 7 and 8, were selected which will produce the largest temperature transients in the canopy. Since these are not probable conditions, only five temperature cycles of each condition were selected to be run at constant pressure. The first, Condition 7, is a subsonic cruise in a cold atmosphere followed by a supersonic cruise of Mach 2.2 in a standard atmosphere for 10 minutes. The temperature extreme is from -65 to 190°F. The cycle was defined as follows: soak at -65°F for one hour, increase air temperature as quickly as possible to 190°F and hold for 20 minutes, decrease air temperature as quickly as possible to -65°F and hold for 20 minutes, and then repeat.

The second, Condition 8, is a 160°F soak followed by a supersonic cruise at Mach 2.2, in a standard atmosphere for 10 minutes. The cycle is the same as the previous cycle, except the low temperature is 160°F and the high temperature is 245°F.

Load Conditions

The applied load was based on an internal canopy pressure of 13.2 psi. This is the ultimate internal pressure condition assumed for a canopy per Reference 5. Two load values were calculated, one for specimens with 1/4 inch bolts and the second for the specimens with 3/16 inch bolts. The load that was applied to the specimens with 1/4 inch bolts was calculated as follows:

$$(13.2\ \text{PSI})\ (15.9\ \text{IN.})\ (3.50\ \text{IN.}) = 735\ \text{LB.}$$

where 15.9 inches is the canopy radius
and 3.50 inches is the specimen width.

The load per 1/4 inch diameter bolt was 367.5 pounds per bolt and the load per inch of width was 210 pounds per inch.

The load that was applied to the 3/16 inch diameter bolts was 228 pounds per bolt. The load per inch of width was 114 pounds per inch. These loads were used for Tests 1 through 5 and were doubled for Test 6.

TEST RESULTS

Life Cycle One (Cyclic Load Tests No. 1, 2 and 3)

Test Number 1 was a simulation of a subsonic cruise, standard atmosphere. The estimated time to complete, based on six minutes per cycle was 91.6 hours. The actual time to complete was approximately 110 hours. A test load of 1191 pounds was achieved. The capacity of the cooling agent (CO_2) tanks, permitted an uninterrupted run of approximately 24 hours.

The test was run 16 hours per day, 5 days per week, and was monitored. The coolant was supplied automatically to keep the temperature at -5° ± 10°F. An automatic shutoff valve stopped the test when the tanks ran out of coolant. Inspection of the specimens was accomplished three times per day at each eight-hour interval. This test was completed without incident.

Test Number 2 was delayed because the bushings pulled out of the -521 configuration at cycle Number 325 and caused the time to complete the test to slip from the estimated 87.4 hours to 110 hours. This occurred at the end of the specimen without the retainer. The bushings were reinstalled using one inch diameter washers under the bolt heads. This procedure was duplicated for the remaining specimens utilizing 1/4 inch bolts. The test was resumed and completed without further incident for the full 874 cycles.

Test Number 3 precipitated a failure to the -533 specimen on the first cycle. The holes had been drilled improperly on the non-test end of the specimen which produced a shear-out failure. The specimen could not be repaired and was replaced with an aluminum spacer. The test was completed as planned without further incident.

Electrical heaters were used for this test. The selected load, temperature and cycles were achieved. Table 3 shows the temperature distribution within the environmental box for Cycles 1 and 10 of this test.

TABLE 3. TEMPERATURE DISTRIBUTION FOR TEST NO. 3, LIFE CYCLE 1

THERMOCOUPLE NUMBER	TEMPERATURE (°F)	
	CYCLE 1	CYCLE 10
1	164	167
2	160	163
3	161	164
4	154	160
5	162	166
6	153	157
7	150	156
8	160	163

Cyclic Temperature Tests (Numbers 4 and 5)

Test Number 4 was completed as required with the following variations. The initial low temperature was held for 60 minutes. The target time for cold to hot temperature was 12 minutes. The actual time varied from 13 to 25 minutes. The high temperature was held for the specified 20 minutes. Cool down time required 13 to 18 minutes. The load of 1191 pounds was accomplished although the pressure regulator had to be continually adjusted. The bolt loads were 367.5 pounds per 1/4 inch bolt and 228 pounds per 3/16 inch bolt.

This test was stopped on the fourth cycle because the loading cylinder ran out of stroke before maximum load was reached. The combined stretching of all the specimens was the cause of the bottoming out. No permanent set was observed in the specimens after the completion of the test. The specimens had been marked to measure permanent elongation. Adjustment of the hydraulic jack permitted continuation of the test. The five cycles were completed without further incident.

Test Number 5 caused permanent damage to several specimens as described. The time to heat from 160°F to 245°F varied from 5 to 25 minutes. The 245°F was held for the specified 20 minutes. Time to cool to 160°F varied from 13 to 18 minutes. The load of 1191 pounds was accomplished for the five temperature cycles.

Observation at the completion of five cycles showed bubbles in the interlayer of the specimens fabricated with the Sierracin S-130 interlayer. Figure 12 shows typical bubbling in two of these specimens.

Further observations revealed delamination in the bolt area of Specimens -525, -529 and -531. This delamination occurred at the end of the specimen where the acrylic ply was not cut back as shown in Figure 13 for the -531 configuration.

No crazing was observed.

Life Cycle Two Through Four

Test Numbers 1, 2 and 3 were repeated three times to complete Life Cycles 2, 3 and 4. No changes were observed in the specimens. These tests completed 7256 load cycles on the specimen assembly.

Cyclic Temperature Test Number 6

Test Number 6 was accomplished after Life Cycle Four. This test loaded the specimens to twice the operational load at the high temperatures seen in Test 5. Thus, the specimens with the 1/4 inch attachments were loaded to 1470 pounds and the specimens with the 3/16 inch attachments were loaded to 912 pounds. The maximum temperature of 245°F was limited by the thermal capability of the environmental box. The required 24 cycles were completed without incident. The temperature distribution for the eight thermocouples is shown in Table 4.

Post-test observations revealed an increase in the number of bubbles in Specimens -527 through -547 but no additional delamination was observed.

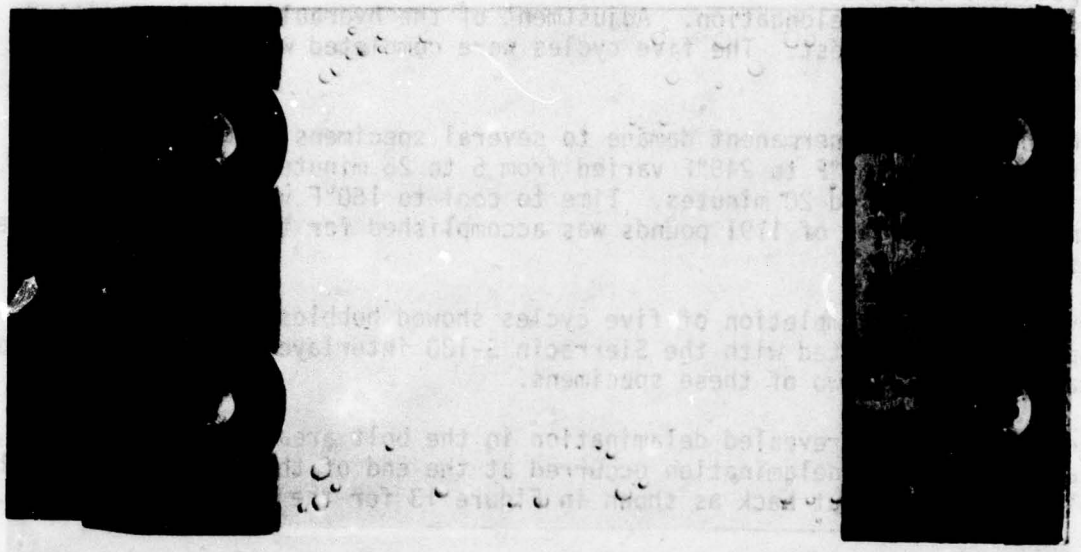
POST-TEST OBSERVATIONS

The specimens were removed from the test fixture and inspected. A description of the test specimens is given in Table 5.

Compressive yielding of the acrylic ply occurred under the washers.

No measurable creep had occurred.

-537



-543

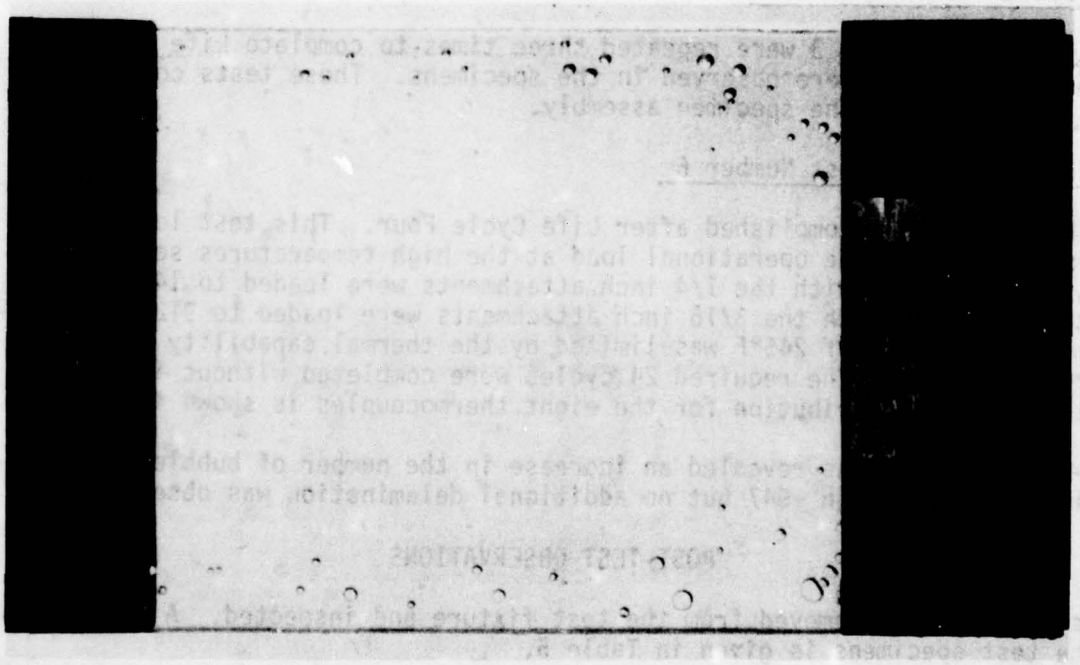


Figure 12. Interlayer Bubbling (-537 & -543)

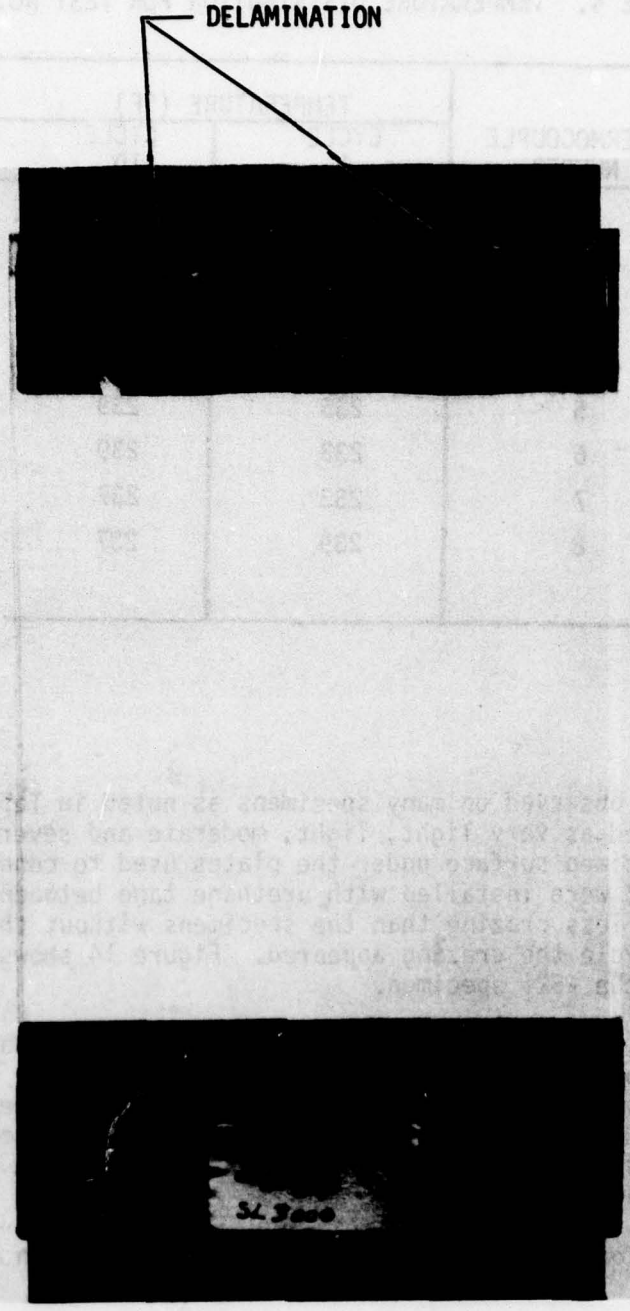


Figure 13. Delamination of Acrylic Ply at Bolt Holes (-531)

TABLE 4. TEMPERATURE DISTRIBUTION FOR TEST NO. 6

THERMOCOUPLE NUMBER	TEMPERATURE (°F)	
	CYCLE 1	CYCLE 10
1	243	238
2	241	242
3	246	247
4	240	243
5	235	239
6	233	239
7	233	237
8	239	237

Surface crazing was observed on many specimens as noted in Table 5. The degree of crazing is defined as very light, light, moderate and severe. All crazing occurred on the specimen surface under the plates used to connect the specimens. Those specimens that were installed with urethane tape between the plate and specimen, exhibited less crazing than the specimens without the tape. It is not known at what cycle the crazing appeared. Figure 14 shows the degree of surface crazing in the -521 specimen.

The surface crazing existing on these specimens is believed to have resulted from contamination of the polycarbonate combined with tension stress and high temperature. The asymmetrical loading of the specimens induced maximum tension stress on the specimen surface that interfaces with the connecting plates. The calculated tension stress on the connecting plate side of the -521 specimen was approximately 3500 psi.

No bushing deformation or bolt hole elongation was visible in any of the specimens.

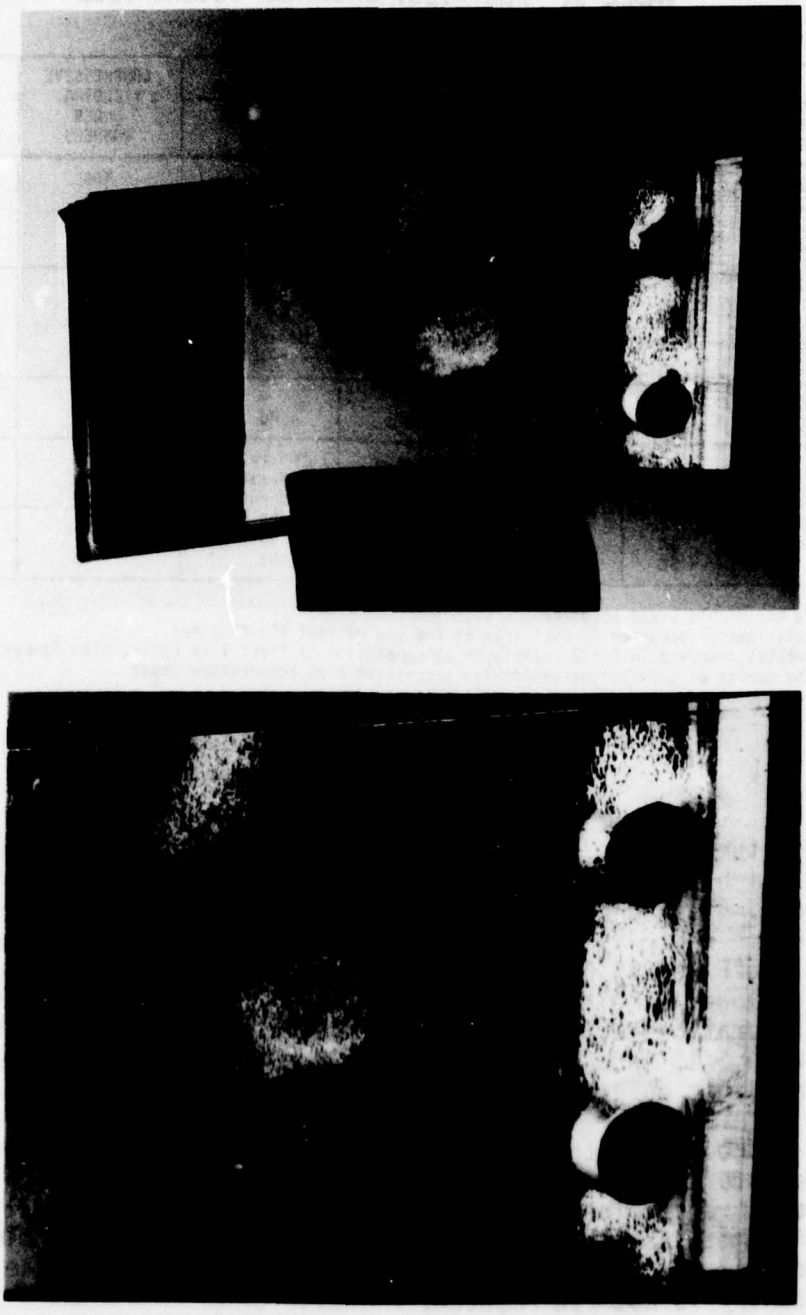


Figure 14. Surface Crazing.(-521 Configuration)

TABLE 5. POST-TEST SPECIMEN DESCRIPTION

CONFIGURATION OF 25943266	MFG	TAPE UNDER BOLTS	CRAZING		COMPRESSIVE YIELDING UNDER WASHERS	REMARKS (1)
			NON-RETAINER END	RETAINER END		
-521	SK		Severe	Moderate	Yes	
-523	SK		Severe	Severe	Yes	
-523	SMU	Yes	No	No	Yes	
-525	SK	Yes	Moderate	Light	Yes	
-525	SMU		Severe	Severe	Yes	(2)
-527	SK		Moderate	Moderate		
-529	SK		Moderate	Moderate		
-529	SMU	Yes	Very Light	No		(2)
-531	SK		Moderate	Moderate		
-531	SMU	Yes	Very Light	Very Light		(2)
-533	TEX		-	-		
-535	TEX		No	No		
-537	SK		Severe	Moderate	Yes	(3)
-539	SK		Severe	Moderate	Yes	(3)
-541	SK		Severe	Moderate	Yes	(3)
-543	SK		Light	Light		(3)
-545	SK		Light	No		(3)
-547	SK		Light	Light		(3)

(1) No measurable creep occurred.
(2) Delamination occurred in bolt area at the end without the retainer.
(3) Bubbles observed in S-130 interlayer at completion of first life cycle, high temperature test. The number of bubbles increased with successive high temperature tests.

CONCLUSIONS

The results of these tests verify the structural integrity and durability for the edge attachment area of a laminated windshield configuration as defined in Figures 1 and 2. The adequacy of the design was substantiated for an 8000-hour aircraft lifetime which is equivalent to 7256 pressure cycles at temperatures ranging from -65°F to 245°F and loads based on an ultimate canopy pressure of 13.2 psi. The loads condition resulted in a specimen load of 210 pounds per inch for configurations with 1/4 inch bolts, and 114 pounds per inch for configurations with 3/16 inch bolts. These tests were similar to the tests conducted on monolithic polycarbonate as reported in Reference 3.

Delamination did occur at the non-retainer end of one group of specimens during the high temperature, cyclic temperature tests. This delamination was a result of high temperature combined with compression induced in the acrylic ply by the bolt head. Asymmetrical loading by the single shear arrangement induced a load that tried to pull the bolts through the specimens. Extending the acrylic to the edge of the canopy is not recommended.

High temperature combined with the bolt load resulted in compressive yielding of the acrylic ply under the washers. This method, as noted above, is not a design concept.

Bubbles occurred in the S-130 interlayer. The bubbling occurred during the Life Cycle One, high temperature, cyclic temperature test and grew with subsequent high temperature tests. The use of this interlayer as fabricated for these specimens is not recommended for laminated transparencies.

The specimens had been marked to permit creep measurements. No measurable creep was observed.

Surface crazing occurred in many of the specimens. The crazing occurred under the aluminum connecting plates and was less severe at the end of the specimen that utilized the retainer and spacer. The use of urethane tape under the connecting plates reduced crazing. As noted in Reference 3, the use of an agent such as urethane tape along with a protective coating can significantly reduce the effects of environment on polycarbonate surfaces.

The test assembly was designed to load and test 18 specimens simultaneously under high, low and ambient temperatures. This method assured identical test conditions for all specimens and reduced the test time that would be required for individual testing of each specimen. A disadvantage of this method was the difficulty involved in making periodic inspections of the specimens.

REFERENCES

1. Hassard, R. S., Plastics for Aerospace Vehicles, Part II, Transparent Glazing Material, MIL-HDBK-17A, Part II, January 1973.

2. Husman, G. E., Kuhbander, R. J., Environmental Data and Machining Techniques of Polycarbonates, Technical Report AFML-TR-73-126, June 1973.

3. Irion, J., Specimen Structural Endurance Tests - F16A, Report No: TR 262, Texstar Plastics, November 1975.

4. Reeves, W. R., Structural Design Criteria, General Dynamics Report 16PS007B, March 1976.

5. Critical Item Development Specification, F-16 Transparencies, General Dynamics Report 16ZK002A, February 1976.

HIGH-SPEED BIRD IMPACT TESTING OF AIRCRAFT TRANSPARENCIES

R. H. Magnusson
Douglas Aircraft Company
McDonnell Douglas Corporation
Long Beach, California

HIGH-SPEED BIRD IMPACT TESTING OF AIRCRAFT TRANSPARENCIES

by

RALPH H. MAGNUSSON

Douglas Aircraft Company
Long Beach, California

ABSTRACT

High-speed bird impact tests were made on a full-scale high-performance aircraft windshield mounted in an actual large bomber-type military aircraft test vehicle, and on several simulated aircraft windshields mounted on support fixtures of representative cockpit framing stiffnesses. The full-scale windshield was of three-ply polycarbonate laminate construction. The five simulated aircraft windshields were constructed of 1-, 2-, and 4-ply polycarbonate structure plies, and a 2-ply tempered-glass laminate, all with various high-performance interlayers. Strain gages were attached at strategic locations on the windshields and supporting structure and selected readings were made during testing. Some static loading/dynamic unloading tests were also conducted. From these tests, an accurate determination of deflections resulting from application of specific loads were obtained. Also, dynamic unloading permits the measurement of windshield vibratory/damping response utilizing the gage oscillographs. Effects of various transparency edge design, attachment bolt hole sizes, and support structure stiffnesses were investigated and documented. A tabulation was made as to the relative effectiveness of the various designs in defeating the impact of 4-pound birds at impact velocities up to 970 feet per second.

PRECEDING PAGE BLANK-NOT FILMED

INTRODUCTION

The impact of a bird on windshields of aircraft flying at high speeds represents a major structural problem for today's aircraft. The Douglas Aircraft Company's Windshield Technology Demonstrator Program is part of an effort by the Air Force Flight Dynamics Laboratory Improved Windshield Protection Program to develop technologies that will assist in the design of aircraft transparent enclosures to increase protection against birdstrikes.

This paper presents the high-speed bird impact tests which progressively evaluated a series of candidate alternate B-1 windshield designs. A basic consideration to this test series is the premise that for test results to be truly representative , the tests must be performed on structure which simulates, or otherwise accounts for, actual aircraft structural stiffnesses. This consideration is followed throughout this test series.

An extensive coverage of these series of high-speed bird impact tests may be found in Reference 1.

B-1 Windshield Bird Impact Test Series

The B-1 windshields, as originally designed, were determined to be a very high cost item from the standpoint of installation. Because of common windshield retainers between two or more windshields, each edge of the windshield had to be installed with two rows of attachments, and there was great difficulty aligning the attachment holes between the windshield and structure, due to tight fitting holes. To alleviate some of the problems and reduce installation costs, Douglas modified the design and developed modifications of the edge designs to utilize only one row of attachments installed in loose holes with wet sealant applied. A series of six bird impact shots were made to validate the theories developed. Shots were made with four- and six-pound birds at 562 knots, and it was shown that the theories were valid.

Simulated Aircraft Windshield Bird Impact Test Series

To optimize windshields, structural support and edge designs, a series of five specimens were designed, utilizing materials proprietary to three transparency vendors, for bird impact testing. A total of ten specimens were ordered that measured 36 x 36 inches and were curved to a constant 60-inch radius. Two structural fixtures were designed and built to support these specimens for bird tests. The structural arrangement purposely was sized with varying degrees of stiffness and variable corner configurations. Twenty bird impact tests were conducted at AEDC. To maximize the comparative data required for proper specimen evaluation during the testing, the three vendors laminated various strain gages and thermocouples within each specimen and additional external instrumentation was accomplished by both Douglas and AEDC. The bird impact tests were conducted at the extreme hot or cold temperatures that a B-1 aircraft would encounter in service at velocities up to 562 knots.

TECHNICAL DISCUSSION

This section presents a discussion of the test facilities utilized, and specific requirements and results of this series of high speed bird impact tests.

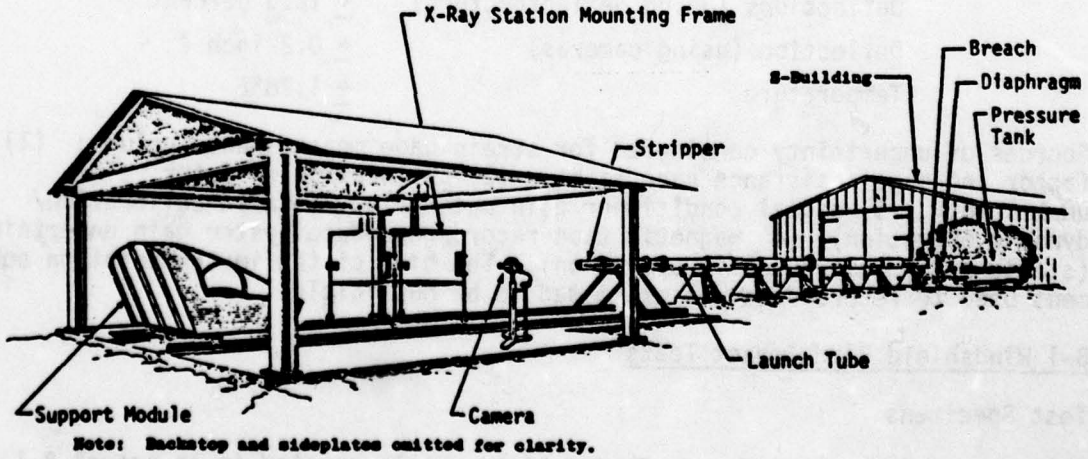
Test Facilities

All tests of this series were performed utilizing the test facilities at Arnold Engineering Development Center (AEDC), Arnold Air Force Station, Tennessee. This facility is operated by personnel employed by ARO, Inc., a subsidiary of Sverdrup & Parcel and Associates, Inc.

The experimental data presented in this paper were obtained in the Range S2 at the AEDC (References 2 and 3). The range consists of a launcher and a launch tube (Figure 1 below). In each shot, the chicken and its sabot were loaded in the breech end of the launch tube immediately forward of a double diaphragm section. The diaphragms were made of 0.019 inch thick Mylar.

The purpose of the sabot was to permit adaptation of the chicken to, and prevent contact with, the bore of the launch tube during launch. The sabots were made of balsa wood having a density that varied from 13.5 to 17 lb/ft^3. The sabot was prevented from traveling on and striking the target by a tapered stripper tube attached to the muzzle of the launch tube.

The test area consists of a 22 x 32 foot covered concrete pad. Two 0.5 inch thick steel plates spaced approximately 3 inches apart serve as the backstop; single 0.25 inch thick steel side plates are rolled into place for personnel protection and to contain debris. The impact point on the windshield panels was located approximately 5 feet from the third X-ray station and approximately 13 feet from the stripper muzzle. The accuracy of the launcher in striking the designated target point with the projectile was ± 1 inch.



Note: Backstop and sideplates omitted for clarity.

Figure 1. AEDC Bird Impact Test Facility. (Range S-3)

Data Reduction

Projectile velocity was determined from three X-ray stations located about 3.5 feet apart along the flight path between the launcher muzzle and the target. The velocity measuring system was mounted on an instrumentation dolly with the first station located approximately one foot from the muzzle of the stripper tube. The X-ray pulsers were triggered when the chicken broke a 24 gauge copper wire in an electrical break-wire system. The time between firings of the pulsers was recorded with a digital chronograph, and using the time together with the distance measured between images of the projectile on the X-ray film (after corrections for point source emission), the velocity was determined.

Strain gage and deflectometer data obtained during the static portion of the static loading/dynamic unloading tests of the B-1 tests only were provided to Douglas in the form of oscillograph traces together with their respective calibration traces. Strain gage data obtained during the dynamic unloading portion of the tests and the actual bird shot tests for both series were digitized, then plotted as a function of time.

Photographic data consisting of motion picture film and still photographs were also transmitted to Douglas for evaluation.

Data Uncertainty

ARO test personnel estimated the total uncertainties associated with data obtained during these tests as follows:

Parameter	Uncertainty
Velocity	± 0.5 percent
Bird Weight	± 0.1 percent
Strain Gage Readings	± 10.0 percent
Deflections (using deflectometers)	± 12.0 percent
Deflection (using cameras)	± 0.2 inch
Temperature	± 1.78°F

Sources of uncertainty considered for strain gage measurement include: (1) gage factor and gage resistance uncertainty, (2) calibration resistor value uncertainty, (3) signal conditioner gain uncertainty (static calibration/dynamic operation), (4) magnetic tape record/reproduce system gain uncertainty (static calibration/dynamic operation). The bias of the instrumentation equipment used to record data was estimated to be negligible.

B-1 Windshield Bird Impact Tests

Test Specimens

The test specimens consisted of windshield panels mounted in an actual B-1 module (prototype crew module X-5). The crew module was mounted in a special support frame which was not anchored to the test area floor, but did not move

during the test shots. The test article was mounted at zero-degree angle-of-attach aircraft attitude. The windshield attach bolts and/or retainer was modified in the several tests to evaluate the various proposed B-1 designs. A series of bird impact and static loading tests were performed on two left-side windshield specimens. The tests included the original R-I design and installation requirements utilizing two rows of tight attachments, then revised for two rows of attachments with loose holes, one row of attachments with tight holes, one row of attachments with loose holes, and one test with every other attachment left out.

The test specimens were furnished by the Air Force and consisted of representative air vehicle windshields mounted in a Prototype B-1 Crew Module at AEDC. Three (3) test specimens were avilable and identified as two (2) left-hand windshields (L3000151-001) and one (1) right-hand windshield (L3000151-002).

The parts available were manufactured by Swedlow, Inc., per Rockwell International (RI) drawing L3000151 (refer to Figure 2). The parts were identified as:

L3000151 -001	Left Hand	SWU 108
L3000151-001	Left Hand	SWU 107
L3000151-002	Right Hand	SWU 105

The right-hand windshield, Number 105, was installed by ARO personnel before the test began and was left in for all shots. The left-hand panel, Number 108, had been installed by Rockwell International personnel during their last B-1 bird impact test entry. Removal of Panel Number 108 after Shot Number 2 and installation of Panel Number 107 was also accomplished by ARO personnel.

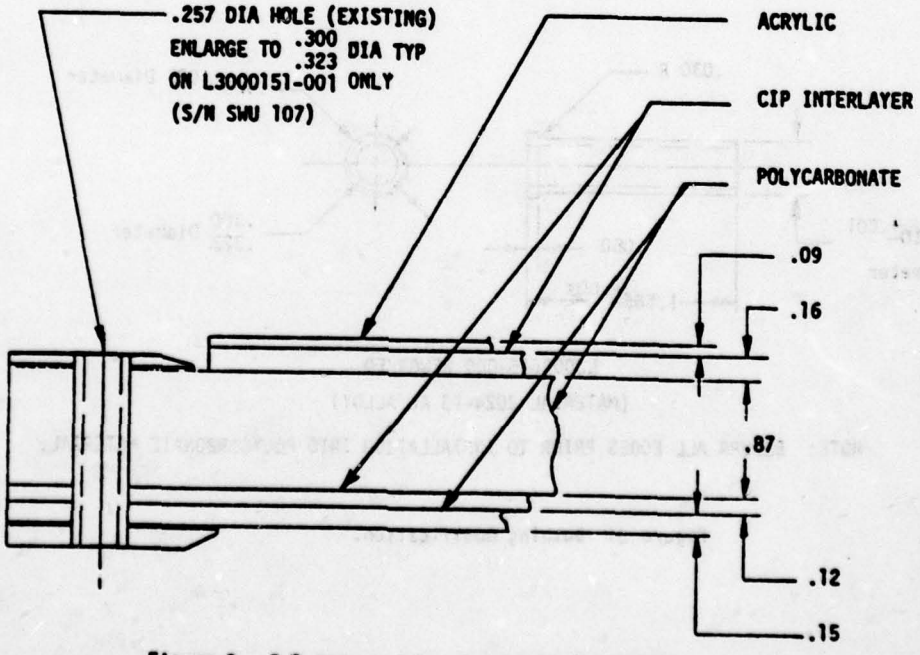


Figure 2. B-1 crew module windshield (L3000151).

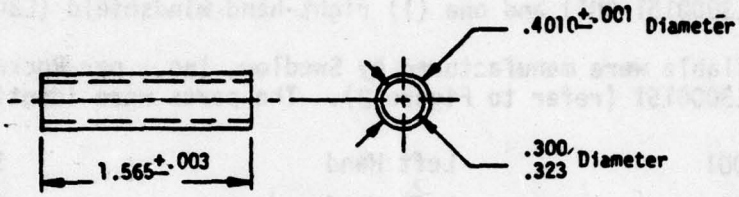
AD-A065 049 AIR FORCE FLIGHT DYNAMICS LAB WRIGHT-PATTERSON AFB OHIO F/G 1/3
CONFERENCE ON AEROSPACE TRANSPARENT MATERIALS AND ENCLOSURES (1--ETC(U)
DEC 78 R E WITTMAN

UNCLASSIFIED AFFDL-TR-78-168 NL

4 OF 10
ADA
065049



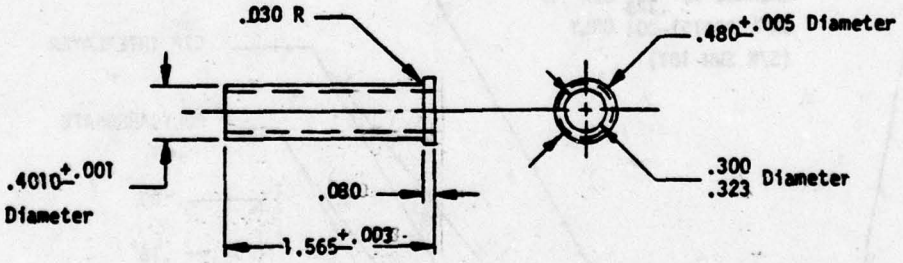
The left-hand part, SWU 107, had the bolt attachment holes enlarged in the bushings to 0.300 - 0.323 diameter by AEDC, as shown in Figure 2 before installation on the crew module. Different configurations of retainers and bushings were used during the tests. Two new sets of bushings were fabricated for use during the test. One of these sets was fabricated according to Rockwell Drawing No. L3000645, and the other set fabricated according to the same drawing but modified per Figure 3. Before each bushing was installed, it was cleaned with alaphatic naptha, followed with cleaning with isopropyl alochol. Dow Corning 1200 primer was applied to each bushing and then the bushing was cemented in the windshield hole with Dow Corning 93-007 sealant.



L3000645-025 REWORKED

(MATERIAL 2024-T3 AL ALLOY ROD)

NOTE: DEBURR ALL EDGES PRIOR TO INSTALLATION INTO POLYCARBONATE MATERIAL.



L3000645-009 REWORKED

(MATERIAL 2024-T3 AL ALLOY)

NOTE: DEBURR ALL EDGES PRIOR TO INSTALLATION INTO POLYCARBONATE MATERIAL.

Figure 3. Bushing modification.

A new set of retainers common to the left hand windshield was fabricated, then reworked per Figure 4 by cutting the retainer as shown. This rework produces the desired effect of removing the restraint of the second row of bolts.

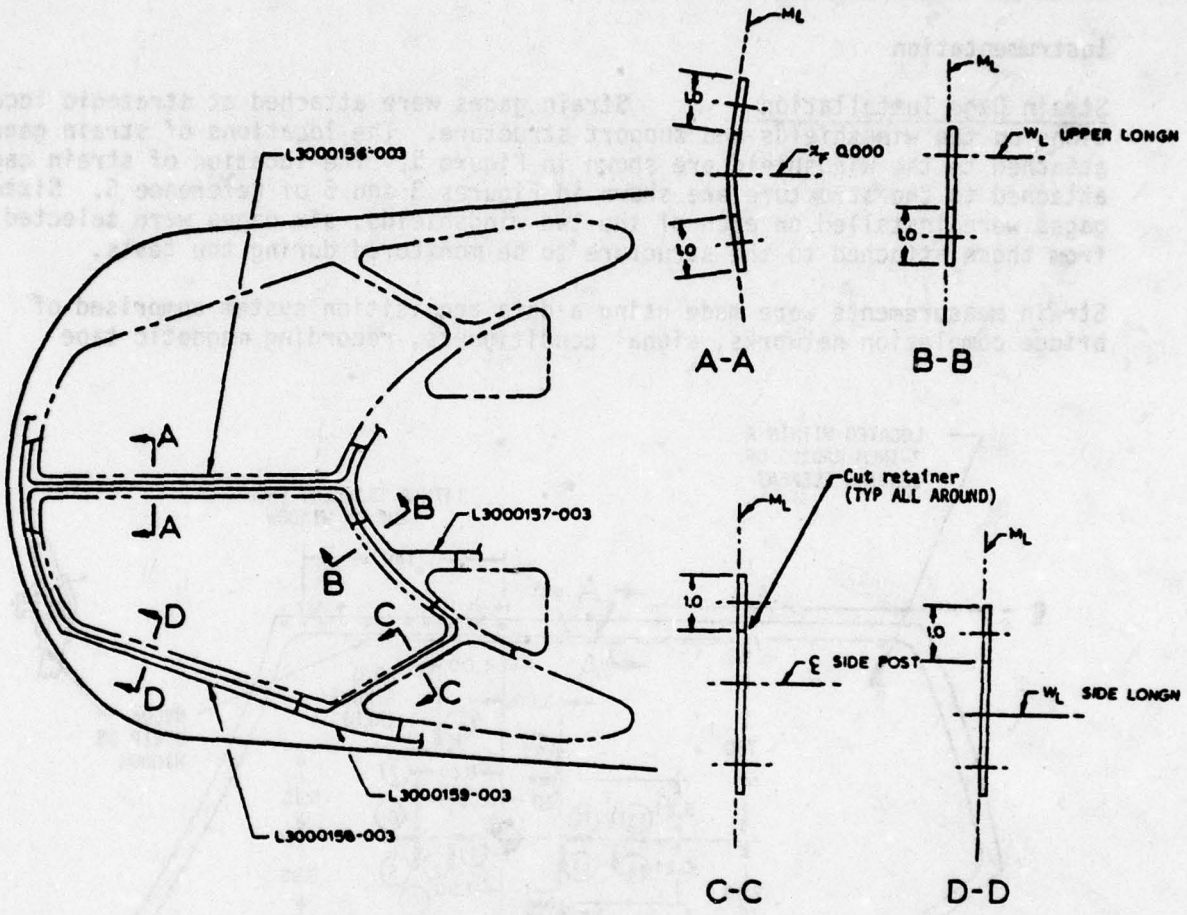


Figure 4. Retainer modification.

As windshield Number 107 was being installed for Shot Number 3, all bolts common to the windshield had Products Research PR 1422 sealant applied around the bolt shank to fill the volume remaining in the bolt hole. The sealant was refurbished when the bolts were removed and reinstalled when for the next shot (Shot Number 4).

During the previous B-1 windshield test (Reference 4) the right-hand longeron, near the centerline of the module, was damaged. A large piece of the longeron was torn off during bird impact and cracks were formed in the web. Prior to this test, most of the damaged section of the longeron was removed and a new section made of steel was installed (Reference ARO Drawing Number VST0409401).

The impact point, shown in Figure 5 below, remained the same for all shots. Four-pound chickens were used as projectiles for the first five shots; a six-pound chicken was used on Shot Number 6. The nominal launch velocity for all shots was 650 miles/hour (953 fps).

Instrumentation

Strain Gage Installation - Strain gages were attached at strategic locations on the windshields and support structure. The locations of strain gages attached to the windshield are shown in Figure 5. The location of strain gages attached to the structure are shown in Figures 3 and 5 of Reference 5. Sixteen gages were installed on each of the two windshields; six gages were selected from those attached to the structure to be monitored during the tests.

Strain measurements were made using a data acquisition system comprised of bridge completion networks, signal conditioners, recording magnetic tape

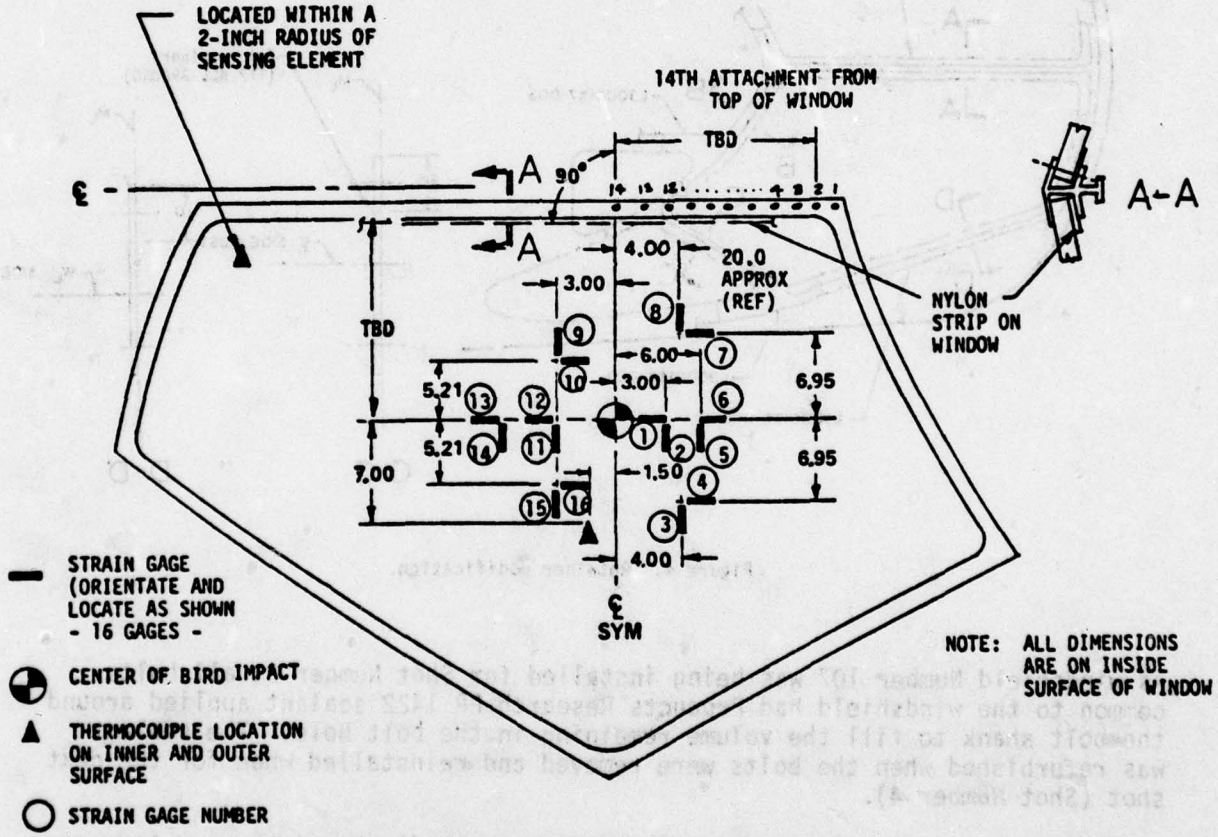


Figure 5. Strain gage and thermocouple locations.

machines and recording oscillographs. Twenty-two recording channels were used in acquiring data on deflection tests and on the actual test shots. These data were presented as oscillograms and were digitized and converted to the desired units. The bandwidth of the recording system was DC to 4 kHz. Calibration of this system was accomplished using known resistances paralleled with the active leg or strain gage, thus producing a bridge unbalance and an output voltage.

Two different strain gage mounting installations were evaluated in this test series. The mounting installation shown in Figure 6 was utilized in Shots 1, 2, and 3. A desirable feature of this installation was thought to be the "shock block". However, the extra mass of the silicone gage sealing, which covered the gage and its leads, resulted in the block tearing loose when the windshield was impacted. The silicone-covered block jumped approximately four inches subsequent to impact; thus hyperextending the strain gage foil leads causing premature gage failure.

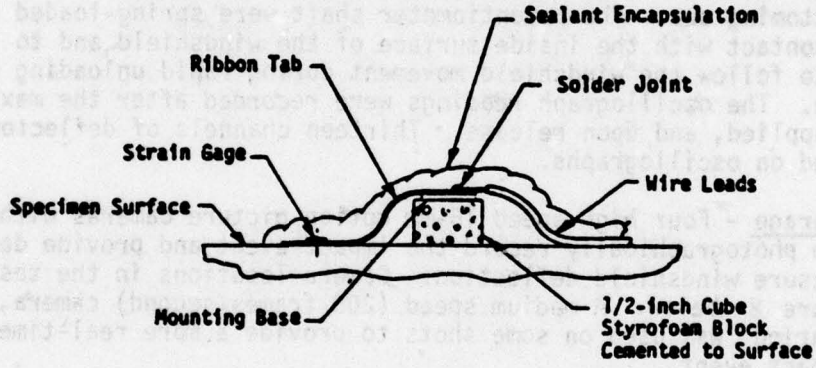


Figure 6. Styrofoam block shock absorber.

The failure of some gages was noticed after Shots 1, 2, and 3, but each gage installation appeared to still be intact after each test. A detailed evaluation of the high-speed motion pictures showed the gage installation jump, upon bird impact, and, because of the high elasticity of the silastic seal, the installation appeared to be normal after the test.

Failed gages were then removed and replaced with the mounting installation shown in Figure 7 for Shots 4, 5, and 6. No gage failures due to inertia effects was sbusequently encountered.

The strain gage mounting installation shown in Figure 7 was utilized in the Simulated Aircraft Windshield Bird Impact Test series.

Deflectometer Recording Equipment - The measurements were made using a Bourns Model 109 linear potentiometer ac the active leg in a wheatstone bridge

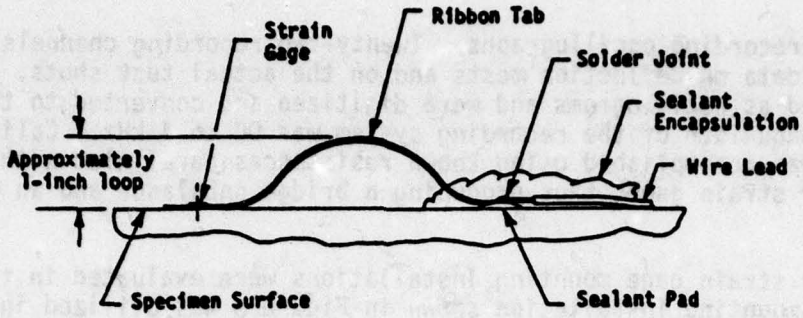


Figure 7. High impact shock resistant gage installation.

circuit. These deflectometers were capable of deflecting at least two (2) inches before bottoming out. The potentiometer shaft were spring-loaded to ensure intimate contact with the inside surface of the windshield and to cause the shaft to follow the windshield movement during rapid unloading of the applied force. The oscillograph readings were recorded after the maximum static load was applied, and upon release. Thirteen channels of deflectometer data were recorded on oscillographs.

Photographic Coverage - Four high-speed 16-mm motion picture cameras with color film were used to photographically record the impact event and provide data from which to measure windshield deflection. Camera locations in the test area are shown in Figure 8 below. A medium speed (200 frames/second) camera, whose location varied, was used on some shots to provide a more real-time record of the impact event.

Still color photographs were made of the test setup, including the interior of the module, deflectometer setup, static loading device, camera setup, inner and outer views of the windshield, and general overall views. Color photographs were also made of the test article after impact to record any damage to the windshields or supporting structure.

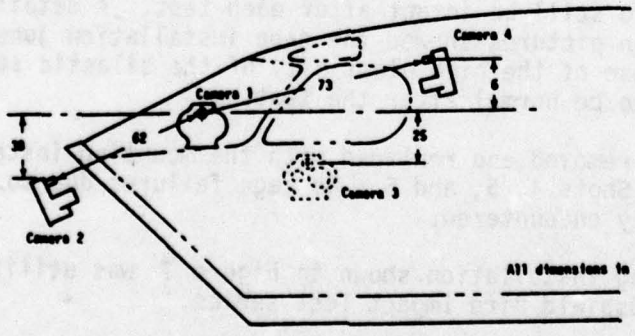


Figure 8. Camera locations.

Static Loading/Dynamic Unloading Tests

Static loading/dynamic unloading tests were conducted before each of the first four shots (refer to Figure 9). The purpose of these tests was to determine the amount of deflection (with use of deflectometers) that occurred at various locations on the windshield and support structure when a known static load was applied. Also, dynamic unloading permitted the acquisition of strain gage versus time data for the determination of the vibratory motion and damping phenomenon of the windshield specimens.

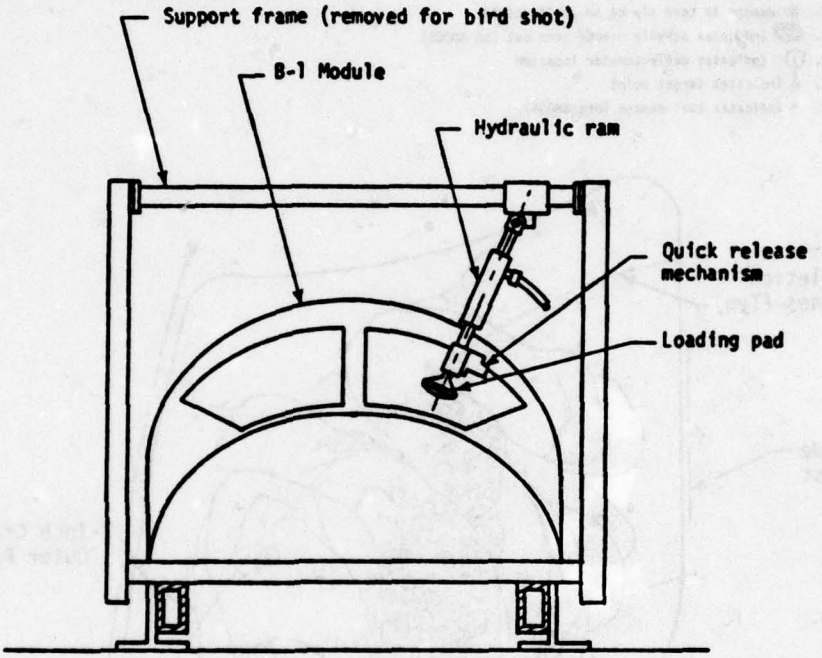


Figure 9. B-1 Windshield Static Loading/Dynamic Unloading Test Setup.

AEDC designed and built the necessary structural members to mount a movable hand operated hydraulic system that is capable of delivering 1500-2500 pounds force normal to the windshield surface at Location A, as shown in Figure 9 The structural members were attached at the longitudinal base legs of L9531899 Module Holding Fixture. Douglas designed and fabricated the release mechanism and loading pad.

The hydraulically operated loading pad was mounted with its axis normal to the impact point. A quick-release mechanism was incorporated as an integral part of the device to remove the load with a minimum of damping action attributable to the device itself. The loading device was calibrated for loads up to 2500 pounds.

The test procedure was to obtain deflection measurements using the deflectometers at one or two load levels, then dynamically release the load and obtain strain versus time measurements and high-speed motion picture coverage of the event. High-speed motion picture coverage was provided to obtain a visual record of the windshield for comparison with deflectometer measurements at points defined in Figure 10.

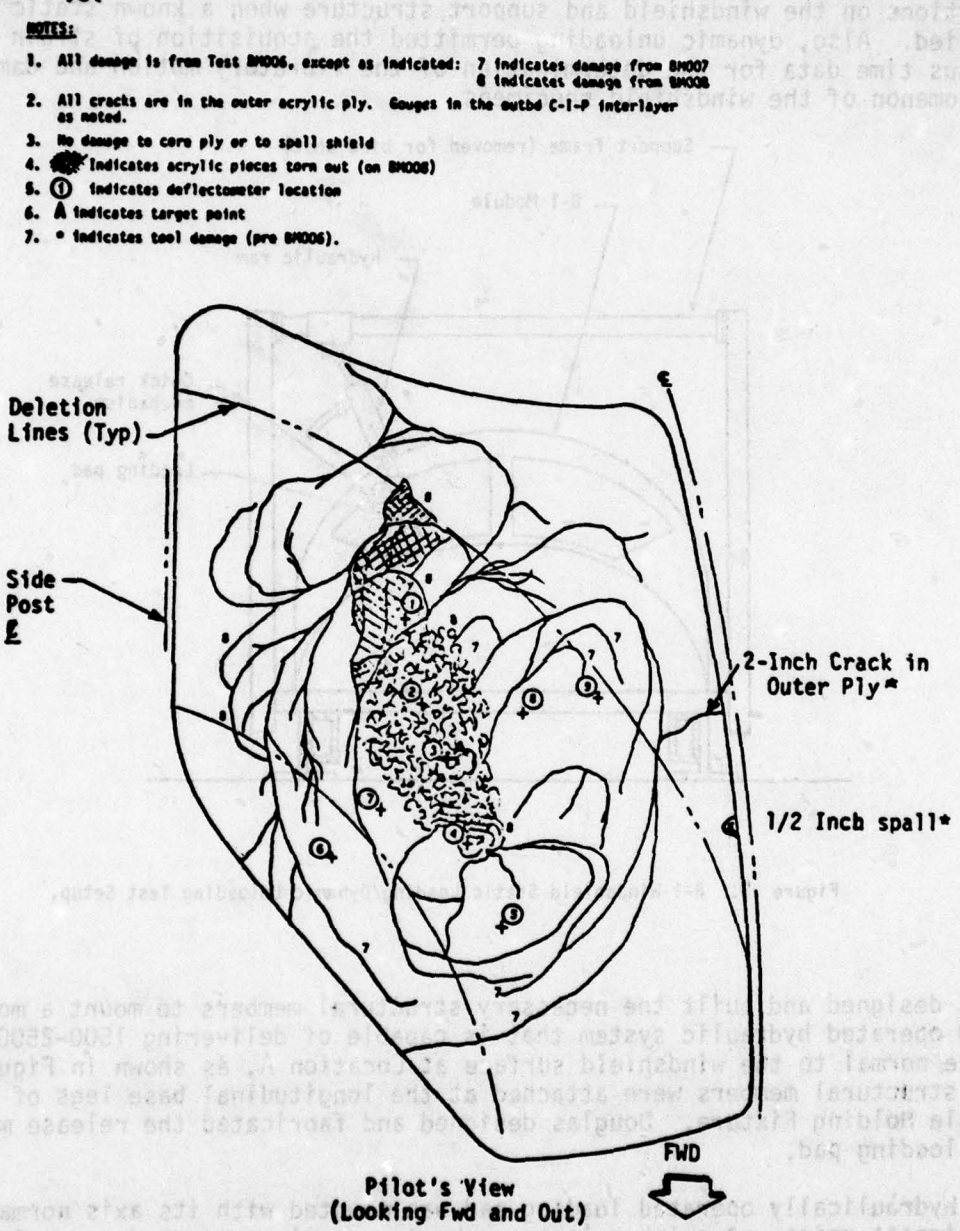


Figure 10. B-1 windshield test specimen (SWU107) test BM006 to BM008. Deflectometer locations and post-test condition.

The results of center deflection measurements taken during the static loading tests prior to each of the first four shots are presented in Table 1. A 1500-pound load was applied to the impact point prior to dynamic release before Shots 1 through 4; a 2500-pound load was applied to the impact point prior to dynamic release before Shots 2, 3 and 4.

Bird Impact Tests

All tests were performed utilizing a complete bird carcass weighing a planned $4.0^{+.2}_{-0}$ pounds. The basic design velocity was 650 ± 17 mph (953 ± 25 fps). Velocities actually achieved are noted in the complete test summary of Table 1.

In the summary of Table 1, it may be seen that on Shot Number 1, the outer acrylic ply of Panel Number 108 spalled and cracked but there did not appear to be any damage to the polycarbonate structural ply. There were several cracks in the polycarbonate inner ply that appeared to emanate from a damaged area that resulted from excessive heat being applied to the windshield during installation of strain gages. On Shot Number 2 (same windshield panel), there was some additional spalling of the outer ply but no visible damage to the structural ply or additional cracking of the inner ply. The progressive damage is shown in Figure 10.

On Shot Number 3, using windshield Panel Number 107, the outer acrylic layer spalled and cracked, but there was no visible damage to the polycarbonate structural ply or cracking of the inner ply. On Shots 4, 5, and 6 (Panel Number 107) there was little additional damage to the windshield; the inner ply did not appear to be damaged. On Shot Number 6 (six-pound chicken), the inner ply cracked but did not spall.

Every other bolt common to the windshield was removed before Shot Number 5. The ends of the top aft retainer (L3000157-003) and the forward end of the lower aft retainer (L3000159-003), which were not secured with bolts, were bent outwards as a result of the hydraulic forces of the bird. As an aid in preventing this from happening on the following shot, bolts were moved from adjacent holes to the ends, leaving two successive holes without bolts. This bolt configuration was successful in securing the ends of the retainer during the impact of Shot Number 6.

Structural damage occurred on Shot Number 6; the spall ply cracked and cracks appeared in the aft longeron and in the outboard sill structure (Figure 11). Also, a few bolts failed, but there was no penetration of the interior of the module by the bird.

Vertical deflection (normal to the windshield) at the impact point are tabulated in Table 1 for all cases.

These test results indicate that a B-1 windshield system design incorporating the Douglas attachment recommendations (one row of "loose" holes) is acceptable for bird impact.

TABLE 1. BIRD IMPACT TEST RESULTS ON X-5 MODULE

SEQ	SHOT NO	PART NO.	STATIC LOADING					BIRD IMPACT						REMARKS		
			TEMPERATURE			LOAD	CENTER DEFL	TEMPERATURE			WT (lb)	V (fps)	CENTER DEFL	RETAINER/ATTACH HOLES CONDITION	TRANSPARENCY COND. AFTER TEST	SUPPORT COND. AFTER TEST
			AMB.	W/S	COCKPIT			AMB.	W/S	COCKPIT						
1	BM004	L3000151-001 SMU-108	71.0°	71.5°	–	15000	.25"	73.5°	83.5°	74.6°	4.00	953	2.15"	Original B-1 instl. (Full retainer-tight holes in bushings. W/S attach bolt torque 80-105"#. Heat bubble damage on inner ply near SG 9.	Outer ply fracture over lg. area near impact. Inner ply fracture start at heat bubble. No damage to core ply.	No structural damage. Bolts did not rotate.
2	BM005	L3000151-001 SMU-108	61.2°	72.0°	68.2°	15000	.25"	48.5°	63.8°	49.2°	4.07	951	2.40"	One bolt design simulation. Retainer cut between attach bolts (1"). Tight holes in bushings. W/S bolt T = 50-60"#	More spalling of outer ply. No further damage to inner ply. No damage to core ply.	No damage.
			55.3°	60.0°	–	25000	.43"									
3	BM006	L3000151-001 SMU-107	60.0°	65.2°	69.8°	15000	.22"	57.6°	64.4°	60.0°	4.02	967	2.05"	Full retainer (2-bolt design.) Bolt holes in bushings are o/s, + sealant. W/S bolt T= 50-60"#	Much crack & spalling of outer ply. No damage to core ply or inner ply.	No damage.
			59.4°	71.7°	71.2°	25000	.38"									
4	BM	L3000151-001 SMU-107	45.0°	55.9°	53.7°	15000	.27"	62.9°	71.0°	68.6°	4.00	936	2.15"	One bolt design simulation. Retainer cut between attach holes. Bolt holes in bushings are o/s, + sealant. W/S bolt T=50-60"#	Additional cracks & peeling of outer ply. No damage to core ply or inner ply.	No damage.
			45.0°	61.0°	56.1°	25000	.46"									
5	BM008	L3000151-001 SMU-107	–	–	–	–	–	62.9°	71.4°	65.7°	4.02	930	2.25"	Same as previous test, except every other w/s attach bolt removed.	Additional cracks & peeling of outer ply. No damage to core ply or inner ply.	Unsupported end of top retainer bent up 1". Also, bottom fwd end of rear retainer bent up 3/4".
6	BM009	L3000151-001 SMU-107	–	–	–	–	–	72.4°	78.4°	74.4°	6.00	970	4.55"	Same as previous test. Bent retainer straightened and replaced.	Additional peeling of outer ply. No damage to core ply. Inner ply cracks originated at point of maximum deflection.	14" crack in radius of long'n above side post. 3" crack in radius of lower sill 12" fwd of side post.

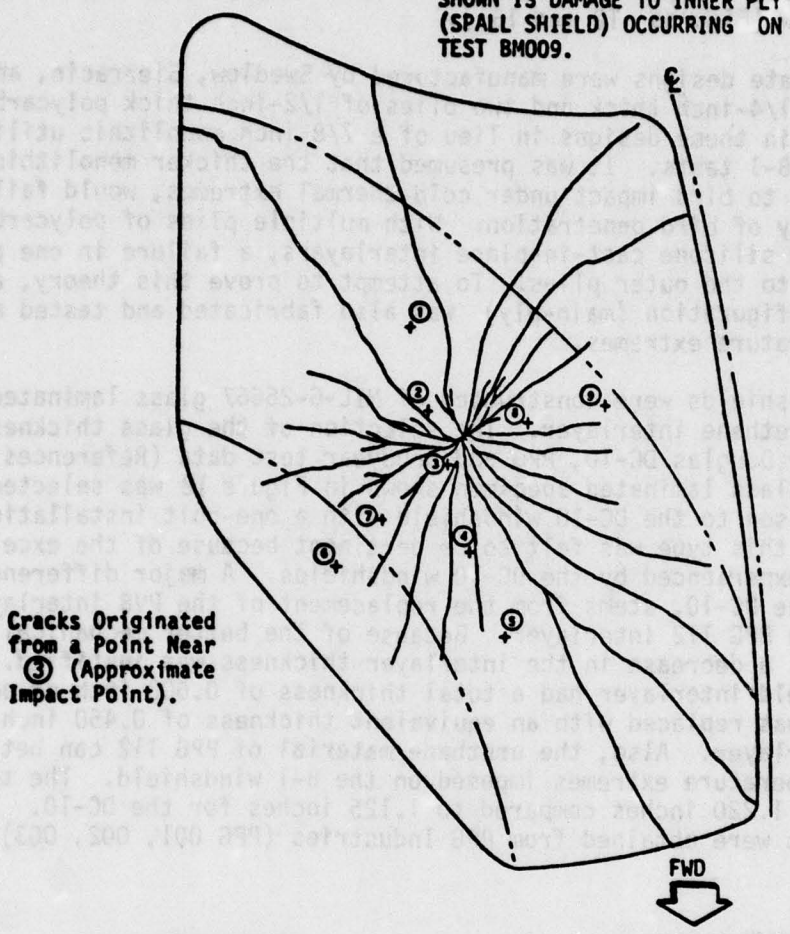


Figure 11. B-1 windshield test specimen (SWU107), inner ply surface, post-test BM009.

Simulated Aircraft Windshield Bird Impact Tests

In order to finalize and optimize all of the structural design aspects for a full sized B-1 alternate windshield design, simulated aircraft windshield test specimens and mounting fixtures were designed for this series of bird impact tests.

Test Specimens

Windshield Specimens - Five windshield configurations were developed and bird impact tested. These parts were 36 x 36 inch square with a 60-inch radius curvature. Glass and polycarbonate laminated windshield configurations were tested. The laminated polycarbonate designs (P/N Z5942640-501, -507 and

P/N Z5942639-503, -505) and the glass laminated design (P/N Z5942639-501) are shown below (Figures 12 and 13).

The polycarbonate designs were manufactured by Swedlow, Sierracin, and PPG. Four plies of 1/4-inch thick and two plies of 1/2-inch thick polycarbonate were selected in these designs in lieu of a 7/8 inch monolithic utilized in the full-size B-1 tests. It was presumed that the thicker monolithic material, when subjected to bird impact under cold thermal extremes, would fail, hence the possibility of bird penetration. With multiple plies of polycarbonate separated with silicone cast-in-place interlayers, a failure in one ply should not propagate to the outer plies. To attempt to prove this theory, a 7/8 inch monolithic configuration (main-ply) was also fabricated and tested at high and low temperature extremes.

The glass windshields were constructed of MIL-G-25667 glass laminated with PPG 112 polyurethane interlayer. The selection of the glass thickness was based on prior Douglas DC-10, PPG and Goodyear test data (References 6, 7 and 8). The glass laminated specimen shown in Figure 12 was selected as a direct comparison to the DC-10 windshield with a one-bolt installation. A comparison of this type was felt to be pertinent because of the excellent service life experienced by the DC-10 windshields. A major difference, when compared to the DC-10, stems from the replacement of the PVB interlayer on the DC-10 with PPG 112 interlayer. Because of the better mechanical properties of the latter, a decrease in the interlayer thickness was justified. The DC-10 windshield interlayer had a total thickness of 0.600 inch of polyvinyl butyral that was replaced with an equivalent thickness of 0.450 inch of PPG 112 urethane interlayer. Also, the urethane material of PPG 112 can better withstand the temperature extremes imposed on the B-1 windshield. The total glass thickness was 1.220 inches compared to 1.125 inches for the DC-10. Three test specimens were obtained from PPG Industries (PPG 001, 002, 003).

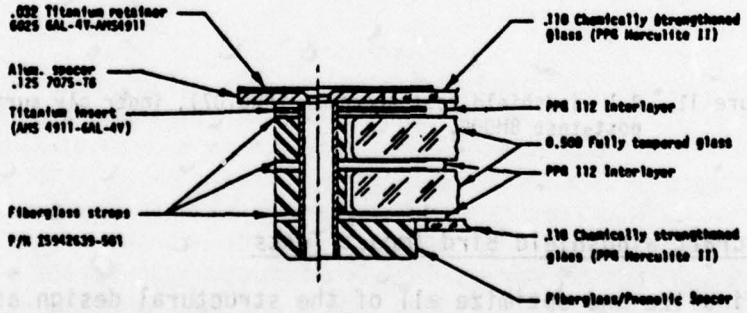


Figure 12. Simulated aircraft windshield design. Laminated glass construction (Z5942639-501).

The four-ply polycarbonate specimen shown in Figure 13a with a two-bolt edge design was selected utilizing R-I test data from testing accomplished at the

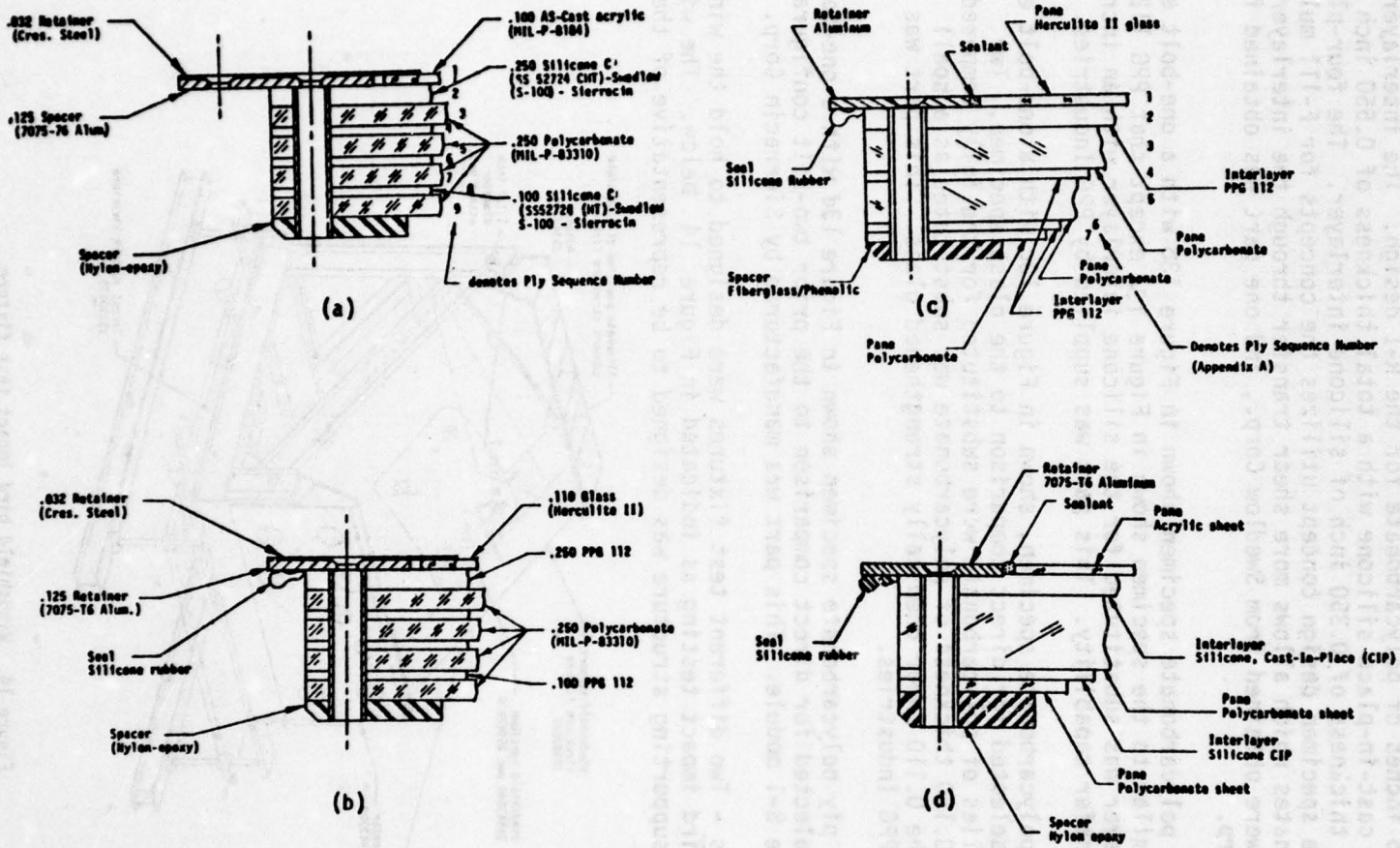


Figure 13. Simulated aircraft windshield designs. Laminated polycarbonate constructions, (a) Z5942640-501; (b) Z5942639-505; (c) Z5942639-503; (d) Z5942640-507.

Canadian National Research Council and AEDC, Tennessee (Reference 5). The total thickness of polycarbonate selected was 1.00 inch compared to a total thickness of 1.025 inches of polycarbonate for the R-I design. The interlayer selected was cast-in-place silicone with a total thickness of 0.550 inch compared to R-I total thickness of 0.350 inch of silicone interlayer. The four-ply polycarbonate specimen design concept utilizes the concepts for F-111 multilayered laminates which allows more shear transfer through the interlayers. Three parts were obtained from Swedlow Corp., and one part was obtained from Sierracin Corp.

The four-ply polycarbonate specimen shown in Figure 13b with a one-bolt edge design is similar to the specimen shown in Figure 13a except that PPG 112 urethane interlayer was substituted for the silicone interlayer with an increase in shear transfer capability. This part was supplied by PPG Industries.

The two-ply polycarbonate specimen, shown in Figure 13c with a one-bolt edge design, was selected for direct comparison to the glass specimen. Two 0.500 inch plies of polycarbonate were substituted for the fully tempered glass and a 0.150 thickness of polycarbonate was substituted as a spall shield for the 0.110 inner chemically strengthened glass. This part was supplied by PPG Industries.

The 7/8 inch ply polycarbonate specimen shown in Figure 13d with a one-bolt edge design was selected for direct comparison to the prior two-bolt configurations tested on the B-1 module. This part was manufactured by Sierracin Corp.

Test Fixtures - Two different test fixtures were designed to hold the windshield for bird impact testing as indicated in Figure 14 below. The windshield edge supporting structure was designed to be representative of the

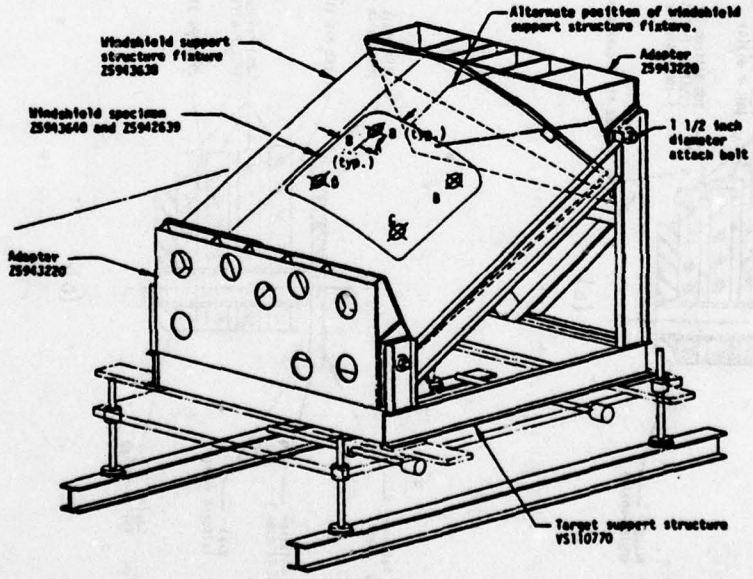


Figure 14. Windshield bird impact test fixture.
(Type "a" - polycarbonate specimens)
(Type "b" - glass specimens)

various support members typical for full sized B-1 windshield installations. The two fixtures were designed to demonstrate relative stiffnesses for a heavy glass windshield installation as well as a lighter weight polycarbonate windshield installation using the two-bolt and one-bolt installation concept and yet allow rotation of the specimens through 180 degrees to shoot Locations A, B, C and D.

In an attempt to assess the need for corner gussets or fittings to meet bird impact requirements, stiff gussets with a large radius were installed at corners near A and B. These gussets had a stiffening flange in the windshield area. At corner D a stiff gusset was installed. At corner C a light strap was installed to tie the two structural members together for pressurization requirements.

A computer windshield sizing analysis was in progress during the design and early bird tests on the 36 x 36 inch windshields. Based on these analyses the glass windshield support structure fixture was modified for five of the last seven bird tests. The lower stiffener flanges were removed on three of the non-centerline support structure near corners B and C. The reduced stiffness is more representative of the actual B-1 structure.

A single row of attachments 1-5/8 inches on center were required to install the glass laminated windshield. Both two-rows and one-row of attachments 1-5/8 inches on center were alternately required to install the polycarbonate windshields.

Figure 15 illustrates representative support structure similar to what may be required depending upon the type of windshield material used (noted at top).

The AEDC/ARO bird impact test equipment included an adjustable test bed, as shown on ARO drawing VS110770 and illustrated in Figure 14 upon which the test setup was installed. There was lateral and vertical adjustment. This arrangement allowed a target point on a windshield to be placed in alignment with the centerline of the bird cannon or in the trajectory of a bird.

The bird shot test procedure required that the two configurations (Z5942638-1 and -501) of the fixture assembly be capable of being removed and reinstalled in a different hole pattern corresponding to 180 degrees rotation (end for end) of a fixture assembly. To permit this rotation, two interchangeable hole patterns were located in each adapter. The end plates in the fixture assemblies had one corresponding hole pattern. A fixture assembly was installed between the two adapters by installing nine 3/8 inch diameter bolts through the fixture assembly end plates and the adapter face plate. There was interchangeability of the 3/8 inch diameter hole patterns between adapters and end plates for either the 0 degree or 180-degree position of the fixture assemblies.

Instrumentation

Strain Gage Installation - Strain gages were installed on all specimens in the locations noted in Figure 15. Sample strain gage output are shown in Figure 16.

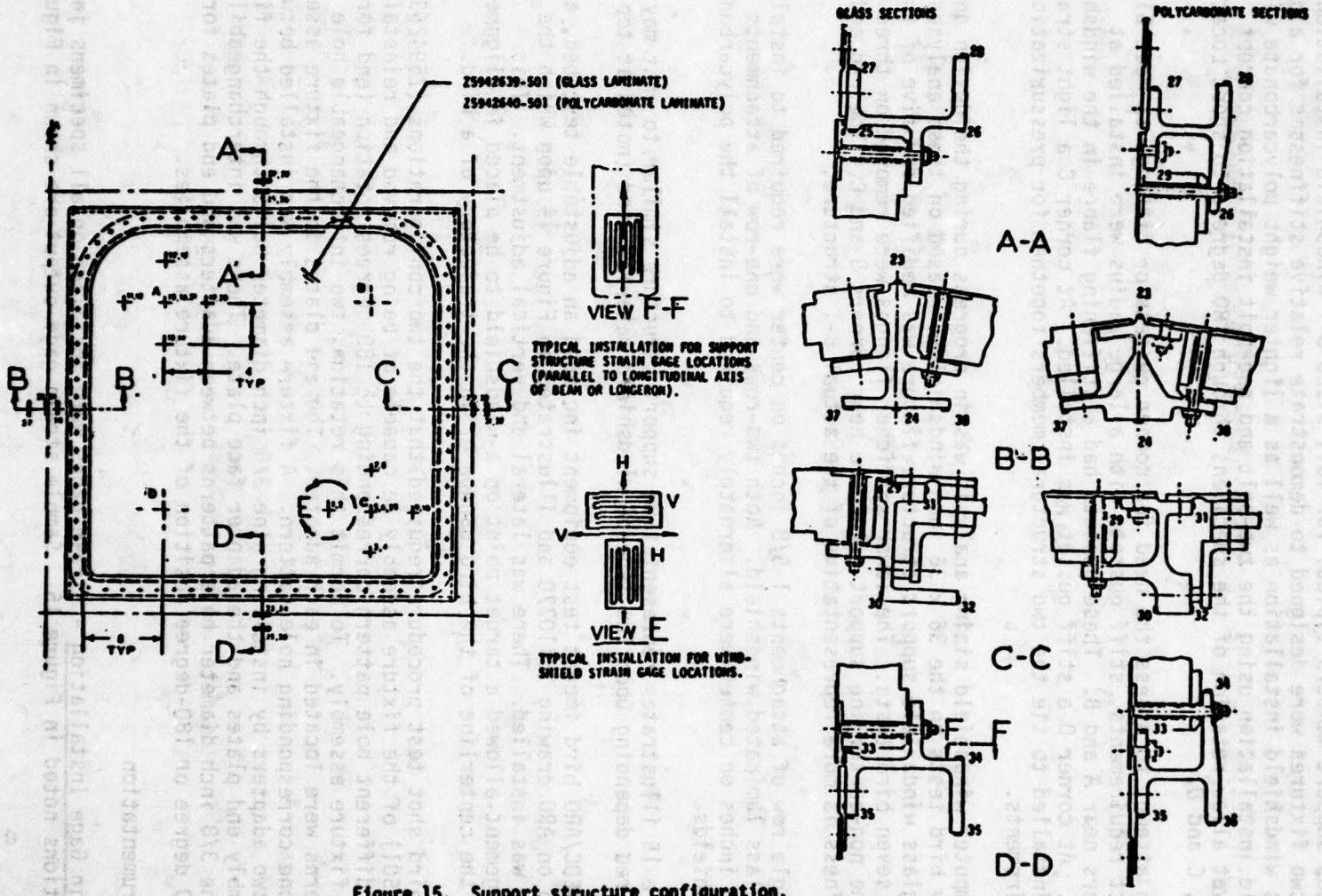
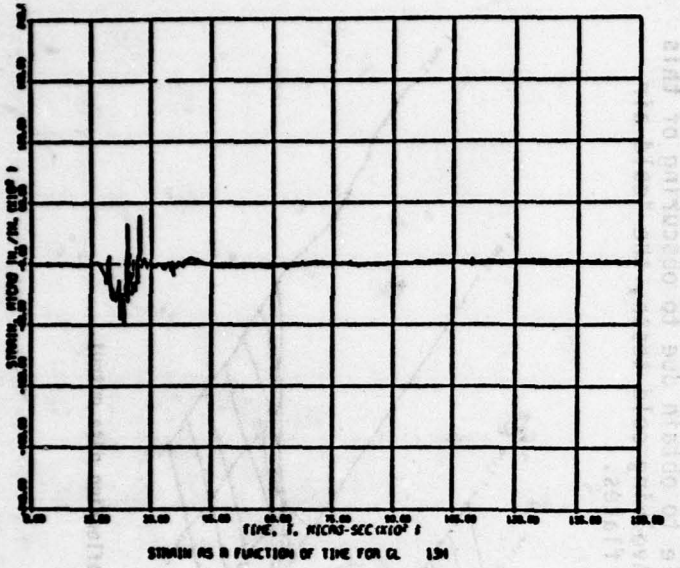
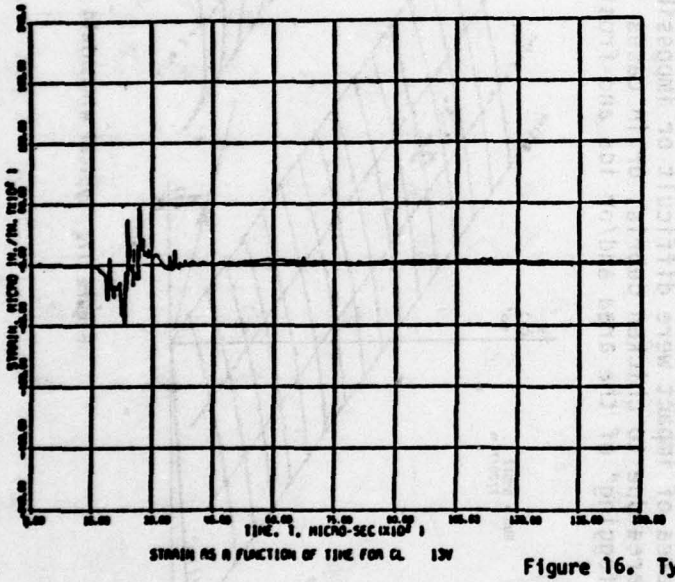


Figure 15. Support structure configuration. Strain gage locations.





STRAIN MAP

SPECIMEN NO. PPG 001 DESCRIPTION Laminated Glass (Z5942639-501)

TEST NO. BM012 SUPPORT STRUCTURE GL

IMPACT VELOCITY 943 FPS IMPACT POINT A

BIRD WEIGHT 4.00 lbs TEMPERATURE - OUTER PLY -28°F

DATE 7-16-76 TEMPERATURE - INNER PLY 7°F

STRAIN GAGE MOUNTED ON -7 SURFACE OF outer PLY

REAL TIME IMPACT 13.20 MICRO-SEC ($x10^2$) FROM + GATE

REAL TIME INERTIA 17.20 MICRO-SEC ($x10^2$) FROM + GATE

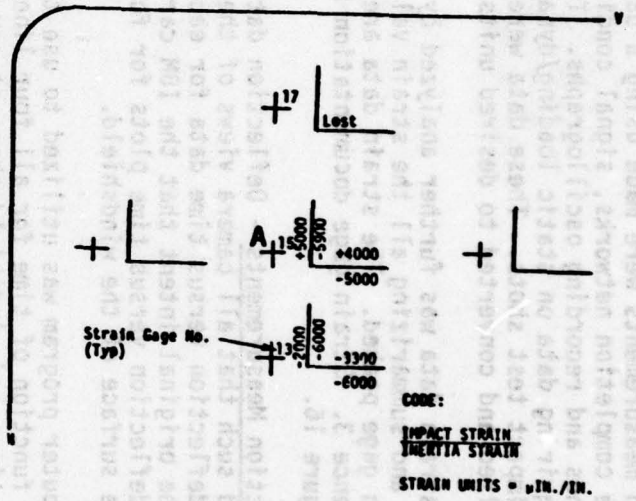


Figure 16. Typical strain gage documentation.

Strain measurements were made using a data acquisition system comprised of bridge completion networks, signal conditioners, recording magnetic tape machines and recording oscillographs. Twenty-two recording channels were used in acquiring data on static loading/dynamic unloading tests and on the actual bird impact test shots. These data were presented as oscillographs and were digitized and converted to desired units and replotted as a function of time.

This strain data was further analyzed by taking time cuts on the digitized plots and summarizing all the strain values as a function of time as each strain gage peaked. The strain data are summarized and presented fully in Reference 3. Strain gage documentation and a typical strain map are as shown in Figure 16.

Deflection Measurements - Deflection data consisted of motion picture film edited such that all camera views of the impact and adjacent areas were reduced into deflection versus time data for each shot and punched on IBM cards. It was the original intent that the IBM cards, thus punched, were to be used to plot deflection versus time plots for four predetermined individual lines on the surface of the windshield.

A computer program was utilized to use these IBM cards and plot deflections (as a function of time for all four lines) to simultaneously show relative deflections and windshield shape at any instant in time. This information could be used to verify the bird impact model described in Section V. A sample output of deflection at time = 0 milliseconds, and time = 3 milliseconds, is shown on Figure 17 below. This latter figure shows a typical lack of deflection detail in the area of impact. This is due to the nature of the deflection data collection process. When the AEDC film analyst can not discern the motion of the target lines, no deflection data could be punched on the IBM cards. On this series of tests, meaningful deflections in the area of impact were difficult or impossible to obtain due to obscuring of this area due to chicken debris, or in cases involving cold tests, the "cold-air fogging" of the area and/or ice and frost flakes.

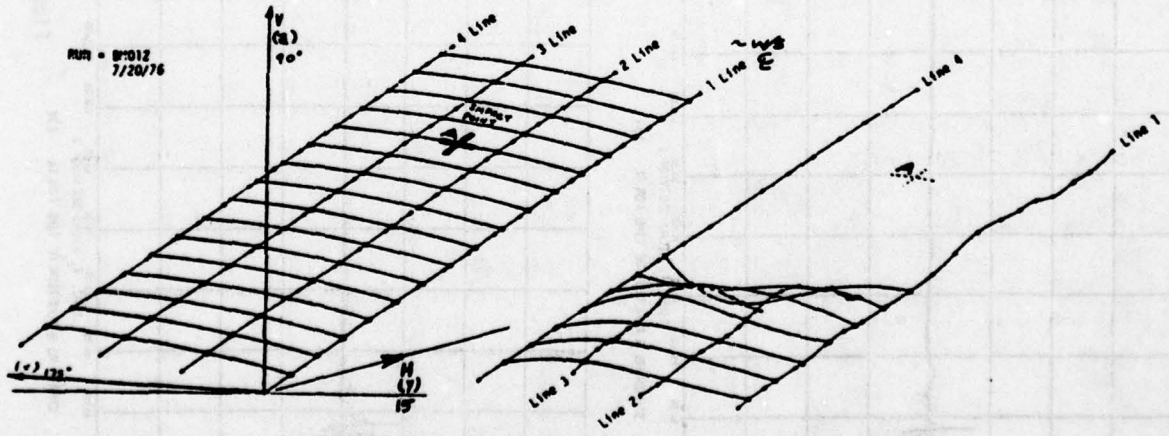


Figure 17. Typical windshield deflection data output.

Photographic Coverage - Four high-speed 16-mm motion picture cameras with color film were used to photographically record the impact event and provide data from which to measure windshield deflection. Camera locations in the test area are shown in Figure 18. A medium speed (200 frames/sec) camera, whose location varied, was used on some shots to provide a real-time record of the impact event.

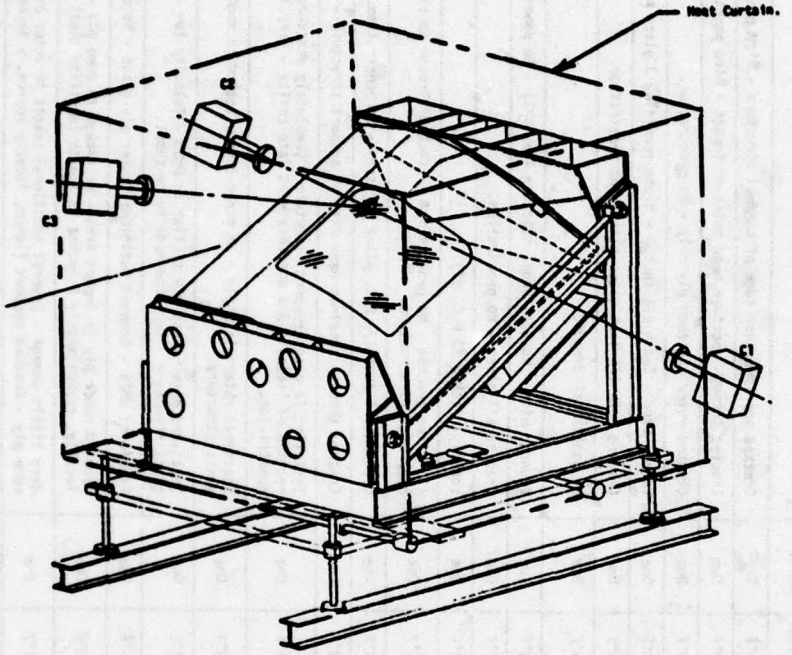


Figure 18. Camera location and heat curtain.

Thermal Requirements - The thermal requirements were chosen as the absolute minimum and maximum temperatures that could be experienced for bird impact. The hot temperatures simulated a hot atmosphere supersonic cruise followed by an emergency descent to 8000 feet and Mach 0.85 followed immediately by bird impact. The cold temperatures simulated a cold atmosphere subsonic cruise followed by an emergency descent to 8000 feet and Mach 0.85 followed immediately by bird impact. The temperatures shown in Table 2 were planned temperatures on the core plies. These temperatures are as close as can be easily obtainable in the laboratory.

A special hood or enclosure was mounted around the test equipment as indicated in Figure 18 including the setup structures noted on ARO drawing VS110770. This enclosure and ducting, as shown on VS110476, did not provide a high heat transfer coefficient on the specimen. Therefore, the temperature range for control had to be -165°F to 330°F. This would require a tremendous amount of LN_2 and probably exceed the propane heater capability. The best alternative, was to orient the VS109354BN-2 manifolds on either side of the 36 x 36 specimen and direct the air onto the specimen. The temperature range for control was approximately -85°F to 250°F. This conserved tremendously on LN_2 and was well within the capability of the propane heaters. Aforementioned manifolds were

TABLE 2. TEST SEQUENCE AND TEMPERATURE REQUIREMENTS (°F)

PART NUMBER	TEST NO.	SPEC. NO.	SHOT LOC.	V (fps)	TYPE OF STR. (FIG 140)	T2-5 O.B.SFC	T6-9 T.C.INT	T10-13 I.B.SFC	ROWS OF BOLTS	REMARKS
Z5942640-501	BM10	SMU 001	A	941	b	-40°F	-20°F	40°F	Two	Cracked specimen near edge of support structure - Bird penetration.
Z5942640-501	BM11	SMU 002	A	960	b	85°F	78°F	93°F	Two	Cracked through specimen near point or impact - Bird penetration.
Z5942639-501	BM12	PPG 001	A	943	a	-55°F	-28°F	7°F	One	Cracked outer 1/2 inch ply only - No penetration.
Z5942639-501	BM13	PPG 001	A	948	a	80°F	80°F	80°F	One	Bagged bird - Depth 4-6 inches - Broke remaining 3 glass plies - No penetration.
Z5942639-501	BM14	PPG 002	C	939	a	87°F	87°F	87°F	One	Cracked both 1/2 inch glass plies - No penetration.
Z5942639-501	BM15	PPG 002	E Center	515	a	90°F	90°F	90°F	One	No additional damage.
Z5942640-501	BM16	SMU 002	C	369	b	82°F	82°F	82°F	Two	Bounced bird - No additional cracking from BM11 - No penetration.
Z5942640-501	BM17	SMU-001	C	737	b	97°F	-	91°F	One	Cracked all plies - No penetration.
Z5942640-501	BM18	SK 001	C	847	b	230°F	190°F	110°F	One	Locally cracked #3 P.C. ply.
Z5942639-501	BM19	PPG 003	C	971	a	220°F	190°F	160°F	One	All plies cracked - No penetration - Cracked through specimen 9-inch length at back edge of structure.
Z5942640-501	BM20	SK 001	A	958	b	74°F	80°F	76°F	One	Cracked all four 1/4 P.C. plies - Passed - No penetration.
Z5942640-501	BM21	SMU 003	A	960	b	-40°F	-20°F	38°F	One	Cracked through specimen near edge of support structure - Bird penetration.
Z5942640-501	BM22	SMU 003	C	846	b	75°F	76°F	71°F	One	Installed in glass support structure - Completely shattered inner P.C. ply - A section of laminate 3 x 6 inches went into cavity - Very little bird penetration.
Z5942639-503	BM23	PPG 004	C	953	c	194°F	159°F	130°F	One	Shattered outer glass ply - No other damage tested in modified glass structure.
Z5942639-505	BM24	PPG 005	C	877	c	205°F	191°F	132°F	One	Shattered outer glass ply similar to BM23 - Velocity low - Tested in modified glass structure - Decision made to re-shoot.
Z5942639-505	BM25	PPG 005	C	951	c	200°F	195°F	145°F	One	Repeat of BM24 - Removed additional outer ply glass - No additional plies cracked.
Z5942640-507	BM26	SK 002	C	939	c	226°F	213°F	143°F	One	Removed outer ply in impact area - No damage to core ply - Cracked support flange locally, approximately 5 inches in length (modified glass str.).
Z5942640-507	BM27	SK 002	B	920	c	-36°F	-41°F	31°F	One	Very little damage - Several additional cracks in outer acrylic ply - No damage to core ply - Cracked support flange, locally approx. 9 inches (modified glass str.)
Z5942639-503	BM28	PPG 004	B	940	b	-30°F	-33°F	38°F	One	Broke both 1/2 inch P.C. core plies aft of impact point - Bird penetrated! (Tested in P.C. structure).
Z5942639-505	BM29	PPG 005	B	931	b	-28°F	-21°F	39°F	One	Much spalling of outer ply of glass with no apparent damage to core plies. (Tested in P.C. Structure).

three feet long and flowed approximately one pound per second. The supply lines were insulated with 2-inch thick fiberglass insulation or equivalent.

The plywood cover on the fixture assemblies produced an enclosed area or cavity below the windshield. Pneumatic lines penetrated the plywood cover or floor of the support structure and either hot or cold air was blown into the cavity of the support fixture. As required, the temperatures were held between 40°F and 110°F from Table 2. It required approximately four to six hours to attain steady state temperatures.

Before the bird tests were conducted, the temperatures through each specimen were monitored until steady-state conditions at the locations shown. As required to meet the conditions shown in Table 2, the thermal conditions were constantly monitored on the recording equipment to ensure that the test setup temperatures were maintained. The temperature tolerance was $\pm$ 10°F, and in the event the temperatures did not match the theoretical requirements, the temperatures internal to each windshield were adjusted.

Bird Impact Tests

All tests were performed utilizing a complete bird carcass weighing a planned $4.0^{+.2}_{-0}$ pounds. The basic design velocity was 650 $\pm$ 17 mph (953 $\pm$ 25 fps). Velocities actually achieved are noted in the complete test summary of Table 2.

The summary of Table 2 is a complete summary of the test results for the 20 bird shots conducted on the simulated aircraft windshield specimens.

The results of the tests indicated conclusively that the corner fittings did not contribute to the success of the specimens withstanding the bird impacts.

The three glass laminated specimens (P/N Z5942639-501) manufactured by PPG were tested at three thermal regimes and it was shown that the specimens withstood the impact of a four-pound bird at V_c = 565 knots.

The one specimen of four - 1/4 inch plies of polycarbonate laminated by Sierracin was successfully tested at V_c = 502 knots at maximum hot temperatures and cracked only one ply. Subsequently, this specimen was tested at V_c = 565 knots at room temperature passed. Since the elasticity of silicone interlayer does not change significantly at the lower temperatures, it is believed that this specimen design would also withstand the bird impact at lower thermal extremes.

The one specimen identified as Z5942639-505, of four - 1/4 inch plies of polycarbonate laminated by PPG was successfully tested at maximum thermal extremes, and it was shown that the specimen withstood the impact of a four-pound bird at V_c = 565 knots.

It is believed the four-ply laminated specimens manufactured by PPG and Sierracin could be successfully installed on a production airplane and would provide a minimum weight windshield. The parts would be reliable, have maximum anti-icing capabilities, and it is believed that good optical quality can be developed by the two vendors.

The 7/8-inch ply of polycarbonate laminated specimen, identified as Z5942640-507 and installed with one row of attachments, was tested at maximum thermal regimes and it was shown that the specimen withstood the impact of a four-pound bird at V_c = 565 knots. It is believed that the 7/8 inch polycarbonate laminate could be installed on a production airplane. This type of laminate cannot be recommended since the 7/8 inch ply is comprised of two or more individual plies fusion bonded that have been adequately tested in the laboratory showing that the fusion bonding delaminates causing possible objectionable visibility problems for a flight crew. Also, because of the stiffness of this configuration, more load is transferred to the support structure locally. The support flange near the impact point was cracked in each of these two tests, but was very possible the cumulative effect of previous shots conducted on each corner.

CONCLUSIONS

A series of bird impact tests on the B-1 windshield and on simulated aircraft windshields, were performed on appropriate support structure. These tests were run with a progressive series of different edge restraints and stiffnesses, and/or various transparency designs at extreme temperature conditions. The specimens involved in these tests utilized all current state-of-the-art transparency structural and interlayer materials commercially available for high-performance aircraft. There were five final candidate windshield designs in this program. A primary point of test specimen evaluation was the determination whether the ensuing specimen failure was cohesive (within a ply itself), or adhesive (at the bond line between interlayer and structural ply). A cohesive failure ensures that the maximum possible load is carried by a particular ply configuration. Of the tested specimens, the two-ply glass design provided the most desired combination of strength and stiffness; however, the weight of this design was prohibitive for high-performance aircraft. The four-ply polycarbonate design, as tested per this report, represents the structural optimum in light-weight windshield design and is recommended as an alternate B-1 windshield design.

REFERENCES

1. Magnusson, R. H. High Speed Bird Impact Testing of Aircraft Transparencies, AFFDL-TR-77-98, February 1978.

2. Sanders, E. J., Results of Further Tests to Evaluate the Bird Impact Resistance of Windshields for the B-1 Aircraft, AEDC-DR-76-43, May 1976.

3. Sanders, E. J., Results of Bird Impact Testing of Prototype B-1 Windshields and Support Structure Design, AEDC-DR-76-100, December 1976.

4. Sanders, E. J., Results of Qualification Testing of Bird Resistance Windshields for the B-1 Aircraft, AEDC-DR-75-87, September 15, 1975.

5. Structural Test Programs, "DVT Crew Module X-5 Bird Impact Tests Strain Gage Instrumentation Package", Rockwell International Report TFD-75-353, May 12, 1975.

6. Lawrence, J. H., Magnusson, R. H., Kelley, R. D., Certification Bird Tests for Windshields and Clearview Windows - Model DC-10, MDC Report J0025, Douglas Aircraft Company, August 1969.

7. Littell, Jr., H. E., Improved Windshield and Canopy Protection Development Program, AFFDL-TR-74-75, June 1974.

8. Ingelse, A. O., Wintermute, G. E., Gaynes, M. H., Waters, E. L., Bird Strike Capabilities of Transparent Aircraft Windshield Materials, AFML-TR-74-234, Part I, December 1975, and Part II, October 1975.

AIRCRAFT TRANSPARENT ENCLOSURE BIRD IMPACT MATH MODEL

P. H. Denke and
G. R. Eide
Douglas Aircraft Company
McDonnell Douglas Corporation
Long Beach, California

PRECEDING PAGE BLANK-NOT FILMED

AIRCRAFT TRANSPARENT ENCLOSURE BIRD IMPACT MATH MODEL

by

P. H. DENKE and G. R. EIDE
Douglas Aircraft Company, Long Beach, California

ABSTRACT

This paper described the Bird Impact Math Model, a computer program designed especially for the purpose of calculating transient dynamic responses of aircraft windshield and canopy systems, composed of laminated transparencies and supporting structures, to bird impact.

The paper briefly describes the theoretical basis of the program, and presents applications to classical problems and actual windshield systems. The approach is based upon a finite element model of the multilayered transparency and supporting structure, subjected to time-varying loads representing bird impact. The equation of motion for the model accounts for geometric and material nonlinearities. The approach to geometric nonlinearities is based upon the method of fictitious forces and deformations. The approach to material nonlinearities is based on the Von Mises yield criterion, and the Pandtl-Reuss equations. The scope of the computing effort is minimized by introducing a modal transformation. The transformed nonlinear differential equation of motion is solved incrementally in time and iteratively within each time step.

Calculated results produced by the program are shown to correlate accurately with exact solutions for simple dynamically loaded structures that exhibit large geometrically nonlinear effects, including snap-through. Linear and geometrically nonlinear analyses of the F-16 canopy subject to bird impact also were attempted. The linear analyses ran successfully, and showed qualitative agreement with test results, but displacements were underestimated, because of geometrically nonlinear effects. The nonlinear analyses of the F-16 canopy were unsuccessful. Reasons for the lack of correlation are discussed, and recommendations for further study are presented.

PRECEDING PAGE BLANK-NOT FILMED

INTRODUCTION

In the past, design verification of an aircraft windshield system subjected to bird impact has been accomplished primarily by test. A reliable analytical tool is needed to support the design process, and to reduce the amount of testing required for substantiation. In particular, a mathematical model is needed that can simulate, in some detail, the response of a windshield system to bird impact, including displacements, internal stresses, and strains. The model should be implemented as a computer program.

The present paper briefly describes the Bird Impact Math Model, a computer program designed for this purpose. Reference 1 contains a complete description of the Math Model, including theory and applications, a user's manual, and a programming manual.

The Math Model was developed as part of the Windshield Technology Demonstrator Program, a research effort conducted by the Douglas Aircraft Company, and sponsored by the Air Force Flight Dynamics Laboratory. This program is part of a larger Windshield Protection Program being conducted by the Flight Dynamics Laboratory, to develop improved technologies, that can contribute to increased resistance of aircraft transparent enclosures to birdstrikes.

A basic requirement established for the Math Model is that it should provide computing capability for both parametric studies and design substantiation analyses, at reasonable cost.

The design features of a typical aircraft windshield or canopy system, and the response mechanism of such a system to impact, also impose requirements upon the Math Model. Ideally, the model should be able to account for:

1. The laminated construction of the transparency, its attachment to the supporting structure, and the presence of the supporting structure itself.

2. The loads produced by the impacting bird, and the interaction between bird and windshield.

3. The transient dynamic response of the structure, including displacements, stresses and strains, as functions of time.

4. The thermal environment, and its effects on material properties and response.

5. The existence of significant amounts of damping in interlayer materials.

6. The effects of high strain rates of material properties.

7. Material nonlinearities.

8. Geometric nonlinearities.

The list covers most of the difficult problems in the field of finite element structural analysis. Translated into terms of computer programming and data processing, this statement means that any program able to do the job is likely

to run for an unacceptably long time, unless it is designed and optimized specifically for the purpose. A literature search revealed no existing special purpose program meeting the requirements. Therefore, the decision was made to develop such a program.

The formulation of the Math Model covers all of the effects mentioned in the preceding list, except bird-windshield interaction, or target compliance. An attempt to account for this phenomenon was thought to be premature, in view of the shortage of related data available at the beginning of the project. Modification of the program to account for target compliance at a later time may be feasible. Also, the accounting of high strain rate effects was not planned as an automated feature of the program, again because of the shortage of related data, and because the necessary complicated calculations would significantly increase the cost of the analysis. The user estimates strain rates, and inputs corresponding material properties.

Not all of the effects covered by the mathematical formulation were converted to computer code, because of time constraints. The effects formulated, but not programmed, include plasticity, thermal loads resulting from damping energy dissipated as heat, and the dependence of material properties on temperature changes occurring after initial impact. Coding in some of these areas is partially completed. The following paragraphs outline the approach, as it is mathematically formulated.

The approach is based on the analysis of a finite element model of the windshield system. The model is a set of nodes connected by elements that have mass, damping and stiffness. Some nodes can have constraints, although the formulation provides for completely unconstrained, and otherwise statically unstable, models.

The model is assembled from four kinds of elements: axially loaded bars, membranes, cells, and point masses. The membrane and cell elements are based on the lumped parameter idealization, in the sense that these elements are themselves composed of bars and shear panels.

In the past, the lumped parameter model has provided satisfactory results in a wide variety of aerospace applications. One advantage of the model is simplicity. The user not familiar with the theory of finite element analysis can easily grasp the concept, and therefore feel increased confidence in applying the results. A second advantage, important in the present application, is that use of the model facilitates the analysis of geometric nonlinearity resulting from element force rotation, by the method of fictitious loads.

The disadvantages of the conventional bar-panel model have been that "lumping" is required, Poisson coupling is neglected, panels should be rectangular, and plate bending and shell bending are difficult to represent. These disadvantages have been overcome, in the present application, by the newly developed membrane and cell elements, which require no lumping, and automatically account for Poisson coupling and skewness. The cell element can be subjected to out-of-plane bending and torsion. Deformations through the thickness are also represented. Plate and shell structures can be modeled. Thus the advantages have been retained, and the disadvantages have been eliminated.

In the formulation, materials are assumed to be isotropic, and to conform to the Von Mises yield criterion, and the Prandtl-Reuss equations, in the plastic range. Unloading is considered. The dependence of material properties on temperature is taken into account. The equation of motion is solved stepwise in time, and material property effects are taken into account by updating the stiffness and damping matrices at each increment.

Loads are applied at nodes of the model as time dependent vectors. When the angle between the transparency surface and the bird trajectory is small, investigation indicates that the bird slides along the surface, producing a "traveling footprint". A module in the Math Model preprocessor automatically generates traveling footprint load vectors.

The formulation accounts for thermal loads resulting from initial thermal gradients, and from temperature changes resulting from heat generated due to damping, without heat transfer.

Two kinds of geometric nonlinearities are considered: nonlinearities resulting from changes in shapes of elements, as when a bar becomes shorter and thicker, and therefore stiffer; and nonlinearities resulting from rotations of element forces. Nonlinearities of the first kind are taken into account by updating element stiffness and damping matrices for each increment. Nonlinearities of the second kind are accounted for by coordinate updating; and within each increment, by the method of fictitious forces and deformations (FF & D).

The formulation of the FF & D method is a feature of the Math Model. A rational basis for the method is established. Changes in element stiffness resulting from element force rotations, appearing in the equation of motion as coefficients, of the unknown displacements, are shown to be precisely replaceable by terms on the right of the equation, representing loads resulting from fictitious element forces and deformations. These forces and deformations exist; they are fictitious only in the sense that they are not considered in linear theory.

A modal transformation is introduced. Such a transformation appears essential to keep computing costs within reasonable limits for large models.

Corrections for equilibrium errors resulting from coordinate updating are also provided.

The transformed nonlinear differential equationoof motion is solved incrementally in time, and iteratively within each increment. The purpose of the iterative loop within the increment is to satisfy the equation of motion, considering the presence of the fictitious load terms.

During any one iteration, the differential equation is linearized. The linearized equation is solved exactly. Approximate numerical integration algorithms are not employed. This approach seems to be quite reliable. No difficulties with loss of accuracy, or singularity of the initial condition equations, were experienced in solving the linearized equations, during any of numerous applications of the final version of the computer program.

The Math Model has been applied to classical problems and to simple structures, linear and nonlinear. The linear applications verify the cell element as a satisfactory building block for finite element modeling. The nonlinear applications show that the Math Model gives accurate results for simple structures exhibiting very large geometric nonlinearities, including snap-through effects.

Applications to statically loaded and vibrating laminated beams show satisfactory correlations with test data for displacements and for stresses within the layers.

Correlations of calculated linear results with test data for the F-16 canopy subjected to bird impact loads show that calculated responses tend to be proportional to measured values, but stresses and displacements are underestimated.

An application of the Math Model nonlinear option to the F-16 canopy produced erroneous results. The difficulty was studied and attributed to the use of an unsuitable modal transformation. The problem is that modes suitable to describe the motion immediately after impact can become unsuitable after coordinates have been updated several times. The difficulty can be anticipated whenever the analysis is extensive enough to require a modal transformation. An analysis presented in Appendix F of Reference 1, Part 1, shows why the difficulty occurs and leads to recommendations for corrective action.

The modal approach to nonlinear analysis undoubtedly can provide satisfactory results, if enough suitable modes are employed. The question remaining to be answered is whether a set of such modes can be found small enough so that the feasible model size will not be unduly limited.

The Math Model in its present form is considered satisfactory for linear analysis of windshield systems subjected to bird impact. The geometrically nonlinear version is operational, but the code needs further optimization. It gives accurate results for simple structures exhibiting pronounced nonlinearities. The applicability to structures having more than a few elements remains to be evaluated, pending development of a better understanding of suitable modal transformations.

The linear code is suitable for parametric studies, and for more detailed design evaluations, depending on the complexity of the finite element models employed. The linear option also can provide useful information for substantiation, if nonlinear effects are small, or if test data permitting the evaluation of such effects are available.

Part 2 of Reference 1, the User's Manual, provides instruction in the use of the Math Model computer program. This part also contains data on typical running times for various modules and options. The times for the linear option are considered acceptable. The times for the nonlinear option indicate the feasibility of the approach, although the code requires further optimization, and the successful use of modes in nonlinear analysis of large models has yet to be demonstrated.

Part 3 of Reference 1, the Programming Manual, describes the approach to

optimizing the code and the details of the program. Appendix H of Part 1 summarizes the basic equations in approximately the order of solution reflected in the program. The strategy of code optimization includes keeping the matrices as small as possible, by employing individual element mass, damping and stiffness matrices in place of assembled structural matrices, and by taking full advantage of the modal transformation.

The linear option of the Math Model computer code is considered to meet the basic intent of the project: to provide a tool for parametric studies and for design substantiation analysis, at reasonable cost. Development of a better understanding of modal transformations applicable to large displacement analysis, plus refinements of the nonlinear code, are expected to provide an economically feasible nonlinear capability. Use of this capability can lead to significant reductions in the costs of bird impact testing required for design verification.

DISCUSSION

The theoretical basis of the Math Model is briefly described and applications are presented.

Structural Elements

The model is composed of four kinds of elements: (1) axially loaded bars, (2) membranes, (3) cells, and (4) point masses. The membrane and cell elements are themselves composed of axially loaded bars and shear panels, or lumped parameter elements. Forces acting upon the bars, membranes and cells are resolved into two different sets of components called "element forces" and "lumped element forces".

Axially Loaded Bars

Figure 1 shows the bar element with its element forces and displacements. The sets of forces on each end are parallel to the global coordinate axes. The force at the middle is parallel to the bar.

This element can be connected to other elements at each end and at its center.

Figure 2 shows the axially loaded bar with its "lumped" element forces. Two lumped axial element forces act on the bar, numbered as shown. The corresponding element deformations, designated $\bar{e}_1$ and $\bar{e}_2$, are equal to the works done by unit values of $\bar{F}_1$ and $\bar{F}_2$, during a virtual displacement. In this simple case, the deformations are equal to the elongations of the two halves of the bar.

The F components and the $\bar{F}$ components are statically equivalent, consequently the relationships among these components can be derived from equilibrium.

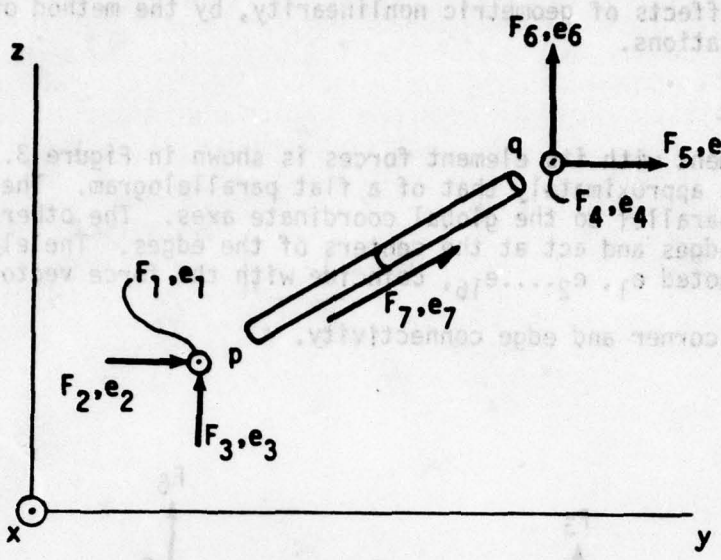


Figure 1 Axially Loaded Bar Element Forces and Displacements

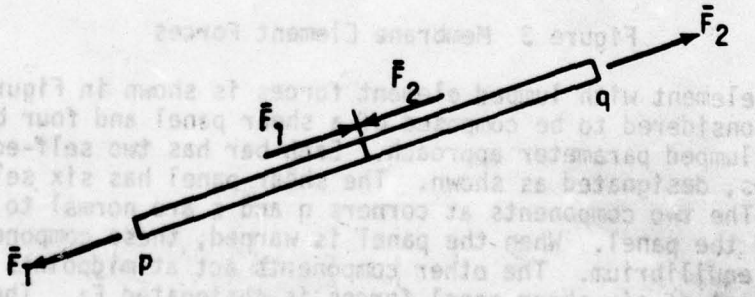


Figure 2 Axially Loaded Bar with Lumped Element Forces

The reason for introducing lumped element forces is that they are useful in formulating the effects of geometric nonlinearity, by the method of fictitious forces and deformations.

Membrane Elements

The membrane element with its element forces is shown in Figure 3. The shape of the element is approximately that of a flat parallelogram. The forces at the corners are parallel to the global coordinate axes. The other forces are parallel to the edges and act at the centers of the edges. The element displacement vectors, denoted e_1, e_2....e_{16}, coincide with the force vectors.

This element has corner and edge connectivity.

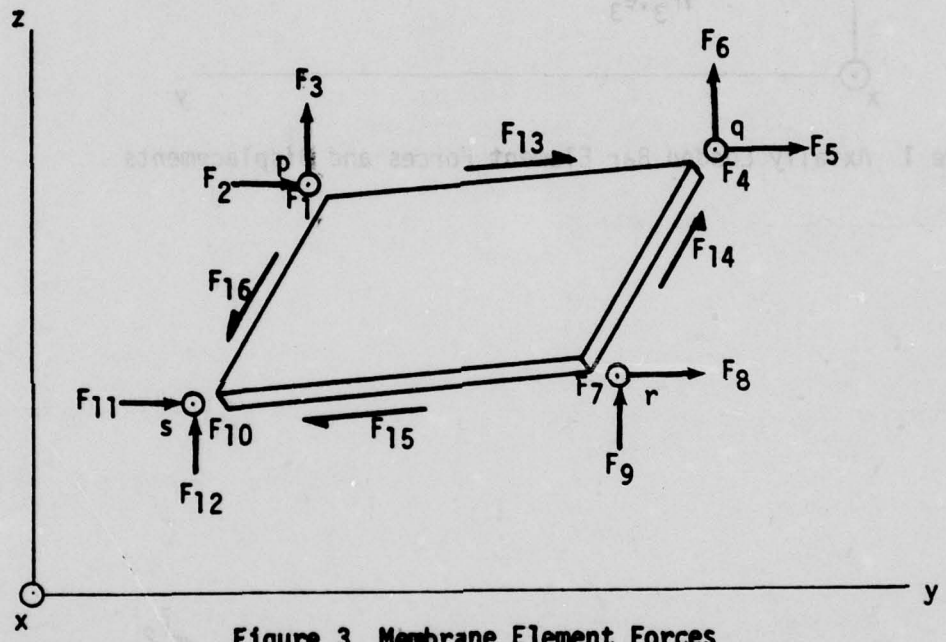


Figure 3 Membrane Element Forces

The membrane element with lumped element forces is shown in Figure 4. The membrane is considered to be composed of a shear panel and four bars according to the usual lumped parameter approach. Each bar has two self-equilibrating element forces, designated as shown. The shear panel has six self-equilibrating components. The two components at corners q and s are normal to the approximate plane of the panel. When the panel is warped, these components are required for equilibrium. The other components act at midpoints of panel edges. The complete set of six shear panel forces is designated F_1. The element force $\bar{F}_1$ has a unit value, by definition, when the vector on edge pq is equal to unity.

The corresponding deformations are designated $\bar{e}_1$, $\bar{e}_2$....$\bar{e}_9$. The deformations

are equal to the works done by unit values of the element forces during a virtual displacement.

Equations relating the F and $\bar{F}$ forces are written on the basis of equilibrium.

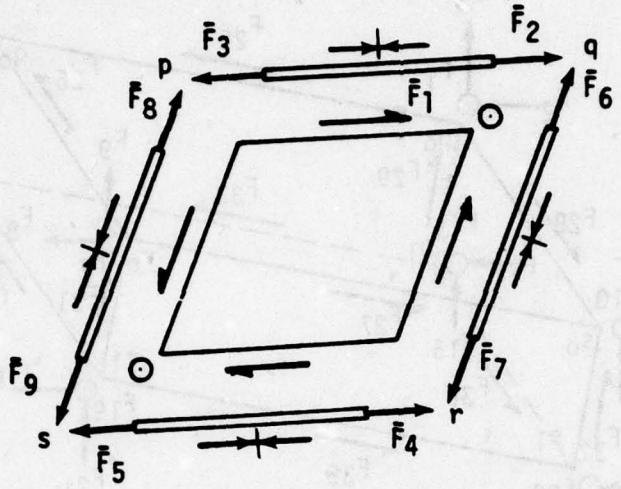


Figure 4 Membrane Element with Lumped Element Forces

Cell Elements

The cell element with its element forces is shown in Figure 5. The surfaces $p_0q_0r_0s_0$ and $p_1q_1r_1s_1$ are approximate parallelograms and are approximately flat and parallel. The edges p_0p_1, q_0q_1, r_0r_1, and s_0s_1 are approximately normal to the upper and lower surfaces. The forces at the corners are parallel to the global coordinate axes. The other forces are parallel to the edges of the cell and act at the centers of the edges. The element displacement vectors e_1, e_2.....e_{36} coincide with the force vectors.

The cell element has corner and edge connectivity.

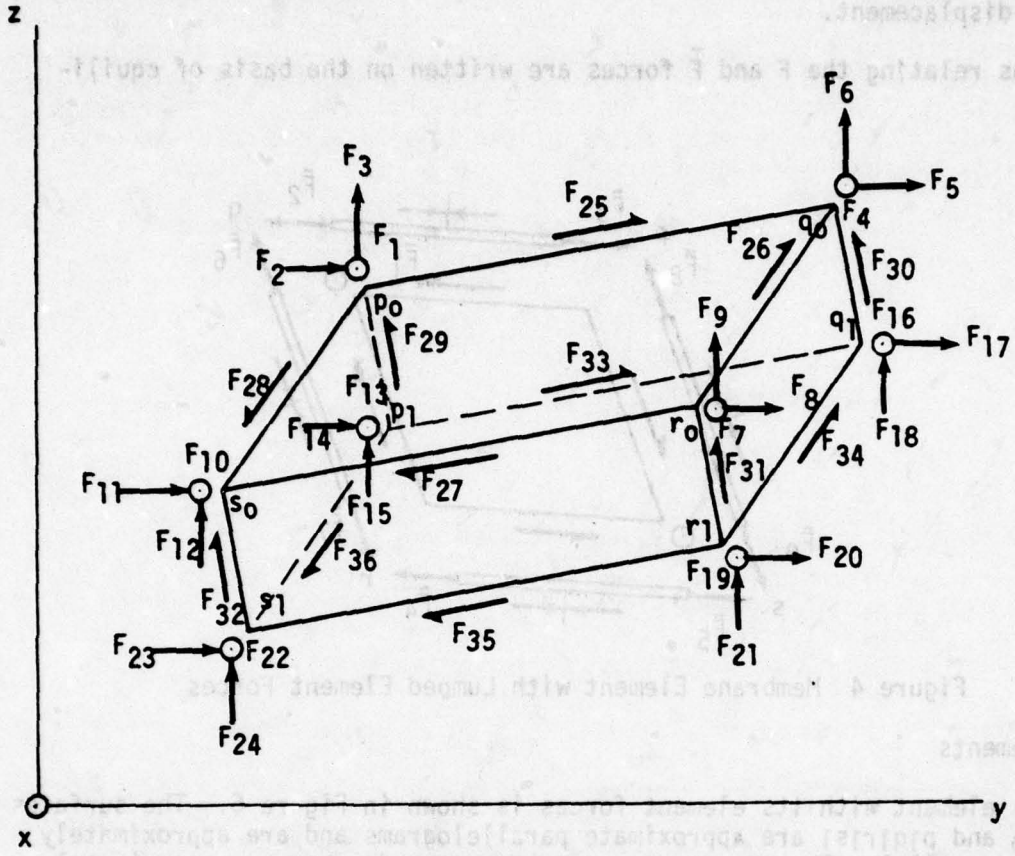


Figure 5 Cell Element Forces

Figure 6 shows the method of lumping the cell element. The thickness of the lumped element is reduced by a factor of $1/\sqrt{3}$, so that the lumped element can have the same bending, torsional, normal and shearing stiffnesses in the elastic range as the actual plate element being represented.

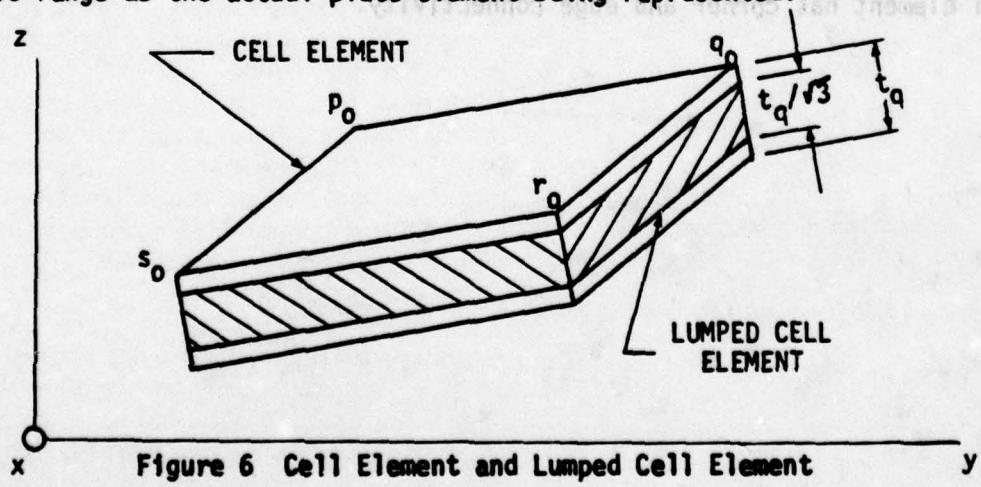


Figure 6 Cell Element and Lumped Cell Element

The lumped elements for the cell and their element forces are shown in Figure 7. The lumped structure is essentially a torque box. Cross-sectional areas of bars and thicknesses of shear panels are selected so that the element will have the proper stiffness. The lumped element of reduced thickness is joined to the upper and lower surfaces of the cell by means of an implied statically determinate linkage.

Each bar of the lumped element has two self-equilibrating element force components and each shear panel has six, as in the case of the membrane, designated as shown. The corresponding element deformations are designated $\bar{e}_1, \bar{e}_2 \ldots \bar{e}_{30}$. The deformations are equal to the works done by unit values of the element forces during a virtual deformation.

Equations relating the F and $\bar{F}$ forces are derived on the basis of equilibrium.

Element Stiffness Matrices

Stiffness matrices for the bar, membrane and cell elements are given in Reference 1, Part 1. Matrices of unassembled deformations resulting from temperature changes are also presented.

The derivations for the bar element are conventional.

The matrices for the membrane element are derived on the assumption that the element is approximately a flat parallelogram, although equilibrium is satisfied for any shape. The matrices automatically account for the effects of Poisson's ratio and membrane skewness. The lumping procedure is also accomplished automatically.

The matrices for the cell are derived on the assumption that the element is approximately a parallelepiped having two parallelogram faces and four rectangular faces. Equilibrium is satisfied for any shape. The matrices account for the effects of Poisson's ratio and skewness. Lumping is automatic.

Element Damping Matrices

Damping matrices for bar, membrane and cell elements are derived from the corresponding stiffness matrices by multiplying by suitable scale factors. This procedure does not imply that the assembled damping matrix for the structure is a scale factor times the assembled stiffness matrix, since each element can have a different scale factor. Damping force vectors for the elements coincide with stiffness force vectors.

Element Mass Matrices

Inertia force vectors for the elements coincide with stiffness force vectors, except that no inertia force vectors are provided at the midpoints of bars, or at the centers of membrane and cell edges. Also, no lumped inertia forces are defined. Mass matrices for the elements are taken from the literature. (Reference 2.)

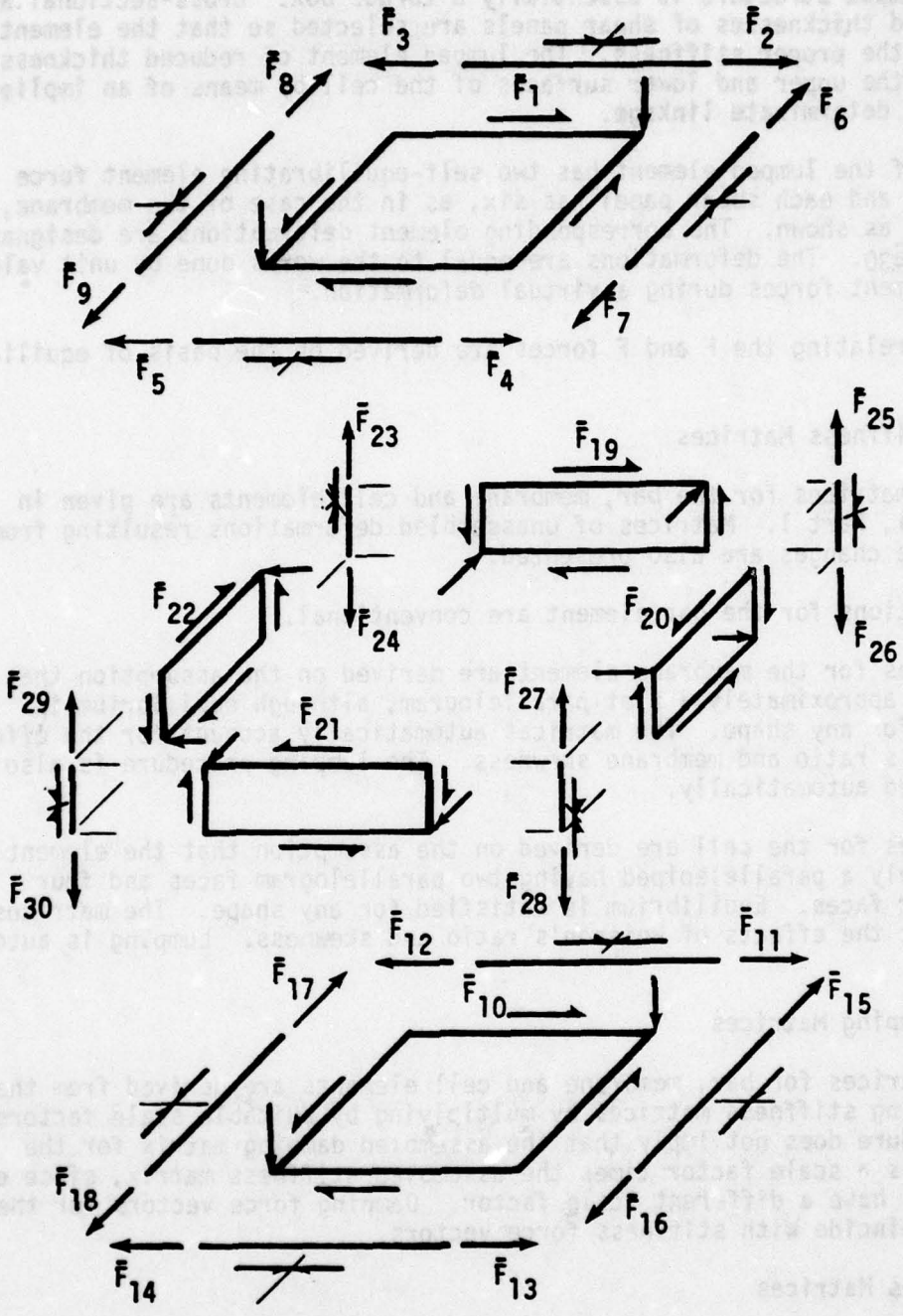


Figure 7. Lumped Element Forces for Cell

Point Mass Element

This element represents a finite mass concentrated at a point. Three components of inertia force and displacement are defined for the element parallel to the global coordinate axes. Point mass elements can be affixed to joints but not to shear nodes.

Material Behavior

The materials comprising the model are assumed to be isotropic. The Math Model can be modified to accommodate anisotropic elastic materials with relatively few changes.

Plasticity is considered in the formulation in deriving element stresses and strains. Load is applied to the structure incrementally in time. The components of strain occurring during an increment are assumed to be related to the corresponding incremental stress components according to the Prandtl-Reuss equations, which satisfy the Von Mises yield criterion. Plastic strains are assumed to occur in any element only as long as the equivalent stress increases. As soon as the equivalent stress starts to decrease (i.e., the element starts to "unload"), the element is assumed to become elastic and to remain elastic thereafter. The equivalent stress in the Prandtl-Reuss equations is equal to twice the octahedral shearing stress.

In windshields and canopies subjected to bird impact, damping effects are not very significant, except in the interlayers of laminated transparencies, and even there they are small, because only the brief period during and immediately after impact is of interest. Consequently linear viscous damping is assumed to simplify the analysis.

In the formulation, temperatures at initial impact are considered to be input, and these temperatures are updated incrementally, assuming that damping energy dissipated during an increment is converted to heat. No heat transfer is considered, because of the brief duration of impact. Thermal stresses are taken into account.

Material stiffness, damping and thermal properties are temperature dependent, and these properties are updated during the solution.

Many material properties are strain rate dependent. The user accounts for this dependence by estimating strain rates expected at various points in the transparency, and inputting corresponding material properties. Strain rate dependence is not automatically taken into account, because such a procedure would greatly increase the cost of the calculation. Furthermore, the roughness of available data concerning the effects of strain rate does not justify a more elaborate approach at this time.

Loads

The loads that the impacting bird produces on the windshield, or canopy, are functions of the bird mass, bird shape, angle of incidence, and relative

velocity of bird and transparency before and after initial impact. The loaded region apparently is not confined to the initial area of impact. Data obtained from F-16 canopy tests indicate that, after initial impact, the bird slides along the surface, applying loads along the path of contact, for an appreciable distance. The problem is complicated by the fact that the transparency displaces during contact, so that the relative velocity may be less or more than it was before contact, depending on whether the surface is retreating from the bird or rebounding into it. This effect is called target compliance.

The effects of target compliance were considered to be beyond the scope of the present investigation. The effects of an area of contact that moves along the surface are considered. Such a moving contact area is called a traveling footprint.

When the complications resulting from target compliance are eliminated, the loads produced by the bird on the transparency can be calculated separately from, and prior to, the transparency response.

Equation of Motion

The equation of motion is written by considering the equilibrium of forces acting upon the structural nodes at any instant of time. These forces include the internal stiffness, damping and inertia forces, the thermomechanical loads, and the reactions. The thermomechanical loads include the bird impact loads, and external loads equivalent to internal forces resulting from unassembled thermal deformations.

The resulting matric differential equation contains geometric nonlinearities produced by large deformations and rotations of the finite elements, and material nonlinearities resulting from plasticity. The effects of geometric nonlinearities resulting from element rotations, appearing in the equation as coefficients of the unknown displacements, are precisely replaced by terms on the right of the equation called fictitious loads. These loads exist; they are fictitious only in the sense that they are not considered in linear theory.

The equation is written in incremental form, corresponding to a short interval of time. Geometric nonlinearities resulting from element deformations, and material nonlinearities, are taken into account by updating element stiffness properties at the beginning of each increment, and by assuming that element stiffnesses are constant during the increment. Geometric nonlinearities resulting from element force rotation are taken into account by coordinate updating, and by solving the linearized equation of motion iteratively within each increment, accounting for the presence of the fictitious load terms, which depend on displacements.

A modal transformation is introduced to reduce the scope of the calculation. The transformed linearized equation of motion is solved by classical differential equation methods. No approximate integrating algorithm is employed.

A linear computing option is provided for linear problems. In this option,

coordinates are not updated, element stiffness properties are not updated, and the equation of motion is solved once per increment.

Details of the derivation of the equation of motion and its solution are presented in Reference 1, Part 1.

Static Linear Correlations, Classical Problems

The results of these studies are offered to provide verification of the cell element as a building block for finite element modelling. In addition, the plate buckling study tends to verify the first order fictitious force terms for shear panels. These results were obtained by solving the familiar static displacement method equation. No modal transformations were employed.

Cell Element, Elementary Loads

Figure 8 shows that the rectangular parallelepiped cell element produces correct displacements for nine elementary loads. The length and width of the element are a and b, and the thickness is h. Young's modulus is E, and Poission's ratio is ν.

The nine loads are shown on the left of the figure. The first three loads represent pure shear on the element, the next three, pure tension. Loads 7 and 8 represent pure bending, while load 9 represents pure torsion.

The flexibility matrix on the right of the figure represents element deformations resulting from unit values of the loads. The rows of the matrix correspond to deformations, the columns to loads. The deformation corresponding to any particular load is defined as the work done by a unit value of the load, during a virtual displacement. For example, the term in Row 4 and Column 4 of the matrix represents the elongation of the element in the direction of P_4, resulting from a unit value of P_4. This term is equal to $b/(ahE)$ which is correct. Similarly, the term in Row 4, Column 5, represents the elongation in the direction of P_4, resulting from a unit value of P_5. This value is $-\nu/(hE)$, which is also correct.

All of the terms in the flexibility matrix are correct, and none are missing, which shows that the element gives correct deformations for all nine elementary loads with correct Poisson's coupling in the linearly elastic case.

The same kind of check was made for the skewed cell element shown in Figure 9. The figure shows the planform dimensions. The thickness of the element was unity. The skewed element was subjected to nine loading conditions corresponding to the loads applied to the parallelepiped. Joint B was constrained from moving in all three directions, Joint A was constrained from moving in the y and z directions, the joint directly under B on the lower surface was constrained from moving in the y direction. Displacements were calculated according to the element algorithms in all corner joint unconstrained degrees of freedom and in all edge shear node degrees of freedom for the nine loading conditions. The results were compared with values calculated from classical plate theory, and were found to check to within at least six significant figures, showing that the element correctly accounts for the effects of skewness, as well as Poisson coupling.

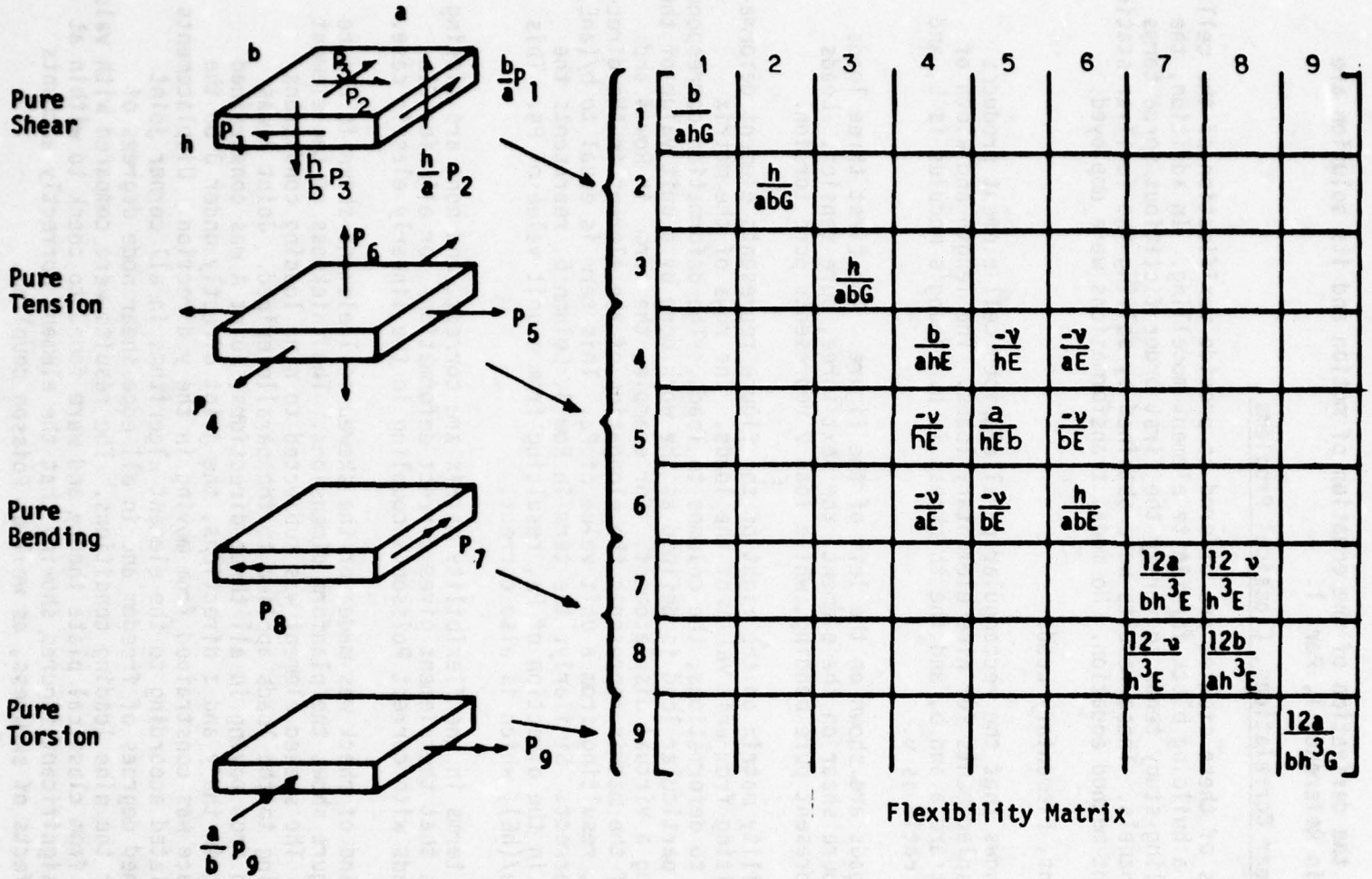


Figure 8 Validity of Parallelpiped Cell Element for Simple Loads

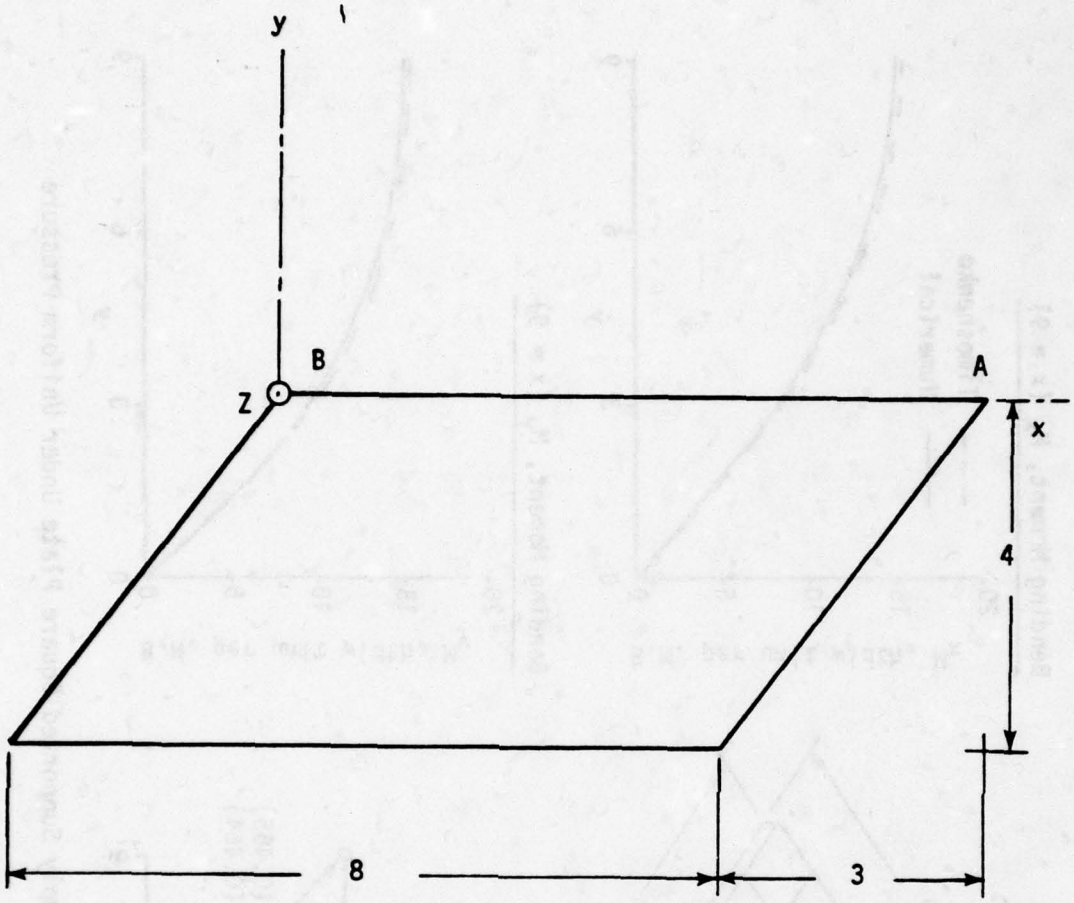


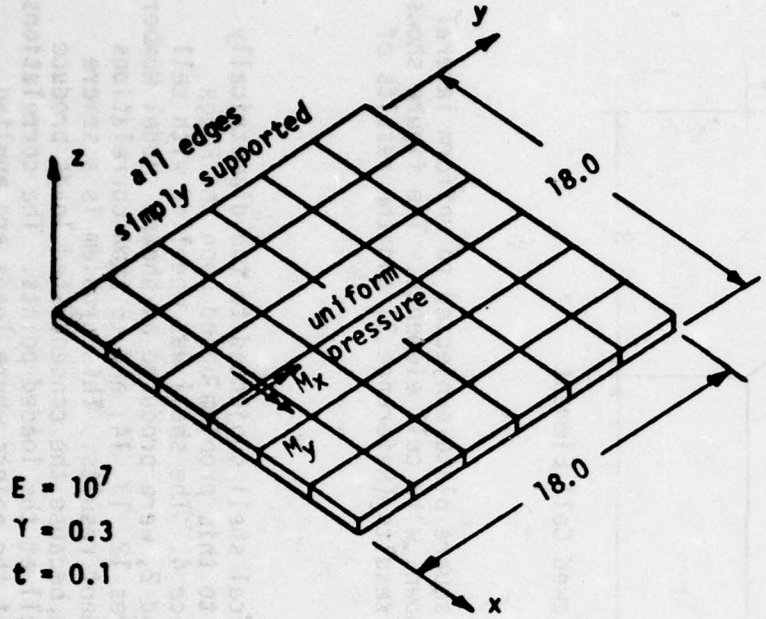
Figure 9 Skewed Cell Element

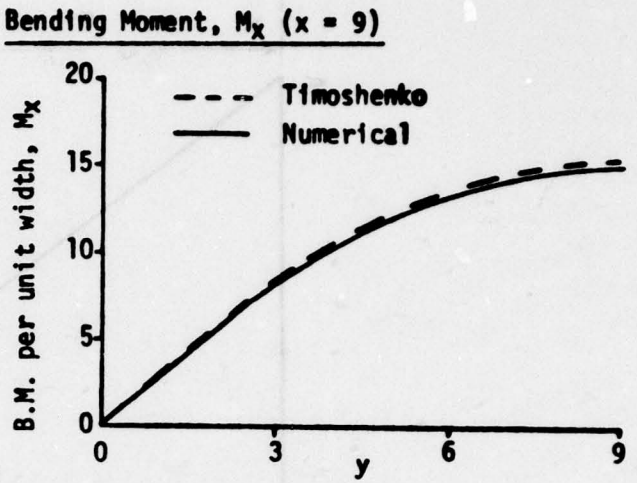
Flat Plate, Uniform Pressure

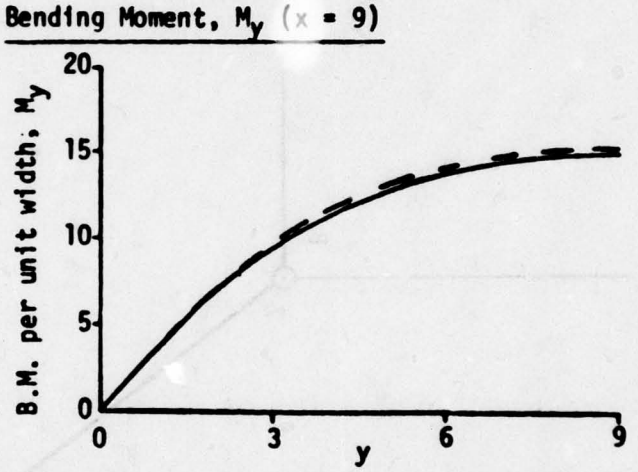
Figure 10 shows a simply supported square plate subjected to uniform lateral load. The plate was modelled as shown, with cell elements. The figure shows good agreement between theoretical results (Reference 3) and the results of the finite element analysis.

Pinched Cylinder

Figure 11 shows a circular cylindrical shell subjected to two diametrically opposed loads. A precise solution to this problem based upon the Függe shell equations is given in Reference 4. The shell was modelled with cell elements. Two models, Numbers 1 and 2, were produced as shown. Model Number 2 had a slightly finer grid. Figures 12, 13, 14, and 15 show correlations between theoretical and finite element results. This problem is a severe test of the finite element approach, because the concentrated loads produce infinite bending moments in the shell at the loaded points. The correlations are generally quite close, except at the points where loads are applied.







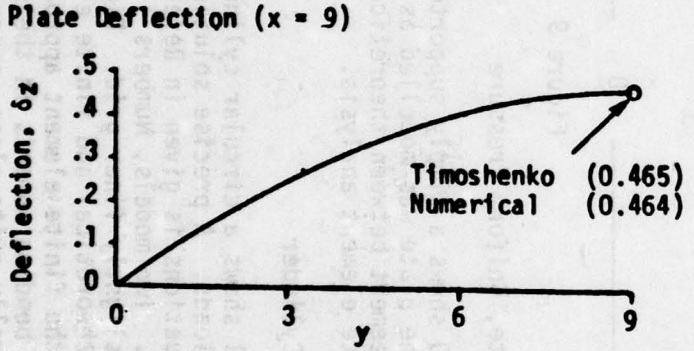


Figure 10 Static Analysis - Simply Supported Square Plate Under Uniform Pressure

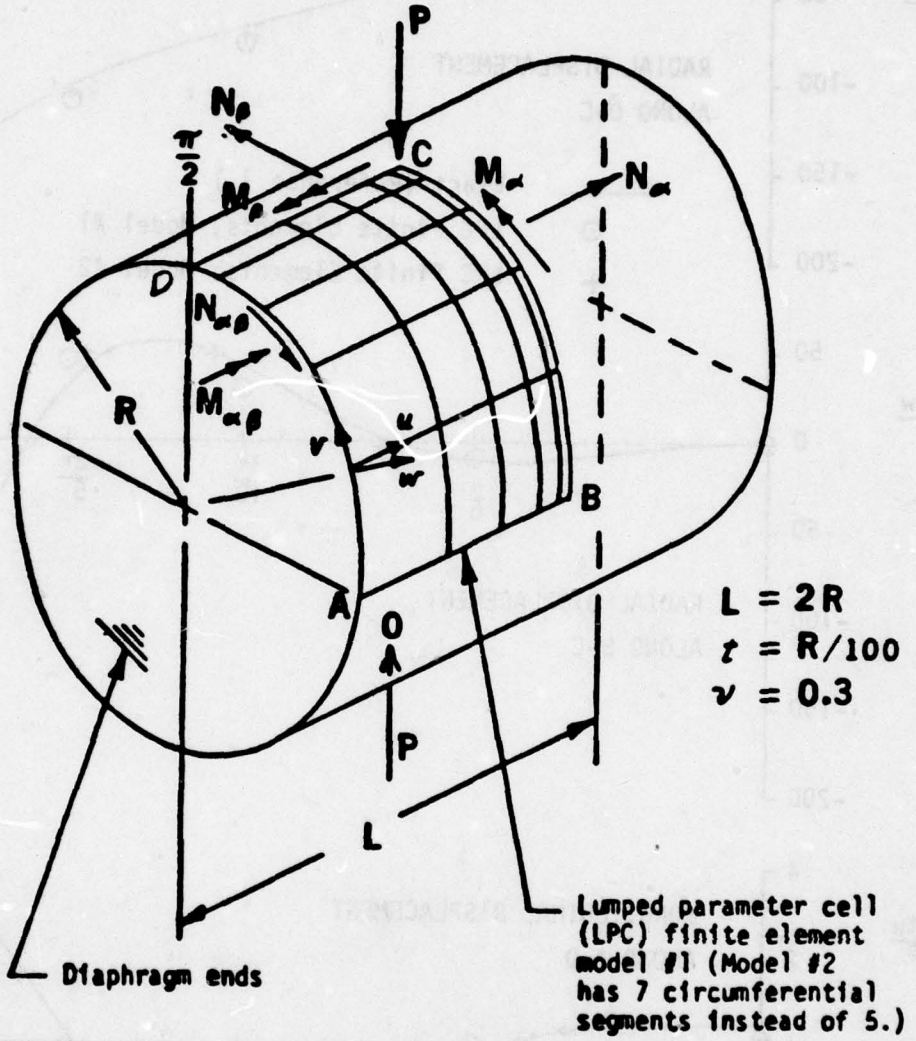


Figure 11 Pinched Cylinder Model

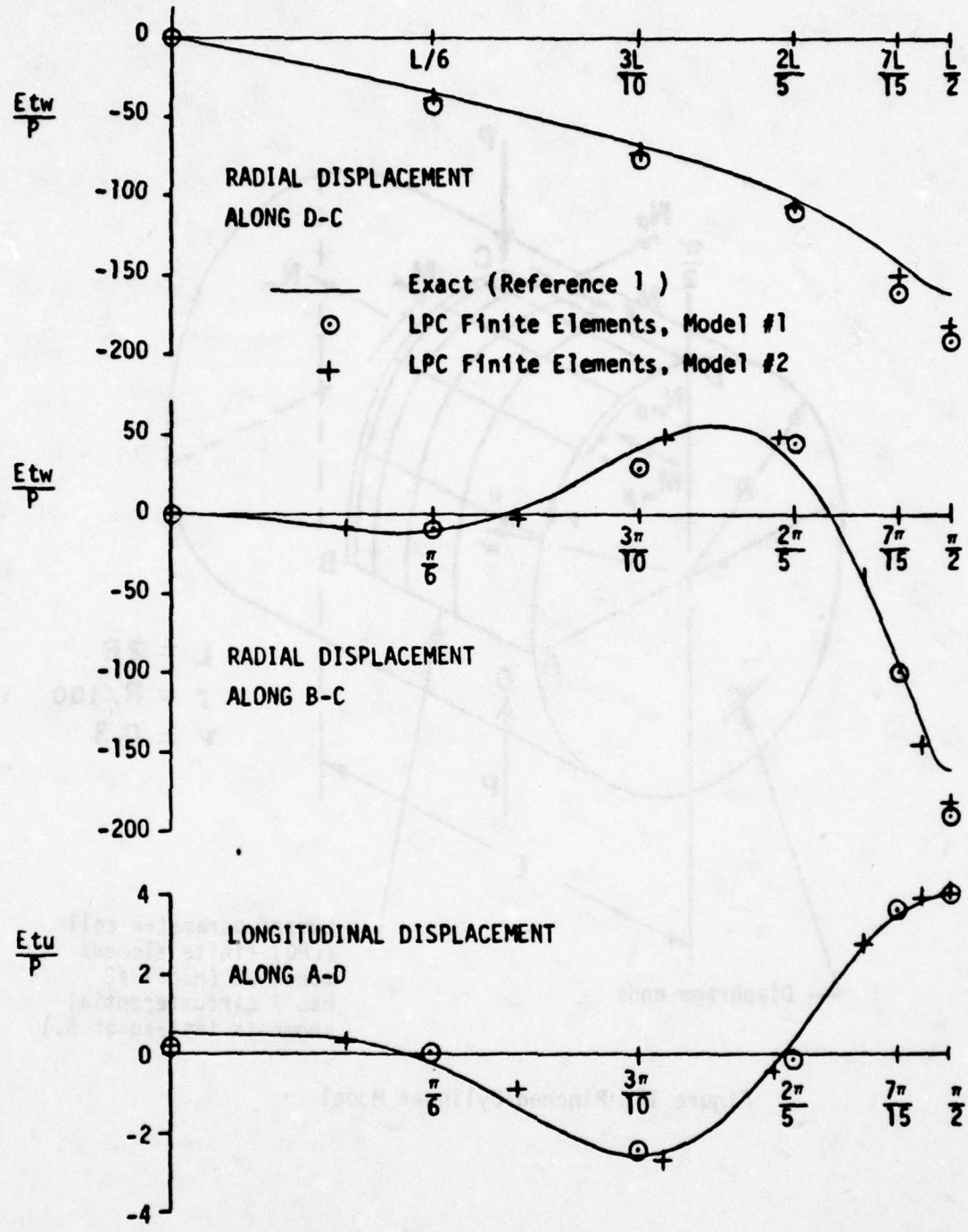


Figure 12. Pinched Cylinder Displacements

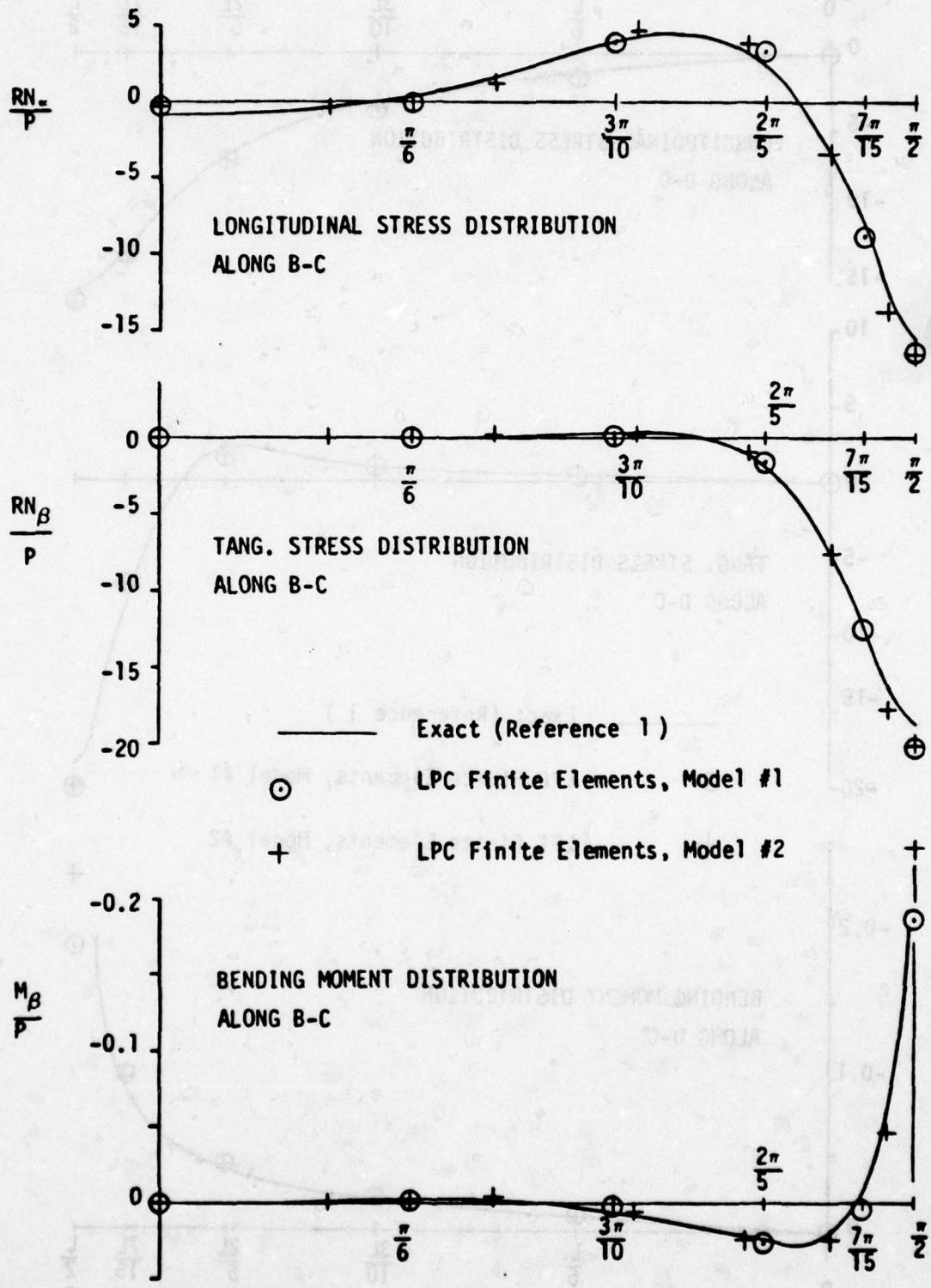


Figure 13 Stresses and Moments on Section B-C

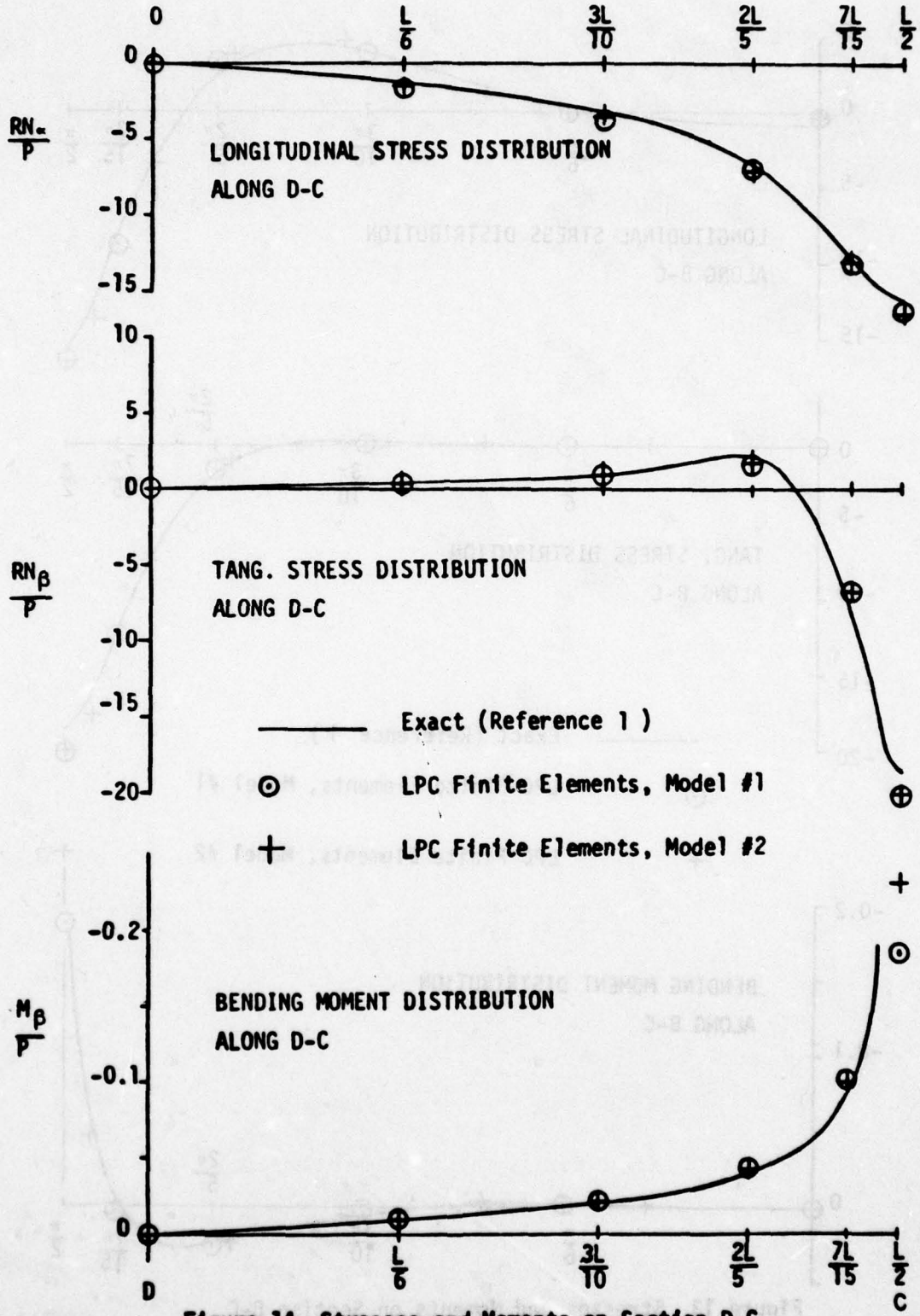


Figure 14 Stresses and Moments on Section D-C

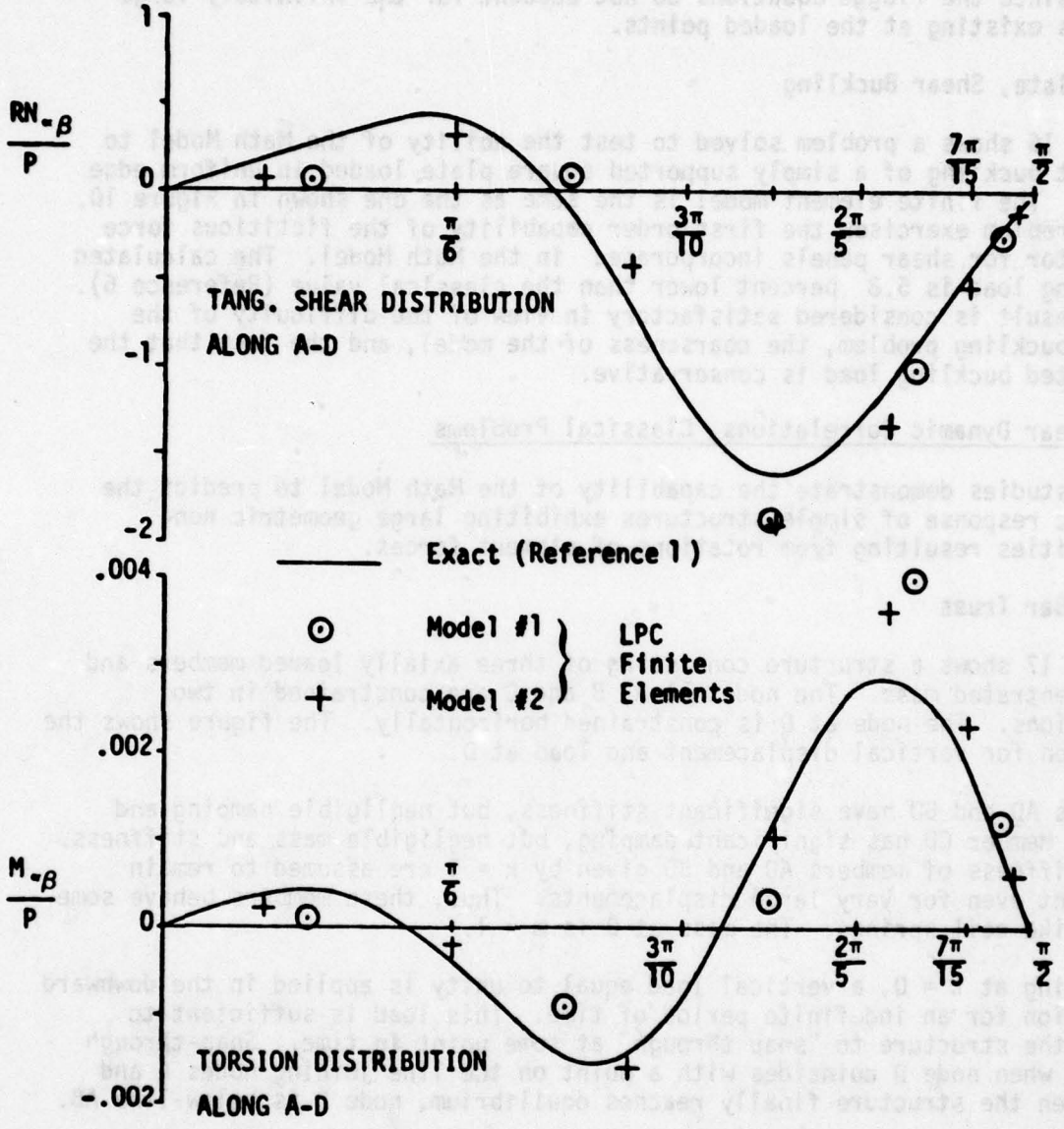


Figure 15 Shear Stress and Torsional Moment

At these points the finite element radial displacements are about 12 per cent too high, while the bending moments, of course, are bounded rather than infinite. However, the theoretical results are also in error at this point since the Flügge equations do not account for the infinitely large strains existing at the loaded points.

Flat Plate, Shear Buckling

Figure 16 shows a problem solved to test the ability of the Math Model to predict buckling of a simply supported square plate loaded in uniform edge shear. The finite element model is the same as the one shown in Figure 10. This problem exercises the first order capability of the fictitious force generator for shear panels incorporated in the Math Model. The calculated buckling load is 5.8 percent lower than the classical value (Reference 6). This result is considered satisfactory in view of the difficulty of the shear buckling problem, the coarseness of the model, and the fact that the predicted buckling load is conservative.

Nonlinear Dynamic Correlations, Classical Problems

These studies demonstrate the capability of the Math Model to predict the dynamic response of simple structures exhibiting large geometric nonlinearities resulting from rotations of element forces.

Three Bar Truss

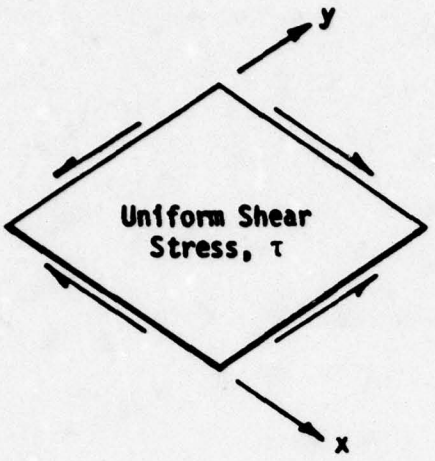
Figure 17 shows a structure consisting of three axially loaded members and a concentrated mass. The nodes at A, B and C are constrained in two directions. The node at D is constrained horizontally. The figure shows the notation for vertical displacement and load at D.

Members AD and BD have significant stiffness, but negligible damping and mass. Member CD has significant damping, but negligible mass and stiffness. The stiffness of members AD and BD given by $k = 1$ are assumed to remain constant even for very large displacements. Thus, these members behave somewhat like coil springs. The mass at D is $m = 1$.

Beginning at $t = 0$, a vertical load equal to unity is applied in the downward direction for an indefinite period of time. This load is sufficient to cause the structure to "snap through" at some point in time. Snap-through occurs when node D coincides with a point on the line joining nodes A and B. When the structure finally reaches equilibrium, node D is below line AB.

The problem is solved for two values of damping, of member CD. In the high damping case, the damping parameter is $c = 2$. In the low damping case, $c = 0.05$. All dimensions, loads and other parameters are understood to be in consistent units.

The problem was solved exactly, to provide a basis of comparison for results given by the Math Model. The exact result for the vertical motion of point D is given by the solution of the differential equation $m\ddot{\Delta} + c\dot{\Delta} + K(\Delta)\Delta = P$, (1)



Buckling Stress (psi)

Theoretical τ_B = 2606

Numerical τ_B = 2455 (5.8%)

Buckling Mode

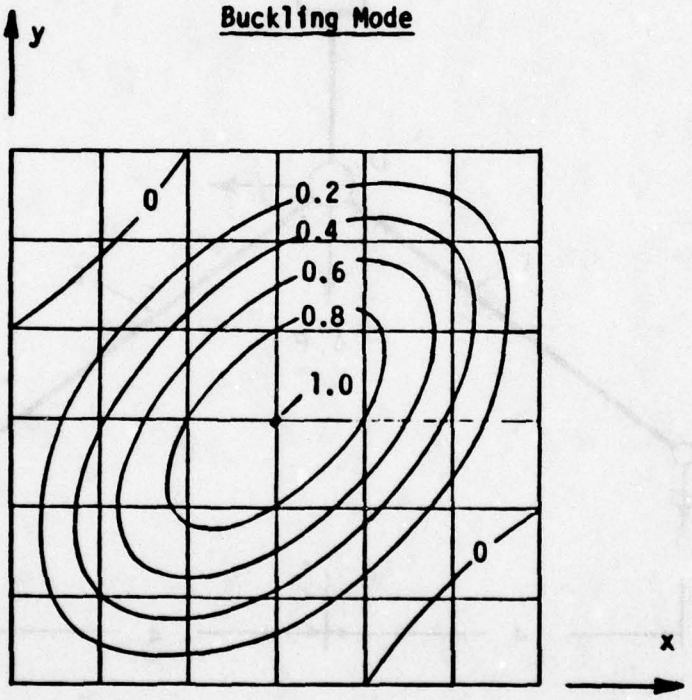


Figure 16 Buckling Analysis, Simply Supported Square Plate Under Uniform Shear

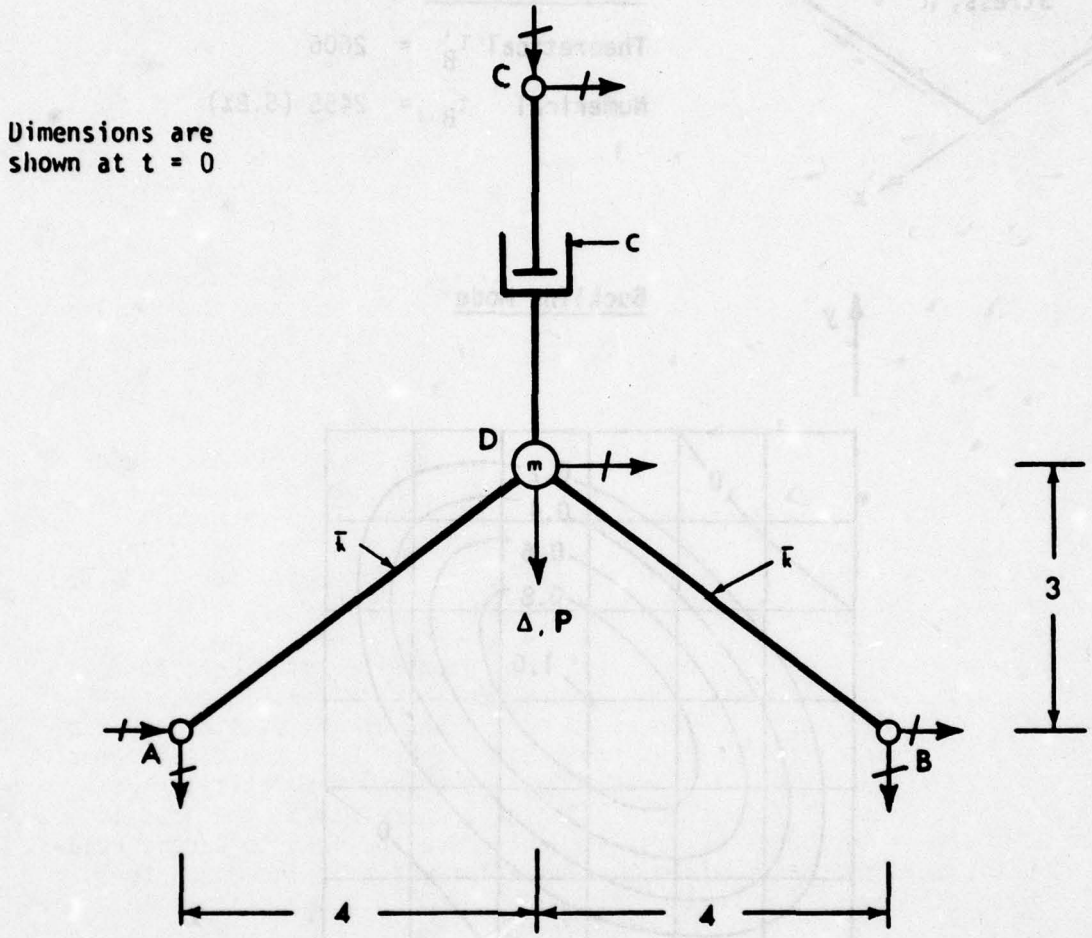


Figure 17 Three Bar Truss

where $m = 1$, (2)

$c = 2$ (high damping), (3)

$c = 0.05$ (low damping), (4)

$$K(\Delta) = \frac{2(3-\Delta)(6-\Delta)}{[16 + (3-\Delta)^2]^{1/2}\left\{5 + [16 + (3-\Delta)^2]^{1/2}\right\}} \quad (5)$$

and $P = 0$ for $t < o$, (6)

$P = 1$ for $t > o$. (7)

The stiffness $K(\Delta)$, given by Equation 5, can be found by writing the equation for the force produced by bars AD and BD on node D, in terms of the displacement Δ. The differential equation was solved numerically by a computer code called Continuous System Modelling Program (CSMP). See Reference 7.

Figure 18 shows the results for the high damping case. The solid line is the exact result from CSMP. The points indicated by plus marks show the results given by the Math Model for time increments of $\tau = 1.5$ with five iterations per increment. The agreement is good. The linear solution shown by the dotted lines is grossly in error.

Figure 19 shows results for low damping. In this case the truss oscillates for a long period of time, after snapping through. The solid line again shows the CSMP result. The plus marks and circles show the Math Model results for time increments of $\tau = 0.75$ and $\tau = 0.25$ with five iterations per increment. The results for $\tau = 0.25$ are good. The results for $\tau = 0.75$ are satisfactory for most engineering purposes.

The static response of the three bar truss can be obtained from Equation 1 by setting m and c equal to zero. The load P can then be calculated as a function of the displacement Δ. Figure 20 is a graph of the static response. As the load is increased from zero at point O, to about 0.5, the displacement follows the curve to point A. After this point the load theoretically decreases as displacement is increased. At point B where $\Delta = 3$, the load is again zero. Further increases of displacement cause the load to become negative. At C the load reaches a minimum value after which it increases to zero at a displacement of 6. Further increases of displacement cause the load to increase.

The dashed segment, ABCDE, represents unstable equilibrium. If load were applied by hanging a weight at node D of the truss, the displacement would actually follow the curve OAEF as the weight is increased from zero, because of the instability. The straight line segment AE represents snap-through. Linear response is shown by the dash-dot line.

The static response curve illustrates the pronounced nonlinear character of the problem. The point labeled "Math Model", for $P = 1$, was taken from Figure 18, which gives a value of about 7.07 as the displacement corresponding to static equilibrium.

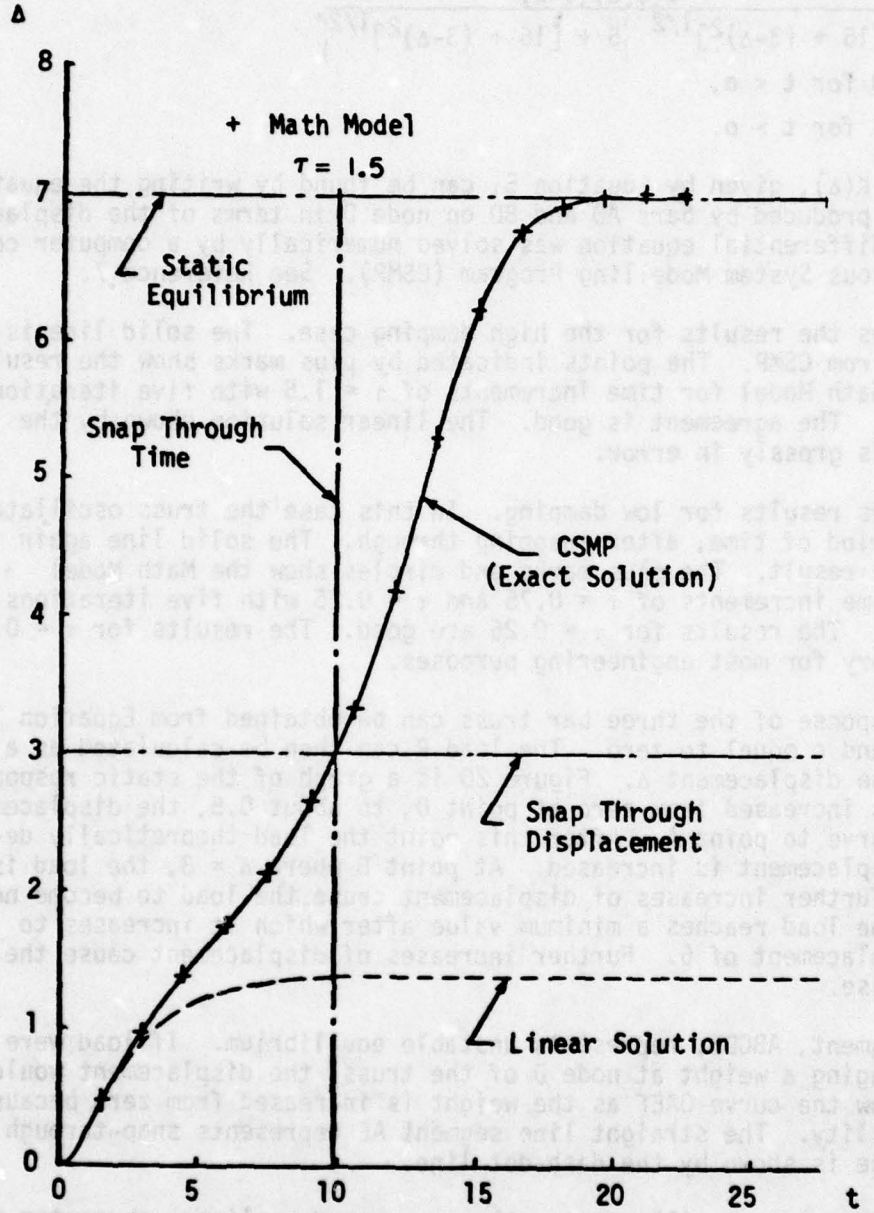


Figure 18 Displacement of the 3-Bar Truss High Damping

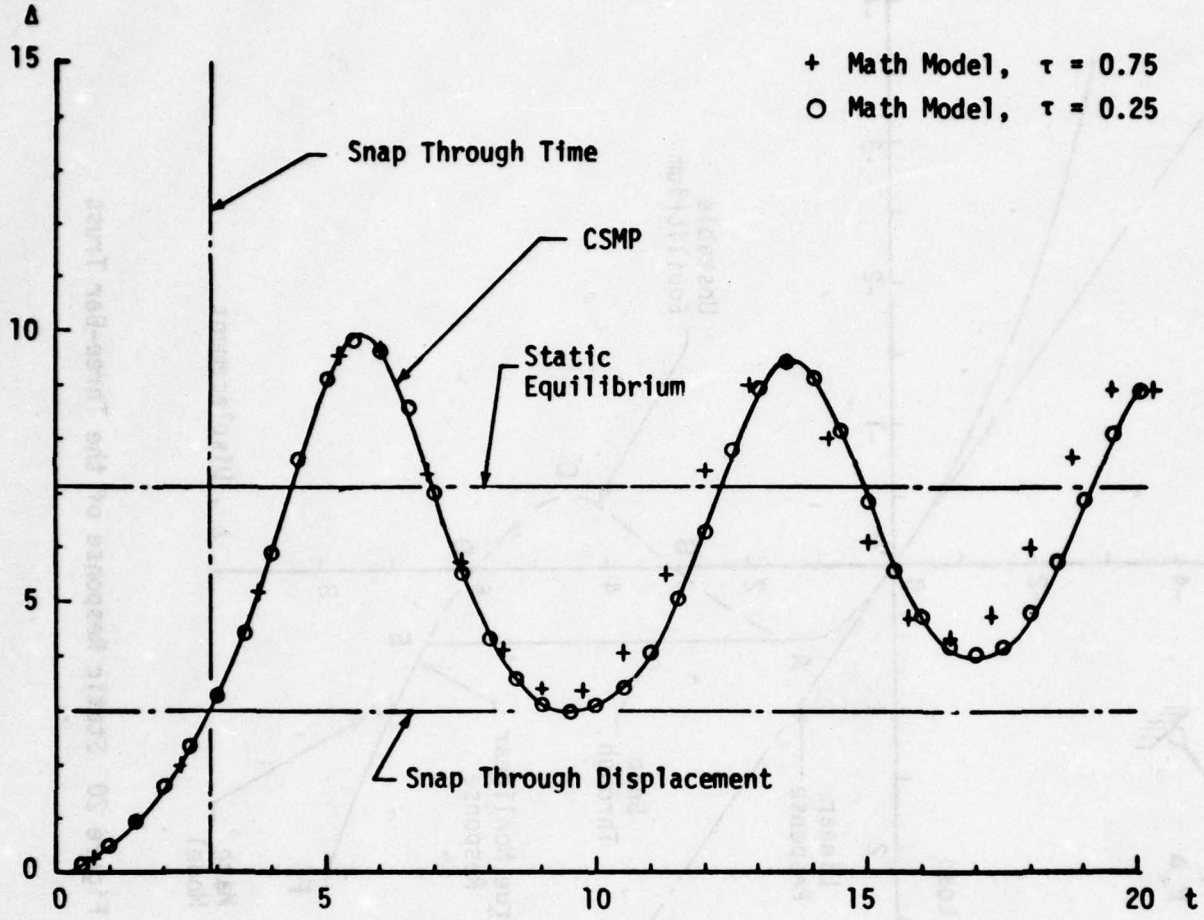


Figure 19 Displacement of the 3-Bar Truss, Low Damping

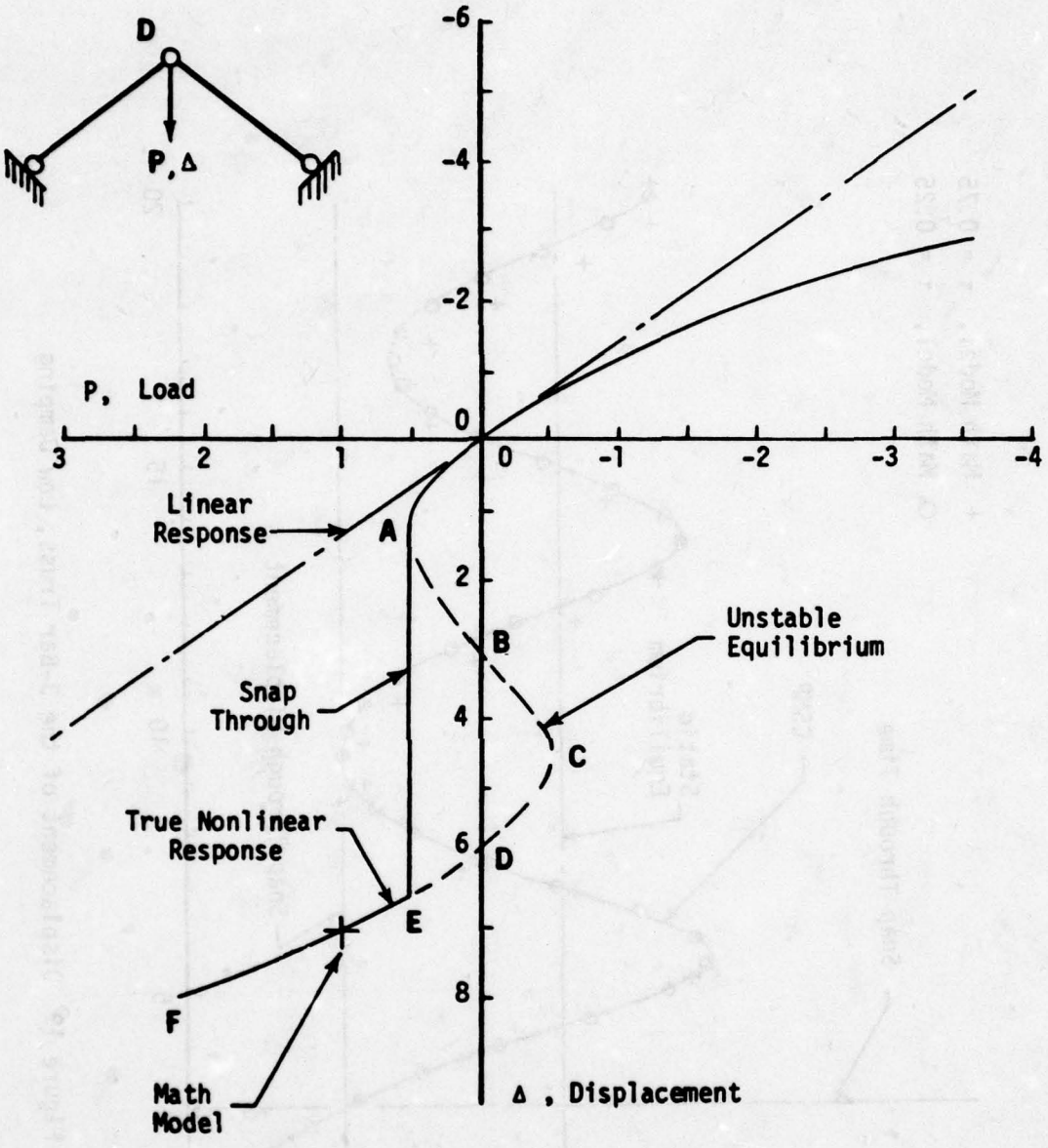


Figure 20 Static Response of the Three-Bar Truss

Flat Truss

Figure 21 shows a structure called the flat truss. Basically, the structure consists of two very stiff bars, AC and CE, hinged at point C, and a mass at C. The bars are supported vertically at A and E, but are free to move horizontally without friction at these points. Bars AC and CE have very small masses and small damping constants. The dotted line CG represents a bar with very small stiffness, mass and damping. The reason for introducing the weak bar CG and the small amount of mass and damping in AC and CE is to prevent singularities in the solution.

The exact solution to this problem can be found easily by calculating the response of the mass M to the load P, since no other forces of any significance are acting, and the acceleration is constant and equal to unity.

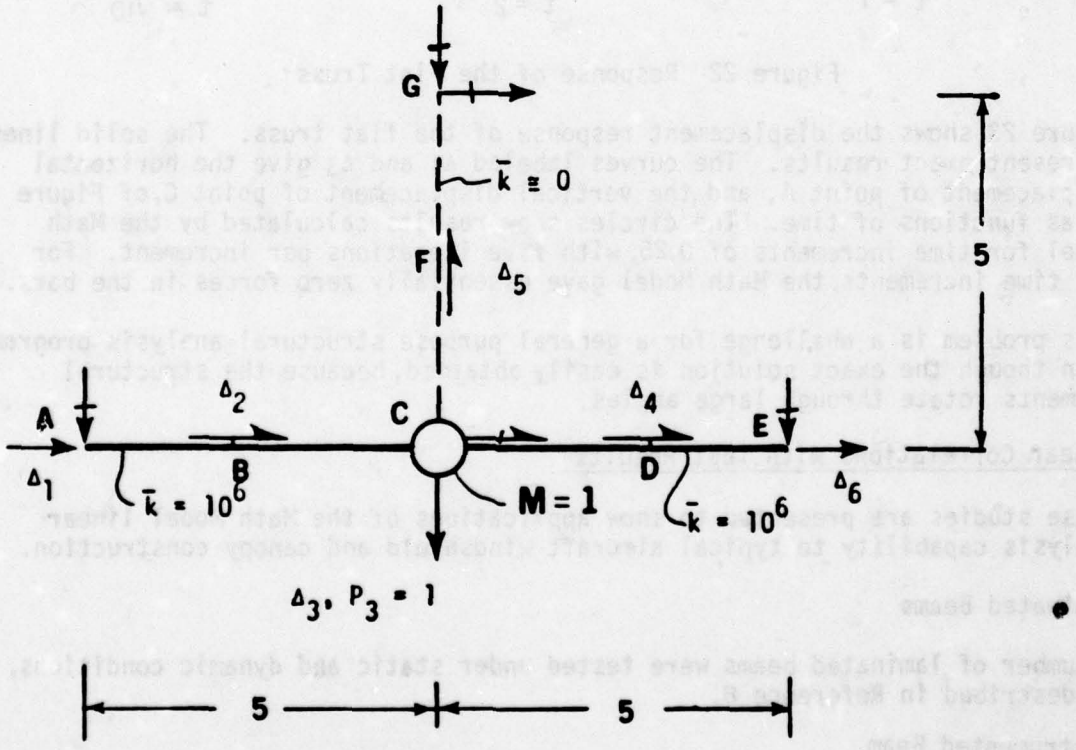


Figure 21 Flat Truss

Figure 22 shows the positions assumed by the structure at three different times. At $t = \sqrt{10}$, the truss has completely folded. At all times the length of each bar is precisely 5 inches, and the bar forces are essentially zero, except immediately after $t = \sqrt{10}$, when the bars suddenly begin to support the full external load, after a brief period of oscillation.

This structure and the 3-bar truss represent two extremes, in that the ends of the flat truss are free to move horizontally, while the ends of the 3-bar truss are prevented from such motion.

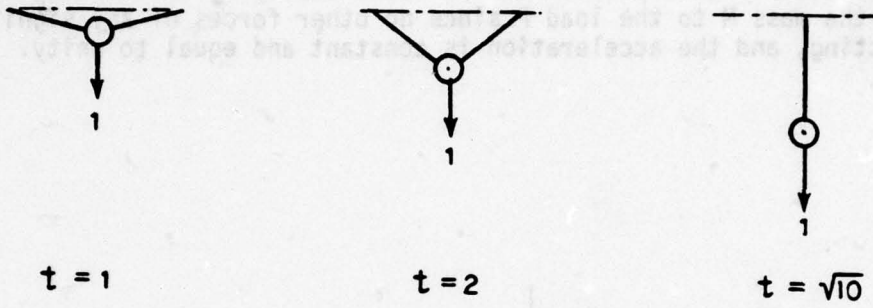


Figure 22 Response of the Flat Truss

Figure 23 shows the displacement response of the flat truss. The solid lines represent exact results. The curves labeled $\Delta 1$ and $\Delta 3$ give the horizontal displacement of point A, and the vertical displacement of point C, of Figure 21, as functions of time. The circles show results calculated by the Math Model for time increments of 0.25, with five iterations per increment. For all time increments, the Math Model gave essentially zero forces in the bars.

This problem is a challenge for a general purpose structural analysis program even though the exact solution is easily obtained, because the structural elements rotate through large angles.

Linear Correlations with Test Results

These studies are presented to show applications of the Math Model linear analysis capability to typical aircraft windshield and canopy construction.

Laminated Beams

A number of laminated beams were tested under static and dynamic conditions, as described in Reference 8.

Instrumented Beam

Figure 24 shows a laminated beam 36 inches long by 8 inches wide, composed of three structural plies and two interlayers. Ply materials and thicknesses are shown in Figure 25 (b). The beam was simply supported at the ends and loaded at the third points.

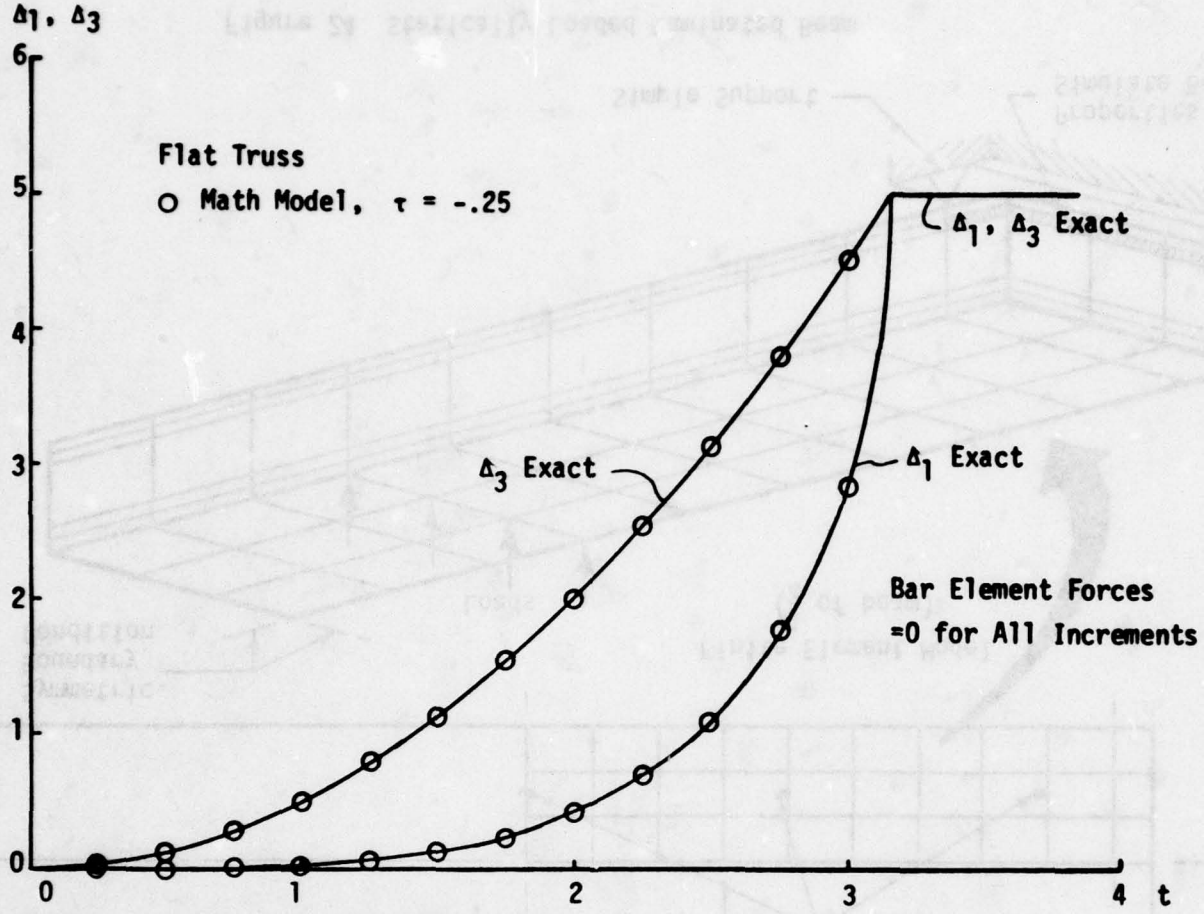


Figure 23 Displacement of the Flat Truss

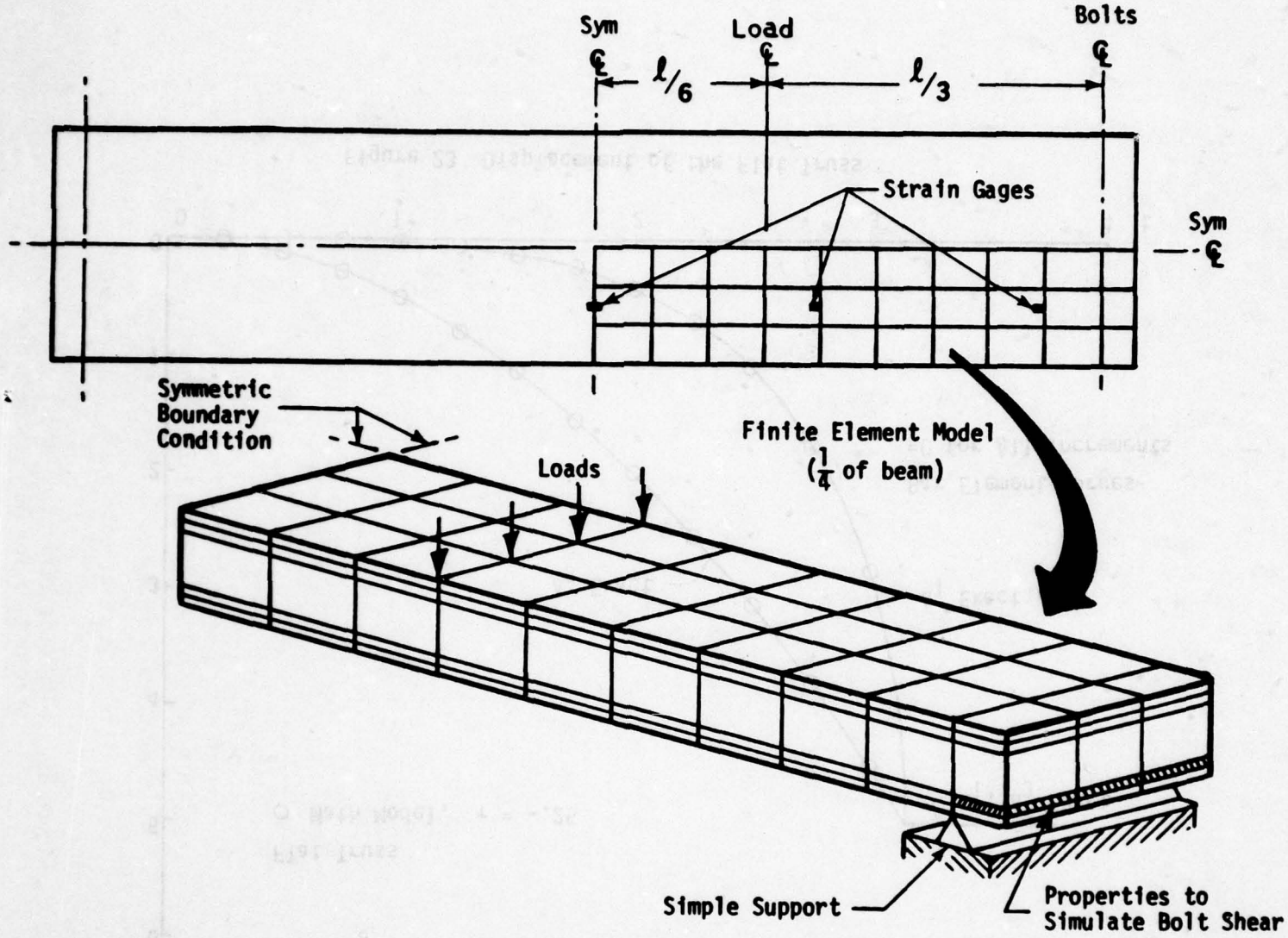
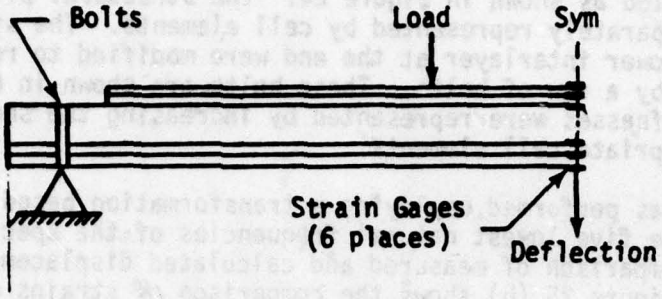
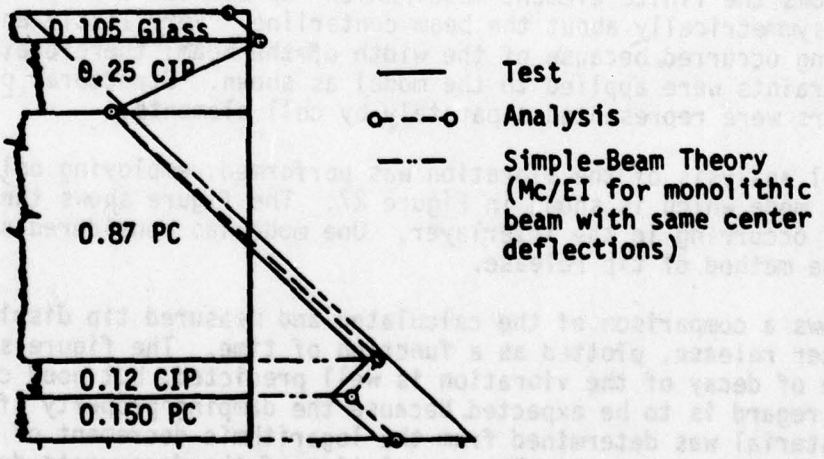


Figure 24 Statically Loaded Laminated Beam



	Test	Analysis
Load (lb.)	1365	1365
Defl. (in.)	2.75	2.80

(a) Static Deflection



(b) Strain Correlations

Figure 25 (a) Static Deflection and (b) Strain Correlations for 36-inch Beam Model

One-fourth of the beam, bounded by longitudinal and transverse planes of symmetry, was modelled as shown in Figure 24. The structural plies and interlayers were separately represented by cell elements. The stiffness properties of the lower interlayer at the end were modified to represent stiffness supplied by a row of bolts. These bolts are shown in Figure 25 (a). The bolt stiffnesses were represented by increasing the shear stiffnesses of the appropriate cell elements.

A static analysis was performed, employing a transformation based on modes corresponding to the five lowest natural frequencies of the specimen. Figure 25 (a) shows the comparison of measured and calculated displacements at the beam centerline. Figure 25 (b) shows the comparison of strains calculated through the thickness of the laminate with test data. These comparisons are considered satisfactory. They demonstrate the capability of the Math Model to produce reliable results for a laminated transparency. The comparisons also support the feasibility of the modal approach to strain and displacement analysis, and show the inapplicability of engineering beam theory.

Damping Beam

The laminated cantilever beam shown in Figure 26 was tested for the purpose of providing data on the damping properties of the interlayer material (Reference 8). The 18 inch by 8 inch beam consisted of two 0.25 inch thick polycarbonate plies separated by a 0.12 inch thick layer of CIP interlayer material. The beam was excited by an initial tip displacement. After release, the beam vibrated freely.

The figure shows the finite element model, which represented a strip 1 inch wide, located symmetrically about the beam centerline. Very little anticlastic bending occurred, because of the width of the beam; therefore, anticlastic constraints were applied to the model as shown. Structural plies and interlayers were represented separately by cell elements.

A linear modal analysis of the vibration was performed, employing only the first bending mode, which is shown in Figure 27. The figure shows the large shear strains occurring in the interlayer. One mode was considered sufficient because of the method of tip release.

Figure 28 shows a comparison of the calculated and measured tip displacement occurring after release, plotted as a function of time. The figure shows that the rate of decay of the vibration is well predicted, but good correlation in this regard is to be expected, because the damping property of the interlayer material was determined from the logarithmic decrement of the motion measured from the curve. The correlation of the decay rate does, however, tend to support the use of viscous damping as part of the theoretical basis of the Math Model, since the correlation is good along the entire curve. The figure also shows that the frequency of vibration is well predicted. Measurements show a test frequency of 12.6 Hertz, compared to a computed value of 12.8. The frequency correlation tends to verify the accuracy of both the stiffness and mass matrices employed in the analysis for cell elements.

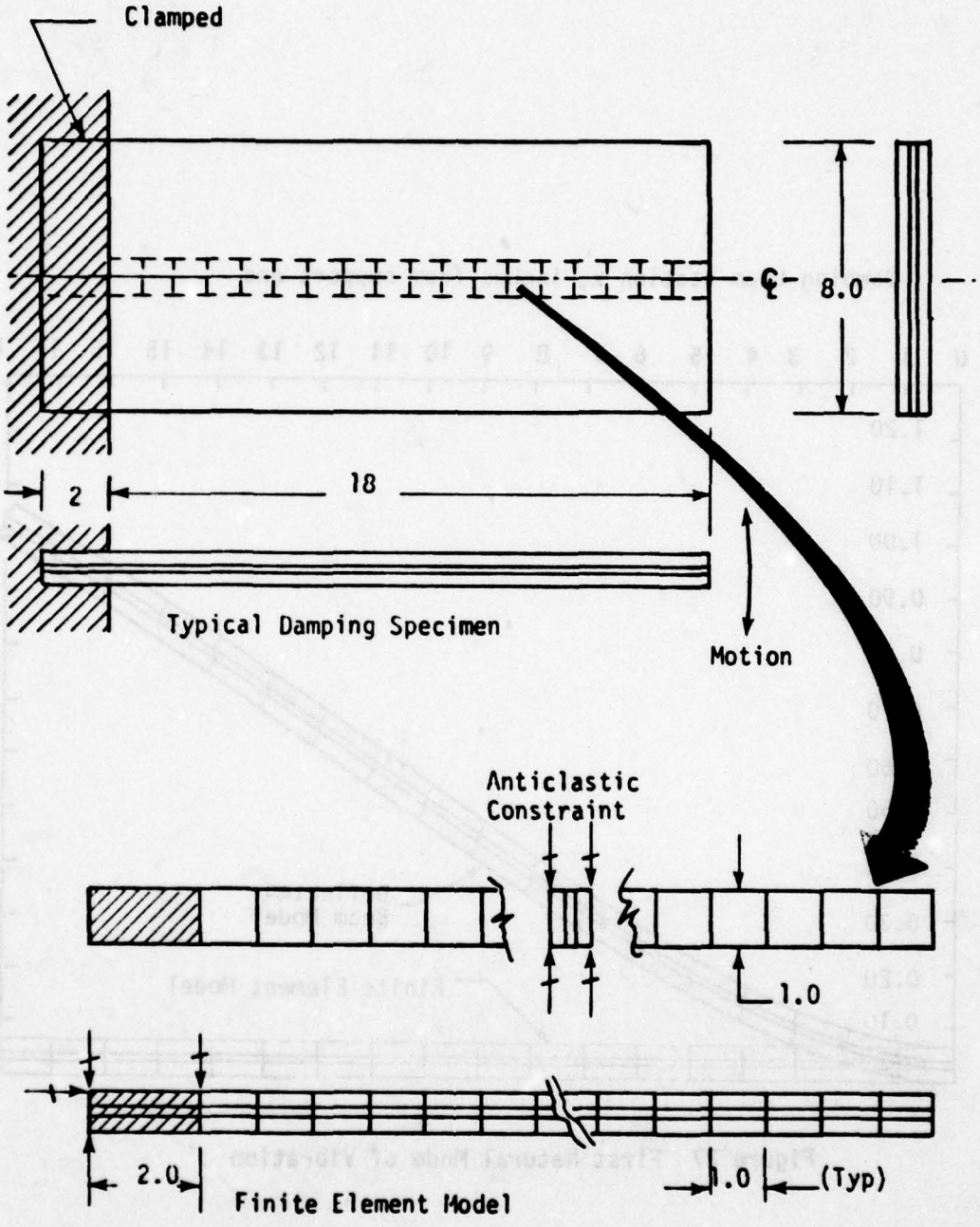


Figure 26 Damping Beam Specimen and Finite Element Model

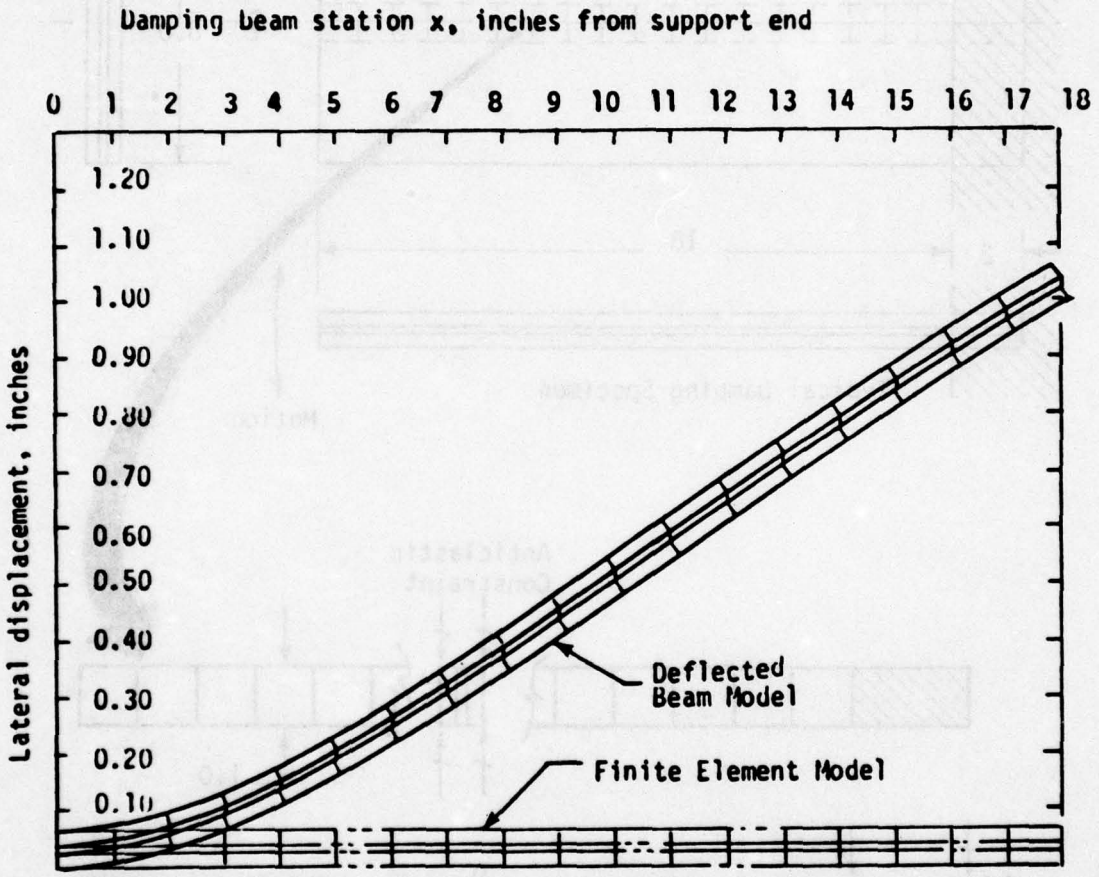


Figure 27 First Natural Mode of Vibration

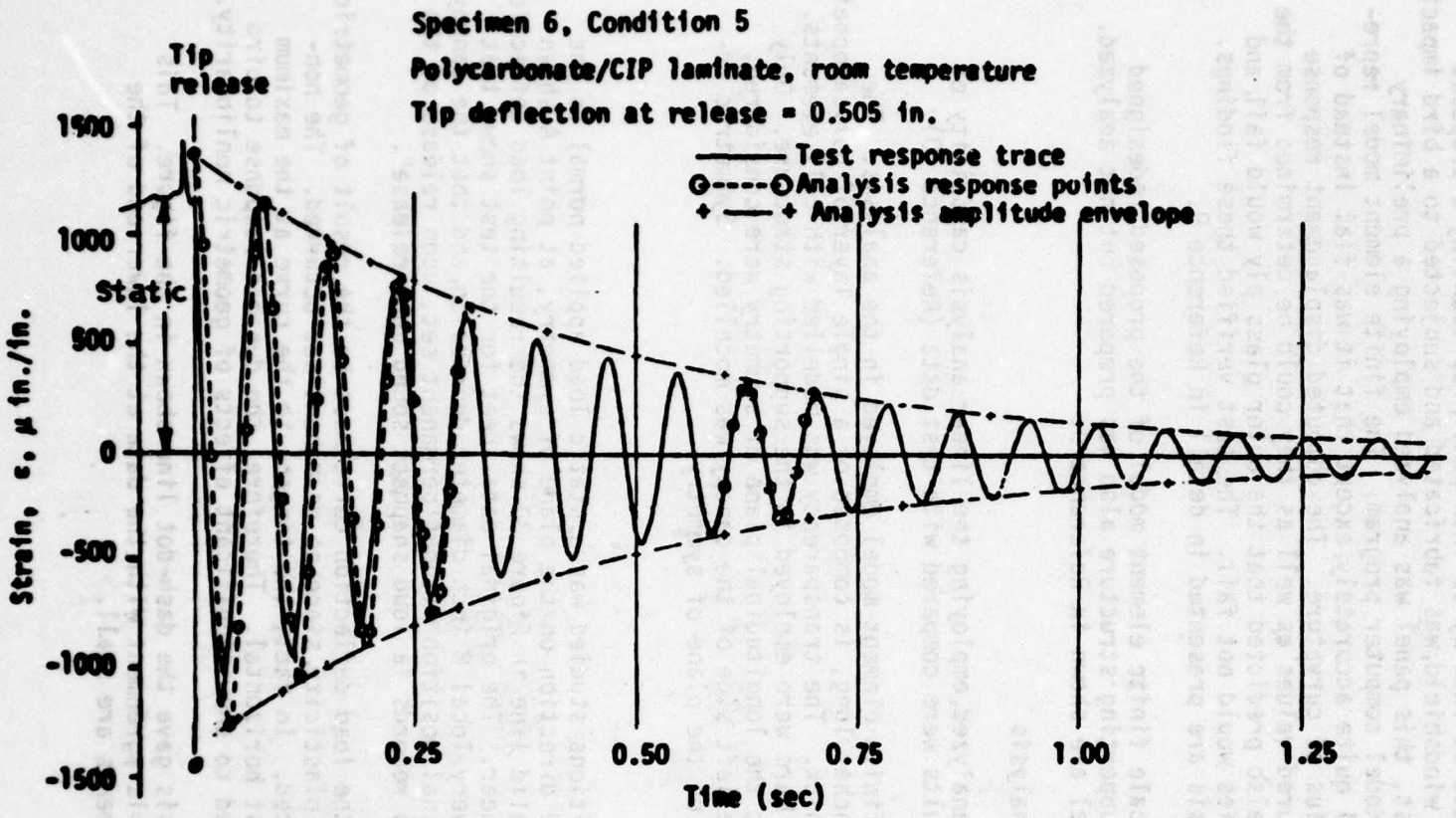


Figure 28 Response of the Damping Beam to an Initial Tip Displacement

B-1 Bird Impact Data

A seven layer laminated 36 inch by 36 inch panel, representing a proposed redesign for the B-1 windshield, was fabricated and subjected to a bird impact test. Before the test, this panel was analyzed employing a preliminary version of the Math Model computer program. The finite element model represented the test panel quite accurately, except that it was flat instead of having a 60 inch radius of curvature. The computed displacement response correlated with measured values as well as they could be determined from the data. The analysis also predicted that the outer glass ply would fail, and the polycarbonate plies would not fail. The test verified these findings. Results of the analysis are presented in detail in Reference 9.

A reaslistic large scale finite element model of the proposed redesigned B-1 windshield and supporting structure also was prepared but not analyzed. Sketches of this model are shown in Reference 9.

F-16 Canopy Linear Analysis

The F-16 canopy was analyzed, employing the linear analysis capability of the Math Model. Results were compared with test data (Reference 10).

Figure 29 shows the finite element model employed in the analysis. The canopy, roughly 90 inches long, is composed of a single layer of polycarbonate, nominally 1/2 inch thick. The transparency was modelled with cell elements. Cells, membranes and bars were employed in the supporting structure. Only loads symmetric about the longitudinal plane of symmetry were considered; consequently only the left side of the canopy was modelled. Symmetric reactions were applied on the plane of symmetry.

Static Loading

One of the test conditions studied was a static load applied normal to the surface in the inward direction on the plane of symmetry, at point A shown in Figure 29. The solid line in Figure 30 shows the resulting load deflection curve, which is nonlinear. The original data sheet for the test shows that the load produced a very local 8 inch diameter depression, and that the canopy returned to its original position without permanent set, upon release of the load. The sheet also records "a loud snapback sound upon release".

The nonlinearity of the load deflection curve must be the result of geometric nonlinearity, and not plasticity, since no permanent set occurred. The nonlinearity is pronounced. In fact, the tangent to the curve at the maximum applied load is almost horizontal. Therefore, the dynamic response to bird impact can be expected to show significant effects of geometric nonlinearity.

The Math Model analysis gave the dash-dot line shown in the figure. This result is in reasonable agreement with the data at the lower end of the curve where displacements are small.

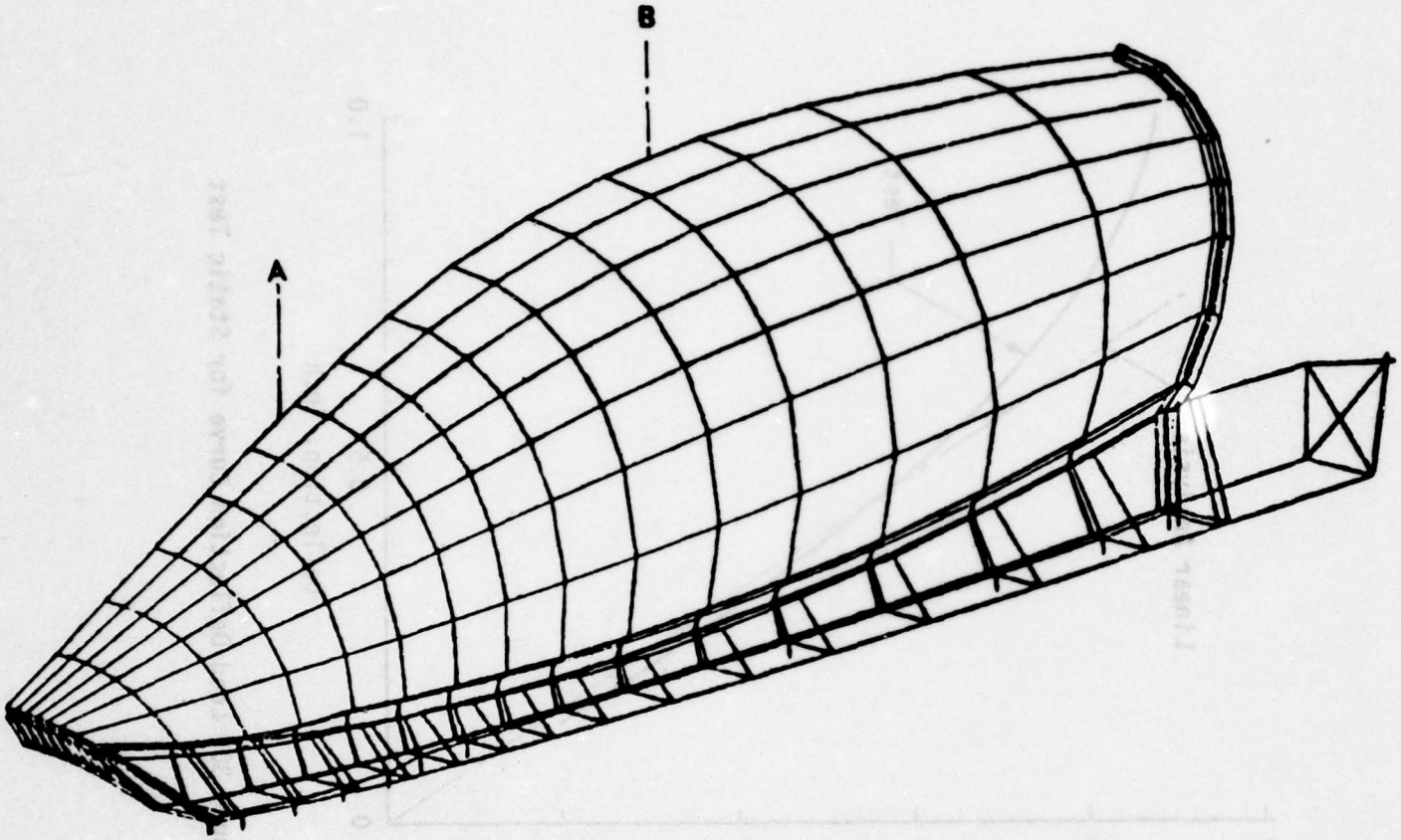


Figure 29 Half-shell Finite Element Model of the F-16 Canopy

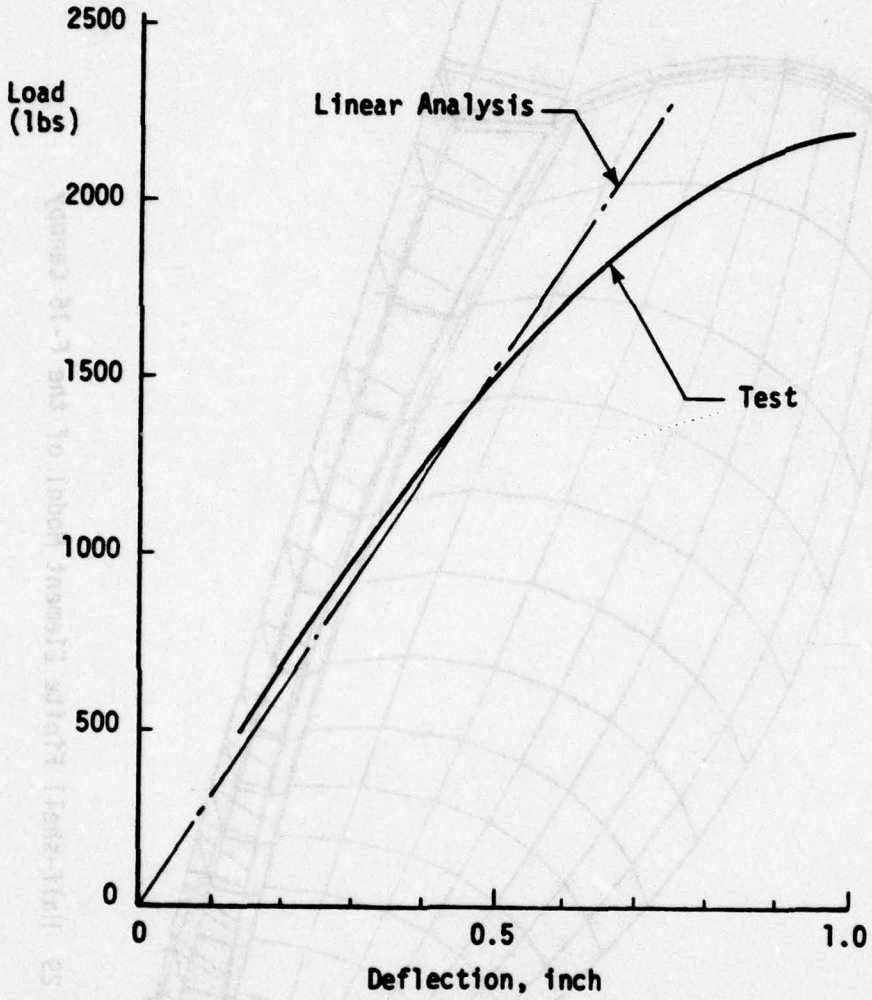


Figure 30 Load Deflection Curve for Static Test

Bird Impact Loading

The results of numerous bird impact tests were analyzed. In these tests, initial impact was at point A, shown in Figure 29. Bird weights ranged from two to four pounds, and bird velocities varied from 150 to 350 knots approximately.

High speed motion pictures of the tests showed that, after initial impact at point A, a wave was produced in the surface that traveled aft along the plane of symmetry. This wave was quite pronounced, and did not diminish in amplitude until it passed a point, roughly indicated by point B in Figure 29, about halfway between the point of initial impact and the back of the canopy. When failures occurred, they tended to occur in the region of point B.

In the first applications of the Math Model, load was applied only in the region of point A, for a time period called the "squash up" time, that depends on the length and speed of the bird. The method of calculating the magnitude of the load, its dependence on time, and its spatial distribution, is given in Reference 11. The results of these analyses showed a very weak traveling wave that rapidly diminished in amplitude as it progressed aft. The calculated stress distributions, which showed maximums at point A, did not correlate with the observed occurrence of failures in the region of point B. The loads that were applied in these early studies are subsequently called "stationary footprint" loads, because the load vectors remain in the region of initial impact.

In view of the failure of the stationary footprint approach, the "traveling footprint" hypothesis was advanced. In this approach, the load vectors are assumed to travel aft, keeping pace with the bird, as it slides along the surface toward the rear of the canopy. The traveling footprint loads are calculated by a method described in Reference 1, which is a modification of the approach of Reference 11.

Several traveling footprint analyses of the F-16 canopy were performed. In the case described in the following paragraphs, the bird weight was 4 pounds, and the bird speed was 340 knots. The solution provided by the linear incremental option of the Math Model employed a transformation based on the lowest 30 natural vibration modes of the finite element model shown in Figure 29. Figure 31 shows the results. Vertical displacements are plotted at points along the canopy centerline for different times, which are shown in seconds. The figure shows a strong traveling wave peaking at the crown of the canopy.

Figure 32 shows equivalent stresses on the canopy inner surface centerline for the same test. When the equivalent stress, equal to twice the octahedral shear stress, reaches the ultimate tensile stress determined in a uniaxial tensile test, failure occurs according to an accepted failure theory. The figure shows that the equivalent stress is maximum at Fuselage Station 136. Thus, the linear analysis indicates maximum stress in the aft part of the canopy, and not at the point of impact, in agreement with test results.

The linear analysis agrees qualitatively with test results, but unfortunately

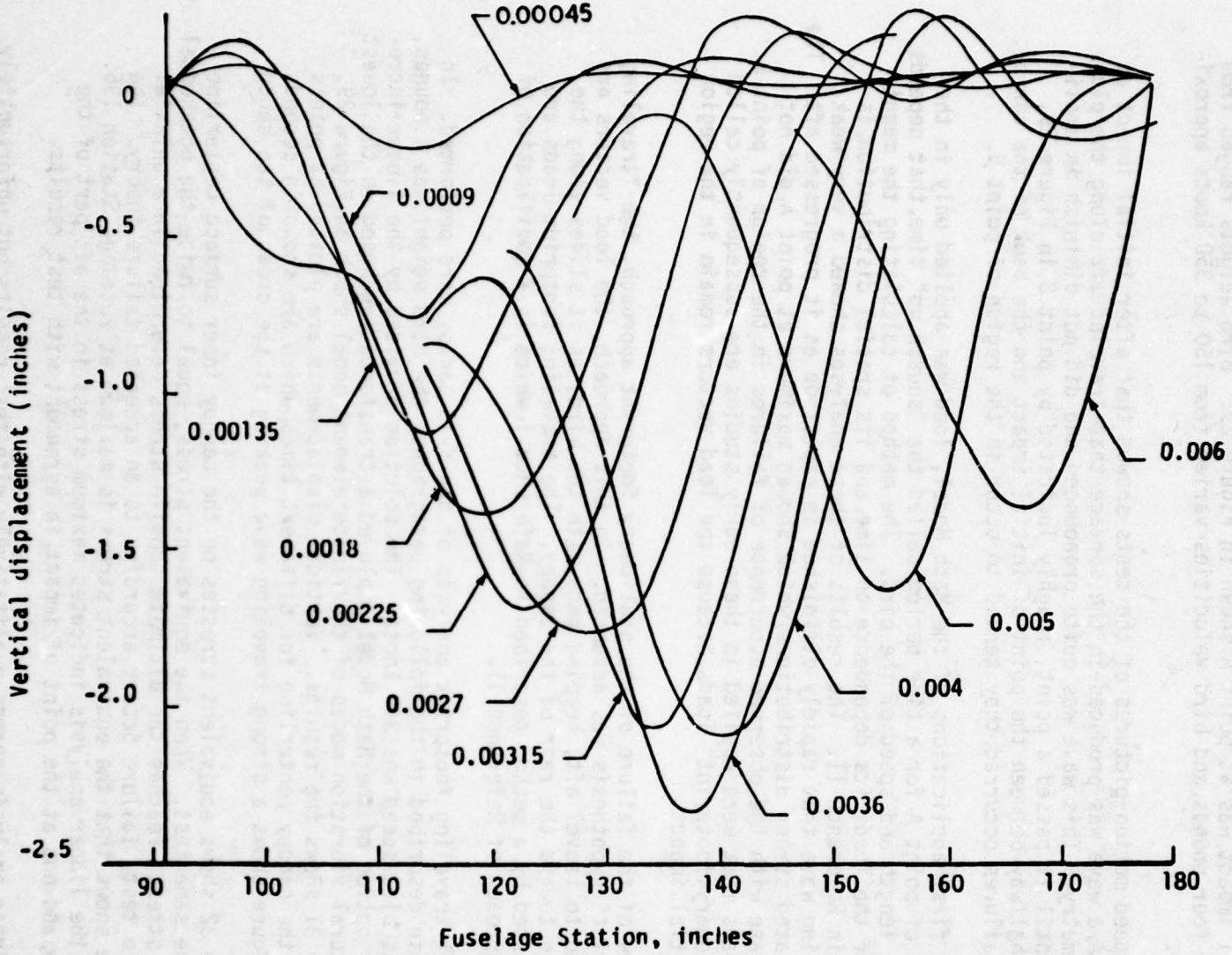


Figure 31 Vertical Displacement on the Plane of Symmetry, as a Function of Fuselage Station and Time

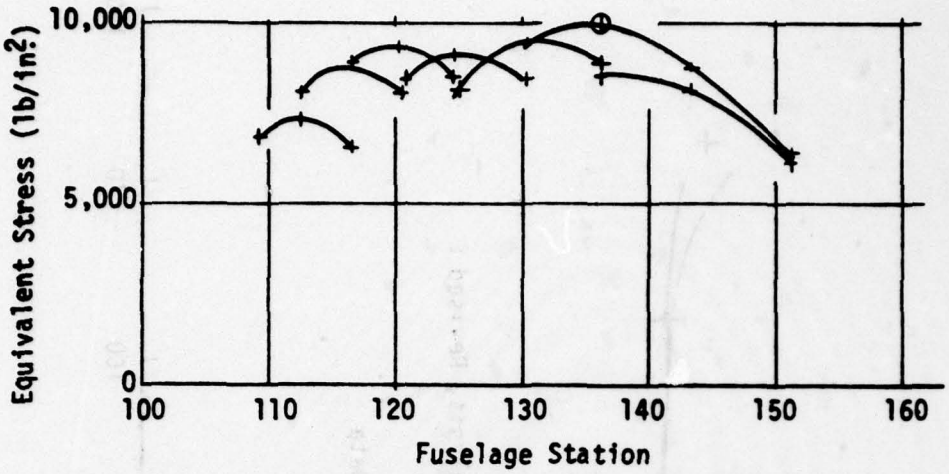


Figure 32 Equivalent Stress on the Plane of Symmetry, Inside, as a Function of Fuselage Station and Time

predicted displacements and stresses are generally too low. Figure 33 shows the envelope of the traveling wave derived from Figure 31, compared to the envelope determined from the high speed motion pictures. The linear analysis tends to agree with test results, in that maximum displacement occurs well aft of the point of initial impact. The test results, however, are greater than linear analysis results by a factor of 3.6. Also, the test results drop off more rapidly after reaching the peak than the analysis shows.

Subsequent testing of specimens taken from the canopy indicated that the value of Young's modulus, E, used in the analysis was too high. Re-analysis with a lower value of E gave the dash-dot curve shown in Figure 33, but the maximum test displacement is still 2.8 times greater than the analytical maximum.

The large discrepancy between linear results and observed displacement is believed to be a geometrically nonlinear effect in view of the fact that the static tests results, shown in Figure 30, show a pronounced geometric nonlinearity. Figure 34 shows a possible mechanism of nonlinear wave propagation. Shortly after impact, according to this hypothesis, snap-through occurs, producing a wave of greater amplitude than linear theory predicts. This wave travels aft to some point near the rear of the canopy, where it snaps out and becomes a linear wave. Such a mechanism would explain the observed discrepancy since, snap-through behavior is well known to have the capability of producing much larger displacements than linear theory predicts. For example, see Figure 18 showing displacements of the three-bar truss.

Nonlinear Analysis of the F-16 Canopy

The traveling snap-through wave hypothesis can be tested by applying the Math Model nonlinear incremental option to the problem. Such an analysis was attempted, but the attempt was unsuccessful. A difficulty was encountered which could not be overcome in the available time.

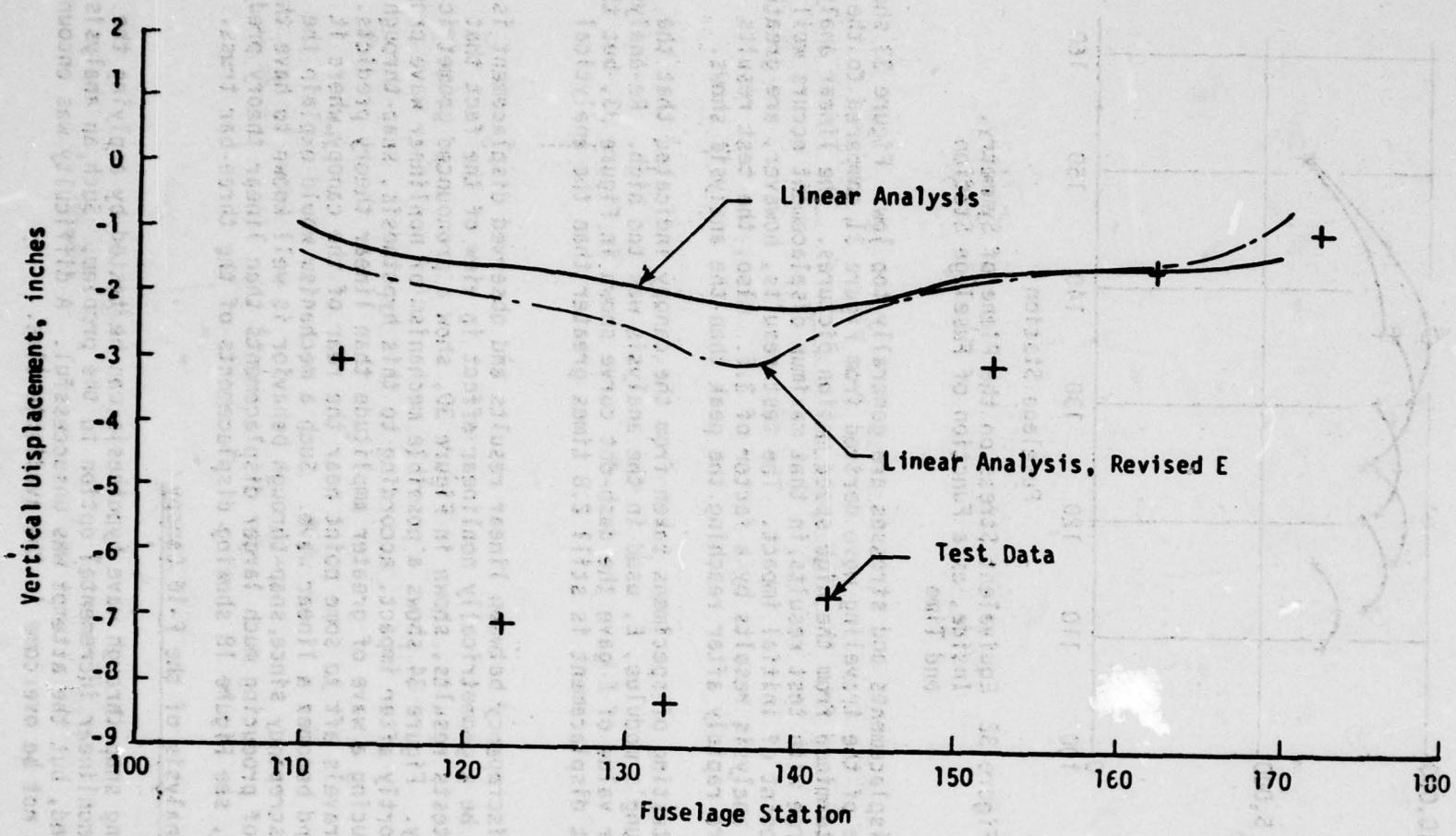


Figure 33 Envelope of Traveling Wave

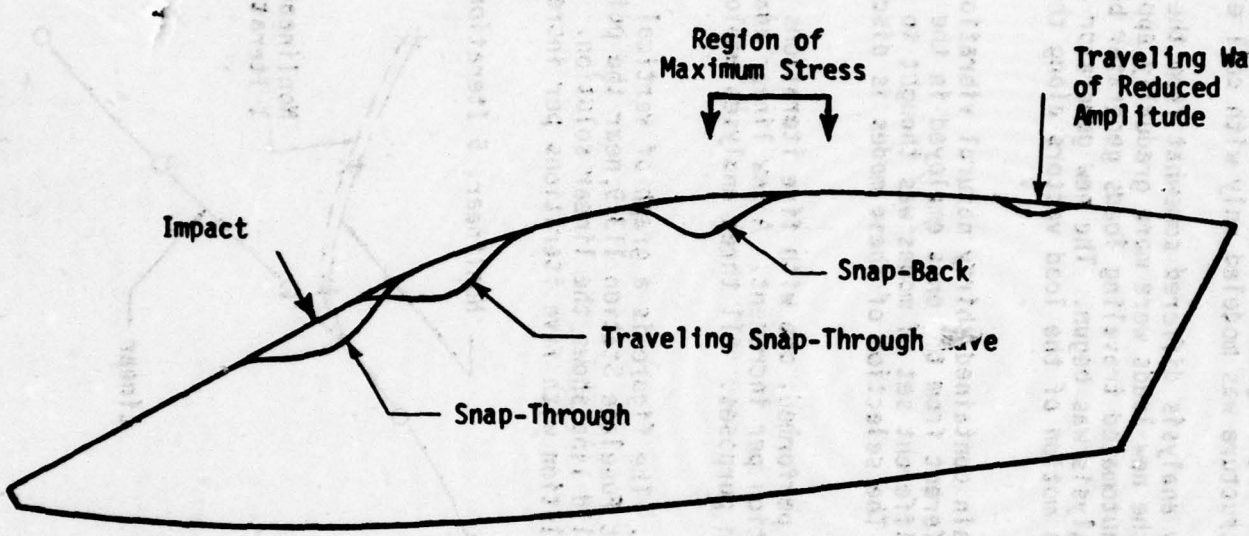


Figure 34 Possible Mechanism of F-16 Canopy Response: Traveling Snap-through Wave

The nonlinear option was applied to the same test condition discussed previously in connection with the linear analysis, in which the bird weight was 4 pounds, and the bird speed was 340 knots. The model employed for this study was similar to the one shown in Figure 29, except that more transverse stations were added aft of point B, giving more detail in the rear part of the canopy. Also, the entire structure was modeled only with cell elements.

The loads applied in the new analysis differed somewhat from the loads of the previous study, in that the new loads were more gradually applied, as a result of the fact that an automated traveling loads generator became available just before the new analysis was begun. The new generator allowed a smoother and more continuous motion of the load vectors along the top of the canopy.

The modal transformation again contained thirty natural vibration modes, but the modes selected were different from the ones employed in the previous linear analysis, because a different set of modes was thought to be needed for the nonlinear problem. The selection of these modes is discussed in Reference 1.

Two nonlinear analyses were performed; one with five iterations per increment, and one with only one iteration per increment. A new linear analysis also was performed for comparison purposes. All three analyses employed the same set of modes.

Figure 35 shows the results. The figure is a graph of vertical displacements at the canopy centerline, at Fuselage Station 113.9, near the point of initial impact, versus time. The solid line shows the linear solution. The dash-dot line shows the nonlinear solution with five iterations per increment, while

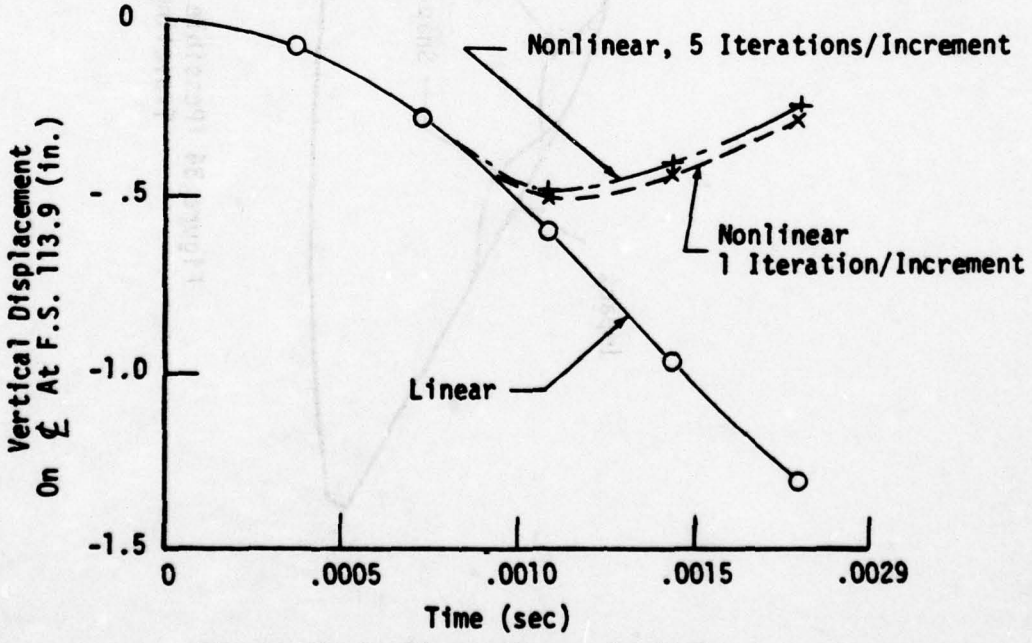


Figure 35 Nonlinear Canopy Analysis

the dotted line shows the nonlinear solution with one iteration per increment. The nonlinear curves at first follow the linear curve, but as displacements increase, the nonlinear results depart from the linear values and decrease toward zero. This result is the opposite of what is expected, since the nonlinear results should be greater than the linear. The nonlinear results are undoubtedly incorrect.

This matter was studied, and the conclusion was drawn that the difficulty probably lies in the selection of modes and not in the theoretical basis of the Math Model, or in the computer program. The subject is discussed in Reference 1, where a possible explanation of the difficulty is presented. Further study of the use of modal transformations for nonlinear analysis is recommended.

Running Times

The Math Model computer program includes a preprocessor, the incremental solution, with linear and nonlinear options, and a postprocessor. These modules and the associated running times are discussed in detail in Parts 2 and 3 of Reference 1. For the analysis of the F-16 canopy described in the preceding paragraphs, the nonlinear module with five iterations per increment, required about 430 CPU seconds/increment and 310 IO seconds/increment on the CDC Cyber 74 computer employing 160,000 decimal words of care. These times are quoted as an indication of the feasibility of the nonlinear code. This code in its present form is not optimized. Its efficiency can be improved considerably.

REFERENCES

1. Denke, P. H., Eide, G. R., and Morris, R. C, Aircraft Windshield Bird Impact Math Model, Part 1 - Theory and Applications; Part 2 - User's Manual, Part 3 - Programming Manual, AFFDL-TR-77-99, Parts 1, 2 and 3, December 1977.

2. Przemieniecki, J. S., Theory of Matrix Structural Analysis, McGraw-Hill Book Company, New York, 1968.

3. Timoshenko, S., and Woinowsky-Krieger, S., Theory of Plates and Shells, McGraw-Hill Book Company, New York, 1959.

4. Lindberg, G. M., Olson, M. D., and Cowper, G. R., "New Developments in the Finite Element Analysis of Shells", DME/NAE Quarterly Bulletin, No. 1969 (4).

5. Pickard, J., FORMAT - Fortran Matrix Abstraction Technique, Volume V, Engineering User and Technical Report, AFFDL-TR-66-207, Volume V, October 1968.

6. Timoshenko, S., and Gere, J. M., Theory of Elastic Stability, McGraw-Hill Book Company, New York, 1961.

7. IBM Application Program, System/360 Continuous System Modeling Program User's Manual, Program Number 360 A-CX-16X.

8. Rhodes, G. F., Damping Static Dynamic, and Impact Characteristics of Laminated Beams Typical of Windshield Construction, AFFDL-TR-76-156, September 1977.

9. Lawrence, J. H., Jr., et al., Windshield Technology Demonstrator Program - Detail Design Options Study, AFFDL-TR-77-1, December 1976.

10. Coker, M. J., Hoffman, J. B., Lawrence, J. H., Jr., Windshield Technology Demonstrator Program - Canopy Detail Design Options Study, Douglas Aircraft Company Report MDC J7176, April 1978.

11. Barber, J. P., Wilbeck, J. S., and Taylor, H. R., Bird Impact Forces and Pressures on Rigid and Compliant Targets, UDRI-TR-77-17, March 1977.

SESSION IV

MATERIALS TESTING AND AIRCREW VISUAL STUDIES

Chairman: I. Wolock
Naval Research Laboratory
Mechanics of Materials
Branch
Washington, D.C.

LABORATORY SCREENING TESTS: A COST EFFECTIVE APPROACH TO AIRCRAFT TRANSPARENCY DESIGN

B. S. West and P. E. Johnson
University of Dayton
Research Institute
Dayton, Ohio

PRECEDING PAGE BLANK-NOT FILMED

LABORATORY SCREENING TESTS: A COST EFFECTIVE APPROACH TO AIRCRAFT TRANSPARENCY DESIGN*

Blaine S. West and Paul E. Johnson
University of Dayton Research Institute

ABSTRACT

Design refinement of aircraft transparencies for bird impact resistance through the testing of full scale flight hardware is expensive in terms of dollars, manpower, and calendar time. This paper describes the development of mechanical properties tests for the express purpose of screening candidate laminated transparency configurations in the laboratory. The tests were devised to evaluate both center panel impact and edge impact conditions and the specimens were tested at loading rates varying from near static to 2000 in/minute. These tests have been used to evaluate more than one hundred F-111 laminated transparency design configurations for three different vendors (Sierracin/Sylmar, Swedlow Inc., and PPG Industries). Load-displacement time histories and high-speed motion picture coverage (5000 frames per second) were used to assist in the evaluation of test results. Test results were used to finalize the transparency cross-section, edge design, fastener selection, retaining strip material and configuration, and bearing strip design for the full scale test articles.

INTRODUCTION

The use of flight hardware for developing bird resistant crew enclosure structural systems is expensive in terms of time and money. Further, it often involves the sacrifice of flight hardware items for which there is a limited supply. Thus, the use of developmental tests at some reduced level is not a new concept.

Historically, the most common intermediate level test has been the bird impact testing of flat plates. Laboratory tests, in general, have not attempted to duplicate the combined loading state or the high strain rate conditions experienced during an actual bird impact event. Furthermore, from the Air Force's point of view, it is important to note that these tests have not been standardized. Therefore, any comparisons of capability among the various design options from which to choose has been difficult, if not impossible.

---

* The studies reported in this paper were performed for the Air Force Flight Dynamics Laboratory under Contracts F33615-75-C-3134 and F33615-76-C-3103.

PRECEDING PAGE BLANK-NOT FILMED

The screening test development and application reported herein is believed to be unique. The unusual features associated with this effort are as follows.

1) Test development and application was performed by an independent testing laboratory using Air Force funds.

2) The tests were developed specifically for the F-111 crew module taking into account known failure modes and design deficiencies associated with the BIRT transparency system.

3) Participation by transparency manufacturers was on a voluntary basis.

4) All screening test specimens were supplied and paid for by the manufacturers and remained the manufacturers' property.

5) All testing was paid for by the Air Force and test results became public information.

6) Care was taken by the Air Force and the University of Dayton to protect proprietary information associated with each manufacturer's design.

OBJECTIVE

The objective of this study was to develop relatively inexpensive laboratory test specimens and procedures which would be useful for screening candidate F-111 windshield transparency configurations for bird impact resistance.

TEST DEVELOPMENT

The F-111 crew module retrofit hardware was used as the baseline structure for defining the important transparency design parameters to be exercised. This structure consists of the MCAIR crew module, the BIRT [1] transparency, and the UDRI [2] arch reinforcement package. The qualification test results, including high speed (5000 frames per second) film coverage, for the flight hardware birdstrike qualification tests were studied. Structural response and failure mode as a function of impact location was categorized. From these results it was determined that the limiting structural component was the aft arch edge of the BIRT transparency during impact in the vicinity of the aft arch-center beam juncture. It was further determined that the important structural parameters for characterizing transparency performance are the structural integrity of the transparency edge and the stiffness of the center panel configuration.

For purposes of evaluating the capability of the candidate screening tests to discriminate between candidate designs, it

was deemed desirable to use two design configurations during the test development. The BIRT (PLEX 55 MOD) and Task II [1] configurations (reference Figure 1) were selected for this purpose. The Task II configuration was a leading candidate during the BIRT transparency development reported in Reference 1 and therefore it was expected to exhibit comparable capabilities. In addition, the use of the BIRT configuration was expected to provide additional information on the influence of design details on its performance during bird impact.

Initially, five tests were designated for evaluation as potential screening tests. The specimen design and the rationale for their selection is given in Reference 3. The tests, together with a brief description, are:

1) Simply Supported Three Point Flexure Test - utilized center panel configuration with geometry in accordance with ASTM D790-71; 16:1 span-to-depth ratio; width twice nominal thickness.

2) Short Beam Shear Test - utilized aft arch edge attachment cross-section; span-to-depth ratio 5:1; three point loading; variable end fixity.

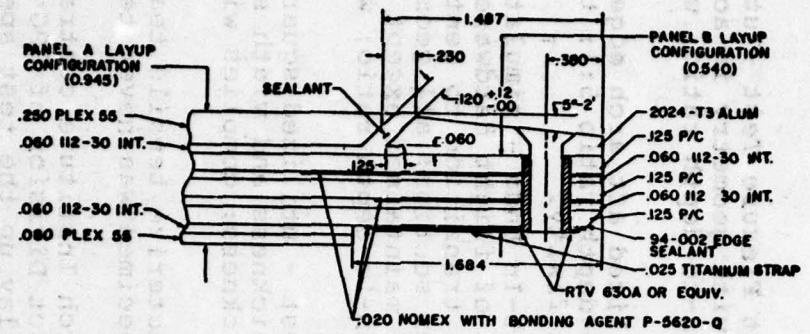
3) Long Beam Flexure with Built-In Ends - simulated actual transparency edge treatment of flight hardware in aft arch area at both ends with transition to center panel geometry through beam center section; all geometries and manufacturing processes maintained except for curvature; nominal 16:1 span-to-depth ratio; width to include two fasteners.

4) Longitudinal Compression Test - utilized square prism shaped geometry with the thickness and width set equal to the nominal laminate thickness; complies with ASTM D695.

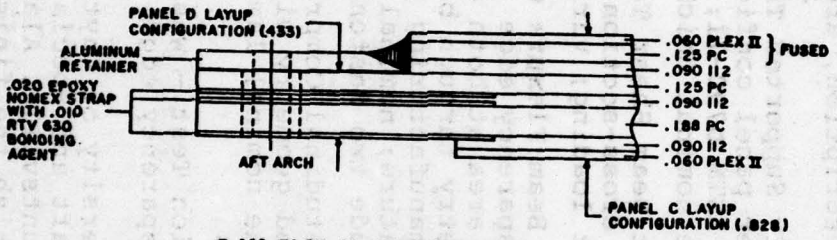
5) Tension Test - was to characterize tensile tear-out at transparency edge. This specimen was never tested.

The University of Dayton Research Institute contracted with the Aircraft and Specialty Product Division of PPG Industries, Inc., Huntsville, Alabama, to lay up the test specimen panels and furnish the finish machined test specimens. The University requested that the processing of the test specimen panels be identical (excluding curvature) to the processing techniques used in the fabrication of the actual aircraft transparencies. The finish machining of the test specimens was conducted in a manner to produce surfaces with low residual stress. The thickness of the specimens was not machined.

The University's high performance electrohydraulic closed-loop test system shown pictorially in Figure 2 was used to strain each test specimen. This system is centered around an



CURRENT F-111 BIRT WITH PLEXIGLASS 55 MODIFICATION CONFIGURATION



F-111 TASK II CONFIGURATION

Figure 1. BIRT and TASK II Transparency.

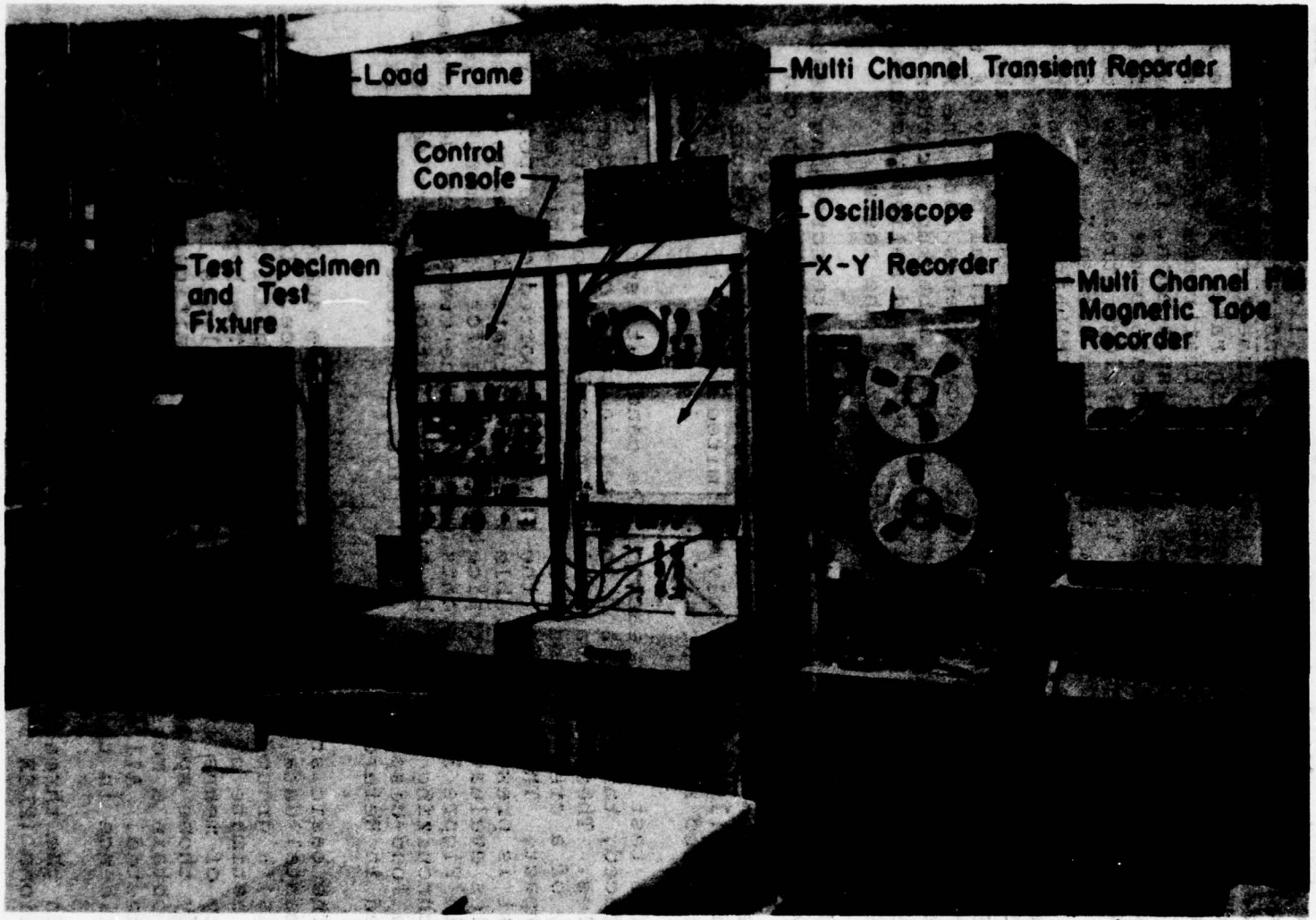


Figure 2. MTS Equipment.

electrohydraulic closed-loop test machine capable of being programmed in load, strain, and displacement control. With the machine in the displacement control mode a linear ramp function was used to strain each test specimen. Considering the geometry and loading of each specimen, the displacement rate was adjusted to produce the desired engineering strain rate. The machine is capable of producing displacement rates that range from less than 0.05 in/min to 5000 in/min. Ram displacement is measured using a Linearly Variable Differential Transformer (LVDT) while the specimen reacts against a four-arm bridge strain gage load cell. Included as part of the test system are an X-Y recorder, a multichannel FM tape recorder, and a multichannel transient recorder. Load and displacement data is recorded directly on the X-Y recorder for the low and medium speed tests. For the high-speed tests the data is stored in the digital memory of the transient recorder for playback at reduced speeds into the X-Y recorder. The FM tape recorder is used as a backup recorder on the high-speed tests. In addition, high speed motion picture coverage was used for a large percentage of the tests.

The test matrix for each of the candidate screening tests is shown in Table 1. Five specimens were tested at each condition to permit a statistical analysis of the test results. Because of the cost associated with the long beam flexure specimens with built-in ends, only a limited number of these specimens were procured and tested.

The test data for each of the candidate screening tests was reduced, tabulated, and analyzed in terms of a number of test variables. These test variables were selected to reflect the ability of a crew enclosure system to withstand a high energy bird impact. The data for the simply-supported three point flexure test is presented in Table 2 to illustrate the range of test variables evaluated. A typical test curve for Specimen A-7 is shown in Figure 3. The events noted on the curve were determined by synchronizing time on the high speed motion picture coverage and the load-displacement (time) plot. Complete test data is reported in Reference 3.

The basic statistical tool used in the analysis of the experimental data was an analysis of variance. In this type of analysis, a group of means are tested for equality based on a pooled estimate of the random error. When the hypothesis of equality of means is rejected, a second analysis is performed to identify those specific means which are significantly different and to obtain a measure of the magnitude of the difference which was detected. All tests were performed at the 95 percent level of confidence in this analysis.

In the three-point flexure experiments, two windshield configurations (PLEX 55 MOD (BIRT) and Task II) were tested at each

TABLE 1

TEST MATRIX

SIMPLY-SUPPORTED, THREE-POINT FLEXURE TEST MATRIX SPAN-TO-DEPTH RATIO = 16/1		
Maximum Fiber Strain Rate[1] ($min.^{-1}$)	Current F-111 BIRT with Plexiglass 55 Modification Edge Configuration	F-111 Task II Edge Configuration
0.0482	5[2]	5
4.82	5	5
48.2	5	5

COMPRESSION TEST MATRIX		
Engineering Strain Rate[1] ($min.^{-1}$)	Current F-111 BIRT with Plexiglass 55 Modification Edge Configuration	F-111 Task II Edge Configuration
0.0482	5[2]	5
4.82	5	5
48.2	5	5

SHORT-BEAM SHEAR TEST MATRIX SPAN-TO-DEPTH RATIO = 5/1		
Maximum Fiber Strain Rate[1] ($min.^{-1}$)	Current F-111 BIRT with Plexiglass 55 Modification Edge Configuration	F-111 Task II Edge Configuration
0.964	5[2]	5
9.64	5	5
96.4	5	5

NOTES:

1. Strain rate calculated for homogeneous and isotropic beam with the test specimen dimensions and for small deformations.
2. Denotes number of specimens tested at each strain rate.
3. All tests were conducted at 73°±2°F and 60±5 percent relative humidity.
4. Short-beam shear tests were modified as described in Reference 3.

LONG-BEAM FLEXURE WITH BUILT-IN ENDS TEST MATRIX				
Displacement Rate (in/min)	Bending Moment to Transverse Shear Ratio[1] (in-lb/lb)			
	3.78[3]	3.36[2]	2.10[2]	1.65[2]
2.0	2	1[4]	2	1
200.0	2	2		
2000.0	2	1		

NOTES:

1. Calculations assume small deformations.
2. Four point loading, bending moment to transverse shear ratios calculated for outer supports where the bending moment is maximum.
3. Three point loading, two fastener configurations tested at each displacement rate as specified in Reference 3.
4. Denotes number of specimens tested at each displacement rate.
5. Outer support span set at 16 times nominal laminate thickness.
6. All tests conducted at 73±2°F and 60±5 percent relative humidity.

TABLE 2

TEST DATA FOR THREE POINT FLEXURE DEVELOPMENT TEST

Spec. No.	Windshield Configuration	Max. Fiber Strain Rate[1] (min^{-1})	Accumulated Work to 5% Max. Fiber Strain (in-lb)	Accumulated Work to 10% Max. Fiber Strain[2] (in-lb)	Secant Stiffness at 2% Max. Fiber Strain (lb/in)	Secant Modulus of Elasticity at 2% Max. Fiber Strain (psi)	Ultimate Flexural Strength[3] (psi)	Strain at Fracture of Interior[5] Plexiglass Layer (in/in)
A-3	PLEX 55 MOD	.0482	780	1990	455	262,430	12,270	.039
A-11	"	.0482	830	2090	439	241,870	12,170	.057
A-30	"	.0482	910	2380	478	271,800	13,730	.071
A-31	"	.0482	900	2220	478	271,940	12,850	.055
A-37	"	.0482	800	-	422	233,200	12,690	.065
Mean (Std Dev)			840 (60)	2170 (170)	454 (24.5)	256,250 (17,780)	12,740 (620)	.057 (.012)
A-7	PLEX 55 MOD	4.82	880	2260	500	276,610	14,230	.037
A-10	"	4.82	1060	2590	574	317,740	14,390	.045
A-29	"	4.82	1040	2610	599	337,360	15,030	.038
A-34	"	4.82	1110	2610	612	340,190	14,600	.044
A-40	"	4.82	1000	2460	570	315,100	14,520	.042
Mean (Std Dev)			1020 (90)	2510 (150)	571 (43.3)	317,400 (25,430)	14,550 (300)	.041 (.004)
A-1	PLEX 55 MOD	48.2	1040	2580	587	317,210	14,580	.041
A-2	"	48.2	1040	2640	607	334,140	15,180	.038
A-8	"	48.2	980	2490	556	297,320	14,120	.043
A-9	"	48.2	1020	2540	584	316,670	13,990	.040
A-41	"	48.2	1030	2520	560	310,020	14,390	.044
Mean (Std Dev)			1020 (20)	2550 (60)	579 (21.0)	315,070 (13,340)	14,450 (470)	.041 (.002)
C-1	TASK II	.0482	490	1270	327	201,870	10,590	.062
C-3	"	.0482	470	1310	321	201,300	10,720	.068
C-11	"	.0482	460	1240	317	195,730	11,240	.056
C-34	"	.0482	460	1360	314	195,740	11,750[4]	.088
C-40	"	.0482	460	1330	316	195,380	11,760[4]	.088
Mean (Std Dev)			470 (10)	1300 (50)	319 (5.2)	198,000 (3,280)	11,210 (550)	.072 (.015)
C-10	TASK II	4.82	500	1430	383	237,470	13,450	.037
C-32	"	4.82	570	1490	385	237,570	13,220	.045
C-35	"	4.82	560	1480	373	230,600	13,460	.046
C-36	"	4.82	600	1350	386	238,560	13,960	.048
C-41	"	4.82	500	1750	387	231,920	13,740	.035
Mean (Std Dev)			560 (70)	1500 (150)	383 (5.7)	235,220 (3,670)	13,570 (290)	.042 (.006)
C-4	TASK II	48.2	710	1770	426	260,000	12,980	.041
C-7	"	48.2	790	1810	423	261,500	14,100	.039
C-13	"	48.2	750	1900	429	274,600	14,890	.039
C-33	"	48.2	710	1800	426	263,020	13,970	.041
C-38	"	48.2	700	1790	420	257,720	13,950	.040
Mean (Std Dev)			710 (20)	1810 (50)	425 (3.7)	263,370 (6,300)	13,980 (680)	.040 (.001)

[1] Stress and strain calculations based on homogeneous and isotropic beam with the test specimen dimensions.

[2] Interior plexiglass layer of all specimens failed prior to 10% strain, however maximum fiber strain based on original specimen configuration.

[3] Strength calculations per paragraph 10.2 ASTM D790-71.

[4] Ultimate stress occurred at fracture of interior plexiglass layer.

[5] Maximum fiber strain occurred in laminate interior layer for all specimens.

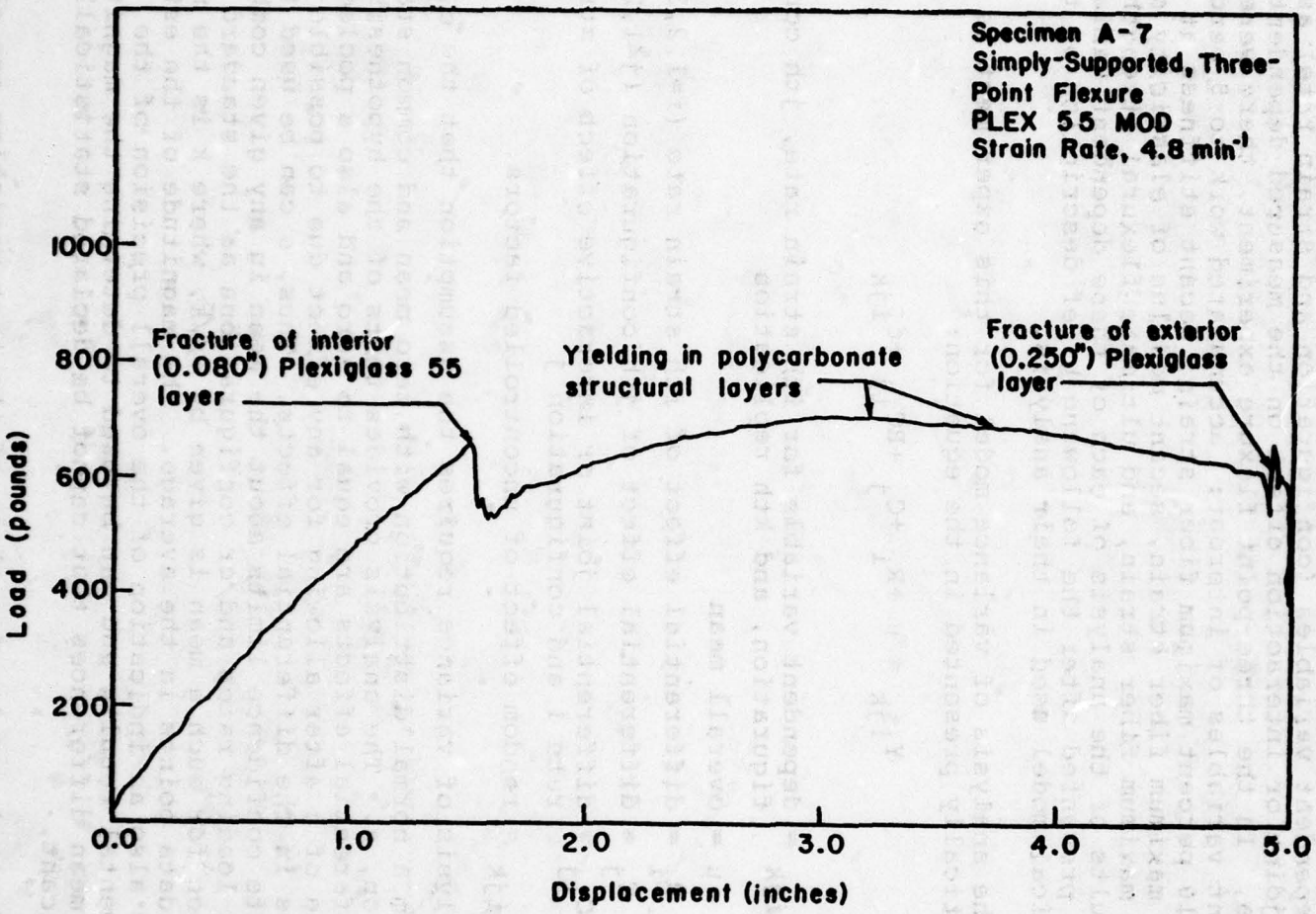


Figure 3. Test Curve for Specimen A-7.

of three maximum fiber strain rates (0.0482, 4.82 and 48.2 min^{-1}). Five specimens were tested at each combination of configuration and strain rate. This type of experiment is known as a factorial experiment with replications and permits an evaluation of each of the independent variables (configuration and strain rate) as well as the joint or interaction effect on the measured dependent variable. In the three-point flexure experiment, there were five dependent variables of interest: accumulated work to 5 percent and to 10 percent maximum fiber strain, secant stiffness at 2 percent maximum fiber strain, secant modulus of elasticity at 2 percent maximum fiber strain, and ultimate flexural strength. The results of the analysis of each of these dependent variables will be presented after the following brief description of the statistical model used in their analysis.

The analysis of variance model for this experiment is mathematically presented in the equation:

$$Y_{ijk} = \mu + R_i + C_j + RC_{ij} + \varepsilon_{ijk}$$

where

Y_{ijk} = dependent variable for ith strain rate, jth configuration, and kth replication

μ = overall mean

R_i = differential effect of ith strain rate (i=1,2,3)

C_j = differential effect of jth configuration (j=1,2)

RC_{ij} = differential joint or interactive effect of strain rate i and configuration j

ε_{ijk} = random effect of uncontrolled factors.

The analysis of variance requires the assumption that the ε_{ijk} are from a normal distribution with zero mean and common standard deviation, σ. The analysis provides tests of the hypothesis that the differential effects are equal to zero and also a pooled estimate of σ after allowing for any effect due to possible differences in the differential effects. Thus, σ can be used to calculate confidence limits about the mean in any given combination of loading rates and/or configurations as the standard deviation for such a mean is given by $\sigma/\sqrt{k}$, where k is the number of data points in the average. The magnitude of the estimate of σ is also an indication of the overall precision of the experimental results and can be used to determine the magnitude of the mean differences that cannot be declared statistically significant.

Typical results for three of the test variables are shown in Figures 4, 5, and 6. These figures show that there exists in general, a statistically significant difference as a function

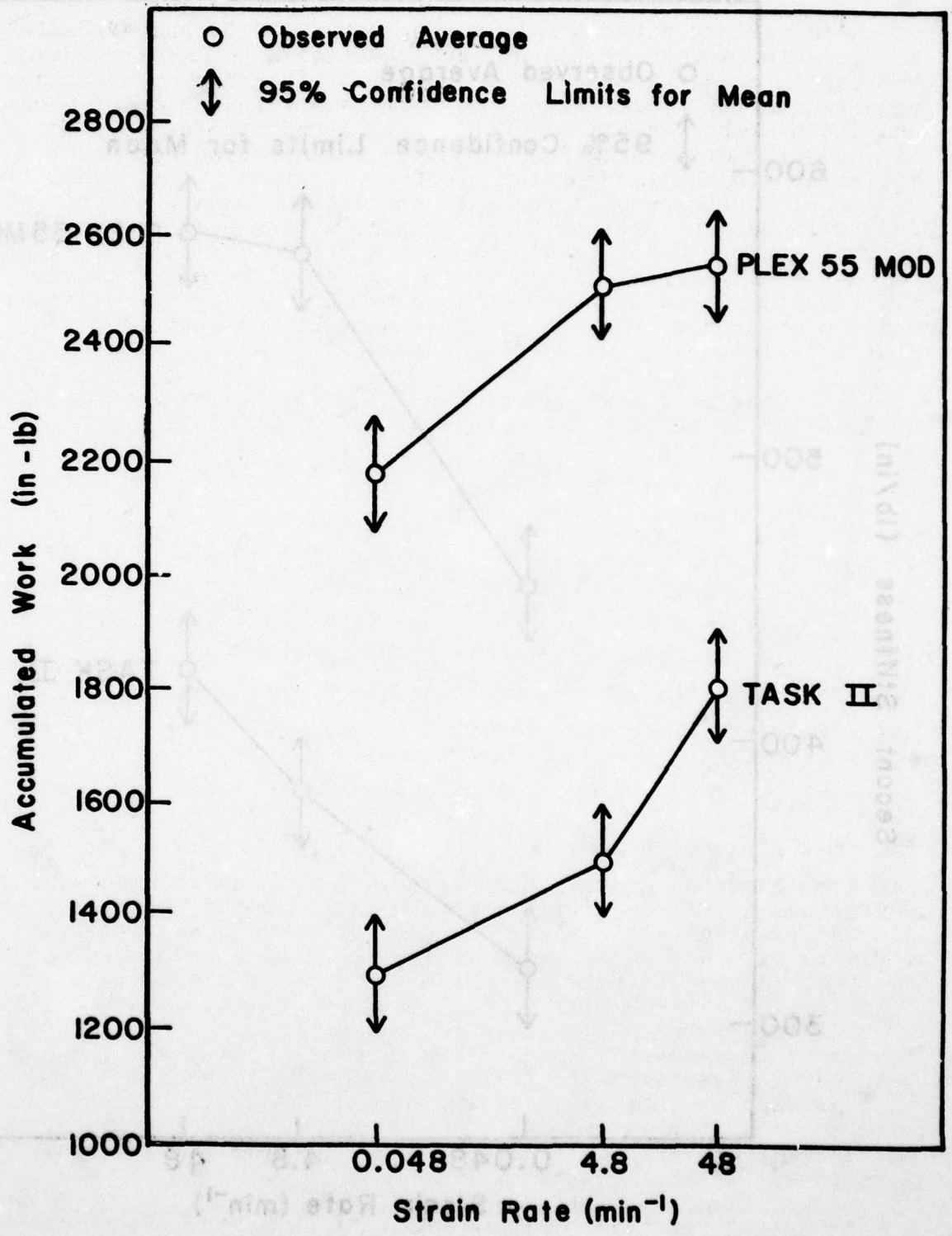


Figure 4. Statistical Results.

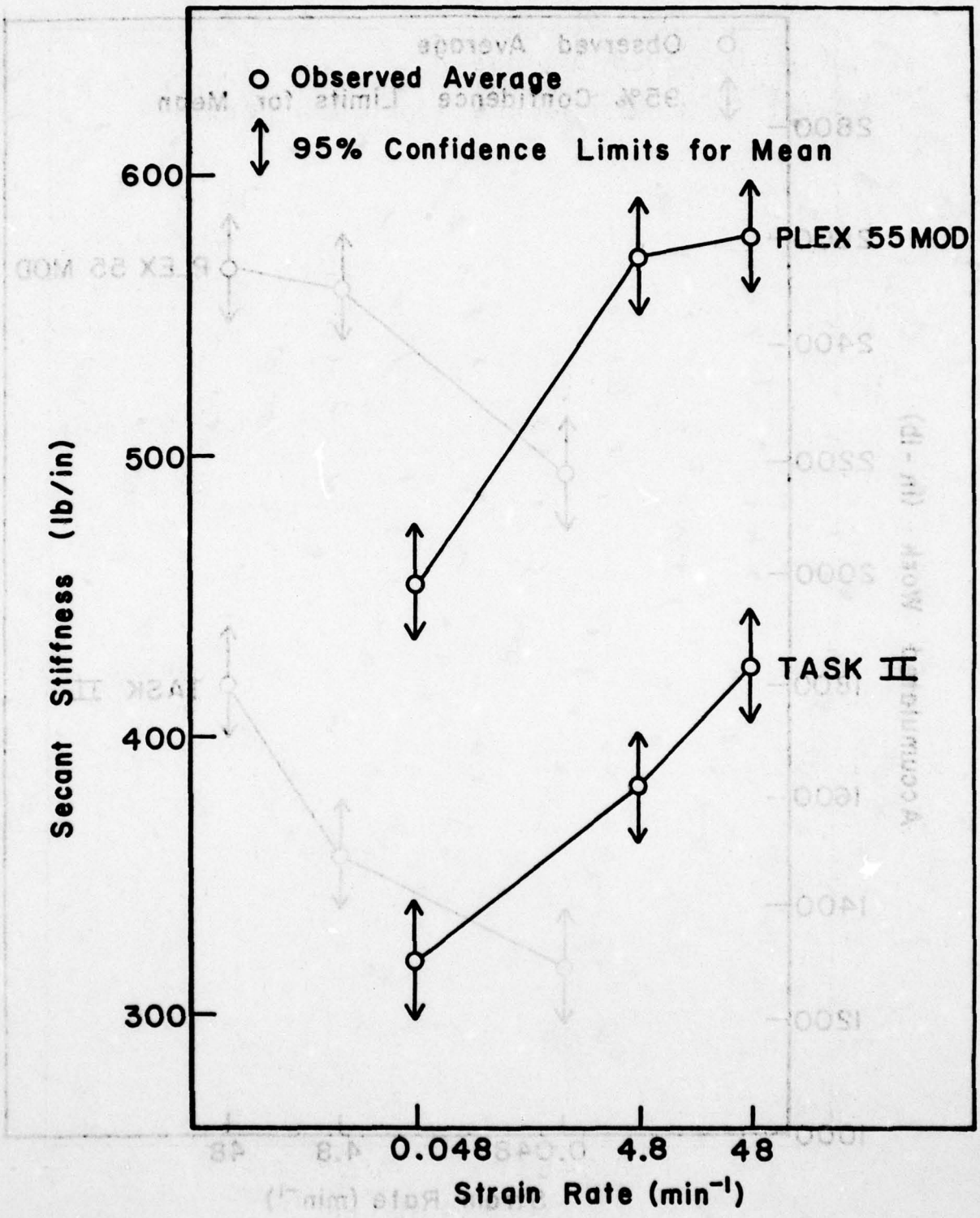


Figure 5. Statistical Results.

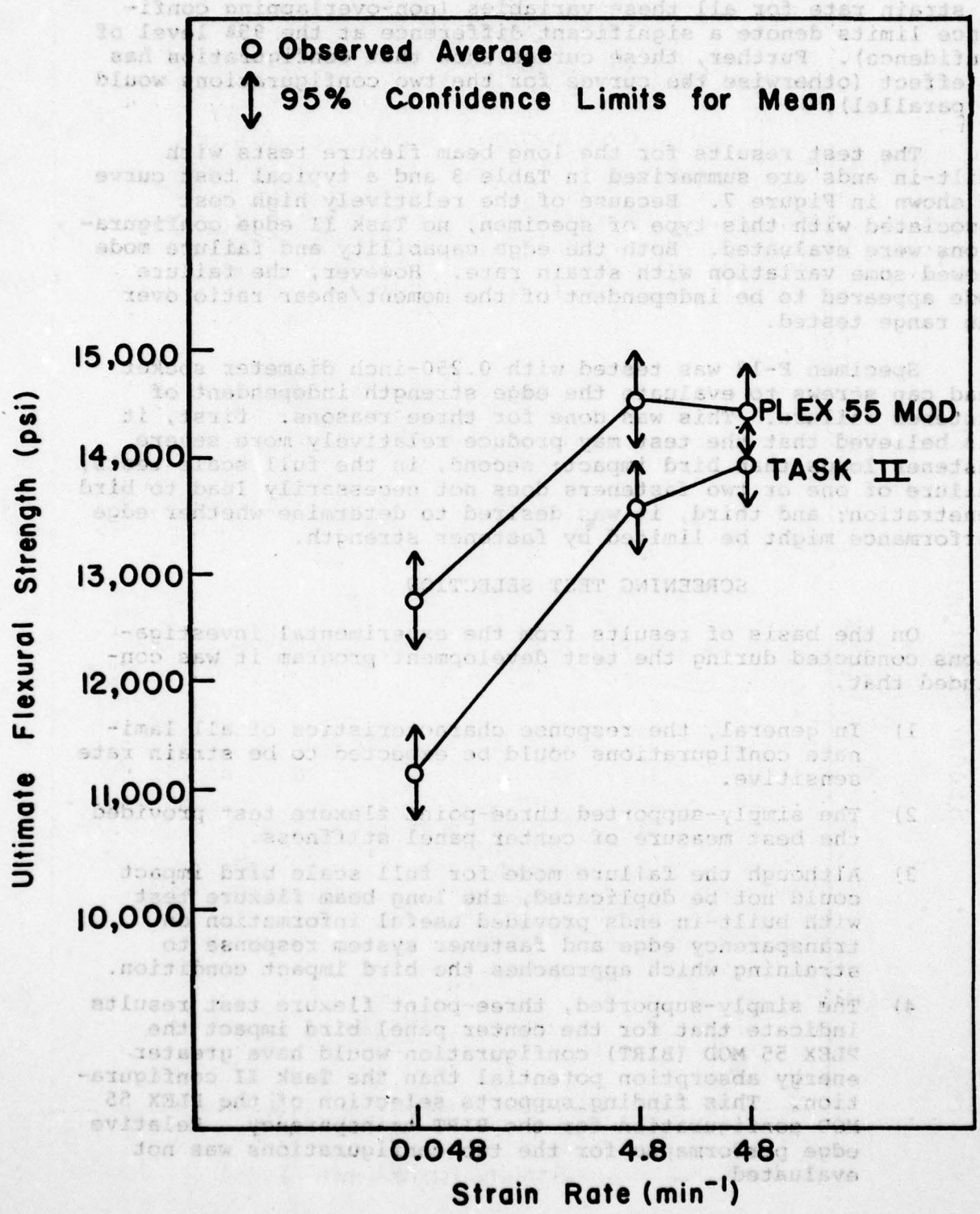


Figure 6. Statistical Results.

of strain rate for all these variables (non-overlapping confidence limits denote a significant difference at the 95% level of confidence). Further, these curves show that configuration has an effect (otherwise the curves for the two configurations would be parallel).

The test results for the long beam flexure tests with built-in ends are summarized in Table 3 and a typical test curve is shown in Figure 7. Because of the relatively high cost associated with this type of specimen, no Task II edge configurations were evaluated. Both the edge capability and failure mode showed some variation with strain rate. However, the failure mode appeared to be independent of the moment/shear ratio over the range tested.

Specimen E-17 was tested with 0.250-inch diameter socket head cap screws to evaluate the edge strength independent of fastener failure. This was done for three reasons: first, it was believed that the test may produce relatively more severe fastener loads than bird impact; second, in the full scale tests, failure of one or two fasteners does not necessarily lead to bird penetration; and third, it was desired to determine whether edge performance might be limited by fastener strength.

SCREENING TEST SELECTION

On the basis of results from the experimental investigations conducted during the test development program it was concluded that,

1) In general, the response characteristics of all laminate configurations could be expected to be strain rate sensitive.

2) The simply-supported three-point flexure test provided the best measure of center panel stiffness.

3) Although the failure mode for full scale bird impact could not be duplicated, the long beam flexure test with built-in ends provided useful information on transparency edge and fastener system response to straining which approaches the bird impact condition.

4) The simply-supported, three-point flexure test results indicate that for the center panel bird impact the PLEX 55 MOD (BIRT) configuration would have greater energy absorption potential than the Task II configuration. This finding supports selection of the PLEX 55 MOD configuration for the BIRT transparency. Relative edge performance for the two configurations was not evaluated.

TABLE 3

TEST RESULTS, FIXED-FIXED BEAM DEVELOPMENT TEST

Specimen Number	Moment/Shear Ratio (in-lb/lb)	Displacement Rate (in/min)	Failure Load (in)	Failure Deformation (in)	Work Accum. to Failure (in-lb)	Type of Failure (5)	Notes
E-5	3.78	2.0	3350	3.4	5040	P	1
E-14	3.78	200.0	1050	1.2	590	F	1,2
E-9	3.78	2000.0	2000	2.0	1780	F	1,2
E-19	3.78	2.0	2600	2.6	3300	P	
E-4	3.78	200.0	2450	2.2	2300	F	
E-15	3.78	2000.0	3000	2.6	3830	C	
E-17	3.78	1600.0	2950	2.5	3670	P	3
E-12	3.36	2.0	3000	2.2	3300	P	
E-6	3.36	200.0	3350	2.2	3760		4
E-11	3.36	200.0	3900	2.1	3670	P	
E-2	3.36	2000.0	4250	2.4	4960	P	
E-16	2.10	2000.0	3750	0.8	1540	F	
E-7	2.10	2000.0	4300	0.9	2040	F	
E-8	1.65	2000.0	5400	1.1	3520	F	

NOTES:

1. Specimens tested with a pin extension relative to ends of torqued collar of 0.0 (flush) to 0.5 threads.
2. Fastener failure occurred at the end of the hexagonal torque recess on the threaded shank of the pin. Remaining fastener failures occurred at the start of the thread engagement of the collar as described in Paragraph 2.4.5 of the text.
3. Tested with 0.250 inch dia. socket head cap screws (SHCS) in place of 0.190 inch dia. fasteners.
4. Complete fracture beneath loading nose.
5. Failure symbols definition: P = Pullout failure around aluminum bushings
   F = Fastener failure, see note 2
   C = Combination pullout and fastener failure

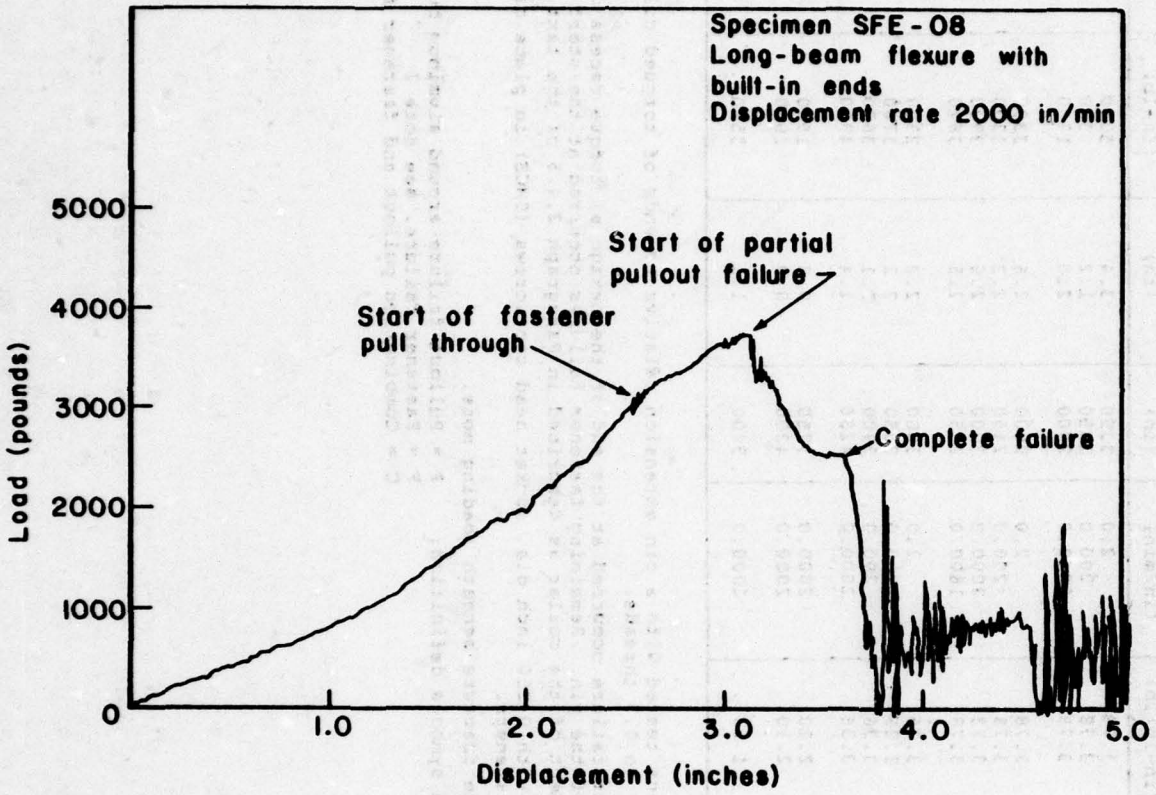


Figure 7. Fixed-Fixed Beam Test Results

5) The Plexiglass plies contribute appreciably to the overall laminate stiffness and energy absorbing characteristics. The laminates respond not as a homogeneous beam and not as a stackup of independent beams, but at some intermediate condition. Thus, the interlayer shear modulus is an important mechanical property in determining overall laminate behavior.

6) Comparison of results for specimens E-15 and E-17 indicates that the capability of the BIRT edge is not limited by fastener failure.

It was concluded that the use of the simply-supported, three-point flexure test and the long beam flexure test with built-in ends could provide useful information in screening candidate design configurations. Furthermore, a number of specific areas for possible improvement in the BIRT transparency edge performance were defined. These were: 1) improved adhesive bonding of the retaining strip and bearing strip, 2) elimination of or improved bonding of the Nomex reinforcements, 3) increased thickness of the bearing strip, 4) use of fasteners without a tool slot in the head, 5) configuration of the retainer strip to minimize the effects of the bird hydrodynamic forces, and 6) improved strength and ductility of fasteners.

SCREENING TEST APPLICATION

The selected screening tests were used to evaluate F-111 windshield and canopy candidate configurations under the alternate design development program (ADBIRT) initiated by the Air Force in June 1976. During the period September 1976 to April 1978, the University of Dayton has performed 104 F-111 screening tests for three transparency manufacturers: Sierracin/Sylmar, Swedlow Inc., and PPG Industries. These tests are summarized by type and manufacturer in Table 4.

Each manufacturer was responsible for defining candidate design configurations for testing. Freedom to vary basic configuration, material, edge design details, and fastener system was left to the discretion of the manufacturer within the general constraints established by the Air Force.

Copies of all raw data was made available to the manufacturer for his tests. In addition, the data was reduced, summarized, and interpreted by University of Dayton personnel. These results were reported orally to the appropriate manufacturer and to the Air Force. In addition, all results are documented in AFFDL-TR-76-101, Volume II (UDRI-TR-76-44, Volume II).

Test results for all tests are summarized in Tables 5 through 8. Pertinent observations, relating to the laboratory

TABLE 5

THREE POINT FLEXURE SCREENING TEST RESULTS

Laminate Configuration	Mean Bending Stiffness[1] (lb/in)/in	
	0.0482 min^{-1} Max. Fiber Strain Rate	48.2 min^{-1} Max. Fiber Strain Rate
BIRT with PLEX 55 MOD	246	313
Task II	130	181
S/S[2] 2 ply, SP int.	121	160
S/S 3 ply, SP int.	75	96
S/S 2 ply, S-100 int.	38	48
S/S 3 ply, S-100 int.	14	21
Swedlow 2 ply, silicone, 6622 int.	78	93
Swedlow 2 ply, 6640 int.	34	89
Swedlow 2 ply, 6622 int.	139	174
Swedlow 2 ply, 6640, 6641 int.	102	130
Swedlow 2 ply, 6641 int.	135	176
Swedlow 2 ply, 6641M int.	120	152
PPG 2 ply, 112-30 int.	-	188[3]
PPG 3 ply, 112-30 int.	-	132[3]
PPG 3 ply W Plex Inbd., 112-30 int.	-	249[3]
PPG 2 ply, 112-15, 112-30 int.	-	171
PPG 2 ply, silicone, 112-30 int.	-	126
PPG 2 ply, .125 Plex; .120 112-30 int.; .187 P/C; .060 112-30 int.; .250 P/C	-	159
PPG 2 ply, .125 Plex; .090 112-30 int.; .187 P/C; .090 112-30 int.; .250 P/C	-	170
PPG 3 ply, .125 Plex; .060 112-30 int.; .125 P/C; .030 112-30 int.; .125 P/C; .030 112-30 int.; .080 Plex	-	183
PPG 3 ply, .125 Plex; .090 112-30 int.; .125 P/C; .060 112-30 int.; .125 P/C; .090 112-30 int.; .125 P/C	-	176
PPG 3 ply, .125 Plex; .060 112-30 int.; .150 P/C; .030 112-30 int.; .150 P/C; .060 112-30 int.; .150 P/C	99	135

NOTES:

(1) Simply-supported, three-point flexure test (16/1 span/depth ratio). Secant stiffness at 2% max. fiber strain. Stiffness adjusted to BIRT specimen test fixture span assuming simple beam theory (48.2 min^{-1} span = 15.32 in., 0.0482 min^{-1} span = 15.55 in.).

(2) S/S = Sierracin/Sylmar design.

(3) These test specimens were fabricated from actual windshield transparencies. The longitudinal axis of the specimens was parallel to the center beam.

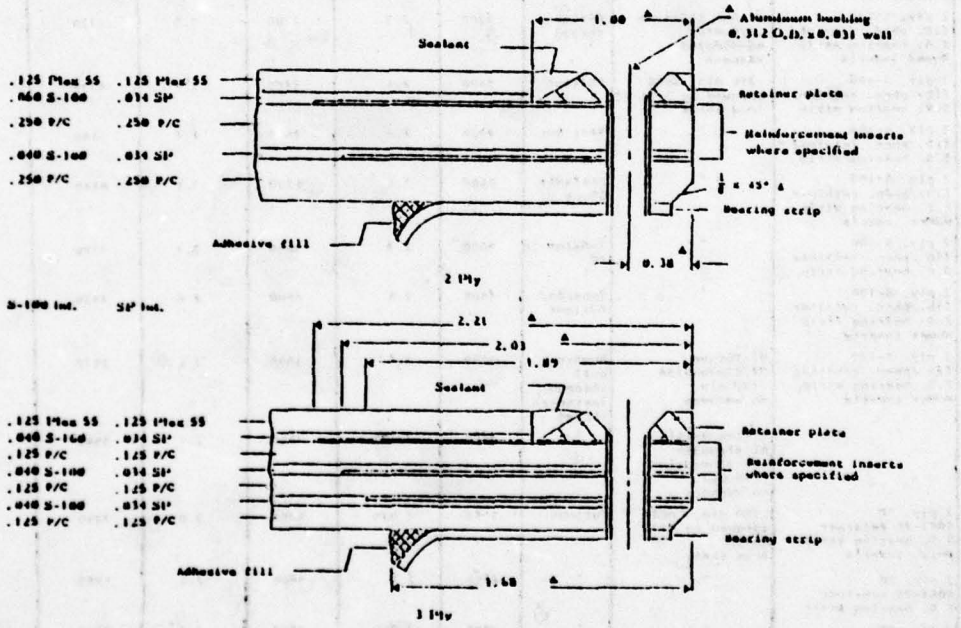
TABLE 6

SIERRACIN FIXED-FIXED BEAM

Specimen Number	Specimen Configuration	Fastener Configuration	Failure Type	Ultimate Load (lb)	Ultimate Deformation (in)	Failure Load (lb)	Failure Deformation (in)	Work Accumulated to Failure (in-lb)
FD999-B1	2 ply,S-100 fib./phen. retainer S.S. bearing strip	Hi-Lok titanium .190 dia. dimpled washers	Fastener Thread	1800	1.9	1800	1.9	1800
FD999-B4	"	"	"	2275	1.925	2200	2.0	1840
FD999-B6	" 4061-T6 bearing strip	"	"	2000	1.775	2000	2.0	1770
FD1009-B2	2 ply, SP 4061-T6 retainer S.S. bearing strip	"	"	1800	1.8	1800	1.8	1590
FD999-B7	2 ply, S-100 fib./phen. retainer & bearing strip	"	"	1975	1.95	1800	2.0	1700
FD993-B3	3 ply, S-100 fib./phen. retainer S.S. bearing strip	"	"	3300	2.4	3300	2.4	2620
FD993-B5	"	.250 dia. SHCS torqued to 5 ft-lb short shank	" "	3700	2.2	3700	2.2	2740
FD999-B6 retest	2 ply,S-100 fib./phen. retainer no bearing strip	Hi-Lok titanium .190 dia. dimpled washers	Fastener/ thread pullout	1925	2.4	1800	2.0	2000
FD999-C4	2 ply, S-100 fib./phen. retainer S.S. bearing strip Nomex inserts	Hi-Lok titanium .190 dia. no-dimpled washers	Fastener thread	2200	2.5	2200	2.5	2320
FD993-B4	3 ply, S-100 fib./phen. retainer S.S. bearing strip	.250 dia. SHCS torqued to 5 ft-lb long shank	Pullout	4400	2.6	4400	2.6	4320
FD999-B5	2 ply, S-100 fib./phen. retainer S.S. bearing strip	"	Tear Out	4600	2.4	4600	2.4	3840
FD999-C1	2 ply, S-100 fib./phen. retainer S.S. bearing strip Nomex inserts	"	Fastener Shank	6500	3.1	6500	3.1	8140
FD999-B2	2 ply, S-100 fib./phen. retainer S.S. bearing strip	"	Tension in PC	4600	2.4	4600	2.4	3780
FD993-C2	3 ply, S-100 fib./phen. retainer S.S. bearing strip Nomex inserts	"	Tension/ Pullout	4800	2.6	4800	2.6	4420
FD993-C5	3 ply, S-100 fib./phen. retainer S.S. bearing strip Nomex inserts	Hi-Torque Hi Elongation .190 dia. no washers	Bushing pull through/ fastener thread	3000	2.6	3000	2.6	2970
FD993-C4	"	Hi-Lok H-111 Hi strength low elongation .190 dia. no washers	"	3850	2.725	3800	2.7	3580
FD1009-C3	2 ply, SP 4061-T6 retainer S.S. bearing strip poly. inserts	.250 dia. SHCS torqued to 45 in-lb long shank	Pullout	5050	2.925	5000	3.0	7290
FD1009-B1	2 ply, SP 4061-T6 retainer S.S. bearing strip	"	"	4850	2.8	4800	2.8	5950
FD1010-C7	3 ply, SP 4061-T6 retainer S.S. bearing strip poly. inserts	"	"	4800	3.0	4800	3.0	5880
FD1010-B3	3 ply, SP 4061-T6 retainer S.S. bearing strip	"	"	4400	2.7	4400	2.7	4740
FD999-C2	2 ply, S-100 fib./phen. retainer S.S. bearing strip Nomex inserts	.250 dia. SHCS torqued to 45 in-lb long shank	Fastener Shank	5000	2.8	5000	2.8	6330

TABLE 6 (Concluded)

Specimen Number	Specimen Configuration	Fastener Configuration	Failure Type	Ultimate Load (lb)	Ultimate Deformation (in)	Failure Load (lb)	Failure Deformation (in)	Work Accumulated to Failure (in-lb)
ED1009-C1	2 ply, SP 6061-T6 retainer S.S. bearing strip poly. inserts	-	-	5175	2.9	5100	2.9	6580
ED993-C1	3 ply, S-100 fib./phen. retainer S.S. bearing strip Nomex inserts	-	Tension/ Pullout	5000	2.8	5000	2.8	5800
ED1010-R1	3 ply, SP 6061-T6 retainer S.S. bearing strip	-	Pullout	4300	2.8	4300	2.8	4860
ED1010-C3	3 ply, SP 6061-T6 retainer S.S. bearing strip poly. inserts	-	-	4700	2.7	4700	2.7	5160
ED1009-R3	2 ply, SP 6061-T6 retainer S.S. bearing strip	-	-	4900	2.85	4900	2.8	6990



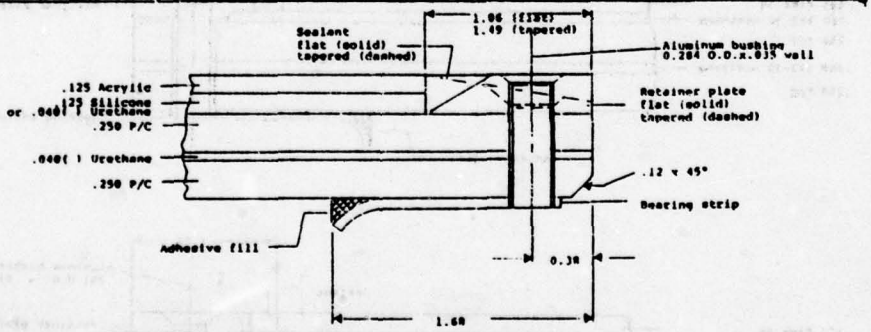
A Dimensions common to all Sierracin/Sylmar configurations

All Dimensions are inches

TABLE 7

SWEDLOW FIXED-FIXED BEAM

Specimen Number	Specimen Configuration	Fastener Configuration	Failure Type	Ultimate Load (lb)	Ultimate Deformation (in)	Failure Load (lb)	Failure Deformation (in)	Work Accumulated to Failure (in/lbs)
SFE-03	2 ply, 2-.040 (6022) urethane, flat fib./ phen. retainer, .063 S.S. bearing	NAS 1221-7 E 10 bolt ML 1386-6 nut AN960 D10 washer 2-threads protruding	Fastener head	2700	2.475	1700	3.300	4600
SFE-02	2-ply, 1-.125 sil., 1-.040 (6622) urethane flat fib./ phen. retainer .063 S.S. bearing	HLT413LP-6-10 bolt HL1386-6 nut AN960 D10 washer Flush	Fastener at end of hex torque recess	770	1.075	770	1.075	420
SFE-05	2-ply, 2-.040 (6622) urethane, tapered fib./phen. retainer, .063 S.S. bearing	HL117-6-16 bolt MB21043-7 nut AN960 D10 washer 3-threads protruding	Fastener pull thru/ pullout	3750	3.125	2520	3.600	6560
SFE-06	Same as SFE-05	Same as SFE-05	Fastener pull thru/ pullout	3800	3.050	2450	3.500	6450
SFE-04	Same as SFE-03	.250 dia SHCS torqued to 45 in-lb	Fastener shank	4950	2.713	4950	2.713	5600
SFE-13	2-ply, 2-.040 (6640) urethane, flat fib./ phen. retainer, .063 S.S. bearing	HL21PB-6-18 bolt HL1386-6 nut Flat washers 3-threads protruding	Fastener shank	3200	2.650	2700	2.825	3450
SFE-15	2-ply, 2-.040 (6641) urethane, flat fib./ phen. retainer, .063 S.S. bearing	Same as SFE-13	Fastener shank/ thread	2400	2.700	2400	2.700	3050
SFE-12	Same as SFE-13	Same as SFE-04	Pullout	4500	2.525	4500	2.525	3910
SFE-14	Same as SFE-15	Same as SFE-04	Pullout	5050	2.875	4750	3.100	6630
SFE-11	2-ply, 1-.125 MT sil., 1-.040 (6622) urethane, flat fib., phen. retainer .063 S.S. bearing	HL21PB-6-18 bolt MB21043-3 nut 3-threads protruding	Fastener shank	3550	2.750	3550	2.750	4040
SFE-10	Same as SFE-11	Same as SFE-17	Fastener shank	3400	2.750	3400	2.750	3600
SFE-16	Same as SFE-17	Same as SFE-04	Pullout	4950	2.675	4950	2.675	5220
SFE-18	Same as SFE-17	HLT413LP-6-18 bolt MB 21043 nut Flat washers 3-threads protruding	Fastener thread	1250	1.300	1200	1.475	990



GENERAL NOTES:

1. Bearing Strip
   a. S.S. = 0.063 MIL-S-5059 Comp 301 CRES
2. Fastener
   a. .250 SHCS = 0.250 dia Socket Head Cap Screws
      UTS = 170,000 psi min.
3. All specimens tested at 1000 in/min displacement rate

All dimensions are inches

AD-A065 049 AIR FORCE FLIGHT DYNAMICS LAB WRIGHT-PATTERSON AFB OHIO F/G 1/3
CONFERENCE ON AEROSPACE TRANSPARENT MATERIALS AND ENCLOSURES (1--ETC(U)
DEC 78 R E WITTMAN

UNCLASSIFIED AFFDL-TR-78-168 NL

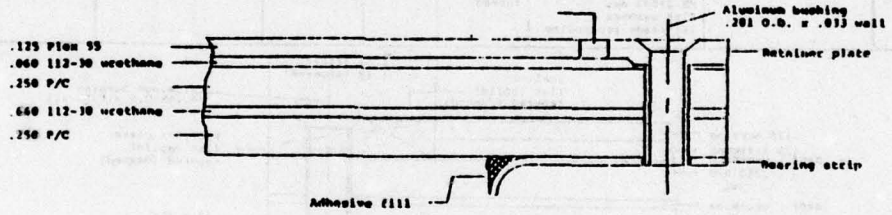
5 OF 10
ADA
065049

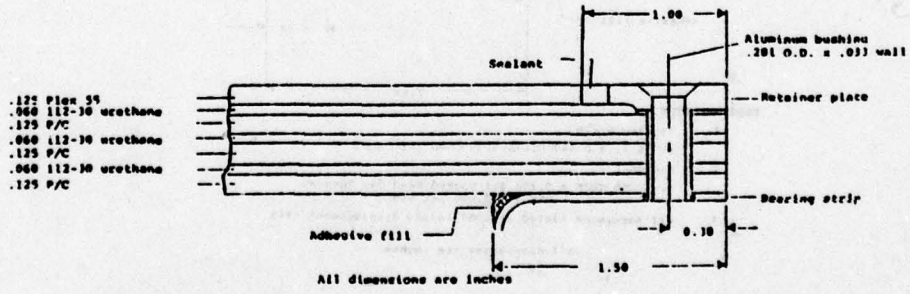


TABLE 8

PPG FIXED-FIXED BEAM

Specimen No.	Specimen Config.	Fastener Config.	Failure Type	Ultimate Load (lb)	Ultimate Deform. (in)	Failure Load (lb)	Failure Deform. (in)	Work Accum. to Failure (in-lb)
2-A	0.125 Plex 55 0.060 112-30 0.250 P/C 0.060 112-30 0.250 P/C	NAS 1221-3E10S AN960-D10 MS 21043-3	Pullout/ Fastener	3500	3.275	3500	3.275	9640
2-B	Soft Al. retainer S.S. bearing strip	0.250 SHCS	Pullout	3500	2.625	3500	2.625	4290
2-1-C	Same as 2A & 2B but with Hard Al. retainer	Same as 2A	Fastener head	3050	2.325	1350	3.300	4920
4-A	0.125 Plex 55 0.060 112-30 0.125 P/C 0.060 112-30 0.125 P/C	0.250 SHCS	Pullout	3100	2.325	3000	2.550	3700
4-B	0.060 112-30 0.125 P/C Soft Al. retainer S.S. bearing strip	Same as 2A	Pullout	2950	2.750	2950	2.950	4490
4-1-C	Same as 4A & 4B but with Hard Al. retainer	Same as 2A	Fastener head	1900	2.440	1450	2.900	1830
1-A	0.125 Plex 55 0.060 112-30 0.250 P/C 0.060 112-30	HLT413LP-4-17 AN960-D10 MS21043-3	Fastener shank	2950	2.525	2950	2.525	3260
1-B	0.250 P/C Phenolic/glass retainer S.S. bearing	Same as 2A	Pullout/ Fastener	2750	2.625	1050	3.300	4410
1-HC	0.125 Plex 55 0.060 112-30 0.250 P/C 0.060 112-30	Same as 1A	Fastener	3200	2.450	3200	2.450	3890
1-HD	0.250 P/C Soft Al. retainer w RTV 630 S.S. bear. w HE 17924 A/B	Same as 2A	Fastener shank	1750	2.725	3360	2.900	4650





GENERAL NOTES:

1. Bearing Strip
   a. S.S. = 0.030 1/4 H Stainless Steel
2. Fasteners
   a. 0.250 SHCS = 0.250 dia. Socket Head Cap Screw
      UTS = 170,000 psi min

screening tests and subsequent full scale bird qualification tests, tests, are summarized below.

1) Laminate stiffness can be varied over a wide range for the same basic configuration by varying interlayer material and thickness.

2) Acrylic outer and inner plies have a significant influence on structural response prior to their failure.

3) The bearing strip and retaining strip have a significant influence on edge performance. Proper design and bonding procedures can alter edge strength by a factor of two.

4) Important design parameters affecting bearing strip design are bending stiffness, width, tear-out strength, and adhesive bonding strength.

5) Important design parameters affecting retaining strip design are length, stiffness, bolt pull-through resistance, tensile strength, and adhesive bonding strength.

6) Fastener strength, ductility, and head geometry are important design parameters.

7) Edge bending loads and fastener tensile load can be effectively relieved through controlled broaching of the fastener through the retaining strip.

8) For the F-111 aft arch edge, tensile tear-out of the inside polycarbonate ply is an important failure mode. Thus, inside ply thickness, bearing strip tear-out strength, and bearing strip adhesive strength are important (edge distance on the polycarbonate is not a design variable).

9) Reinforcing strips imbedded in the interlayer can be used to increase strength. However, if bonding is poor the net result will likely be a decrease in edge capability.

10) A relatively tight fit on fasteners, bushings, etc. tends to result in better edge performance.

11) A large amount of inelastic behavior prior to failure generally indicates a good edge design within the limits imposed by the materials used.

CONCLUDING REMARKS

The tests conducted here and comparison with prior and subsequent full scale bird impact tests have demonstrated that:

1) Simple, properly designed laboratory tests can define design deficiencies and provide useful information for correcting these deficiencies.

2) The screening tests performed provided qualitative data which generally correlated with capability exhibited during full scale bird impact tests on flight hardware.

3) Performance is better characterized if tests are conducted at intermediate or high strain rates.

4) Such standardized tests can provide the Air Force with information for evaluating the potential success of candidate design configurations and thus reduce the amount of full scale developmental testing required.

5) A good design is a proper blend of all components such that they complement each other to form a well behaved structural unit. Thus, a "good fastener", a "good retainer strip", etc., can only be defined in terms of the characteristics of all the parts comprising a transparency edge.

REFERENCES

1. Littell, H. Edward, Improved Windshield and Canopy Protection Development Program, AFFDL-TR-74-40, May 1974.

2. West, Blaine S., Design and Testing of F-111 Bird Resistant Windshield/Support Structure, Volume I - Design and Verification Testing, AFFDL-TR-76-101, October 1976.

3. Johnson, Paul E., Design and Testing of F-111 Bird Resistant Windshield/Support Structure, Volume II - Mechanical Properties Testing, UDRI-TR-76-44, University of Dayton Research Institute, Dayton, Ohio, December 1976 (currently being revised to include latest test data. Will be published as AFFDL-TR-76-101, Volume II).

THE FRACTURE TOUGHNESS OF POLYCARBONATE: A PRELIMINARY REPORT

S. A. Sutton
Naval Research Laboratory
Mechanics of Materials Branch
Washington, DC

PRECEDING PAGE BLANK-NOT FILMED

THE FRACTURE TOUGHNESS OF POLYCARBONATE:

A Preliminary Report

by

Stephen A. Sutton

Naval Research Laboratory
Code 8433
Washington, D.C. 20375

ABSTRACT

Polycarbonate has become a material of great interest and of some controversy in aircraft transparency applications. The application of fracture mechanics to this material provides a powerful means to characterize its toughness. The plane strain fracture toughness, Kic, or the plane stress fracture toughness, Kc, (these are referred to collectively as "Kc/Kic fracture toughness" in this paper) provide a valuable assessment of toughness to be used for material selection or structural design purposes.

This paper reports the progress of an investigation to provide a definitive Kc/Kic fracture toughness profile of polycarbonate subjected to a variety of environmental and loading conditions. A baseline series of Kc/Kic fracture toughness tests was conducted to determine how well and under which conditions Kc/Kic fracture toughness testing can be applied to this material.

Early results indicate that polycarbonate is a suiteable material on which to perform Kc/Kic fracture toughness tests. The data shows a marked dependence of Kic and Kc upon loading rate, thickness, and testing temperature and indicate that reproducible results can be obtained.

PRECEDING PAGE BLANK-NOT FILMED

I. INTRODUCTION

The characterization of the fracture toughness of stretched acrylic was recently completed by the author [1]. The purpose of the stretched acrylic research was two-fold: firstly to determine the fracture behavior of the material as characterized by its Kc/Kic fracture toughness and influenced by a variety of loading parameters, and secondly to develop guidelines to be used in a subsequent revision of MIL-P-25690 which is the current specification for "K-factor" tests (actually the K-factor is a Kc). This paper describes the background, experimental procedure, and the results of a series of baseline tests to extend this research to polycarbonate. The early tests reported in this paper are designed to provide a definitive set of data illimination the behavior of the material under a variety of thicknesses, temperatures, and relatively high loading rates.

Fracture toughness is defined as a particular way of measuring a very important strength property of a material: its "toughness". Fracture mechanics defines this toughness as the resistance of a material to the propogation of a sharp crack.

There are three distinct concepts in fracture mechanics of interest. The Stress Intensity Factor (K) is a number that provides a measure of the intensity of the stress field in the small area immediately surrounding a sharp crack in a body under load. The value of K that will cause the crack to propogate suddenly in an "unstable" manner is called the Critical Stress Intensity Factor (Kic or Kc). The Plane Strain Stress Intensity Factor (Kic) applies to materials whose thickness is greater than a certain minimum (for the thru-crack configuration shown in figures 1 and 2). The Kic is considered a material property and is independent of thicknesses above the lower limit.

The measure of toughness for thin specimens is affected (increased) by the thinness of the specimens, and the critical stress intensity is given as the plane stress fracture toughness, Kc. This Kc measure is not considered a unique material property since it is thickness dependent. Therefore it is always preferable to test specimens of sufficient thickness to insure a valid Kic measure.

Fracture toughness has excellent portability in that the toughness measures from various sources can be easily and accurately compared, and can be used in a variety of design situations. A more thorough treatment of the fundamentals of fracture toughness and its particular application to aircraft transparency design is given in references 3, 5, and 6.

FRACTURE TOUGHNESS AND DUCTILITY

The relationship between fracture toughness and ductility (as measured by the yield stress) needs to be noted. Many research projects (eg. [4,8]) have assessed the effect of various parameters upon the strength of polycarbonate and a favorite, and indeed important, parameter is the yield strength, which may be measured by a number of standardized tests. Very often these endeavors will determine that the yield strength is decreased as a result of certain factors, such as the application of high forming temperatures. In effect the material is rendered more ductile by these factors as reflected in a decreased yield stress. However, a decrease in yield strength will quite often lead to an increase in fracture toughness. Again the correlation between ductility and high fracture toughness is relatively common knowledge.

The problem arises when the word "yield" is dropped from the beginning of "yield strength" and reports are made of the "strength" being adversely affected by certain factors when in fact the "fracture strength" is being favorable affected. Of course there is no guarantee that the fracture toughness is not adversely affected simply because the yield stress is, but this relationship should always be kept in mind when dealing with "yield" strength and "fracture" strength.

III. MATERIAL AND EXPERIMENTAL

The techniques in specimen design and preparation, testing, and interpreting the results developed in the stretched acrylic research [1] were extended to polycarbonate which has the advantage of providing a technique that evaluates these two materials on an equal basis.

MATERIAL

The material used in these present baseline series of tests is a standard, aircraft grade polycarbonate. The difficuly with obtaining material of various thicknesses to be used in a highly controlled research program is that one is never really sure whether the results from different thicknesses are actually a result of the thickness, or if they are a result of the differrent processing technique for the different thicknesses. In these early tests it is important to assure that the material does not vary from test to test.

To solve this problem, three sheets of 3/4-inch polycarbonate were chosen that were produced under identical conditions, and this material was then machined to provide the thinner specimens of 1/4-inch, 1/2-inch, as well as the original 3/4-inch. The machining was very carefully done to avoid any heat build-up in the material. Specimens of each thickness were distributed among these three sheets and position in the sheet noted for future reference.

One of the problems encountered in Kc/Kic fracture toughness testing is in the variability of the results, or scatter. The best technique for coping with this inherent scatter is to conduct a set of identical tests and average the results to provide a single, very reliable data point. In the present set of tests the following methodology was adopted to reduce the influence of scatter in the tests. Whenever a toughness test was performed, it was performed identically (ie. same thickness, loading rate, environment, etc.) on a set of specimens (usually 6 in number), and the specimens were evenly distributed from among the three original sheets of the polycarbonate. The results were then averaged to provide one averaged data point. The result is that "material" is kept very consistent throughout the testing program and the variance in the toughness can better be assured to come from the changes in thickness, loading rate, or temperature and not from material variation among the specimens.

SPECIMENS

The compact tension specimen that proved very valuable in the earlier stretched acrylic research was used in the polycarbonate tests. This is a popular and reliable fracture mechanics specimen that has been well analyzed by Srawley, et.al. [3,6] and is very similar to the ASTM E399 specification for the compact tension specimen [5]. The geometry is shown in figure 1 and an overall dimension of 2-inch by 2-inch was chosen with a H/W ratio of 0.6.

The precrack was prepared by first machining a square-bottomed notch and then initiating the sharp natural crack that extended from approximately 4 to 8 mm beyond the base of the notch. The ability to easily produce this sharp natural precrack in polycarbonate has traditionally been a vexing problem. The technique developed to precrack the polycarbonate in this current research proved reliable and fewer than 5% of the specimens so precracked were unuseable. In addition, the precracks were quite even and their depth could be reliably controlled.

These cracks were produced by a small razor blade held in a light-weight, self-aligning fixture (figure 3) that is designed to allow the blade to penetrate only a small, fixed distance (approximately 1 mm) into the material. The impact was produced by a small, light hand-held hammer, and although a mechanical impact device such as a falling weight might produce slightly more consistent results, the manual technique worked very well.

There are a few critical points to this technique. The only razor blade found satisfactory was a stainless steel commercial "injector" blade and a single blade would generally produce 5-10 good precracks. The blade holding fixture must be relatively light weight (about 150 grams), self aligning, and must not allow the blade to penetrate beyond a certain small, fixed depth. This is shown schematically in figure 3.

It was found, interestingly, that this technique that works well for polycarbonate does not produce acceptable results in the stretched acrylic.

LOADING APPARATUS

The loading apparatus used in these polycarbonate tests is shown schematically in figure 2. The fixture is similar in principle to that used in the previous stretched acrylic tests, but was modified to provide more accurate load control and data measurement at the higher loading rates necessary to assure an unstable fracture (as opposed to slow-growth type fracture) in the ductile polycarbonate. The primary actuator is a servo-controlled (load control) hydraulic actuator where the force applied to the specimen and the opening displacement (and of course time) can be

measured continuously during the test.

This testing system is capable of accurately measuring failures that occur in about 1/10 of a second which is the upper bound for loading rate in these current tests, but has the potential for somewhat higher rates. This speed represents a two order-of-magnitude increase over those used for the stretched acrylic tests and better represents the impact loading conditions often seen in service for these materials.

The tests were performed under a completely automated computer-controlled testing system. Briefly, a large time-shared computer with which the experimenter interacts, remains in global control of the experiment. The actual real-time experimentation, however, is relegated to a smaller satellite mini-computer that is dedicated to the real-time portion of the experiment (ie. the breaking of the specimen). The larger "host" computer retains global control of the satellite across a communication link (that could be, for example, a telephone line) and the host handles all the background activities such as operator communication, pre- and post-processing of the raw data, and storage and display of the final, processed results.

This data acquistion system is the subject of independent papers that are cited in the references [2,7,9].

IV. TESTS AND RESULTS

These tests are intended to be a baseline set of Kc/Kic fracture toughness tests for polycarbonate. They are carefully cotrolled tests on a fixed material the purpose of which is to determine under what conditions valid Kc and/or Kic measurements can be obtained. The limits at which the material can be sucessfully and practically tested, and any immediately obvious problems that may occur over these ranges of experimental parameters is explored.

THICKNESS

Three thicknesses were chosen for these tests: 1/4-inch, 1/2-inch, and 3/4-inch. The 3/4-inch specimens appear to produce the plane-strain condition required for a strictly accurate Kic determination (as reflected in the data presented below), while the 1/4-inch material apparently does not produce this condition. Therefore the measure of toughness derived from the thick specimens represents a valic Kic, while the thin specimens yield a Kc value that is a measure of toughness but is affected (increased) by geometry factors in the thin specimens.

The 1/2-inch specimens represent a practical testing thickness since they are thin enough to produce a well-behaved, even precrack, yet thick enough to be in plane strain and produce a valid Kic value, as demonstrated by the results discussed below.

LOADING RATE

Loading rates were chosen to produce failures in the range of 0.1 to 10 seconds. Technically the loading rate in these tests is expressed as a K-rate, the rate at which the stress intensity factor (K) increases with time. This rate is proportional to the slope of the force-time trace for the test. Although K-rate is the technically correct measure of loading rate, time-to-failure will often be used below since it provides a better qualitative measure of the duration of the test.

The time-to-failure lower limit of 0.1 seconds represents a constraint of the testing machine, while the 10 second limit represents a very rough upper limit on time-to-failure beyond which there is too much slow growth in the material (see SLOW CRACK GROWTH below).

TEMPERATURE

Testing temperatures ranging from 30 to 180 degrees F (0 to 82 degrees C) have been investigated in these initial baseline tests. The specimens were brought to this temperature by placing the precracked specimens in an air bath for one-half hour before being removed for immediate testing (within 10 seconds). This range of temperatures is generally representative of those experienced in service and processing.

A high temperature aging tests were attempted where the material was held at elevated temperatures for a relatively long period of time and then tested at room temperature. The tests were not sufficiently productive on the current material because the 3/4-inch polycarbonate used, having been fusion bonded from thinner material, had already experienced severe high temperature aging and further attempts at aging apparently did little to affect the toughness beyond what had already been done. Thorough aging investigations will be performed later in the project on polycarbonates of varying degrees of processing history and environmental exposure (both laboratory and in-service).

DATA

Figures 4 through 7 display the polycarbonate data from tests which were conducted at the various temperatures, loading rates, and thicknesses discussed above. In these figures a standard convention of plotting the K-rate logarithmically has been adopted.

In these graphs each specimen is represented as a separate data point and the straight lines are drawn between the averaged values. This means that each averaged value is the average from approximately six seperate specimens prepared and tested identically, as discussed earlier.

Figure 6 displays the results for the 3/4-inch specimens. Note that toughness increases with increasing temperature and with decreasing loading rates, which is the general behavior expected since the ductility increases with higher temperature and lower loading rates (ie. longer times-to-failure).

Figure 5 displays the results from the 1/2-inch material which coincide well with the 3/4-inch data (figure 7). This is an important observation and assures that the 1/2-in and 3/4-inch specimens are behaving in plane strain.

Figure 4 displays the 1/4-inch results. The superposition of these results on the 1/2-inch or the 3/4-inch results (figure 7) reveals that the 1/4-inch material gives a higher toughness. Again, this is due to the 1/4-inch material being in plane stress.

SLOW CRACK GROWTH

The difficulty in testing polycarbonate, which is a relatively ductile material, is that it has a tendency toward slow crack growth. Kc/Kic fracture toughness is a measure of the "instability" toughness of a material. An instability is the sudden and catastrophic propagation of the crack which is usually preceeded by some slow crack growth. The amount of slow crack growth preceeding the instability depends upon the amount of ductility surrounding the crack tip and any factor that increases this ductility will increase the amount of slow crack growth.

Thin specimens exhibit higher ductility in the crack tip region and this causes an increase in slow crack growth. Higher temperatures and/or lower loading rates (ie. longer times-to-failure) also result in increased ductility and, therefore, increased slow crack growth.

As a practical matter, too much slow crack growth will invalidate the Kic value since the crack will advance too close to the boundary of the specimen before instability occurs. In these current tests, the maximum slow crack growth allowed was arbitrarily set at approximately 2 mm.

For this reason, the 1/4-inch material could not be tested at 180 degrees F since instability did not occur, and the 180 degree F tests on the 1/2-inch and 3/4-inch material at the medium loading rate were impinging upon the maximum allowable slow-growth and should be regarded as possibly invalid values.

One of the primary objectives of this current set of baseline tests is to determine the allowable limits for these factors that effect the slow crack growth (eg. thickness, temperature, and loading rate) which will ultimately limit testing to within certain ranges of these parameters.

COMPARISON TO STRETCHED ACRYLIC

In an effort to obtain a comparison between the polycarbonate and the stretched acrylic when tested under identical conditions and on the same testing system, a small number of stretched acrylic specimens were tested and compared to the results of the polycarbonate tests. Figure 9 shows the results compared to room temperature testing at the two loading extremes.

The polycarbonate is considerably tougher than the stretched acrylic in these tests and its toughness apears to be decreasing at a slightly higher rate with K-rate than the stretched acrylic. These toughness results for the stretched acrylic compare well with the results obtained in the previous research on this material [1].

A word of caution is urged, however, in that these polycarbonate tests are somewhat preliminary and it is premature to allow this single figure to lead one to believe that polycarbonate is so clearly tougher than stretched acrylic.

SCATTER

Scatter is a notorious problem in Kc/Kic fracture toughness testing that was amply demonstrated by the provious work in stretched acrylic [1]. Scatter is measured by calculating a co-efficient of variation (Cf) for each set of identically-tested specimens, and then averaging the Cf's for all such sets to arrive at an "average Cf". The average Cf for the previous stretched acrylic tests was approximately 0.08, while the average Cf for the polycarbonate, however, was only approximately 0.05.

The relatively small scatter is significant in that any standardized Kc/Kic fracture toughness test for polycarbonate can yield values in which there is equal confidence based on a smaller number of samples.

V. SUMMARY

The most significant and important conclusion that can be drawn from these baseline tests is that polycarbonate can successfully and practically prepared and tested with reproducable Kic and Kc results. The 1/2-inch and 3/4-inch specimens tested at these moderately high loading rates yield a valid plane strain Kic value. The Kc/Kic fracture toughness of polycarbonate is markedly affected by changes in temperature and loading rate and this generally conforms to what is expected for this material.

The goal of future work will be to determine the manner in which various environmental and processing variables affect the toughness of the material. Tests will continue over the same range of loading rates and temperatures and most tests will be conducted on a fixed thickness yielding a valid Kic value (probably near 1/2-inch) although other thicknesses will be used as well.

The result will be a large, definitive data base providing much-needed information to be used in the assessment of the use of this material in aircraft transparency applications, and also providing the capability for use in design situations.

REFERENCES

1. Sutton, S. A., "Fracture Toughness of Stretched Acrylic Plastic", to be published J. of Testing and Evaluation.

2. Sutton, S. A., "A Model for Computer-Based Data Acquisition and Control", Experimental Mechanics, vol. 17, April 1977.

3. Brown, W.F., Jr., and Srawley, J.E., "Pane Strain Crack Toughness Testing of High Strength Materials," ASTM STP 410, Am. Soc. for Testing and Materials, 1966

4. Hassard, R.S., "Design Criteria: Transparent Polycarbonate Plastic Sheet", Tech. Rep't. GERA-1815, Goodyear Aerospace Corporation, April 1972.

5. 1976 Annual Book of ASTM Standards, Part 10, American Society for Testing and Materials

6. Srawley, J.E., "Pane Strain Fracture Toughness," Fracture, Vol. 4, Ch. 2, pp. 45-68.

7. Sutton, S.A., "REMOS: A Remote Communications Operating System for Real-Time Applications", to be published.

8. Golden, J.H., et.al., "The Effect of Thermal Pretreatment on the Strength of Polycarbonate", J. of Applied Poylmer Science, vol. 11, pp. 1571-9, 8 August 1967.

9. Sutton, S. A., "An Automated Portable Data Acquisition System for Materials Testing Applications", in preparation.

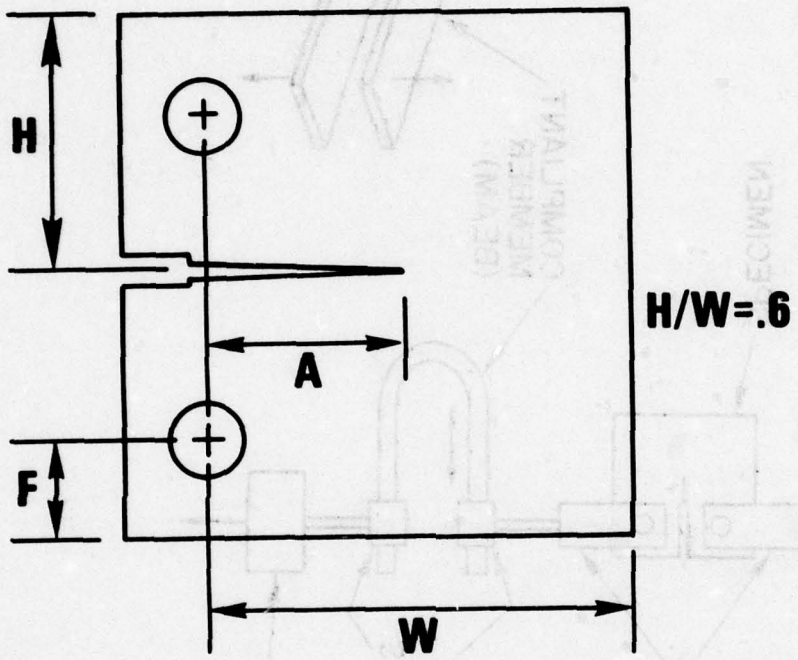


Figure 1. Compact Tension Specimen

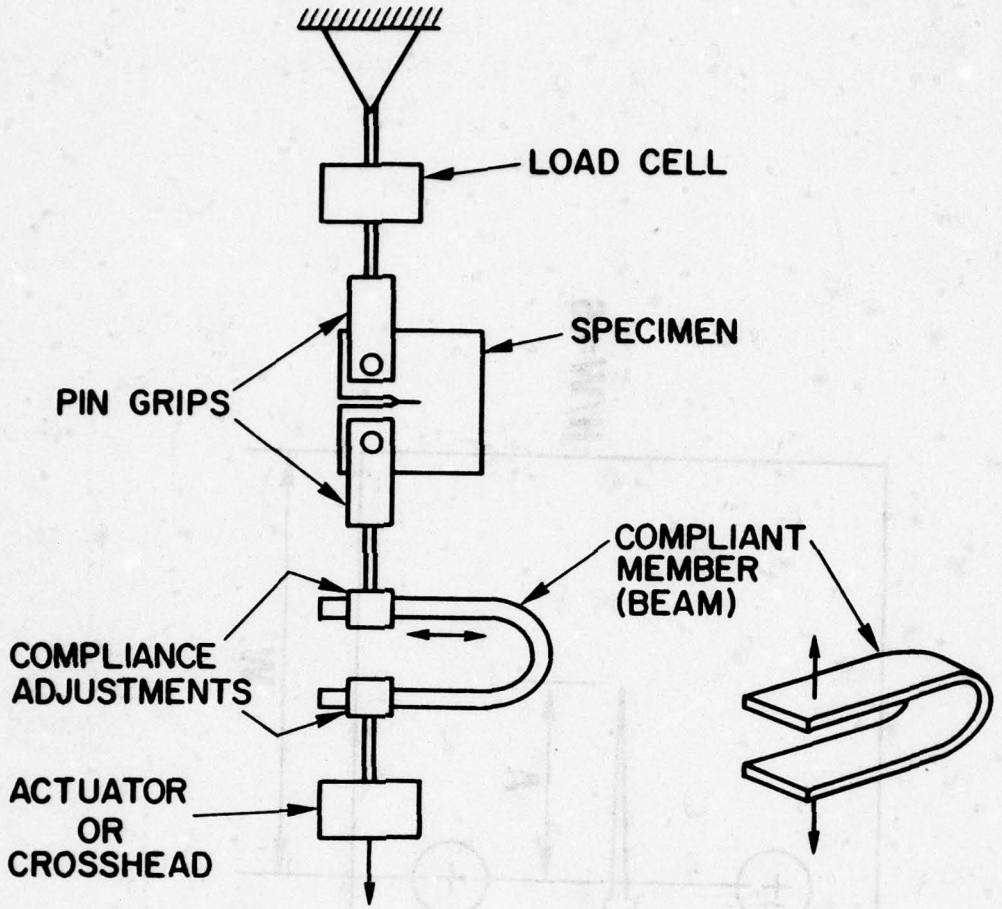


Figure 2. Loading/Testing Machine Configuration

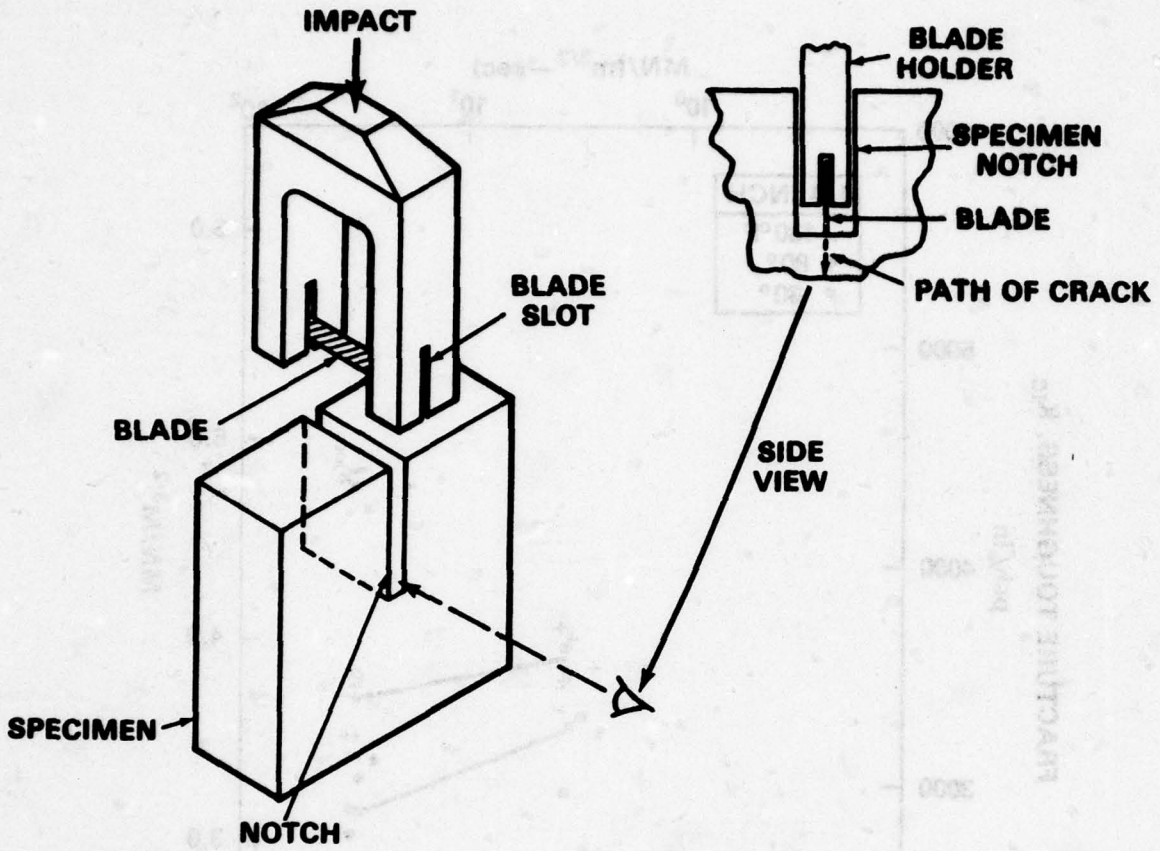


Figure 3. Pre-cracking Schematic

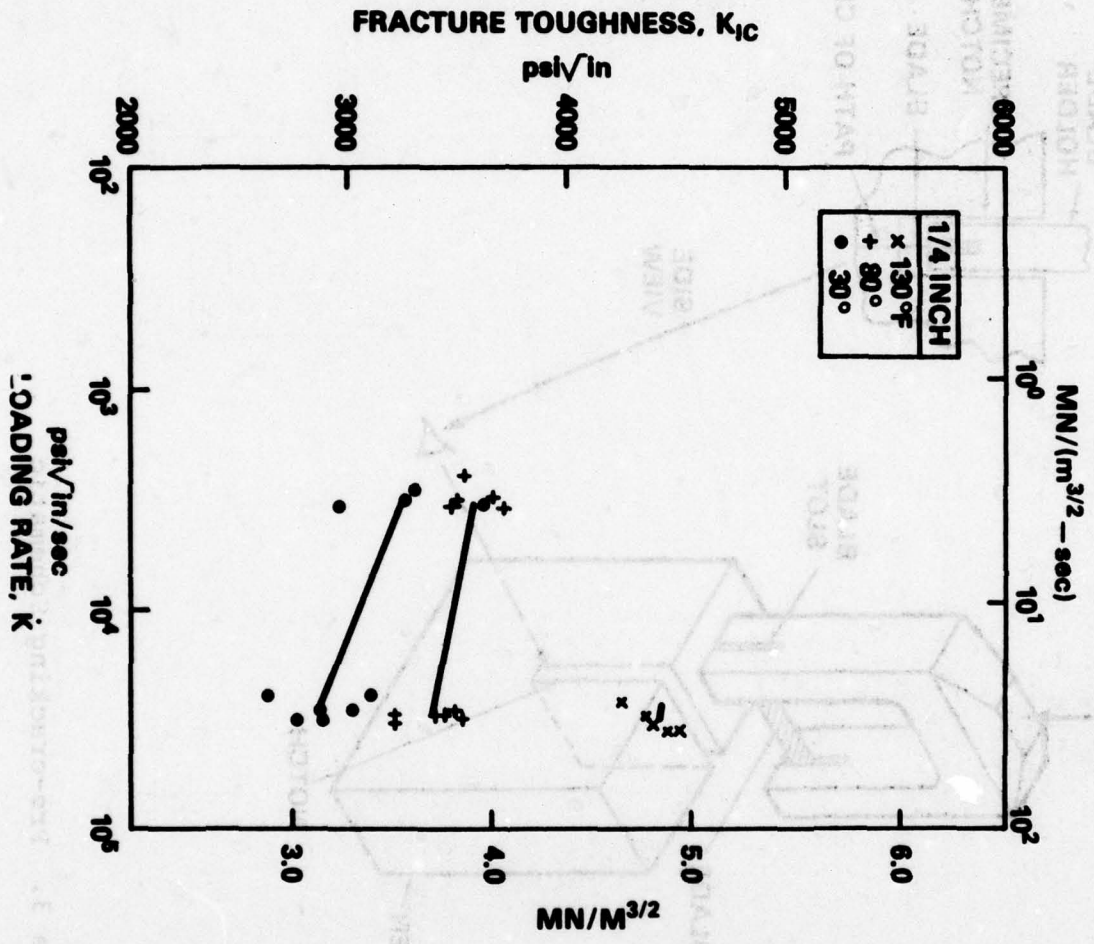


Figure 4. Fracture Toughness (Kic) vs. Loading Rate (K-rate) for 1/4-inch Material, Assorted Testing Temperatures

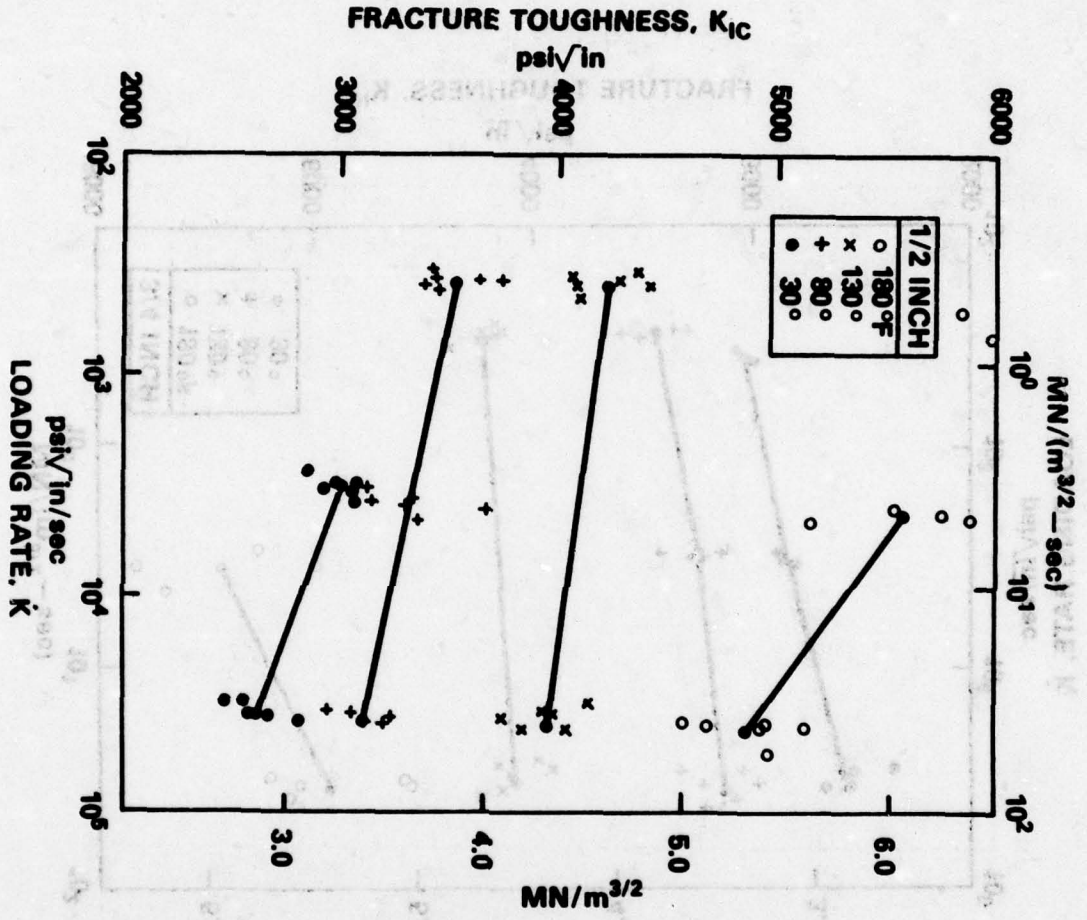


Figure 5. Fracture Toughness (Kic) vs. Loading Rate (K-rate) for 1/2-inch Material, Assorted Testing Temperatures.

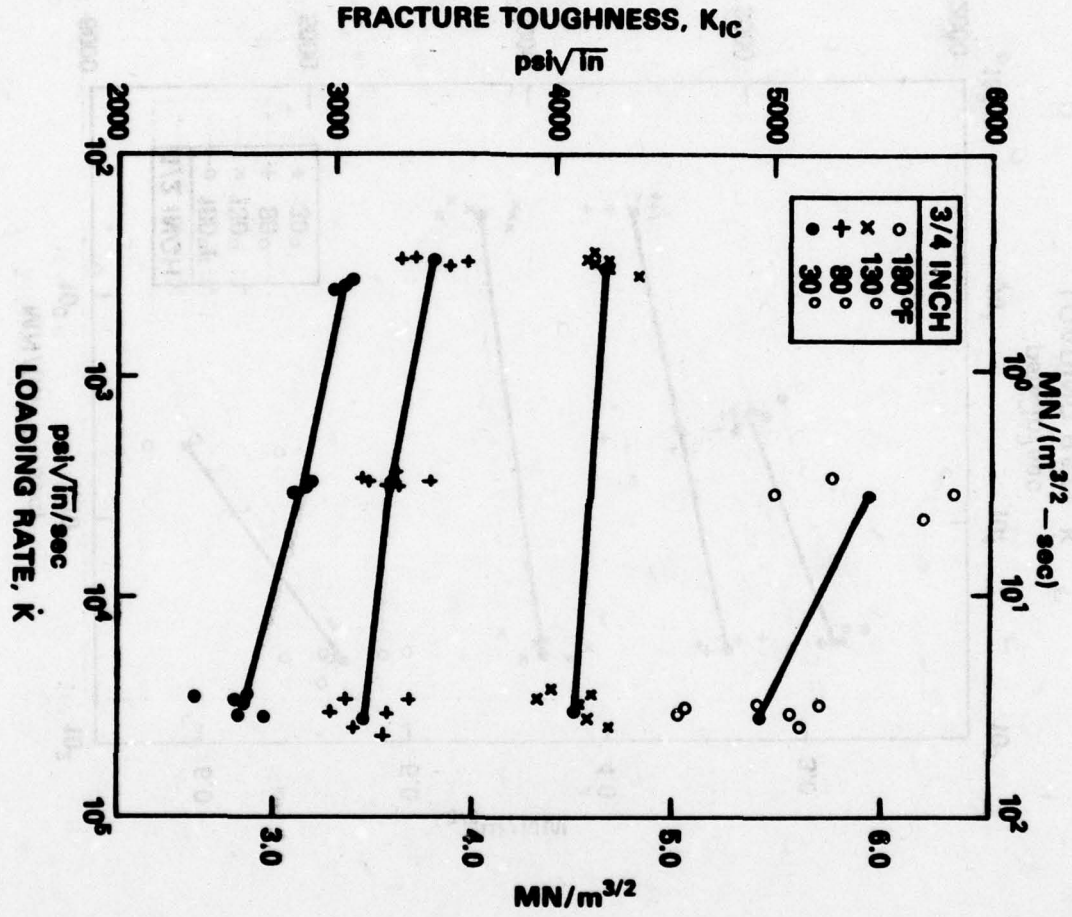


Figure 6. Fracture Toughness (Kic) vs. Loading Rate (K-rate) for 3/4-inch Material, Assorted Testing Temperatures

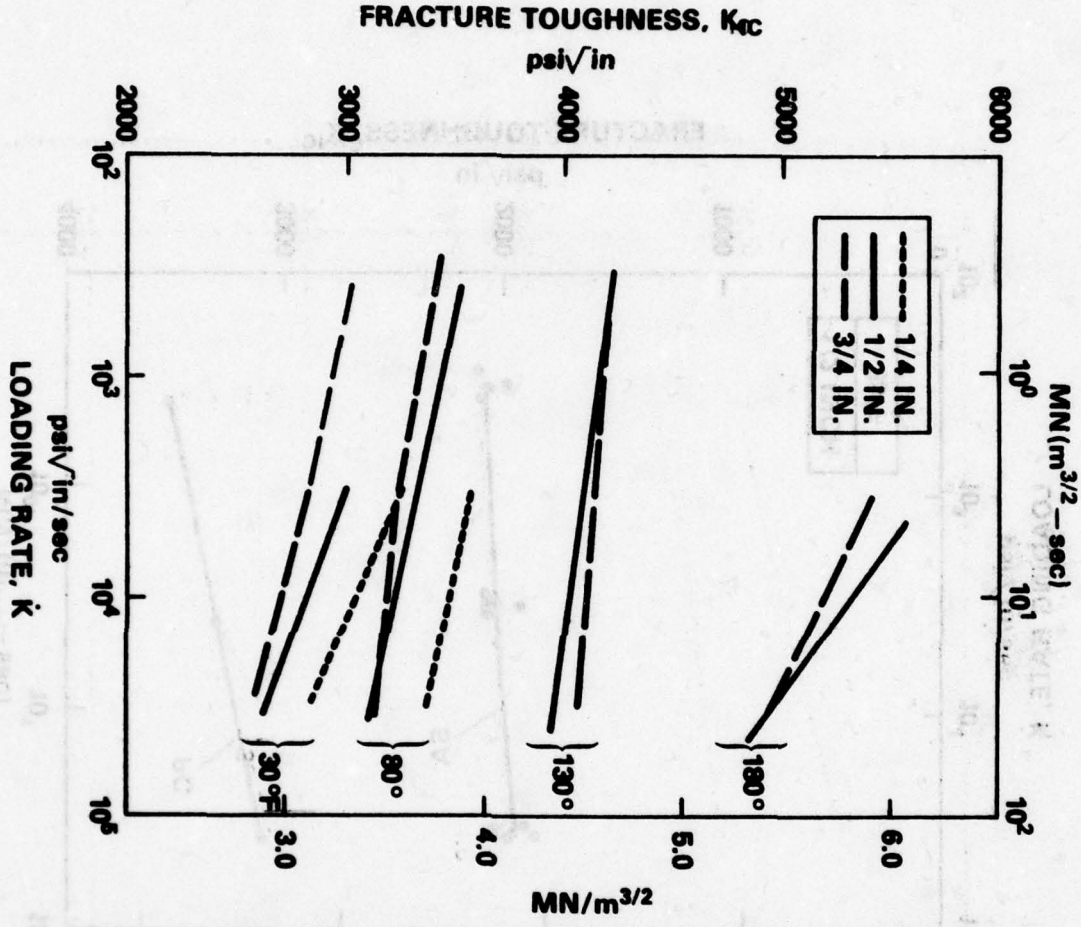


Figure 7. Fracture Toughness (Kic) vs. Loading Rate (K-rate) for all Tickness, Assorted Testing Temperatures

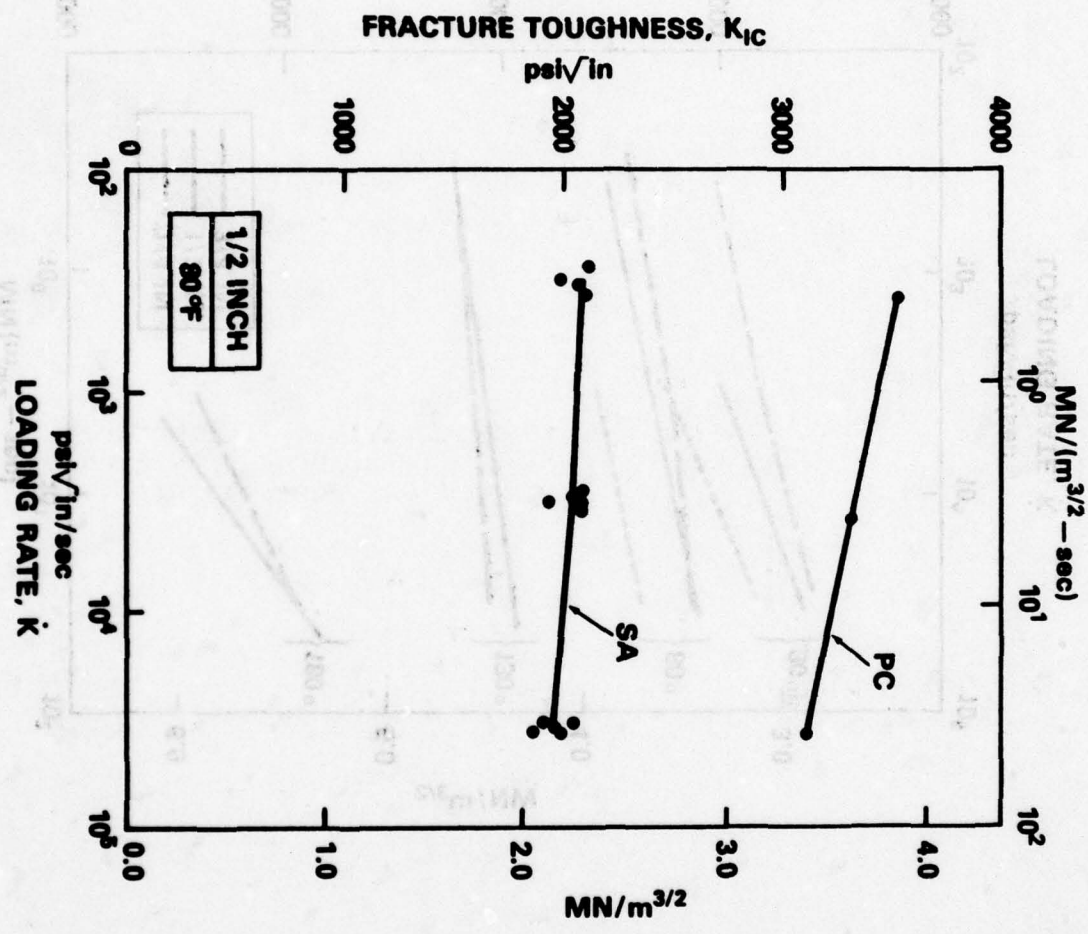


Figure 8. Fracture Toughness (Kic) vs. Loading Rate (K-rate) for Polycarbonate vs. Stretched Acrylic.

ABRASION TESTING OF TRANSPARENT PLASTICS

J. E. Mahaffey
PPG Industries, Incorporated
Aircraft and Specialty Products
Pittsburgh, Pennsylvania

ABRASION TESTING OF TRANSPARENT PLASTICS

J. E. Mahaffey
PPG Industries, Inc.

Abstract

The abrasion resistance of transparent plastics is a very important material property where these materials are used on the exterior or interior surfaces of aircraft transparencies. Abraded surfaces of aircraft windshields can significantly reduce pilot vision under certain flight conditions and seriously impair pilot performance and flight safety. The abrasion resistance of transparent materials is difficult to evaluate in the laboratory. Several types of abrasion test methods have been developed over the years but no one test is considered to provide an adequate assessment of the resistance of transparent plastics to abrasion considering the different types of abrasion a transparent enclosure may encounter in service.

To obtain the most information pertaining to abrasion resistance of transparent plastics, PPG Industries uses several different types of abrasion tests including both impingement and rubbing type abrasion. This paper describes each of the several methods in detail and reviews the salient features of each test. Abrasion resistance test data generated on several types of transparent plastic materials using these test methods are presented. The plastic substrates tested include cast acrylic, stretched acrylic, polycarbonate and CR-39 allyl diglycol carbonate plastic. Abrasion resistance data are also presented on polycarbonate coated with several types of protective coatings designed to improve the abrasion and environmental resistance of the material. The significance of the data generated by these tests will be summarized.

PRECEDING PAGE BLANK-NOT FILMED

INTRODUCTION

Scratch and abrasion resistance is an important property of transparent materials used in aircraft transparencies, particularly transparent plastics because of the relatively low resistance of these materials to abrasion compared to glass. For most opaque materials, abrasion resistance is important primarily from the standpoint of aesthetics and environmental resistance. An additional factor, abrasion, is critical for transparent materials, in that it impairs the optical quality of the material. Consequently, abraded surfaces of aircraft transparencies can significantly reduce pilot vision and therefore have a serious effect on pilot performance and flight safety.

The abrasion resistance of transparent plastics is difficult to evaluate in the laboratory. Scratch and abrasion testing of these materials has, in fact, been a controversial subject for many years. A large number of scratch and abrasion tests have been developed and evaluated within the industry. ASTM Committee D-20 has been involved in this activity for several years. More recently, ASTM Subcommittee F7.08 has been working on abrasion test methods specifically applicable to aircraft transparencies which utilize exposed transparent plastic components.

Of all the abrasion test methods available today it is believed that no one test provides an adequate assessment of the abrasion resistance of transparent plastics, due primarily to the different types of abrasion actually encountered by an aircraft transparency in service. The increased use of plastics with protective coatings, particularly coated polycarbonate, makes the use of more than one abrasion test important because of the possible interaction between the coating and the substrate.

For these reasons, PPG Industries uses four types of tests in evaluating the abrasion resistance of transparent plastics for both rubbing and impingement type abrasion. This paper describes the four test methods, reviews abrasion test data generated on several types of transparent plastics using these test methods, including coated polycarbonate, and discusses the significance of the test results.

It should be noted that abrasion resistance is only one important property of these types of materials. The effect of other environments such as temperature, humidity, and solar radiation is equally important.

TEST METHODS

The following is a description of the four abrasion test methods used by PPG Industries for transparent plastics. While there are several other test methods which could be used, it is believed that these provide a good basis for determining the abrasion resistance of plastic materials.

Bayer Abrader

This test was recently developed by Bayer A.G., West Germany as a rubbing type abrasion test for transparent plastics. Figure 1 is a photograph of the equipment used for this test. The test specimen is 4 x 4 inches square and is positioned in a 4 x 4 inch cavity of the test bed so that the specimen surface is flush with the bottom of the test bed. One kilogram of 6/14 quartz silica sand is placed over the specimen. A mechanical linkage to an electric motor moves the test bed in a back and forth motion and 4 inch stroke length at a frequency of 150 cycles per minute (300 strokes per minute). This action causes the silica sand to remain virtually at rest inducing a rubbing type abrasion on the specimen. A regulator is used to control the speed of the apparatus which works in conjunction with a counter to automatically control the number of cycles. The degree of abrasion is controlled by the number of cycles used which usually ranges from 50 to 300 cycles for transparent plastics. The criteria for measuring the degree of abrasion is the increase in haze induced as determined using a Gardner pivotal sphere hazemeter in accordnace with ASTM D-1003.

The Bayer Abrader is a relatively new abrasion test method. Testing to date, however, shows that results are reproducible and that the test is a good rubbing type abrasion test. This test method is currently being considered as a standard abrasion test for transparent plastics by ASTM Subcommittee F7.08, "Aerospace Transparent Materials and Enclosures."

PPG Salt Abrader

The salt abrader was developed by PPG Industries several years ago to simulate ice crystal impingement on aircraft windshields encountered when flying through certain types of clouds. The test consists essentially of impacting the plastic test specimen with minute salt crystals at a high velocity. The basic component of the apparatus, illustrated in Figure 2, is a commercial sandblast gun used to sandblast trademarks and other identification onto glass. Salt was selected as the abrasive medium because it has a MOH hardness similar to ice crystals and is readily available. The salt crystals of controlled size are impacted on the specimen in cycles of 1/2 second duration controlled by an accurate timer control coupled with a counter which automatically controls the number of cycles. The degree of abrasion induced per cycle is controlled by the air pressure delivered to the sandblast gun. The test provides an abraded area of one inch in diameter. Specimen size is 3 x 3 inches square which is of sufficient size to obtain four abraded areas per specimen. The degree of abrasion induced is also measured by the increase in haze.

The salt abrasion test is believed to be an effective test for impingement type abrasion for transparent plastics particularly ice crystal impingement and also sand/dust impingement. This test is also being considered as a standard abrasion test for transparent plastics by ASTM Subcommittee F7.08.

Taber Abraser

The Taber Abraser test is a fairly well known abrasion test which has been in use for several years. It is currently specified in ASTM test methods, industry, and governmental specifications for abrasion testing of several different types of materials. Most people who have been involved in abrasion testing of materials are familiar with this test. ASTM D-1044, which was developed specifically for abrasion testing of transparent plastics, utilizes the Taber Abraser. The Taber Abraser apparatus is illustrated in Figure 3. The test consists of two standardized abrasive wheels which remain fixed, to which a predetermined load is applied. The specimen to be tested, usually 4 x 4 inches square, is fixed to a turntable which rotates at 70 revolutions per minute. The rotating specimen causes the two abrasive wheels to rotate abrading the specimen in a circular pattern approximately 1/2 inch wide and 2-1/2 inches inside diameter. Like the preceding two test methods, increase in haze in the abraded area of the specimen is used to measure the effect of this type of abrasion.

Proposed Abrasion Test

A relatively new rubbing type abrasion test for transparent plastics is currently being evaluated to provide additional abrasion resistance data for these type materials. The apparatus consists of a lead block with a felt pad attached to the base of the block. The center of the block is hollowed out to accommodate the abrasive medium. The block is attached to a motor driven mechanical linkage which moves the block in an oscillating motion over the specimen surface. A fine mesh alundum abrasive is continually applied to the specimen surface through a small slit in the felt pad. The test can be conducted both wet and dry where the wet tests consist of a variety of solvents or cleaning liquids in combination with the abrasive.

This test was designed primarily to simulate abrasion on transparent materials induced by cleaning. The abrasive used is similar to the hardness of dust which accumulates on the transparency and the load simulates the force usually used in cleaning. The primary advantage of this test for transparent plastics is that solvents which may come into contact with the transparency can be included in the abrasion test.

The degress of abrasion induced by this test is determined by a subjective visual examination of the degree of scuffing of the specimen surface using a scale of 0 to 100, where 0 denotes no effect and 100 extensive surface damage. The increase in haze can and has been used as a criterion for abrasion with good correlation to the subjective evaluation.

TYPICAL ABRASION TEST DATA

Figures 4 through 8 present typical test data generated using the four types of abrasion test methods. Figure 4 shows the abrasion resistance of several transparent plastic materials which are currently used or have been used in aircraft transparencies based on the Bayer rubbing abrasion test. Note that the ranking of these materials relative to abrasion resistance is similar to that generally accepted for these materials e.g., CR-39 plastic has the highest resistance to abrasion, polycarbonate the poorest, with the acrylics falling in between. It also can be noted that as the number of cycles increases the magnitude of increase in haze tends to flatten out which indicates additional cycles will have a polishing effect with little increase in haze.

The resistance to abrasion of polycarbonate coated with three different protective coatings is illustrated in Figure 5. These coatings are representative of several types of commercially available protective coatings for polycarbonate which are being evaluated by PPG Industries. Based on this test, it can be seen that the abrasion resistance of the coated polycarbonate is generally superior to the uncoated plastic materials listed in Figure 4. In the case of these three coatings, the haze induced by this test is increasing at a greater rate as the number of cycles approaches 300. It is believed the coatings are starting to be eroded by the quartz silica sand and that eventually the coating would be removed.

Test data generated using the PPG Salt Abrader is presented in Figures 6 and 7. Figure 6 shows salt abrasion test data for the same uncoated transparent plastics listed in Figure 4 for the Bayer abrasion test. Note that the order of ranking of abrasion resistance obtained in this test is the same as that observed in the Bayer test (Figure 4). The magnitude of the increase in haze as a function of the number of cycles is significantly different, however, particularly for polycarbonate. The surfaces of this material are rapidly eroded by this impingement type abrasion compared to acrylic and CR-39 plastic which correlates with previous service experience where these materials have been used on the exterior surfaces of aircraft transparencies.

Figure 7 illustrates the abrasion resistance of the same protective coatings on polycarbonate listed in Figure 5. These test results illustrate the significance of more than one type of abrasion test. The order of ranking of abrasion resistance based on the Bayer test was coating A, B and C with coating A the least abrasion resistant. In the salt impingement test, coating B showed the least resistance to this type abrasion by a significant margin while coatings A and C were comparable. It was evident from the examination of the coating B specimens that the protective coating was eroded from the specimen surface after a relatively short time period exposing the bare polycarbonate to the salt abrasion. Based on this test, coating B is considered a doubtful candidate for use on the exterior surface of an aircraft transparency even though Bayer abrasion

tests indicated the coating to be superior to acrylic in abrasion resistance. Coating C was clearly superior to the other two coatings based on these two types of tests.

Typical Taber Abraser abrasion test data for several monolithic transparent plastics and coated polycarbonate are listed in Table 1. These tests were conducted in accordance with ASTM D-1044 which specifies a 500 gram load on the abrasive wheels and 100 revolutions of the specimen. The same general ranking of abrasion resistance for the uncoated plastics obtained with the salt and Bayer rubbing abrasion tests was also obtained with the Taber Abraser. The Taber Abraser data for the three coated polycarbonate materials, however, did not correlate with data obtained in the two previous abrasion tests. In fact, ranking of abrasion resistance of the three coated polycarbonate materials was completely different for all three tests. This is another illustration of how the apparent abrasion resistance of a material, particularly coated plastics, can vary depending on the abrasion test used. It also shows the importance of using more than one test in evaluating the abrasion resistance of these type materials.

In using the Taber Abraser some investigators use more than the 100 cycles specified in ASTM D-1044. Figure 8 shows Taber Abrasion test results for several plastic materials, both coated and uncoated for up to 1,000 cycles. Note that the increase in haze for Plexiglas 55 at 200 cycles is relatively high (30%) compared to the other materials. As the number of cycles increases, however, the haze values level off and actually decrease to a point where the haze at 1,000 cycles is less than the haze at 100 cycles. This is not an unusual phenomenon in abrasion testing. As the number of cycles is increased above 100 the abrasive wheels actually have a polishing effect on the acrylic. The selection of 100 cycles as a standard for ASTM D-1044 for transparent plastics is probably fairly realistic.

DISCUSSION

Of the four abrasion tests used, the Bayer Abrader and the salt abrader are considered to be the most important in evaluating the abrasion resistance of transparent plastics used in aircraft transparencies. The Taber Abraser and the proposed test are used to complement these two tests. The Taber Abraser is used primarily because it is a well known standard test and data generated by this test can be used to compare with existing data. The advantage of the proposed test is that it provides an indication of abrasion resistance in combination with a solvent.

A comparison of the type abrasion induced by the Bayer rubbing abrasion test and the salt impingement test is provided in Figure 9. Figure 9a is an electron microscope photomicrograph at a magnification of 200 of cast acrylic abraded with the Bayer abrader. The surface damage consists essentially of a series of fine scratches of various lengths and occasionally there is evidence of a gouge in the acrylic induced by a particle of sand. Figure 9b is cast acrylic, also 200 magnification, abraded with the PPG salt

abrader. In this case the acrylic surface is actually eroded in a fairly uniform manner as opposed to the scratch type damage in Figure 9a. These photographs provide a good illustration of the difference in surface damage induced by these two types of tests.

The use of abrasion test data in predicting how a material will perform in service is very difficult. Like most other types of accelerated laboratory environmental tests it is difficult to correlate these data with actual service life. The greatest value of data of this type is screening or comparing the abrasion resistance of coated and uncoated plastics. Very often significant weaknesses in a material or material combination can be detected by these types of tests. This is probably the most important use of abrasion test data.

The comparison of abrasion test data of a relatively new material to similar data for a material which has been used previously in aircraft transparencies can provide an indication of how the new material will perform in service. For example, acrylic has been used on the interior and exterior surfaces of aircraft transparencies for many years. While the abrasion resistance of this material leaves a lot to be desired, a material which demonstrates a significant improvement in abrasion resistance in laboratory tests compared to acrylic should prove to be better in abrasion resistance in service. Because of the many variables involved, and the effect of other environmental parameters, it is difficult to make accurate predictions of service performance. The use of more than one type of abrasion test provides additional data upon which a more accurate assessment can be made.

In the final analysis, the best way to evaluate abrasion resistance, like many other properties, is actual flight service tests using full-scale transparencies. While this is an expensive and time consuming procedure it is the only method of determining how a material or combination of materials will perform in service. Laboratory tests, however, whether they are abrasion tests or other environmental tests, are very useful and necessary to eliminate materials with obvious undesirable properties and to select the best material for a particular application.

TABLE 1

TABER ABRASER TEST RESULTS*

SUBSTRATE	HAZE INCREASE (%)
CR-39 PLASTIC	3.8
PLEXIGLAS 55	19.8
PLEXIGLAS II	24.2
STRETCHED ACRYLIC	29.5
POLYCARBONATE	36.4
COATED POLYCARBONATE	
COATING A	10.9
COATING B	0.3
COATING C	4.2

*100 CYCLES, 500 GRAM LOAD

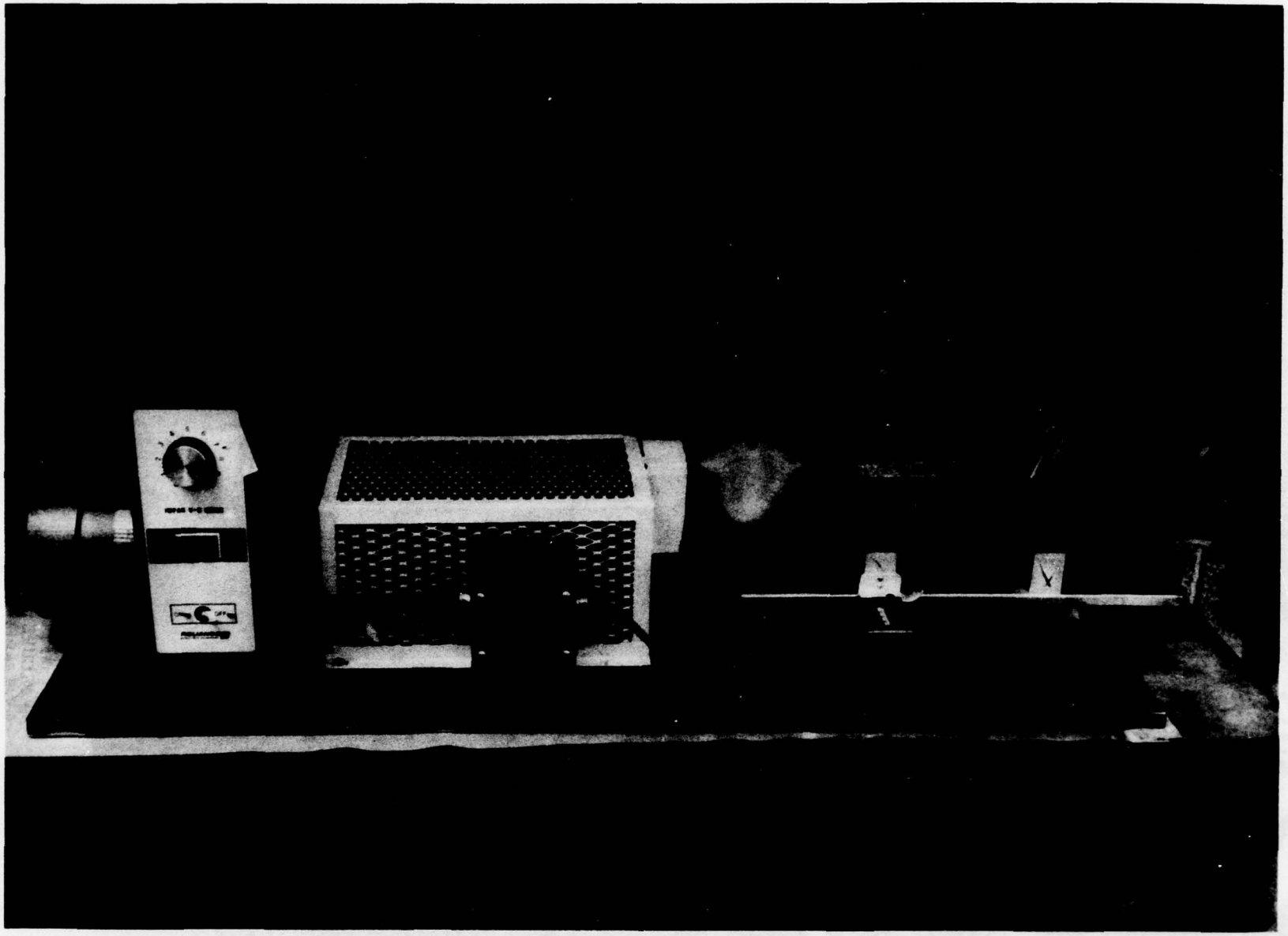


FIGURE 1. BAYER ABRADER

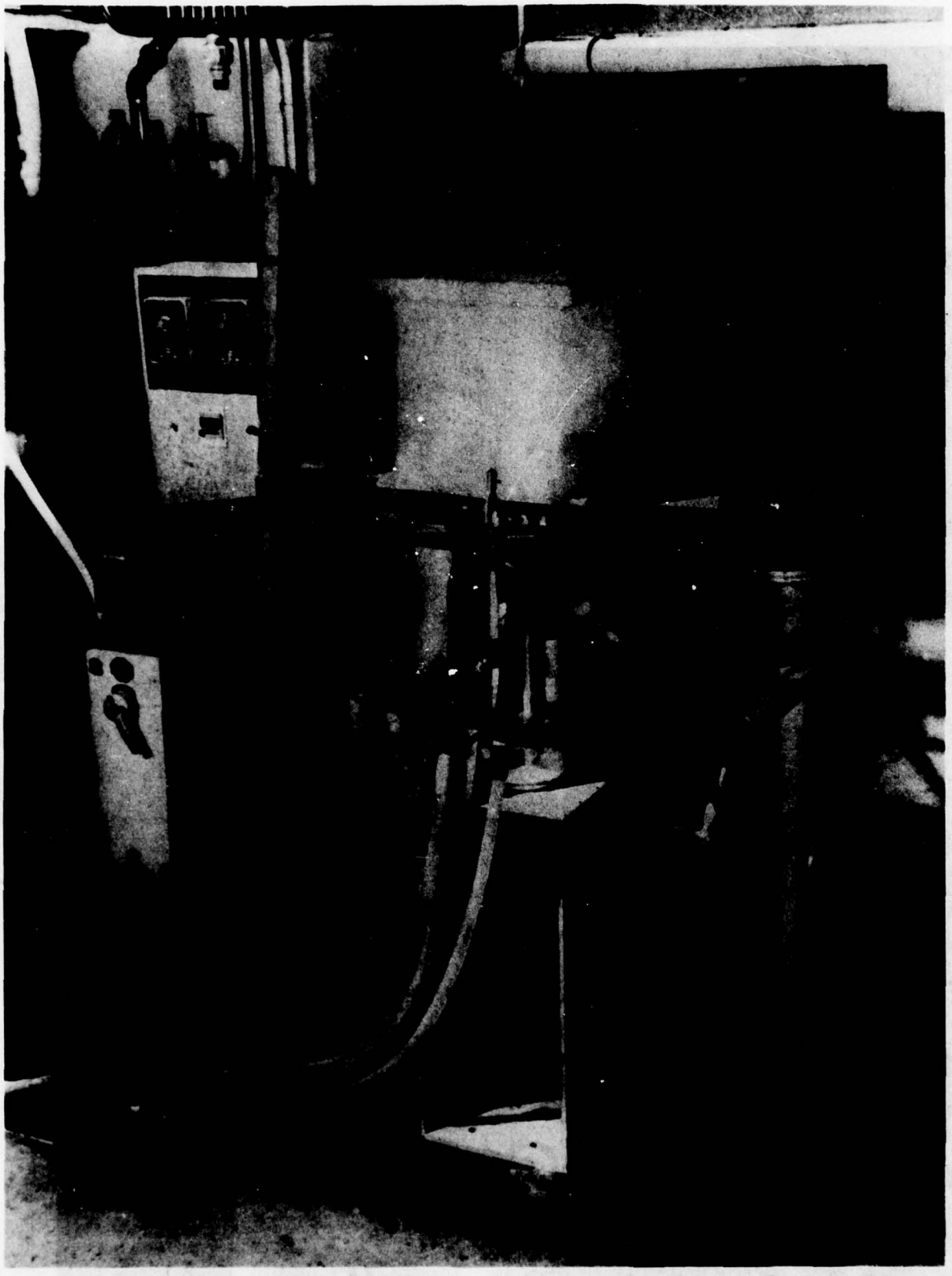


FIGURE 2. PPG SALT ABRADER

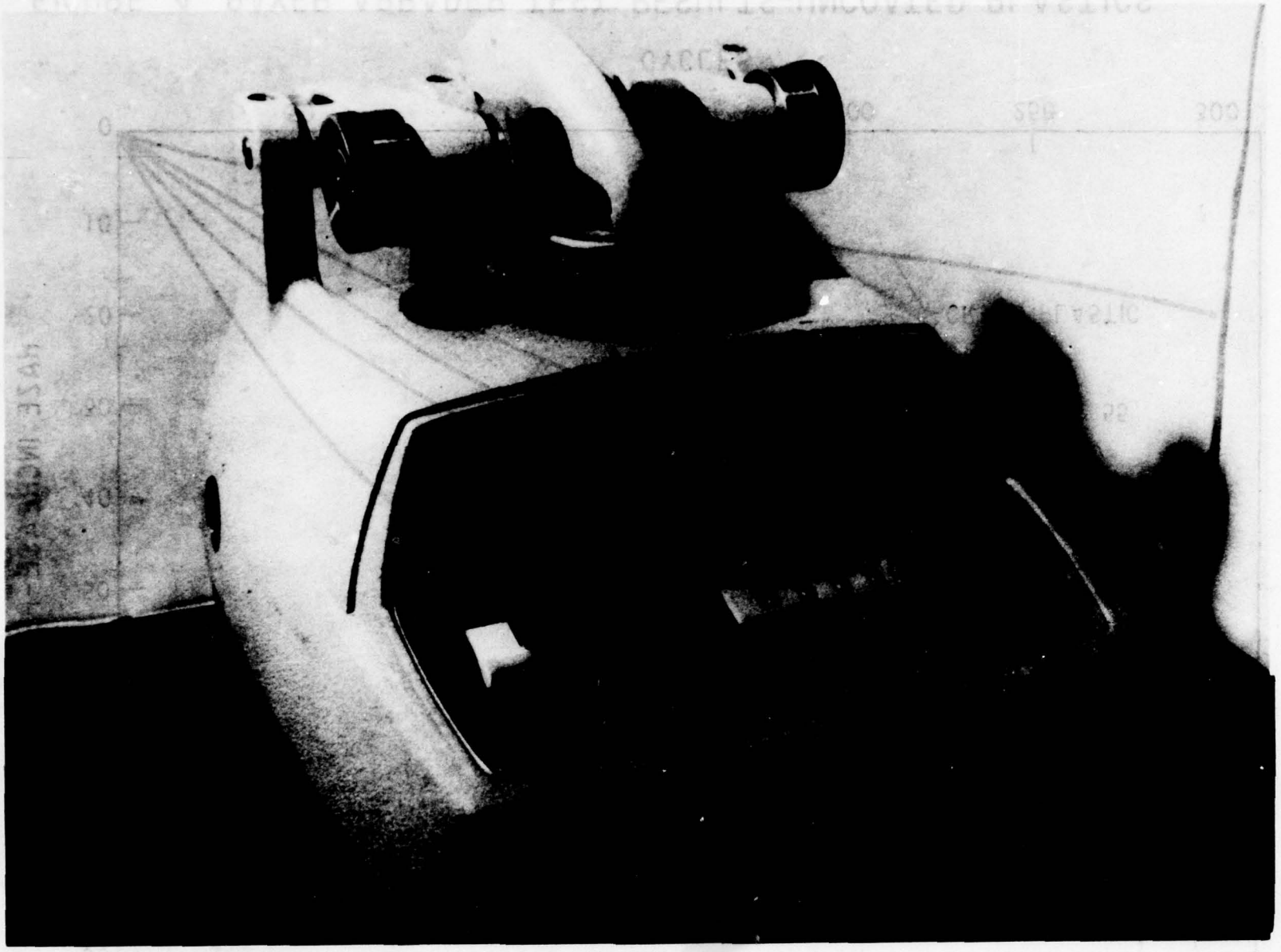


FIGURE 3. TABER ABRASER

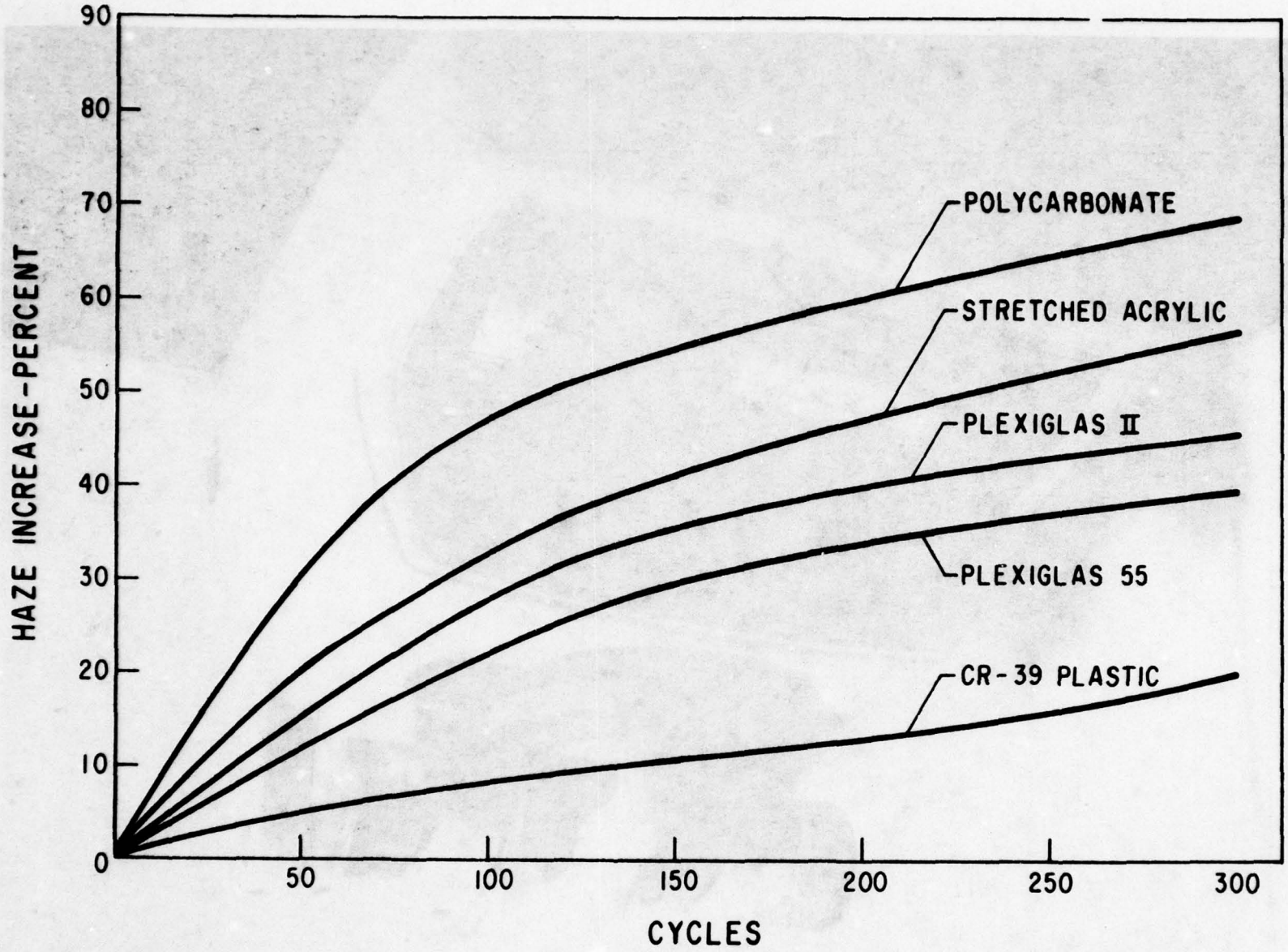


FIGURE 4. BAYER ABRADER TEST RESULTS-UNCOATED PLASTICS

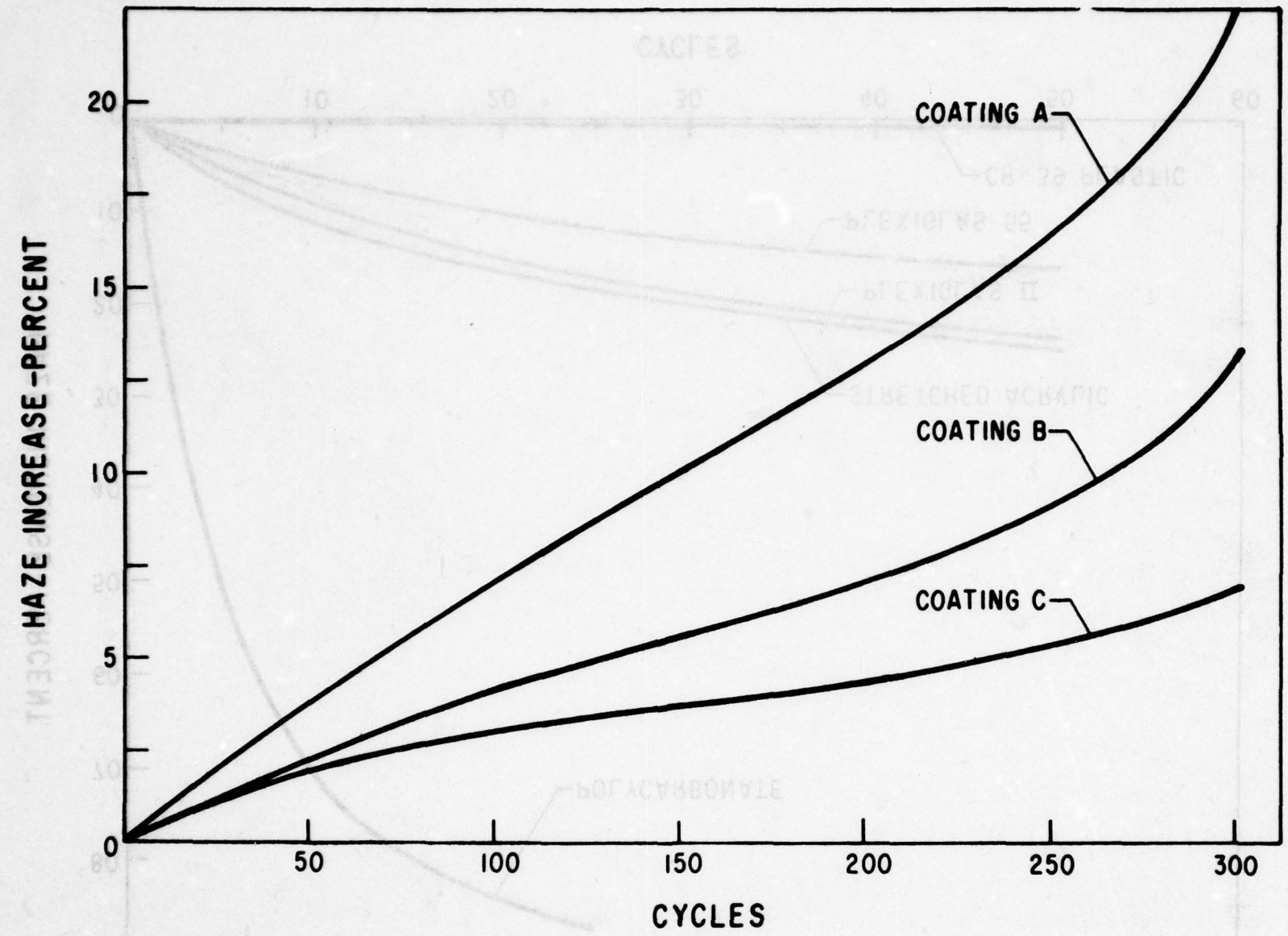


FIGURE 5. BAYER ABRADER TEST RESULTS-COATED POLYCARBONATE

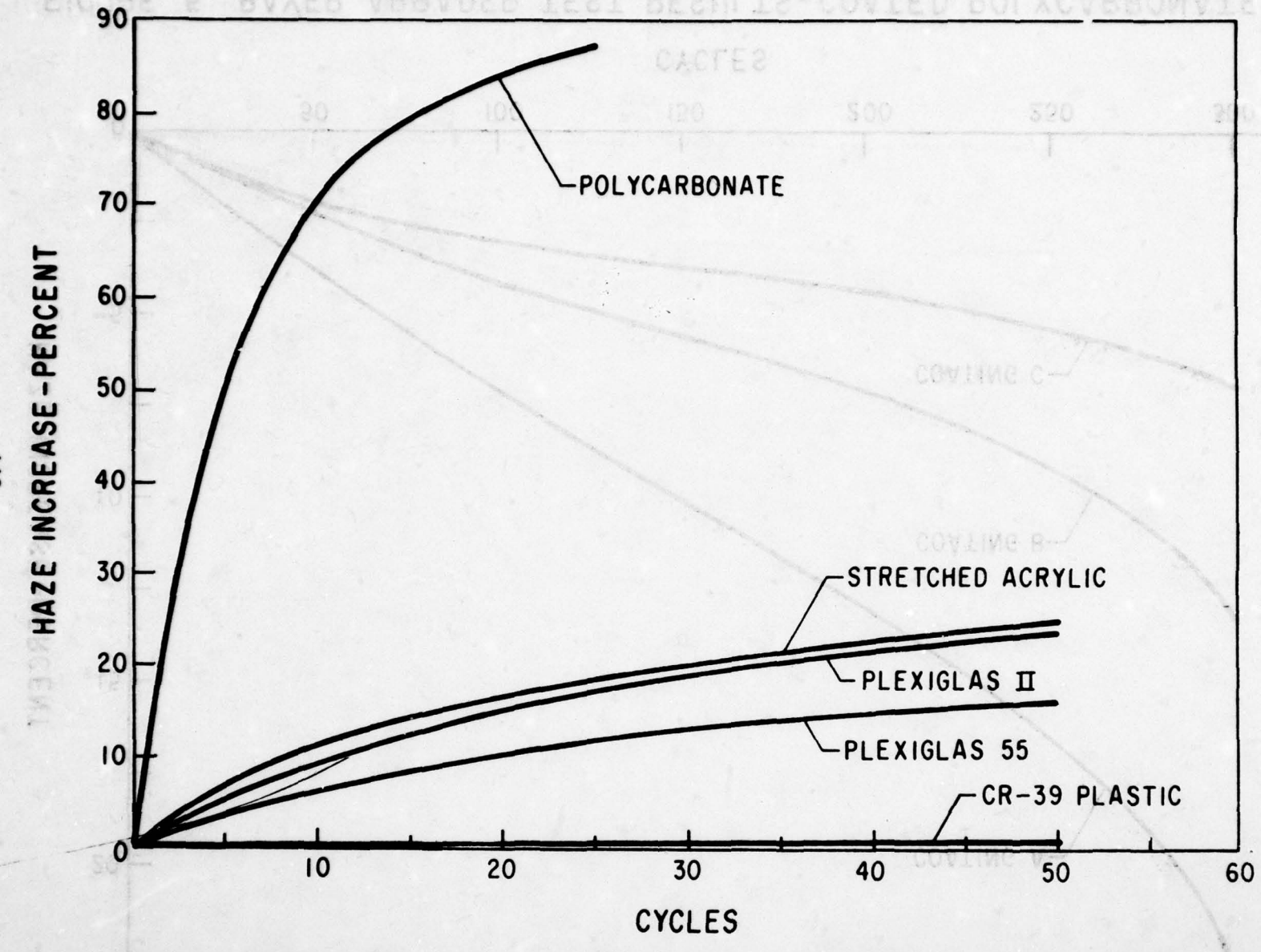


FIGURE 6. PPG SALT ABRADER TEST RESULTS-UNCOATED PLASTICS

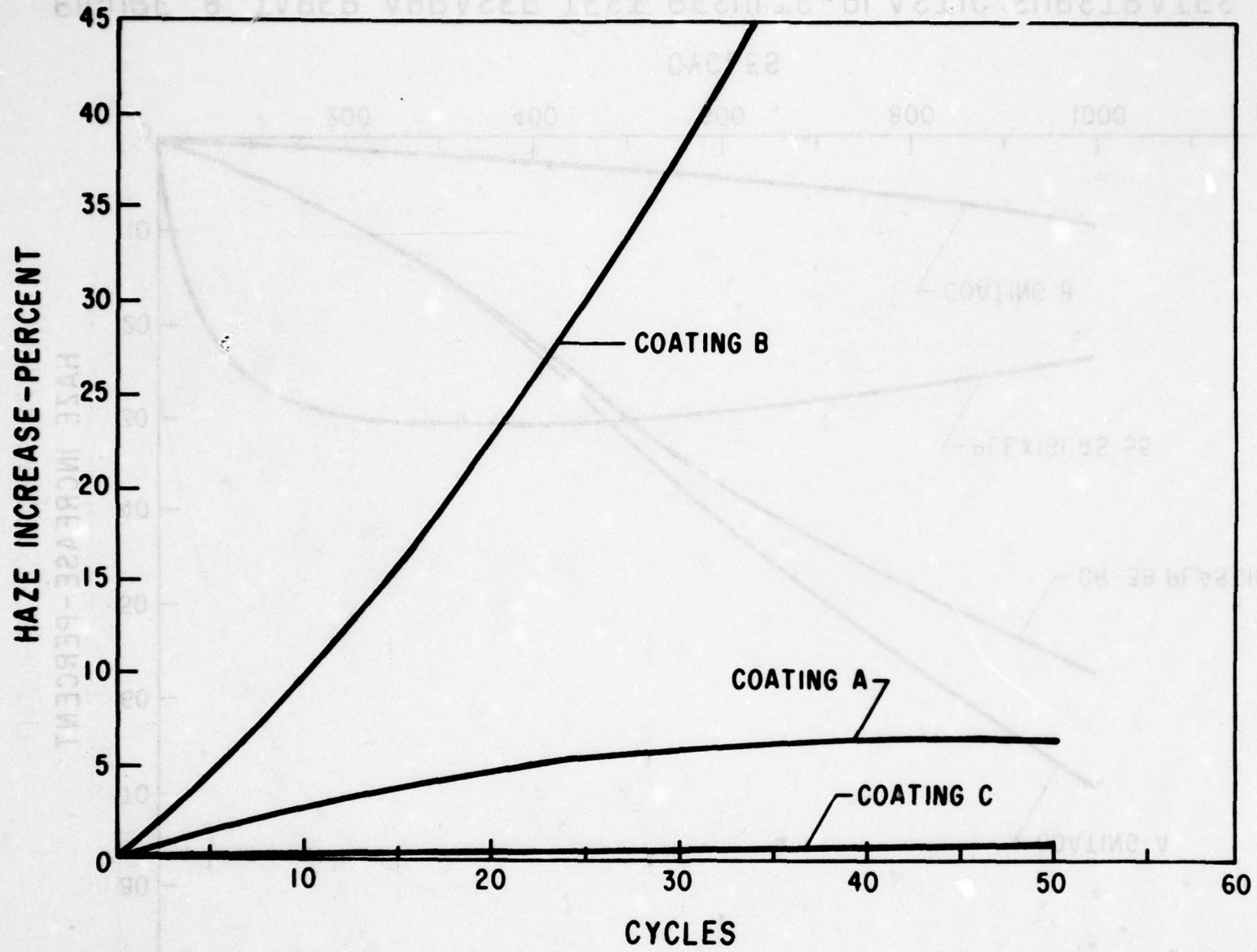


FIGURE 7. PPG SALT ABRADER TEST RESULTS-COATED POLYCARBONATE

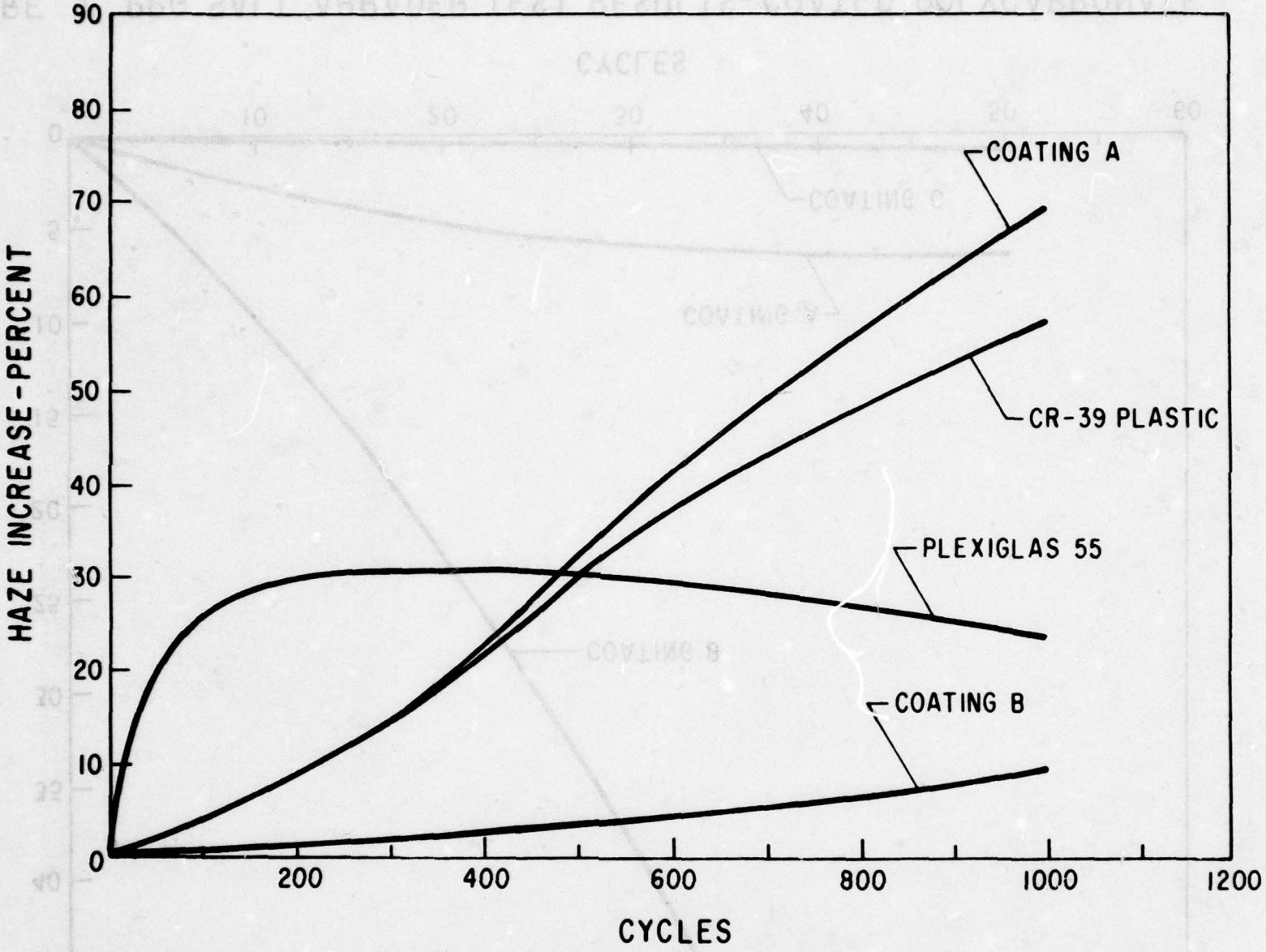


FIGURE 8. TABER ABRASER TEST RESULTS-PLASTIC SUBSTRATES

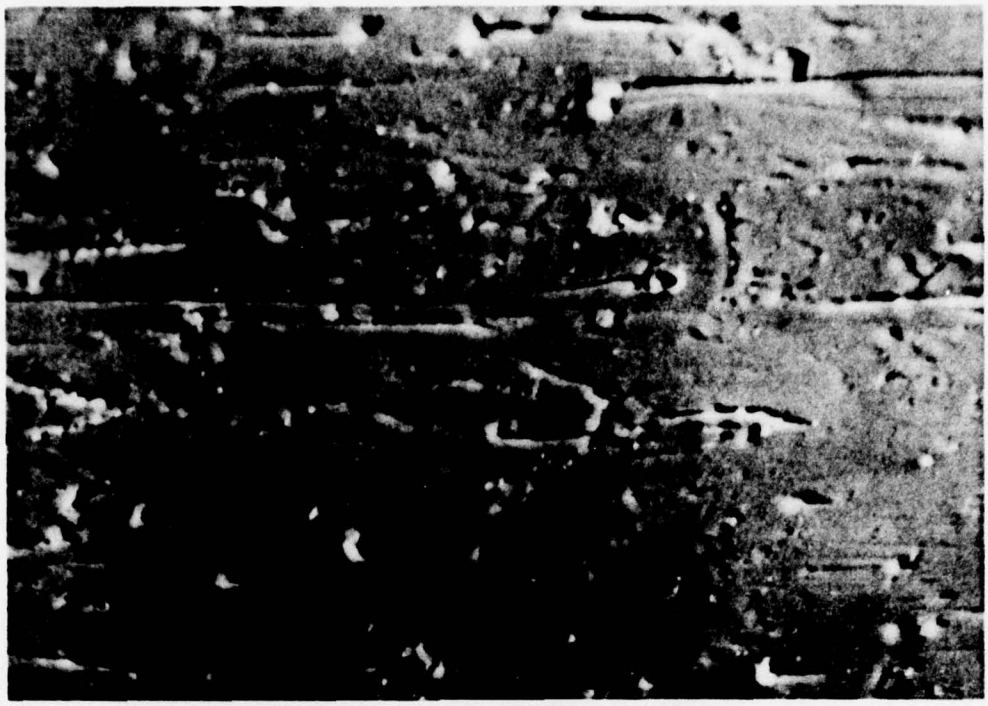


FIGURE 9A. BAYER ABRASION SPECIMEN PHOTOMICROGRAPH

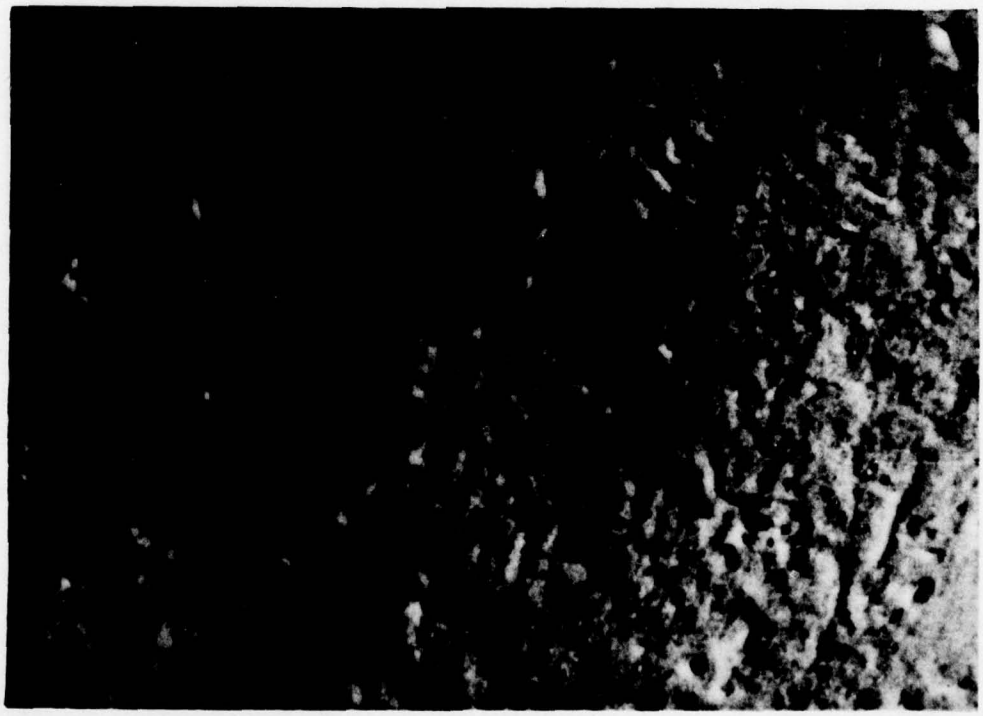


FIGURE 9B. SALT ABRASION SPECIMEN PHOTOMICROGRAPH

A METHOD OF VISUAL INSPECTION OF AIRCRAFT TRANSPARENCIES

Capt. R. G. Eggleston
Aerospace Medical Research Laboratory
Wright-Patterson Air Force Base, Ohio

PRECEDING PAGE BLANK-NOT FILMED

A METHOD OF VISUAL INSPECTION OF AIRCRAFT TRANSPARENCIES

Robert G. Eggleston

Aerospace Medical Research Laboratory
Human Engineering Division
Wright-Patterson AFB, Ohio

Historically, the visual inspection process has typically lacked structure and definition, and has consequently varied considerably in its implementation among aircraft transparency quality control inspectors. Thus, visual quality judgments rendered in the visual inspection process are likely to be unreliable. In this study, a systematic visual inspection procedure was used to assess the severity of distortion in a controlled viewing situation. Experienced quality control inspectors evaluated the severity of distortion observed in a sample of F-111 forward transparencies. The psychophysical scaling method of Magnitude Estimation was used to provide structure to the inspection process. This method requires an inspector to rate the perceived severity of distortion for each windshield against an arbitrarily selected standard windshield. Appropriate numerical values are assigned to the windshields by the judges to represent the relationship of the windshields to the standard. It was found that experienced quality control inspectors could use the Magnitude Estimation procedure to reliably scale the F-111 windshields. In general, the Magnitude Estimation procedure was highly suited to the task of evaluating aircraft windshields for distortion and could easily be used to evaluate other parameters of the visual quality of aircraft transparencies, such as rainbowing and multiple imaging.

INTRODUCTION

To insure acceptable optical quality, aircraft transparencies are customarily submitted to a visual evaluation which is generally performed by experienced quality control inspectors. Each transparency is normally evaluated for the extent of various local defects such as reams, dents, bubbles, and scratches. The extent and severity of large scale optical aberrations such as distortion and multiple imaging are also evaluated. When assessing localized defects, the visual inspection process is straightforward. After visually locating the deficiency, the quality control inspector determines whether or not it is within tolerance. Any defect found to exceed the established acceptance criteria results in the transparency being rejected. Generally, the most rigorous criteria are applied to aircraft canopies and forward facing windscreens.

When windscreens are inspected for visual quality in terms of complex optical aberrations like distortion, the visual inspection process has typically lacked structure and definition, and has consequently varied considerably in its implementation among quality control inspectors. In general, little attention seems to have

PRECEDING PAGE BLANK-NOT FILMED

been given to developing a systematic visual inspection procedure. Perhaps this is due to the fact that the visual evaluation of aircraft windscreens for distortion is normally performed as an adjunct to standard photographic assessment techniques. Unfortunately, even though quantitative measures of distortion can be derived from photographs, these measurements do not provide a complete or an adequate description of distortion. The photographic measurement procedures simply have not been sufficiently well developed to capture the total, or global extent of distortion. Consequently, these photographic-based measures are of little value in determining how variations in the distortion pattern may differentially degrade the out-of-cockpit vision of an aircrew member.

Visual inspection has the advantage of allowing the inspector to consider the total extent of distortion, including its severity, location, and pattern, when judging the acceptability of an aircraft windscreen. This advantage cannot be realized, however, unless the inspection is performed in a systematic manner. Recently, Gomer and Eggleston (1) applied the psychophysical method of Magnitude Estimation (ME) to the visual inspection of F-111 bird impact resistant windscreens, in an effort to standardize the inspection process. Using the ME procedure in a controlled viewing situation, a group of experienced quality control inspectors and Air Force F-111 pilots were able to successfully scale eleven F-111 windscreen panels in terms of the perceived severity of distortion, multiple imaging, and rainbowing. The ME procedure was efficient and did not require any alterations to the facilities normally used for visual inspection at the fabrication plant. In general, the perceptual judgments of the severity of distortion were highly consistent across both pilot and experienced quality control inspectors. This consistency was probably realized because of the structure given to the visual inspection task by the ME procedure.

Unfortunately, Gomer and Eggleston were unable to assess the reliability of the judgments rendered under the ME procedure due to time constraints in their study. The present study was performed to determine if an inspector is able to rate the optical quality of an aircraft windscreen consistently over time. As in the Gomer and Eggleston study, quality control inspectors and Air Force pilots rated F-111 bird impact resistant windscreens in terms of the severity of optical distortion. In the present study however, the same set of nine windscreen panels were evaluated twice, thus an inspector's ratings for a given panel could be compared across the two visual inspection sessions.

METHOD

Subjects

Four of the original twelve quality control inspectors and the Air Force F-111 pilots used in the Gomer and Eggleston study were available for this experiment. The results of a previously administered optometric examination indicated that all of the subjects satisfied class II flying standards with respect to visual acuity, convergence, and stereopsis (2).

Apparatus

Nine bird impact resistant F-111 windscreen panels (5 left seat and 4 right seat) were evaluated in the manufacturer's laboratory. Each panel was mounted on a holding fixture and oriented at an installation angle of 21.6 degrees with regard to the pilot's horizontal line of sight. A viewing ring (10 cm inside diameter) was positioned at the pilot's design eye reference to define a boundary for acceptable head movements during the observation of a front illuminated stringboard. An opaque template was placed over each windscreen to mask the peripheral regions of the transparency for which the manufacturer was not required to adhere to the optical specifications. In this manner, perceptual judgments of the severity of distortion would not be influenced by the apparent severity of the problem in these border areas. Figure 1 shows the general viewing arrangement.

Magnitude Estimation. Stevens' (3) procedure for acquiring direct estimates of subjective magnitudes was used to derive a perceptual scale of distortion. Although there are several approaches, it was decided that variability of the data would be reduced by providing a standard stimulus (in this case a windscreen) and by arbitrarily assigning its subjective magnitude a numerical value of 10. It was then possible to record an observer's impression of the relative magnitude of a given optical problem in each of the remaining windscreens. Should the subject perceive twice as much distortion for example, in a particular windscreen when compared to the standard, he would designate its value as 20. Likewise, should he perceive half as much he would assign the number 5 to that windscreen. This procedure takes advantage of the ease with which a person can match numbers to the psychological magnitudes of stimulus events, and was identical to that used in the Gomer and Eggleston (1) study.

Distortion Judgments. The subjects were instructed to rate each windscreen panel against the standard panel in terms of the perceived overall severity of distortion. The following factors were to be considered by the subject when making distortion judgments: (1) the degree to which the grid lines appeared to deviate from vertical and/or horizontal, (2) the extent of divergency or convergency in what should have been parallel grid lines, (3) the amount of shimmer or waviness in individual grid lines, (4) the presence of noticeable breaks or gaps in the pattern, (5) line blurring, and (6) the proportion of the total visual area incorporated by the windscreen in which distortion (as defined above) was perceived.

Pictorial examples of each factor were furnished, although relative weights were not assigned a priori by the experimenters. Also, the subjects were not restricted from evaluating other dimensions of distortion which they deemed to be important. However, they were instructed not to make a distinction between a left seat (pilot) and a right seat (co-pilot) windscreen. It was emphasized repeatedly to the subjects that they should be consistent in their comparative judgments.

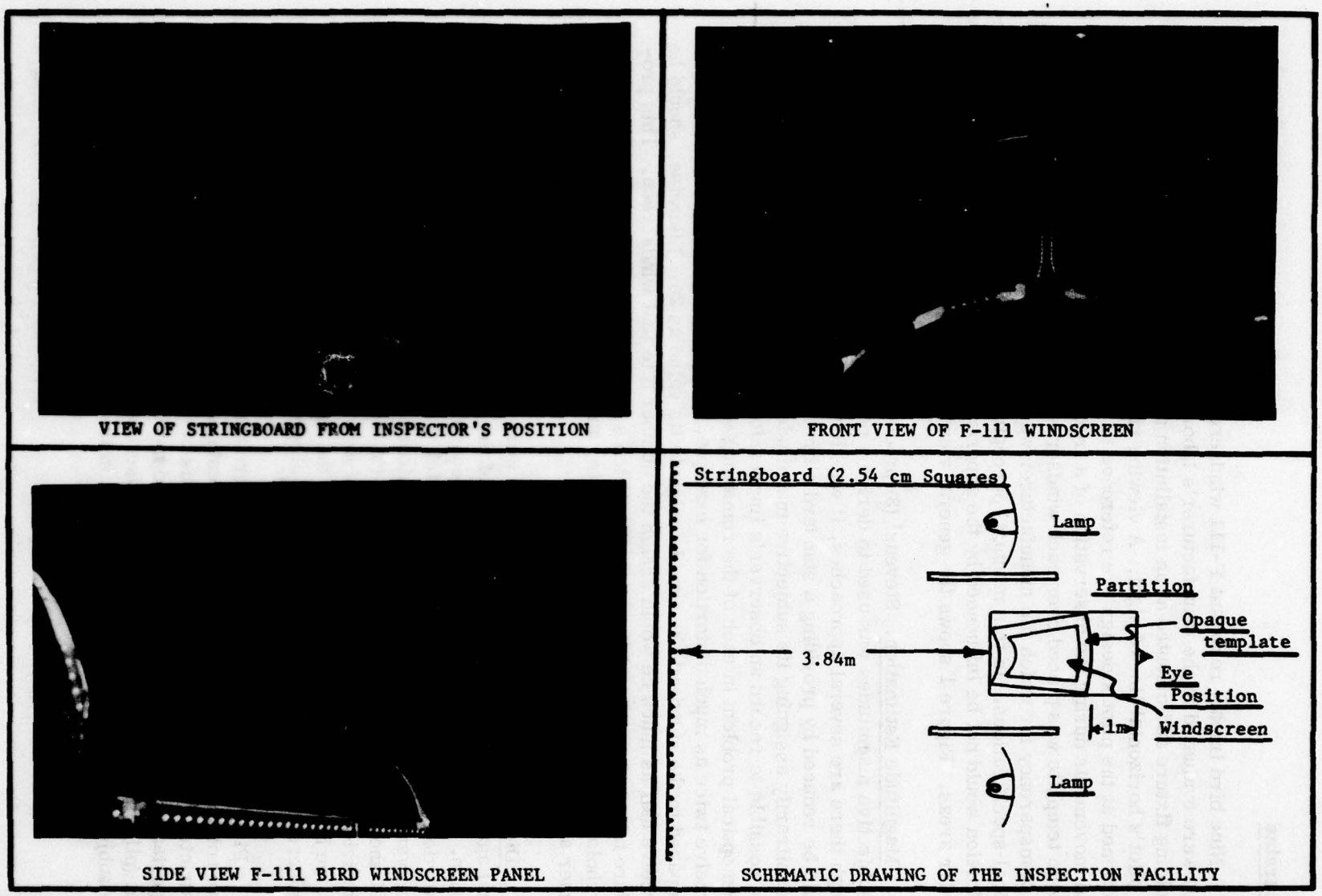


Figure 1. A composite view of the visual inspection arrangement

Procedure

The subjects individually entered the experimental room from a well-illuminated staging area. Upon reaching the standard windscreen, they had 75 s to cycle between the standard and a comparison windscreen, and to form their impression of the relative severity of distortion. The inspector reported his judgment to the experimenter and proceeded to follow the same procedure with the next comparison windscreen. After comparing four windscreens with the standard panel in this manner, the subject left the room and returned to the staging area where the next subject was notified. The subjects were instructed not to discuss the numerical values they had assigned to the windscreens.

The set of four comparison windscreens were changed after the last subject in the sequence had made his judgments and a new set were brought into position. Once all of the windscreen panels had been compared with the standard, the inspectors left the experimental area for approximately three hours, after which time they returned to perform the same comparisons again, using an identical judgment procedure. The order of presentation and the placement of the comparison windscreens with respect to the standard were randomized within and across the two experimental sessions. No windscreen identification numbers were visible to the subject at any time during the experiment.

RESULTS

A logarithmic transformation was performed on the rating data to compensate for any differences in scale factor introduced by the four subjects. Using this transformed data, a correlational analysis was performed to determine the degree of relationship between the perceptual judgments of an inspector across the two experimental sessions. These results are presented in Figure 2.

The correlation coefficients ranged from .704 to .874 for the four subjects, thus showing good stability in the perceptual judgments of distortion for each subject across inspection sessions.

DISCUSSION

Distortions are inherent in any aerodynamically efficient windscreen design. Aircraft windscreens with varying radii of curvature, installed at shallow rake angles usually produce the severest levels and the greatest pattern variations of distortion. Typically, distortion is apparent in terms of deviations of a target object and variable changes in the apparent size of the target. This latter effect is a result of differential magnification throughout the windscreen. These different effects on the perception of a target object, along with others, suggest that there are many parameters of distortion responsible for what is seen through an aircraft windscreen. Consequently, if distortion is treated as a unitary variable, as it was in this study, a quality control inspector must integrate the various aspects of

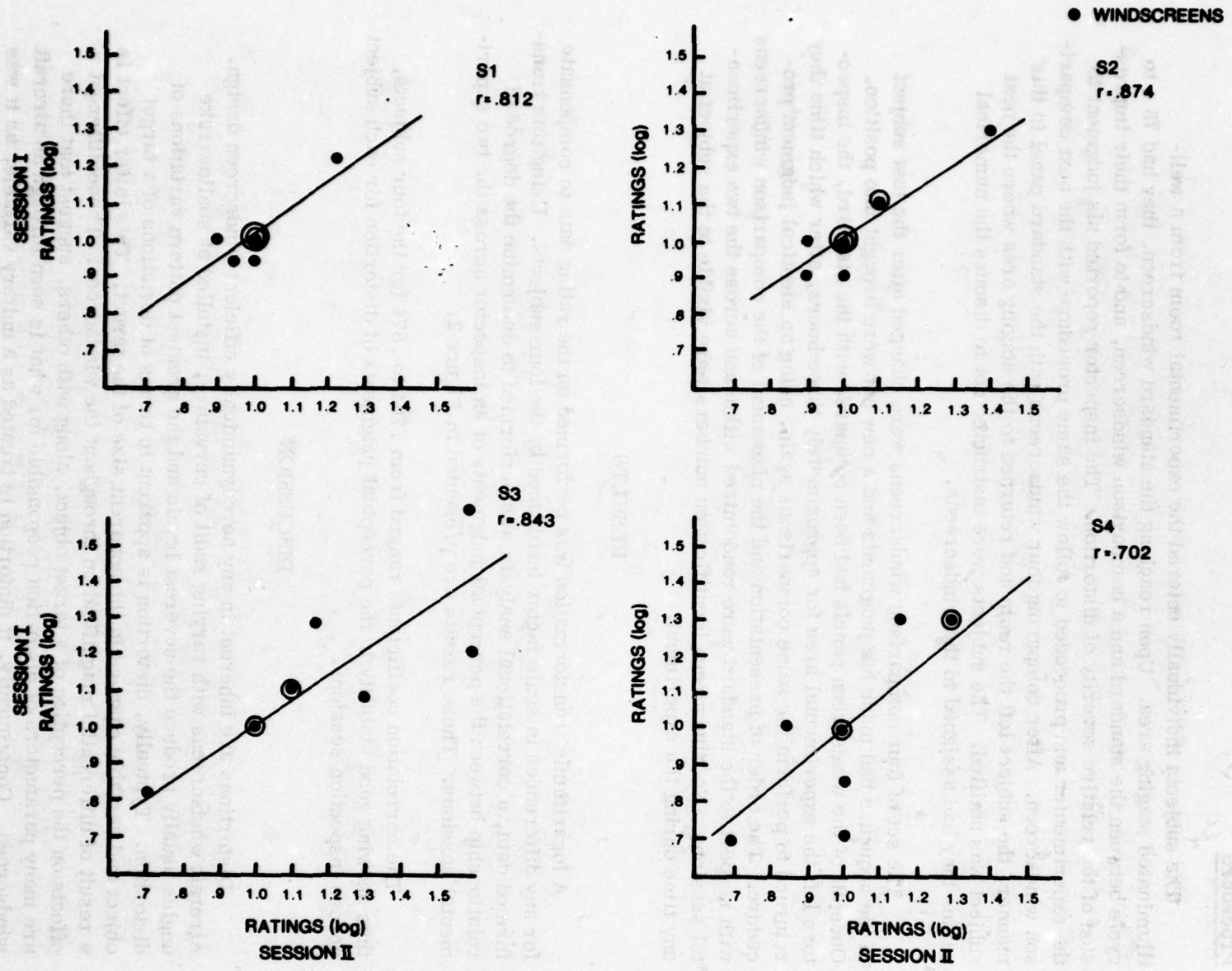


FIGURE 2. A COMPARISON OF DISTORTION JUDGEMENTS BETWEEN RATING SESSIONS

distortion in arriving at his judgment about its overall apparent severity. Clearly, this is a most difficult task. However, the Magnitude Estimation judgment procedure makes it somewhat easier by requiring the inspector to make a relative comparison between the distortions found in two aircraft windscreens. Nevertheless, the visual inspector is still required to subjectively weigh each aspect of distortion, consciously or unconsciously, and determine which windscreen produces the most severe visual effect.

Being a psychophysical phenomenon, perceived distortion can be influenced by changes in the inspector himself, as well as changes in the judgment situation. Altering the room lighting, target object, instructions, or performing the inspection in groups as opposed to individually, will each affect the judgments rendered by a quality control inspector. Judgments may also be affected by increases in fatigue and/or stress experienced by the inspector. All of these factors can potentially reduce the reliability of the visual inspection process.

In the past, the evaluation of aircraft windscreens for visual quality has been performed in essentially a laissez faire manner. Reliability of the judgments rendered in this situation are generally quite low. The reliability of perceptual judgments is better when a standardized inspection procedure is used. As the results of this study demonstrated, reliable judgments of perceived distortion were obtained with the Magnitude Estimation procedure. Furthermore, there was also good compatibility among the four inspectors. The inter-rater correlations were all between .71 and .88 except for one.

Since the distortion ratings for all of the inspectors were substantially in agreement, it is reasonable to pool their judgments and compare the mean ratings for the two experimental sessions. Calculating the coefficient of stability for this data produced an r value of .898 which is higher than the coefficients found for any of the individual inspectors (see Figure 2).

The results of this study are encouraging, as they clearly indicate that reliable judgments of a complex variable like distortion can be obtained by using a systematic, standardized visual inspection procedure. Furthermore, Gomer and Eggleston (1) found a significant positive correlation between magnitude estimates of the perceived severity of distortion and a composite index of distortion provided by the photographic measurement techniques of displacement grade and lens factor. This suggests that these photographic measurements may capture the salient aspects of windscreen distortion.

Considering the data from the present study, along with the findings of the Gomer and Eggleston study, it is recommended that the Magnitude Estimation judgment procedure be used when aircraft windscreens need to be inspected for optical quality. Normally, a windscreen considered to represent the minimum acceptable optical quality should be designated as the standard. It is suggested that the quality control inspector be provided with information indicating the range of magnitudes

that can be expected prior to performing the ME task. This is probably best done by showing the inspectors photographs depicting the effects of the variable to be investigated. It is also suggested that all ratings be made privately, thereby minimizing any unwanted influences which could result from social pressures imposed by a group of judges. If the Magnitude Estimation procedure is used as suggested, maximum reliability should be achieved in the visual evaluation process, particularly when judgments are pooled across three or more quality control inspectors.

It should be noted that no comment has been made regarding the acceptability of aircraft windscreens possessing various amounts of distortion. The Magnitude Estimation judgment procedure allows windscreens to be scaled reliably according to the perceived severity of distortion. It does not, however, provide a means for determining whether or not a given level of distortion is acceptable.

The issue of acceptance is important and must be addressed. At present, subjective opinions rendered by Air Force pilots are used to establish the accept/reject criterion for aircraft windscreens with respect to distortion. Standards of acceptance do not exist for multiple imaging and rainbowing, other than that they should not be "clearly objectionable". Obviously, changes are needed to improve the validity of the acceptance standards for aircraft transparencies. Although subjective pilot opinions are necessary, they should be supplemented with data reflecting how mission performance is affected by different levels of the various optical variables. Research currently underway in the Aerospace Medical Research Laboratory is aimed at finding visual and psychomotor performance decrements resulting from various levels of windscreen induced distortion, multiple imaging, haze, and rainbowing. Data from these studies should be instrumental in establishing valid standards of acceptance for aircraft transparencies based on relevant Air Force mission requirements.

REFERENCES

1. Gomer, F.E., and Eggleston, R.G. Perceived Magnitudes of Distortion, Secondary Imaging, and Rainbowing in Aircraft Windshields. Human Factors, In press, 1978.

2. Mahlman, H.E. Handbook of federal vision requirements and information. Chicago: Professional Press, 1971.

3. Stevens, S.S. Psychophysics: Introduction to its perceptual, neural, and social prospects. New York: Wiley, 1975.

F-111 WINDSCREEN PHORIAS

Lt. Col. B. D. Targove
Aerospace Medical Research Laboratory
Human Engineering Division
Wright-Patterson Air Force Base, Ohio

and

Major W. F. Provines
School of Aerospace Medicine
Physiological Optics
Brooks Air Force Base, Texas

PRECEDING PAGE BLANK-NOT FILMED

F-111 WINDSCREEN PHORIAS

Lt Col Bertram D. Targove
Aerospace Medical Research Laboratory
Human Engineering Division
Wright-Patterson AFB, Ohio

Major Wayne F. Provines
School of Aerospace Medicine
Brooks AFB, Texas

It has been hypothesized by vision scientists that varying magnitudes of windscreen distortion induce varying magnitudes of hyperphoria. Displacement grading is a current method of quantifying F-111 windscreen distortion.

In order to test this hypothesis, three F-111 windscreens of varying displacement grading were evaluated for windscreen induced hyperphoria. "L" had a low displacement grading. "M" had a higher displacement grading but was just within the displacement grading specification. "H" had a displacement grading significantly higher than the specification. Two Helium-Neon lasers, separated by 6.4 cms, were yoked in order to simulate a pilot's binocular line of sight. The windscreens were articulated so as to facilitate an induced phoria measurement at 22 representative locations throughout each of the three windscreens. A throw distance of 10 meters from windscreen to measuring surface was utilized. At 10 meters, a vertical separation of 1 cm between the two laser spots was calculated as 0.1 of a prism diopter (almost exactly 1.0 milliradian).

The maximum induced windscreen phoria level for L was 0.2 prism diopters, M was 0.25 prism diopters and H was 0.55 prism diopters. The mean phoria levels for the 22 locations were L = .0455, M = .1227 and H = .1364. Standard deviations were L = .0554, M = .0813 and H = .1115. An analysis of variance, followed by a post hoc comparison, indicated that the mean of L was significantly lower (95% confidence level) than M or H. No other significant differences between means were found. In comparing the induced vertical phoria variability of the 22 locations measured for each windscreen, it was found that H had twice the variability of induced vertical phoria compared to L and a one-third greater variability compared to M.

The data appear to indicate that if a binocular specification for vertically induced hyperphoria is appropriate, mean induced vertical hyperphoria findings are probably not meaningful as a pass/fail criterion. However, the British method of considering only the maximum vertical hyperphoria value as a criterion would appear to have some merit. In addition, it may be that windscreen vertical phoria variability may be at least as important as the maximum vertical phoria value. The use of twin lasers is not recommended for this evaluation. Time, space and equipment demands might be prohibitive. The use of binocular photographs appears to

PRECEDING PAGE BLANK-NOT FILMED

be a satisfactory method of both evaluating the maximum vertical induced phoria and induced vertical phoria variability.

INTRODUCTION

The F-111 is a USAF aircraft having a low altitude, high speed flight profile. The windscreen (W/S), geometrically configured and structurally designed to meet the aerodynamic demands of this profile, presents certain opticovisual difficulties.

The F-111 W/S configuration presents a low slant angle from the horizontal resulting in a high angle of incidence of 68.4°. It presents a complex curvature best described as conical with radii of curvature varying horizontally from 18" to 31". Early W/S's were 0.945" thick and consisted of multilayered plastic materials in order to provide an acceptable level of bird impact resistance. Those design factors resulted in numerous optical and visual effects due to Snell's law of refraction.

Targove (in press), based on a paraxial optical analysis of the boresight segment of the F-111 W/S, reported a significant potential for deleterious binocular vision effects. The analyses predicted that variable prismatic deviation and variable meridional magnification would result in induced optical phoria and meridional aniseikonia.

A phoria or heterphoria may be described as the tendency of the eyes to turn or deviate in relation to one another. The direction can be in, out, up, or down. This condition results from internal neuro and/or muscular factors, or can be induced by some external action such as the placement of a prism before only one eye. Compensation for the phoria may be made by the retinal fusion reflex in order for the individual to maintain single binocular vision. Aniseikonia as defined by Shapero et al., 1960, is the relative difference in size and/or shape of the two retinal images.

Present optical distortion specifications for the F-111 W/S include displacement grading (D.G.) and lensing which are derived from line grid photographs taken from the pilot's design eye position through the normally installed transparency. Displacement grading may be defined as the maximum linear drift of a grid line away from true horizontal or true vertical. Lensing, either magnification or minification, is determined from line grid expansion or shrinkage from the true grid spacing. Measurement techniques and magnitude limits are characterized by a technique developed by Thompson, 1970.

PURPOSE

The purpose of this study was to investigate the association between the magnitude of displacement grading found in selected F-111 windshields and the tendency for these W/S's to induce a vertical phoria. Preference was given to the D.G. measure of distortion since a preliminary study indicated that it was the factor responsible for induced phorias.

EQUIPMENT

An articulating windshield holding fixture was fabricated to support the windshield. It consisted of a vertically fixed cylindrical stand upon which were mounted two one-milliwatt helium neon lasers. The lasers were fixed so that the beams horizontally separated by 6.4 cm exited at the pilot's design eye position. Adjustment could be made to maintain accurate beam separation and parallel alignment.

A support platform was fulcrumed at the design eye position to allow for elevation and azimuth movements. The platform was configured to hold an F-111 W/S at an angle conforming to the normal aircraft installation angle. Dials in one degree gradations were designed to display accurate W/S positioning. Azimuth changes could be made by manually moving the platform to the indicated dial position. Elevation positions were controlled by a hydraulic pump. With the dial indicators at 0 degrees azimuth and 0 degrees elevation, the twin laser beams simulated the pilot's binocular lines of sight in forward gaze through the windshield boresight. Vertical and horizontal movements of the platform allowed transmission of the beams through any area of the windshield, simulating the pilot's complete binocular field of view.

The laser beam projection target consisted of a 25 cm X 25 cm white square upon which were drawn one mm thick black horizontal lines separated by one cm. With the target placed at 10 meters from the W/S each line represented a deviation of 0.1 prism diopter.* With this setup any vertical deviation of the twin beams induced by the W/S could be quantitatively determined.

PROCEDURE

Three left hand F-111 W/S's manufactured by PPG Industries were selected for their low, moderate and high representation of displacement grading values** as shown in Table I. The W/S with low and moderate D.G. values were from an RDT&E test sample removed from the aircraft after at least one year of operational service. The W/S with high D.G. had never been installed. The W/S's are coded L, M, and H to denote the D.G. values.

---

*1 prism diopter (Δ) = tan 1/100 = 0.57^{0} = 9.9 milliradians.

**Current D.G. specification calls for a maximum value of 150.

TABLE I

WINDSHIELD USED FOR PHORIA STUDY

L serial # 503931	D.G. 125
M serial # 504990	D.G. 140
H serial # 605295	D.G. 170

The W/S to be evaluated was placed on the articulating fixture and swung away from the laser beams so that beam alignment could be made without passing through the transparency. Induced phoria readings were then made in 5 degree azimuth and elevation steps throughout the entire W/S. Deviation of the laser beams were recorded as absolute vertical differences to an accuracy of .05$^{\Delta}$. The W/S was again swung away from the laser beams to assure beam alignment. The remaining two W/S's were evaluated in a like manner. The first W/S was then repositioned on the fixture. Five positions were rechecked, compared to the initial readings and determined to be repeatable to 0.05$^{\Delta}$.

RESULTS

With the 5 degree azimuth and elevation steps induced phoria findings for 22 positions could be determined within the optical zones of each W/S. These positions were arbitrarily numbered as shown in Figure I.

The raw data (absolute vertical difference between right and left laser beam deviation) are presented in Table II. Analysis of the data is presented in Table III. An analysis of variance supplemented by post hoc analyses indicated that W/S L had a significantly lower (95% confidence level) mean than either W/S M or W/S H. This was the only significant difference in means. In comparing the induced phoria variability, W/S H showed twice the variability compared to W/S L and a one-third greater variability compared to W/S M. In W/S L all positions showing induced phorias were of a greater base down prism effect before the left eye thus causing an upward fusional movement of the left eye in relation to the right to maintain single binocular vision. W/S M and W/S H were of predominately the same prism effect with the exception of one reversal (position 17) in W/S M and two reversals (positions 16 & 17) in W/S H. Reversals were of a greater base down prism before the right eye thus causing upward fusional movement of the right eye compared to the left.

Half of the positions measured in W/S L, over three-fourths in W/S M and almost all positions in W/S H revealed an induced phoria effect.

Since the possibility existed that even higher phoria values could exist between the evaluated positions than those found, uncertainty existed as to whether or not the values of 0.2$^{\Delta}$ in W/S L, 0.25$^{\Delta}$ in W/S M and 0.55$^{\Delta}$ in W/S H represented the true maximum values. Additional data was sought by a saturated search throughout the optical zone of each transparency. No greater values were found in W/S L or W/S H, however in W/S M, at 5^{0} left azimuth and minus 12^{0} elevation a value of 0.3$^{\Delta}$ was elicited.

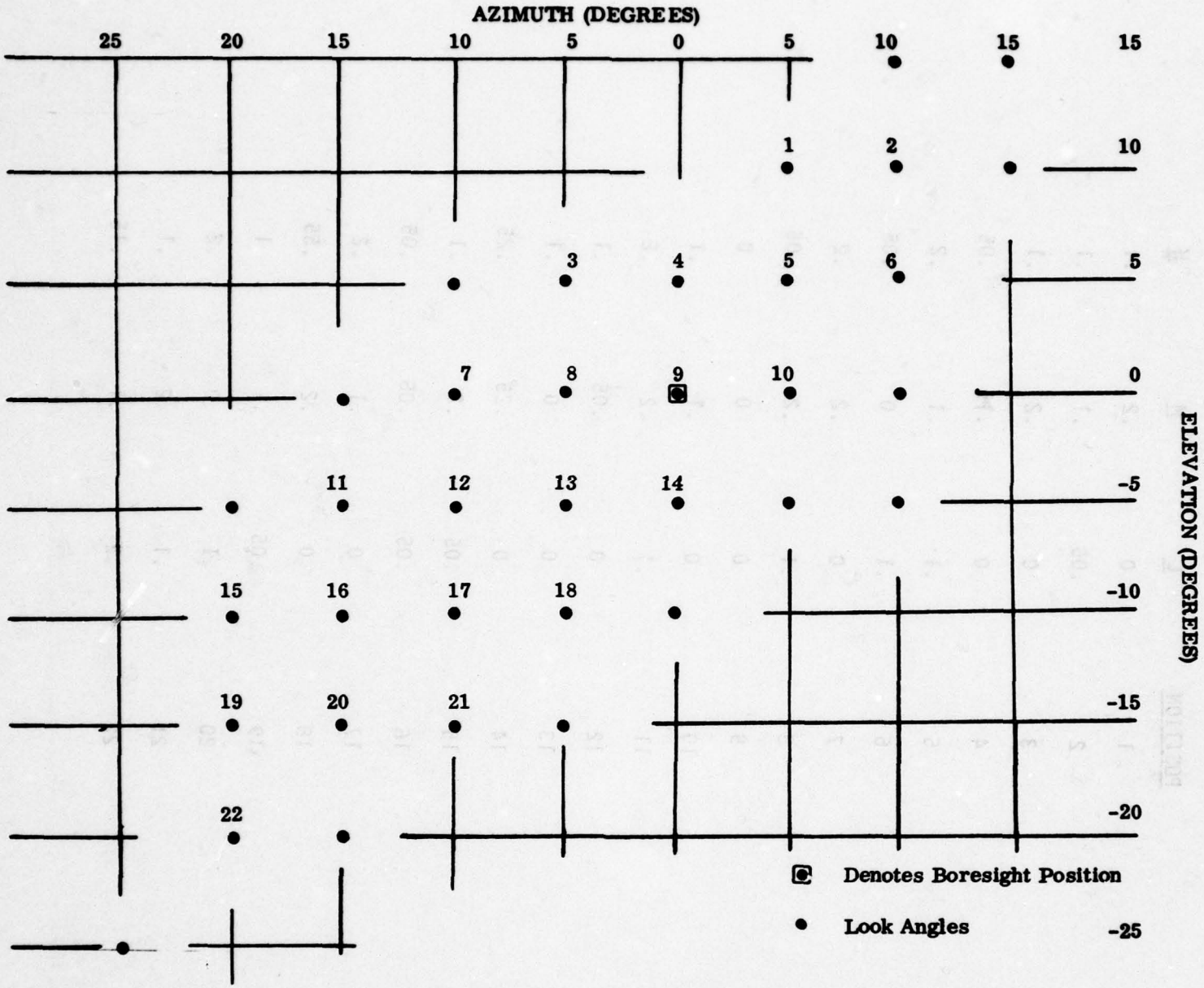


Figure 1. Positions of Induced Phoria Readings Within Windshield Optical Zone

TABLE II

POSITION	L	M	H
1	0	.2	.1
2	.05	.1	.1
3	0	.2	.1
4	0	.15	.05
5	.1	.1	.2
6	.1	0	.05
7	0	.2	.2
8	.1	.2	.05
9	0	0	0
10	0	.1	.1
11	.1	.2	.2
12	0	.05	.1
13	0	0	.1
14	0	.25	.25
15	.05	.2	.1
16	.05	.05	.05
17	0	.1	.2
18	0	.2	.55
19	.05	.1	.1
20	.1	0	.2
21	.1	.2	.1
22	.2	.1	.15

TABLE III

DATA ANALYSIS OF 22 WINDSCREEN POSITIONS

WINDSCREENS	MEAN DEVIATION	MAX. PHORIA	% POSITIONS SHOWING PHORIAS	REVERSALS
L (D.G. = 125)	0.05^{Δ} (S.D. = $.06^{\Delta}$)	0.2^{Δ}	50	0
M (D.G. = 1.40)	0.12^{Δ} (S.D. = $.08^{\Delta}$)	0.25^{Δ}	78	1
H (D.G. = 170)	0.14^{Δ} (S.D. = $.11^{\Delta}$)	0.55^{Δ}	96	2

DISCUSSION

The effects of a phoria upon the visual system are diverse, whether internally mediated or induced. The visual system most often can compensate for a low or moderate phoria. However, as the phoria increases complaints begin to arise. Common symptoms include eye strain, visual fatigue, headaches, etc. Horizontal phoria compensation is relatively large as compared to vertical compensation which falls into a very limited range. Acceptable limits of induced phoria due to prism imbalance are not clear-cut and are somewhat dependent upon factors such as the binocular fusional amplitude, the visual task and fatigue.

An overview of the data analysis indicates a trend of increased induced vertical phoria with higher D.G. values. However, analysis reveals that the mean phoria findings are probably not a meaningful criterion. The phoria variability appears to have more merit. Borish, 1970, reports some adaptation to a sustained vertical phoria, indicating that the visual system will more readily adapt to a constant vertical prism imbalance than to a varying condition.

Nevertheless, a criterion based on the maximum phoria value may be worthwhile. A 0.25 prism vertical imbalance is the maximum permitted in ophthalmic lens prescriptions as specified by the American National Standards Institute, 1972. Corney, 1973, recommended for aircraft W/S's a maximum vertical imbalance of 10mm (0.29^{Δ}) based on the British Military specification that binocular deviation not exceed this limit. The F-111 W/S D.G. maximum limit of 150 to 155, although empirically established, has with few exceptions correlated well with operational aircrew acceptance. A W/S with a D.G. near this limit resulted in a maximum phoria value of 0.3^{Δ}. If indeed binocular specifications for vertical phorias in aircraft W/S's are deemed to be necessary requirement, the relationship of the above factors merit careful consideration.

Magnification or lensing has been shown to be a crucial factor in the F-111 W/S configuration. Although the specific visual effect is uncertain, should the magnification be meridional and unequal to the two eyes, aniseikonia will result, thereby altering binocular depth perception. Ogle, 1962, reported that induced vertical phorias are in some ways additive to aniseikonia. This suggests that D.G., besides creating untoward visual symptoms, may potentially act in concert with lensing to produce a visual spatial warpage effect. These interactions deserve careful investigation.

SUMMARY

F-111 W/S distortion specifications address displacement grading and lensing characteristics. Incremental increases in D.G. were shown to induce upon the visual system corresponding incremental increases in binocular stress. This stress expressed as induced vertical phoria has been verified clinically to bring on adverse symptoms. The visual effects of W/S lensing is conjective but deserves exploration due to the potential inducement of depth perception errors, acting above or together with the D.G. factor.

ACKNOWLEDGMENT

Sincere appreciation is extended to Capt. William Waessner and Capt. Robert Eggleston for their contributions in support of this study.

REFERENCES

1. American National Standards Institute, Z80.1 Committee. Requirement for First Quality Prescription Ophthalmic Lenses. U.S. Gov't Printing Office, 1972.

2. Borish, Irvin M. Clinical Refraction. Third Edition, Ch. 21, The Professional Press, Chicago, 1970.

3. Corney, N. S. Optical Requirements for Aircraft Transparencies. Paper presented at the Conference on Transparent Materials and Enclosures, Las Vegas, 1973 (AFML-TR-73-126, June 1973).

4. Ogle, Kenneth N. In The Eye. Vol. 4, Visual Opters and the Optical Space Sense, Ch. 17, Academic Press, New York, 1962.

5. Shapero, et al. Dictionary of Visual Science. Chilton Co., Phil & New York, 1960.

6. Targove, B. D. Paraxial Opticovisual Analysis of the F-111 Windscreen. Paper to be presented at the Aerospace Medical Association Meeting, New Orleans, 1978.

7. Thompson, K. E. Optical Evaluation of the F-111 Windshield. Report FZM-12-10952A, General Dynamics, Fort Worth Division, Fort Worth, TX, 20 May 1970.

THE EFFECTS OF WINDSCREEN DISTORTION UPON PILOT APPROACH AND LANDING PERFORMANCE

W. L. Welde
Aerospace Medical Research Laboratory
Visual Display Systems Branch
Wright-Patterson Air Force Base, Ohio

THE EFFECTS OF WINDSCREEN DISTORTION UPON PILOT APPROACH AND LANDING PERFORMANCE

William L. Welde

Aerospace Medical Research Laboratory
Human Engineering Division
Wright-Patterson AFB, Ohio

ABSTRACT

A flight test was conducted with a modified NC-131H TIFS (Total In-Flight Simulator) aircraft to quantitatively assess the effect that various levels of windscreen distortion have upon pilot night approach and landing performance. Four highly qualified Air Force C-131 pilots flew visual approaches and simulated landings under three experimental conditions of minimal, moderate, and severe windscreen distortion levels, and one baseline condition of zero distortion. The flight test was accomplished at Niagara Falls airport. The experimental task consisted of flying a heads-down ILS instrument approach to a point two miles from the runway threshold, at which time the pilot transitioned to a night visual approach and simulated touchdown five feet above the runway. After training, each subject pilot performed five approaches with each of three specially fabricated distortion panels that were installed inside the evaluation cockpit, and a similar number of approaches under the no distortion condition. A repeated measures counterbalanced experimental design was employed to minimize the effects of learning and fatigue. Other intervening variables, such as turbulence and crosswind effects were controlled by utilizing the unique capabilities of the TIFS aircraft.

Task performance was assessed from 27 channels of digitally recorded flight parameter data. Pilot comments were also recorded at the conclusion of each approach. The results validated the findings of a parallel study conducted in a Boeing 727 visual simulator. The results indicated that as windscreen distortion increased, there was a degradation in task performance in the final touchdown phase with a definite break in performance occurring between the minimal and moderately distorted windscreen conditions. Distortion caused difficulty for the pilot to precisely determine his altitude above the runway or aircraft rate of descent, thus producing longer and harder landings. Windscreen distortion was found to impact the vertical cues much more than the lateral cues required for runway alignment.

PRECEDING PAGE BLANK-NOT FILMED

INTRODUCTION

Experience in the design and use of windscreens for modern high performance aircraft has led to a need for practical minimum optical specifications which will assure acceptable and safe visual task performance by pilots. Windscreen developments have demonstrated that previously accepted optical standards are difficult to achieve primarily due to current windscreen design considerations, such as (1) complex curvatures to maximize unobstructed field of view for the pilot, (2) installation at high angles of incidence to provide optimum aerodynamic sloping, (3) the use of radar reflective coatings, and (4) composition of thick and multilayered materials to provide aircrew protection against the hazards of bird strikes.

Air Force pilots flying F-111 aircraft have reported significant interference effects with specific in-flight visual tasks from a number of optical variables present in the polycarbonate bird impact resistant windscreen, such as distortion, surface haze, rainbowing, multiple images, internal reflections, and transmission loss. The most complex of these variables to optically characterize, as well as to assess the effects from the standpoint of human visual system performance and ultimately in-flight visual task performance, is distortion. The resultant overall effect of distortion upon pilot task performance varies considerably upon such salient factors as severity of the distortion, type of distortion (e.g., banding, shimmer, line blurring), location in the windscreen, exposure duration, ambient illumination (day versus night), flight visibility conditions, nature of the flying task (target detection versus tracking), task criticality, and individual perceptions. Comments from pilots indicate that the manifestations of distortion cause blurred vision, alterations in the geometric shape of objects such as the runway, targets to jump, changes in the rate of movement, magnification and minification of targets, clinical effects (headaches, fatigue), and in some extreme cases, even cause the target to disappear.

Since 1976, personnel of the 6570th Aerospace Medical Research Laboratory (AMRL), Human Engineering Division at Wright-Patterson AFB, Ohio have been engaged in a significant research effort to relate the aforementioned windscreen optical variables to quantifiable physiological and psychophysical metrics. The specific objectives of AMRL's Windscreen Program are to define and evaluate the interaction between the optical variables and pilot visual task performance in order to (1) define production quality and control tests and procedures, (2) develop visual performance design criteria and tradeoff information for future military aircraft transparencies, and ultimately (3) formulate specifications for the optical quality of aircraft transparencies. One of the initial priorities in this windscreen research was to quantitatively assess the effect that various levels of windscreen distortion have upon pilot night visual approach and landing performance. This flight task is generally considered to be the worst case with respect to the distortion variable. Accordingly, parallel experimental studies on the effects of windscreen distortion upon pilot approach and landing performance were conducted in a flight simulator and a flight test aircraft.

The simulator study was accomplished by The Boeing Company of Seattle, Washington under the direction of Dr. Conrad L. Kraft in a 727-200 aircraft flight simulator. (1) The external visual scene was provided by a computer image generation system. Eight C-141 operational Air Force pilots served as subjects in this windscreen study. The distortion flight test program was conducted by the Calspan Corporation of Buffalo, New York under the direction of AMRL and supported by the Air Force Flight Dynamics Laboratory. This is the report on the flight test program to quantitatively assess the effects of various levels of windscreen distortion upon pilot night visual approaches and landing performance.

METHOD

Apparatus

The flight test was flown in a specially modified Convair NC-131H research aircraft that was capable of simulating the flight characteristics, responses, and feel of virtually any large aircraft. The aircraft, designated as TIFS for Total In-Flight Simulator, was designed and modified by the Calspan Corporation (formerly the Cornell Aeronautical Laboratory) for the Air Force Flight Dynamics Laboratory at Wright-Patterson AFB, Ohio. TIFS was built around the airframe of the C-131B military aircraft version but upgraded to the civilian equivalent of the Convair 580 turboprop transport. The fuselage was extensively modified to include a second evaluation cockpit mounted below and forward of the original crew station. The evaluation cockpit, consisting of two side-by-side pilot positions, was accessed in-flight from the main cabin via a crawlway. Changes to the aerodynamic flight control system included the addition of side force generation surfaces mounted vertically above and below the wing surfaces approximately midway between the engine nacelles and the wingtips. The aircraft's original Fowler flaps were also modified and partly replaced by direct lift flaps. A hybrid digital/analog computer flight simulation system and a flight data recorder system were installed in the cabin of the fuselage.

For the purpose of this study, the TIFS aircraft was flown as a fly-by-wire C-131 with authentic control feel provided by electrohydraulic feel servos attached to the evaluation pilot's cockpit controls. The evaluation pilot's cockpit was configured with the standard yoke flight control and a right hand throttle quadrant. Cockpit instruments included the basic two-axis Attitude Director Indicator (ADI), the Horizontal Situation Indicator (HSI), altimeter, airspeed, vertical velocity, and appropriate engine instruments. A "touchdown" indication was provided to the pilot subject in the left seat by the illumination of a light located above the ADI on the forward instrument panel and an auditory signal in the headset when wheel height above the runway reached five feet as determined by radar altimeter.

Windscreen distortion was simulated in the flight test with 2 by 4 foot flat acrylic transparent panels. Pittsburgh Plate Glass Company (PPG) had originally developed and fabricated eleven optically distorted windscreen panels of known

properties that fundamentally represented a continuum from a minimal degree of apparent distortion to extremely severe distortion. These panels were then photographed against a black grid board with white lines at an angle of 40° from the vertical and a distance of 202 inches. Through a psychophysical scaling process using the 8 X 10 inch photographs of these eleven windscreen distortion panels, twenty individuals rated image quality from the least to the greatest amount of distortion present in the PPG panels. The ratings resulted in two paired sets of three distortion panels each, which represented approximately equal gradations of minimal, moderate, and severe distortion. The one set of three panels was employed in the Boeing simulation study and the second set was used in the flight test program. These windscreen distortion panels were installed in brackets above the glare shield of the left seat pilot's position inside the evaluation cockpit at a 40° angle of incidence and a design eye viewing distance of 21 inches. Through the use of grid board photographs, the actual TIFS evaluation cockpit canopy for the left side was assessed as possessing virtually no inherent distortion characteristics.

A Microwave Landing System (MLS) providing precision glide slope, localizer, and distance information was utilized in the flight test. The MLS receiver was installed in the evaluation cockpit and the portable transmitter was positioned at the departure end of the runway. A digital data acquisition system recorded 58 channels of data at a rate of 50 samples per second, regarding aircraft states, pilot control activity, and aircraft position relative to the runway. Of these recorded parameters, 27 channels of data that were deemed the most germane to assessing pilot flight task performance were selected for data processing. (2)

Procedure

The flight test was flown on runway 28 Right at Niagara Falls International Airport between the hours of 7:30 p.m. and 4:00 a.m. This runway environment was selected after a careful survey of various Air Force bases and civilian airports because of the absence of possible altitude and flight path cues such as: (1) city or other ground lights (roadways), (2) VASI, which is a Visual Approach Glide Slope Indicator System, and (3) runway centerline strobe lights. The entire approach from the outer marker at 4.1 NM to the runway was flown over farmland that was sparcely lighted.

The runway was 9,130 feet in length and 150 feet in width at a mean sea level elevation of 590 feet. The desired touchdown point was 700 feet beyond the approach end of the runway. This point was clearly delineated at night by a lighted taxiway intersecting at the right side of the runway. During the course of the flight test the high intensity approach lights were stabilized at the middle setting of step three and the runway edge lighting at the lower step two level. The TIFS right landing light was utilized throughout the approach, but the left landing light was not illuminated because of side lighting effects on the subject pilot's instrument panel and canopy.

The experimental flight task was initiated by the pilot subject in the left seat engaging the evaluation cockpit flight controls and assuming control of the aircraft on the downwind leg. Heading vectors for intercepting the MLS localizer at the outer marker were provided to the subject by the safety pilots, who closely monitored flight progress. The aircraft was configured for 130 KIAS with the gear down and the Fowler and direct left flaps set at 15°. The test director in the right seat of the evaluation cockpit placed a large cardboard panel above the subject's glare shield to obscure his forward vision through the windscreen. The subject's task was to intercept the ILS localizer and 2.5° glide slope and fly a strictly heads-down instrument approach with reference to the ADI flight director needles, the HSI, and the airspeed indicator. At a point two NM from the runway, the ADI flight director needles were driven out of sight, the cardboard panel was removed from the left windscreen, and the test director advised the subject to complete the approach visually.

A bias was used in the ILS localizer signal to cause the aircraft to be positioned either to the right or to the left of centerline approximately 400 feet when the localizer needle was flown precisely centered at the two NM instrument to visual transition point. The glide slope signal was not biased from the actual angle. The purpose of the localizer bias was to increase the difficulty of the flight task by forcing the subject to make definite control inputs to visually align the aircraft with the runway centerline, and also to avoid the possibility of the subject merely holding aircraft attitude and rate of descent down to the runway. In addition, the altimeter and vertical velocity instruments were covered so this information was not available to the subject in his visual approach, which if used would have invalidated the data. The specific intent was to insure that the subject flew the aircraft from the two NM point through the landing phase by employing only those visual cues provided by the lighted runway environment as viewed through the four experimental windscreen conditions.

Actual touchdowns on the runway were not accomplished by the subject for two considerations. The primary reason was that the TIFS aircraft gross weight exceeded the maximum permissible landing weight for the major portion of each flight. Also, the eye height of the subject in the evaluation cockpit was somewhat lower for landing than that encountered when flying a standard C-131. Therefore, when the aircraft descended to a wheel height of five feet above the runway, a "touchdown" light illuminated at the top of the subject's forward instrument panel and, additionally, a characteristic tire squeal was heard in the headset. At this moment, the safety pilots simultaneously disengaged the evaluation cockpit flight controls, assumed full control of the aircraft, and executed a go-around without actually touching down. The safety pilots always maintained the prerogative to take control of the aircraft whenever they observed a potential hazard to flight safety. This action was occasionally necessitated during the subject's final phase of landing due to low airspeed, high sink rates, significant deviation from the runway centerline or unusual aircraft attitude. The landing criteria for the subject was to touchdown on the centerline at 700 feet down the runway opposite the taxiway at a minimum of 125 KIAS.

The unique capabilities afforded by the TIFS research aircraft were utilized profitably in neutralizing or, at least, standardizing certain environmental effects, such as crosswind and air turbulence, that traditionally plague flight test studies due to the inherent variability of these uncontrolled factors across experimental conditions. For example, the requirement to fly the aircraft in either a crab angle or wing down manner in order to maintain track towards the runway centerline because of the crosswind effect was eliminated by adjusting the side force generation surfaces on the TIFS aircraft. A radio call was made to the control tower to determine the wind direction and velocity at the beginning of each approach. Also, the experimental trials were conducted in a standardized condition of light clear air turbulence. If natural turbulence was not present, which often was the case, a taped set of random signals was played into the TIFS variable stability system to produce a realistic light motion turbulence.

The weather conditions encountered on the data collection flights were excellent with a predominantly clear or high scattered cloud condition, visibility varying between 7 to 20 miles with a mean around 15 miles. Several flights were cancelled due to ground fog or rain. The entire flight test, including equipment calibration, training, and data collection flights, was accomplished over 23.8 flight hours in 14 sorties and approximately 130 approaches.

Experimental Design

A repeated measures experimental design was employed in this study, in which all four pilot subjects flew five approaches with each of the three experimental conditions of minimal, moderate, and severe windscreen distortion levels, and the baseline condition of zero distortion (no panel installed). A completely counterbalanced design was established for the presentation order of windscreen distortion conditions (none, minimal, moderate, severe) time of night flown (early or late flight), and the direction of offset from runway centerline (left or right). Thus, the effects of learning and fatigue were minimized through counterbalancing. Each subject initially flew a minimum of five approaches for training prior to data collection for the purpose of becoming familiar with the experimental procedures. Since the TIFS aircraft was flown with the basic force and response characteristics of a C-131B, transfer of training was maximized for the subjects.

Subjects

Four highly qualified Air Force pilots assigned as flight test pilots to the 4950th Test Wing at Wright-Patterson AFB, Ohio voluntarily served as experimental subjects in this study. They ranged in age from 28 to 40 years (mean = 34 years). The subjects' total flying time varied from 1350 to 3630 hours (mean = 2270 hours). Flying time in the C-131B aircraft, in which they were currently operational, ranged from 120 to 840 hours (mean = 390 hours). All subjects were administered an optometric examination that confirmed they possessed normal uncorrected visual acuity, convergence, and stereopsis.

RESULTS

The pilot approach and landing flight task performance was assessed by means of a series of one-way analyses of variance statistical tests. (3) In each analysis, windscreen distortion (with repeated measures on subjects) was treated as the independent variable. With the data collapsed across four subjects and five trials each, the following recorded parameters were selected as the dependent variables in the analyses:

RMS Pitch Angle
RMS Roll Angle
RMS Pitch Rate
RMS Roll Rate
RMS Yaw Rate
Average Indicated Airspeed
RMS Indicated Airspeed
RMS Flight Path Angle
RMS Vertical Velocity
RMS Heading Error
RMS MLS Localizer Error
Absolute Average MLS Localizer Error
Absolute Average Glideslope Error
RMS Elevator Force
RMS Aileron Force
RMS Rudder Force
MLS Distance at Touchdown or Takeover
MLS Localizer Error at Touchdown or Takeover

In order to maximize the sensitivity of the statistical analyses, approach performance was divided into four distinct geographical segments: (1) visual breakout at two NM to one NM from runway threshold, (2) one NM to runway threshold, (3) runway threshold to touchdown (simulated) or takeover by the safety pilots, and the (4) touchdown or takeover point.

The average initial conditions or aircraft status at the instrument to visual breakout point at two NM were determined for the 80 experimental approaches. Breakout occurred at approximately 2.12 NM distance from the runway threshold and a 1.09^{o} absolute MLS localizer error, which indicated the aircraft was an average of 440 feet either to the left or right of runway centerline at breakout. The aircraft mean altitude above ground was 640 feet at an indicated airspeed of 133.4 knots and a flight path angle of -2.7^{o}.

For the first segment consisting of breakout to one NM from runway threshold, no significant differences (i.e., $p \leq .05$) in pilot performance were detected as a function of windscreen distortion for any of the dependent variables treated. In the second segment from one NM to runway threshold, only a single variable resulted in

a statistically significant difference in pilot flight task performance. As shown in Table 1, which presents the mean scores on each dependent variable found to be statistically significant, RMS roll angle systematically increased with a corresponding increase in windscreen distortion. The third segment from runway threshold to touchdown or takeover produced four variables with significant differences, as seen in Table 1. The three RMS variables of indicated airspeed, vertical velocity and flight path angle exhibited similar trends. The lowest scores were associated with

TABLE 1

STATISTICALLY SIGNIFICANT ($p \leq .05$) PILOT FLIGHT TASK PERFORMANCE PARAMETERS FOR WINDSCREEN DISTORTION LEVELS

	Windscreen Distortion			
Segment/Parameter	None	Minimal	Moderate	Severe
1 NM to Runway Threshold				
RMS Roll Angle	1.74	2.00	2.06	2.29
Runway Threshold to Touchdown or Takeover				
RMS Indicated Airspeed	1.38	1.13	1.97	2.24
RMS Vertical Velocity	1.59	1.45	2.22	2.57
RMS Flight Path Angle	0.41	0.38	0.57	0.66
Absolute Average MLS Localizer Error	0.05	0.04	0.04	0.07

the none and minimal windscreen distortion levels and the highest RMS values linked with the moderate and severe distortion conditions. A definite trend towards significantly degraded task performance was manifested between the minimal and moderate distortion levels. Absolute average MLS localizer error did not differentiate among the various levels of windscreen distortion with much precision. Severe distortion produced the most error, whereas the amount of error for none, minimal, and moderate distortion was for all practical purposes equal. The fourth segment, on which analyses were accomplished and presented in Table 2, dealt with the MLS localizer error in feet from the runway centerline and the distance down the runway from the threshold at touchdown or takeover. Absolute average MLS localizer error for the none, minimal, and moderate windscreen distortion conditions was similar, but considerably greater runway centerline deviation occurred with severe distortion. Furthermore, by examining Table 2, it can be seen that a

TABLE 2

AIRCRAFT POSITION ON THE RUNWAY
AT TOUCHDOWN OR TAKEOVER

Performance Parameter	Windscreen Distortion			
	None	Minimal	Moderate	Severe
Absolute Average MLS Localizer Error	6.5'	4.9'	6.1'	13.2'
Runway Distance Beyond The Desired 700' Point	274'	213'	882'	1246'

significant difference in touchdown distance was associated with the lower distortion levels of none and minimal than that encountered with the moderate and severe distortion conditions. However, in all cases, the touchdown or takeover distance was beyond the desired 700 foot point.

Table 3 depicts the number of occasions that the safety pilots felt compelled to assume control of the TIFS aircraft because of a hazard to safety of flight. Of the 80 approaches flown, safety pilot takeover occurred on 39 trials. A Chi Square test was applied to the takeover data to determine whether the number of incomplete touchdown attempts differed as a function of windscreen distortion. No significant difference was detected, although it is apparent from Table 3 that considerably more takeovers resulted when any windscreen distortion panel was installed.

TABLE 3

NUMBER OF SAFETY PILOT TAKEOVERS
PRIOR TO SIMULATED TOUCHDOWN

Pilot	Windscreen Distortion				
	None	Minimal	Moderate	Severe	Total
A	1	4	3	3	11
B	3	3	2	1	9
C	0	0	5	4	9
D	1	3	3	3	10
Total	5	10	13	11	39

DISCUSSION

The pilot performance data for the approach and landing flight task reflected greater differences in the quality of performance among the four windscreen distortion conditions as the aircraft neared the touchdown point. The effects of greater windscreen distortion levels resulted in increased erratic aircraft control and degraded landing performance. On four of the seven recorded parameters that were found to be statistically significant, pilot performance was found to deteriorate sharply when flying with the moderate and severe windscreen distortion conditions. It appears that with these two higher distortion levels the pilots become less assured of themselves and, thus, become overly cautious and yet more variable in their performance. Longer and harder landings resulted from inferior and erratic control of airspeed, vertical velocity, flight path angle, and roll angle. Conceivably, the distorted visual scene afforded by the moderate and severe windscreen panels caused the pilots to find the visual cues required for night landings less reliable. This would naturally lead to a situation of more variable control inputs as the pilot attempted to find the proper attitude and rate of descent for landing.

Comments from the pilot subjects indicated that distortion caused them to feel unsure of their precise altitude above the runway and more hesitant regarding when to round out for landing. The pilots confirmed that they compensated for the higher distortion conditions and unreliable vertical cues by maintaining a slightly higher airspeed than normal throughout the landing phase. Although the pilots encountered multiple images from the approach lights when viewing the runway through the greater distortion levels, they expressed they had considerably more difficulty with depth perception cues than with those references used in runway alignment.

Results from this flight test study validated earlier findings from the Boeing simulation experiment regarding the degradation in approach and landing performance for the moderate and severe windscreen distortion levels. Further research is being conducted at AMRL to quantitatively characterize distortion found in the current production of military aircraft transparencies in order to relate the effects of distortion with pilot flight task performance found in these two studies.

REFERENCES

1. Kraft, C.L., Anderson, C.D., Elworth, C.L., and Larry, C. Windshield Quality and Pilot Performance. AMRL-TR-77-39, October 1977.

2. Reynolds, P.A. Calspan Data from the Windshield Distortion Flight Tests. TIFS Memo No. 807, October 1976.

3. Schori, Thomas R. Windshield Distortion Program: Inflight Evaluation. University of Dayton Research Institute Memo, April 1977.

PREDICTION OF WEATHER-RESISTANCE OF TRANSPARENT PLASTICS BY MULTICONDITION ACCELERATED EXPOSURE

J. M. Kolyer
Rockwell International Corporation
Autonetics Strategic Systems Division
Anaheim, California

PRECEDING PAGE BLANK-NOT FILMED

PREDICTION OF WEATHER-RESISTANCE OF TRANSPARENT PLASTICS BY MULTICONDITION ACCELERATED EXPOSURE

J. M. Kolyer
Rockwell International Corporation

ABSTRACT

The key factor in degradation of plastics by weather is ultraviolet (UV) light. Therefore, acceleration of the weathering process is achieved customarily by increasing the rate of deposition of UV light on samples. For indoor (cabinet) tests, the generally-accepted method is to maintain a constant level of simulated noon summer sunlight. This is a time-compression procedure which is used in commercial instruments such as the Weather-Ometer and Xenotest.

A limitation to the usual procedure is that only one set of arbitrary conditions is maintained during an exposure period. Thus, the relative effects of light intensity, temperature, and humidity are not distinguished. In contrast, we exposed samples to 24 different combinations of the weather factors at one time. This was accomplished by grouping Pyrex/quartz environmental chambers, differing in temperature and humidity, about a single xenon lamp. Light intensity was controlled by the lamp-to-chamber distance.

Plastics studied were polycarbonate and polystyrene. The prediction methodology was as follows: (1) Extensive accelerated data were obtained by the above multicondition procedure. Increasing degrees of yellowness and loss in tensile strength were measured. (2) Weather conditions at the outdoor exposure test sites were analyzed into "environmental cells", each with a range of UV light intensity, temperature, and humidity. (3) Based on the accelerated data, degradation rates were assigned to the above "cells". (4) Increments of degradation were predicted by multiplying the total time the weather spent in each "cell" by the degradation rate for that "cell". (5) The latter increments were summed using Weibull or log-normal mathematical models.

Successful predictions were achieved for exposure in Phoenix or Miami, and the relative importance of weather factors was made clear. It was concluded that multicondition accelerated exposure is a new and important technique.

PRECEDING PAGE BLANK-NOT FILMED

I. INTRODUCTION

In general, the key factor in degradation of plastics by weather is ultraviolet (UV) light. Therefore, acceleration of the weathering process is achieved by increasing the rate of deposition of UV light on samples. Figure 1 diagrams the common procedures. One method uses natural sunlight which is concentrated about 8 times by front-surface mirrors on follow-the-sun mounts (Desert Sunshine Exposure Tests, Inc.; Reference 1). The more common method, used in indoor (cabinet) tests, "compresses" exposure time by maintaining simulated noon summer sunlight on a 24-hour basis. This time-compression procedure is the principle of commercial cabinet instruments such as the Weather-Ometer (Reference 2) and Xenotest (Reference 3). References 4 and 5 are reviews of recent developments in accelerated testing. The subject also was briefly reviewed in our paper given at the last Conference on Aerospace Transparent Materials and Enclosures (Reference 6).

Both the sunlight-concentration and time-compression methods have their pros and cons. The time-compression method has the disadvantage of imperfect simulation over the entire solar spectrum but the advantages of convenience and precise control of variables. Our work has involved appraisal of both methods in prediction methodology, but only results with the time-compression method are reported here.

A limitation to the usual time-compression procedure is that only one set of arbitrary conditions, intended to simulate a particular exposure site, is maintained inside the cabinet. Thus, the relative contributions of light intensity, temperature, and humidity are not distinguished. A long succession of exposures would be needed to give enough degradation rate data for predictions for various climates. In contrast, we exposed samples to 24 combinations of the basic weather factors at one time, as will be described below. In effect, we operated "twenty-four miniature Weather-Ometers" simultaneously. Therefore, our procedure is referred to as "multicondition accelerated exposure" as opposed to the customary single-condition method.

The present results were obtained in a study of accelerated/abbreviated test methods for the weather-resistance part of the Encapsulation Task of the Department of Energy's Low-Cost Silicon Solar Array Project and was performed under Contract No. 954458 from the Jet Propulsion Laboratory.

II. EXPERIMENTAL PROCEDURE

A. Plastic Films Studied

The films studied were:

(1) polystyrene, 0.13 mm (5 mils) thick, non-UV-stabilized, clear, biaxially-oriented

(2) General Electric's Lexan 8740 polycarbonate, 0.13 mm (5 mils) thick, non-UV-stabilized.

Note that unstabilized Lexan was used to provide rapid degradation data for mathematical modeling. Lexan for outdoor use, e.g., in aircraft windshields, is always stabilized.

B. Multicondition Accelerated Exposure

Full details are given in Reference 7. The essence of the procedure is that plastic film samples were hung in 24 separate rectangular Pyrex tubes, each with a different combination of UV light intensity, air temperature, and relative humidity. Eighteen of the Pyrex tubes were placed inside quartz tanks through which water was circulated. These tanks were grouped around a 2500 watt xenon lamp as shown in Figure 2. Pyrex was chosen as the tube material because it attenuates UV light at around 300 nanometers, where the lamp emits too strongly. Light intensity was established by the lamp-to-sample distance, and air temperature was regulated by water circulated through the quartz tanks. The relative humidity was controlled at 0% by Drierite desiccant, at 50% by a glycerol-water solution (Reference 8), or at 100% by deionized water placed in the bottom of the tubes. A shutter, diagrammed in Figure 1, was raised and lowered to provide alternating 12-hour periods of light and shade for six of the tubes. Spectroradiometric data established the level of UV radiation, integrated from 300 to 400 nanometers, in terms of "typical noon sunlight" based on measurements made at 1 PM, June 30, 1976, at Anaheim, CA. In addition to the 18 illuminated tubes, 6 tubes representing dark conditions, not diagrammed in Figure 1, were immersed in constant-temperature baths. These 24 different environmental conditions are listed in Table 1.

A view of the exposure cabinet and power supply for the xenon lamp is shown in Figure 3. Figure 4 shows the interior of the cabinet with the quartz chambers grouped about the lamp.

C. Outdoor (Natural) Exposure

Films were exposed at 45°S on racks near Phoenix, AZ (Desert Sunshine Exposure Tests, Inc.) and at Miami, FL (South Florida Test Service, Inc.). To find the effect of season on initial rates of degradation, exposures were started at different times. Polystyrene exposure began in Miami on October 20, 1976. Lexan exposures at both sites began in early fall of 1976 (September 1 in Miami, September 12 in Phoenix), on December 22, 1976, or on June 21, 1977.

D. Measurement of Degradation Due to Weathering

Among several properties checked, yellowness (as measured by optical transmission at 360 nanometers) and tensile strength were selected for mathematical modeling and prediction. The optical property was easily and precisely measured, while tensile strength is considered a critical mechanical property whose decrease indicates extensive polymer degradation.

Absorbance at two wavelengths, 360 and 600 nanometers, was determined on the films with a Cary 16 Spectrophotometer. In the tensile test, strips 0.20 inch (0.5 cm) wide were pulled at a crosshead speed of 2 inches/minute (5 cm/minute) for Lexan and 0.2 inches/minute (0.5 cm/minute) for polystyrene. An Instron testing machine was used. See Reference 7 for full details. All data points are the means of 5-10 replicates.

III. RESULTS AND DISCUSSION

A. Prediction Methodology

Steps in making a prediction were as follows:

(1) Based on multicondition accelerated data, a mathematical equation to model the course of degradation was selected. The equation had one or more parameters analogous to rate constants in chemical kinetics.

(2) To cover the expected range of weather conditions, a matrix of "environmental cells" was constructed with the dimensions (a) UV intensity, (b) air temperature, and (c) relative humidity. Using the accelerated data, "rate constant" values were assigned to each cell.

(3) Weather conditions were defined for a given exposure site for 7-9 AM, 9-11 AM, 11 AM-1 PM, 1-3 PM, and 3-5 PM of the "typical day" of each month.

(4) Using the above "environmental cell" matrix, "rate constant" values were assigned to each time period of each typical day.

(5) Two-hourly increments of degradation throughout each typical day were summed using the model equation. The result is the increment of degradation applicable to each month.

(6) Monthly increments of degradation were summed over the total exposure period to obtain the prediction.

B. Predictions for Yellowing of Films

1. Polystyrene

The results are discussed in terms of the six prediction steps outlined above.

(1) Figures 5-8 illustrate Weibull plots of the yellowness data for the 18 illuminated conditions of accelerated exposure. Since yellowing is caused by UV light, it was negligible for the 6 dark conditions. Also, data with the shutter operated were in line with the rest, indicating that the yellowing reaction proceeded negligibly slowly in the dark periods. In the figures, the abscissa represents exposure time, while the ordinate represents yellowness numerically expressed as $A_{360} - A_{600} - 0.0139$. This quantity is the increase in absorbance at 360 nanometers due to exposure. The absorbance at 600 nanometers, A_{600}, is subtracted to correct for light scattering and reflection losses which vary from sample to sample, thus putting all determinations on the same basis. The value 0.0139 is the inherent $A_{360} - A_{600}$ value for unexposed film and is subtracted because we wish to work with the increase in A_{360} due to weathering.

The data points in Figures 5-8 define straight lines well enough to justify use of the Weibull model as the equation for use in prediction. The Weibull model is:

$$\ln\left(\frac{1}{p}\right) = \log_e\left(\frac{1}{p}\right) = \lambda t^{\beta} \qquad (1)$$

where P is fraction of some original property, λ is the scale parameter, β is the shape parameter, and t is exposure time. In the present case P is the transmittance T, which is related to absorbance A by the equation $A = \log_{10}(\frac{1}{T})$.

Equation (1) may be rewritten as:

$$\log_{10}(A_{360} - A_{600} - 0.0139) = \log_{10}(\frac{\lambda}{2.3}) + \beta \log_{10} t \qquad (2)$$

Equation (2) is represented by the linear plots in Figures 5-8, which have the form $y = mx + b$ where

$$y = \log_{10}(A_{360} - A_{600} - 0.0139),$$

$$mx = \beta \log_{10} t, \text{ and}$$

$$b = \log_{10}(\frac{\lambda}{2.3}).$$

Thus β is the slope of the line and has the value 0.90 in all four cases.

In conclusion, the Weibull equation with $\beta = 0.90$ is a good model for this set of accelerated data. The Weibull equation is commonly used in reliability studies (Reference 9). It has previously been proposed as a model for the degradation of plastics due to weathering (Reference 10).

(2) Since the points for different humidity levels fall along the same line, humidity can be neglected as a variable in the yellowing reaction. Also, the mean monthly humidity varies little (Table 3). Thus the matrix is simplified to two dimensions instead of three. The "rate constant" $\lambda/2.3$ from equation (2) is equal to the value of $A_{360} - A_{600} - 0.0139$ when $t = 1$ because $\beta \log_{10} t$ in equation (2) becomes 0 when $t = 1$. Therefore, by reading values at the $t = 1$ intercept, the graphs of Figures 5-8 provide the following rate data:

UV Intensity Relative to Noon Summer Sunlight	Air Temp., °C	$\lambda/2.3$, hour^{-1}
0.66	18.3	0.00108
0.66	55.3	0.00173
1.00	26.1	0.00177
1.00	60.3	0.00245

To interpolate and extrapolate these data, an Arrhenius type relation between $\lambda/2.3$ and the absolute temperature was assumed. The relation of $\lambda/2.3$ to light intensity was linear as expected. Using graphical methods, the data were arranged in 260 two-dimensional "cells" for the temperature range 15 to 40°C and for UV intensity in 0.1 increments. Each cell was assigned a "rate constant" value.

(3) Miami weather-station data (Reference 11), coupled with test-site data (Reference 12), provided temperature averages during daylight hours for each month. Next, UV intensities were estimated. The data of Reference 13, page 137, were taken as a working approximation of seasonal variation, and the data of the same reference, page 124, were used to estimate intensity variation during the day. These literature data were used to assign relative UV intensity values with reference to July noon sunlight = 1.00. Thus, the key assumption was made that our cabinet provided the UV level of July noon sunlight in Miami. All these approximations were necessary because precise daily measurements of the outdoor UV intensity were not available. However, the need for such data has been recognized (Reference 14) and test services are preparing to take spectroradiometric readings routinely. With precise outdoor data to correlate with cabinet UV data, much more accurate predictions will be possible in the future.

(4) The summary of Miami weather data is shown in Table 2. By looking up $\lambda/2.3$ values in the 260-cell matrix described above, a "rate constant" was assigned to each of the two-hourly periods in Table 2.

(5) The following equation, explained in Reference 7, was used to sum the five two-hourly increments of degradation over the typical day of each month:

$$\log_{10}\left(\frac{1}{P}\right) = \left[\left(\begin{matrix}\lambda/2.3 \text{ for} \\ 7\text{-}9 \text{ AM}\end{matrix}\right)^{1/\beta} t + \left(\begin{matrix}\lambda/23. \text{ for} \\ 9\text{-}11 \text{ AM}\end{matrix}\right)^{1/\beta} t \right.$$

$$\left. + \ldots \left(\begin{matrix}\lambda/2.3 \text{ for} \\ 3\text{-}5 \text{ PM}\end{matrix}\right)^{1/\beta} t\right]^{\beta} \qquad (3)$$

where P = fraction of original transmittance at 360 nanometers, $\beta = 0.90$, and t = 1/12 day. The result was a list of $\lambda/2.3$ values by month.

(6) To sum increments of degradation over each exposure period, equation (3) was used again, but this time the $\lambda/2.3$ values were for each month and t was equal to exposure days during each month.

Predicted vs. actual data points are plotted in Figure 9. Considering the assumptions necessary, especially concerning UV intensity, agreement between predicted and real values is good. Although the Weibull model seems appropriate, the lognormal model (Reference 15) has also been applied successfully to fit outdoor weathering data.

2. Lexan

Accelerated exposure gave about 20 times the expected rate of yellowing for Lexan. This result was explained by a mismatch of the solar spectrum and the xenon lamp at about 295-300 nanometers, which is the wavelength region responsible for yellowing (Reference 16). One set of approximate spectral measurements at 300 nanometers indicated that the new xenon lamp was 40 times as intense as sunlight. As the lamp aged, its efficiency in yellowing Lexan decreased because the lamp output at 300 nanometers decreased. Polystyrene yellowing rate was unaffected presumably because the most damaging wavelength in this case is 319 nanometers (Reference 6), at which a match of sunlight and lamp intensities was maintained.

The accelerated data up to about $\log_{10}\left(\frac{1}{P}\right) = 0.5$ could be represented by a Weibull plot with slope = $\beta = 1$. This is the exponential model, a special case of the Weibull model:

$$\log_{10}\left(\frac{1}{P}\right) = \left(\frac{\lambda}{2.3}\right) t \qquad (4)$$

Humidity played a minor role, accounted for by interpolation to the average levels at the exposure sites.

By a similar procedure to that described in detail for polystyrene above, values of $\lambda/2.3$ were assigned to the typical day of each month in Miami and also in Phoenix. In this case, λ represents the rate constant for a zero-order chemical reaction in which $\log_{10}(\frac{1}{P})$ is the chromophore concentration.

Predicted vs. actual values are plotted in Figure 10 for Miami and in Figure 11 for Phoenix. Note that a mismatch of lamp and sunlight at the critical wavelength made it necessary to use the 300-day actual data point as the reference for predictions. Hence, the form of the predicted curves, not their absolute values, is significant.

C. Predictions for Loss of Tensile Strength

1. Polystyrene

The accelerated test data were less extensive for tensile strength than for yellowing. Therefore, the same UV intensity and temperature effects as for yellowing were assumed. The plot of accelerated data at 0% relative humidity could be approximately represented by the Weibull equation:

$$\log_{10}(\frac{1}{P}) = (\frac{\lambda}{2.3})\, t^{0.77}$$

Predicted values are compared to actual results in Figure 12. Again, agreement is good.

2. Lexan

Accelerated data approximately fitted the Weibull equation with $\beta = 0.55$. Agreement with outdoor data was fair after 300 days: $\log_{10}(\frac{1}{P}) = 0.79$ predicted vs. 0.62 found in Miami, and 0.76 predicted vs. 0.57 found in Phoenix. Unlike yellowing, tensile strength loss was not hyperaccelerated. The explanation is that light of two wavelengths, 295 and 330 nanometers, is responsible for degrading Lexan (Reference 16). It is believed the 295 or 300 nanometer region was responsible for yellowing while the 330 nanometer region caused chain-scission of the polymer, apprehended as loss of tensile strength. Though the xenon lamp's intensity was too high at

295-300 nanometers, it was well-matched with sunlight at 330 nanometers and changed negligibly with aging at this wavelength.

D. Relative Effect of UV Light, Temperature and Humidity on Other Properties

Multicondition accelerated exposure is useful for establishing the effect of individual weather variables on the overall degradation rate. For example, we followed the loss of gloss of Lexan as judged by transmittance of the film at 600 nanometers. The loss of gloss causes light-scattering and lowers the optical transmission. In the twenty-four accelerated conditions, significant loss of gloss occurred only under UV light and at 100% relative humidity. This result shows that moisture can play a key role in UV degradation. Temperature was also influential. Similar effects were indicated for polystyrene but to a lesser degree. On the other hand, the formation of surface carbonyl groups on polystyrene, also requiring UV light, was little affected by moisture level. In contrast, degradation of certain solar cells proved to be dependent on moisture and temperature but not at all on UV light. These examples, summarized in Table 3, demonstrate the usefulness of the multicondition method in judging the relative effects of basic weather factors.

IV. CONCLUSION

The conclusion is that multicondition accelerated exposure is an important technique. It provides the extensive degradation rate data necessary for making relatively precise outdoor lifetime predictions and identifying cost-effective materials. The same set of accelerated data can be interpreted for various exposure sites. Of course, there is no "royal road" to accelerated weather testing, as all workers in the field realize. Our multicondition method must be considered useful for monolithic materials such as plastic films. Composite structures, involving interfaces, are liable to be debonded by temperature/humidity cycling. For example, blistering of paint films in Miami may result from dew-soaking overnight followed by sun-baking during the day. Our fixed-condition method does not simulate this situation. Instead, a Q-Panel tester (Reference 17) or UVCON device (Reference 18) would be appropriate. For cold climates, freeze-thaw cycles may have to be simulated. In general, a judicious combination of test methods must always be chosen for any given material and exposure site. For any method involving solar simulation by lamps it is essential to match light intensity with that of the sun, or at least to obtain the data to correct for a mismatch, at the critical wavelength(s) causing photochemical degradation.

REFERENCES

1. G. A. Zerlaut, "Accelerated Outdoor Weathering Employing Natural Sunshine," Proceedings, Institute of Environmental Sciences, 21st Annual Meeting, Anaheim, CA, April 13-16, 1975.

2. Atlas Electric Devices Co., "Atlas Fade-Ometer and Weather-Ometer," Bulletin No. 1300B, undated, received 1976.

3. Original Hanau Quartzlampen GMBH, "Xenotest 1200," brochure, U.S. distributor Batson Machinery, Inc., undated, received 1976.

4. R. Metzinger and R. A. Kinmonth, Jr., "Accelerated Weathering in the '70s: Laboratory Weathering," Modern Paint and Coatings, December 1975.

5. R. A. Kinmonth, Jr., "A Correlation Review - Published Results from 1962-1977," Atlas Sun Spots (published by Atlas Electric Devices Co.), Vol. 6, Issue 16, Autumn 1977. Note: This is one of a continuing series of literature reviews.

6. J. M. Kolyer, "Stability of Transparent Materials Under Worldwide Climatic Conditions," Conference on Aerospace Transparent Materials and Enclosures, Atlanta, Georgia, November 18-21, 1975, pgs. 405-432.

7. J. M. Kolyer and N. R. Mann, Interim Report on Accelerated/Abbreviated Test Methods, Study 4, Task 3 (Encapsulation) of the Low-Cost Silicon Solar Array Project for the Period April 1, 1976 through October 24, 1977, JPL Contract 954458, ERDA-JPL-954458-77/2, Distribution Category UC-63, prepared October 24, 1977.

8. "Standard Recommended Practice for Maintaining Constant Relative Humidity by Means of Aqueous Solutions," E104-51, 1974 Annual Book of ASTM Standards, pgs. 846-852.

9. N. R. Mann, R. W. Schafer, and N. E. Singpurwalla, Methods for Statistical Analysis of Reliability and Life Data, Wiley, 1974.

10. J. E. Clark and J. A. Slater, "Outdoor Performance of Plastics III, Statistical Model for Predicting Weatherability," National Bureau of Standards Report 10 116, October 30, 1969.

11. National Oceanic and Atmospheric Administration/Environmental Data Service, Bulletin: Local Climatological Data, Monthly Summary, 1976-1977.

12. South Florida Test Service, Inc., Miami, FL, weather data bulletins, 1976-1977.

13. L. R. Koller, Ultraviolet Radiation, 2nd Edition, Wiley, 1965.

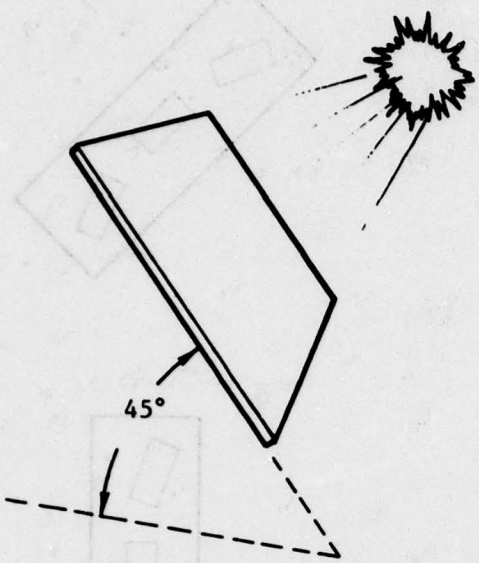
14. J. L. Scott, "Seasonal Variations - Nemesis of Repeatable/Reproducible Accelerated Outdoor Durability Tests?," Federation of Societies for Coatings Technology Symposium, Cleveland, OH, literature received 1976.

15. C. Bennett and N. L. Franklin, Statistical Analysis in Chemistry and the Chemical Industry, Wiley, 1954.

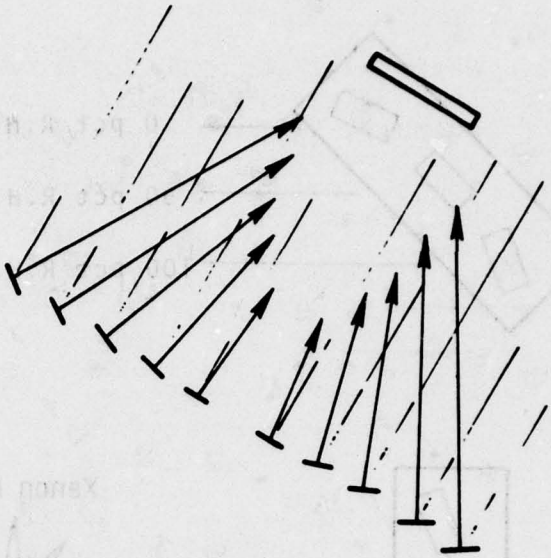
16. General Electric Co., "Weatherability of Lexan Polycarbonate," undated brochure received 1975.

17. Q-Panel Co., Cleveland, OH, literature received 1976.

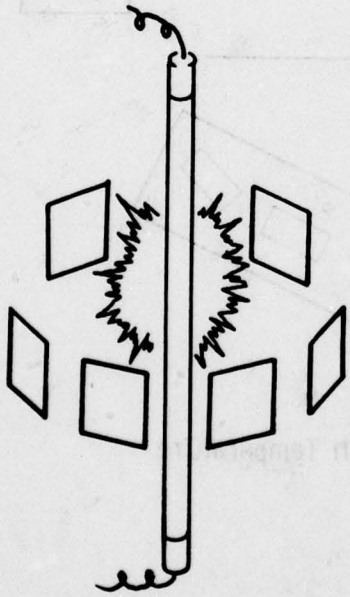
18. Atlas Electric Devices Co., Atlas Sun Spots (bulletin), Vol. 5, Issue 13, Autumn 1976.



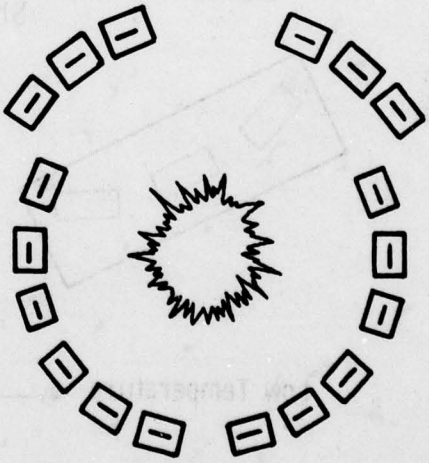
Conventional Outdoor Exposure. Sample faces south.



Sunlight Concentration. Sample, upside down, on follow-the-sun mount with mirrors. (Desert Sunshine Exposure Tests, Inc.)



Time-Compression. Samples, in the same cabinet, rotate around xenon lamp (Weather-Ometer).



Multicondition Time-Compression. Samples, in separate environmental chambers, ranged around xenon lamp.

Figure 1. Methods of Exposure Testing

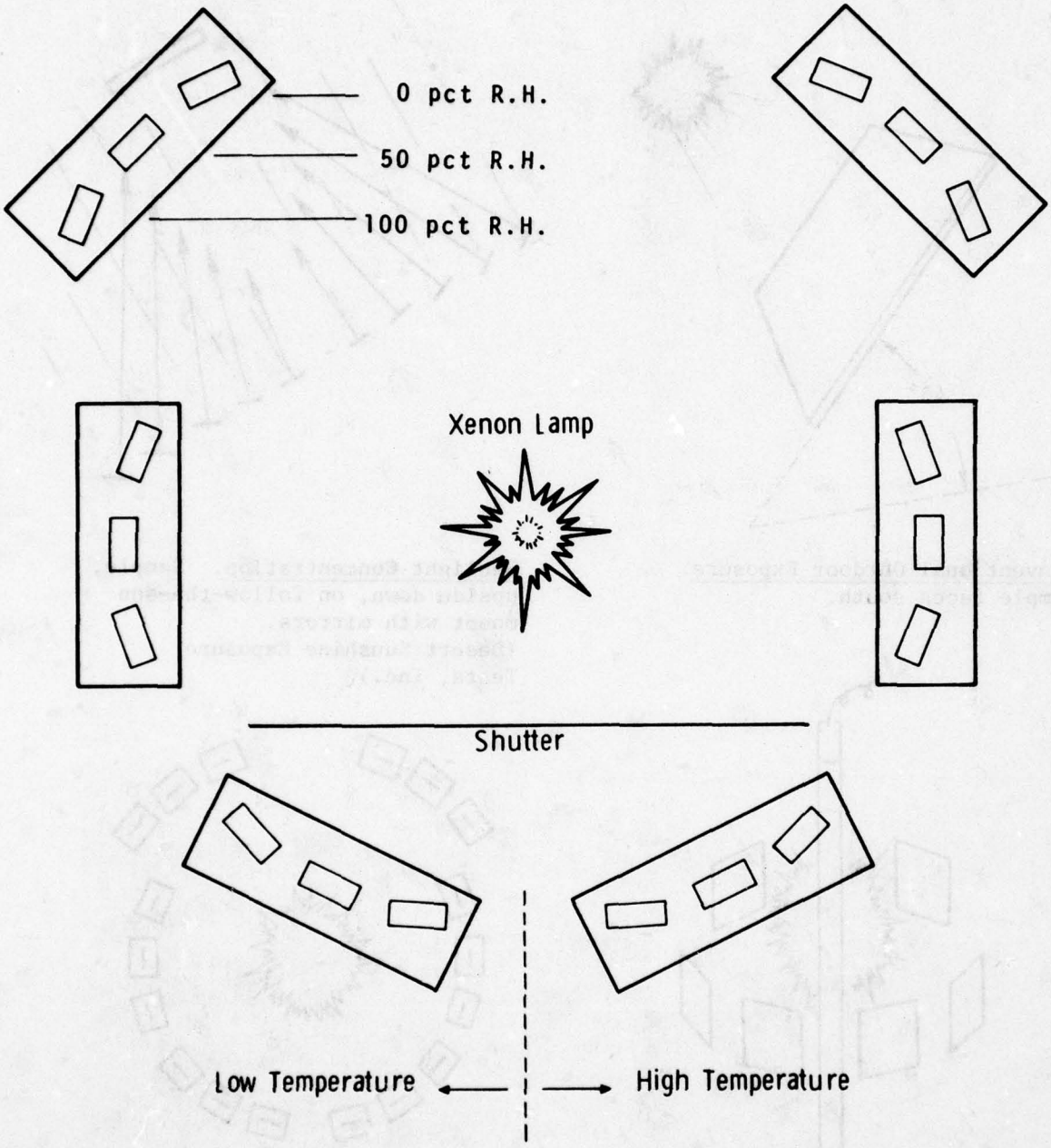


Figure 2. Diagram (Top View) of Apparatus for the Eighteen Illuminated Conditions of Multicondition Accelerated Exposure

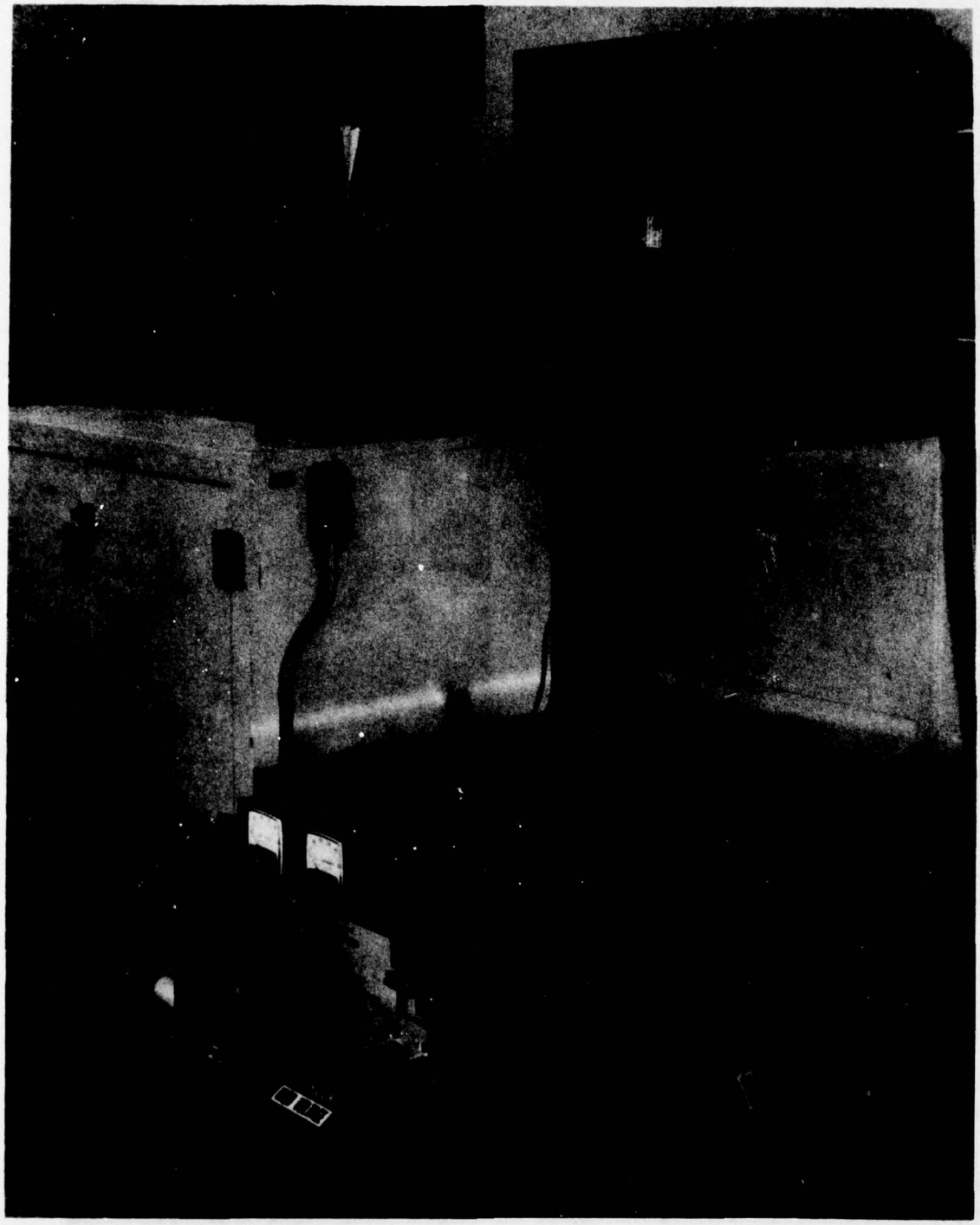


Figure 3. Apparatus for Multicondition Accelerated Exposure

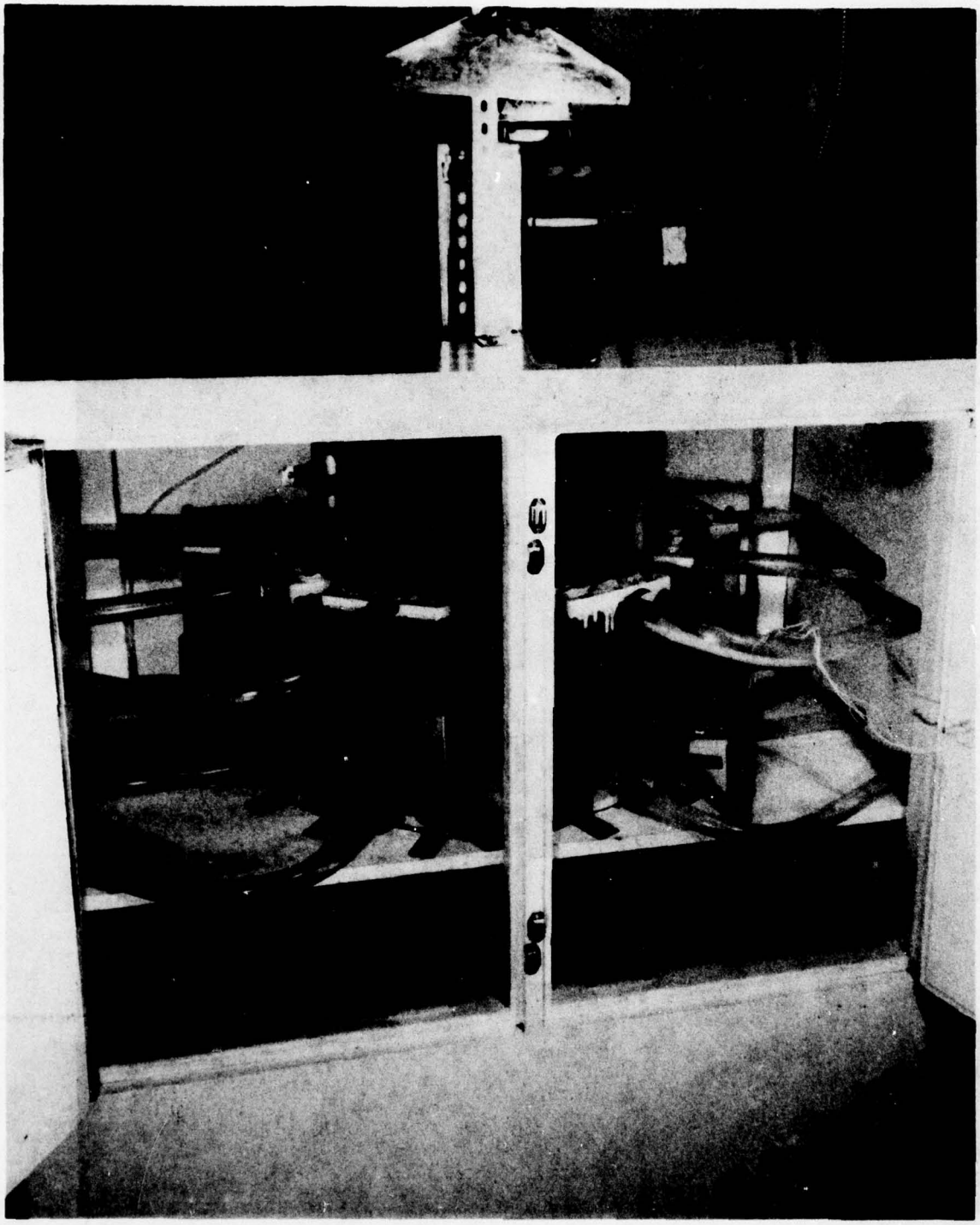


Figure 4. Interior of Cabinet, Showing Xenon Lamp Surrounded by Quartz Tanks

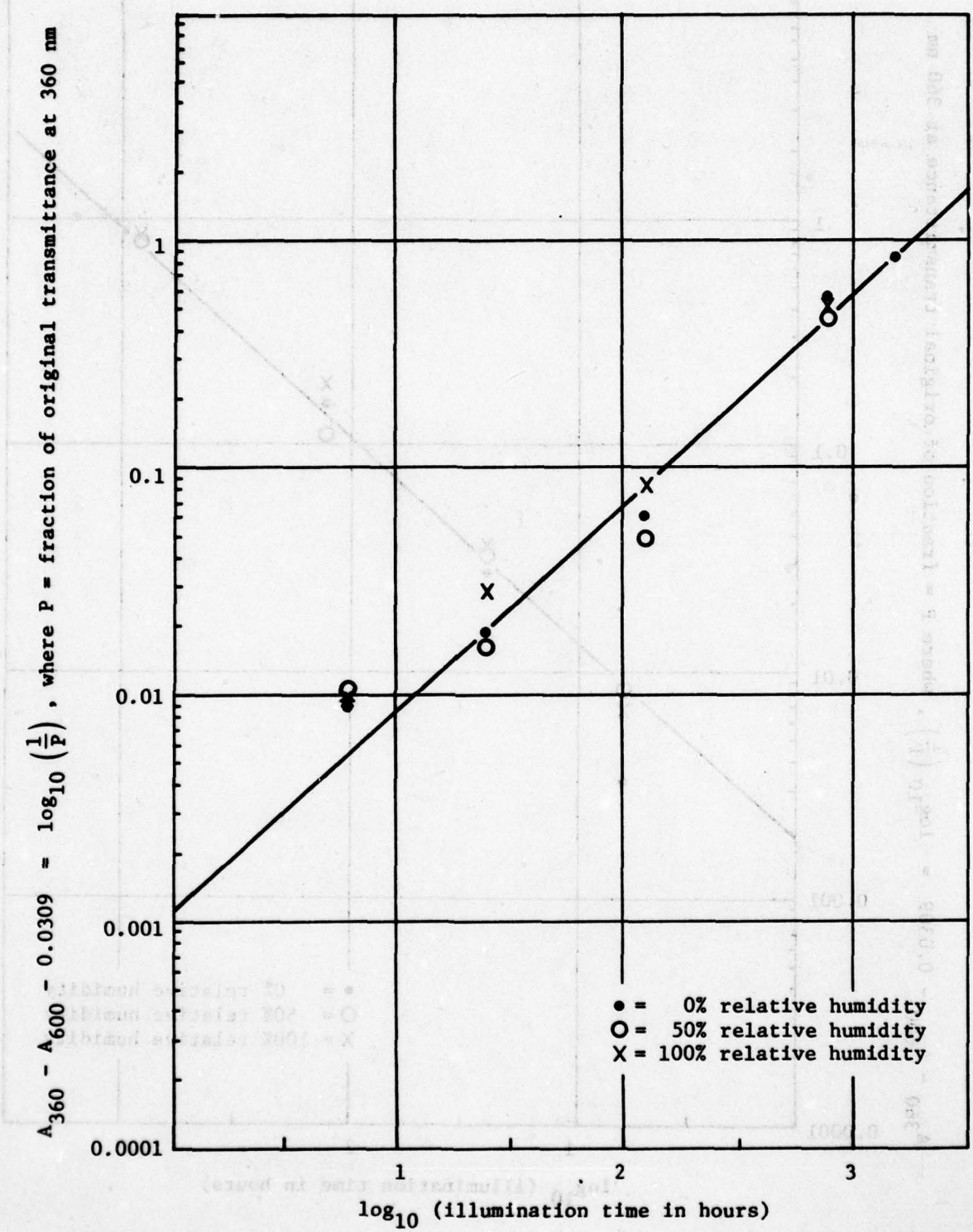


Figure 5. Accelerated Exposure Data for Polystyrene, 0.66 Relative UV Intensity, 18.3°C

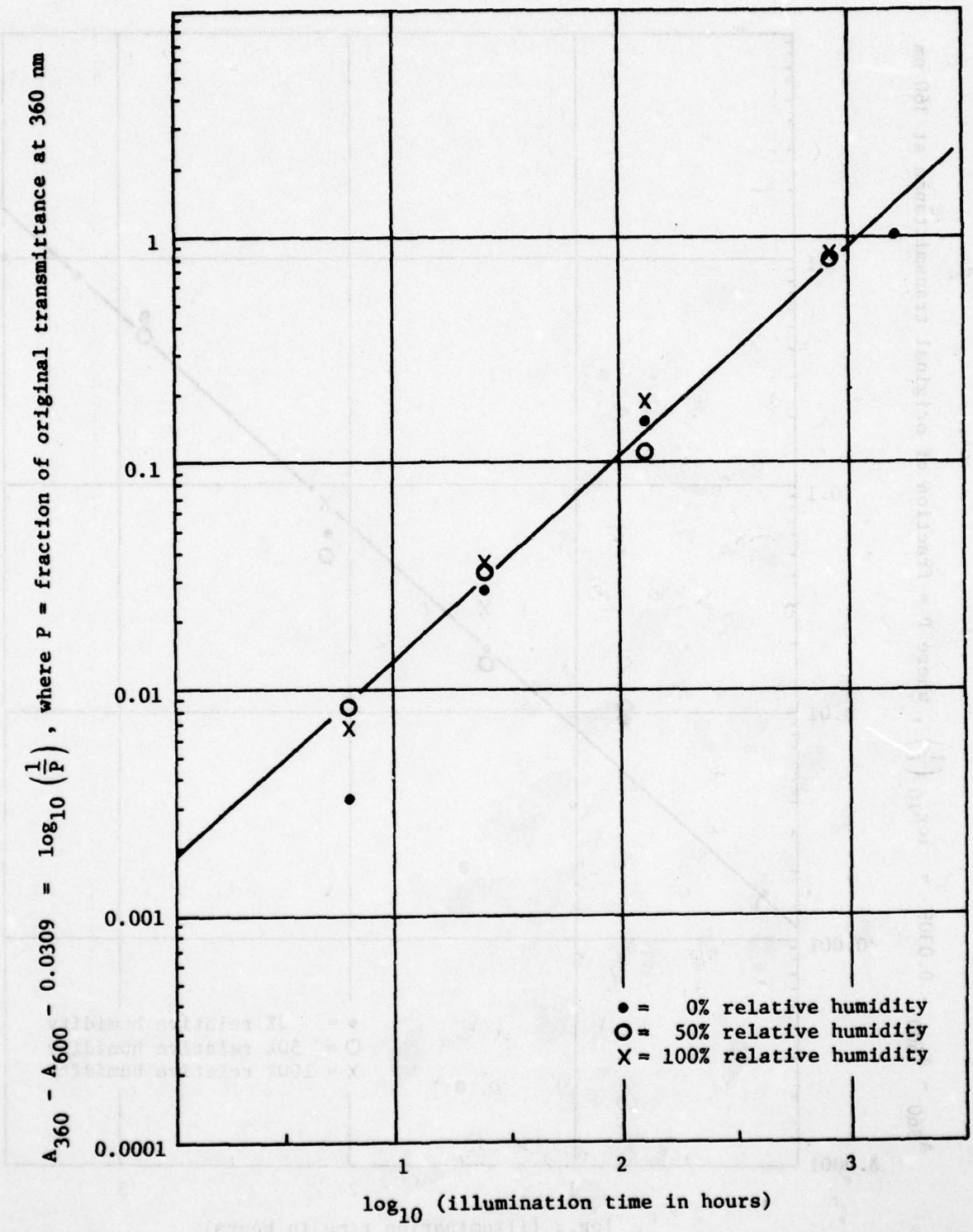


Figure 6. Accelerated Exposure Data for Polystyrene, 0.66 Relative UV Intensity, 55.3°C

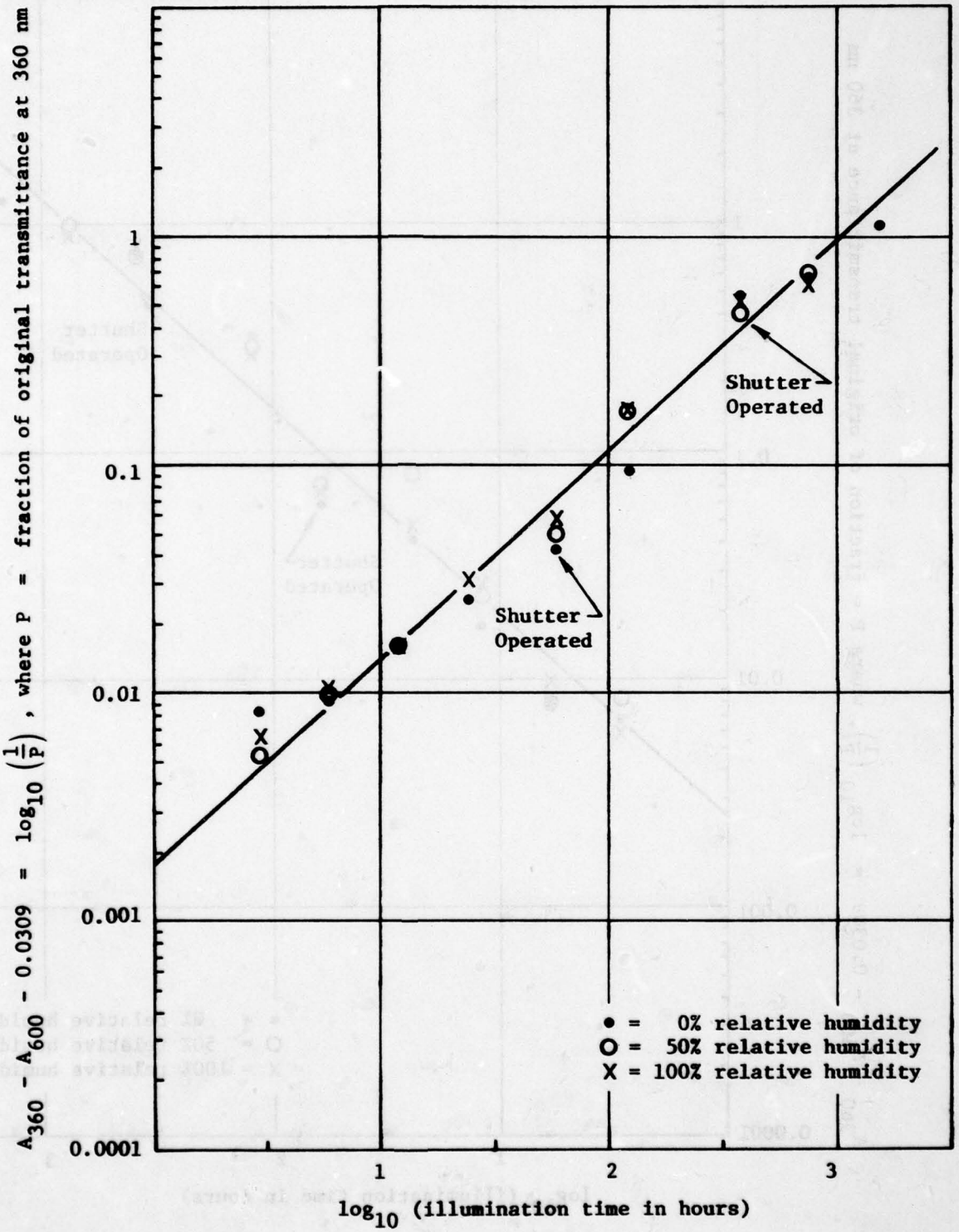
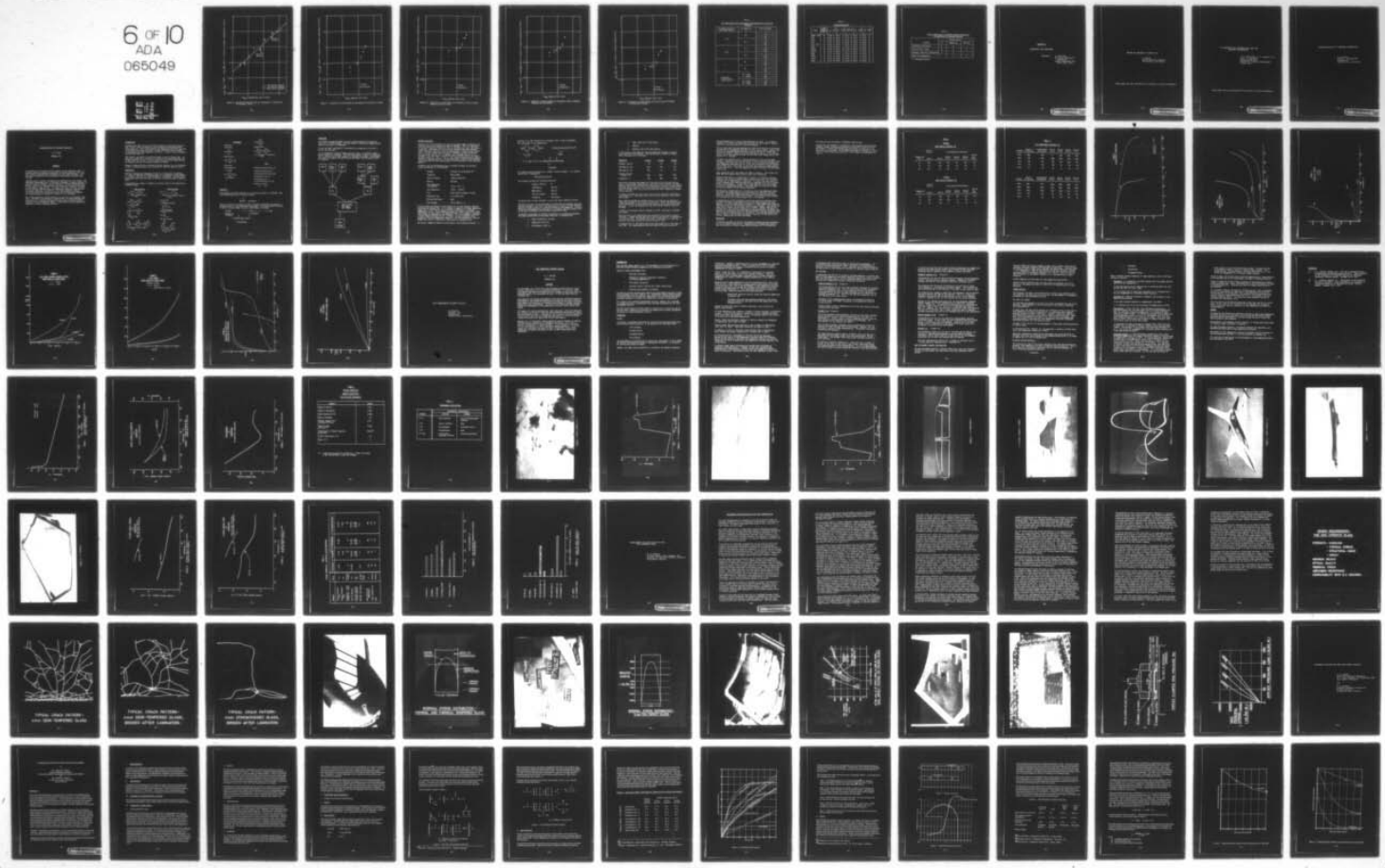


Figure 7. Accelerated Exposure Data for Polystyrene, 1.00 Relative UV Intensity, 26.1°C

AD-A065 049 AIR FORCE FLIGHT DYNAMICS LAB WRIGHT-PATTERSON AFB OHIO F/G 1/3
CONFERENCE ON AEROSPACE TRANSPARENT MATERIALS AND ENCLOSURES (1--ETC(U)
DEC 78 R E WITTMAN

UNCLASSIFIED AFFDL-TR-78-168 NL

6 OF 10
ADA
065049



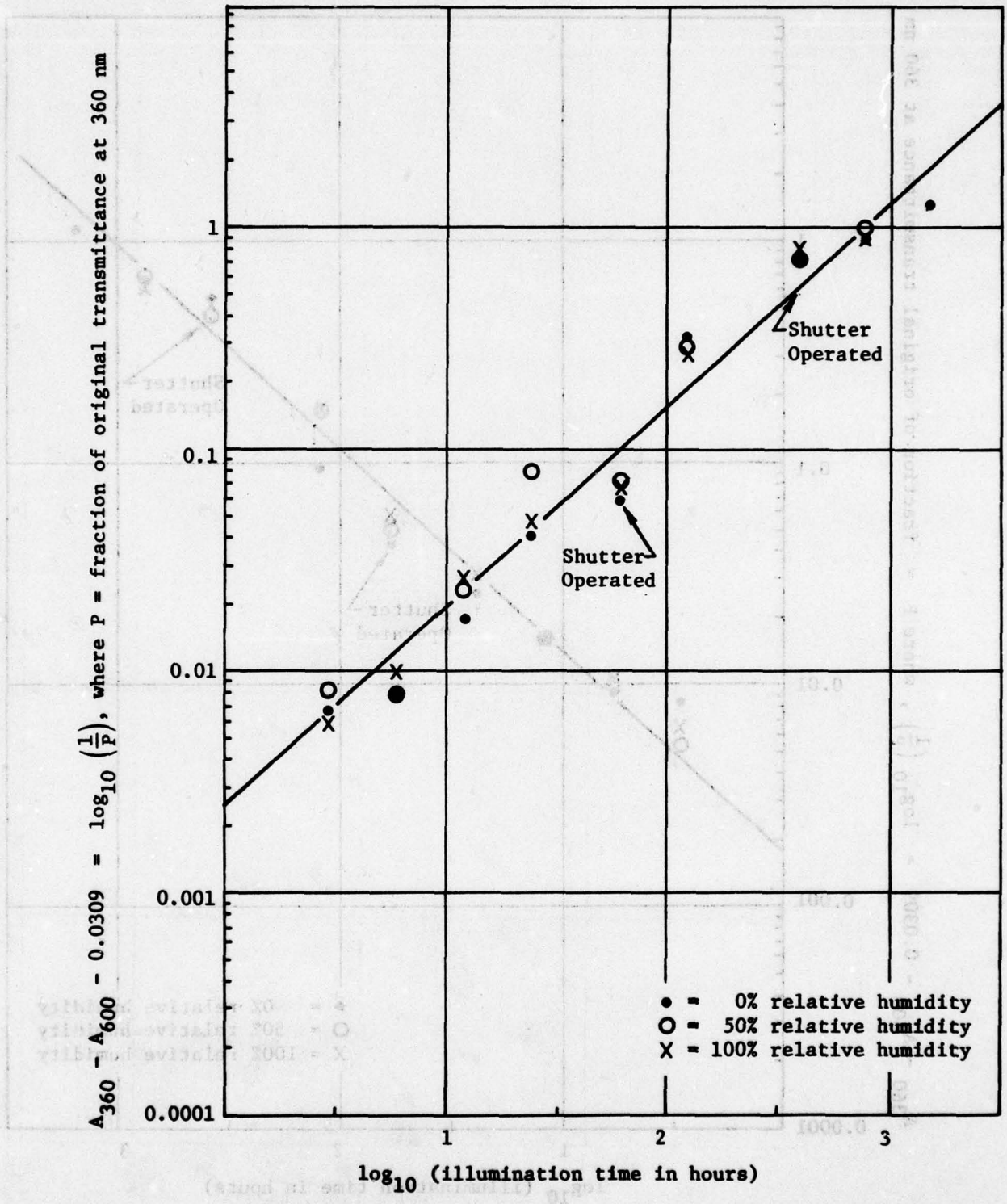


Figure 8. Accelerated Exposure Data for Polystyrene, 1.00 Relative UV Intensity, 60.3°C

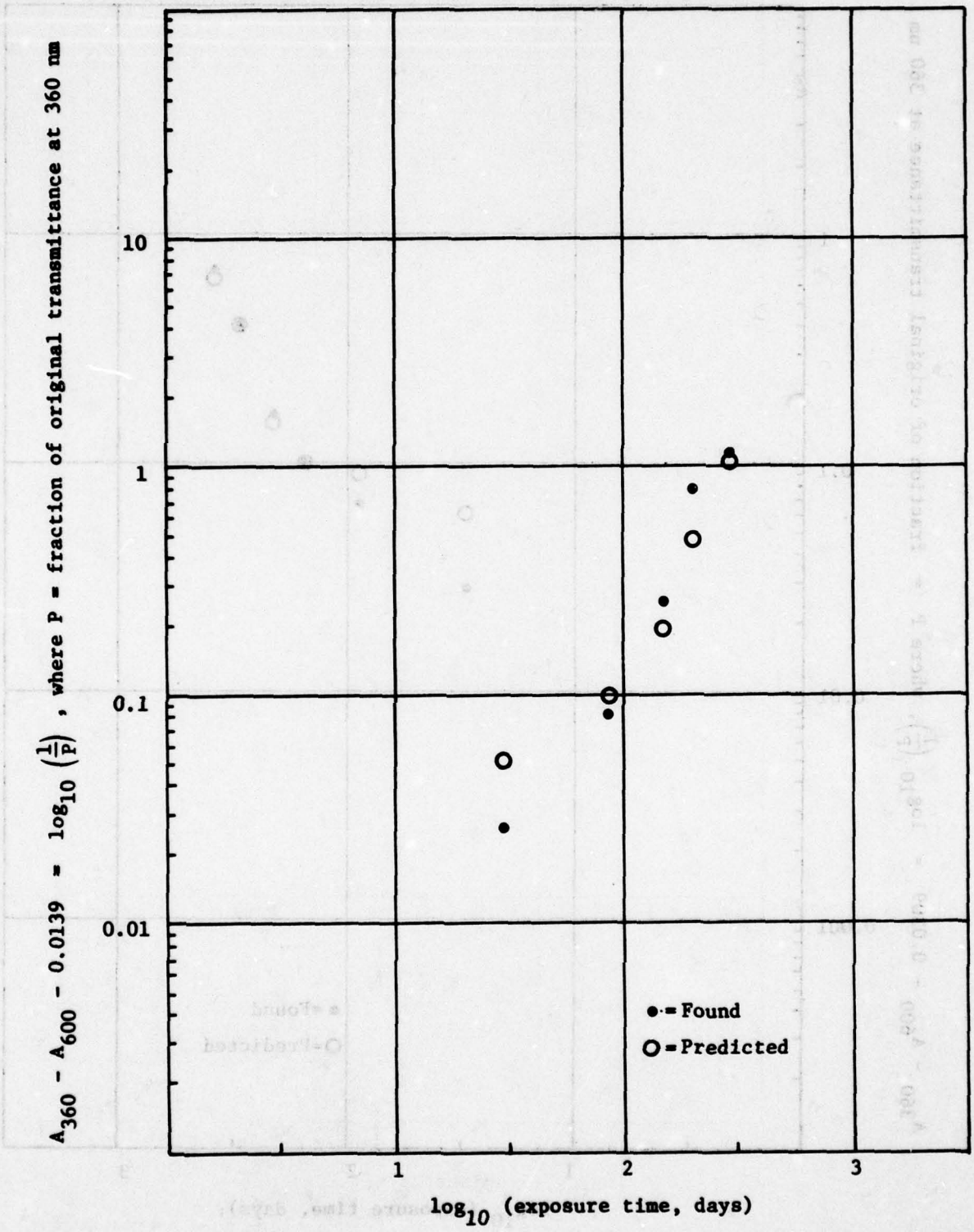


Figure 9. Predicted vs Actual Values for Yellowing of Polystyrene in Miami

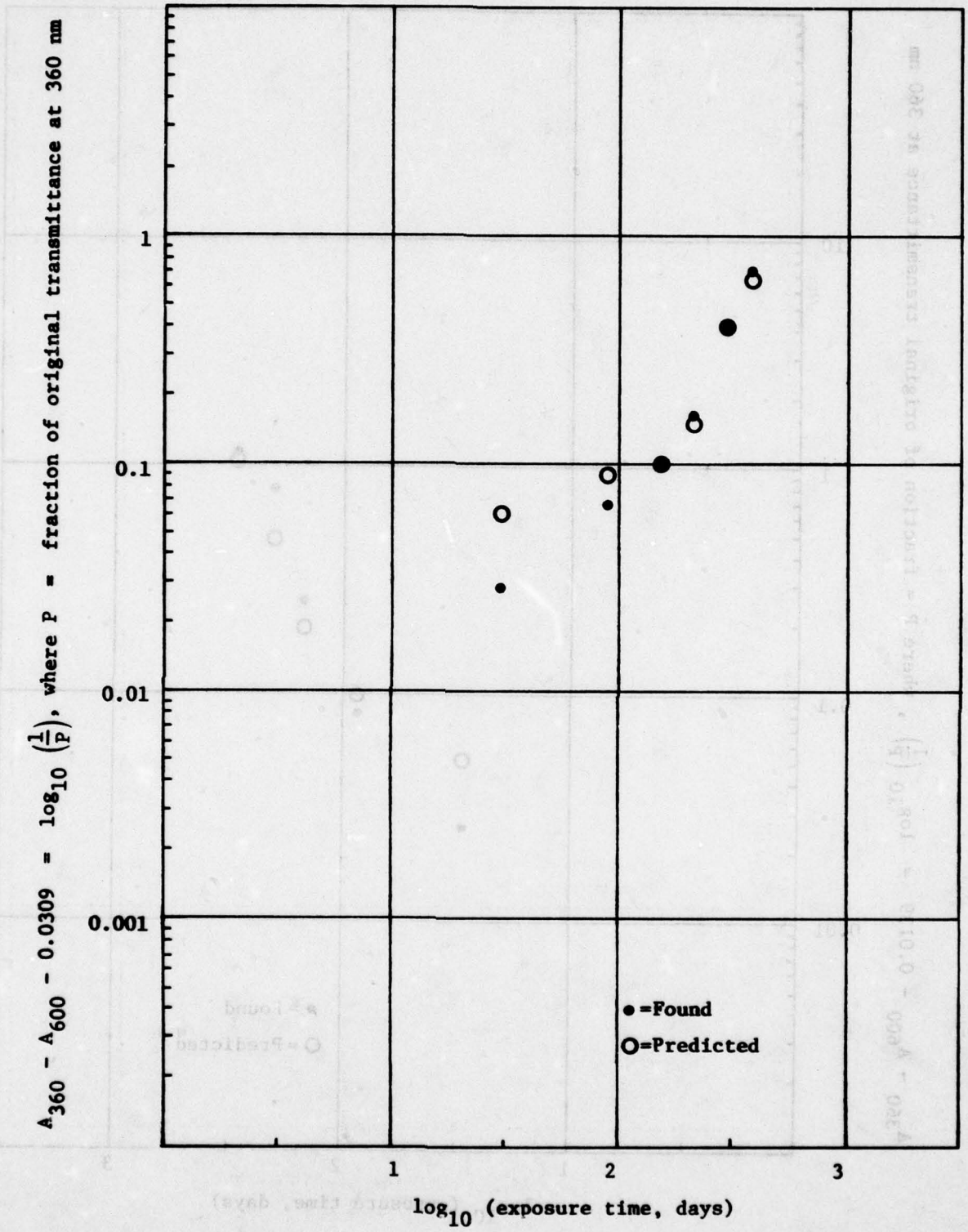


Figure 10. Predicted vs Actual Values for Yellowing of Lexan in Miami (Exposure started 9/1/76)

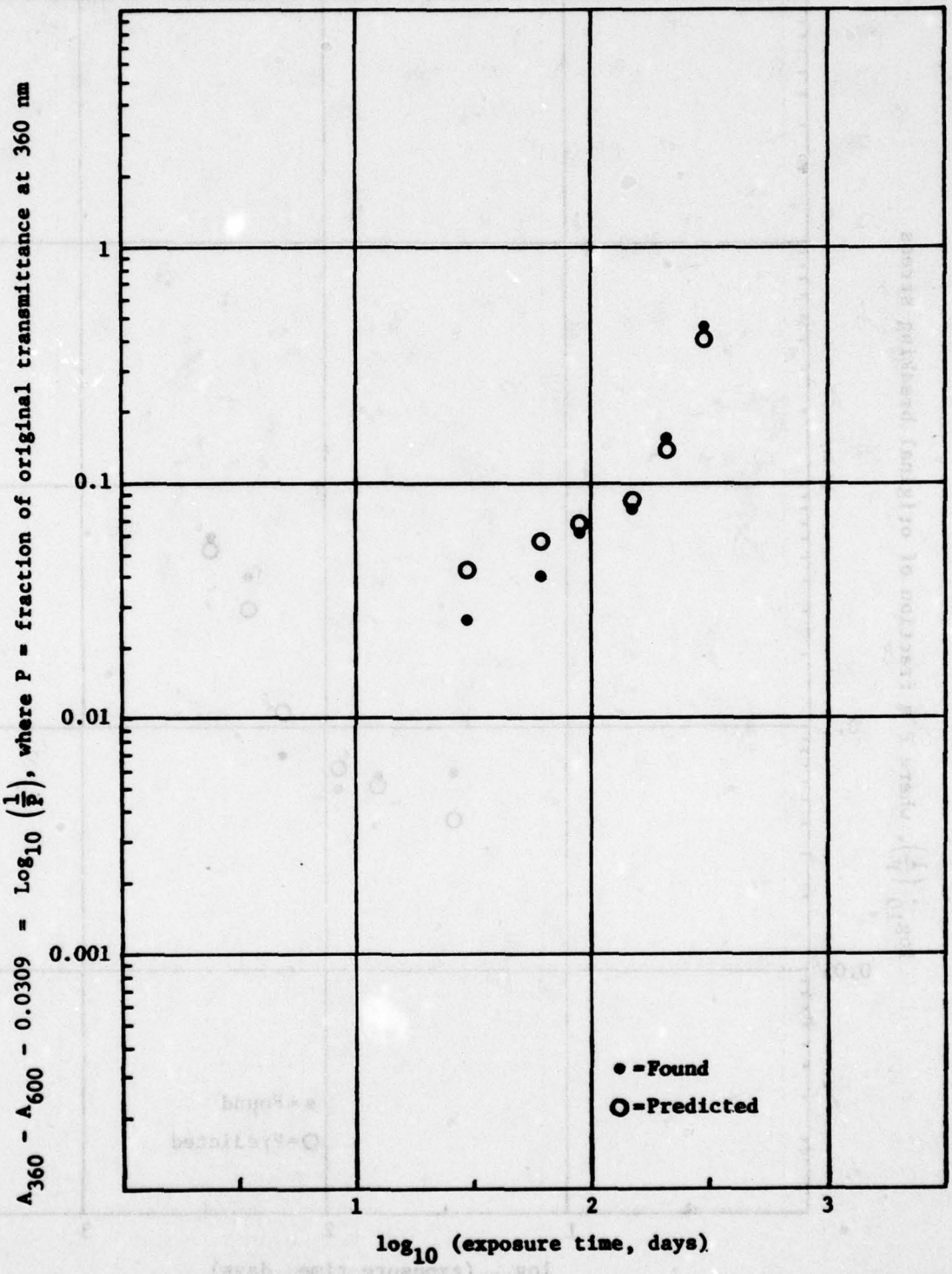


Figure 11. Predicted vs Actual Values for Yellowing of Lexan in Phoenix (Exposure started 9/12/76)

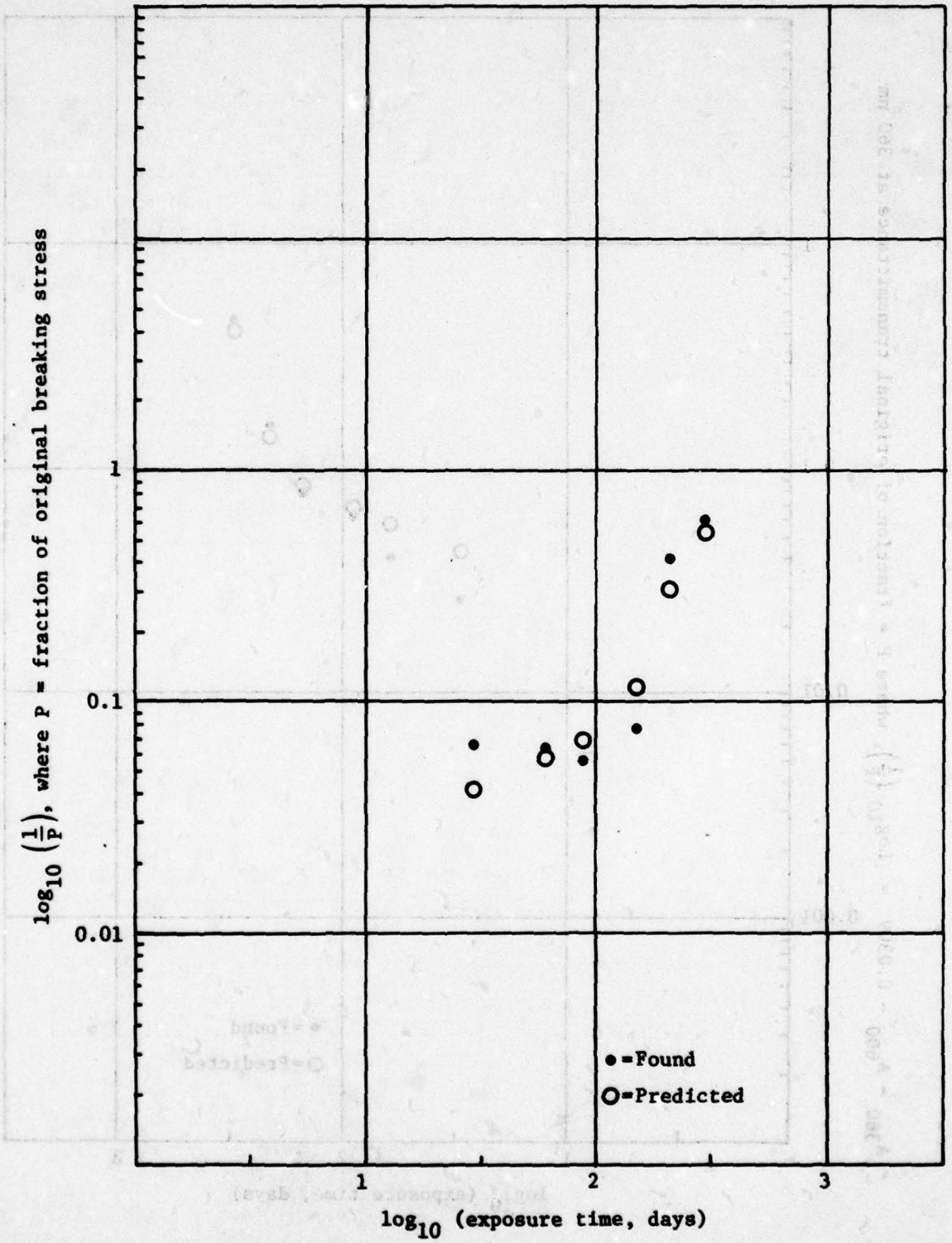


Figure 12. Predicted vs Actual Values for Loss of Tensile Strength of Polystyrene in Miami

Table 1.

The Twenty-Four Fixed Conditions in Multicondition Accelerated Exposure

UV Intensity Relative to Noon Summer Sunlight	Air Temperature °C	Relative Humidity %
1.00	26.1	0
		50
		100
	60.3	0
		50
		100
0.66	18.3	0
		50
		100
	55.3	0
		50
		100
0	40	0
		50
		100
	80	0
		50
		100
Alternating (1.00 for 12 hrs., 0 for 12 hrs.)	26.1 (light) 6.7 (shade)	0
		50
		100
	60.3 (light) 43.9 (shade)	0
		50
		100

Table 2.

Miami Weather Data

Month	Mean Relative Humidity %	7 - 9 AM UV	7 - 9 AM T,°C	9 - 11 AM UV	9 - 11 AM T,°C	11AM-1PM UV	11AM-1PM T,°C	1 - 3 PM UV	1 - 3 PM T,°C	3 - 5 PM UV	3 - 5 PM T,°C
Sept. 1976	76	0.09	27	0.44	29	0.67	31	0.49	31	0.07	31
Oct.	75	0.04	24	0.20	27	0.31	29	0.23	29	0.03	29
Nov.	75	0.02	22	0.10	24	0.16	26	0.11	26	0.02	26
Dec.	75	0.01	19	0.06	22	0.09	24	0.07	24	0.01	24
Jan. 1977	70	0.02	16	0.09	19	0.14	22	0.10	22	0.01	22
Feb.	71	0.03	18	0.14	21	0.22	23	0.16	23	0.02	23
March	69	0.05	23	0.26	26	0.40	28	0.29	28	0.04	28
April	69	0.09	23	0.46	25	0.71	27	0.52	27	0.07	27
May	71	0.12	25	0.60	27	0.92	29	0.67	29	0.10	29
June	74	0.14	27	0.69	29	1.06	31	0.77	31	0.11	31
July	74	0.13	28	0.65	30	1.00	32	0.73	32	0.10	32
Aug.	75	0.12	28	0.60	30	0.90	32	0.66	32	0.09	32

Table 3.

Relative Importance of Weather Factors Disclosed by Multicondition Accelerated Exposure

Property	Weather Factor		
	UV	Temperature	Moisture
Yellowing, Polystyrene	X	X	
Loss of Gloss, Lexan	X	X	X
Carbonyl Formation, Polystyrene	X	X	
Solar Cell Degradation		X	X

X = Pronounced Effect

SESSION V

MATERIALS AND PROCESSES

Chairman: E. Morrisey
Air Force Materials Laboratory
Wright-Patterson Air Force Base, Ohio

PRECEDING PAGE BLANK-NOT FILMED

REPORT ON PROGRESS OF ASTM F7.08

R. Morrow
Hughes Aircraft Company
Los Angeles, California

This paper was not available for printing in this proceedings.

PRECEDING PAGE BLANK-NOT FILMED

AN IMPROVED CHIP RETARDER AND SEAL FOR AIRCRAFT WINDSHIELDS

S. H. Herliczek, J. C. Burwell, Sr.,
and J. G. Marriott
Libbey-Owens-Ford
Automotive Products Development
Toledo, Ohio

This paper was not available for printing in this proceedings.

PRECEDING PAGE BLANK-NOT FILMED

CHARACTERIZATION OF URETHANE INTERLAYERS

E. M. Brown
Swedlow, Incorporated
Engineering
Garden Grove, California

PRECEDING PAGE BLANK-NOT FILMED

CHARACTERIZATION OF URETHANE INTERLAYERS

E. M. Brown

SWEDLOW, INC.

ABSTRACT

The versatility of aircraft from the subsonic to the supersonic range created a need for windshield interlayers of varying characteristics. PVB and silicone contribute good interlayers for their specific needs. With the advent of added bird strike capability the urethane interlayer came into use.

Urethanes offer a variety of properties by manipulation of the formula. Because each transparency has its individual uniqueness in design, Swedlow has developed several formulae to allow selection of the most desirable properties. Selection of these materials was based on the required attributes of interlayers. They include: (1) clarity and color stability, (2) good tensile and shear modulus across the temperature range, (3) good adhesion to various substrates, (4) stability in elevated temperature range, (5) ability to be used without heat except for de-icing and de-fogging, (6) variable modulus as required by design for bird resistance.

Two of these materials provide properties at each end of the property spectrum. The physical and mechanical characteristics of these materials may be used as is, or one may be blended with the other to provide the best characteristics as dictated by design. These properties are discussed and compared to current interlayer materials.

PRECEDING PAGE BLANK-NOT FILMED

INTRODUCTION

Urethanes have come into use on aircraft windshield interlayers because of their clarity, ease in processing, high strength and broad temperature range capability. They provide better high temperature capability than PVB for strength and ageing, and higher strength with equivalent performance at low temperatures when compared to silicone. In short, their performance overlaps both materials.

This material can readily be tailored to meet a specific design need. Because each windshield is different in design and its requirements may vary to meet important criteria like bird proofing, the physical properties may be changed to provide the necessary bending stiffness.

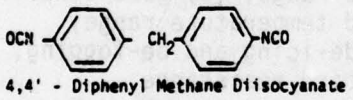
Because of these variations required by design, Swedlow, Inc. has developed a family of urethanes that can be tailored to a specific design criteria.

COMPOSITION

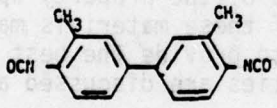
Urethane elastomers are composed principally of three basic ingredients: 1) a resin of polyether or polyester type, 2) an isocyanate of the aromatic or aliphatic type, and 3) a chain extender or crosslinker. These are combined under controlled conditions to provide a urethane polymer of specific detail.

Listed below are a number of commercial materials used in the production of urethane polymers.

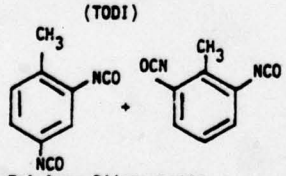
AROMATIC ISOCYANATES



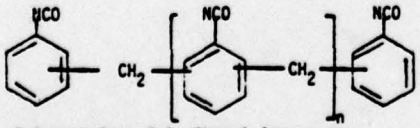
4,4' - Diphenyl Methane Diisocyanate
(MDI)



Bitolyene Diisocyanate
(TODI)

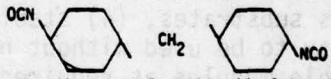


Tolylene Diisocyanate
(TDI)

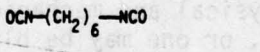


Polymethylene Poly Phenyl Isocyanate
(PAPI)

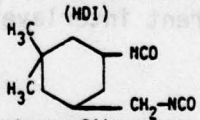
ALIPHATIC ISOCYANATES



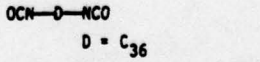
4, 4' - Methylene Bis (Cyclohexyl Isocyanate)
(H_{12} MDI)



Hexamethylene Diisocyanate
(HDI)

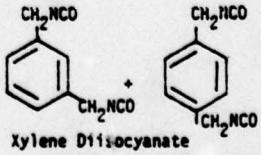


Isophorone Diisocyanate
(IPDI)



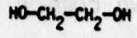
D = C_{36}

Dimer Acid Diisocyanate
(DDI)

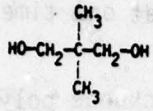


Xylene Diisocyanate
(XDI)

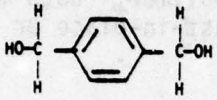
CHAIN EXTENDERS



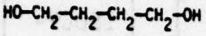
Ethylene Glycol



Neoprentyl Glycol



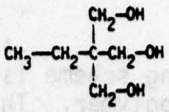
P-Xylene Glycol



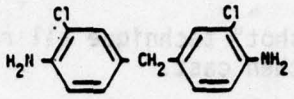
1,4 Butanediol



1,4 Cyclohexanediol

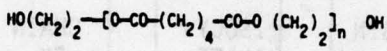


Trimethylolpropane

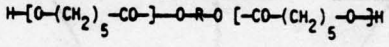


4,4' – Methylene-bis – (2-Chloroaniline)
(MOCA)

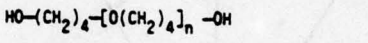
RESINS



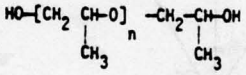
Polymethylene Adipate Glycol Ester



Polycaprolactone Glycol Ester

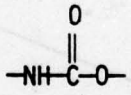


Poly (oxytetra methylene) Glycol Ether



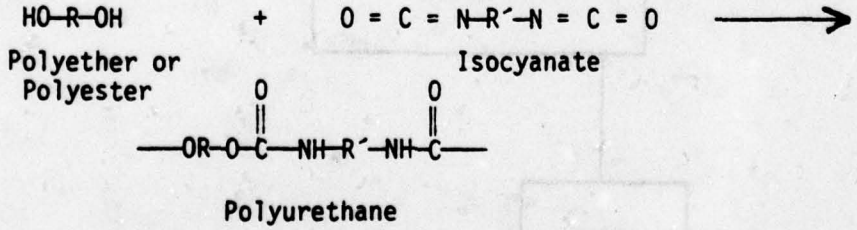
CHEMISTRY

Polyurethanes are often referred to as isocyanate polymers or urethanes. They are characterized by the following linkage.



(Urethane)

They are typically the reaction product of hydroxyl-terminated polyethers or polyesters and di or polyfunctional isocyanates. The formula below is typical of one of the most common reactions which produce a urethane.



Polyether or Polyester

Isocyanate

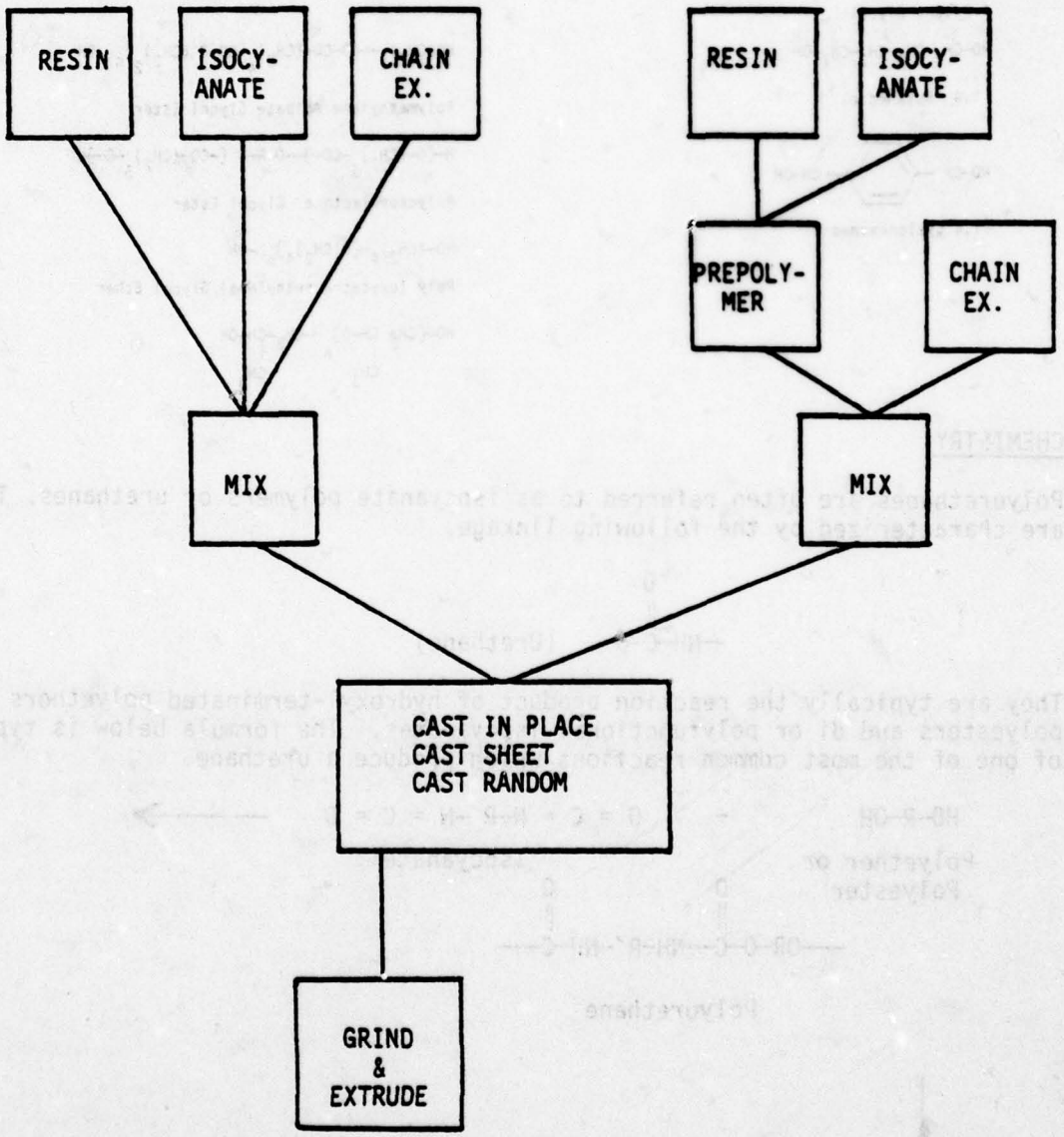
Polyurethane

PROCESSING

The urethane processing scheme is one of ratioing and mixing liquids and curing to a finished polymer. This end polymer is made by two common methods known as "one shot" or "prepolymer"

In the "one shot" technique all raw materials are combined at one time in the mix and then cast.

In the "prepolymer" route we combine the basic resin, or backbone polymer with an excess of isocyanate. The resulting product is known as a prepolymer. This is reacted with a chain extender to complete the polymer. Both methods will result in products that may be cast into sheet, cast-in-place or used in extrusion.



MATERIAL SELECTION

From the list of raw materials you can see the great number of possible combinations that can be created to produce a urethane. This list represents only a small fraction of materials that are available for use in the industry. In addition, these materials can be used in products other than urethane creating polymers that may in fact be combinations of several types of materials. For this reason, when thinking of urethanes, it must be realized, that the product may not be all urethane, and the properties, be it all urethane or not, may have no correlation with a specific product with which you may be familiar. This, in fact, is the reason urethanes receive negative response in some applications. On the other hand, it says that the engineer using these materials must become aware of the limitations of each individual material.

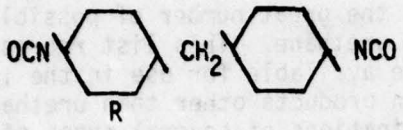
In general the high performance type of urethane elastomer can provide a range of properties in the following:

Hardness	-	50 Shore "A" to 80 Shore "D"
Elongation	-	50% to 600%
Tensile Strength	-	2,000 to 8,000 PSI
Modulus	-	Variable
Cold Temperature Brittlepoint	-	-20 to - 65 + °C
High Temperature	-	+100°C (+212°F)
Color	-	Water white to opaque to brown
Compression Set	-	15 to 50% @ 70°C
Abrasion Resistance	-	Good
Tear Strength	-	100 to 1000 P.L.I.

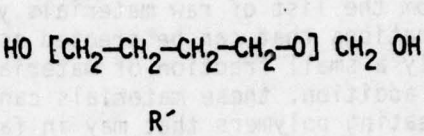
As can be seen the urethane's prime assets are its high strength, abrasion resistance and flexibility. It is limited, in general, for higher temperature usage, and in some formulas can be bothered by hydrolysis at elevated temperatures or U.V. It has moderate solvent and chemical resistance. These limitations, are not always to be expected though, as by change in structure, these potential drawbacks can be eliminated. It is not uncommon to develop a higher temperature material but in doing so one may compromise other properties like cold temperature capability. As with any material, specific demands may result in trade-offs in other material characteristics.

One typical commercial material can be shown in the following structure. It

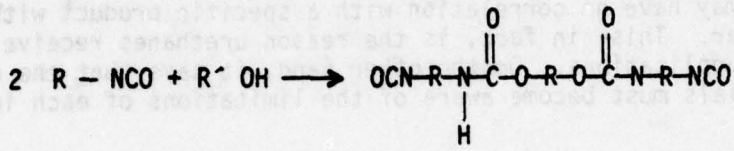
consists of H_{12} MDI reacted with a polyether resin to form a prepolymer. This prepolymer is sold commercially.



(H_{12} MDI)

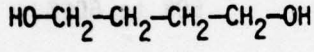


(PTMG)



Prepolymer

This material may be reacted with a number of chain extenders. For instance one can use 1,4 Butanediol.



This product provides the following properties:

Hardness, Shore D	-	42
100% Modulus	-	1800 psi
300% Modulus	-	4000 psi
Tensile Strength	-	4500 psi
Elongation	-	380 percent

By substitution of chain extenders, we can alter these properties further.

Additional variation can be developed by altering the ratio between the resin and the isocyanate. In Figure 1 we show the two curves of the same commercial material (X) when plotted in a penetrating mode on a TMA apparatus. In curve Xm we show what happens when the quanity of iscoyanate has been reduced. Here we can see a difference in melting point transition of 90°C.

In Swedlow's development of urethane interlayers, we selected raw materials that would provide the following good properties in transparencies.

1. Light transmission, low haze
2. Temperature stability
3. Environmental stability

4. Offer simplicity of fabrication

5. Adhesion

6. Moderate tensile and shear modulus

In the process, three materials were developed that provided a range of properties across the spectrum. They were SS-6622, SS-6640 and SS-6641. Their properties are as indicated:

PROPERTIES	SS-6622	SS-6640	SS-6641
Hardness, Shore A	88	55	85
100% Modulus, PSI	1120	166	851
300% Modulus, PSI	1930	178	957
Ultimate Tensile Strength, PSI	7300	2422	3500
Elongation, %	530	650+	650+

During the interlayer development for bird strike it was obvious that because of the different frame designs, different ranges of bending stiffness would be required for the ideal bird proof window. To meet this need Swedlow developed several materials like the SS-6640 and SS-6641 which could be combined in various ratios providing properties that were incrementally between the two materials.

In Figure 2 we show the stress-strain curve of the three basic materials at room temperature. From these curves the variation achieved by each formula can be seen.

When comparing SS-6622 and SS-6640 (Figure 3) at high and low temperature ranges the extremes of the formulas can be noted. These urethane types tend to be thermoplastic so the plots are more nearly alike at the elevated temperatures. In the cold temperature area the different formulas show their extremes.

In Table 1 we show bond tensile strengths on 0.040" interlayers of SS-6640 and SS-6641.

Bond tensiles at cold temperatures were consistent and offered no unusual surprises. SS-6640 had bond tensiles of 600 psi and 3000 psi at temperatures of -20°C and -65°C. The SS-6641 had values of 2000-2500 psi at both temperatures with some evidence of brittle failure at -65°C.

In exposure to U.V. the samples were precut and exposed on all four edges to the light. This edge exposure effect was noted on the bond strength at

elevated temperature but not at room temperature or below. In a standard windshield, of course, the edge would be sealed and the extreme of exposure would be in the discoloration of the polycarbonate.

Five ply bond shear data was developed on 0.040" thick interlayers and tested as described in the proposed ASTM test for five ply bond shear. Control bond tensiles at room temperature provided a value of 238 psi for SS-6640 and 787 psi for SS-6641. These results are presented in Table 2. They show uniformity across the temperature range with no significant changes due to oven ageing or U.V. exposure.

In Figure 4 we show the plot of load vs deflection on the five ply shear testing. Plotted also is the curve of the silicone interlayer SS-5272. Across the temperature range from -65°C to +110°C, we can see that the SS-6640 provides comparable and better failure values while the modulus closely brackets the silicone curve. The SS-6641 on the other hand shows its higher modulus at both -65°C at R.T. The high temperature values are typical of this thermoplastic type.

Shear properties after oven ageing are shown in Figure 5. The original and after 500 hours ageing curves show no significant differences.

Because delamination is a common mode of failure in windshields, and many materials with differing coefficients of expansion are used, the interlayer stiffness at low temperatures is important. In Figure 6 we show curves of several commonly used windshield materials as reported by Mr. Bain of Boeing at the last conference. In addition to those materials, we have included the plots of SS-6640 and SS-6641. These same types of curves can be demonstrated with Gehman Tortional Modulus apparatus.

Both materials demonstrated their flexibility across the temperature range. The SS-6641 had higher modulus (less deflection) as compared to the PVB formulas. The SS-6640 showed outstanding flexibility and characteristics which are normally only shown with silicones. The stiffening point between this urethane and the silicone showed only a 5° difference.

In demonstration of the differences that can be achieved in bending stiffness for bird impact requirements, we show the curves produced for three materials in five ply shear testing (Figure 7). These camples were composite laminates where only the urethane interlayers are different. Here we see the upper curve, SS-6641, and the lower curve, SS-6640. Between these we have plotted one of the possible combinations of the two materials, SS-6641M. Its position with respect to each curve may be changed as required by design. Beam bending data also demonstrated this difference. Plotting mean bending stiffness, as shown in the University of Dayton's study on Bird Resistance Windshields, demonstrated the same differences.

CONCLUSION

In the data provided, we believe the urethanes presented are good candidates for use in subsonic applications. Depending upon the temperature profile, when placed behind silicone or deep behind the outer ply in a windshield,

they would be good candidates in supersonic applications.

We hope that you recognize in the technical data presented that properties somewhere between SS-6640 and SS-6641 may be obtained by modification of the formula. Further modifications may be utilized, as required, to go beyond the data presented. We at Swedlow encourage the designer to inquire if he has a particular need, and we will do our utmost to accommodate the inquiry.

TABLE 1

SS-6640

BOND TENSILE STRENGTH, PSI

Temperature (°C)	Acrylic/ Acrylic Control	Polycarbonate/Polycarbonate Control	100 Hrs @ 70°C	300 Hrs @ 70°C	500 Hrs @ 70°C	300 Hrs U. V. Tower
25	300	232	238	311	294	240
70	135	168	128	137	155	115
110	105	110	100	121	126	77

SS-6641

BOND TENSILE STRENGTH, PSI

Temperature (°C)	Acrylic/ Acrylic Control	Polycarbonate/Polycarbonate Control	100 Hrs @ 70°C	300 Hrs @ 70°C	500 Hrs @ 70°C	300 Hrs U.V. Tower
25	935	949	787	955	929	874
70	305	255	302	---	373	---
110	38	100	---	70	87	45

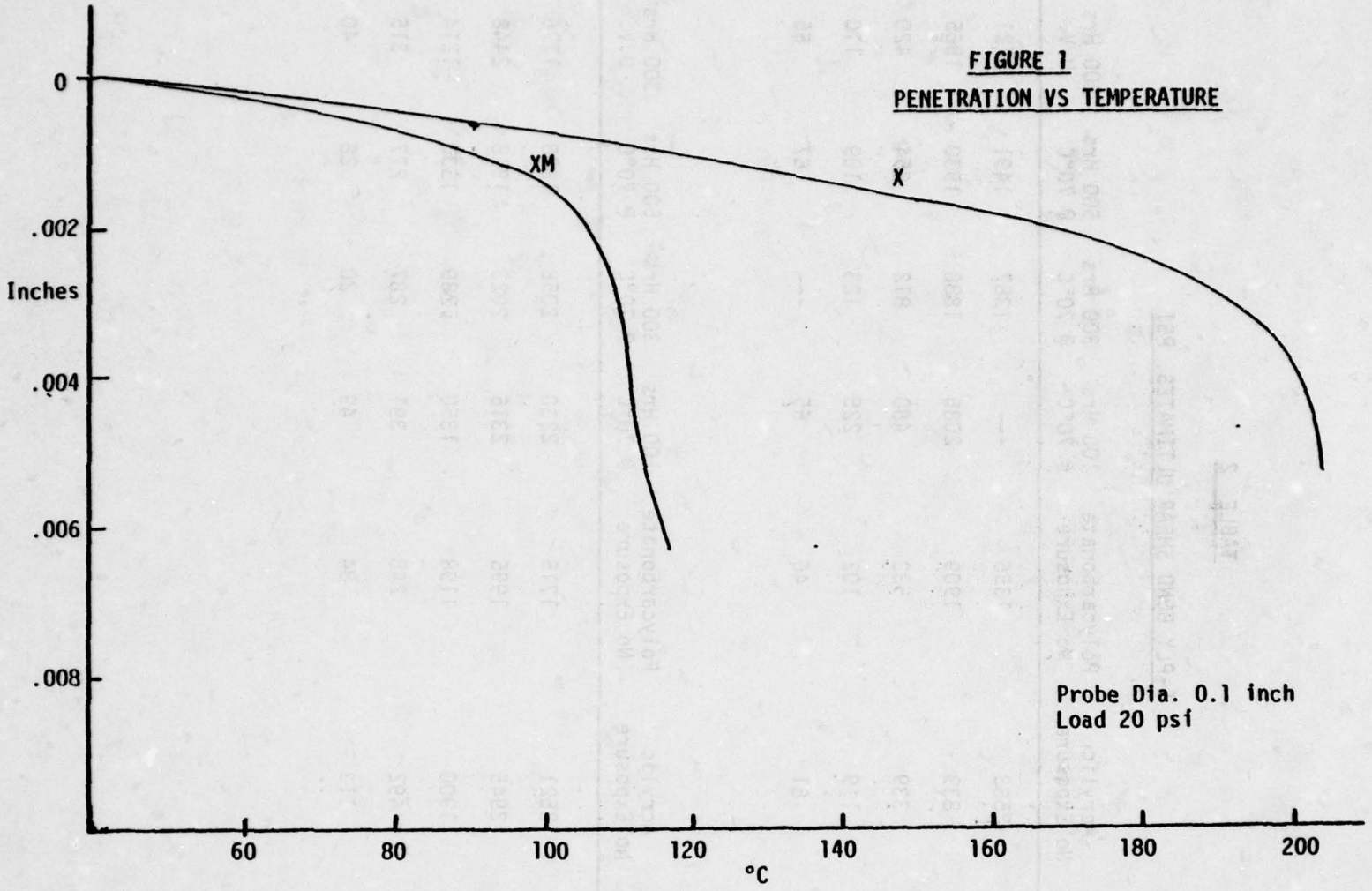
TABLE 2

5-PLY BOND SHEAR ULTIMATES, PSI

SS-6640	Acrylic No Exposure	Polycarbonate No Exposure	100 Hrs @ 70°C	300 Hrs @ 70°C	500 Hrs @ 70°C	300 Hrs U.V.
-65°C	2583	1356	---	1387	1491	1721
-20°C	839	1909	2086	1888	1930	1865
25°C	339	533	480	812	854	420
70°C	119	102	225	123	109	110
110°C	81	46	65	---	67	65

SS-6641	Acrylic No Exposure	Polycarbonate No Exposure	100 Hrs @ 70°C	300 Hrs @ 70°C	500 Hrs @ 70°C	300 Hrs U.V.
-65°C	2521	1715	2230	2058	1858	1776
-20°C	2945	1995	2316	2023	1818	2448
25°C	1900	1198	1358	1289	1330	1214
70°C	492	248	391	287	277	315
110°C	113	84	49	20	28	40

FIGURE 1
PENETRATION VS TEMPERATURE



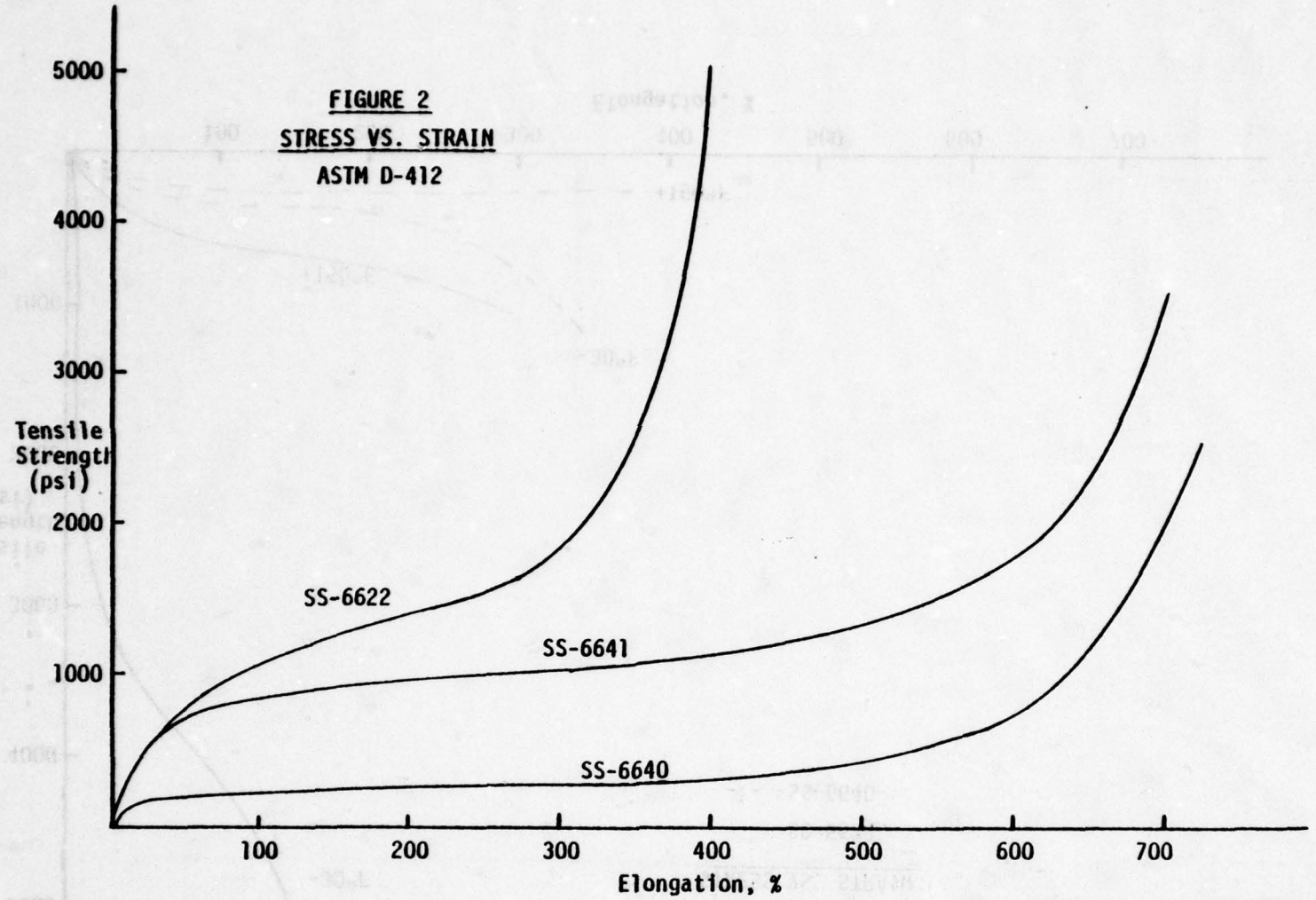

FIGURE 2
STRESS VS. STRAIN
ASTM D-412
5000
4000
3000
Tensile
Strengt
(psi)
2000
1000
SS-6622
SS-6641
SS-6640
100
200
300
400
500
600
700
Elongation, %

FIGURE 3

STRESS VS. STRAIN

—— SS-6622

- - - -SS-6640

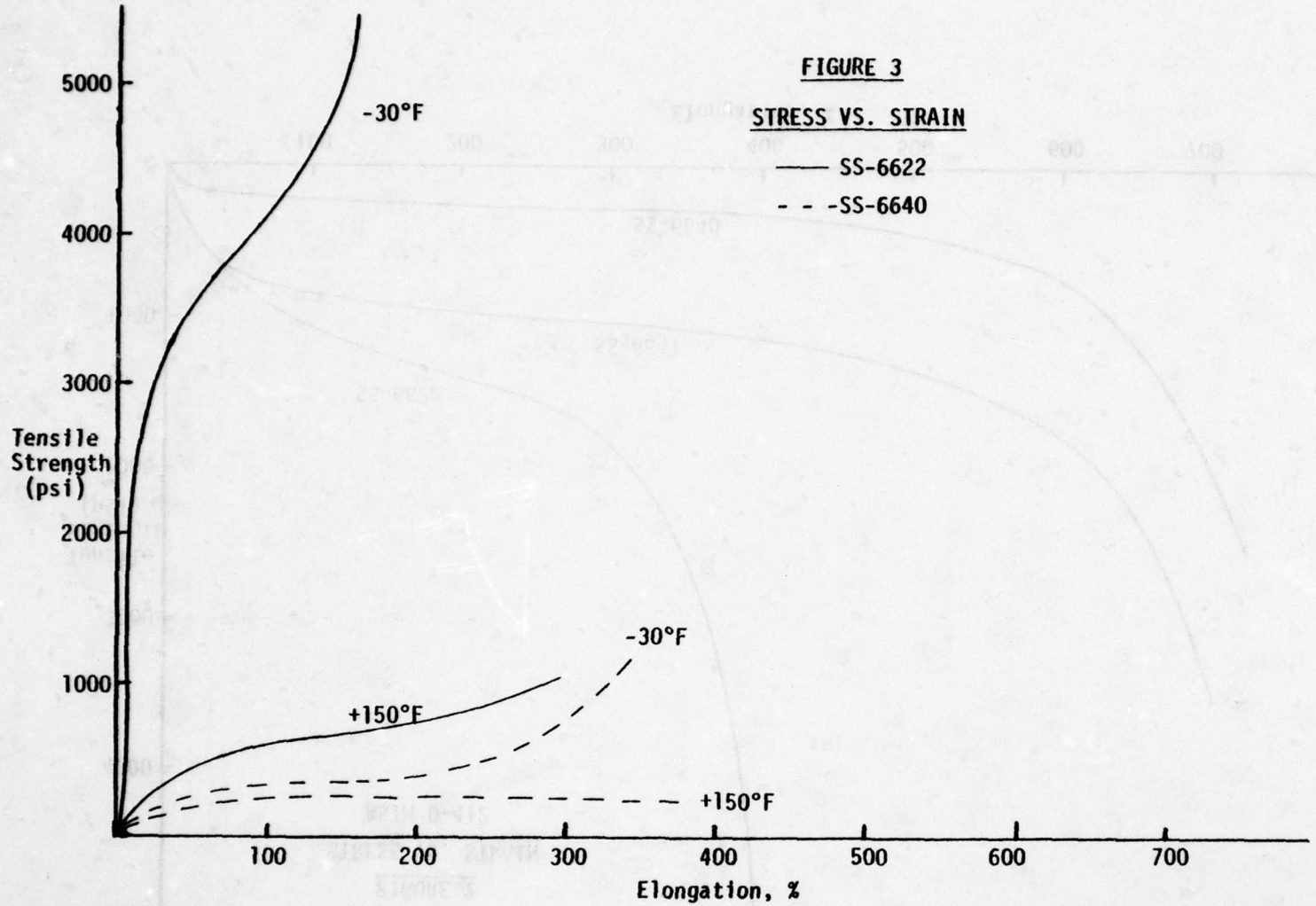


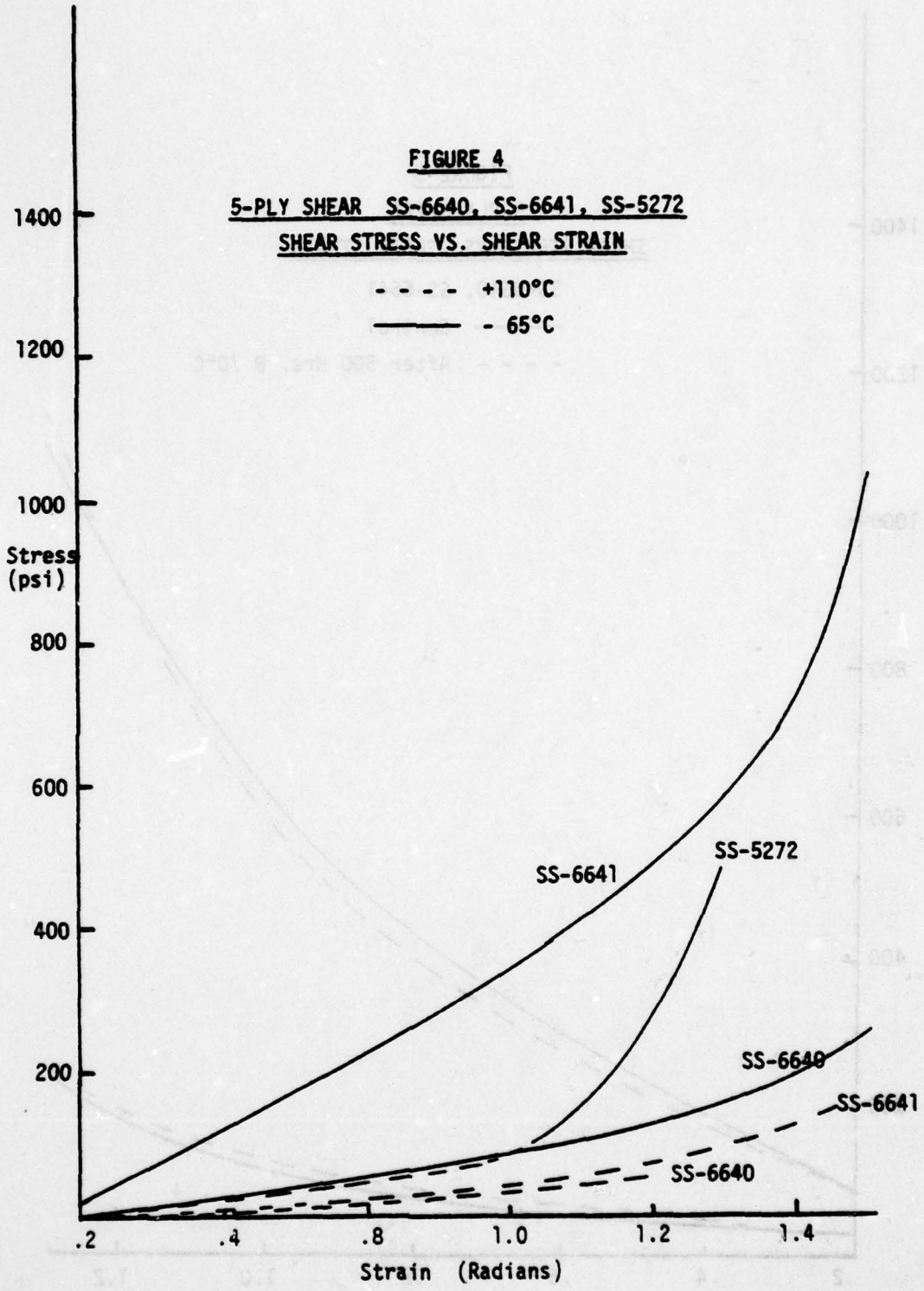
FIGURE 4

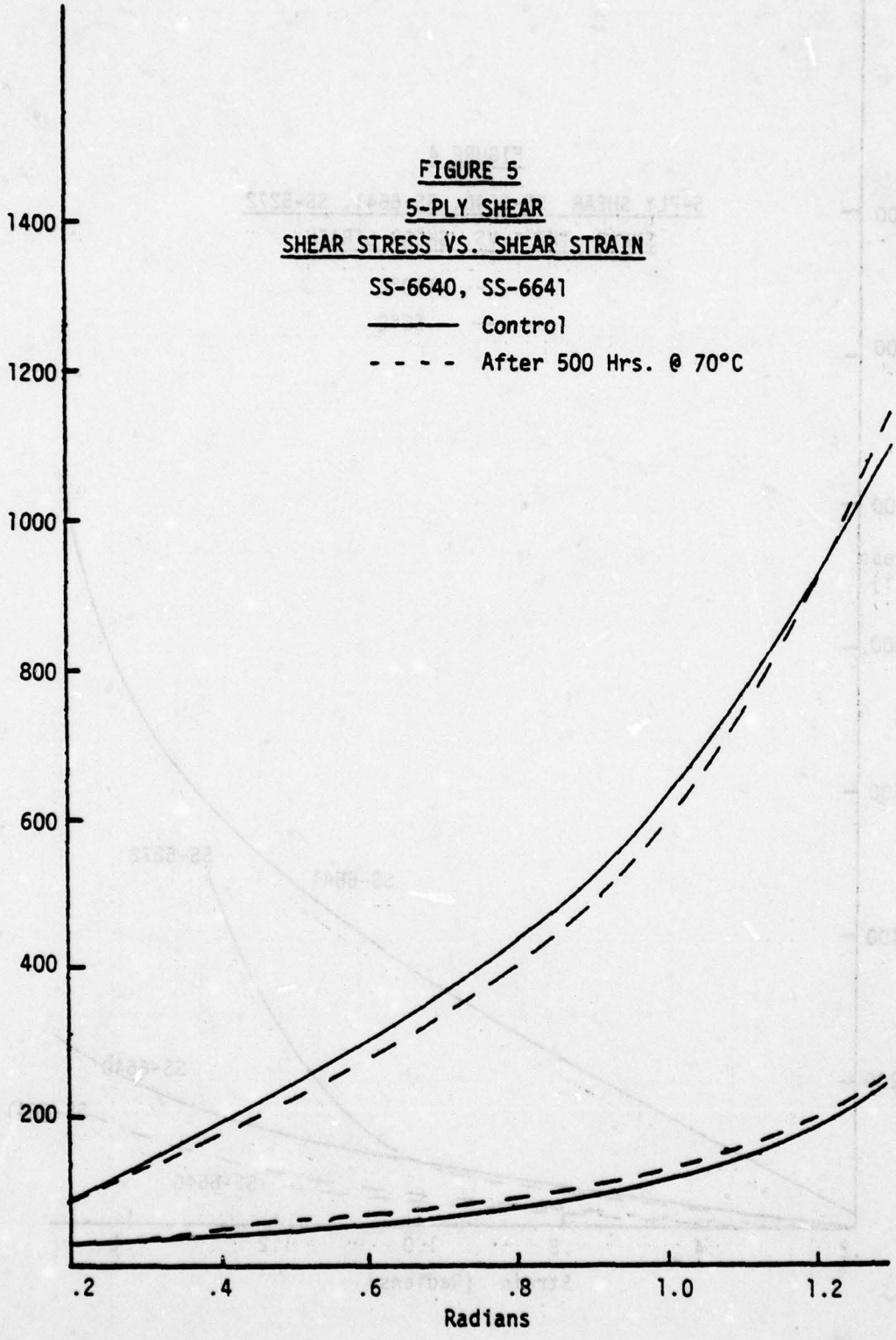
5-PLY SHEAR SS-6640, SS-6641, SS-5272

SHEAR STRESS VS. SHEAR STRAIN

- - - - +110°C

——— - 65°C




FIGURE 5
5-PLY SHEAR
SHEAR STRESS VS. SHEAR STRAIN
SS-6640, SS-6641
Control
After 500 Hrs. @ 70°C
1400
1200
1000
800
600
400
200
.2
.4
.6
.8
1.0
1.2
Radians

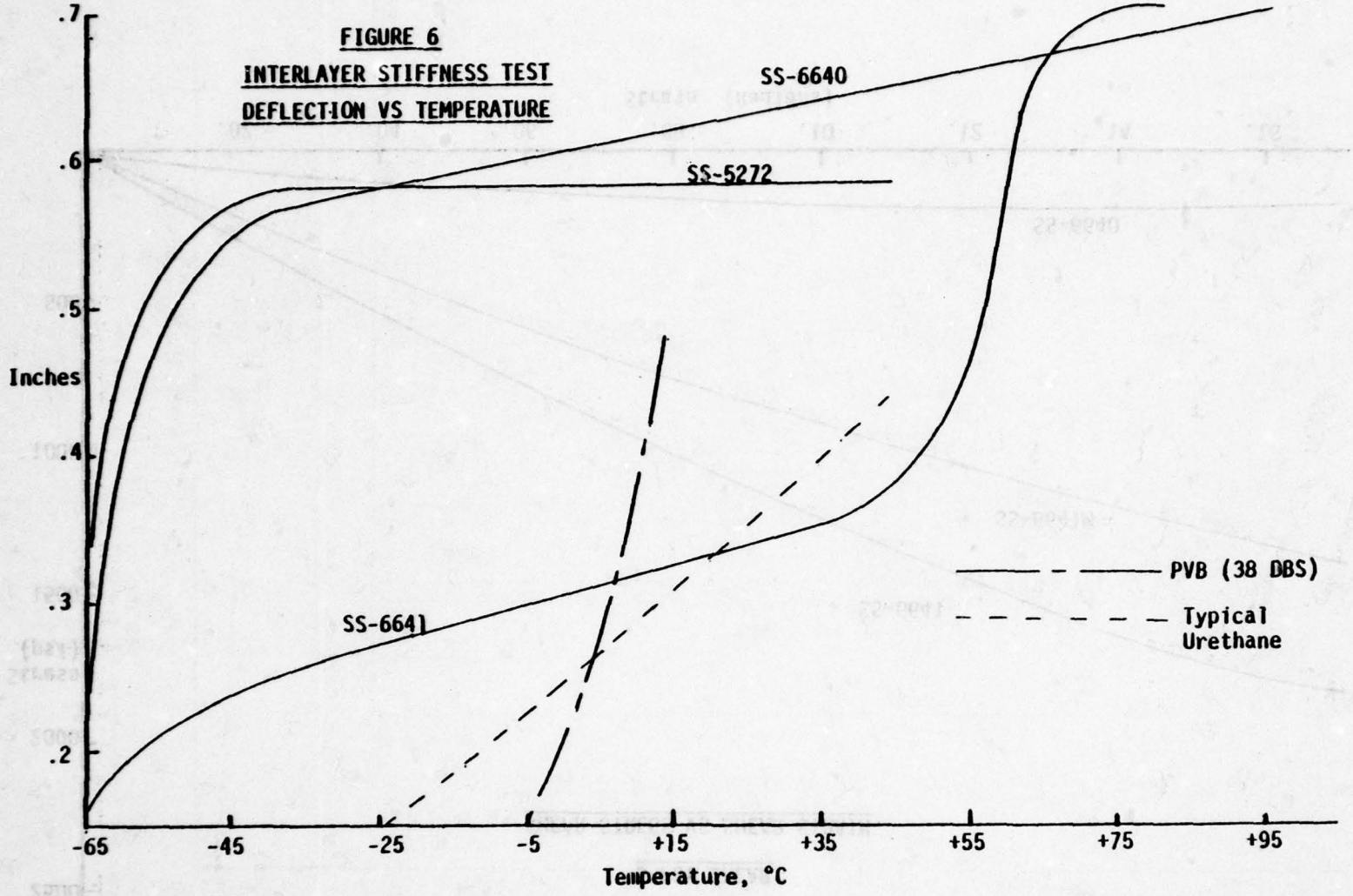
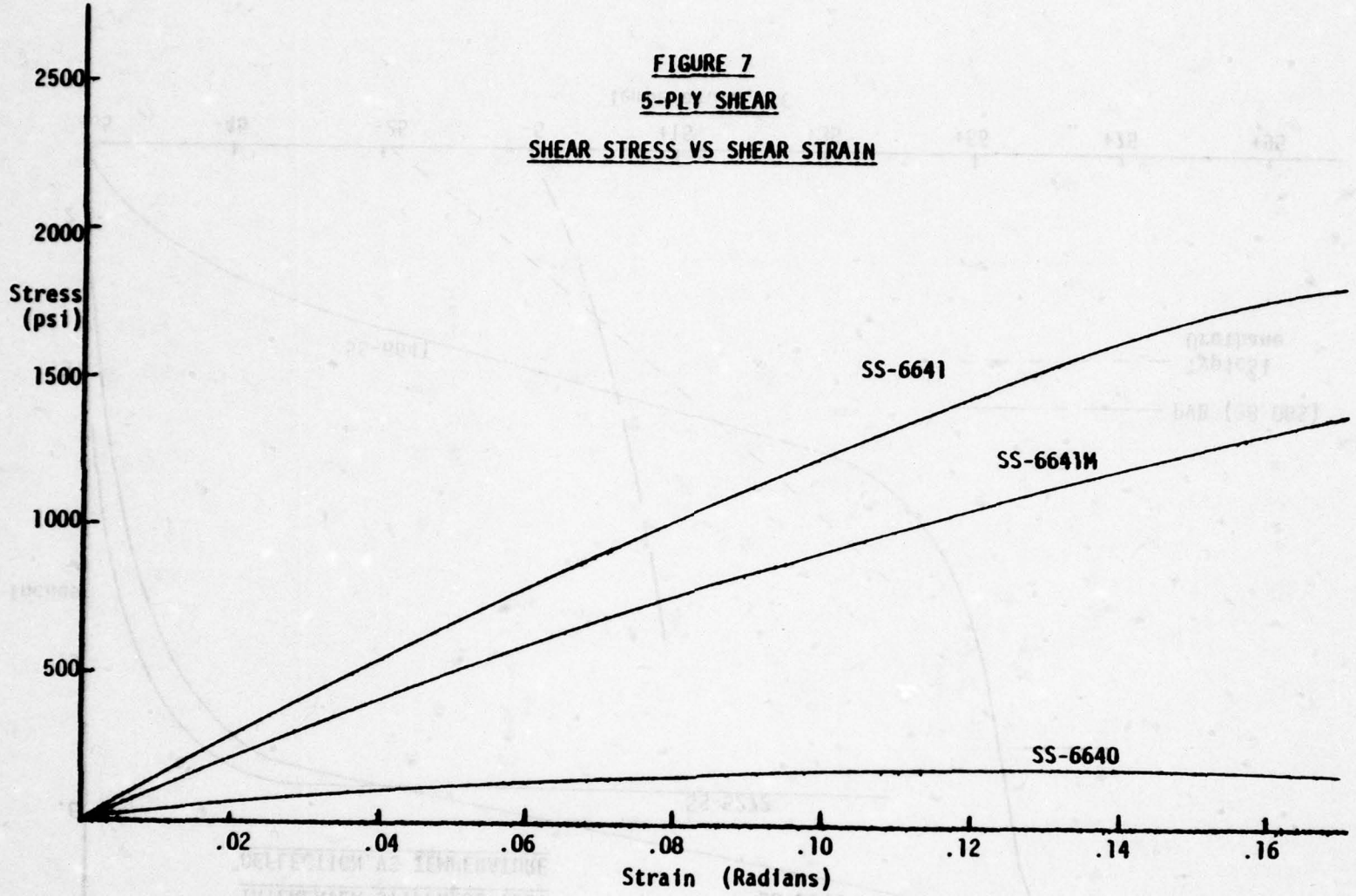

FIGURE 6
INTERLAYER STIFFNESS TEST
DEFLECTION VS TEMPERATURE
SS-6640
SS-5272
SS-6641
PVB (38 DBS)
Typical Urethane
Inches
.7
.6
.5
.4
.3
.2
-65
-45
-25
-5
+15
+35
+55
+75
+95
Temperature, °C

FIGURE 7

5-PLY SHEAR

SHEAR STRESS VS SHEAR STRAIN



HIGH TEMPERATURE AIRCRAFT GLAZING

R. Shelton
Swedlow, Inc.
Engineering
Garden Grove, California

HIGH TEMPERATURE AIRCRAFT GLAZING

R. C. Shelton

SWEDLOW, INC.

ABSTRACT

The development of aircraft with high performance capabilities has placed rigorous requirements on the transparent enclosures. In the past, these requirements have been met through the use of materials such as as-cast and stretched acrylic, cast polyester and glass; in both the monolithic and laminated form.

Later material and process developments which provided increased temperature performance of the transparent enclosures included the heat shield concept, which enabled utilization of stretched acrylic beyond its thermal relaxation temperature, and polycarbonate. The heat shield concept was made possible through the development of high temperature resistant cast-in-place interlayers.

This paper will review the materials, other than glass, which have been and are currently being used to fabricate the transparent enclosures for today's high performance aircraft. Included will be a review of how these materials can be used to fabricate the transparent enclosures of aircraft with performance characteristics beyond the current requirements.

Swedlow, Inc. is continually seeking materials and/or processes to improve the upper service capability of transparent enclosures. As a result, several new materials are being evaluated. To be included in this paper will be a discussion of a few of the more promising materials. This discussion will highlight the known desirable properties, such as high temperature and impact resistance, as well as their known undesirable properties.

PRECEDING PAGE BLANK-NOT FILMED

INTRODUCTION

Over the past twenty years or so, the development of high performance aircraft has placed increasing demands on the transparent enclosures.

Typical of these requirements are:

- High heat resistance
- Retention of physical properties (Integrity at elevated temperature)
- Bird impact resistance
- Excellent optical quality with large viewing areas
- Excellent environmental resistance

In order to provide transparencies meeting the requirements expected of these high performance aircraft, Swedlow, Inc. implemented company-funded programs to evaluate materials and material combinations, and to develop fabrication processes necessary to produce high temperature resistant transparencies.

As a result of our extensive development activity, Swedlow, Inc. continues on a production basis to manufacture heat shielded transparencies for high-performance aircraft.

The heat shield concept has been proven in service to be a practical way to utilize today's materials and provide high temperature resistant transparent enclosures for high-performance aircraft.

DISCUSSION

HISTORY

In the past, transparent enclosures for aircraft have been fabricated using the following plastic materials, in the monolithic and laminated forms.

Cast Polyester

As-Cast Acrylic

Stretched Acrylic

Polycarbonate

The development of stretched acrylic meeting the requirements of MIL-P-25690, has greatly influenced the design of transparent enclosures - as evidenced by its excellent service history.

However, its upper service capability is limited by the thermal relaxation

temperature. Normally, stretched acrylics are not recommended for continued use above approximately 220°F. There is evidence that, with a suitable temperature gradient and pressure, stretched acrylic can be utilized to temperatures in excess of 250°F.

Figure 1 shows the time - vs - temperature relationship for stretched acrylic, 0.312 inch thick, with 8.0 psi internal pressure. There are undoubtedly other instances where stretched acrylic has been exposed to temperatures in excess of 250°F, although documentation is not readily available.

Recognizing this upper temperature limit for stretched acrylic, and, since there was not a high-temperature resistant material that could be utilized in the monlithic form, led to the development of high temperature resistant castable interlayers and provided the successful application of the heat shield concept (Reference 1). This development was necessary because the available sheet laminating materials were unsatisfactory.

- Conventional polyvinyl butyral lacked the required temperature resistance, and
- Silicones, which had the necessary temperature resistance, required processing conditions beyond the capability of the stretched acrylic.

Swedlow has developed several castable interlayers, each tailored for specific applications.

For High-Temperature use, Swedlow's castable silicone interlayer, SS-5272Y(HT), is used. It has excellent optical properties, clarity, adhesion to transparent face sheets and toughness. It is a low modulus material that retains its flexibility at depressed temperatures.

Figure 2 shows the excellent retention of tensile strength and elongation at temperatures from -160°F to +300°F.

Figure 3 shows the excellent retention of tear strength at temperatures from -160°F to +300°F. Additional properties are shown in Table 1.

In addition, we have an interlayer coded SS-5272Y (TR), a modification which extends the thermal capabilities of SS-5272Y (HT) to 450°F.

As discussed earlier, development of the heat shield was necessary because of the lack of a high-temperature resistant monolithic material. One of the many materials evaluated that appeared to possess the required properties for use as a monolithic high temperature resistant material, was polycarbonate.

It offered higher impact resistance and improved heat resistance as compared to stretched acrylic. However, it was soon recognized that polycarbonate is susceptible to surface attack and damage and requires a means of protection. Considerable effort has been expended, by many firms,

in developing and evaluating a means of protecting polycarbonate. In applications where the superior impact resistance of polycarbonate is essential, surface protection is still required, and is being provided by the application of thin protective coatings or a material such as acrylic.

APPLICATIONS

To demonstrate the ability of currently available materials to satisfy the needs of high temperature resistant transparent enclosures, refer to Table 2. This table describes several aircraft whose performance characteristics required high temperature resistant transparent enclosures.

General Dynamics F-111 (Figure 4)

The transparencies for the F-111 were originally designed of laminated, chemically tempered glass. Prior to qualification of the laminated glass transparencies, the F-111 was equipped with both monolithic stretched acrylic and heat shielded stretched acrylic transparencies produced by Swedlow, Inc. The F-111 was the first production use of the laminated acrylic heat shield.

Currently, F-111 transparencies consist of laminated polycarbonate to provide added bird-impact resistance, with protective layers of as-cast acrylic.

Figure 5 shows a typical temperature profile that the current bird-proof transparencies must meet.

Grumman F-14 (Figure 6)

The first production high performance aircraft to have their transparencies designed of heat shielded stretched acrylic, was the F-14. (Reference 1). Figure 7 shows a typical temperature profile that the heat shielded side windshields are required to withstand. The requirements for the canopies are similar.

The F-14 heat shielded, stretched acrylic transparencies (Figure 8), continue to enjoy excellent service performance. Swedlow, Inc. has delivered in excess of 2200 transparencies. (Windshield side panels, forward and aft canopies).

The latest report we have is that as of March, 1978, over 350 F-14's have made more than 92000 flights involving approximately 143,000 flight hours. The maximum flight time on any individual aircraft is over 1000 hours.

As previously reported, (Reference 1), there have been incidents of crazing of the outer as-cast acrylic heat shield, attributed largely to the edge restraint of the transparencies. It is our understanding that this has been corrected through the redesign of the edge restraint.

It should be noted that with a heat shielded transparency any damage that occurs to the outer as-cast acrylic has no effect on the structural stretched acrylic, because of the castable silicone interlayer.

McDonnell Douglas F-15 (Figure 9)

Transparencies for the F-15 were originally designed using polycarbonate (acrylic clad and abrasion resistant coated). Because of in-service problems the material was changed to monolithic stretched acrylic.

The windshield was originally constructed of as-cast acrylic faces, fusion bonded to a polycarbonate structural member. This construction was discontinued due to the cracking of the outer as-cast acrylic layer.

The windshield was changed to monolithic polycarbonate, with an abrasion resistant coating, the same as the canopies. The A. R. coated polycarbonate construction was discontinued due to the loss of adhesion after U.V. exposure as well as rain erosion and ice crystal abrasion.

Because of the problems experienced with the polycarbonate, McDonnell Douglas changed all F/TF-15 transparencies to monolithic stretched acrylic, (Figure 10). The monolithic stretched acrylic transparencies have been tested to Mach 2.5, and F-15's so equipped have flown at Mach 2.5. Swedlow, Inc. has delivered in excess of 1,300 transparencies for the F/TF-15 aircraft, and, to date, there have been no reported problems associated with the use of stretched acrylic in this application.

General Dynamics F-16 (Figure 11)

Transparencies for the F-16 are monolithic polycarbonate, abrasion resistance coated. At this time, the main difference from the original design is thickness of the polycarbonate. Based on the F-15 transparency results, degradation of the abrasion resistant coated polycarbonate, in service, can be anticipated.

Rockwell B-1 (Figure 12)

The windshields (Figure 13) for the B-1 aircraft were originally constructed of laminated polycarbonate to provide added bird-impact resistance, with an outer layer of as-cast acrylic for environmental protection, and to carry the required anti-ice coating.

The final configuration differs only in regard to the outer layer -- it being chemically tempered glass. (Reference 2).

EDGE ATTACHMENT LAMINATE AND ADHESIVES

The edge attachment materials currently being used, nylon and fiberglass, satisfy the requirements when fabricated using high temperature resin systems.

Figure 14 shows the tensile strength of Epoxy Nylon (Swedlow Code X6N-225) and Epoxy Fiberglass (Swedlow Code X6G-298) vs temperature. Figure 15 shows the bearing stress of Epoxy Nylon (X6N-225) and Epoxy Fiberglass (X6G-298) - vs - temperature. Both of these materials have been proven in service - the epoxy nylon on the General Dynamics F-111, RIC B-1, the F-14, and the epoxy fiberglass on the General Dynamics F-111 laminated acrylic transparencies.

Several adhesives are available for high temperature application.

Swedlow's HO-614 modified epoxy has been proven satisfactory for use in service as the adhesive on the F-111 and the F-14 laminated acrylic transparencies.

FUTURE ACTIVITY

The preceding has been a brief discussion of several ways currently available materials are being utilized to satisfy the requirements of transparent enclosures on high performance aircraft.

But what lies ahead?

The continued development of aircraft with higher performance has led to the question - "What material(s) will be utilized in the future to fabricate the transparencies?"

To begin with, the heat shield concept will continue to play a vital role in high temperature resistant transparencies, in combination with high-temperature resistant castable interlayers. However, a monolithic member of high temperature resistant, tough material would be more efficient. Therefore, we as transparency fabricators, are continuing our development and evaluating means of providing the high temperature resistant transparent enclosures necessary for the future aircraft.

Included in this activity is the development of interlayers and the evaluation of plastic sheet.

As discussed earlier, Swedlow, Inc. has developed a castable silicone interlayer with temperature capability to 450°F.

Additional information concerning the development and characterization of urethane interlayers was presented in the preceding paper by Mr. E. M. Brown of Swedlow and will not be repeated here.

POTENTIAL GLAZING MATERIALS

The following are some of the plastic materials that have been evaluated as potential high temperature resistant transparent glazing materials. This is by no means all the materials evaluated, but are some that appeared, at first, to possess desirable qualities.

- Polyolefin

- Polyamide
- Polysulfone
- Polyphenylsulfone

Table 3 contains typical properties of these materials, with a brief description as follows.

Polyolefin is a chemically resistant polymer with the lowest specific gravity of any thermoplastic.

It has good clarity and is reported able to withstand 260°F for long periods and 400°F for short times.

In its current form it lacks good resistance to U.V. exposure and is not yet recommended for continuous outdoor exposure.

Polyamide has improved resistance to chemicals and solvents as compared to polycarbonate.

It has good strength retention at temperatures over 200°F.

It is reported able to be used continuous at temperatures of 175°F.

Polysulfone is a heat resistant high performance thermoplastic. It has high strength and low creep under load at elevated temperatures. With its high heat distortion temperature, it is capable of long term use at 300°F to 350°F. It retains its notched izod strength over a wide temperature range, as well as in thicknesses up to 1/2 inch. When tested unnotched, it will bend but not break. After long term aging at 300°F, the notched izod strength is reduced slightly, from 1.3 ft-lb/in notch to 0.8 ft-lb/in notch.

It reportedly has good resistance to mineral acids, alkali and salt solutions but is attacked by ketones, aromatic and chlorinated hydro carbons. Polysulfone, in its current form lacks good resistance to U. V., and is not yet recommended for continuous outdoor exposure, but offers considerable potential.

Polyphenylsulfone is a high performance thermoplastic with a heat distortion temperature 55°F above polysulfone, capable of long term use at temperatures in excess of 375°F. It retains excellent notched izod strength over a wide temperature range, from 12 ft-lbs/in, at R. T. to 8 Ft-lbs/in at -40°F. After long term aging at 400°F its room temperature notched izod strength is 2.0 ft-lbs/in. The reduction is similar to that exhibited by polycarbonate after long term aging at 250°F (16ft-lbs/in to 2 ft-lbs/in). Polyphenylsulfone has better resistance to environmental stress-cracking with chlorinated hydro carbons than polysulfone or polycarbonate. It is resistant to mineral acids, alkali and salt solutions. It also has good resistance to

hydro carbon oils and chlorinated hydro carbons. Polyphenylsulfone is attacked by ketones, esters and aromatic hydro carbons. Polyphenylsulfones, like polysulfone, lacks good resistance to U.V. and is not yet recommended for continuous outdoor exposure.

Figure 16 shows the relative heat distortion temperatures of these materials with stretched acrylic and polycarbonate included as reference materials.

Figure 17 shows the relative impact strengths of these materials as determined by notched izod. Again, stretched acrylic and polycarbonate are shown as reference materials, including the effect of thermal conditioning on polycarbonate.

It is evident, based on the materials discussed herein, that an immediate solution to the problem of a monolithic, high temperature resistant enclosure material is not imminent. The polyolefin and polyamide materials lack the required temperature capability and U.V. resistance to be used without protective layers. This would be a step backward from what is available with laminated acrylic.

The polysulfone and polyphenylsulfone both suffer from lack of U.V. resistance. If this lack of U.V. resistance can be overcome, the polyphenylsulfone would then show real promise as a high temperature resistant enclosure material.

SUMMARY

The materials and fabrication procedures required to supply high temperature resistant enclosures are available, by utilizing the heat shield concept. Excellent service performance is attained through the use of proven production materials and processes.

Polycarbonate, with adequate surface protection is finding application where its superior impact resistance is essential.

The edge attachment materials, (reinforced laminates and adhesives), are available and being used on high temperature enclosures.

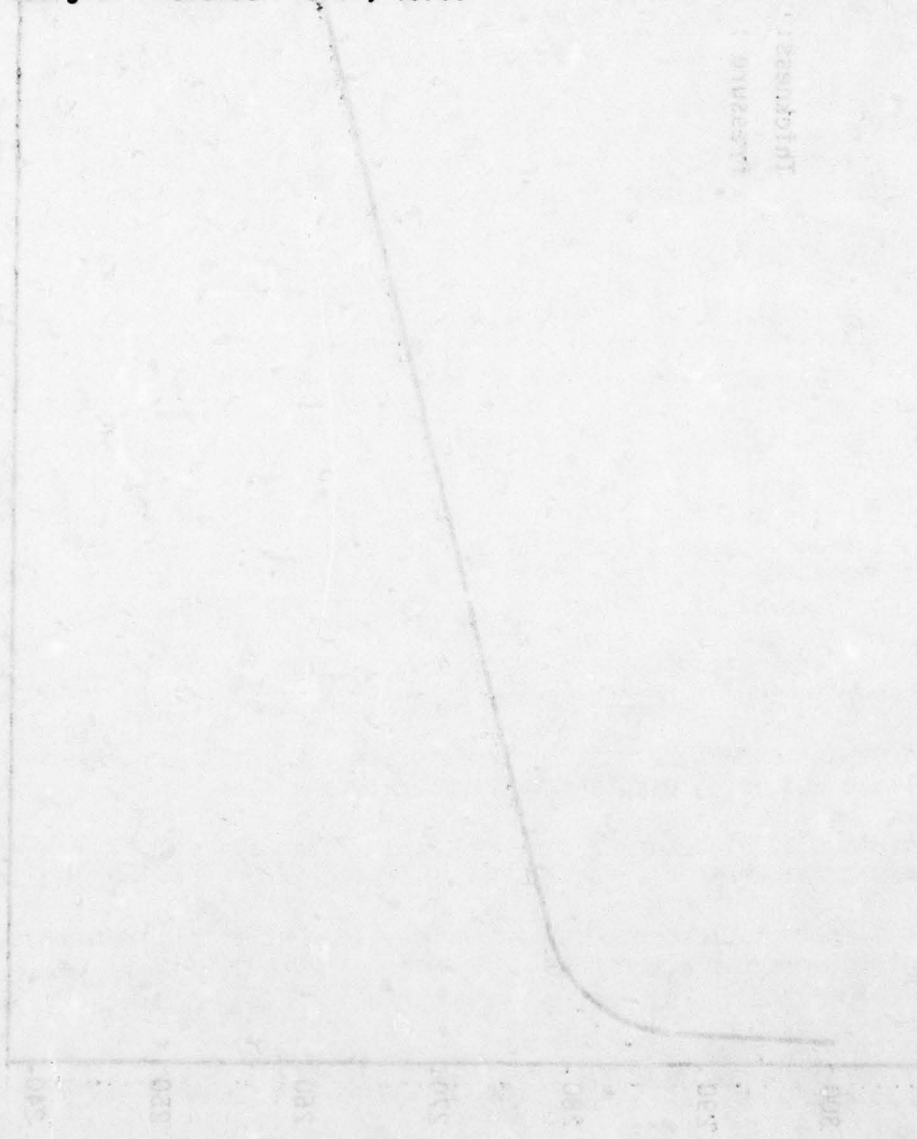
Improvement of high temperature resistant interlayers and the evaluation of the new transparent glazings is a continuing effort by Swedlow, Inc.

It is our aim to lead the way in the development of high temperature resistant enclosures for aircraft.

REFERENCES

(1) R. C. Shelton, Swedlow, Inc. "The Use of Laminated Acrylic Transparencies on High-Performance Aircraft." Paper presented at the Conference on Transparent Materials for Aerospace Enclosures, Atlanta, Georgia. November 18-21, 1975.

(2) R. C. Shelton, Swedlow, Inc. "Development of The Windshield for the B-1 Aircraft." Paper presented at the Conference on Transparent Materials for Aerospace Enclosures, Atlanta, Georgia. November 18-21, 1975.



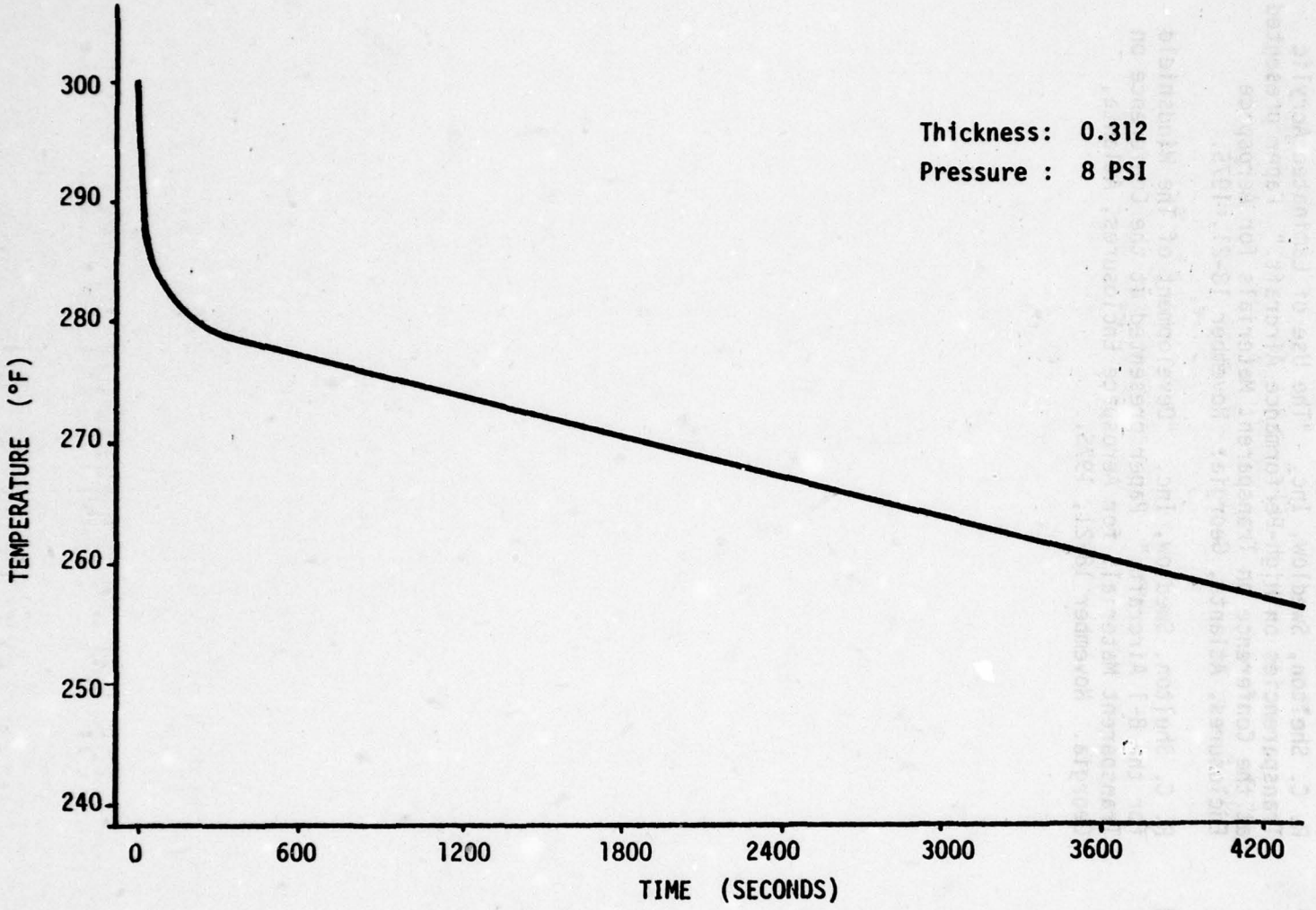


FIGURE 1 - OPTICAL DEFORMATION LIMIT OF STRETCHED ACRYLIC UNDER PRESSURE

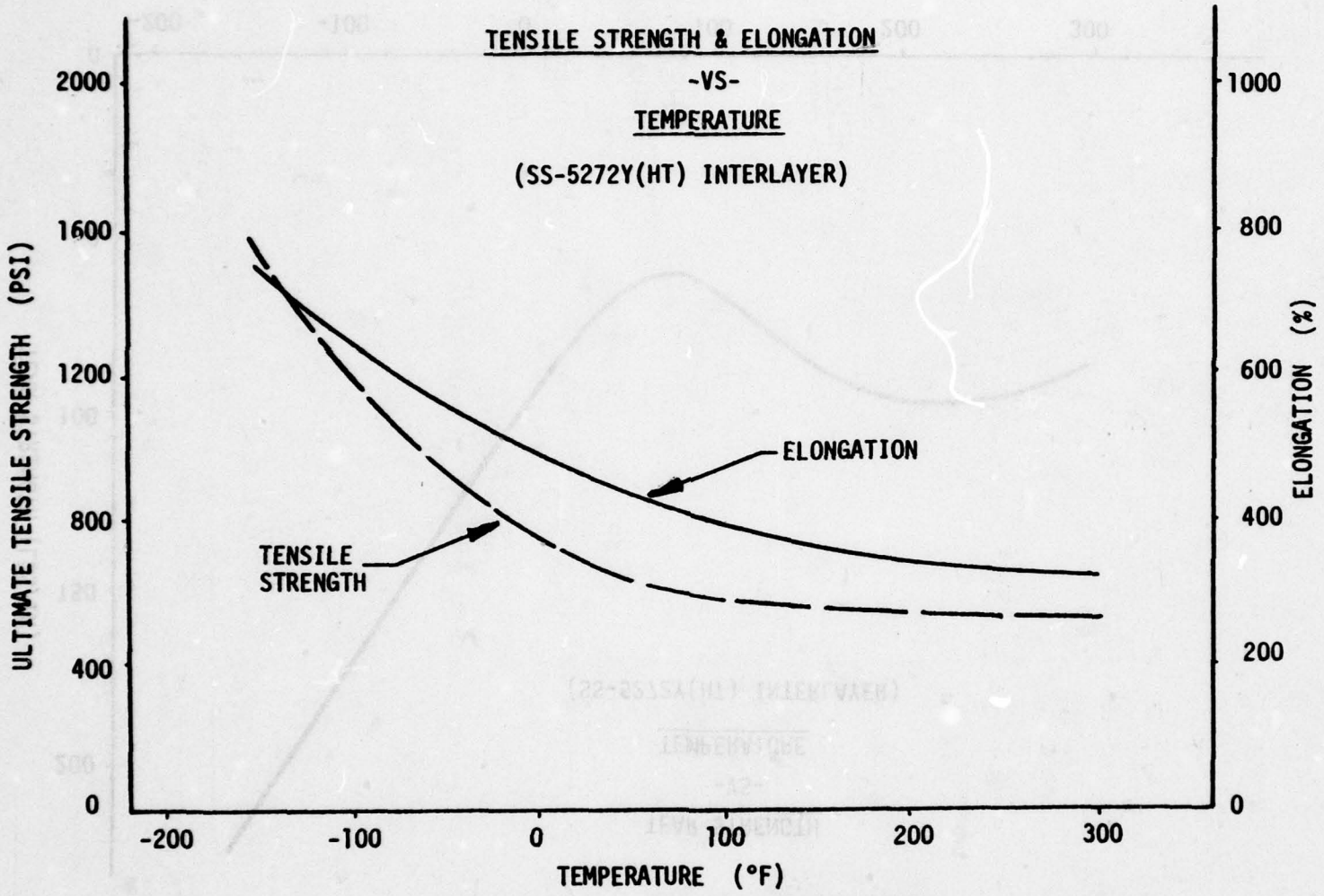


FIGURE 2 - TENSILE STRENGTH AND ELONGATION OF SS-5272Y(HT)

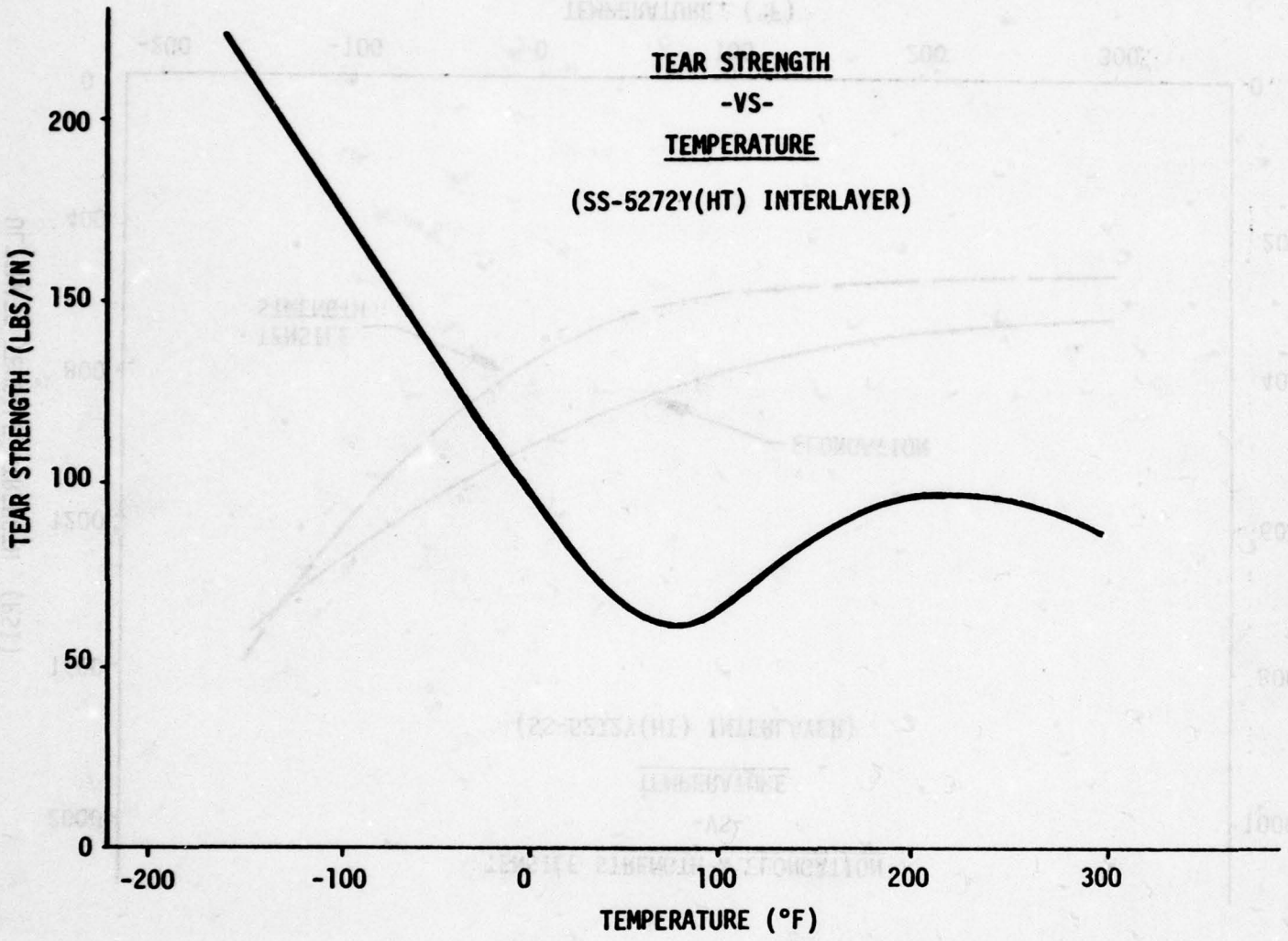


FIGURE 3 - TEAR STRENGTH OF SS-5272Y(HT)

TABLE 1

TYPICAL PROPERTIES

SWEDLOW SS-5272Y(HT)

CAST-IN-PLACE INTERLAYER

PROPERTY	RESULT
Specific Gravity	1.02
Index of Refraction	1.409
Water Absorption (%)	0.028
Shore A Hardness	43
Thermal Conductivity ($BTU/HR/FT^2/^oF/IN$)	0.76
Specific Heat ($BTU/LB/^oF$)	0.345
Coefficient of Thermal Expansion ($IN/IN/^oF$)	$212X10^{-6}$
Light Transmission % (1)	90
Haze % (1)	2

(1) Interlayer evaluated as a composite. 0.188" MIL-P-8184, 0.188" SS-5272Y(HT), 0.250" MIL-P-25690.

TABLE 2

TRANSPARENCY APPLICATIONS

AIRCRAFT	TRANSPARENCY CONSTRUCTION	
	ORIGINAL	CURRENT
F-111	Glass Laminate	Acrylic/Polycarbonate Laminate
F-14	Acrylic Laminate	Same
F-15	Polycarbonate	Stretched Acrylic
F-16	Polycarbonate	Same
B-1 W/S	Acrylic/Poly-carbonate Laminate	Glass/Polycarbonate



FIGURE 4 - GENERAL DYNAMICS F-111

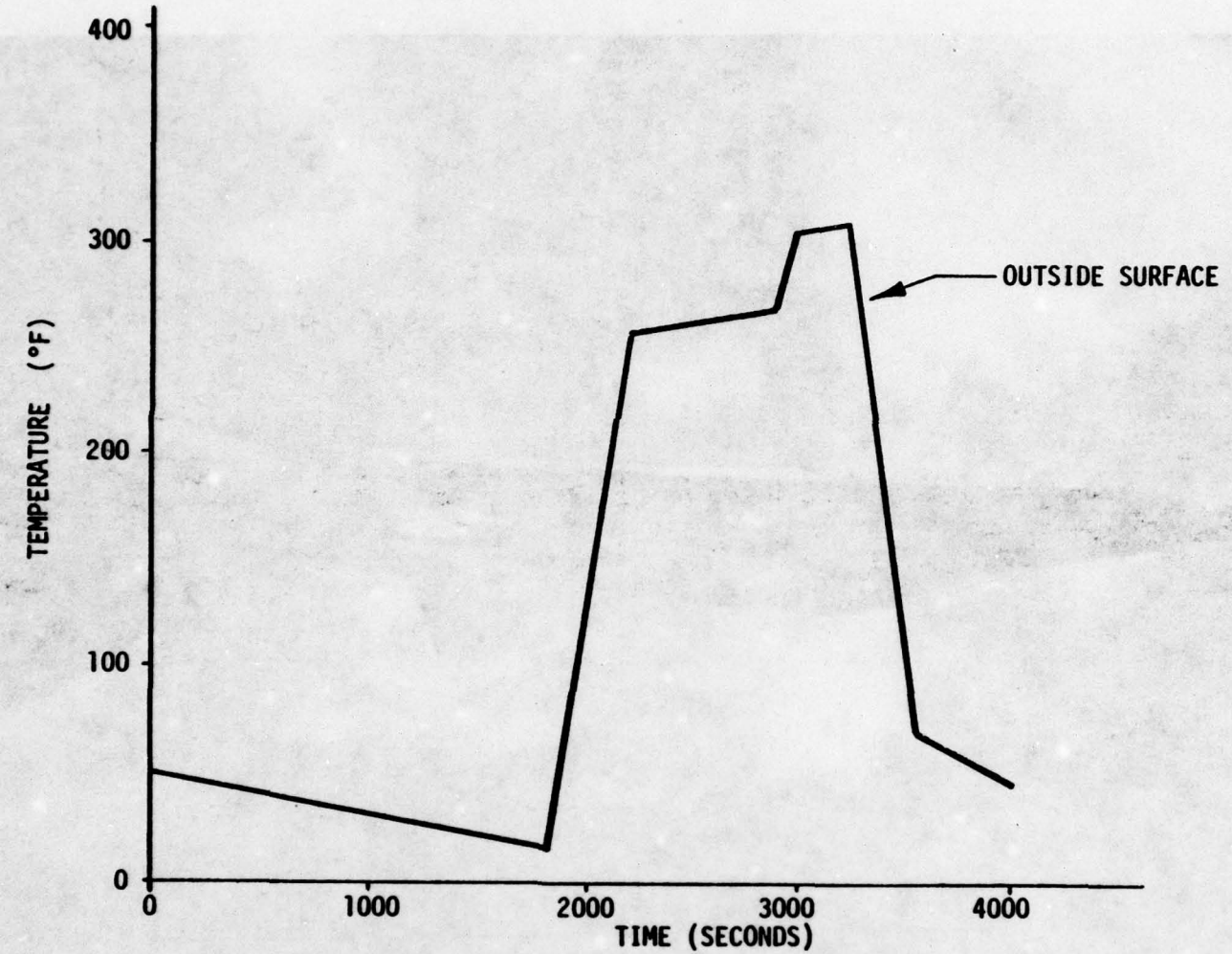


FIGURE 5 - F-111 WINDSHIELD TEST TEMPERATURE PROFILE

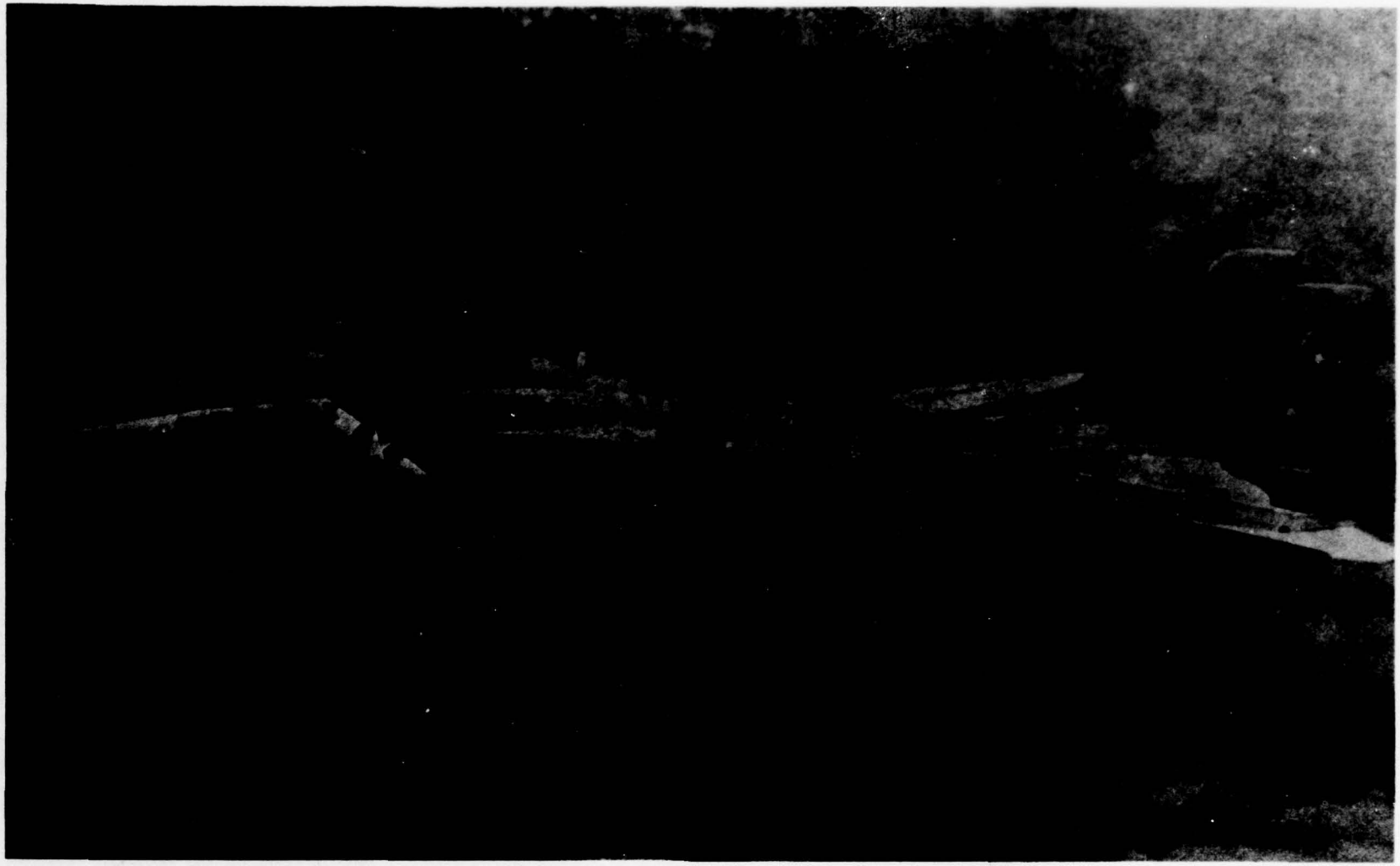


FIGURE 6 - GRUMMAN F-14

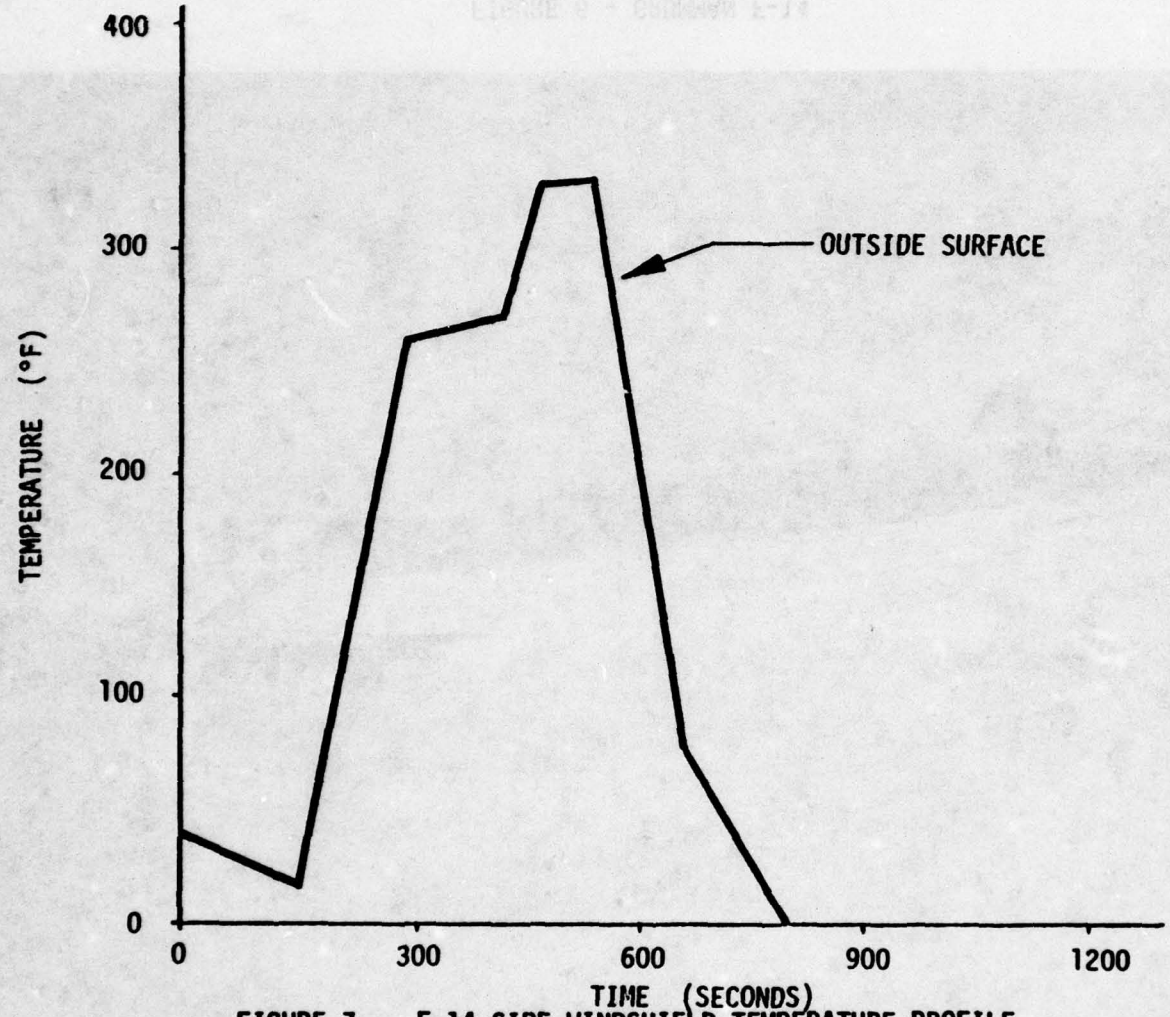


FIGURE 7 - F-14 SIDE WINDSHIELD TEMPERATURE PROFILE

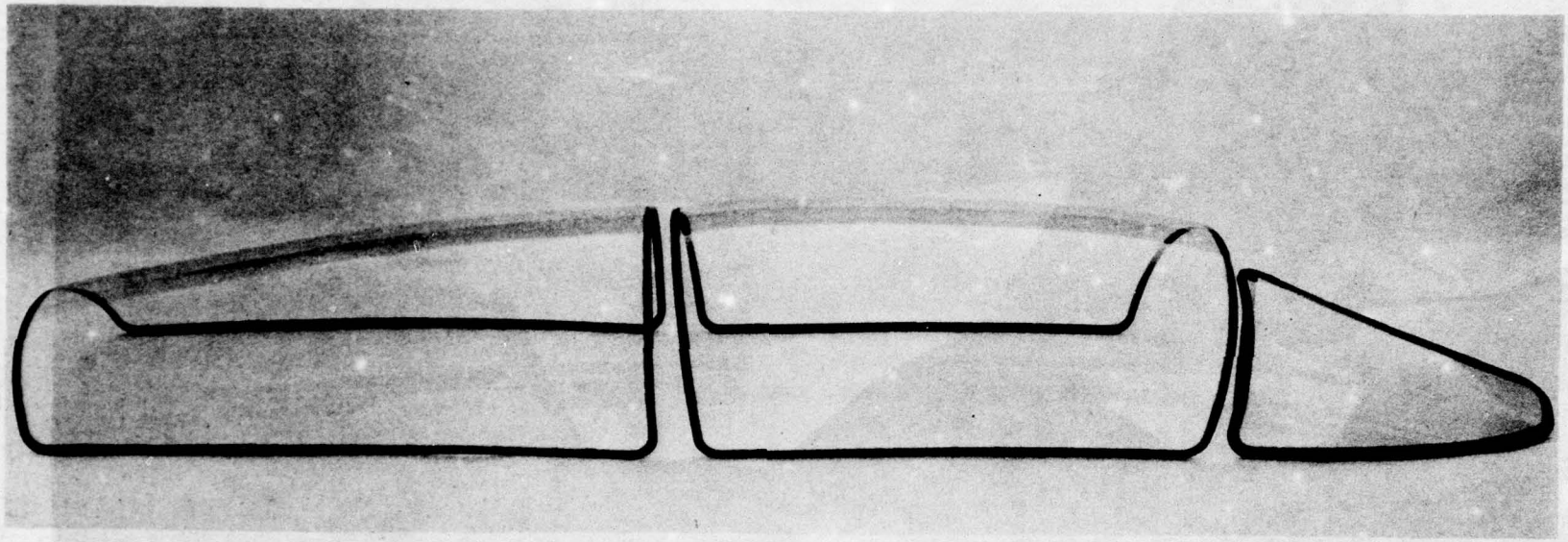


FIGURE 8 - F-14 TRANSPARENCIES

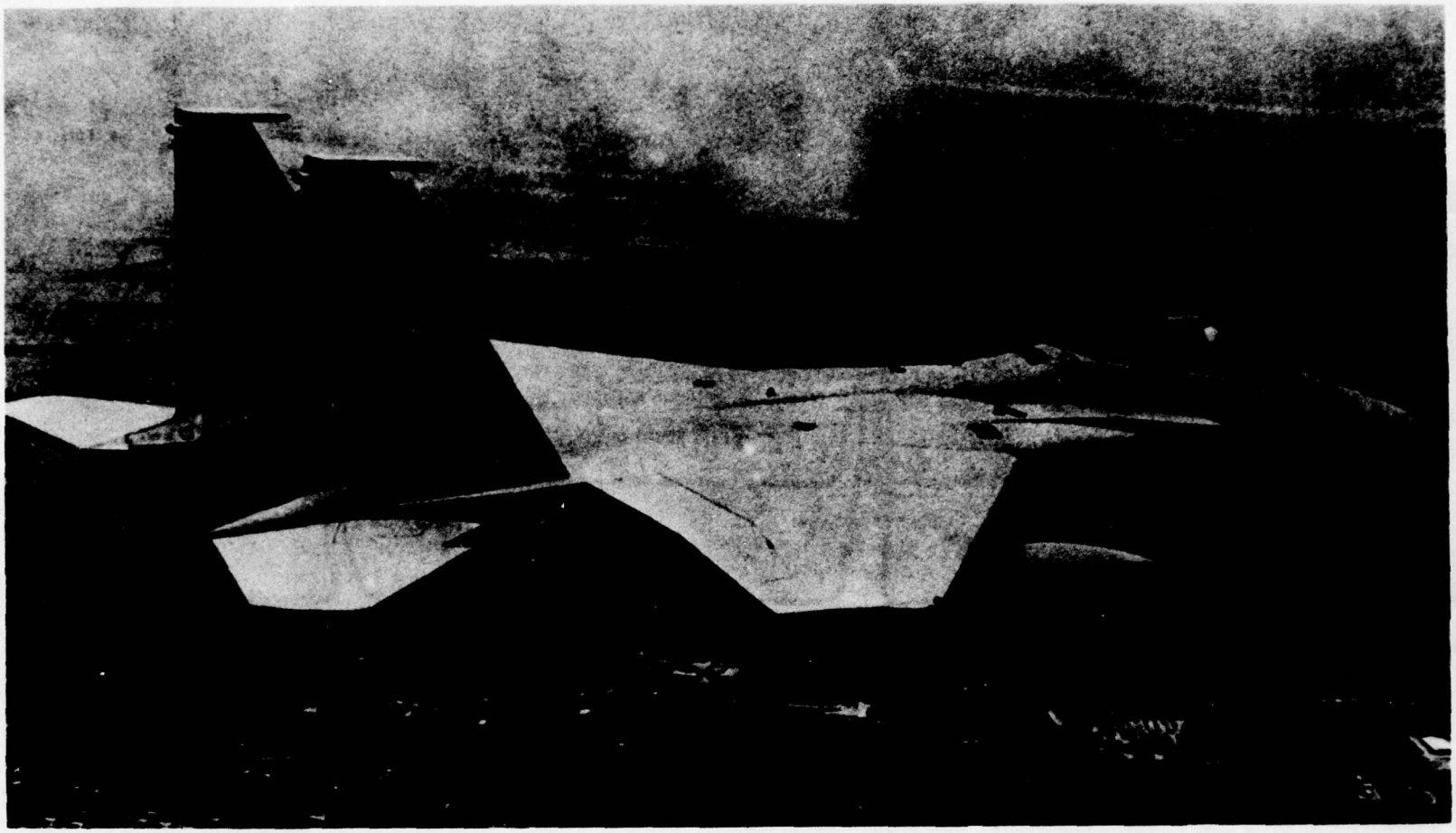


FIGURE 9 - McDONNELL DOUGLAS F-15

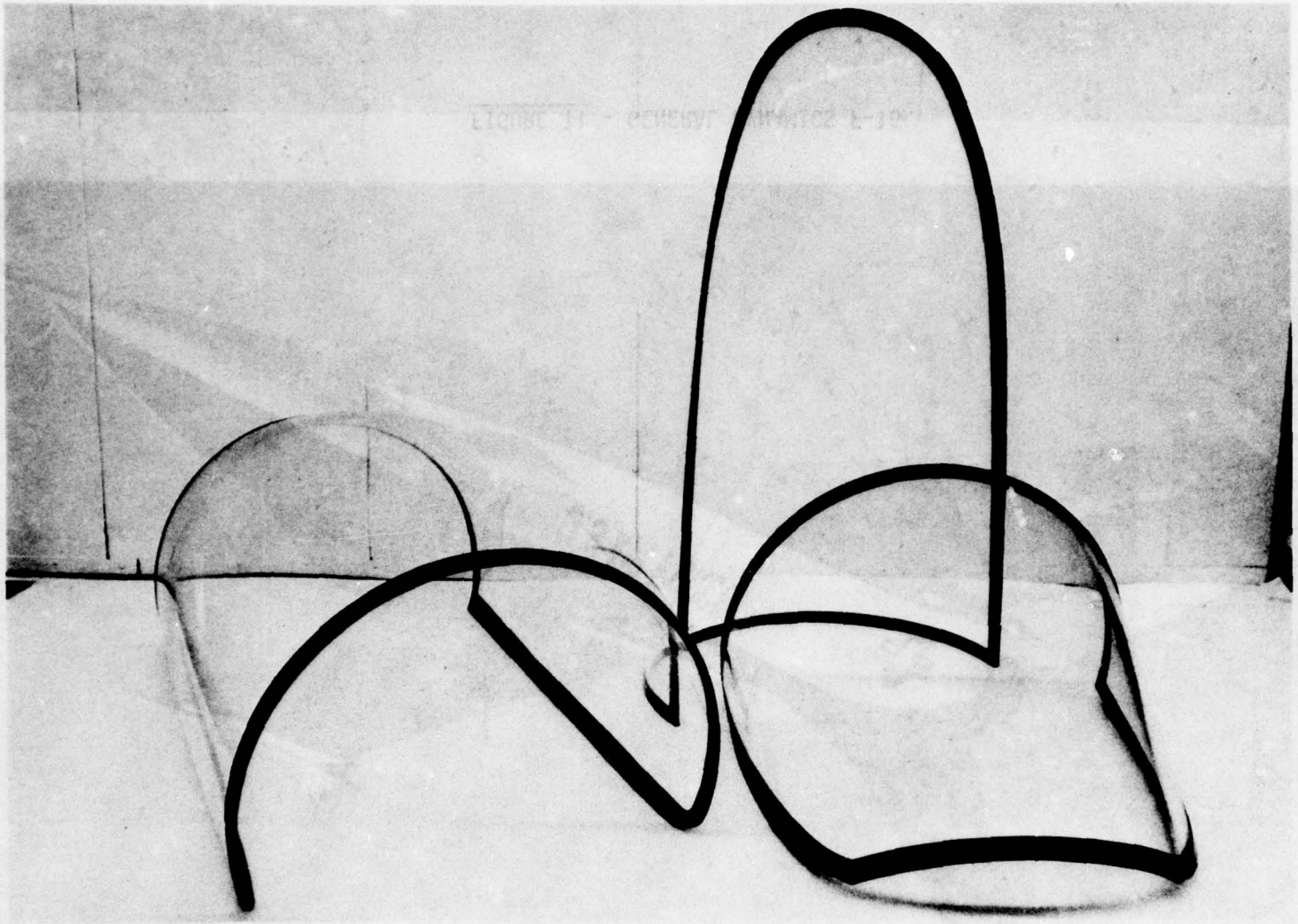


FIGURE 10 - F-15 TRANSPARENCIES



FIGURE 11 - GENERAL DYNAMICS F-16

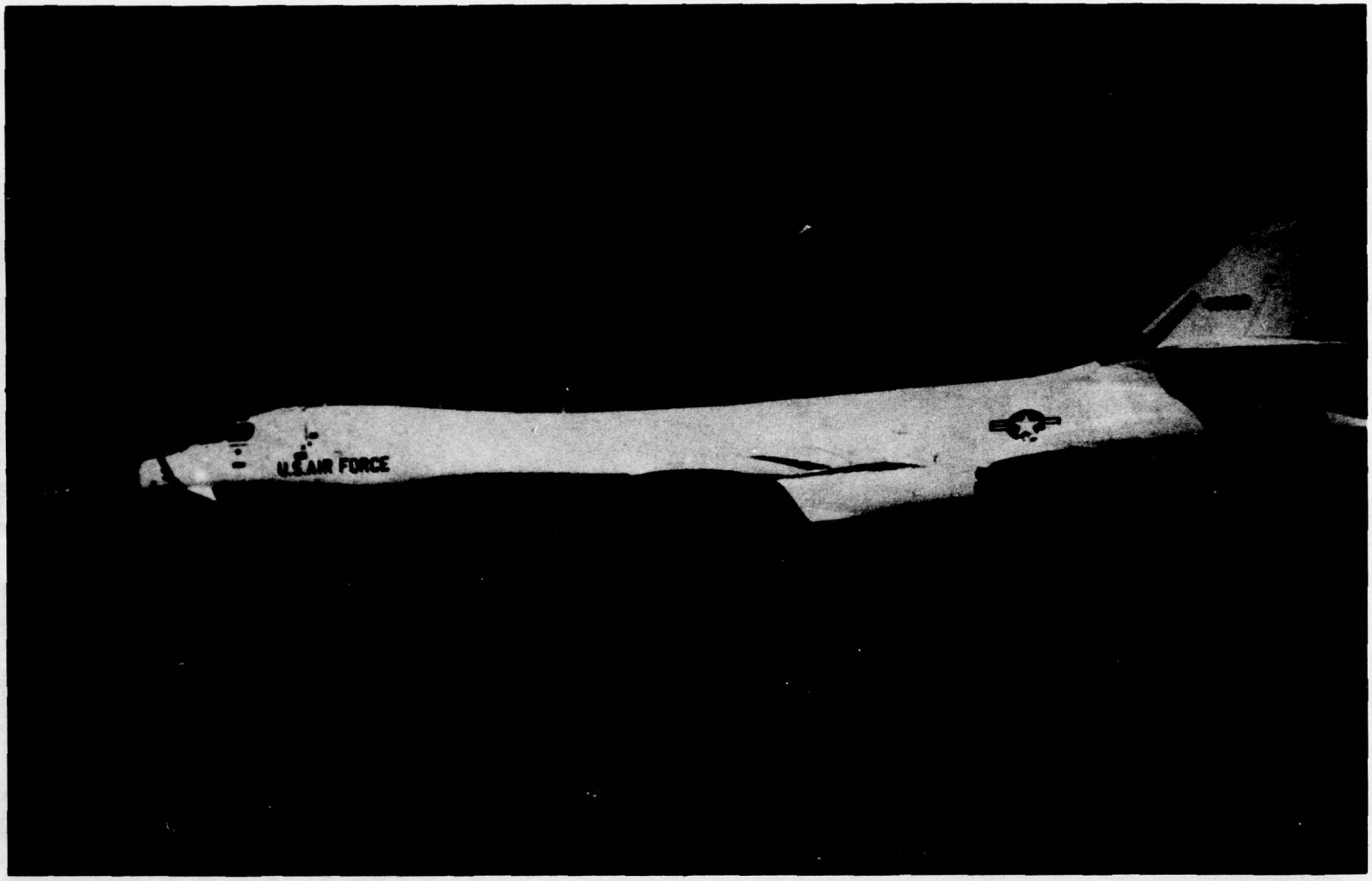


FIGURE 12 - ROCKWELL B-1

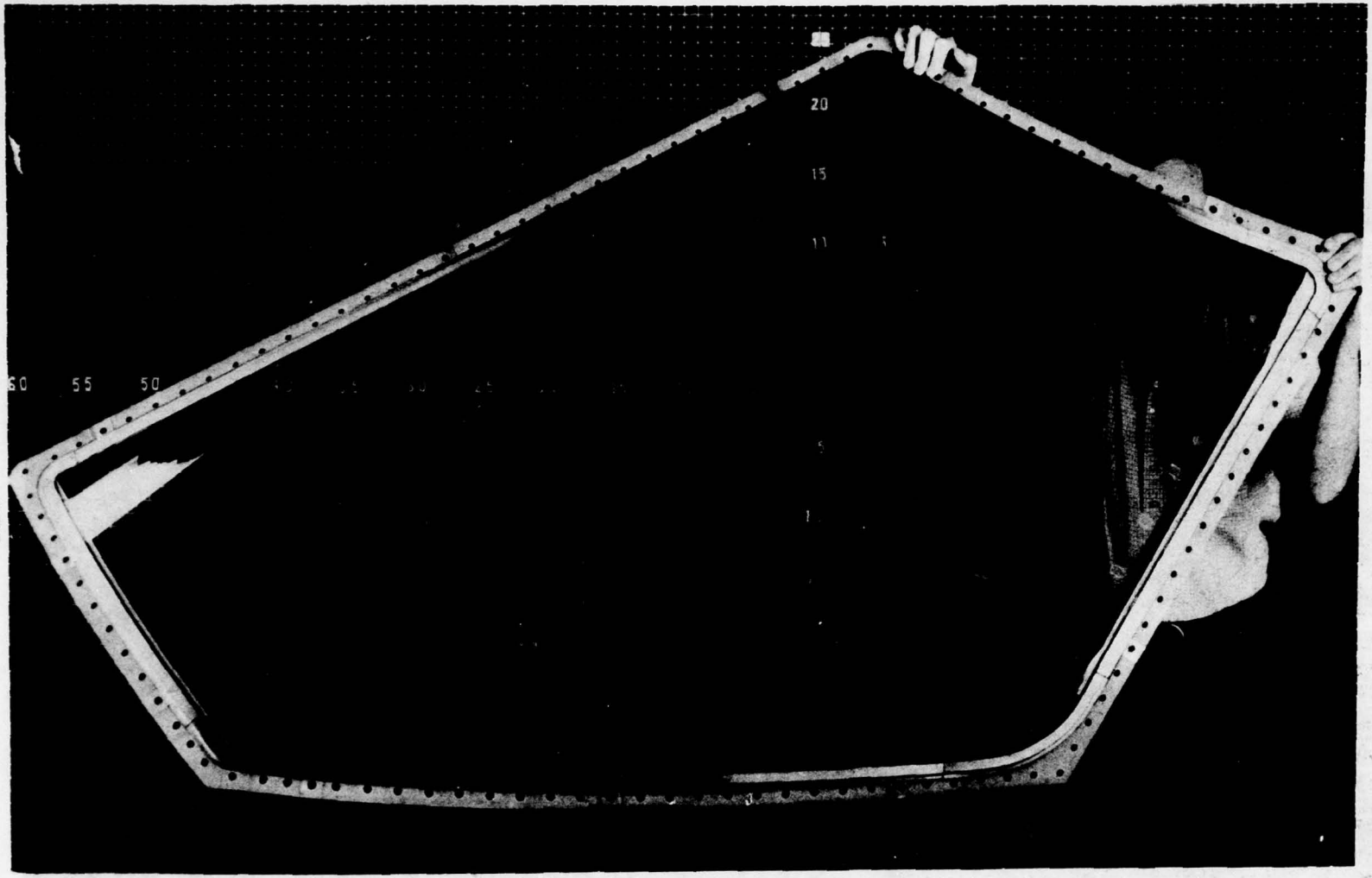


FIGURE 13 - B-1 WINDSHIELD

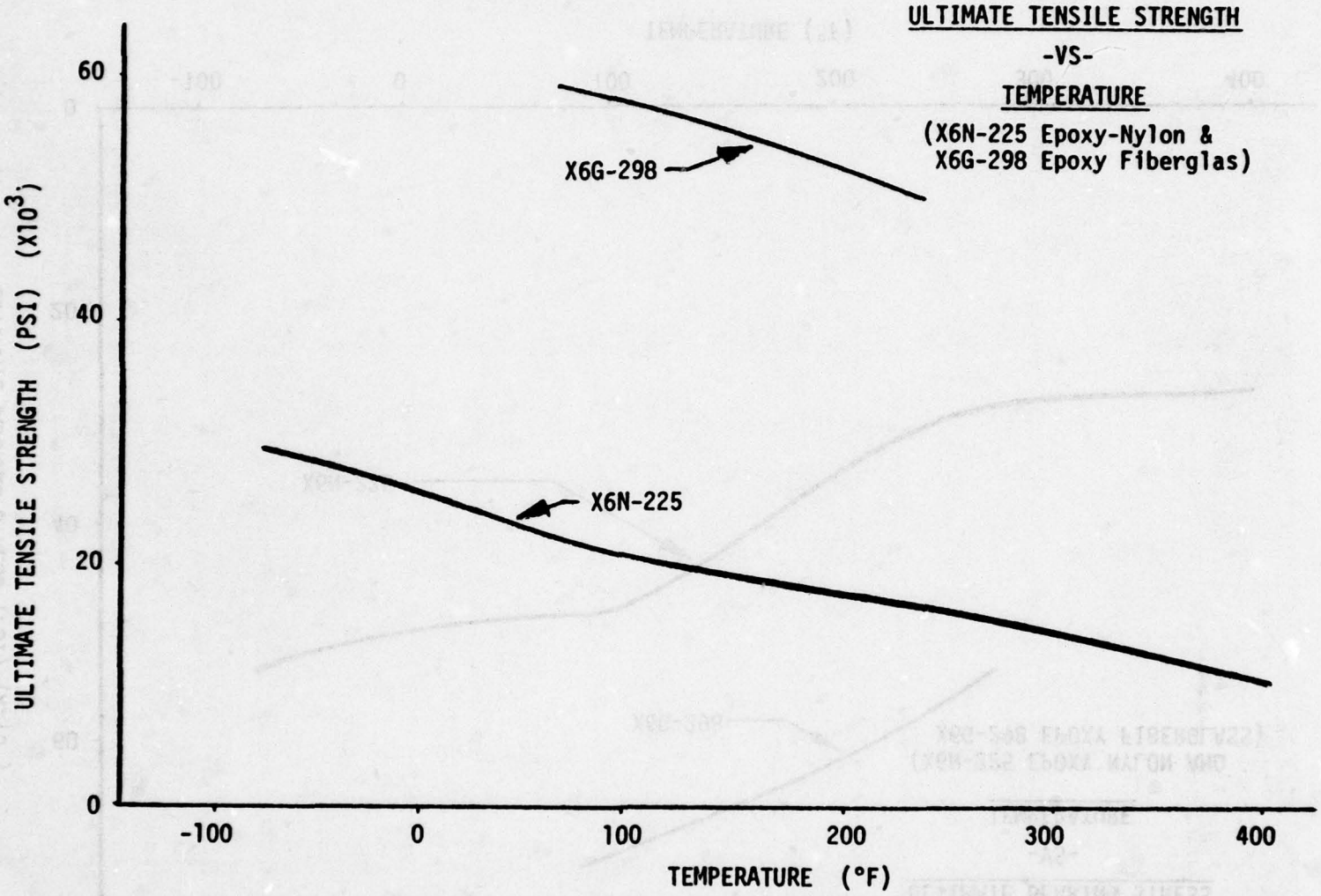


FIGURE 14 - ULTIMATE TENSILE STRENGTH OF EPOXY-NYLON AND EPOXY FIBERGLAS

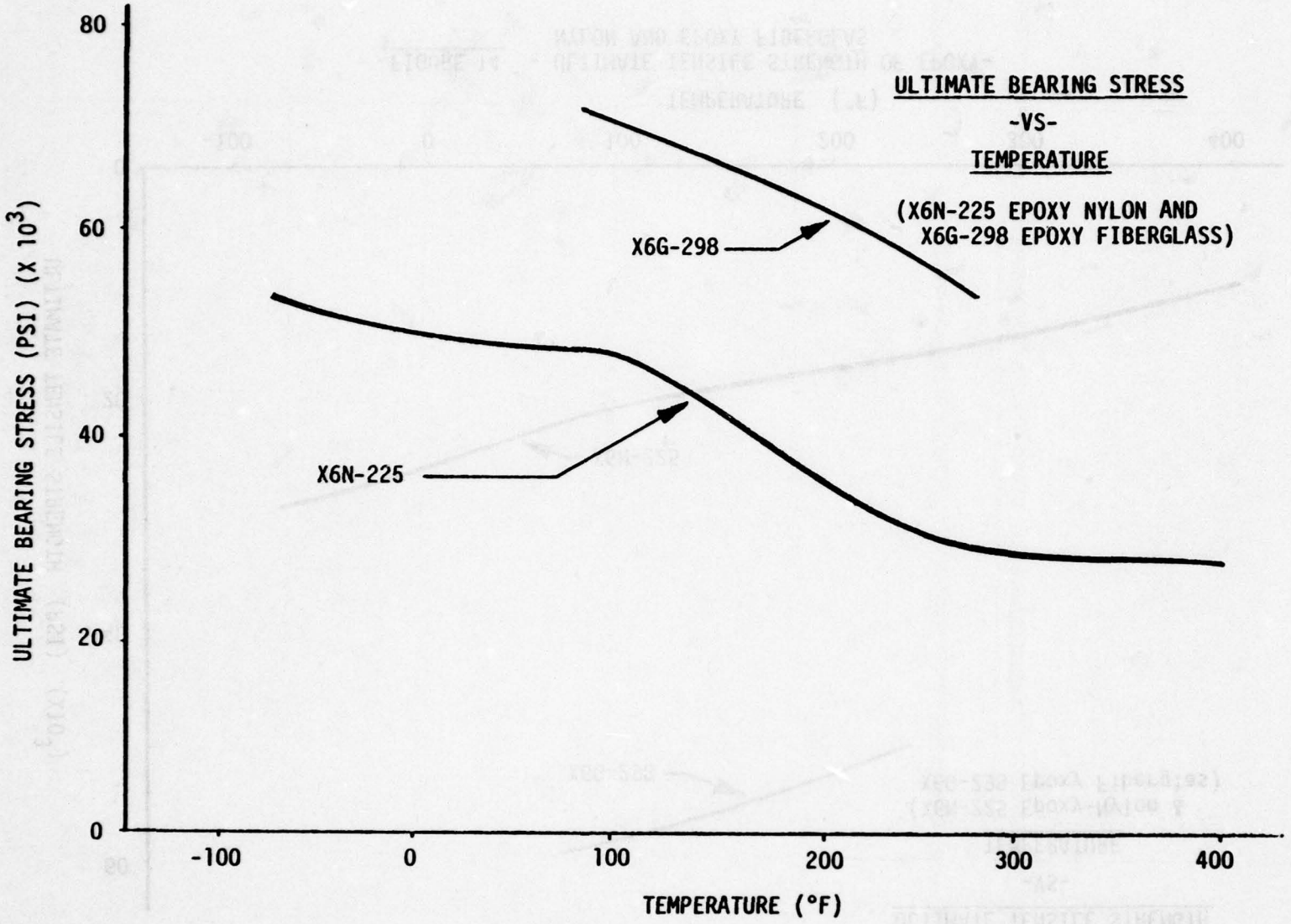


FIGURE 15 - ULTIMATE BEARING STRESS OF EPOXY NYLON AND EPOXY FIBERGLASS

TABLE 3

TYPICAL PROPERTIES - POTENTIAL GLAZING MATERIALS

PROPERTY	UNITS	MATERIALS			
		POLYOLEFIN	POLYAMIDE	POLYSULFONE	POLYPHENYLSULFONE
Tensile Strength - Yield	psi	4,000	10,700	10,200	10,400
Tensile Strength - Break	psi		7,900		9,000
Elongation - Yield	Percent		9		7
Elongation - Break	Percent	15	70	75	60
Tensile Modulus	psi	210,000	280,000	360,000	310,000
Flexural Strength	psi		12,800	15,400	12,400
Flexural Modulus	psi		299,000	390,000	330,000
Notched Izod Impact	Ft-lbs/ in of Notch	0.8	1.1	1.3	12.0
Heat Deflection Temperature	°F	240	255	345	400
Light Transmission	Percent	90	85	70	80
Haze	Percent	<10	5	<10	<10

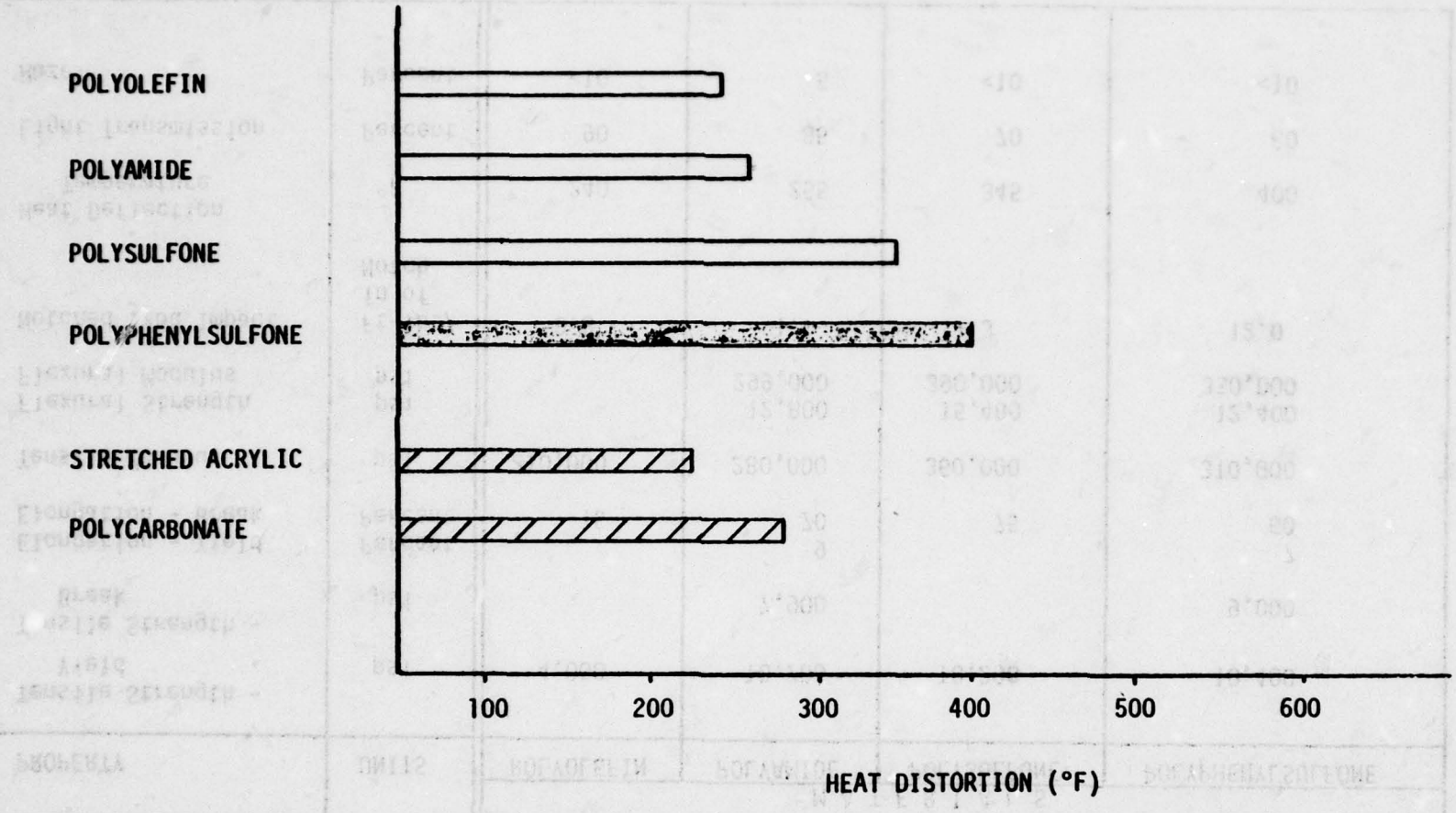
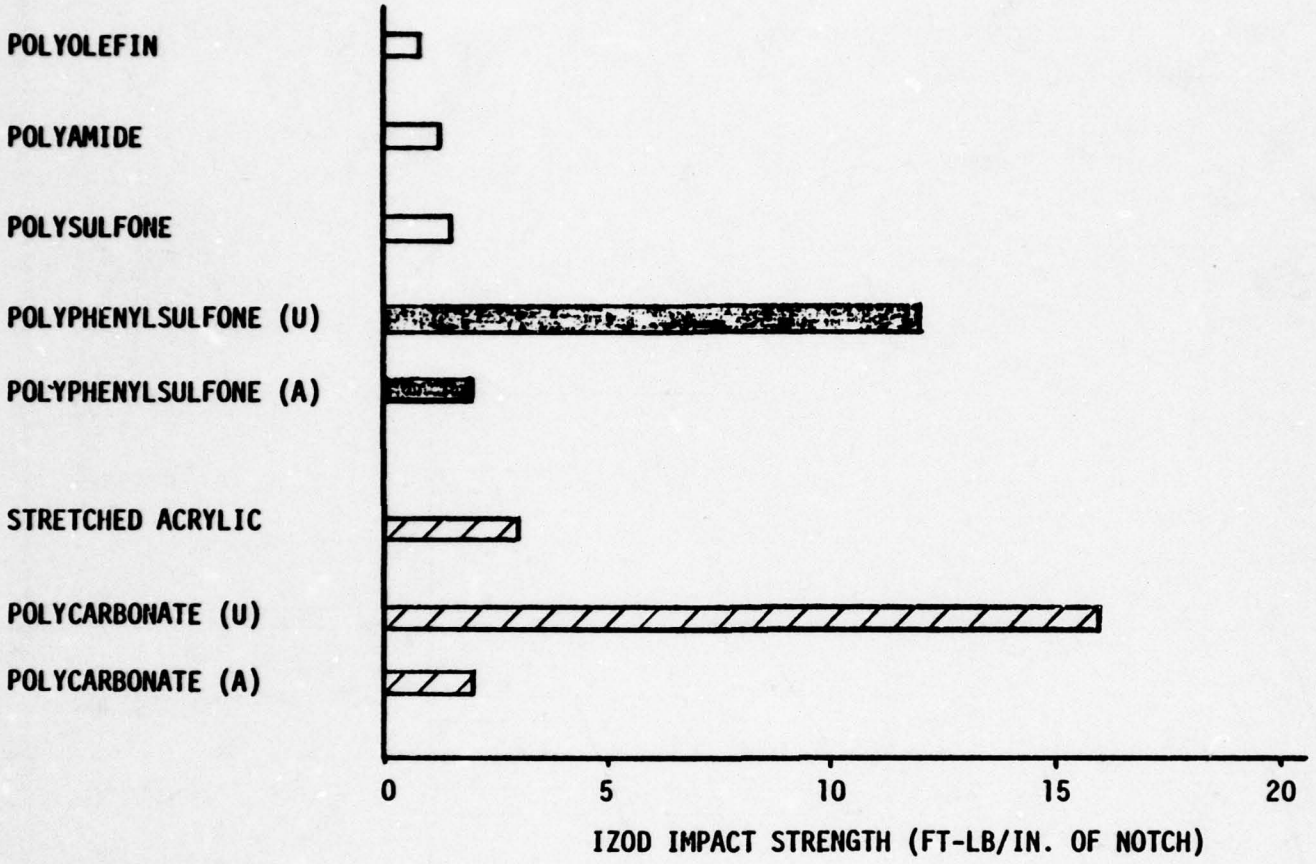


FIGURE 16 - HEAT DISTORTION TEMPERATURE OF POTENTIAL GLAZING MATERIALS



(U) UNAGED

(A) THERMALLY AGED

FIGURE 17 - NOTCH IZOD IMPACT STRENGTH OF POTENTIAL GLAZING MATERIALS

DEVELOPMENT AND APPLICATION OF THIN HIGH STRENGTH GLASS

W. G. Roberts
Triplex Safety Glass Company, Ltd.
Aircraft and Special Products Division
Birmingham, England

PRECEDING PAGE BLANK-NOT FILMED

DEVELOPMENT AND APPLICATION OF THIN HIGH STRENGTH GLASS

Thin high strength glass is required for the facing plies of glass and composite windshields, and for lightweight constructions, particularly on helicopters. The design requirements are listed in Fig. 1, and are, in fact, similar for both cases.

Thin glass, particularly in large sizes, needs an appreciable strength level to survive the various operations involved in windshield manufacture. Particular attention is required to edge finishing, especially if high degrees of tempering are subsequently involved. Once in service, it is subjected to a variety of thermal stresses, from exposure to extremes of ambient temperature and high speed, and from the temperature gradients set up by electrical deicing systems.

Facing plies can, sometimes inadvertently, end up carrying fairly high stresses from fuselage pressurisation, particularly on glass/plastic composite constructions, which may be additive to differential stresses caused by the expansion mismatch of materials, or any hoop tension stresses picked up from the surrounding structure. In helicopters, the use of relatively flexible structure around the transparency may impose a combination of bending and racking stresses, particularly under manoeuvre loading.

For many years, the main structural case in forward facing windshield design has been bird impact. On all modern aircraft the windshield is designed to withstand the limiting impact without damage to the structural plies, and in such cases the facing ply has a minor role. There is, however, a growing interest in bird impact resistance for helicopter windows where thin glasses may be used essentially as structural plies. From an operational point of view, impact with hail is a more serious design case for facing glasses. Windshield damage from hail has been a rare occurrence on the narrow body jet transports, due to the universal use of relatively thick semi-tempered glass; experience on wide body jets has not been quite so favourable. It is thought likely that demonstration of hail resistance will become part of the qualification process in the future.

There is a specialist interest in resistance to impact from particles of silica carbide, which is now being used to provide very high friction surfaces to facilitate aircraft ground operation. A somewhat similar problem has arisen in Japan where certain Airline Operators have had considerable problems when inadvertently flying through airborne clouds of volcanic particles.

The use of thin glass for the outer ply of a windshield ensures a high degree of abrasion resistance, and excellent compatability with all types of electro-conductive coating, at minimum weight, but there are other limiting factors with very thin glass constructions. They must retain

PRECEDING PAGE BLANK-NOT FILMED

the optical quality required for high performance aircraft windshields and it is also important that vision through the glass should not be seriously impaired after fracture, which has a limiting effect on the choice of thickness and temper.

The conventional method of thermal tempering of glass employs forced jets of air to produce the rapid cooling required. There are varying degrees of temper, primarily related to the degree of heat transfer employed. "Full temper" is an expression in common usage, and is somewhat inadequately defined in Mil.G. 25667 as producing a centre tension in ¼" thick glass of approximately 2,800 millimicron/inch (units of photoelastic retardation). This is equivalent to an induced stress in the centre of the glass of about 10,000 lbs/square inch. It is probably of more practical interest to define the strength of the glass in bending in terms of Modulus of Rupture. Fully tempered glass usually has a Modulus of Rupture of between 25,000 and 30,000 lbs. per square inch with the surface compression stress induced by tempering being about 17,000 lbs. per square inch.

The conventional aircraft windshield design uses one or more load bearing components of full temper glass laminated to, and protected by, thinner facing plies, which invariably have a lower degree of temper so that in the event of damage in service, from hail or thermal stress, for instance, the windshield can retain an adequate level of residual vision in non-icing conditions until it can be changed. Full temper glass breaks with a characteristic heavy dicing pattern, which can totally obscure forward vision; the amount of dicing is a function of the degree of temper, or more precisely the amount of induced centre tension. It is also a function of glass thickness and hence for a given fracture pattern, the strength will be greater in a thin glass than in a thicker one. In practice, the particle size and degree of residual vision obtained on fracture can also be affected by externally induced stresses, particularly from bending under differential pressurisation. It can also be demonstrated that the fracture pattern exhibited by a face ply that has been laminated with PVB to a thicker structural ply is different to that for an unlaminated glass of the same degree of temper. Comparison between Figs. 2 and 3 shows the beneficial effects of lamination on residual vision.

Two intermediate levels of tempering are commonly used. Historically, the term "strengthened" has been used in the U.K. to define the minimum level of temper such that the glass still breaks essentially as annealed glass. "Semi-tempered" will be familiar to most as the standard referred to in Mil.G. 25667, and was probably intended as the highest possible level of temper consistent with some retention of residual vision. It should be emphasised that these are visual standards rather than strength levels, and are, in fact, best defined by visual standards. Figs. 3 and 4 illustrate the two levels, in 4 mm glass samples, deliberately fractured ½" from one edge, after lamination to 12 mm structural plies.

Facing plies have usually been around 3/16" thick; in Europe where metric glass thicknesses are available, 4, 5 or 6 mm are commonly used. Facing plies of ⅛" (3 mm) are also employed, and there is a growing use of ⅛" in helicopter glazings. As a general rule, the thinner the glass, the lower the degree of temper induced. The achievable strength is dependent on the heat capacity of

the glass, hence its thickness, and it also becomes progressively more difficult on thinner glass to retain adequate flatness, or control of curvature on curved constructions. In recent times, considerable advances have been made using novel support and transfer mechanisms for the glass during bending and tempering. Fig. 5 shows the flat and curved visor glazings of the Concorde SST; each of the 6 glazings consist of two plies of 0.1" glass, tempered to a Modulus of Rupture of about 22,000 lbs. per square inch. These glasses actually have a semi-structural role; although not loaded by cabin pressurisation, it is essential they withstand aerodynamic pressure loading during supersonic flight.

The practial use of really thin high strength glass received a boost in the mid 60's with the introduction of curved, glass-faced acrylic constructions on modern jet transports. The radical difference in stiffness between the glass and acrylic materials demanded the glass be as thin as practicable, thinner in fact than the conventional thermal tempering process could provide, bearing in mind that this same difference in stiffness also necessitates using relatively higher bending strengths. It is relevant to note that bending and tempering technology at that time was also a constraint on the use of tempered glass for the structural plies of these large curved windshields.

The need was met by chemically tempered glass initially .085" thick, although other thicknesses are *now* available. The process of ion-exchange is now well-known, and produces a significantly different pattern of internal stress distribution, as shown in Fig. 6. This also demonstrates the "area rule", i.e. for equilibrium the total "compression" area under the curve must be equal to the "tension" area. In general terms, chemical tempering can impart much higher strength levels, and bending strengths in excess of 50,000 lbs. per square inch have been reported. However, because of the "area rule", it is difficult to "tune" the glass for very high strength, or adequate depth of compression, without inducing a very high centre tension, and thus compromising the residual vision.

Hence a practical limitation is imposed on using glass thinner than about .08" unless residual vision can be sacrificed as a requirement. In the early 70's, considerable use was made of chemically tempered glass only .05" thick, which by virtue of its strength and flexibility could be "elastically formed" to match the curvature of the main structural plies. Fig. 7 demonstrates the almost total lack of residual vision in a Boeing 747 glass windshield of this type, following failure of the outer .05" facing ply in service. The only forward vision is, in fact, through a small area at the original site of delamination where the glass fragments have become detached.

In the late 60's, Triplex developed an improved thermal tempering process, now known as "Ten Twenty", to achieve much higher levels of induced stress. Essentially this requires much higher rates of heat transfer from the surface of the heat-softened glass during quenching. The resulting stress patterns are similar to the conventional tempered product, retaining the typical

parabolic distribution and deep neutral axis. The uniformity of tempering gives a further benefit in virtually eliminating any visual effect in polarised light. Ten Twenty glasses are now produced with strengths of up to 50,000 lbs. per square inch and have found wide applications including Concorde, DHC7, the A300B, Boeing 747, and AV8A Harrier, and they are now also being used by the European Space Agency to provide viewing windows in Sky Lab.

The Ten Twenty process has obvious application to the tempering of thin glass. For a given thickness, higher strengths can be obtained than by conventional thermal means, but even more importantly, an equivalent strength level can be achieved in much thinner glass. The ratio of induced surface compression to centre tension is higher than conventional, which means that for a given centre tension, (and hence level of residual vision) a higher strength glass can be obtained. The typical stress pattern of a 3 mm Ten Twenty face ply is shown in Fig. 8. The induced surface compression gives a Modulus of Rupture of 27,000 to 30,000 lbs. per square inch, yet the centre tension is low enough to give a high degree of residual vision. Fig. 9 shows a Boeing 747 windshield with a 3 mm outer face ply that has been deliberately broken with a spring loaded punch to demonstrate the resulting pattern of cracking.

Considerable attention has been paid to the hail impact resistance of Ten Twenty face plies, in fact, the chosen strength level for Boeing 747 is a careful compromise between maximum hail resistance and good residual vision. The mechanism of facing ply failure is still not totally understood despite considerable testing carried out by Triplex using the facilities of the Royal Aircraft Establishment at Farnborough.

The threshold speed to break the glass is primarily related to thickness with degree of temper playing a significant but less important role. Fig. 10 illustrates the trends established to date on thermally tempered Soda Lime float glass. It also shows, for reference, two isolated test results obtained using .05" and .085" Corning Chemcor which may indicate a similar trend. Boeing 747 windshields have now accumulated over 650,000 flying hours since the introduction of 3 mm Ten Twenty face plies. During that time, there has only been one known hail incident which happened to an S.A.A. 747 SP Aircraft in May 1977. It was climbing out of Vienna, Austria, passing through 15,000 feet, when it encountered moderate turbulence with heavy hail, and was struck three times by lightning. The facing plies on both windshields were cracked, and other damage included shattered inboard and outboard landing light covers and dented leading edges and cowls. Fig. 11 illustrates the degree of residual vision of the Left Hand windshield. The senior training Captain of S.A.A., who happened to be flying the aircraft, later reported "The approach was commenced during dusk to dark conditions in clear visibility, and bearing in mind we had no landing lights, I could detect no undue or visual distortion during the approach, round-out or landing."

The manufacture of thin curved tempered glass components is a delicate compromise between heat softening the glass for forming and tempering whilst maintaining close control of shape. The Ten Twenty process, after considerable development, has the capability of bending and tempering individual glasses with high precision, such that the two components can be successfully brought together in the subsequent laminating process and still meet high optical standards. Ten Twenty has also been developed for laminated car windshields where the inner and outer components are, in fact, deliberately tempered to different levels, which again illustrates the accuracy of bending involved.

An obvious application of this technology is in lightweight helicopter windshields and a series of trials have recently been carried out to establish the bird impact characteristics of thin laminates. Fig. 12 shows the impact at 203 mph of a 2 lb. bird on a typical construction of two 3 mm Ten Twenty glasses, mounted at 40° to the line of flight. The previous shot at 181 mph caused no damage.

With the development of higher strength, considerable additional work has been needed to improve test procedures for measurement of strength, and this work has now been extended to include the thinner glasses. The conventional 4 point bend test is widely used on rectangular beams, typically 8" x $1\frac{1}{2}$". This method is simple and inexpensive, but it is difficult to eliminate edge effects. Plate bending under differential pressure has the fundamental attraction of closely simulating the end use of the product as a pressure bearing structural ply. On some aircraft programmes, such as Concorde, tests have been carried out on actual full size components, carefully strain-gauged, to determine first the location, and then the magnitude of maximum principle stresses under pressurisation. These calibrations can then be used for destructive sampling, or for proof-testing of all components to a high percentage of the design load.

For more repetitive testing, for instance to establish variability over a large batch, simpler plate bending specimens are used. The Ring-on-Ring method is an extension of 4 point bending theory, and provides in the central area, a zone of nominally equal bending stress. It has been found in practice, however, to be somewhat impractical, being sensitive to specimen geometry and flatness, and relatively expensive. Probably the simplest procedure employed by Triplex uses 12" x 12" square plates, clamped on all four edges over a $\frac{3}{4}$" width, and pressurised from one side by a diaphragm. Provided the specimens are of reasonable thickness, a good correlation with plate bending theory can be obtained, although it is still advisable to derive precise stress calibrations with strain-gauging techniques. These demonstrate that care must still be taken with clamping procedures if comparative results are to be obtained.

It is well known that plate bending produces a linear calibration provided deflection does not exceed roughly half-thickness, beyond which diaphragm tension produces a stiffening effect. This can be taken into effect in the

calibration, particularly if strain-gauge checks are made. Significant errors can be introduced, however, once the maximum principle stress begins to move away from the centre of the squares towards the corners, as happens on relatively thin specimens. This is probably the main drawback with square clamping methods for thin glass, leading inevitably to a circular clamping arrangement.

In designing a practical test technique that can be used for thin glasses from say .08" up to 0.250", it is obviously desirable not to have a pre-determined specimen size. The principle employed is to test a small area of a relatively large, inexpensively prepared specimen, with the further benefit that the same relatively large specimens can be used to determine residual vision characteristics after breakage. The Triplex test equipment is shown in Fig. 13. The glass under test is clamped between two 2" wide rubber faced annular rings with differential pressure being applied to the central 6" diameter area through a specially shaped rubber diaphragm. The clamping force is kept at a constant level throughout the test by hydraulic means, and is preset so that the total downward load on the upper ring is considerably in excess of the upward applied load on the glass. In practice, this gives a slight reduction in encastration with applied load, but this is minimised by the wide clamping width of at least 10 times the glass thickness.

The equipment has been calibrated by strain-gauge techniques. Fig. 14 shows the variation of maximum stress with applied load for a range of glass thickness; it is interesting to note the calibration is linear for the thicker substances, whereas diaphragm tension effects are evident for 3 mm glasses and thinner. Clamping itself produces a small applied stress, but this is entirely repeatable and can therefore be taken into account.

Although the centre of the circular area is confirmed by the strain-gauging to be the position of maximum stress, the break position tends to vary in a random manner within a small central area. This is to be expected as glass always breaks in tension from a surface flaw.

DESIGN REQUIREMENTS- THIN HIGH STRENGTH GLASS.

STRENGTH - HANDLING
- THERMAL STRESS
- STRUCTURAL LOADS
- IMPACT

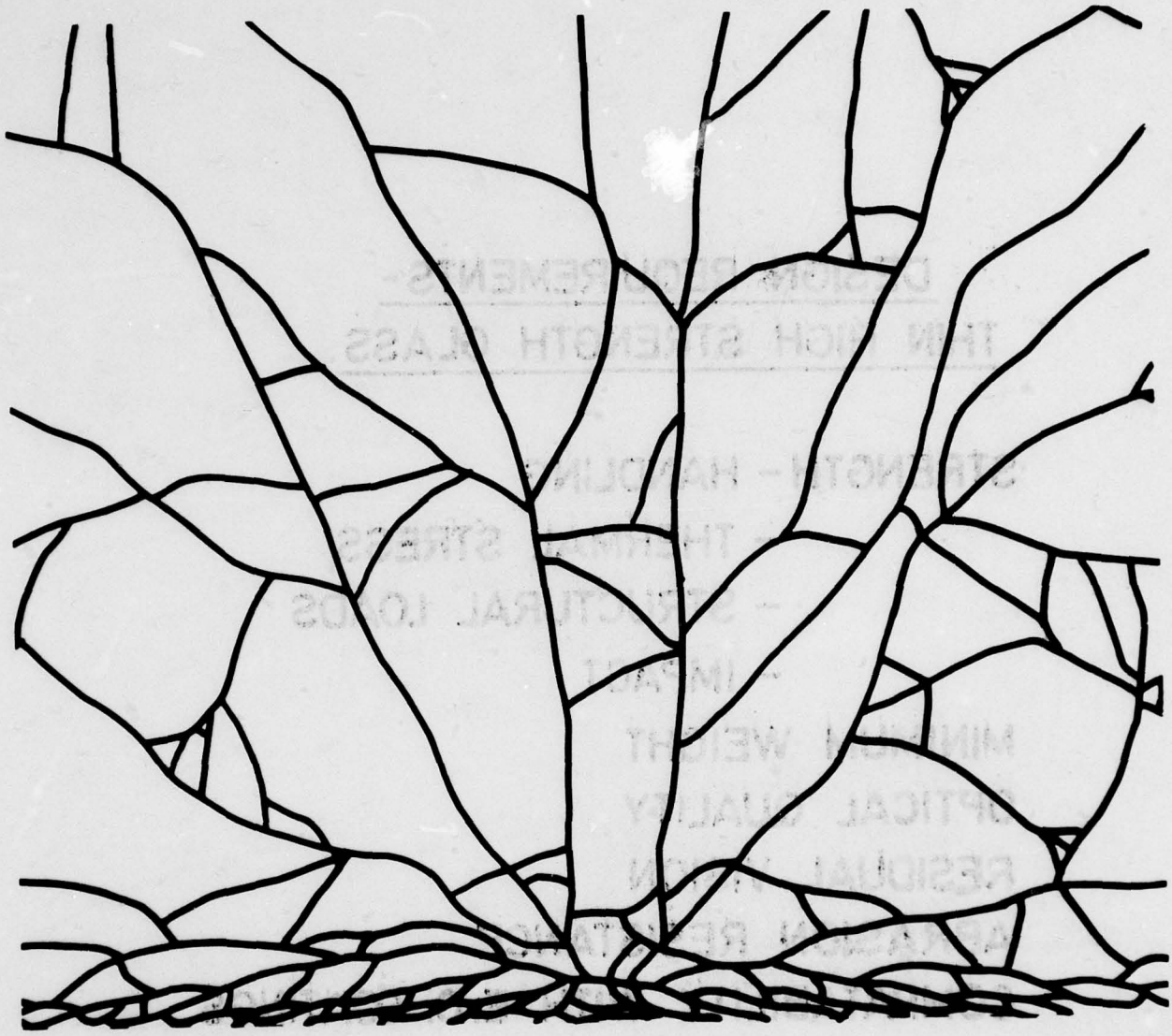
MINIMUM WEIGHT

OPTICAL QUALITY

RESIDUAL VISION

ABRASION RESISTANCE

COMPATABILITY WITH E.C. COATINGS



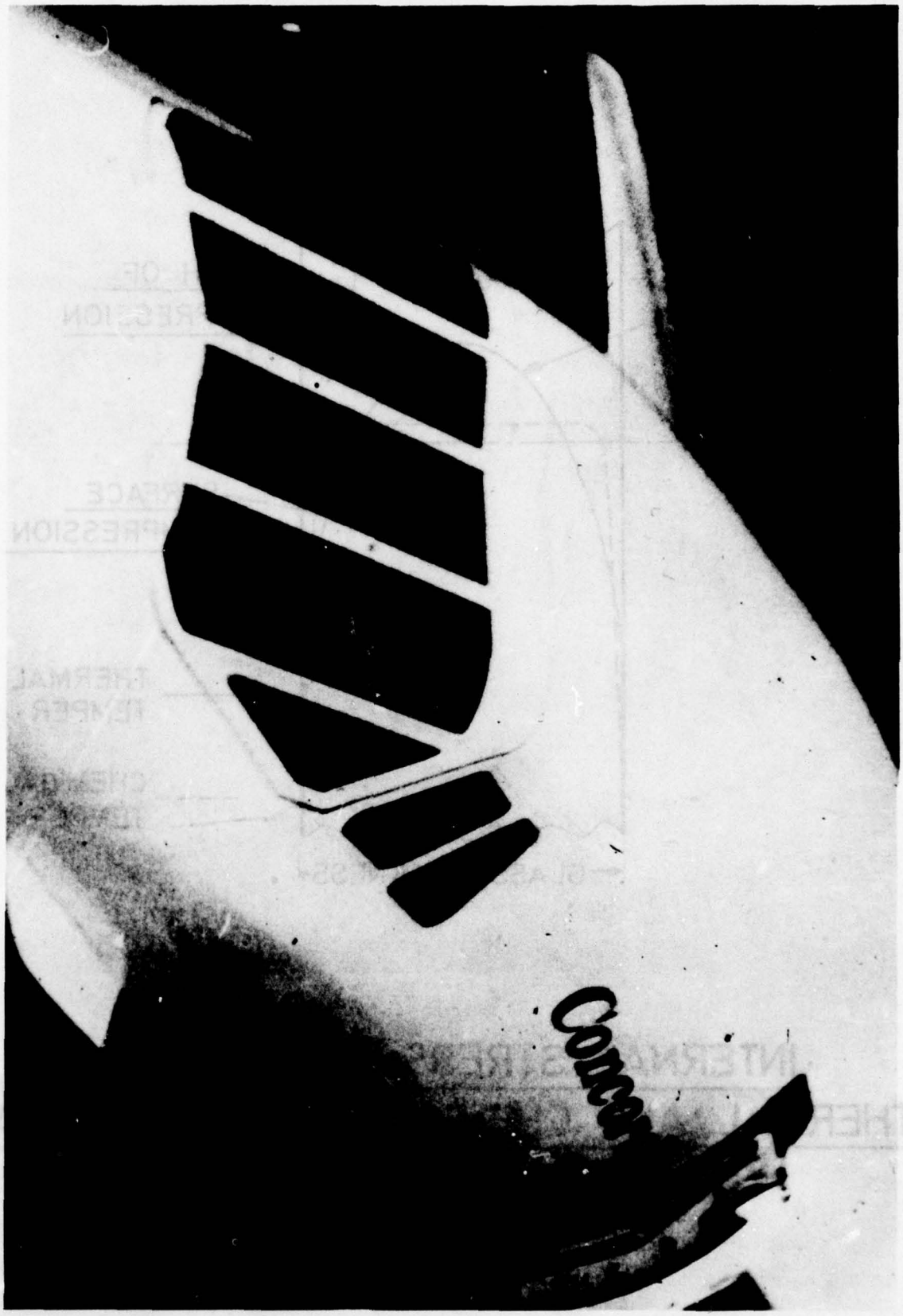
TYPICAL CRACK PATTERN -
4mm. SEMI-TEMPERED GLASS.

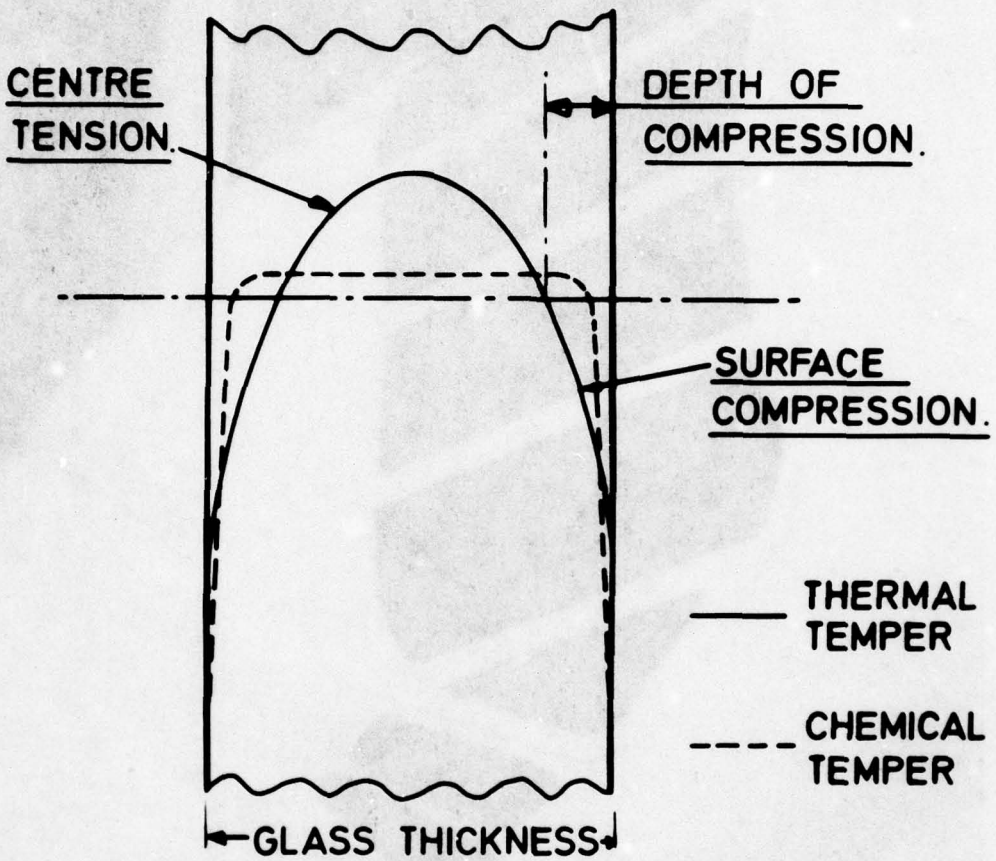


TYPICAL CRACK PATTERN -
4mm. SEMI-TEMPERED GLASS,
BROKEN AFTER LAMINATION.

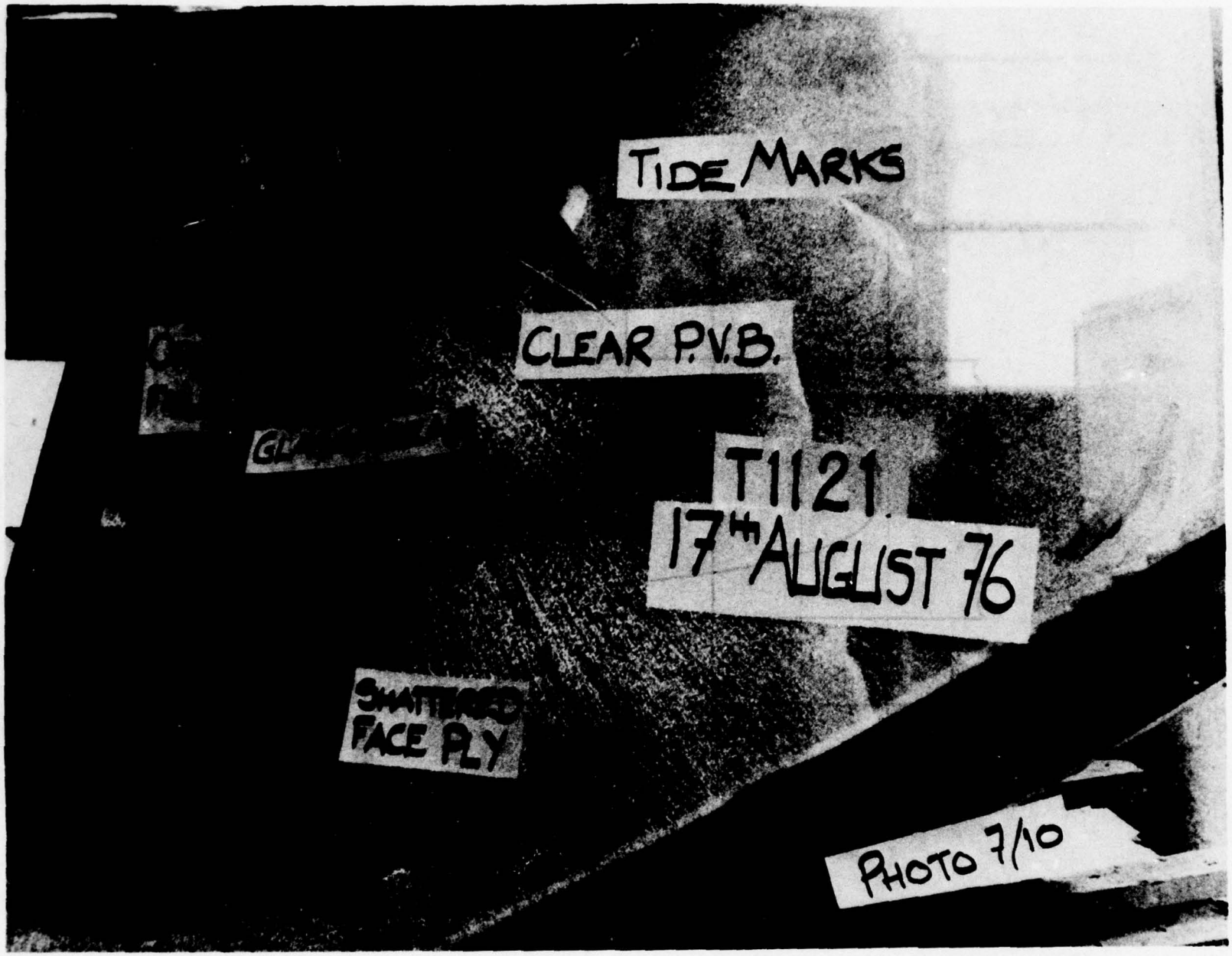


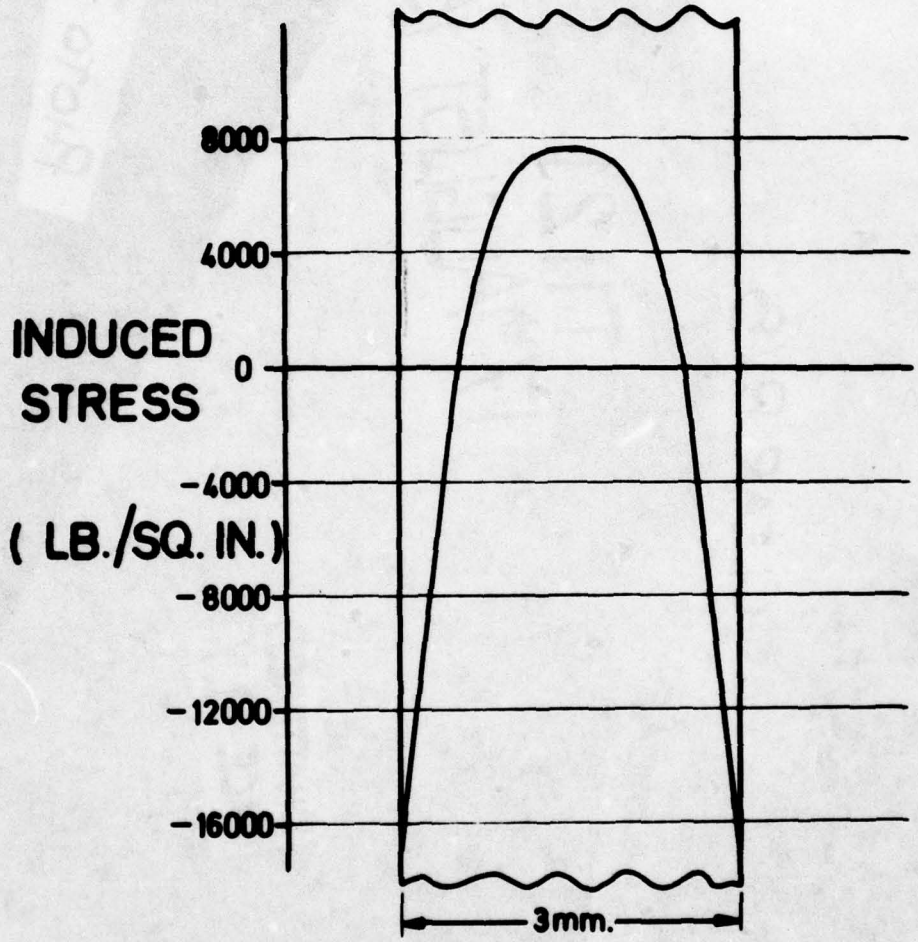
TYPICAL CRACK PATTERN-
4mm. STRENGTHENED GLASS,
BROKEN AFTER LAMINATION.


Comet



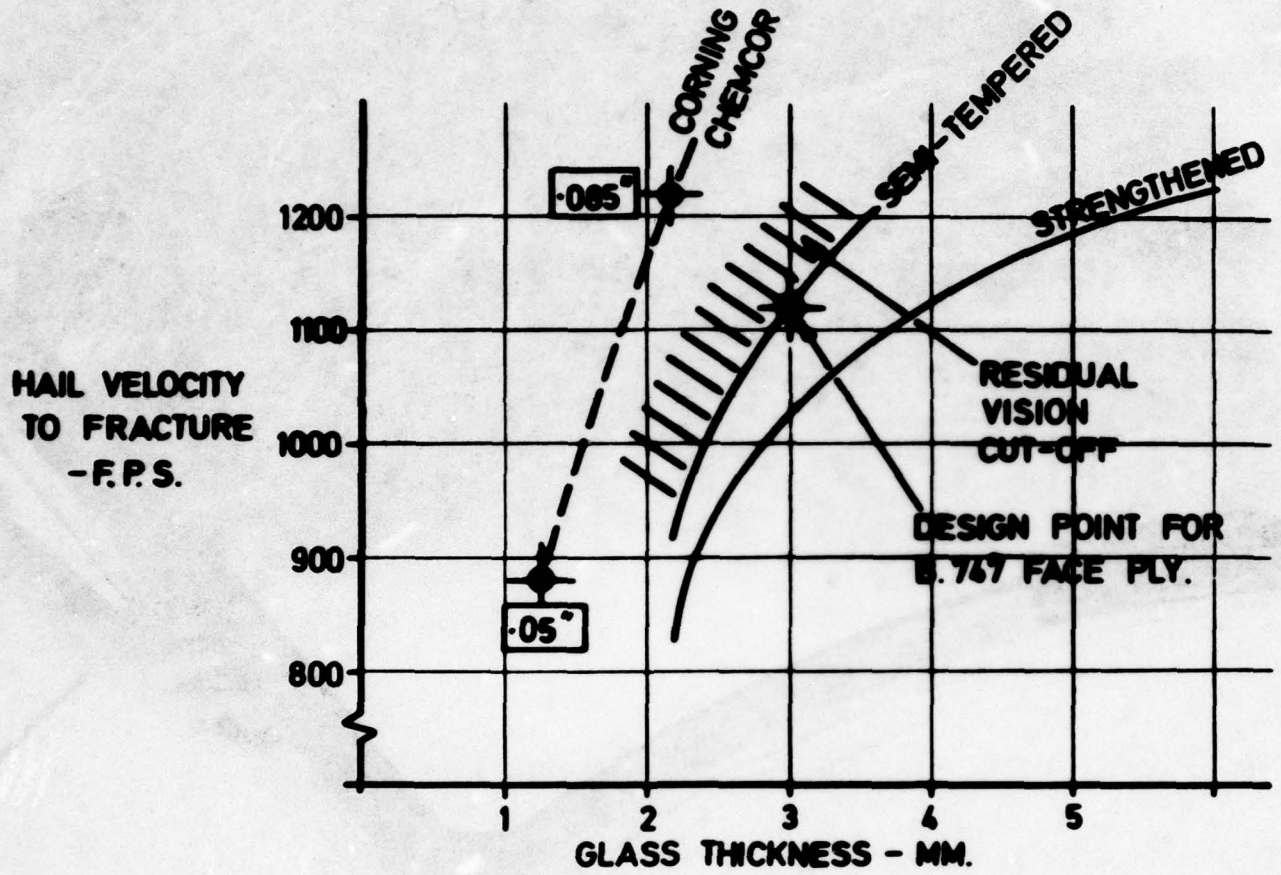
INTERNAL STRESS DISTRIBUTION - THERMAL AND CHEMICAL TEMPERED GLASS.


TIDE MARKS
CLEAR P.V.B.
T1121
17th AUGUST 76
SHATTERED FACE PLY
PHOTO 7/10



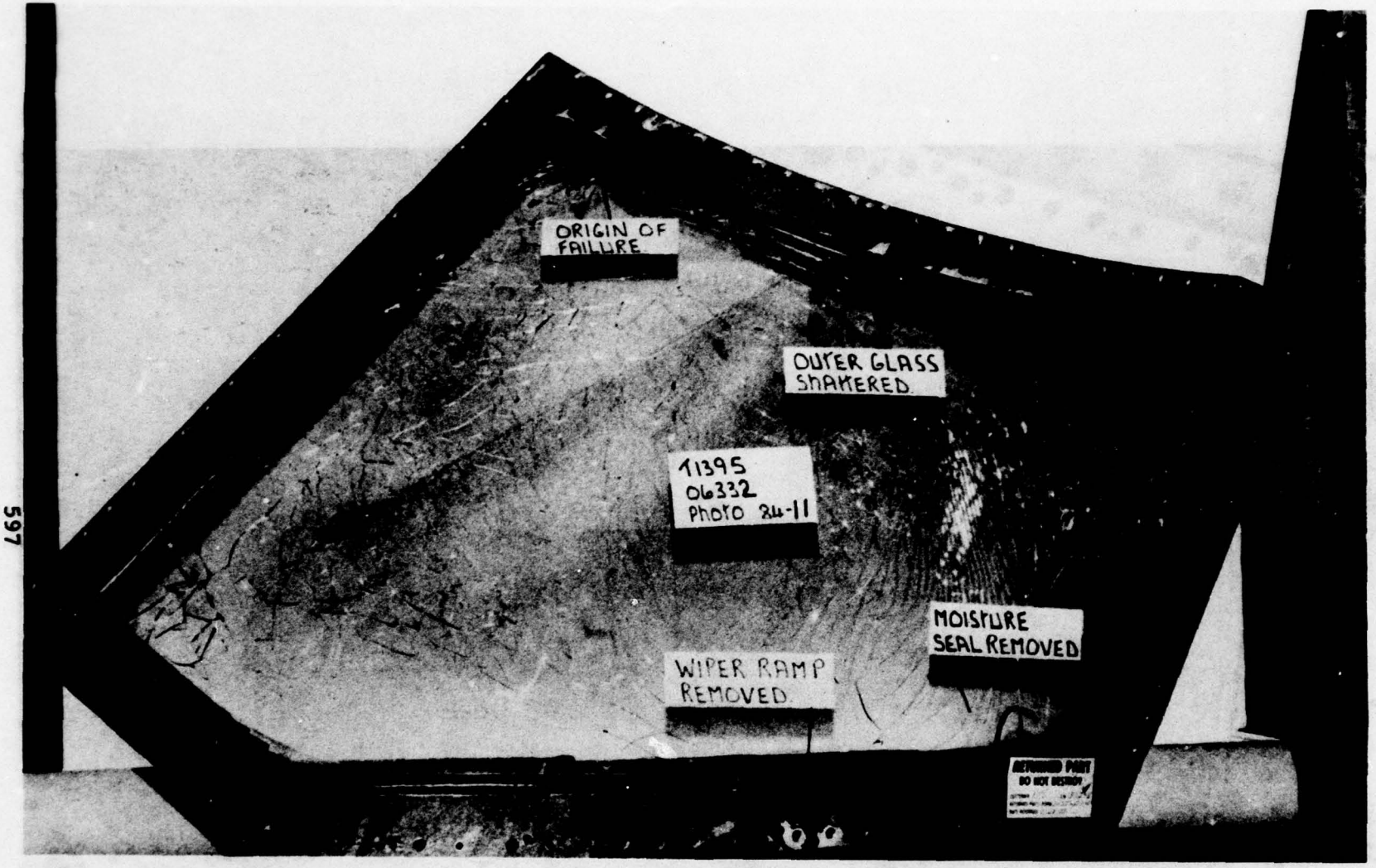
INTERNAL STRESS DISTRIBUTION-
3 mm. 'TEN-TWENTY' GLASS.

1130J
1130J

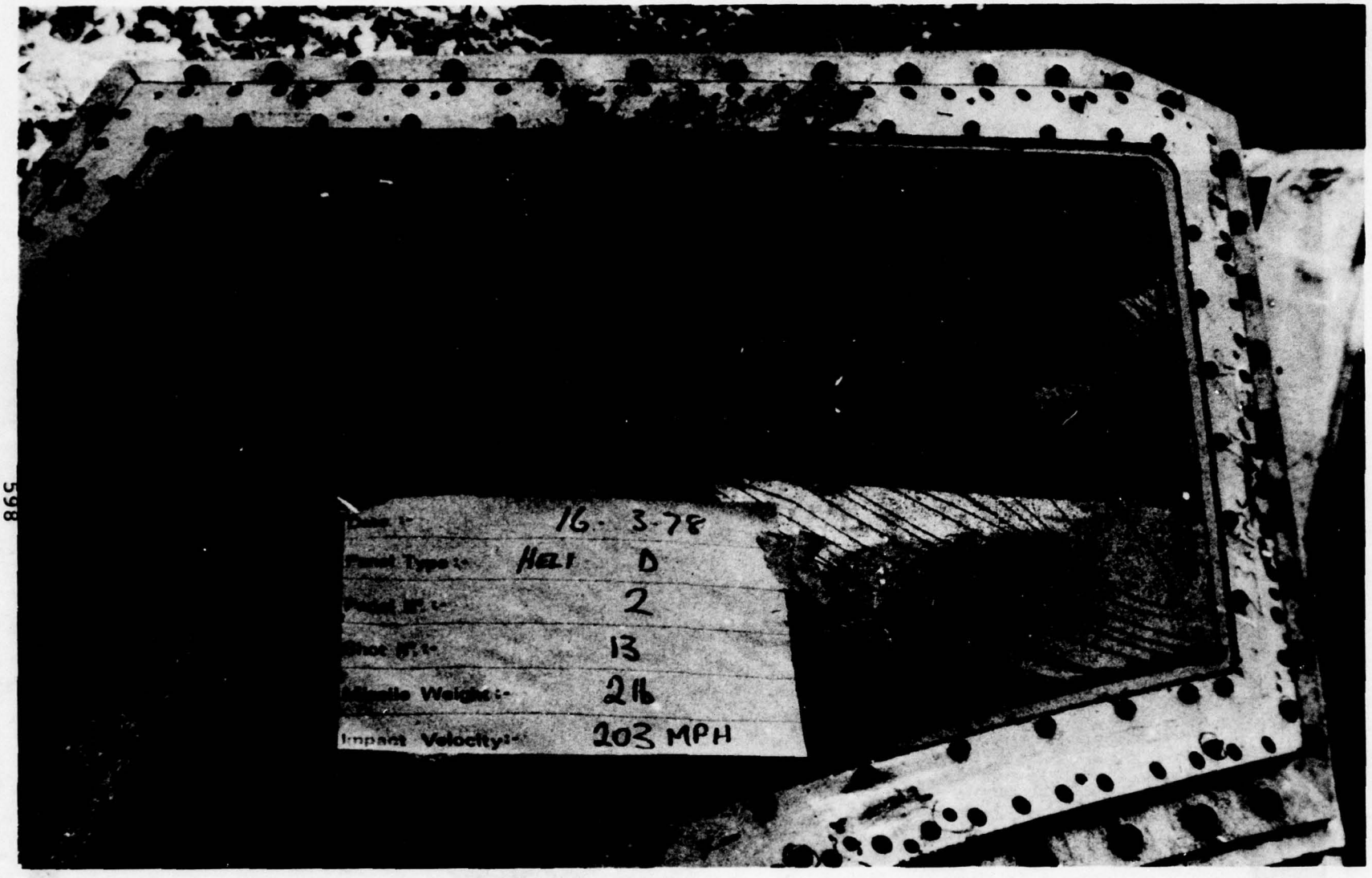


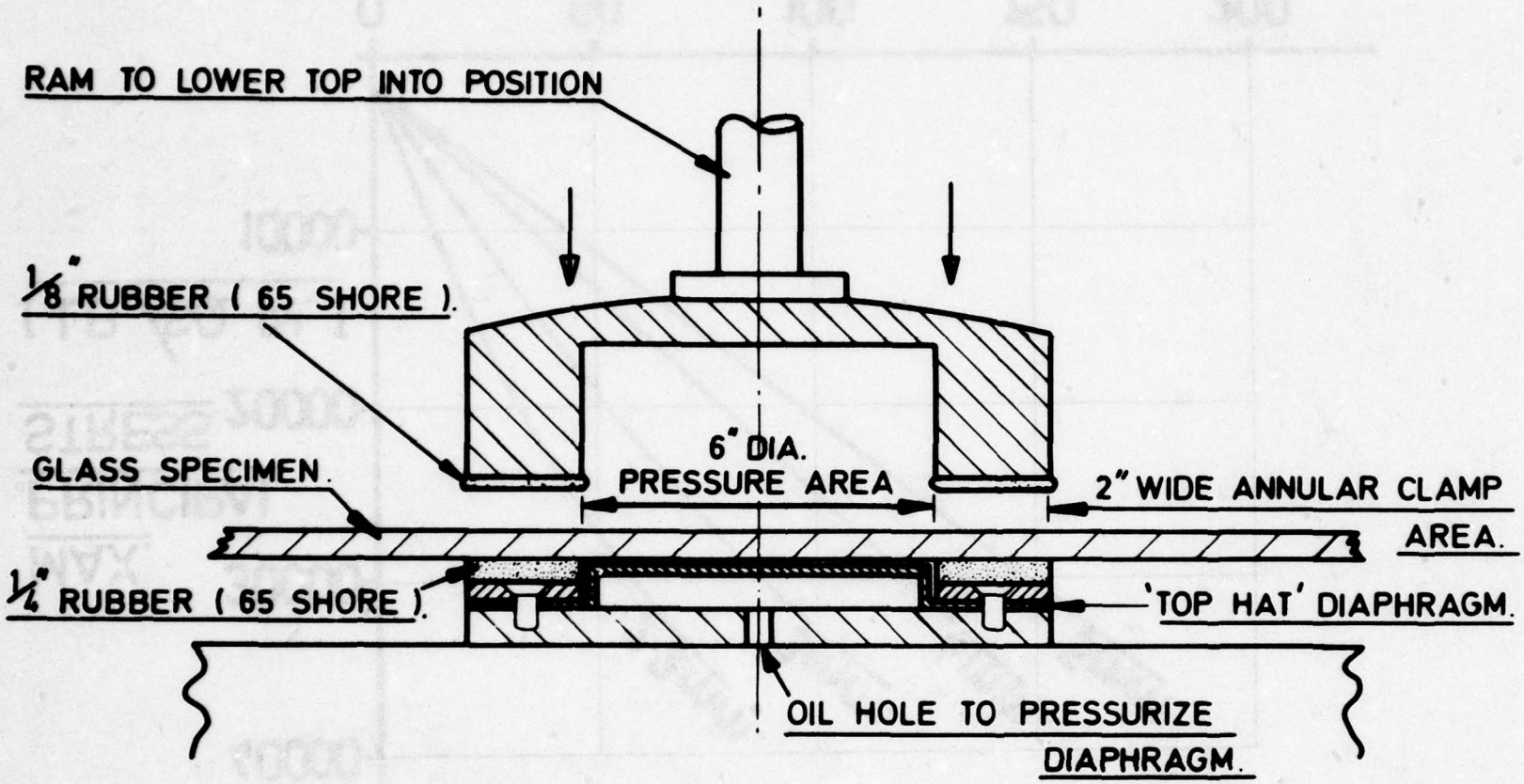
1·0" DIA. HAIL AT 40° IMPACT ANGLE TO LINE OF FLIGHT.

HAIL IMPACT TESTING ON FACING PLIES.


ORIGIN OF FAILURE
OUTER GLASS SHATTERED
11395
06332
PHOTO 24-11
MOISTURE SEAL REMOVED
WIPER RAMP REMOVED

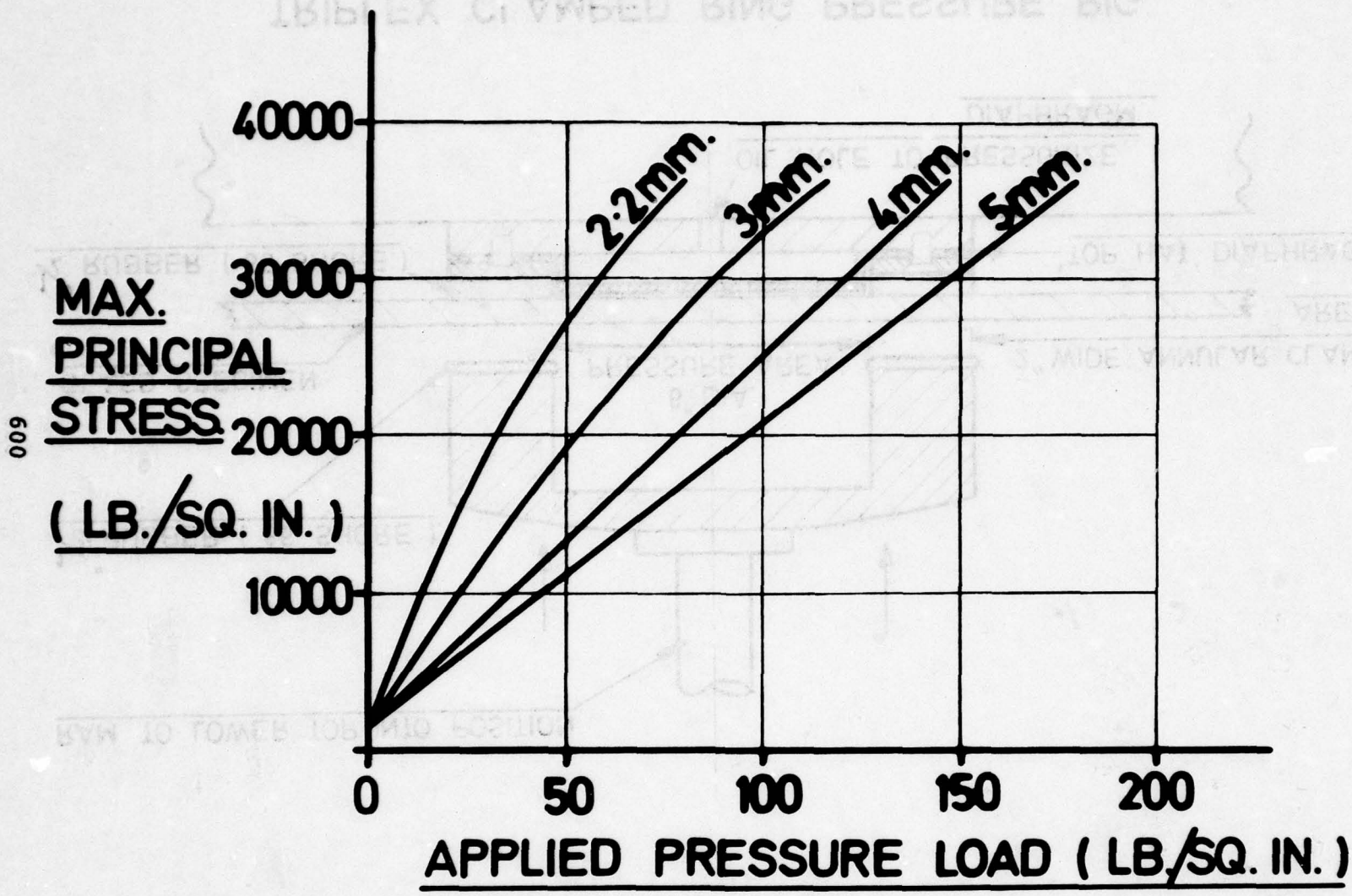
597


16. 3-78
HE1 D
2
13
21b
203 MPH



599

TRIPLEX CLAMPED RING PRESSURE RIG.


40000
30000
20000
10000
MAX. PRINCIPAL STRESS. (LB./SQ. IN.)
2·2mm.
3mm.
4mm.
5mm.
0
50
100
150
200
APPLIED PRESSURE LOAD (LB./SQ. IN.)

SUPERHARD COATINGS FOR ARMY HELICOPTER GLAZINGS

T. E. Condon
Applied Technology Laboratory
U. S. Army Research and Technology Labs
Fort Eustis, Virginia

and

R. S. Hassard
Goodyear Aerospace Corporation
Arizona Division
Litchfield Park, Arizona

SUPERHARD COATINGS FOR ARMY HELICOPTER GLAZINGS

by

Mr. Thomas E. Condon
Applied Technology Laboratory
US Army Research & Technology Laboratories (AVRADCOM)
and
Mr. Richard S. Hassard
Goodyear Aerospace Corporation
Arizona Division

ABSTRACT

Army helicopter glazings have been particularly susceptible to windshield damage from wiper abrasion and dust clouds generated by the rotor vortex as evidenced by Army operational service experience. The life expectancy of Army acrylic windows has been estimated at 300 to 600 hours of service before replacement was necessary. The purpose of this effort was to develop a transparent hard coating which would extend the service life of new glazings and possibly, through resurfacing, some panels already in service.

This paper concerns the development of candidate coatings capable of solving the Army's problem of frequent glazing replacement. Most hard coatings marketed have utilized silicic acid chemistry as a source of submicron silica. This is no exception. If the silica from the silicic acid is considered the only source of hard filler, then the best formulation will depend on a property balance which will resist windshield wiper abrasion and provide adequate coating flexibility and adhesion. Further adjustment of the formulation for hydrolytic stability, flow, and ultraviolet (UV) resistance may diminish the allowable filler content. If desired, further hardening to a "superhardness" may be accomplished by inserting a small quantity of submicron aluminum oxide or silicon dioxide powders into the formulation, but not without problems.

Although "superhardness" is attainable, it is not necessarily the answer to all erosion problems. Increased hardness improves resistance to windshield wiper abrasion, but it also embrittles the coating toward a lesser resistance to particle impingement.

Through all of these considerations, superior transparent coatings have been developed for helicopters which can be extended to other plastic glazings.

PRECEDING PAGE BLANK-NOT FILMED

I. INTRODUCTION

A review of Army helicopter transparencies operational service experience determined that these transparencies have a high frequency of replacement and a poor in-service performance record. Current efforts in reliability and maintainability (R&M) of Army aircraft have re-emphasized the recognition of the requirement to reduce current maintenance and procurement costs due to repetitive replacements of Army helicopter transparencies.

II. PHILOSOPHY

Transparent hard coatings have had marginal acceptance because of inherent weaknesses which have not completely overcome the extreme environments of aircraft exposure. It was the purpose of this development to alleviate the greatest deficiency, which was believed to be "hardness." The approach was to add physically hard particles of submicron size to a resin synthesized through silicic acid chemistry.

III. CRITERIA OF FLIGHTWORTHY COATINGS

The criteria of the flightworthy coatings is the successful completion of laboratory environmental testing and, finally, flight testing in both temperate and frigid climates.

IV. PROBLEMS, OPERATIONAL

1. REPLACEMENT COSTS

The past record of performance of Army helicopter transparencies has been poor. Previous studies have revealed that in a review of 412 windshields, one windshield was replaced in every 307 flying hours. Other data showed a 500- to 650-hour MTR (mean-time-to-replacement) for the UH-1D windshield. One of the most common failure modes and causes for repair or replacement of the windshield was visual impairment from scratching. The scratching was from all sources, including windshield wiper abrasion, dust clouds from the rotor vortex and in-flight impingement.

For the period of April 1971 through March 1972, Army UH-1H transparency inspection actions were grouped and recorded. One hundred-sixty replacements for the UH-1H right-hand windshield were installed at a total cost of $131,508, including 2,058 maintenance man-hours and the purchase price of the assemblies. Additionally, 213 replacements of the roof window of the same ship model cost $127,128 including 2,396 man-hours and the purchase price of the assemblies. These replacement expenditures represent only two transparencies on one model aircraft in an Army inventory which consists of six different helicopter models with a total of 73 different window assemblies.

2. SAFETY

The most important function of windshields is to provide the maximum amount of undistorted visibility for the pilots Use of wipers or improper cleaning methods, in conjunction with any grit, easily scratches the plastic surface. Rework of scratches produces inferior optics and is not acceptable in the primary vision area of the windshield. Logistically, spare replacement transparencies are not always immediately available. The two windows previously mentioned are located in the pilot's primary field of vision and receive more attention than others which have defects, specifically scratches, but have to be "lived with" until replacements are available.

Although delayed replacement keeps the total cost down, it still leaves Army helicopters operating with critically degraded transparencies in some aircraft cabin areas. An option is to replace these designs with laminated glass or with a glass/plastic design. Although solving the scratching problem, this will increase the possible modes of failure for the particular windshield and result in a penalty which is paid in weight, initial investment and replacement cost, shatter resistance (pilot safety), and formability.

3. MAINTENANCE

The type of field level maintainability of future Army aircraft transparencies is an important consideration. Consider just the maintenance man-hour times involved. It takes eight hours to remove and replace a UH-1 windshield, which constitutes major aircraft downtime from an operational standpoint. Delaminations of laminated transparencies are not considered to be field repairable. Consequently, the need for a coating to improve the abrasion/scratch resistance of plastic windshields is essential to improving the record of performance of Army helicopter transparencies. Replacement of windshield transparencies for scratches from wipers, alone, occurs as the third most frequent windshield maintenance action, although scratches are the most frequent pilot's complaint concerning performance or condition of cockpit transparencies. Only the lack of spares sometimes precludes the replacement of these transparencies. On non-cockpit windows, scratching accounts for 38 percent of the failure modes.

4. SUMMARY

As a result of the past poor performance of Army helicopter transparencies, a program to develop an abrasion-resistant coating for helicopter plastic windshields was initiated. The objective of this program was to improve the reliability and maintainability of Army helicopter windshields and minimize the field maintenance problem with its associated life cycle costs.

The following coating development effort was accomplished by the Goodyear Aerospace Corporation, Arizona Division, under Army Contract DAAJ02-76-C-0004. The objective of the program was to verify and further evaluate the formulas and coatings developed under Army Contract DAAJ02-73-C-0062 with the Marks Polarized Corporation. Additionally, 10 UH-1 windshields will be coated and a 6-month Army field evaluation will be conducted.

The initial contractual effort determined that the formulas and coatings developed under Contract DAAJ02-76-C-0062 were not suitable for use on Army helicopter transparencies. Through material substitutions and reformulation, three new formulations were produced and laboratory tested. The best performing of these coatings has been selected for use in the previously-planned 6-month Army field service evaluation. The technical portion of this paper will describe the highlights involved in the development of these three new formulations.

V. PROBLEMS, DEVELOPMENTAL

1. CHOICE OF COATING CONSTITUENTS

a. General

This paper concerns itself more with problem areas and highlights of information acquired during the development of superhard coatings. These problems revolved around choice of coating constituents in conjunction with the silicic acid chemistry, surface compatibilities, crosslinkers, cure, coating thickness and mar resistance.

b. Binder Choice

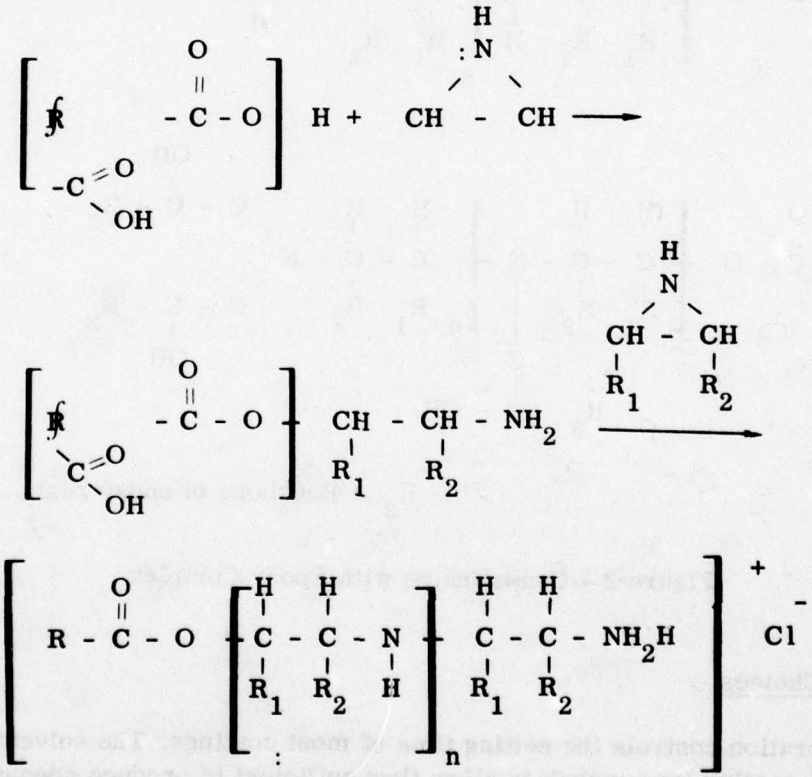
None of the coatings, which utilized polyvinyl alcohol (PVA), survived the humidity test adequately. Another binder was sought which would, in theory, be more hydrolytically stable. A literature search produced the choice of a water soluble, amine terminated acrylic polymer with properties of:

Viscosity	4000-7000 cps
Color	5 max (Gardner)
pH	5-5.6 .

Because XD-7080™, co-cured with a bisphenol-A base resin, was reported to react in coatings which exhibited good ultraviolet and chemical resistance, could be reduced with water; had a long work life; and was known to have good adhesion to a wide range of substrates, it was chosen as a substitute for PVA. Because the material is obtained in the form of a hydrochloric acid salt of the amine terminated polymer, its pH would be expected to be compatible with the polysilicic acid solutions of low pH.

The chemistry of XD-7080 curing agent provides for the reaction of acrylic acids with an imine. The result is an amino ethyl ester terminated with a primary amine. Hydrochloric acid is reacted with the primary amine to form an amine salt which renders the polymer water soluble.

The formulation is shown in Figure 1.



R = Backbone of the acrylic monomers
R_1 and R_2 = Proprietary

Figure 1 - XD-7080 Amino Hydrochloride Salt

™ XD-7080 - trademark of Dow Chemical Co., Midland, Michigan.

When mixed with an epoxy, the epoxy is suspended in the form of an emulsion in the water solution and effectively remains isolated from the primary amine groups (NH2). This phenomenon accounts for the extended pot life. Once the combination is applied as a film, the water and hydrochloric acid start to evaporate, the ionic charge is dispersed and the epoxy is free to react with the primary amine $N\begin{matrix}H\\H\end{matrix}$ to form a cross-linked binder (see Figure 2).

Mixtures with the polysilicic acid and the silica powder, prior to cure, provide a compatible acidic resin system.

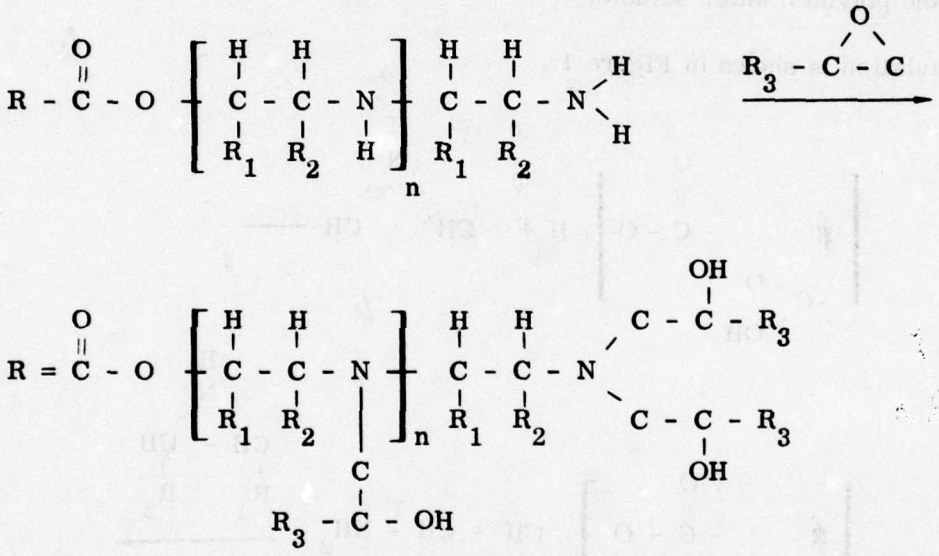


Figure 2 - Crosslinking with Epoxy Complex

c. Solvent Choices

Solvent evaporation controls the setting time of most coatings. The solvent must remain in the coating long enough to allow flow sufficient to produce adequate adhesion, gloss, and leveling. It must evaporate fast enough to prevent sagging and inadequate film thickness.

The relationship between evaporation rate and solvency is always critical with blends of different solvent types. Such was the case for superhard coating formulations.

Besides the organic solvents present in the composition, there were also water and acetic acid, which should be taken into consideration. Solvents rarely evaporate at the same rate; therefore, the composition and resulting solvency change as the blend evaporates. Film properties can vary widely because of this phenomenon. Retained solvent can affect coating properties such as clarity, gloss, adhesion, water resistance, and hardness. Because different solvents are contained in the coating raw materials list, the evaporation rates realistically concern mixtures rather than separate acids, alcohols and water. Table 1 concerns volatile losses of three different polysilicic acid compositions along with the XC-7080/DER-332™ binder. The associated graph of Figure 3 plots these figures along with some of the earlier unfilled coatings using these constituents and comparing them to Abcite.™

TABLE 1 - VOLATILE LOSS OF POLYSILICIC ACIDS AND XD-7080/DER-332 BINDER

		Volatile content (percent)	Volatile components lost in: 30 min (percent)	60 min (percent)	90 min (percent)
Raw material	Epoxy binder	36.4	37.1	39.8	41.2
	Polysilicic acid - A	71.5	57.3	71.3	76.9
	Polysilicic acid - B	81.8	72.2	88.1	89.3
	Polysilicic acid - C	82.4	77.7	87.4	88.8
Superhard coating	Formulation no. 129	88.5	33.9	55.3	74.6
	Formulation no. 130	88.5	33.9	55.4	72.3
	Formulation no. 136	88.7	32.7	54.3	72.0
	Formulation no. 147	92.4	47.1	71.4	88.2
	Abcite (Code-705)	90.3	39.9	66.0	86.4

™XD-7080/DER 332 - trademarks of Dow Chemical Co., Midland, Michigan.

™Abcite - trademark of E.I. DuPont de Nemours, Co., Inc., Wilmington, Delaware.

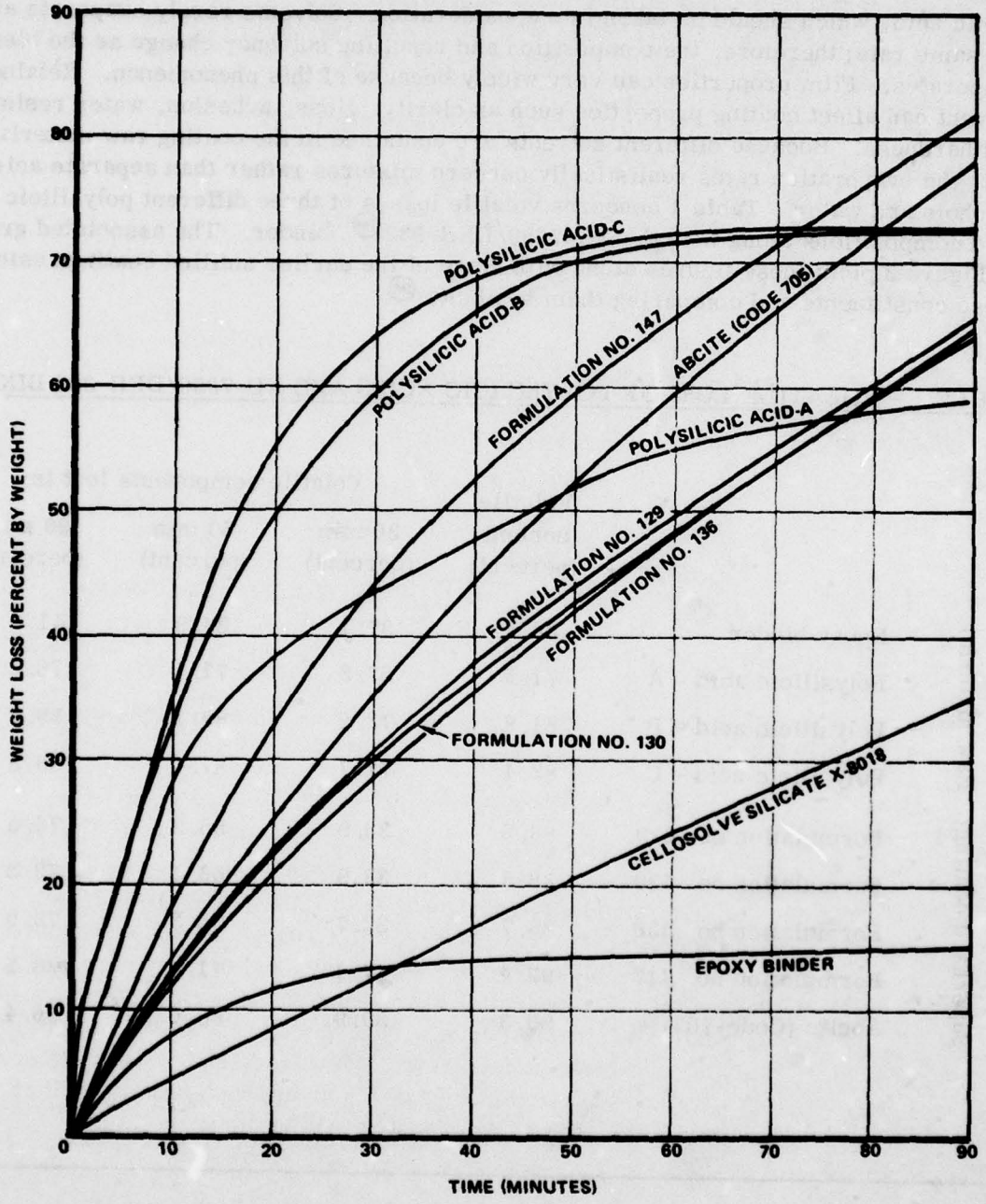


Figure 3 - Evaporation Rate Analysis

Solvent evaporation rate is not an absolute value in practical situations because it depends upon environmental conditions. Temperature, air movement, the presence of a solute, surface area, and humidity are factors that affect the evaporation of a single solvent.

The following test method was found to give reproducible results. In all cases available equipment was used.

Step 1: Foil-backed blotters were cut from Whatman™ No. 54 filter paper and standard aluminum foil so that the resulting blotter assembly would fit the balance pan of a Type H6T Mettler™ balance.

Step 2: The foil-backed blotter assembly was placed on the balance pan and weighed. Then, with the use of a hypodermic needle, approximately 2 cc of a liquid in question were applied onto the blotter and immediately weighed to determine the initial amount of liquid added.

Step 3: With both doors of the balance left open, and with the balance left on "full release", periodic readings were taken.

Step 4: Data was recorded on a form which listed: Δ time, time, weight, Δ weight, and percent Δ weight. Readings were usually taken every 5 minutes for a period of not less than 90 minutes (see Figure 3).

Step 5: Values collected were then translated into data which was plotted as percent weight loss versus time.

d. Fillers

By screening many submicron sized materials, two oxides were chosen as candidate fillers in their finest form. Fumed aluminum oxide and silicon dioxide are well known as fillers, but each posed dispersal problems in coatings. These particular coating fillers are used more as thickeners than hardeners and depend more on coagulation or gelation properties than as colloidal suspensions in small concentrations. Figure 4 compares the surface charges of each with respect to the pH of an aqueous solution along with the range in which the isoelectric point (zero charge) occurs and particles drift together into a coagulation. Figure 5 is an approximation which shows the variations in viscosity which also can be expected with an increase in pH.

™ Trademark of W & R Balston Ltd, England.

™ Trademark of Mettler Instrument Corp., So. San Francisco, California.

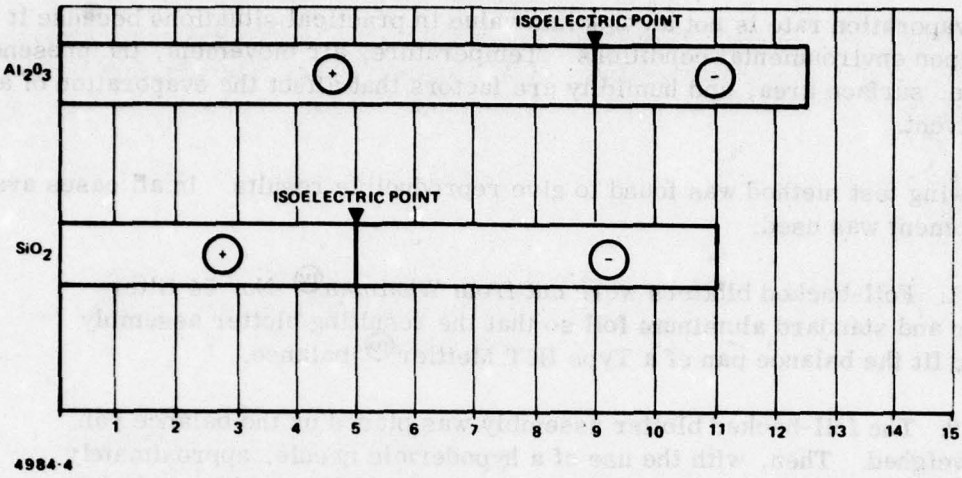


Figure 4 - Charges versus pH

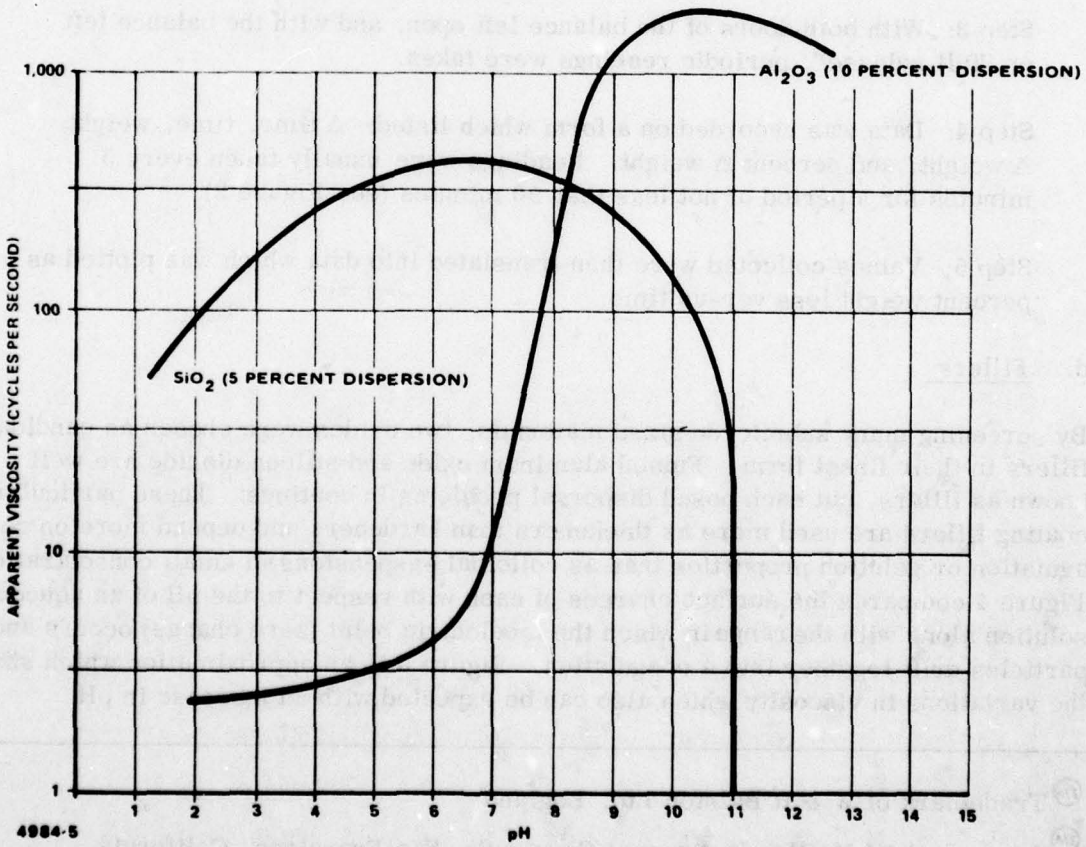


Figure 5 - Apparent Viscosity versus pH

The viscosities can be reduced by reducing the quantity of filler, which may provide better flow characteristics of the coating, but of more importance are the hardness and light transmitting characteristics of the coating itself. The alumina tends to be hydrophobic to aqueous solutions and may need surface treatment for proper wetting and optical continuity. The silica is hydrophylic and absorbs water molecules to the point of complete gelation if the filler concentration is sufficiently high.

Both fillers appear to be compatible with an acidic system with a pH below 4.5 and have comparatively low viscosities in small concentrations. A choice is premature at this point because it will depend upon haze and hardness determinations after the fillers have been balanced into a cured resin system.

Because submicron sized particles were chosen as fillers, some means was necessary to quantitatively determine the amount and average particle size which could be consistently separated from a liquid suspension. Three fillers were chosen from Table 2. The nominal particle sizes of 0.007 (EH-5), 0.014 (M-5), and 0.020 (Aluminum Oxid "C") represented a range of particle sizes which could be used to determine solids content versus time for a predetermined centrifuge speed.

TABLE 2 - PROPERTIES OF VARIOUS FILLERS

	Aluminum Oxid "C"	Alon	Fumed silica M-5	Fumed silica EH-5
BET surface area (m^2/gm)	100 ±15	100	200 ±15	390 ±40
pH (4 percent aqueous suspension)	4.0-5.0	4.1-4.6	3.5-4.2	3.5-4.2
Nominal particle size (microns)	0.020	0.030	0.014	0.007
X-ray structure	Primarily gamma	90 percent gamma	Amorphous	Amorphous
Surface charge	+	+	-	-

(TM) Cab-O-Sil EH-5 - trademark of Cabot Corp., Boston, Mass.

(TM) Aluminum Oxid "C" - trademark of Degussa Inc., Teterboro, N. J.

(TM) Cab-O-Sil M-5 - trademark of Cabot Corp., Boston, Mass.

Reproducibility of filler concentrations was obtained by standardizing the shearing speed (Waring blender), time, and percentage of solids added to water by weight. The percentage of solids used for this determination was 4 percent. Curves for centrifuge speeds of 4500 and 9000 rpm were established by running filler suspensions of different particle sizes for various time spans at these velocities and weighing the solids content of the remaining suspension. The latter was accomplished by weighing a small portion of the suspension, evaporating all the water, and weighing the residue. Figures 6 and 7 show the results of these determinations.

Considering the nominal particle sizes from Table 2, the curves of Figures 6 and 7, and a centrifuge time of 15 minutes, the plot of percentage of retained filler versus nominal particle size resulted in a straight line, independent of other variables for a given centrifuge speed as shown in Figure 8. By extending the same slope for the one point of Aluminum Oxid "C" at 4500 rpm, parallel slopes for intermediate centrifuge speeds can be estimated.

Using the standard equation for a straight line, $Y = mx + b$, the Y intercept of the 9000 rpm/15 min curve is 132 percent and is equal to b. The slope was calculated to be -6500, therefore the equation becomes $Y = -6500x + 132$ for a centrifuge speed of 9000 rpm. The Y intercept, however, will vary with speed. Utilizing the 4500 rpm and 9000 rpm lines and plotting a separate line of Y_I intercept versus speed, (2 points), its slope may be calculated and its intercept determined from the new line. The coordinates of the two points would be (9000, 132) and (4500, 204). The slope becomes -0.016 and the intercept 270, or

$$Y_I \text{ Intercept} = -0.016R + 270 \quad ,$$

where R equals the speed/15 minutes. Substituting the Y_I intercept for b in the original equation, a new equation appears which is

$$Y = -6500x - 0.016R + 270 \quad .$$

From this equation, the centrifuge speed and time can be determined for any percentage of particles desired in the remaining suspension. As an example, if it is desired to retain 50 percent of the particles in suspension after centrifuging for 15 minutes, the centrifuge speeds required would be

$$R = \frac{-6500(x) - y + 270}{0.016} \quad ,$$

where

R = Centrifuge speed for 15 min period
(x) = Nominal particle size
(y) = Particle retention required (percent).

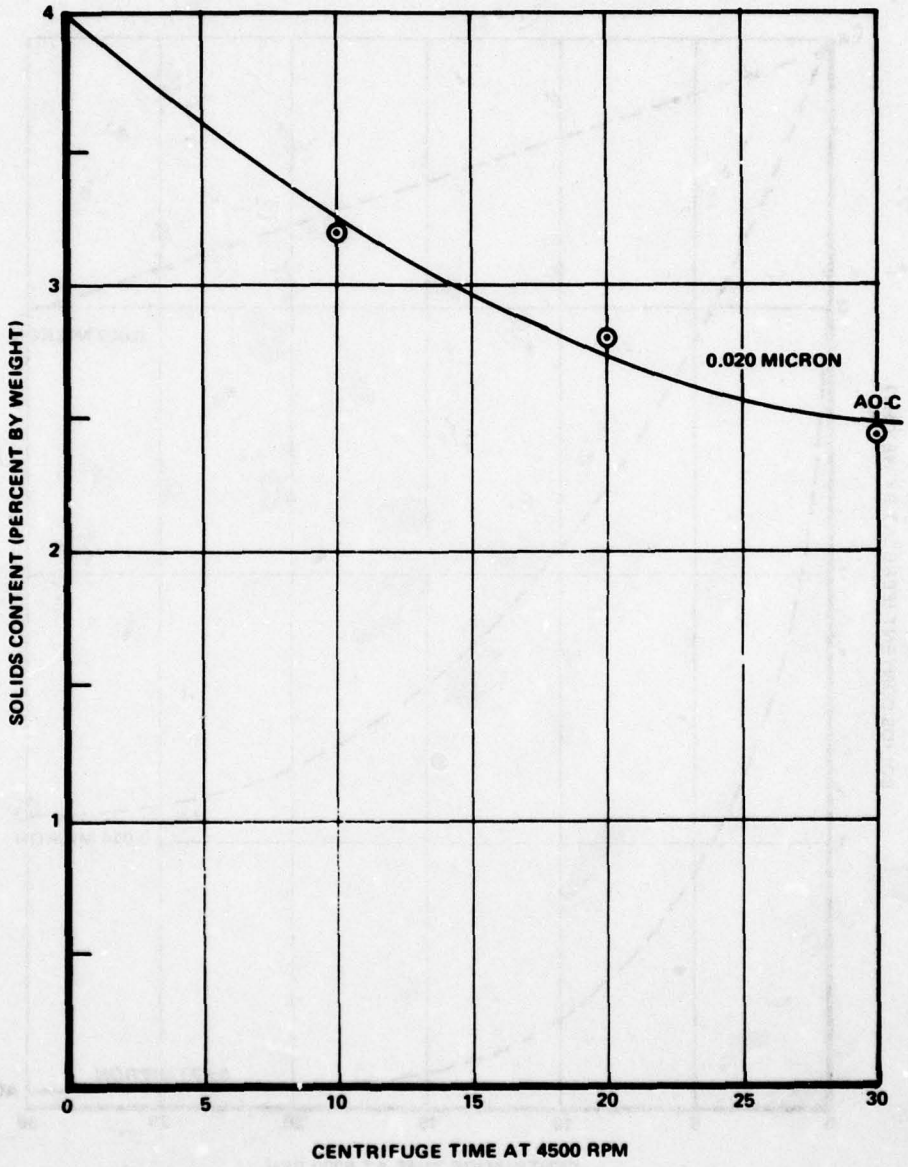


Figure 6 - Suspension Solids Content versus Centrifuge Time at 4500 RPM

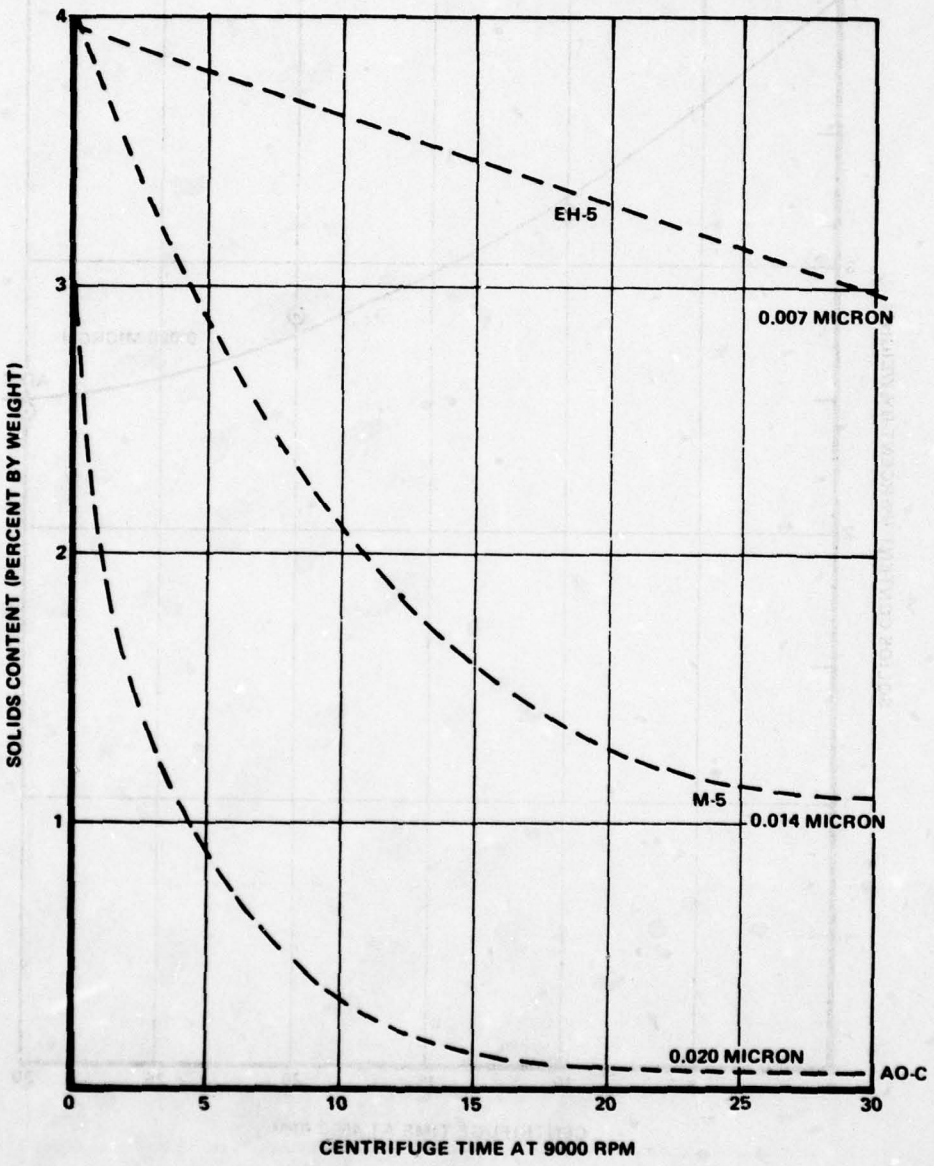


Figure 7 - Suspension Solids Content versus Centrifuge Time at 9000 RPM

AD-A065 049 AIR FORCE FLIGHT DYNAMICS LAB WRIGHT-PATTERSON AFB OHIO F/G 1/3
CONFERENCE ON AEROSPACE TRANSPARENT MATERIALS AND ENCLOSURES (1--ETC(U)
DEC 78 R E WITTMAN

UNCLASSIFIED AFFDL-TR-78-168 NL

7 OF 10
ADA
065049



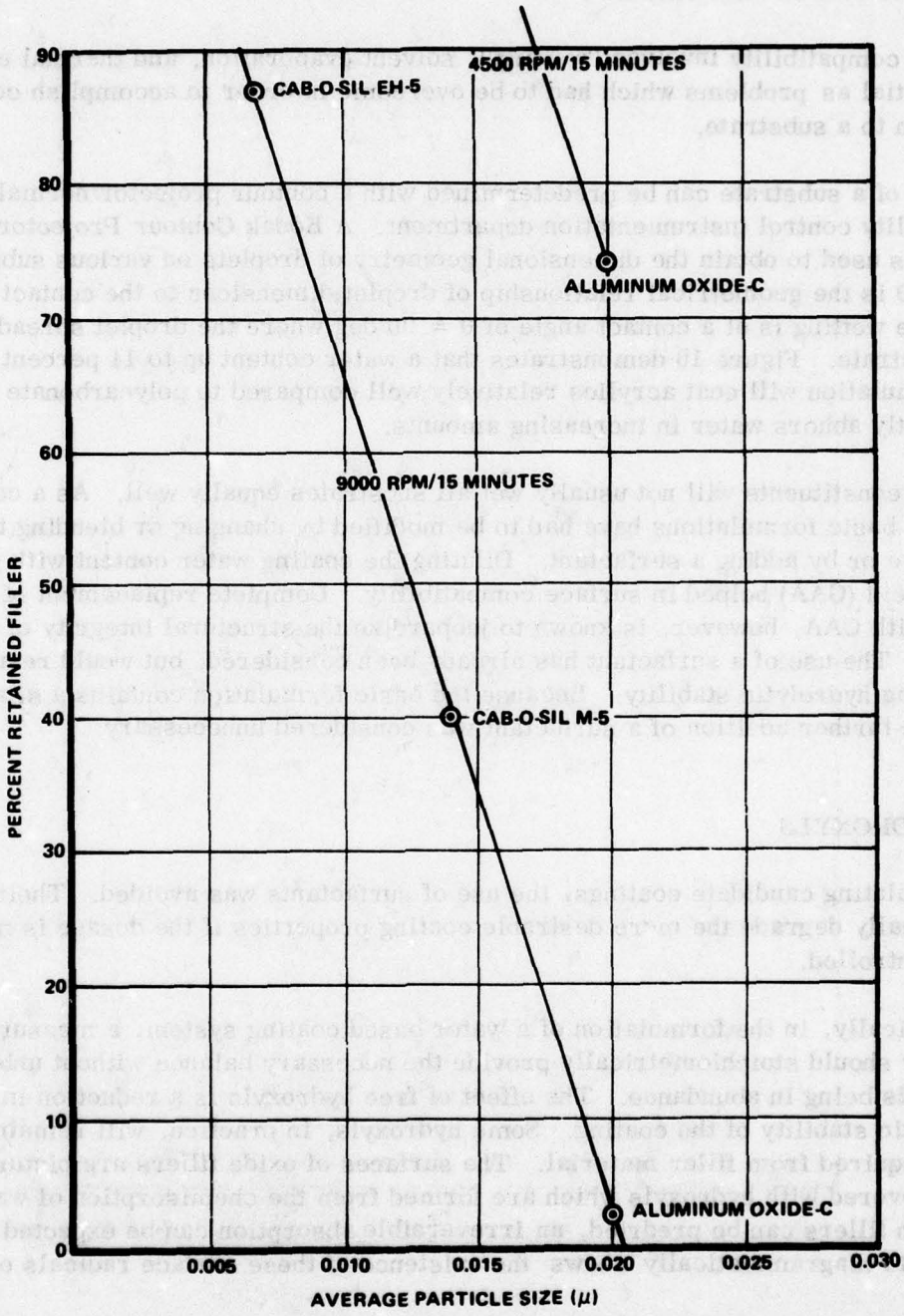


Figure 8 - Percentage of Retained Filler versus Average Particle Size

2. SURFACE COMPATIBILITY

Surface compatibility involves "wetting", solvent evaporation, and thermal expansion differential as problems which had to be overcome in order to accomplish coating adhesion to a substrate.

Wetting of a substrate can be predetermined with a contour projector normally found in a quality control instrumentation department. A Kodak Contour Projector(TM) Model 14-5 was used to obtain the dimensional geometry of droplets on various substrates. Figure 9 is the geometrical relationship of droplet dimensions to the contact angle. Ultimate wetting is at a contact angle of $\theta = 90$ deg where the droplet spreads out on the substrate. Figure 10 demonstrates that a water content up to 14 percent in a coating formulation will coat acrylics relatively well compared to polycarbonate which apparently abhors water in increasing amounts.

Coating constituents will not usually wet all substrates equally well. As a consequence, basic formulations have had to be modified by changing or blending the solvent structure or by adding a surfactant. Diluting the coating water content with glacial acetic acid (GAA) helped in surface compatibility. Complete replacement of the free water with GAA, however, is known to jeopardize the structural integrity of polycarbonate. The use of a surfactant has already been considered, but would result in films exhibiting hydrolytic stability. Because the basic formulation contains a silane coupling agent, a further addition of a surfactant was considered unnecessary.

3. HYDROXYLS

In formulating candidate coatings, the use of surfactants was avoided. Their usage can actually degrade the more desirable coating properties if the dosage is not carefully controlled.

Theoretically, in the formulation of a water based coating system, a measured weight of water should stoichiometrically provide the necessary balance without unbound hydroxyls being in abundance. The effect of free hydroxyls is a reduction in the hydrolytic stability of the coating. Some hydroxyls, in practice, will remain with those acquired from filler material. The surfaces of oxide fillers are pictured as being covered with hydroxyls which are formed from the chemisorption of water. Although fillers can be predried, an irreversible absorption can be expected to remain. Figure 11 diagrammatically shows the existence of these surface radicals on silicon dioxide.

(TM) Kodak Contour Projector - trademark of Eastman Kodak Co., Rochester, N.Y.

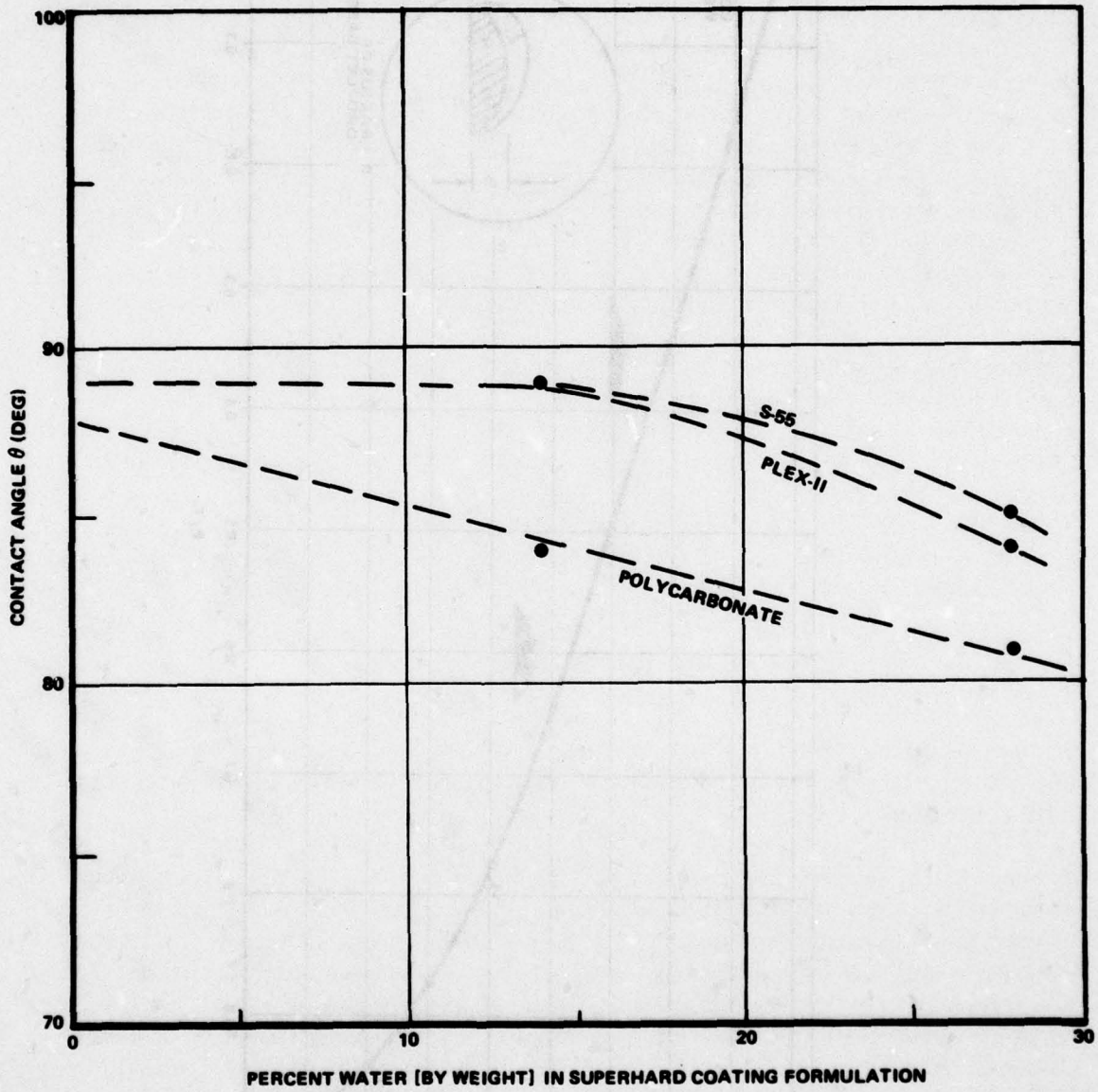


Figure 9 - Percentage of Water (by Weight) in Superhard Coating Formulation

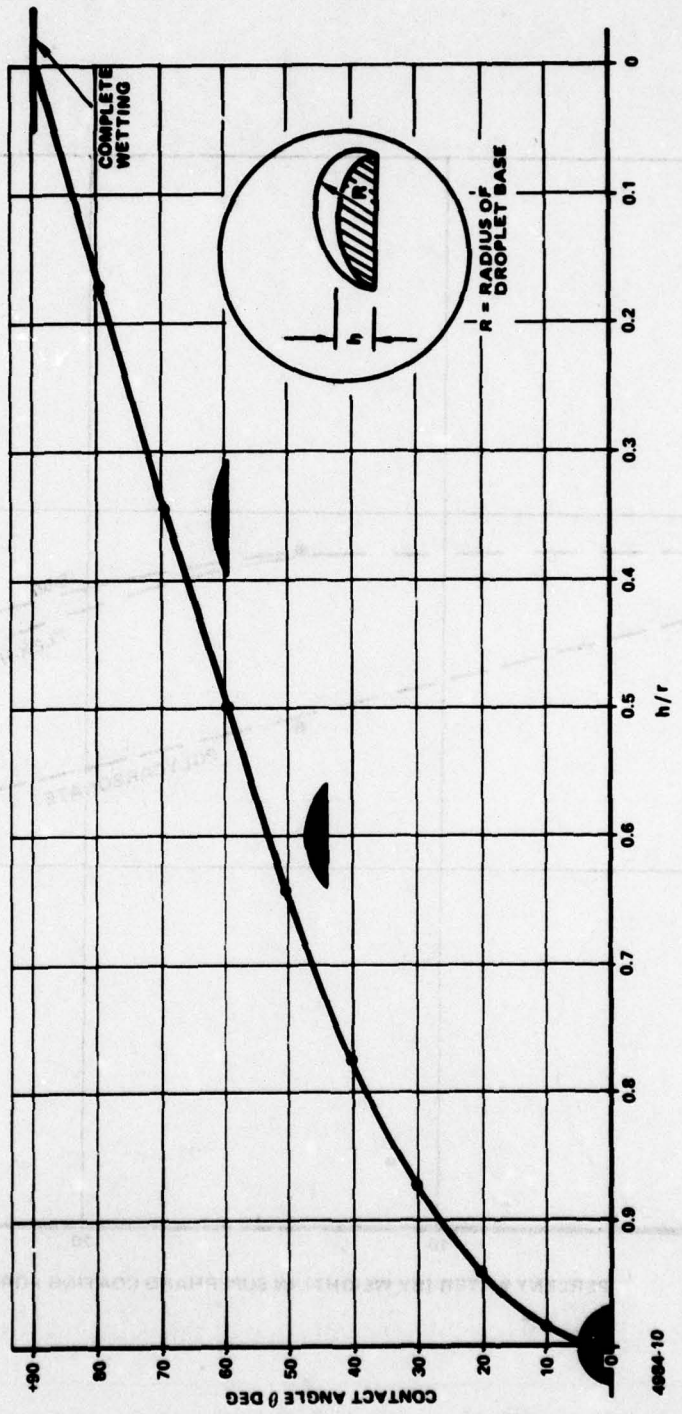


Figure 10 - Contact Angle θ versus Ratio of h/r

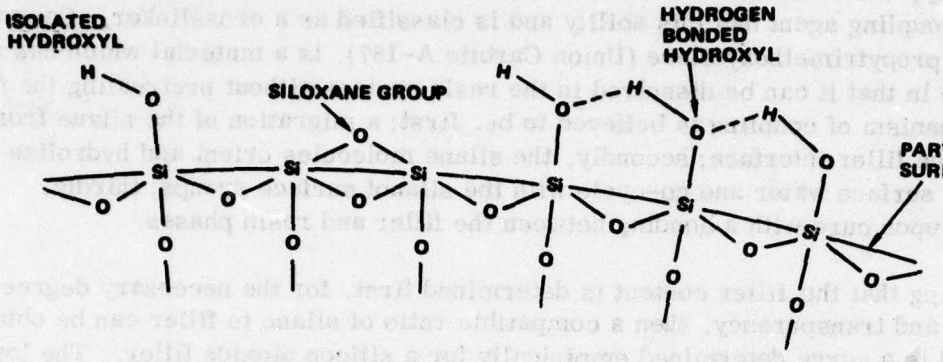


Figure 11 - Typical Groups which Can Occur on the Silicon Dioxide Aggregrate, Determining Its Surface Chemistry

Any drying which will remove hydroxyls after formulation is very limited because a temperature below 100° C is required when coating stretched acrylic. Figure 12[a] demonstrates the reversible dehydration which is not accessible except for coating substrates, such as polycarboantes, which are stable at higher temperatures.

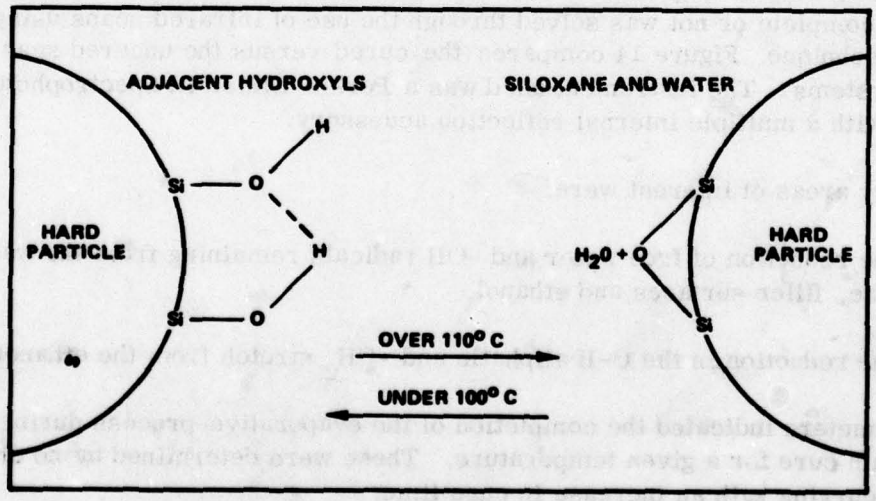


Figure 12 - Reversible Dehydration of the Silicon Dioxide Surface

[a] Adapted from "CAB-O-SIL Properties & Functions" Cabot Corp., Boston, Mass.

Essentially, OH radicals which remain should be bound in some manner. The use of a silane coupling agent has this ability and is classified as a crosslinker. Gamma-Glycidoxypropytrimethoxysilane (Union Carbite A-187), is a material which has an advantage in that it can be dissolved in the resin system without pretreating the filler. The mechanism of coupling is believed to be, first; a migration of the silane from the resin to the filler interface; secondly, the silane molecules orient and hydrolize with the bound surface water and co-cycle with the silanol surface groups; thirdly, condense upon cure with a bonding between the filler and resin phases.

Considering that the filler content is determined first, for the necessary degree of hardness and transparency, then a compatible ratio of silane to filler can be obtained. Figure 13 is a curve determined empirically for a silicon dioxide filler. The lowest percentage of haze is the criteria for an acceptable level with a resulting silane to silica weight ratio of 3:1.

The silane plays a dual role in that it not only crosslinks the filler to the resin system, but also the resin system to some substrate surfaces. The silane will therefore be in both filled and unfilled systems.

4. OPTIMUM CURE DETERMINATION

Cure has been mentioned from the standpoints of removing water and hydroxyl groups and condensing the resin system into a hard coating. The problem of knowing whether a cure was complete or not was solved through the use of infrared scans using a multiple reflection technique. Figure 14 compares the cured versus the uncured scan of one of the resin systems. The instrument used was a Perkin-Elmer IR Spectrophotometer ™ Model 700 with a multiple internal reflection accessory.

The primary areas of interest were:

1. The reduction of free water and -OH radicals remaining from the water base, filler surfaces and ethanol.

2. The reduction in the C-H aliphatic and $-CH_2$ stretch from the ethanol.

These parameters indicated the completion of the evaporative process during cure and the maximum cure for a given temperature. These were determined by no change in the scan occurring with an increase in cure time.

™ IR Spectrophotometer - trademark of Perkin-Elmer Corp., Norwalk, Conn.

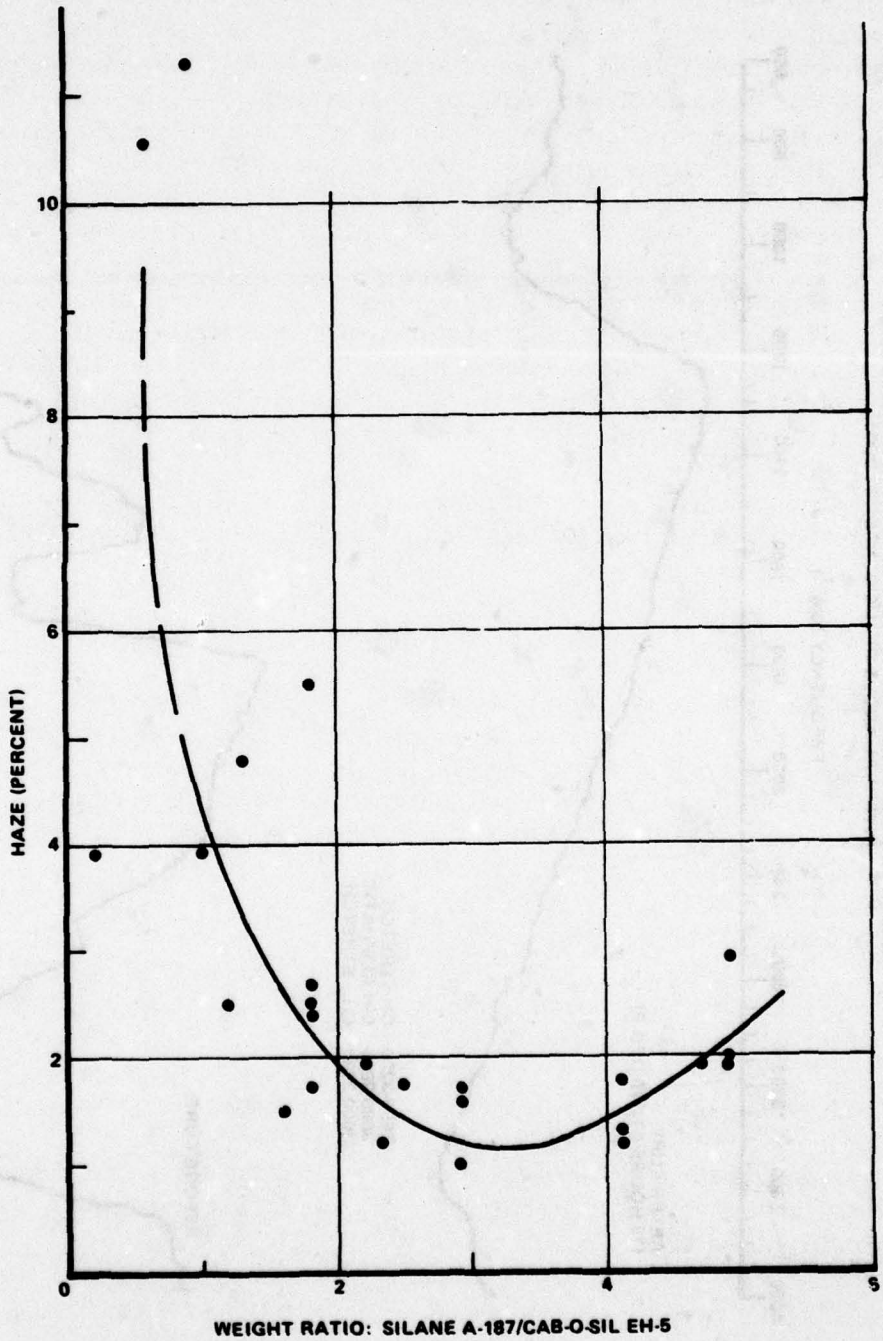


Figure 13 - Weight Ratio: Silane A-187/CAB-O-SIL EH-5

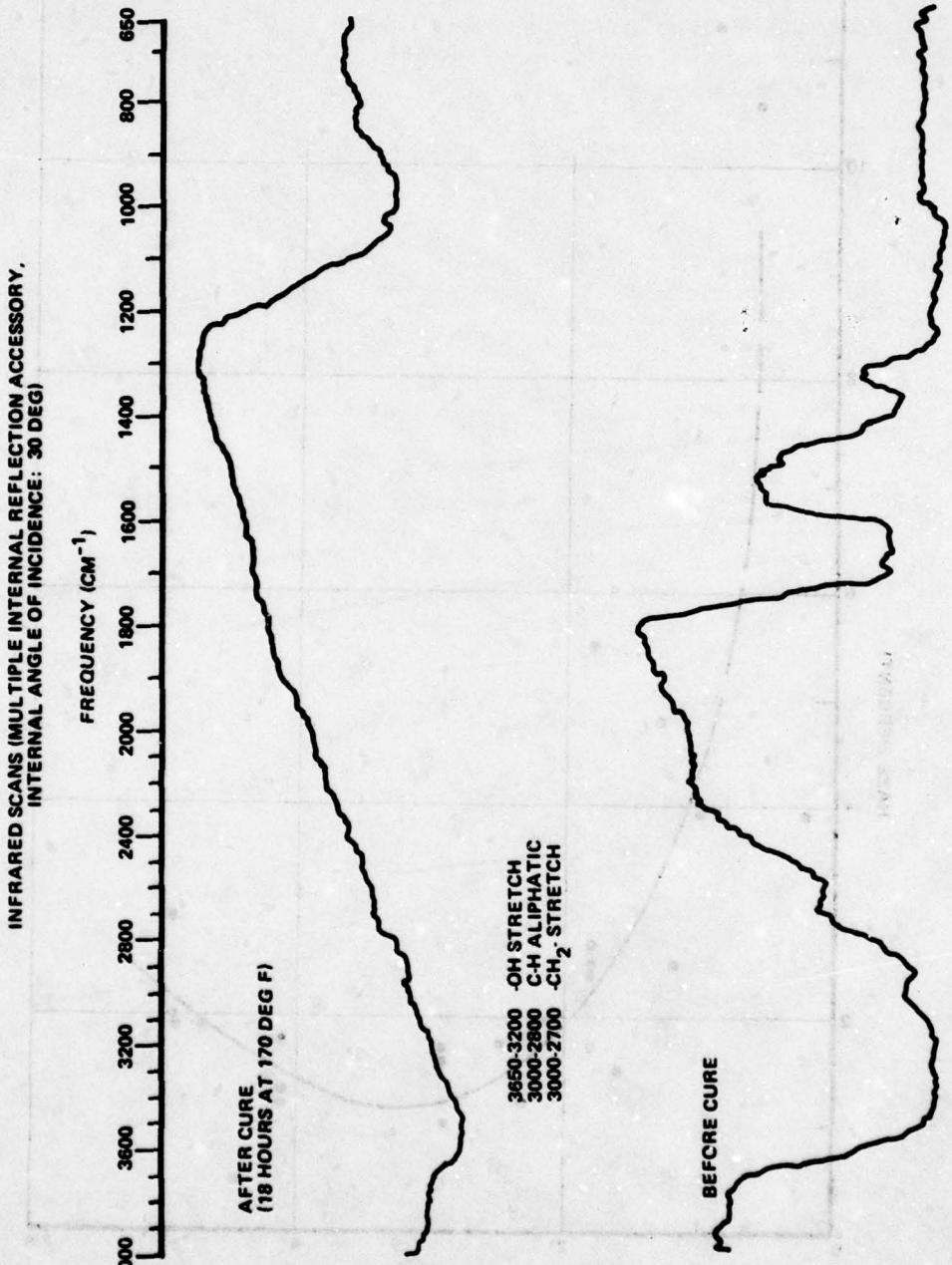


Figure 14 - Infrared Coating Cure Profile

5. COATING THICKNESS DETERMINATION

Controlling coating thickness on a flat sheet is not difficult. Coating a contoured canopy may offer problems. Flow coating or dipping are the more obvious methods, with flow coating probably being more economical, depending upon the pot life of the material.

Sagging of coatings is common in water reducible coating systems. The use of a filler as a hardener also helps in making the film more thixotropic, and less likely to be thin at the top and thick at the bottom of a flow-coated or dipped part. A coating approximately 3 to 5 microns in thickness is considered adequate. Coatings heavier than these dimensions may exhibit rule lines as shown in Figure 15. These are theorized as being caused by the circulation currents of the evaporating solvents which concentrate bubbles into parallel lines to the direction of flow as shown diagrammatically in Figure 16.

Measuring thicknesses of coatings is difficult to do nondestructively; although specimens may be taken from the selvage area if the coating is considered as being uniform. Two methods have been used. One utilized an unprimed area or a strip of release tape over which the coating would flow. Once cured, the film was carefully stripped and physically measured with a Pratt & Whitney Supermicrometer,(TM) Model B.

The second method was much more revealing in that the use of a scanning electron microscope (Cambridge Stereoscan 600(TM)) not only allowed an accurate thickness measurement of the coating, but also the coating surface condition and hard particle distribution, merely by changing the specimen orientation. Figure 17 is a typical edge photograph with the linear reference tab.

Figure 18 compares the surfaces of unfilled and filled coatings in which the clusters of filler and voids are evident.

The specimens are cut from the part in a selvage area as squares $1/2 \times 1/2$ in. These are cemented to a target holder and placed in an accessory metal-sputtering equipment. Dielectric specimens have to be coated with a thin conductive film which does not interfere with the contour features being examined. Once plated, the specimens may be mounted in the electron microscope, and through standard procedures, positioned, focused, and photographed.

(TM) Supermicrometer - trademark of Pratt & Whitney Machine Tool Div. of Colt Industries, West Hartford, Conn.

(TM) Stereoscan 600 - trademark of Cambridge Instrument Co., Morton Grove, Ill.

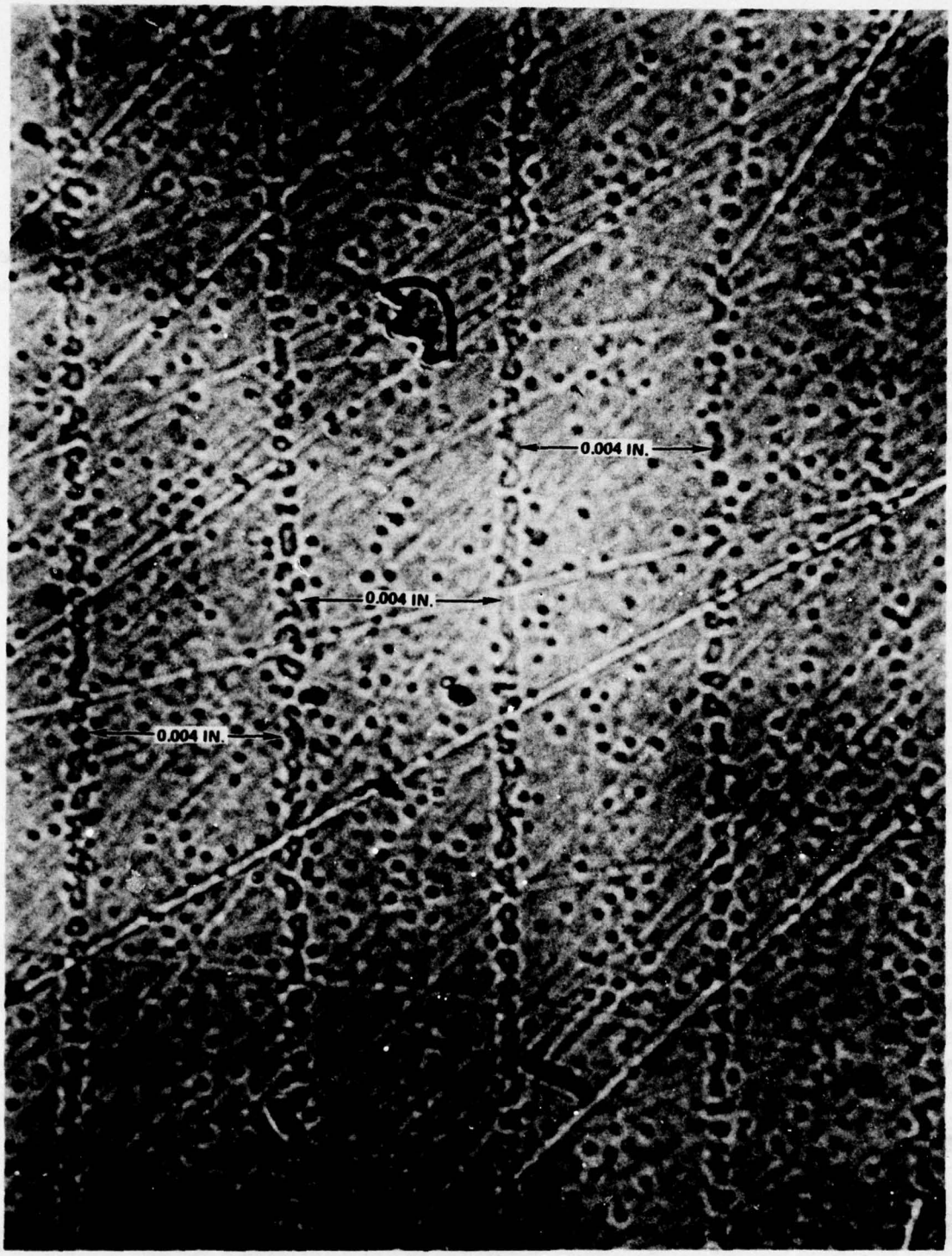


Figure 15 - Rule Lines in Primer

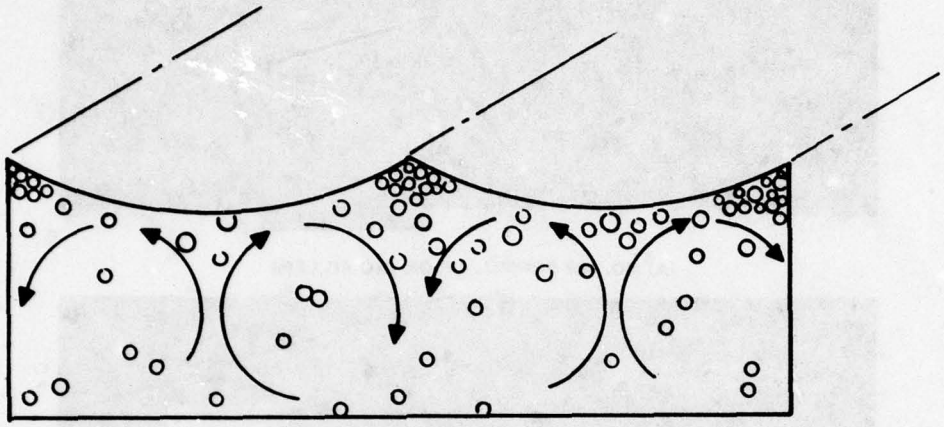


Figure 16 - Vortex Currents During Solvent Evaporation

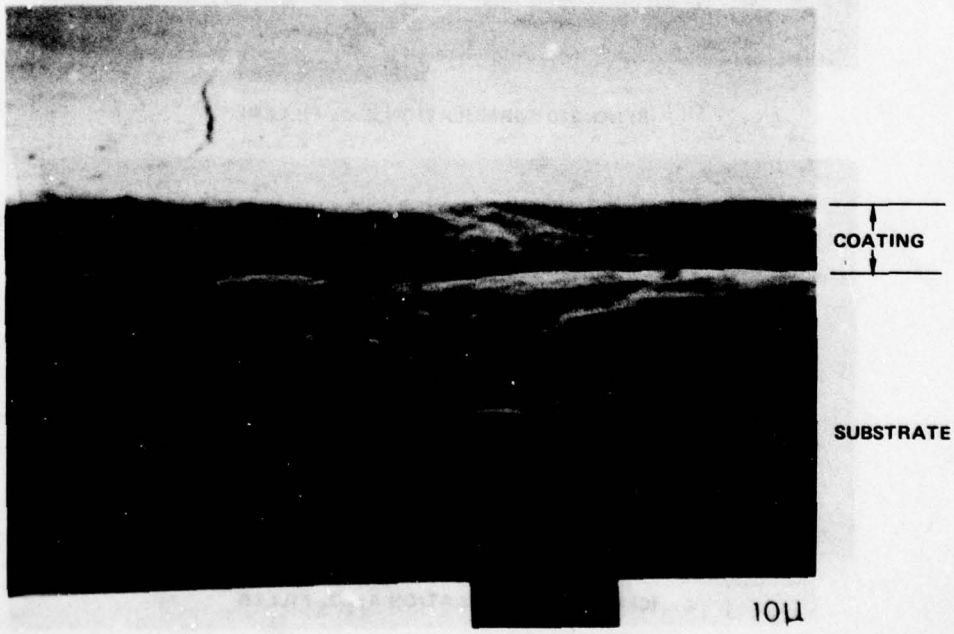
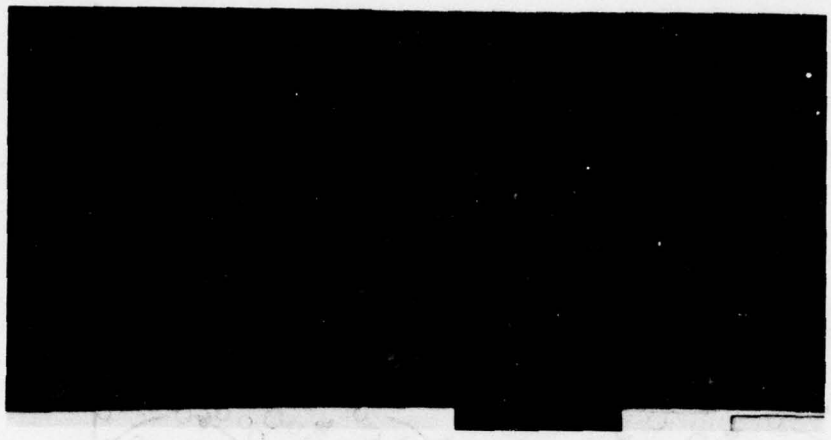
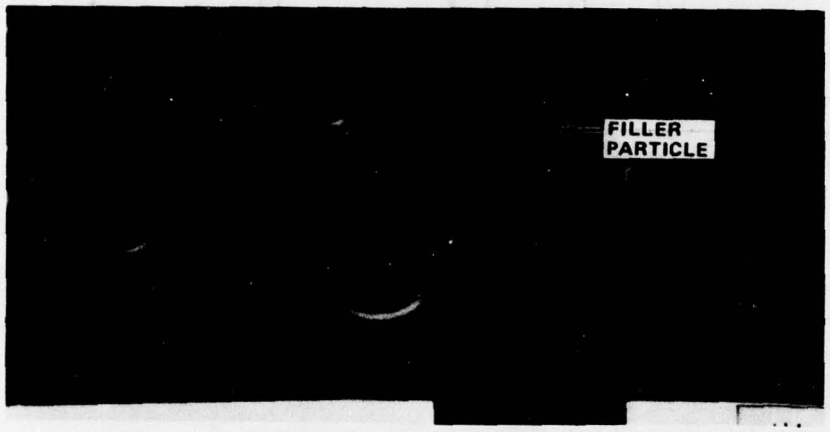


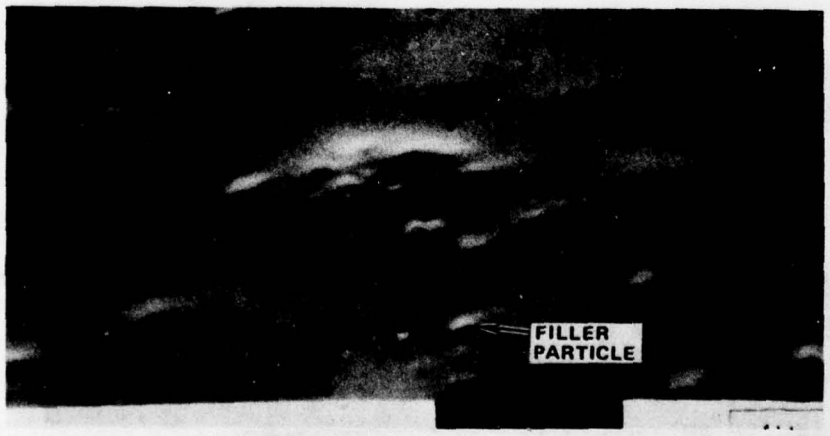
Figure 17 - Electron Microphotograph of Coating Thickness at 83 Deg Angle



(A) NO. 188 FORMULATION (NO FILLER)



(B) NO. 210 FORMULATION (SiO_2 FILLER)



(C) NO. 214 FORMULATION Al_2O_3 FILLER

Figure 18 - Electron Microphotographs of Filled and Unfilled Transparent Hard Coatings on Stretched Plex 55 Substrate (Black Marker Represents 4 Microns in Length)

6. THE MECHANICS OF ABRASION

Mar resistance is a more inclusive term for abrasion which involves hardness, slip, scratch, and impingement variables. Scratching, although primarily a horizontal force, first requires a break in the coating. A smooth surface which tends to be frictionless (slip) resists penetration. Figure 19 is an electron microphotograph showing fissures started with steel wool. Although the coating is broken, it cannot be seen without magnification. A good slip property undoubtedly helped. Hardness also acts against penetration and the two together resist windshield wiper abrasion.

Because the fracture mechanisms are essentially 90° out of phase, the coating formulation has to be a tradeoff which will most closely meet the probabilities of scratching versus impact.

VI. FORMULATIONS

The three formulations are shown in Table 3; all are based on the chemistry of alkyl silicates.

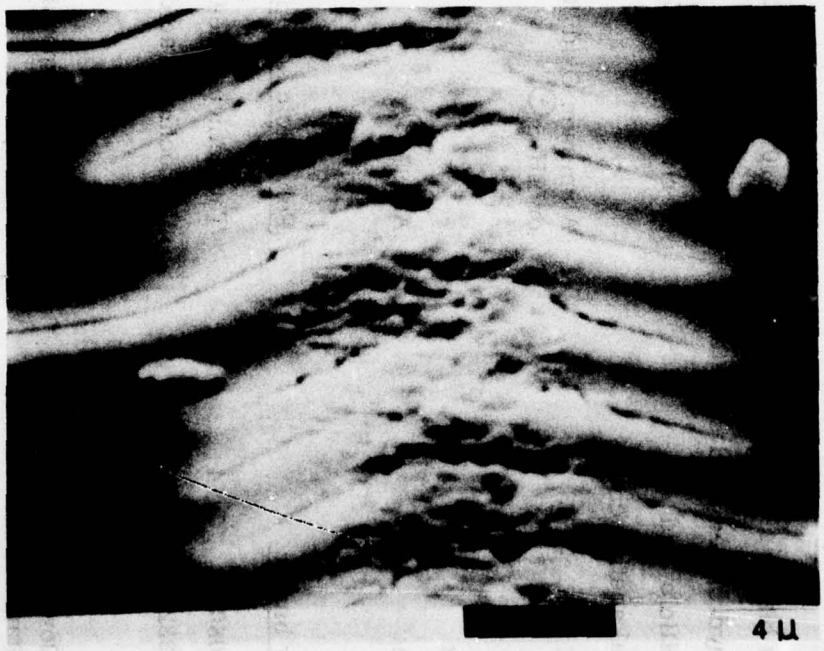


Figure 19 - Minor Coating Penetration from Steel Wool

TABLE 3 - GOODYEAR AEROSPACE COATING FORMULATIONS IN PARTS BY WEIGHT

Components	Commercial designations	Coating codes No. 188	No. 210	No. 214
Epoxy binder	XD-7080/DER 332 ①	7.5	7.5	7.5
Pre-hydrolyzed ethyl silicate	Silbond H-4 ②	5.7	5.7	5.7
Polysilicic acid	(Derived from TEOS)	25.1	25.1	25.1
Glacial acetic acid	-	29.4	29.4	29.4
Filler	Aluminum Oxid "C" ③ or EH-5 ④	-0-	21.0 (1.98 % EH-5)*	18.8 (2.5 % Aluminum Oxid "C")*
Water	-	29.4	8.4	10.6
Silane	A-187 ⑤	2.9	2.9	2.9
		100.0	100.0	100.0

Epoxy binder

XD-7080	71.4
DER 332	28.6
	100.0

Polysilicic acid preparation

Tetraethyl orthosilicate	83.7
Hydrochloric acid (15%)	16.3
	100.0

Agitated until exotherm ceases
Allowed to stand 24 hours before compounding

① Dow Chemical Co.
② Stauffer Chemical Co.
③ DeGussa Inc.
④ Cabot Corp
⑤ Union Carbide Corp.

*Water suspension, percentage by weight.

Notes:

1. Allow evaporation at room temperature for 1/2 hour.
2. Oven cure at +190 deg F for 16 hours for a stretched acrylic substrate.
3. Avoid skin and eye contact; use only with adequate ventilation.

VII. CHEMISTRY OF ALKYL SILICATES

The explanation of the forming of SiO_2 crystalites from tetraethyl orthosilicate is a basic concept, but the process of hydrolysis is more complex.[a] Crystalline silica in the form of SiO_2 is never really produced. Many intermediate species of polysilicates are formed during hydrolysis. As the reaction proceeds, the polysilicates grow in molecular weight and chain length, until most or all of the ethyl groups are driven off and a nonlinear network of -Si-O-Si- remains.

This chemical process of hydrolysis is the basis for application of ethyl silicate products as binders. By partially hydrolyzing tetraethyl orthosilicate under carefully controlled conditions, a stable mixture of polysilicate "pre-polymers" can be made. These materials can be stored for a limited period of time and when ready for use as binders, can be hydrolyzed to completion by adding the proper amount of water and changing the pH to an unstable range by using a gel agent. Most of the water for 100 percent hydrolysis is present in these binders; a change in pH will push the reaction to completion.

The stoichiometric equation for partial hydrolysis is as follows:

$$Si(OR)_4 + 2\,xH_2O \xrightarrow{H^+ \text{ or } OH^-} \underbrace{\left|Si(OR)_{4(1-x)}(O)_{2x}\right|}_{\text{polymer}} + 4\,x\,ROH$$

where

$$x = \frac{\text{Degree (percent) of hydrolysis}}{100}$$

$R = C_2H_5$ (ethyl group) for ethyl silicate.

It is imperative that a small amount of acid or base be added to catalyze the hydrolysis.

The mechanism of hydrolysis of ethyl (or other alkyl = R) silicate is as follows:

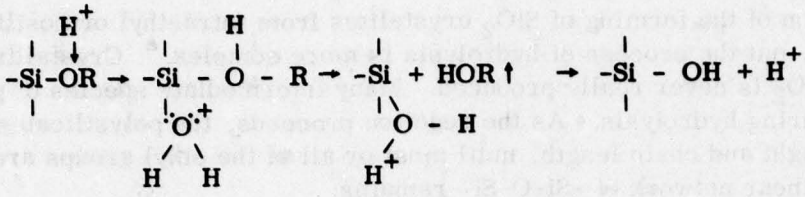
Acid hydrolysis:

$$\text{-Si-OR} + H_2O \xrightarrow{H^+} \text{-Si-OH} + ROH$$

---

[a] Discussion of chemical process of hydrolysis adapted from technical literature of Stauffer Chemical Co., New York, N. Y.

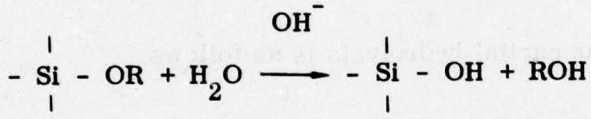
Mechanism:



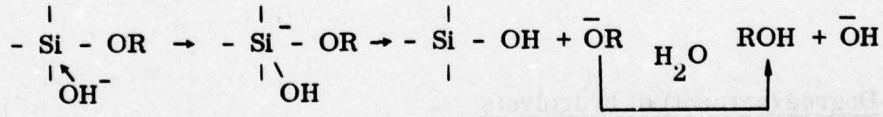
In this reaction, a silicic acid ester is generated, along with an alcohol, which leaves the reaction. A hydrogen (or Lewis acid) ion (H^+) is consumed and regenerated with no net loss or gain, thus perpetuating the reaction.

This same reaction takes place with a base:

Base hydrolysis:

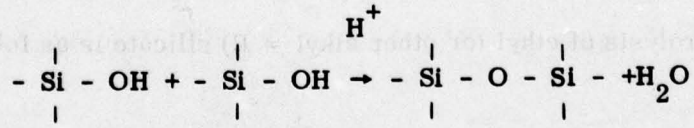


Mechanism:

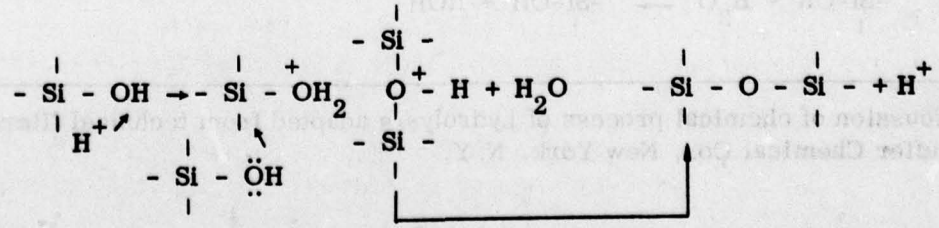


For alkyl silicate polymers to form, the following condensation reactions must occur:

Acid condensation:



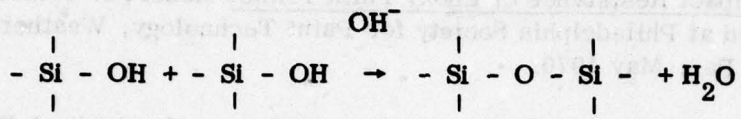
Mechanism:



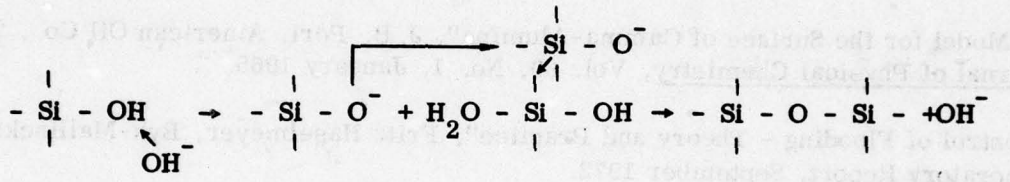
In this reaction, two silicic acid esters react to form a dimer (or higher polymer), generating H_2O, which continues the hydrolysis reaction. Again there is no net loss or gain of the H^+ ion.

Similarly:

Base condensation:



Mechanism:



VIII. CHOICE OF COATING

All three coatings were subjected to severe environmental tests which are documented in the final report for this project which is now in publication.

Goodyear Aerospace No. 210 formulation would rank first in performance and is this company's choice as the more reliable coating. The No. 188 coating appears less hard, and the No. 214 coating exhibits a haze problem which limits the amount of aluminum oxide which can be added.

Currently, the No. 210 coating has only been applied and tested on stretched Plex 55. Extension of the formulation for use on as-cast acrylic will require either modification of the formulation or the development of a primer compatible with coating and substrate or both.

IX. CONCLUSIONS

The development of the No. 210 superhard coating for helicopter transparencies is expected to alleviate the problem of abrasion and extend the service life approximately threefold.

A coating designed to totally resist impingement may not be scratch resistant and vise versa. A tradeoff of properties is represented in the No. 210 coating developed through the problem areas discussed.

BIBLIOGRAPHY

Silane Coupling Agents As Integral Blends in Resin-Filler Systems, S. Sterman and J. G. Marsden, Product Development, Silicones Div., Union Carbide Corp., based on SPI Reinforced Plastics Meeting, Chicago, February 1963.

Molecular Basics for Impact Resistance of Epoxy Paint Films, Robert J. Moore, Shell Chemical Co., presented at Philadelphia Society for Paint Technology, Weathering Seminar, Philadelphia, Pa., May 1970.

"Infrared and Gravimetric Study of Surface Hydration of Gamma-Alumina", J. B. Peri, American Oil Co., The Journal of Physical Chemistry, Vol. 69, No. 1, January 1965.

"A Model for the Surface of Gamma-Alumina", J. B. Peri, American Oil Co., The Journal of Physical Chemistry, Vol. 69, No. 1, January 1965.

"Control of Flooding - Theory and Practice", Fritz Haselmeyer, Byk-Mallinckrodt, Laboratory Report, September 1972.

Mechanism of Paint Chipping, Howard S. Bender, General Motors Research Laboratories, Federation of Societies for Paint Technology, Boston, Mass., October 1970.

Ethyl Silicate Binders, Peter G. Carpenter, Specialty Chemical Division, Stauffer Chemical Co., Paint and Varnish Production, July 1972.

Modified Silica Gels as Absorbents and Catalysts, Robert L. Burwell, Jr., Chemtech, June 1964.

"Synthetic Silicas, Important Pigments to the Paint Industry, William Georgov and Alexander A. Chasan, J. M. Huber Corp., Journal of Paint Technology, Vol. 43, No. 557, June 1971.

Copolymers, Polyblends, and Composites, Norbert Platzer, Chemtech, February 1974.

Brittle Materials, A General Introduction, E. Smith, Dept. Metallurgy, Univ. of Manchester, G. B., Materials Science & Engineering, Switzerland, Vol. 15, (1974).

Abrasion Resistant Finishes, Sidney B. Levinson, D. H. Litter Co., Ltd. Eighth Biennial Western Coatings Technology Symposium, San Francisco, Calif., February 1966.

"Particle Size Distribution Measurement in the 200 to 1200 Å Range", Ted Lee and C. W. Weber, Union Carbide Corp., Analytical Chemistry, Vol. 39, No. 6, May 1967.

Handbook of Surface Preparation, Snogren; Palmerton Publishing Co., Inc., 1974.

Paint Testing Manual, Gardner/Sward; 13th Edition, 1972; ASTM-STP 500.

Superhard Transparent Coatings, Marks Polarized Corp., April 1975; USAAMRDL-TR-75-22, Eustis Directorate.

Exploratory Development of Heat and Abrasion Resistant Coatings for Transparent Plastics, July 1976; AFML-TR-76-115, Air Force Systems Command.

"Synthetic Silicas, Important Pigments to the Paint Industry, " William Georgov and Alexander A. Chasan; J. M. Huber Corp.; Journal of Paint Technology, Vol 43, No. 557, June 1971.

Abrasion Resistant Coating for Transparent Plastics, Loren Haluska and George Galic; Dow Corning Corp.; 1976.

McCutcheon's Functional Materials, McCutcheon Division, MC Publishing Co., New Jersey, 1977 Annual.

McCutcheon's Detergents and Emulsifiers, North American Edition, McCutcheon Division, MC Publishing Co., New Jersey, 1977 Annual.

"Infrared Spectroscopy - Its Use in the Coatings Industry"; Infrared Spectroscopy Committee of the Chicago Society for Paint Technology. Publisher: Federation of Societies for Paint Technology, Philadelphia, Pa., 1969.

TL 1078-OM-8111: Stereoscan 600 Scanning Electron Microscope Instruction Manual, Issue II, Vol. II. Morton Grove, Ill., Cambridge Instrument Co., Inc.

DIAMOND TURNING OF F-111 WINDSCREENS: FEASIBILITY STUDY PHASE I

Major T. T. Saito
Air Force Materials Laboratory
Wright-Patterson Air Force Base, Ohio

and

J. Taboada and Major B. R. Altschuler
USAF School of Aerospace Medicine
Brooks Air Force Base, Texas

PRECEDING PAGE BLANK-NOT FILMED

DIAMOND TURNING OF F-111 WINDSCREENS: FEASIBILITY STUDY PHASE I.

Theodore T. Saito, Ph.D. Major USAF
Air Force Materials Laboratory (LTE)
Wright-Patterson AFB OH 45433

J. Taboada, Ph.D.
Laser Effects Branch (RZL)
Radiation Sciences Division
USAF School of Aerospace Medicine
Brooks AFB TX 78235

B. R. Altschuler, D.D.S., Major, USAF
Dental Investigation Service
USAF School of Aerospace Medicine
Brooks AFB TX 78235

ABSTRACT

Diamond turning of optics is using a single point diamond tool on a precision lathe under precisely controlled machine and environmental conditions to fabricate an optical component. The technology has been used to make many high precision optics. The F-111 windscreen is in the shape of a frustrated right circular cone, a geometry compatible with diamond turning. Phase I of the feasibility study demonstrated the machinability and polishability of the F-111 windscreen material.

Two flat 15 cm square samples of the F-111 windscreen material were diamond turned and then polished. The diamond turning was performed on a Moore machine at Union Carbide's Y-12 plant. The Lawrence Livermore Laboratory polished the sample with lustralox plastic grade on polytex supreme. Extensive pre-machining and post-machining tests are described including the lateral shearing interferometric techniques developed by one of the authors. Optical distortion and haze were significantly reduced after machining and polishing.

Diamond turning of windscreens may offer attractive cost savings by reducing shrinkage during fabrication and allowing recycling of windscreens rejected because of excess haze. Diamond turning may also provide revolutionary optical designs to reduce distortion through decentering techniques. The plans for Phase II of the feasibility study, to machine and polish actual curved windscreen sections, will also be described.

PRECEDING PAGE BLANK-NOT FILMED

INTRODUCTION

The F-111 utilizes a layered plastic windscreen to give protection from bird strikes. These Bird Impact Resistance Transparencies (BIRT) have been installed and used in operational aircraft. The 8 August 1977 issue of Aviation Week reported, "The greatest problem faced by F-111 crews during peacetime training missions is the threat of bird strikes in the windshield area. Bird strikes have caused more F-111 accidents than all other causes combined. ... Most F-111's at Upper Heyford have been modified with a new, thicker, polycarbonate windshield, sufficiently strong to resist any bird that is not large enough to break the windshield frame."

The heavyweight windscreen is a composite of polycarbonates about 8.4 mm (0.25") thick with an interlayer about 0.76 mm (0.030") thick sandwiched between 6.4 mm (0.25") thick outside, and 2.0 mm (0.08") thick inside acrylics. The material we used for this study had three polycarbonate layers, four interlayers and was about 25 mm (1") thick. The purpose of the acrylic is to give the windscreen resistance to damage from abrasion from ground crew cleaning and other surface damage which could be inflicted more easily in the soft polycarbonate.

The windscreen is in the shape of a frustrated 5° oblique circular cone with the cone half angle of approximately 5°. The base of the cone has about an 85 cm radius, a 132 cm height, and at the top a radius of about 45 cm. If one assumes a radius at the top of the cone of 45.7 cm (18") and a circular arc whose length is 660 mm (26"), each section subtends about one-fourth of a circle.

The BIRT windscreen has created some problems. Optical Spectra reported August 1977 (p-17), "Because windscreens need to be slanted, curved and multilayered in order to provide good aerodynamic performance and birdstrike protection, they often produce optical problems adversely affecting the capabilities of the pilot. ...The ultimate aim is to develop more precise and demanding specifications for the fabrication of the windscreen."

Even if the windscreen was perfect, that is the windscreen was described by two concentric cones with perfectly straight sides, visible distortion would be present. These distortions are a result of the curvilinear geometry of the windscreen. Captain Rick Seid has investigated theoretically the reduction of distortion by moving the inside cone with respect to the outside cone (1). The "decentering" theoretically can reduce distortion.

Another problem is shrinkage and is costly in that of five F-111 windscreens that start production, only about one is accepted. With good molds, the shrinkage rejection can be reduced to 2:1. One of the reasons for rejecting the windscreens is the waviness in the surface. Even those windscreens accepted often have a significant degree of waviness.

This paper reports our efforts to utilize diamond turning and polishing to help solve some F-111 windscreen problems. Diamond turning is the use of a diamond tool on a precision lathe under very precisely controlled machine and environmental conditions to fabricate a finished optical component (2).

Since the shape of the F-111 windscreen is compatible with diamond turning we initiated Phase I of our feasibility study.

The objectives of Phase I were to investigate the machinability and compatibility of the F-111 acrylic with diamond turning and polishing and what type of improvement of optical properties such as transmission distortion, surface figure, and haze could be achieved. Since flat geometrics could be fixtured and machined easier than the frustrated cone geometry, we worked with flat pieces.

This paper will describe the test parts, premachining tests, diamond turning post machining tests, optical polishing, and post machining-polishing tests, and make conclusions while giving a brief outline of the planned Phase II of the effort.

TEST PART DESCRIPTION

The USAF School of Aerospace Medicine (USAFSAM) provided two flat pieces of F-111 windscreen material. Each sample was approximately 30 cm (12") square and had a small hole drilled in the surface of one corner to serve as a fiducial mark. A coordinate system was defined as follows. With the piece on a table with the fiducial mark up and in the lower left hand corner, the fiducial mark was defined as the origin of an x-y coordinate system such that the windscreen was in the positive x, positive y quadrant. Sample #1 was 27 mm thick and sample #2 was 24 mm thick.

PREMACHINING TESTS

Transmission optical distortion of the F-111 windscreen samples was measured by using a lateral shearing interferometric technique developed by Taboada, and reported elsewhere (3).

The optical system for distortion mapping is illustrated schematically in Figure 1. An Ar-ion laser beam (≃600 mW) is spatially filtered by (SF), apertured to 2 cm by (VAP1) and recollimated by lens L1. The collimated beam is received by the lens L2, L3 combination which introduces a slight $\pm$ power. Through the interference of the front and back reflections from a shearing plate (SP), a fringe pattern is generated that is directly related to the net lens power 1/L of the system (L1, sample, L2, L3) by the expression:

$$\frac{1}{L} = \frac{\lambda}{d\Delta x}$$

where λ (wavelength) = 514 nm; d, the shear; and Δx, the fringe spacing. A parameter proportional to $1/\Delta x$ is measured by sweeping the fringe pattern, with a rotating mirror (RMC), across a 100 μm resolution detector consisting of pinhole aperture (A), microscope (M), and photodiode (PD). The periodic fringe signal is low-frequency filtered by (EF), monitored with an oscilloscope (OSC), and frequency measured with a counter (FC). Aperture A and the test region are at approximate conjugate image planes. A photograph of the actual apparatus showing the sample under test is shown in Figure 2.

Calibration is obtained by placing known low-power lenses in the test region between L1 and L2. Remarkably linear response is observed, viz 0.00141 diopters/Hz ± 1% as shown in Figure 3. A two-dimensional rectilinear scan of a portion of a windscreen sample is illustrated in Figure 4.

A scan was made of the best portion of sample #1 and a plot of the distortion lines projected onto the vertical coordinate plane is shown in Figure 5. The observed distortion is slightly within standards for ophthalmic lenses, being approximately 0.06 diopters, but it could be detected visually by translating the sample across the line-of-sight.

Haze measurements were also made of the samples with a Gardner hazemeter. Haze was about 5% and transmission about 87%.

The samples were then sent to the Lawrence Livermore Laboratory (LLL) where three different interferometric systems were used to measure the flatness: the Davidson 127 mm (5") diameter interferometer, the 457 mm (18") diameter Fizeau interferometer and the 100 mm (4") diameter Zygo interferometer.

Davidsons Tests

The Davidson interferometer had a 127 mm (5") aperture utilizing the 546.1 nm (green) mercury line, and viewed the surface at a normal angle of incidence. Therefore each fringe represented equal contours separated by 273.1 nm (10.75 μ"). Figure 6 shows a typical result of flatness measurement on a 127 mm diameter circle located approximately at x = 15 mm and y = 65 mm. Fringes were only visible over a portion of the interferogram because the sample was so far out of flat. The fringes which are visible over about a 18 mm x 90 mm rectangular strip depicted astigmatic power and at least two saddle points. All four surfaces demonstrated similarly poor optical flatness.

Fizeau Tests

Tests were then made using the 460 mm (18") diameter Fizeau interferometer. Since the light source was a helium-neon laser operating at 632.8 nm each fringe was 316.4 nm (12.5 μ"). Figures 7 and 8 show the front surface interferograms of both the cabin and plane side of both samples, respectively. Attempts to measure the homogeneity of the windscreen samples with the Fizeau interferometer failed. Although it was possible to get fringes when using a flat 460 mm (18") diameter mirror, the fringes would vanish when the plastic was inserted between the mirror and the Fizeau splitter.

Zygo Tests

Attempts to measure the homogeneity of the plastic with the 100 mm (4") diameter Zygo interferometer also failed. Insertion of the windscreen between the interferometer and a flat mirror obliterated the fringes present from the flat mirror. The poor surface flatness caused the loss of fringes.

Polariscope Tests

The windscreen material was also tested in a Photo-Elastic Incorporated 305 mm (12") diameter Polariscope which utilized the 546 nm mercury line for a light source. The parts were surprisingly free of birefringence in the center. The corners and edge had more birefringence as shown in Figure 9. The rotational angle was measured at four different corners and the average values were used to calculate the retardance. The first piece had a value of 51 nm/cm and the second piece a value of 67 nm/cm.

DIAMOND TURNING

Diamond turning was performed by the Union Carbide's Y-12 plant at Oak Ridge, Tennessee, under USAFSAM Project Order 77-3. One of the two pieces was sawed into smaller samples approximately 15 cm (6") square. A suffix A will designate such portion of the sample. Sample 1-A was diamond turned on both sides using a vacuum chuck to hold the part in the center of the spindle. Sample 2-A was machined on center on one side and fly-cut on the other. Sample 2-A was held in a potting fixture. Y-12 had extreme difficulty in lapping a windscreen surface flat, a requirement for using the vacuum chuck.

Sample 2-A was mounted using rubber gel and allowed to cure over the weekend. It was then machined and checked immediately while still in the fixture. The flatness was checked with a Davidson interferometer. The flatness, shown in Figure 10, was then checked after 24 hours. The flatness deteriorated from 1.2 μm to 1.8 μm peak-valley in 24 hours. Removing the part from the fixture decreased the flatness by a factor of 10. Sample 2-A was then mounted in a frame to give it a more rigid support and was machined again.

Y-12 measured the surface finish with a two-beam microinterferometer. The surface of sample 2-A has a 38 nm (1.5 μ") peak-valley finish near the center of the side machined on center. This is as good a surface finish as many diamond turned copper mirrors.

POST MACHINING TESTS

The samples were then returned to LLL. We measured the samples on the 10 cm (4") diameter Zygo interferometer using a 632.8 nm laser beam. The surfaces were improved in flatness but still deviated grossly from perfect flatness as can be seen in Figure 11. Fringes could now be seen across the entire aperture. Furthermore not only could fringes be seen in transmission but also an interferogram could be taken of the surface flatness looking <u>through</u> the plastic. Sample 2-A had better flatness than sample 1-A.

While testing the sample we noticed that the flatness was drastically affected by light finger pressure on the sample.

Nomarski differential interference contrast photo-micrographs were taken of the surfaces, and are shown in Figure 12. Sample 2-A turned on center had the best surface.

OPTICAL POLISHING

Sample 1-A was optically polished by Mr. Phillip Baker of LLL in order to obtain better clarity. The plastic was mounted to an aluminum backer. Between the flat aluminum plate which served as the backer was a 6 mm (1/4") thick rubber pad. It was polished with Lustralox Plastic grade, in tap water, on polytex supreme. The polytex supreme was mounted on a conventionally machined piece of flat aluminum using the adhesive provided on the back of the polytex. The windscreen surface became flatter during the polishing. Furthermore no "springing" was noticed after unmounting the plastic. Mr. Baker felt that the piece could be polished flat to better than 5 rings (2 1/2 waves in the visible) in several hours. He was puzzled about the problems of obtaining flatness by diamond turning. In addition to polishing sample 1-A, Mr. Baker cleaned one surface of 2-A. The surface was cleaned using Lustralox Plastic Grade in water and a Kaydry paper cloth. Mr. Baker hypothesized that a residue from the cutting oil was causing the cloudy appearance.

POST MACHINING POLISHING TESTS

Sample 1-A was scanned as previously described for transmission optical distortion. The results are shown in Figure 13. The distortion was markedly improved with distortion excursions reduced from 0.06 diopters to less than 0.02 diopters in regions away from the edges. Distortion could no longer be detected visually. Haze was reduced from 5% as previously observed to about 1.6%.

CONCLUSIONS AND PHASE II STUDY

The F-111 windscreen material is compatible with the diamond turning and polishing process described in this paper. Furthermore the optical properties are significantly improved through this technique.

If this technique can be applied to the actual F-111 windscreen, there are several benefits which might occur. First, shrinkage might be reduced by diamond turning those windscreens rejected because of waviness.

Significant cost savings might be possible by recycling windscreens retired from the field because of excess haze. Windscreen rapidly deteriorate when not cleaned with the proper procedure. The cleaning scratches cause haze. These scratches can be removed with precision machining. At the "Transparent Window Workshop" held in Dayton, Ohio, on 22 September 1977, discussion regarding recycling windscreens indicated that no cost effective methods were known for the plastic windscreens.

Diamond turning can produce the "decentered" windscreens theoretically analyzed and developed by Seid (1). Therefore, a whole new family of windscreen designs may now become feasible.

In addition to diamond turning the windscreens, additional payoffs may develop from machining and polishing electroless nickel masters. Since

glass is presently not compatible with the diamond turning process, it might be possible to deposit electroless nickel on the masters and then diamond turn them. In addition to getting straighter masters, another dimension of windshield design emerges. If the fabrication process repeatedly introduces axisymmetric distortions into the windscreen, the distortions can be compensated by diamond turning. Furthermore, additional optical distortions might be reduced bu contouring the windscreen.

Phase II of this application study has been initiatied as a cooperative effort with the USAF (AF Materials Laboratory, AF Flight Dynamics Laboratory, and Aerospace Research Laboratory) and Y-12. Since the largest diamond turning machine available, the Ex-Cell-O at Y-12, is not capable of machining the entire F-111 windscreen, a section of the windscreen will be taken from two windscreens. After the Air Force makes initial tests, Y-12 will measure the windscreens' straightness and roundness and then diamond turn the conical shape with a single degree-of-freedom cut. A decentered windscreen will also be fabricated. Polishing will be performed and then post machining-polishing tests will be made. We look forward to the successful completion of Phase II and an application of diamond turning technology to revolutionize windscreen technology.

ACKNOWLEDGEMENT

We are grateful for the contributions of Mr. Phil Baker of LLL for polishing the sample, and Mr. Jones Arnold of Y-12 who diamond turned it. Mr. Warren Hays assisted in the polariscope measurements. We are thankful for helpful discussions with Captain Rick Seid regarding his decentering theory and results. Major Wayne Provines obtained the sample and contributed the haze measurements, Major Charles Hatsell and Dr. Ralph G. Allen, Chief, Laser Effects Branch (USAFSAM/RZL), were very helpful in coordinating this effort.

REFERENCES

1. Rick Seid. Private communication, 1977.

2. Saito, T. T. Machining of Optics: An Introduction. Appl. Phys. 14:1773 (1975), and also see Proceedings of the Society of Photo-Optical Instrumentation Engineers (SPIE), Vol. 93, Precision Machining of Optics SPIE, Bellingham, Washington (1976).

3. Taboada, J. Lateral Shearing Interferometric Technique for Transparency Distortion Analysis. Appl. Opt. 16:2603 (1977). See also Air Force Invention No. 12265, J. Taboada, inventor.

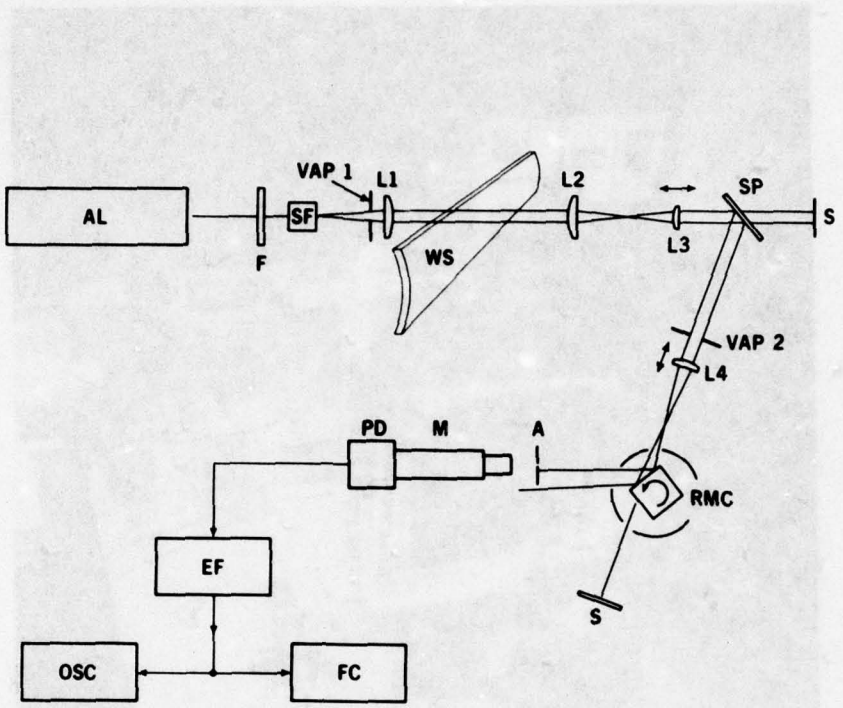


Figure 1. Optical arrangement for lateral shearing interferometer with digital electronic readout. A-100 μm pinhole aperture. AL-Argon Laser, 0.6 W, λ= 514 nm. EF-electronic bandpass filter. F-neutral density filter. FC-frequency counter, 3 sec sampling period. L1, L2, L3, L4-lenses. M-microscope. OSC-oscilloscope. PD-photodiode. RMC-rotating mirror cube, 1 rev/sec. S beam stops. SF-spatial filter, VAP1, VAP2-variable apertures. WS-windscreen sample. (From Reference 3.)

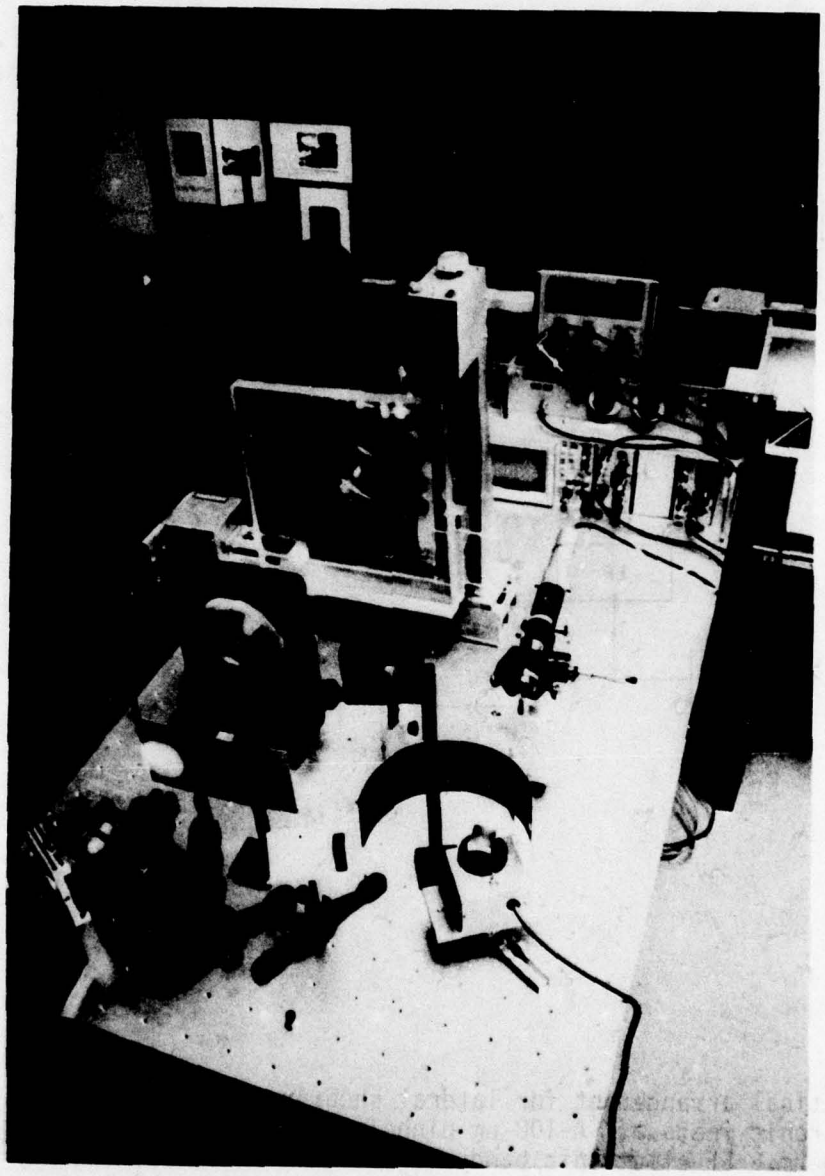


Figure 2. Photograph of actual laboratory apparatus.

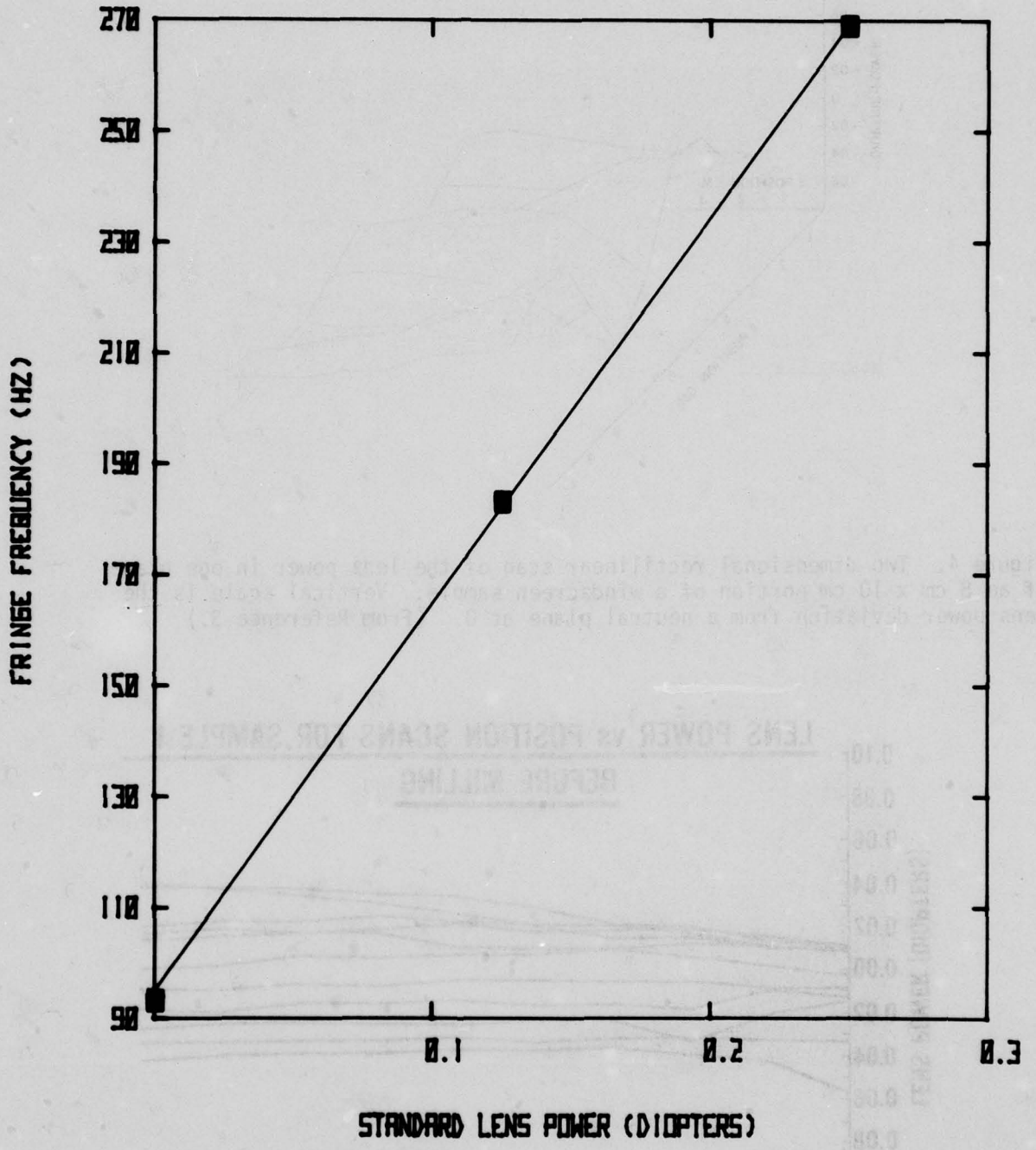


Figure 3. Interferometer readout calibration to standard ophthalmic lenses. (From Reference 3.)

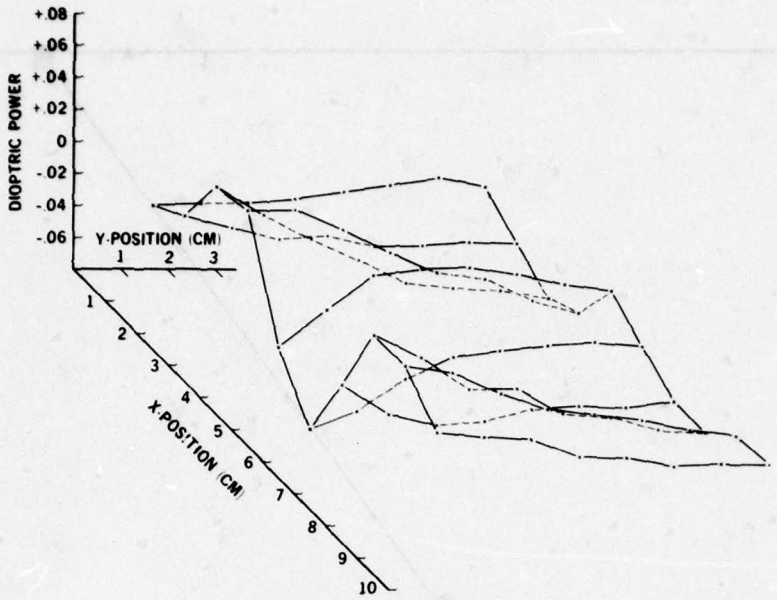


Figure 4. Two dimensional rectilinear scan of the lens power in one plane of an 8 cm x 10 cm portion of a windscreen sample. Vertical scale is the lens power deviation from a neutral plane at 0. (From Reference 3.)

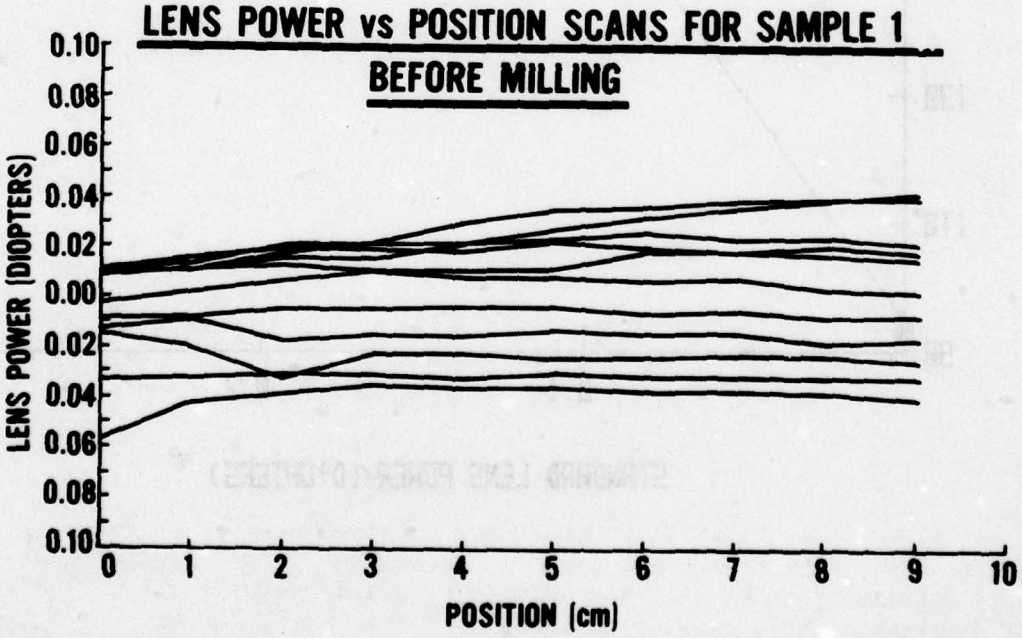


Figure 5. Lens power vs position scans for sample #1 before milling.

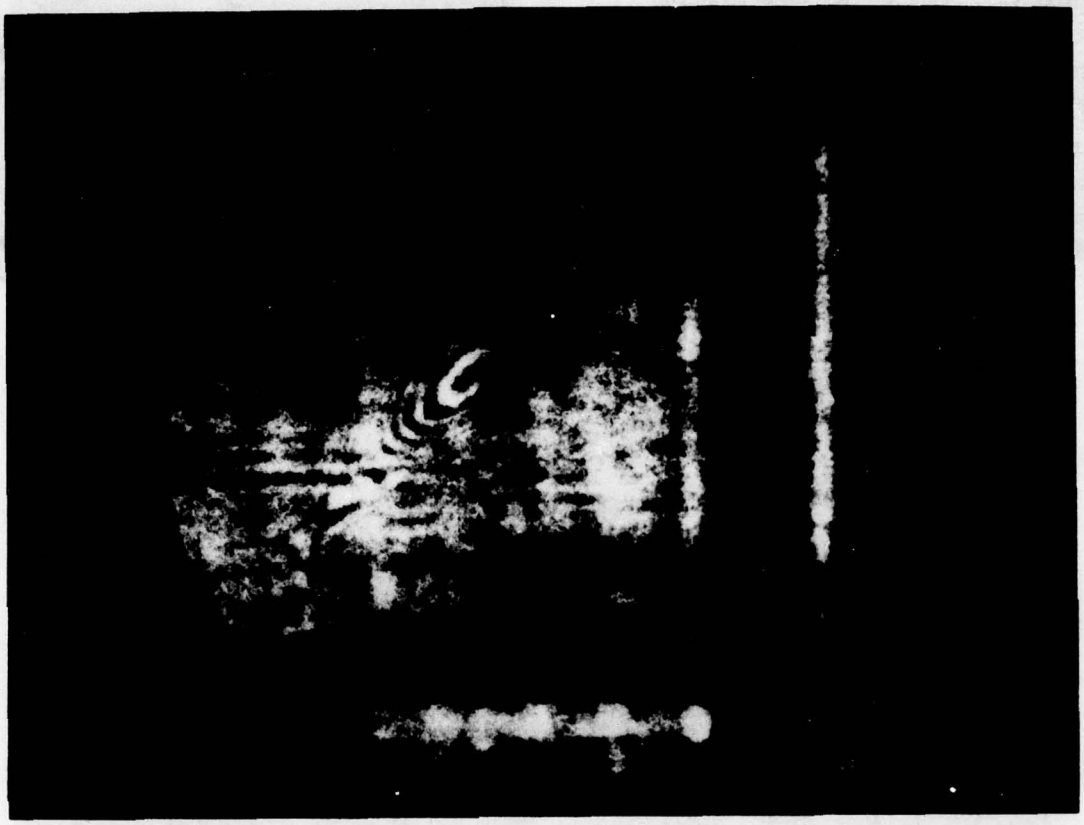


Figure 6. Flatness of Panel #2: This interferogram was taken on the Davidson interferometer (each fringe is 0.27 μm or 10.75μ") with the center of the 5" aperture located at the coordinates x = 0.5" and y = 2.5". The surface deviates grossly from being flat.

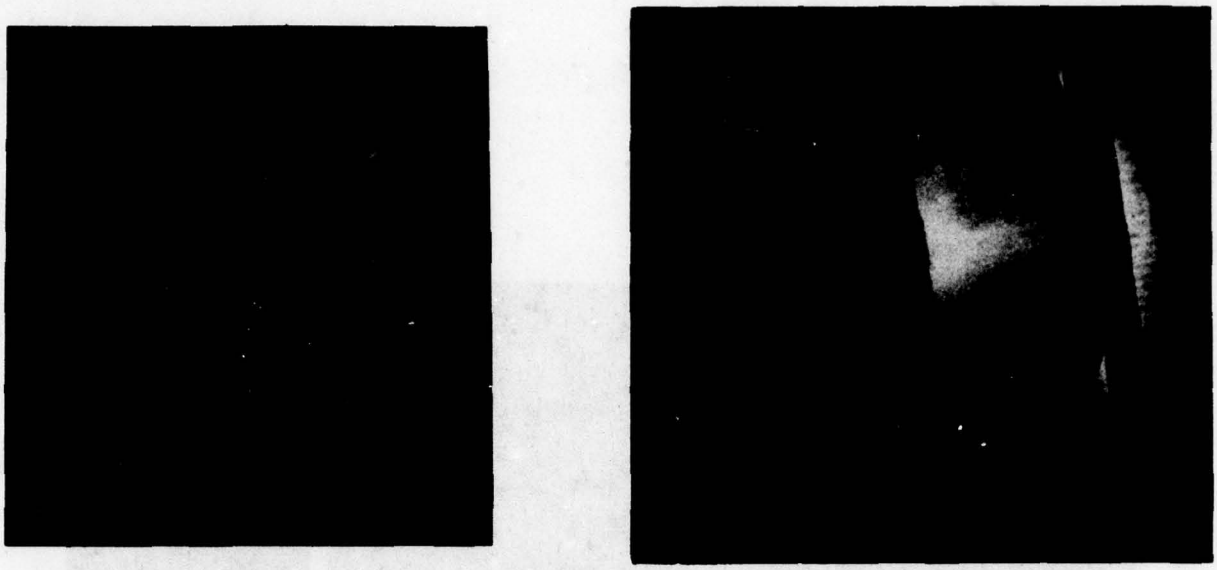


Figure 7. Fizeau interferograms of the cabin and plane side of sample #1.

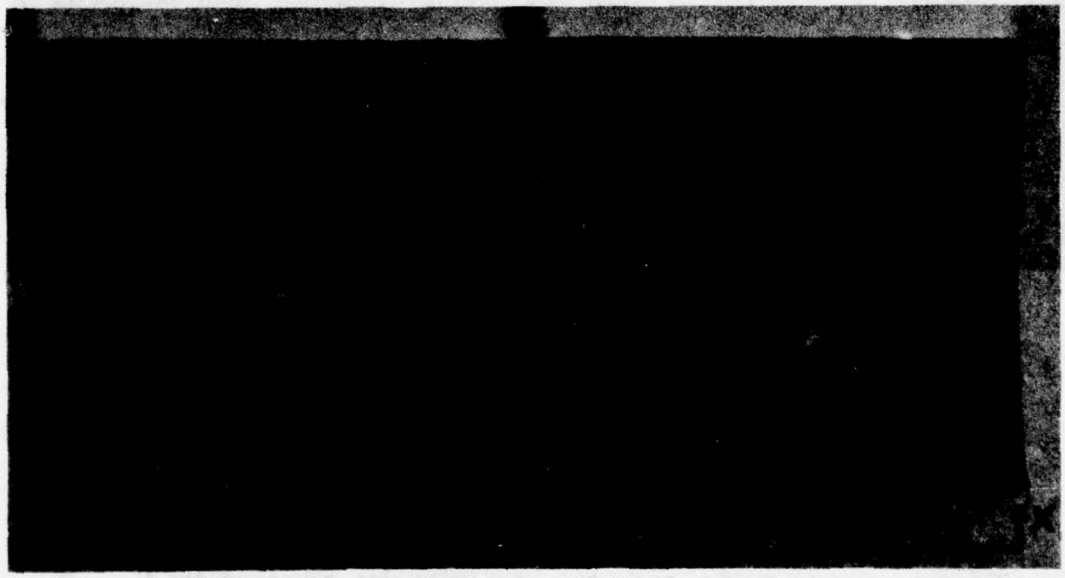


Figure 8. Fizeau interferograms of the cabin and plane side of sample #2.

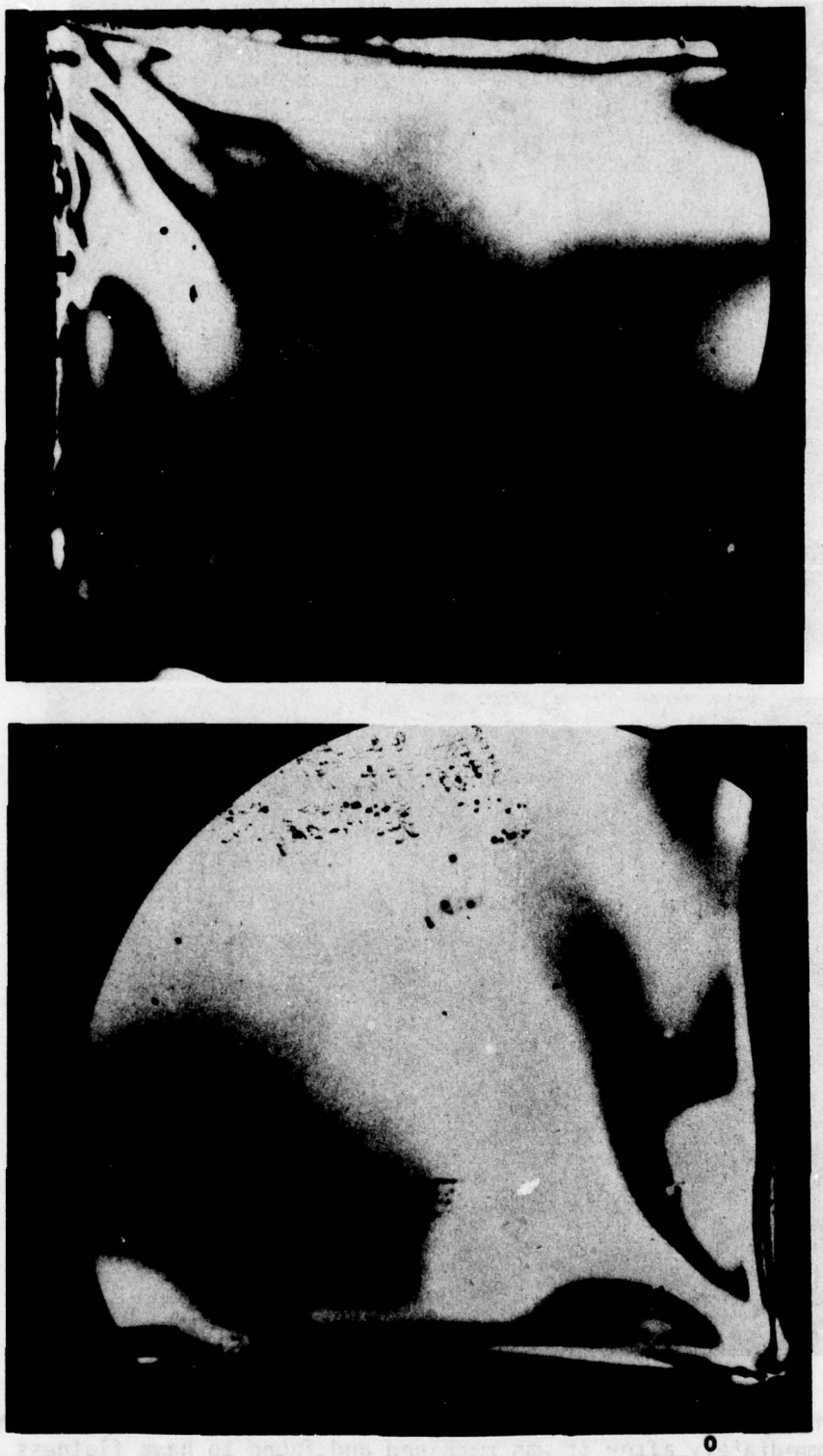


Figure 9. Photographs of polariscope investigation at 5461 Å of F-111 windscreen samples 1 and 2. Photographs show about a 23 cm x 23 cm section near the fiducial mark.

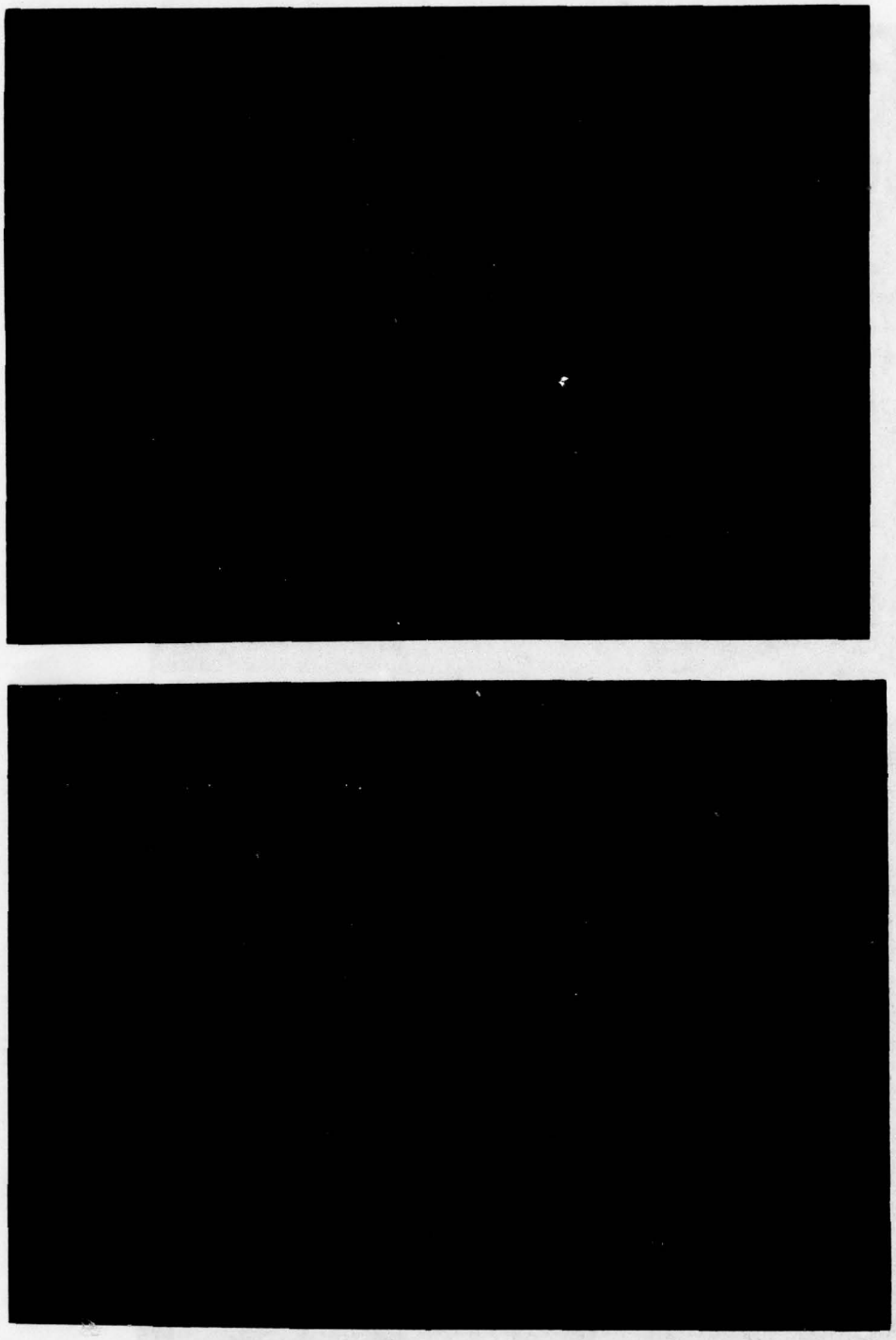


Figure 10. Stability test on sample 2-A. (a) The figure quality of the sample was inspected immediately after it was machined and found to have flatness errors of about 48μ". (b) The same surface was again inspected a day after it was machined and found to have flatness errors of about 72μ". (NOTE: This surface was remachined after the photographs were made.)

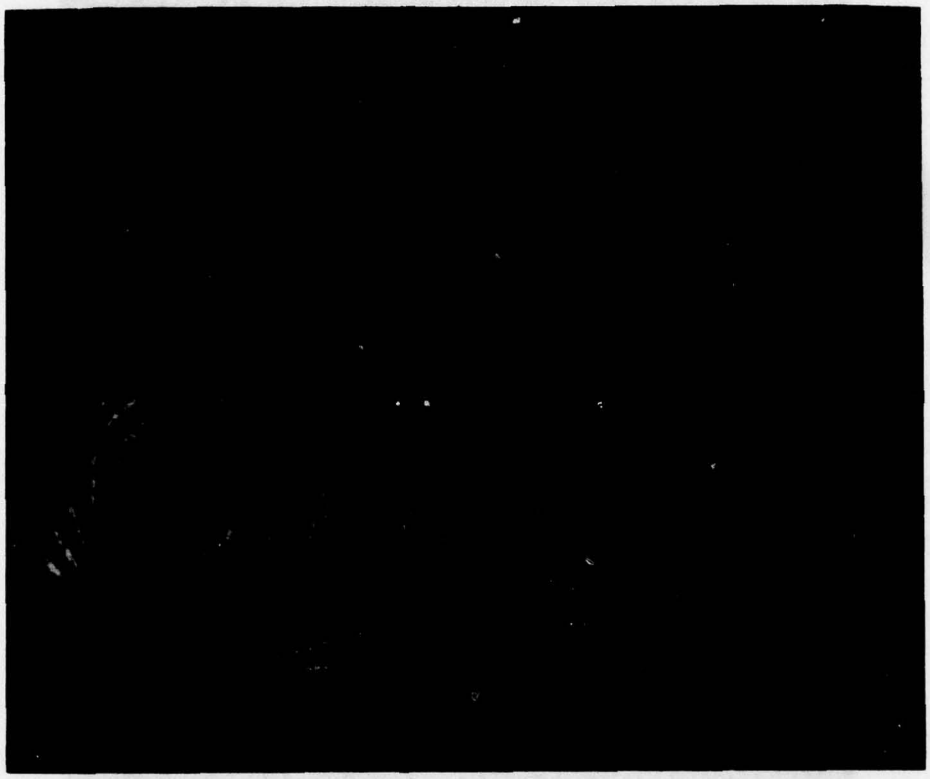


Figure 11. Zygo interferogram of sample 2-A, post machining.

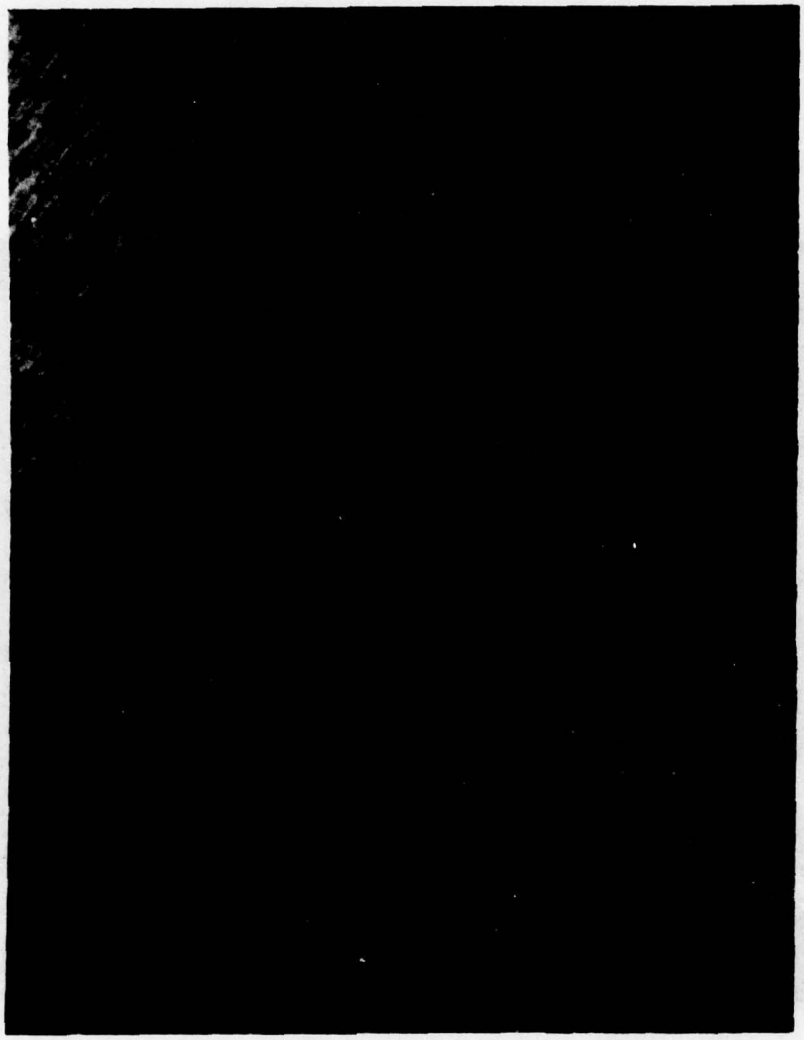


Figure 12. Nomarski differential interference contrast photo-micrograph of sample 1-A surface.

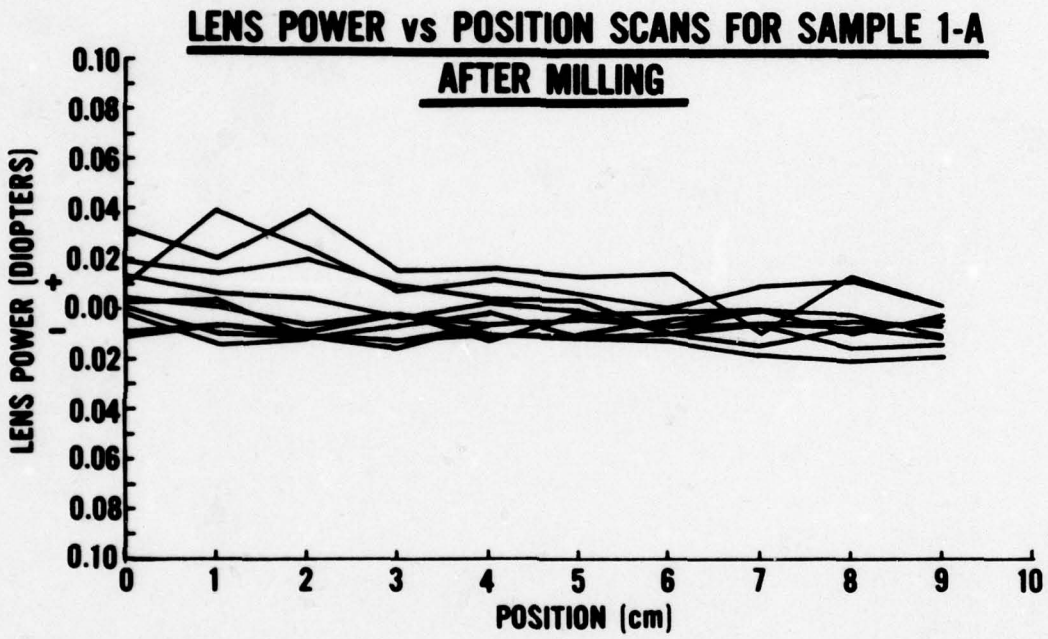


Figure 13. Lens power vs position scan for sample 1-A after machining and polishing.

SESSION VI

DESIGN AND PERFORMANCE - PART I

Chairman: M. R. Pollock
The Boeing Company
Materials Technology
Seattle, Washington

PRECEDING PAGE BLANK-NOT FILMED

BRITISH AIRWAYS EXPERIENCE WITH BOEING 747 COCKPIT AND CABIN WINDOWS

K. B. Armstrong
British Airways
Structures Group
London Airport, Hounslow, England

PRECEDING PAGE BLANK-NOT FILMED

BRITISH AIRWAYS EXPERIENCE

WITH BOEING 747 COCKPIT AND CABIN WINDOWS

Keith Armstrong
British Airways

ABSTRACT

British Airways, has had the benefit of considerable operational experience with the Boeing 747, and this paper highlights such experience as related to the various types of windows fitted to this aircraft. Similar experiences with other aircraft are also discussed.

Particular reference is made to the No. 1 windshield, and also No. 2 and No. 3 cockpit windows of the B.747, which have shown a tendency to develop in-plane cracking from the rebated edge of the outer ply after relatively few flight hours. Some suggestions are offered for possible solutions, in terms of raw material specification improvement and attention to detail design.

Similar proposals are made for cabin windows, which also exhibit a high replacement cost.

Suggestions are offered for improvements to the temperature control system, and a cockpit window warranty incentive scheme is outlined to provide encouragement to manufacturers to increase the life of their product concurrently with the size of their profits.

PRECEDING PAGE BLANK-NOT FILMED

SUMMARY

This paper covers the experience of British Airways, with all types of windows on the Boeing 747 but also refers to other types of aircraft. No. 1 windows of Sierracin and Triplex types are mentioned but we have insufficient experience with PPG windows to permit valid comment on this type.

Particular reference is made to the serious problems with the No. 2 and No. 3 windows of both Sierracin and Swedlow manufacture which suffered in-plane cracking from the rebated edge of the outer ply after very few flight hours. Suggestions are offered for possible solutions in terms of raw material specification improvements and attention to detail design. A small design change resulting in considerable improvement in window life is mentioned.

The high cost of cabin window replacement, due to in-plane cracking, is also dealt with, and similar solutions to those proposed for the No. 2 and No. 3 windows are recommended.

A warranty incentive scheme is suggested for the cockpit windows to provide encouragement to manufacturers to increase the life of their products and the size of their profits at the same time.

Some suggestions are offered for improvements to the temperature control system.

1.0. INTRODUCTION

British Airways have had service experience with No. 1 windows of Sierracin and Triplex manufacture and No. 2 and No. 3 windows of Sierracin and Swedlow manufacture. Cabin windows have almost entirely originated from Goodyear. To the best of my knowledge we have not yet fitted any PPG No. 1 windows and certainly we have no significant experience with this type.

Whilst the performance of our No. 1 windows appears to have followed the general trend of worldwide experience, we seem to have had more than our share of in-plane cracking problems with No. 2 and No. 3 windows.

We have had extensive in-plane cracking problems with outer cabin windows, and a vast amount of seal leakage and bowing of cabin windows, both inner and outer, resulting in the inner and outer panes touching each other. The in-plane cracking is largely attributed to water absorption at the window edge and a lack of any clamping pressure with this particular design.

Crazing remains an ever present problem and a frequent cause of window removal. We are far from satisfied with the existing specifications MIL-P-8184 and MIL-P-25690. It is my view that these specifications could and should be more detailed and that better materials could be produced.

This could be done either by an improvement of the specification in terms of mechanical properties, leaving the raw material manufacturers the same compounding and treatment freedom they have at present, or by specifying the material and its treatment in more detail as is usually done with a metallic alloy. In the metal case it is more usual to specify alloy content, treatment, and also mechanical properties. Because stretched acrylic materials are required for a wide variety of purposes it might be helpful to specify several types. This would take account of the fact that fracture toughness may be reduced in order to achieve a higher reversion temperature. A grading system related to usage could provide more effective materials for particular purposes.

2.0. NO. 1 WINDOWS

2.1. SIERRACIN

Originally only the Sierracin type was available and the performance of the early versions was poor. As a result of a vast development effort by Sierracin on the window itself and a considerable number of modifications to the window heat controller, these windows now have a good performance and one window fitted to a British Airways aircraft has exceeded the target life of 10,000 hours. The basic difficulty of this window is the provision of a heating film and interlayer material that can tolerate the thermal expansion coefficient difference between the main acrylic plies and the outer glass.

These difficulties have been overcome to the point where the Sierracin window is performing well and a new heating film and interlayer are expected to result in further significant improvements.

2.2. TRIPLEX

Since the Sierracin window was originally designed by Boeing, at a time when the weight of glass windows was excessive, there have been considerable developments in glass technology and both Triplex and PPG are now able to offer windows only slightly heavier than the original acrylic design.

Because the main plies are glass and the outer plies are also glass, the thermal expansion problem is inherently less with the all-glass windows and their chance of achieving longer lives should, in theory, be greater. They have their own problems associated with the bending of thick plates of glass to the required optical quality.

Triplex were the first to arrive at the 10,000 hour milestone and are, so far, the only manufacturer to achieve 18,000 hours with their window Serial T.1006 fitted to British Airways aircraft G-AWNO.

Many other Triplex windows have since crossed the 10,000 hour mark or are coming close to it. The following hours had been achieved at 31st December, 1977, (Table 1).

TABLE 1 HIGH LIFE TRIPLEX WINDOWS

DETAILS OF WINDSHIELDS WHICH HAVE FLOWN MORE THAN 10,000 HOURS

AIRLINE	AIRCRAFT	W/S SERIAL NO.	HOURS FLOWN AT 31.10.77	ESTIMATED HOURS FLOWN AT 31.12.77	COMMENTS
BA	G-AWNO	T.1006	16,824	17,500	B747 Fleet Leader.
CP	C-FCRB	T.1012	13,928	14,500	
CP	C-FCRB	T.1043	13,928	14,500	
JL	JA9123	T.1046	13,459	14,000	
SB	N901SW	T.1044	13,079	13,600	
AC	CF-TOC	T.1039	12,965	13,500	
SQ	9V-SQC	T.1040	12,074	12,600	
AF	N18815	T.1052	11,346	11,900	
JL	JA8114	T.1059	11,183	11,700	
JL	JA8113	T.1053	10,988	11,500	
BA	G-AWNA	T.1042	10,215	10,800	
JL	JA8122	T.1028	9,806	10,400	
CP	C-FCRD	T.1085	9,802	10,400	
AC	C-GAGA	T.1111	9,407	10,000	
NW	N611US	T.1087	9,332	10,170	
JL	JA8123	T.1079	12,242		Removed
KE	N749WA	T.1032	11,472		Removed

SEASONAL FAILURE PROBLEMS

The overall failure pattern worldwide shows a peak in the failure rate during the northern hemisphere cold period each year. See Boeing graph (Fig. 1). British Airways had a particularly bad patch in January/February 1976, but this failure peak has occurred every January since 747 operations began. It seems to apply more to the acrylic type windows, as one would expect, from the differences in thermal expansion coefficients mentioned earlier. A list of failures is given in Table 2.

2.3. WEATHER SEALS

Maintenance of weather seals has been found to be important, and the Maintenance Manual calls for inspection of window sealing compound and renewal as required. The British Airways Manual emphasizes the need to maintain the weather seals to avoid moisture ingress.

2.4. STATE-OF-THE-ART

Whilst the operators always seek longer life, lower price, and lower maintenance costs. I think that it would be fair to say that, if 10,000 hours could be achieved as an average life, this would be acceptable. There are no air-safety problems with No. 1 windows. Development needs to continue, but the target is in sight.

It is possible that an increase in ramp warmup time, together with a controlled rate of cooling at the end of each flight, could increase the life of the No. 1 windows. The present temperature controllers themselves seem to have reached a fairly reliable state after a number of modifications.

A purchasing scheme that might be of interest is attached as Appendix A.

3.0. NO. 2 & NO. 3 WINDOWS

These caused considerable concern during 1975/76. A number cracked in service at very low hours and more than half of these were reported by British Airways. (See Table 3). Originally this defect was attributed to the cutting of a groove in the rebate of the outer ply by a seal flash trim tool. However, this may not have been the only cause, for two reasons;

1. Serial No. 840 was made after the seal flash trim tool problem was corrected and it cracked in service.

2. One window made by Swedlow also cracked in service with British Airways.

These problems were disturbing because in several cases the majority of the outer ply departed in-flight. When this type of failure occurred it usually did so at very low hours. A large number of windows have been removed at 12,000 hours and upwards with no defects other than crazing and bubbling, whereas windows that failed by cracking did so in as little as 461 hours. Serial No. 187 was inspected by Mr. D. R. Scott, of British Airways, only 4 days before failure. He is a Development Engineer with a fair amount of experience on 747 windows and he studied the window carefully because of its low Serial Number. He was looking for this type of cracking and found none. 4 days later it failed. This made containment of the problem by inspection impossible except by a preflight inspection. Even this may be inadequate as the crew report indicated that it was noticed on the descent, implying that it had not been noticed at the start of the flight. (See Photo, Fig. 2).

For these reasons there was a greater safety problem with No. 2 and No. 3 windows and effort was directed to finding the cause of the in-plane cracking failures. The most likely causes seemed to be residual stresses due to bad machining or solvent penetration into the rebate radius due to flying windows, which had been replaced in service, before the sealant had fully cured. The latter cause was known to exist and the solution proposed was to paint the machined edges of existing windows held in Stores with PR 1422 and to recommend that the prime manufacturer should amend his drawings to call for a similar treatment. This action has been taken and no further in-flight failures have occurred in a period of 18 months.

The in-plane cracking may have been aggravated by the rather sharp radius in the rebate coupled with a rebate cut to more than half of the outerply thickness. Rebating beyond half thickness is not considered good practice. However, only the radius could be changed at this stage, the other points could only be noted for avoidance in new designs.

It is worth noting that the in-plane cracking failure almost always occurred from the temperature sensor edge. One window showed cracking on the opposite edge as well and both these edges contain the bus-bars. No failures have so far been found along the shorter edges. Only one window showed some in-plane cracking on the inner ply. It is possible that the problem is related to the local heat increase at the bus-bars and could also relate to the moisture content of the acrylic at the time of installation. A number of the failures are known to have been in Stores for several years. (See Figure 4).

No. 2 and No. 3 windows also suffer bubbling fairly frequently, and this problem also applies to both Sierracin and Swedlow windows. (See Photo Fig. 3). The interlayer material seems very soft and it would be interesting to know if the problem is one of adhesion, or of plasticizer migration in the interlayer. It could also be due to air entrapment or more likely due to gases produced by overheating. Temperature has to be sensed by surface contact through a 0.1 in thickness of interlayer, which has considerable thermal lag. Temperature overshoots could easily occur in this system and are considered to be a likely cause of the problem. Improvements in the temperature control system for No. 2 and No. 3 windows would be helpful, they could probably solve the bubbling problem.

Bubbling remains a continuing nuisance and the cause of a number of removals which often occur outside the warranty period but before crazing becomes a problem.

4.0. CABIN WINDOWS

We have a considerable number of windows, sometimes 10 to 20 in one aircraft and in extreme cases as many as 80 which have leaking seals and suffer from condensation. This results in water absorption into the inner face of the outer pane and the outer face of the middle pane. Boththese faces expand, causing the outer pane to bow inwards and the inner pane to bow outwards. Because they are mounted only 1/4 in apart in a common seal, they frequently touch as a result of absorbed condensation. (See Figs 5A and 5B). 80 window replacements cost 16,000 dollars plus labour costs.

Although new seals, (65B-07671-4), have been available for some time, they are only changed when condensation makes it necessary. On G-BDPV, 43 windows were bowed with condensation when only 2,000 hours from new. Inspection of seals on two sample windows showed wrinkles due to incorrect installation. Both windows had nicotine stains and were severely bent due to water absorption. Neither of these windows showed in-plane cracking, but the service life of 2,022 hours was probably too short for this to occur, and in any case the windows seemed to have become increasingly wet without having dried out at any time. It is during the drying process that the damaging tensile stresses in the transverse direction occur.

British Aerospace have found that if samples of stretched acrylic are placed in an environment of 95% R.H. and 45°C for several weeks and then dried in an air circulating oven at 70°C, interlaminar separation will occur during the drying process.

The wet condition of these windows occurred although the new type seal 65B-07671-4 was fitted in both cases. The problem has been identified as creep of the seal in service. Although the -4 seal is better than the original -3, further redesign has been found necessary. Another new seal 65B-07671-5 has been produced and it is hoped that this design will solve the leakage problem. The -5 seal has been subjected to extensive testing by Boeing. British Airways aircraft G-BDXE, delivered on 28th March, 1978, is our first to be fitted with -5 seals on the production line.

Associated with the moisture from the condensation is the frequent occurrence of in-plane cracking at the edge of cabin windows, which often occurs before a window would be removed for crazing. Such cracking inevitably renders rework of the windows impossible. (See Fig. 6).

There is clearly a connection between water and in-plane cracking whatever other factors are involved. Edge sealing of cabin windows with PR 1422 or a similar material could well be an advantage. Damage is probably due to repeated wetting and drying. Drying of the outer edge resulting in tensile stresses in the transverse direction is considered more dangerous than wetting. British Airways apply PR. 1422 to the edges of re-worked windows and although very few have been removed none have yet been found with in-plane cracking.

A possible source of a solution is to improve the transverse properties of stretched acrylic, but here a balance has to be struck between strength and brittleness when an increase in cross-link intensity is being considered. A transverse strength in excess of 1/5 of the longitudinal strength results in cracks running out-of-plane. (Ref. 1). It is essential that cracks run in-plane because this prevents catastrophic failure and allows plenty of time for delamination to be discovered during maintenance checks. Experience with passenger cabin windows has been that delamination does proceed in-plane whereas with the thicker No. 2 and No. 3 windows (para 3.0) it runs catastrophically out-of-plane.

It is also of interest that design is of fundamental importance to the occurrence of in-plane cracking. For example, the DC.8 has its inner and outer panes bolted together and with the clamping force involved no in-plane cracking has ever occurred. The DC.10 has a similar design to the 747 and considerable in-plane cracking has already been found. Whilst this can be borne in mind for future design, it would be a very expensive solution on existing aircraft. Nevertheless, improved design is possible as a solution to the problem.

Crazing is another cause of removal, which could be reduced by incorporating new and more effective ultraviolet stabilizers in larger quantities. This problem is due to the greater intensity of radiation in the 290- to 310- nanometer band at the high cruise altitude of long range aircraft. See Figure 7, (Rohm and Haas). Because this band of radiation is cut off by the atmosphere at ground level, out-door exposure tests are not very helpful for the assessment of the life of acrylic windows used at high altitude. Water absorption also encourages crazing. The threshold crazing stress is reported to be reduced by 1,000 p.s.i. for every 1% of water absorbed. It is important, therefore, to produce materials with the lowest practicable water absorption.

5.0. CONCLUSIONS

1. The No. 1 window no longer presents any safety problems and an MTBR of 10,000 hours seems probable.

2. The No. 2 and No. 3 windows were a cause of great concern when the first version of this report was written in November, 1976. The in-plane cracking problem on these windows appears to have been solved but the following points should be borne in mind for future design.

(a) Build the acrylic window into a metal frame so that the sealant can cure when the acrylic is free of stress.

(b) Design the width of the sealant gap to allow for expansion and contraction of the window within the strain limits of the sealant. This would reduce sealant failure and consequent moisture ingress.

(c) Rebates should be less than half the panel thickness in depth.

(d) A large machined radius is beneficial.

(e) Use Nylon or Terylene monofilament sealant removal cords.

(f) Polish machined edges if a safe and beneficial method can be found.

(g) Seal machined edges on all stretched acrylic parts.

(h) Use the best possible machining techniques.

(i) Keep torque on attachment bolts to a minimum.

(j) Move thermostat to a lower stress area, (e.g. a corner), and by punching out some of the layers of PVB bring it closer to the heating film.

(k) If cracks are to continue in-plane, and not run out at the edge, the transverse strength of stretched acrylic must not exceed 1/5 of the longitudinal strength, (Page 114 Ref. 1). Tests to cover this should be included in the stretched acrylic specification. Each sheet thickness needs to be tested because different thicknesses can have different transverse properties. This leads to the conclusion that in-plane cracking must be prevented by design and machining techniques (methods a to d and f to h above), rather than by improvement of the transverse properties. In fact the problem appears to be due to thick stretched acrylic (5/8") having better transverse properties than thin stretched acrylic. (In-plane cracks in cabin windows (3/8" thick) remain in-plane).

(l) No. 2 and No. 3 windows also suffer from surface crazing and improvements in resistance to crazing would help to prolong the life of some windows. This might be achieved by the addition of one of the better U/V stabilisers now on the market, or by any additives that could reduce water absorption.

3. Cabin windows are suffering from crazing and in-plane cracking to an unacceptable degree.

Solutions could be in the following areas;

(a) Craze resistance could be improved by;

(i) The use of better U/V stabilisers. MIL-P-8184 could specify a reduced U/V transmittance.

(ii) Possibly by the use of additives to reduce water absorption.

(iii) Better control of the cross-link density.

(b) In-plane cracking can only be prevented by design if craze resistance is to remain unaffected. The possibilities for improvement are;

(i) Sealing of the edge.

(ii) Clamping of the edge.

(iii) The use of leakproof seals.

(iv) The use of seals bonded to the window with a suitable adhesive.

4. Improved quality control tests are required because materials to the present specifications appear to have widely differing water absorption and craze resistance characteristics.

Effort needs to be devoted to solving the bubbling problem with the No. 2 and No. 3 cockpit windows.

The cost of spares could also be reduced by an arrangement whereby Boeing received a royalty for their design and development work from the window or other component manufacturer. Such an arrangement could save duplication of storage, inspection, and tied-up capital and hence permit a significant reduction in prices to the airlines.

The solution of the crazing and the in-plane cracking on cabin windows is an urgent requirement, especially at a time when the economic position of many airlines is not good and the high running cost of aircraft only aggravates the situation. The cost of cabin window replacement and refurbishing could easily be halved by immediate application of the latest polymer technology and, where necessary, the use of alternative designs, improved sealant, and suitable edge sealing at the production stage.

A vital step to achieve the aim is the rewriting of MIL-P-8184 and MIL-P-25690 to call for the necessary molecular structure, treatment, and ultraviolet stabilizer content that will give the properties required (Ref. 2). Improved quality control tests may also be necessary, in particular to ensure that the required cross-link density and water absorption limits are achieved.

MIL-P-8184 should state the chemical composition, curing and heat treatment conditions and the mechanical properties required of the basic "as cast" material. Several types with different degrees of cross-linking could be specified. MIL-P-25690 should, ideally, specify several types of stretched acrylic, heat treated and stretched to meet particular needs, e.g. a high reversion temperature is not required for passenger cabin windows. The most suitable type could then be chosen for each particular end use. (See Appendix B).

Improved specifications are a matter of urgency because until they are written, the raw material manufacturers will not have the required basis to work from. Once this has been done, it will be up to the aircraft manufacturers and operators to specify the use of the correct grades of the improved materials.

It is within the capability of the present technology to produce an improved acrylic material, and it is up to us all to see that it is defined and specified as soon as possible.

RECOMMENDATIONS

Further research is required in the following areas;

1. The compilation of a Design Manual to enable the best possible use to be made of acrylic materials. Examples should be quoted of previous errors in design and how they may be avoided.

2. The evaluation of the mechanical properties required of acrylics for particular end uses to enable the number of types required to be specified and their properties to be tabulated.

3. The effect of water content on stretched acrylics needs to be studied in depth to enable the effects on long term properties to be predicted. (Ref. 3). A test after water immersion needs to be included in the tensile tests for Specification approval.

4. The effect of U/V radiation on stretched acrylic needs to be studied in a chamber capable of simulating the range of atmospheric pressure and humidity experienced in long range airline flying. Such results should be compared with the usual outdoor weathering tests.

REFERENCES

1. The New Science of Strong Materials, J. E Gordon, Penguin Books (1968).

2. "Fracture Mechanics of Stress Cracking and Crazing", L. J. Broutman, SPE Journal, March, 1965.

3. Anisotropic Fracture of a Hot-Stretched Acrylic Thermoplastic, Keith Williams, published in Fracture 1977, Vol. 3, ICF 4, Waterloo, Canada, June 19 24, 1977.

APPENDIX A
LIFE EXTENSION–INCENTIVE WARRANTY SCHEME

There would appear to be a need for this sort of scheme on certain aircraft parts such as cockpit windows, although similar schemes could profitably be applied to any expensive short-life components.

The object of the scheme is to provide the manufacturer with a clear financial incentive to reduce the COST of his components to the operator. At this point I would like to introduce the broad and apparently reactionary concept that *price is unimportant and cost is all important.* What matters is *COST* which is *price/life* or some refinement of this, such as the formula below originally used for floor panels.

$$C = \frac{P e^{KL}}{L} \pm xw \qquad (1)$$

where

- C = cost/year
- P = price
- L = life
- K = rate of interest expressed as a decimal
- x = cash value of weight in £/lb
- w = weight increase or decrease about a given datum
- e = exponential function (2.718)

The problem has to be looked at from both sides. In their own ways, both manufacturer and operator are in business to make a profit, and this needs to be appreciated and is simply summed up by the saying, "No deal is a good deal unless both sides make a profit." To return to aircraft cockpit windows, the *PRICE* is frightening enough to the operator but the *COST* can be more so, although it may be less obvious. The manufacturer wants to make a large number of items to spread his development and tooling costs, and the operator wants to buy as small a number as possible. The operator wants the manufacturer to spend money on development to improve the life of the product and thereby *reduce* his sales and profits. Clearly once the life equals the warranty period life has no incentive whatever to do this. The purpose of this note is to show that by offering the manufacturer a *higher price* for a *longer life* the operator can obtain a *lower cost* for himself. In this way both sides can be satisfied.

LIFE INCENTIVE PRICING FORMULA

$C = \frac{PT}{LT}$ = cost to the operator which he seeks to minimize

$$PT = \left(\frac{PS \cdot LT}{LD}\right) \qquad LT \geq LD \text{ Applicable Within Warranty Period} \qquad (2)$$

$$PT = PS\left[1 + \left(\frac{LT}{LD} - 1\right) \cdot M\left(1 \ \frac{PC}{PS}\right)\right] \qquad LT > LD \text{ Applicable When LT Exceeds Warranty Period} \qquad (3)$$

where

PS = listed selling price
PC = cost price
PT = total price
L = life (years)
M = bonus rate (say 0.5)
C = cost to operator per year
LD = life (datum)
LT = life (total)

For the purpose of graphs (figs. A-1, A-2, and A-3) to follow, assume

M = 0.5
LT = 1 to 4 years
PS = 1
PC = 0.8, 0.9
LD = 1

CALCULATIONS FOR FORMULAS (2) AND (3)

The first formula (2) applies up to the end of the warranty period and just states that the operator pays proportionally to the life obtained.

The second formula (3) applies beyond the warranty period and defines the advantage to the manufacturer of increasing the life of his product. Obviously the value of the bonus rate M would be negotiable and the profit margin would have to be declared and seen to be reasonable. The value of M could be chosen, depending on complexity of the product and cost of tooling, to provide an adequate development incentive to the manufacturer.

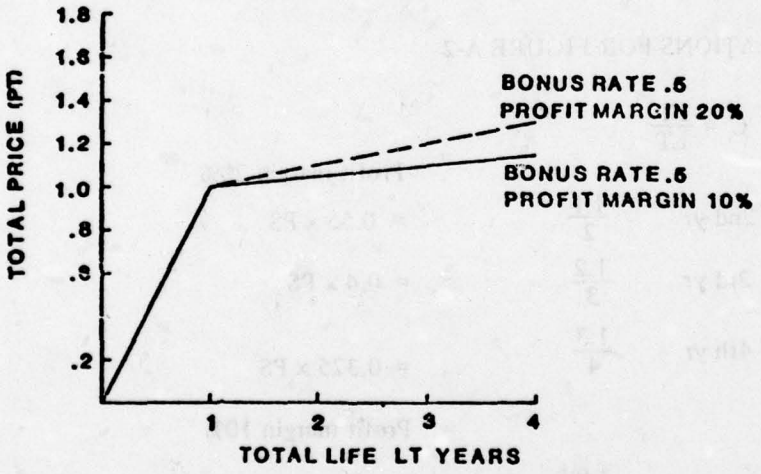


FIGURE A-1 - VARIATION OF TOTAL PRICE TO OPERATOR

CALCULATIONS FOR FIGURE A-1

$$PT = PS \left[1 + \left(\frac{LT}{LD} - 1\right) \quad M \left(1 - \frac{PC}{PS}\right)\right]$$

at end of	2nd yr 1 + (1 x 0.5 x 0.2)	= 1.1 x PS	
	3rd yr 1 + (2 x 0.5 x 0.2)	= 1.2 x PS	Profit margin 20%
	4th yr 1 + (3 x 0.5 x 0.2)	= 1.3 x PS	
	2nd yr	= 1.05 x PS	
	3rd yr	= 1.1 x PS	Profit margin 10%
	4th yr	= 1.15 x PS	

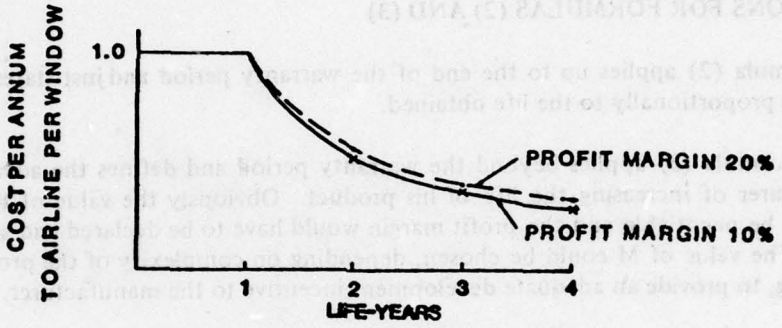


FIGURE A-2 COST TO OPERATOR

CALCULATIONS FOR FIGURE A-2

$$C = \frac{PT}{LT}$$

Profit margin 20%

at end of 2nd yr	$\frac{1.1}{2}$	= 0.55 x PS
3rd yr	$\frac{1.2}{3}$	= 0.4 x PS
4th yr	$\frac{1.3}{4}$	= 0.325 x PS

Profit margin 10%

$\frac{1.05}{2}$	= 0.525 x PS
$\frac{1.1}{3}$	= 0.367 x PS
$\frac{1.15}{4}$	= 0.288 x PS

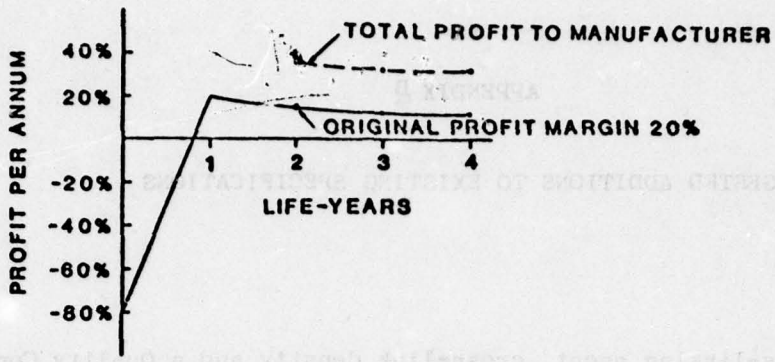


FIGURE A-3 PROFIT TO MANUFACTURER

CALCULATIONS FOR FIGURE A-3
20% original profit margin
Profit per annum

1st yr	20%	
2nd yr	$\frac{20\% + 1 \times 10\%}{2}$	= 15%
3rd yr	$\frac{20\% + 2 \times 10\%}{3}$	= 13.35%
4th yr	$\frac{20\% + 3 \times 10\%}{4}$	= 12.5%

At the end of the second year and after, the manufacturer, having reutilized his equipment and labor in the manufacture of other lines, can make a total profit almost twice his original and from figure A-2 it can be seen that the operator can more than halve his *cost*. A scheme of this type is clearly capable of arrangement to give real benefits to both sides. All costs and savings have not been included in the interests of simplicity; e.g., the cost of tooling has been omitted because this is sometimes amortized over the initial production run and not necessarily loaded onto later spares. Likewise, additional savings to the operator such as reduced stockholdings and service delays have also been omitted.

CONCLUSION

It is not thought that the incentive scheme proposed will apply to more than a few high-cost short-life items. Nevertheless, it could assist in bringing about real improvements in some areas and is submitted for consideration and discussion.

APPENDIX B

SUGGESTED ADDITIONS TO EXISTING SPECIFICATIONS

MIL-P-8184

1. Specify cross-linking agent, cross-link density and a Quality Control Test.
2. State catalyst used for polymerisation.
3. Type of U/V stabiliser and quantity required.
4. Type of water repellent additive and quantity required.
5. Artificial weathering test using 290-310 nM U/V.
5. Water content at which mechanical properties are to be measured.
6. List a number of types for different end uses with appropriate cross-link densities.

MIL-P-25690

1. List a number of types for different end uses and specify properties required of each type.
2. Specify percentage stretch for each type.
3. Define a ratio between transverse and longitudinal strength which will ensure that in-plane cracks run in-plane.
4. Specify water content at which mechanical properties are tested.
5. Add Quality Control Checks for 1. and 2.
6. Reduce U/V transmittance 50%.
7. Add artificial weathering tests using 290-310 nM U/V.

TABLE 2 - NO. 1 WINDOW. LIST OF FAILURES

DATE OF FIT	DATE OF REMOVAL	A/C	DEPART STATION	ARRIVAL STATION	HOURS FLOWN	BRAKE LNDGS	CAUSE/TYPE OF FAILURE	REMARKS	INCIDENT RPT. REF.
	11-5-71	NC	Local Test Flight		Not Rec.	Not Rec.	Shattered	Low level positioning for approach.	EEA.S.4.10111
	21-3-72	NA	JFK	JFK	Not Rec.	Not Rec.	2 loud bangs shattered	A/C returned to New York. OAT not recorded altitude 37,000 ft.	EEA.S.4.11128 1-10A022
	25-12-72	NH	BEIRUT	BEIRUT	4508	1081	Shattered	OAT not recorded.	Unreferenced. EEA.S.4.12267
	16-1-73	NB	LHR	MIAMI	4407	Not Rec.	Delaminat-ion	OAT - 55°C	EEA.S.4.12265 MIA.158L
	21-1-73	NK	LHR	JFK	3412	Not Rec.	Loud bang severe delam.	OAT - 12°C	EEA.S.4.12342 1-10A-013
	22-1-73	NI	FRANK-FURT	BEIRUT	2917	Not Rec.	Crack & ext ensive delam	Window progressively delaminated all over.	EEA.S.4.12263 OPE.OCC.031
	17-1-74	NH	DARWIN		202	44	Shattered taxying out		GGE781/226-6 EEA.S.4.241
	5-4-74	NJ	LHR	ROME	5548	1142	Delam & shattered	OAT not recorded.	EEA.S.4.490 46.445
	10-7-74	NH	TORONTO	PREST WICK	6015	1272	Shattered in flight	OAT-49°C	PIK.INC.25/74 EEA.S.4.684
	1-9-74	NG	DARWIN	MELBOU-RNE	6380	1238	Delam in flight	OAT not recorded.	CTE.272.226 EEA.S.4.828
11-11-73	27-1-75 29-6-75 5-2-76	NN EBE SAN		JO-BURG	4550	956	Delaminat-ion	Capts No. 1 originally removed for delam and one US sensor. Refitted twice Serial T.1029.	

TABLE 2 CONTD.

DATE OF FIT	DATE OF REMOVAL	A/C	DEPART STATION	ARRIVAL STATION	HOURS FLOWN	BRAKE LNDGS	CAUSE/TYPE OF FAILURE	REMARKS	INCIDENT REPORT REF.
	20-2-75	NN	LHR	CHICAGO	4592	983	Delm followed by arcing & shattering	OAT - 55°C T.1002	ORD/E/039 EEA.S.4.1389
	30-6-75	ND	LHR	WASHINGTON	BOTH SCREENS SHATTERED		Hailstones shattered screen.	HAIL	IAD.E.137
	25-7-75	NO	BOSTON	PHILADELPHIA	6531	Not Rec.	Outer layer shattered.	Hailstorm. T.1033	EEA.S.4.1832 1-078
	23-8-76	NP	LHR	TORONTO OAT not Rec.	3493	762	Previous Delm suddenly spread & window shattered.	Triplex. T.1050.	INC/ACC/7622 EEA.S.4.1918
	16-7-75	NM		MELBOURNE	1301	390	Arcing on pushback shattered.	Triplex. T.1123.	CTE.208 EEA.S.4.1917
	5-1-76	PU	DELHI	TEHERAN	3914	775	Prev Delm Shattered in cruise.	OAT - 12°C Triplex T.1072. 6 cold trips just before failure.	Unreferenced EEA.S.4.055
	14-1-76	NE	BAHRAIN	ZURICH	5976	1226	Delm & arcing shattered.	OAT - 40°C No cold trips near date of failure.	OPO.2.1.2034 EEA.S.4.072
	16-1-76	NI	ANCHORAGE	LHR	8788	2015	Outer layer shattered with loud bang.	OAT - 69°C 12 cold trips near date of failure.	OPO.2.2.2035 EEA.S.4.108
	22-1-76	NF	LHR	CHICAGO	4731	1023	Outer layer shattered.	OAT - 76°C. 12 cold trips near date of failure.	INC/ORD/01 EEA.S.4.133

TABLE 2 CONTD.

DATE OF FIT	DATE OF REMOVAL	A/C	DEPART STATION	ARRIVAL STATION	HOURS FLOWN	BRAKE LNDGS	CAUSE/TYPE OF FAILURE	REMARKS	INCIDENT REPORT REF
5-1-75	13-2-76	NC		ANCHOR AGE	4681	1013	Delam in flight.	Capts No. 1 Serial 2453.	
27-1-75	17-2-76	NN		MIAMI	4485	902	Outer pane shattered	Capts No. 1. Serial 2495.	
24-5-75	10-3-76	NA		LHR	3366	654	Outer layer delam.	Capts No. 1. Serial 2585.	
11-2-76	1-6-76	NH		BOSTON	1399	280	Gasket damaged.	Capts No. 1 Serial 2387. Removed because of noisy air leak. Seal probably damaged on installation.	
24-11-74	14-6-76	NI		LHR	6218	1317	Delam in flight. Glass departed.	Serial 2450. F/O's No. 1.	
28-12-76	30-6-76	NL		SINGA-PORE	6177	1411	Delam outer ply missing.	Serial 2549. Capts No. 1.	
19-4-74	22-7-76	PZ	CHICAGO	LHR	6662	1984	Sparks & arcing foll-owed by loud bang & delam.	F/O's No. 1. OAT -47°C. Serial 2118.	EEA.S.4.1028 OPO.2.2.2211
8-6-74	3-9-76	NG	JO-BURG	NAIROBI	9761	1994	Arcing & out er pane shtd	Serial 2222 F/O's No. 1	EEA.S.4.1040
12-12-74	16-9-76	PU	WASHING-TON	LHR	7249	1442	Outer pane shattered.	Serial T.1105 Capts No. 1	EEA.S.4.1039
	27-12-74	NL	JO-BURG	NAIROBI	5816	1216	Arcing foll owed by delm & loud bang shattered.	OAT - 17°C	F.317 EEA.S.4.1203

TABLE 2 CONTD.

DATE OF FIT	DATE OF REMOVAL	A/C	DEPART STATION	ARRIVAL STATION	HOURS FLOWN	BRAKE LNDGS	CAUSE/TYPE OF FAILURE	REMARKS	INCIDENT REPORT REF.
	12-2-76	NH	LHR	ANCHOR-AGE	6601	1335	Loud bang followed by delm in flgt.	OAT - 69°C. L.H. S/N 2536. No cold trips before failure.	ANC.A1.03.76 EEA.S.4.183
	12-2-76	NH	LHR	ANCHOR-AGE	4935	987	Delm in flgt 11 mins after LH.	OAT -- 69°C. Serial No. 2471 R.H. No cold trips before failure.	ANC.AI.03.76
	17-2-76	NN	LHR	MIAMI	4485	803	Capts No. 1 window shattered in flight.	10 cold trips just before failure. OAT estimated -50°C.	
	13-2-76	NC	LHR	ANCHOR-AGE	4681	1013	Creaking, loud bang, delm & shattered in flight.	OAT - 68°C. L.H. Serial No. 2453. 6 cold trips just before failure.	
	20-2-76	NE	ANCHOR-AGE	LHR	4629	1213	Delam elec sparking in bottom LH corner. Creaking noise, Glass remd intact but misted up on landing run.	OAT-64°C. 11 cold trips just before failure.	
9-4-76	23-9-76	PV		LHR	2049	375	Delm beyond limits.	Serial T.1281. Capts No. 1.	

TABLE 2 CONTD.

DATE OF FIT	DATE OF REMOVAL	A/C	DEPART STATION	ARRIVAL STATION	HOURS FLOWN	BRAKE LNDGS	CAUSE/TYPE OF FAILURE	REMARKS	INCIDENT REPORT REF.
20-2-75	17-1-77	NN	MIAMI	PREST-WICK	8,693	1,765	Delam and shattered in flight.	Serial No. 2488. OAT -68°C.	PIK/INC/67/76
17-7-75	10-1-77	NM	NAIROBI	ZURICH	6,626	1,530	Shattered in flight.	Serial No. 2915 OAT -63°C.	ZRH/114/646
13-10-75	20-1-77	NK	DELHI	HONG-KONG	5,536	1,245	Shattered in flight.	Serial No. T.1158	Unreferenced
2-5-75	17-2-77	NF	LHR	ANCHOR-AGE	7,564	1,550	Arcing on interlayer, severe delaminat-ion.	Serial No. 2640 SAT -66°C	ANC/AI/04, 77
25-7-75	17-2-77	NO	BAHR-AIN	LHR	7,207	1,454	All glass missing.	Serial No. 2847	I.010A
Original Fit.	12-2-77	PV	YYZ	JFK	3,664	730	Shattered in flight.	Serial T.1186	
16-6-75	12-8-77	ND	JFK	LHR	8,873	2,096	Shattered in flight.	Serial No. 2831 OAT -50°C	B.747/2868
22-7-76	5-8-77	PZ	ORD	LHR	4,043	710	Heating Fault.	Serial No. T.1302.	

TABLE 2 CONTD.

DATE OF FIT	DATE OF REMOVAL	A/C	DEPART STATION	ARRIVAL STATION	HOURS FLOWN	BRAKE LNDGS	CAUSE/TYPE OF FAILURE	REMARKS	INCIDENT REPORT REF.
29-6-76	10-5-77	NL	WASHING-TON	LHR	3,915	798	Large delam on top edge.	Serial No. 2899	
5-10-75	8-9-77	NA	SYDNEY	MEL-BOURNE	7,977	1,760	Shattered in flight.	Serial No. 2770.	B.747/2902
23-12-76	17-9-77	NH	SYDNEY	MEL-BOURNE	3,128	641	Shattered in flight.	Serial No. T.1204	
1-9-76	5-5-77	AYV			2,046	633		Serial No. 2886	
23-8-75	30-9-77	NP	ANCHOR-AGE	HANEDA	9,457	1,951	Shattered in flight.	Serial No. 2742. Heat switched off by crew when overheat light came on.	B.747/2936
18-5-75	17-10-77	NB	BERMUDA	LHR	10,484	2,118	Delam.	Serial No. 2753. OAT -62°C.	B.747/2946
23-12-75	9-1-78	NG	LHR	ANCHOR-AGE	9,058	1,897	Delam.	Serial No. 2891. OAT -66°C.	EEA.S.4.032
4-1-76	12-12-77	PU	DELHI	LHR	8,923	1,800	Delam.	Serial No. 2466. OAT -59°C.	EEA.S.4.063
QANTAS	31-1-78	NA	LHR	BAHRAIN	11,336	3,477	Shattered in flight.	Serial No. T.1042. Previous service with Qantas OAT -50°C.	B.747/3058.

TABLE 2 CONTD.

NOTE:- **'NG and 'PU showed glass cracked at top edge only. Complete glass layer remained attached to the interlayer. This is a new form of failure indicating some adhesion improvement between the heating film and the interlayer.**

TABLE 3 CONTD.

NOTE:- G-BDPZ on lease from Aer Lingus.

* Note to Serial 401.

"On 23.8.74 loud hissing reported during descent. No evidence of leak found at Chicago."

On 22.2.76 sound of air leak reported on descent between 10,000 ft and 7,000 ft.

Nuts torqued up at Chicago.

TABLE 3 - NO. 2 & 3 WINDOWS IN-PLANE CRACKING FAILURES

WINDOW POSITION	DATE OF MANU-FACTURE	DATE OF FIT	DATE OF REMOVAL	HOURS FLOWN	BRAKE LNDGS	SERIAL NO.	FAILURE LOCATION & REMARKS	AIRCRAFT
No 3 LH	11.5.70	21.6.74	11.1.75	2349	491	475	Stored by BA for several years. Failed in flight.	G-AWNK
No 3 LH	6.8.70	16.6.74	9.9.75	5330	1066	401 *		G-AWNG
No 3 RH	16.9.70	17.7.75	20.8.75	482	98	455	Spare from Air India pool.	G-AWNH
No 2 RH	9.11.70	23.11.75	13.1.76	461	90	458	Failed in flight.	G-AWNF
No 2 RH	23.8.73	13.1.76	9.5.76	1432	280	840	Near temp sensor. Warranty Claim.	G-AWNF
No 2 RH	20.6.71	29.11.76	17.5.76	1808	494	664	Spare from Singapore Airlines pool. Temp sensor side. Warranty claim.	
						SWO		G-AWNA
No 3 LH	May '74	11.7.75	8.7.76	4056	897	3007	Temp sensor side & opposite. Warranty claim.	G-AWND
No. 3 LH	20.11.69	23.11.75	18.6.76	3558	1364	187	Temp sensor side. Stored by B.A. for several years.	G-AWNB
No 3 LH	5.1.70	20.3.71	25.8.76	12645	2926	363	At centre near temp sensor. Original fit.	G-BDPZ
No 3 RH	July 70	20.3.71	17.9.76	12936	3977	430	Early stages of cracking along bus bar edges. Silicone sealant used. Original fit.	G-BDPZ

NOTE:- The majority of failed windows have been stored in high humidity parts of the world or for long periods of time.

Failures always occur from one of the two sides containing bus-bars and usually from the temperature sensor side.

747 NO. 1 WINDSHIELD REMOVAL EXPERIENCE

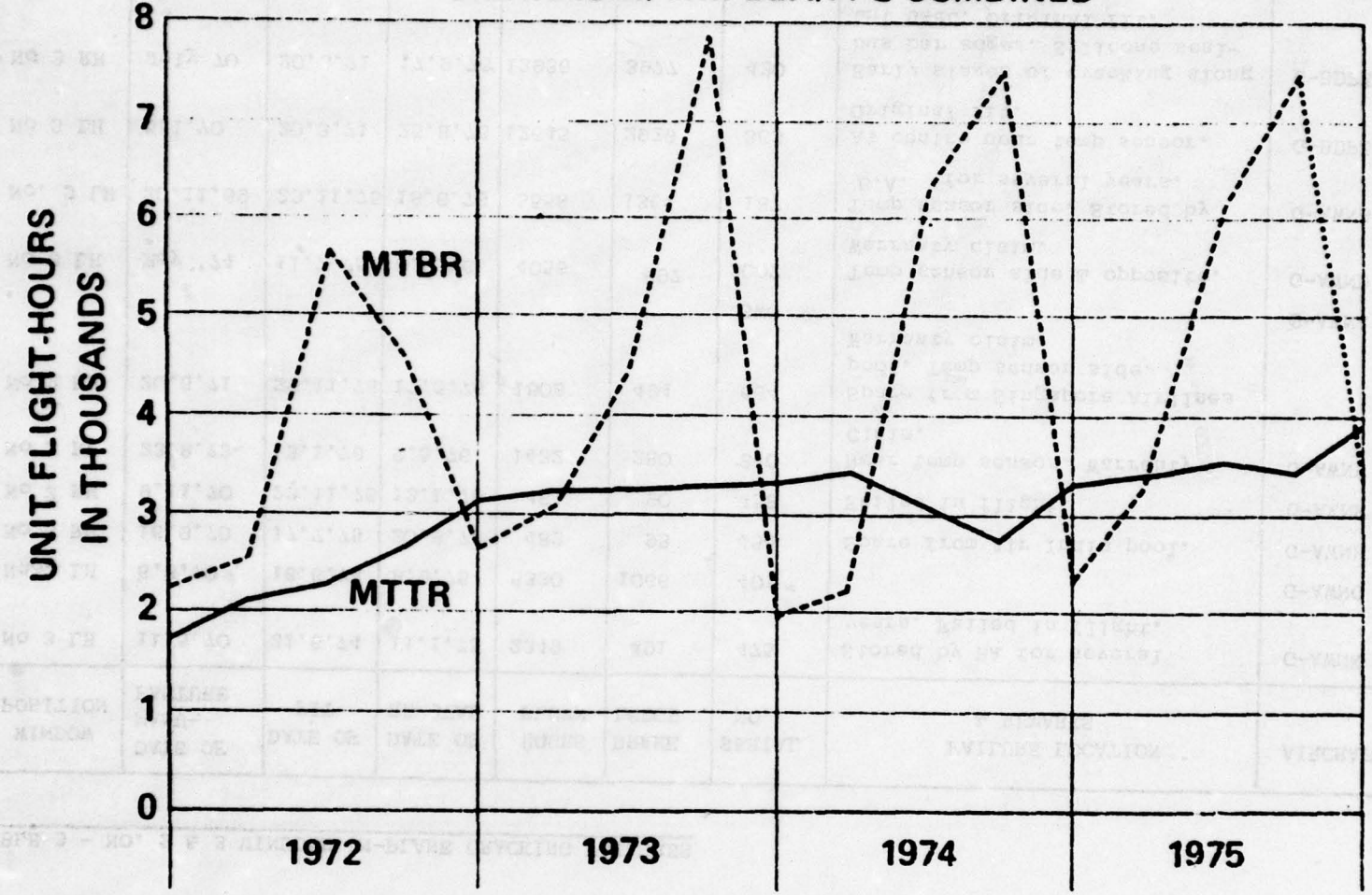


FIG: 1

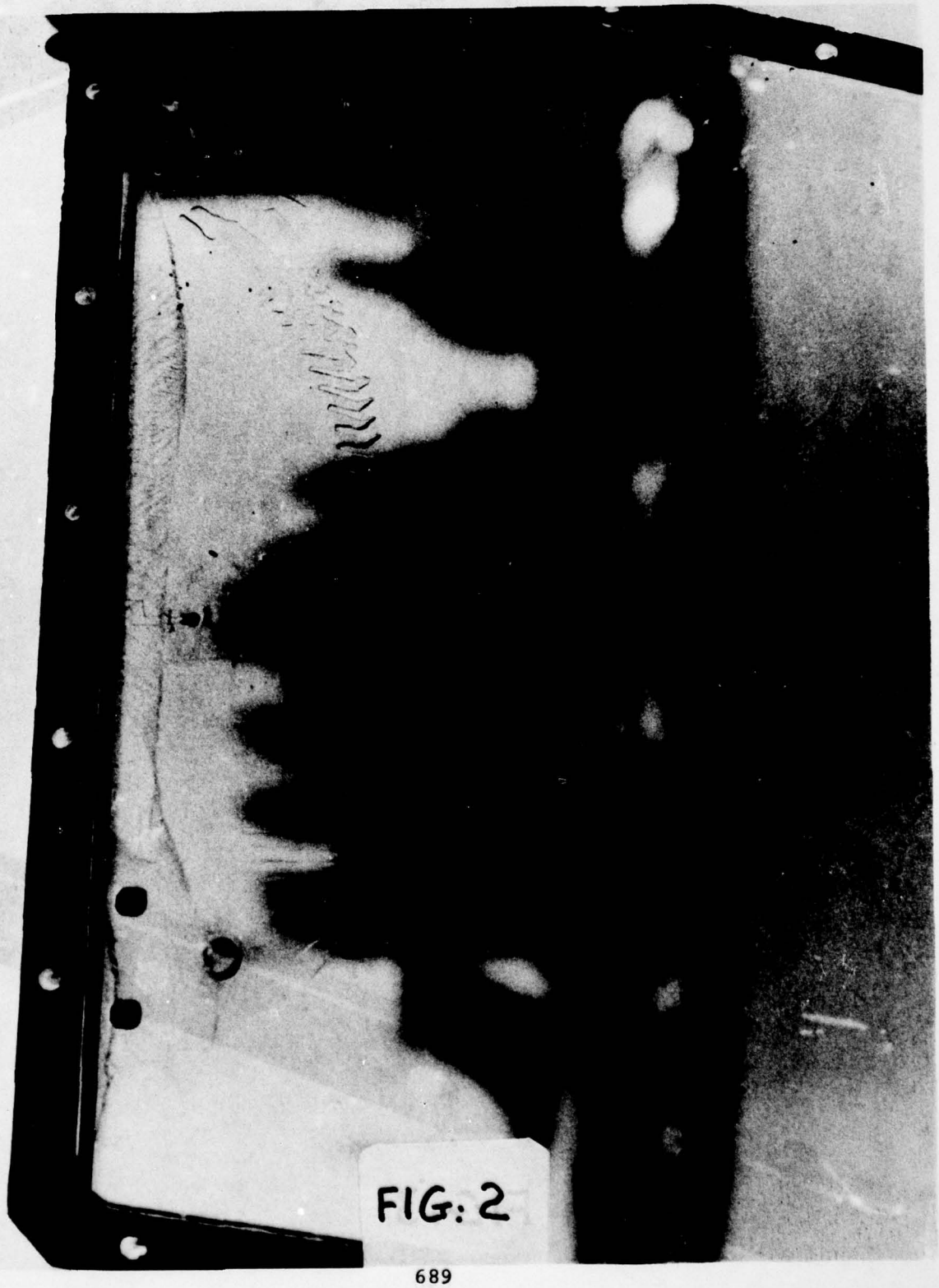


FIG: 2

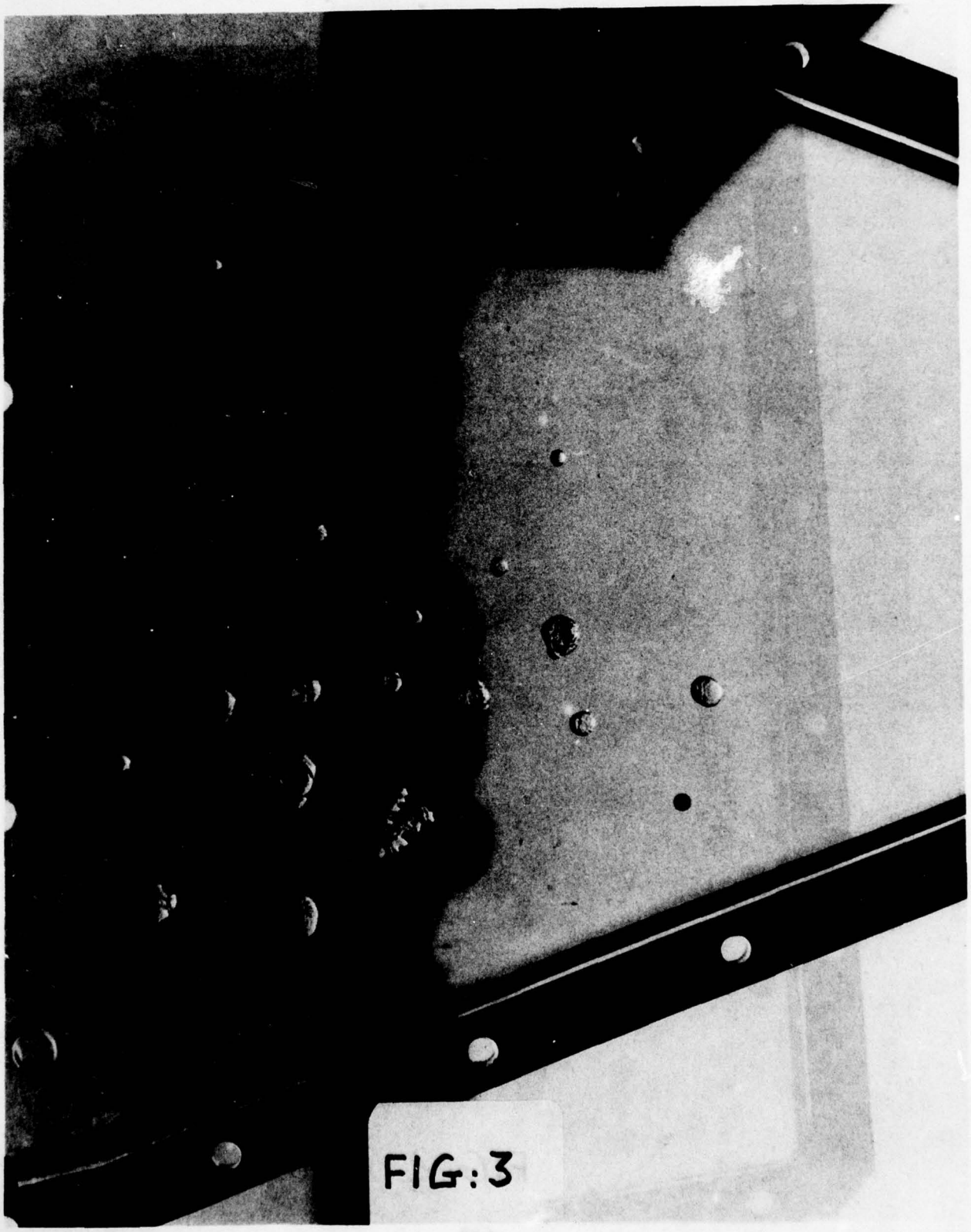
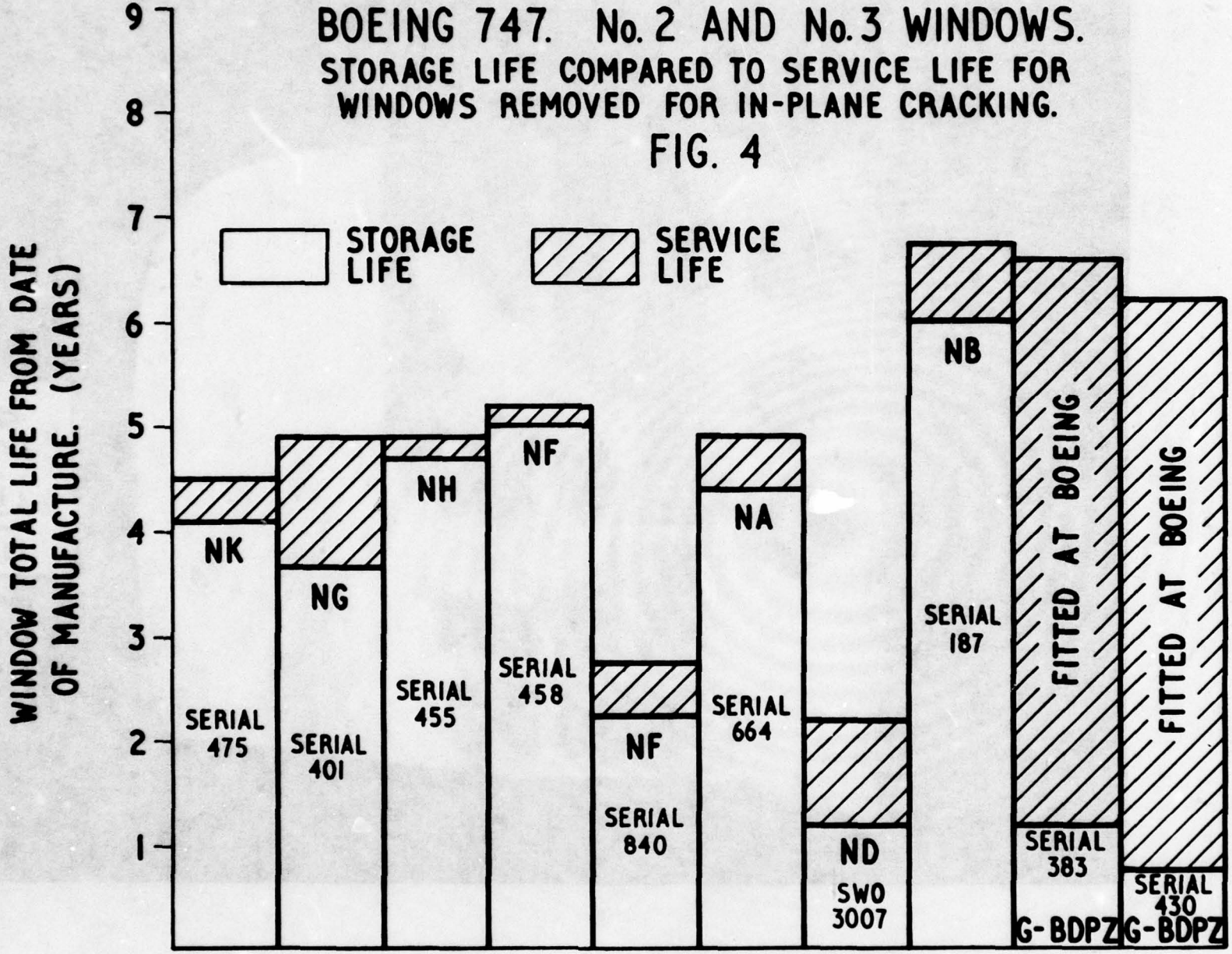


FIG:3

BOEING 747. No. 2 AND No. 3 WINDOWS.

STORAGE LIFE COMPARED TO SERVICE LIFE FOR WINDOWS REMOVED FOR IN-PLANE CRACKING.

FIG. 4



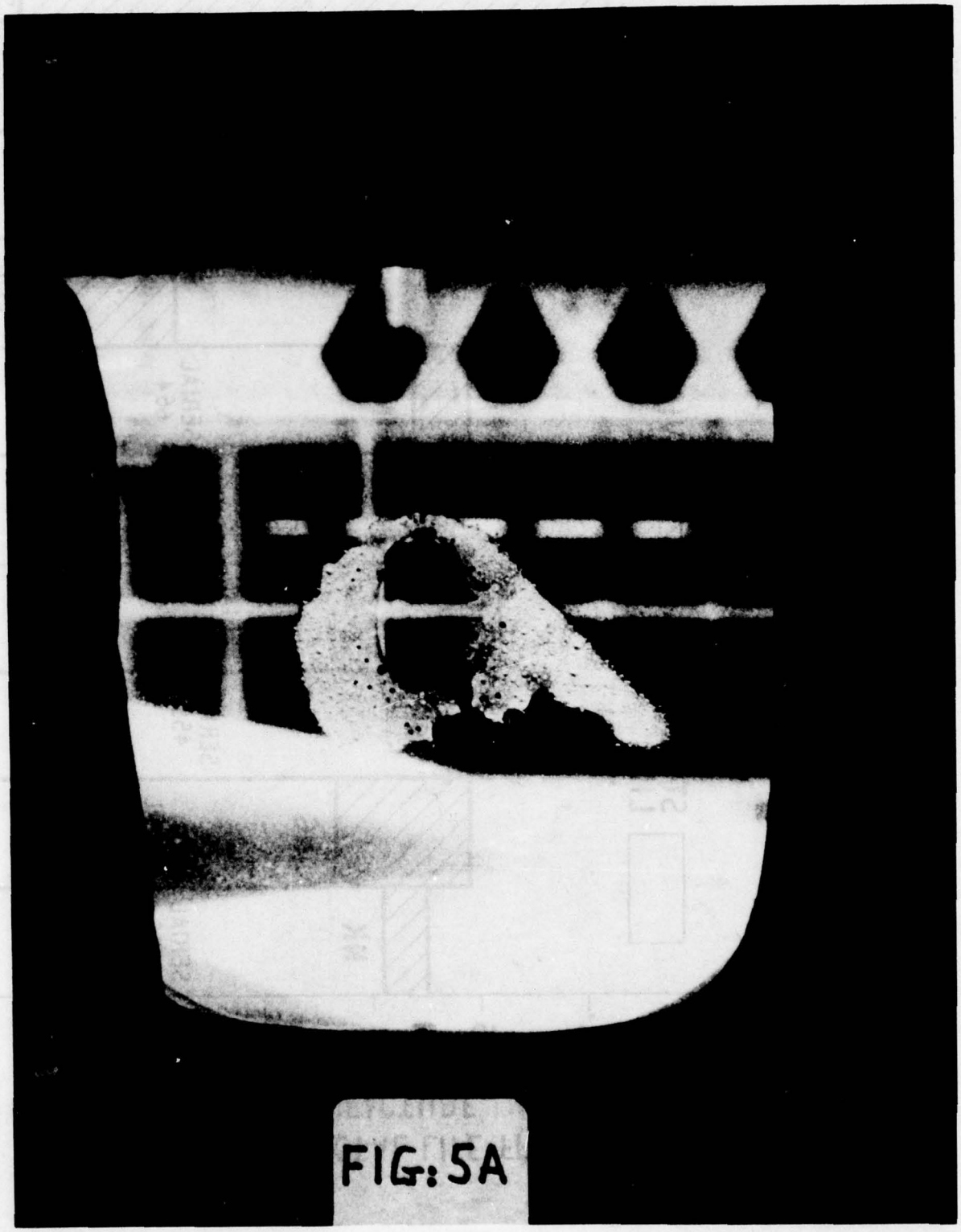


FIG. 5A

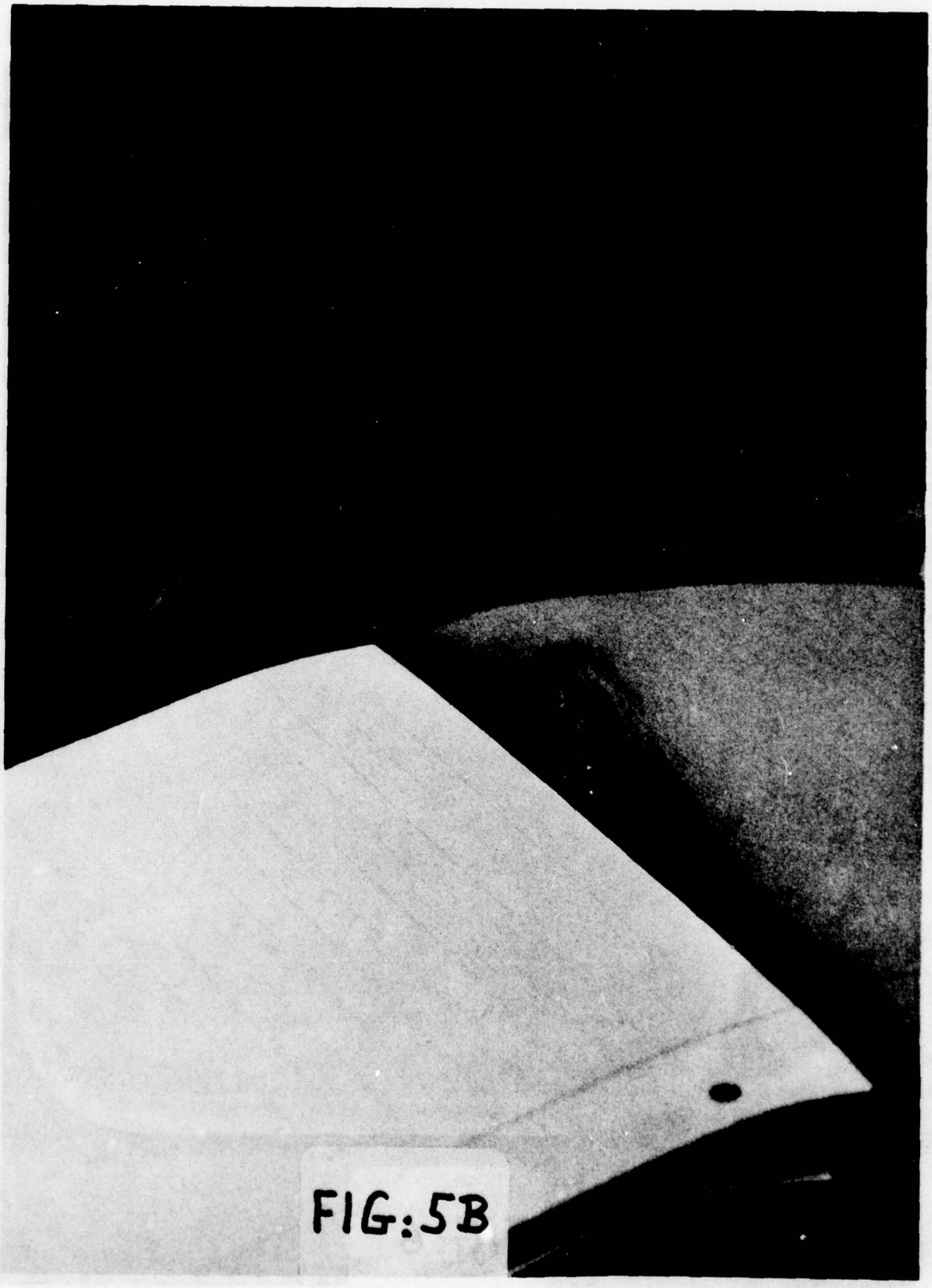


FIG:5B

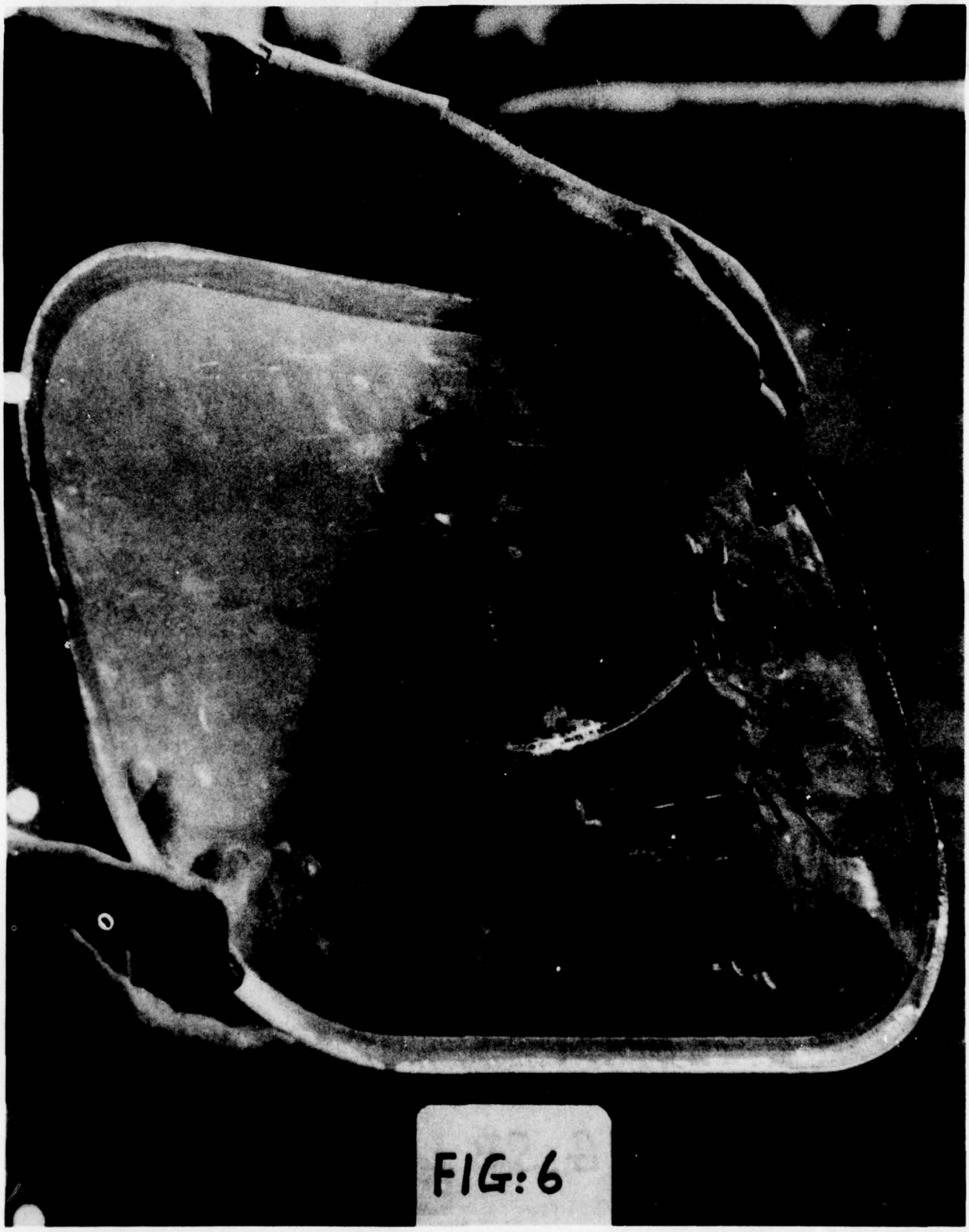


FIG: 6

PROBABLE RELATIVE DAMAGE VALUES FOR VISIBLE AND ULTRAVIOLET LIGHT

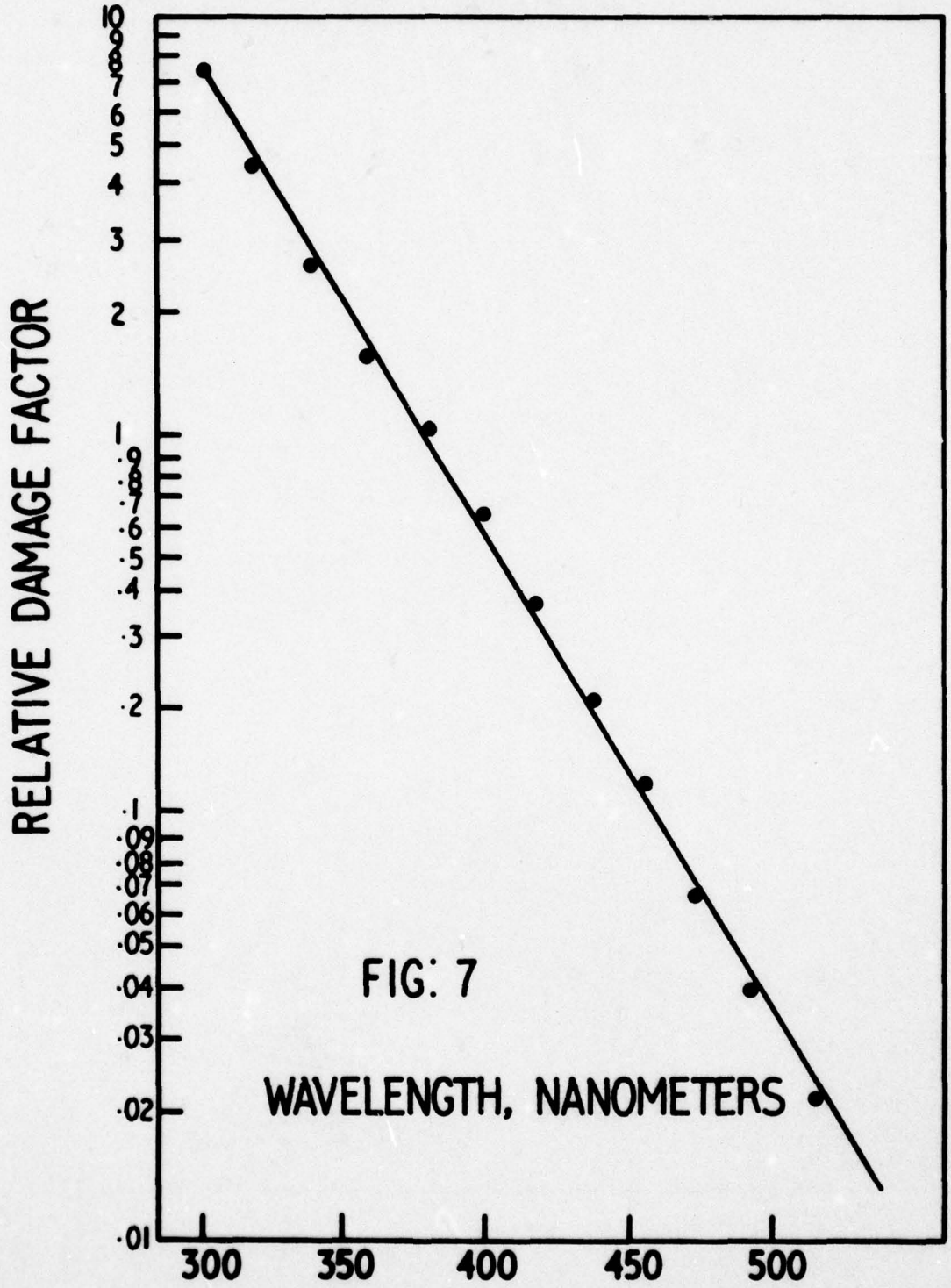


FIG. 7

DC-8-60/DC-9. WINDSHIELD ATTACHMENT

J. Christensen
Scandinavian Airlines
Maintenance Engineering
Copenhagen Airport, Denmark

PRECEDING PAGE BLANK-NOT FILMED

DC-8-60/DC-9. WINDSHIELD ATTACHMENT

1. Introduction

At a certain time we were convinced that appearance of the -500 windshield panels would sufficiently decrease windshield failures to make the problem possible to live with.

Experience has shown that this was unfortunately not true. On the first slide I have calculated average life of all DC-9 -1 windshields to be appr. 4590 hrs. On the -500 panels, which have so far been removed, average life is appr. 5600 hrs (Fig. 1).

Within SAS we have the idea that proper solutions to technical problems require understanding of the nature of these problems.

Although we have at several occasions asked Douglas and the windshield manufacturers for a full explanation of the windshield failure modes, we have never received such explanation, but I may add that we think we understand it.

By today we have information about more than 500 windshield failures. In this table I divide failures into the two groups: Internal and external failures (Fig. 2).

Our present ideas are that all internal failures, i.e. burnt spot, arcing, cracked outer pane, delamination, sensor failures, chips, and solder joint failures are caused by excessive strain applied to the PVB along the edge of the outer glass ply by windshield heat and by the combined action of cabin differential pressure and windshield attachment.

I should have liked to comment on many other aspects of windshield failure modes, but time allotted does not permit that.

However, there is some observations I will like to mention:

We consider it an established fact that replacement of one DC-8-60/DC-9 windshield panel - irrespectively of position - increases the probability of failure of the others. I call this induced failures. Induced failures would always belong to the "internal" group. The same goes for repeated low time failures of panels installed in the same position.

PRECEDING PAGE BLANK-NOT FILMED

We have statistical information which indicates that this phenomenon is part of the cause of more than 50% of the failures. I have connected this problem with another observation, namely that the windshield attachment bolts very often are found loose.

2. Cabin Pressure/Windshield Attachment

I shall now attempt to give an explanation to the part of the delamination mechanism, which is caused by cabin pressure and by the windshield attachment.

A. PVB Deformations at Common Retainers

By accident we discovered deformation of the PVB on a side windshield panel removed after cracked outer pane during cruise. An almost identical deformation was observed on another panel, which had had sensor failure during flight. The deformations, which are shown on the slide, are mainly in the area covered by the common retainer, but they are not confined to these areas (Fig. 9).

This made us examine other windshields, which had been removed due to failure. The results vary with the circumstances under which the windshields failed. But generally they look very much like what is shown on the slide.

When heat has been disrupted with full cabin pressure acting on the windshield, it appears that they will be bigger than on windshields, which have been replaced without preceeding shut-off of heat during flight.

To try to explain this a piece of PVB was heated to about 40°C and then given a deformation, which was subsequently maintained while the PVB was cooled to about -15°C for sufficient time to get this temperature throughout the PVB. When the load after that was relieved and the PVB heated to about 20-30°C, it maintained part of the deformations given to it.

When load was applied and relieved at a constant high or low temperature, permanent deformation would disappear after some time.

B. Insert Displacement at Horizontal Retainers

The deformations at the horizontal retainers differ somewhat from what is observed at the common retainers.

Very often, however, it can be observed that the insert has been tilted as shown (exaggerated) on next slide (Fig.10).

This indicates that the retainer/seal system deflects excessively.

C. Cabin Pressure

Cabin pressure applies a load of approximately one metric ton (0.616 kp/cm^2) on a center windshield panel. According to laws for flat plate bending, this causes the center ply (and the other plies of course) to deflect. At the center of the sides, the angular deflection will be about 0.14°. The reactions will have a distribution along the edges as shown on the slide (Fig.11).

The maximum value at the center would be: 10.8 kp/cm

The load is through the PVB and the insert transmitted to the retainer and back to primary structure.

If this load is applied to the edge of the retainer, it will deflect approximately 0.56° or 4 times center ply angular deflection.

When the PVB is cold (10°C or less) its modulus of elasticity is above 60,000 lbs/sq.in. = 4220 kp/cm^2, (Fig.12) and the load is taken up by elastic deformation of the PVB between the insert and the retainer.

But if the PVB is hot (38°C or above), its modulus of elasticity is only 70 lbs/sq.in. = 4.9 kp/cm^2, and the PVB would consequently not be capable of taking up the applied load on the available surface.

The load must consequently be taken up by elastic deformation of the insert (Fig.13).

We suppose that the insert alone transmits the load to the retainer and that it is simply supported by the retainer and fixed in the PVB.

Calculations show that the insert would then get a deflection, which correspond quite well with the found PVB deformations.

3. Failure Theory

The observed deformations could be produced by the insert being simply supported on the retainer. This condition may be present, when the PVB is heated to about 40°C by sun radiation immediately before take-off. As cabin pressure increases, some of the PVB will be displaced and will not come back later. However, elastic forces in the insert and the pan will bring the insert back to almost original position, when cabin pressure has been relieved. During subsequent flights - when the PVB is not hot at take-off - the normal load path no longer exists due to the missing PVB. In this condition a high bending moment is applied to the insert when cabin pressure is applied. This moment will create strain in the PVB below the edge of the outer glass ply. This strain is believed to be a contributing factor for the evolution of delamination.

4. Induced Failures

It is obvious that strain in the PVB along the edge of the windshield panel increases, if bending moment on the insert between structure and retainer decreases.

I will now try to explain the phenomenon induced failure using this observation. One particular thing about induced failures is that when a side panel, e.g. the left, is replaced, we have often observed that the center panel and the right panel will start to delaminate at the RH common retainer and vice versa, and that when a center panel is replaced, LH and RH panel will start to delaminate at the outboard retainers.

A somewhat popularized explanation for this is given on this slide (Fig.14).

The upper figure symbolizes a cross section of the 3 windshield panels when subject to cabin pressure just after installation.

However, we have observed that the seal system is yielding indicated by the loose attachment bolts. This is shown in the next figure, where we have got an angular deflection of the inserts and thus reduced moment on the insert at the retainer end and increased moment in the PVB. This condition may cause failure of one panel, e.g. the left.

In the next line left panel has been replaced. The increased moment on the left side of the c enter panel will cause a reduction of the deflection of this panel also at the right retainer. Moment from the insert on the retainer will thus decrease and the retainer will consequently tilt about the single line of bolts.

This will increase strain in the PVB for both center and RH panel, and they will therefore fail sooner than would otherwise be expected.

The last figure illustrates in the same way what happens if a center panel is replaced.

5. Theory for Repeated Failures

Repeated failures of panels installed in the same position presumably occur when permanent deformations of the PVB below the common retainer have taken place on the neighbour panel. (Fig. 15).

When the failed panel is replaced, bolts in the common retainer are retorqued thus increasing the bending moment, transmitted to the insert of the neighbour panel. (Fig.16).

This to some extent improves conditions for this panel at this retainer. However, when cabin pressure is applied, it causes higher than normal pressure load on the silicone sealant between insert and retainer, and the silicone sealant will yield caused by this load, as the PVB adjacent to the high pressure area is already missing, this will allow the retainer to tilt reducing moment on the insert of the newly installed windshield.

A condition with high strain in the PVB around the insert in the new panel has now been established, and the normal failure pattern has been initiated.

6. Conclusion

The combined action of the following design deficiencies starts a never ending chain of windshield failures.

A. Too weak retainer

B. Too soft seals

C. Use of PVB as load carrying member along windshield edge.

The resulting induced and repeated failures are involved in about 2/3 of all DC-8-60/DC-9 windshield failures. Retorque may relieve this situation somewhat, but basic design deficiencies prevent drastic improvements.

7. Recommendations

I recommend that MDC and the windshield manufacturers initiate design of new windshield edge attachment systems.

A proposal based on SAS experiences and discoveries is offered (Fig. 17).

-oOo-

DC-9 AVERAGE LIFE OF FAILED WINDSHIELDS				
POS	DASH NO	NO W. SH.	AV. HRS.	% INCR.
LH	-1	84	4506	
LH	-501	66	5088	13
CTR.	-1	72	5430	
CTR.	-501	46	5697	5
RH	-2	105	4081	
RH	-502	35	5841	43
ALL	-1/-2	261	4590	
ALL	-501/-502	147	5600	22

FIG. 1

DC-9 WINDSHIELD - FAILURE DISTRIBUTION									
	INTERNAL FAILURES						EXTERNAL FAILURES		
	BURNT SP ARCING CRACK	DELAM	SENSOR	CHIPS	SOLDER JOINT	TOTAL	OVERH	OTHER	TOTAL
1969	13	5				18	3	3	6
1970	20	19				39	2	3	5
1971	39	10				49	6	4	10
1972	25	8				33	2	4	6
1973	11	6	2		1	20		7	7
1974	27	10	10	2		49	6	6	12
1975	21	3	5	1	1	31	5	2	7
1976	32	19	9	3	1	64	4	2	6
1977	25	14	8	1	1	49	1	3	4
TOTAL	213	94	34	7	4	352	29	34	63

FIG. 2

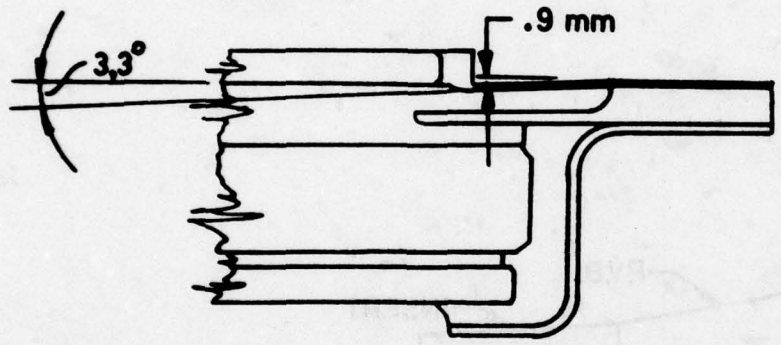


FIG.9 TYPICAL P.V.B. DEFORMATION

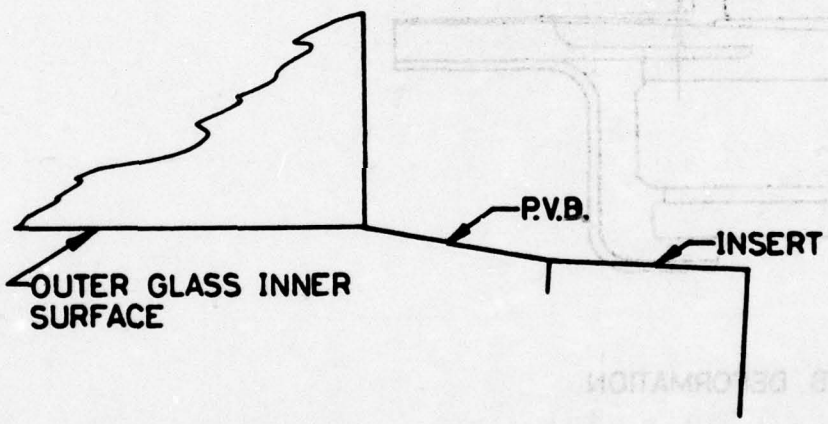


FIG.10 P.V.B. INSERT DEFORMATION AT HORIZONTAL RETAINERS

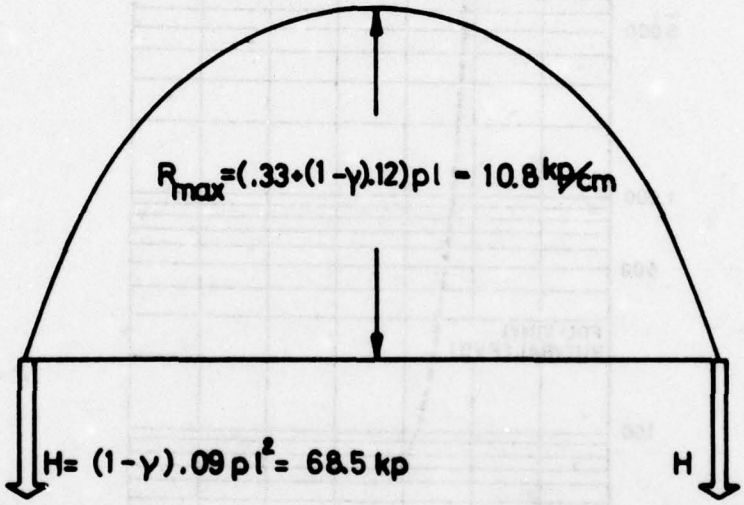


FIG.11 DISTRIBUTION OF REACTIONS ALONG EACH SIDE OF CENTER WINDSHIELD CENTER PLY. (DIF. PRESS=.616 kp/cm^2)

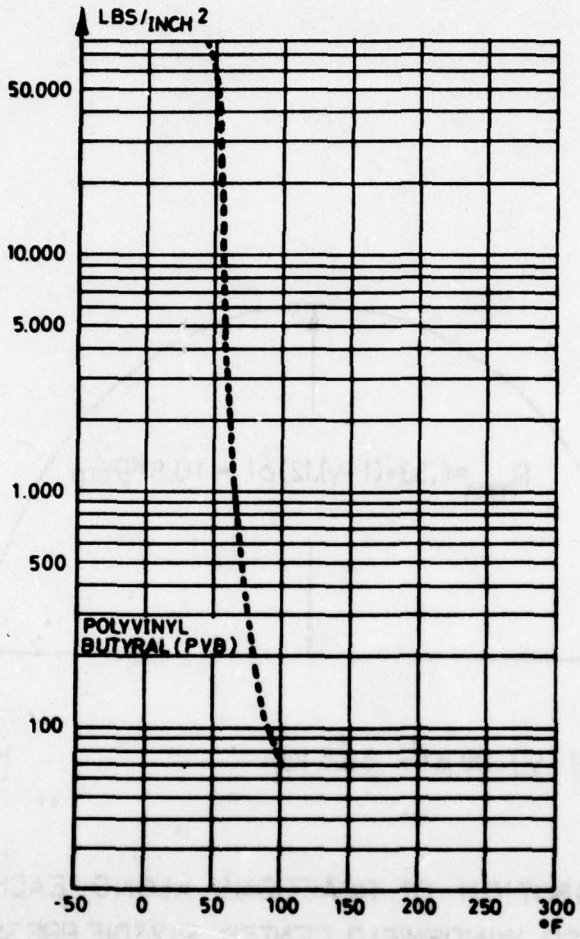


FIG. 12 TENSILE MODULUS OF PVB INTERLAYER.

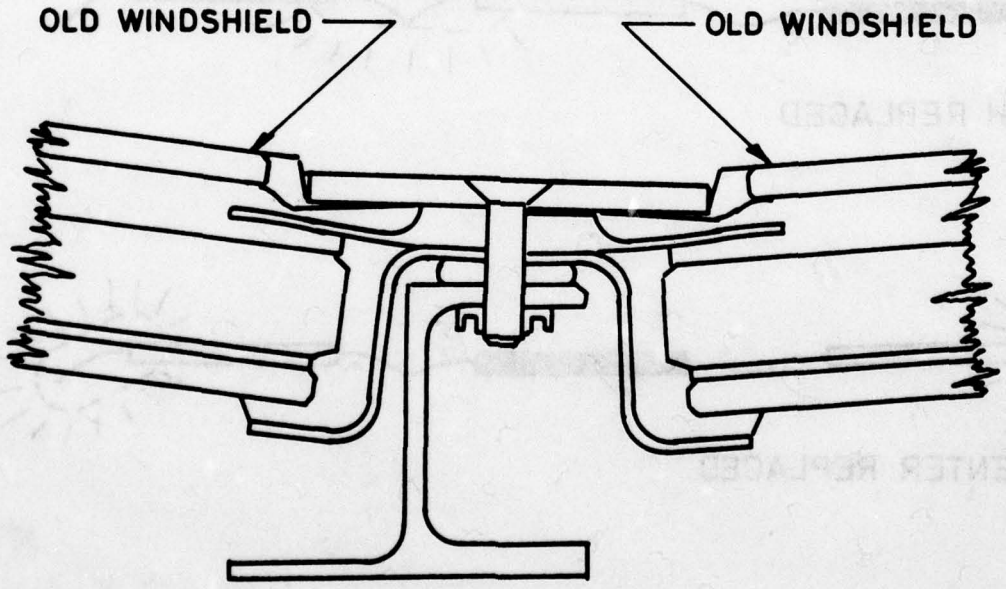


FIG.13 WITH CABIN PRESS.

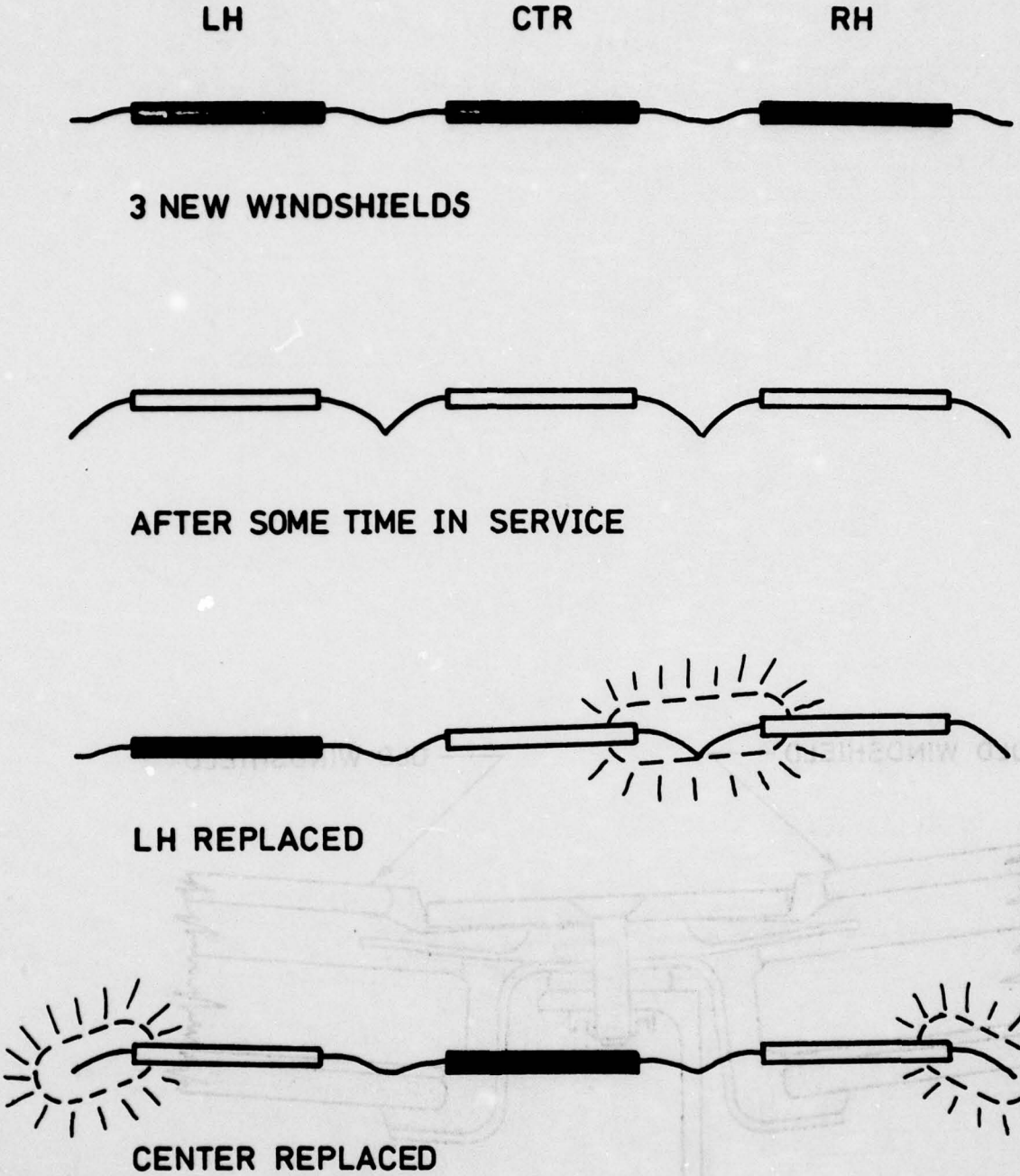


FIG.14. INDUCED FAILURE

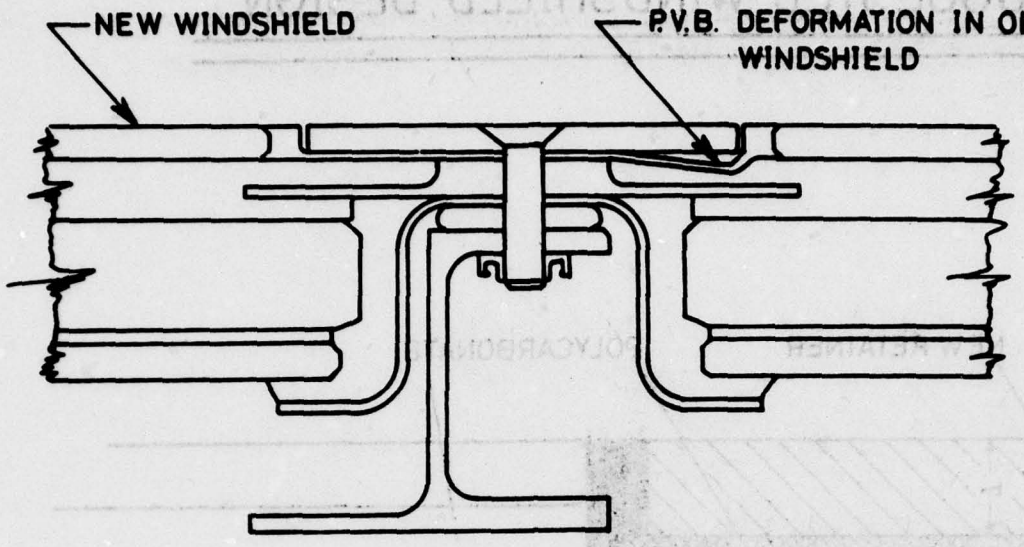


FIG.15 WITHOUT CABIN PRESS.

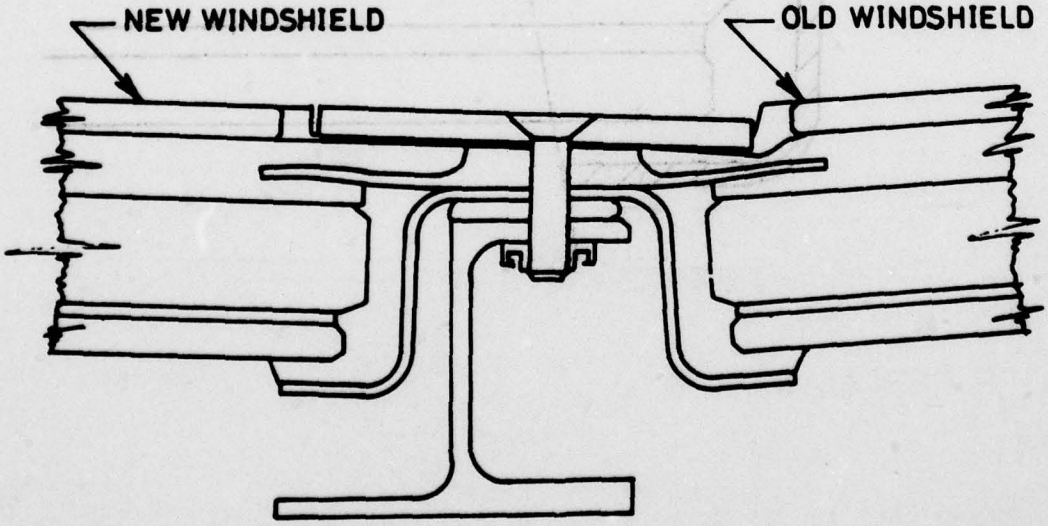


FIG.16 WITH CABIN PRESS.

SUGGESTED WINDSHIELD DESIGN

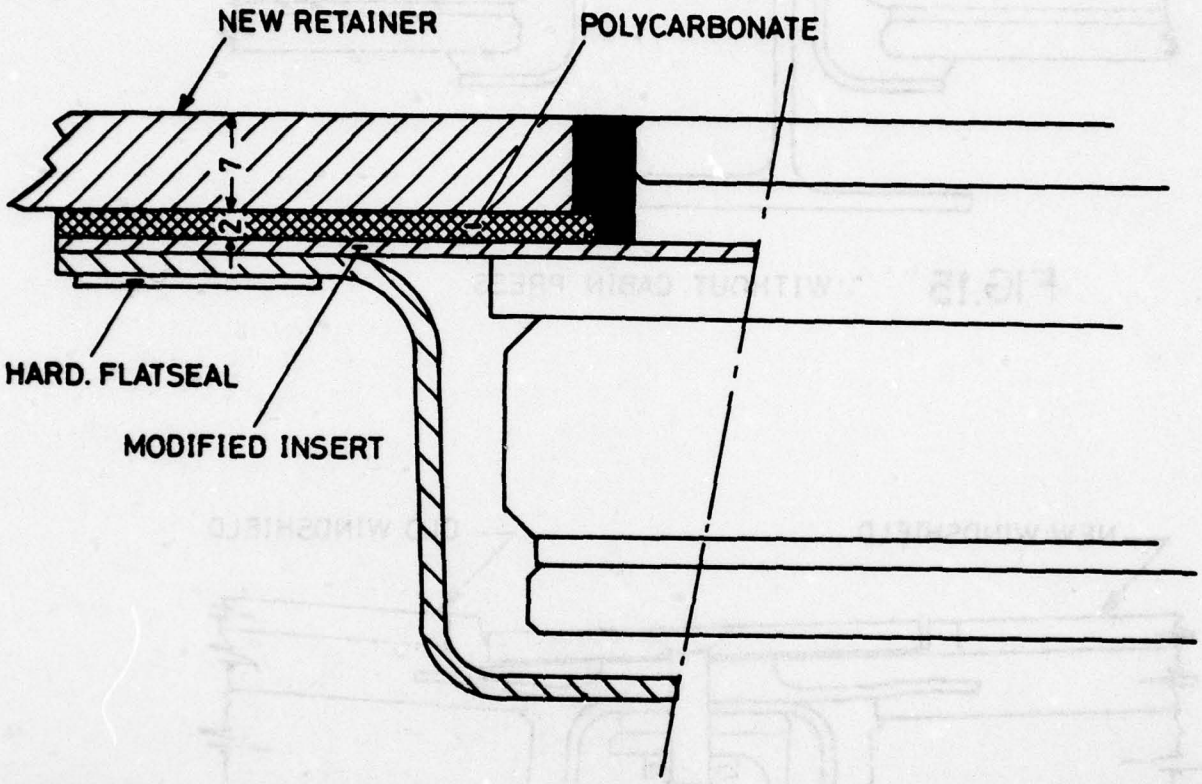


FIG.17

WINDSHIELD DESIGN FOR MILITARY AIRCRAFT

P. S. Christie
Boeing Aerospace Company
Boeing Military Airplane Development
Seattle, Washington

WINDSHIELD DESIGN FOR MILITARY AIRCRAFT

Peter Christie
Structures Technology
Boeing Military Airplane Development

ABSTRACT

The configuration of the forward fuselage is influenced by the shape of the windshield. The windshield shape (flat, single curvature, or double curvature) is influenced by considerations of aerodynamic drag, weight, cockpit interior noise, windshield initial cost, and long term maintenance costs. Since most current aircraft cabins are pressurized for high altitude flight, the lightest and lowest cost shape of the cabin is that having a circular, or double lobe, cross section. The curved windshield blends into the circular cross section and provides reductions in drag and in cockpit noise levels. Today, curved windshields are five to ten times more expensive than flat windshields, but it may be possible to reduce their cost with alternate design approaches. Hence, the key to a low cost forward fuselage is a low cost, long life, curved windshield.

The all-plastic windshield is investigated for both electrical and hot air anti-icing, for precipitation static effects, lightning strike, radar cross section control, and for scratch resistance. The application of all-plastic windshields to 14 current military and general aviation aircraft is shown.

The advantages and limitations of hot air anti-icing and rain removal are discussed. The desirability of improving hot air anti-icing leads to the search for alternate air distribution systems. One novel concept of hot air control is shown, with application to several recent military aircraft proposed.

Cross sections of all-plastic windshields from both military and general aviation aircraft are shown.

PRECEDING PAGE BLANK-NOT FILMED

The Shape of the Forward Fuselage

The configuration of an aircraft forward fuselage, shown in Figure 1, involves considerations of (1) pilot vision, (2) sufficient space for cockpit equipment, nose gear stowage, and radome antenna installation, and (3) the aerodynamics of the nose and cab which affect the forebody drag, the rain, hail, and ice contact on the windshield, and the cockpit noise level due to flow separation at windshield corner posts. The slope of the windshield affects the size of the windshield, the weight of the windshield for bird proofing, pilot optics, and head up display (HUD) optics.

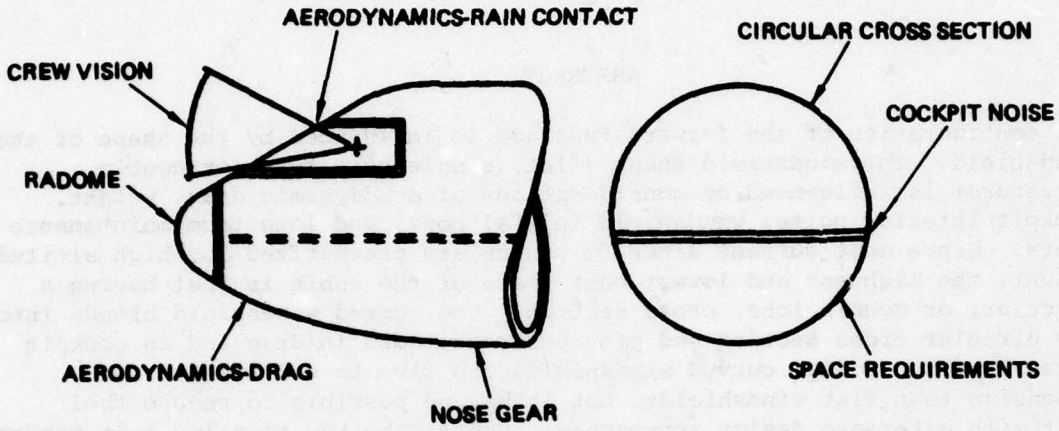


Figure 1. Fuselage Configuration Requirements

It is desirable to blend the windshield into the nose so that there is no change of direction of the airflow at the base of the windshield. When the windshield juts abruptly up from the nose it increases the amount of water and ice that is deposited on the windshield due to inertial action when the airflow changes direction. The blended windshield minimizes water contact, and may allow the removal of windshield wipers. If wipers are not required, it may be possible to remove the outer glass ply of laminated acrylic windshields, thus eliminating thermal strain problems between glass and plastic. An example of a blended windshield is shown in Figure 2. This is the Partenavia P68B, a six-passenger, twin engine commuter aircraft made in Naples, Italy. The windshield aerodynamics result in no rain contact during flight. The windshield and side windows are combined into a single window.

Since almost all aircraft are designed for high altitude flight, cabin pressurization is required. The lightest and lowest cost shape of the cabin for internal pressure laods is a circular, or multilobe, cross section.

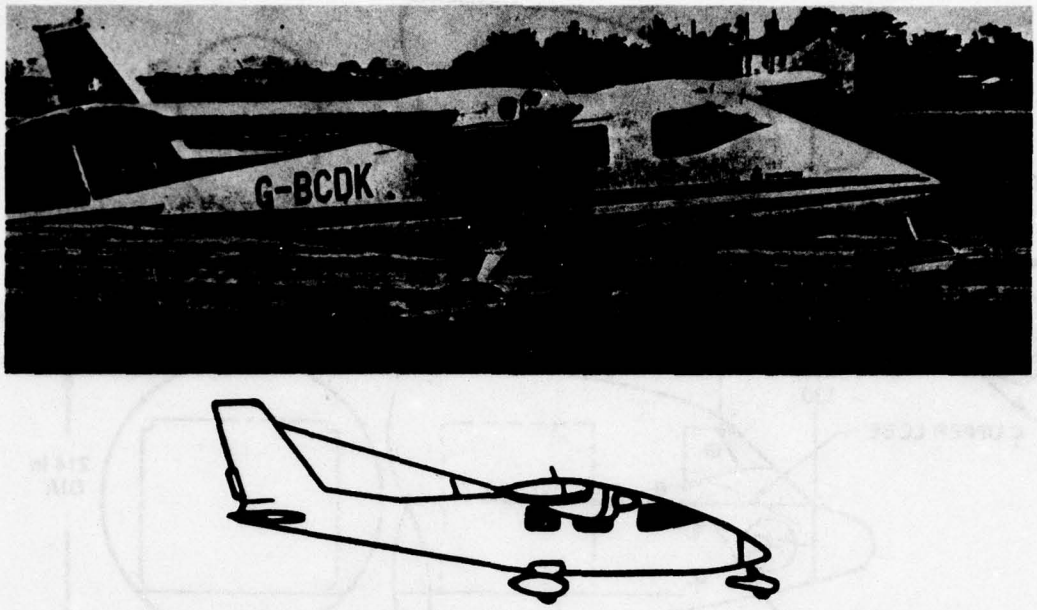


Figure 2. Partenavia P68B (Photo From Flight International)

This shape not only provides the least expensive manufacturing costs, but also minimum maintenance costs for the life of the airplane. When the circular cross section is used, it allows the option of designing the windshield and support structure so that pressure loads are carried through the windshield in hoop tension, rather than in flat plate bending, thus eliminating the large cutout in the pressure shell at each window, and producing a lighter design.

An application of the circular cross section cabin to a wide body military transport is shown in Figure 3. In this design, the circular cross section tapers from the constant section at Station 400 to the forward end of the cargo deck at Station 300. Forward of Station 300, a double lobe cross section is used in order to locate the side windows as close as possible to the pilot's eye, and hence, reduce their size. The pilot's floor serves as a continuous cross tie for lateral pressure loads from each lobe. The upper lobe is a section of a cone forward of Station 202, allowing the installation of a single curvature windshield, which is blended into the nose.

A single curvature windshield is preferred over a double curvature windshield for several reasons. Out of contour manufacturing problems cause higher residual stresses during installation clamp-up due to the increased local stiffness of double curvature windshields. A single curvature windshield allows the option of either a laminated glass or plastic design. A double curvature windshield is considered to be more expensive than single curvature, due to the difficulty of accurate forming.

A curved windshield provides all of the advantages of low aerodynamic drag, reduced cockpit noise, and the opportunity to build a low cost body.

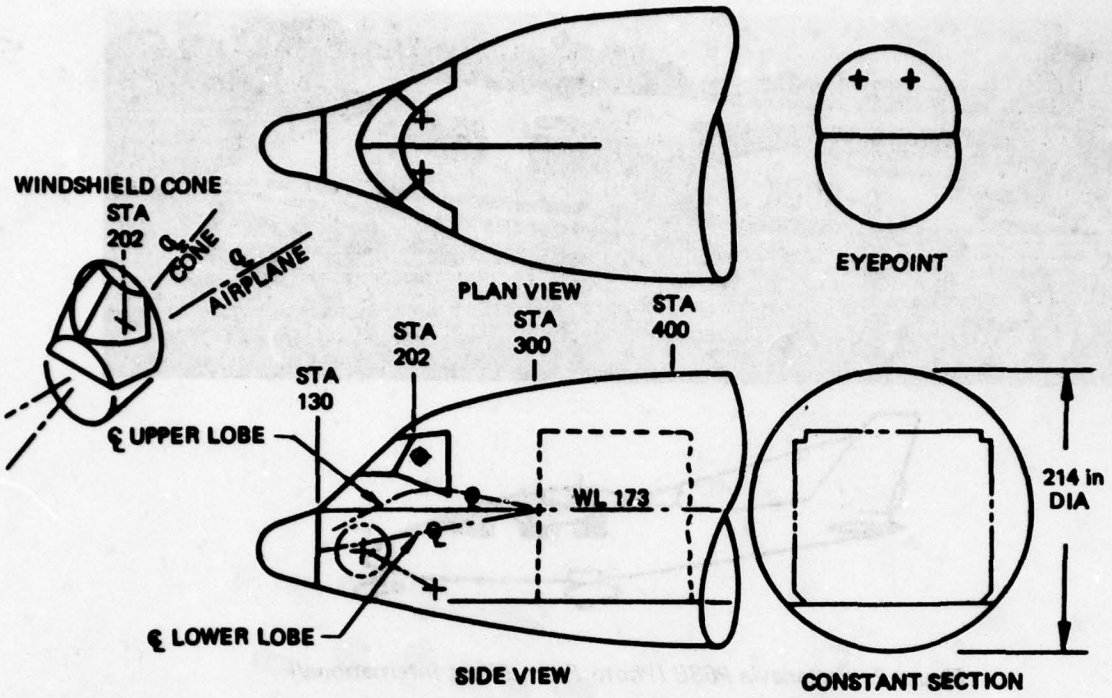


Figure 3. Nose Configuration of Short Range Freighter

Curved windshields are roughly five to ten times more expensive than flat windshields, and hence, the designer must have a high level of confidence in his ability to devise a long-life design so that maintenance costs are minimized.

All-Plastic Windshields

The lightest and least expensive windshield is made of plastic, either single ply or laminated stretched acrylic. Three material characteristics of plastic currently result in the use of the all plastic windshield being limited to small aircraft. These are low thermal conductivity, low static charge drainoff, and low scratch resistance. The most severe limitation is the low thermal conductivity because it requires the use of a very thin face ply for electrical anti-icing, resulting in a subsequent interaction between the electrical coating and the static charge on the outer surface, as explained later.

As cockpit size increases from fighters to side-by-side trainers to transports, the windshield size increases. At some point the hot air anti-icing used on fighters and some executive jets becomes inefficient for the removal of ice, and electrical heat must be used. Because the thermal conductivity of acrylic is one-fifth that of glass, the acrylic face ply must be .050 to .060 thick in order to meet the heat transfer requirements during anti-icing. By comparison, glass face plies are .11 to .25 thick in order to provide adequate hail resistance.

AD-A065 049 AIR FORCE FLIGHT DYNAMICS LAB WRIGHT-PATTERSON AFB OHIO F/G 1/3
CONFERENCE ON AEROSPACE TRANSPARENT MATERIALS AND ENCLOSURES (1--ETC(U)
DEC 78 R E WITTMAN

UNCLASSIFIED AFFDL-TR-78-168 NL

8 OF 10
ADA
065049



It is necessary to make a large number of calculations to determine the maximum heat requirements needed to maintain the windshield outer surface at 35°F. The heat load varies with airplane speed, flight altitude, ambient pressure and temperature, droplet size and density, and windshield slope, size, distance from the nose, and wetness of the outer surface. In Figure 4 is shown the results of calculations at the centerline of the airplane for a specific curved windshield configuration undergoing continuous icing at 7000 feet. Convection of heat is seen to be the major cause of heat transfer, and exists during all phases of flight, in good and bad weather. Evaporation of water absorbs the second largest amount of heat during continuous icing.

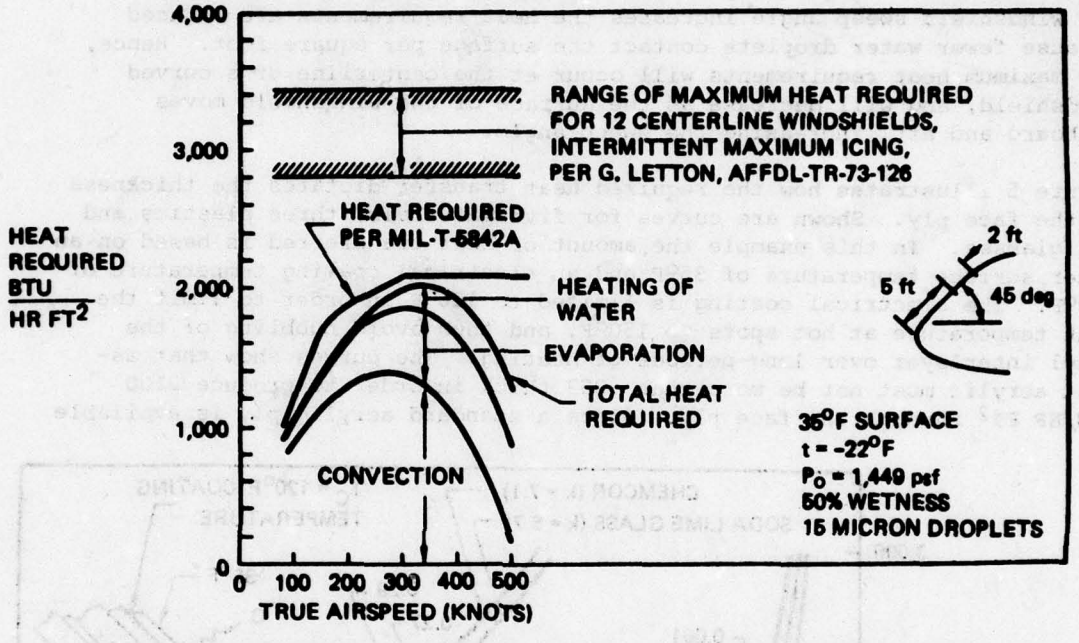


Figure 4. Heat Required at the ℄ for Continuous Maximum Icing at 7,000 ft

The amount of heat required to evaporate a portion of the water is directly dependent on the degree of wetness of the windshield. One of the advantages of plastic is that it does not run as wet as does glass, which can be 100% wet, and therefore, the heat loss due to evaporation from a plastic surface is much less than from a glass surface. When the plastic windshield is kept clean and polished, the water will bead up and run in rivulets, rather than spreading a film of water over the entire surface. Hence, the surface of the water that is exposed to evaporation is reduced. Sierracin used 20% wetness in their analysis of the Cessna Citation, while Northrop used 60% for the F-5A. The data in Figure 4 is based on 50% wetness.

During the day the sun provides a heat input to the windshield of 360 BTU/HR FT^2, a portion of which reduces the heat required for deicing. The heat required at night is therefore more severe. It can be seen on Figure 4 that the heat required to anti-ice increases with speed then reduces as

aerodynamic heating gradually increases the temperature of the air at the windshield. Thus, the maximum heat demands can be avoided by flying faster, or slower, than the peak heat demand speed, shown in Figure 4 to be about 340 knots.

Also shown is the heat flow requirement of MIL-T-5842A, which specifies 2100 BTU/HR FT^2 for flight above 300 knots true air speed. At the top of Figure 4 is a band representing the maximum heating requirements of 12 hypothetical centerline windshields having varying geometry, and undergoing intermittent maximum icing. This data, calculated by George Letton, and reported in AFML-TR-73-126, is based on windshields having zero sweep angle, which is the geometry at the centerline of a curved windshield. As the windshield sweep angle increases the heat requirements are reduced because fewer water droplets contact the surface per square foot. Hence, the maximum heat requirements will occur at the centerline of a curved windshield, and will decrease as the surface of the windshield moves outboard and aft, increasing the sweep angle.

Figure 5 illustrates how the required heat transfer dictates the thickness of the face ply. Shown are curves for five materials, three plastics and two glasses. In this example the amount of heat transferred is based on an outer surface temperature of 35°F and an electrical coating temperature of 120°F. The electrical coating is limited to 120°F in order to limit the peak temperature at hot spots to 150°F, and thus avoid bubbling of the vinyl interlayer over long periods of heating. The curves show that as-cast acrylic must not be more than .053 thick in order to produce 2100 BTU/HR FT^2 through the face ply. Since a standard acrylic ply is available

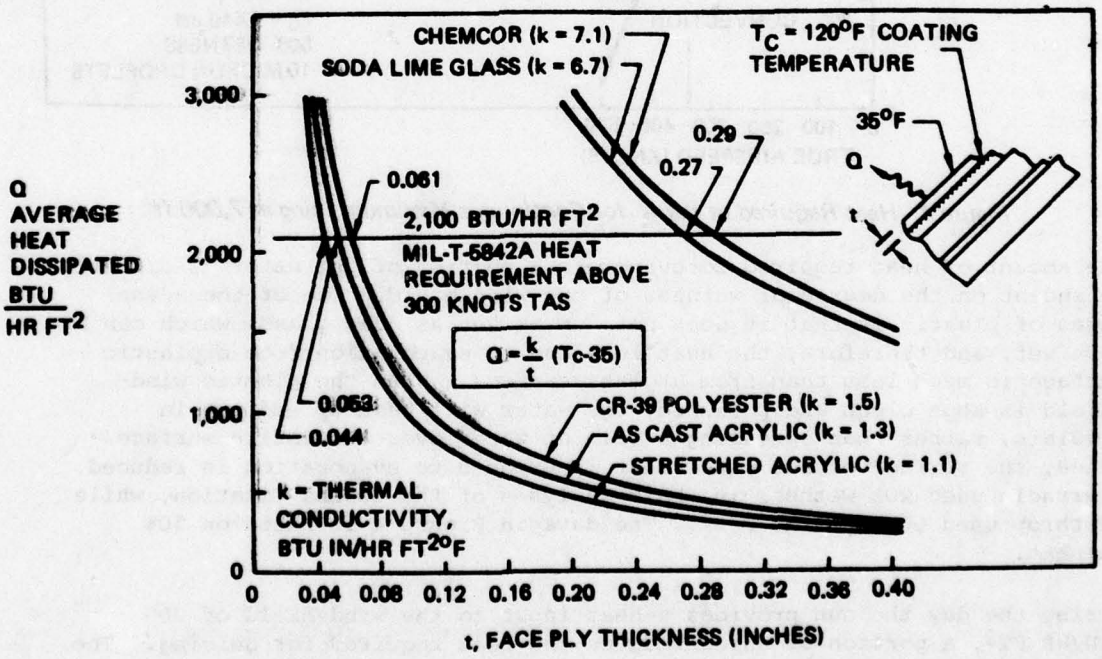


Figure 5. Face Ply Thickness Versus Average Heat Dissipated

at .055 (+.005, -.015) it is just about possible to meet the heat requirement with as-cast acrylic. Although thinner gages of acrylic are available, they have poorer optics and are subject to damage by shop handling. Figure 5 also shows that stretched acrylic must be .044 thick, while CR-39 polyester can be .061 thick and still meet the heat requirement. The much higher conductivity of soda lime glass and Chemcor show up to advantage here, since they can be .27 and .29 inches thick, respectively.

The data in Figure 5 is based on the average dissipation of power throughout the windshield. Manufacturing tolerances on coating thickness result in thicker than average coatings being deposited locally, resulting in reduced resistance and higher local temperatures. Figure 6 shows that the electric field lines tend to converge on the lower resistivity area, causing the equal potential lines to squeeze together. Since the power dissipated per square is the same, the smaller the area of the square, the hotter the surface. Hence, hot spots may tend to be located adjacent to regions of thicker coatings. Industry practice is to limit the range of average power/peak power to the 60% to 70% range ($.6 \leq Km \leq .7$). For the configuration in Figure 4, a Km = .6 means that the as-cast acrylic face sheet must be .040 inch thick in order to limit the coating temperature to 150°F. In order to use .055 inch as-cast acrylic, the tolerance on coating thickness must be tightened until Km = .88.

The need exists for higher thermal conductivity acrylics to improve the heat transfer capability of plastic face plies. No test data currently exists to define the length of time required to bubble vinyl interlayers at 150-160°F. The current data in MIL-HDBK-17A gives data above 190°F (40 hours or less), but data to 10,000 hours is needed.

Precipitation Static Effects

One of the characteristics of plastic is that it tends to retain a static charge to a greater extent than glass does. When the intensity of the charge is great enough, it will seek the grounded airframe by either flashing over to the windshield sills and posts, or by burning through the faceply to the electrical coating. When the electrical coating is very close to the outer surface, as is the case with an .050 as-cast acrylic faceply, the charge may burn through the faceply before it flashes over to the surrounding frame, ruining the windshield in the process.

The magnitude of P-static effects are dependent on windshield area, airplane speed, and windshield slope, as shown schematically in Figure 7. Charging current increases directly as surface area and speed increases. The initially uncharged airborne particle exchanges a charge with the airframe when it is deflected on impact. In the case of rain, snow, or ice crystals, aerodynamic heating gradually reduces the mass of the particle as speed increases until complete melting and evaporation occurs at about Mach 2.2, resulting in no exchange of charge.

Charging current increases non-linearly with increase in windshield slope. During 1970, the Air Force Avionics Laboratory at Wright Field sponsored flight tests of an F-4 with radome instrumentation designed to measure charging current at various stations on the radome, Figure 8. The frictional charging of the radome by precipitation was measured during

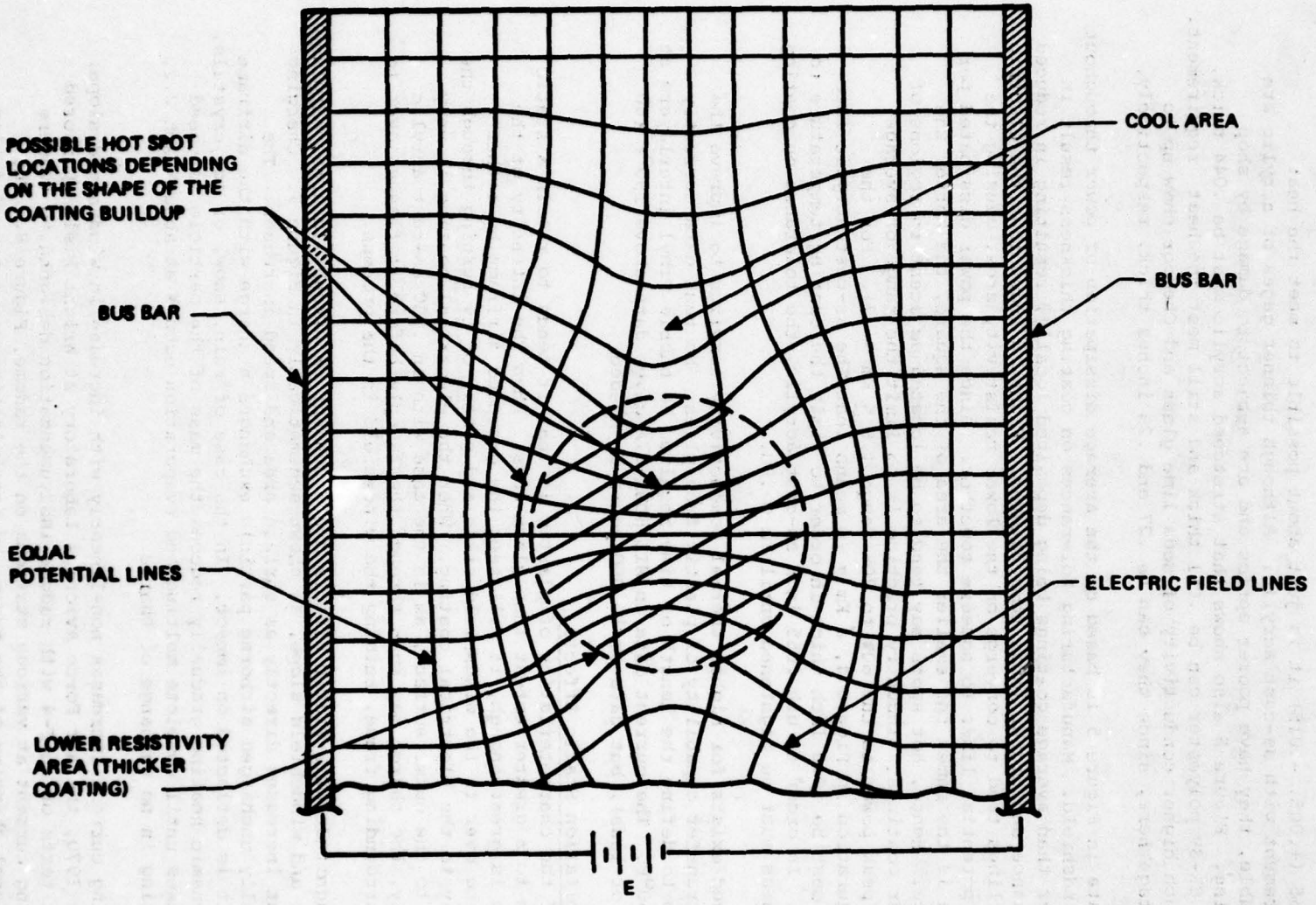


Figure 6. Hot Spots Caused by Manufacturing Tolerances on Coating Thickness

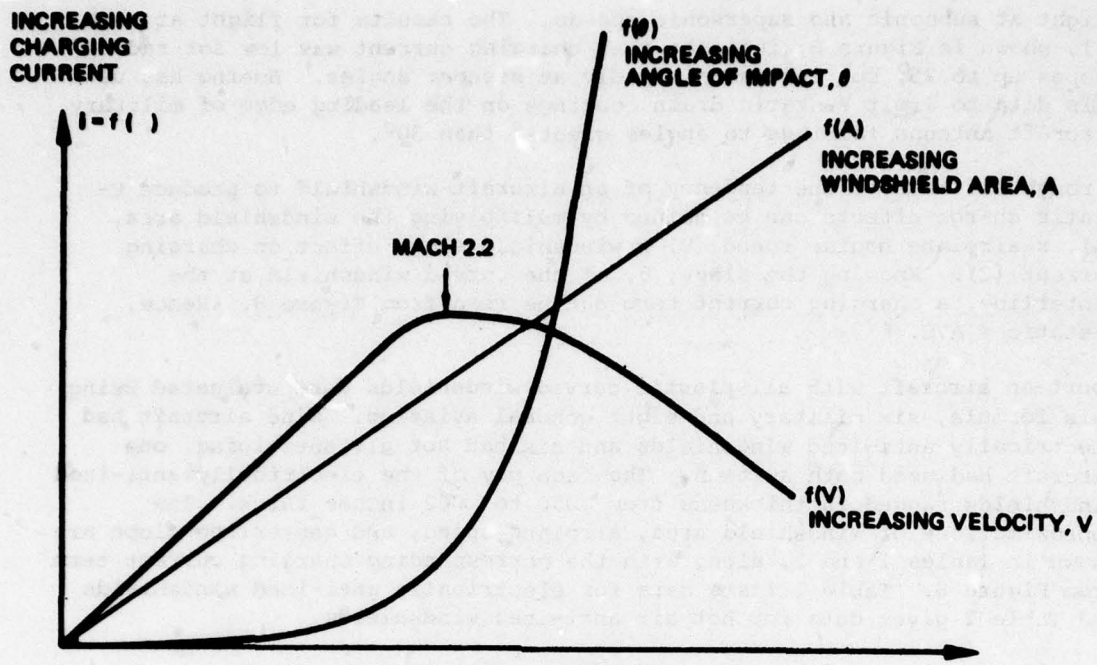


Figure 7. P-Static Charging Effects

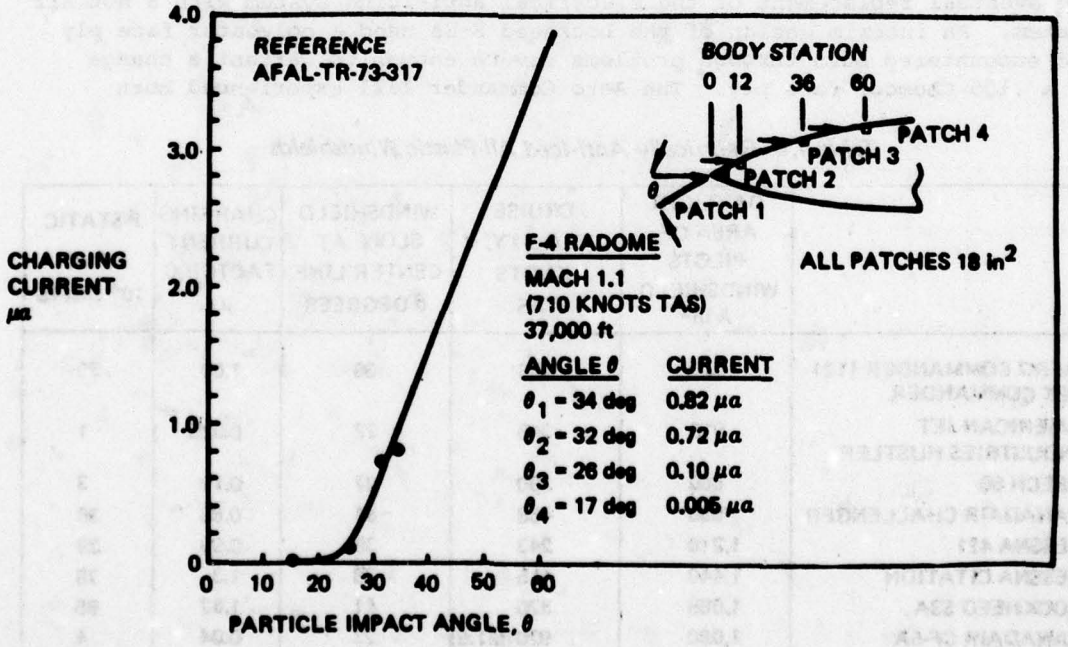


Figure 8. Charging Current Versus Particle Impact Angle

flight at subsonic and supersonic speeds. The results for flight at Mach 1.1, shown in Figure 8, indicate that charging current was low for radome slopes up to 25°, but increased rapidly at steeper angles. Boeing has used this data to limit P-static drain coatings on the leading edge of military aircraft antenna fairings to angles greater than 30°.

A rough estimate of the tendency of an aircraft windshield to produce P-static charge effects can be gained by multiplying the windshield area, (A), x airplane cruise speed (V) x windshield slope effect on charging current (C). Knowing the slope, θ, of the curved windshield at the centerline, a charging current term can be read from Figure 8. Hence, P-static = AVC.

Fourteen aircraft with all-plastic curved windshields were evaluated using this formula, six military and eight general aviation. Nine aircraft had electrically anti-iced windshields and six had hot air anti-icing, one aircraft had used both systems. The face ply of the electrically anti-iced windshields ranged in thickness from .050 to .062 inches thick. The approximations of windshield area, airplane speed, and centerline slope are shown in Tables 1 and 2, along with the corresponding charging current term from Figure 8. Table 1 lists data for electrically anti-iced windshields and Table 2 gives data for hot air anti-iced windshields.

The P-static term for electrically anti-iced windshields is plotted in Figure 9, and shows relatively high values for the Cessna Citation and Lockheed S3A, and relatively low values for the Canadair CF-5A, Beech 60 Duke, and American Jet Industries Hustler. The original design of the Citation experienced burn through of the plastic face ply, resulting in the eventual replacement of the electrical anti-icing system with a hot air system. An interim design of the Lockheed S-3A used a polyester face ply and encountered burn through problems severe enough to warrant a change to a .105 Chemcor face ply. The Aero Commander 1121 experienced burn

Table 1. Electrically Anti-Iced All-Plastic Windshields

	DAYLIGHT AREA OF PILOTS WINDSHIELD, A in^2	CRUISE VELOCITY, V KNOTS TAS	WINDSHIELD SLOPE AT CENTER LINE, θ DEGREES	CHARGING CURRENT FACTOR, C μa	P-STATIC = AVC 10^4 UNITS
AERO COMMANDER 1121 JET COMMANDER	820	435	36	1.09	39
AMERICAN JET INDUSTRIES HUSTLER	910	348	22	0.025	1
BEECH 60	650	230	27	0.19	3
CANADAIR CHALLENGER	890	458	34	0.88	36
CESSNA 421	1,210	243	35	0.99	29
CESSNA CITATION	1,440	415	38	1.3	78
LOCKHEED S3A	1,085	370	41	1.62	65
CANADAIR CF-5A	1,080	920(M1.6)	23	0.04	4
HFB HANSAJET	1,048	443	32	0.86	31

Table 2. Hot Air Anti-Iced All-Plastic Windshields

	DAYLIGHT AREA OF PILOTS WINDSHIELD A in^2	CRUISE VELOCITY, V KNOTS TAS	WINDSHIELD SLOPE AT CENTERLINE, θ DEGREES	CHARGING CURRENT FACTOR, C μa	P-STATIC = AVC 10^4 UNITS
CESSNA CITATION	1,440	415	38	1.3	78
GENERAL DYNAMICS F-111	1,440	1,167 (M2.0)	20	0.01	2
LEARJET	1,004	495	33	0.77	38
McDONNELL F-15	1,455	1,432 (M2.5)	27	0.19	40
NORTH AMERICAN A5	1,409	1,204 (M2.1)	21	0.015	3
ROCKWELL B-1	1,736	920 (M1.6)	25	0.08	13
(No. 1 PROTOTYPE—HOT AIR FOR RAIN REMOVAL AND PARTIAL ANTI-ICE)					

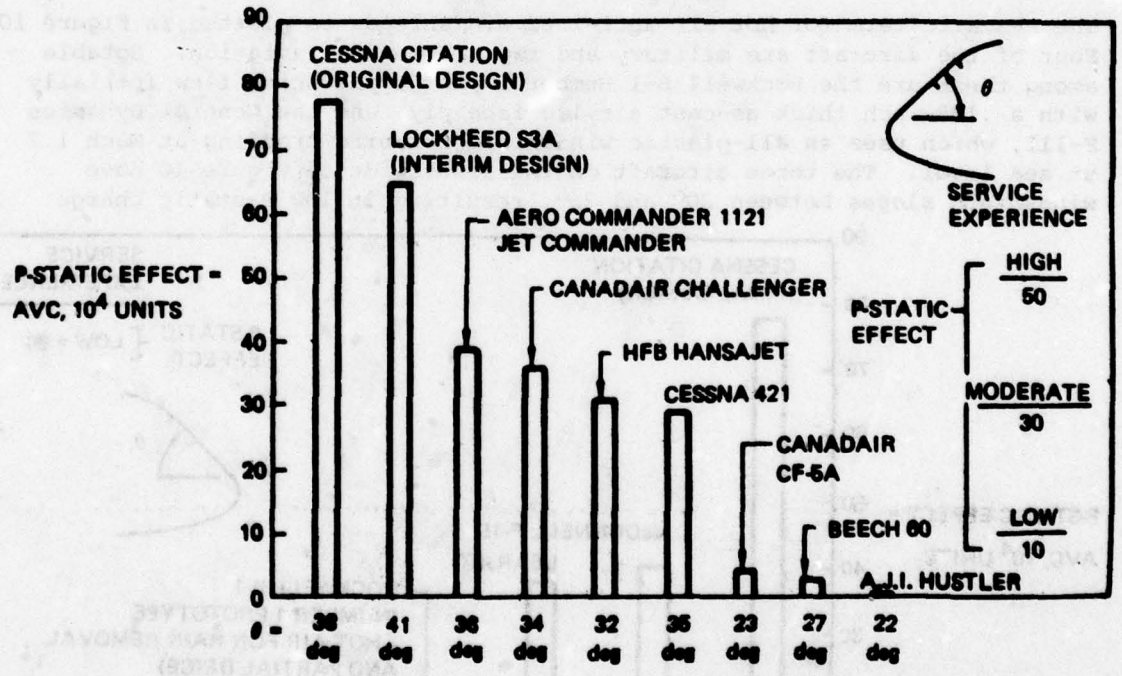


Figure 9. Electrically Anti-Iced All-Plastic Windshields

through of the laminated outer pane of its double pane design, resulting in the replacement of the outer pane with an electrically heated laminated glass pane. Service experience with the HFB Hansajet has resulted in the need to apply P-static drain polishes regularly, as reported by P. J. Sharp in AFML-TR-73-126. The Cessna 421 has experienced burn through of the face ply sufficiently often to cause Cessna to be actively seeking a solution for its double curvature windshield. The Canadair CF-5A, designed by Northrop, has not experienced burn through, except at the sensor, which was located in the .062 inch face ply, .030 inch from the outer surface. This was fixed by painting a ring of silver acrylic around the sensor and grounding it. Northrop has removed the electrical anti-ice system from the F-5E because of recurring electrical shocks to the ground crew and pilot. The Beech 60 Duke has had a few isolated incidents of burn through, but it is not a problem, and the windshield is considered to be a successful design. Both the Lockheed S-3A and the A.J.I. Hustler have windshields of similar area, and have similar cruise speeds. But the P-static effect is 100 times greater on the S-3A because of its steeper windshield slope. A suggested scale of P-static effect is shown in Figure 9, wherein a value of 10 is judged to be a low effect, 30 is a moderate effect and 50 is a high effect. A review of the service history of each airplane is required in order to validate the accuracy of this scale.

The P-static term for hot air anti-iced windshields is plotted in Figure 10. Four of the aircraft are military and two are general aviation. Notable among these are the Rockwell B-1 Number 1 prototype, which flew initially with a .188-inch thick as-cast acrylic face ply, and the General Dynamics F-111, which uses an all-plastic windshield for bird proofing at Mach 1.2 at sea level. The three aircraft on the right side of Figure 10 have windshield slopes between 20° and 25°, resulting in low P-static charge

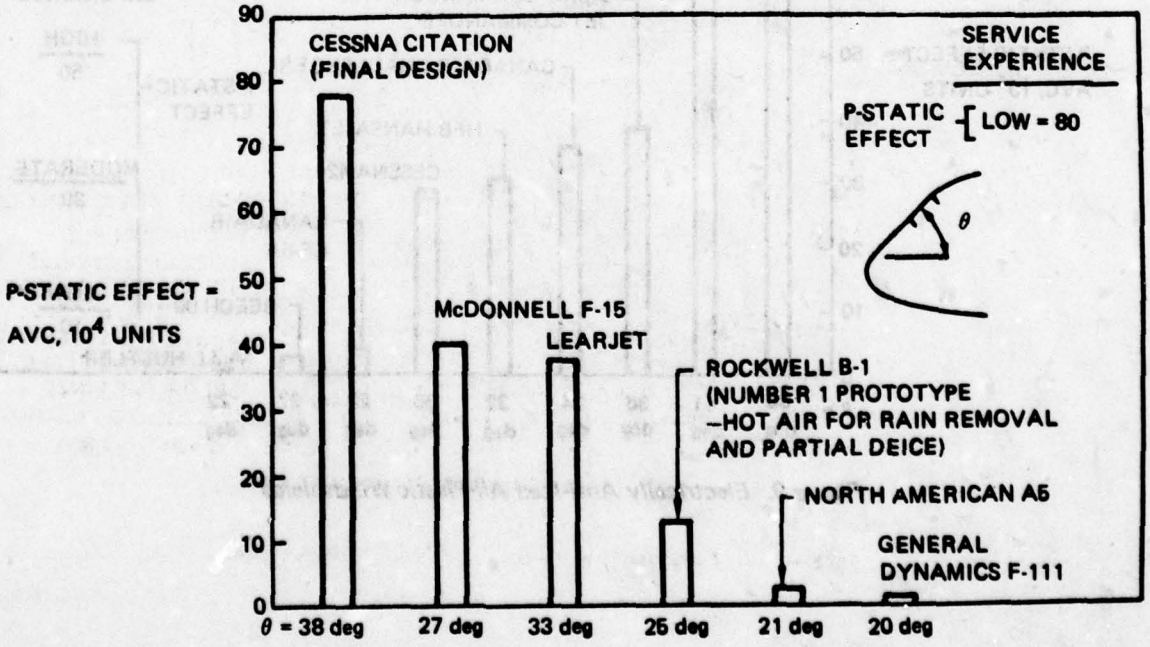


Figure 10. Hot Air Anti-Iced All-Plastic Windshields

effects. No P-static problems have been reported for any of these six windshields and it is believed that they are much more tolerant of P-static effects due to the absence of the electrical anti-ice coating. A suggested scale of 80 for a low P-static effect is shown in Figure 10.

The rough estimate of P-static = AVC indicates that there are significant differences in P-static sensitivity between different aircraft configurations. In order to illustrate these differences, the nine electrically deiced windshields are plotted in Figure 11, with windshield area and aircraft velocity in each axis. It is desired to lay a series of windshield slope lines on this graph, but their location can only be judged by the service history of the aircraft shown. Using the value of P-static = 30 x 10^4 from Figure 9 as a moderate value, curves of constant slope have been drawn. The charging current associated with each angle has been taken from Figure 8. In order to use the curves, the designer would enter the graph knowing the area, velocity, and slope of his design.

If his windshield slope was, say, 30° and his area and velocity placed him well above the 30° line, he should expect to have high P-static charge effects. If he is well below the 30° line his windshield should experience low P-static charge effects. A review of the service history of each airplane shown is required in order to validate the accuracy of these curves.

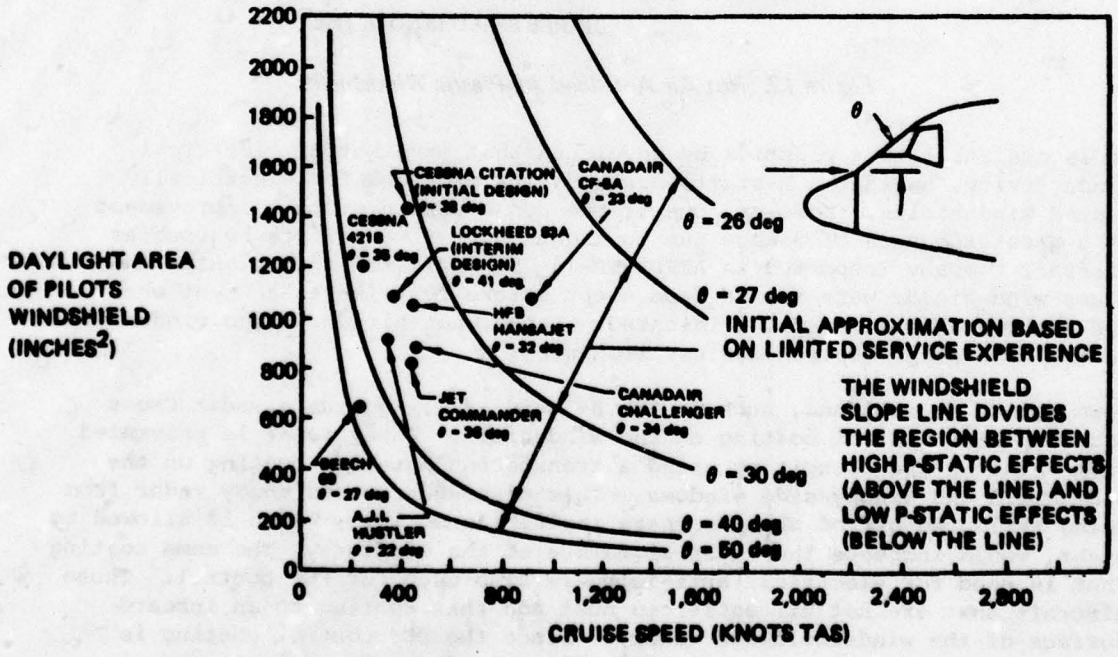


Figure 11. Electrically Anti-Iced All-Plastic Windshields

Similarly, the hot air deiced aircraft are shown in Figure 12, with the constant slope curves based on a value of P-static = 80 x 10^4. If the service history of these aircraft indicate low P-static effects on windshield durability, then the curves could be raised until some other P-static effect, such as radio interference, was encountered.

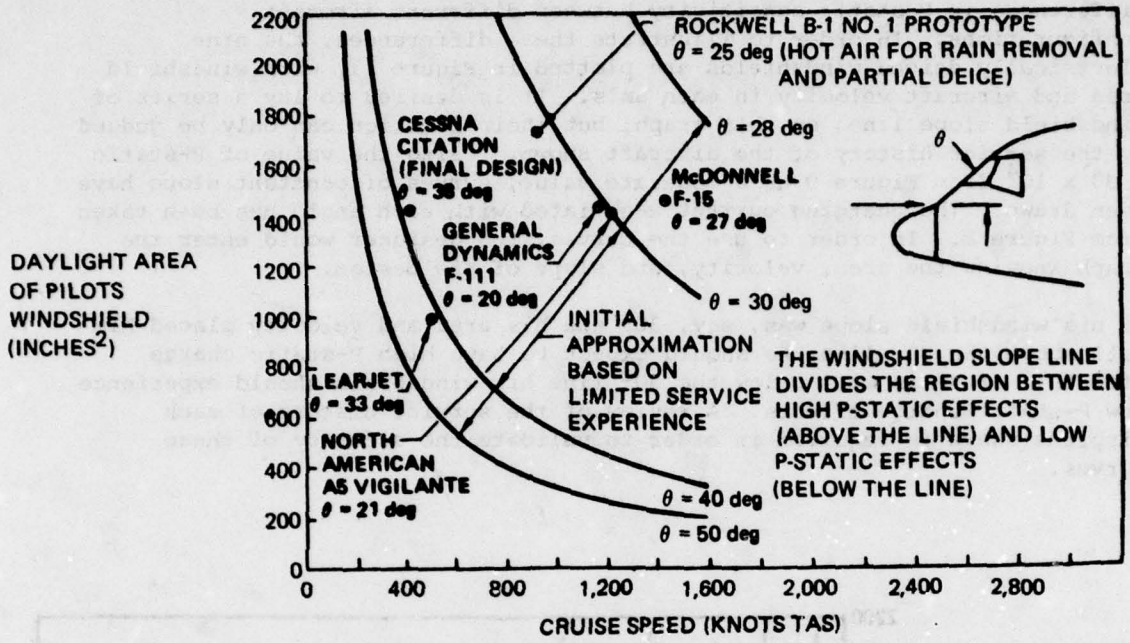


Figure 12. Hot Air Anti-Iced All-Plastic Windshields

It is desirable that plastics be developed that have better electrical conductivity, so that a P-static drain can be provided for electrically heated windshields. However, one of the consequences of this improvement is a greater chance of damage due to lightning strike. Tests by Douglas Aircraft Company (reported in AFFDL-TR-76-75) indicated that plastic and glass windshields were immune from swept stroke restrike attachment when the electrical coating was eliminated. Hence, hot air anti-iced windshields have a natural protection against lightning.

Some military airplanes, such as the B-1 and F-111 require a Radar Cross Section (RCS) control coating on the windshield. Enemy radar is prevented from entering the cockpit by using a transparent metallic coating on the windshield and canopy/side windows. This coating prevents enemy radar from being reflected off of sharp corners inside the cockpit, which if allowed to occur, would increase the radar signature of the airplane. The same coating that is used for electrical anti-icing is also used for RCS control. Those aircraft that are hot air anti-iced must add this coating to an inboard surface of the windshield and canopy. Since the RCS control coating is usually grounded, it must be located well away from the outer surface in order to prevent P-static charge burn through on those windshield configurations that would develop high P-static charge.

Scratch Resistance

For those aircraft that do not use hot air for anti-icing and rain removal the primary cause of scratching of the plastic face ply is the windshield wiper, Figure 13. Other causes of scratching include in-flight contact with dust, which can be reduced with low windshield slopes and blended designs, and scratches due to improper ground maintenance.

PLASTIC IS SCRATCHED BY

1. **WINDSHIELD WIPER ABRASION**
2. **IN-FLIGHT CONTACT WITH DUST PARTICLES**
3. **CLEANING DURING MAINTENANCE**

SOLUTIONS TO SCRATCHING PROBLEM

1. **RAIN REPELLANT USED IN PLACE OF WIPERS**
2. **HOT AIR RAIN REMOVAL, OR SPECIAL WIPER DESIGN**
3. **HARD PLASTICS, SUCH AS CR-39 POLYESTER**
4. **HARD COATINGS, SUCH AS DOW CORNING ARC**
5. **TRAINING OF MAINTENANCE PERSONNEL**
6. **COVERS FOR WINDSHIELD AND CANOPY WHEN AIRCRAFT IS PARKED OUTSIDE**

Figure 13. Scratching of Plastic Windshields

Many military and commercial aircraft use a rain repellant system, such as the Boeing developed Rainboe, as the primary means of clearing rain, with wipers used only during taxi and low speed flight. On some aircraft, such as the Northrop F-5, rain repellant is the only means of clearing rain. Almost all general aviation aircraft have no rain removal system for their all-plastic windshields. When the plastic is kept clean and polished, the water beads up and blows off at low speed. Adequate vision between the beads exists during taxi. Only a few general aviation aircraft have wipers, (Beech King Air, Piper Cheyenne and Navajo) and these aircraft have electrically heated, laminated glass windshields.

Solutions to wiper scratching include the use of hot air for rain removal (as used on the Lockheed C-141 and Douglas DC-8, as well as many smaller aircraft), the use of water pumped to the wiper blade as a lubricant (as used on an interim design of the Lockheed S-3A), and the potential use of specially designed wiper blades, now in development. Since the wiper represents a source of drag its elimination is desirable, particularly on long range aircraft.

Additional solutions that have been applied in the past include the application of hard plastics, such as CR-39 polyester, for face plies, and the addition of hard coatings to face plies. CR-39 is a hard, brittle, notch sensitive, plastic that can be hot formed to single curvature shapes, prior to lamination. It has been used on a number of helicopter designs, as well as on general aviation aircraft. Its most recent application was on an interim design of the Lockheed S-3A. CR-39 is also widely used for shatterproof sunglasses and prescription lenses.

A successful hard coating remains to be developed, although coatings now in development may show promise. Sustained load tests at 100% continuous humidity at Boeing on coated and uncoated stretched acrylic specimens resulted in coated specimens developing crazing sooner than uncoated specimens, indicating that the coating tended to embrittle the surface.

The training of ground personnel to avoid touching the all-plastic windshield is necessary to prevent scratches caused by incorrect cleaning. Owners of Learjets have placed DO NOT TOUCH WINDSHIELD signs on the instrument panel glare shield to warn ground personnel. Military and general aviation aircraft have similar usage rates, about 600 hours/year. This contrasts significantly with commercial transports, which average 2200-3400 hours/year, with some operators flying over 5000 hours/year. Thus, the military airplane spends over 90% of its life on the ground, usually parked on flight lines where it is exposed to sun, rain, industrial pollutants, and wind borne dust. The sun deteriorates electrical coatings, especially certain types of gold coatings. The sun also deteriorates moisture seals, which protect the electrical coatings and bus bars.

Windshield and canopy covers have been observed on general aviation aircraft and on Russian military aircraft. More widespread use of covers would extend windshield life.

Contraction of Plastic at Low Temperatures

The coefficient of thermal expansion of acrylic is seven times greater than glass and three times greater than aluminum. As a result of this difference between the windshield materials and the airframe, thermal loads are induced in the windshield and airframe during high altitude flight at low temperatures. The acrylic contracts relative to the aluminum frame, inducing tension stress in the acrylic and compression stress in the aluminum. A non-clamping edge attachment relieves this problem, but also prevents the use of a hoop tension load path for cabin pressure loads. Some manufacturers, such as General Dynamics and Rockwell, are using the hoop tension approach and designing the windshield and support frame for both hoop loads and thermal loads.

A glass faced stretched acrylic windshield must be heated continuously during flight in order to reduce the thermal loads in the interlayer, which lead to delamination and eventual premature windshield replacement. This means that the airplane electrical system must continually expend power to maintain the windshield within its pre-set temperature limits, regardless of whether icing conditions exist or not. Major airframe manufacturers and commercial operators have generally concluded that the life of both composite and laminated glass windshields is significantly extended when the windshield operates with heat on at all times. This use of energy is not needed on a hot air anti-iced all-plastic windshield, since the hot air system is used only as required for ice and rain removal.

Advantages and Limitations of Hot Air Anti-Icing

The main advantages of hot air anti-icing and rain removal is the application of heat directly to the outer surface and the elimination of wipers, Figure 14. The use of hot air for these purposes is limited to turbine engine aircraft, which have an air supply available. However,

ADVANTAGES OF HOT-AIR ANTI-ICING

1. HEAT IS APPLIED DIRECTLY TO THE OUTER SURFACE OF THE WINDSHIELD.
2. THIN FACE PLY CAN BE REMOVED, REDUCING THE POTENTIAL FOR INTERLAYER OVERHEAT DAMAGE.
3. P-STATIC BURN THROUGH ELIMINATED.
4. LIGHTNING STRIKE ELIMINATED.
5. WINDSHIELD WIPERS CAN BE REMOVED, REDUCING SCRATCHING AND AIRFRAME DRAG.
6. REDUCED ENERGY USAGE, SINCE HOT AIR IS ONLY REQUIRED DURING RAIN AND ICING.

Figure 14. Hot Air Anti-Icing

combustion heaters are in service on piston engine aircraft for cabin heating and their use could be extended to this occasional duty. The heat is applied directly to the ice and frost, rather than through a low conductivity plastic face ply. Elimination of the face ply reduces the potential for interlayer overheating, but maximum surface temperatures must be limited to about 225°F in order to prevent relaxation of the stretched acrylic. Use of a thick plastic face ply as a heat shield for the stretched acrylic is a design option, but laminated plastic windshields do not use them. This is an area where the low conductivity of plastic can be used to advantage.

The removal of the electrical coating eliminates P-Static burnthrough and eliminates the possibility of lightning strike. The elimination of the wipers reduces the possibility of scratching. The low wetting characteristic of plastic results in beading of water. The elimination of wipers also reduces drag, which is especially important on long range aircraft. Hot air anti-icing results in less energy usage over the life of the airplane than does electrical anti-icing.

Hot air anti-icing is limited to windshields 25 to 35 inches in height, Figure 15, since the air temperature drops with distance from the nozzle. However, both the F-15 and the F-111 have windshields about 41 inches long, and use hot air successfully.

LIMITATIONS OF HOT AIR ANTI-ICING

1. WINDSHIELD HEIGHT LIMITED TO 25 TO 35 INCHES.
2. ENGINE BLEED AIR SUPPLY IS LIMITED DURING DESCENT.
3. COMMERCIAL TRANSPORT CABIN REQUIRES LARGE AIR SUPPLY, DEPENDING ON EFFICIENCY OF CABIN SEALING SYSTEM.
4. BLEED AIR IS ALSO REQUIRED TO DEICE WING LEADING EDGE AND ENGINE INLET
5. AIRPLANE LANDING TECHNIQUE CAN LIMIT THE AIR AVAILABLE FOR DEICING OR RAIN REMOVAL.

Figure 15. Hot Air Anti-Icing

Engine bleed air is used for environmental control of the cabin, and for deicing the wing leading edge and engine inlet. Since there is a limit to the air available from the engine, there may not be enough excess air available for anti-icing and rain removal. When the pressure cabin is large, as in a modern commercial transport, the leakage rate at door and window seals can result in a high demand for bleed air, depending on the efficiency of the cabin sealing system. The lowest air supply occurs during descent and loiter, when the engines are at idle RPM, which coincides with the region of maximum icing below 22,000 feet. Airplane landing technique also has an effect on the anti-icing system, since an airplane that lands with power on can continue to anti-ice and clear rain, whereas an airplane that chops the engines at the threshold cannot. Solutions to this problem include the use of a combustion heater, or a boost fan in series with the bleed air system, or use of the APU.

Aircraft that are Best Suited for Hot Air Deicing

Aircraft with a single crewman, such as fighters, or with the crew seated in tandem, such as trainers or medium range bombers (North American A5) have the smallest windshields and are most easily anti-iced with hot air.

The next best suited for hot air is the twin engine aircraft with the crew seated side by side in a small cockpit or passenger cabin. The twin engined airplane must be designed for safe flight on one engine, and hence has ample engine bleed air available during normal twin engine operation. The small cockpit, or passenger cabin, minimizes the air required for environment control, as well as minimizing the amount of leakage from the cabin. The types of aircraft that fit this description are the Navy antisubmarine warfare aircraft, such as the Lockheed S-3A, Navy attack aircraft, such as the Grumman A6A, a medium range bomber or tactical fighter, such as the General Dynamics F-111. and an executive jet, such as the Learjet or Cessna Citation. All of the above twin engine aircraft use hot air for anti-icing and rain removal except the S3A.

Larger, four engine aircraft have also used hot air for anti-icing and rain removal. The Rockwell B-1 has a hot air system installed as a backup for the electrical anti-icing system. Both the Lockheed C-141 and Douglas DC-8 use hot air for rain removal. Initial versions of the Boeing KC-135 used hot air for rain removal.

The probability of experiencing both the loss of one engine and an icing encounter on the same flight is very remote. But this extreme flight condition can be designed for by switching all available air to the pilots windshield so that maximum visibility can be maintained during the critical landing phase when ice and rain removal is most necessary.

A New Hot Air Distribution Concept

In trying to improve the efficiency of hot air systems, either the temperature of the air must be increased, or the mass flow increased by increasing the velocity (increased pressure), or alternate methods of hot air distribution must be considered. One possible method of distributing the air more uniformly is shown in Figure 16. In this concept the hot air is passed through a rotating slotted tube which moves back and forth across the windshield, subjecting the cleared area to the same temperature of air

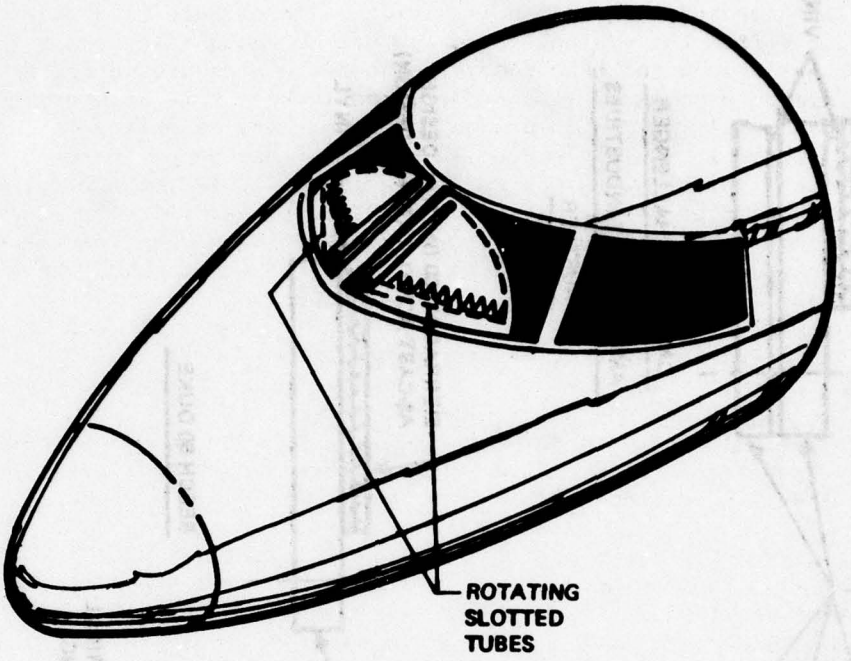


Figure 16. Hot Air Distribution Concept

throughout. The tubes would be stored together externally at the windshield center post, or separately at the base of the windshield. Both rain and ice would be cleared with this system.

It is proposed to flight test this concept on a military airplane that is currently using an electrically anti-iced composite windshield. In this approach, the windshield vendor would supply the copilots windshield without the glass face ply and electrical anti-icing. The hot air system would be installed on the copilots windshield. Flight tests under icing conditions would take place, with vision assured through the electrically anti-iced pilots windshield.

Composite windshields have been used on three of the most recent military airplanes, the Lockheed S3A, Rockwell B-1, and Boeing YC-14. One of these airplanes may be a good candidate for flight testing this system.

Cross Sections of All-Plastic Windshields

Details of electrically anti-iced all-plastic windshields are shown in Figure 17. The basic load carrying ply is stretched acrylic, with vinyl interlayers, and a variety of material used for face plys. Note that electrical anti-icing of all plastic windshields has been applied mainly in the general aviation field.

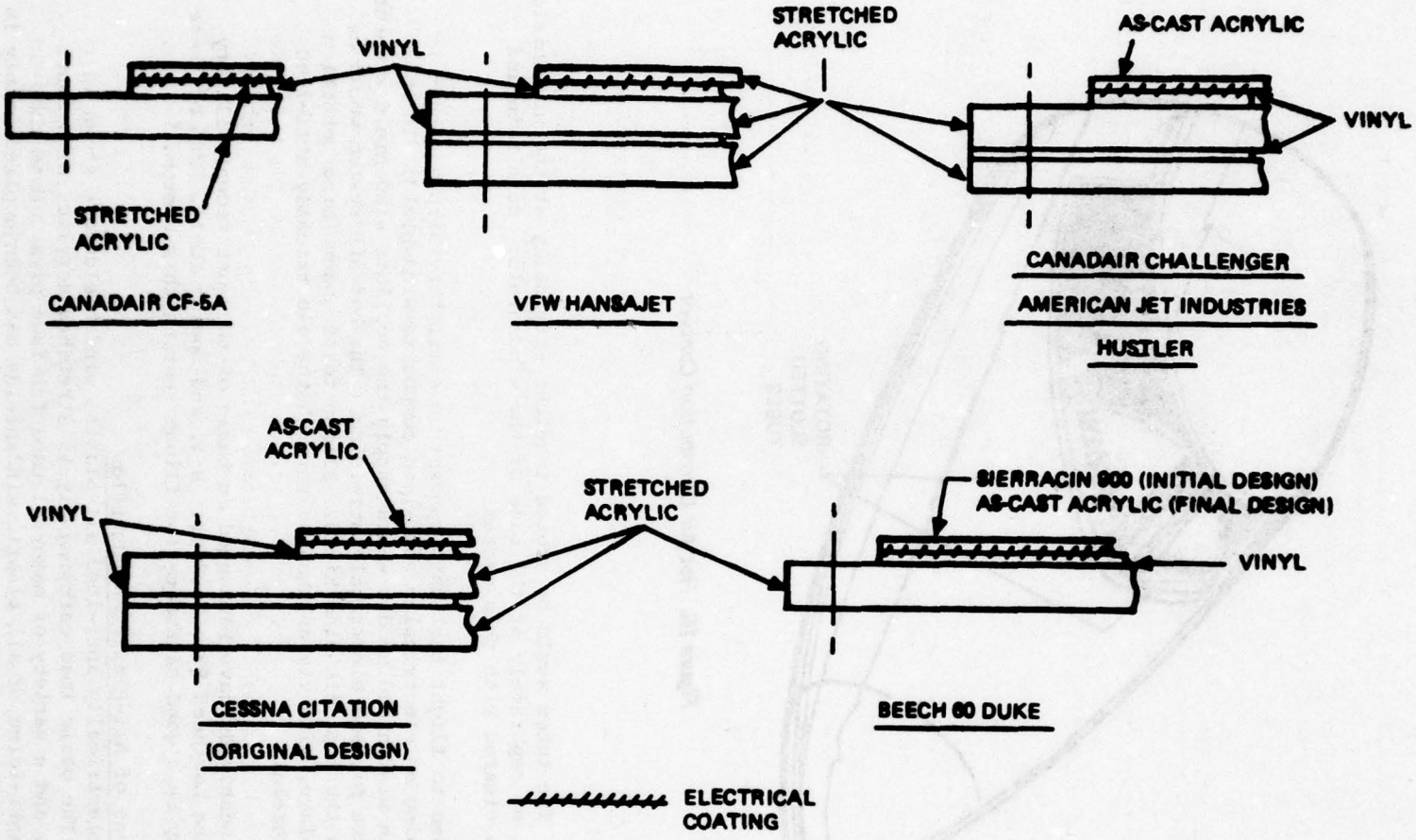


Figure 17. Electrically Anti-Iced All-Plastic Windshields

Hot air anti-iced all-plastic windshields are shown in Figure 18, most of them military aircraft. Both polycarbonate and stretched acrylic have been used for the main plys. A variety of interlayers have been used, depending on flight temperature requirements. As-cast acrylic has been used for the face ply.

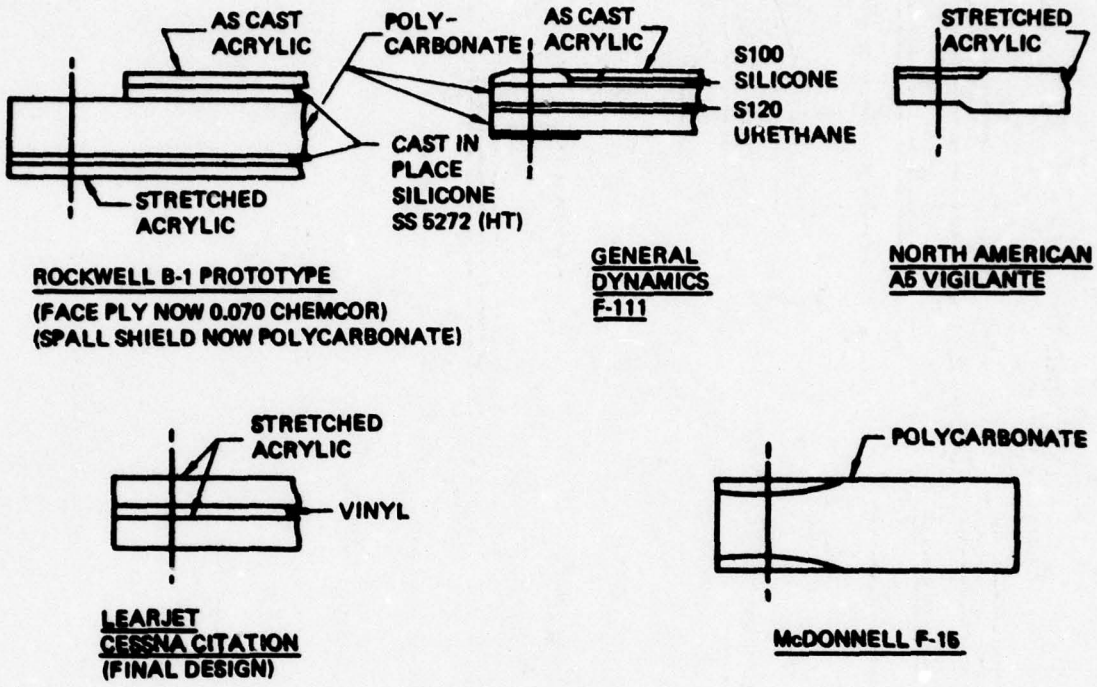


Figure 18. Hot Air Anti-Iced All-Plastic Windshields

Conclusions

A low cost forward fuselage depends upon the use of a curved windshield in order to provide a circular cross section pressure cabin. The all-plastic windshield can provide a low cost, long life design when hot air is used for rain removal and deicing. Widespread use of this design on military fighters, trainers, attack aircraft, and a few medium bombers may be extended to aircraft with larger windshields through use of the rotating tube air distribution concept. All-plastic windshields require trained ground personnel in order to avoid accidental scratches. Since military aircraft spend over 90% of their life on the ground their windshields should be protected from the sun. More widespread use of protective covers should be emphasized.

Acknowledgment

Recognition must be given to the many Boeing engineers who contributed specialized knowledge to this report, and to the airframe and windshield industry personnel who provided valuable service data. The opinions expressed are the responsibility of the author.

DESIGN, DEVELOPMENT AND TESTING OF A LIGHTWEIGHT BIRD-PROOF COCKPIT ENCLOSURE FOR THE F-111

J. B. Olson
Sierracin Corporation
Sylmar Division/Engineering
Sylmar, California

PRECEDING PAGE BLANK-NOT FILMED

DESIGN, DEVELOPMENT AND TESTING OF A LIGHTWEIGHT BIRD-PROOF COCKPIT ENCLOSURE FOR THE F-111

Jan B. Olson
Chief Engineer

SIERRACIN/SYLMAR

ABSTRACT

When the cockpit transparencies were originally specified for the F-111, limitations imposed by then-available transparent materials prevented simultaneous attainment of all desired characteristics. The high temperature environment and weight restriction were primarily responsible for selection of a glass/silicone/glass laminate with essentially no bird impact resistance. Several instances of aircraft and some crew losses, coupled with emergence of polycarbonate as a viable aircraft glazing material, prompted the Air Force to fund a program with the original glass supplier to develop a birdproof retrofit windshield. This program resulted in a windshield that vastly exceeded the bird requirement in the central area, but was not properly matched to the structure, resulting in a failure to meet the design goal at the critical aft edge. Also, it was somewhat heavy, precluding retrofit to particularly weight sensitive versions of the aircraft, and initially suffered from optical problems, including the infamous "rainbow" phenomenon.

At that time, Sierracin proposed and the Air Force funded a program to remove these limitations by refining the design, including a thinner, simpler cross section having a better balance of center-to-edge performance and employing less optically sensitive processing.

This program was conducted as a cooperative effort involving the Air Force Flight Dynamics Laboratory, the University of Dayton and Sierracin/Sylmar. It was extremely successful in that all goals were met or exceeded, including achievement of lighter weight transparencies with improved resistance to bird impact and thermal exposure. This achievement was the result of the development of some very innovative design concepts, particularly in the area of the aft edge where extremely high impact loads must be transmitted from a very limber windshield to necessarily rigid aircraft framing.

This paper recounts the significant aspects of the program, including evaluation of novel design concepts, developmental testing and final bird impact, pressure-thermal cycle and flight evaluation verification testing.

PRECEDING PAGE BLANK-NOT FILMED

INTRODUCTION

Background

Certain characteristics of the F-111 aircraft (Figure 1) are unusual and relevant to this paper in that they create stringent demands on the cockpit transparencies. Included among these are that it:

- --has a radar penetration mission in which it flies very fast at extremely low altitudes where birds and high skin temperatures occur
- --has a large transparent frontal area because of the side-by-side seating
- --uses an ejectable crew module with its own strict weight and balance restrictions
- --has windshields with extremely low viewing angles, hence severe optical criticality.

When the aircraft was initially designed in the early 1960's, the only usable transparent materials which were capable of maintaining required properties at the high skin temperatures were glass and silicone.

Accordingly, the original design consisted of two plies of thin, strengthened glass laminated together with a silicone interlayer (see Figure 2). The glass plies carried pressurization loads in hoop tension with these loads uniformly introduced through titanium straps bonded to both surfaces of each glass ply. The adjacent crew module structure was designed to interface with the resulting metal edge.

This "all-glass" design ultimately yielded good optical quality, but was apparently quite difficult to manufacture and therefore very expensive. More importantly, this cross section, which is not significantly thicker than that of an automobile windshield, has virtually no bird impact resistance. This weakness combined with the F-111's high-speed, "nap-of-the-earth" mission and large transparent frontal area has resulted in the confirmed loss of at least six aircraft and two crew members to bird strikes. The birds that wreaked this havoc were as small as 1 1/4 ounces, which is less than 2% of the mass of the traditional four pound bird which all commercial and many military aircraft are required to resist.

These high losses to what, in most cases, would represent minor bird impacts on more conventional designs prompted the Air Force to initiate a program to develop bird-proof windshields and canopies retrofittable to the existing structure. While the program was prompted by critical need, it was the emergence of polycarbonate as a viable aircraft glazing material that made a practical solution appear feasible.

Initial Bird-Proofing Program

The initial program to bird-proof the F-111 was conducted by the supplier of the original all-glass parts. The resulting designs, shown in Figures 3 and 4, were polycarbonate laminates protected by acrylic facing plies with urethane interlayers used throughout. The temperature limitations of this thermoplastic urethane interlayer dictated the otherwise excessive thickness and weight of the outer ply in order to provide sufficient thermal insulation. It would appear, from a comparison of this cross section with that of the original glass laminate, that a similar edge design philosophy was employed based on load-bearing straps around the edges attached to each structural ply. To anyone familiar with the fabrication of optical grade polycarbonate laminates, it will be readily appreciated that this is an extremely difficult design, particularly at the extreme viewing angle of the F-111 windshield (reference Figure 5).

The original program included ten shipsets of windshields and canopies for flight evaluation. These initial parts suffered from severe optical problems including a phenomenon known as "rainbowing." Rainbowing results from the passage of polarized skylight through areas of high residual stress in the photo-elastically sensitive plastic plies. It is apparent at low altitudes, but becomes much more acute at high altitudes where the skylight is more completely polarized. An example of rainbowing is shown in Figure 6 with a polarizer superimposed to facilitate photography. When severe, rainbowing is considered quite objectionable by F-111 pilots.

Most of the thickness growth of the bird-proof retrofit over the original thin, all-glass laminate was outward, necessitating fairings to reconcile the new protruding mold line with that of the original capsule. The thicker design with the accompanying fairings was about 65 lbs. heavier than the glass design that it replaced. This weight increase precluded the adoption of this retrofit on one F-111 model, and inhibited the future growth potential of others without an extremely expensive capsule recertification program. This fact, coupled with optical problems and high acquisition cost, caused some alarm within the Air Force.

DISCUSSION

Advanced or Lightweight Bird-Proofing Program (ADBIRT)

The concern caused by the limited applicability, high acquisition cost and threat of optical problems apparently inherent in the early design invited competitive consideration. In light of this concern, Sierracin examined the problem and then presented an unsolicited proposal to the Air Force based on a simplified design concept which offered potentially significant reductions in weight, cost and optical problems. These initial Sierracin designs, shown in Figures 7 and 8, had the following features relative to the initial bird-proof designs shown in Figures 3 and 4:

--a high temperature interlayer, Sierracin S-100 silicone, eliminated the interlayer's thermal limitation, allowing the acrylic outer ply to

be reduced to a thickness dictated by the polycarbonate's thermal limits. (Subsequent reduction in thermal profile allowed it to be further reduced to the practical minimum, 1/8 inch.)

--these same high temperature properties of the silicone lifted processing restrictions, permitting use of an alternate manufacturing concept which promised better optical quality with little or no rainbow-producing residual stress.

--the protective inner ply of acrylic and its attaching interlayer were replaced by a ductile protective coating, Sierracin S-233, which had performed well in service on the interior surfaces of other polycarbonate transparencies, including those of the early F-15's and bird-proof A and T-37's.

Certain features of the original bird-proof design were retained in the initial Sierracin proposal for the sake of minimizing requalification testing, particularly bird testing. These included the numbers and thicknesses of the polycarbonate structural plies and retention of the reinforced plastic straps, or inserts, around the periphery.

Subsequently we learned that, although the original design had greatly exceeded the 4 lb., 500 knot design requirement in the center, it fell short of meeting that requirement at the edge by over 70 knots. Figure 9 broadly surveys that windshield's bird resistance capability. Realizing that impact energy is a function of velocity squared, this represents a disparity in center-to-edge capability of well over three-to-one. Put another way, the edge area of this design limits the windshield's bird resistance capability to less than 1/3 of that potentially inherent in its cross section, for which the weight penalty is paid over the entire area.

In spite of this accepted deficiency in the initial bird-proof design, the 500 knot requirement was to apply to our program. Not only was our windshield expected to be simpler and lighter, but now we were aware that it must also be stronger than its predecessor.

This revelation completely changed the nature of our program. What began as a straightforward effort to simply refine a proven design was transformed into a program requiring fundamental development leading to technical breakthrough. Instead of preserving much of the early design, we started from scratch with essentially no preconceived notions.

Because the need for basic development work was unforeseen at the time of our proposal, it was also unfunded by the Air Force. Sierracin management, however, recognized the fundamental approach as the only one likely to be successful, and underwrote our additional program costs.

Design Approach

As mentioned previously, the principal weakness in the previous design was at the aft arch support, particularly near the centerpost where the impact angle is most unfavorable. We therefore directed our initial activities

at cross sections and edge details which would maximize edge strength and compatibility with the torsionally stiff aft arch. We were prepared to sacrifice some of the excessive impact capability in the central area if necessary to accomplish this.

To more fully utilize polycarbonate's inherent bird impact resistance, we sought to take advantage of its tremendous ductility. As Figure 10 attempts to depict, this has the adverse effect of "trapping" more of the bird's kinetic energy resulting in higher loads at the critical aft edge. It also makes the problem of retaining the limber windshield to the rigid arch structure without edge failure considerably more difficult. The problem is further compounded by the need to interface with support hole spacing and edge distances chosen for the metal edge of the all-glass design, and totally inappropriate to conventional all-plastic design practice. It was obvious that new concepts of edge attachment and structural interaction were needed to overcome this dilemma.

Preliminary Laboratory Test Phase

The initial phase of the program involved gathering data on the dynamic response characteristics of various candidate composite beams and edge concepts. Figure 11 shows some of the coupons used in this activity. Variations tested included varying thicknesses and numbers of polycarbonate plies, interlayers of differing properties, edge designs with and without inserts and numerous bushing and edge member concepts.

Much of this testing and considerable valuable assistance in predicting and interpreting performance was ably provided by Mssrs. Blaine S. West and Paul E. Johnson of the University of Dayton under separate Air Force contract. Figure 12 shows some selected data attesting to the edge strength improvement achieved in this phase of the program. The edge design finally selected contains considerable, although somewhat subtle, novelty for which patent coverage is currently being sought.

Full-Scale Qualification Test Program

The next phase of the program involved bird testing of full-scale transparencies installed in actual crew modules at Arnold Engineering Development Center (AEDC) in Tullahoma, Tenn.

We selected the most producible of the designs that emerged from our laboratory test program as likely candidates. It was also the most limber design as it used the low modulus silicone interlayer throughout. We knew that this design's flexibility would result in more trapped energy, but we hoped that our much stronger edge would overcome the higher resultant edge loads.

It didn't, and the performance of this first design was a big disappointment! After passing slower speed shots, it failed at 410 knots, and it was back to the drawing board.

Additional Developmental Testing

Fortunately, this test did provide us with a much needed data point which enabled us to more accurately predict the required dynamic response characteristics. We hurriedly obtained needed data from additional testing in our own laboratory which enabled us to select new candidate cross sections for exploratory bird testing.

Six weeks after the 410 knot failure, we were back in bird test at AEDC with one each of these three windshield designs (two laminated and one monolithic polycarbonate mainply), plus a monolithic-mainply canopy. This quick recovery was a tremendous accomplishment, for which I take this opportunity to thank all those at Sierracin who contributed.

The results of this very instructive comparative bird test series are summarized below, and can generally be described as ranging from dismal failure to spectacular success.

1. Monolithic design - both windshield and canopy failed catastrophically. This confirmed previous data which suggests that thick polycarbonate (over 1/4 inch) performs less well than thin, and monolithic polycarbonate performs less well than an equivalent laminate. Accordingly, the monolithic approach was eliminated from further consideration on this program in spite of its other advantages.

2. Copolymer interlayer design - this part failed in an acceptable manner (i.e. broke, but would not have incapacitated the pilot or prevented return of the aircraft), and represented the best aft arch area bird impact performance to have been achieved on the F-111 program to that point in time. We now had a qualifiable design.

3. Polyurethane interlayer design - this design, shown in Figure 13, was spectacularly successful! The part withstood the design impact at the critical location near the aft arch. The actual velocity was 2% low at 489 knots, but within test tolerance. There was some cracking of the faceply and central polycarbonate ply, but the inner ply and all edge members and bonds, while exhibiting gross plastic deformation, were intact and attached! This was most gratifying as all design concepts, including some quite novel ones, performed as planned - a somewhat rare occurrence in this business. Needless to say, this design was selected for completion of the qualification testing.

   The performance of this design was so outstanding that it was suspected of being a fluke (movies showed that the bird had yawed in flight), so the shot was repeated later in the program. The performance in this second test (491 knots actual) was identical - breakage of the outer two plies, but only plastic deformation of the inner ply and edge attachments. We seemed to have found that optimum state where, at the extreme load condition, all critical components almost, but don't quite, fail.

4. Canopies - canopies representing reduced versions of the above three designs were evaluated and the results roughly paralleled those of the windshields; i.e. the monolith failed as previously mentioned, and both thermoplastic-interlayered versions passed without problems. The design that represents a scaled-down version of the selected windshield was chosen for the canopy and is shown in Figure 14.

Final Qualification Testing

The remainder of the qualification program was performed on the selected design, consisting of impacts at less critical locations plus a cyclic pressure/thermal fatigue life test with a verification bird test after completion. This portion of the program went smoothly, with all requirements being met with ease. With the exception of the long duration life test, this program was conducted from start to finish in only ten months, including all coupon fabrication, laboratory testing, tooling, fabrication of windshields and canopies, 18 bird shots, and additional unforeseen design and test activities.

SUMMARY

At the end of that time, all goals had been met and a bird-proof transparency system with no significant weight penalty over the original nonbird-proof design was qualified and available to the Air Force. This system is retrofittable to all models of the F-111 with no module recertification required.

Note in Table 1 that the Sierracin lightweight bird-proof transparencies almost equal the weight of the very unbird-proof all-glass panels. The nominal system weight increase is primarily due to the addition of the fairings, and even this 12 lb. difference could be eliminated, but little incentive exists to go further at this time.

As of this writing, the status of this program is that the Air Force has awarded Sierracin a production contract and rate tooling is underway with the first shipset of parts to be delivered in May.

CONCLUSION

The design resulting from this program is probably the most efficient in terms of bird impact resistance vs. weight of any aircraft transparency system to date. The technical success of this program has not only provided us with new insights into optimizing polycarbonate design, but could also be a model in the establishment and management of a program where technical breakthrough is the desired result. With the exception of unlimited funding and time (and when have we ever had those?), all factors conducive to a successful technical endeavor were present in the structuring and management of this program, namely:

1. the top priority dedication of a group of engineers with relevant specialized technical expertise,

2. a program managed by the technically responsible groups at both ends,

3. a customer (the Air Force, ably backed-up by the University of Dayton) who provided counsel, experience and support, but gave the technical specialists a free hand to innovate with a minimum of constraints or preconceived notions,

4. a clear understanding of the end objectives, with a minimum of definition as to the route to be taken, and

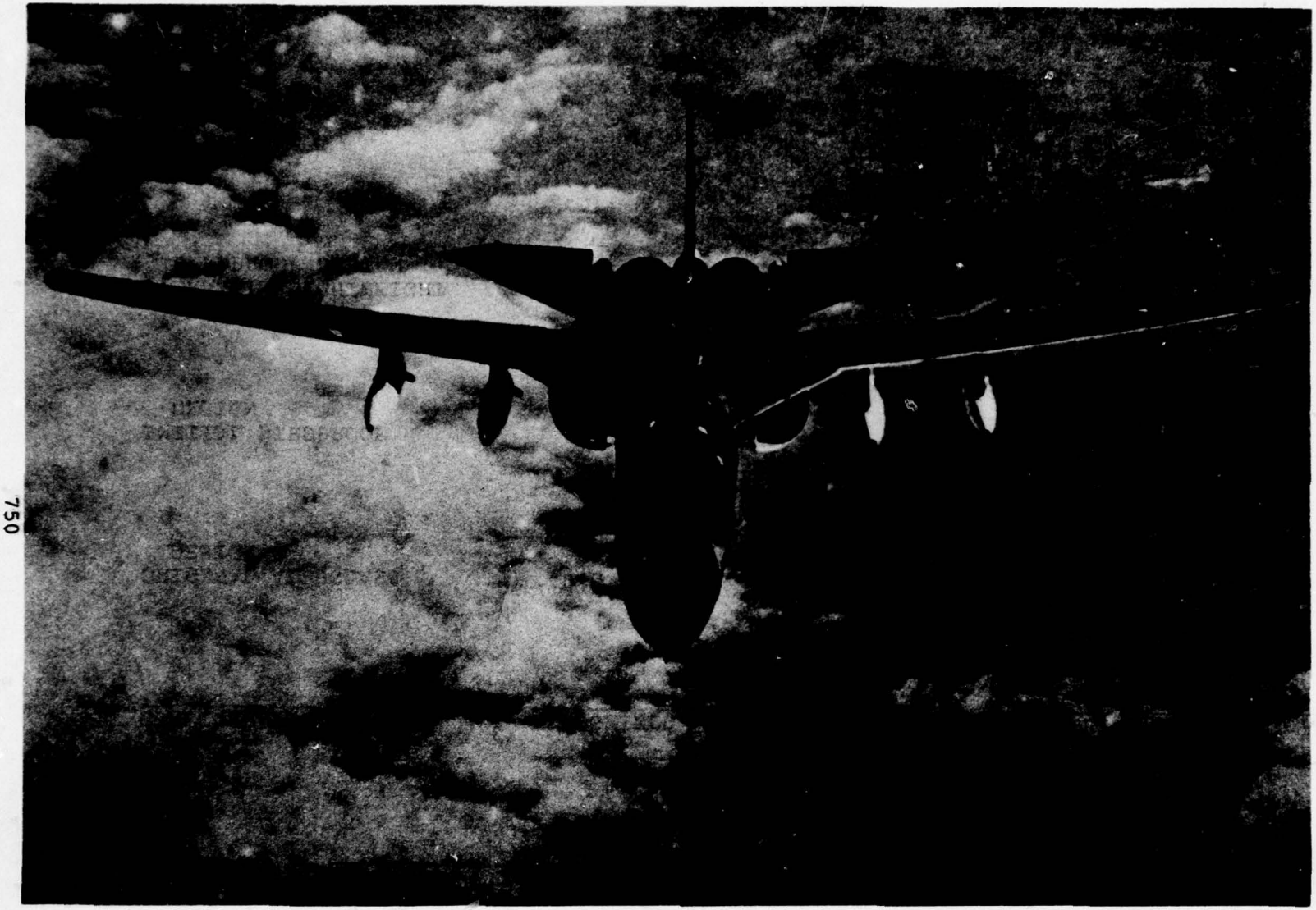
5. a contract and management support that was sufficiently elastic to allow conversion of an initial failure into a useful data point which led to ultimate success.

ACKNOWLEDGEMENTS

Sierracin wishes to express gratitude to the Air Force for the opportunity of participating in this challenging program. In particular, we wish to thank Mr. Robert E. Wittman and Capt. Forrest L. (Woody) Pretzer of the Flight Dynamics Laboratory (AFFDL/FEW) for their support and confidence in the conduct of this program.

TABLE 1 - WEIGHT COMPARISON OF F-111 TRANSPARENCY SYSTEMS

CONFIGURATION	WEIGHTS				
	WINDSHIELD	CANOPY	HARDWARE	SHIPSET	WEIGHT PENALTY
ORIGINAL ALL-GLASS DESIGN	40.5 lbs.	39.5 lbs.	-	160 lbs.	-
INITIAL BIRDPROOF DESIGN	63 lbs.	45 lbs.	9 lbs.	225 lbs.	+65 lbs.
SIERRACIN LIGHTWEIGHT BIRDPROOF DESIGN	48 lbs.	33.5 lbs.	9 lbs.	172 lbs.	+12 lbs.



750

FIGURE 1
FRONTAL VIEW OF F-111 AIRCRAFT

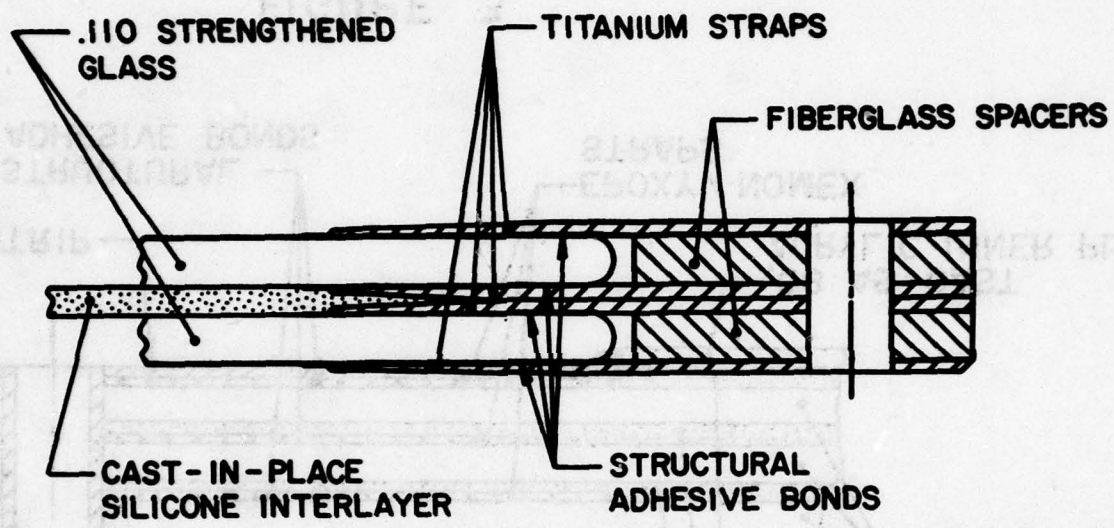
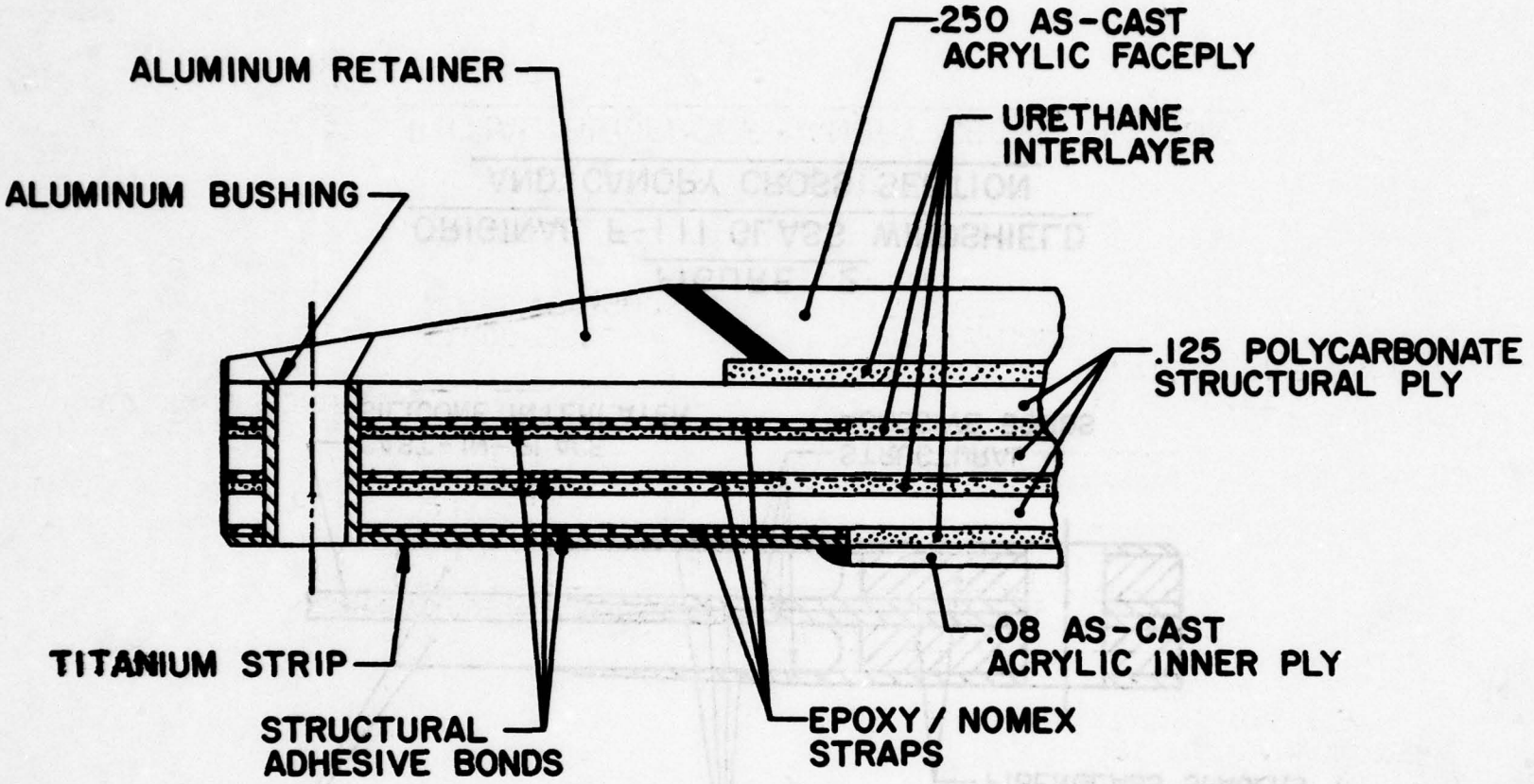


FIGURE 2
ORIGINAL F-111 GLASS WINDSHIELD
AND CANOPY CROSS SECTION



752

FIGURE 3

INITIAL BIRDPROOF WINDSHIELD CROSS SECTION

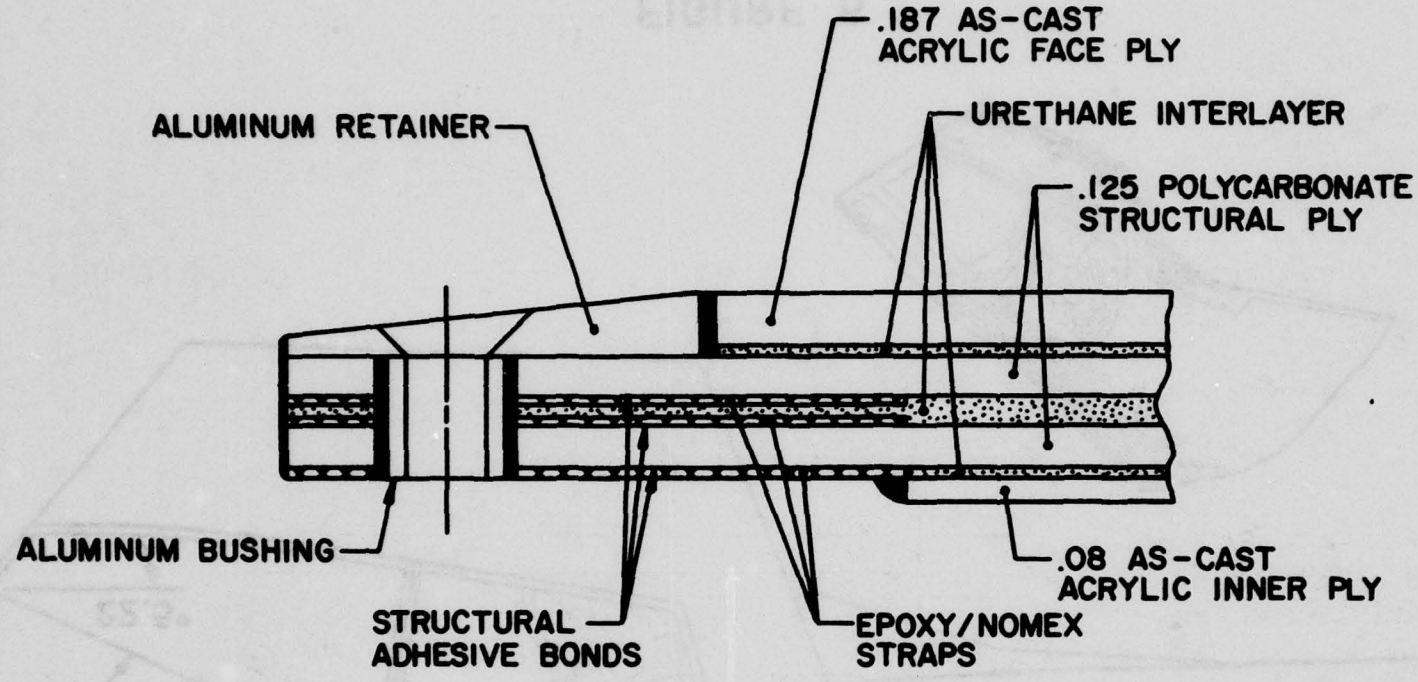


FIGURE 4

INITIAL BIRDPROOF CANOPY CROSS SECTION

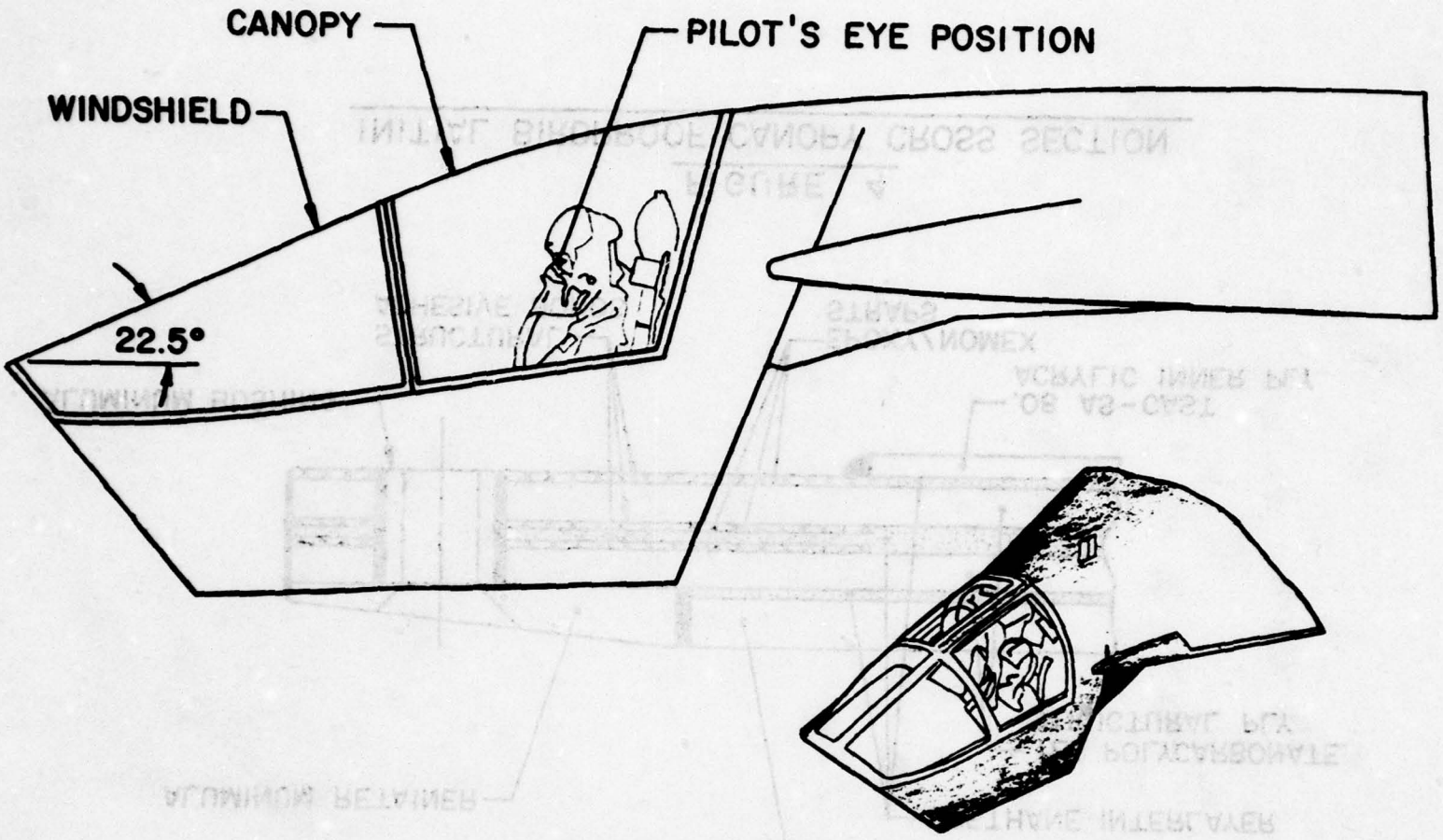
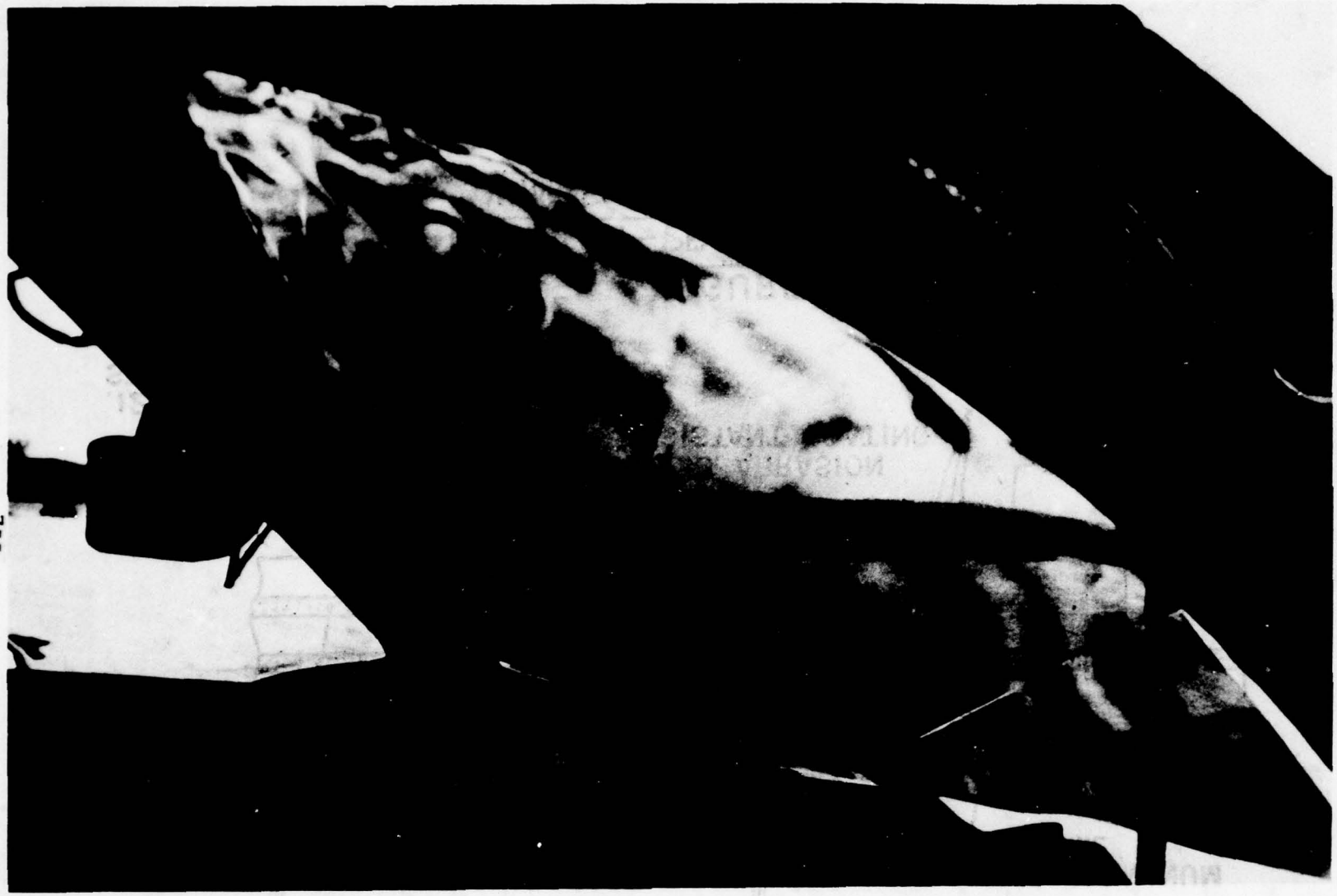


FIGURE 5
F-111 CREW MODULE LAYOUT



755

FIGURE 6

"RAINBOWING" EXAMPLE - F-111 WINDSHIELD

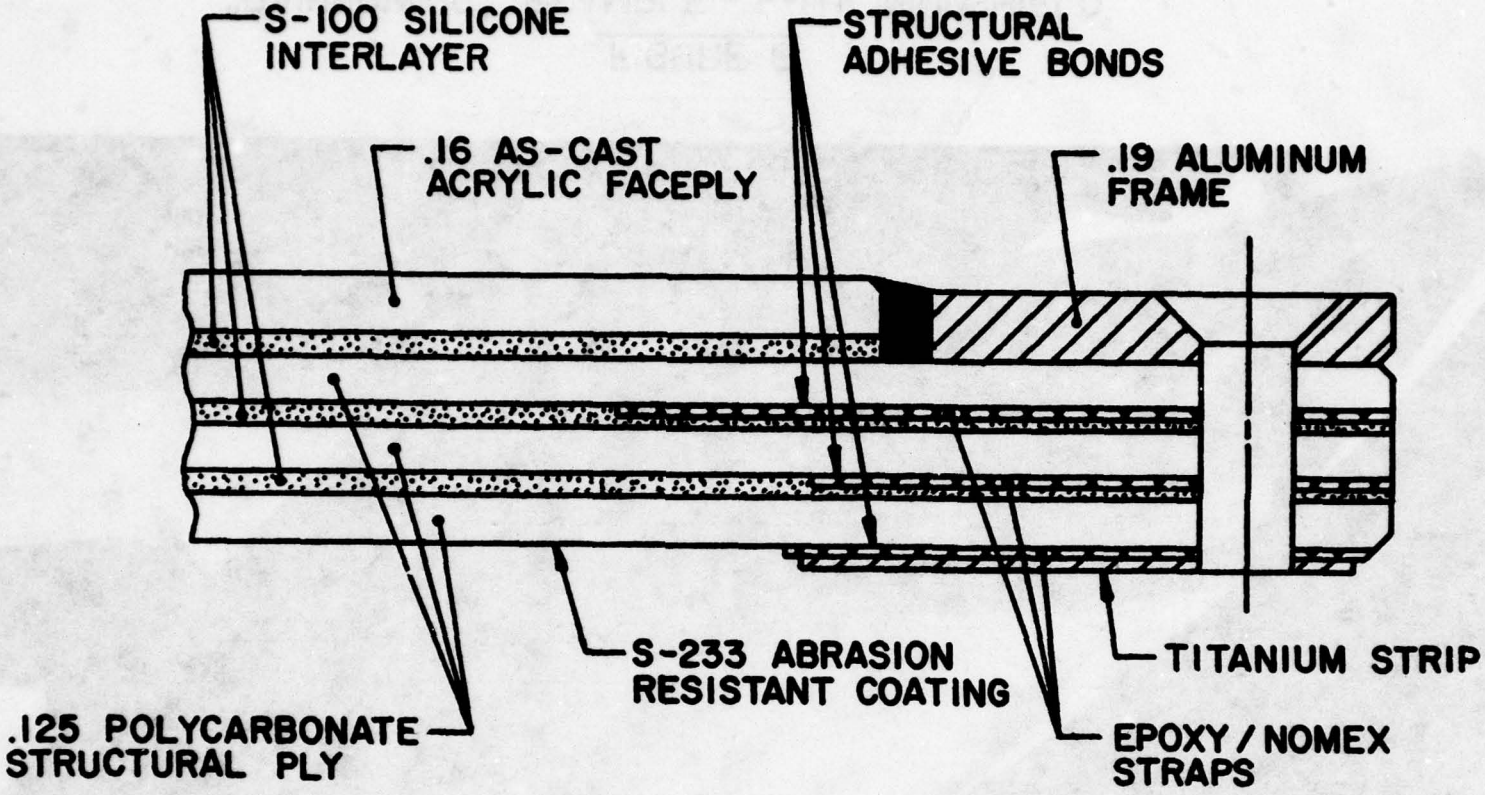


FIGURE 7

INITIALLY-PROPOSED SIERRACIN WINDSHIELD CROSS SECTION

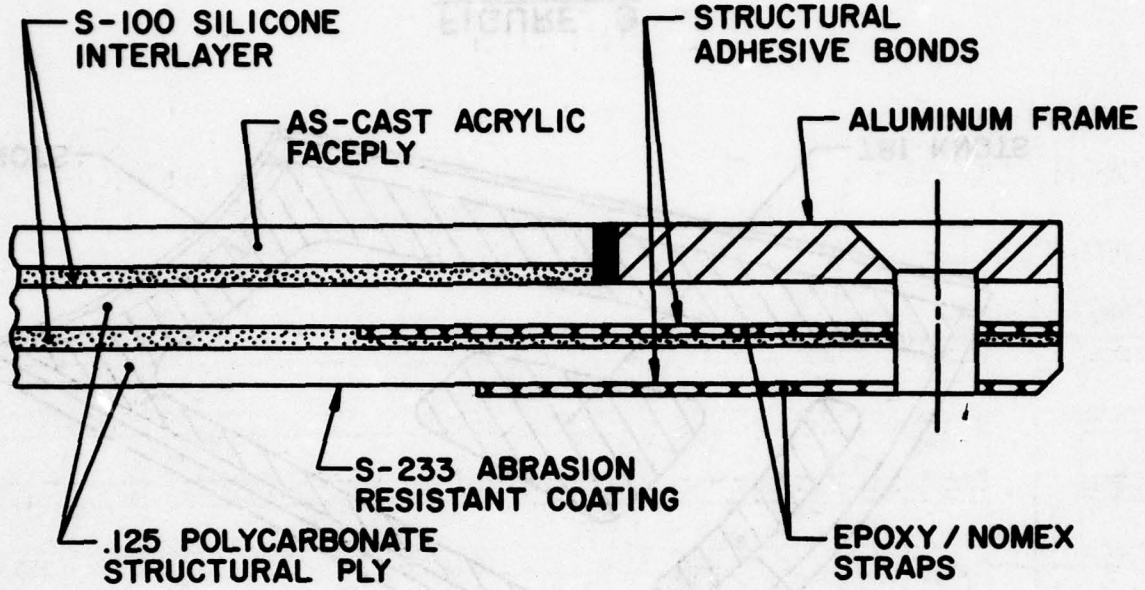


FIGURE 8

INITIALLY-PROPOSED SIERRACIN

CANOPY CROSS SECTION

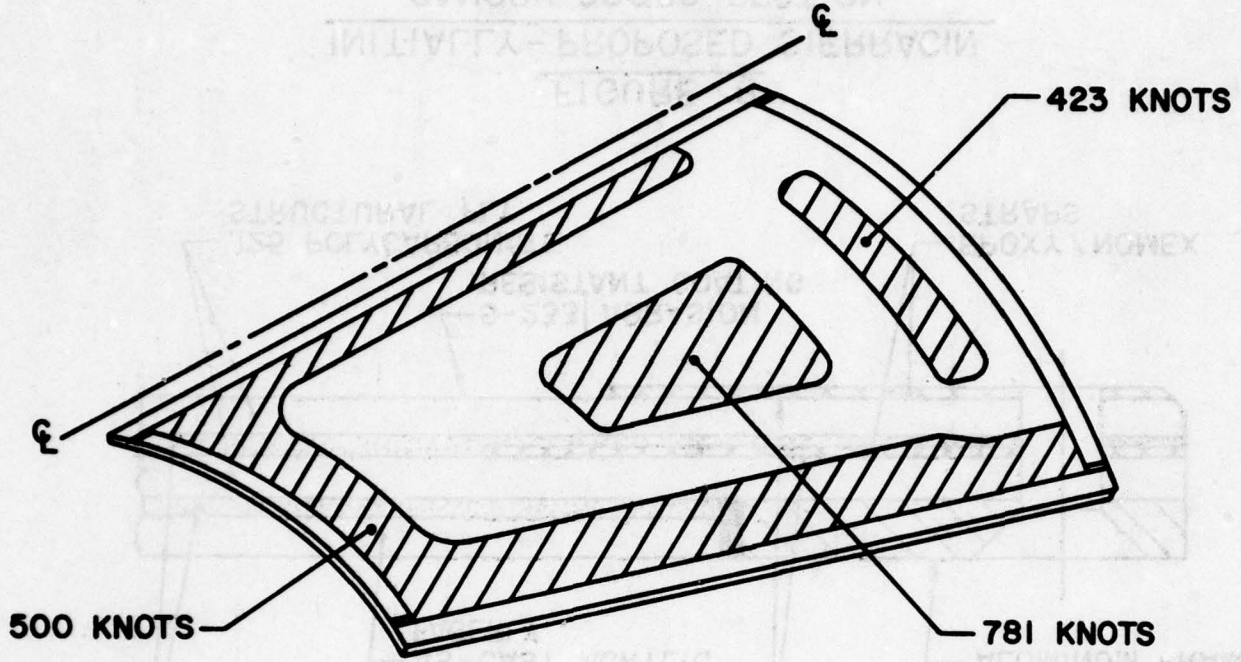
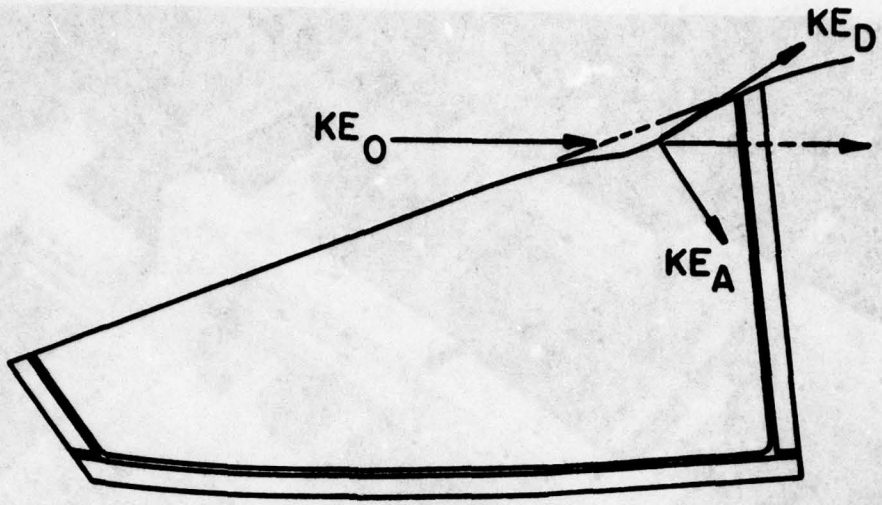
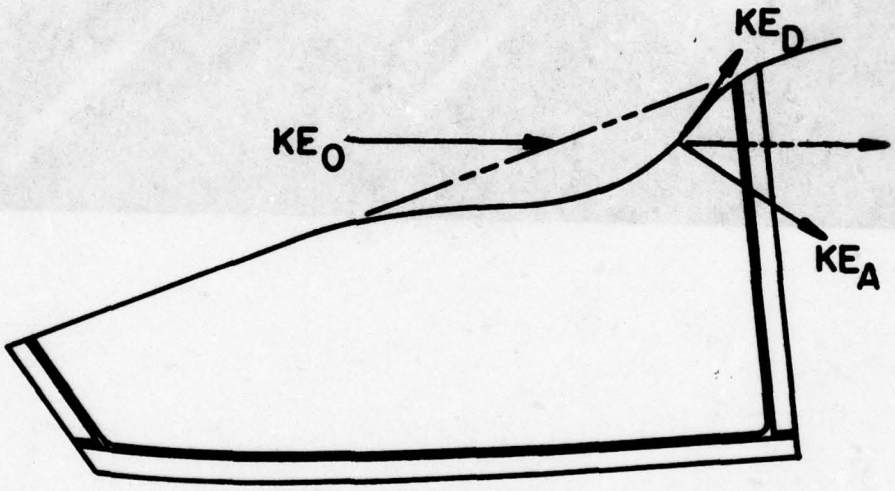


FIGURE 9
BIRD PERFORMANCE SURVEY OF
INITIAL BIRDPROOF DESIGN



STIFF WINDSHIELD



"FLEXIBLE" WINDSHIELD

KE_0 = INITIAL BIRD KINETIC ENERGY

KE_D = KINETIC ENERGY OF DEFLECTED BIRD

KE_A = KINETIC ENERGY IMPARTED TO WINDSHIELD SYSTEM

FIGURE 10
EFFECT OF DEFLECTION ON IMPACT LOADS

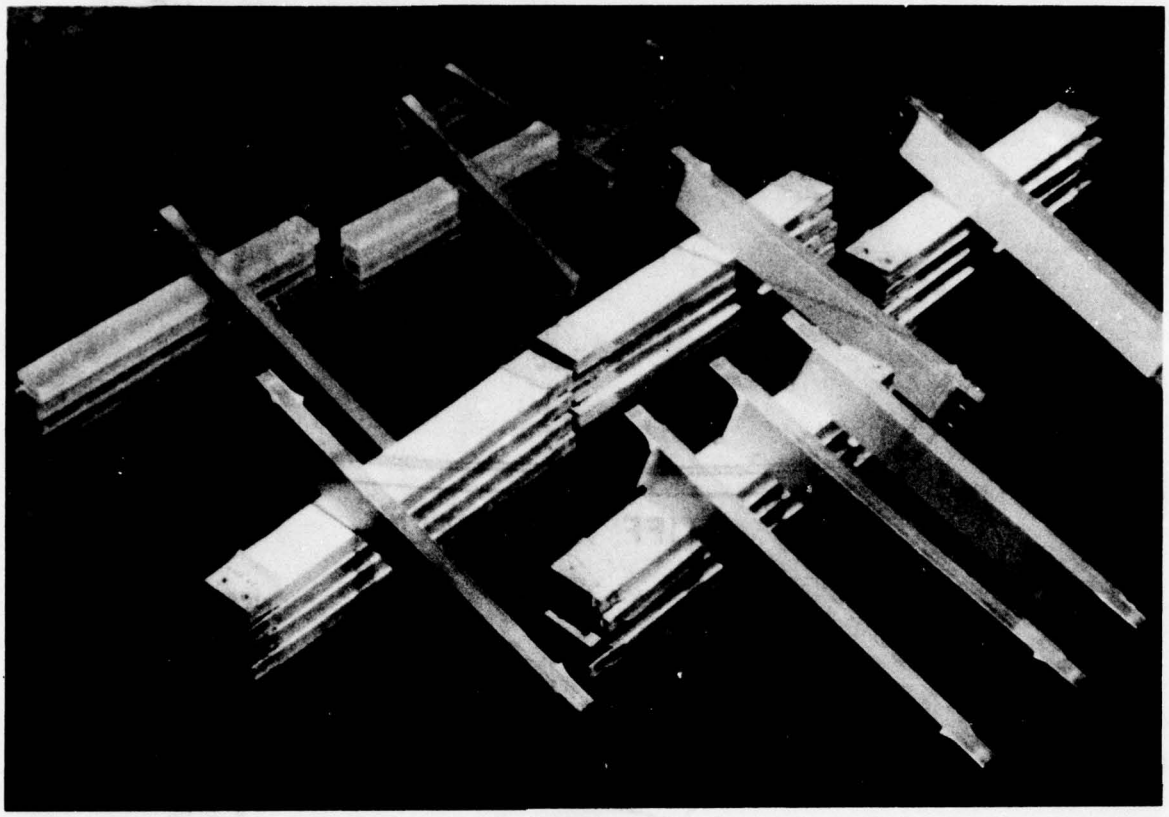


FIGURE 11

REPRESENTATIVE BEAM TEST COUPONS

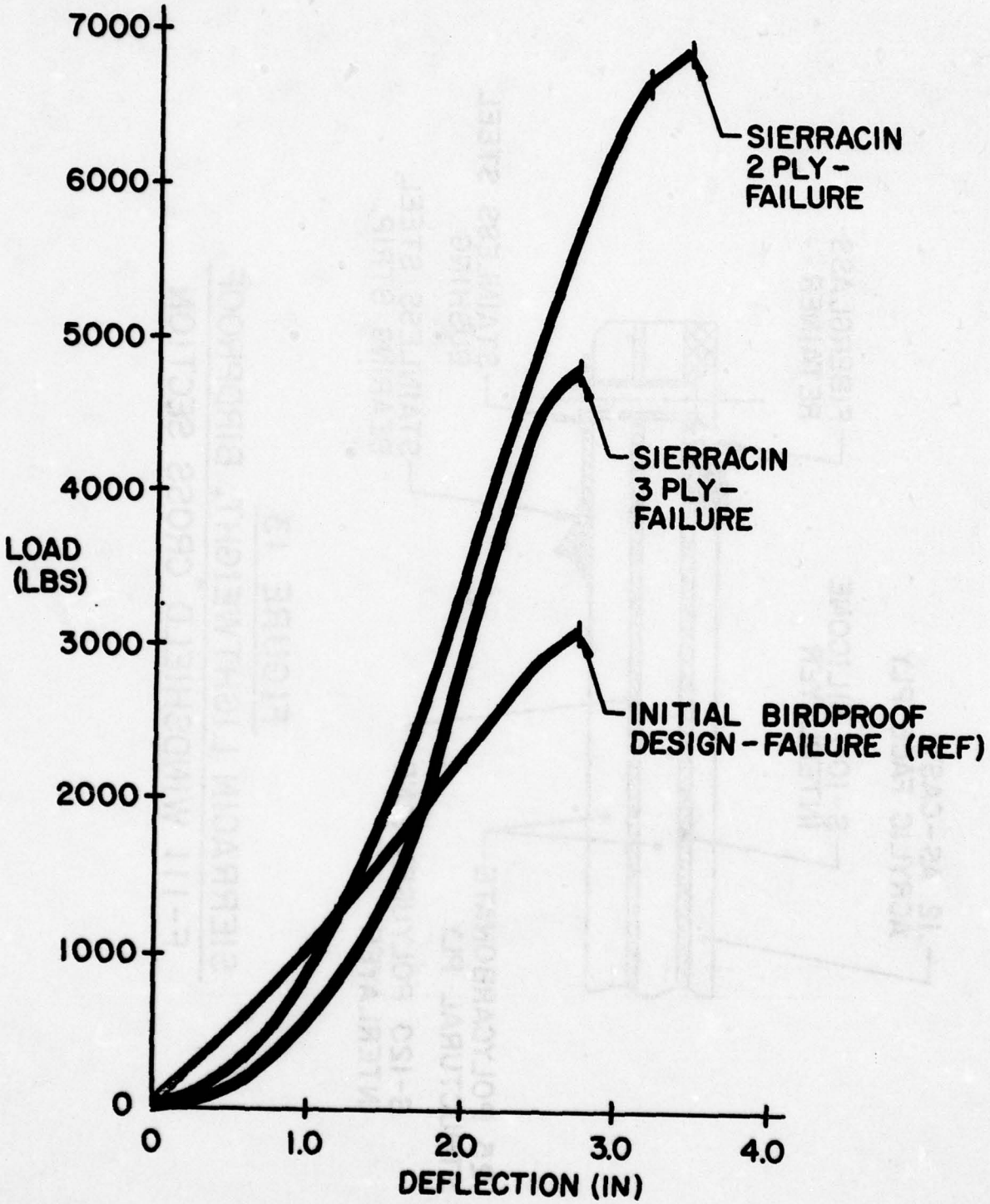


FIGURE 12
F-111 BEAM TESTS

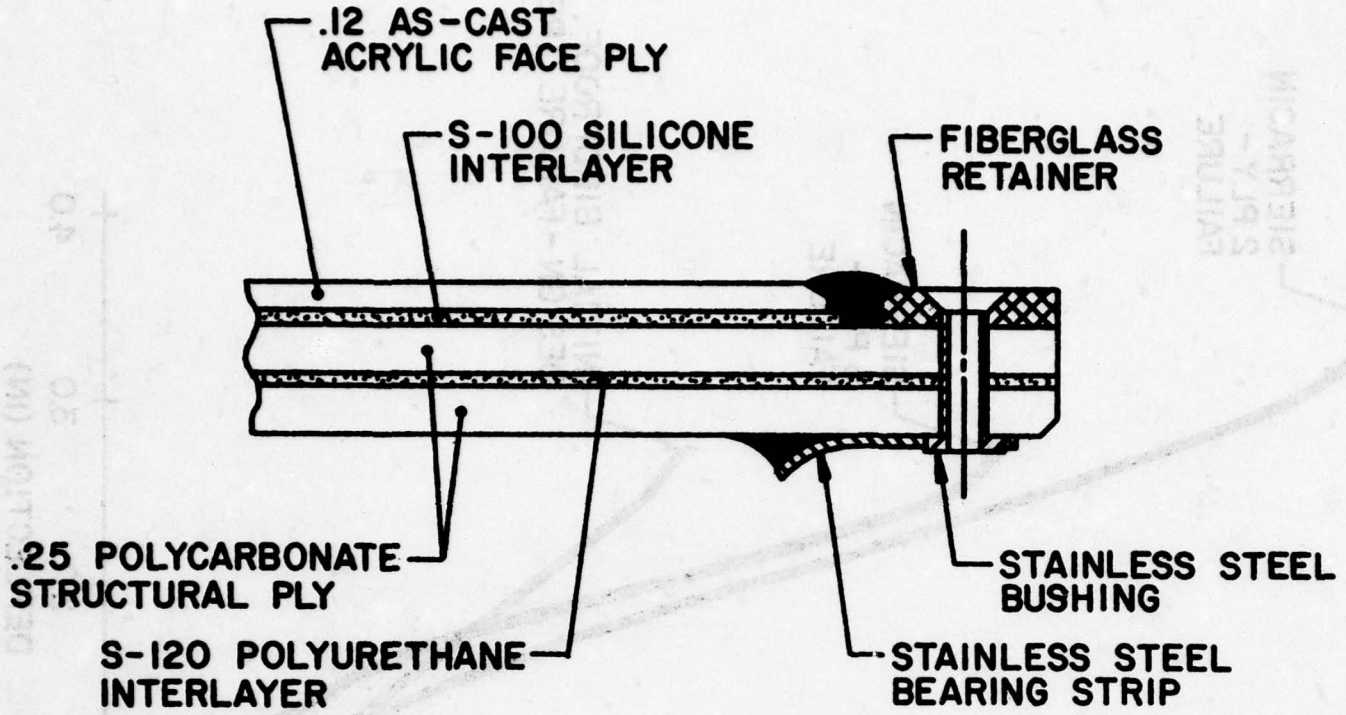


FIGURE 13

SIERRACIN LIGHTWEIGHT, BIRDPROOF

F-111 WINDSHIELD CROSS SECTION

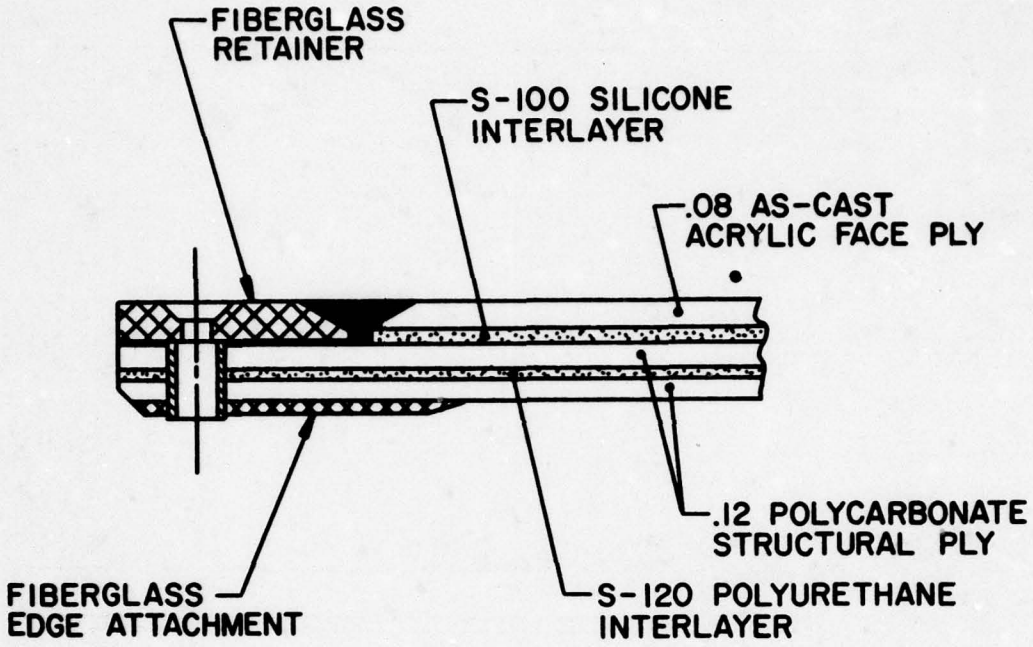


FIGURE 14

SIERRACIN LIGHTWEIGHT, BIRDPROOF

F-111 CANOPY CROSS SECTION

GLASS/PLASTIC TRANSPARENT ARMOR FOR HELICOPTERS

W. C. McDonald
Goodyear Aerospace Corporation
Arizona Division
Litchfield Park, Arizona

PRECEDING PAGE BLANK-NOT FILMED

GLASS/PLASTIC TRANSPARENT ARMOR FOR HELICOPTERS

by

Wilson C. McDonald, Goodyear Aerospace Corporation

Gordon R. Parsons, Army Materials and Mechanics Research Center

ABSTRACT

This paper covers the continuing development of transparent glass/plastic armored glazings for helicopters. During the 1975 conference in Atlanta, the initial UH-1 helicopter armor effort was discussed. This paper covers the latest programs which have been undertaken to scale up the protective level of helicopter transparencies over the work previously reported. Primary emphasis has been placed on upgrading the ballistic protection level of current inventory aircraft and on generating sufficient data to enable designers of new aircraft to incorporate transparent armor. Additional UH-1 windshields with improved ballistic capability were fabricated and flight tested at the Army Yuma Proving Ground, Yuma, Arizona; and at Ft. Rucker, Alabama. These two locations provided the climate extremes desired for the flight test program. In addition to the UH-1 programs, several other novel approaches have been undertaken to demonstrate how transparent armor can be used effectively to protect aircrewmen. The results of these programs clearly represent a significant advancement in the state-of-the-art of armored glazings and should be of considerable interest to design personnel and safety and survivability groups.

PRECEDING PAGE BLANK-NOT FILMED

I. INTRODUCTION

Recent advances in the state-of-the-art of transparent armor have made the incorporation of such armor practical. The helicopter is playing an increasingly important role in modern warfare. With its expanded combat area mission requirements such as rescue, search, attack, and close-proximity missions, the helicopter is exposed to more hostile fire than ever before. The standard transparent windows and windshields, which represent sizeable vulnerable areas, offer virtually no ballistic protection and when penetrated often generate considerable injurious spall.

High-performance glass/plastic composites have been developed which, for the first time, provide ballistic protection at an areal density and thickness significantly lower than prior state-of-the-art laminated glass armor. In addition, the new glass/plastic composites eliminate the backside spalling of injurious fragments upon ballistic impact.

II. TECHNICAL APPROACH

1. GENERAL

This paper discusses several programs that have been undertaken by the Army to demonstrate that the glass/plastic armor is now ready for installation on helicopters. It also shows that various types of installations can be considered.

1. Composite armor can be made curved or flat, as a direct replacement for present glazings.

2. Parasitic panels of composite armor can be installed behind present canopies, windshields, and windows when space and weight is a critical factor.

3. Panels may be added close to the pilot in the form of a protective hood to provide the protection needed at the lowest possible weight.

Two very interesting programs were sponsored over the last several years by The Army Materials and Mechanics Research Center (AMMRC), Watertown, Massachusetts. Mr. Gordon Parsons was the Army technical coordinator, and Goodyear Aerospace Corporation in Litchfield Park, Arizona, performed the work on these programs.

2. UH-1 PROGRAM NUMBER 1

UH-1 Program Number One resulted in the fabrication of a number of sets of curved and flat transparent armor panels for the UH-1 helicopter. This program was divided into three phases.

Phase I included the design of the armor installation, as well as ballistic and environmental testing to document performance. Manufacturing drawings and instructions for the armor installations were prepared.

Phase II consisted of the fabrication of eight shipsets of the transparent armor and hardware in accordance with the drawings.

Phase III effort included the environmental testing of three shipsets of the full-scale parts produced in Phase II. One additional shipset of transparent armor was installed in a UH-1H helicopter to verify the adequacy of the design and installation procedures and to allow flight test evaluation. The remaining four sets, which included curved windshield panels and flat door windows, were delivered to AMMRC, Watertown, Massachusetts, where they have been used in numerous tests.

The composite makeup as specified by AMMRC was as follows:

Material	Thickness (inches)
Soda-lime annealed glass	0.250
Polyvinyl butyral (PVB) interlayer	0.060
Soda-lime annealed glass	0.125
Cast-in-place interlayer	0.100
Polycarbonate with Goodyear Aerospace abrasion-resistant coating	0.125
Total thickness	0.660
Composite weight 6.5 lb/ft^2	

A successful flight test program was conducted at the U.S. Army Proving Ground (YPG), Laguna Field, Yuma, Arizona, for longer than six months. In additional to flight testing in all types of weather to obtain the required environmental exposure, pilots were requested to submit their comments after each test flight. Nearly all pilots interviewed stated they would want the transparent armor on their aircraft in combat. The more each pilot flew the aircraft, the more complimentary he became.

3. UH-1 PROGRAM NUMBER TWO

In 1977 a second program was sponsored to scale up the protection level of the armored glazings. Thicker windshields of the following construction were produced:

Material	Thickness (inches)
Soda-lime annealed glass	0.375
Cast-in-place interlayer	0 060
Soda-lime annealed glass	0.375
Cast-in-place interlayer	0.100
Polycarbonate with Goodyear Aerospace abrasion-resistant coating	0.187
Total thickness	1.097

Composite weight 11.8 lb/ft^2

During each of the UH-1 armor programs, Goodyear Aerospace conducted a wide range of environmental tests to ensure composite adequacy. The testing of the heavier armor produced in program number two was as follows.

4. ENVIRONMENTAL TESTING MATRIX

a. General

Tests covering high temperature, low temperature, temperature shock, humidity, and ultraviolet (UV) stabilization were selected because they represent the most severe conditions proposed by established military specifications. Although some of these tests may not represent actual environmental conditions of helicopter glazings, every attempt was made during the testing program to comply with the intent of the specification.

Several panels 36 × 36 inches in size were prepared. One set was exposed to the humidity test and the other set to high temperature, low temperature, and temperature shock. Smaller panels, 12 × 12 inches in size, were exposed to UV and outdoor weathering to confirm that no degradation is experienced under these conditions.

b. High-Temperature Testing

Several panels during the test program were subjected to high-temperature testing as outlined in MIL-STD-810C, Method 501, Procedure 1.

This test requires the item to be placed in a test chamber in which the temperature is raised slowly (18 deg F per minute or less) to 160 deg F. This temperature is maintained for 48 hours. The test chamber temperature is then lowered slowly to ambient and stabilized.

The panels subjected to this test repeatedly passed with no evidence of cracking, clouding, delamination, or other visible signs of degradation.

c. Low-Temperature Testing

The panels were tested in accordance with MIL-STD-810C, Method 502, Procedure 1.

Low-temperature testing requires the test item to be placed in a chamber and the temperature lowered at a rate not exceeding 18 deg F per minute until -40 deg F is reached.

The low temperature is maintained for 24 hours. The panel is then returned to ambient temperature and examined.

The panels successfully passed this test at -40 F without damage.

Because previous testing has shown that glass breakage can occur at low temperatures, every precaution was taken to ensure success. All glass edges were hand dressed to eliminate chipped areas and to provide a smooth, stress-free glass. The temperature was lowered slowly over a three-hour period to -20 F and held overnight to determine the effect of this temperature on the composite. A window in the test chamber permitted periodic inspections, and no degradation was evident. The second day, the temperature was lowered to -30 F and held for 5 hours. Again, inspection revealed that the panels were undamaged.

The temperature was then lowered to -40 F and held overnight. The panel was then returned to ambient over a period of several hours and removed from the chamber. The two panels showed no evidence of any deterioration.

Light transmission and haze were checked before and after completion of the tests. The results are shown in Table I.

TABLE I - LOW-TEMPERATURE TEST DATA

Characteristic	Before test	After test
Light transmission average (percent	72.2	72.5
Haze average (percent)	1.0	1.0

d. Humidity Testing

A panel was run through the humidity tests outlined in MIL-STD-810C, Method 507, Procedure 1

This test requires the test items to be exposed to 149 deg F and a relative humidity of 95 percent. The temperature is gradually raised from ambient to 149 F. This temperature is maintained for not less than six hours. The relative humidity is maintained at not less than 85 percent while the temperature is reduced in 16 hours to 86 F. These steps are repeated for a total of 10 cycles for not less than 240 hours. The two 36- × 36-inch panels were examined at the conclusion of the test, and both had several small corner and edge delamination areas not exceeding 1/2 × 1 inch. The panels otherwise exhibited good appearance.

Light transmission and haze readings taken on the panels before and after the humidity testing are shown in Table II.

TABLE II - HUMIDITY TEST DATA

Characteristic	Before humidity tests	After test
Light transmission average (percent)	72.3	72.0
Haze average (percent)	1.0	1.9

e. Temperature Shock Testing

This test was run in accordance with MIL-STD-810C, Method 503, Procedure 1.

In this test, the armor composite is placed in an oven and heated to 160 deg F for not less than 4 hours or until the test item stabilizes. At the conclusion of this time, the transparent armor panel is transferred within 5 minutes to a cold chamber which has been stabilized at -60 deg F. This temperature was suggested by Goodyear Aerospace as the point where stress levels are at or near the maximum that a glass/plastic composite will tolerate. The panel is held at the low temperature for 4 hours or until stabilized and then returned to the +160 F chamber within 5 minutes, where it is stabilized. The entire cycle is repeated two more times before the test is concluded.

The thermal shock test is the most severe test to which a glass/plastic composite is exposed.

During this test, two panels, 36 × 36 inches, survived the complete cycle at -60 deg F.

f. Ultraviolet Stabilization Testing

The accelerated exposure to ultraviolet radiant energy was run on two 12-in. × 12-in. panels.

Panel number one was placed in the Goodyear Aerospace test chamber. This chamber is 8 × 36 × 50 inches in size. The chamber bulb type, placement, and reflector correspond to that described in FTMS No. 506, Method 6024. The chamber, however, does not utilize a rotating turntable, circulating controlled hot air, or fog generating source.

Panel number two was placed on the Goodyear Aerospace outdoor weathering rack positioned for standard 45 deg south exposure.

The panels were examined and tested for light transmission and haze prior to test exposure and after 36 days (864 hours) and 345 days (8280 hours) of exposure. The results are shown in Table III.

g. Conclusion

This testing program has shown that glass/plastic composites can be produced which will pass high temperature, low temperature, thermal shock, humidity, and ultraviolet stabilization tests. The program has also indicated there is a very critical balance that must be maintained when designing composites and selecting the materials to be used.

TABLE III - ULTRAVIOLET RADIATION TEST DATA

Panel no.	Light transmission (average percent)			Haze (average percent)		
	Original	After 864 hr	After 8280 hr	Original	After 864 hr	After 8280 hr
1 (accelerated exposure)	72.0	72.2	72.4	2.4	3.6	3.4
2 (outdoor exposure)	72.1	72.2	72.4	2.4	3.1	3.8

There is evidence that panels exposed to high humidity for extended periods and then exposed to extreme thermal shock may show signs of delamination and some glass breakage. In this regard, it is difficult to visualize a situation where a helicopter or other low-flying aircraft would encounter both of these conditions in the short time as specified by MIL-STD-810C. It is recognized that MIL-STD testing imposes severe conditions to accelerate natural exposure effects

A field testing program was initiated which will evaluate glass/plastic UH-1 windshields under actual conditions in two entirely different environments (Ft. Rucker, Alabama, and Yuma, Arizona). This testing is needed to establish a realistic test program for future programs involving glass/plastic composites. This field testing will run for approximately one year, and test results will be available by late 1978.

4. FABRICATION AND OPTICAL EVALUATION

a. General

Three shipsets of UH-1 transparent armored windshields, P/N 3149000-100, were fabricated. The windshields were complete with all framing necessary for direct attachment to the existing fuselage. Except for relocation of the free air temperature gauge, use of longer windshield attachment screws, and an extension of the present windshield wiper bushing, the armored windshields can be directly substituted for the current standard acrylic windshields.

b. Refined Glass Forming Procedures

Because of the large variations in glass contours experienced in the previous contract, on the second program Goodyear Aerospace fabricated new tooling and formed all glass to more closely controlled tolerances. This simplified the mating of the glass and the plastic backing and enhanced the overall optical quality of the windshields.

c. Design Analysis Approach

In addition to the design analysis of the windshield composites already discussed, a new structural investigation of the windshield framing and fuselage mount area was undertaken. The investigation was conducted to analytically verify the structural adequacy of the transparent armor installation.

To summarize, it was concluded that no structural problems are caused by the armored windshield installation. Because the armored windshields are much more rigid than the standard acrylic windshields, the armored parts aid in stabilizing the helicopter frame structure. The aircraft, with relocation of the battery to the aft position, stays within the allowable center of gravity limits established for the aircraft.

The transparent armor windshields weigh 99 pounds each, while the original Plexiglas windshields weigh 10 pounds each. Total weight increase per shipset resulting from the installation of the armored windshields was therefore 178 pounds.

d. Optical Test Evaluation

All windshields produced were measured for thickness in nine locations to verify that an acceptable tolerance was held which would permit acceptable optics to be achieved (see Figure 1 for typical results).

Optical deviation measurements were taken in accordance with MIL-G-5485C, Paragraph 4. 5. 2. 1 (see Table IV).

Optical distortion evaluation was accomplished in accordance with MIL-G-5485C, Paragraph 4. 5. 3 (single- and double-exposure photographs). A data summary of the windshield optical properties, including distortion measurements, is presented in Table IV. A typical windshield photograph is shown in Figure 2. In addition, each set of windshields was mounted on a frame simulating the UH-1 mounting, and photographs were taken outdoors to demonstrate the optical quality.

The optical quality was considered very good for composites of this thickness and curvature.

TABLE IV - UH-1 GLASS/PLASTIC ARMOR WINDSHIELDS OPTICAL TEST EVALUATION

Panel no.	Light transmission (percent average)	Haze (percent average)	Optical deviation (minutes average)	Optical distortion (slope)
1 RH	81.0	1.3	2.9	Slope 1 in 8 lower RH corner
1 LH	80.5	0.9	3.2	Slope 1 in 8 lower LH corner
2 RH	81.4	0.7	3.6	Slope 1 in 16 lower RH corner
2 LH	80.6	0.9	1.8	Slope 1 in 12 lower LH corner
3 RH	81.0	1.5	2.4	Slope 1 in 16 lower RH corner
3 LH	81.1	1.3	2.4	No significant slope

Light transmission — in accordance with Federal Test Method Standard 406, Method 3022.

Haze — in accordance with Federal Test Method Standard 406, Method 3022.

Optical deviation — MIL-G-5485C, Paragraph 4.5.2.1.

Optical distortion — in accordance with MIL-G-5485C, Paragraph 4.5.3 (double-exposure photograph).

e. Flight Test Evaluation

(1) General

With the completion of the three sets of armored windshields, P/N 3149000-100, each part was inspected and bought off by representatives of the Army.

Shipset number one was installed in a helicopter fuselage located at Goodyear Aerospace, Litchfield Park, Arizona, in September 1977. These parts are facing south and are being monitored periodically for resistance to the severe temperature and UV radiation exposure experienced in this desert area.

Shipset number two was delivered to the test airfield at Fort Rucker, Alabama, where the windshields were installed in August 1977 on a UH-1 aircraft being used on various flight test programs. The rather wet and humid conditions experienced in this area complement the testing conducted at the two other locations to provide the weather extremes experienced in most areas of the world.

Shipset number three was delivered to the U. S. Army Proving Ground (YPG), Laguna Field, Yuma, Arizona, and installed in June 1977 on a helicopter. These armored windshields have been exposed to the hot climate conditions of that area and were evaluated by various pilots assigned to fly the aircraft on numerous missions. The flight test evaluation at both test facilities was scheduled over a one-year period.

(2) Installation of Test Articles

The installation of the windshields at the Yuma Proving Ground showed that armored types can be installed as a direct replacement of the standard units. Modification of the windshield wiper arm to accommodate the greater part thickness, and relocation of the free air temperature gage, are the only modifications that should be required on the UH-1 if production lots of windshields are ordered in the future. The installation pointed out that there is some contour variation from one UH-1 aircraft to another. This discovery has made it necessary to redesign the edge band to allow for more flexibility of the part's edge during bolting of the windshield to the airframe.

(3) Flight Test Evaluation

After the armored windshields were installed, the weight and balance of the ship were checked and found to be within acceptable limits with the battery located in its aft position.

The first flight test was made at Yuma on June 29, 1977. These flights are scheduled to continue for approximately one year with each pilot reporting his observations.

Figure 3 shows the steps of installation, balancing, and flight test recorded at the U. S. Army Proving Ground, Laguna Field, Yuma, Arizona.

(4) Reports

Personnel at both Yuma and Fort Rucker have been assigned to monitor the condition of the windshields and report pilot comments during the flight test program. These reports will be transmitted to Mr. Gordon Parsons, AMXMR-ER Technical Supervisor, Army Materials and Mechanics Research Center, Watertown, Massachusetts.

III. OTHER HELICOPTER ARMOR INSTALLATIONS

In addition to the UH-1 transparent armor installation discussed in this paper, Goodyear Aerospace has participated in several other interesting programs with Eustis Directorate, U. S. Army Mobility Research and Development Laboratory, For Eustis, Virginia.

These programs have demonstrated several novel approaches in providing aircrew protection on existing aircraft without the need for extensive modifications.

As shown in Figure 4, armor panels were fabricated for the AH-1G which allowed for a quick-attach approach. This concept permits the panels to be installed rapidly for combat missions and removed easily when not required. Taking into account the areas most often struck by bullets or fragments, it was possible to minimize the size of the panels to reduce weight and still greatly enhance the survivability of both the aircrew and the aircraft.

Another interesting concept demonstrated by Fort Eustis is shown in Figures 5, 6, and 7. Transparent armor panels were fabricated by Goodyear Aerospace and built into a hood assembly at Fort Eustis.

This concept permits the pilot's head to be protected from all angles without severely restricting his movements. Such hoods can be designed to move forward and aft or to swing upward and aft to permit pilot access into the aircraft.

Placing the armor this close to the aircrewman permits a few square feet of material to offer maximum protection at the lowest possible weight.

Concepts such as these are often the only practical method of providing additional protection for aircrewmen flying older types of aircraft.

IV. CONCLUSIONS

The following conclusions are offered:

1. Transparent glass/plastic armor has reached the state of development where it can be furnished in single curvature or flat panels.

2. Composites designed for helicopter use have been fabricated and have demonstrated protection against ground fire from 30 caliber M2 ball-type rounds and other threats.

3. The survivability of aircraft and aircrews can be greatly enhanced with glass/plastic transparent armor.

4. Freedom in composite design permits the armor thickness and weight to be scaled up or down to meet specific threat and weight goals.

5. The plastic backing ply prevents spalling which minimizes injuries from flying particles and increases panel integrity under multiple hits.

6. Glass/plastic composites are thinner than ballistic-grade laminated glass and are lighter in weight, reducing installation problems.

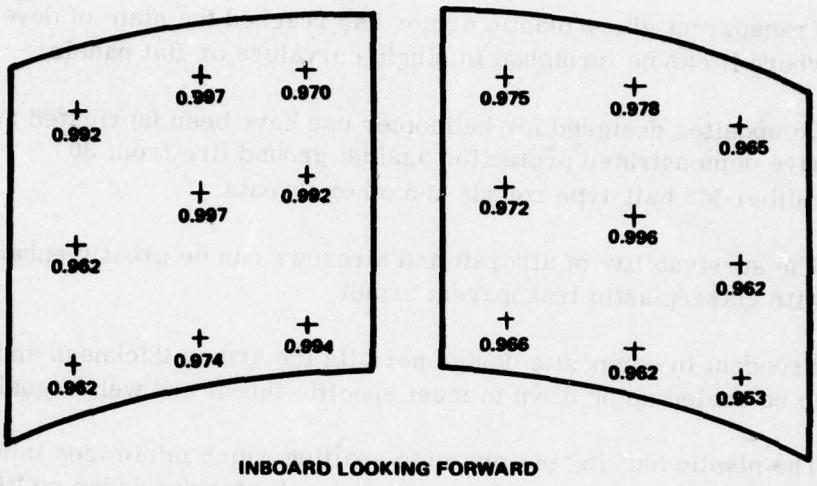


Figure 1 - UH-1 Windshield Thickness Measurements - Windshield Set No. 1

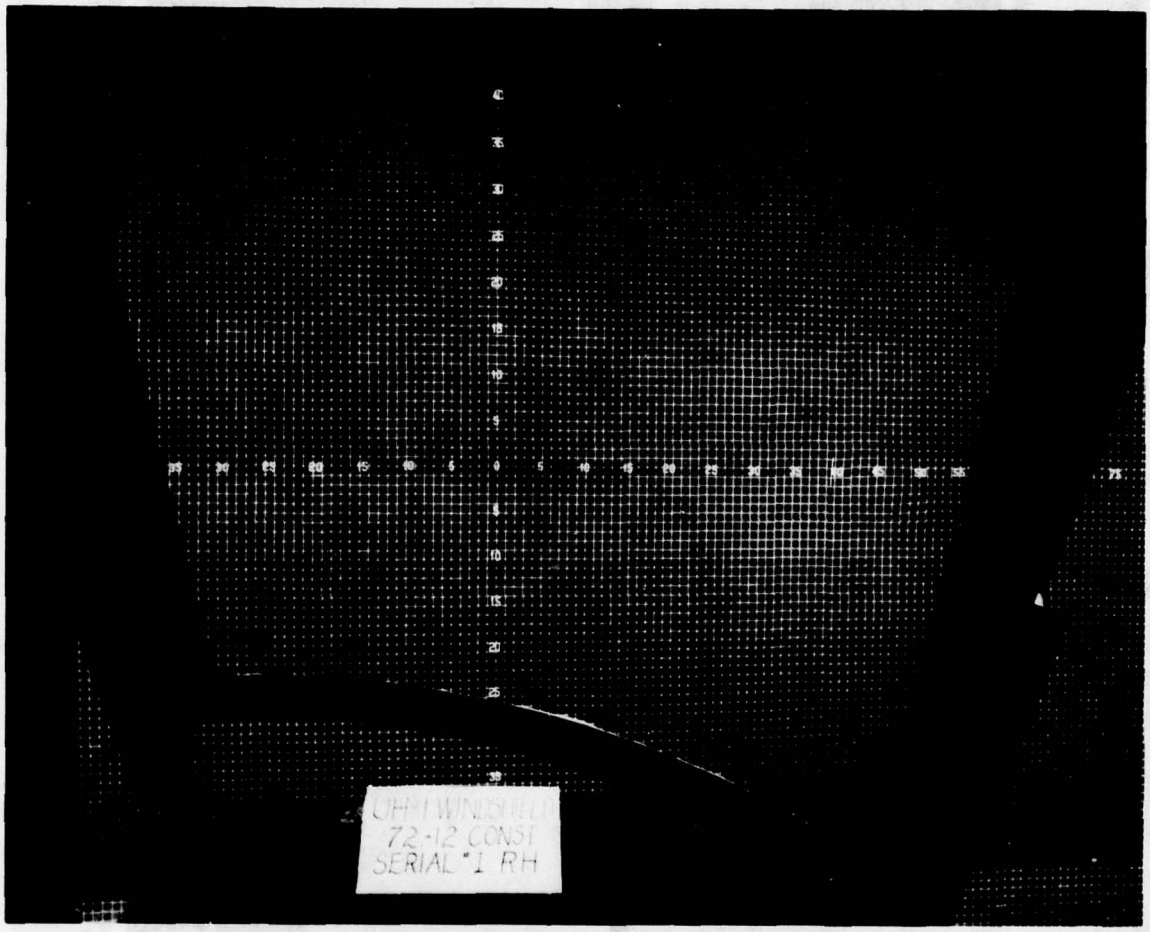
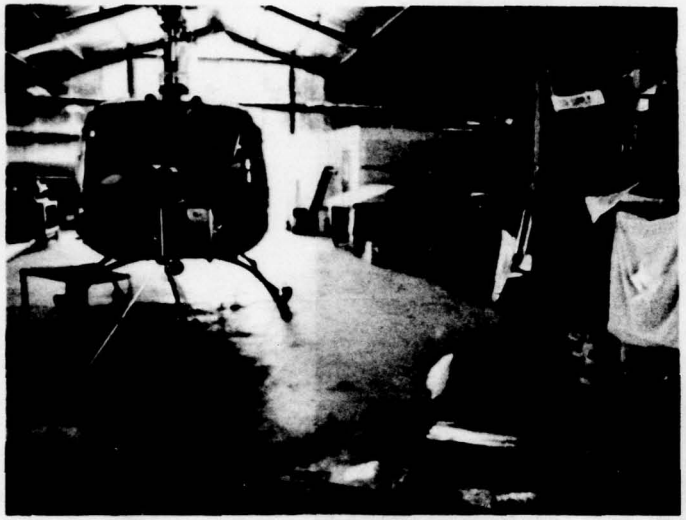
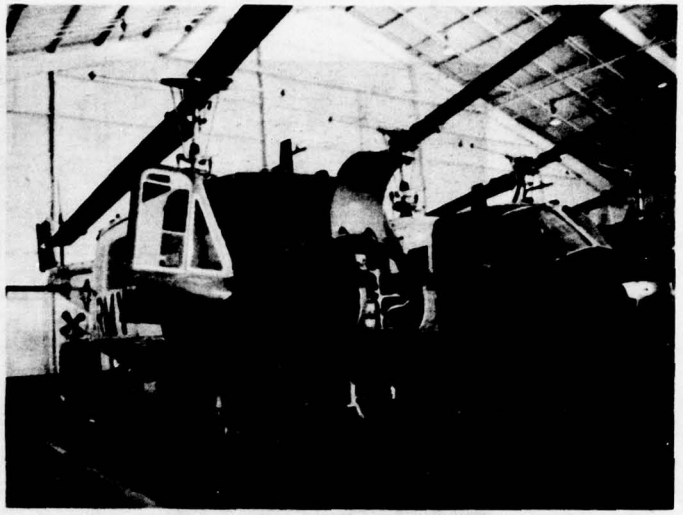


Figure 2 - Single-Exposure Photograph, Windshield S/N 1 (LH)



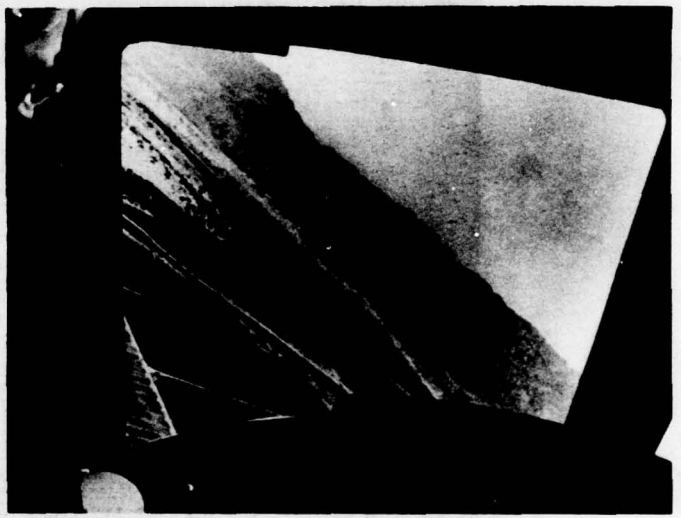
(1) REMOVE STANDARD WINDSHIELDS AND REPLACE WITH ARMORED WINDSHIELDS



(2) WEIGH AND BALANCE AIRCRAFT PER TM55-405-9



(3) OPTICAL EVALUATION RH ARMORED WINDSHIELD DURING FLIGHT TEST AT YUMA, ARIZONA



(4) OPTICAL EVALUATION LH ARMORED WINDSHIELD DURING FLIGHT TEST AT YUMA, ARIZONA

Figure 3 - Installation, Balancing, and Flight Test Procedure

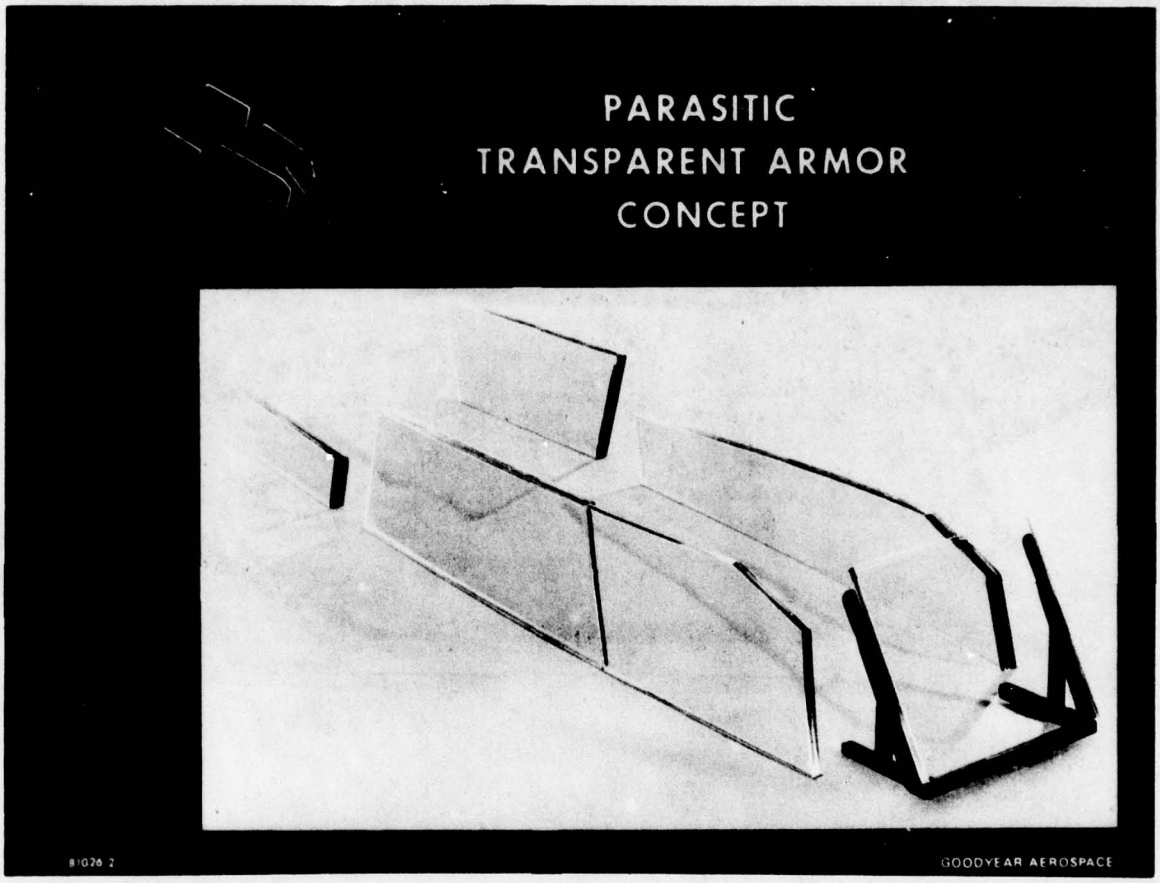


Figure 4 - Transparent Armor Panels Designed for Mounting inside the Present AH-1G Canopy and Windshield

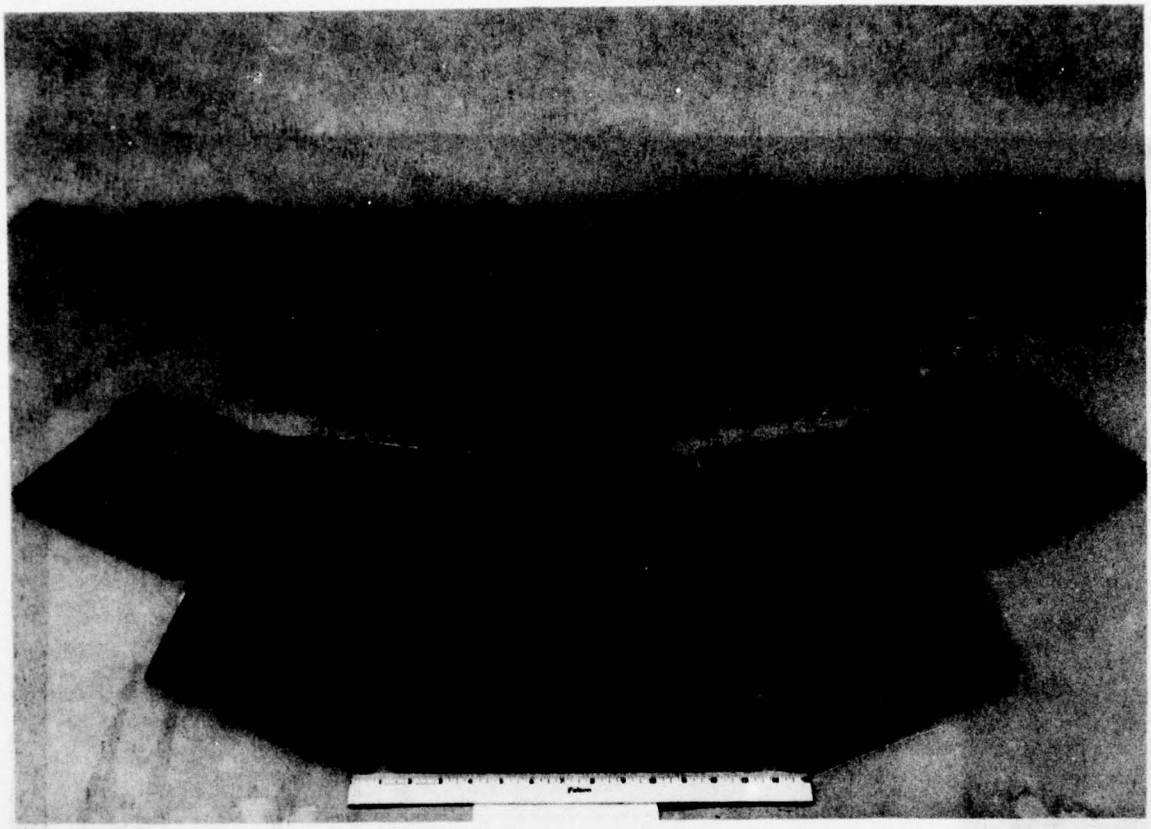


Figure 5 - Transparent Armor AH-1G Hood Panels before Mounting

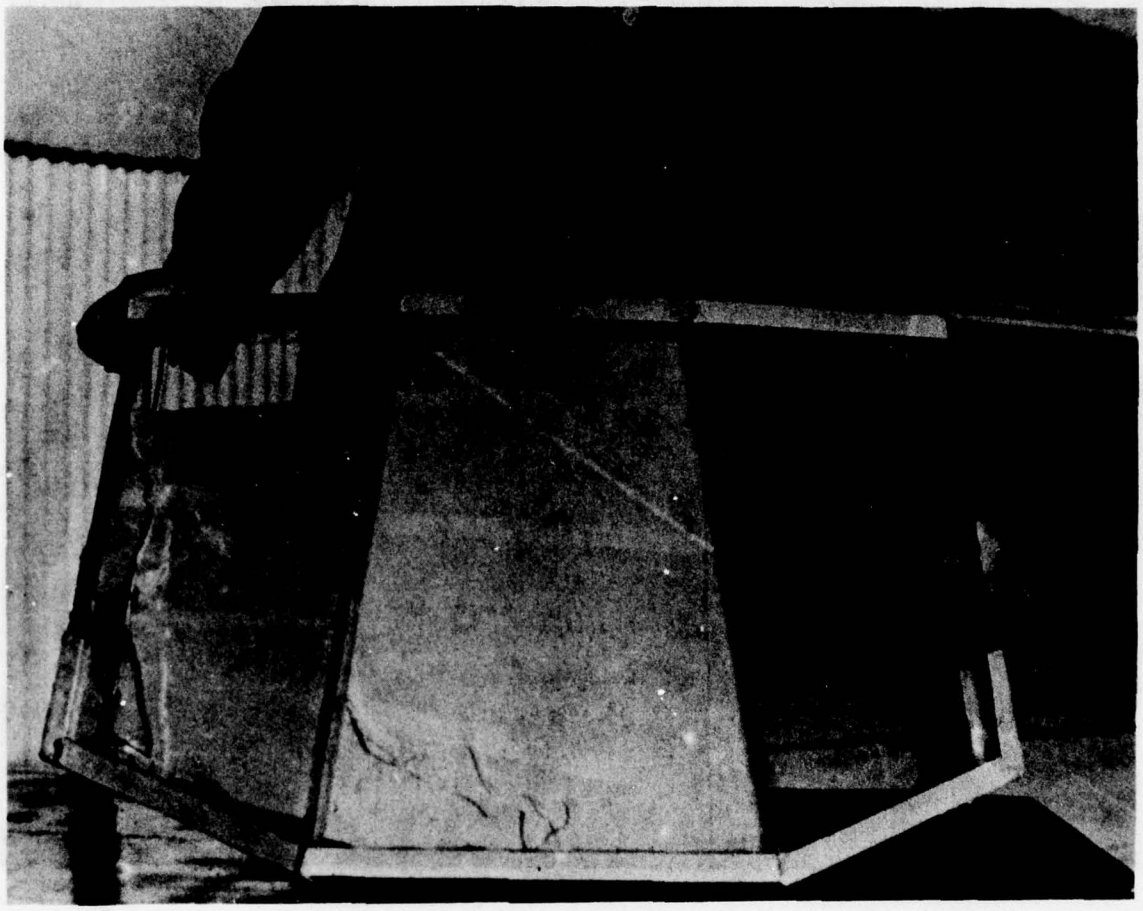


Figure 6 - Front View of AH-1G Armored Hood Assembly

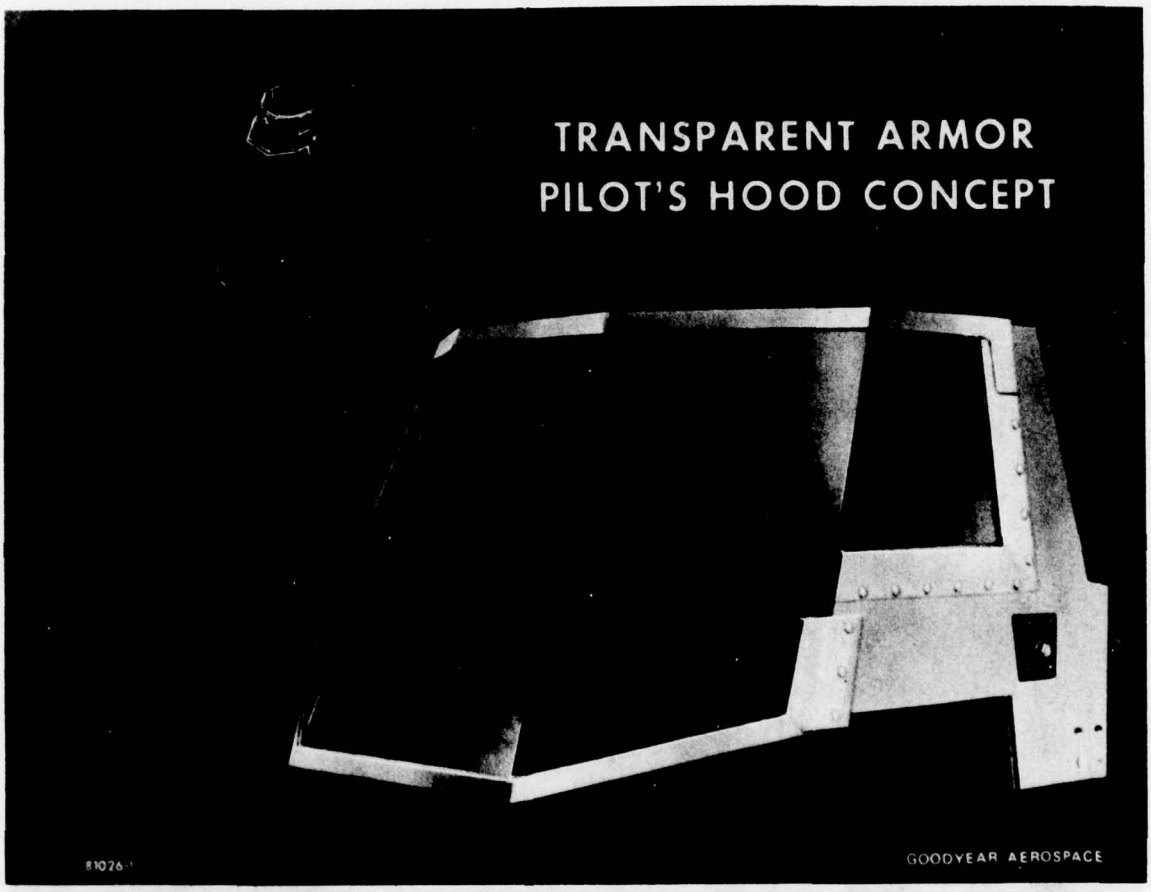


Figure 7 - Side View of AH-1G Armored Hood Assembly

DESIGN, DEVELOPMENT, AND QUALITY ASSURANCE TESTING OF B-1 SIDE AND UPPER CREW MODULE WINDOWS FOR AIRCRAFT NO. 4

R. E. Shumaker
Goodyear Aerospace Corporation
Arizona Division
Litchfield Park, Arizona

DESIGN, DEVELOPMENT, AND QUALITY ASSURANCE TESTING OF B-1 SIDE AND UPPER CREW MODULE WINDOWS FOR AIRCRAFT NO. 4

R.E. Shumaker
Goodyear Aerospace Corporation
Litchfield Park, Arizona

ABSTRACT

Previous papers on B-1 transparencies presented at the 1973 and 1975 Air Force Symposiums dealt primarily with the windshield. This paper reviews the development of the side and upper windows as they were redesigned for the aircraft No. 4 forward escape hatch.

The final design of the side window is a 5-ply acrylic-polycarbonate-acrylic laminate, while the upper window is a 3-ply acrylic-polycarbonate laminate with an abrasion-resistant coating applied to the cockpit surface of the polycarbonate main structural ply. These transparencies are of special interest because they represent yet another application of polycarbonate to an advanced high-performance aircraft glazing.

In this paper, a review first is made of the original side and upper window designs utilized on the Nos. 1 to 3 aircraft. The window design changes incorporated on aircraft No. 4 to improve durability, service life, and functional performance then are discussed and illustrated with cross section sketches, photographs of parts, design requirements, and the materials selected for fabrication.

Finally, the major requirements of the drawings and specifications are highlighted with some of the various aspects of quality assurance testing required for production hardware. Some of the topics covered include: polycarbonate fusion bonding and interlaminar shear strength testing, optics, interlayer testing, electrical – including thermal uniformity testing – and edge attachment adhesive testing.

PRECEDING PAGE BLANK-NOT FILMED

INTRODUCTION

Previous papers on B-1 transparencies presented at the 1973 and 1975 Air Force-sponsored symposiums dealt primarily with the windshield. This paper will review the development of the side and upper windows through the redesign for the final production configuration for the forward escape hatch of the No. 4 aircraft. These transparencies are of special interest because they represent yet another application of polycarbonate to an advanced, high-performance aircraft glazing.

Goodyear Aerospace was awarded a contract from Rockwell International in late 1971 to develop side and upper crew module windows for the first three B-1 aircraft for the RDT&E program. The side window design specified was a 3-ply polycarbonate/acrylic laminate with an external abrasion-resistant coating to protect the polycarbonate structural ply and an electrically conductive gold coating on the inboard face ply for defogging. The upper eyebrow window was of monolithic polycarbonate construction, again with an external abrasion-resistant coating to protect the polycarbonate. A gold coating for radar cross section reduction (RCSR) was applied to the cockpit side of the polycarbonate and was covered with a solution-applied abrasion-resistant coating to increase durability. This prototype program was completed successfully in 1973 and was one of the earliest applications of polycarbonate to aircraft transparencies.

Based on the results of Rockwell's structural fatigue testing in late 1975 and early 1976 with the original window designs, and also on the accumulated flight test experience then available with polycarbonate from a number of other programs in industry, it had become evident that several rather significant design changes should be incorporated into the side and upper windows for aircraft No. 4. These were needed to eliminate potential design and durability problems and to realize a more cost-effective production design with lower operational life-cycle costs.

Goodyear Aerospace also was the contractor selected in 1976 for the follow-on program to fabricate the side and upper windows for aircraft No. 4. This new contract required a change in size for the side and upper windows due to the redesign of the crew module escape system required for the final production configuration aircraft. Although window contour lines remained the same, the window size changes required a completely new family of fabrication tools because it also was necessary to maintain a spare part fabrication capability for the original windows to support future logistics requirements for the first three test aircraft.

The new transparencies developed for B-1 aircraft No. 4 are seen in Figure 1.

Highlights of the design evolution of these windows to the final configuration will be reviewed briefly, along with some comments on materials and processing and a look at quality assurance testing requirements.

SIDE WINDOW DESIGN EVOLUTION

Original Design for Aircraft Nos. 1 to 3

The original design specified by Rockwell for the side window is shown in Figure 2. Since low weight was a primary design goal, the window design was oriented to the use of polycarbonate and an abrasion-resistant coating to obtain the best high-temperature strength-to-weight ratio possible with the materials then available.

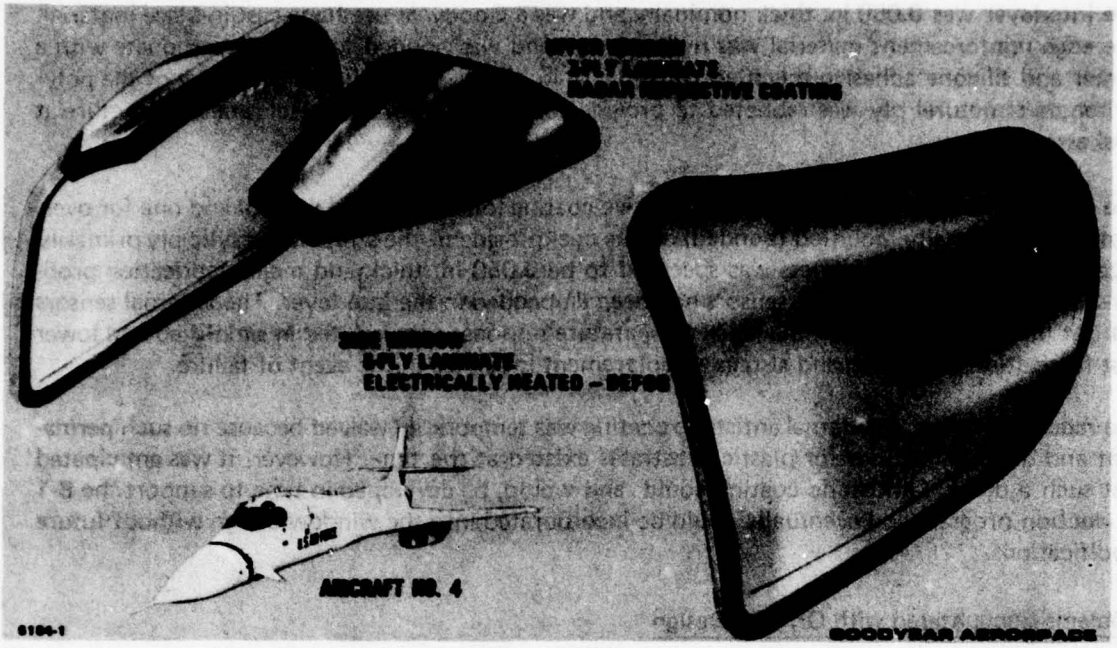


Figure 1 – B-1 Side and Upper Windows, Final Design

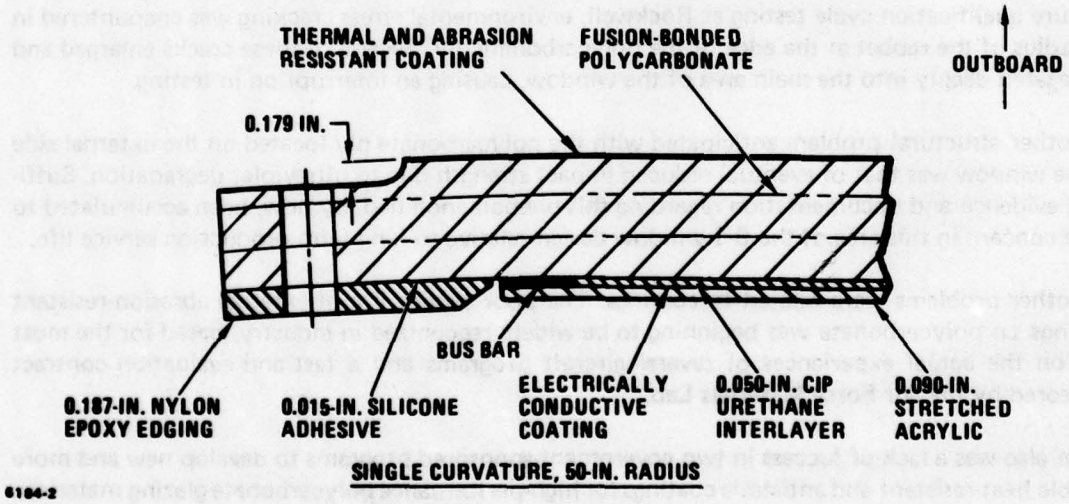


Figure 2 – Side Window Cross Section, Original Design

While conflicting design requirements demanded difficult tradeoffs in the choice of materials, the resulting window construction consisted of a 3-layer fusion-bonded polycarbonate structural ply 0.900 in. thick with a thermal-, abrasion-, and solvent-resistant coating applied on the external surface to provide protection and durability to the polycarbonate. The inboard ply was 0.090-in. stretched acrylic (per MIL-P-25690) and served as the substrate for the vacuum-deposited electrically conductive multilayer gold coating applied to its interlayer side for defogging purposes. Coating power output was nominally 0.45 watt/in.^{2}.

The interlayer was 0.050 in. thick nominally and was a Goodyear urethane cast-in-place material. The edge reinforcement material was nylon epoxy and was bonded to the polycarbonate with a primer and silicone adhesive specified to be 0.015 in. thick. The outboard periphery of the polycarbonate structural ply was rabbeted to provide for a flush fit of the metal retainer structure at final assembly.

The two temperature sensors for the conductive coating (one for normal control and one for overheat) were externally mounted (bonded) on the cockpit side of the stretched acrylic ply primarily because the interlayer thickness was specified to be 0.050 in. thick and major fabrication problems would have resulted if the sensors had been embedded in the interlayer. The external sensors did not have any significant time lag in temperature response and resulted in simplified and lower cost fabrication processing and also easy replacement in service in the event of failure.

The requirement for an external antistatic coating was temporarily waived because no such permanent and durable coatings for plastic substrates existed at the time. However, it was anticipated that such a durable antistatic coating could, and would, be developed in time to support the B-1 production program and eventually could be incorporated into the window design without future modifications.

Problems Encountered with Original Design

During the time period from late 1974 to early 1976, several deficiencies in the original side window design became apparent. Two problems were structural in nature. During full-scale thermal-pressure qualification cycle testing at Rockwell, environmental stress cracking was encountered in the radius of the rabbet at the edge of the polycarbonate ply. Several of these cracks enlarged and propagated deeply into the main area of the window, causing an interruption in testing.

The other structural problem anticipated with the polycarbonate ply located on the external side of the window was that of eventual reduced impact strength due to ultraviolet degradation. Sufficient evidence and documentation regarding this phenomenon had, by now, been accumulated to cause concern in this area of the B-1 window design relative to long-term production service life.

The other problems were related to coatings. The poor service life of external abrasion-resistant coatings on polycarbonate was beginning to be widely recognized in industry, based for the most part on the actual experiences of several aircraft programs and a test and evaluation contract sponsored by the Air Force Materials Lab.

There also was a lack of success in two government-sponsored programs to develop new and more durable heat-resistant and antistatic coatings for high-performance polycarbonate glazing materials.

Redesigned Configuration for Aircraft No. 4 and Production

To correct the problem areas described, the side windows for aircraft No. 4 were redesigned to a 5-ply laminated composite. The redesigned hardware is shown in Figure 3. Contour lines were unchanged. The new shape of the side window resulting from the crew module redesign for aircraft No. 4 is shown in Figure 4, compared to the original window shape. It will be noted the new heated area is much more rectangular in shape; as a result, it was possible to attain much more uniform electrical heating for defogging purposes.

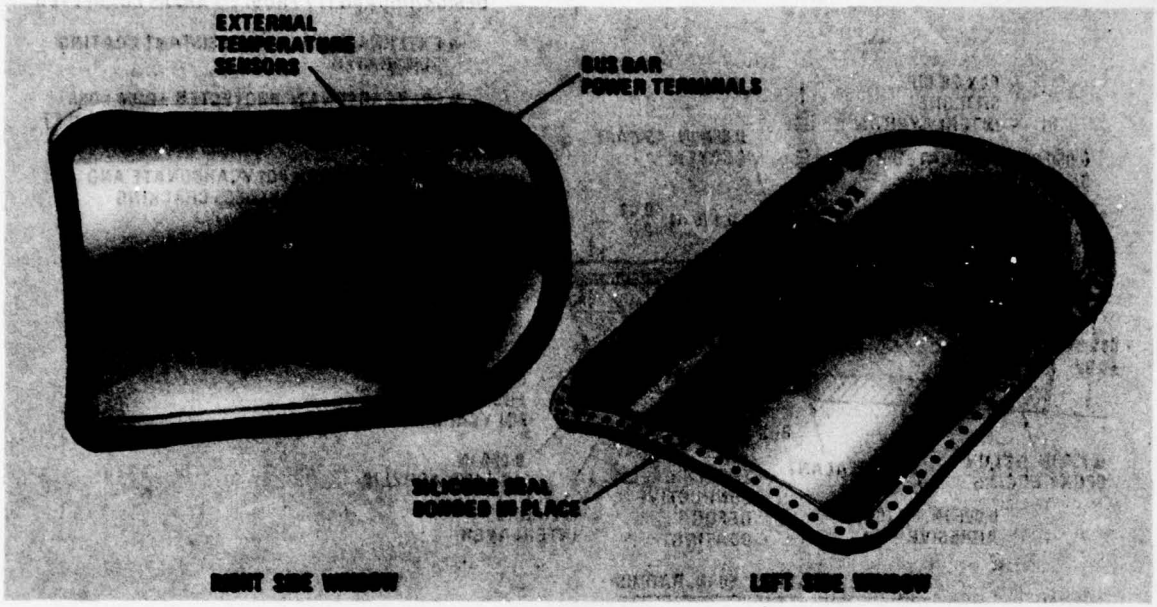


Figure 3 – Side Windows, New Design

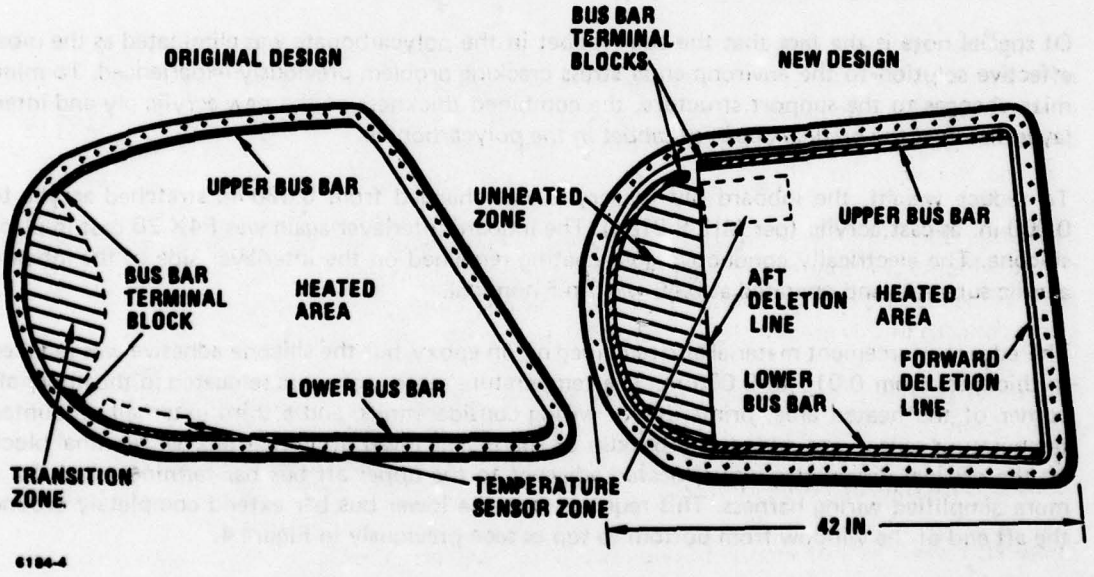


Figure 4 – Side Window Configuration

The new 5-ply acrylic-polycarbonate-acrylic construction for the side window is depicted in Figure 5. The structural ply remains three layers of polycarbonate fusion-bonded together but reduced slightly in thickness from 0.900 in. to 0.870 in. The external abrasion-resistant coating previously used on the polycarbonate was replaced by a thin 0.060-in. as-cast acrylic face ply (per MIL-P-8184) and a Goodyear Aerospace high-temperature-resistant interlayer, cast-in-place F4X-2B silicone. With this design approach, the acrylic and interlayer also serve to protect the polycarbonate from long-term ultraviolet degradation.

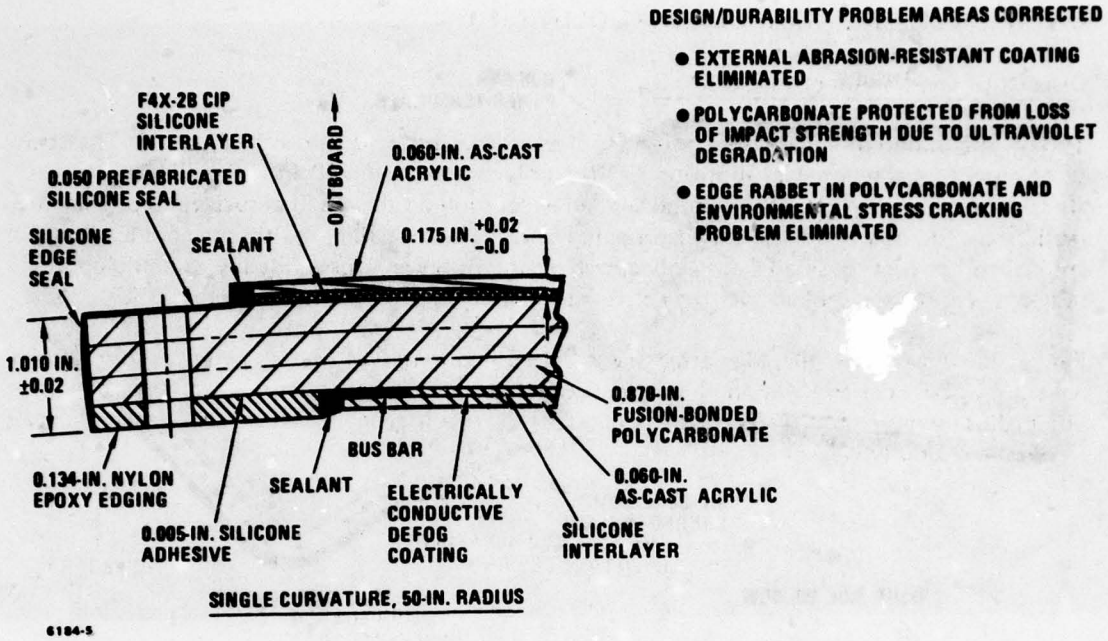


Figure 5 – Side Window Cross Section, New Design

Of special note is the fact that the edge rabbet in the polycarbonate was eliminated as the most effective solution to the environmental stress cracking problem previously experienced. To minimize changes to the support structure, the combined thickness of the new acrylic ply and interlayer matched the original depth of rabbet in the polycarbonate.

To reduce weight, the inboard ply of acrylic was changed from 0.090-in. stretched acrylic to 0.060-in. as-cast acrylic (per MIL-P-8184). The inboard interlayer again was F4X-2B cast-in-place silicone. The electrically conductive gold coating remained on the interlayer side of the inboard acrylic substrate and operated at 0.45 watt/in.^{2} nominal.

The edge reinforcement material also remained nylon epoxy, but the silicone adhesive was reduced in thickness from 0.015 to 0.005 in. The temperature sensor zone was relocated to the upper aft corner of the heated area, primarily for wiring considerations, and a third externally mounted temperature sensor was added as a backup or spare. The lower aft corner bus bar terminal block on the original design also was relocated adjacent to the upper aft bus bar terminal block for a more simplified wiring harness. This required that the lower bus bar extend completely around the aft end of the window from bottom to top as seen previously in Figure 4.

At the beginning of the contract for aircraft No. 4 in early 1976, the requirement for an external antistatic coating still existed for the side windows. Accordingly, an 0.050-in.-thick, type 0319 Chemcor glass external face ply with a 10- to 50-megohm-per-square, permanent static drain coating was specified since no durable coating had yet been developed for plastic. However, early in the new program the antistatic coating requirement was dropped, and with only minor tooling modifications the Chemcor was replaced with the 0.060-in. acrylic in the final design configuration to save approximately two pounds per window in weight.

UPPER EYEBROW WINDOW DESIGN EVOLUTION

Original Design for Aircraft Nos. 1 to 3

The original monolithic design specified for the upper window is shown in Figure 6. The structural ply was again three-layer fusion-bonded polycarbonate, 0.750 in. thick, with a thermal-, abrasion-, and solvent-resistant coating applied in solution on the external surface to provide protection and durability to the polycarbonate. A vacuum-deposited, multilayer gold coating was applied to the cockpit side of the polycarbonate for RCSR purposes. Finally, a liquid abrasion-resistant coating was applied over the gold coating to increase durability and service life.

Except for dimensions, the edge attachment details and materials were the same as for the original side window design including a rabbeted edge on the outboard side of the polycarbonate to obtain flush mounting of the structure. Here too, the requirement for an external antistatic coating was temporarily waived.

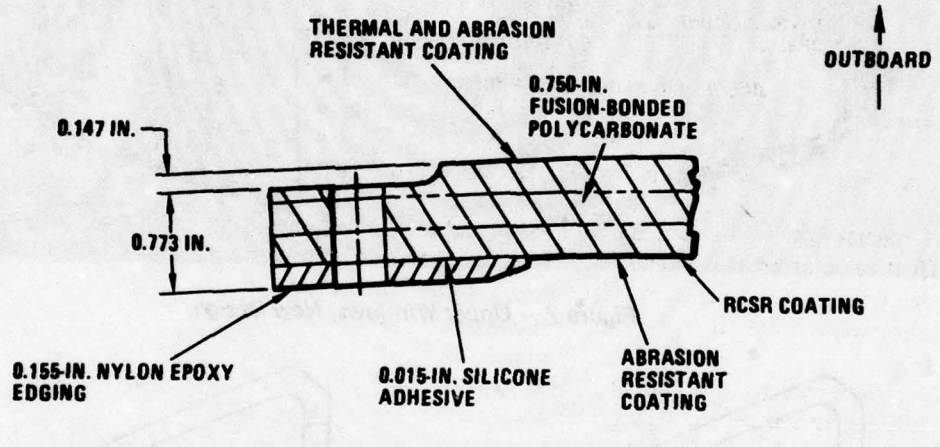


Figure 6 – Upper Window Cross Section, Original Design

Problems Encountered with Original Design

For the most part, the same deficiencies encountered with the original side window design were also experienced with the upper window: environmental stress cracking in the rabbeted area of the polycarbonate, probable long-term reduced impact strength of the polycarbonate due to ultraviolet degradation, and the poor service life of the externally applied abrasion-resistant coatings. Also, while not as important as for the side window, there was no antistatic coating available for the plastic substrates of the production upper window design. This raised the possibility of a costly design fix to incorporate a compound-curved glass ply with antistatic drain coating laminated to the outboard side of the polycarbonate.

Another problem encountered on the upper window cockpit surface was sporadic loss of adhesion of the RCSR coating system in the area immediately adjacent to the nylon epoxy edge reinforcement material. It also was believed that the RCSR coating was vulnerable and subject to scratching and humidity damage with its long-term service life being suspect.

Redesigned Configuration for Aircraft No. 4 and Production

To correct the problem areas, the eyebrow windows for aircraft No. 4 were redesigned to a 3-ply laminated composite. The resulting hardware is shown in Figure 7. Contour again was unchanged. The shape of the redesigned upper window compared with the original window shape is seen in Figure 8.

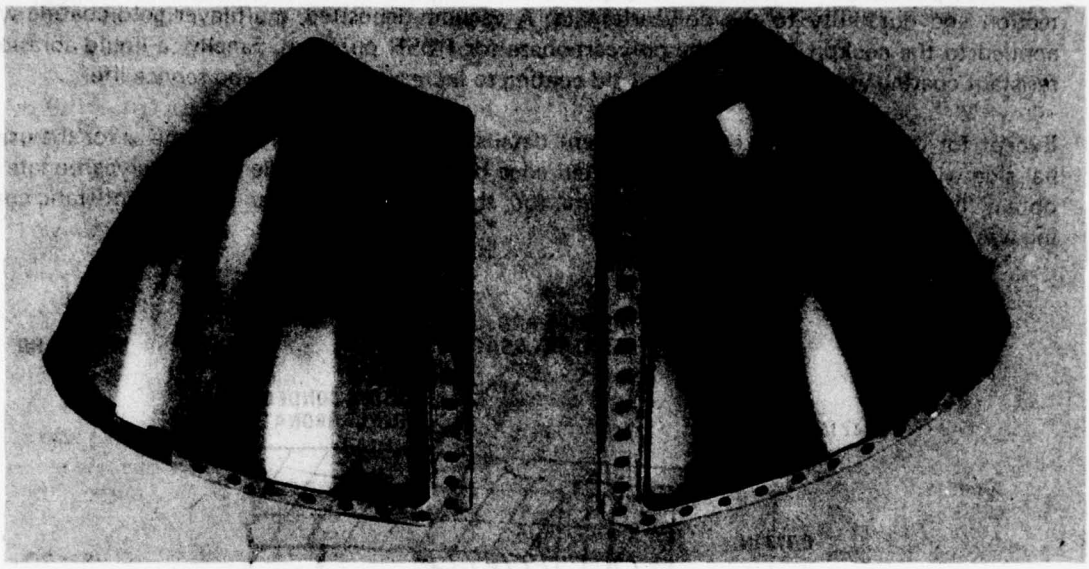


Figure 7 – Upper Windows, New Design

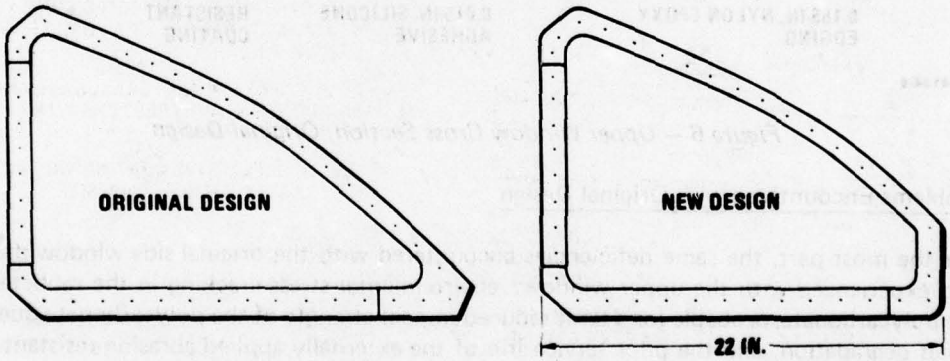


Figure 8 – Upper Window Configuration

The new 3-ply acrylic-polycarbonate composite for the upper window is shown in Figure 9. The structural ply is three layers of fusion-bonded polycarbonate but reduced in thickness from 0.750 to 0.720 in. The edge reinforcement material remained nylon epoxy and the silicone adhesive was reduced to 0.005 in. thick.

The antistatic coating requirement for the small upper window was dropped very early in the new program, and the external abrasion-resistant coating previously used on the polycarbonate was replaced by a thin, 0.060-in. as-cast acrylic face ply (rather than glass) and the cast-in-place F4X-2B silicone interlayer – as was the case for the side window. The acrylic and interlayer again provided long-term protection to the polycarbonate from ultraviolet degradation. This approach also resulted in the elimination of the edge rabbet in the polycarbonate and the environmental stress cracking problem in the same manner as for the side window redesign.

To save weight, an abrasion-resistant coating was specified for the cockpit surface of the polycarbonate where general experience had shown that good adhesion could be maintained. In this location it was not prone to ultraviolet degradation and reasonable service life could be expected.

The other primary feature of the upper window redesign was to relocate the multilayer gold coating for radar cross section reduction from the cockpit side of the window to the interior of the laminated composite where it was safely embedded and protected for long-term service life. To improve light transmission properties of the window, the resistance of the RCSR coating was increased from 15 ohms per square maximum on the original design to 30 ohms per square maximum. This data follows in a later section.

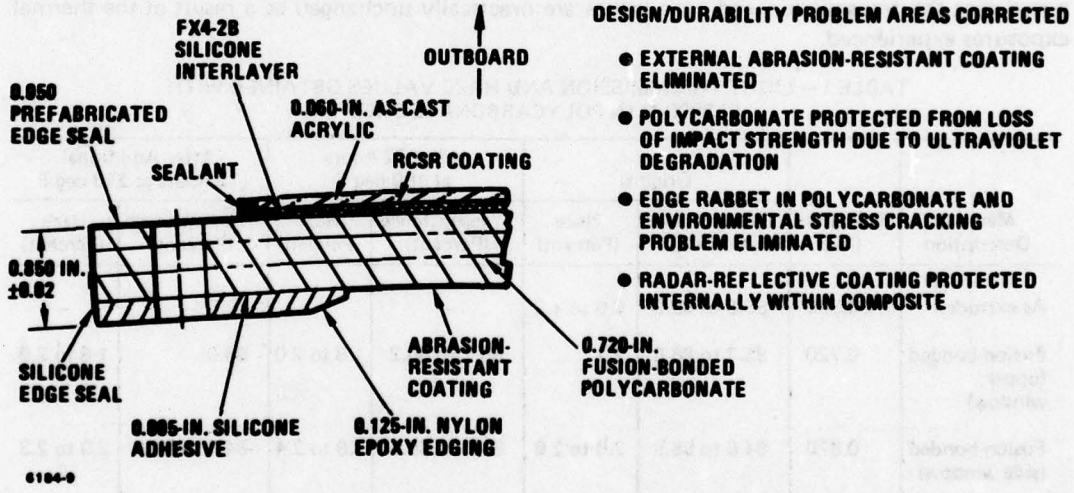


Figure 9 – Upper Window Cross Section, New Design

MATERIALS AND PROCESSING

With just a few exceptions due to the differences in window size and design, the materials and process development activities were similar for the side and upper windows for aircraft No. 4. It should be realized, too, that much of the more difficult development work already had been accomplished on the first contract for the original windows. The primary task this time was to adapt

the developed and proven processes and techniques to the redesigned hardware, taking advantage, of course, of the opportunity to incorporate improvements and/or refinements where possible. This section of the paper will briefly highlight some of the major areas of interest.

Polycarbonate

Material requirements were controlled by MIL-P-83310 and Rockwell Specification No. LB0103-121. To meet light transmission and haze requirements, it was necessary to use General Electric's SL3000-111N polycarbonate as the basic extruded sheet stock. Because this material was not extruded commercially in gauges thicker than 0.375 in., it was necessary for Goodyear to fusion-bond several extruded sheets together to obtain the required thicknesses of the structural plies for the side and upper windows (0.870 and 0.720 in., respectively, with ±0.030-in. thickness tolerance).

This was done by first predrying the individual extruded sheets to remove moisture and then placing three sheets of the required thickness between large 4- x 6-ft. optical cauls or platens. Fusion-bonding was accomplished using a special process for the necessary time-temperature-pressure cycle without the use of any surface primers or adhesives. Because the optical view angle for side and upper windows was not very severe, no grinding and polishing of the polycarbonate was required, either before or after fusion-bonding. Control of the interlaminar shear strength properties will be discussed in the last section of the paper which covers quality assurance testing.

Typical light transmission and haze values for the polycarbonate flat sheet stock are presented in Table I and represent typical ranges obtained from a number of representative sheets. It will be noted that the transmission and haze values are practically unchanged as a result of the thermal exposures experienced.

TABLE I – LIGHT TRANSMISSION AND HAZE VALUES OBTAINED WITH SL3000-111N POLYCARBONATE SHEET

Material Description	Thickness (In.)	Original		After 72 hours at 180 deg F		After Additional 72 hours at 240 deg F	
		Transmittance (Percent)	Haze (Percent)	Transmittance (Percent)	Haze (Percent)	Transmittance (Percent)	Haze (Percent)
As extruded	<0.300	88.8 to 89.0	0.6 to 1.2	–	–	–	–
Fusion-bonded (upper window)	0.720	85.7 to 86.8	2.1	85.7 to 86.2	1.8 to 2.0	86.0	1.8 to 2.0
Fusion-bonded (side window)	0.870	84.6 to 85.5	2.0 to 2.6	85.1 to 85.6	1.8 to 2.4	84.7 to 85.5	2.0 to 2.3

Acrylic Sheet Stock

The cast acrylic sheet stock specified for the side and upper windows was per MIL-P-8184. Because stringent low angle of view optics were not involved and also because a reasonably uniform electrical heating pattern could be obtained without a substrate of constant thickness, it was not necessary to grind and polish the acrylic sheet stock prior to use. Instead, all material was hand-selected to obtain the quality required.

Forming

Acrylic Sheet

Because of its shallow compound curvature, the outer acrylic face ply for the upper window was thermo-formed using conventional processing. With the curvature of the side window being a section of a cylinder with a rather flat 50-in. radius, it was possible to cold bend the 0.060-in.-thick inner and outer acrylic plies to contour along the straight line elements without a thermal-forming cycle. This greatly simplified the handling and processing of the side window detail parts.

Polycarbonate Sheet

The thermo-forming of polycarbonate sheet to obtain the excellent optical quality required for an aircraft transparency without markoff and distortion bands is never an easy task.

In the case of the B-1 side and upper windows, the problem was further complicated by the thick gauges of the blanks (0.870 in. and 0.720 in., respectively) and especially by the contour tolerances imposed on the formed parts. It was necessary to maintain a ±0.030-in. maximum deviation from theoretical contour in the central optical area. The side window polycarbonate forming blank was obtained from a 34- x 47-in. section of material, while the upper window blank was cut from a triangular shaped section of material about 25 in. long.

Using processing techniques developed during the earlier program, the polycarbonate window blanks were formed to acceptable contour at temperatures under 350 deg F, using as short a cycle as possible to minimize thermal exposure time. It also was a standard practice to form the polycarbonate parts right after the fusion-bonding cycle to take advantage of the already-dried-out material. It was thus possible to eliminate the usual drying cycle just prior to forming.

Abrasion-Resistant Coating

The abrasion- and solvent-resistant coating applied in solution form to the inboard polycarbonate surface of the upper window was Goodyear Aerospace Code 705 coating. In this particular case, the coating was applied to the formed polycarbonate blank and cured thermally prior to the interlayer laminating cycle.

Interlayer Material

The design requirement for high-temperature resistance for the side and upper windows dictated a silicone material for the outboard interlayer. Accordingly, for these applications, Goodyear's F4X-2B cast-in-place silicone interlayer was selected. This same material was chosen for the inboard interlayer for the side window on the basis of excellent adhesion to the substrates, compatibility with the electrically conductive coating, general processing characteristics, and anticipated excellent service life.

Characteristic of silicone materials, the F4X-2B interlayer possesses modest mechanical properties at normal operating temperature ranges. However, it retains these properties well at extreme temperatures, providing greater strength at elevated temperatures and a lower modulus at low temperatures than other types of interlayers. The inherently low shear modulus at all temperature ranges significantly helps to accommodate thermal strains. The interlayer also has good optical qualities.

The tensile strength of the F4X-2B interlayer at room temperature is 500 to 600 psi with an ultimate tensile elongation of 450 percent. However, Goodyear considers the shear strength and shear modulus properties of an interlayer to be the two most important design parameters. The shear strength (F_{su}) for the F4X-2B interlayer ranges from 600 psi at –65 deg F to 150 psi at 270 deg F. Shear modulus (G_i) is 50 to 60 psi at –65 deg F and room temperature, and 25 to 30 psi at +270 deg F. Typical curves for shear stress versus shear strain data from –65 to +270 deg F are shown in Figure 10.

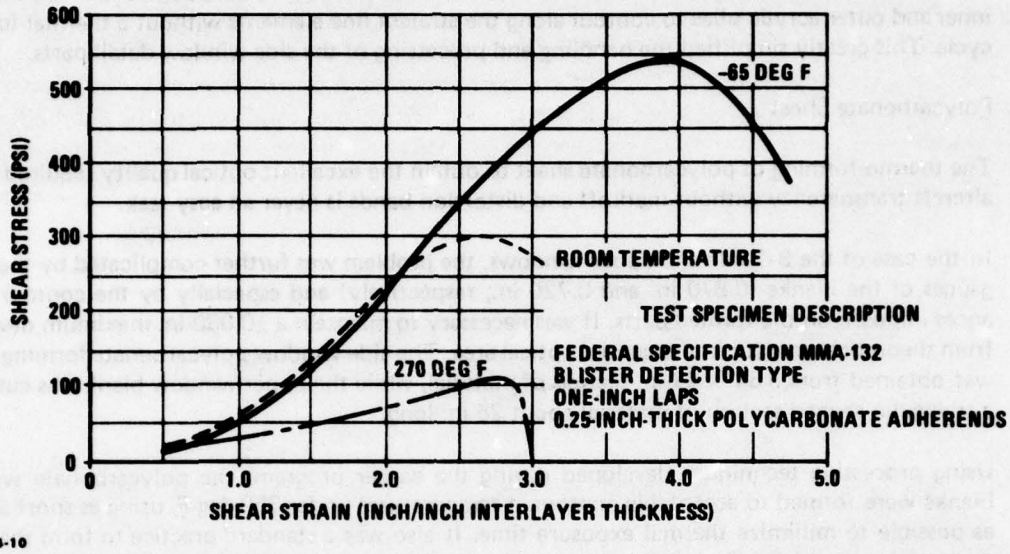


Figure 10 – Typical Curve, Shear Stress versus Shear Strain, F4X-2B Interlayer System

Interlayer Laminating

The choice of the F4X-2B silicone interlayer dictated that laminating operations would be based on cast-in-place processing. Matched male-female casting fixtures with concentric contours were used for the windows. The design of these tools was based on the experience obtained in the earlier program for aircraft Nos. 1 to 3 transparencies. These casting fixtures proved to be very satisfactory in practice, and data presented in the last section of the paper will show that the specification requirements for optical distortion and deviation were attained.

Edge Reinforcement Laminate

The nylon epoxy edge reinforcement laminate was a high-temperature-resistant, high-strength material that met specific Rockwell requirements for tensile strength and tensile modulus in both the warp and fill directions at room temperature and 220 deg F. This material was purchased as a certified subcontract item in prelaminated and cured flat sheets. By using the same edging material used on the windshield panels of the B-1, the cost of qualifying a second edging material for the low quantity of transparencies involved was avoided.

During fabrication, the individual detail edging strips were cut to predetermined pattern sizes and formed to the shallow contours required for the side and upper windows.

Adhesive Bonding of Edge Reinforcement Laminate

The adhesive bonding system developed earlier for transparencies on aircraft Nos. 1 to 3 also was specified for the windows on aircraft No. 4. The adhesive, selected specifically to be compatible with polycarbonate, was an RTV silicone rubber with primer. The cured adhesive bond line was required to be a controlled thickness of 0.005 in. +0.005, −0.003. This was accomplished by using a fine wire spacer technique or by spiral wrapping the detail edging strips with a polyester fishline cord of the correct diameter.

After bonding and clamping, the window assemblies were cured at an elevated temperature. It should be noted that the fishline spacer cord was left in the bond line of the finished windows. This was the preferred technique because the fine wires left voids in the bond when they were extracted prior to final trimming and drilling.

Attach Hole Drilling/Reaming and Finishing

Very stringent requirements were imposed by Rockwell on the edge attachment holes in the B-1 windows and considerable process development was required before the techniques were completely established and the process became routinely repeatable.

The specified requirement for hole diameter was 0.4063 in. +0.0005, −0.0043 and maintaining this tolerance was complicated by the presence of the nylon epoxy edging material bonded to the polycarbonate.

To preclude potential hole cracking problems from environmental exposure and other factors, a wall finish of 63 RMS or better was specified for the polycarbonate portion of the holes.

These requirements were consistently achieved on a production basis. All of the nearly 1000 holes drilled for the aircraft No. 4 windows, including spares and test parts, were acceptable.

Seals and Sealants

After final assembly operations, including trimming, drilling, and contour inspections, were completed for the side and upper windows, three separate sealing operations were performed. First, a prefabricated silicone rubber exterior weather seal, trimmed to size and with holes cut, was bonded to the outboard surface of the polycarbonate in the edge attachment area using a Dow Corning primer and DC-93-006 silicone sealant as an adhesive. The periphery of the outer acrylic face ply and exposed interlayer were next protected with an 0.125-in.-wide application of DC-93-006 sealant applied around the trim edge of the daylight opening area. The inboard acrylic face ply and interlayer trim on the side window also were sealed. Finally, the net trim edge of the polycarbonate structural ply of each window was finished to 125 RMS or better and covered with a thick coating of the DC-93-006 sealant.

Side Window Electrically Conductive Coating Design/Development

The design and development of the multilayer, electrically conductive (EC) gold coating consisted of determining the heated area and coating resistivity pattern, defining the vacuum deposition

parameters, conducting preliminary coating runs, testing the initial parts, and evaluating the test results for "fine tuning" of the chamber setup to achieve the desired resistivity pattern. The resistivity pattern is the primary factor affecting the power density distribution and consequently the temperature distribution or thermal uniformity of the heated panel.

The power density (watts/in.^{2}) distribution is characterized by the use of power constants or K factors which define the relationship of the power density at one location in the heated area to that of another location. Following are the Rockwell requirements for various power constants:

$$K_o = \frac{\text{power density at the overheat sensor location}}{\text{power density at the normal control sensor location}} = 1.00^{+0.07}_{-0.0}$$

$$K_a = \frac{\text{average power density}}{\text{power density at the normal control sensor location}} = 1.00^{+0.0}_{-0.14}$$

$$K_c = \frac{\text{minimum localized power density}}{\text{average power density}} > 0.75$$

$$K_s = \frac{\text{power density at the spare sensor location}}{\text{power density at the normal control sensor location}} = 1.00^{+0.07}_{-0.0}$$

$$K_h/K_o = \frac{\text{maximum localized power density}}{\text{power density at the overheat sensor location}} \leq 1.25$$

$$K_h = \frac{\text{maximum localized power density}}{\text{power density at the normal control sensor location}} = \text{no requirement}$$

Other design parameters specified by Rockwell include: maximum bus-to-bus voltage and resistance shall be 66 volts and 11.95 ohms, respectively; power density shall be greater than 0.36 watt per square inch and less than or equal to 0.70 watt per square inch when total power is 325 watts.

To determine the characteristic power constants for the new side window shape, the power density values were measured at various points throughout the heated area. This was done during early development testing. The power density values were determined by a transient temperature method which compared the rate of temperature rise at the points on the test panel with a calibration curve. This curve was developed by measuring the rate of temperature rise for known values of power density on a calibration coupon having a cross section similar to that of the test panel. The calibration curve, Figure 11, is a plot of the time required for a 30-deg-F temperature rise versus power density input to the calibration coupon. The 30-deg rise was arbitrarily selected as low enough to heat the entire panel before the hottest area became overheated and yet high enough to reduce the sensitivity to instrumentation tolerances. Also it is within the general range of the operational coating control temperature of 110 deg F.

Power density values were determined at 20 uniformly spaced locations throughout the window panel, as indicated in Figure 12, and also at two additional points within the sensing element zone and at the predetermined general locations of the hottest point and coldest point on the window panel. Figure 12 shows the power density values determined for one of the production window panels. Prior to conducting the power density testing, a thermal color paint test was used to indicate the general heating pattern and to locate the hottest and coolest areas of the panel.

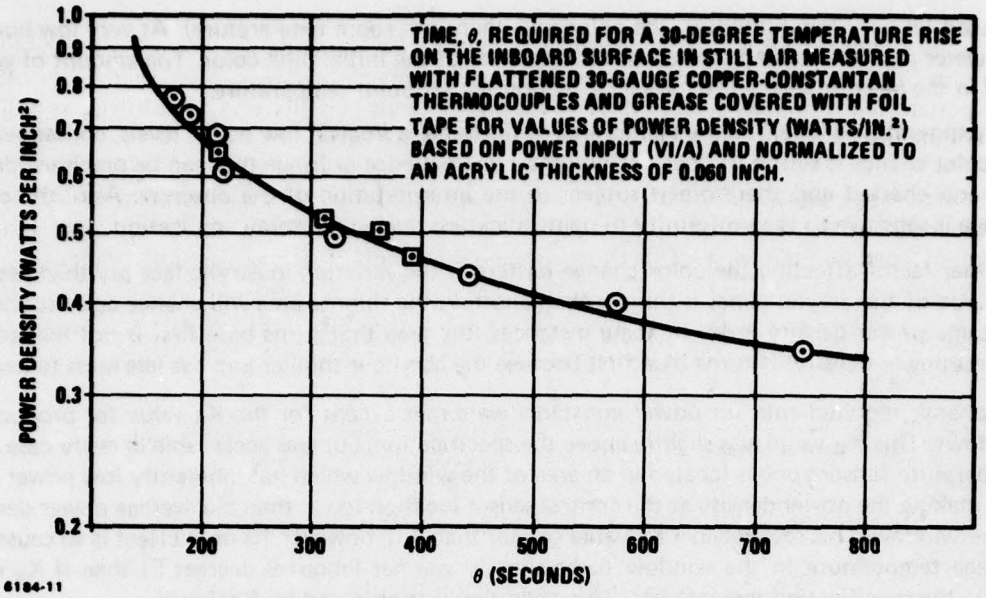


Figure 11 – Calibration Curve, Laminated B-1 Side Window

Thermal color paint is a paint that changes color as the temperature changes. In this case, the color was to change from pastel pink to blue at 104 deg F.

The thermal color paint initially was specified to be used to determine the power density, as well as temperature uniformity. However, several limitations became apparent during development testing. First, the effect of humidity variations caused variations in the temperature at which the color

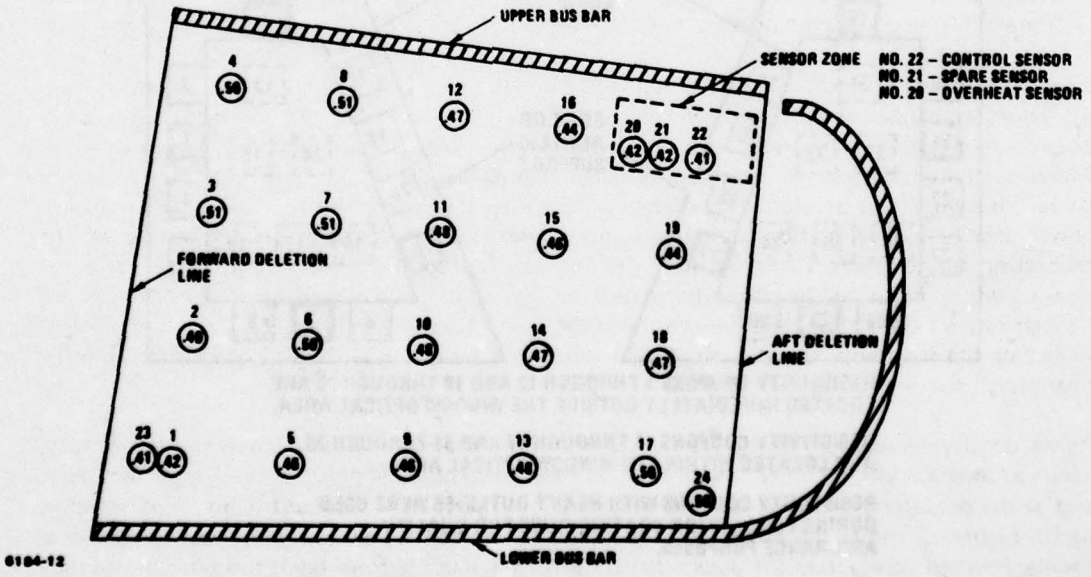


Figure 12 – Representative Left Side Window Power Density Distribution (Watts/In.²)

changed (at very low humidity, the color will change at room temperature). At very low humidity, water had to be added to the paint mixture to get the initial pink color. The amount of water used in the mixture seemed to have an effect on the set point temperature.

The temperature gradient in the heated area of the panel is small at low power levels; consequently, the color change is subtle. It does not present a distinct edge or fringe that can be precisely identified and charted and therefore is subject to the interpretation of the observer. Also, the color change is sensitive to the uniformity of paint thickness during the spray application.

Another factor affecting the color change pattern is the variation in acrylic face ply thickness. If one area of the acrylic panel is thinner than another, the thinner area will change color sooner at the same power density level. In some instances, the area that turns blue first is not the area of highest power density. It turns blue first because the acrylic is thinner and has less mass to heat.

In general, requirements for power constants were met except for the K_a value for production windows. This K_a value was slightly above the specification, but was acceptable in every case. The temperature sensor zone is located in an area of the window which has inherently low power density, making the power density at the control sensor location lower than the average power density in the window. This resulted in a K_a value greater than 1.0; however, its only effect is to cause the average temperature in the window to be slightly warmer (about 9 degrees F) than if K_a were within the specification requirement. This condition was accepted by Rockwell.

Upper Window RCSR Coating Design/Development

In the development of the RCSR gold coating for the upper window, three trial runs were made with witness coupons located as indicated in Figure 13. Each run was made with a slightly different setup to try to get the resistivity as high as possible without exceeding the specified limit of 30 ohms per square.

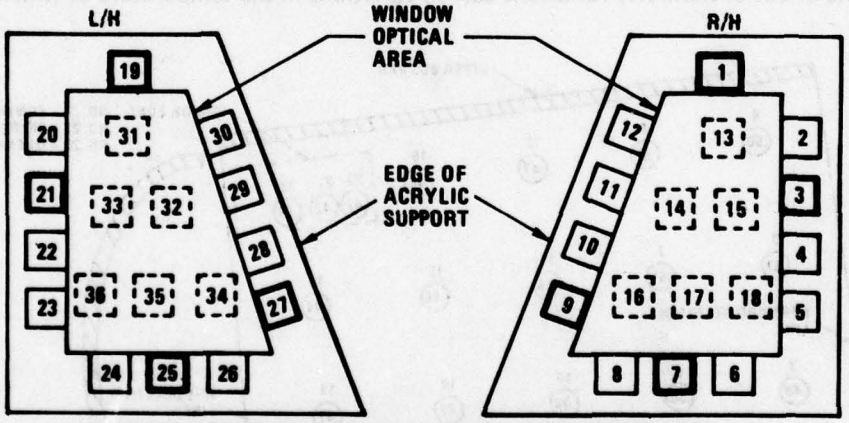


Figure 13 – Location of Resistivity Coupons

As a quality assurance check on the coating resistivity during chamber runs on the actual production windows, witness coupons were located only at points 1, 3, 7, and 9 on the right window and points 19, 21, 25, and 27 on the left window. These coupons were monitored to ensure the RCSR coating on the acrylic face ply was below 30 ohms per square before lamination to the polycarbonate structural ply.

Representative Light Transmission and Haze Data

A brief look at the resulting light transmission and haze values will be of interest after reviewing the various materials and component parts. The specification requirement for light transmission (Illuminant C) was 60 percent minimum and was achieved for both windows. The haze requirement was 5 percent maximum and this was met for the upper window, which had only one interlayer. However, the silicone interlayer has a rather high haze content, and with two interlayers in the side window construction the resulting haze did exceed the maximum allowable. Values up to 6.6-percent haze were experienced in isolated instances.

Typical data obtained during the various stages of fabricating the side and upper windows are presented in Table II.

TABLE II – TYPICAL VALUES OBTAINED DURING FABRICATION OF AIRCRAFT NO. 4 TRANSPARENCIES

	Light Transmission (Percent)	Haze (Percent)
Side Window		
Electrically Conductive-Coated Acrylic (0.060 in.)	72.0	1.0
Formed Polycarbonate (0.870 in.)	84.7	2.4
3-Ply Laminate with EC-Coated Ply	62.5	4.5
5-Ply Laminate	63.0	5.5
Upper Window		
RCSR-Coated Acrylic (0.060 in.)	74.7	1.3
Formed Polycarbonate (0.720 in.)	86.8	1.6
3-Ply Laminate with RCSR-Coated Ply	68.5	4.4

PROCESS CONTROL AND QUALITY ASSURANCE TESTING OF PRODUCTION WINDOWS

Because of the critical structural capacity and high-performance nature of the side and upper windows, quality assurance testing for this program was somewhat more extensive than normal. Early in the development effort, formal process control and material specifications, as well as Quality Assurance Acceptance Test Plans/Procedures (ATP) were prepared by Goodyear Aerospace. Rockwell quality assurance requirements were included in the ATP and its approval of these documents was required prior to the fabrication of any production parts.

This section will highlight some of the most important quality assurance requirements and test procedures used. Obvious and routine inspections such as thickness and other dimensional verifications, contour checks, light transmission measurements, and workmanship examinations will not be covered.

Polycarbonate Testing

Three types of quality assurance tests were conducted on the fusion-bonded polycarbonate stock used for the main structural plies of the windows. Two tests, the unnotched Charpy impact test and the beam flexure test, were conducted for every window produced. The third test, torsional shear, was only performed if an area of suspected low adhesion or contamination was encountered during test in the fusion-bond lines of the beam flexure specimens.

Test coupons were cut from the parent fusion-bonded polycarbonate sheet immediately adjacent to the area from which each individual window panel blank was obtained. The test coupons accompanied their related window panel through all thermal processing cycles and were exposed to the same chemical and solvent environment as the actual window. One face of the upper window test coupons had the inboard surface abrasion-resistant coating applied.

Unnotched Charpy Impact Test

This test was intended to detect any brittle failure tendencies in the polycarbonate structural ply. The test procedure was per ASTM 256, Method B, except that the specimens were unnotched. Three specimens, each 0.5 in. wide x 0.238 in. thick x 4.95 in. long, were machined for every window panel manufactured. One original surface of the fusion-bonded test specimens was retained when machining the 0.238-in. thickness. This surface for the upper window test specimens was to be the abrasion-resistant coated face representative of the cockpit surface and during test was positioned opposite the impact face.

The specimens were tested at an energy level equivalent to 70 foot-pounds per inch of thickness (16.7 foot-pounds for the 0.238-in.-thick specimens). No brittle failure of the test specimens was permitted.

Beam Flexure Testing

This test was used to ensure that a minimum level of interlaminar shear strength was maintained in the fusion-bond lines of the polycarbonate. In this test setup a typical maximum outer fiber tensile stress of approximately 24,000 psi was developed in the polycarbonate at ductile yield which corresponded to an interlaminar shear stress at the fusion-bond lines of about 3100 psi for the side window and 2600 psi for the upper window.

Three test specimens were prepared, each 1 in. wide x 6 in. long x the fusion-bonded thickness for each window. Each specimen was tested to ductile yield at room temperature by 4-point bending with a 5-in. support span as seen in the photograph of Figure 14. The load was applied at two points two inches apart, centered between the two support points, at a rate of 0.05 in. per minute. For upper window test specimens, the load was applied to the specimen surface upon which the abrasion-resistant coating had been applied.

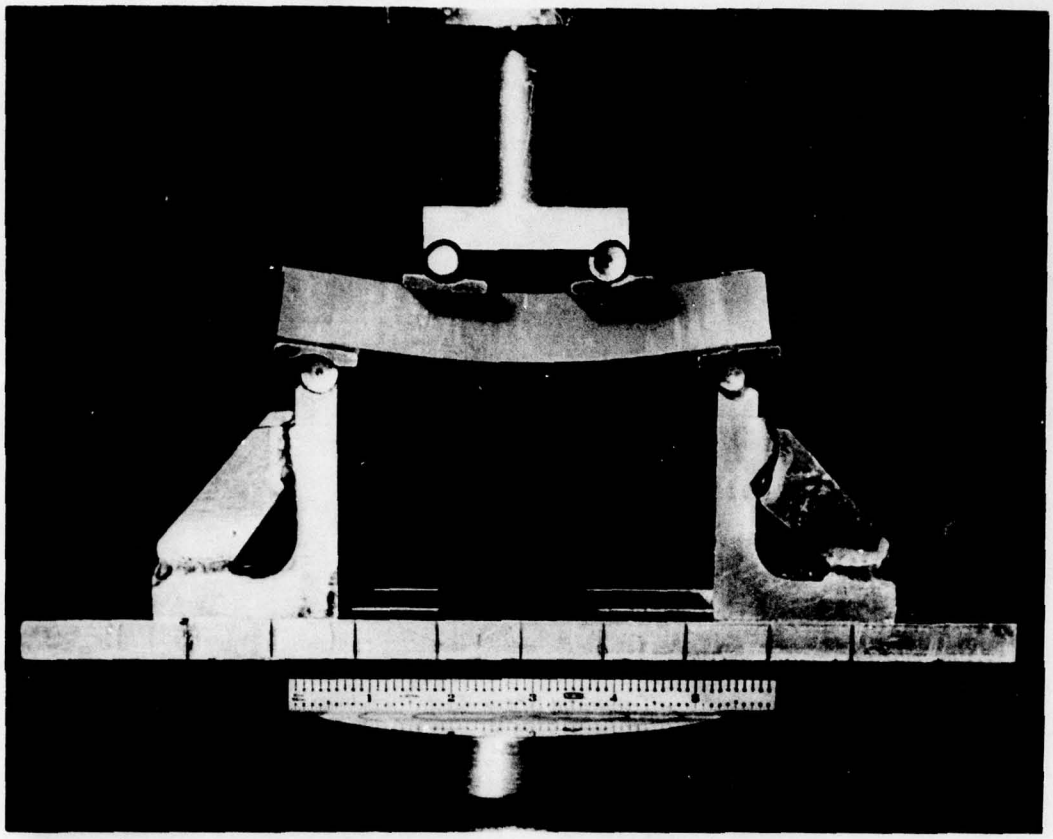


Figure 14 – Beam Flexure Testing

Load was applied until a ductile-yield failure occurred and was visually confirmed. At the first appearance of strain marks on the tension surface of the specimen, the load was immediately removed before any further deflection could take place.

No brittle failure was permitted. Any shear failure occurring at any of the fusion-bonded interfaces which exceeded an area of 0.25 $in.^2$ was cause for rejection of the window assembly. Smaller area failures at the fusion-bond lines were restricted to one per specimen and a torsional shear test then was required.

Torsional Shear Testing

In the event such a shear or delamination failure was experienced at a fusion-bond line, a torsional shear test was then required to establish quantitatively the actual shear strength of the fusion-bond line in question.

Material for the torsion shear specimens was taken from the beam flexure specimen within 0.5 in. of the failure area and a torsional shear strength no less than 8000 psi at yield was to be realized.

The test specimen design is shown in Figure 15 and a photograph of the test setup is seen in Figure 16.

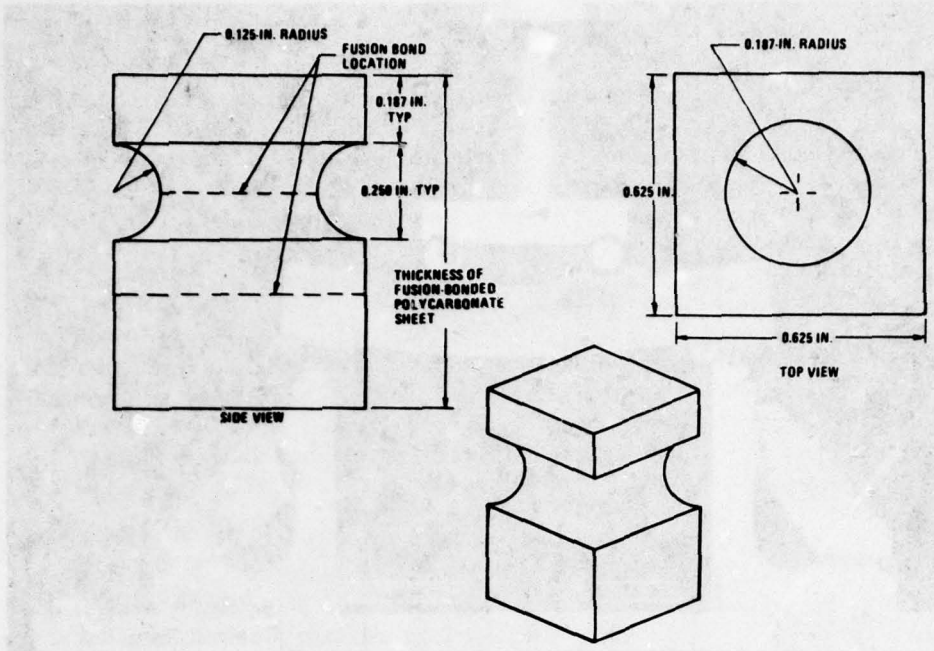


Figure 15 – Torsional Shear Test Specimen

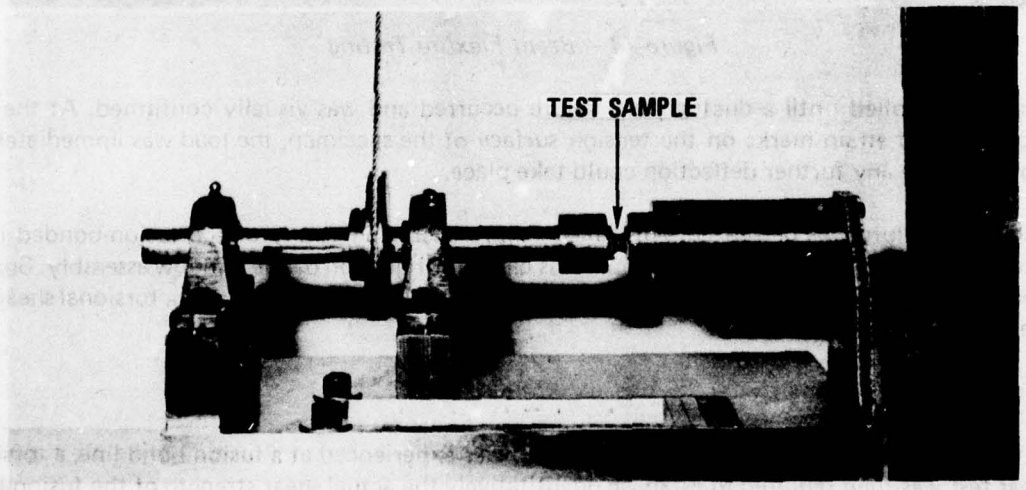


Figure 16 – Torsional Shear Test Setup

On several occasions, small and local fusion-bond line failure areas were experienced during beam flexure testing. The failure areas were usually only pin-head in size and always had a tiny foreign particle present in the center of the failed area when examined microscopically. However, no subsequent failure was ever experienced during the ensuing torsion shear test, thus verifying the structural integrity of the fusion-bonded material.

This torsion shear test for polycarbonate was developed by John Kimerly and associates of Rockwell and is described by Rockwell Specification No. LF0001-007. This apparently is the first test method to be developed that can obtain an accurate measure of the true fusion-bond strength at a reasonable cost. Mr. Kimerly described this test method at a recent meeting of the ASTM Subcommittee F7.08 for Aerospace Transparent Enclosures and Materials, and it is understood the method has been proposed as a standard ASTM test.

Abrasion-Resistant Coating Adhesion Test

Upon completion of the coating cure on the upper window polycarbonate substrate, the adhesion of the abrasion-resistant coating was checked at room temperature in the excess trim area. The standard ½- x ½-in. scribed grid test area with 3M Company No. 250 tape and a fast 90-deg "snap" removal technique was used to verify coating adhesion to the polycarbonate substrate.

Interlayer Adhesion

Two types of quality assurance control tests were used to verify interlayer adhesion: flatwise tensile strength and 180-deg-angle tensile peel tests. The test coupons were fabricated simultaneously with the actual window panels, using the same materials and batches of interlayer resin. The coupons then accompanied the windows through the prescribed processing thermal cycles to be as representative as possible.

Flatwise Tensile Strength

This test procedure was used to monitor the flatwise tensile strength of the window laminate comprising the polycarbonate structural ply and the electrically conductive-coated inboard acrylic face ply.

Five test specimens, each 2 x 2 in. as shown in Figure 17, were tested at room temperature at a load rate of 0.05 in. per minute. An average test value of 140 psi was required.

Interlayer/Scrim Cloth 180-Deg Tensile Peel Testing

This test method was used to verify the silicone interlayer adhesion to the other interface materials in the side and upper windows; namely, the outboard acrylic face ply and polycarbonate in the side window and the RCSR coating in the upper window.

The specimen for this test required a 4- x 7-in. substrate with a No. 116- or 120-style fiberglass cloth strip embedded in the interlayer, which was cast in place to a thickness of 0.100 to 0.150 in. After completion of the interlayer cure cycle, three strips, each one inch wide, were cut through the interlayer. The test specimens were loaded into the tensile test machine and the extended cloth edge was folded back and gripped so as to apply load at 180 deg (parallel) to the substrate surface during the ensuing tensile peel test at room temperature. Load was applied at a rate of two inches per minute.

A cohesive failure of the interlayer was required, with no evidence of delamination.

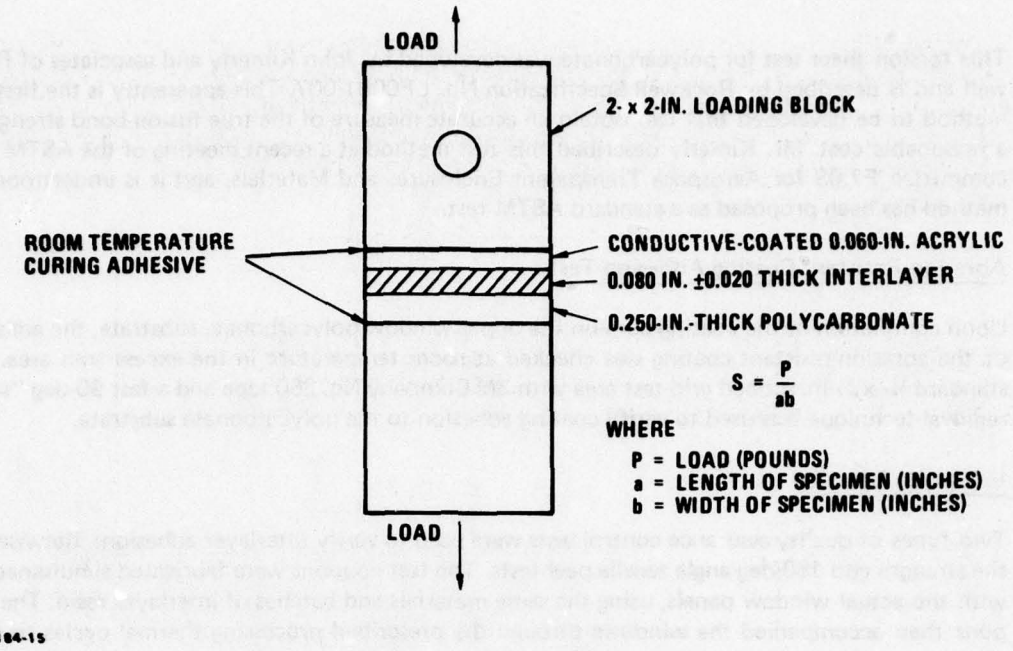


Figure 17 – Flatwise Tensile Test

Edge Attachment Adhesive Bonding Control Tests

One double-lap shear test sample, as shown in Figure 18, was bonded and cured simultaneously with each window assembly. The adhesive and primer materials utilized for the test sample were from the same batch-container as used in the manufacture of the window assembly. Five test specimens one inch wide were cut from the parent test sample and tested in tension at 150 deg F (after a 30-minute soak) with a test machine head travel rate of 0.05 inch per minute. The minimum adhesive lap shear strength of any specimen was required to be 400 psi.

Optical Quality Requirements

The optical quality requirements for the side and upper windows are listed in Table III. Discussion here will be confined to distortion and angular deviation.

Because of the rather perpendicular angle of view associated with the side and upper windows as installed in the aircraft, attainment of the optical requirements was not nearly as difficult as for the low-angle-of-view main windshield. However, it seems that every different window configuration has its own particular problems; and in the case of the side window, the major effort to achieve the required optics centered around maintaining parallelism of the window surfaces during lamination of the three plastic plies and two interlayer materials.

Optical Distortion Inspection, Side and Upper Windows

Each window was photographed at its installation position using a special holding fixture positioned to locate the nearest edge of the window approximately five feet from the grid board to ensure that one photograph would provide total coverage on the grid board. To facilitate photography, the camera was located approximately 10 inches farther away from the pilot's eye position

than normal. Using this setup, single- and double-exposure photographs were taken to inspect and verify optical quality. In the case of the side window, photographs also were taken with the conductive coating under full operating power. The grid line slope limits of 1:10 for the side window and 1:6 for the upper window assemblies were consistently achieved. Typical grid board photographs of two production windows are seen in Figures 19 and 20.

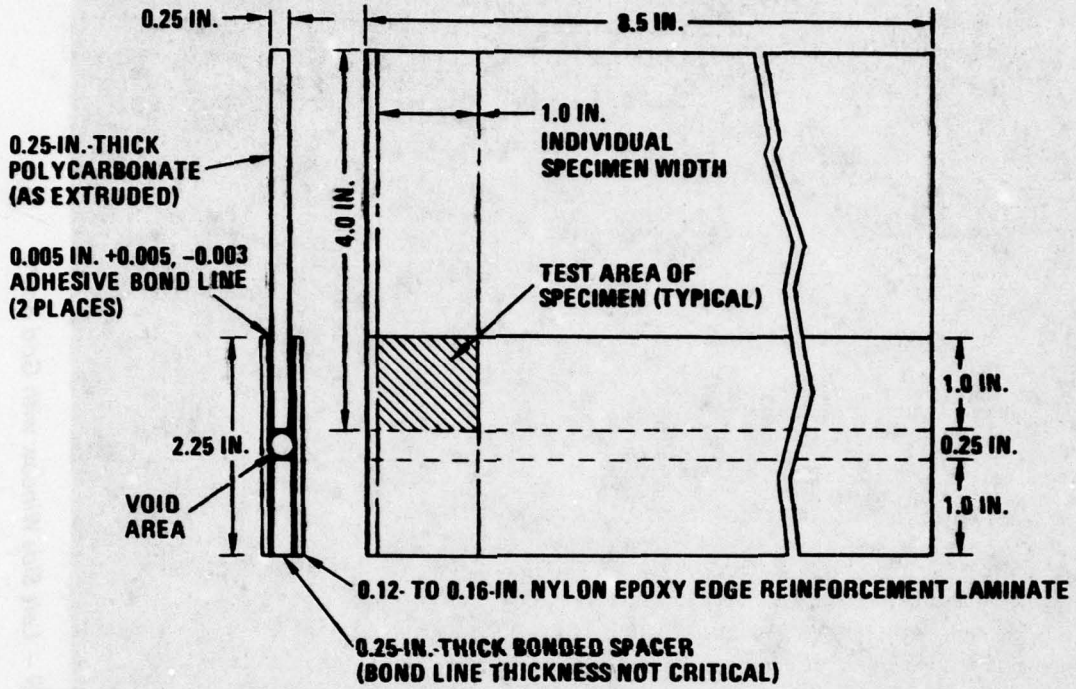


Figure 18 – RTV Adhesive Bond Control Sample

TABLE III – OPTICAL QUALITY REQUIREMENTS

Window Type	Zone	Optical Distortion (Maximum Slope)	Minor Optical Defects	Angular Deviation (Minutes of Arc)	Light Transmittance Percent (Minimum)	Haze Percent (Maximum)
Side	1	1:10	4	4	60	5
	2	1:6	4	NA	60	5
	3	NA	NA	NA	60	5
Upper	1	1:8	2	NA	60	5
	2	1:6	2	NA	60	5

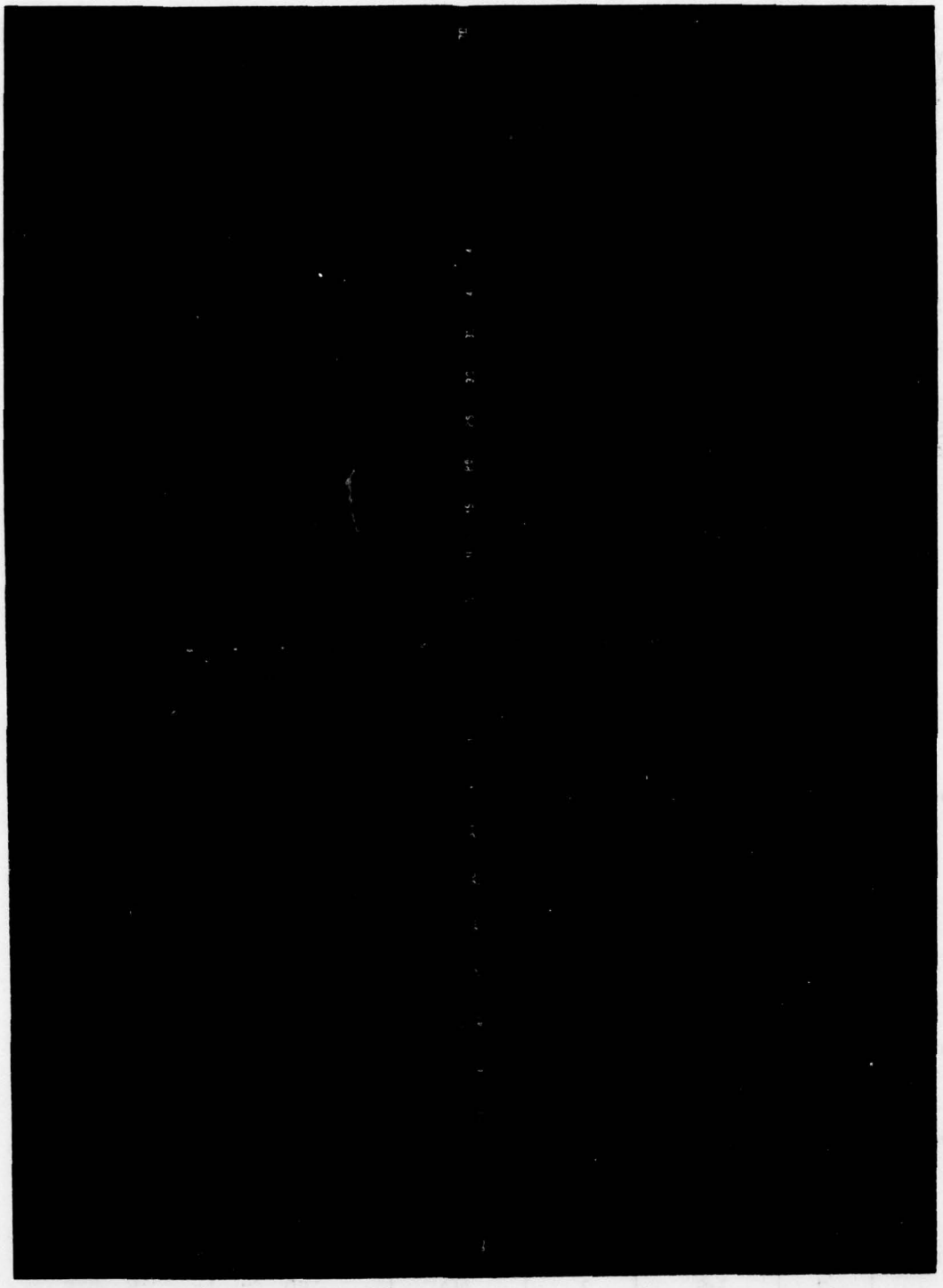


Figure 19 – Left Side Window with Grid Board

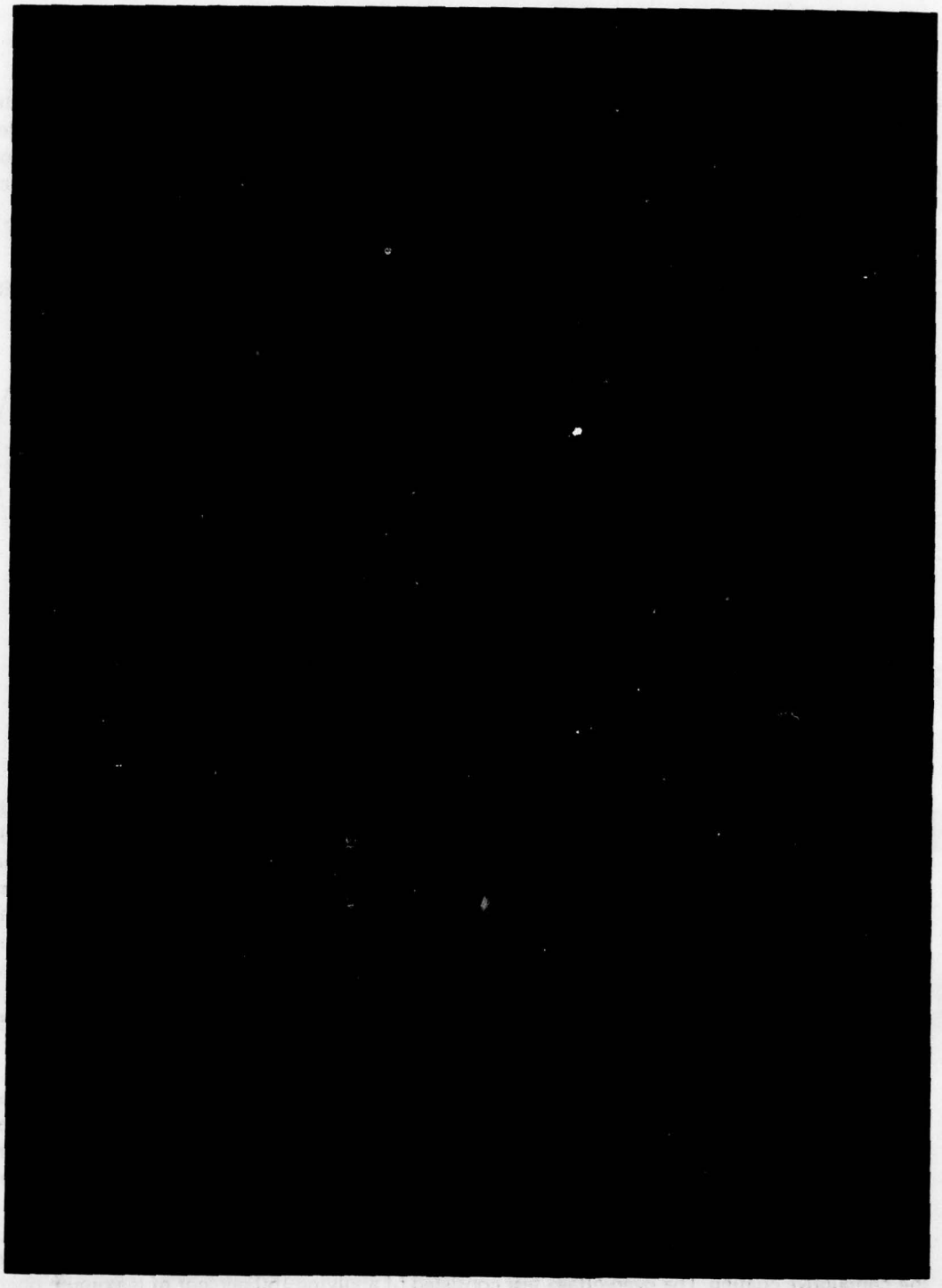


Figure 20 — Left Upper Window with Grid Board

Angular Deviation Inspection, Side Window

The basic setup for measuring the angular deviation of the side window is shown in Figure 21. In actual practice a gimbaled fixture was utilized to quickly establish the 90-deg angle between telescope and window surface at each measurement point in the Zone 1 critical optical area. Except for several points very near the edge on two of the windows, the four-minute maximum angular deviation requirement was consistently achieved.

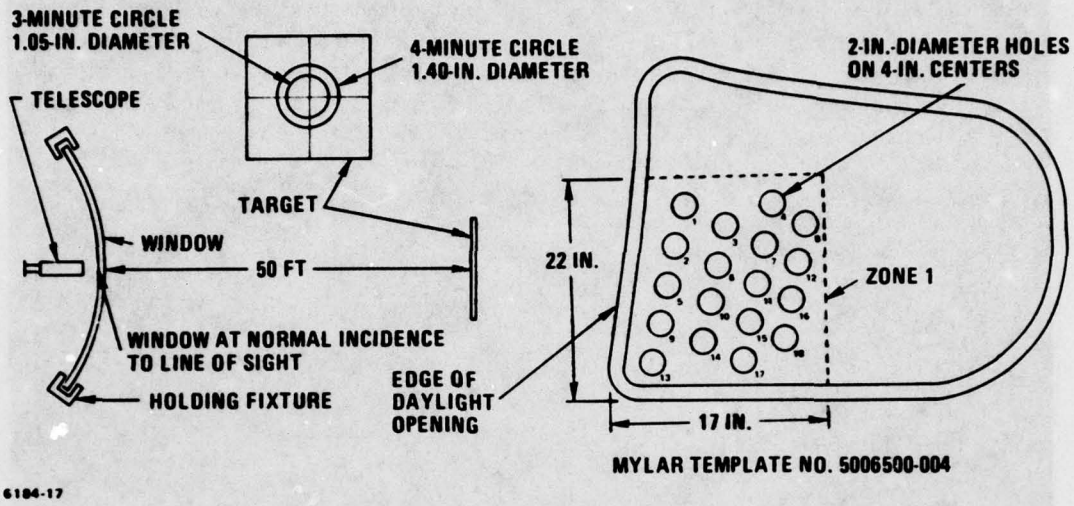


Figure 21 – Angular Deviation Test

Quality Assurance Electrical Testing

Quality assurance testing of the side window electrically-conductive coating was conducted both on the monolithic acrylic panel after coating application and also on the window panel after laminating. The electrical tests prior to laminating were primarily to verify that the applied coating was acceptable and consisted of bus-to-bus resistance, polariscope survey, overvoltage, and thermal paint examination. The electrical tests conducted after laminating and final assembly verified the quality of the completed window and consisted of bus-to-bus resistance, sensing element resistance, polariscope survey, overvoltage, insulation resistance, dielectric withstanding voltage, thermal paint, power density distribution and power constants, and cold soak thermal shock at -65 deg F with full electrical power. The maximum allowable bus-to-bus resistance was 11.95 ohms in order to satisfy the minimum allowable power density requirement of 0.36 watt/in.^{2}.

The resistance of each sensing element was measured both before and after installation on the side window assembly and again just prior to shipment to verify that the sensing element was undamaged and within the manufacturer's specified temperature/resistance tolerance range. Calibration at 110 deg F was provided by the manufacturer, as was certification that each sensing element met the one-minute, 10-volt DC test requirement.

The polariscope (polarized light) visual survey indicates any strains, damage, or internal flaws in the conductive coating. The overvoltage test consisted of applying 150 percent of maximum operating voltage for a period of three seconds with no damage allowed as a result. The insulation resistance tests required application of 500 VDC between all mutually insulated window circuits for

a period of one minute or until the resistance value stabilized, whichever came first. The insulation resistance between all mutually insulated circuits was required to be greater than 75 megohms. (This test was required both before and after the dielectric withstanding voltage test.) The dielectric withstanding voltage test consists of applying 1000 VDC between all mutually insulated circuits for a period of one minute with no evidence of breakdown or flash-over and no leakage current exceeding 2 milliamperes. The thermal paint, power density distribution, and power constants tests were conducted as previously discussed.

The side window cold soak thermal shock test started with a two-hour soak in a test chamber running at -65 deg F. At this time the window was removed from the cold chamber and, as quickly as possible, the maximum operating voltage (66 volts) was applied for a period of one hour or until control temperature was reached, whichever occurred first. No evidence of degradation of the conductive coating or temperature sensors was allowed as a result of this test. Figure 22 shows a side window panel being electrically powered after the cold soak period. Frost will be noted on the unheated area at the aft end of the window.

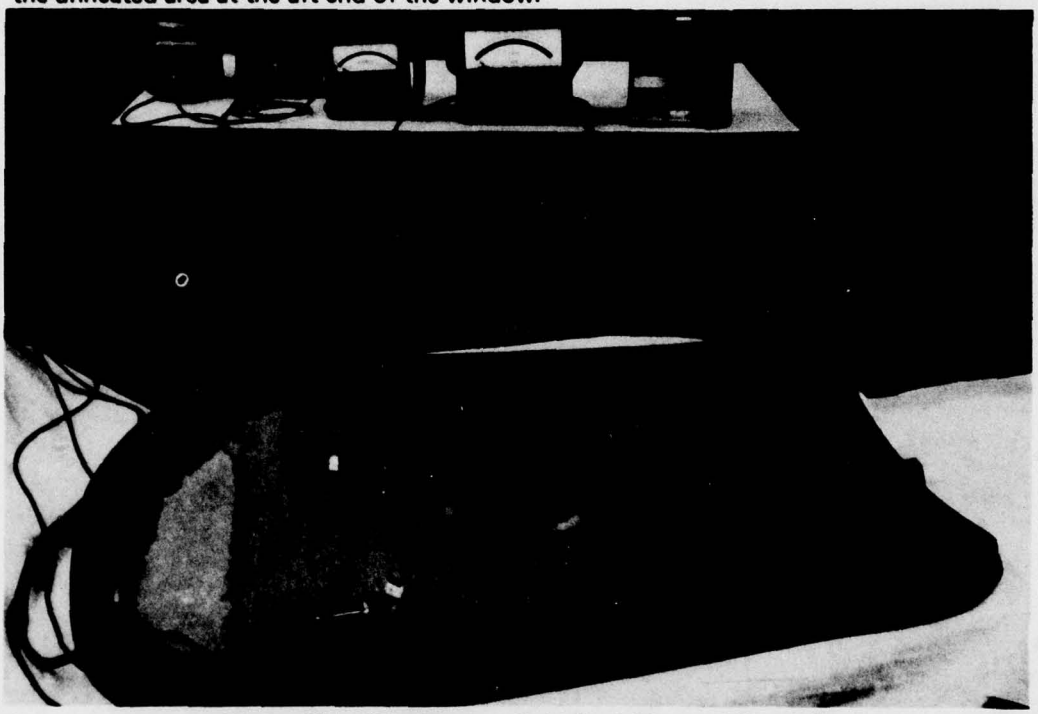


Figure 22 – Side Window Cold Soak Thermal Shock Test

Weight

With the existence of all the other dimensional controls stipulated, no specific maximum weight requirements were imposed. However, complete records were maintained to monitor the resulting weight of the windows throughout the manufacturing effort. The average weights experienced were as follows for the four shipsets of hardware fabricated:

Side window (one panel)	51.8 lb
Upper window (one panel)	10.5 lb.

The maximum deviation from the averages was 0.6 pound for a side window and 0.4 pound for an upper window.

SESSION VII

DESIGN AND PERFORMANCE - PART II

Chairman: K. E. Thompson
General Dynamics
Fort Worth Division
Fort Worth, Texas

PRECEDING PAGE BLANK-NOT FILMED

AIRCRAFT WINDSHIELD IMPROVEMENTS

W. C. Townsley
PPG Industries, Incorporated
Aircraft and Specialty Products
Huntsville, Alabama

PRECEDING PAGE BLANK-NOT FILMED

Abstract

AIRCRAFT WINDSHIELD IMPROVEMENTS

William C. Townsley

PPG Industries, Inc.

Aircraft & Specialty Products

Aircraft windshields have historically provided a failsafe, reliable, optically good shield against the environment surrounding the flight envelope. The major complaint among aircraft users has been low service life for a high cost, sophisticated item.

Over the past several years, PPG has devoted a significant portion of its development efforts toward improving the service life of aircraft windshields. This paper presents the most recent improvements and provides service life data when available.

Specific topics of discussion include: (1) PPG 112 Interlayer; (2) Heat Vulcanized Silicone Edge Sealant; (3) Edge Heating; (4) Improved Sensing Elements; and (5) Glass/Plastic Refurbishment Programs.

PRECEDING PAGE BLANK-NOT FILMED

Aircraft windshield improvements have been a subject discussed many times at many different places over the years. I was once told by a commercial pilot, after I informed him that I worked for PPG in the windshield production plant at Huntsville, that I might feel that airplane windshields were the most sophisticated devices on the aircraft, but to him they were simply something for him to look through. As long as they served that purpose under all flying conditions he was satisfied. What did concern him was when the windshield caused him to have to pay attention to it. If the windshield began to delaminate, cold chip, arc, fail to heat, or make his warning light come on, this is what made him mad. The reason it made him mad was because he had to divert his attention from his important flying functions to an abnormal situation. Both as a passenger on aircraft and as a developer of better windshields, I can sympathize with this pilot.

During the past several years, PPG has devoted a large part of its development effort toward increasing the service life of aircraft windshields. Several papers have been presented by various manufacturers covering subject matter, in the developmental stages, offering great hope to the end users for more flight hours for your dollar. What I will be discussing with you today are the major areas of improvement on actual production parts and how they are affecting service life. The items covered are in existance now on flying aircraft and have all been put into use in the last four years. I will also tell you the problems that we have experienced with some of the improvements and what has been done to correct these problems.

SENSING ELEMENTS

In 1974, PPG introduced an improved version of the resistance wire sensing element used in most heated windshields. The old type element in use since the 1950s consisted of fine resistance wires embedded in the PVB interlayer material. The new type takes the same wires, wraps them around a polycarbonate core and then fusebonds a thin ply of acrylic on either side of the polycarbonate. The lead wires are insulated which serves to totally isolate the sensing system from the heating system. The main advantages of this element are that it is about half the size of the old element, thus increasing the clear viewing area and allowing a more precise location at the control point; it is compatible with all substrates, not just PVB; and it is electrically isolated, thus reducing the possibility of shorting. We are currently using this element in over 90% of windshields produced by PPG that use resistance elements.

The reliability of the new element has been exceptional. Windshield removals attributed to element failure have been almost non-existant. Isolated reports of element bubbling have occurred which can be duplicated under test conditions by applying high voltage to the element. These are apparently caused by controller malfunction.

Most reports we receive of windshield heating problems result in replacing the controller as well as the windshield.

HEAT VULCANIZED SILICONE SEAL

The second major improvement, a heat vulcanized silicone edge sealant system was introduced on production windshields in 1974. We commonly refer to it as H.V. silicone.

The first generation of weather seals was simply an extension of the PVB interlayer over the edge of the glass. PVB and most other interlayers are degraded by environmental exposure. It was not long before it became apparent that PVB was not a good material to be exposed to the environment. It became brittle, cracked, shrunk, and admitted mositure to the heating film.

The second generation weather seal was a rubber bumper adhered next to the glass edge and backed up by PVB. This was an improvement, but still did not provide the protection necessary.

The third generation of sealant materials and one still in wide use throughout the industry is the polysulfides. These were originally developed and used as fuel tank sealants. They have many good properties and when properly applied will provide a reasonably good seal against moisture. It has been PPG's experience that long exposure to flight conditions causes the polysulfides to crack, erode, and lose adhesion to the glass edge. A regular maintenance program for seal inspection and repair is recommended for maximum windshield service life. One of the major problems with the polysulfides is the relatively poor erosion resistance. Efforts to combat this weakness have resulted in forming a sacrificial overlay of sealant over the basic seal. This method is used on the BAC 747 and L-1011 main windshields to decrease moisture problems.

H.V. silicone, our current generation of sealing system, has been an excellent improvement to reduce moisture penetration. Its main advantages over polysulfide systems are: 1. Better erosion resistance 2. Better moisture penetration resistance 3. Better flexibility (elongation 400%) 4. Excellent adhesion properties to glass, interlayer, and other substrates and 5. It is totally void of entrapped air.

PPG purchases raw silicone stock, adds curing and priming agents, and extrudes shapes required to fill voids where moisture must be prevented. H.V. silicone is applied prior to the autoclaving operation and is cured under high temperature and pressure during autoclaving. The resulting seal is without equal in today's state of the art.

H. V. silicone is used on over half the windshields produced by PPG at Huntsville. Through the contacts of our Sales and Technical support personnel many aircraft manufacturers have requested that we switch to H.V. silicone to increase service life. There are numerous windshields that could be improved with H.V. silicone application that still use less effective systems. These are primarily military aircraft where purchase contracts specify that parts be supplied to drawing and specification requirements that were in effect during the early years of the aircraft's production.

Of the thousands of windshields flying with H.V. silicone only a handful have been removed because of seal failure. Inspection of H.V. silicone seals on sales returns for other reasons show that the seals are still in excellent shape. A conservative estimate based on field reports and inspection of sales returns shows seal life of H.V. silicone to be a minimum of 50% better than polysulfide systems.

I've stated the positive values of H.V. silicone but there are some limitations to its use. It cannot currently be used with stretched acrylic windshields because of the required fabricating processes. Field repair is difficult because conventional polysulfides will not adhere to H.V. silicone. This is not a major drawback because, due to its long service life, field repair has not been necessary. Also, H.V. silicone is more expensive to apply than the polysulfides. The initial expense is insignificant compared to the increased life it provides the windshield.

PPG 112 INTERLAYER

The third major improvement and we feel the most exciting one, is the development of PPG 112 interlayer for use in a variety of windshield applications.

PPG 112 interlayer is produced in sheet form by our Chemical Division at Barberton, Ohio. It is compatible with glass, polycarbonate, as-cast and stretched acrylic as well as PVB interlayer. Compared with PVB interlayer, it offers greater adhesion to all common windshield substrates; it has much better low and high temperature tensile properties which allows a thinner, weight saving, fail safe section in all glass designs; and it has totally eliminated the need for edge stress relieving systems such as slip planes and parting mediums common to PVB designs.

We are currently manufacturing production parts with a single sheet of 112 interlayer in combination with PVB interlayer for the Grumman Gulfstream, Douglas DC-8, DC-9, and DC-10, Fokker F-27 and F-28, British Aircraft BAC-111, and Boeing 747. Figure 1 is a cross section drawing of the Boeing 747 main windshield. The Mitsubishi MU-2 and the new Rockwell 700 aircraft use windshields with glass and all 112 interlayer. The Embraer 110 and Lockheed L-1011 use a

AD-A065 049 AIR FORCE FLIGHT DYNAMICS LAB WRIGHT-PATTERSON AFB OHIO F/G 1/3
CONFERENCE ON AEROSPACE TRANSPARENT MATERIALS AND ENCLOSURES (1--ETC(U)
DEC 78 R E WITTMAN

UNCLASSIFIED AFFDL-TR-78-168 NL

9 OF 10
ADA
065049



glass/stretched acrylic combination windshield with 112 interlayer. The F-111 and A-10 use 112 interlayer in combination with polycarbonate and as-cast acrylic in their bird resistant designs.

In 1974 and 1975 we placed several test windshields with single plies of 112 interlayer in combination with PVB interlayer into flight service. Figure 2 is a summary of the current status of these windshields. The only failure at this point is the SAS-DC-10 windshield which was removed due to a cracked inboard glass ply unrelated to the 112 interlayer located against the outboard ply.

It is still too early to predict the total impact of the use of 112 interlayer on service life. From test flight windshield data it appears that the 10,000+ flight hour windshield for commercial jets may become the norm rather than the rarity they have been in the past.

Service life, reliability, and decreased costs per flight hour are the big advantages of 112 interlayer. As with most new developments, we have had some problems associated with its use and have solved these problems.

Early in our production of parts using 112 in combination with PVB interlayer we had reports of optical interference during night landing. It was described as a "halo" or "orangepeel" effect stemming from point source runway lights. We recognized prior to production of the parts containing the combination interlayers that the orangepeel level was inherently greater than in parts with all PVB or all 112 interlayer. This is due in part to the slight index of refraction difference between the interlayers. Both company pilots and FAA representatives inspected our original test flight parts at Douglas and Grumman and found the optics acceptable.

Because of the field complaints we at PPG began an extensive program to improve our in-house processing of components to decrease the degree of orangepeel. The parts produced today are far better for orangepeel than parts produced in 1974 and 1975. Current production parts cannot be distinguished from parts containing all PVB or all 112 interlayer except by a trained eye under special lighting conditions. We strongly feel that the most critical pilot would find the optics of the parts with the combination interlayers comparable with the single interlayer optics.

There have been isolated reports of excessive delamination on some 112/PVB parts. Investigation of returned units revealed a manufacturing problem that we were able to recognize, correct, and control to prevent a recurring problem.

We are proud of the overall performance of 112 interlayer and of our positive response to the isolated problems that it has caused some operators. We don't anticipate additional problems but you can be assured of a professional response if they do occur.

EDGE HEATERS

The fourth major improvement is the development of edge heating for aircraft parts. We make no claims to be the originator of the use of edgeheaters. That distinction belongs to others including Ernie Pearce of Continental who began to use surface mounted heaters on his Boeing standard body jets before we began producing windshields with Aircon® edgeheaters built into the part.

The need for edgeheating on non-rectangular heated glass lites became apparent on the No. 1 windshields on Boeing standard body jets. The conductive coating of the Nesa® glass is not able to supply enough heat to the acute angle corners of the windshield to prevent delamination.

Several methods of edgeheating are employed on the No. 1 windshield which is shown in Figure 3. Some operators use a stick on type heater mounted to the inboard surface of the glass powered by a separate power supply and controlled by a sensor built into the heater. Manufacturers use two types. One is a strip heater encased in silicone rubber that is mounted under the outboard retainer and operated off the windshield power and sensor. The other is one used exclusively by PPG and consists of tiny resistance wires embedded in the interlayer prior to lamination of the windshield. This edgeheater design also uses the windshield power and sensing circuits. This system which we call Aircon® has been in use on production windshields for Boeing jets since late 1974.

Reports from Boeing and the airline operators indicate that service life on windshields equipped with edgeheaters is increasing. Because of the worldwide use of Boeing jets by scores of operators, accurate detail data on service life is quite difficult to collect and report. We know the trend is positive but quantitative data is not yet available.

We have had one area of complaint with the Aircon edgeheaters which I will discuss and include our plan for improvement. We have had removals of windshields because of broken wires while the windshield was in service. Once the wire is broken intermittent sparking is visible as the current arcs across the break. Although this is not a structural problem, it is distracting to some pilots and removal has been ordered. The degree of magnitude of the broken wires is very small compared to the number of windshields in service, but any complaint from pilots is of great concern to PPG. Of the more than 5000 pilot and copilot windshields shipped with Aircon®

edgeheaters less than 1% have had broken wires. Working through Boeing, PPG has repaired and returned the majority of the removed parts for re-installation.

To reduce the occurrence of broken wires we have plans to change the wire used on the edgeheaters to one with the same resistance but made from an alloy which has a greater tensile strength. The wire is on order and we expect to have it incorporated into production parts by July 1, 1978.

We have negotiations in progress with Boeing to incorporate an Aircon edgeheater on the No. 2 sliding window for the same aircraft. We understand that Boeing is surveying the users of Boeing aircraft to determine the need for edgeheating the No. 2 windshield. We have made instrumented test parts and are ready to begin production on a phased basis. Based on our test data, we expect this action to offer the same kind of improvement in service life that we have seen on the No. 1 windshield. The No. 2 window design uses the stronger alloy wire that we will use in the new No. 1 windshield design.

GLASS/PLASTIC REFURBISHMENT PROGRAMS

The last windshield improvement that I would like to discuss with you involves the refurbishment of removed glass/plastic L-1011 windshields not manufactured by PPG. The design of the windshield before and after refurbishment by PPG is basically the same - two structural plies of stretched acrylic with an outboard heated glass ply laminated to the stretched acrylic. (See Figure 4.)

PPG was awarded a contract by Lockheed in 1977 to refurbish six right hand L-1011 windshields. We received six units during 1977 and completed the refurbishment with the shipment of the last unit in February 1978.

PPG's refurbishment approach was to remove the outboard glass and interlayer from the stretched acrylic carcass and relaminate a .120" thick ply of Nesatron coated Herculite II® chemically tempered glass to the stretched acrylic with 112 interlayer. The chemically tempered glass offers high strength to combat the large stresses in glass/plastic laminates. The 112 interlayer offers a much increased flexible adhesive system to both the glass and stretched acrylic. The heating film of Nesatron® coated glass has proven integrity on other large windows such as the Boeing 747.

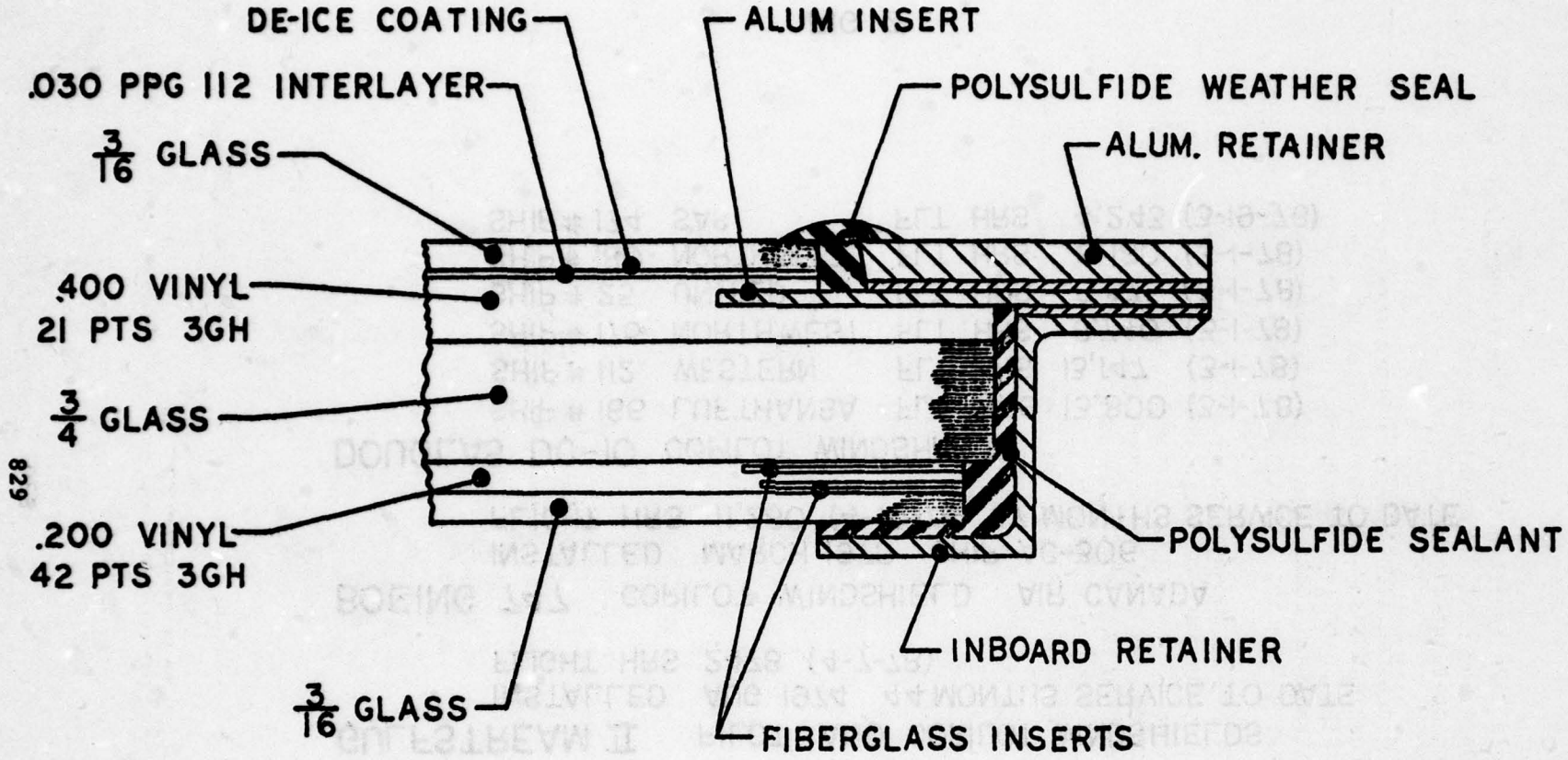
Of the six windshields furnished Lockheed, two have been installed. The other four have been shipped to airlines and we will be following their performance with great interest. We are currently negotiating with Lockheed for additional refurbishment contracts.

In summary, I would like to leave with you the thought that PPG is committed to produce the best windshield possible consistent with the ever improving state of the art.

The items I have discussed today are real improvements to production windshields. I have not discussed the development items that we are currently working on to improve service life. These too are significant, exciting, and look promising. When they are transformed from promising into the real world they will be reported.

One last thought - PPG as a manufacturer of all types of aircraft windshields welcomes feedback on the performance of these windshields. All the ground testing in the world does not duplicate actual flight service. We can only correct problems and offer improvements if we know what the problems are.

Thank you for your attention and let us hear from you.



BOEING 747

MAIN WINDSHIELD

FIG. 1

PPG 112 INTERLAYER
TEST WINDSHIELD STATUS
MARCH 1, 1978

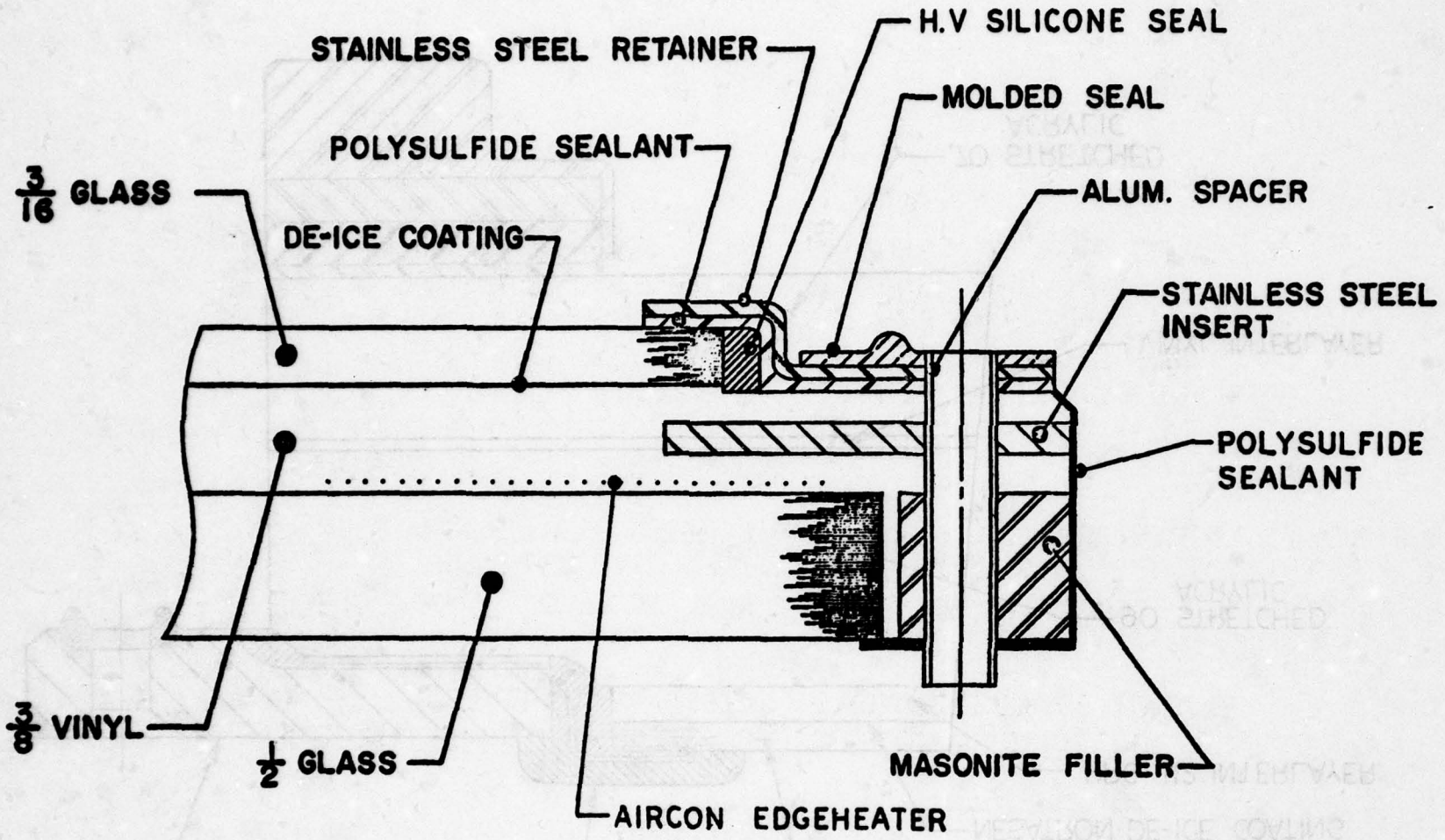
GULFSTREAM II PILOT AND COPILOT WINDSHIELDS
INSTALLED AUG 1974 44 MONTHS SERVICE TO DATE
FLIGHT HRS 2478 (4-7-78)

BOEING 747 COPILOT WINDSHIELD AIR CANADA
INSTALLED MARCH 1975 SHIP AC-306
FLIGHT HRS 11,280 (4-10-78) 37 MONTHS SERVICE TO DATE

DOUGLAS DC-10 COPILOT WINDSHIELD

SHIP # 166	LUFTHANSA	FLT HRS	13,800 (3-1-78)
SHIP # 112	WESTERN	FLT HRS	13,147 (3-1-78)
SHIP # 175	NORTHWEST	FLT HRS	8,740 (3-1-78)
SHIP # 25	UNITED	FLT HRS	8,675 (3-1-78)
SHIP # 180	NORTHWEST	FLT HRS	8,180 (3-1-78)
SHIP # 174	SAS	FLT HRS	4,243 (3-19-76)

FIG. 2

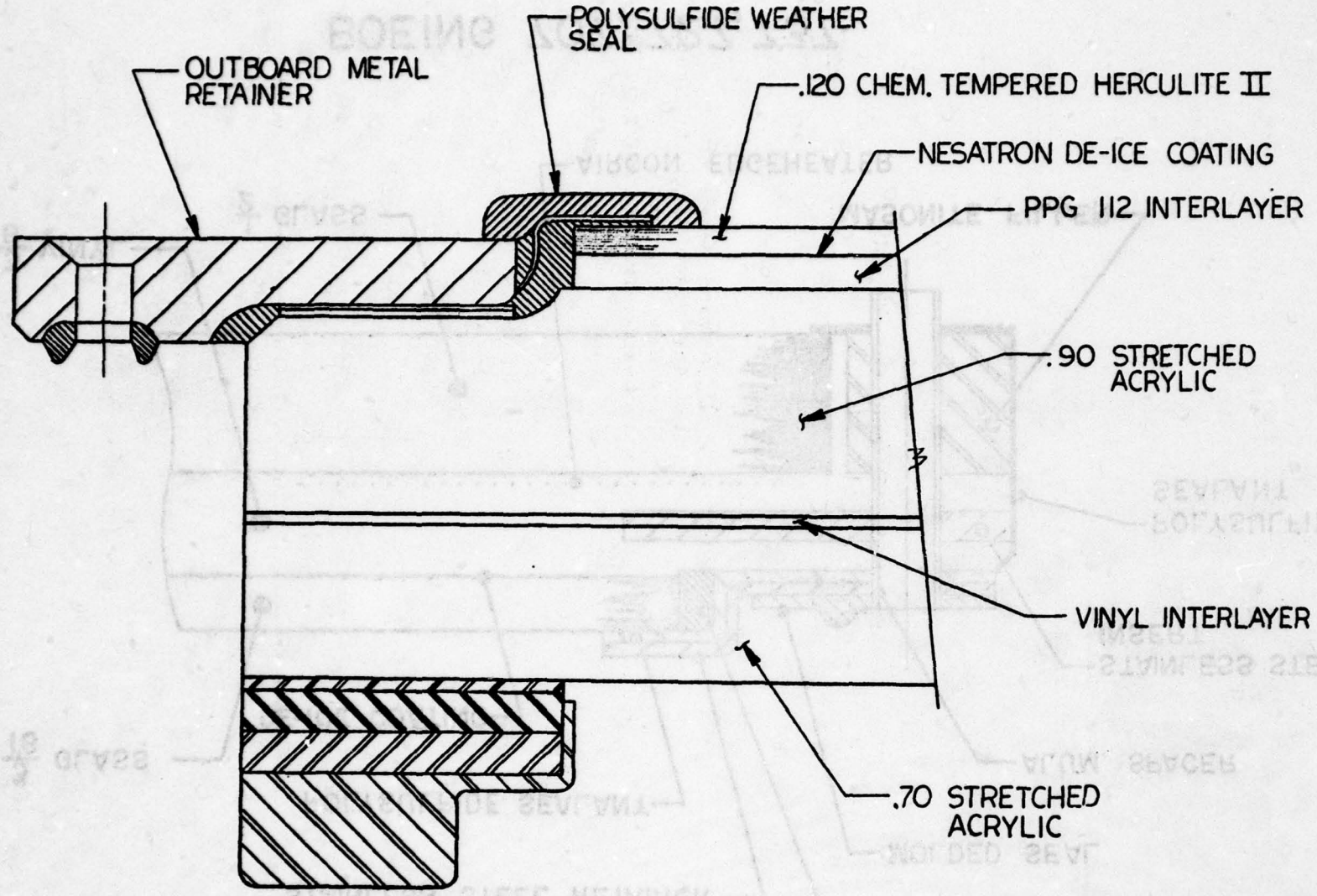


831

BOEING 707, 727, 737

MAIN WINDSHIELD

FIG 3



832

LOCKHEED L-1011
MAIN WINDSHIELD
FIG. 4

THE USE OF EXPLOSIVE CORD FOR 'THROUGH CANOPY' ESCAPE SYSTEMS

G. W. Underwood
British Aerospace Aircraft Group
Headquarters (Research)
Kingston-Upon-Thames, Surrey, England

The Use of Explosive Cord for 'Through Canopy' Escape Systems

by

G. W. Underwood, British Aerospace Aircraft Group,
Headquarters (Research)

Abstract

The need for fast and reliable crew emergency escape systems is an important requirement for high performance military aircraft. Low level flight conditions can now demand a speed range from supersonic to zero (the latter for VTOL aircraft) and in either of these extremes crew survivability in an emergency depends increasingly on the speed by which a safe exit can be made from the aircraft.

The main body of this paper records some of the technical aspects of the Research and Development carried out into explosive cord 'through canopy' escape systems by Hawker Siddeley Aviation Ltd. (now part of British Aerospace) over the period of 1964 to the present day.

Reference is made to the fact that this Research and Development has resulted in the adoption of linear explosive cord (MDC) systems for a number of aircraft types now in service and that current work is showing a possible new and exciting potential for its application to the new generation of strike aircraft.

PRECEDING PAGE BLANK-NOT FILMED

THE USE OF EXPLOSIVE CORD FOR 'THROUGH CANOPY' ESCAPE SYSTEMS

1. INTRODUCTION

The low level flight conditions in high performance Military Aircraft now cover a speed range from supersonic in some cases to zero for VTOL Aircraft.

Crew survivability as one approaches either end of this speed range depends increasingly on the speed by which a safe exit can be made from the aircraft.

A considerable amount of work in the area of escape systems has been done both in the United States and the UK since the end of World War Two as the old method of unassisted crew escape was found to be difficult if not impossible in most emergency flight environments.

Various escape systems have been considered and several very different methods adopted for service aircraft. Two methods involving 'through canopy' systems, in which the canopy was deliberately broken to enable rapid egress of the crew, were the subject of two papers given at a symposium on optical transparencies organised by the Society of British Aerospace Companies Limited in the UK in June 1971. The one paper was from the USA covering the work on frangible glass canopies (Ref. 1) and the other was from the UK in which the main accent was given to the explosive cord technique adopted for 'as cast' acrylic transparencies (Ref. 2) on the Hawker Siddeley (now British Aerospace) VTOL Harrier strike aircraft.

The excellent behaviour of the Harrier escape system in service has prompted a more detailed R & D activity in the UK on this method of escape. Work has been continuing up to the present day which has resulted in the adoption of linear explosive cord (known in the UK as miniature detonating cord - MDC) systems for a number of in service aircraft and for such systems to have first consideration in the new British Aerospace Aircraft Group for possible new strike aircraft applications.

1. (continued)

This paper does not attempt to go over all the old ground covered previously beyond that necessary to set the scène, but concentrates on a number of the parameters which have been investigated of the use of MDC on 'as cast' acrylic, 'stretched acrylic, and certain other materials including brief reference to the present activity on polycarbonate.

2. AIMS AND OBJECTIVES

The early objectives of an MDC system were limited to one of the following two main aims because no previous escape method in common use appeared to have a chance of success:-

Either: To enable aircrew to escape when the aircraft crashes and is submerged under water (i.e. the 'ditched' case).

Or: To enable aircrew to escape when the aircraft crashes and turns over onto its back on the ground.

It was thus considered not as the primary means of escape but additional to a more conventional method.

The later and much broader premise has been:-

To provide a fast, controlled break of the aircraft transparency or crew hatch in such a time and manner that, in seat ejection, the crew member is uninjured by the primary break up and by debris and blast of detonation.

The reasons why MDC systems might potentially satisfy this general premise (and subsequently proven) are as follows:-

(a) Virtually zero time delay when operated.

(b) Could enable escape from an inverted aircraft on the ground and probably when an aircraft had 'ditched' in water (i.e. the original aims mentioned earlier) by action of the aircrew or,

2. (continued)

should the crew be injured, by simple action by rescuers.

(c) Could be simple, likely to be reliable, and could probably be contained wholly on the transparency assembly.

(d) Would have a light weight.

(e) Would have a low component and installed cost.

(f) Could be 'triggered' either electrically or mechanically and if by the latter would be totally divorced from the aircraft electrical system.

(g) Might in certain circumstances be capable of being fitted to existing transparencies by retrospective action.

(h) Has the potential in new aircraft projects of being the prime and only means of escape thereby reducing weight, complexity, and volume required for other types of systems.

(j) Would have low battle damage probability over other types of systems.

All the above aims appeared feasible (and subsequently met) but certain aspects required particular attention as potential disadvantages for an MDC systems. These were as follows:-

(i) Differing from mechanical canopy jettison, MDC might not be capable of withstanding long term flight environmental conditions without failure or degredation in performance.

(ii) Because explosives are the intrinsic part of the system, crew injury and/or damage to aircrew survival equipment might not be sufficiently remote as to be acceptable against primary or secondary effect of blast or component particles - the latter applying not only to the MDC itself but also to the broken transparency particles.

2. (continued)

(iii) Such a system might not be satisfactory on all types of transparencies to an acceptable degree of reliability, particularly due to the very different toughness and crack propagation properties of the various materials at varying temperatures.

(iv) The installation of MDC on the canopy would result in some loss of vision and this might not be to an acceptable standard for aircrew operational requirements.

(v) Canopies with MDC fitted may require more careful handling by ground staff to avoid installation damage.

3. <u>The Overall Approach - an Historical Background</u>

The major part of this paper is concerned with some of the more important research and development carried out by Hawker Siddeley Aviation (now a part of British Aerospace Aircraft Group) in developing MDC escape systems. Prior to considering the details of the R & D. it is perhaps useful to summarise the activities in general terms against approximate time scales in *brief note form.*

1944-46. The Royal Aircraft Establishment at Farnborough issued technical notes on the possibilities for the use of 'Explosive Cord Devices' for the rescue of personnel from crashed aircraft and for providing aircraft emergency escape.

1960-63. HSA activity limited to preliminary small scale investigations on the potential uses for MDC.

1963-65 Serious consideration given to MDC systems for underwater escape - demonstration in test tank for Buccaneer Naval strike aircraft (dummy and live subjects). Close links established with RARDE (Royal Armaments Research and Development Establishment) on manufacture and development of MDC for possible airborne escape systems.

3. (continued)

1965-70 MDC system developed for prototype forerunner of the Hawker Siddeley (now British Aerospace) Harrier VTOL strike aircraft. Systems developed for various other aircraft types involving 'ground' demonstrations on full size 'as cast' acrylic canopies. R & D approach was somewhat 'ad hoc' necessitated by urgency of investigations but considerable background information was obtained.

1970-73 Further development on more scientific lines towards optimising MDC for 'as cast' acrylic transparencies. Aircraft with MDC now in service including the Harrier. Satisfactory service experience led to choice of MDC system for a new high performance strike/trainer - subsequently to become the Hawker Siddeley (now British Aerospace) Hawk. Preliminary investigations commenced on materials other than 'as cast' acrylic .

1973-76 Monolith 'as cast' acrylic investigations completed. Detail study of MDC on 'stretched' acrylic monolith carried out.

1976-77 Main activity concentrated on investigating possible hazards to aircrew, and alleviation thereof, from lead splatter. 'Stretched' acrylic work extended in scope.

1977 - Present Day:

Further work on MDC developments and applications with particular accent on polycarbonate and laminated transparencies.

4. THE RESEARCH AND DEVELOPMENT PROGRAMME

4.1. 'As Cast' Acrylic Application

All the aims and objectives of para. 2. were investigated to enable fitment of an MDC system to conventional aircraft and also to unconventional V/STOL strike aircraft - hence a speed range of high subsonic to zero had to be covered.

4.1. (continued)

The various items of a complete system are shown in Figure 1.

By 1971 HSA had, by a somewhat ad-hoc approach, developed satisfactorily, but not necessarily optimised, MDC systems for possible application to a number of aircraft. All the developed systems employed a round or 'D' section cord, the cord basically consisting of a lead sheath encasing a core of an explosive the ends of which were hermetically sealed. The detonator was a small mechanical device developed by HSA which could be fired as a result of seat movement, or by gas pressure from the charges in the seat, or by independent action of aircrew or rescuers.

The developments of the system up to 1971 have been covered in fair detail in Hudsons' paper at the June 1971 Transparency Symposium in the UK (Ref. 2) to which reference is made earlier, hence it is unnecessary for the information given in that paper to be repeated here. However, it is perhaps worthy of note that even though the system was not necessarily optimised, all the main aims listed in para 2 appeared, from test results, to have been achieved. By 1973 service experience with the VTOL Harrier had substantiated most of the findings in practice as recorded in two papers, both given by members of the Royal Air Force Institute of Aviation Medicine (IAM) at an AGARD conference held in September of that year (Refs. 3 and 4). Lives were being saved under flight conditions in which no other escape system was likely to be successful and the potential disadvantages, listed in para 2, did not appear to be creating major criticism or anything requiring major modification. However, two aspects were considered desirable. An overhead MDC pattern as well as peripheral cord was recommended to assist break up of the transparency into small enough pieces to reduce the possibility of crew injury when ejecting through the debris, and some additional protection was found to be necessary to a part of the survival equipment.

4.1. (continued)

In 1971, therefore, time for a more scientific approach was made possible and for the following two years the following aspects were investigated in some detail:-

(i) A Study of Stress Wave Propagation on Beams and Simple Plates - Theory and Experiment

A reasonably satisfactory match between theory and experiment was obtained for small specimens but was not applicable to large specimens and the work was discontinued. Nevertheless the experimental work carried out to determine values of physical constants for use in the theory established very useful data on pressure/time profile for dynamic loading due to MDC detonation on the acrylic surface and on wave propagation in acrylic beams and plates.

(ii) An Investigation of Primary Fracture

This investigation was carried out in three parts.

(a) Ballistic Pendulum Impulse measurements and Energy Distribution

This work investigated the effects of changing the cord parameters as shown in Fig. 2 and thereby assisted in optimising the intrinsic fracture potential of cords for various applications.

The ballistic pendulum was designed to convert the impulsive energy produced by detonation of a length of MDC into an approximately equal amount of potential energy. The pendulum consisted of a hardened steel anvil (against which the MDC was 'fired') suspended from two light alloy links which were allowed to freely swing from a steel pivot bar. The pivot bar rotated on two self aligning low friction bearings, the angle of rotation being measured via

4.1. (ii) (a) (continued)

a potentiometer. Test repeatability was found to be quite satisfactory with this apparatus which was, in itself, found to be a very valuable tool both in this and later series of tests.

(b) Primary Fracture Study

Employing the information learned from (a) above, high speed photography at rates of up to 8×10^6 frames per second (the facility being provided by the RAE) was used to record primary fracture immediately under and close to MDC on detonation in both 'as cast' and 'stretched' acrylic materials. The results indicated that primary fracture was completed in about 5×10^{-6} seconds and nearby fractures in 60×10^{-6} seconds after detonation of the MDC.

(c) The influence of wave interaction on the fracture of acrylic in the region of MDC.

A hypothesis was formulated and proved by test to give an understanding of the formation of cracks as a result of wave interaction.

(iii) Investigation of Secondary Cracking

It had been established earlier that secondary cracking in the acrylic was dominated by flexural wave systems and extensive investigations were carried out to study the ability of various MDC configurations to generate such waves. The outcome indicated that increased wall thicknesses could improve the flexural output of the MDC cord by as much as 50% without reducing its primary fracture capability. Tests were also carried out on cords from 'overseas' sources but none were found to be superior to the RARDE cords that formed the main part of the programme.

4.1. (continued)

(iv) Development of Techniques for System Installations

This work was carried out under five investigations as follows:-

(a) Review of Explosive Components

A study, with selected experimental work, was carried out in an attempt to optimise RARDE MDC cords in those aspects not studied before, including such items as explosive content and type and methods of joining MDC. Very little change was indicated as necessary to improve the RARDE cords already in use. Certain explosive pellets were found to be fairly satisfactory for ensuring detonation if multiple branching of MDC was necessary in a system but further work in this area was considered desirable for future action as an insufficient degree of reliability had been obtained.

(b) Peripheral Loop Investigations

Flexural wave investigations were extended from the previous small scale tests to tests on curved shells using high speed photography to 'capture' the passage of the waves across the transparency. Surface strain measurements were also taken. An example of a photographic record showing a stress wave on the transparency is given in Figure 3.

(c) Overhead Pattern Investigations

This programme was geared to aspects of using an overhead pattern to give a controlled break up of the canopy 'crown' and of a split 'clamshell' type of fracture. Most work was geared to 'as cast' acrylic but from limited testing on 'stretched' acrylic the first real indication was given that the the clamshell method would probably have special merit for 'stretched' acrylic transparencies.

4.1. (iv) (continued)

(d) Crack Initator Investigations

Various forms and types of crack initiators were investigated in a wide range of tests on plates and shells. Specially designed loops in an otherwise straight run of MDC were found to be one of the simplest and also acceptable means of crack initiation.

(e) Multi Point Detonation

A first look was made into possible ways of developing suitable explosive delay devices to permit phasing of MDC detonations in a total system context.

By the end of 1973 HSA, whilst accepting that more work could be done to optimise MDC systems for application to 'as cast' acrylic transparencies, considered that they had accumulated a a fair amount of knowledge. Photographs of a canopy exploding and a fracture pattern are presented in Figs. 4 and 5. Their experience was such that they had confidence in tackling most applications of a similar nature in new designs or for retrospective fit on current 'in service' transparencies with minimum development and proving of the basic systems.
It was decided therefore, only to tie up a few loose ends on the application of MDC to 'as cast' acrylic and to commence an investigation in some detail on the use of MDC for 'stretched acrylic transparencies.

4.2. Stretched Acrylic Application

The limited work carried out on the effects of MDC on 'stretched' acrylic material prior to 1973 had indicated that a breakup of the material in the form of small pieces, as achieved with 'as cast' acrylic, was not a feasible approach. A cutting action had been achieved, however, and it was decided to concentrate on two possible approaches to canopy break-up - the provision of a 'minimum aperture' through which the crew man could eject or the breakup of the total canopy in a 'clamshell' manner, i.e.

4.2. (continued)

the canopy breaking along its centre line and at the edges hence opening outwards in a clamshell manner.

Prior to investigating either of these methods it was necessary for a back up investigation to be carried out to explore the detail practical problems drawing information, when relevant, from the test series prior to 1973.

Three detailed investigations on small specimens were carried out followed by tests on large scale specimens to investigate modes of canopy fracture.

4.2.1. Transparency Material Qualification Tests

Tests were carried out on small specimens (i.e. approx. 12" x 6") of two types of stretched acrylic material against the following parameters:-

(i) Material thickness up to approximately 0.5 in.

(ii) Three types of MDC (circular thin-walled; circular thick-walled; and 'chevron' shaped).

(iii) Flat and curved acrylic specimens (i.e. the effect of a forming operation).

(iv) Effect of temperature.

The more important conclusions were that both materials behaved in a similar way and the fracture resistance increased as temperature increased. Tests on the curved (i.e. formed) specimens indicated that fracture of the material occurs more readily when the line of fracture is at right angles to the curvature and furthermore, they had lower resistance to fracture than for flat un-formed material.

4. 2. (continued)

4. 2. 2. MDC Qualification Tests

Tests were carried out on flat 'stretched' acrylic to investigate the following:

(i) The cutting, fracturing and dispersive effects of employing four shapes of MDC cord - thinwall and thickwall circular, Chevron, 'D' Section and Ribbon.

(ii) A general appreciation of the possible hazard to aircrew and damage to aircrew equipment from the types of MDC under consideration from the debris due to detonation.

The test methods employed for (i) above involved ballistic pendulum (as described previously in para 4.1(ii) and ejection velocity techniques. The ejection velocity technique took the form of a simple test rig in which the acrylic specimens (to whichwere attached the particular MDC being investigated) were set up at 45° to the horizontal. This allowed high speed photography to establish the velocity of the ejected particles, with the distance to which they were ejected giving an indication of the force exerted by the MDC.

The test methods employed for (ii) above involved splatter tests on wood, fabric and gelatine targets placed at realistic distances from the MDC explosive.

The general conclusion was that whilst all cords could satisfactorily cut through the material up to 0. 5 in. thick (the maximum thickness tested) the type of cuts showed different characteristics as shown in Fig. 6. and different splatter damage was evident. No single recommendation was made as the information was required as background to any future 'real' application when a choice could be made to meet a particular installation. An encouraging result was that the acrylic ejection velocity and distance thrown was likely to meet the need for the transparency particles to be cleared outwards rapidly from the oockpit area in an aircraft installation. Subsequently a limited exercise on 0. 75 in. thick small specimens was carried out and a satisfactory cutting action established.

4.2.3. MDC Attachment

It was necessary to investigate both the peripheral and overhead systems for the application of MDC on small scale specimens in which considerable value was obtained by referring back to the experience of the 'as cast' acrylic work carried out previously.

Peripheral System:

Previous experience on 'as cast' acrylic transparencies had already shown that the most satisfactory system both for MDC effectiveness and to reduce the possible hazard to aircrew from the lead splatter was to incorporate a metal retaining/backing plate. The plate positioned and pressed the MDC against the transparency material without the need for an adhesive, the plate itself being positively attached to the inside of the canopy side or edge metal members.

This test series confirmed that the previous finding also applied to stretched acrylic, the backing plates giving substantially improved fracture and fragment ejection than for such a system without backing plates. Furthermore, light alloy materials could be used to minimise size and weight of the plates if more desirable than the previous thin steel material but care in design was necessary, particularly if chevron cord was used, to ensure that the plate did not fracture or bend sufficiently to increase the internal debris hazard.

Overhead System:

When an MDC overhead pattern is to be applied to a transparency the backing plate method is obviously not acceptable for optical and practical reasons. The problem then becomes one of choice of MDC capable of cutting the material (but having acceptable splatter characteristics) and of providing a good bond of the MDC to the canopy.

This series of tests investigated the bonding problem as the other parameters had received attention in other parts of the programme. Of the adhesives investigated, a two-part epoxy polyamide was found to satisfy the test

4.2.3. (continued)

requirements although it was established that some reduction occurred in the performance of the MDC both in terms of fracture capability and ejection potential.

The evaluation of the bonding included vibration and temperature testing, the parameter levels being related to those expected to be experience by a strike aircraft of the Harrier type.

The vibration tests were carried out using moving coil vibrators covering both high frequency cycling (110-500Hz at a 6g peak acceleration) and low frequency cycling (5-110 Hz).
Excitation was applied separately along the direction of the three principle axes with a minimum time of 50 hours for any particular direction.

The temperature testing took the form of cycling the specimens from + 90°C to -40°C to + 90° C, to a total of 400 cycles.

It had not been anticipated that either the vibration or temperature would effect the MDC itself (based on early work by RARDE), however, on completion of the tests all cords were detonated as a check for satisfactory operation. From a bonding point of view the tests, not unexpectedly, indicated that care was needed on bends and at the end of bond lines to ensure that debonding did not commence as once started this could extend quite rapidly under repeated loadings. In addition, useful information was obtained on the compatability of the MDC cord with a polythene sleeving which was found to be a useful way of protecting and strengthening the basic cord.

4.2.4. Large Scale Specimen/Canopy Investigation

Following the investigations on small scale specimens as described in para's. 4.2.1. to 4.2.3., it was necessary to apply the knowledge gained to large specimens and hence cover the case for a 'real' application to a complete aircraft canopy.

4. 2. 4. (continued)

The test specimens were both flat and curved of up to 0. 5 in. thick - the latter being actual aircraft canopy specimens. The tests covered both 'Acceptable Aperture' and 'Clamshell' systems in which both circular and chevron cords were evaluated.

Testing was related to the thermal conditions expected in flight and/or on the ground with no assistance given to the ejection of the canopy pieces from internal cockpit pressurisation or external aerodynamic suction - hence meeting the worst condition of zero height and zero speed which would be a critical case for VTOL aircraft.

The programme was carried out in two parts, the first to investigate the fracture properties of large specimens at laid down temperature extremes and the second being to investigate further the system for controlled break-up of the overhead part of the transparency to enable faster clearance of the debris from the cockpit area.

The temperature testing was carried out under the following conditions:-

(i) Soaked at +100°C followed by MDC operation at +90°C

(ii) Soaked at -50°C followed by MDC operation at -40°C

(iii) Canopy stabilised with outer face of the acrylic at 100°C and the inner face at +70°C.

All specimens were fitted with thermocouples and tests were conducted in a specially constructed environmental chamber. The results indicated that of the two particular cords tested both were capable of meeting (ii) and (iii) but only the chevron cord fully met (i) with 0. 5 in thick material. This in itself was not considered to be too disappointing as condition (iii) was considered to be the more realistic flight case.

4.2.4. (continued)

The temperature test programme had produced sufficient information on the type and control of breakup which could be obtained. The'minimum aperture' approach was given some attention but most of the further activity was concentrated on the 'clamshell' type system. A limited programme was mounted in which a full installation of MDC was applied to a few canopies in which changes were made to the overhead pattern in an attempt to speed up the progress of dispersing the canopy debris from the cockpit area.

The final results indicated that in the most straightforward 'clamshell' system, dispersion of the broken canopy particles outside the area of the cockpit was achieved 0.3 seconds from detonation in still air. With the adoption of a more complex MDC pattern over the crown of the canopy the dispersion in 0.2 seconds was achieved but further work on joints and patterns was considered necessary if this type of system was to be optimised. The break up of a canopy can be seen in Fig. 7.

Thus by the end of 1976 sufficient information was considered to have been obtained to enable the design teams to incorporate MDC on stretched acrylic transparencies in which the material was up to 0.5 in. thick with minimum development. However, one aspect was considered to require further and more specific investigation than previously, this being in the area of possible crew hazards from the effect of lead splatter. By the end of 1977 testing of of small scale specimens had indicated the probability of success with 0.75 in. thick material.

4.3. MDC Splatter Hazards

Reference has been made earlier in this paper to tests which were done at various stages in the development of MDC systems because of the very understandable concern that many persons expressed over the possible hazard to aircrew from the effects of detonation of the cord. In the case of the HSA developed systems this has been in the main associated with lead splatter.

As this paper is being given to aircraft transparency experts it is unnecessary to go into any great detail on the not inconsiderable attention paid particularly to this aspect in 1977.

4.3. (continued)

It is probably sufficient to record that a programme was carried out in which an anthropomorphic dummy was used which had an easily replaceable 'test' head, the latter being cast in polyurethane foam. The dummy was fitted with various types of flying helmets, clothing and equipment and positioned relative to a cockpit canopy (fitted with the appropriate types of MDC) in the same manner as on a particular strike aircraft (Ref. Figs. 8A & 8B). In a fairly extensive programme attention was paid both to the possibilities of physical damage to aircrew and the damage of their survival equipment - a programme in which the Institute of Aviation Medicine (IAM) was particularly interested and involved.

The test results in detail are only of direct relevance to the equipment and the specific aircraft investigated hence are not given in this paper. It would be relevant, however, to say that whilst the writer has no evidence of serious injury to aircrew who have escaped by using their MDC system in the UK, certain precautions may need to be taken dependant on the system employed and the pilots/aircrew position in the cockpit relative to the position and type of the MDC. The claim is not made that no hazard exists, only that the hazards have to date been able to be minimised by careful design and to a level which appears to be acceptable to the UK Authorities.

4.4. Current Investigations and the Effect of MDC on Materials other than Acrylic

4.4.1. Preliminary Work

During the course of the earlier work on 'as cast' and 'stretched' acrylic the 'world scene' on aircraft transparencies indicated that in the future it was possible that certain other materials would find favour for future aircraft applications.

For strike aircraft canopies, glass was having some consideration and, in particular, polycarbonate was having considerable attention in the USA.

4.4.1. (continued)

Simple tests were, therefore, carried out to establish whether the types of cords used in the acrylic investigation might be acceptable for the newer canopy materials. A few small test samples were employed to examine the effect (at room temperature) of MDC on thin laminated toughened glass, thin monolith polycarbonate and a 0.5 in. polycarbonate sheet to which had been directly bonded a thin sheet of as'cast'acrylic.

In all cases fracture was found to be possible but as the UK considered that their requirements could probably be met for some time to come by the use of acrylic, any major programme of MDC on other materials was deferred except for one on a fibre-glass crew escape hatch which was successfully concluded.

4.4.2. Current Programme

The current view in the United Kingdom on future strike aircraft requirements has indicated to our transparency designers that new materials or mixed material composites may be necessary. Surface temperatures attained in high speed flight has been the main reason, but possibly more severe requirements to cover bird impact conditions are also likely to have to be met. In addition, the trend towards 'one piece' combined canopy and windscreen units with no windscreen arch (as exemplified on the General Dynamics F16) has found such favour by some pilots that pressure is being brought to bear by aircrew for aircraft designers to provide them with these all round view capabilities in future.

A combination of all the above transparency trends gives a most challenging situation to our teams involved in aircrew escape systems - and particularly so to those who believe in MDC escape systems. The challenge has been accepted, however, and the work is currently in hand evaluating various

4.4.2. (continued)

combinations of materials as well as monoliths in polycarbonate (with and without protective coatings) and stretched acrylic in thicknesses greater than those evaluated in the previous Company programme.

This work is in its early stages and is currently confined to small scale specimens but, by drawing on the past experience of the MDC team, fairly rapid progress is expected to be made. The provision of large scale test specimens is likely to be the greatest holding factor. It must be recorded that the willingness to co-operate by providing small scale test samples at no cost to the Company by Texstar Plastics, PPG Industries Inc., and Swedlow Inc. is greatly appreciated.

The limited results obtained to date are showing considerable promise and it has already been demonstrated that, with very little modification in one type of cord, a polycarbonate monolith approximately 1 in. thick can be satisfactorily fractured under certain specified conditions. It is not proposed to give further information in this paper as the results will be first and progressively given to those companies who supplied the Company with the samples.

The result of the test on the 1 in. thick polycarbonate is perhaps particularly significant to those persons who advocate a 'one piece' windscreen and canopy assembly. One of the problems with such a unit on an aircraft is that if the total assembly has to be jettisoned as part of the crew escape sequence in an emergency, the aircrew are likely to be subject to very severe buffet possibly resulting in severe physical injury. If, however, only a portion of the canopy/windscreen unit can be broken in a controlled manner by an MDC system, not only will the whole escape sequence be much faster but the crew should have some measure of protection from the wind blast by the forward 'windscreen' portion of the transparency remaining on the aircraft. This is an exciting

4. 2. 2. (continued)

and important possibility but further work in our present test series will need to be completed before such a possibility can be claimed as reality.

5. Conclusions

So where does this leave us?

Since Hawker Siddeley Aviation (now part of British Aerospace) commenced its MDC 'through canopy' escape system work in about 1963, confidence has grown in its ability to provide probably the fastest, lightest and most efficient type of system and one which may have many applications in the future. These applications are not seen as being confined purely to strike aircraft canopies as the potential for such systems may be attractive for many categories of aircraft including helicopters and for some retrofit action.

During the course of the research and development programmes the Company registered certain Patents which are referenced in the Appendix to this Paper. A brief description is given of the main aspects covered by each Patent.

Confidence in MDC escape systems has been shown to be well founded in the case of the VTOL Harrier aircraft from which a number of successful escapes have been made under conditions which could almost certainly not have been met by any other system. Not only has successful operation been demonstrated but component life is satisfactory and handling problems have been minimal. In addition to the Harrier, MDC is now a standard fitment on a number of 'in service' military aircraft, the latest of these being the British Aerospace Hawk as shown in Figs. 9A and B.

Hawker Siddeley Aviation and the British Aircraft Corporation, as a result of recent UK Government nationalisation policy, are now joined together as part of the newly formed British Aerospace Corporation. Such is the level of confidence in MDC escape systems, supported by service experience, that those Divisions of the British Aerospace Aircraft Group responsible for the design of new strike aircraft, are giving first consideration to the possible use of such systems in their new projects.

5. (continued)

The systems developed to date are probably not fully optimised. Nevertheless, successful operational systems have been developed but research continues to be needed and it is the intention to continue with R & D in this field.

One thing is certain, the research team engaged on this work over the years has gai ned a very great deal of experience - experience which will be invaluable in the future work.

It is their not inconsiderable success that has enabled some of the results of their work to date to be recorded in this Paper.

6. Acknowledgments

The Author wishes to acknowledge that much of the R & D work has been carried out with the support of the Procurement Executive of the Ministry of Defence.

He wishes also to express his appreciation to the 'MDC team' for their great support and activity in this field of research and in particular to the B. Ae. Brough and Kingston Sites and to the various Branches of the Ministry, RARDE, and the I. A. M. who admirably played their part in the activity.

Finally the Author's thanks are due to the Technical Director of British Aerospace Aircraft Group for permission to give this Paper but points out that the views expressed therein are his own and not necessarily those of the Company.

References:

1. Wittman R.E. "Chemically Strengthened Glass for Frangible Aircraft Canopies." SBAC Optical Transparency Symposium, London, June 1971.

2. Hudson G.T. "Escape Through Aircraft Transparencies." SBAC Optical Transparency Symposium, London, June 1971.

3. Barwood A.J. Group Captain. "Clearance of Ejection Path by the Use of Explosive Cord." AGARD Conference, September 1973.

4. Reader D.C. Squadron Leader. "Ejection Experience from VTOL Military Aircraft." AGARD Conference, September 1973.

APPENDIX

CREW ESCAPE SYSTEMS

Hawker Siddeley Aviation (now part of British Aerospace) Patents

Case 1427 Crew Escape System

British Patent No. 1. 383. 511.
Corresponding Patents in France, Germany, USA.

Provides a canopy transparency break-up system comprising peripheral miniature detonating cord (MDC) held in place by sprung, segmented retaining plates and further incorporating crack initiating loops. End-on mechanical detonation is also provided.

Case 1430 MDC - D - Cord

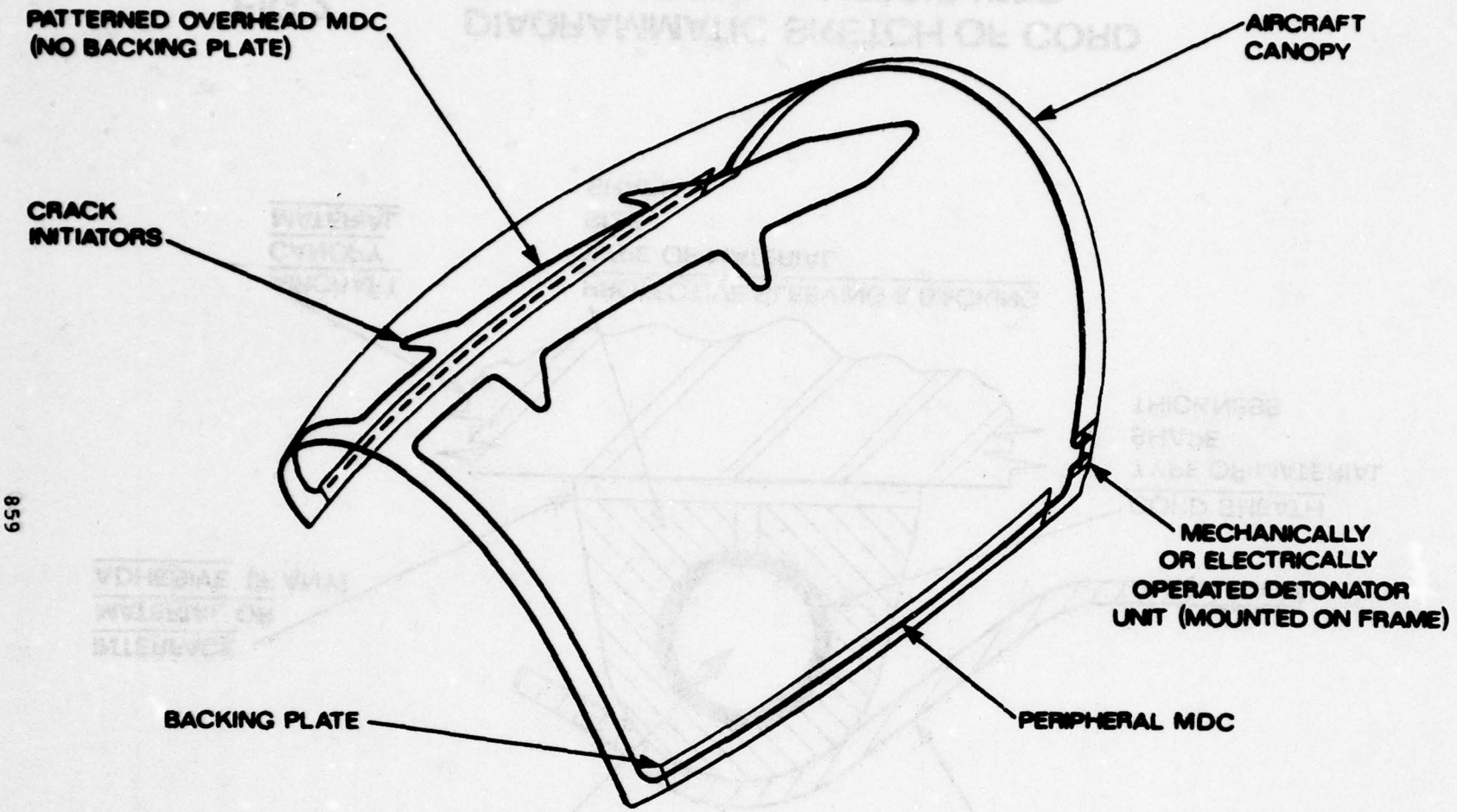
British Patent No. 1. 383. 512.
Corresponding Patents in France, Germany, USA.

A D-section miniature detonating cord in which the semi-circular portion, but not the flat face, incorporates several layers of lead tape which acts as a blast - containing and reflecting material to direct the blast effect of the detonation through the flat face.

Case 1440 Pattern MDC

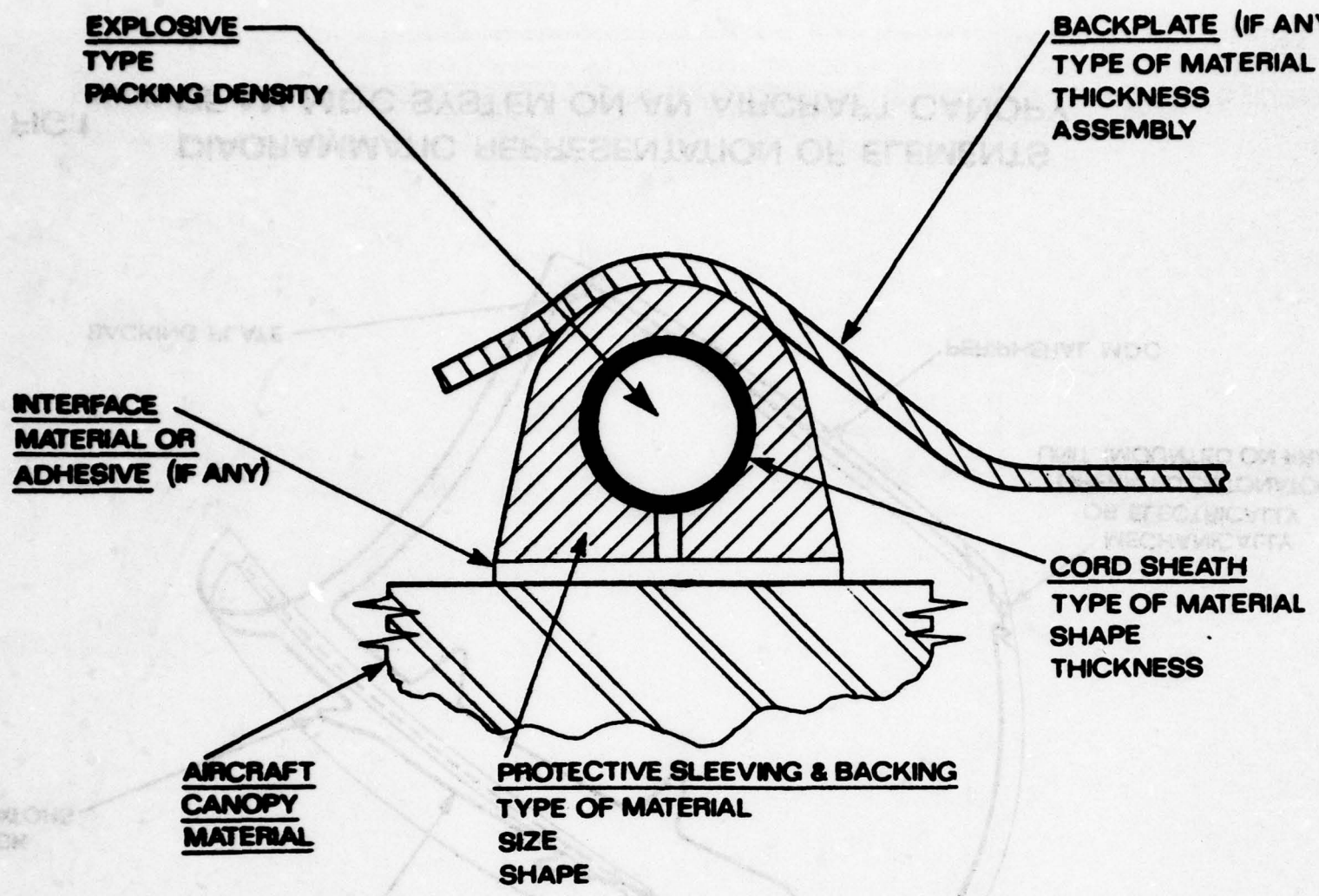
British Patent No. 1. 383. 513.
Corresponding Patents in France, Germany, USA.

An extension of the peripheral system of Case 1427 in which miniature detonating cord is laid in a loop extending from the peripheral run and into the region at the top of the transparency through which the crew member will pass on ejection. The loop further incorporates crack initiating loops and the cord is adhesively applied by a process covered by the Patent.



859

FIG.1 DIAGRAMMATIC REPRESENTATION OF ELEMENTS OF AN MDC SYSTEM ON AN AIRCRAFT CANOPY



860

FIG.2 DIAGRAMMATIC SKETCH OF CORD PARAMETERS INVESTIGATED

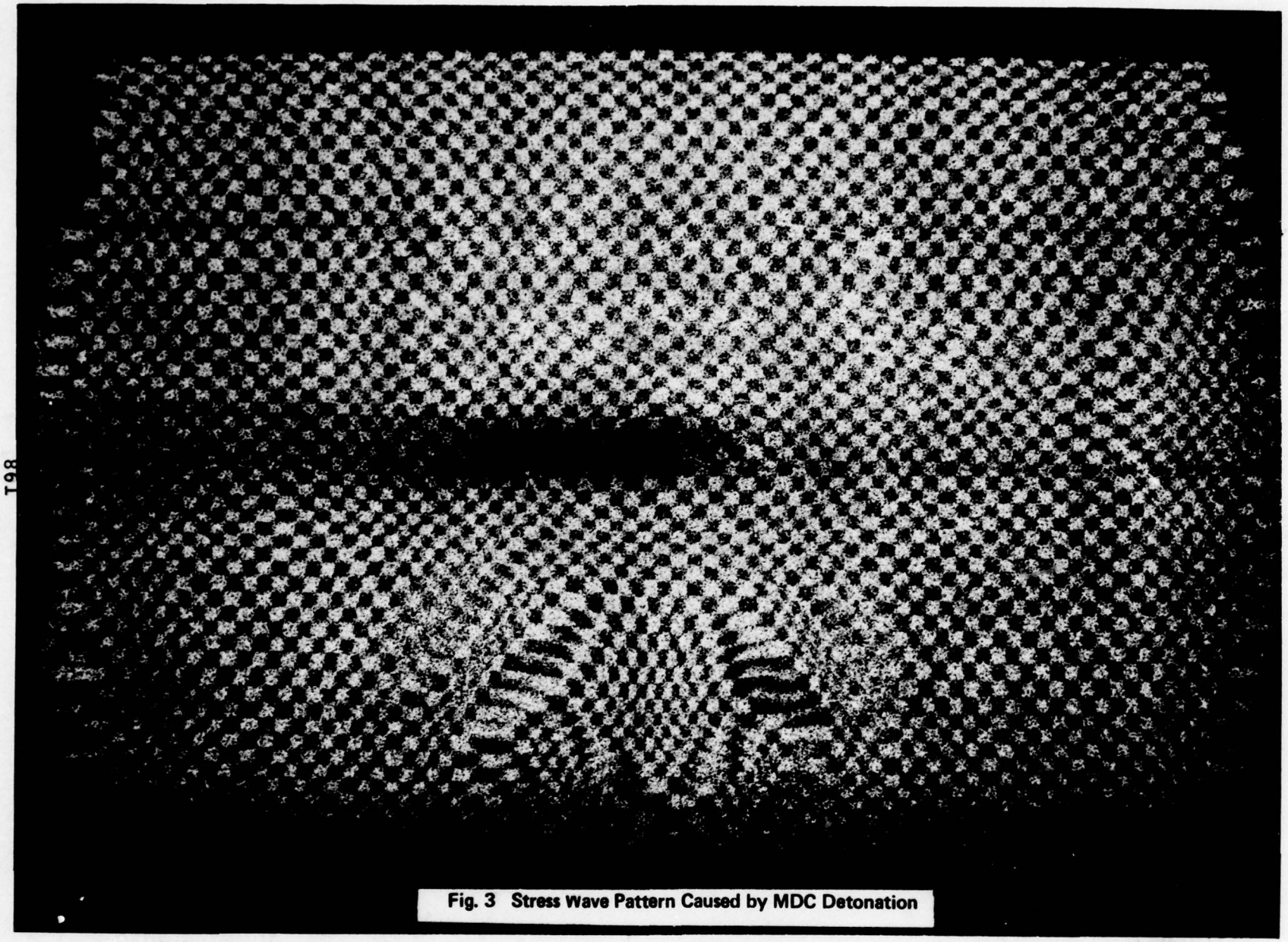


Fig. 3 Stress Wave Pattern Caused by MDC Detonation

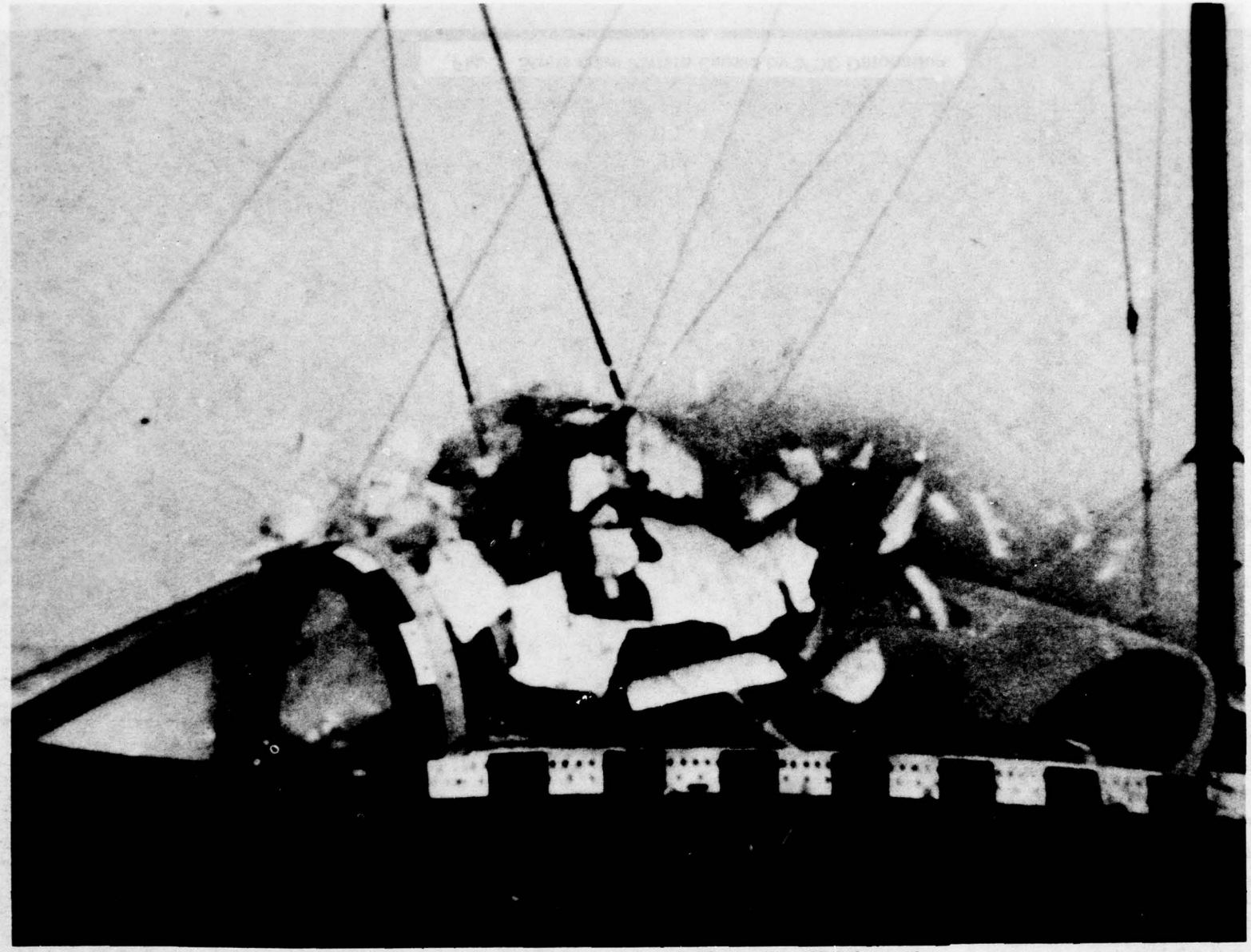


Fig. 4 An 'as cast' Acrylic Canopy Approx. 0.04 sec. after MDC detonation

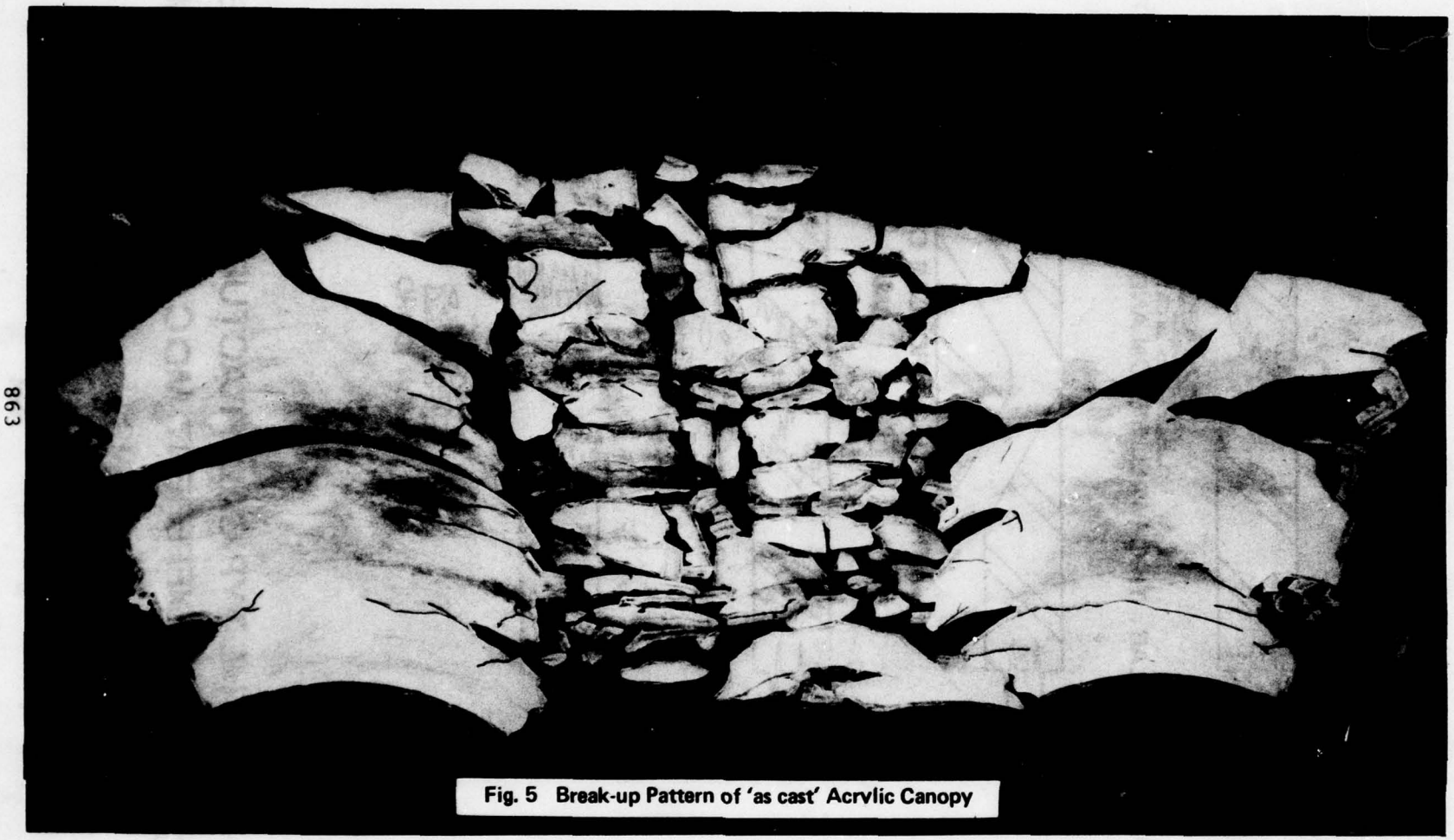
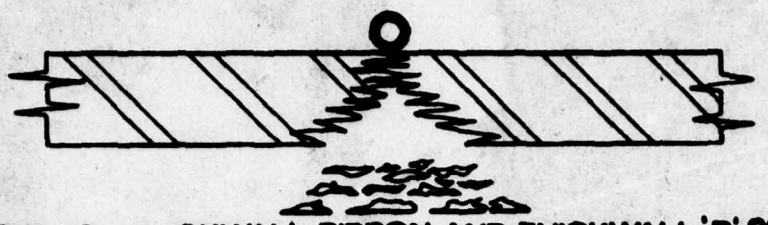
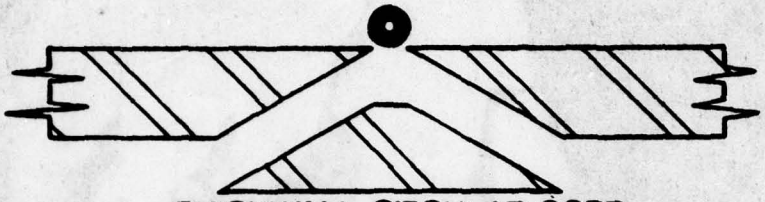


Fig. 5 Break-up Pattern of 'as cast' Acrylic Canopy



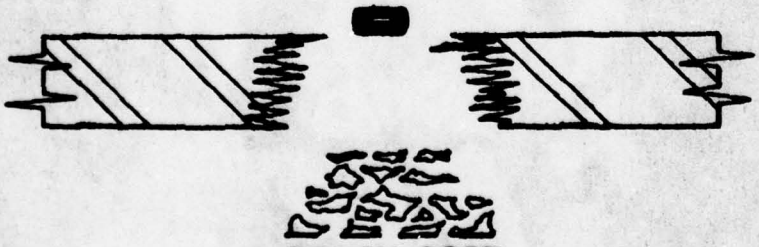
THINWALL CIRCULAR, THICKWALL RIBBON AND THICKWALL 'D' SECTION CORDS.



THICKWALL CIRCULAR CORD.



CHEVRON CORD.



RIBBON CORD.

FIG.6 THE TYPICAL FRACTURE CHARACTERISTICS FOR DIFFERENT MDC/STRETCHED ACRYLIC COMBINATIONS.

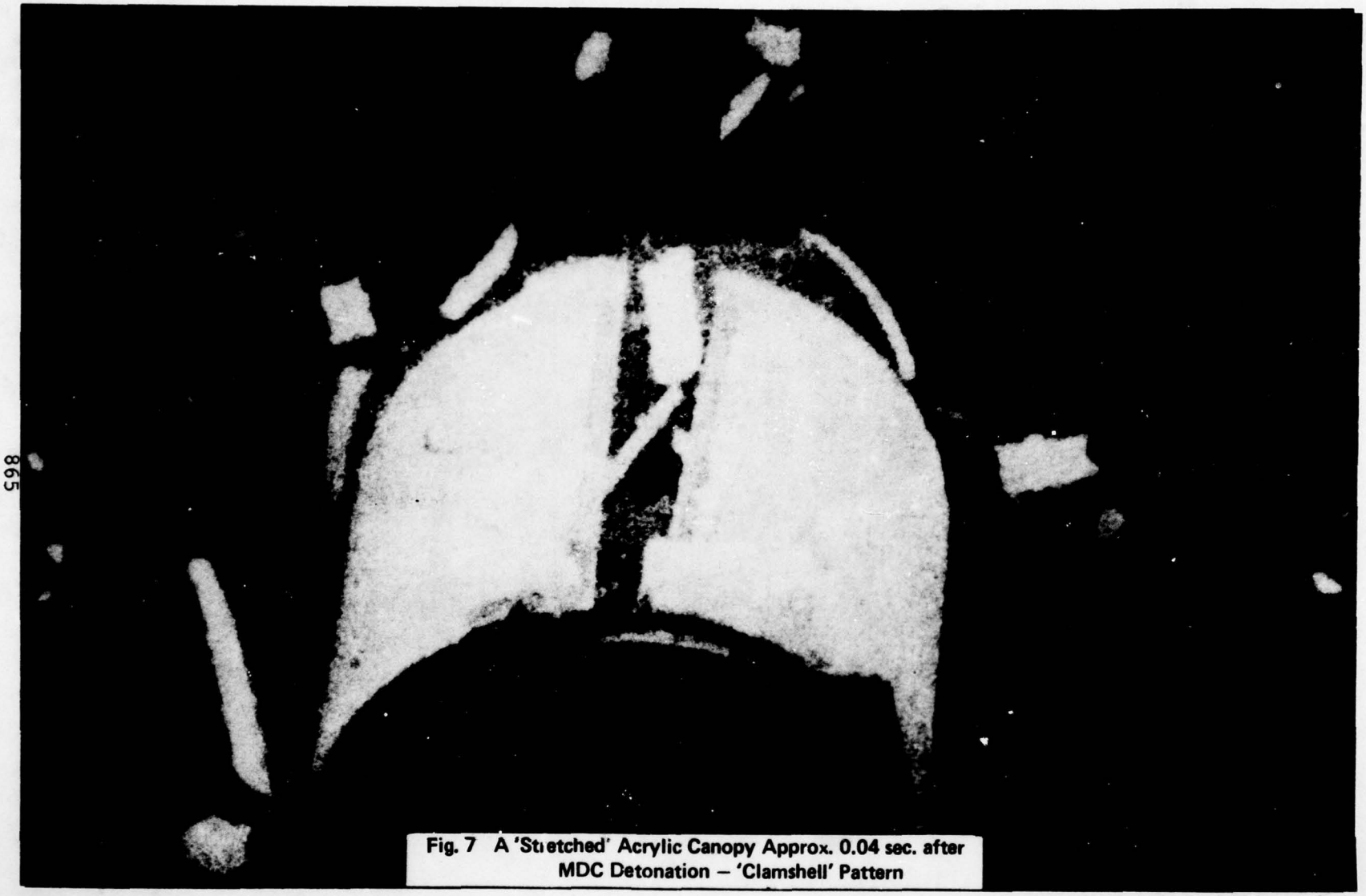


Fig. 7 A 'Stretched' Acrylic Canopy Approx. 0.04 sec. after MDC Detonation – 'Clamshell' Pattern

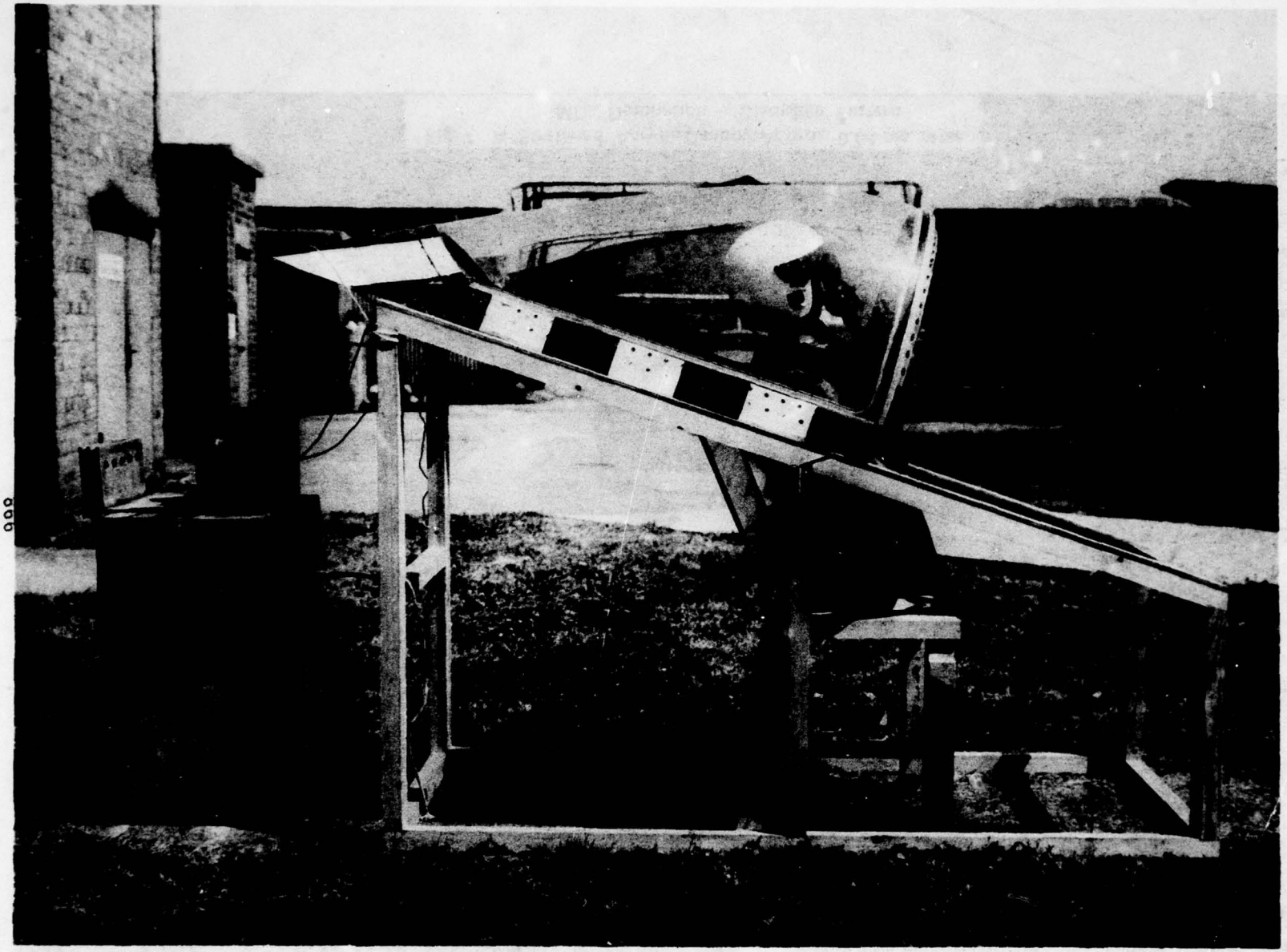


Fig. 8A Dummy Pilot/'MDC' Canopy Test Set Up



Fig. 8B Dummy Pilot's Head (Cast in Polyurethane Foam)

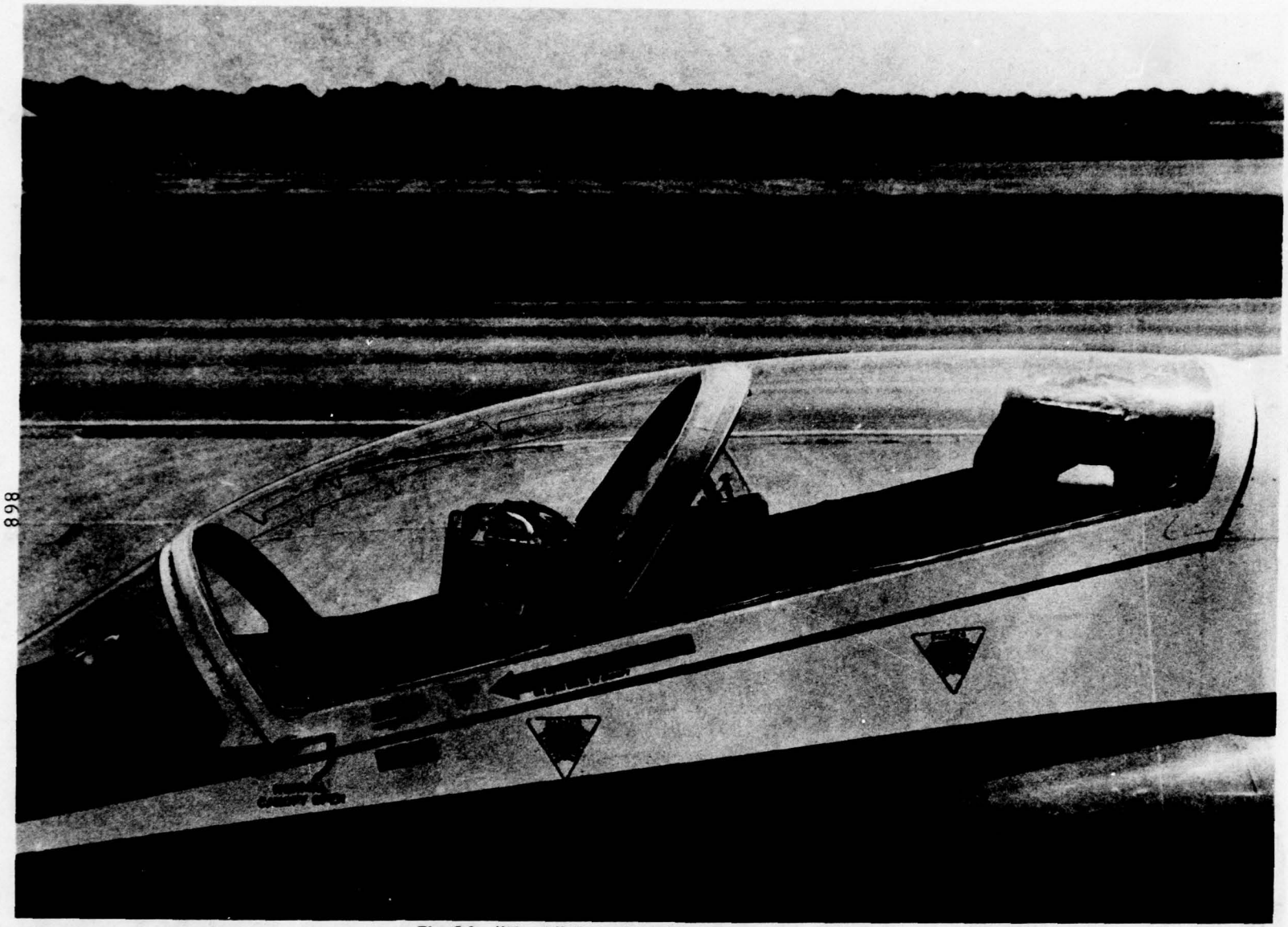


Fig. 9A "Hawk" Canopies with MDC Peripheral and Overhead Pattern



Fig. 9B General View of British Aerospace "Hawk"

THE WINDSHIELD DEVELOPMENT OF A MODERN WIDE-BODY TRANSPORT

C. R. Mercer
Lockheed-California Company
Engineering
Burbank, California

PRECEDING PAGE BLANK-NOT FILMED

THE WINDSHIELD DEVELOPMENT OF A MODERN WIDE-BODY TRANSPORT

by Charles R. Mercer
Lockheed-California Company

ABSTRACT

The development of a wide-body transport windshield system entails the successful integration of good design philosophy, a myraid of requirements and divergent disciplines, and a wide variety of test programs. Hopefully the result is a successful, well accepted, reliable, cost effective design.

This paper provides a review, after almost six years of airline experience, of these elements as they apply to the L-1011 TriStar. Major test programs are discussed. In-service problem areas are defined and the remedial measures and resulting increase in overall reliability improvement is reviewed. Operational comments are included with particular emphasis on visibility aspects. The paper concludes with some comments on future windshield system design challenges.

PRECEDING PAGE BLANK-NOT FILMED

INTRODUCTION

The decision to proceed with design of an entirely new airplane entails many challenges and "unsolved opportunities." Since the L-1011 was designed without constraint from prior model continuity, we had the opportunity to fully exploit the state-of-the-art and take full advantage of the rapid advancement in materials and design technology in the transparency area.

Now may I share with you some highlights of this technically exacting program.

DISCUSSION

The fundamental criteria that established the key requirements for the L-1011 windshield design were:

- A wide-body single-deck fuselage.
- A three-man crew using a separate third crew member station with optional forward-facing capability.
- A single set of throttles (thrust levers) accessible to both pilots and the third crew member. Ergonomics thus dictates a distance between the two pilots of approximately 42 inches. In fact all the current transport aircraft, e.g. B-707, DC-8, B-727, B-737, and DC-10, use this dimension.
- A pilot eye reference height in the neighborhood of 19-feet above ground level, dictated by gear and fuselage geometry.

A basic requirement for any windshield system is to provide the best possible overall vision. One might say that the optimum windshield is one that is "invisible." Of course it must also keep out the elements - wind/rain/hail - retain a comfortable, habitable environment for the crew, require no maintenance and add neither cost nor weight to the airplane. Fanciful you say? Orville and Wilbut compromised on the wind/rain/hail and weren't troubled by limitation on the operating envelope. The Apollo Astronauts on the other hand had an altogether different view. Their compromise was at the other end of the scale - but what an ambitious and exciting operational envelope. Today's commercial transport pilot operates between these two extremes - more shirt sleeve than the Wright Brothers - a more limited operational envelope than the Astronauts.

DESIGN CRITERIA

The provision of excellent external vision together with adequate internal vision for unobstructed instrument view and the provision of maximum usable instrument panel space is a highly important and critical requirement.

The final L-1011 design was the result of application of a variety of criteria, some regulatory, some advisory in nature; and some innovative thinking. The FAA defines the certification requirements for windshields in

Part 25 of the Federal Air Regulations (FAR), with policies and guidelines for the vision envelope provided in Civil Airworthiness Manual (CAM) 04b.

The IATA 15th Annual Technical Conference on All Weather Landing and Takeoff, held in Lucerne, Switzerland (April 1963), established criteria for over-the-nose vision that have found universal acceptance.

An additional well recognized and comprehensive reference is SAE Aerospace Standard AS 580.

The decision of whether to use flat or curved transparency panels needs to carefully consider the geometry requirements for good external visibility together with maximum internal instrument vision and optimum panel space. This was undoubtedly one of our most difficult and carefully conducted trade-off studies. The final decision to select a composite material and a cylindrical curved design was reached only after review and assessment of many parameters: (It should be noted that the order of importance of these was the subject of many well-argued, and sometimes heated, debates.)

- Weight

  It was concluded that a curved composite windshield offered a substantial weight saving over a flat windshield providing approximately the same vision envelope. The curvature permitted the cabin pressure to be carried in the transparent panel by a combination of hoop tension and bending rather than by bending alone. In addition, use of the curved windshield permitted significant weight savings in the shell structure adjacent to the windshield.

- Drag

  Evaluations of carefully conducted wind tunnel testing convinced us that a curved windshield can provide a measurable reduction in drag (up to four-tenths of a drag count).

- Cockpit Internal Noise

  Preliminary analysis indicated that a curved windshield would reduce aerodynamic noise. Subsequent flight tests conducted at 10,000 feet confirmed that the curved windshield is appreciably quieter than an equivalent flat windshield because it eliminates "break-away" airflow noise at the sideposts.

- Design Risk

  The known shatter-resistance characteristics of stretch-oriented acrylic plastic and the availability of thin optical-quality tempered glass provided us a solid design base. An aggressive and timely test program reinforced our belief that the existing state-of-the-art technology could enable us to produce a successful design. Many excellent papers have documented the materials

development and design considerations associated with our program and that of the Boeing 747.

- Instrument Panel Space and Vision

Several flat windshield configurations as well as various curved arrangements were analyzed, using mockups and graphics. Figure 1 shows an external comparison, and Figure 2 shows the improvement in instrument panel space attributable to the curved configuration. Vision improvement as affected by sidepost location will be discussed later.

- Optics

Flat, laminated plate glass windshields have excellent optical quality. It was obvious that, at least initially, the large, curved, composite plastic windshields for the L-1011 could probably not have optical distortion limits as tight as those for flat windshields.

Considerable test evaluation indicated that a central area distortion limit of 1:20 maximum would be acceptable for all flight conditions. Early windshields using flat cold-wrapped .050" thick (Chemcor) glass for the outer abrasion shield exhibited a border distortion due to the glass "edge pinch" effect. When the glass manufacturers developed the glass forming process to where excellent optical quality "formed" glass was available, a tougher 0.085" thick formed glass outer ply was incorporated and the optical quality of these windshields was excellent. Optical evaluation of windshields with a formed 0.105" thick glass outer ply indicates that excellent optical quality continues to be maintained.

- Bird Impact Capability

It was concluded that a curved windshield is superior to a flat design due to the arch characteristics which more easily allow the bird to be "bounced" rather than "bagged." It is obvious that a flat glass panel design can be strengthened to provide "bounce" capability but at a substantial additional penalty to the already higher weight requirement of the flat design. This bounce capability is desirable in that bird strike capability is not dependent on maintaining a heated vinyl interlayer for bagging. In addition, the composite acrylic panel has much greater resilience and shatter resistance than glass. The bird impact tests discussed later substantiated the curved windshield's outstanding structural capability.

DEVELOPING THE DESIGN

Fail-safe design is dictated by the fact that loss or blowout of a complete panel is unacceptable. The configuration using two separate acrylic plies (Figure 3) provides full fail-safe capability following failure of either one of the plies.

An outer layer of chemically strengthened glass provides protection from windshield wiper abrasion and dust. In addition the inner surface of the glass provides an ideal location for the electrical conductive heat coating required for anti-ice and defog capability.

In framing and mounting the windshield we established a somewhat unique design approach to take maximum advantage of the curved composite strength by eliminating the conventional heavy framing around the windshield cutout.

Figure 4 indicates the manner in which the windshield post functions and how hoop tension loads are carried in the skin and through the windshield itself. This avoided the normal isolation of the windshield from fuselage structure. In the post areas the tension loads remain in the windshield and its framing plate, requiring the post to take only beam bending resulting from fuselage pressurization and bird strikes. The bushing design assures optimum load distribution and transfer between frame and windshield.

A general view of the original detail design may be obtained from a cross section of the main windshield (Figure 3). This shows:

- Two stretched acrylic plies, .90 inch and .70, bonded together with an .050 PVB interlayer
- The .050 inch thick Chemcor outer glass ply bonded to the acrylic with an .075 inch thick PVB interlayer. Note the separator slip joint.
- Bus bar and electrical conductive heat coating
- Anti-static external coating on the Chemcor glass to "drain" static buildup
- Sensor and terminal design
- Rubber and spacer design
- The aerodynamic seal - dry for quick installation and removal
- The pressure seal - also dry for quick installation and removal
- The hard-coated inner acrylic surface
- Insulation

Figure 5 shows the similarity but some differences of the side window design:

- Conductive coating location
- Sensor location
- No outer glass layer
- No hard coat

Sidepost Location

Recognition of the extreme importance of the key forward viewing area as it relates to collision avoidance led us to position the main sideposts as far aft as possible. This resulted in an unobstructed side vision angle of 50° instead of the more conventional 30°. Figure 6 shows that very important end product - the vision diagram. Note also the ambinocular photo taken with the FAA Binocular Cockpit Visibility Camera.

The aft post location, coupled with the very wide cockpit, made it obvious that a "clear vision" openable side window was impractical at best. From his position (21 inches off the centerline and positioned forward for optimum over-the-nose vision) the pilot was unable to move sufficiently outboard to effectively utilize an openable window and still reach the controls to adequately fly the airplane. We were again faced with a major tradeoff decision.

We elected to eliminate the openable window and to demonstrate an equivalent level of safety to satisfy the FAR "clear vision window" requirement. As a part of this demonstration a comprehensive and thorough hail impact test program was developed and accomplished. The deletion of the openable side window caused us to design and develop a simple, and we feel desirable, flight station escape system. An easily opened hinged overhead hatch, accessible via the first observer's fixed seat and a built-in ladder, together with five inertia descent reels, provides rapid, safe, and easy egress to either side of the aircraft in an emergency. Figure 7 shows this escape system.

Many past windshield designs had failed to provide adequate horizontal and vertical reference to assist the pilot during the final phases of approach and landing. Therefore the glareshield was extended in an unbroken horizontal line for the maximum width possible and the forward edges of the sideposts were so aligned that they appeared vertical to the pilot. In addition a subtle, but effective, refinement of all the post geometry creates the illusion of an "optical impression center." This is evident in Figure 8.

Adverse weather protection required:

- Anti-icing and defogging of the main windshields and defogging of the side windows. This was accomplished by application of electric power to a conductive coating. The coating is deposited on the windshield's inner glass surface as shown in Figure 3. The side window heat coating is located on the outer face of the inner acrylic ply. A blower was installed to aid in defogging the inner windshield face during rapid warmup from a cold soak condition and to act as a backup in the event of anti-ice system malfunction. Figure 9 shows the control panel in the cockpit.

- Windshield washers and wipers systems with individual controls for each pilot. These are provided for cleaning dirty windshields and removing rain.

- A rain repellant system, also provided with individual pilot controls, to provide an alternate or supplementary rain removal capability. The rain protection system is shown in Figure 10.

MOCKUPS

Mockups played a significant part in our development program:

- The mockups shown in Figures 1 and 2 aided in our flat versus curved windshield selection. The effects on cockpit vision, post requirements, structural and trim concepts as well as instrument panel space comparisons were investigated using several mockups of this type.

- The full scale movable cockpit mockup is shown in Figure 11. This was - and is - one of our most valuable design tools. In its fixed position, four large movable screens allowed vision evaluation for:

  - Landing VFR from 100 foot decision height
  - Landing with 100 foot DH and 1200 foot RVR
  - Landing with 50 foot DH and 700 foot RVR
  - Level flight VFR at 33,000 feet

  In addition, a "blind-fold" can be attached to facilitate cockpit lighting evaluation. We accomplished our initial instrument lighting qualification tests using this device.

The complete cab can also be mounted on a dolly establishing the actual 19 foot high ground relationship as shown in Figure 11. The attitude is controllable in pitch thus allowing simulation and evaluation of the effects of sunlight and night lighting at various aircraft attitudes while being towed around the airport.

TEST PROGRAMS

Several major test programs contributed to the overall design effort:

Bird Impact Tests

The windshield's ability to withstand the impact of a four pound bird at closure velocities of 350 knots TAS (minimum) was clearly established in a comprehensive test program and demonstrated to the FAA. Figure 12 shows the test setup at our Rye Canyon Research Facility. A full scale actual flight station segment was used to assure structural conformity. Testing throughout a wide temperature range from ambient to sub-zero confirmed the ability of the curved composite windshield to "bounce" the bird rather than "bagging" it.

Hail Impact

The absence of a clear vision side window established the need to demonstrate an ability to withstand severe hail impact and still assure that adequate forward visibility would always be sufficient to safely continue flight and land the airplane. Initial ground tests were conducted at the rain tunnel facility at the Lockheed-Georgia Company (refer to Figures 13 and 14). These tests were FAA witnessed and confirmed our selection of the chemical temper, central core tension, and case depth of the outer Chemcor glass layer.

Subsequent in-flight testing confirmed the existence of adequate residual visibility for safe landings following breakage of the outer glass ply. A typical mosaic break pattern is shown in Figure 15. Hail encounters in service with windshields utilizing .050 thick Chemcor reaffirmed the desired landing vision capability. (It may be noted that experience shows that use of the .085 thick Chemcor glass has practically eliminated hail-caused breakage.)

Fail-Safe

This test was conducted on an L-1011 main windshield to demonstrate the fail-safe capability of the main and side windshields.

Phase I was conducted to qualify the windshields in accordance with Federal Aviation Regulations, Part 25, Paragraph 25.775. Test results demonstrate that the L-1011 windshields can withstand maximum flight pressure differential and temperature effects with a major load-carrying member of the windshield failed.

Phase II was an additional Lockheed requirement, and demonstrated that the windshields could withstand over twice the maximum flight pressure differential at 70°F internal and -50°F external temperatures after the failure of a major load-carrying windshield element. See Figure 16. Although not directly applicable, but of particular interest in this area was a test conducted by the supplier (Sierracin) which demonstrated the windshield's capability to sustain the impact of several .357 magnum bullets fired at close range into the windshield inner surface. In each case the inner ply retained the bullet and the windshield integrity was safely maintained. Figure 17 is a photograph of a section of the L-1011 windshield used in the test.

Life Cycle

Two windshield panels were used for this test. The first panel demonstrated its structural integrity by successfully withstanding the structural qualification tests; however the heating film failed during the thermal shock test. The second panel endured 100 simulated typical flight cycles demonstrating its life expectancy. Prior to the life cycle tests, the panel was successfully subjected to thermal shock test and a pressure cycling test. A change in the outer interlayer configuration required that the pressure cycling test be repeated on the second panel. The only noticeable discrepancy in the second panel was seal extrusion from between the panel and retainer.

The tests were then repeated on the forward and aft side windows. Both demonstrated their ability to withstand all of the structural requirements of the test program. Delamination and bubbling in the vinyl interlayer was detected in both panels, however this condition did not diminish the structural capabilities of either panel.

NOTE - A new windshield life test facility allowing real world environmental testing was developed by Sierracin-Sylmar in 1974 to evaluate Boeing 747 design improvements. A joint effort between Lockheed and Sierracin expanded the facility to incorporate an entire L-1011 cab structure. For a comprehensive report of this facility see "At Last, a Meaningful Windshield Life Test," by Jan B. Olsen.

OPERATIONAL DEVELOPMENT

Pilot acceptance of the curved windshield was excellent from the very start, with no particular problem areas evident until delamination of the outer glass ply occurred during our flight test program, well before the FAA airplane certification date. We had been flying without windshield heat for some weeks due to development problems with the windshield heat control system. In clear air at 33,000 feet altitude the pilots heard a loud sharp noise. Their initial reaction was to duck down. They reported that the separation edge lines looked like cracks and the shattered glass around the edges looked like ice. They elected to descend to a more comfortable (for their peace of mind) altitude. After landing the windshield was examined carefully. The PVB exposed surface was smooth and clear. In fact only the edge area provided visual evidence of the glass loss and of course a fingernail pressed into the vinyl surface was evidence that the surface was truly PVB.

We recognized immediately that a program providing windshield characteristics and constuction details to pilots would be well advised. Ground schools, a Field Service Digest article, and customer training sessions proved effective in explaining the new and previously unknown features to crews.

A second important, but not unexpected, experience was the initial hail impact outer glass failure. The immediate concern of the pilots was loss of vision. However they found that there were areas where the glass sloughed-off and adequate vision was available to land safely.

Once again we realized that more training and information were in order and as a result we produced a training film "Hail Encounter Procedures." Today we find that with the .085 inch thick chemically strengthened windshields hail encounter rarely results in breakage, in fact I know of only one or two cases. There have been some .085 breaks for other causes.

An early question concerned operation of a curbed windshield in rain - particularly in the approach and touchdown phase. Experience now confirms that absolutely no problem exists. In fact pilots have indicated the curved design is substantially superior to the flat panel design in this regard.

Internal reflections can present a problem unless they are effectively dealt with. The horizontal glareshield aft edge is the cutoff for unwanted reflections in the windshield. The center pedestal area forward of the throttle quadrant aft edge is adequately shielded. The aft area of the center pedestal will reflect light sources into the upper outboard main panel areas. These are acceptable but can be eliminated by careful selection of edge lighted panel control.

RELIABILITY IMPROVEMENT PROGRAM

The introduction of the L-1011 into airline service in the Spring of 1972 was accompanied by the normal amount of maintenance and reliability problems. A comprehensive reliability improvement program was established and a qualified and representative team selected to track and assure prompt remedial action.

SIGNIFICANT SERVICE PROBLEMS

- Burnout of the conductive coating - caused primarily by moisture penetration of the edge seal and edge delamination. The successful remedial action for preventing moisture penetration was to improve sealing by:

  a. Addition of a peripheral titanium "Z" strip around the glass edge. See Figure 3. Note that the "Z" strip replaced metal tabs previously used to conduct buildup from the P-static drain coating.

  b. A wide band of polysulfide sealant - this weather seal is most effective when the sealant at the "Z" glass interface is a large hump.

  c. A .12 inch undercut of the PVB interlayer between the glass face ply and the acrylic provides additional effective area for the polysulfide sealant which is well protected from erosion by the "Z."

  An edge delamination problem was effectively countered by:

  a. Increasing the rigidity of the windshield laminate by changing to a more rigid PVB interlayer between the acrylic plies. This reduces the deflection and thus delamination stresses.

  b. Increasing the thickness of the PVB interlayer between the glass and the acrylic from .075 and .100 inches which in turn reduces the shear stresses at the conductive coating/bus bar.

- Chemcor Breakage

  The .050 inch thick chemically strengthened glass face plies were subject to frequent breakage from hail, FOD, or tool impact. The L-1011 used a flat cold-wrapped sheet of Corning 0313 temper with case depth and central core tension that are compatible with a

large mosaic break pattern to assure adequate residual visibility. Corning's improvement of the optical quality of preformed glass enabled us to shift to an .085 inch thick preformed glass face ply with deeper effective case depth and greater strength. This change was made in March 1975. The optical quality is excellent and the breakage for all causes has been greatly reduced. Hail breakage has been almost entirely eliminated. Eventual use of .105 inch thick material should result in even greater ability to reduce glass breakage from all causes.

- Air Leaks

  Air leaks between the glass and acrylic and between the sill and the frame have been eliminated by addition of a beaded gasket and improvement of the alignment and attachment of the dry seal, see Figure 3.

- Miscellaneous

  a. Improved terminal connection has reduced or eliminated a problem associated with overheated power terminals.

  b. An open sensor problem has been remedied with an improved sensor connection.

CURRENT DEVELOPMENTS

- We are currently service testing windshields with preformed .105 inch thick Chemcor face plies and expect to go forward with production incorporation at an early date. The new glass has double the case depth of .085 and is very much stronger.

- We are also conducting a service test to evaluate Pittsburg Plate Glass as an alternate source for main windshield panel rework. These windshields will utilize outer glass of .120 PPG Herculite II with an indium oxide heat film system and an interlayer of .150 PPG 112 urethane.

- A totally unanticipated and unusual in-service problem has been failure of the Chemcor glass outer layer as a result of several flights through volcanic plumes. In an effort to understand this phenomenon, tests have been conducted utilizing silicon carbide particles to simulate similar damage experienced by S3A Viking aircraft while operating in an aircraft carrier environment. Apparently jet-blast driven anti-skid paint particles of silicon carbide have caused failure of .050 chemically strengthened face plies. In the silicon carbide particle tests using a particle size equal to the largest particle that can pass through 20 wire/in mesh screen, both .105 Chemcor and .120 Herculite withstood 160+ knot particle impact without breakage.

CONCLUSION

The windshield system design is maturing in a satisfactory fashion. Development and improvement is a continuing process as can be seen by reference to Figure 18, Mean Time Between Failures (MTBF) and Mean Time Until Removal (MTUR). This improvement in MTBF and MTUR speaks well for the basic design and also for the very considerable effort expended by many dedicated people and facilities in the continuing search for improvement.

In attempting to cover a program of this scope many facets and areas have either been briefly mentioned or omitted. This is regrettable. However much has been written and many excellent reports are readily available to anyone who wishes to delve deeper into the subject.

A final word with a look to the future - we need to turn our efforts toward:

- Continued work in the elimination of unwanted reflection (mainly internal) which carries the promise of greatly improving the operational environment.
- Integration of advanced head-up displays (HUD) into the basic windshield design; a challenge for a joint avionics/transparency design effort.
- Continued material development to further reduce post size or eliminate post requirements in the entire critical vision area for the commercial transport.
- Development of a workable anti-fog coating or surface characteristic that is long lasting.



FRONTISPIECE

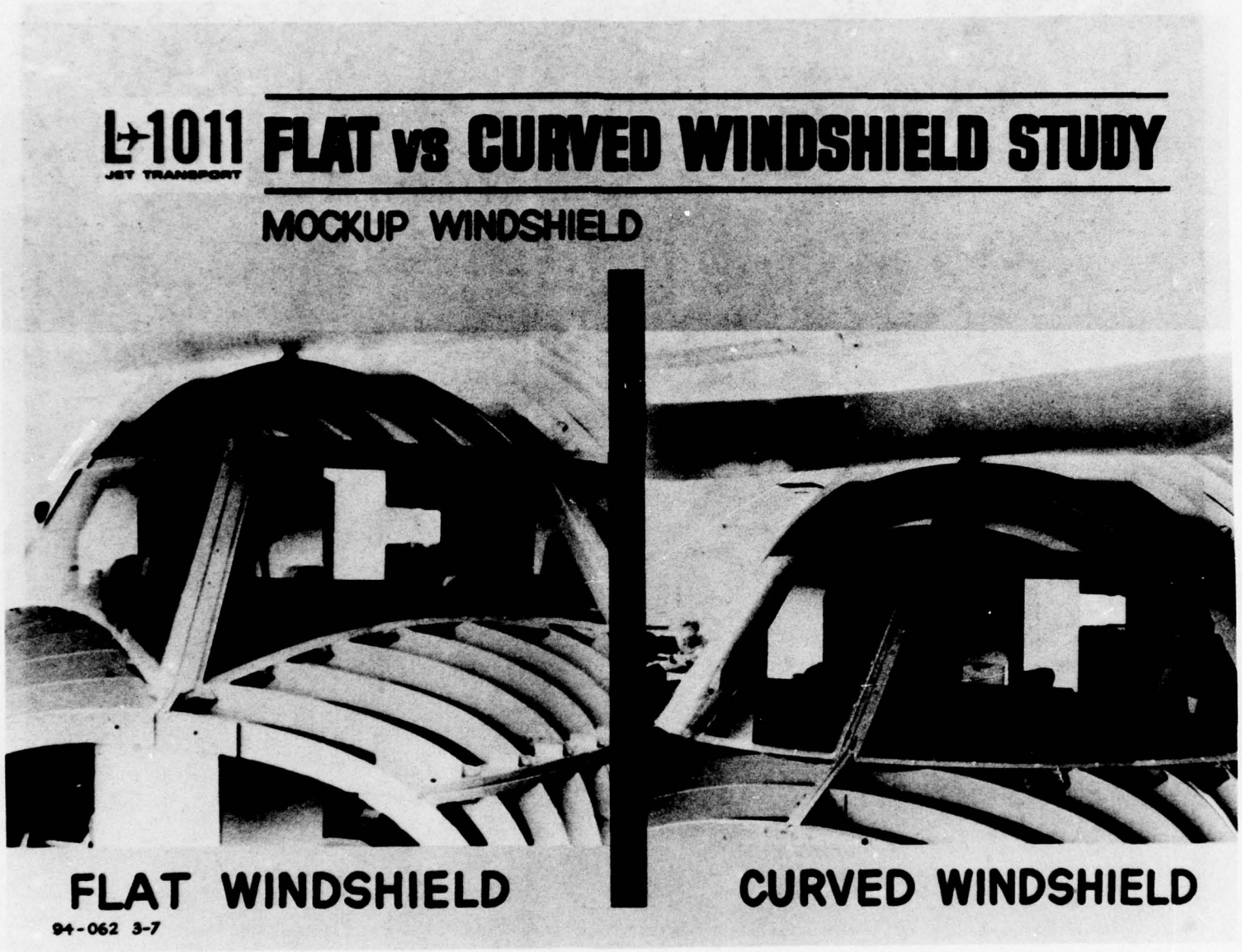


Figure 1. Flat vs Curved Windshield Study — Mockup Windshield

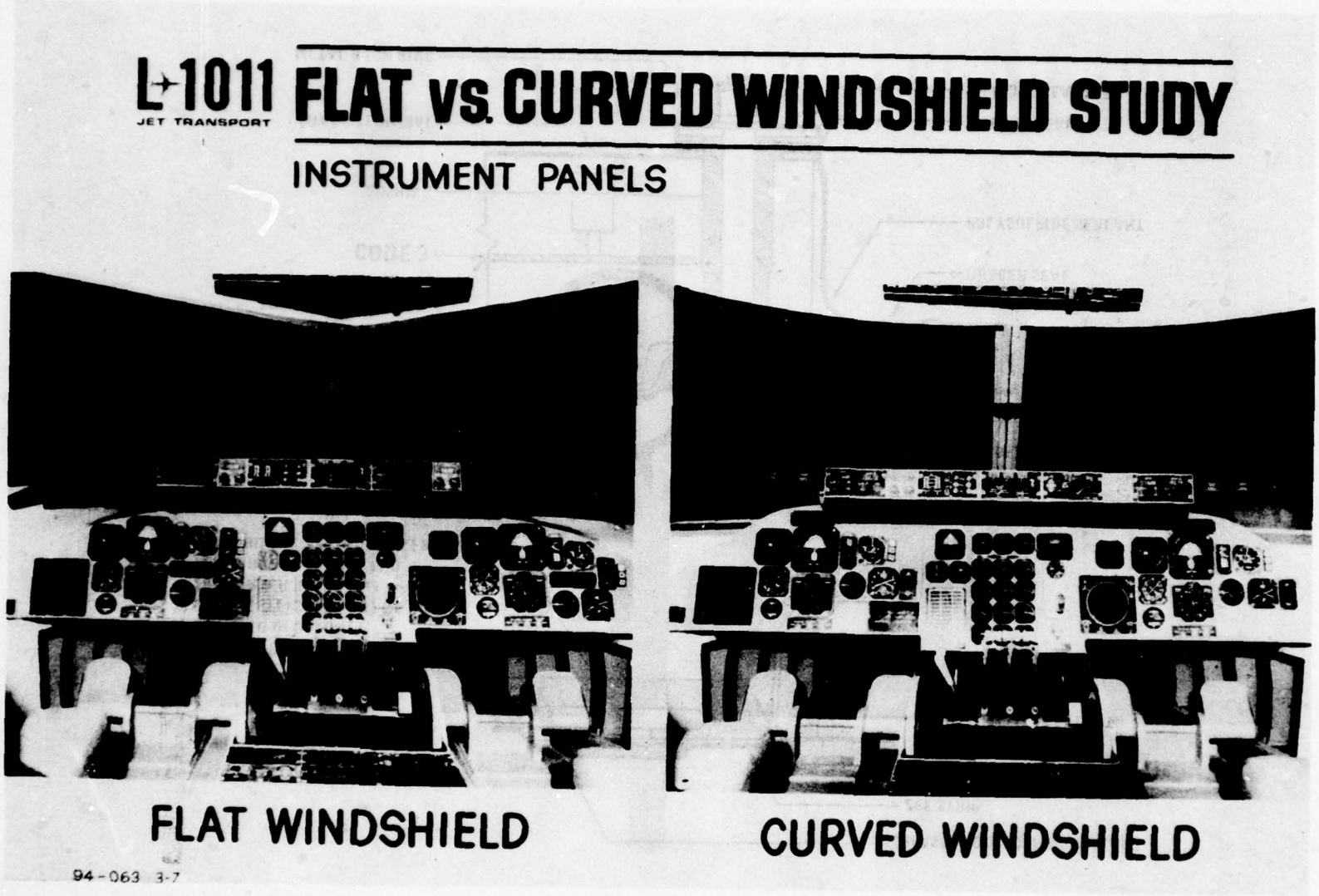


Figure 2. Flat vs Curved Windshield Study — Instrument Panels

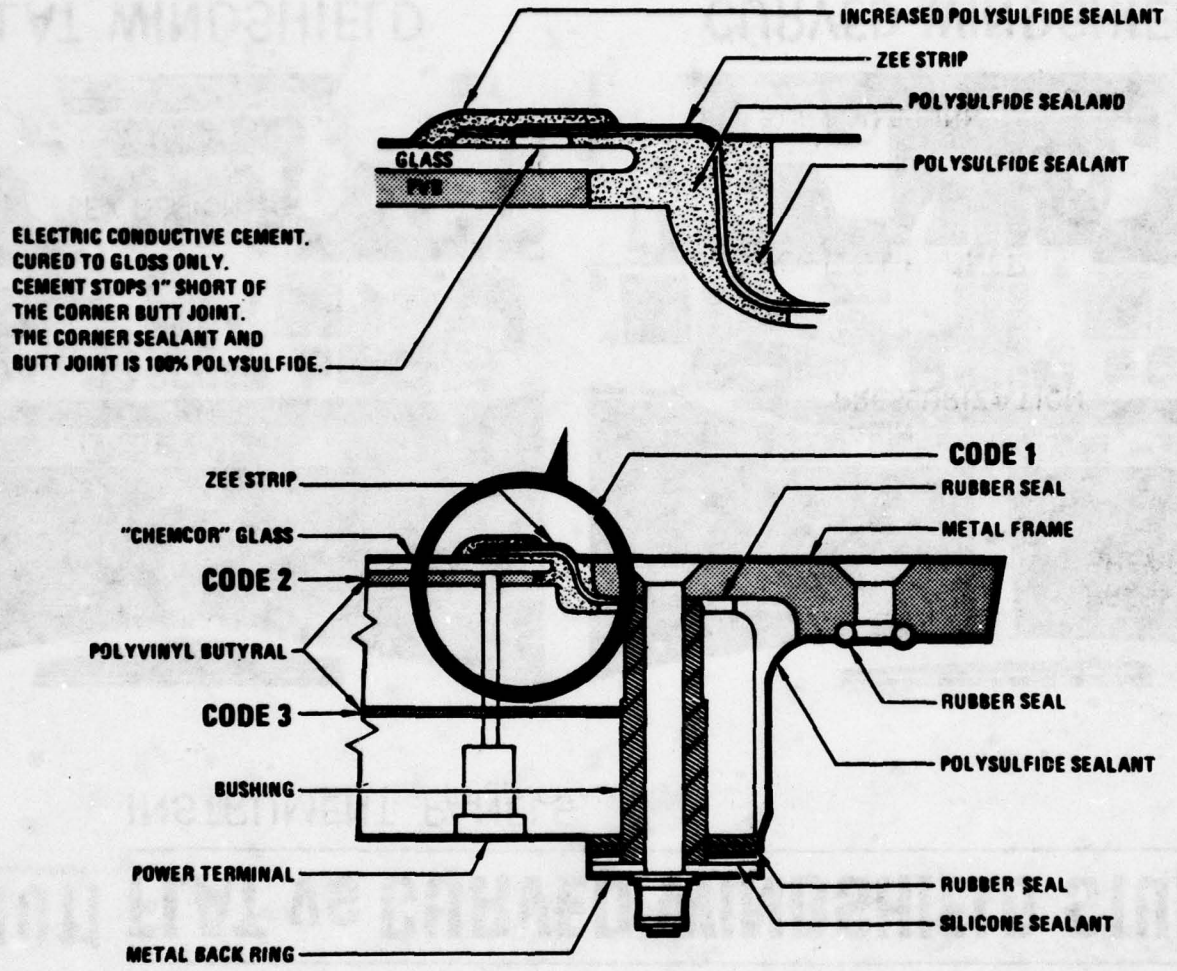


Figure 3. Cross Section Main Windshield Design Detail

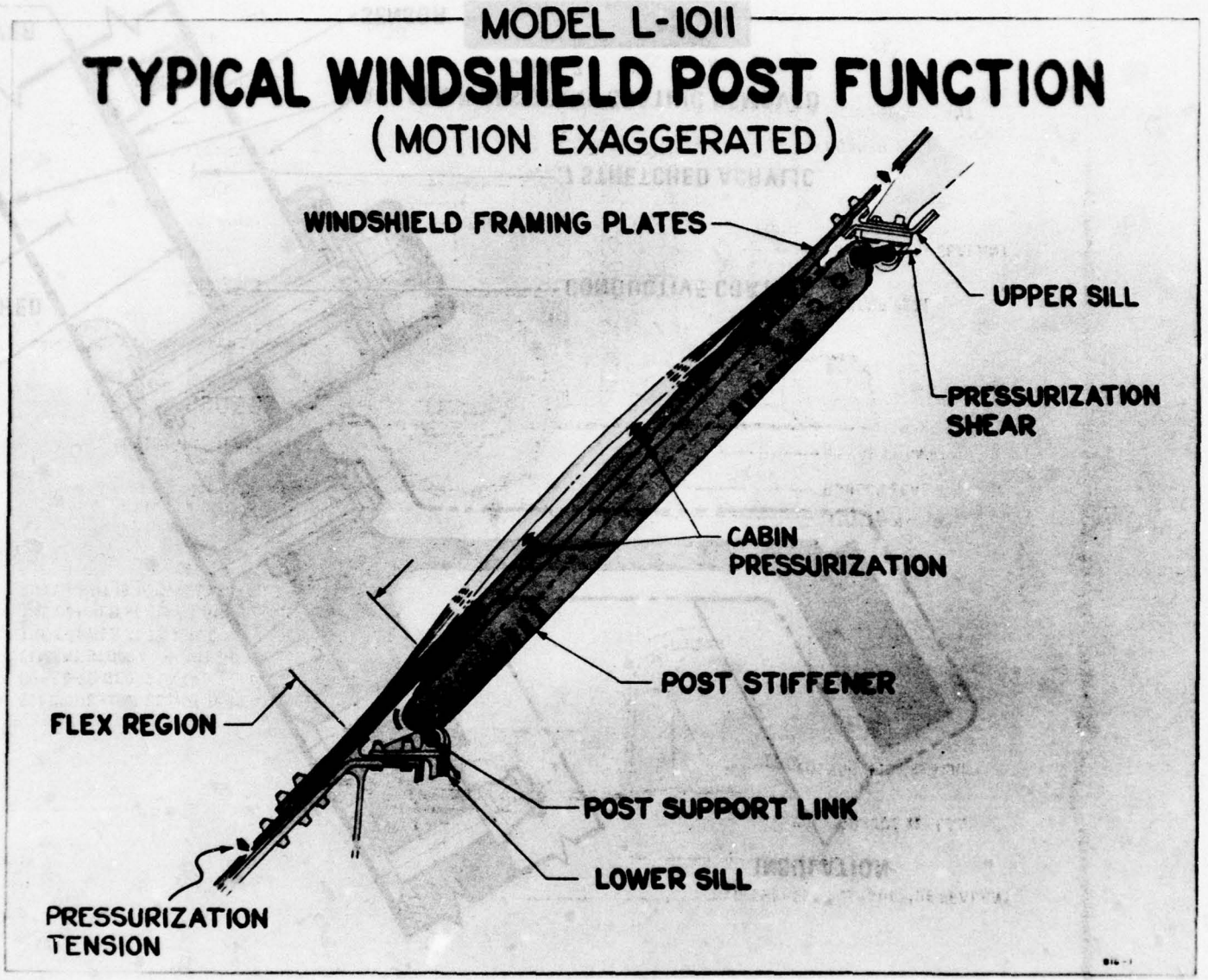


Figure 4. Typical Windshield Post Function

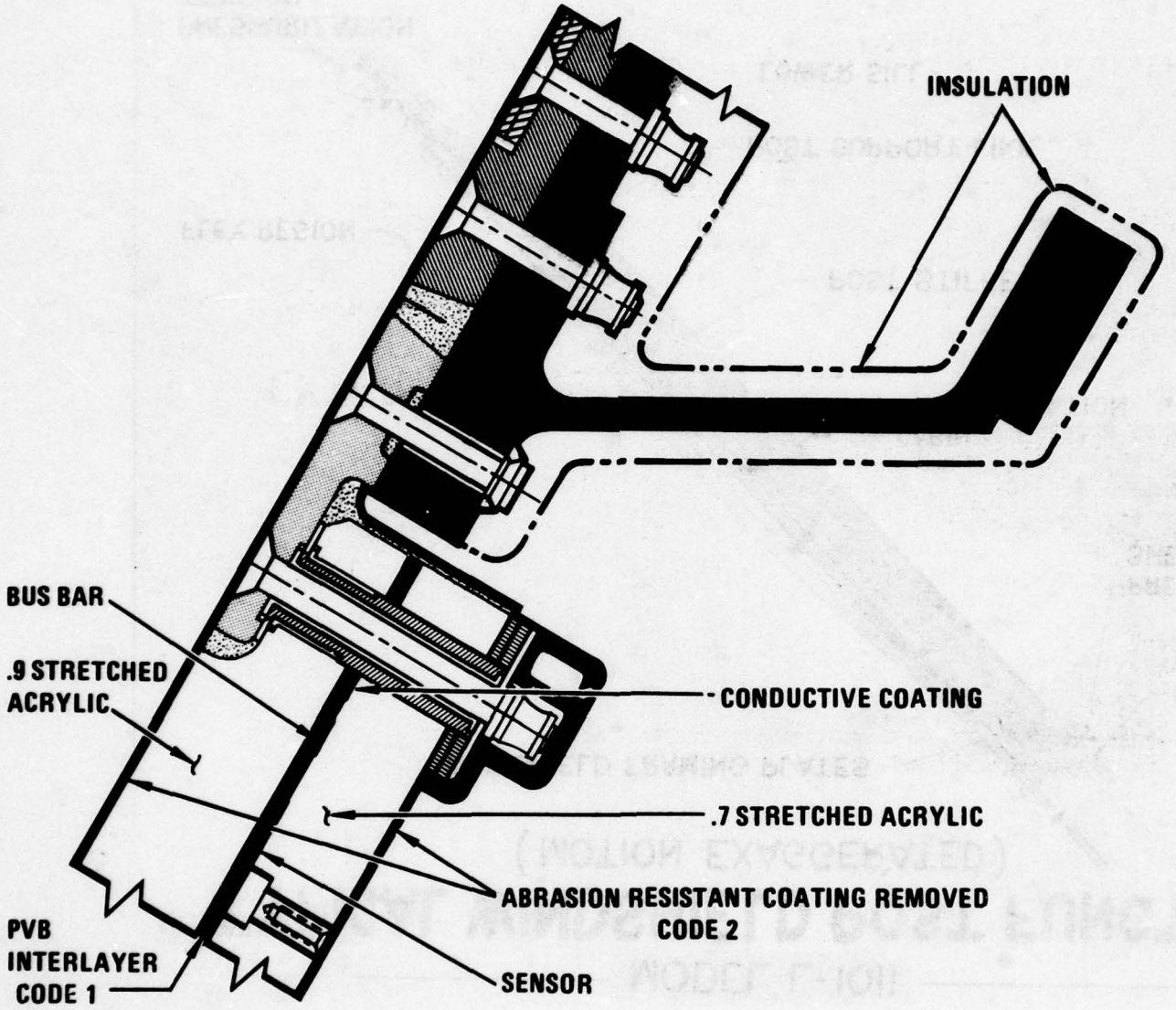


Figure 5. Cross Section — Side Windshield Design Detail

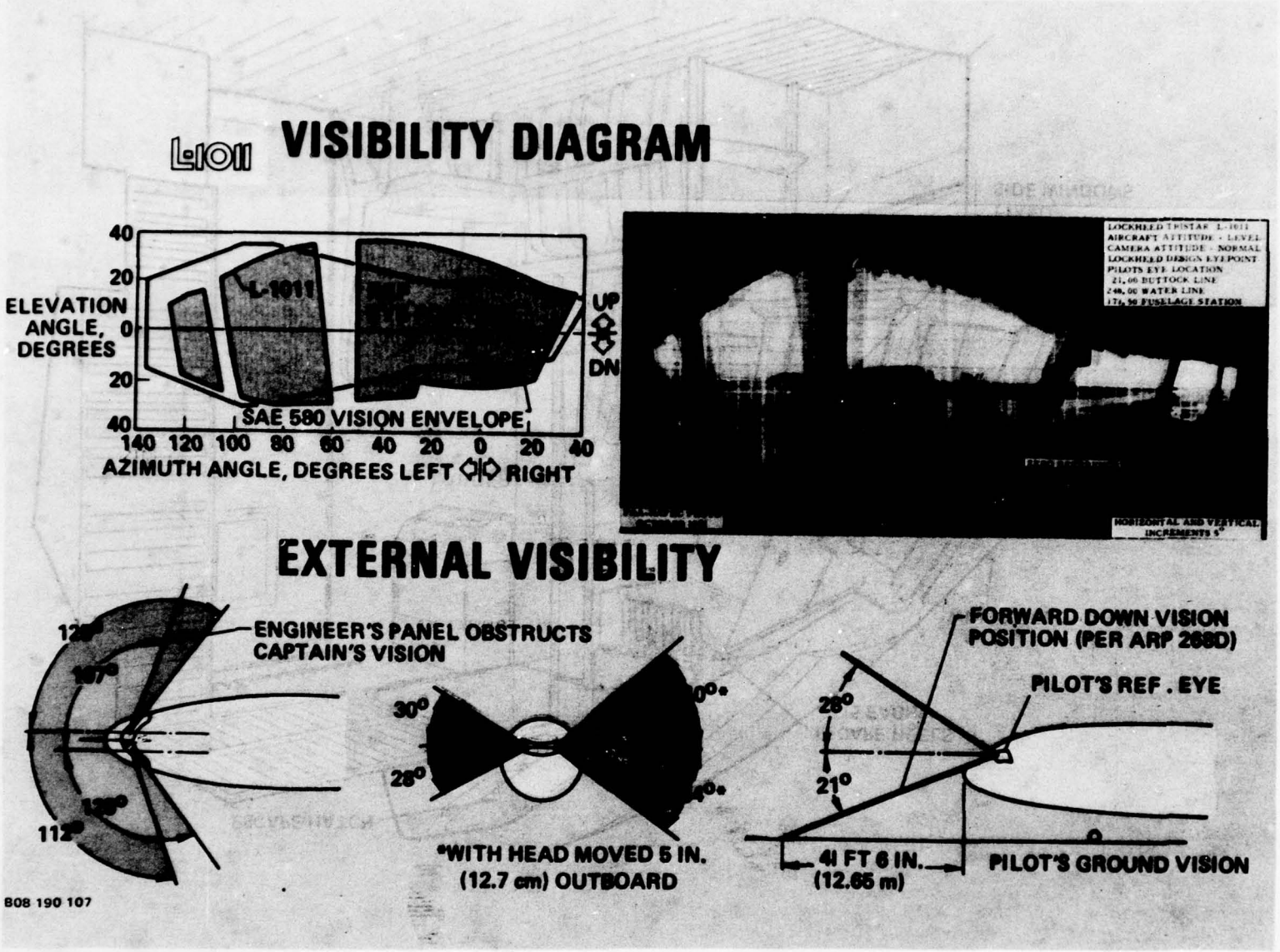


Figure 6. Visibility Diagram

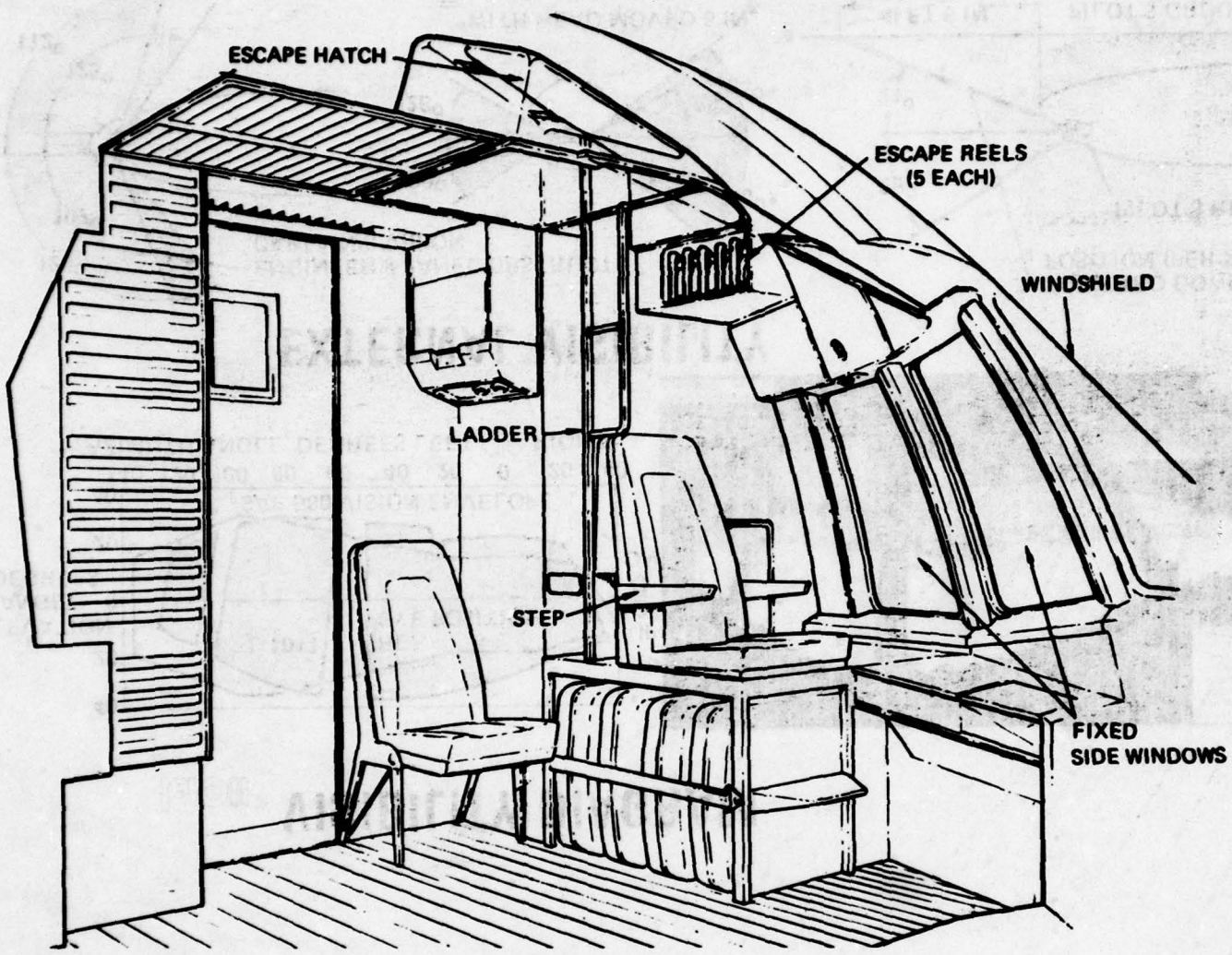


Figure 7. Cockpit Escape System

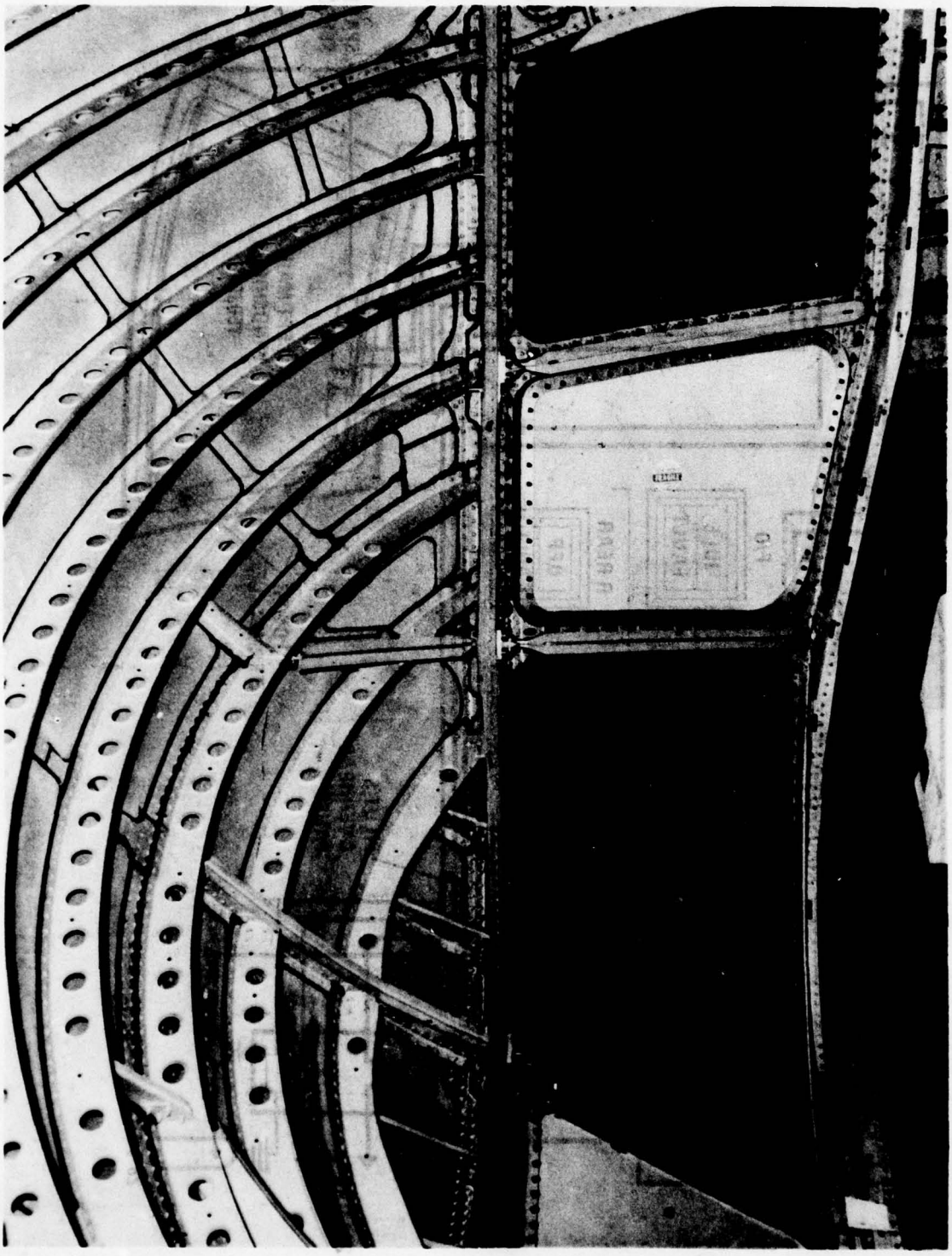


Figure 8. Cab Structure

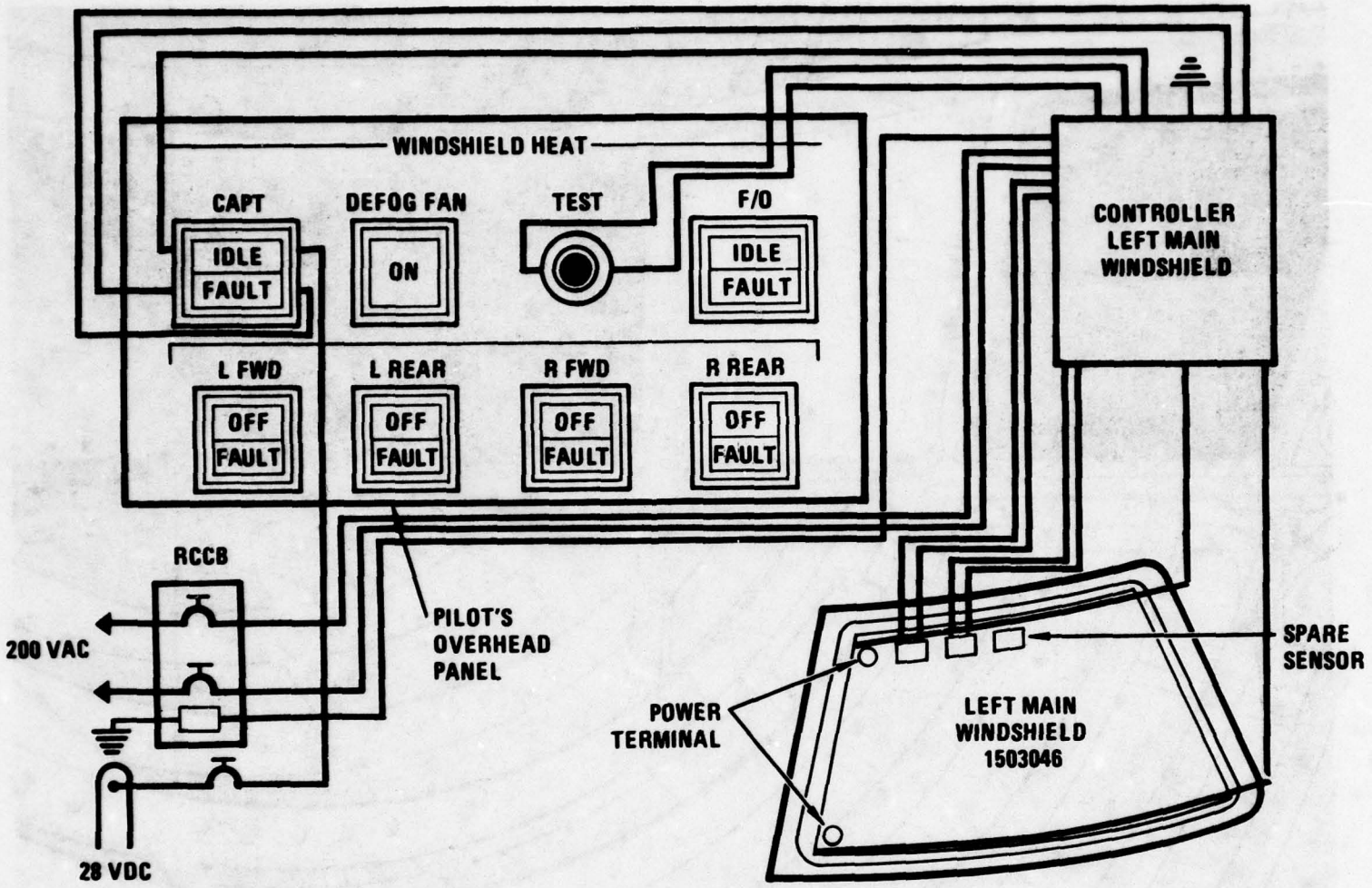


Figure 9. Windshield Heat System

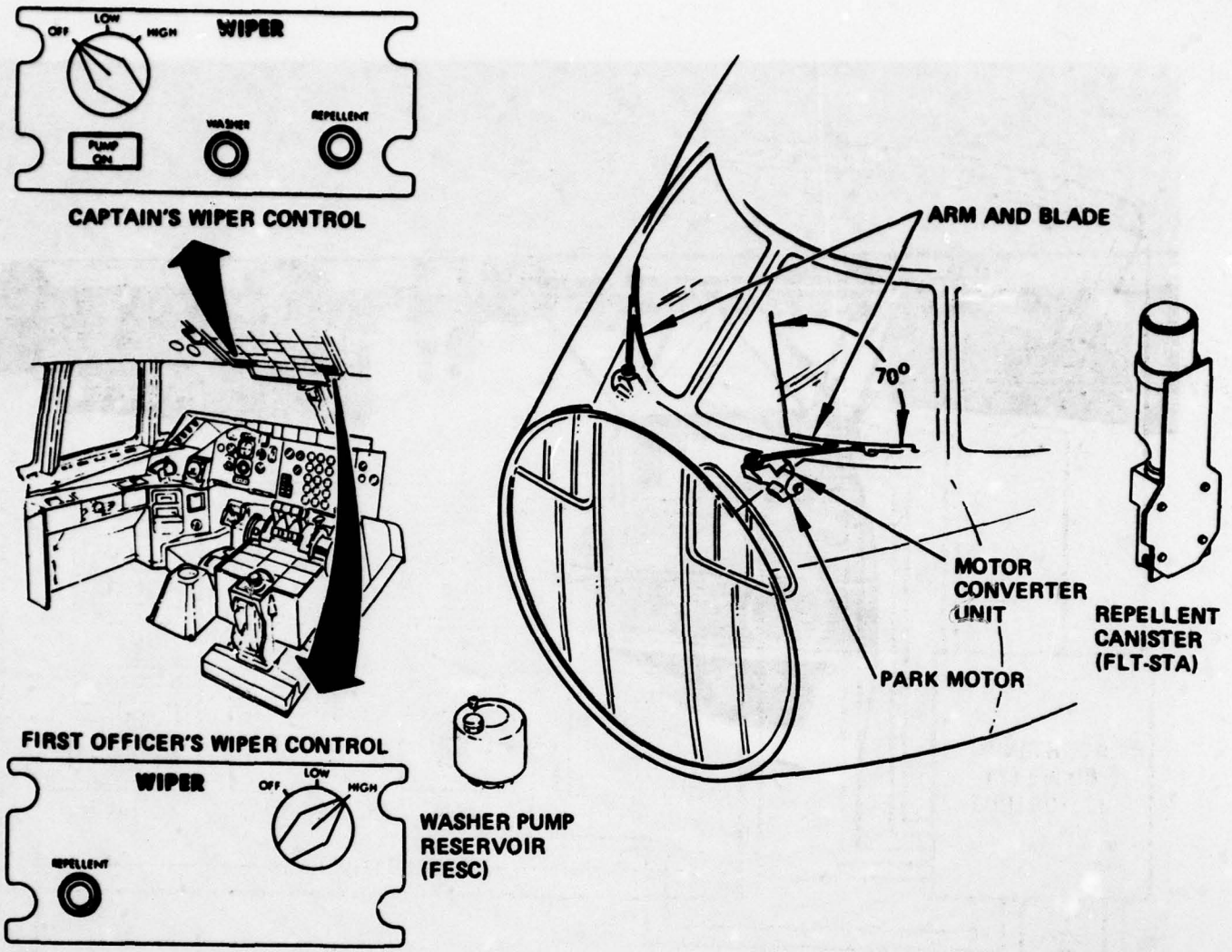


Figure 10. Windshield Rain Protection



Figure 11. Flight Station Lighting Mockup



Figure 12. Bird Test

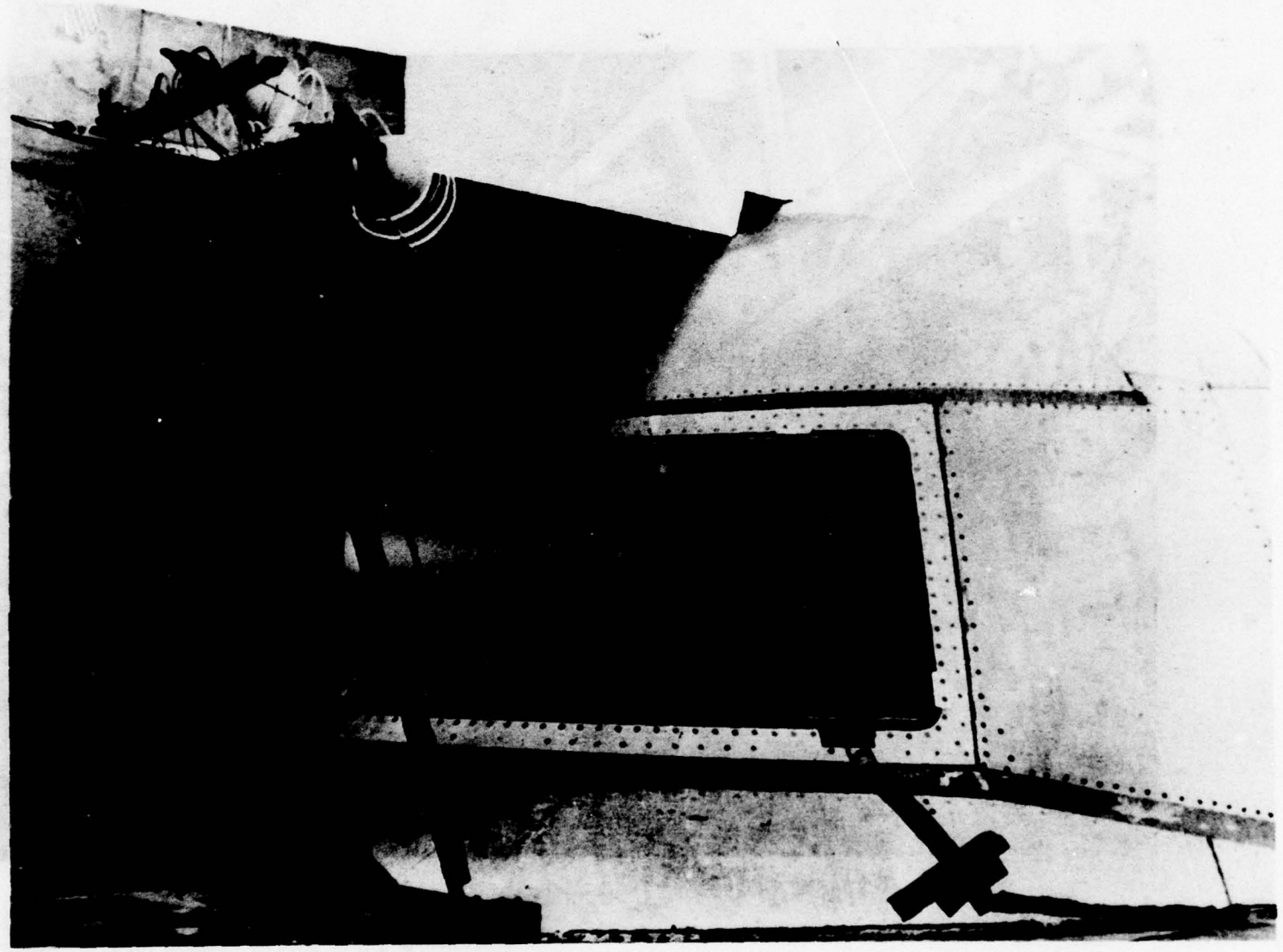


Figure 13. Hail Test Rig

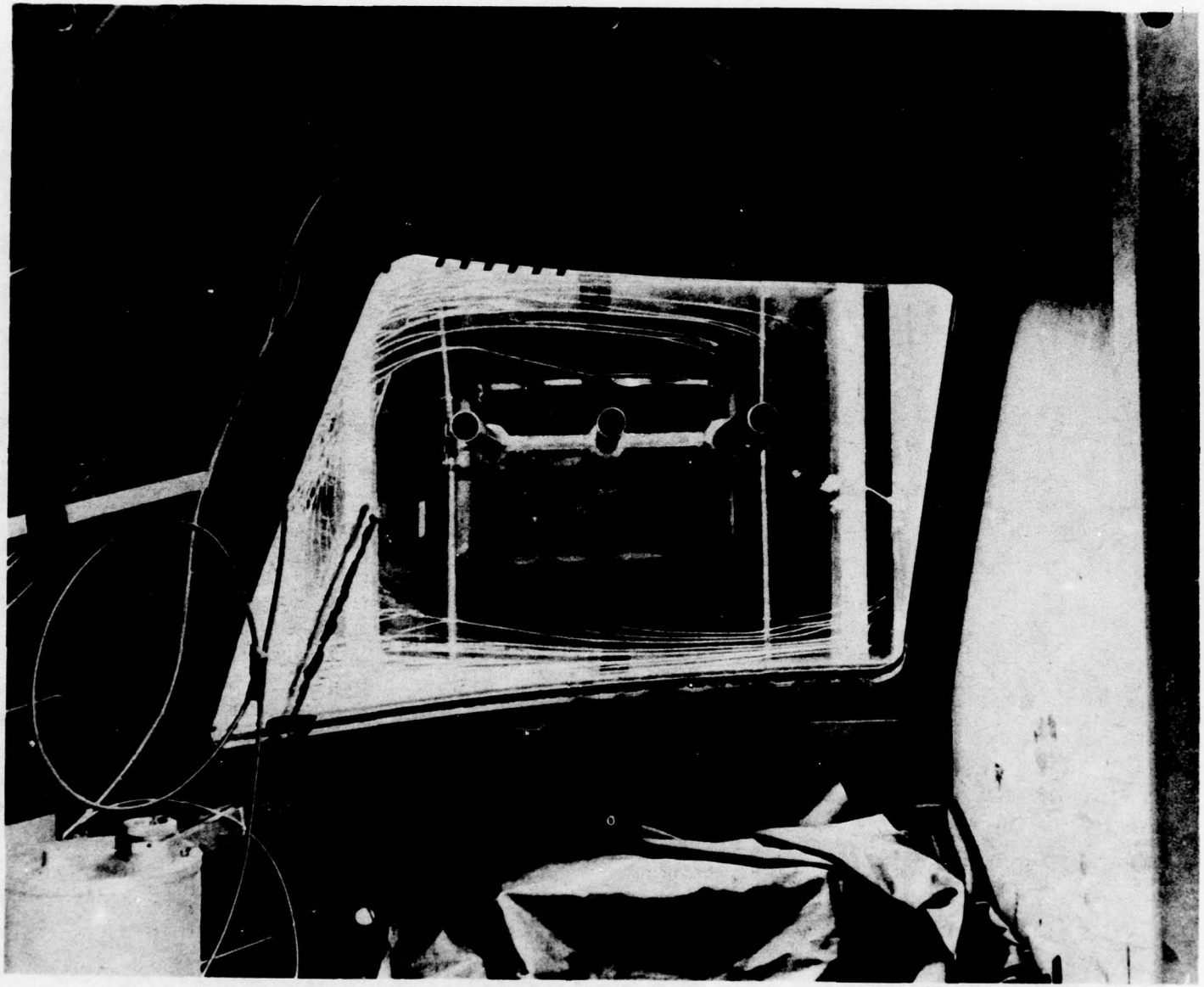


Figure 14. Hail Test - Internal View

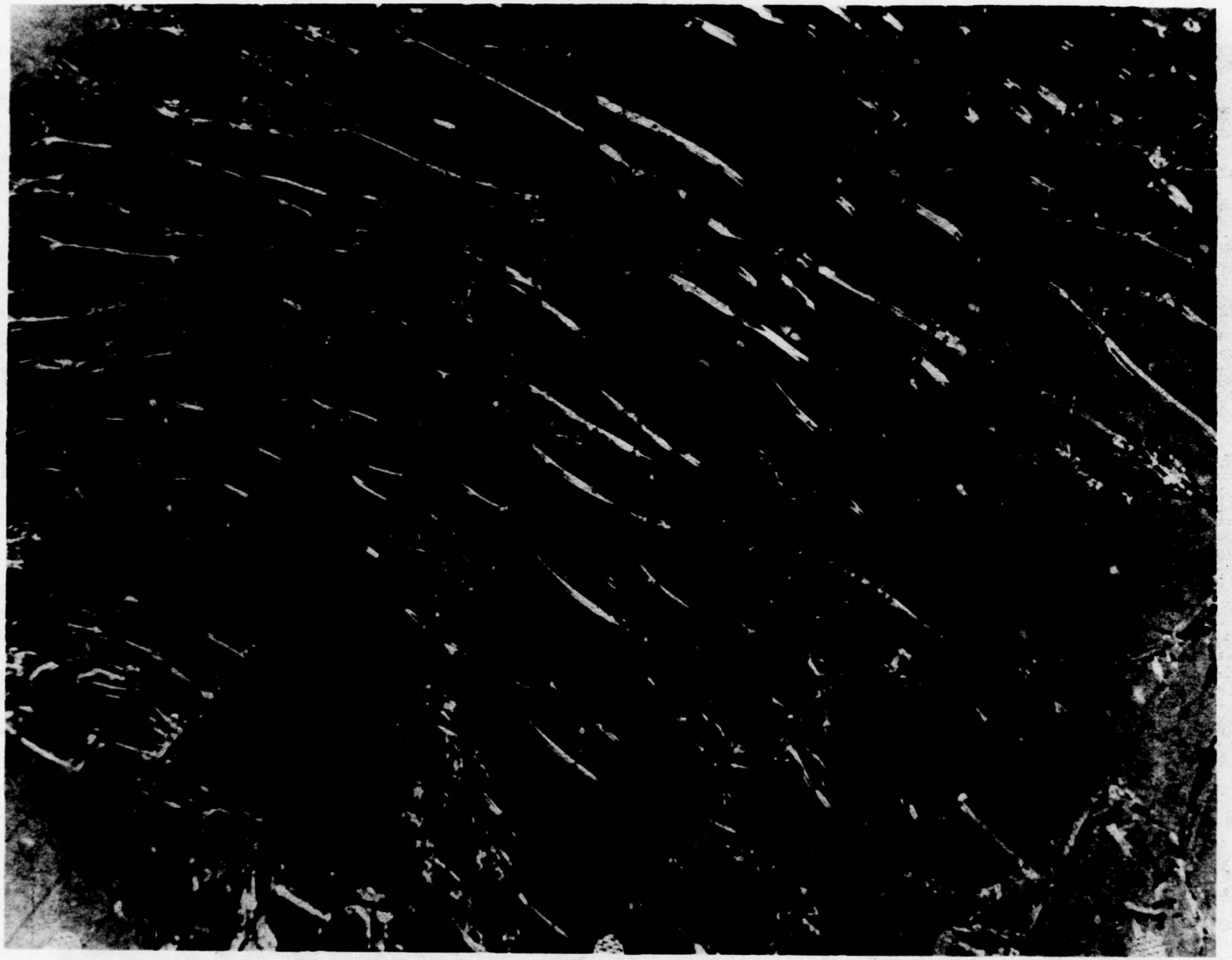


Figure 15. Broken Chemcor

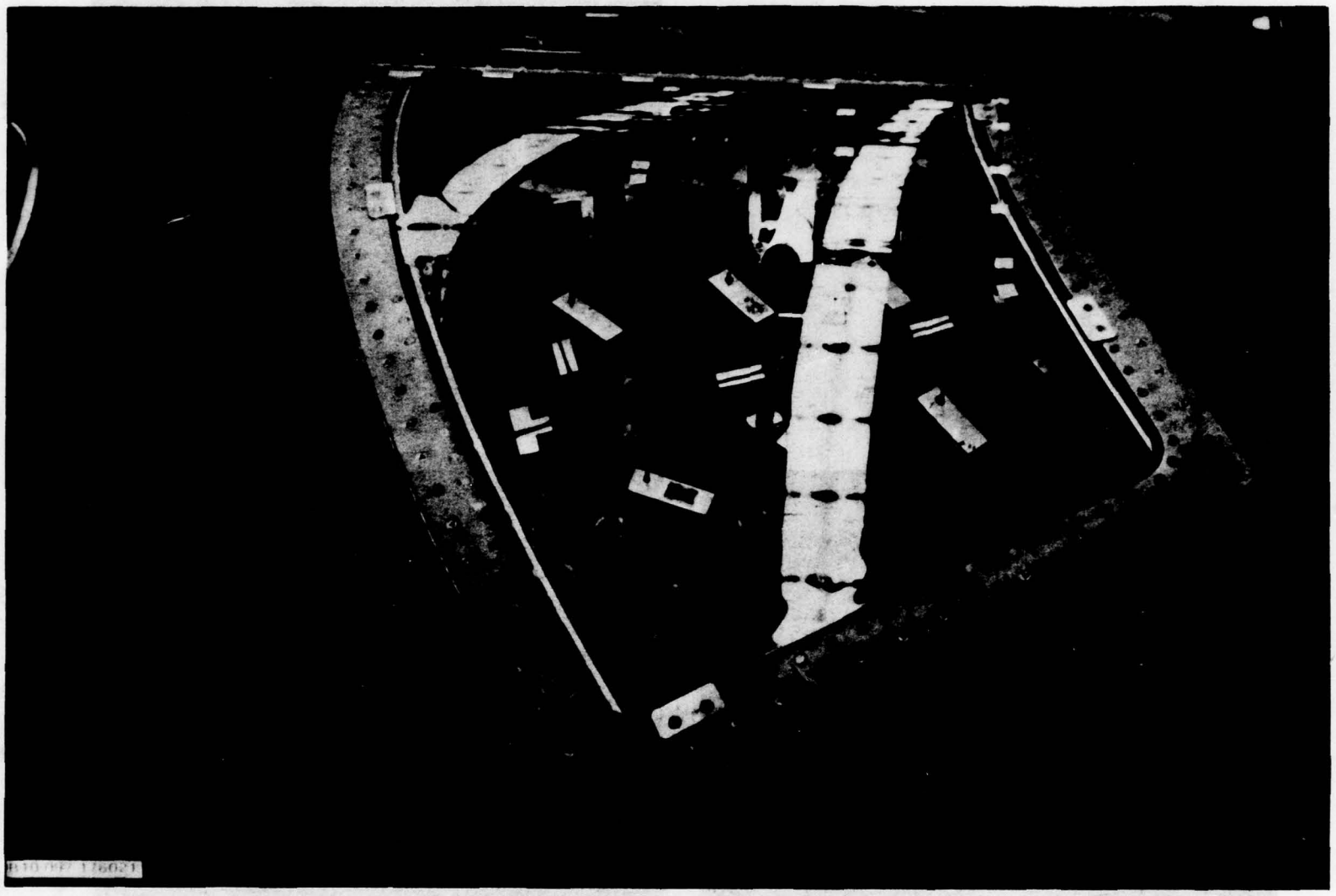
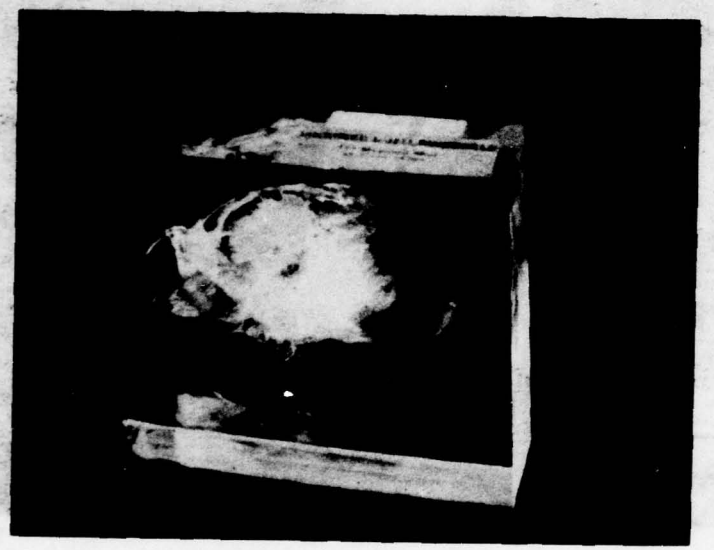


Figure 16. Cycle Test







LOCKHEED L-1011 WINDSHIELD

357 Magnum Shot
at close range

Figure 17. Bullet Impact

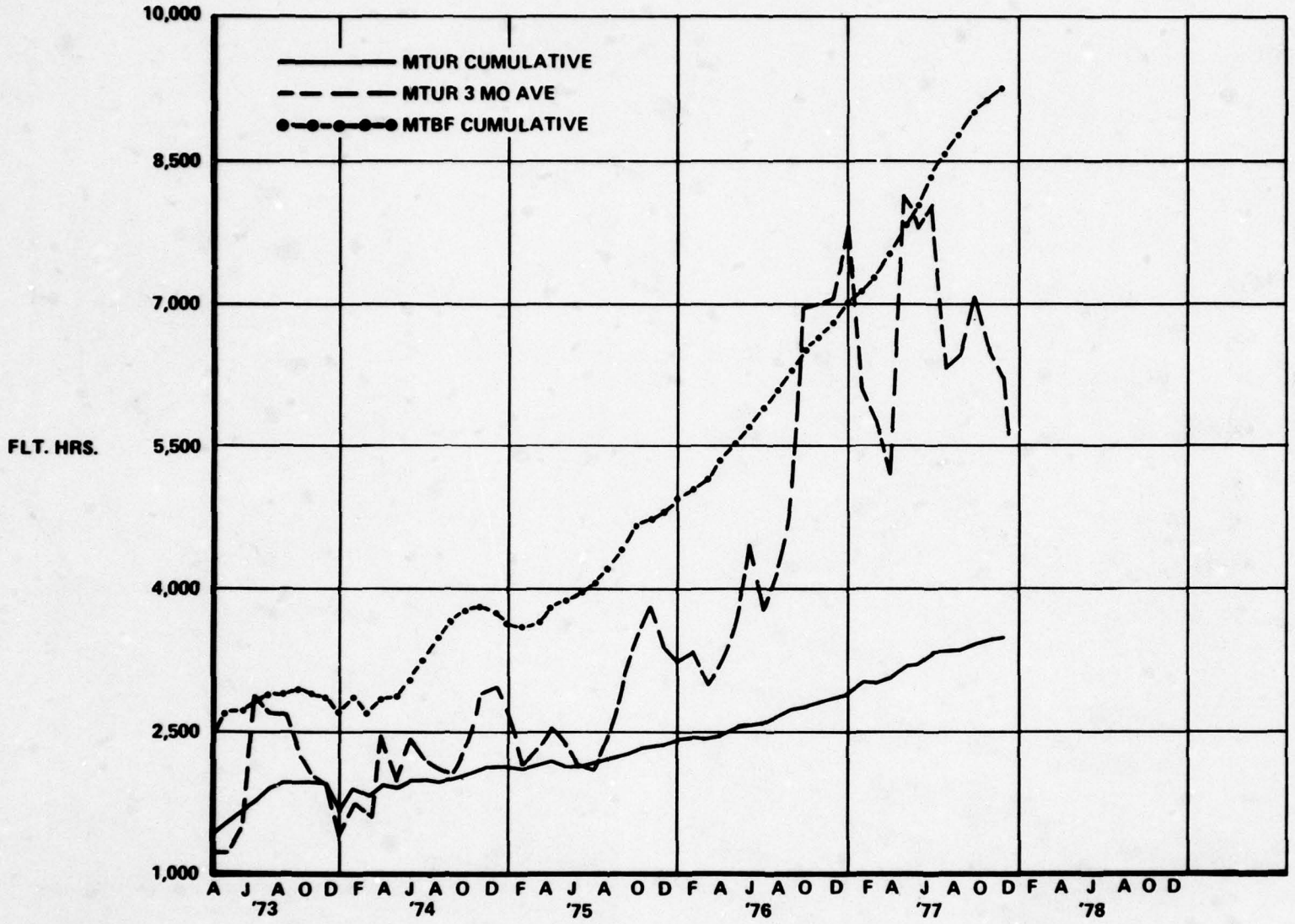


Figure 18. Mean Time-Between Failure/Until Removal

AIRCRAFT TRANSPARENCY FAILURE AND LOGISTICAL COST ANALYSIS

S. Brown
Rockwell International
Los Angeles Division
Los Angeles, California

PRECEDING PAGE BLANK-NOT FILMED

AIRCRAFT TRANSPARENCY FAILURE AND LOGISTICAL COST ANALYSIS

By

Syd Brown

Advanced Design

Engineering Specialties

Rockwell International Los Angeles Division

ABSTRACT

The concern for increasing costs in the maintenance of Transparency Systems has prompted the Air Force Flight Dynamics Laboratory to sponsor this study contract. The objective of this study is to identify the high-cost/high-maintenance transparency components, identify cause of failures, and recommend corrective programs to reduce cost of ownership to the Air Force Logistics Command.

The study involves the review of 20 selected aircraft in current Air Force inventory to establish an intensive data base relating to transparency maintenance activity and associated logistical support costs. During this phase, a collection of detailed design characteristics, methods of construction, test and qualification, and costing information was assembled. From these data, the basis for design improvements is currently being determined.

During the course of this study, field audits of Air Logistic Centers, selected Air Force operational bases, airframe manufacturers, and transparency suppliers were made. Inquiries were made to identify and evaluate the available facilities, maintenance programs and procedures, and testing capabilities. These data, in conjunction with the design characteristics, are being used to determine the impact that aircraft performance, environmental, and weathering factors may have on the failures of transparency components.

The approach used in the identification of candidate improvements is to focus on the high-cost contributors to maintenance and repair. Trade studies will be made to ascertain if significant reductions in life-cycle costs can be achieved.

At the time of the presentation of this paper, the program will be approximately two-thirds complete. Therefore, the findings and conclusions are considered to be preliminary in nature.

PRECEDING PAGE BLANK-NOT FILMED

INTRODUCTION

The Air Force's continued effort to increase the reliability, and reduce the cost of maintaining aircraft transparency systems (windshield, canopies, cabin windows) has prompted the Flight Dynamics Laboratory to sponsor this program. It is directed at surveying the maintenance and installation procedures at the five Air Logistics Centers (ALC's) and eight selected Air Force operational bases for the purpose of identifying the high-cost, high-frequency maintenance items of transparency components for 20 selected aircraft in current Air Force inventory.

This program is an extension of two previous contracts (References 1 and 2) that were conducted to study failure modes, maintenance procedures, and the associated logistical support costs for transparency systems. The extent of the analysis developed in these previous studies was to search historical maintenance and logistical cost records, and categorize the physical transparency characteristics, failure modes, frequency of failures, and costs in a readily identifiable and inclusive statement of the problem.

The intent of this study is to expand the research of the transparency problems in greater depth, identify and recommend changes in maintenance procedures, and recommend design improvements that will reduce failures and cost of maintenance.

BACKGROUND

With continued progress being made in the science of flight technology and the dramatic increase in performance capability of aircraft in current inventory and those being planned for the next generation, the cost of maintaining this equipment is approaching astronomical figures. Current estimates indicate the cost of maintaining the total Air Force fleet is approaching two billion dollars per year. It is for this reason that the Department of Defense is placing greater emphasis on weapon system design-to-cost and life-cycle cost improvements in the area of maintenance and logistical support. An essential part of any aircraft is its transparency system. The large amount of funds being expended on transparency systems is shown in Figure 1.

The annual costs are categorized by aircraft type for the time span of July 1976 through June 1977. The total annual cost of approximately five million dollars is for the 20 study aircraft. If all models in current inventory were included, the annual cost indicated would be significantly higher. To further demonstrate the huge expenditure, a 10 year projection (Figure 2), adjusted for inflation and aircraft attrition, indicates that approximately $68,500,000 will be spent. This estimate does not include other models or the new weapon systems that will be phased in during that time span. The cost data shown in these charts were extracted from (Reference 3) K051 (IROS), "Increased Reliability of Operational Systems."

In view of the large sums being expended in maintaining these transparencies, this study is programmed to develop cost effective design and repair concepts aimed at reducing logistical support costs.

PROGRAM OBJECTIVES

The objective of this study is to develop a program to reduce logistical costs of transparency systems. It will be accomplished by conducting a detailed study of the reliability, maintainability, and logistical support characteristics of 20 study aircraft. The approach will be to:

1. Identify high-cost/high-maintenance system components - A search will be made to determine those components whose reported maintenance has resulted in an unusually high frequency of failure, and resulted in high maintenance costs. This means will be used in selecting the candidates that present the greatest potential in cost reduction.

2. Conduct an in-depth failure analysis - A detailed failure analysis will be conducted to determine the failure modes that are causing the greatest incident rate of maintenance actions. Past records of the DO-56 tracking system network (Reference 4) will be scanned to extract the maintenance information contained in the various data collection programs. These data will be assembled to provide a maintenance history of each component.

3. Define the most significant design parameters affecting cost and reliability of transparency systems - During the searching process, a concentrated effort will be made to identify the design parameters that significantly affect the functional operations of the transparency components or support systems. Special emphasis will be placed on determining the impact on operational cost and reliability.

4. Recommend corrective programs to achieve significant savings in life-cycle costs - Utilizing this analysis, failure causes will be identified and system improvements and recommendation for changes in procedures will be proposed. These proposals will be thoroughly analyzed and, through trade studies, the cost effectivity of these changes will be determined. From these trades, corrective programs that achieve significant savings in life-cycle cost will be recommended to the Air Force.

PROGRAM REQUIREMENTS

The program, as outlined in the contractual Statement of Work (SOW), (Reference 5), is a 16-month study, phased in three tasks as shown in Figure 3. The phased tasks are:

Task I - Collection of data/information
Task II - AFLC field audit of procedures and cost data
Task III - Transparency analysis

Task I, the collection of data and information, provides a baseline of the physical characteristics and design specifics to provide the transparency designer with a means to identify and effect candidate improvements. During this phase, data pertaining to qualification testing and procedures are gathered to support cost trade studies. These data include information to evaluate structural and thermal integrity, reliability, resistance to bird impact, environmental weathering effects, and optical quality factors. The collection of data used as reference material includes the Air Force technical orders that describe the maintenance and repair procedures that are currently in use by both the AFLC and operational bases.

Task II, the field audit of AFLC and selected operational bases, is concurrently accomplished to correlate the actual maintenance activity with maintenance efforts recorded in AFM-66-1 (Maintenance Data Collection System), Reference 6. The previous studies made indicated that descriptive data contained within AFM-66-1 are not always adequate to fully describe the nature and types of failures recorded. The audits were principally structured to provide the supplementary information through a questionnaire submitted prior to visitation to each facility.

Task III is the transparency analysis phase. During this phase, the data collected in Tasks I and II defining the transparency characteristics will be assembled and analyzed to ascertain which design parameters are the most cost effective, and those that are the least cost effective. The data will be categorized by aircraft transparency type, mission and design characteristics, and a determination of the types of failures and relative frequencies will also be established. In addition, a comparison of the reliability and maintainability costs for each aircraft type with the basic design parameters for each transparency will be evaluated. From the foregoing, corrective programs for those transparency systems that are considered to be cost effective will be identified and proposed to the Air Force.

The principal difference between this program and the antecedent programs is that specific design improvements and revisions to existing procedures will be developed upon completion of this study. The suggested changes will be cost effective recommendations that will result in significant reduction in logistical support cost by substantially reducing the failures of transparency components.

STUDY AIRCRAFT

The list of aircraft included in this study is shown in Figure 4. They represent a wide variety of transparency configurations and concepts including laminated glass panels, stretched acrylic, polycarbonates, composite panels, etc.

The sampling of the study aircraft varies from very low speed helicopters to high-performance vehicles such as F-4, F-111, and F-15 fighter-type aircraft. The data on these selected aircraft provide a comprehensive coverage of maintenance problems that are being experienced in operational service.

TRANSPARENCY/SUPPORT SYSTEMS

The definition of transparency systems, as considered in this study, is listed in Figure 5. They include three categories:

1. Transparency components
2. Interactive support systems
3. Support structures

The transparency components consist of the primary elements of windshield panel assemblies, canopy transparency and frame assemblies, and cabin windows. The Interactive Support Systems include only the major components of the subsystem. For example, sensors, bus bars, controllers, and toggle switches for anti-icing systems; integral and adjacent ducts, diffusers and control valves for defogging; actuators, links, and latches are included. Ancillary items such as wiring, switches, tubing, etc, are not included. Support structure considers only those members that form an edge member, adjacent contact with edge member, or part of a frame assembly.

EVALUATION PROCESS

The normal approach utilized in a maintenance-type study is to conduct a reliability type analysis that is keyed to frequency of failures with interactive review of maintainability, logistics, and cost. In view of the Air Force-demonstrated concern for cost, this program focuses on the identification of high-cost contributors with interactive review of maintainability, reliability (frequenct of failures), and logistics. The end results of both approaches are essentially the same. However, the selected approach will result in a quicker identification of problems for achieving the stated objectives.

Figure 6 diagrams the steps utilized in developing a detailed failure analysis and identification of candidate improvements. Logistical support cost, ranked by work unit code, is inserted into the Maintenance Analysis Model (MAM) program (Reference 7). At the same time, maintenance data from AFM-66-1, Maintenance Data Collection System (MDCS), (Reference 7), are inputed into the MAMS program. The output results in a tabulation of How Malfunctioned, When Discovered, Action Taken, Maintenance Man-Hours, Flight Hours, and Logistical Costs for each selected work-unit code. Figure 7 is a sample page of the print-out format of the Maintenance Actions and various Parameters used to identify and determine failure modes. The MAM's printout

will vary from 30 to 200 pages of print-out, depending on the complexity of the transparency configuration.

When failure modes as extracted from AFM-66-1 are inadequate, alternate data sources from field audit trip notes and collected reference material are used to supplement the analysis, and it is from this array of data that candidate items are established.

CANDIDATE IMPROVEMENT SELECTION CRITERIA

The decision to proceed with a cost trade study, or to document and file the study results, is determined by the following considerations:

1. Study aircraft will be in Air Force for at least 10 more years
2. Design improvement will achieve substantial reduction in annual maintenance costs
3. Design improvement will pay for itself within 3 years of implementation (goal)
4. Design improvement will achieve a significant saving in life-cycle cost over a 10-year period

If one or more of Items 2 through 4 appear to be achievable, a trade study will be implemented to ascertain the estimated cost saving of the proposed changes.

COST-EFFECTIVE TRADE STUDY

Having determined the candidate improvements, the task of meeting the selection criteria must be verified. In order to ensure that the proposed changes are viable, a valid cost comparison representing the existing maintenance effort and the cost estimated for the revised concepts or approaches will be made. The current costs and procedures must be carefully examined to factor inflationary cost increases, aircraft attrition rates, and to correct discrepant inputs that inadvertently find their way into the maintenance tracking system. This will be accomplished by correlating collected field audit data with the information gained through verification calls with field audit contacts.

The assessments of the proposed changes will account for both the nonrecurring development costs and the recurring manufacturing costs, and costs associated with the modification effort. Care will be exercised to account for the developmental and specialized testing and requalification noted in Figure 8.

If the trade studies based on a comparable time span result in reduced maintenance and reduced cost, the proposed changes in design or in procedure will be recommended for incorporation into the appropriate weapon system.

CURRENT MAINTENANCE PROBLEMS

During the field audit surveys, many discussions were held with maintenance personnel to evaluate procedures and to identify available facilities and testing capabilities. These people were also asked to relate their experiences in the inspection, repair, and replacement of transparencies, and to describe the impact of environmental and weathering factors that contribute to the recorded failures.

The following is a collection of the most common maintenance problems:

1. Sealants and aero smoothing - One universal complaint of the operational bases was the long sealant cure time required after replacement of windshields or canopies. Depending on the sealant material and the transparency installation, approximately 24 to 72 hours of cure time are required. A great deal of pressure is imposed on maintenance personnel to return aircraft to flight status sooner.

2. Scratching/crazing/delaminations - These are the most prevalent complaints of flight crews regarding the optical qualities of transparencies. When a squawk is registered, Quality Control will review Technical Order Manual criteria to ascertain if replacement of the component is required. In instances where these criteria fall within a grey area, and a decision for replacement is judgemental, a flight test crew will be consulted to determine final disposition.

3. Moisture penetration of transparent panels - The onset of peripheral delaminations is generally caused by moisture penetration of the edge members. Since this type of delamination is most prevalent, maintenance people believe that improved edge attachment member sealing would greatly reduce this type of failure.

4. Transparency cracks - These are principally caused by stress concentrations due to the misalignment of holes in the transparent panel and edge attachment members. In the cases where replacement panels are back-drilled to ensure proper alignment, the drilling process will sometimes cause local stress risers. Improvements in these areas are needed.

5. Electrical anti-icing systems - In many aircraft with this type of system, the activation of deicing operation is initiated by a simple three-position toggle switch. Under adverse conditions, an overtemperature condition may result and cause cracking of the outer ply. This problem is also attributed to faulty controllers and temperature sensing devices. The unanimous opinion of people in the field is that significant reduction in maintenance man-hours can be achieved by design improvement of these items.

6. Canopy rigging and alignment - The replacement of canopy type transparencies is the cause of an extremely large expenditure of man-hours. The problem is one of adjusting to a wide range of tolerances when the canopy assembly is removed from aircraft for rework. To maintain proper interface with position of the windshield arch and its hinging and attaching points, a complicated series of measurements are made to accomplish proper fit. In some aircraft, this procedure is so difficult that canopies must be sent to the depot where tooling fixtures, accurate enough to control tolerances, are available. This operation is, of course, costly in man-hours and time required for handling and logistics stocking.

7. Fastener attachment - The replacement of transparent assemblies is often complicated by a large variety of types and sizes of fasteners. In many windshield configurations, access to the attachment fasteners, particularly the lower row, is severely restricted. Consequently, selection of appropriate fasteners could reduce installation time and problems.

8. Access to windshield panels - In some aircraft, access to windshields requires the removal of instrument glare shields and associated wiring and plumbing. One aircraft also requires the cutting of electrical wire bundles to complete the removal of the shield assembly. In some fighter aircraft, access to the instrument area is most easily achieved through the removal of windshield side panels. It was suggested that quick-type disconnects be incorporated to ease the removal of glare shields.

The complaints, as noted in the foregoing, are a portion of the problems that are being assembled and reviewed during the Task II analysis phase.

TRANSPARENCY SYSTEM COMPARISON

One of the objectives of this study is to examine each aircraft model or category to determine and document the differences, if any, in transparency configuration. Figure 9 represents a very brief summary of some data that were collected and are being assembled, to show the relationship that some of the most commonly accepted maintenance parameters have with the various transparency concepts. Examination of these data appears to indicate that there is a characteristic range of values that is predictable and can be associated with the different type aircraft. A most important consideration in the assembly of this information is to establish a data base for predicting probable maintenance problems. With the availability of this type of information, the problems presently being experienced may be significantly reduced in the design of the next-generation aircraft.

FAILURE ANALYSIS

The program described is still in the stage of being implemented. At this time, the effort has progressed to the Task III analysis phase, so, hard and factual results are not yet available. Since this phase is the principal difference between this study and the preceding studies, a preliminary analysis is presented. It is provided for the purpose of demonstrating the type of evaluation and study results that are anticipated.

A number of transparency systems included in the study group, such as the B-52, KC-135, C-5, etc, contain wind-shields constructed of glass and PVB laminates. These windshields also include electrical type anti-icing systems having similar temperature controllers and sensing devices. Examination of the AFM-66-1 maintenance data indicates a great deal of similarity in the reported failure modes. Thus, an example analysis applicable to this family of transparencies is presented. Figure 10 lists the components affected and the failure modes extracted from AFM-66-1.

Following the steps outlined in Figure 6 (the evaluation process), the KC-135 series was selected on the basis of being a high-cost contributor, and having a high-frequency failure in items previously mentioned. Figure 10 (failure analysis), lists the components affected, the mode of failure, and the possible candidate improvements. The listed candidate improvements must be cost traded to ascertain if the suggested changes warrant consideration.

PRELIMINARY TRADE STUDY RESULTS

Using the methods previously described (figure 8), projections were made to determine the KC-135A costs for field maintenance, special repairs, packaging and shipping, and spares support for the 1978-88 timespan. Examination of failure analysis of those aircraft reviewed to date indicates that correction factors of 1.5 to 2.5 must be applied to the reported K051 values. These corrections are necessary to account for the inaccuracies in the reporting methods and for the empirical adjustments made in the calculations of K051 data. The expenditures for field maintenance and spares were accordingly adjusted. The projections were estimated by the application of escalation factors that account for the inflationary trend to the 1977 maintenance costs. The escalation factors were obtained from AFR-173-10, volume 1, USAF Cost and Planning Factors (reference 8). The factor to update from 1976-77 to 1978 is 1.1587, and from 1978 to mid-1983 is 1.225. In combination, the escalation factor is 1.419. Figure 11 depicts, in building block form, the total costs projected for the 10-year timespan from 1978-88 for existing concept.

Field maintenance	$ 8,859,000
Special repairs and shipping	150,000
Spares support	14,776,000
Total projected KC-135A 10-year maintenance cost	$23,785,000

The candidate design improvements, as listed in Figure 10, suggest that some limited amount of redesign of windshield panels, to minimize the thermal gradient problems, would be beneficial. These changes include alteration of ply thickness, change to a more flexible interlayer to improve adhesion, and edge-member revision to reduce moisture penetration. Since the basic concept is being retained, it is assumed that a minimal number of bird-strike shots will be required, and that a reasonable portion of requalification can be accomplished by the analytical process on the basis of similarity of design.

Another high-cost contributor identified was the anti-icing system. The suggested improvement is to incorporate a modern solid-state device for increasing the reliability of temperature control. A parallel approach is to improve the warning devices to preclude over-temperature conditions. The desired result is to achieve a time-delay sensitive enough to prevent thermal shock in adverse temperature extremes. The costs estimated for these items were based on Rockwell's experience with the T-39A Controller Modernization Program.

The estimated cost for the nonrecurring development effort is $400,000. This estimate is based on engineering man-hours and allowances discrete tasks, as shown in Figure 8. The estimate for the recurring procurement, fabrication, and installation phase is $9,544,000. This estimate is based on a fleet retrofit using field modification kits and accounts for manufacture, installation, and specialized services and equipment.

Although the suggested design improvements are being incorporated to reduce this problem, some continued maintenance must be expected for the revised concept. To ensure that a valid trade is realized, the criteria for the determination of the expected field maintenance effort and required spares support was conservatively estimated. For this example, the mean time between failures (MTBF) was increased by 100 percent. Considering the corrective improvements, the selected MTBF percentage is considered to be achievable.

Referring to Figure 11, the replacement costs and the projected 10-year allowance for field maintenance and spares support are:

Replacement cost	$ 9,944,000
Field maintenance	3,612,000
Spares support	3,879,000
Total replacement and projected 10-year maintenance cost:	$17,435,000

The results of this comparison indicate a reduction of $6,350,000 in existing maintenance cost can be realized. Consequently, it will be recommended that the candidate changes listed in Figure 10 be considered for incorporation in the KC-135A series aircraft.

CONCLUSIONS

The data assembled in this study to date and the data collected from previous studies, conclusively indicate that significant savings are possible in the expense of maintaining current inventory transparencies. Although these statistics and trends have been recognized in previous years, the potential benefits of improved design concepts have not been fully recognized in terms of total life-cycle costs.

Having identified the problems and associated costs, the obvious steps are to develop ways of negating these trends. During the course of this program, Rockwell has reviewed data collected from both Air Force and industry, and has established a logical and systematic approach to identify, assess, and analyze a solution that can reverse these trends.

It is believed that viable and practical solutions to a number of these problems will be available at the conclusion of this program. Another important benefit to be realized will be transparency design criteria that can be implemented in the next-generation weapon systems.

REFERENCES

1. J. H. Carlson, "Windshield/Canopy/Support Structure (WCSS) Life Cycle Cost and Failure Analysis," AFFDL-TR-75-115, September 1975

2. C. S. King, "Windshield/Canopy Cost and Failure Analysis," UDRI-TR-76-69, October 1976

3. IROS, "Increased Reliability of Operational Systems," K051

4. Department of the Air Force, "Product Performance System (D056)," AFLCM 171-45, April 1971

5. Air Force Contract F33615-77-C-3060, Part II, Section F of the Schedule, Description/Specification, 20 April 1977

6. MDCS, "Maintenance Data Collection System," AFM-66-1

7. MAMS, "Maintenance Analysis Model Program," Rockwell International, Los Angeles Division

8. USAF Cost and Planning Factors, AFR-173-110, Vol 1, 6 February 1975

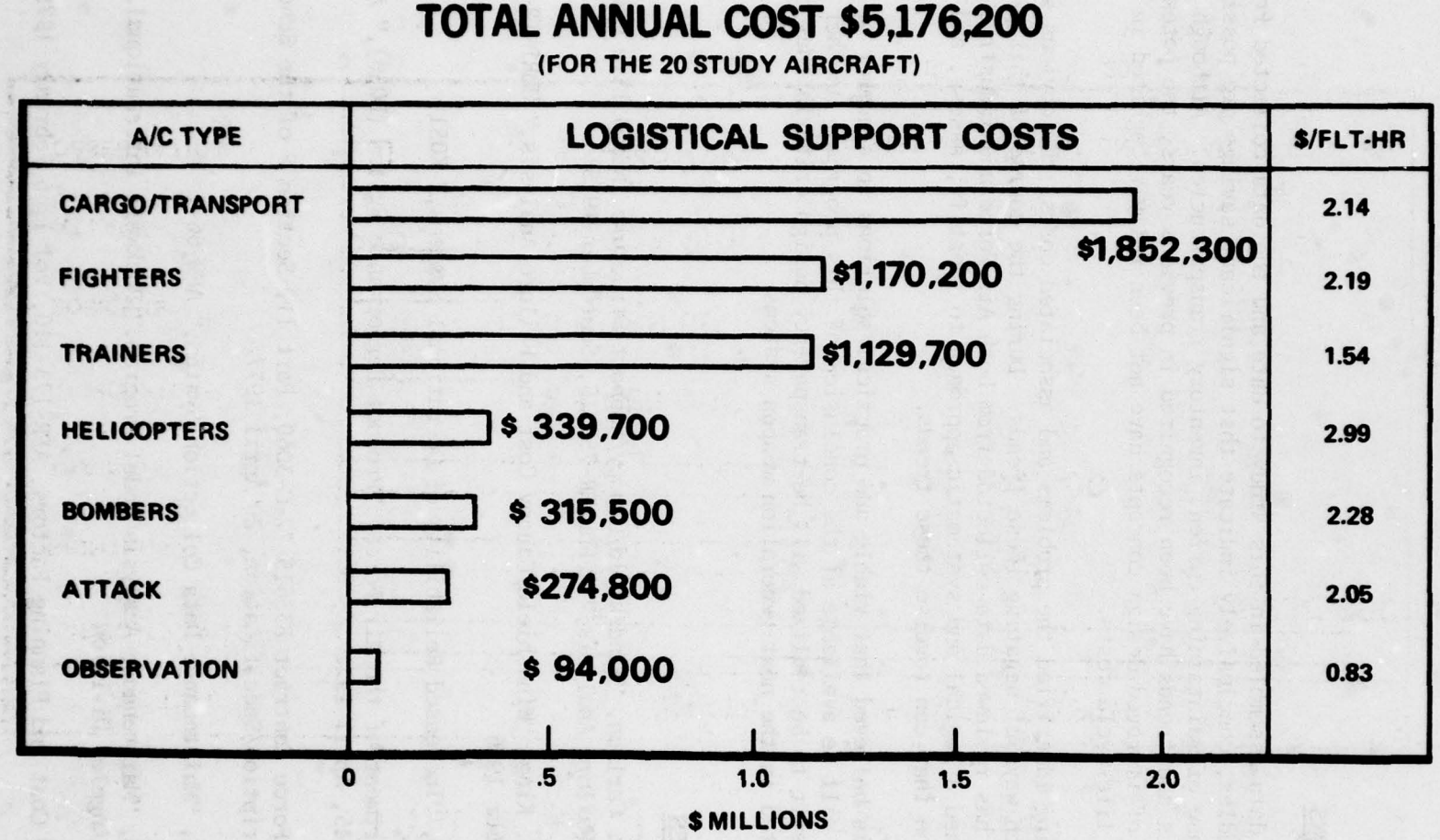


Figure 1. Annual Maintenance Cost in 1977 Dollars

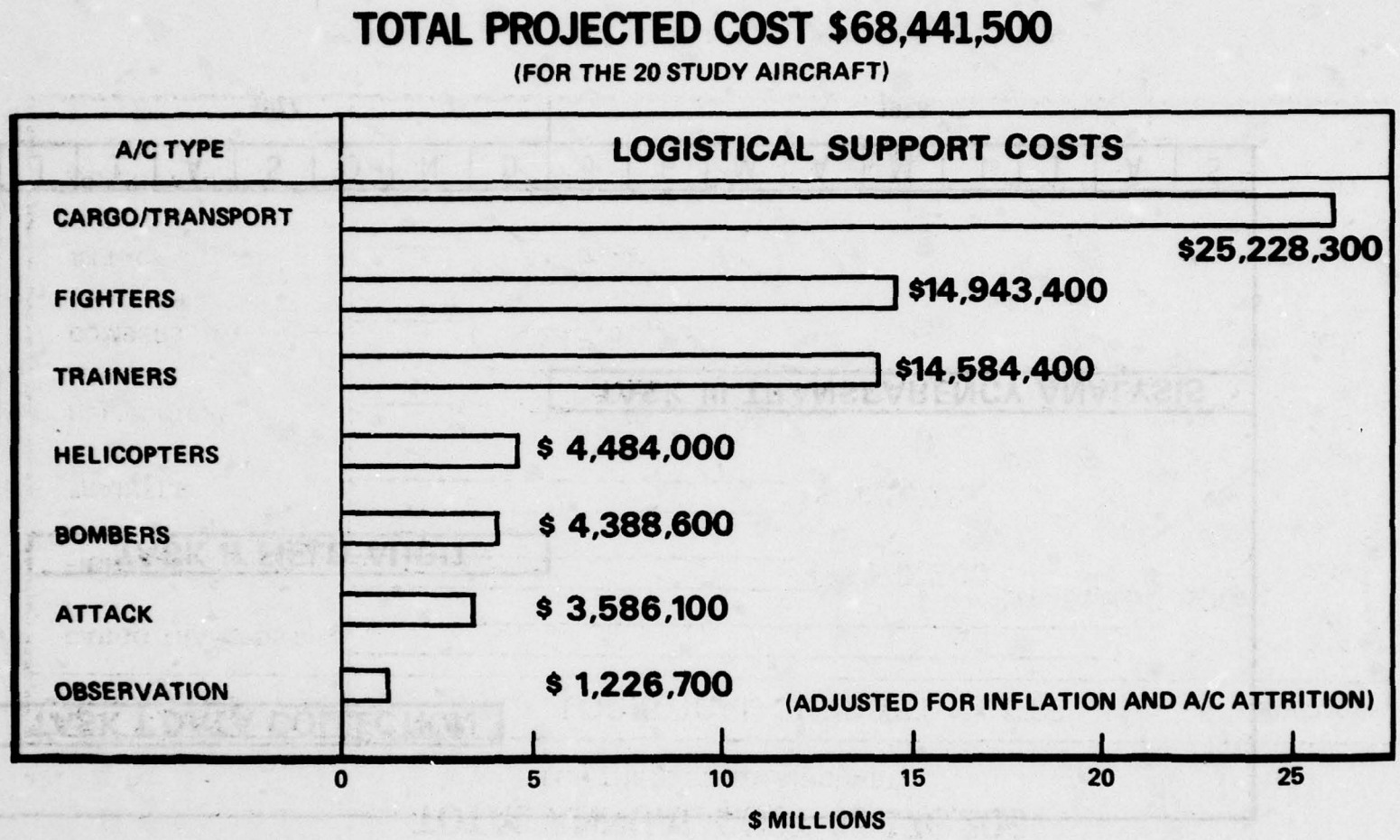


Figure 2. Projected 10-Year Maintenance Costs in 1978-88 Dollars

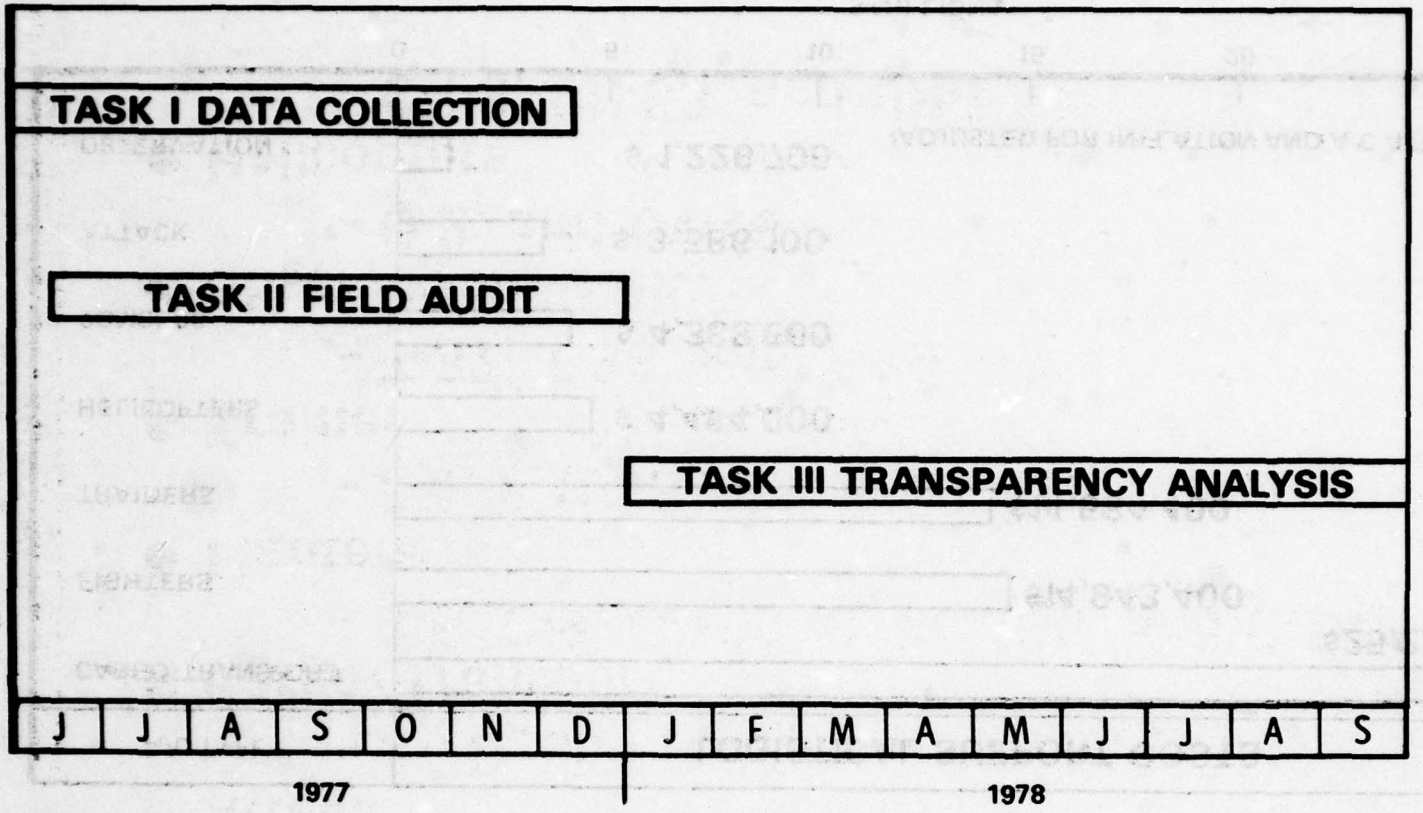


Figure 3. Program Requirements

- **Bombers**
  - B-52, B-57, and FB-111
- **Attack**
  - A-7D, and A-37
- **Cargo/Transport**
  - C-5, C-9, C-130, C/KC-135, and C-141
- **Fighters**
  - F-4, F-15, F-105, and F-111
- **Trainers**
  - T-37, T-38, and T-39
- **Observation/Utility**
  - O-2, and OV-10
- **Helicopters**
  - CH-3, CH-53, and UH-1

Figure 4. Study Aircraft

- **Transparency components**
  - **Windshields**
  - **Canopies**
  - **Cabin windows**
- **Interactive support systems**
  - **Anti-icing**
  - **Defogging**
  - **Rain removal**
  - **Operating and actuation systems**
- **Support structures**

Figure 5. Transparency/Support Systems

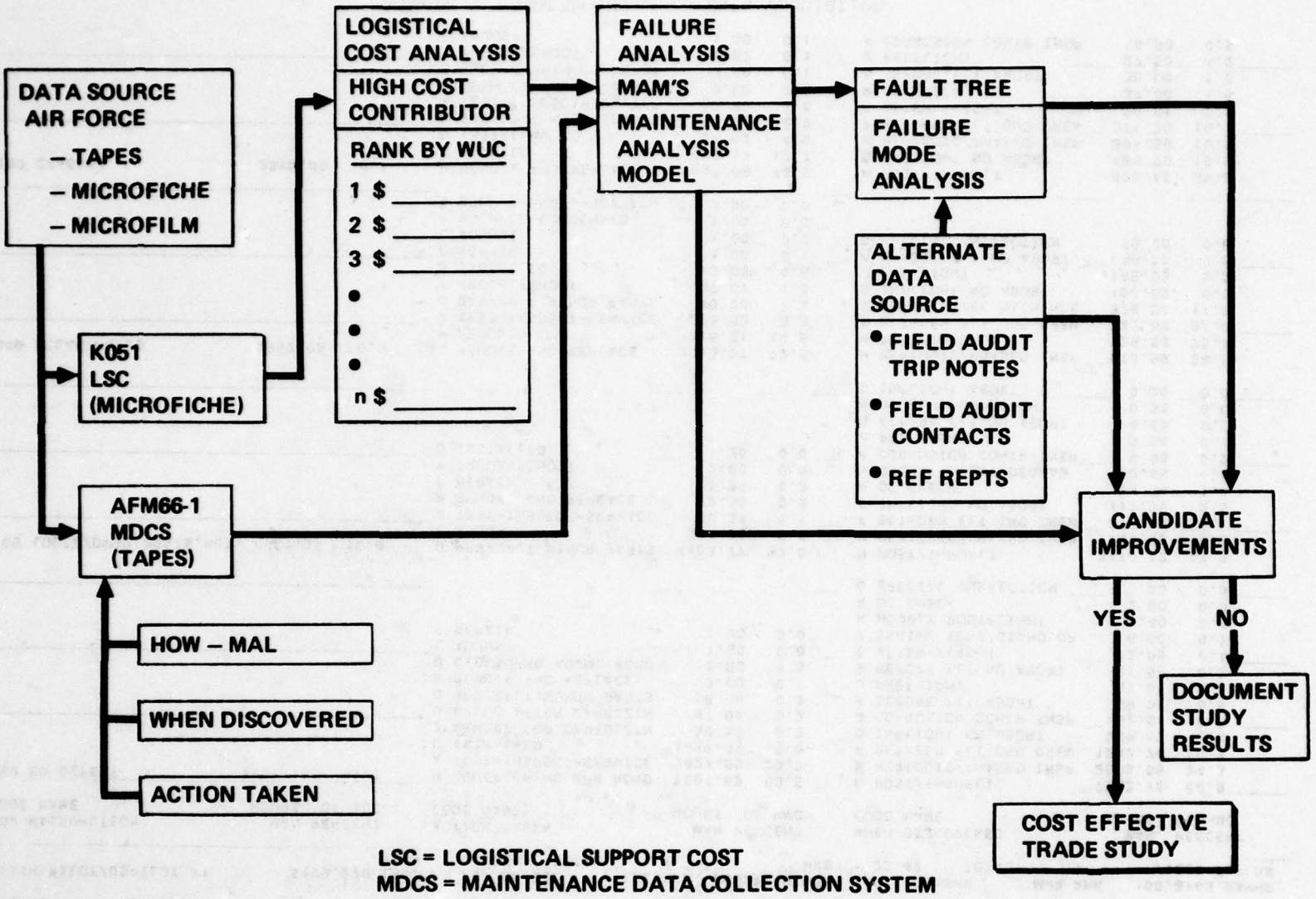


Figure 6. Evaluation Process

DESIGN/COST MAINTENANCE ANALYSIS MODEL

KC/C-135 TRANSPARENCY WUCS ONAC AND SHOP 1/76-6/77 - MARSHALL STA 11-C3 MAR. 18, 1978 PAGE 1

	FLIGHT HOURS	NO. OF FLIGHTS	LSC/YEAR	MANHOURS	MANHOURS/1000 FLIGHT HOURS
TOTAL	283,930	179,705	$850,348	121,987.68	429.63

1114H PILOT/COPILOT #1 $179,226 LSC/YEAR | PCT OF LSC 21.08 TOTAL | LSC RNK 1 | 28624.79 MAN HRS | PCT OF MHR 23.47 TOTAL | MHR RNK 1 | 100.8163 MANHR /1000 FLT HR

HOW MALFUNCTION CODE NAME	MAN HOURS	PERCENT OF WUC	ACTION TAKEN CODE NAME	MAN HOURS	PERCENT OF HMC	WHEN DISCOVERED CODE NAME	MAN HOURS	PERCENT OF HMC
799 NO DEFECT	11947.55	41.7	H EQUIP CK NO RPR RQRD	7581.62	63.5	H POST/THRUFLT	7262.10	60.8
			X TEST-INSPECT-SERVICE	2827.60	23.7	M PERIODIC/PHASED INSP	2908.65	24.3
			Q INSTALLED	1437.39	12.0	F BETWEEN FLT GND CREW	1282.20	10.7
			T REMOVE FOR CANIBLZTN	30.17	0.3	D INFLIGHT NO ABORT	289.17	2.4
			U RPLCD AFTER CANBLZTN	27.01	0.2	4 CORROSION CONTR INSP	62.51	0.5
			G RPR/RPLT MINOR PARTS	26.64	0.2	A BEFORE FLT ABORT	58.01	0.5
			R REMOVE AND REPLACE	12.00	0.1	J PREFLIGHT	37.51	0.3
			J CLBRTD-NO ADJMT RQRD	2.83	0.0	B BEFORE FLT NO ABORT	21.50	0.2
			L ADJUST	1.30	0.0	E AFTER FLIGHT	12.00	0.1
			F REPAIR	1.00	0.0	X ENGINE TEST STAND OP	6.50	0.1
						K HOURLY POSTFLIGHT	4.40	0.0
						R QC CHECK	2.00	0.0
						Q SPECIAL INSPECTION	1.00	0.0
105 LOOSE/DMGD BOLTS,NUT	4461.17	15.8	G RPR/RPLT MINOR PARTS	4103.77	92.0	H POST/THRUFLT	2110.12	47.3
			L ADJUST	280.16	6.3	M PERIODIC/PHASED INSP	1793.65	40.2
			X TEST-INSPECT-SERVICE	50.34	1.1	F BETWEEN FLT GND CREW	315.64	7.1
			R REMOVE AND REPLACE	12.30	0.3	D INFLIGHT NO ABORT	111.75	2.5
			F REPAIR	11.30	0.3	R QC CHECK	64.34	1.4
			Y TROUBLESHOOT	2.00	0.0	N GROUND ALERT-DEGRAD	50.68	1.1
			Q INSTALLED	1.30	0.0	4 CORROSION CONTR INSP	9.00	0.2
						J PREFLIGHT	5.00	0.1
						B BEFORE FLT NO ABORT	0.50	0.0
						K HOURLY POSTFLIGHT	0.30	0.0
						C INFLIGHT ABORT	0.20	0.0
846 DELAMINATED	2857.08	10.0	R REMOVE AND REPLACE	2075.27	72.6	M PERIODIC/PHASED INSP	813.99	28.5
			P REMOVED	415.21	14.5	H POST/THRUFLT	725.83	25.4
			X TEST-INSPECT-SERVICE	265.82	9.3	F BETWEEN FLT GND CREW	622.69	21.8
			G RPR/RPLT MINOR PARTS	40.20	1.4	S DEPOT LEVEL MAINTNCE	328.00	11.5
			Y TROUBLESHOOT	37.67	1.3	D INFLIGHT NO ABORT	186.53	6.5
			Q INSTALLED	16.00	0.6	J PREFLIGHT	148.03	5.2
			F REPAIR	4.00	0.1	B BEFORE FLT NO ABORT	16.00	0.6
			L ADJUST	1.00	0.0	Q SPECIAL INSPECTION	16.00	0.6
			9 BNCH CK-CONDENNED	1.00	0.0			
			1 BNCH CK-NRTS-NOT ATH	0.90	0.0			
190 CRACKED	2313.49	8.1	R REMOVE AND REPLACE	1694.08	73.2	H POST/THRUFLT	920.46	39.8
			P REMOVED	409.11	17.7	D INFLIGHT NO ABORT	460.75	19.9
			Q INSTALLED	103.02	4.5	M PERIODIC/PHASED INSP	391.55	16.9
			G RPR/RPLT MINOR PARTS	66.01	2.9	F BETWEEN FLT GND CREW	371.70	16.1
			X TEST-INSPECT-SERVICE	32.80	1.4	E AFTER FLIGHT	58.01	2.5
			A BNCH CK AND REPAIRED	3.50	0.2	R QC CHECK	37.00	1.6
			B BNCH CK-RTN TO DEPOT	2.00	0.1	A BEFORE FLT ABORT	36.00	1.6
			Y TROUBLESHOOT	1.67	0.1	J PREFLIGHT	27.50	1.2
			L ADJUST	1.30	0.1	4 CORROSION CONTR INSP	10.50	0.5

Figure 7. MAM Maintenance Data Tabulation

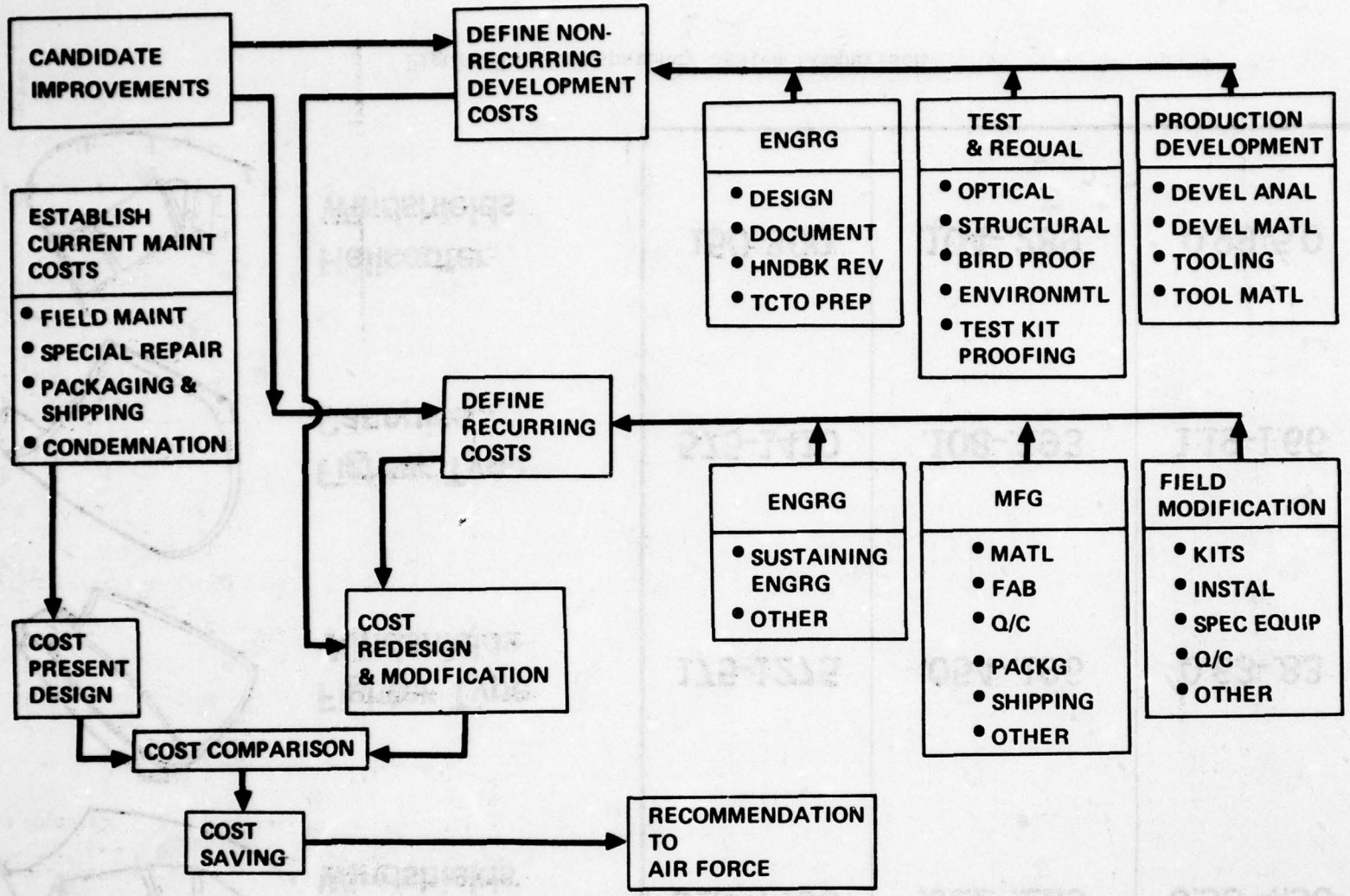
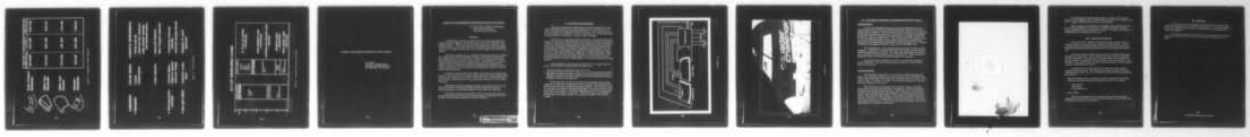


Figure 8. Cost-Effective Trade Study

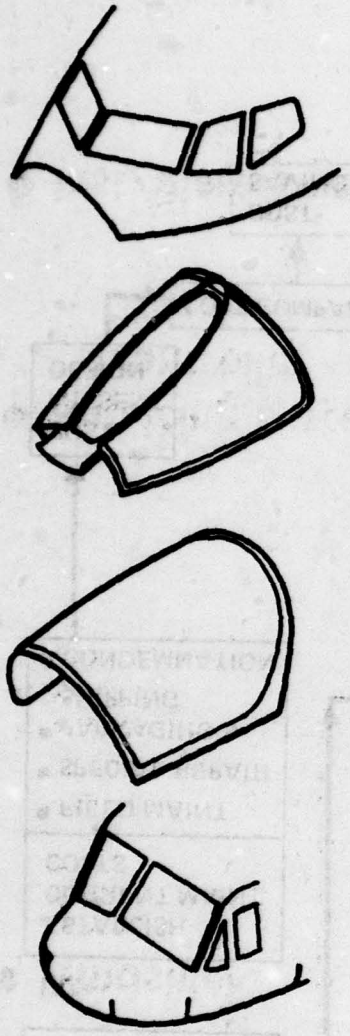
AD-A065 049 AIR FORCE FLIGHT DYNAMICS LAB WRIGHT-PATTERSON AFB OHIO F/G 1/3
CONFERENCE ON AEROSPACE TRANSPARENT MATERIALS AND ENCLOSURES (1--ETC(U)
DEC 78 R E WITTMAN

UNCLASSIFIED AFFDL-TR-78-168 NL

10 OF 10
ADA
065049



END
DATE
FILMED
4-79
DDC



	MEAN TIME BETWEEN FAILURE	MAINT MANHOURS/ FLT HRS	LOGISTICAL SUPT COST ($/FLT HR)
Cargo/Transport Windshields	915-4400	.022-.285	0.93-4.58
Fighter Type Windshields	175-1275	.054-.196	0.63-.83
Fighter Type Canopies	575-1410	.108-.393	1.19-1.66
Helicopter Windshields	150-300	.104-.289	0.99-5.0

Figure 9. Transparency System Comparison

COMPONENT	FAILURE MODES	CANDIDATE IMPROVEMENTS
• Windshield	- Cracks - Delaminations	- Revise outer ply - Improved flex interlayer - Edge member redesign and improved sealing
	- Loose fasteners	- Improved fasteners - More frequent inspection
• Anti-icing system controller	- Internal failure - Failed to operate - Incorrect voltage	- Incorporate improved controller - Improved warning devices
• Inst/glare shield	- Extensive access hours	- Redesign for quick disconnect

Figure 10. Failure Analysis

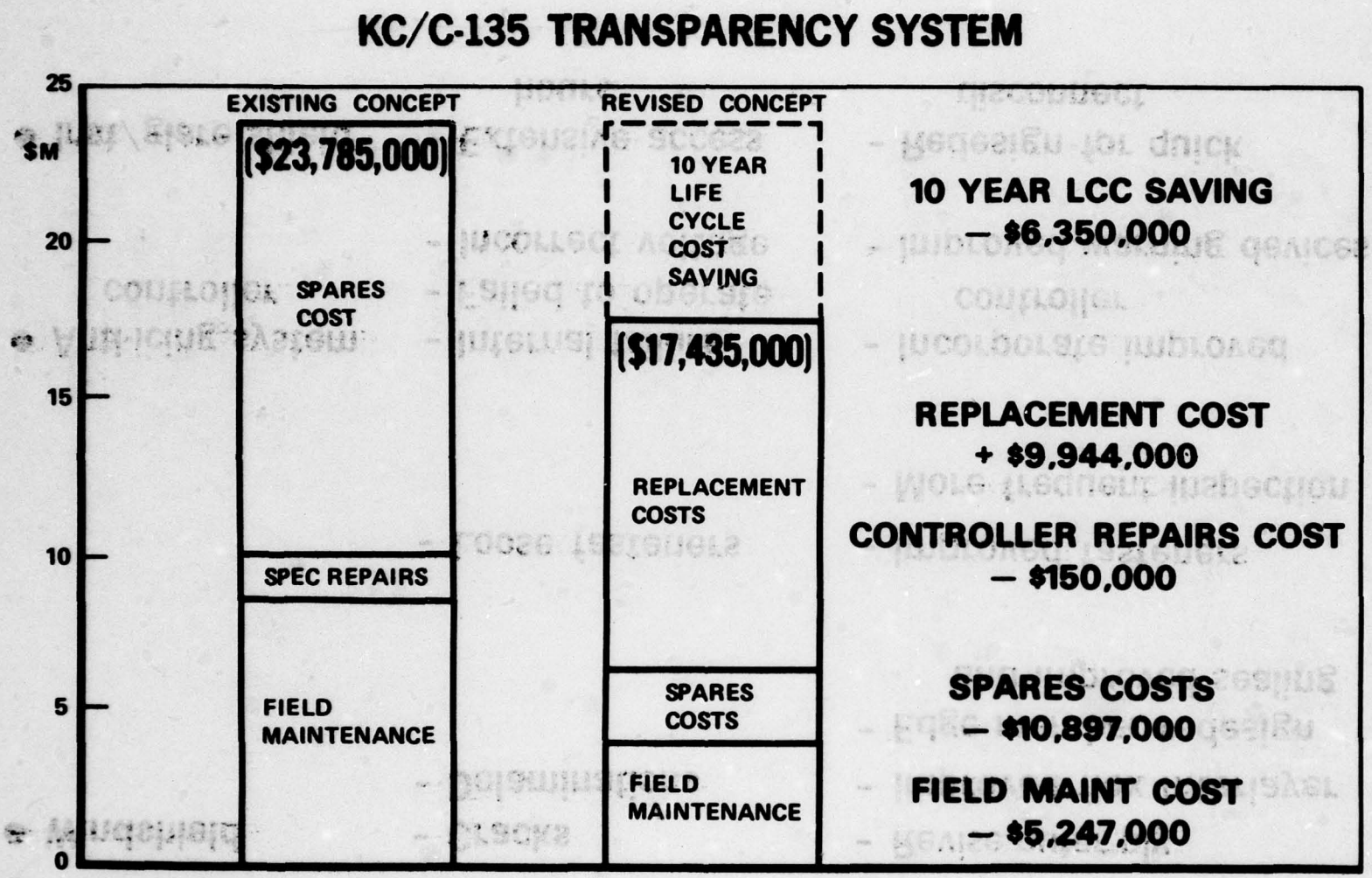


Figure 11. Preliminary Trade Study Results

AIRCRAFT TRANSPARENCY/CONTROLLER SYSTEM APPROACH

E. Goller
Sierracin Corporation
Thermal Systems Division
Los Angeles, California

AIRCRAFT TRANSPARENCY/CONTROLLER SYSTEM APPROACH

By Eric Goller, Engineering Manager
Sierracin Corporation
Thermal Systems Division

Abstract

Traditionally, airframe manufacturers have obtained heated windshields from one supplier, and the associated electronic controller from another supplier. This leaves the airframe manufacturer with the responsibility for all or most of the technical coordination and system debugging, and in case of system malfunction, the warranty situation can become very cloudy.

Sierracin has pioneered in supplying complete transparency systems. By employing this system acquisition concept, the airframe manufacturer and subsequent users have one point of contact in negotiating any product improvement and/or warranty considerations. The supplier of a transparency/controller system must coordinate requirements regarding size, weight, attachments (both electrical and mounting) and cooling with the airframe manufacturer and also match the windshield and controller requirements and performance.

Provision must be made for P-static protection to the transparency system, either glass-faced or plastic-faced, and also keeping voltage surges out of the aircraft electrical system. Fail-safe modes, normal operating and overheat conditions must be considered and accounted for in the system approach.

Placing the heated transparency system requirements with one supplier allows them to evaluate tradeoffs that will ensure the most cost-effective approach for providing optimum service life and reliability.

This paper will discuss examples of this system approach and enumerate the performance and contractual advantages of this approach to the benefit of the airframe manufacturer and his customers.

PRECEDING PAGE BLANK-NOT FILMED

I. Introduction and Discussion

The major components comprising an aircraft windshield de-icing system (See Exhibit #1) are the heated windshield and the electronic controller necessary to actuate the windshield heaters. The expertise necessary for design and manufacture of these components has, in the past, been so diversified as to eliminate a common source of supply.

The Sierracin Corporation has developed the required capabilities to design, manufacture, and furnish these two components within its corporate structure. Sierracin's Sylmar Division has long been a leader in the fabrication of aircraft heated transparencies, while the Thermal Systems Division has the capability to design and manufacture sophisticated electronic control devices. A blending of these proficiencies has produced a unique resource. Currently Sierracin is supplying a complete windshield system for the Canadair CL-600 Challenger Executive Jet (See Exhibit #2). This marks the first time that any single supplier has assumed full technical, manufacturing and warranty responsibility for an entire windshield de-icing system.

The advantages to the airframe manufacturer of a single source of supply for the entire de-icing system are significant:

- One technical and contractual source of contact
- System performance warranty rather than individual component warranty
- Matched componentry design resulting in optimum system performance
- Integrated system tests assure satisfactory system performance prior to delivery to airframe manufacturer

In the past when a failure occurred in the windshield and separate suppliers furnished the windshields and their controls, the airframe manufacturer was placed in an awkward warranty position. Did the failure occur as a result of a problem in the windshield itself, or was it caused by a malfunction of the controller? Usually enough doubt existed that a contractual tug-of-war could continue ad nauseam. With total system responsibility resting with one supplier, there is no doubt who shoulders the warranty burden.

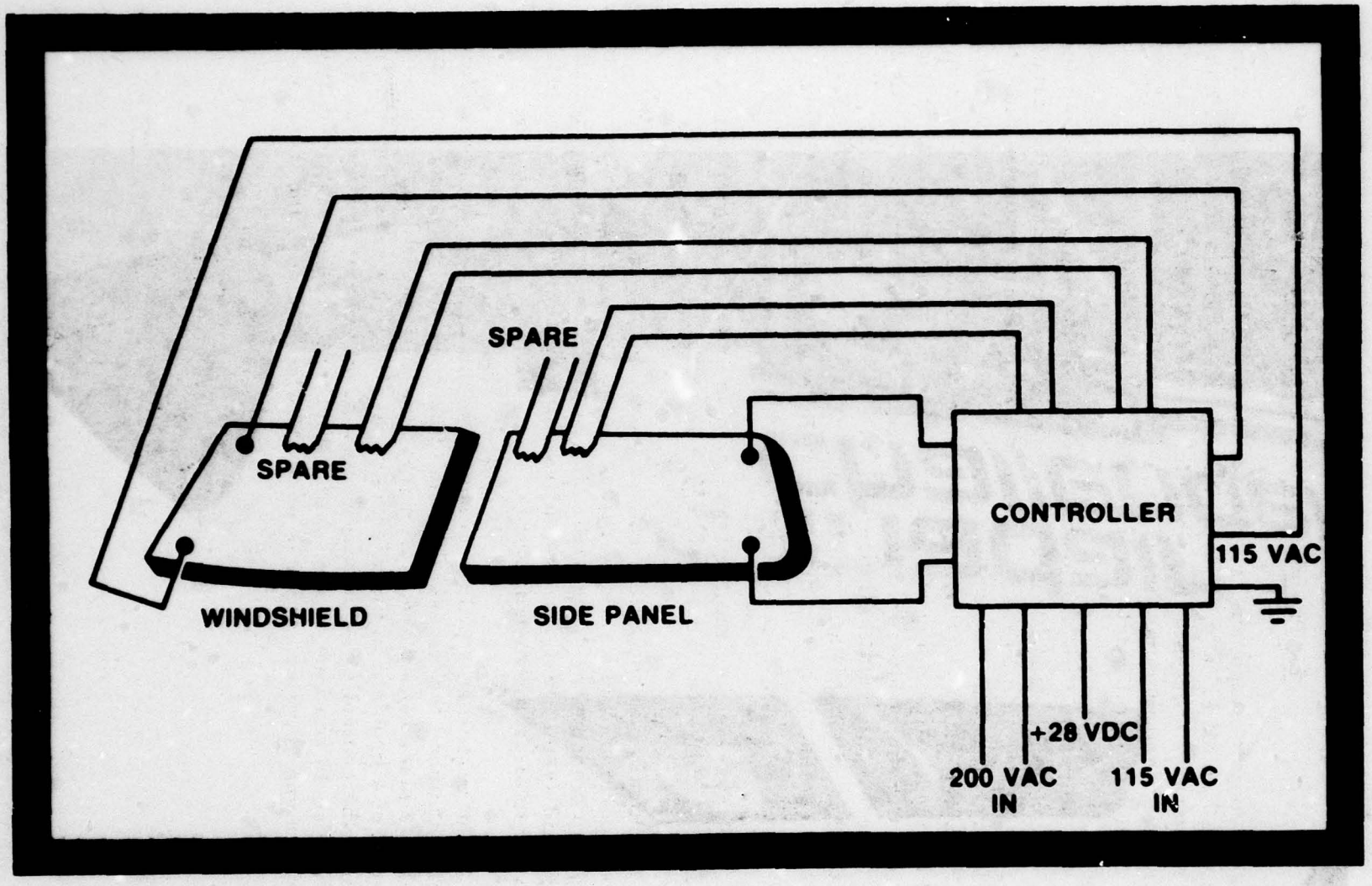

SPARE
SPARE
CONTROLLER
115 VAC
WINDSHIELD
SIDE PANEL
+28 VDC
200 VAC
IN
115 VAC
IN

EXHIBIT #1



EXHIBIT #2

II. Description of Challenger Transparencies/Controller System

Transparencies:

The CL-600 windshields and side panels (See Exhibit #3) are currently in test for bird impact qualification at National Research Council of Canada (NRC) at Ottawa. These transparencies incorporate a novel approach employed by Canadair for maximizing crew vision. Canadair has designed the CL-600 to have no sideposts; the windshield frame simply overlaps the side panel, acting as a splice plate. This concept allows the transparencies to carry pressurization loads in hoop tension and thereby simplifies and lightens the total assembly by eliminating mounting structure in the airplane, in addition to providing maximized vision area for the flight crew.

The windshield is a fail-safe plastic laminate with stretched acrylic mainplies. Provision for drawing off P-static have been incorporated into both the windshield and controller. The anti-icing heating film operates at a power density of 4.0 watts/square inch at 200 volts AC. Optical quality is excellent, even at the critical installation angle of 33 degrees.

Side panels for the Canadair CL-600 are also fail-safe stretched acrylic laminates. The anti-fog heating film produces 1.2 watts/square inch at 115 volts AC.

Controller System:

Two controller assemblies are furnished for each Challenger aircraft. Each assembly consists of a windshield temperature controller (for 1/2 the windshield) and an anti-fog heater controller (one side panel), and is about 8" wide x 6" deep x 4" high. This includes cooling fins, since no external cooling air is provided.

The design of the controllers is such that any single component failure will not result in overheating the windshield. Ultimate windshield protection was a prime design objective. Solid state power switching for On/Off control provides increased reliability. Specific circuitry protects against spikes and transient voltage so that nuisance tripping will be minimized. Automatic fail-safe operation is featured to turn power Off in the event of overcurrent, overtemperature at the windshield sensor and excessive duration of power loss. A push-to-test feature provides a check of the units operation at anytime upon demand.

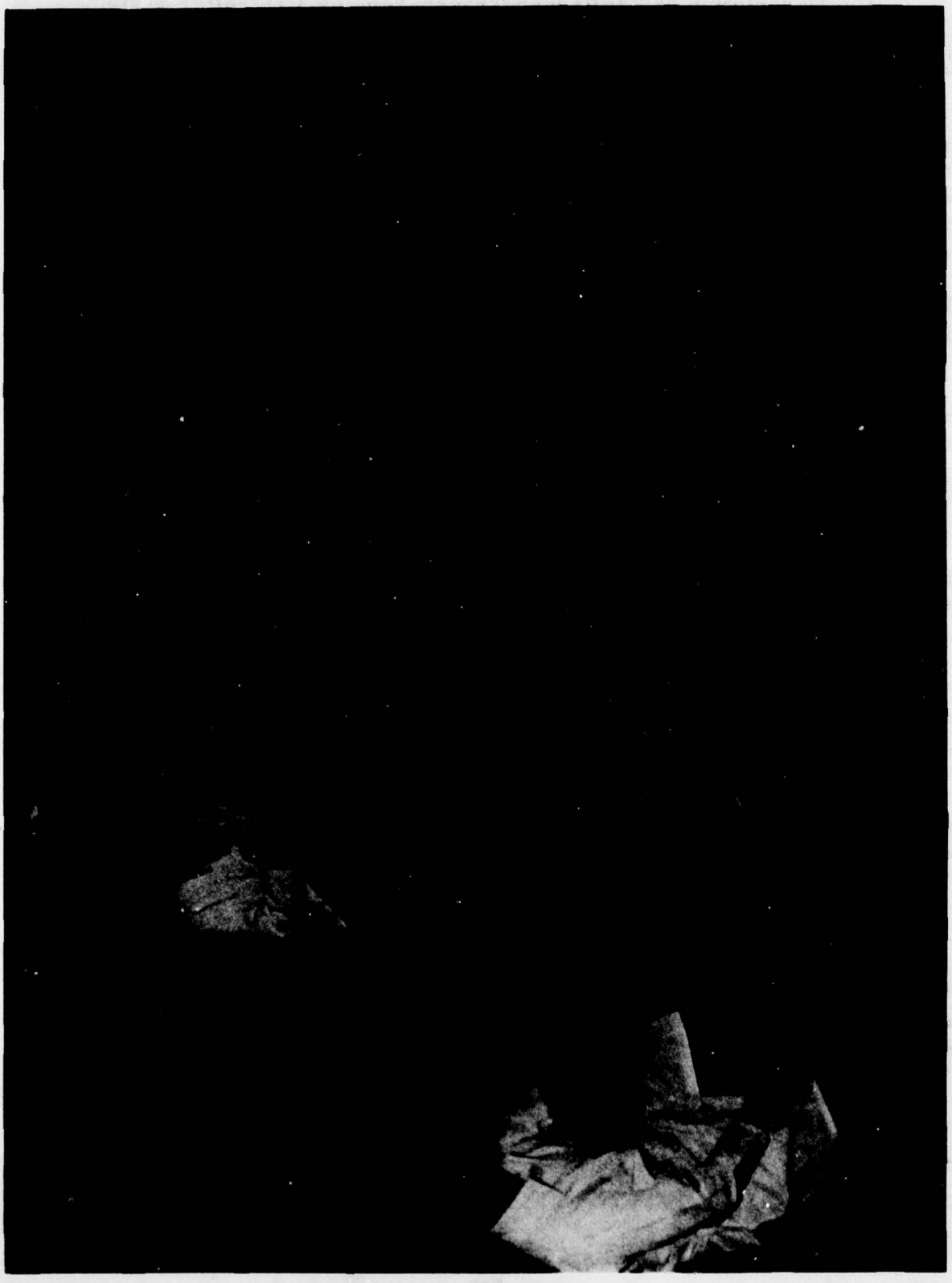


EXHIBIT #3

The windshield controller utilizes 200 V, 1 phase, 400 Hz power and has 3.4 kw capability while the side panel anti-fog heater controller has 115 V, 1 phase, 400 Hz power and has 1.5 kw capacity.

The controller has functioned successfully under extremely severe environmental conditions of temperature, altitude, humidity, vibration, shock, and EMI by passing qualification testing. The unit is now mated to a windshield and is undergoing systems test.

III. System Considerations

Development of a complete windshield de-icing system within one company requires careful planning, design and implementation. This is necessary from the conceptual phase through the component design phase, component fabrication and test and finally component mating and systems test.

Continuous contact between groups within the involved divisions at Sierracin has resulted in a steady feedback of design criteria originating with the windshield. This interaction of design detail has produced more closely matched components from windshield to sensor to controller. For example, it has been possible to adjust controller design criteria quickly as a result of windshield test results.

An analysis was made by Sierracin to determine what systems testing would be required. The objective of systems testing is to verify systems performance. In order to satisfy this objective the following tests were defined:

- Thermal chamber tests to simulate de-icing conditions on the system
- Controller fail-safe operational testing (as a part of the system):

  Overcurrent
  Power loss
  Overtemperature

- Life cycling

Only after meeting customer requirements as evidenced within systems tests will Sierracin be satisfied that the final system product will be worthy of delivery to the customer.

IV. Summary

For the first time, one supplier has manufactured an entire windshield de-icing system for an airframe manufacturer. This eliminates the need for the airframe manufacturer to debate warranty effectivity with component suppliers.

The systems approach during design, development and test of windshields and controllers will result in a performance tailored de-icing system.

*U.S.Government Printing Office: 1979 — 657-002/352